

AFAPL-TR-65-108

aerospace expandable structures

conference transactions

sponsored by:

air force aero propulsion laboratory
in cooperation with
archer daniels midland company
25, 26, 27 may, 1965
minneapolis, minnesota

Technical Report No. AFAPL-TR-65-108

AD681406

CLEARINGHOUSE FOR FEDERAL SCIENTIFIC AND TECHNICAL INFORMATION	
Hardcopy	Microfiche
\$11.00	\$3.25, 803 pp, AD
ARCHIVE COPY	

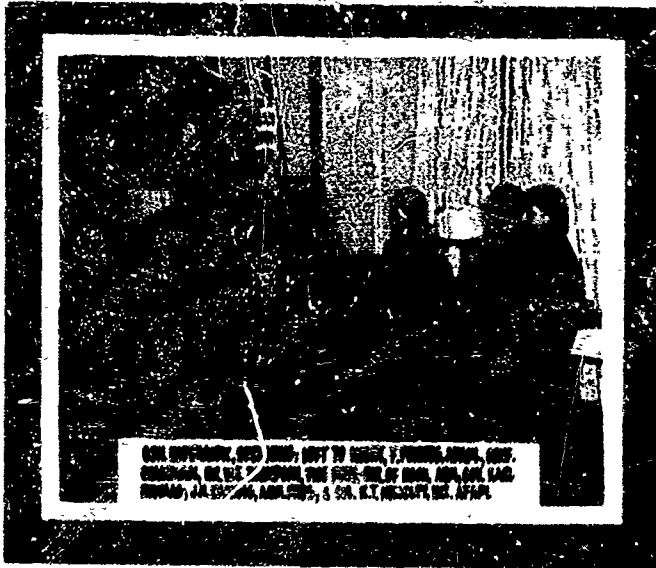
Code 1

Distribution of this document is unlimited

NOTICES

When Government drawings, specifications, or other data are used for any purpose other than in connection with a definitely related Government procurement operation, the United States Government thereby incurs no responsibility nor any obligation whatsoever; and the fact that the Government may have formulated, furnished, or in any way supplied the said drawings, specifications, or other data, is not to be regarded by implication or otherwise as in any manner licensing the holder or any other person or corporation, or conveying any rights or permission to manufacture, use, or sell any patented invention that may in any way be related thereto.

Copies of this report should not be returned to the Research and Technology Division unless return is required by security considerations, contractual obligations, or notice on a specific document.

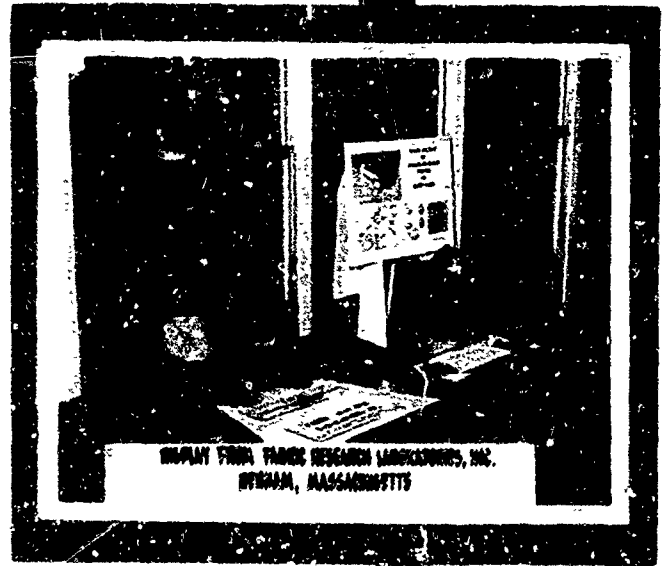


COLL. SUPERVISOR, BIRD KING; LEFT TO RIGHT: J. F. WOOD, JR., MGR. COMM. DIV. OF THE AIR FORCE; DR. R. L. BROWN, JR., MGR. AIR FORCE LAB. WINDMILL, J. A. BROWN, MGR. AIR FORCE, & COL. R. T. HESS, JR., AFAPL



EXPANDABLE STRUCTURE EXHIBITED ON THE LAFAYETTE CLUB GROUND

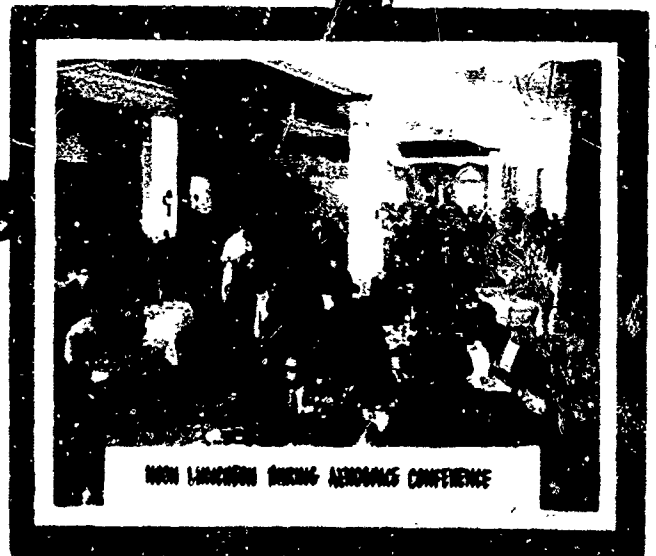
2nd AEROSPACE EXPANDABLE STRUCTURES CONFERENCE



DISPLAY FROM FABRIC RESEARCH LABORATORIES, INC. WYHAM, MASSACHUSETTS



CONFERENCE IN SESSION IN THE MAIN BALLROOM OF LAFAYETTE CLUB



NOON LUNCHEON DURING AEROSPACE CONFERENCE

**SECOND
AEROSPACE EXPANDABLE STRUCTURES CONFERENCE**

25, 26 and 27 May 1965

Sponsored By

AIR FORCE AERO PROPULSION LABORATORY

In Cooperation With

ARCHER DANIELS MIDLAND COMPANY

**In
Minneapolis, Minnesota**

FOREWORD

This conference presents technical contributions summarizing the status of current, significant research in the field of expandable structures. It is our hope that these contributions will encourage the undertaking of new research in expandable structures. This conference has been designed to provide a forum of authorities to critique current research and to propose new research and applications for expandable structures which are necessary to advance the art.

Publication of this report does not constitute Air Force approval of the report's findings or conclusions. It is published only for the exchange and stimulation of ideas.

RICHARD T. HEMSLEY
Colonel, USAF
Director, AF AeroPropulsion Laboratory

ABSTRACT

This report contains a presentation of technical contributions summarizing the status of current, significant research in the field of expandable structures. The report is based upon the discussions at the Second Aerospace Expandable Structures Conference held 25-27 May 1965 at the Lafayette Club, Minnetonka Beach, Minnesota. The subject matter has been arranged in six sessions in the order of presentation at the conference, followed by six papers which were not given at the conference.

CONFERENCE ORGANIZATION

Honorary Chairman

Colonel Richard T Hemsley
Director, Air Force Aero Propulsion
Laboratory

Chairman

Fred W Forbes
Air Force Aero Propulsion Laboratory

Escort Officers

1st Lt A J Zappanti
2nd Lt P W Lauderback
Air Force Aero Propulsion Laboratory

Conference Management Staff

G R Ault, ADM Research
J A Wickland, ADM Public Relations
M Steeg, ADM Public Relations
D F Benson, ADM Employee Relations
J Rusinko, ADM Advertising
C Hall, ADM Research
K Reamer, ADM Research
J Falconer, ADM Research
G A Stein, ADM Research
W J McKillip, ADM Research
C E Sondergelt, Printing, AFSC
M McMurtrie, Technical Publications, AFSC

Exhibit Management Staff

W R Davidson, GCA Corporation
M Mandish, GCA Corporation
I W Russell, GCA Viron Division
D T Hiel, GCA Viron Division
R R Rochon, GCA Viron Division
N S Hansen, GCA Viron Division

CONFERENCE SITE

The conference was held at the Lafayette Club located in a beautiful setting on Lafayette Bay of Lake Minnetonka, Minnetonka Beach, Minnesota.

EXHIBITS

Exhibits of interesting structures, equipment and materials pertinent to the conference are located on the porch behind the front of the conference hall and on the lawn between the club house and the lake. The exhibits are presented for your interest by:

Air Inflatable Products Corp,
Samford, Connecticut

Fabric Research Laboratories, Inc
Dedham, Massachusetts

GCA Viron Division, A Division of GCA Corp,
Minneapolis, Minnesota

Hughes Aircraft Company
Culver City, California

Narmco Research and Development Division
Whittaker Corporation
San Diego, California

G T Schjeldahl Company
Northfield, Minnesota

Space General Corp
Del Monte, California

University of Cincinnati, College of Design,
Architecture, and Art
Cincinnati, Ohio

US Air Force Aero Propulsion Laboratory
Research and Technology Division
Air Force Systems Command
Wright-Patterson Air Force Base, Ohio

US Army Engineer Research and Development
Laboratories, Corps of Engineers
Fort Belvoir, Virginia

ACKNOWLEDGEMENT

Special acknowledgement is given to William E. Thompson, Vice President in charge of Research, Archer Daniels Midland; Gerald R. Ault, Conference Arrangement Chairman, ADM; and John Wickland, Conference Public Relations, ADM, for their efforts in the arrangement and running of this Second Aerospace Expandable Structure Conference. Mr. Warren R. Davidson, GCA Corporation, is also commended for his efforts in arranging the technical displays exhibited at the conference.

The front cover of this report was designed by Tom Rotroff, Department of Industrial Design, College of Design, Architecture, and Art, University of Cincinnati.

EXPANDABLE STRUCTURES FOR OUR
GROWING SPACE PROFICIENCY

Brigadier General Joseph S. Bleymaier
Deputy Commander for Manned Systems
Hq, Space Systems Division (AFSC)

Good morning, ladies and gentlemen. I welcome the opportunity to participate in this second Expandable Structures Conference. Our sister organization, the Research and Technology Division, has direct responsibility for expandable structure research; but we in the Space Systems Division have uses for the results of this research. Our partnership, therefore, is a close and, I hope, a continuing one.

Some of you who are pilots, or ex-pilots, may have heard the story of the nearsighted flyer who, despite his affliction, had an excellent record. He could readily see the instruments but couldn't distinguish objects 15 to 20 feet ahead of him. He was asked how he could possibly land an airplane under those conditions.

"Oh," he explained, "I bring the plane in on instruments. Then when I know I'm getting close to the runway I just watch the co-pilot."

He was asked, of course, what possible good it did to watch the co-pilot.

"Simple," said the old expert. "When I see him flinch and cover his eyes with his arms, why I just flare out and there we are, safe and sound on the deck."

Although I don't recommend this as a flying safety technique, I would suggest to you this morning that while our outlook on space today is limited we are not turning back from our responsibilities or opportunities. If we watch each other -- if we apply the results of our research and technology in a timely, practical manner, we'll produce systems that will give us all the space proficiency we require or desire.

For example, a full-size expandable structure, for possible use in space as a solar collector, a shelter, or even a space station is being built and will be tested this fall at the Aero Propulsion Laboratory at Wright-Patterson Air Force Base.

This 25-foot long, 10-foot diameter honeycomb structure is being built here in Minneapolis by the Viron Division of the Geophysics Corporation, under an Aero Propulsion Laboratory contract. The entire structure is compressed into a small package held together at the front and rear bulkheads by explosive bolts.

A follow-on program involving an extension of this technology into a 75-foot diameter structure is already planned.

The advanced solar turbo electric concept program being conducted by the sponsor of this conference also has significance to military and NASA projects. This program is aimed at providing a 52-foot diameter expanded solar collector and associated energy conversion equipment which could provide 15 kilowatts of electrical power for future space systems.

Another potentially useful project being conducted by the Aero Propulsion Laboratory is the development of expandable crew transfer tunnels/airlocks and space "maintenance hangars."

Prototype transfer tunnels are to be developed and tested for possible application to manned systems, such as our Manned Orbiting Laboratory. The use of expandable components could, quite obviously, effect considerable savings in payload volume. As a matter of fact, there are expandable structure experiments planned for early MOL flights.

A keynote address is supposed to sound a note of challenge -- and, ladies and gentlemen, you have a challenge clearly before you. A few years ago we complained that our space ambitions were rapidly being overcome.

We have, for example, the Titan III space launch system -- capable of an assortment of orbits, a variety of trajectories, and payloads ranging from 5,000 to 25,000 pounds.

On the fourth test flight of the Titan III, May 6th, we put the upper stage -- which we call the transtage -- into three successive orbits, exactly as planned. We released the two satellites the bird was carrying, and then we carried out a fourth ignition which put the vehicle into a final 1,500 to 2,000 mile orbit.

This fourth "burn" was the first ever accomplished in space, and let me tell you how close we came to meeting the parameters. We planned a perigee of 1,502 nautical miles; we achieved 1,500 miles. We were shooting for an apogee of 2,007 miles; we got 2,015 miles. The orbital period we programmed was 156.5 minutes; the actual orbital pass time clocked out to be 156.7 minutes. The eccentricity, or deviation from the circular, was calculated to be .049. It proved to be exactly that.

In addition to hitting the mark on this bonus test, we came extremely close to putting the payloads into the intended orbits -- the experimental Lincoln Laboratory communications package into a 1,700 to 11,000 mile elliptical orbit, and the radar calibration satellite into a 1,700 mile circular orbit.

This fourth and final test of the Titan III "A" configuration (without the two large solid motors) climaxed a remarkable series -- the first flight being 95 per cent successful and second and third flights producing the most accurate orbits ever attained by U.S. space vehicles.

Next month we will launch the first Titan III-C. With 2.4 million pounds of thrust from the first-stage large solid propellant motors, we propose to put a 21,000 pound payload into space. Counting the weight of the transtage vehicle, this will amount to nearly 30,000 pounds on orbit!

We have, therefore, a pretty good launch system going for us. The real demanding challenge facing us today is for functional, meaningful, practical payloads. The use of expandable techniques and technologies affords us an opportunity to take added advantage of the greater weight-lifting capabilities now available to us by simultaneously minimizing the pre-orbit volume and weight of our payloads.

Certainly, there is an abundance of possible payloads in our space future -- payloads for both military and nonmilitary purposes. One very important one on the horizon is the one I have already mentioned -- the Manned Orbiting Laboratory.

The MOL, if approved, clearly has the potential of serving as a proving ground in space, both for men and for equipment; and as a point of sensible departure to systems supporting military missions. Once its initial "laboratory" functions are satisfied, the MOL system -- encompassing the Gemini B plus the Titan III transtage -- could translate into a true work-oriented manned orbiting vehicle. As such, this mission-designed system may well qualify as our first experimental space vehicle -- the "X-1" of space.

The outlook, therefore, is both promising and exciting.

The MOL, during its development and early uses, may serve not only as a carrier for experiments with expandable structures, but may well benefit from the expandable arts as applied to the construction and furnishings of the vehicle itself.

This is what I mean by the importance of close and continuing rapport on the part of the R&T Division and its laboratories, the Space Systems Division, and our industry associates.

Ten years ago only a few engineers were pursuing expandable structures research for aerospace applications. Today this research has "expanded" far beyond the imaginations of even its most ardent supporters. During the past two years, some \$45 million has been spent in research programs.

The view ahead is for perhaps fewer programs, but programs that are more intensive and directed toward practical applications. A number of these programs promise to culminate in actual space experiments.

This, of course, is the objective of all our efforts -- to produce systems that will work, and that will work for us, in space. We have an excellent foundation for progress in the past 10 years of aerospace achievements. The Titan III provides us a new dimension of booster versatility and flexibility. The Manned Orbiting Laboratory affords us a new threshold to manned space capabilities.

There's no question about it, our space dexterity is expanding. You have helped; you can continue to help. No matter how distant or difficult our objectives, we have the skills and the resources to do the job.

And as you in this industry have so amply demonstrated, both of these attributes are expandable.

Thank you.

TABLE OF CONTENTS

SESSION I

Expandable Structures Design Concepts for
Astronaut Transfer Mr. L. Jurich
Mr. F. W. Forbes
Captain J. Schofield
Mr. V. F. Hribar

Development and Optimization of a Resin System
for Rigidization Mr. W. J. McKillip
Mr. R. H. Leitheiser
Mr. L. M. Clemens
Mr. C. N. Impola
Mr. J. Lee

Application of Expandable Honeycomb to
Fabrication of Space Structures. Mr. I. W. Russell
Mr. C. Koons

SESSION II

Lightweight, Expandable Support Shelter Systems. Mr. J. M. Alexander

Bare Base Development Concepts. Mr. K. H. Merkel
Mr. J. M. Alexander
Mr. G. C. Born

'Ratio' Automated Assembly Technique for
Space Structures. Mr. P. Slysh

Chemical Rigidization of Preformed Flexible Foams. Mr. J. F. Hanny

Maintenance Technology for Space Systems. Mr. C. B. May

SESSION III

Structural Considerations for an Expandable
Lenticular Satellite Mr. J. L. Humble

Application of Inflatable Structures to Station
Keeping of Passive Communications Satellites Mr. J. E. Cooper

Development of Manufacturing Techniques for a
Metal Fabric Reinforced Re-entry Paraglider Mr. J. F. Keville

Bending of Unfurlable Tubular Structures in Space Dr. G. G. Herzl

TABLE OF CONTENTS (Cont'd)

Development and Evaluation of a Rigidized Inflatable
Microwave Reflector Mr. K. F. Gibson
Mr. G. M. Peace

SESSION IV

Sodium Silicate as a Versatile Structural Material . . . Mr. H. I. Hoffman

Inflatable Thermal Radiation Shield for Space Application. Mr. J. E. Marshall

A Predistributed Foam for Rigidizing Membrane
Structures in Space Mr. N. Jouriles

Semirigid or Nonrigid Structures for Space Applications . Mr. P. M. Knox
Mr. R. Omer Moses

Buildings in Barrels-(Part III) Mr. S. B. Swenson

Metal Fabrics for Aerospace Expandable Structures. . . . Mr. W. D. Freeston Jr.

Simulation of Meteoroid Impact Effects on
Expandable Structures. Lt. A. J. Holten

SESSION V

Development of an Expandable Airlock Utilizing Elastic
Recovery Principles. Mr. J. Williams
Mr. N. O. Brink

Potential Applications for Expandable and Inflatable
Structures for Re-entry Vehicles Mr. R. P. Wykes

Compression Tests of Wire-Film Cylinders Mr. E. Rottmayer

Design Criteria for Inflated, Expandable Beams Used as
Structural Members in an Advanced Concept Paraglider . . . Mr. R. A. Toni
Mr. J. F. McNulty

Development of Space Expanded and Rigidized Solar
Energy Collectors. Mr. S. Schwartz

SESSION VI

Aluminum Foil Expandable Structures. Mr. S. Motta

Fabrication and Pressurization Technology for
Improvement of Surface Accuracy of Passive
Communications Satellites. Mr. D. C. Grana
Mr. W. E. Bressette

TABLE OF CONTENTS (Cont'd)

Development and Evaluation of a Rigidized Inflatable Microwave Reflector	Mr. K. F. Gibson Mr. G. M. Peace	M S A
SESSION IV		
Sodium Silicate as a Versatile Structural Material . . .	Mr. H. I. Hoffman	A
Inflatable Thermal Radiation Shield for Space Application.	Mr. J. E. Marshall	D T
A Predistributed Foam for Rigidizing Membrane Structures in Space	Mr. N. Jouriles	
Semirigid or Nonrigid Structures for Space Applications .	Mr. P. M. Knox Mr. R. Omer Moses	S C
Buildings in Barrels-(Part III)	Mr. S. B. Swenson	
Metal Fabrics for Aerospace Expandable Structures. . . .	Mr. W. D. Freeston Jr.	S
Simulation of Meteoroid Impact Effects on Expandable Structures.	Lt. A. J. Holten	R A
SESSION V		
Development of an Expandable Airlock Utilizing Elastic Recovery Principles.	Mr. J. Williams Mr. N. O. Brink	C O H E:
Potential Applications for Expandable and Inflatable Structures for Re-entry Vehicles	Mr. R. P. Wykes	
Compression Tests of Wire-Film Cylinders	Mr. E. Rottmayer	D O:
Design Criteria for Inflated, Expandable Beams Used as Structural Members in an Advanced Concept Paraglider . . .	Mr. R. A. Toni Mr. J. F. McNulty	
Development of Space Expanded and Rigidized Solar Energy Collectors.	Mr. S. Schwartz	
SESSION VI		
Aluminum Foil Expandable Structures.	Mr. S. Motta	
Fabrication and Pressurization Technology for Improvement of Surface Accuracy of Passive Communications Satellites.	Mr. D. C. Grana Mr. W. E. Bressette	

TABLE OF CONTENTS (Cont'd)

Membrane Analysis of Pressurized Thin Spheroid
Shells Composed of Flat Gores and Its
Application to Echo II Mr. H. Bahiman
Mr. J. M. Thole

Astronaut Maneuvering Unit Technology Mr. Peter N. Van Schaik

Deployment System for the Pegasus Meteoroid
Technology Satellite Mr. E. R. Ganssle

ADDITIONAL PAPERS
(Not Included in Brochure)

Structural Behavior of Tapered Inflated Fabric
Cylinders Under Various Loading Conditions Mr. L. Kovalesvsky
Mr. F. L. Rish

Satelite Applications for Expandable Space Structures . . Mr. H. S. Zahn

Recent Applications of Inflated Structures to
Aerospace Vehicles Dr. R. S. Ross

Correlation of Analytical and Experimental Results
of Cylindrical Shells Under Newtonian Pressure Distribution. Mr. N. C. Lycurgus
Mr. W. R. Midgley

High-Temperature Protective Re-entry Coatings for
Expandable Structures Mr. M. T. Conger
Mr. T. W. Chalmers

Dual Wall Inflatable Structures for Space
Oriented Applications Mr. H. Q. Bair
Mr. W. H. Fischer

SESSION I

EXPANDABLE STRUCTURE CONCEPT OF CREW TRANSFER TUNNEL FOR SPACE VEHICLES

F. W. Forbes,
Aero Propulsion Laboratory, Wright-Patterson AFB, Ohio

J. Schcfield, Captain, U. S. Air Force,
Aero Medical Laboratory, Wright-Patterson AFB, Ohio

V. F. Hribar,
Materials Sciences Laboratory, Aerospace Corporation

L. Jurich,
Goodyear Aerospace Corporation

SECTION I - INTRODUCTION

For several years the Air Force has been studying a number of future manned space station concepts that would use existing re-entry capsule hardware. These concepts have ranged from a simple re-entry module to sophisticated systems of long mission capability and rendezvous and docking facilities. During these studies it became apparent that a structural requirement would arise for crew transfer tunnels, air locks, and space maintenance hangars. To satisfy this requirement, the Air Force initiated both in-house and contractual research and technology programs. Throughout this effort, the Aerospace Corporation has served as an active consultant.

The development of a crew transfer tunnel that would connect a re-entry vehicle to a cylindrical crew module was selected as an initial objective. Once this objective was defined, a materials survey was conducted to tentatively select a structural system and materials best suited for this particular application. This survey indicated that a multi-ply elastic recovery structure should be used.

The in-house program was initiated by fabricating a wood mockup of a crew transfer tunnel, which was tested in a zero-g aircraft to provide human factors data. This effort was followed by a contract awarded to Goodyear Aerospace Corporation to design, fabricate, and test an expandable crew transfer tunnel. The tunnel configuration being developed under this contract is similar to the wood mockup. The contract effort also includes design studies of air locks, an alternate crew transfer tunnel configuration, and space maintenance hangars as possible experiments for future flight testing.

The purpose of this paper is to summarize the results of both Air Force and contractual initial development of the expandable crew transfer tunnel.

SECTION II - DESIGN CONSIDERATIONS

1. GENERAL

The general design of the expandable crew transfer tunnel was specifically derived under the major constraints imposed by human factors considerations. In addition, it was required that the tunnel design be consistent with mission requirements. Therefore, the design was oriented to provide crew transfer between currently planned spacecraft and orbital laboratories.

2. HUMAN FACTORS

The human factors design requirements were established by Air Force in-house programs. By a cooperative effort between the Aero Propulsion Laboratory, the Aero Medical Laboratory, and the Materials Laboratory, a wood mockup of the tunnel geometry was fabricated. This mockup was flown in the KC-135 zero-g aircraft and thoroughly evaluated relative to human factors requirements in zero-g transfer.

The tunnel mockup was attached to a mockup of the left half of a two-man spacecraft. Entry from the tunnel into the spacecraft was through a 17- by 30-in. elliptical hatch located in the main entry hatch of the spacecraft. Entry from the other end of the tunnel into a simulated orbital laboratory was through a 22-in. -diameter circular hatch. Two ropes were placed 21 in. apart to serve as handrails from one hatch to the other.

The subject wore a full-pressure suit. The critical dimensions of the suited subject were:

Weight, 171 lb (66 percentile)
Stature, 179 cm (74 percentile)
Chest breadth, 36 cm (99 percentile)
Chest depth, 24 cm (70 percentile)
Biacromium, 47 cm (85 percentile)
Cervical height, 153 cm (70 percentile)

The human factors flight evaluation consisted of:

1. Three unpressurized-suit transfers from the spacecraft to the laboratory
2. Two unpressurized-suit transfers from the laboratory to the spacecraft, one of which included a turnaround at the laboratory
3. Six pressurized-suit transfers from the laboratory to the spacecraft. One included a turnaround at the laboratory; another, the carrying of a specimen case; the last,

the transfer of a "completely disabled" shirt-sleeved astronaut

4. Four pressurized-suit transfers from the spacecraft to the laboratory. One included a turnaround at the laboratory; another, a turnaround at the spacecraft; the last, the carrying of a specimen case

Transfers in an unpressurized suit presented no difficulties. Transfers in a pressurized suit required more time and were more cumbersome but were completed with little difficulty. Figure 1 shows the typical mode of transfer in a pressurized unit. The results of these transfer tests can be summarized as follows:

1. No problems were encountered in passing through the 17- by 30-in. elliptical hatch.
2. A specific technique must be worked out for transferring packages and equipment through the hatches.
3. The two handrails were effective locomotion aids to crew transfer and should be incorporated in tunnel design.
4. The tunnel geometry, represented by the mockup, was entirely compatible with effective crew transfer. However, a final tunnel design should have no sharp protuberances that might snag the umbilicals or the space suit and should have a nonabrasive liner to avoid space suit damage.

There are other human factors requirements to be met in any tunnel design. Nontoxic materials must be used in tunnel construction to avoid contamination of the artificial environment. Interior tunnel lighting may be required. Low-intensity lighting would appear to be adequate but should be evaluated in actual transfer experiments.

3. MISSION REQUIREMENTS

a. General

Human factors requirements were used largely to establish tunnel geometry and the locomotion aids required for effective crew transfer. Mission considerations were then used to evolve the final design of the tunnel. Mission aspects considered included launch pad and boost requirements, orbital operations, and mission termination.

b. Launch Pad Requirements

The tunnel should incorporate a modular design approach. This approach would permit, prior to mounting on the launch vehicle, (1) prepackaging of the tunnel, and (2) on-the-ground checkout and repair, if necessary. In addition, the packaged tunnel would be relatively easy to install on or remove from the spacecraft, and the canister would protect it during hold or countdown.



COMPLETELY WITHIN TUNNEL



ENTERING LABORATORY HATCH



EXITING FROM SPACECRAFT HATCH



TAUT ROPE USED AS LOCOMOTION AID

Figure 1 - Crew Transfer Experiment under Zero g

c. Boost Requirements

The packaged tunnel and packaging canister should impose a minimum effect on the aerodynamics of the launch vehicle. A flight canister would require sufficient insulation to prevent aerodynamic heating from damaging the packaged tunnel. During this critical phase of the mission, a malfunction may necessitate abort. Accordingly, for compatibility with mission abort requirements, the design should incorporate provisions to jettison the packaged tunnel and canister from the launch vehicle. In addition, the packaged tunnel must be qualified for the following environmental conditions encountered during the boost phase:

Noise, (see Table 1)

Vibration, (see Table 2)

Shock, 150 g, 2.5-millisecond sawtooth pulse

Acceleration, 5 g forward longitudinal, 2 g lateral

TABLE 1 - NOISE AT VEHICLE SURFACE

Sound level (db)	Frequency (cps)
136	18.75 to 37.5
137	37.5 to 75
138	75 to 150
139	150 to 300
140	300 to 600
141	600 to 1200
139	1200 to 2400
134	2400 to 4800
128	4800 to 9600

TABLE 2 - RANDOM VIBRATION SPECTRUM

Acceleration spectral density (g ² /cps)	Frequency (cps)
1.0	10 to 80
6.0	200 to 300
3.0	360 to 1000
0.1	2000

d. Orbital Flight

When an orbital path is achieved, the packaging canister will be ejected, and the packaged tunnel will deploy to its expanded volume automatically. To initiate crew transfers, the tunnel will be pressurized to its design pressure of 7-1/2 psi. The orbital mission lifetime will be 45 days at altitudes from 100 to 300 naut mi. To withstand conditions encountered in the orbital environment, the tunnel materials must meet the following requirements:

1. Provide a 0.995 probability of zero meteoroid penetrations
2. Maintain interior surface temperatures within 50 to 100 F
3. Be suitable for operations in hard vacuum of 10^{-6} to 10^{-7} torr
4. Absorb 10^6 rads of Van Allen electron radiation without serious degradation

e. Mission Termination

At mission termination, the re-entry vehicle will separate from the orbital module prior to re-entry. Accordingly, the design must incorporate provisions to jettison the transfer tunnel after the final transfer from the laboratory module to the re-entry vehicle.

4. DESIGN CONFIGURATION

A modular design of the expandable crew transfer tunnel was jointly derived by the Aero Propulsion Laboratory, the Aero Medical Laboratory, and Goodyear Aerospace. This design was evolved to combine the human factors requirements and the mission requirements into a single overall design objective.

Basically, the design incorporates an expandable tunnel geometry simulating that geometry used on the mockup for human factors evaluation. The expandable structure has a rigid floor, which in turn is integrated with the packaging canister. In essence, the tunnel floor forms the lower half of the packaging canister and is connected to the upper half of the canister by frangible bolts for canister ejection. The advantages of this design are:

1. No attachments are required between the packaging canister and the launch vehicle.
2. Mounting attachment points are required only at the hatch connections, thus simplifying installation and removal.
3. The ejection systems are simplified. Requirements for launch abort and mission termination are combined into a single system.

Figures 2, 3, 4, 5, and 6 show the operational sequence from prelaunch to mission termination. Figure 2 shows the prepackaged tunnel module attached to the spacecraft and laboratory hatches. Figure 3 shows design

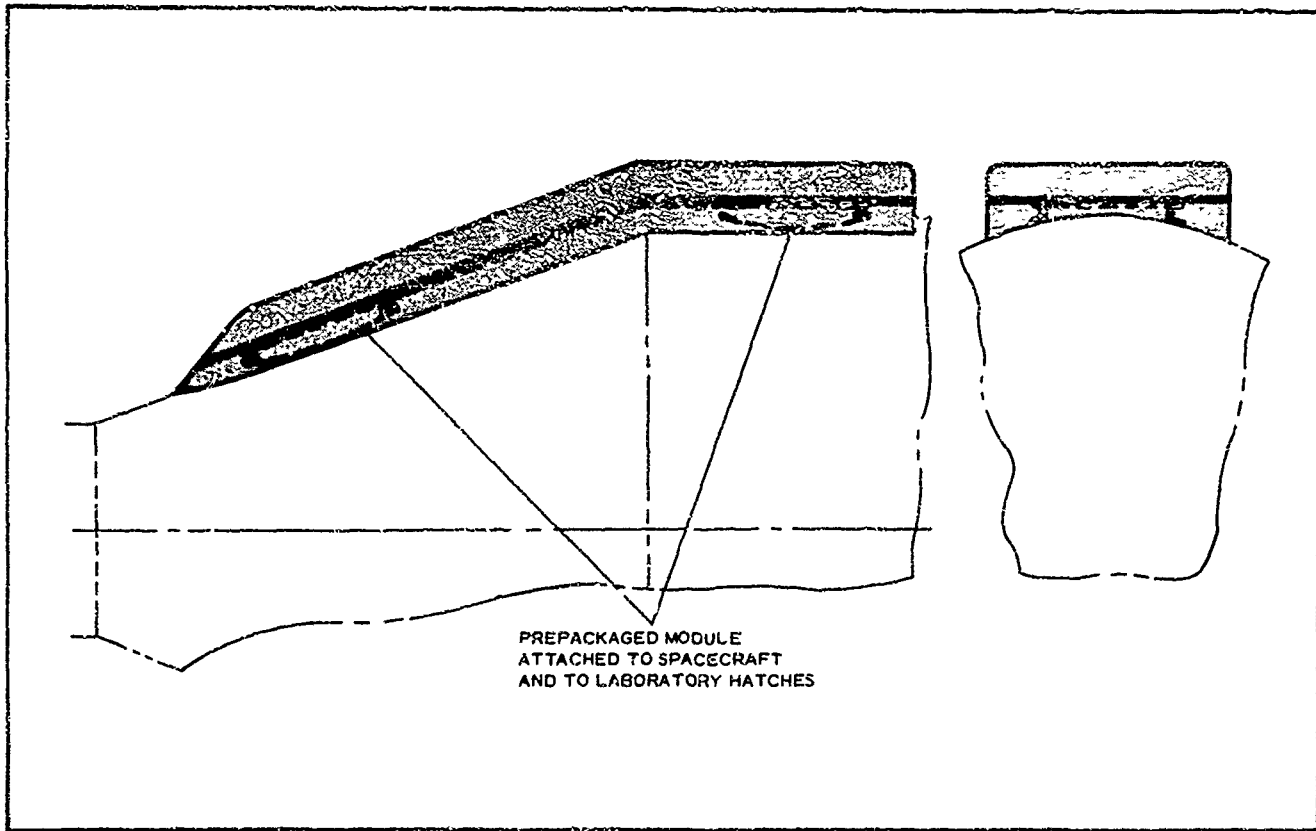


Figure 2 - Launch Configuration of Prepackaged Tunnel

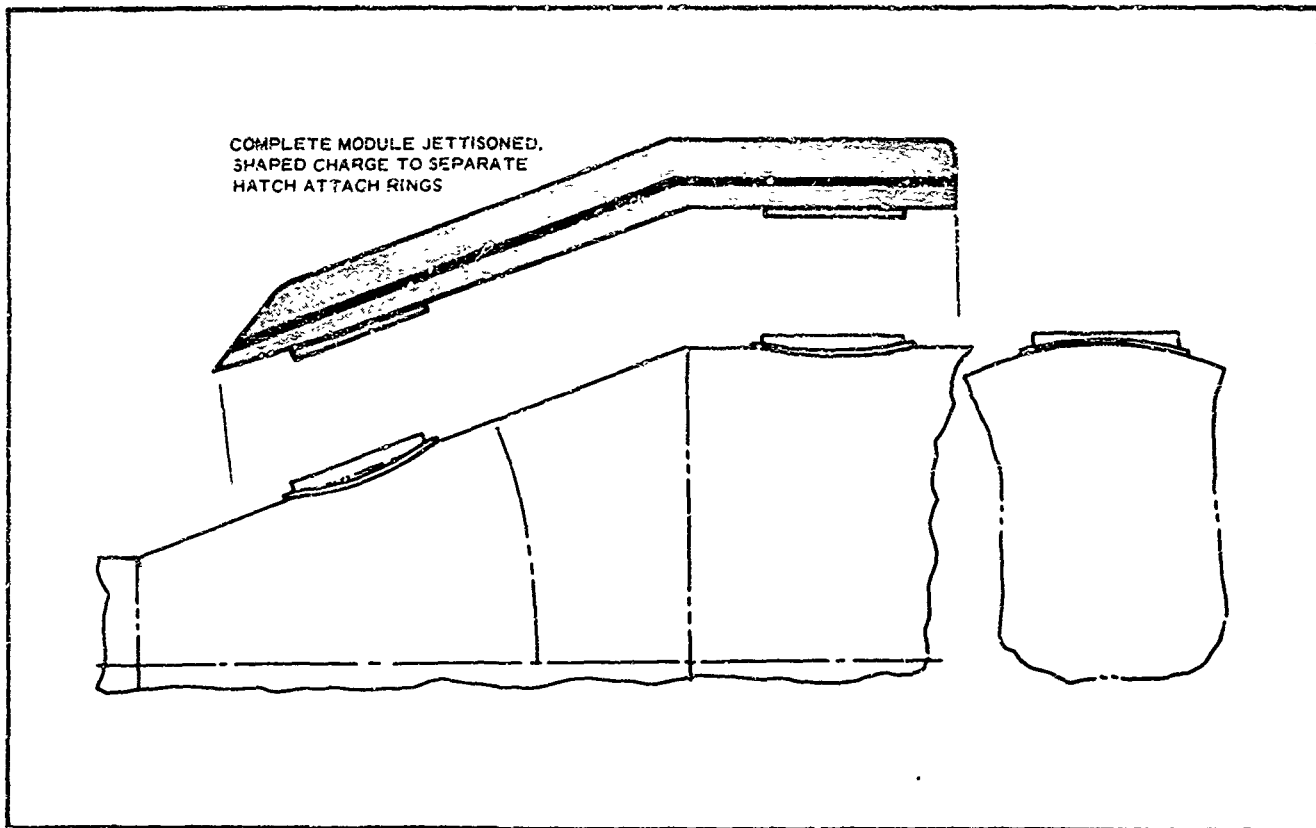


Figure 3 - Tunnel Ejection at Launch Abort

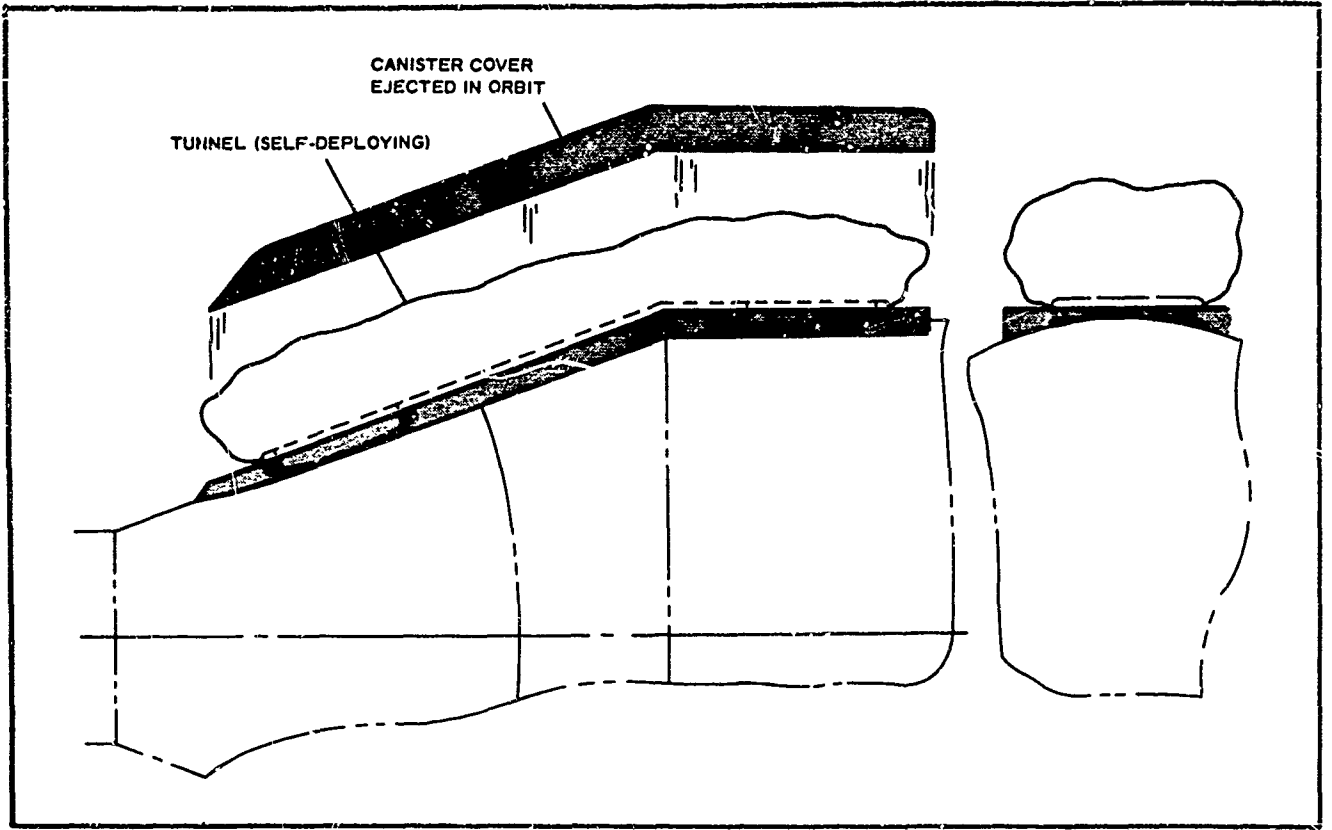


Figure 4 - Canister Ejection and Tunnel Deployment

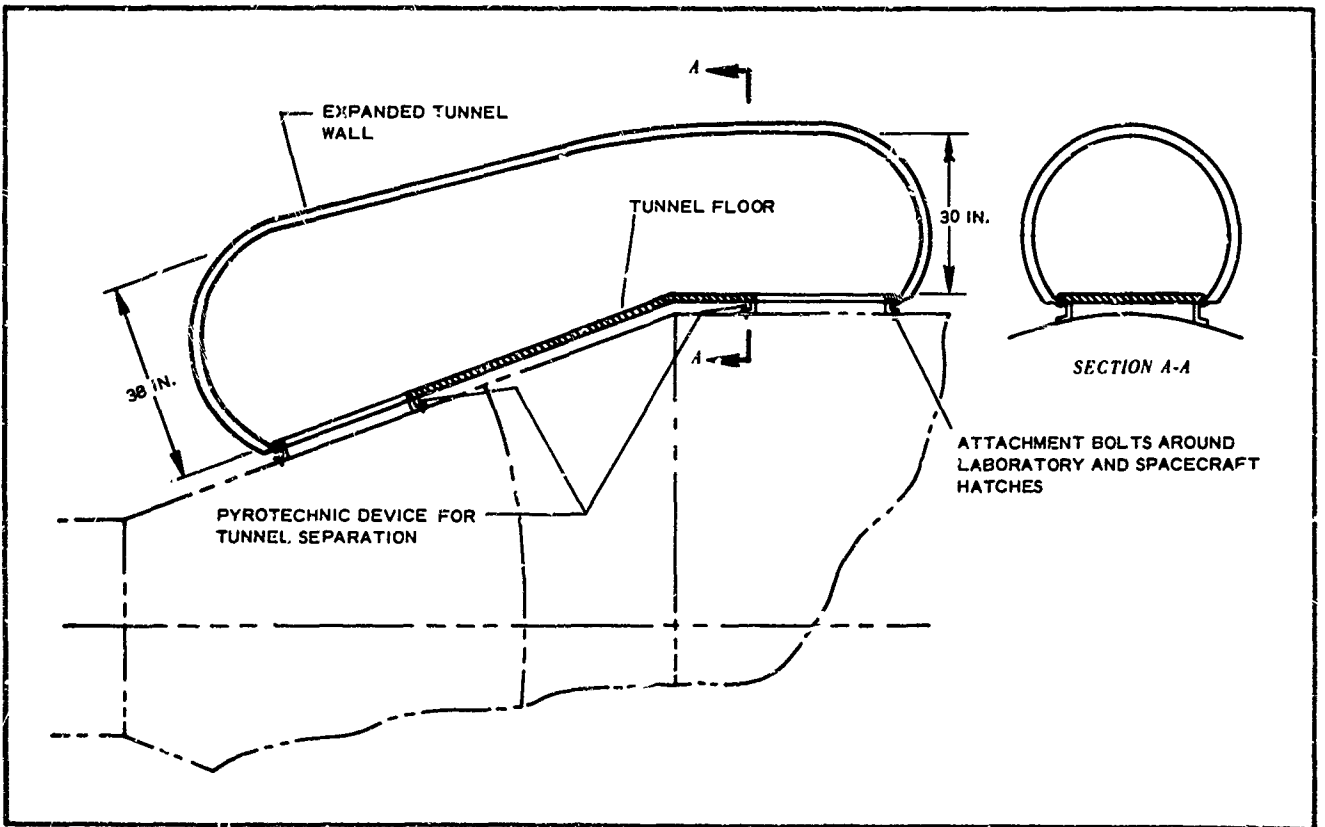


Figure 5 - Deployed Tunnel

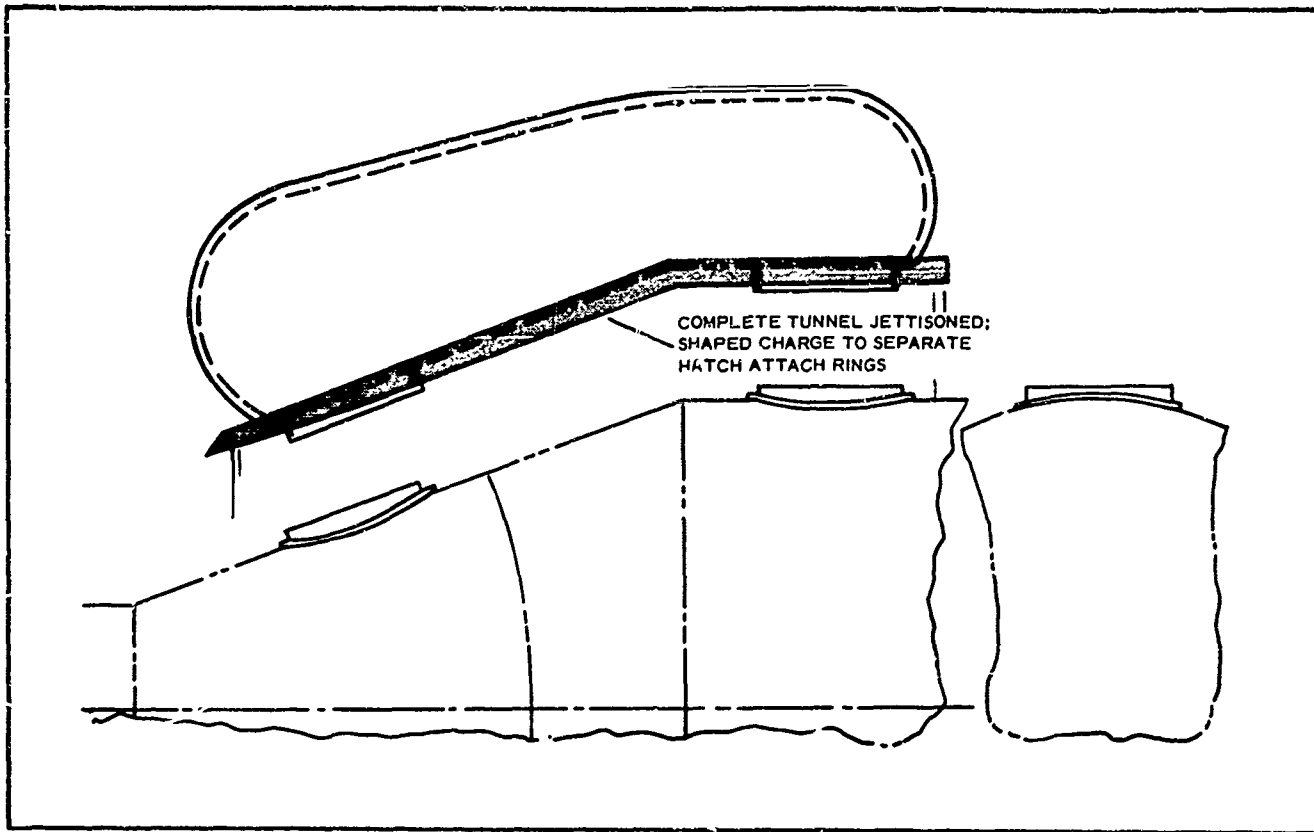


Figure 6 - Tunnel Jettisoned at Mission Termination

provisions to meet abort requirements at launch. The hatch attach rings incorporate a shaped charge to burn through the rings. In the event of abort, the canister and the packaged tunnel will be jettisoned as a single unit.

Deployment of the packaged tunnel in orbit is shown in Figure 4. The frangible bolts used to attach the canister cover to the tunnel floor will be activated, ejecting the canister cover and initiating tunnel deployment. The elastic recovery characteristics of the tunnel should then deploy the structure to its expanded volume. Figure 5 shows the geometry of the fully expanded tunnel. At mission termination, the expanded tunnel will be ejected, permitting separation of the re-entry vehicle (see Figure 6). The jettisoning system will be the same as that used for launch abort.

SECTION III - EXPANDABLE MATERIALS AND ENVIRONMENTAL COMPATIBILITY

1. MATERIALS COMPOSITE

A materials survey was conducted by the Air Force to determine if current technology could be applied to an expandable crew transfer tunnel for use in a space environment for an extended period of time. This research indicated

that the concept of an expandable tunnel was feasible and that such a structure could be fabricated from several different combinations of materials and material techniques.

The materials approach selected to best meet the overall requirements of tunnel design was a material composite. Figure 7 depicts the composite, which is comprised of four distinct layers bonded together into a homogeneous structure. The inner layer is an unstressed pressure bladder, whose only function is to maintain pressure tightness and to transmit pressure loads to an adjacent structural layer. The structural layer carries structural loads resulting from internal pressure. The flexible foam layer performs a dual function. It acts first as a micrometeoroid barrier, protecting the pressure bladder from penetration. A secondary function is deployment and shaping of the structure through the use of stored energy inherent in the foam compressed for packaging. The outer cover also does a dual job. It is used as a smooth base for the application of a thermal coating and also encapsulates the total composite for evacuation and compression prior to packaging for launch.

2. PRESSURE BLADDER

The pressure bladder is a laminate of three individual sealant layers (see Figure 8). The inner layer is a laminate of Capran film sandwiched between two layers of lightweight nylon cloth. This layer is bonded with polyester adhesive to a second layer of closed-cell vinyl foam 1/16 in. thick. The outer sealant is a close-weave nylon cloth coated with a polyester resin. The total weight of the bladder composite is about 0.13 psf and is independent of design pressure.

Tests were conducted on the pressure bladder to determine permeability rate, possible toxicity, and environmental effects due principally to vacuum. Permeability was determined with oxygen as a test gas at 7.5 psia using a Dow cell. The measured rate was less than 10^{-4} psf per day. Relating this rate to the tunnel design, the anticipated gas loss is 0.02 lb per day, substantially less than the maximum allowable of 1 lb per day. A survey of toxic materials known to be used in the construction of the pressure bladder indicated the possible presence of toluene, xylene, methyl ethyl ketone, methylene chloride solvents, and toluene diisocyanate. Although carbon monoxide was not known to be contained, tests for it were also included. The bladder material was exposed to 5 psia of oxygen for 24 hr prior to a chemical analysis and check for toxic gases. Test results indicated that all the above contaminants were below the threshold limits established by the National Bureau of Standards for occupational exposure.

The principal environmental effect for which the bladder was checked was a hard vacuum. This check was made first to ensure that delamination of the composite bladder would not occur, and second to determine the degree of off-gassing to be expected. The bladder construction technique proved successful both in preventing delamination and in minimizing off-gassing. Off-gassing stabilized in about 96 hr with a 6.3-percent weight loss.

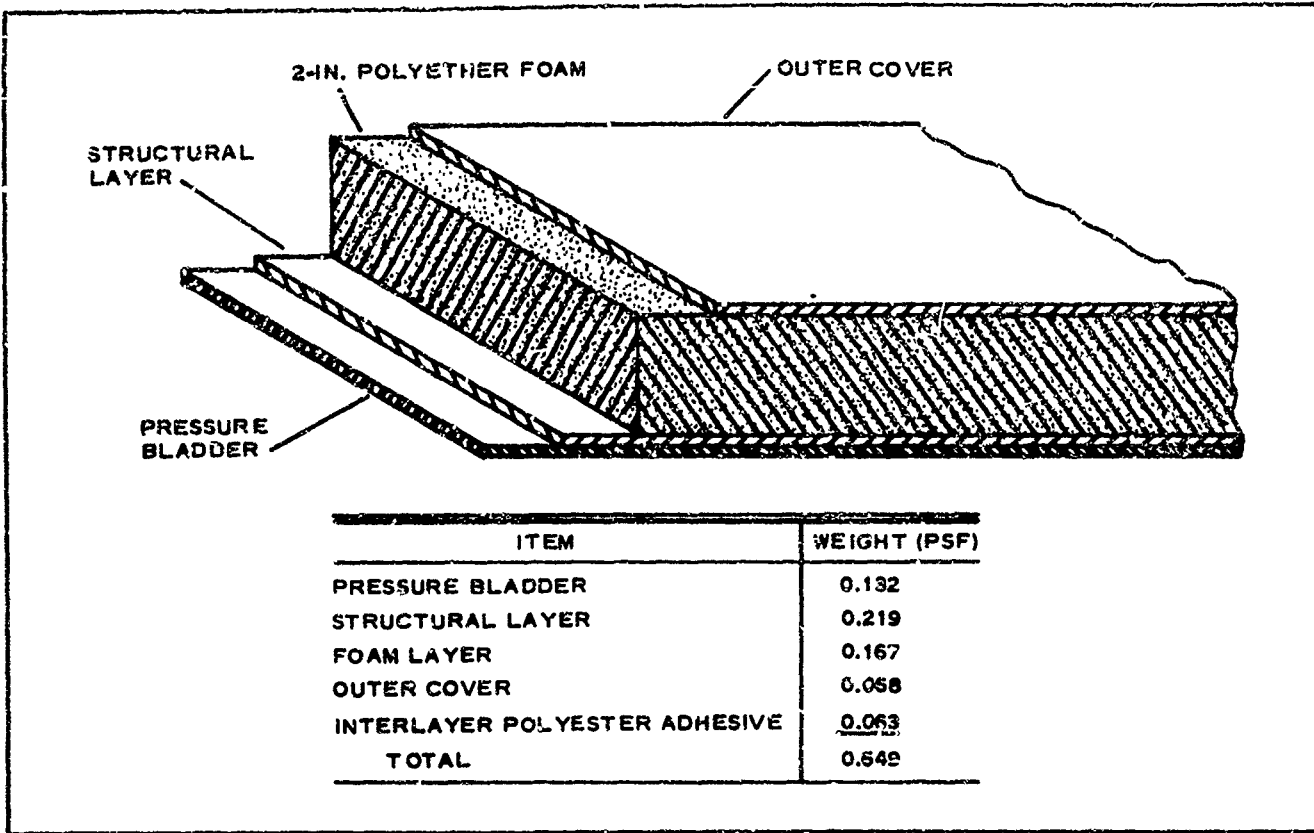


Figure 7 - Tunnel Composite Wall

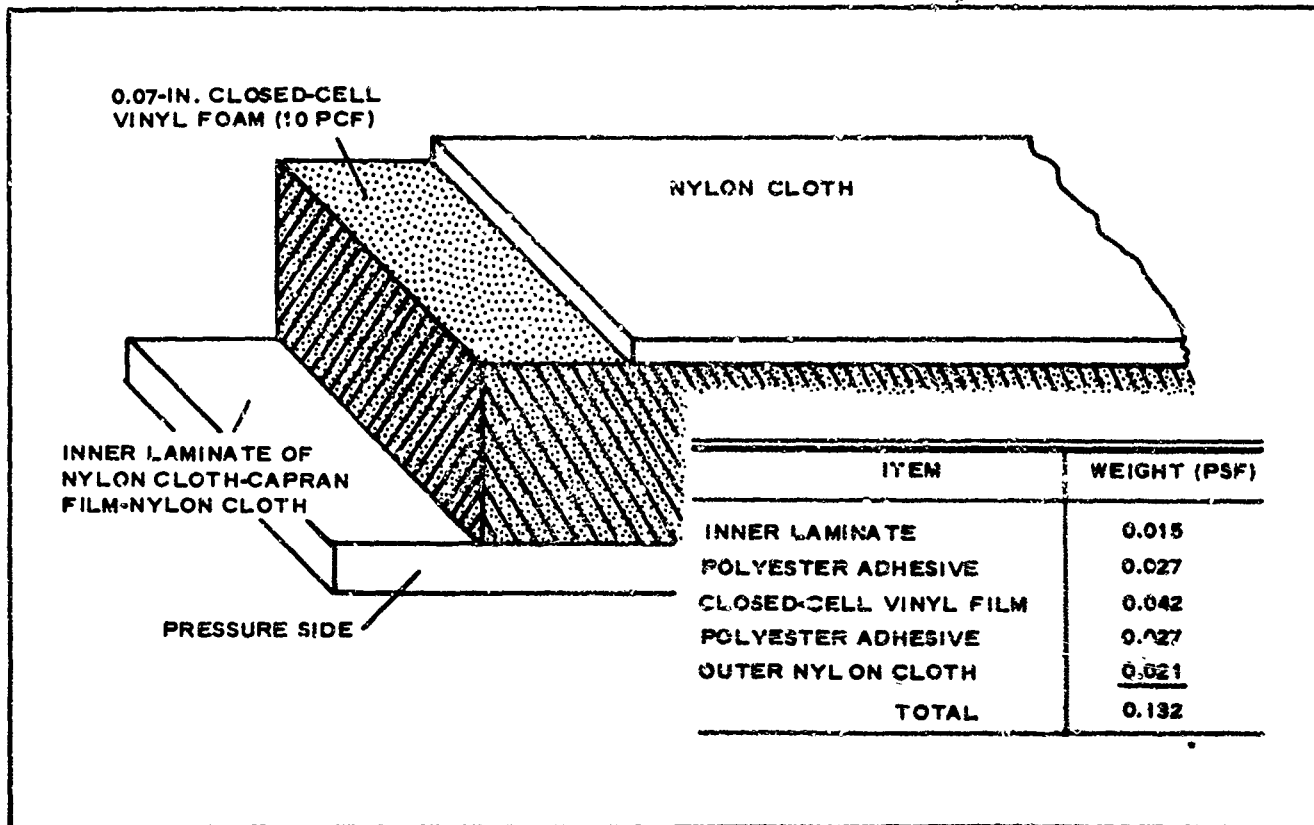


Figure 8 - Pressure Bladder

3. STRUCTURAL LAYER

The structural layer is a four-ply laminate of Dacron bonded to a polyester resin, then cured under heat and pressure. The design pressure of 7.5 psia, which along with a safety factor of five and allowance for creep rupture, requires a load capability of 1070 lb per inch. This load must be carried entirely by the structural layer. The basic structural concept of the multi-ply technique is that joints in the individual plies are staggered in such a way as to offer an essentially seamless construction. Strip tensile tests of this technique indicate an 85-percent load capability, as compared to that of the parent structural cloth. The degradation in strength is attributed to the "locked-in" crimp of the bonded polyester joint. A similar degradation also is incurred in elastomer-coated fabrics and is attributed to the same effect. Even in a mechanically sewn joint, seam efficiencies beyond 85 percent are unlikely. It thus appears that a 100-percent structural efficiency for a fabric structure is not attainable. However, because the structural weight of an overall composite is only 25 percent of the total, the weight penalty incurred by an 85-percent structural efficiency is not significant.

Particular emphasis was placed on the design and development of a structural joint between the rigid floor of the tunnel and the structural layer. The technique that evolved from this investigation (see Figure 9) uses an epoxy resin rigid bond. The locked-in crimp effect was again found in this joint design, resulting in an efficiency of 50 percent. Attempts to improve joint efficiency by using a more elastic epoxy bond were not successful and only resulted in shear failure of the joint. A polyester resin bond similar to that used

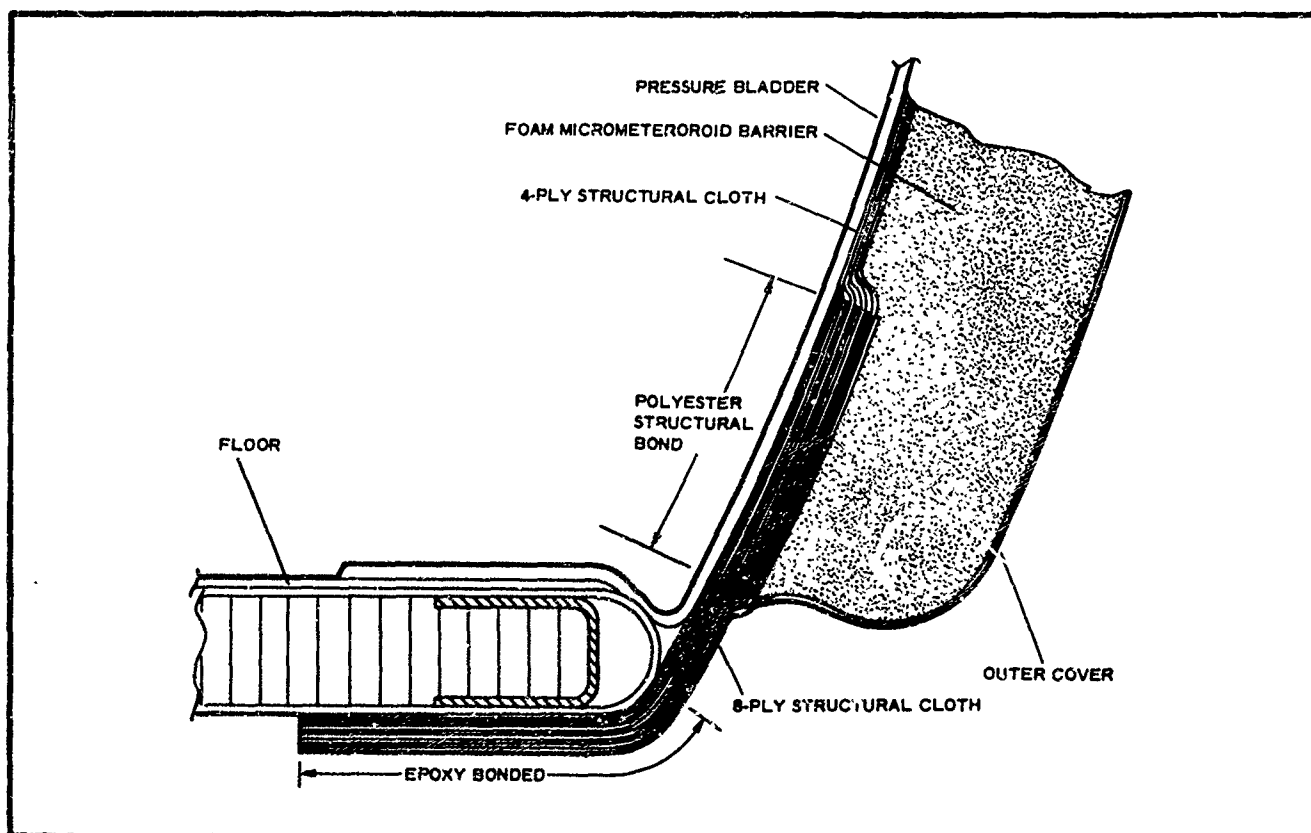


Figure 9 - Structural Joint Between Expandable Wall and Rigid Floor

3. STRUCTURAL LAYER

The structural layer is a four-ply laminate of Dacron bonded to a polyester resin, then cured under heat and pressure. The design pressure of 7.5 psia, which along with a safety factor of five and allowance for creep rupture, requires a load capability of 1070 lb per inch. This load must be carried entirely by the structural layer. The basic structural concept of the multi-ply technique is that joints in the individual plies are staggered in such a way as to offer an essentially seamless construction. Strip tensile tests of this technique indicate an 85-percent load capability, as compared to that of the parent structural cloth. The degradation in strength is attributed to the "locked-in" crimp of the bonded polyester joint. A similar degradation also is incurred in elastomer-coated fabrics and is attributed to the same effect. Even in a mechanically sewn joint, seam efficiencies beyond 85 percent are unlikely. It thus appears that a 100-percent structural efficiency for a fabric structure is not attainable. However, because the structural weight of an overall composite is only 25 percent of the total, the weight penalty incurred by an 85-percent structural efficiency is not significant.

Particular emphasis was placed on the design and development of a structural joint between the rigid floor of the tunnel and the structural layer. The technique that evolved from this investigation (see Figure 9) uses an epoxy resin rigid bond. The locked-in crimp effect was again found in this joint design, resulting in an efficiency of 50 percent. Attempts to improve joint efficiency by using a more elastic epoxy bond were not successful and only resulted in shear failure of the joint. A polyester resin bond similar to that used

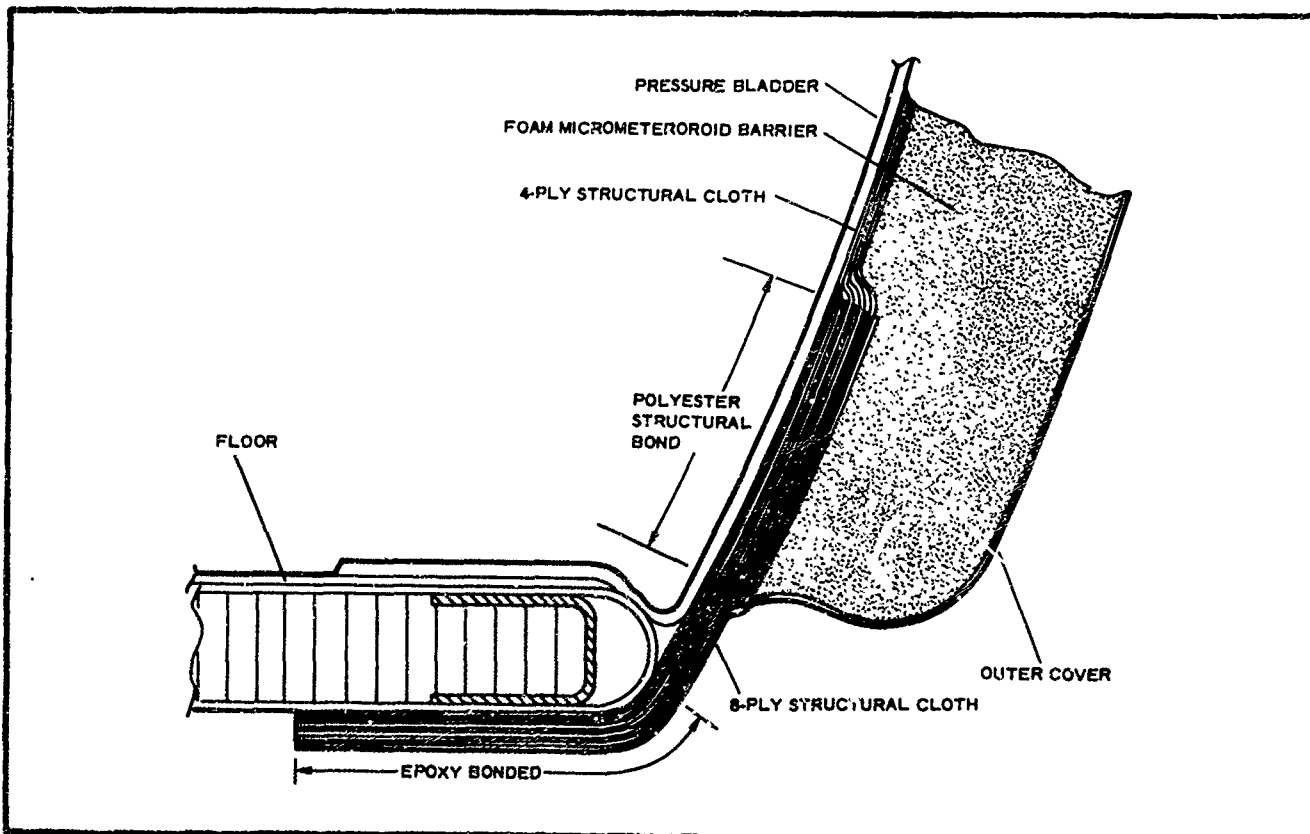


Figure 9 - Structural Joint Between Expandable Wall and Rigid Floor

in the multi-ply wall was also tested, but was wholly inadequate for the required bond. Consequently, the rigid epoxy bond technique was adopted as the required design technique and resulted in an eight-ply bond to the structural floor joined to the four-ply structural layer with a polyester resin bond. Strip tensile tests of this overall joint design indicated that the full load capability of 1070 lb per inch could be carried by both the joints and the basic four-ply structural layer.

Structural tests have been conducted to investigate environmental effects due to vacuum and high-energy radiation (Van Allen electrons). Strip tensile tests on Dacron have indicated negligible effects of hard vacuum on the structural characteristics. Similar tests on fabrics irradiated with 10^6 rads of 1.3-mev gamma radiation have also indicated negligible degradation. Accordingly, there is no reason why synthetic fiber structures should not be used in structural space applications, if their physical characteristics are known and related to the operational environment.

4. FOAM LAYER

The tunnel will be protected from micrometeoroid penetration by a two-inch layer of flexible polyether foam. Flexible foam of 1 pcf density has been selected as a suitable barrier material, based on hypervelocity particle impact tests conducted by Goodyear Aerospace and on tests conducted at the micrometeorite testing facility at Wright-Patterson AFB. Both series of tests (the latter conducted at 27,000 fps with an average particle mass of 0.005 g) indicate that a two-inch foam barrier is equivalent in barrier effectiveness to single-sheet aluminum 0.20 in. thick (2.7 psf). Figure 10 shows the Air Force near-earth micrometeoroid environment spectrum in terms of particle mass and accumulative particle flux. When the previously mentioned test results are correlated with single-sheet aluminum penetration theory, the critical penetrating flux level is about 5.23×10^{-7} particles/sq ft-day. Relating the critical flux with the exposed surface area of the deployed tunnel (130 sq ft) and the mission time (60 days), the probability of zero penetration is 0.995.

While the primary function of the foam will be as a micrometeoroid barrier, it can serve also as a tunnel deployment aid. During packaging, the foam layer will be compressed to about 10 percent of its original thickness and will be restrained by the packaging canister. Upon deployment in orbit, the canister will be jettisoned, and the elastic recovery characteristics of the foam will shape the tunnel to its fully expanded volume. Figure 11 shows the recovery characteristics of the foam under vacuum conditions and for varying temperatures. From Figure 11 it can be seen that the packaged structure must be insulated against extreme cold if full recovery is to be achieved.

Environmental effects should be evaluated to establish compatibility with the environment. Of principal concern are the effects of vacuum, temperature, and high-energy radiation. The effect of foam recovery in a vacuum has already been discussed. Off-gassing induced by vacuum was negligible; it amounted to a 0.4-percent weight loss and stabilized in 1.5 hr. Expected temperature extremes have not yet been established. High-energy radiation is not expected to present any problem because the foam tolerance is about an order of magnitude higher than the anticipated dose of 10^6 rads.

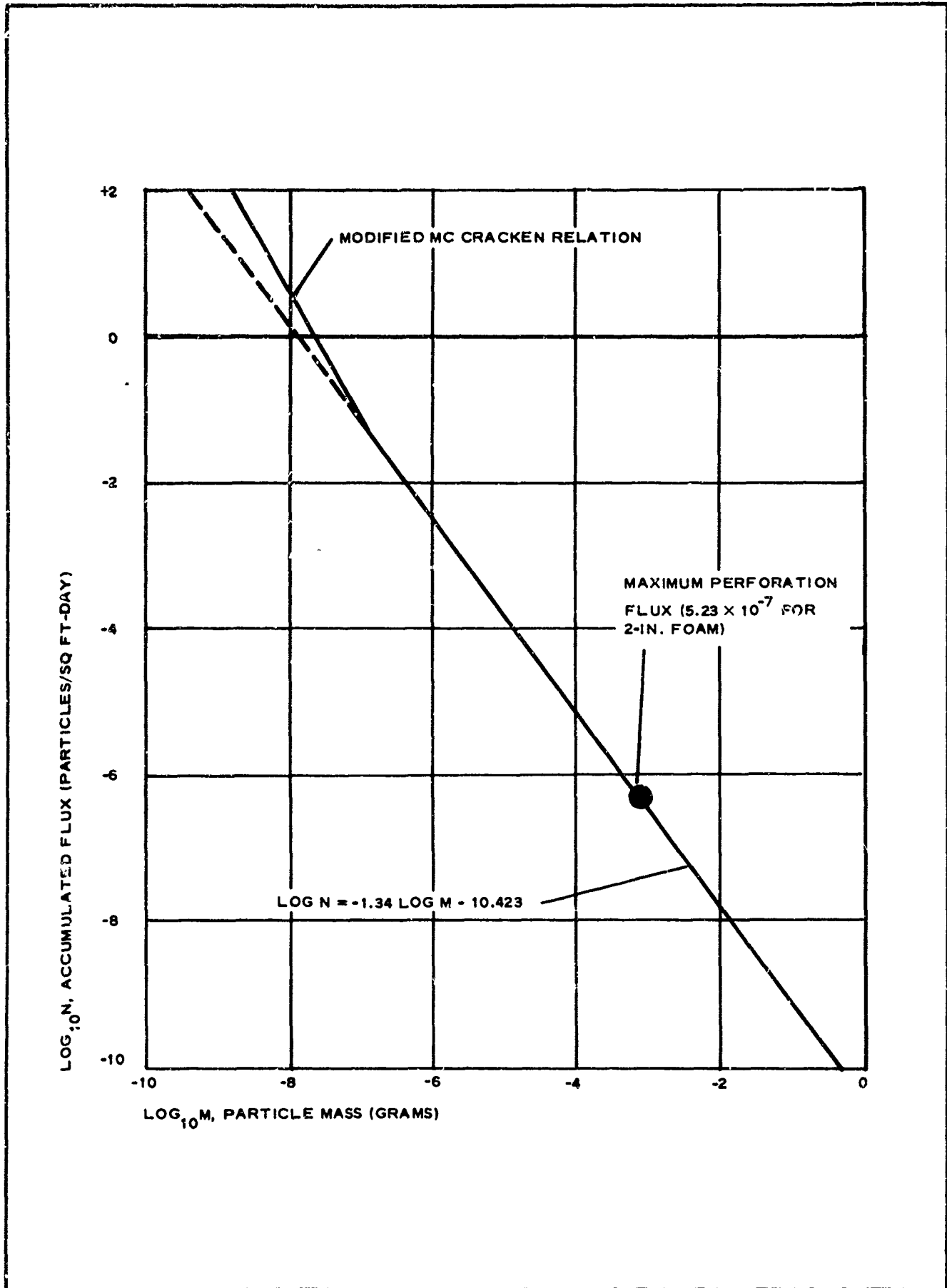


Figure 10 - Near-Earth Micrometeoroid Environment

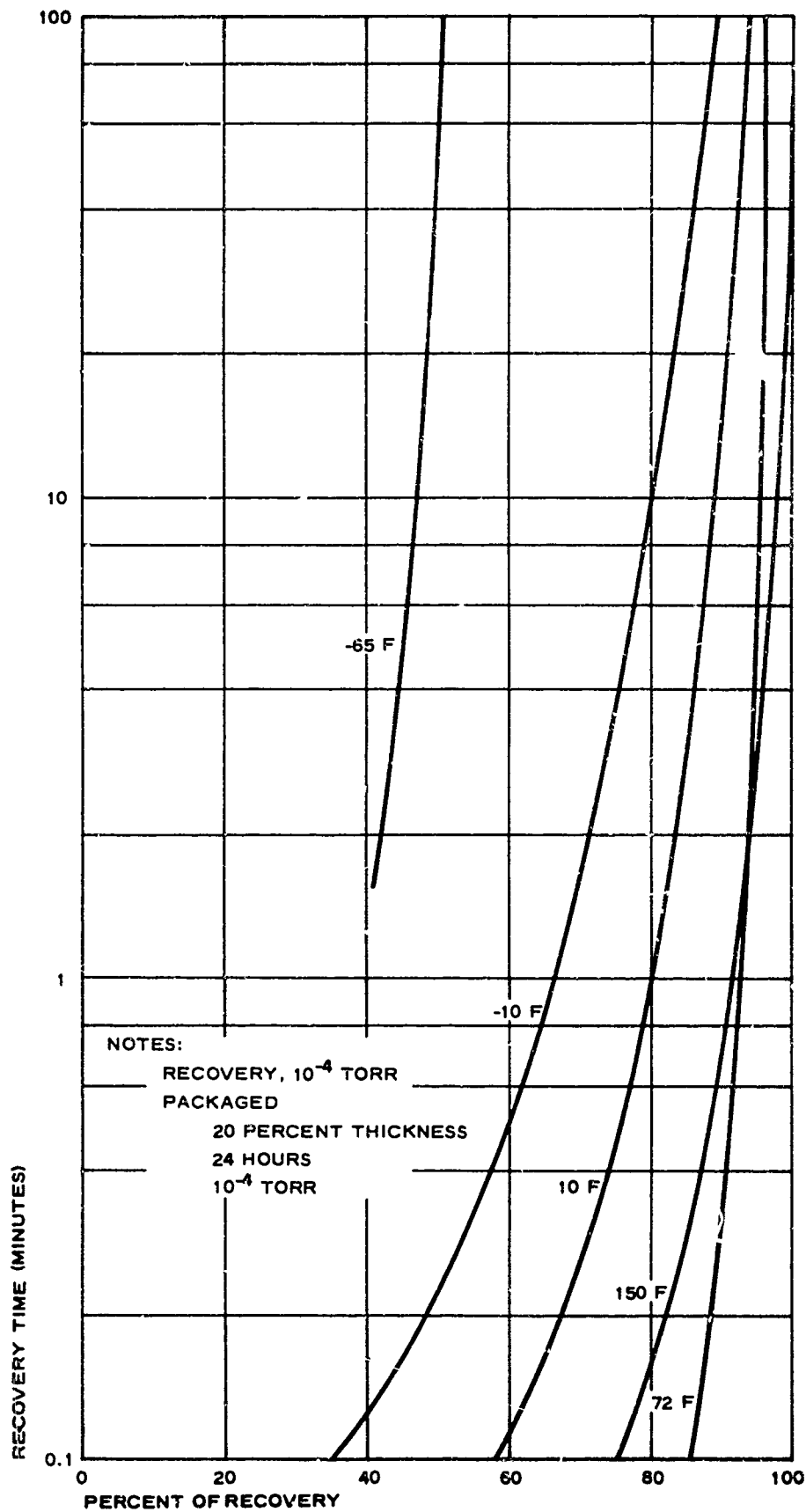


Figure 11 - Foam Thickness Recovery versus Time

5. OUTER COVER

The outermost layer of the composite wall structure encapsulates the wall and provides a smooth base for the application of a thermal coating. The construction of this layer is shown in Figure 12.

Inasmuch as the outer cover encapsulates the composite wall, it serves as an aid in packaging the tunnel prior to launch. By a vacuum technique, the wall thickness can be compressed from the fully expanded 2 in. to about 3/8 in., suitable for folding and subsequent packaging in the canister. Also, a certain amount of air will still be trapped in the composite wall, even after evacuation. This air can be used as a thickness recovery aid, augmenting the elastic recovery characteristics of the compressed foam. Thus, full recovery of the wall thickness, even under adverse temperatures, will be ensured.

Zinc oxide in a silicone resin will be used as a thermal coating on the outer surface. It will provide an absorptance (α_s) of 0.17, an emissivity (ϵ) of 0.75, and an α_s/ϵ of 0.23. The purpose of this coating will be to maintain material temperatures within acceptable limits during full solar flux. Maximum temperatures will be limited to about 60 F; minimum temperatures will be limited by the emissivity of the coating, the thermal conductance of the composite wall, and the heat capacity of the structure. A computer program is currently underway to evaluate these factors relative to orbital inclination, orbital altitude, and orientation of the tunnel relative to the earth. The objective of this program is to establish temperature gradients of the composite wall. These gradients will be used to establish minimum and maximum temperatures and

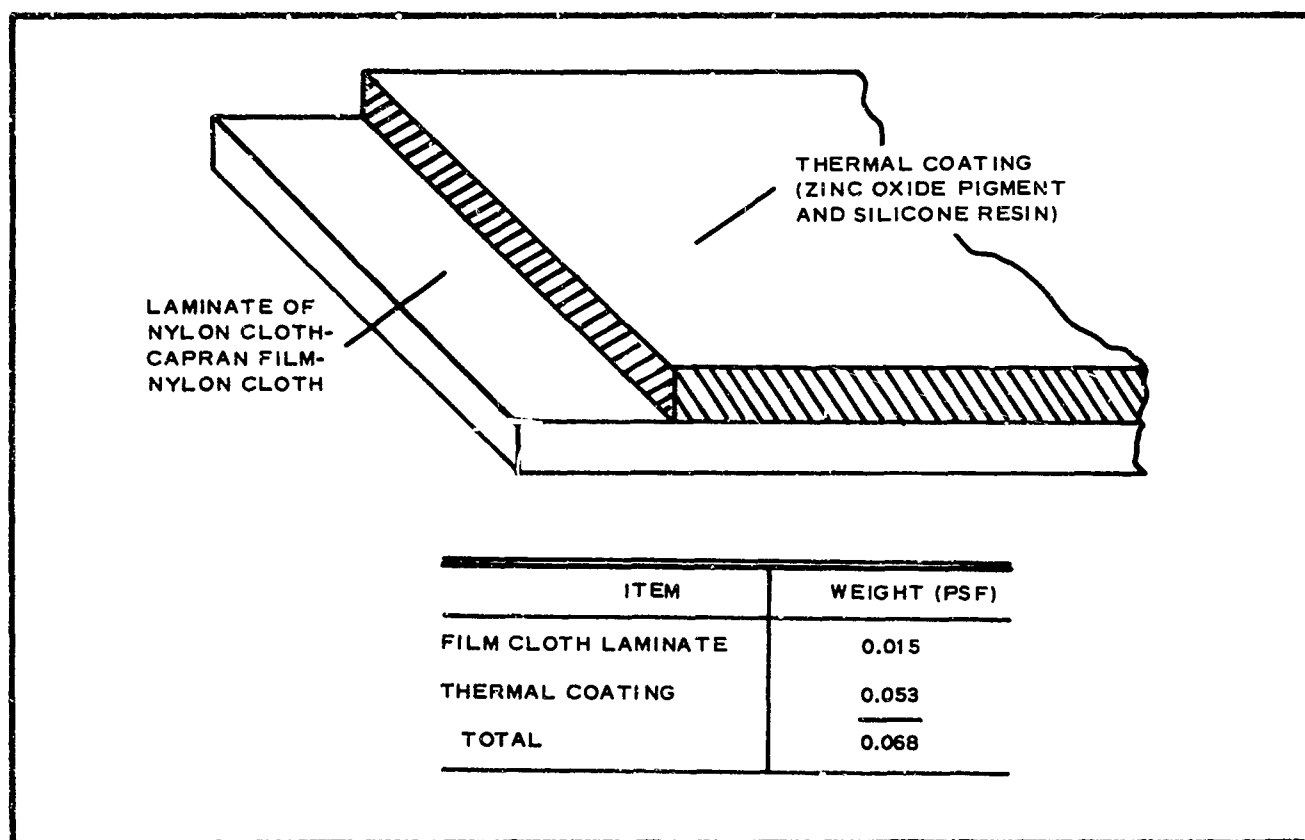


Figure 12 - Outer Cover of Composite Wall

will permit the correlation of material thermal characteristics with the expected temperature extremes.

Environmental effects compatibility requires the consideration of combined vacuum and ultraviolet radiation, the thermal environment, and high-energy radiation from Van Allen electrons. The portion of the outer cover most sensitive to the orbital environment will be the thermal coating. The combined effect of vacuum and ultraviolet radiation will cause some degradation of the coating. The α_s/ϵ ratio is expected to increase by roughly 10 percent for a 60-day mission, resulting in a slight increase in materials temperature. Off-gassing due to vacuum is a minute effect, causing less than 0.5-percent weight loss and stabilizing in 1.5 hr. Thermal effects relative to extremes in temperature are still to be evaluated, but no problems are anticipated. And finally, the silicone elastomer of the coating is expected to absorb 10^6 rads of electron radiation. However, the tolerance of this elastomer to high-energy radiation is on the order of 10^7 to 10^8 rads.

SECTION IV - PLANNED TEST EVALUATION

1. GENERAL

Pending completion of fabrication, the tunnel will be subjected to a series of tests to evaluate the application of such structures to actual space missions. These tests will involve gas leakage, structural integrity, deployment, and crew transfer under conditions of no gravity.

2. GAS LEAKAGE

Gas leakage of the tunnel will be evaluated primarily from the standpoint of leakage, and/or permeability, through the composite wall. The hatch ports will be sealed off with aluminum plates and "O"-ring seals. Similarly, the rigid floor will be sealed carefully at joints, edges, and connections to pinpoint any leakage of the expandable material.

The leakage characteristics of the tunnel will first be established prior to folding and packaging. This will permit the definition of a reference leak rate to account for possible degrading effects of folding and packaging. After a reference is established, the tunnel will be folded and packaged, simulating the launch requirement. It will remain packaged for 24 hr, then deployed and inflated with air to the 7.5-psia design pressure. The tunnel will remain pressurized for seven days, during which time the pressure will be monitored and the leak rate determined from the variations in pressure.

3. STRUCTURAL INTEGRITY

The structural integrity of the tunnel will be checked with a "time under load" test at proof pressure (10 psi) and a cyclic load test from zero to the design pressure (7.5 psi). For the "time under load" test, the proof pressure will be maintained continuously for seven days. During this period, unusual deformations or possible areas of stress concentration will be noted. The cyclic load test is intended to simulate possible cycles of pressurization and depressurization in orbital applications. Sixty cyclic load tests will be conducted. These tests will also be observed for possible deformations, particularly at the floor joint.

4. DEPLOYMENT

Full-scale tunnel deployment tests will be conducted in the 40- by 80-ft vacuum facility at the Arnold Engineering and Development Center. These tests are intended to simulate packaging, canister ejection, and subsequent tunnel deployment in orbit. The tunnel will be packaged in its canister, and the canister will be attached to a special test rig and placed in the vacuum facility. The deployment sequence will be initiated under 10^{-4} torr by jettisoning the canister previously attached with frangible bolts. With the canister jettisoned, the stored energy inherent in the packaged tunnel should deploy the tunnel to its final expanded configuration automatically. The entire sequence of deployment will be filmed.

5. ZERO-G CREW TRANSFER

The tunnel will be finally evaluated and checked out from a human factors standpoint under conditions of no gravity. These tests will be conducted in the KC-135 zero-g aircraft at Wright-Patterson AFB, which is capable of simulating zero g in multiple trajectories, each up to 30 sec in duration. The objective of these test flights will be to check out the tunnel geometry and the locomotion devices needed for effective transfer through the tunnel. During these tests the tunnel will be unpressurized; it will depend only on the inherent stiffness of the material to maintain the expanded tunnel geometry.

Tests will simulate astronaut transfers in both pressurized and nonpressurized suits. Transfers will be conducted from both ends of the tunnel simulating either entry from or return to a parent vehicle. Further, the astronaut will be encumbered by umbilicals to determine their effect on effective transfer. The ability to transfer equipment also will be evaluated; simulated equipment packages of approximately one cubic foot in volume will be used. And finally, tests will be conducted to determine if an incapacitated astronaut can be pulled through the tunnel.

DEVELOPMENT AND OPTIMIZATION OF RESIN SYSTEMS
FOR EXPANDABLE HONEYCOMB

W J McKillip, L M Clemens, R H Leitheiser, J Lee, C N Impola

Archer Daniels Midland Research Center, Sponsored Research Group

INTRODUCTION

As man explores the expanse of outer space, the need to accommodate him with life support systems becomes critical. The specialized field of expandable spacecraft structures has received serious consideration within the past few years as an area of research and development which could service this critical need. These structures are constructed principally of flexible materials that allow packaging without resorting to hinges or other mechanical schemes that can only provide flexibility in localized regions. Once carried to their space destination and expanded from a collapsed form they may be rigidized by a number of techniques. Many of these techniques will be discussed at this conference. The approach under research and development at ADM laboratories has been a chemical rigidization system. The initially flexible system, a cloth or honeycomb structure impregnated with resin, is converted to a rigid resin-fiber reinforced composite when exposed to a controlled release of a gaseous reactant and/or catalyst.

The feasibility of utilizing an isocyanate terminated prepolymer as a resin impregnant for gas catalysis rigidization has been demonstrated under AF Contract No 33(657)-10409. A continuation of this effort, AF 33(615)-1243, showed improved utility and performance. At present, ADM is continuing the research and development of urethane resins in order to further optimize the system and make it operational and reliable for space use. In addition, polyester and epoxy resin systems have been developed which are capable of rigidizing when gassed with a catalyst. Perhaps these systems could be the topic for a future presentation. The engineering, fabrication and operation of rigidified structures is the primary objective of ADM's current AF contract. Other papers, however, to be presented at this symposium will present these aspects in detail. This paper will discuss the results of ADM's resin development program, with special emphasis on the correlation of molecular configurations of the polymer with the physical properties observed. Basic knowledge about such physical properties as modulus and yield strength, in tension and in compression, resin shrinkage, and resin cure rate is important for evaluating a rigidizing resin system for space expandable structures.

Thus the overall program is divided into two general areas of investigation:

1. The determination of the molecular structure which will give the best balance of the important properties.
2. The determination of which molecular structural arrangement will maintain the highest possible performance under actual environmental service such as long term exposure to space conditions during the operational phase. This phase of the program has been recently initiated in the ADM Laboratories and will not be reported herein.

These programs have been sponsored by the Aero Propulsion Laboratory, Wright-Patterson Research and Development with Mr Fred W Forbes as contract monitor.

SUMMARY AND CONCLUSIONS

The property data in Table 1 indicate that the experimental gas-cured urethane prepolymers currently under evaluation surpass anything previously prepared in this laboratory or anything that is currently revealed in the state-of-the-art.

Systems available at this time demonstrate improved properties. Data reported on 3-ply 181 glass laminates which were moisture cured averaged yield strengths of 47,000 psi and flexural modulus of 3,000,000 psi.

Small laboratory prototype structures, impregnated with resin and gassed with water vapor containing specific catalysts, can be rigidified in hard vacuum within 1/2 hour. Resin gel times under one minute have been recorded when pre-mixing resin and water containing .55% trimethyl amine.

Statistical design experiments have shown that flexural strengths can be substantially increased in several ways:

1. By employing polyethers containing acyclic rings, thus increasing backbone rigidity in the final polymer.
2. By using polyethers with a functionality of four or more in each recurring unit, consequently increasing cross-linking density.
3. By maintaining a proper balance between $\text{OH}/\#$ and polyol functionality.
4. By adding polar compounds to the resin systems, thereby bridging polar sites in the polymer.

It has also been shown that the cure rate of isocyanate terminated prepolymers is influenced by several factors:

1. Replacing TDI in the prepolymers with *m*-phenylene diisocyanate results in a resin with terminal NCO groups with enhanced reactivity due to the absence of the deactivating *o*-methyl group. Further enhancement can be obtained by using chlorinated *m*-phenylene diisocyanate.

2. Choice of a proper catalyst greatly speeds the water vapor cure. Suitable combination of catalysts lead to synergistically faster cure times.

In the new resin systems storage stability and handling characteristics remain adequate.

BACKGROUND

The use of isocyanate terminated prepolymers as moisture cured protective coatings suggested them as logical candidates for vapor phase rigidization. The initial prepolymers evaluated were commercially available moisture-cured one component systems. These systems did demonstrate feasibility and were reported on previously.^{1,2}

Polyethers

These initial resins were composed of linear poly(propylene oxide)ethers, short chain diols, trimethylolpropane and toluenediisocyanate. In these formulations the linear polyether and short chain diols were used as chain extenders while the trimethylol propane afforded branched sites for cross-linking. Physical properties derived from these systems were deficient and did not meet design goals.

Replacement of linear polyethers (hydroxyl value 260) with Allied's Actol 51-530 (hydroxyl value 530) led to improved physical properties. Other commercially available poly(oxypropylene oxide) adducts of glycerol (3-functionality), and sort (6-functionality) were formulated and evaluated. Flexural strengths obtained from 3-ply 181 moisture cured glass laminates averaged 18,000 psi with these polyethers.

Replacements of straight chain polyols with acyclic polyols prompted the major breakthrough sought for in the improvement of physical strength.³ A methoxylated derivative of cyclohexanone, 2,2,6,6-tetramethyloxy-cyclohexanol, was propoxylated with PO to a OH# of 540. Prepolymers containing this polyether exhibited the following strength data on 3-ply 181 glass laminates that were cured with water vapor:

bending yield strength	34,000 psi
flexural modulus	2,000,000 psi

From the wide spectrum of physical data accumulated under the AF program, it was then possible to investigate rather closely the correlations of the observed physical properties of cured specimens with the molecular configurations of the urethane resins contained therein. To do this an experimental program designed for statistical analysis was devised. In this program polyether structural moiety, hydroxyl number, and diisocyanate was varied in order to confidently predict structure-property correlation. 27 Experiments were proposed and executed to obtain data--(Table 2). Table 5 shows the composition and properties of the prepolymers synthesized and evaluated for this study. These results will be discussed in the following section.

Isocyanates

Aromatic diisocyanates were preferred in resin formulation over aliphatic diisocyanates because of the increased reactivity and rigidity in the polymer backbone due to the aromatic ring. Very slight changes in physical strength data have been observed in prepolymer systems wherein only the aromatic diisocyanate has been changed. The change in diisocyanate had profound influence on another important aspect of this system, i.e., cure time.

In the initial phase of this program, the commercially available diisocyanate, 2,4-toluene diisocyanate (TDI), was used in prepolymer formulation.

The use of TDI in generating the prepolymer left the relatively unreactive 2-position NCO substituent as the free terminal isocyanate available for further polymerization. Accordingly, cure rates were slow; however in comparison to other vapor-curable type resin systems evaluated the isocyanate prepolymer rigidization was considerably faster, Table 4.

In ensuing efforts to enhance cure rate, 2,4-toluene diisocyanate was replaced with *m*-phenylene diisocyanate. The reactivity was found to be *m*-phenylene diisocyanate > 2,4-toluene diisocyanate in agreement with literature data⁴. Theoretical discussion for these observations will be discussed in the Resin Discussion Section.

RESIN DISCUSSION

Correlation of Molecular Structure with Physical Property

Once chosen, the polyurethane resins have a number of inherent features that make them desirable as reinforcing resins for the structural applications under consideration. It is instructive to consider some of these general qualities.

One obvious attractive feature that the polyurethane-prepolymer system has is the high degree of control that can be exercised on the cross-linking index. In the vapor phase rigidization technique, the degree of cross-linking can be maintained low initially to ensure impregnability and wetting characteristics. Then in the gassing (curing) process, a high degree of polymerization and cross-linking can easily be obtained. Thus as one increases the netting index, i.e., the amount of cross-linking, the rigidity of the polymer increases, since these cross-links provide more points for load transfer from one polymer chain to another.

Another feature inherent in the final polymer is the strong intermolecular forces that result from the urea and urethane linkages in the polymer. These strong intermolecular forces provide good stiffness in the polymer chain, which is manifested by the fact that polyurethanes possess a significant amount of a crystalline phase. Crystallinity and molecular orientation are accompanied by the development of enhanced strength properties, such as tensile and flexural modulus. As can be seen from the molar cohesive energy data⁵ in Table 5, the urethane and urea group are strong contributors to intermolecular interactions.

Another structural contribution toward chain rigidity is the incorporation of the rigid aryl substituent introduced via the aromatic diisocyanate. As pointed out previously, substituent changes on the ring itself, shows little effect on physical properties. This, of course, would not have been the case had the less rigid aliphatic diisocyanate been employed.

With these general properties of polyurethanes in hand, it is of interest to consider other variables which affect physical properties of the composite.

Polyether

The program analysis indicates that modification of the polyether configuration has a profound effect on physical properties. Results have shown that flexural strengths can be substantially increased in several ways:

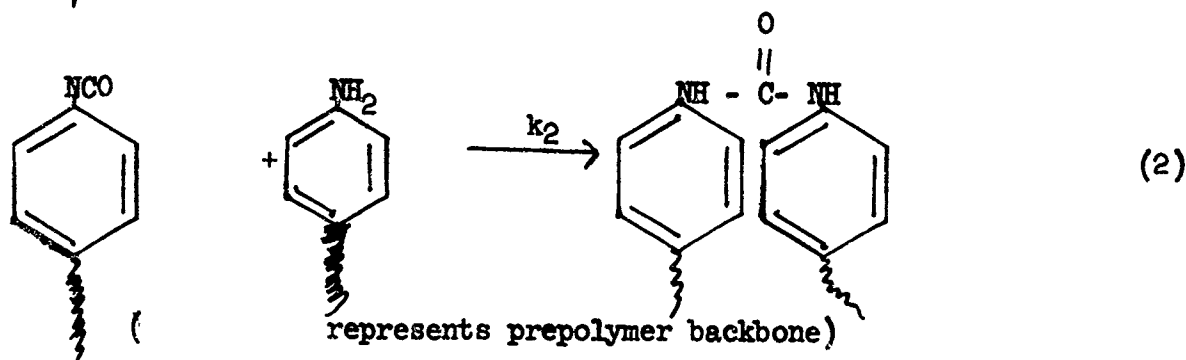
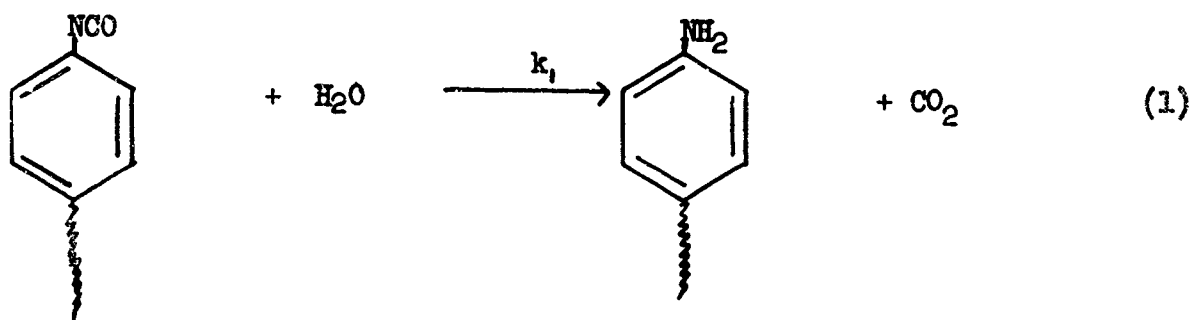
1. By employing acyclic polyols as replacements for straight chain polyols, it can be seen in Table 1 that improved physical strengths were obtained. It is clear that an acyclic ring has fewer conformations available than an open chain molecule and consequently increases the rigidity of the polymer backbone. While searching for resin designs that will give ultimate strength property and rigidity to the cured resin, it must be kept in mind that a certain level of flexibility must be maintained in the prepolymer so that resinous flow characteristics are present. To maintain this latter property the rigid polyol backbone must be suitably extended. This has been achieved by addition of propylene oxide (PO). The ratio of PO to hydroxyl group determines the degree of flexibility which can be so introduced through the resultant ethereal linkages. In the prepolymers, ether links function as flexibilizing groups because they permit small portions of the polymer chains to move independently. Propylene oxide, while functioning as a flexibilizing agent, is nevertheless, because of its pendent methyl substituent, somewhat less flexible than ethylene oxide. The extension of polyols with styrene oxide would result in considerably more restriction of the ether bond rotation. Figures 1 through 3 represent molecular models which illustrate the rigid acyclic polyols extended with propylene oxide and styrene oxide. Inspection of the models indicates limited rotational freedom. Figures 4 and 5 depict open chain polyols extended with PO. Inspection of these models demonstrates more rotational freedom.
2. By using polyethers with a functionality of at least four, a greater cross-linking density was achieved in the cured resin which led to increased strength properties.

Cross-linking density is related to the proximity of active functional groups on a polymer chain. The distance between cross links is termed the netting index. Figures 6 and 7 illustrate the relationship between physical properties and netting index. Enhanced netting index achieved with the polymer systems derived from polyfunctional polyols as listed in Table 2 has been a contributing factor toward achieving product improvement.

3. It has been observed that the proper balance must be maintained between the degree of polyol functionality and hydroxyl number in order to retain the optimum relation between bending strength and modulus. Flexural strengths obtained from the crosslinked resins made from sucrose polyethers bears an inverse relationship to the hydroxyl number - the 3750H# polyether yielding highest bending strengths (Table 6, Fig. 8). The reverse is true for the cross-linked resins made from the α -methyl glucoside polyether and the 2,2,6,6 tetramethylol cyclohexanol polyether. In these instances, the 5300H# polyether yields the higher bending strengths (Table 6, Fig. 8). Sucrose, being octafunctional, apparently over crosslinks at the higher hydroxyl value and develops brittle character.
4. Finally, the correlation of physical strengths with solvent system employed with these resins is currently under investigation at ADM. While the work is far from complete, one interesting result of this study may be seen in Fig. 9. Here the addition of dioctylphthalate to prepolymer prior to moisture cure is shown to increase the flexural strength of the resin-fiber glass laminate. The maximum increase is observed at about 25 weight % of DOP. This increase is ascribed to the ability of the polar DOP molecule to promote secondary valence interactions between polymer chains, thus reducing flexibility. At higher concentrations of DOP, its better-known ability to act as a plasticizer predominates and the flexural values decrease.

Correlation of Molecular Structure and Chemical Properties

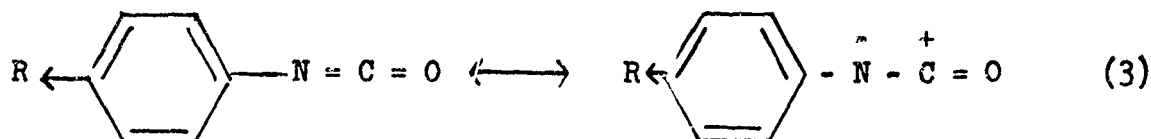
The reaction rates of the aromatic isocyanates present in the prepolymer systems may also be discussed in terms of molecular structure. The curing process is the reaction of the isocyanate with water and may be represented briefly (though very naively) in equations 1 and 2:



It should be pointed out here that Equation 1 is simply representation of what is probably a complex process, and that these two equations merely represent the two major reactions undergone by a moisture-cured prepolymer; side reactions of varying degrees of importance are too numerous to be discussed here. Equation 1 shows the production of an aromatic amine from the isocyanate, and Equation 2 represents the primary crosslinking step: the reaction of the amine with isocyanate to form a urea linkage. Clearly, the condition $k_2 \gg k_1$ must hold to get maximum crosslinking and maximum physical strength. Thus, if $k_2 < k_1$, the resulting polymers would be low in molecular weight and would have little crosslinking. In addition to this condition, the restriction that k_2 be fast is also a prerequisite; otherwise, the cure would be too slow to meet the design goal specifications required in expandable aerospace structures. It is unfortunate that, despite the vast literature on the kinetics of isocyanate reactions⁶, reactions 1 and 2 have scarcely been touched upon. One phase of our continuing program will be to elucidate the kinetics of these reactions.

Despite this gap in our present knowledge, gel time tests have afforded a good approximative method of determining the relative cure times required by the prepolymers derived from various isocyanates. From the data in Table 7, it can be seen that the prepolymers cure, in the order of their precursor isocyanates, as follows: chlorinated m-phenylenediisocyanate (CMPDI) > m-phenylenediisocyanate (MPDI) ~ diphenylmethanediisocyanate (MDI) > toluenediisocyanate (TDI).

This order of reactivity is best discussed in terms of the effect of molecular configuration (structure) on chemical reactivity. In both Equation 1 and Equation 2, one of the reacting species is the isocyanate. Electron withdrawing groups substituted on this aromatic isocyanate will promote the reactivity of the isocyanate by making the carbonyl more positive (Eqn 3), and consequently more receptive



to attack by an active hydrogen compound.

Not surprisingly then, perhaps, the most rapid gel time is observed with CMPDI, since the electromeric electron withdrawing tendency of the chlorine substituent is well known. Indeed, it would appear that on the basis of our still preliminary screening of CMPDI, it is too reactive for the moisture cured system. Thus, laminates prepared from CMPDI prepolymers gave poor flexural values and exhibited severe delamination. The delamination may well be caused by the too rapid evolution of carbon dioxide (Eqn 1) from the sample. An alternative explanation may be that this particular chlorinated prepolymer has poor adherence to glass. The properties of this potentially valuable isocyanate are currently under investigation.

Although the chlorine substituent increases the reactivity of the isocyanate, it might be argued that it also decreases the reactivity of the amine that reacts in the crosslinking step (Eqn 2). It is well known that the chloro-anilines are less basic than aniline. The basicity is, of course, measured in

Hammett-type solvents (such as sulfuric acid-water mixtures) and it may be this basicity difference is levelled in the prepolymer system. An equally possible explanation is that the enhanced reactivity of the isocyanate merely overrides the somewhat decreased reactivity of the amine, particularly in the presence of a catalyst. This latter observation correlates well with the observation that the NCO/OH ratio of 3 or greater had to be maintained in preparing the MPDI prepolymers; at lower values gelation occurred during or shortly after preparation. This indicates that even after one NCO group reacts, the remaining group is still almost as reactive as the first, causing cross-linking and then gelation in the prepolymer. In this regard, the need for a low netting index in the prepolymer has already been pointed out (cf background).

The greater reactivity to water of the MPDI prepolymer as compared to the TDI prepolymer is best explained in terms of steric and electronic effects. Here the electron releasing nature of the methyl group decreases the positive character of the carbonyl carbon, and thus decreases the reactivity of the isocyanate group to attack by active hydrogen compounds. In addition, the steric bulk of the methyl group prevents coordination of the catalyst with the adjacent isocyanate group (refer to Table 7, notice the minor effect of catalysis on gelation) and blocks the approach of the reactant water molecule. The superior performance of MPDI over TDI has also been demonstrated by the shorter cure time required for expandable structures impregnated with ADM's Vapor Set B versus the ADM Vapor Set A, when cured in a simulated space environment.³

The equal reactivity of MPDI and MDI prepolymers is not surprising, since the aromatic isocyanates that make up the resulting prepolymers both have substituents that are only very weakly electron withdrawing, and neither isocyanate is sterically hindered. The drawback to the use of MDI prepolymers in the present application stems from the tendency of these prepolymers to gel in conventional urethane solvents. This is undoubtedly due to the necessarily high functionality of the polyethers employed, coupled with known tendency of MDI to dimerize. The less symmetrical MPDI does not easily dimerize.

Another phase of our current kinetic studies is an intensive investigation of the effect of catalysis on cure time reduction. The pronounced effect of tertiary amines on the rate of the water-isocyanate reaction, Fig 10, Table 8, is consistent with the numerous observations in the literature. Since the curing mechanism is the gassing of a catalyst-water mixture into the resin impregnated structure, it is imperative that the catalyst be volatile. Consequently, our present choice is limited to volatile tertiary amines such as triethyl or trimethylamine. We have observed a synergistic effect when a tertiary amine is used as the gassing catalyst on a structure that has been impregnated with resin containing catalytic amounts of dibutyl tin diacetate (refer to Table 7 for this observation). The inability to maintain prepolymer storage stability with tin additives precludes their use in these systems.

TEST PROCEDURES

Test procedures are vitally necessary as evaluation tools for resin research and development. Due to the specialized nature of the materials to be evaluated, standard equipment and procedures generally were either unavailable or not directly applicable, and therefore had to be developed. Problems which are encountered stem from the fact that the resins to be evaluated are prepared as solutions from which the solvent must be removed prior to attack by the vapor curing agent (usually water). Also, since the cure is accomplished by gaseous agents, the samples must be sufficiently thin (as they are in space structures) to permit permeation of these agents. Thin samples also permit the release of gaseous products of reaction which are formed during curing. These difficulties have been overcome and equipment and methods have been developed to: (1) evaluate flexural strength and flexural modulus, (2) evaluate the rate of cure, and (3) determine shrinkage during cure.

A. Laminate preparation

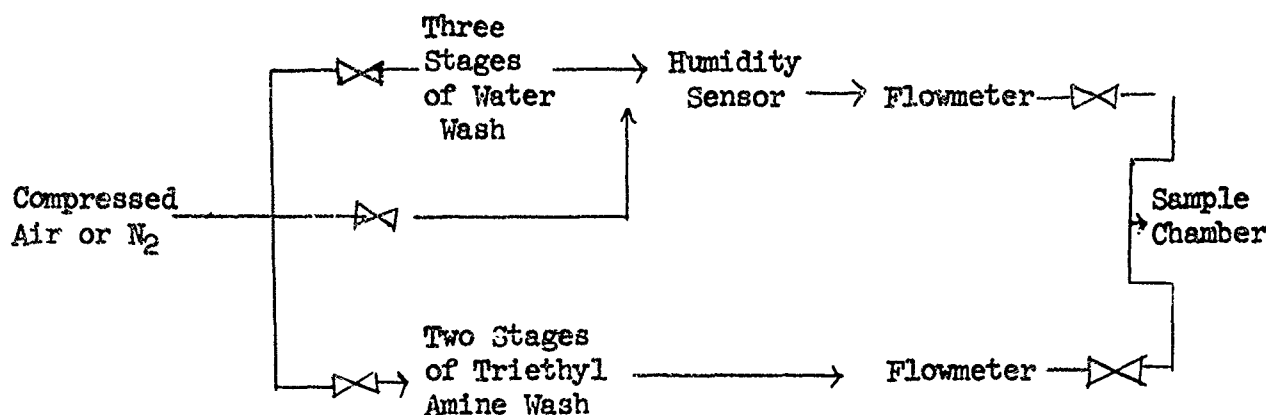
A satisfactory method of preparing laminates for flexural property determination and cure characteristics was the primary requirement for the test procedures subsequently used. In the procedure developed, 5" x 6" pieces of style 181 glass cloth were hand coated with the test resin solution in as uniform a method as possible. These wet sheets were then vacuum dried to remove the solvent. Next, three of the impregnated and dried sheets were consolidated in a press at 65 psi pressure and 80-90°C. Under these conditions of heat and pressure, the dried prepolymer flows to form a single 3-ply laminate with the resin remaining uncured. After cooling to 20°C, the laminate is removed from the silicone greased platens. Laminates of excellent appearance with the majority of the solvent removed, and the resin uncured are produced by this procedure.

B. Flexural Strength and Flexural Modulus

Flexural strength and flexural modulus have been selected as the properties describing the physical strength of the resin. Tensile strength tests on glass-fabric reinforced laminates generally are indicative of the strength of the glass reinforcement component, and consequently of little value in resin development. The 5" x 6" laminates prepared as described in (A) are placed in a chamber swept with water and triethyl amine vapors for 48 hours to obtain complete cure. Test samples ($\frac{1}{2}$ " x 4") are then prepared and tested in an Instron Universal Tester, Model TM. Midpoint loading is used with a span of 2.00 inches and a strain rate of 0.20 inches/min. The flexural samples are always prepared with the length along the warp of the fabric.

C. Rate of Cure

To evaluate rate of cure, equipment has been set up as shown in the following diagram:



The diagram shows a system which saturates with water the main air stream, blends dry air with this stream and finally meters a minute amount of triethyl amine catalyst with the controlled humidity stream into the sample chamber. Assumptions made in using this equipment for rate of cure studies to obtain information for curing space structures are: (1) that the inert elements, O_2 , N_2 , etc., of the air do not affect the function of the curing agent and catalyst; and (2) that the cure of expandable space structures resins will be performed at pressure in a confined volume rather than open to the vacuum of space. Accepting these assumptions, the equipment assembled can apply to flexural samples in the curing chamber set conditions of partial pressure (concentration) of water and triethyl amine, and also the velocity and temperature of cure for any length of time. Samples of uncured laminates prepared as in (A) are placed in the sample chamber and subjected to various times of cure. These samples are then flex tested as in (B), and the physical strength as a function of time determined. Thus, cure expressed as the development of physical properties is determined.

D. Resin Cure Shrinkage

The shrinkage of resins during cure is an important factor which is usually determined by density or dilatometry methods. Due to the presence of solvent in the initial prepolymer and the requirement of diffusing curing agents into the resin and reaction products out of the resin, these usual methods cannot be applied. However, equipment has been designed and built in the Plastics Department of ADM which can detect dimensional changes as small as five-millionths of an inch during curing. A procedure has been developed using this equipment and involves the use of uncured laminates prepared as described in (A). Pins are passed through a piece of laminate at a fixed spacing (usually 1.0 inch), and the sample mounted in the test apparatus.

A pan of water is placed in the chamber with the sample to provide the curing agent, and a readout of the dimensional change as a function of time (cure) is obtained. Extreme care must be exercised to obtain useful information since the absolute dimensional changes are so small. Through the use of the laminating procedure, shrinkage due to solvent removal is minimized and the three-ply structure containing the reinforcement closely approximates the cure shrinkage which would occur in actual space structures.

TABLE 1

PHYSICAL PROPERTIES OF VAPOR CURED PREPOLYMERS

Prepolymer	Hydroxyl	Isocyanate	Solvent	% NCO	% Solids	Flexural Strength	Flexural Modulus	Thickness	% Resin
α Me Glucoside	361	MPDI	BuAc	6.6	49	27,600	1.8×10^6	.042	29
α Me Glucoside	436	MPDI	BuAc	7.5	51	40,377	2.7×10^6	.038	28
α Me Glucoside	539	MPDI	BuAc	8.1	55	39,990	2.37×10^6	.035	32
α Me Glucoside	361	TDI	BuAc	6.25	49	20,000	1.3×10^6	.040	32
α Me Glucoside	436	TDI	BuAc	5.42	49	37,000	2.8×10^6	.035	30
Sucrose	375	MPDI	BuAc	6.5	49	41,480	2.5×10^6	.037	33
Sucrose	450	MPDI	BuAc	7.2	48	24,000	1.58×10^6	.038	36
Sucrose	530	MPDI	BuAc	7.9	46	26,000	1.5×10^6	.040	37
Pentol	359	MPDI	BuAc	6.3	46	31,000	2.31×10^6	.033	
Pentol	445	MPDI	BuAc	5.0	49	28,700	2.8×10^6	.036	21
Pentol	568	MPDI	BuAc	7.31	49	41,000	2.9×10^6	.035	39
Pentol	359	TDI	BuAc	7.0	49				
Pentol	445	TDI	BuAc	7.3	51	24,100	1.92×10^6	.037	
Pentol	568	TDI	BuAc	8.2	55	40,100	2.41×10^6	.040	
α Me Glucoside	436	MDI	-	6.5	50	31,700	1.96×10^6	.040	
α Me Glucoside*	361	MPDI	15% TCP	6.3	50	35,000	2.3×10^6	.035	
α Me Glucoside*	361	MPDI	25% TCP	6.5	50	25,300	1.8×10^6	.035	
α Me Glucoside*	361	MPDI	40% TCP	6.7	50	22,200	1.7×10^6	.039	

12

*Prepolymer formulations contained varying concentration of tricresyl phosphate as polar additive.

TABLE 2

<u>EXPERIMENT NUMBER</u>	<u>POLYETHER TYPE</u>	<u>HYDROXYL NUMBER</u>	<u>DIISOCYANATE</u>
1	AMG	450	MPDI
2	Pentol	540	MDI
3	Sucrose	450	MDI
4	Pentol	450	TDI
5	Sucrose	375	TDI
6	AMG	375	MDI
7	Sucrose	540	MPDI
8	Pentol	375	MPDI
9	AMG	540	TDI
10	Pentol	450	MPDI
11	Sucrose	450	MPDI
12	AMG	540	MDI
13	Pentol	540	MPDI
14	Sucrose	375	MDI
15	AMG	375	MPDI
16	AMG	450	MDI
17	Pentol	450	MDI
18	Sucrose	375	MPDI
19	Sucrose	450	TDI
20	Sucrose	540	TDI
21	Pentol	375	MDI
22	AMG	375	TDI
23	Pentol	375	TDI
24	Pentol	540	TDI
25	AMG	540	MPDI
26	AMG	450	TDI
27	Sucrose	540	MDI

AMG = α -Methyl glucoside
Pentol = 2,2,6,6-tetramethohylcyclohexanol
MPDI = m-phenylene diisocyanate
MDI = 4,4'-Methane diphenyl diisocyanate
TDI = 2,4-Toluene diisocyanate

TABLE 3

COMPOSITION AND PROPERTIES OF PREPOLYMERS

Polyether Polyol	Isocyanate	NCO/OH	Solvent	% NCO	Theo % NCO	% Solids	Gardner-Holt Viscosity	Storage Stability
361-OH α Me G	MDI	2/1	BuAc	6.6	6.65	49	A	ok
436-OH α Me G	MPDI	2/1	BuAc	7.5	7.55	51	A	ok
539-OH α Me G	MPDI	2/1	BuAc	8.1	7.9	55	F	ok
361-OH α Me G	MDI	2/1	BuAc	5.2	5.2	-	-	3-day
436-OH α Me G	MDI	2/1	BuAc	5.15	5.6	-	-	9-day
Styrenoxylated								
Pentol	MPDI	2/1	BuAc	7.35	8.4	68	T	10-day
361-OH α Me G	TDI	2/1	BuAc	6.25	6.4	49	A	ok
436-OH α Me G	TDI	2/1	BuAc	5.42	3.57	49	A	ok
539-OH α Me G	TDI	2/1	BuAc	7.5	-	50	A	ok
361-OH α Me G	MPDI	2/1	CH ₂ Cl ₂	7.5	7.5	52	A	ok
361-OH α Me G	MDI	2/1	BuAc	5.6	5.2	-	-	4-day
361-OH α Me G	MDI	2/1	CH ₂ Cl ₂	-	-	-	-	4-day
445-OH Pentol	MPDI	2/1	BuAc	4.85	7.1	49	A	ok
568-OH Pentol	MPDI	2/1	BuAc	7.31	8.1	49	A	ok
445-OH Pentol	MDI	2/1	BuAc	2.5	5.6	-	-	15-day
568-OH Pentol	MDI	2/1	BuAc	2.0	6.0	-	-	9-day
375-OH Sucrose	MPDI	2/1	BuAc	6.5	6.1	49	D	ok
450-OH Sucrose	MPDI	2/1	BuAc	7.2	8.0	48	G	ok
530-OH Sucrose	MPDI	2/1	BuAc	3.0	-	-	U-V	14-day
530-OH Sucrose	MPDI	2/1	BuAc	7.9	7.9	46	A	ok
375-OH Sucrose	TDI	2/1	BuAc	5.8	6.5	49	A	ok
450-OH Sucrose	TDI	2/1	BuAc	7.5	6.8	49	A	ok
530-OH Sucrose	TDI	2/1	BuAc	8.6	7.2	49	A	ok
445-OH Pentol	TDI	2/1	BuAc	7.3	7.0	51	A	ok
568-OH Pentol	TDI	2/1	BuAc	8.2	7.7	55	A	ok
436-OH α Me G	MDI	2/1	-	6.5	5.7	50	A	ok
359-OH Pentol	TDI	2/1	BuAc	7.0	6.4	49	A	ok
359-OH Pentol	MPDI	2/1	BuAc	6.3	6.4	46	A	ok

TABLE 4

RIGIDIZATION RATES OF GAS CURED SYSTEMS

<u>System</u>	<u>Co-Reactant</u>	<u>Catalyst</u>	<u>Vacuum Cure Time</u>
Isocyanate Terminated Prepolymer*	Water	Triethyl Amine	4-6 hours
Epoxy	1,3-Propylene Diamine	Triphenyl Phosphite	24 hours
Epoxy	--	Triethyl Amine	24 hours
Epoxy	1,3-Propylene Diamine	Borate**	6 hours
Polyester		uv	24 hours
Furfural		Acid	24 hours
Phenyl Silanes		Active Hydrogen	24 hours

*Prepolymers developed under initial contract AF 33(657)-10409

**ADM synthesized accelerator

TABLE 5

MOLAR COHESIVE ENERGY OF ORGANIC GROUPS

<u>Group</u>	<u>Cohesion</u> <u>kcal/mole</u>
-CH ₂ -	0.68
-O-	1.00
-COO-	2.90
-C ₆ H ₄ -	3.90
-CONH-	8.50
-OCONH-	8.74
-HNHCONH-	9.21

TABLE 6

<u>Polyether Type</u>	<u>OH #</u>	<u>Flexural Strength psi</u>	<u>Modulus psi x 10⁶</u>
Sucrose	375	41,479	2.42
Sucrose	450	24,390	1.60
Sucrose	540	22,747	2.69
α -Me G	375	27,600	1.83
α -Me G	450	40,370	2.69
α -Me G	540	39,000	2.36
Pentol	375	30,500	2.30
Pentol	450	29,000	2.80
Pentol	540	41,900	2.93

TABLE 7

PREPOLYMER GEL TIME DATA

<u>Propylene Oxide Polyether Type</u>	<u>OR#</u>	<u>Diisocyanate</u>	<u>Gel Time* (Min)</u>	<u>Gel Time** (Min)</u>
α Me G	540	MPDI	4.8	0.9
α Me G	540	TDI	39.0	> ½ hr
Sucrose	540	MPDI	2.6	0.5
Sucrose	540	TDI	10.0	10.0
Pentol	540	Cl-MPDI	0.5	
Pentol	540	MPDI	5.8	1.8
Pentol	540	TDI	> 30	> ½ hr
α Me G	440	MPDI	6.3	1.8
α Me G	440	TDI	> 1 hr	> ½ hr
Sucrose	440	MPDI	3.5	1.0
Sucrose	440	TDI	> 1 hr	> ½ hr
Pentol	440	MPDI	4.0	2.4
Pentol	440	TDI	> ½ hr	> ½ hr
α Me G	361	MPDI	6.3	1.8
α Me G	361	TDI	> 120	> ½ hr
Sucrose	361	MPDI	2.5	1.0
Sucrose	361	TDI	> 120	> 1 hr
Pentol	361	MPDI	4.0	2.0
Pentol	361	TDI	60	> ½ hr
α Me G	440	MPDI	2.0	
α Me G	440	MPDI	2.1	
α Me G	540	MPDI	1.5	
Pentol ***	286	MPDI	1.5	

* Reactant/water 5 drops/5 g sample, % catalyst .58% Me₃N

** Additional 1% dibutyl tin diacetate added to resin prior to gelation

*** Strenoxylated polyether

TABLE 8

Catalytic Effect on Gelation Time of Prepolymers

<u>Prepolymer</u>	<u>Catalyst (CH₃)₃N</u>	<u>Gel Time (Min)</u>
	0.075%	8
	0.375%	1.5
	0.77%	0.5

REFERENCES

1. I W Fussell, Nels S Hanssen, W J McKillip, Development of An Inflatable Self-Rigidizing Space Shelter and Solar Collector from Honeycomb Sandwich Material, Technical Documentary Report No APF TDR 64-29
2. I W Russell, N Hanssen, W J McKillip, B M Culbertson, R C Slagel, Expandable Self-Rigidizing Honeycomb Structures, Aerospace Expandable Structures Conference Transactions, pp 168-185, (1963).
3. Unpublished Final Report AF 33(615)-1243
4. C E McGinn, R G Spaunburgh, paper presented at the American Chemical Society Meeting, Atlantic City, September, 1956.
5. H Mark, Ind Eng Chem 34, 1343 (1942)
6. J H Sanders, K C Fritsch "Polyurethanes: Chemistry and Technology," Part 1, pp 129 ff (1962).

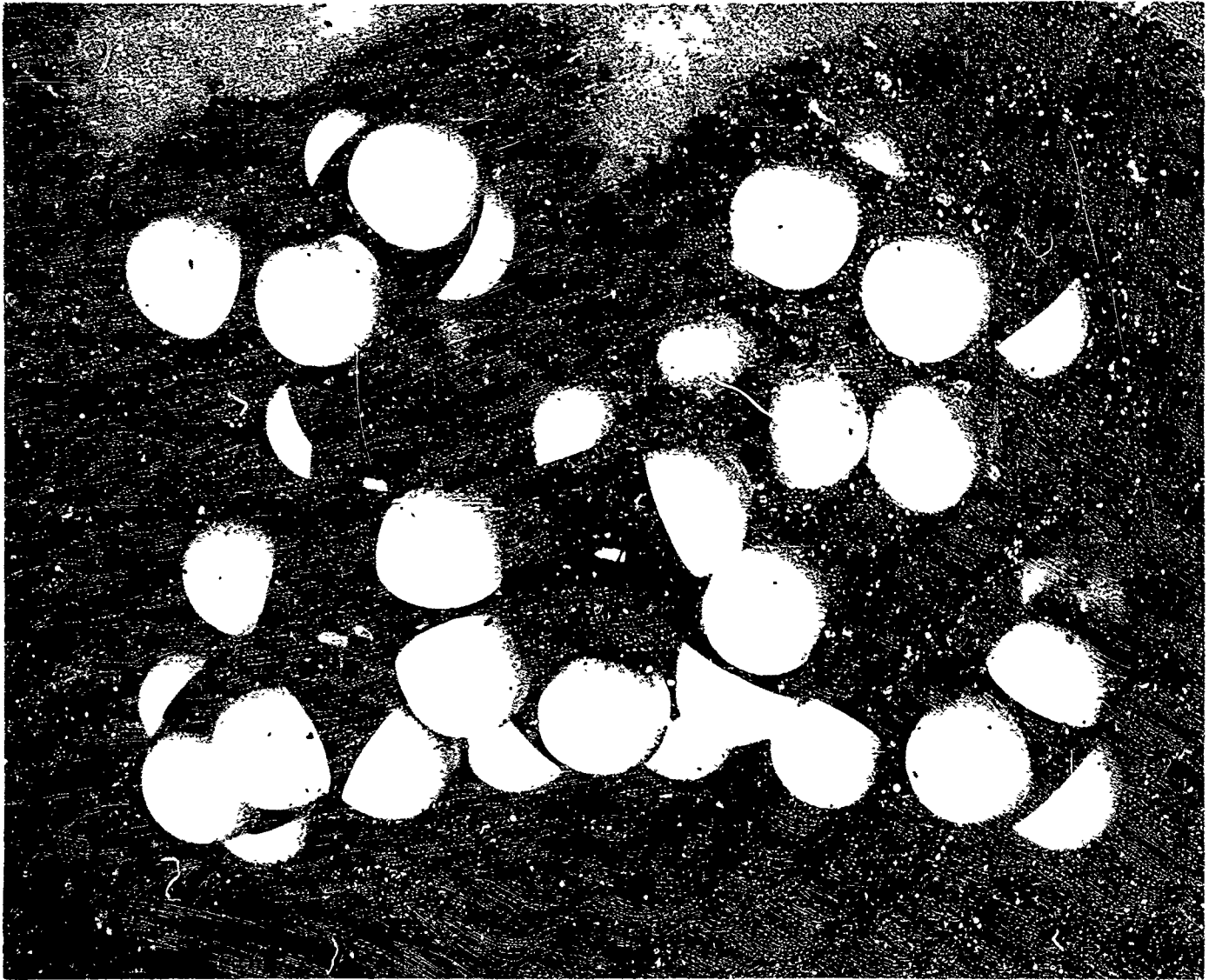


Figure 1 Molecular Model of PO Polyether of 2,2,6,6-Tetra-
methylole cyclohexanol

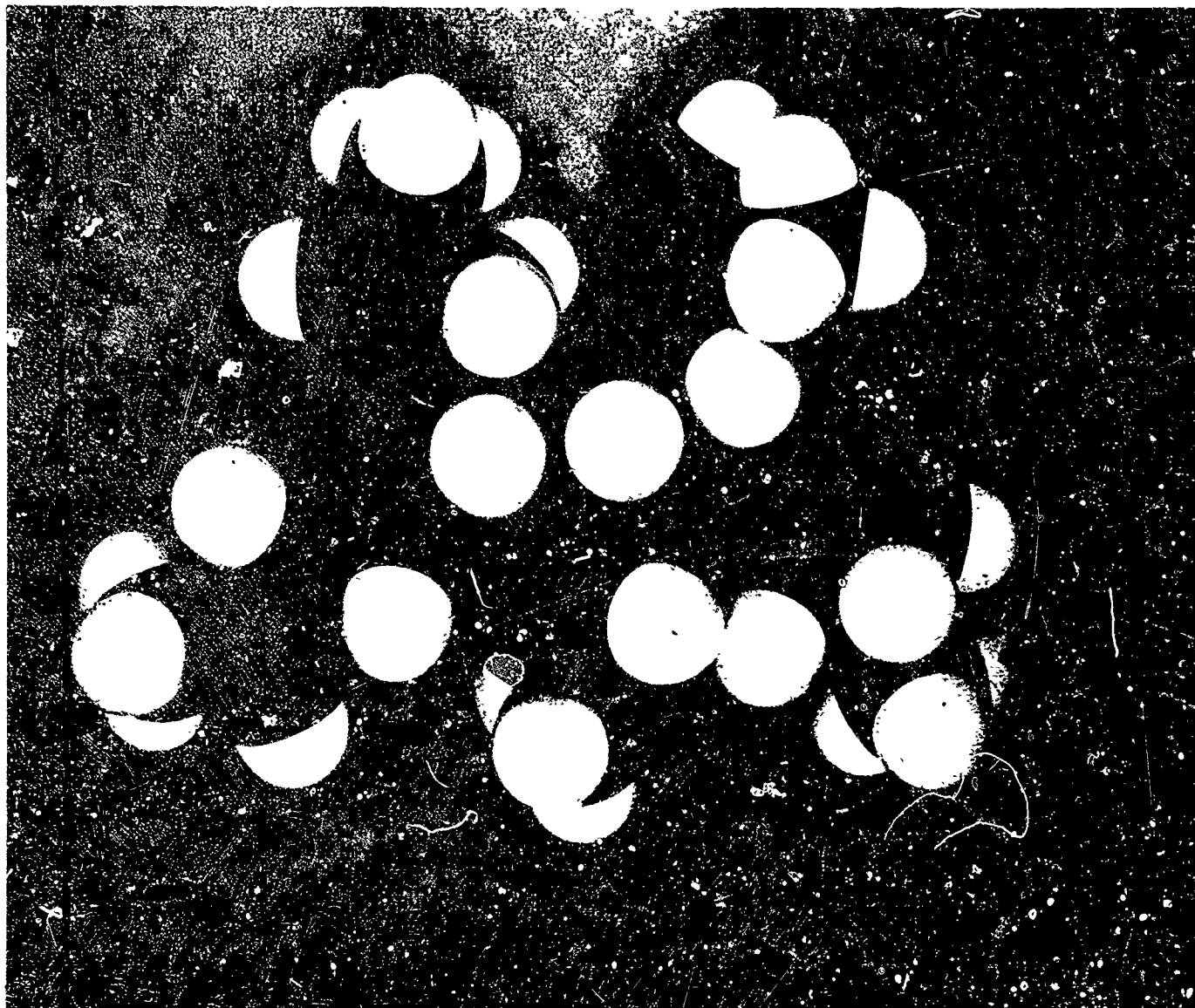


Figure 2 Molecular Model of PO Polyether of α -Methyl Glucoside

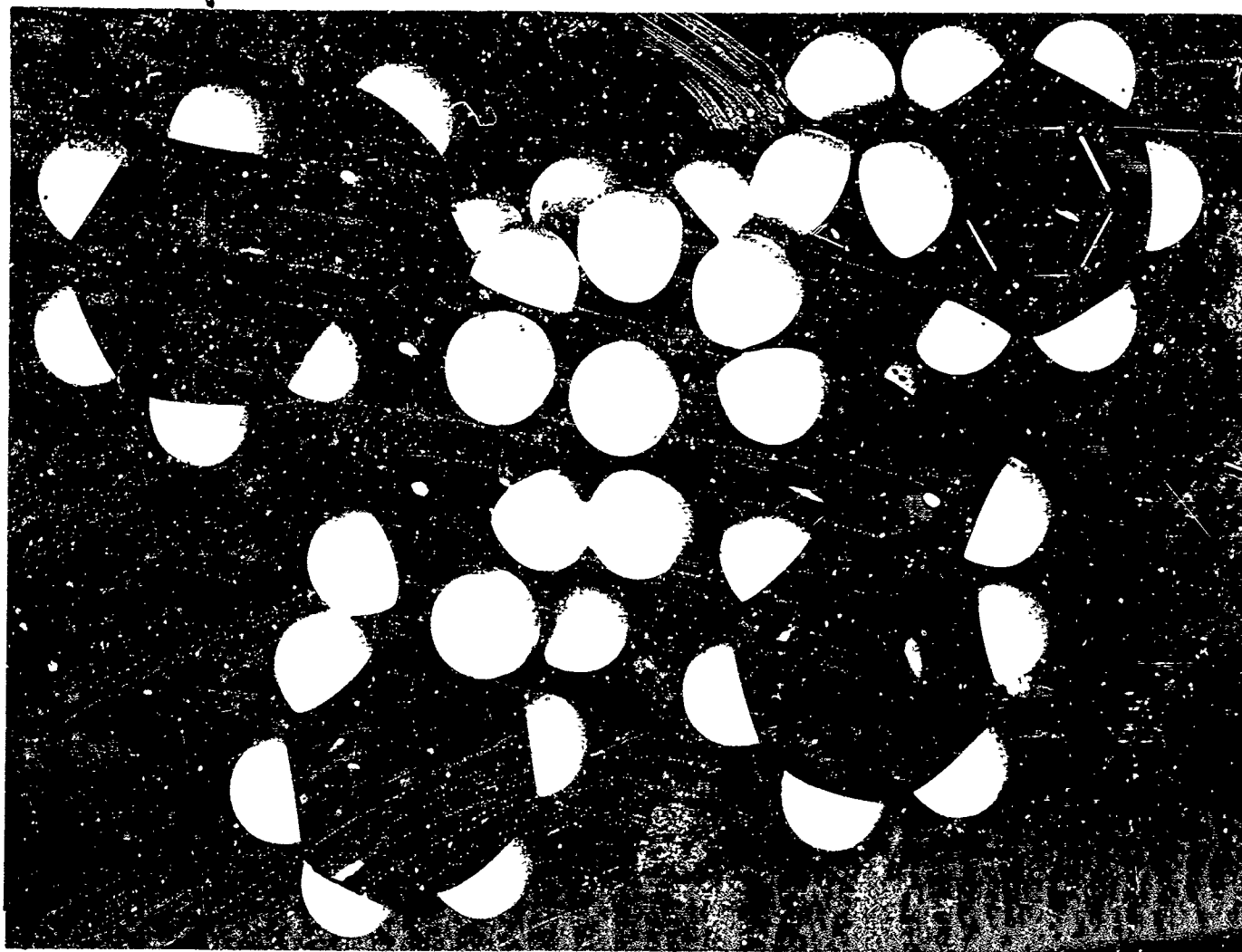


Figure 3 Molecular Model of Styrenoxylated Polyether of
2,2,6,6-Tetramethylcyclohexanol

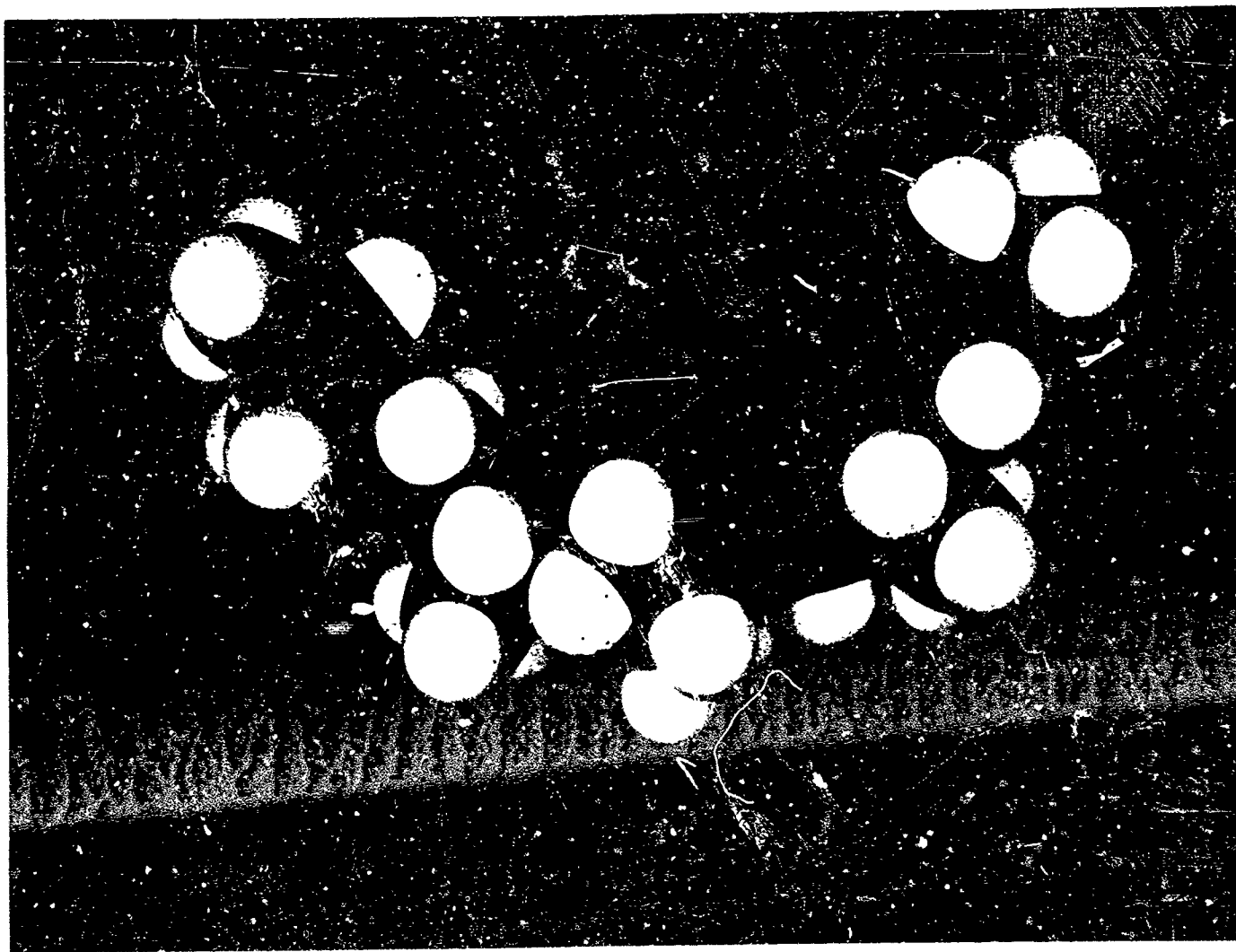


Figure 4 Molecular Model of Poly(propylene oxide)

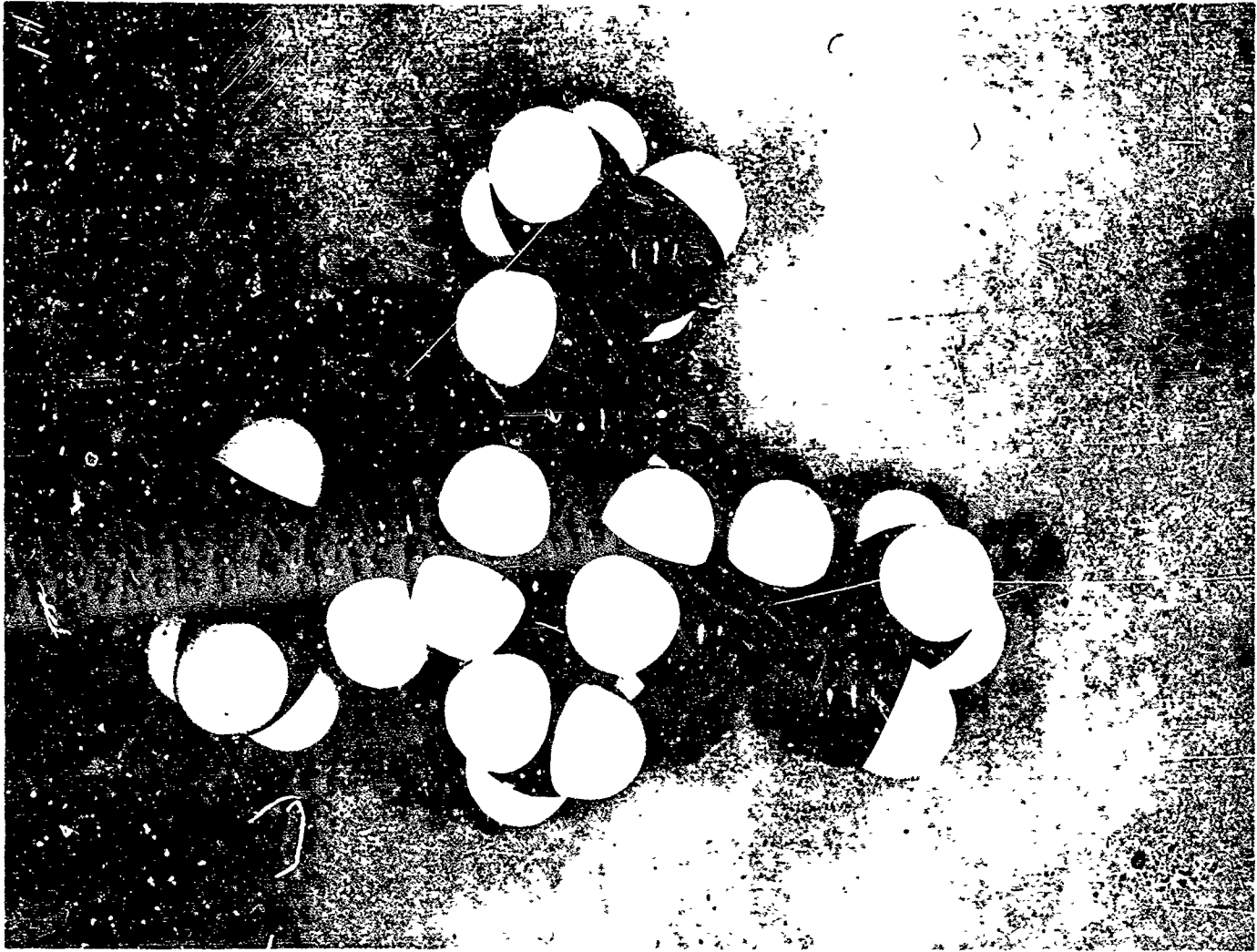


Figure 5 Molecular Model of PO Polyether of Trimethylolpropane

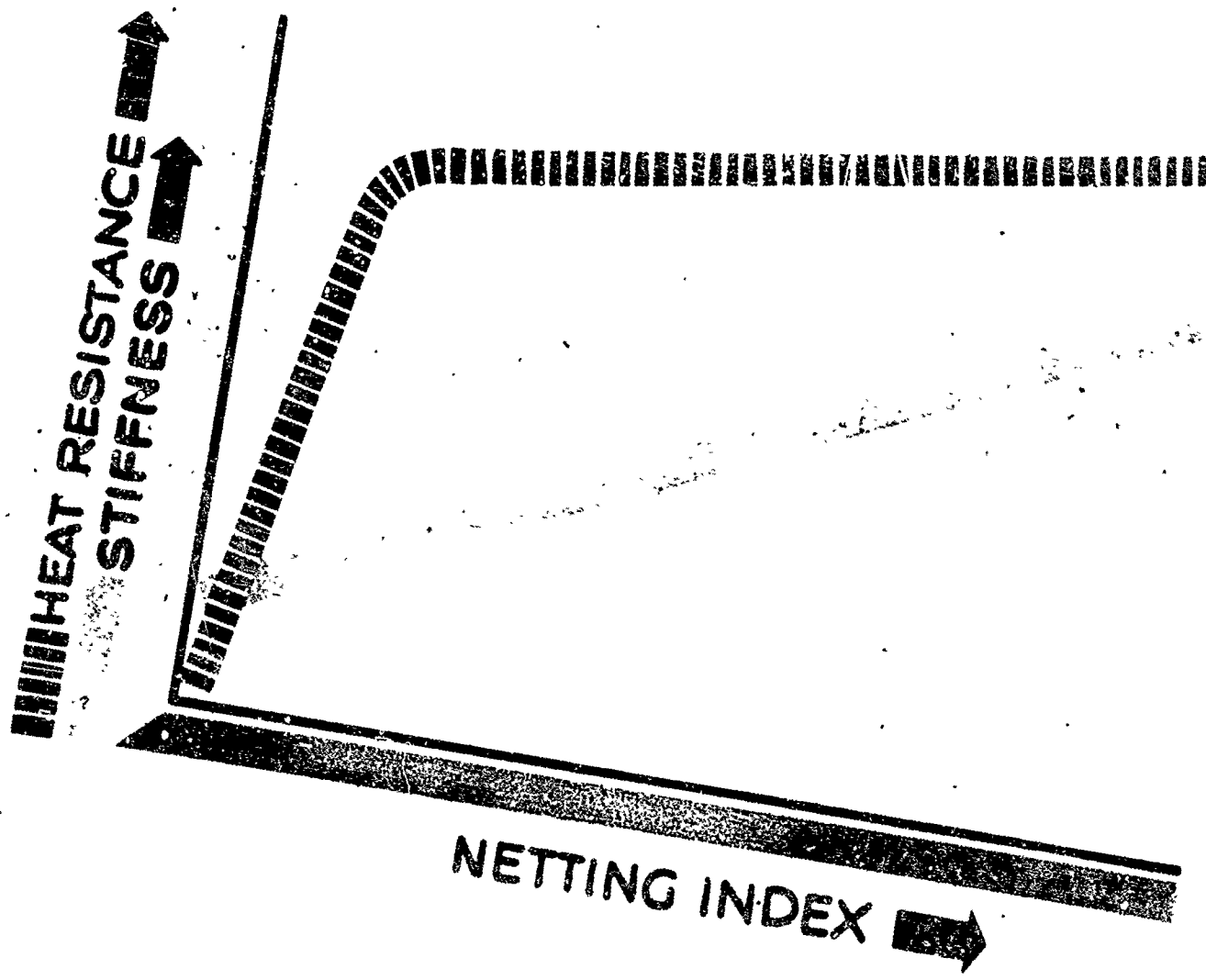


Figure 6
Correlation of Netting Index versus Stiffness in
Polymer

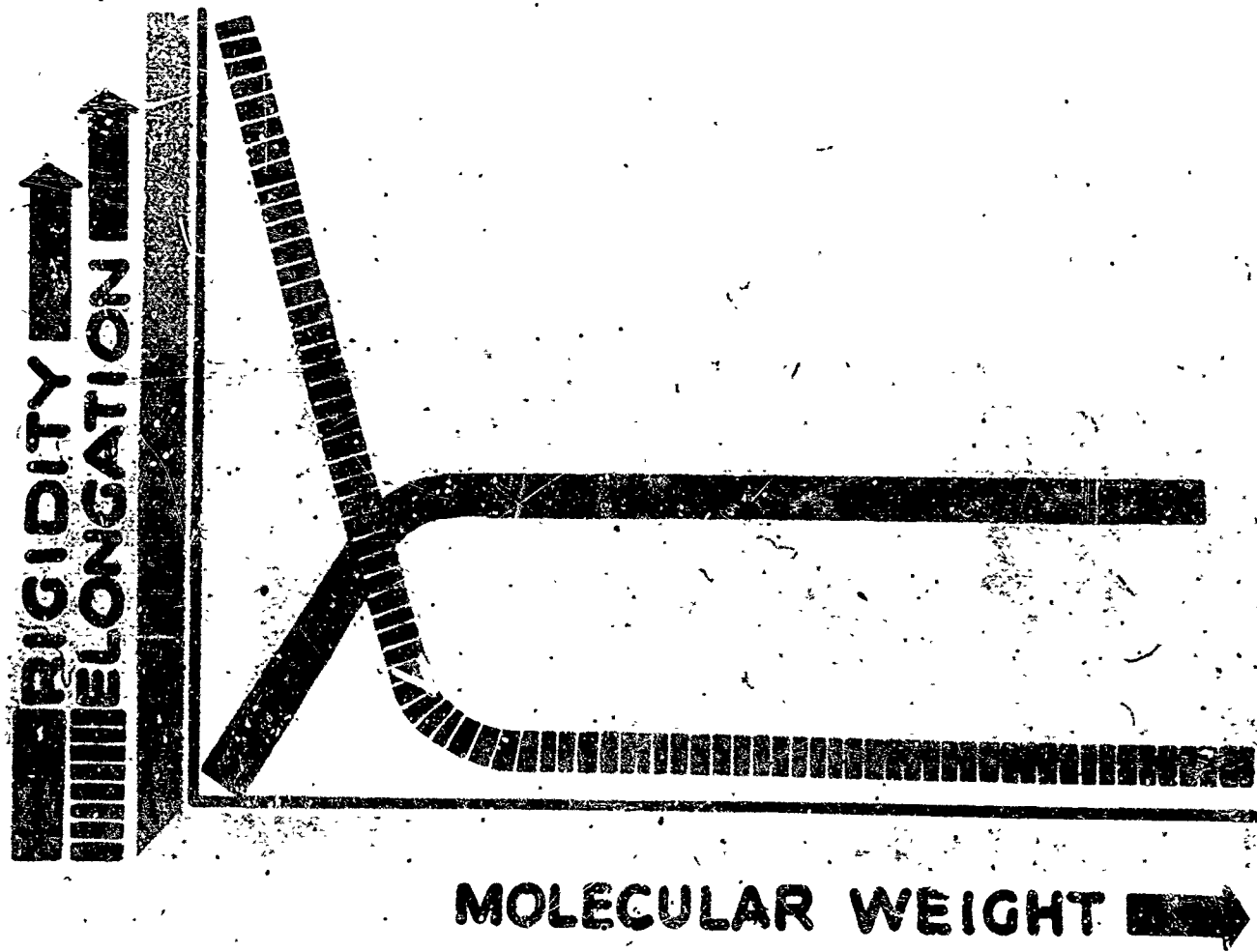


Figure 7 Correlation of Molecular Weight versus Rigidity in
Polymer

△ Sucrose
+ α Me G
○ Pentol

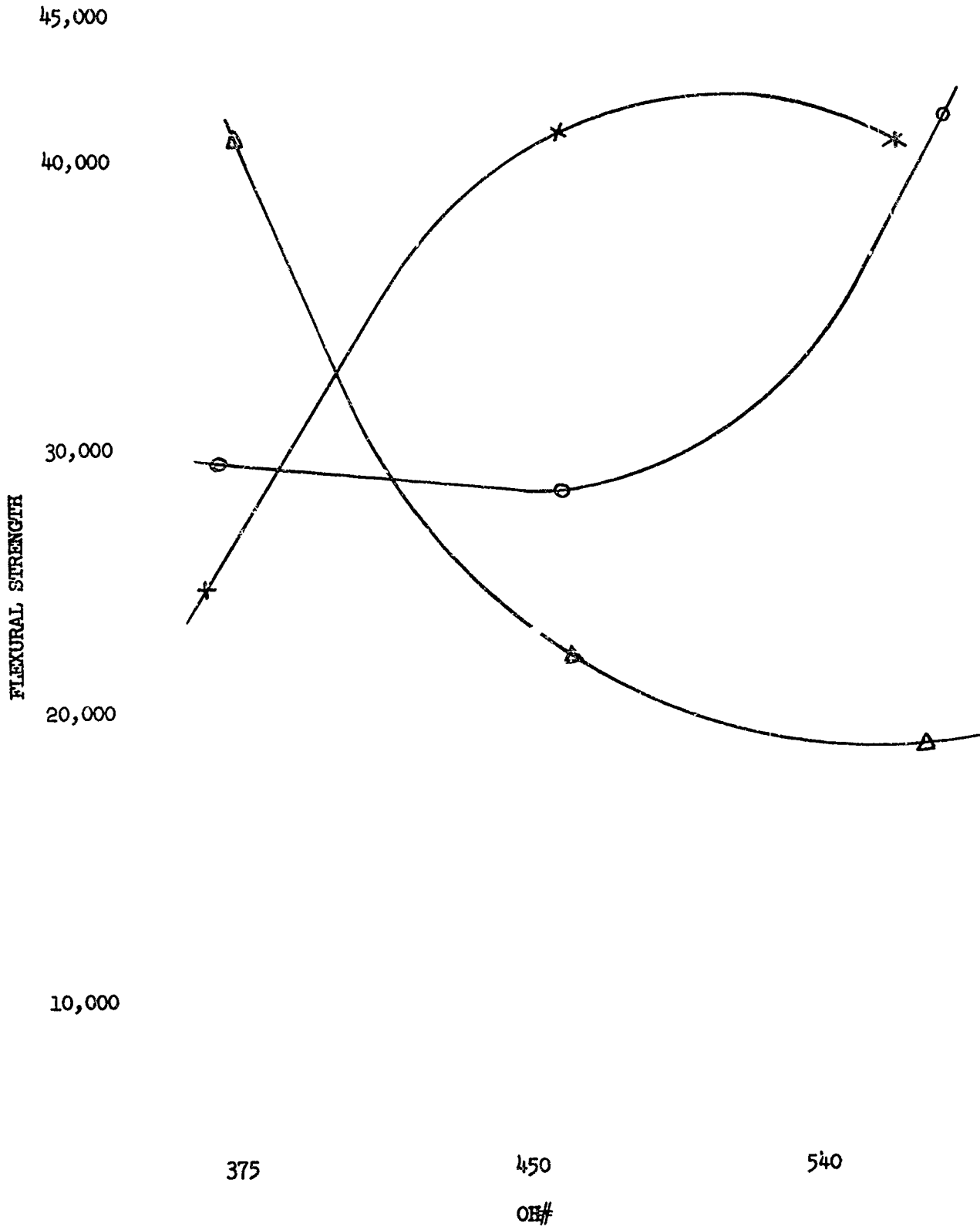


Figure 8 Variation of Flexural Strength versus OH Number in Candidate Polyether Series

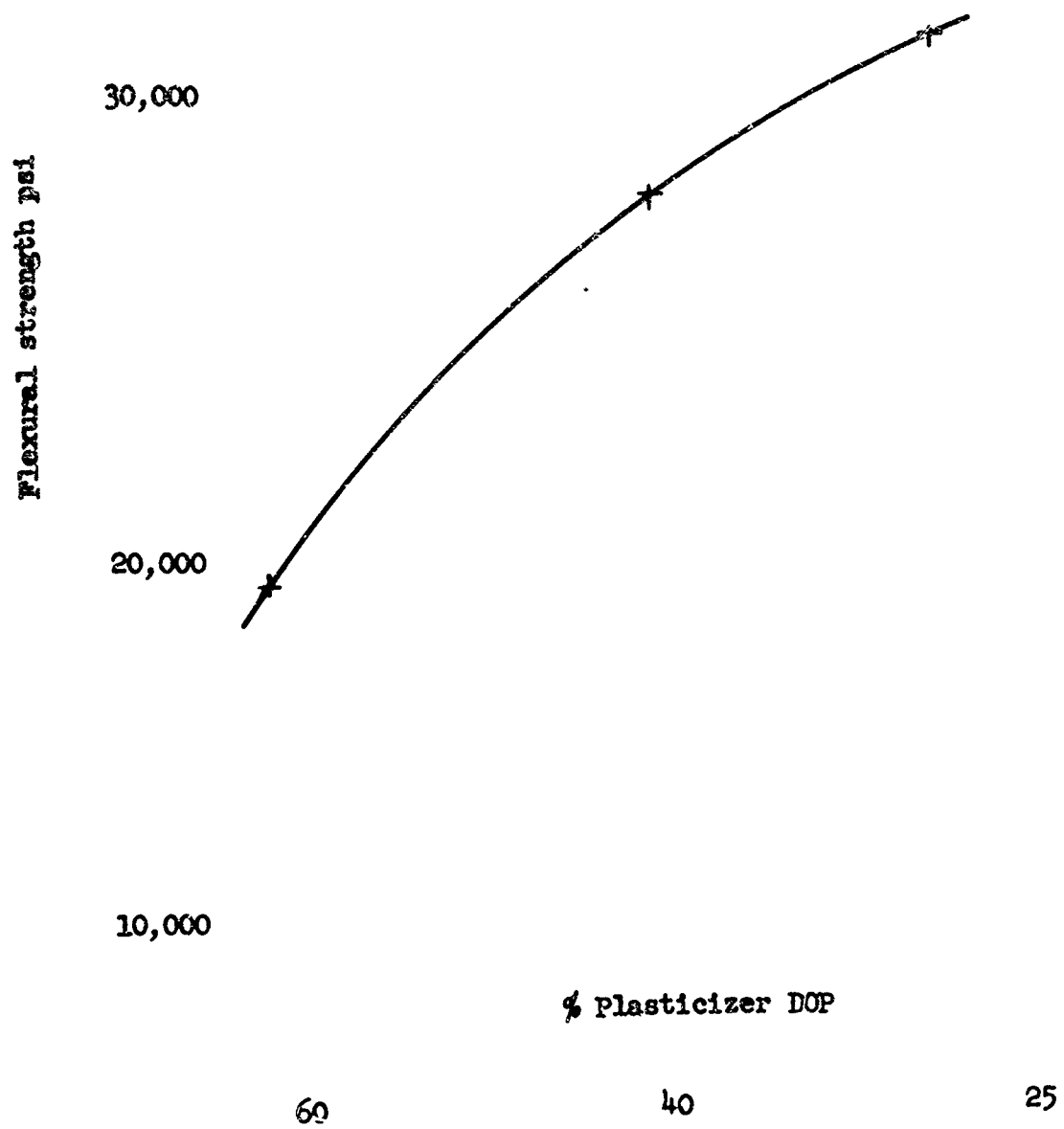


Figure 9 Effect of Varying Weight % Plasticizer Additive on Resin Laminate Flexural Strengths of Urethanes

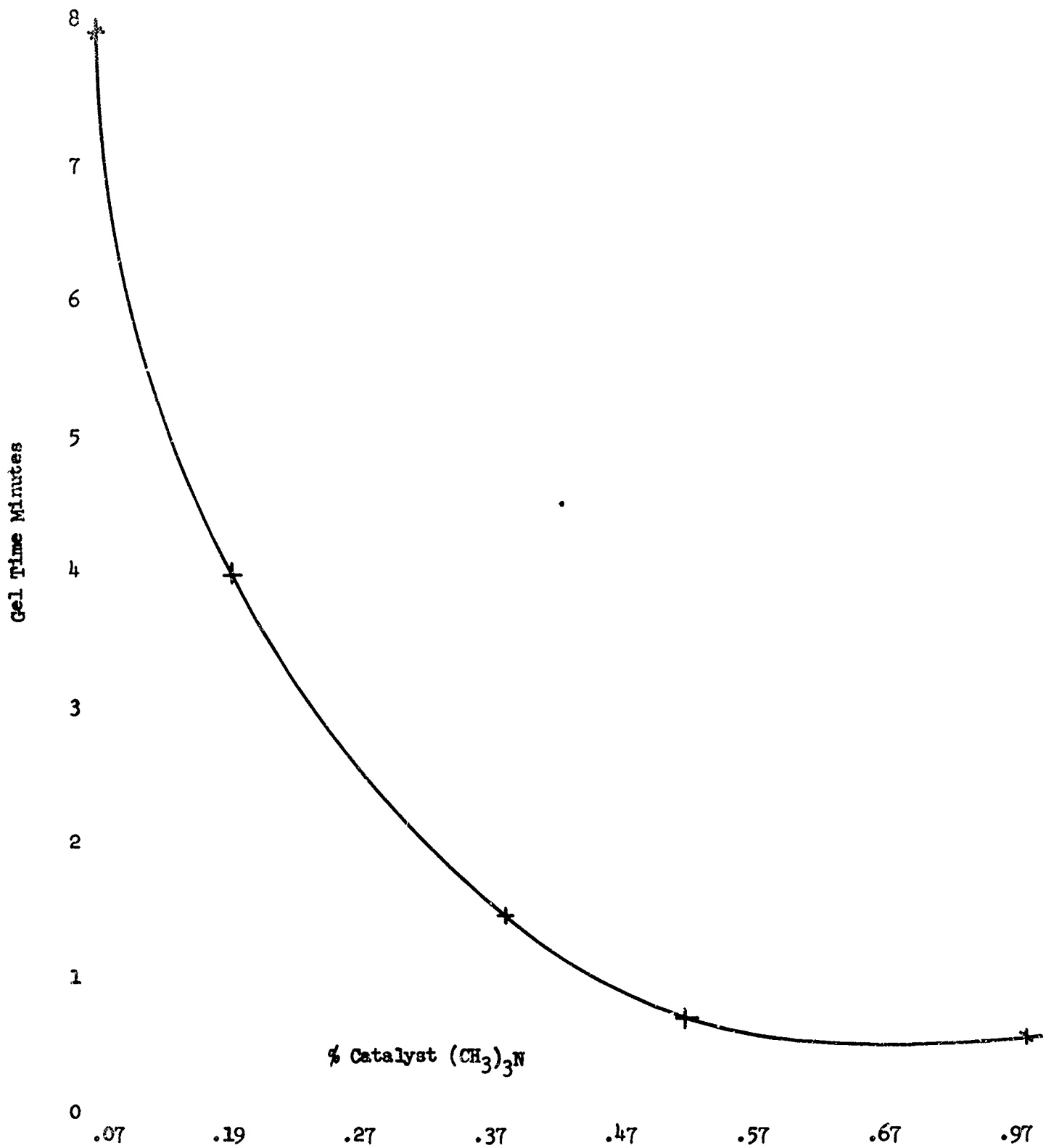


Figure 10 Effect of Catalysis on Gelation Time Evaluation of Urethane Prepolymer

ACKNOWLEDGMENT

The authors wish to express their appreciation to Messrs. Harvey J Richards, Richard E Fries, and Richard P Haugland for their very able technical assistance throughout the course of this work.

THE APPLICATION OF EXPANDABLE HONEYCOMB
TO THE FABRICATION OF SPACE STRUCTURES

Ivan W. Russell

GCA Viron Division

GCA Corporation

Charles Koons

Experimental Fabrication Division

Wright-Patterson Air Force Base

I. INTRODUCTION

The exploration of space will undoubtedly require a wide variety of large structures. Several approaches to producing those large structures become immediately apparent. Small modules or components of the overall structure could be transported into the desired position and assembled into the overall structure. Another approach is to develop an expandable structure which has a small packaging volume and can be transported into the desired position in its fully assembled configuration. Of equal importance to the small packaging volume is the strength-to-weight ratio of the finished structure. Excess weight transported into the space environment means larger rockets and highly increased costs of launch.

GCA Viron Division, in conjunction with several subcontractors, have developed a concept which produces a structure with a low packaging volume and provides high strength with a low weight penalty. This paper will discuss the development phases, materials research, fabrication techniques, experimental development, and actual model space structures which have been fabricated based on the expandable honeycomb concept.

II. STRUCTURAL CONCEPT

Several years ago Mr. F. Forbes and Mr. S. Allinikov of the Air Force Research and Technology Division were investigating methods to produce expandable structures. One of the concepts they originated was to utilize a woven fabric honeycomb material which could be fabricated into structures of essentially any configuration. The structure could then be impregnated with a liquid plastic resin system and still be in a packageable form. Upon deployment into the desired environment, the plastic resin system could be rigidized by vapor phase catalysis,

plasticizer boil-off, or some other technique. There would remain a semi-permanent structure with high strength-to-weight ratio and a number of other advantages. This concept produces results which are comparable to the well known, excellent rigid conventional honeycomb properties.

III. EXPANDABLE STRUCTURES GOALS

The goals listed in the following section are in general oriented toward outer space application. However, this concept is equally applicable to a terrestrial environment and the goals listed are usually also desirable for that application. A high strength-to-weight ratio is desirable since every pound which must be carried into a remote environment normally adds to the overall cost of the completed item. Similarly a high expansion ratio is desirable to provide as small a package as possible. This is especially important in the case of rocket transportation of large structures into the space environment. In that case a restriction of overall dimensions of the packaged item is usually present. It is desirable to require no energy, or very low energy, to expand and rigidize the final structure. The amount of energy required usually directly affects the overall weight and the packaged volume of the structure.

Simplicity of design is a very important factor in structural engineering. This is especially true with expandable structures which are intended for deployment and rigidization in a remote area. The design engineer wants very few required steps between the packaged condition and the final usable condition to feel assured that a high ratio of success can be guaranteed. He also desires to conduct as many proving tests as is possible before the expandable structure is packaged. It is even desirable to have a system where the actual item intended for space use can be inflated, rigidized, inspected, reflexibilized, and packaged for transportation into the space environment.

Any concept chosen for development must be one which can be shown to be applicable for space use through laboratory experimental efforts. The shelf life of a system in its packaged configuration is very important. The structure may be prepared for transportation into the remote area quite some time in advance of the actual use. Similarly, it may be desirable to prefabricate a number of structures for use at a later time. It is known that meteoroids are present in the space environment and the concept should be resistant to that hazard.

The fabrication of accurate structures requires that the structural material have dimensional stability in its final rigidized form. Plastic resin systems are known to shrink during cure but it is desirable to keep that amount of shrinkage to a minimum.

IV. MATERIALS RESEARCH

A. General

Structures fabricated from expandable honeycomb have two major material components. The fabric honeycomb substrate material acts as a carrying agent for the second component, the rigidizing plastic resin. Each component has a discreet function to perform. The fabric, in addition to acting as a substrate material, is the medium for fabricating the structure into the desired shape. The fabric also greatly enhances the physical properties of the rigidizing resin system. The resin system itself serves to tie the individual fibers in the base fabric together and cause them all to act as one unit. It accomplishes this task by encapsulating the individual fibers and acting as a shear surface between each of the individual fibers such that if elongation occurs in one fiber the load is transferred to adjacent fibers.

B. Structural Material

The original intent was to use an actual honeycomb fabric, with hexagonal or square cells, for the fabrication of expandable structures. This configuration would provide a material with no large spans of unsupported fabric in the face material. It should, therefore, be possible to approach the ultimate tensile or compressive strength in the fabric faces before buckling would occur. Also, there would be bi-axial strength since there would be no longer span in one direction than in the other direction. Early investigations showed that there is no actual fabric honeycomb material available as an integrally woven fabric, however, there are several sandwich type fabric materials available.

One such fabric, produced by Raymond Development Industries, incorporates a web type configuration integrally woven between two faces of material. Those webs can only be woven in one direction of the fabric. The finished sandwich, therefore, has considerably more strength in one direction than it has in the other direction. Materials of this nature which have been investigated were not designed especially for inflatable, expandable structures. The loose weave which was used did not provide a material with low enough porosity to make them completely satisfactory for this application. Figure 1 shows an example of this web type material.

Another type of sandwich type fabric material is an outgrowth of the velvet industry. This material, obtained from A. Wimpfheimer and Bro., Inc., Stonington, Connecticut, might be referred to as a drop thread material since it consists of "dropped threads" which are integrally woven into two separate fabrics being simultaneously woven a fixed distance apart. Two pieces of velvet fabric can be produced from this material by cutting the drop threads between the two faces of material. Without cutting those drop threads, a sandwich material is produced which presents a high moment of inertia simply because the faces are far from the neutral axis. The column action of each of the drop threads tends to hold the faces in a fixed position. Variations to this drop thread material can be made by dropping the threads in rows in one direction. Figure 2 shows an example of that fabric. This again provides a unidirectional material. It is also possible to place drop threads in perpendicular rows such that a "quasi-honeycomb" material could be produced. If the drop threads are dense enough, it is conceivable that a tying together action of a plastic resin system might provide a rigid shear resistant wall. These drop threads could also be uniformly scattered at nearly any desired density throughout the material. In that manner, the distance between each of these columns could be varied as desired.

We have produced, in limited quantities, a tailor-made fabric which in cross section looks as is shown in Figure 3. That material can be sewn or bonded from flat woven sheets of fabric. The core is also produced from just a flat piece of material which can be sewn between the two faces as shown. The very great flexibility of design which is available here allows a material to be made up especially for each particular application. One very important point in using sandwich type fabric material in an inflatable expandable structure is that it is necessary to have porosity control in the material so the structure can be inflated into the desired shape. This material lends itself very well to that porosity control in that the faces can be made up from very tight woven fabric or could even have plastic material incorporated directly into the faces. The material can also be tailor-made to meet the strength requirements. In the sketch T_1 , T_2 , and T_3 can all be different or they could even vary throughout a running length of the fabric material. Variable web spacing is possible. One dimensional

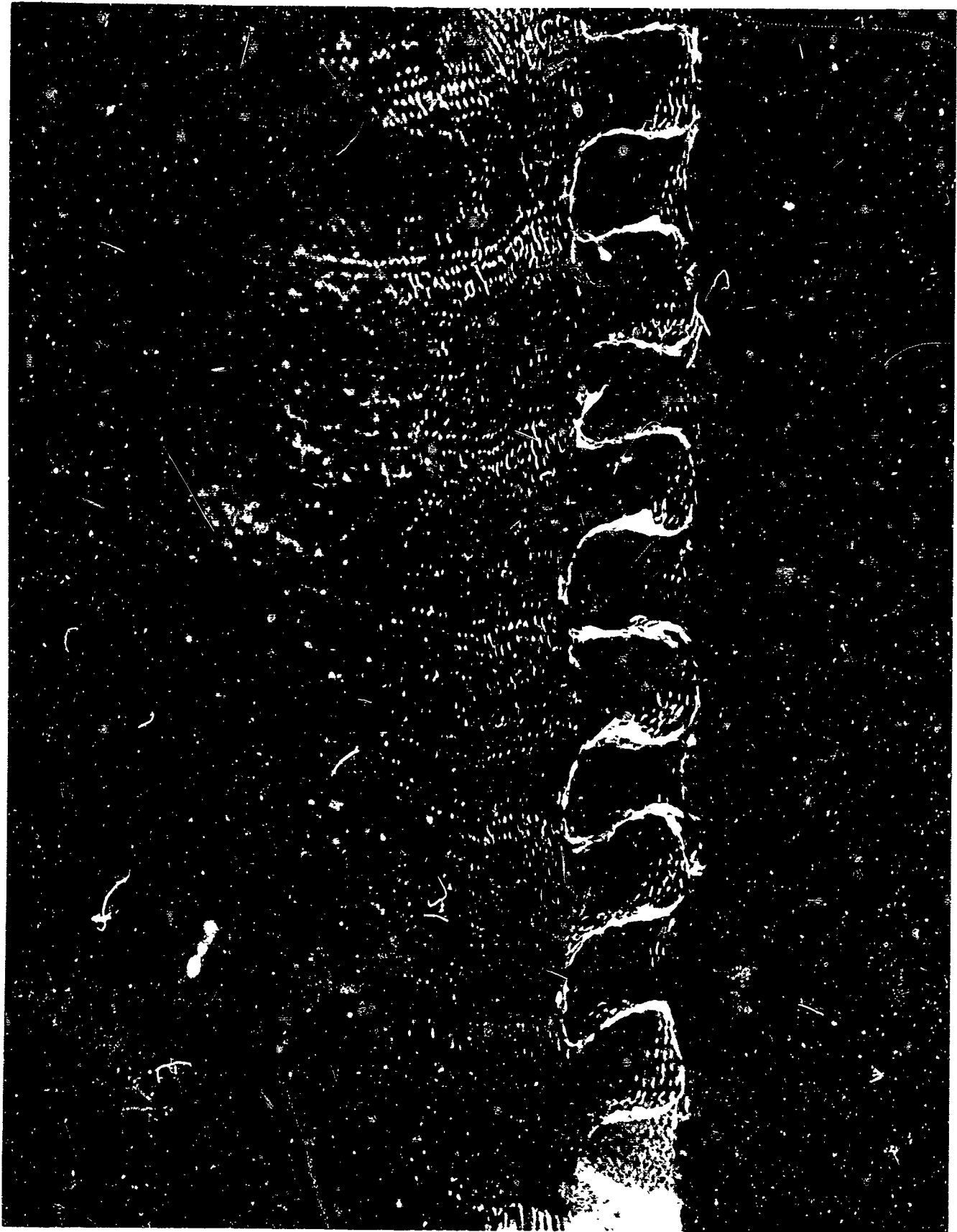


FIGURE 1 - RAYPAN FLUTED FIBERGLASS MATERIAL

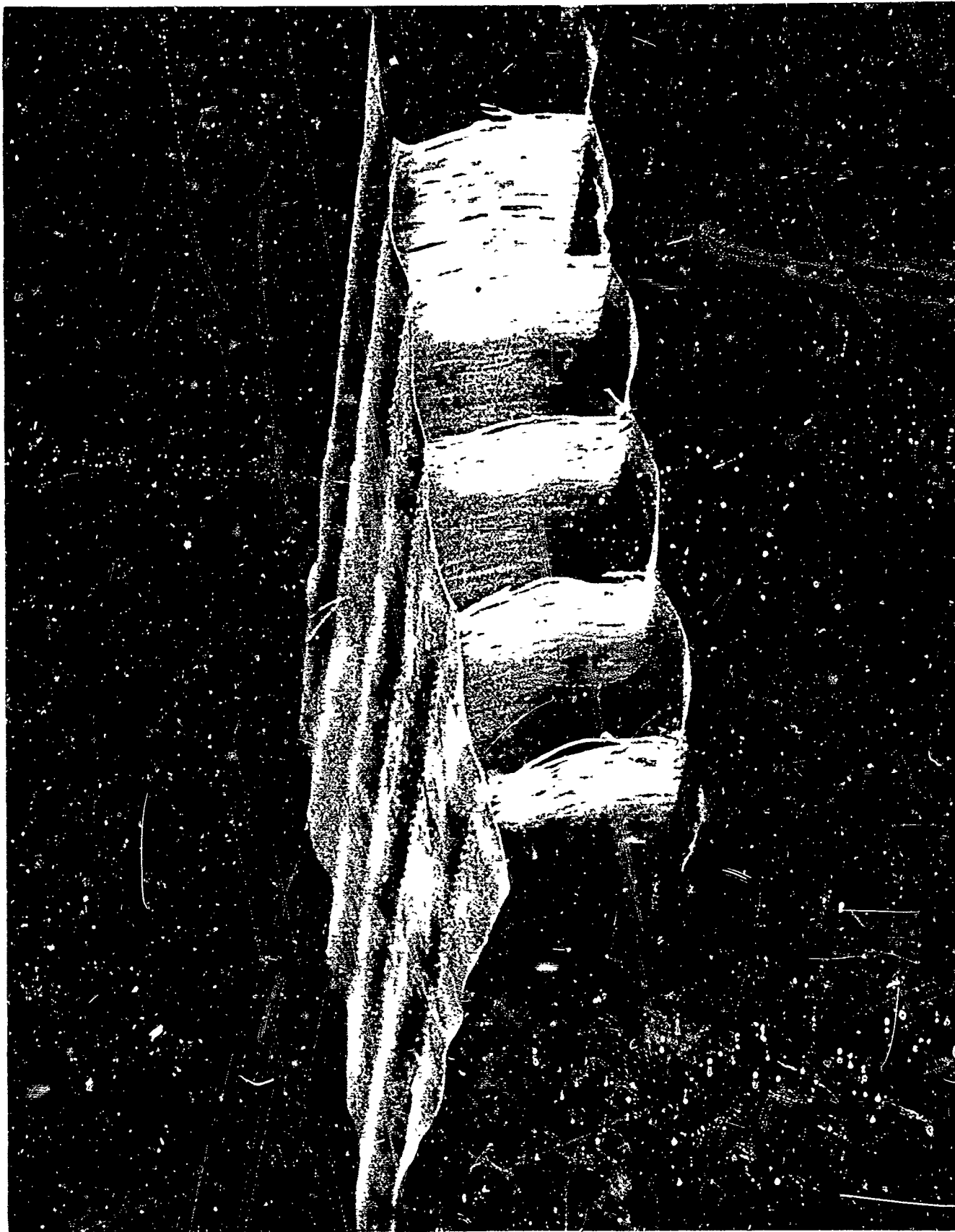


FIGURE 2 - DROP THREAD NYLON MATERIAL

curvature can also be incorporated by making W_1 different from W_2 or W_1 and W_2 could even vary along the fabric. The core configuration could also be one of vertical webs.

Another important aspect in selecting the proper fabric for the fabrication of expandable structures is to make a proper selection of the basic material which goes into the fabric. Probably one of the most important considerations is to obtain as high as possible of a strength-to-weight ratio. Of the materials which can be woven into a fabric, it is known that fiberglass has the highest strength-to-weight ratio. This is closely followed by such materials as Fortisan and some of the other synthetic fibers. Also of high importance is the fact that whatever material is chosen must be able to withstand the environment in which it will be used. Again fiberglass and some of the synthetics withstand the terrestrial or space environment, especially if they are coated with a plastic resin system.

To produce an expandable structure from these fabric materials the problems which will be associated with the actual fabrication must be considered. As a general rule it is easier to fabricate to an exact shape using the lighter weight materials. Resin compatibility for nearly any of the fabrics can be accomplished through proper surface treatments. These surface treatments are mainly used to make a better bond between the surface of the individual fibers and the resin itself. Availability of the material must be considered in the selection of the materials. Some newly developed synthetic fibers or some of the more unique glass fibers are not always available even though they may be desirable for a particular application. Cost of the basic material is also an important factor. Some of the very complicated procedures which must be followed in producing fibers make them very expensive.

C. Plastic Resin System

The plastic resin system which is used in combination with these sandwich type structural materials serves, as one main function, to rigidize the fabric material. As the plastic resin system which encapsulates the individual fibers in the fabric rigidizes, it imparts rigidization to the composite. The resin system acts to tie each of the individual fibers in the overall fabric together such that they will act as one unit. If one of the individual fibers elongates under tension the resin system transfers part of the load to the adjoining fibers. By this mechanism, a uniform distribution of load throughout the load bearing area can be accomplished. The resin system can also be designed to act as a porosity reducer in the fabric material by filling the open spaces between the individual strands in the weave. In order to achieve a satisfactory distribution of load throughout the structural material, it is necessary to have complete and uniform impregnation of the fabric material. This can best be accomplished if the resin system is in a liquid form with a workable viscosity. In addition, it is desirable that the resin system should be easily handled, non-toxic, not affected by laboratory environments, and should require no special storage conditions.

Resin systems which are available to rigidize fabric structures can mainly be classed in three groups. A vapor cured resin system consists of a completely uncatalyzed, long chain molecular system which can be cross-linked with a catalyst provided in a vapor phase. The cross-linking frequency or netting index determines the degree of rigidity. This is a non-propagating system, i.e., every molecule which is to be cross-linked such that it contributes to the three dimensional rigidity must be contacted

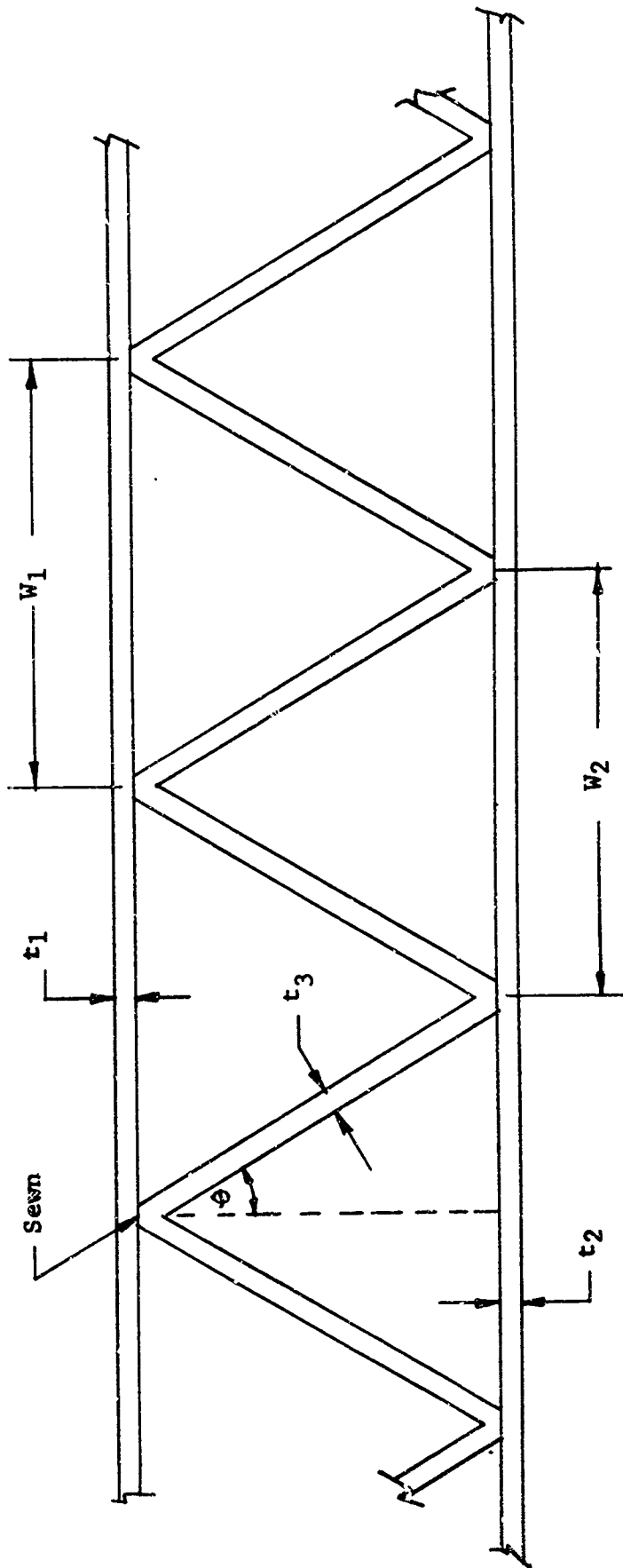


FIGURE 3. TAILOR-MADE SANDWICH MATERIAL

by the vapor catalyst. That catalyst might be supplied from a compressed gas supply or a liquid at pressures below its vapor pressure. Those vapors then can be manifolded such that they are forced through the resin impregnated structural material. The same catalyst vapors can be used as the inflation gas. This type of curing mechanism lends itself very well to an "on command" cure. Examples of this type of resin system are polyurethanes which can be cross-linked with water vapors, polyesters which can be cross-linked with amine vapors, and epoxies which can also be cross-linked with amine vapors.

The plasticizer boil-off system depends only on the evaporation of solvents which have made large molecular structures into a liquid form. This type of system gets its strength from cohesive action or molecular attraction. The resin system, with properly chosen solvents, could have an infinite shelf life. This system itself is extremely simple in that if a resin impregnated structure is placed in a vacuum environment, and the plasticizer has been chosen such that its vapor pressure is sufficiently high, it will automatically cure. The process of cure appears to be a combination of the evaporation of solvents and the migration of those solvents through multiple molecular layers of encapsulating resin. Examples of this type of resin system are gelatin and acrylic. The gelatin system lends itself very well to B-staging into a rubbery and non-tacky packageable item.

An intimately mixed resin system consists of a long chain molecule with the catalyst mixed directly into the liquid resin system. This type resin system has a limited shelf life which possibly could be overcome by storing at low temperature where organic reactions would not take place. Very high strength could be obtained with this type of resin system since the catalyst is previously mixed directly into the resin system and every molecule could theoretically be cross-linked. It appears that this type of resin system could present many very serious problems before it could be shown to be usable for an actual space application. There are also other resin systems such as ultra-violet or high energy radiation cross-linked or heat activated resin systems. These resin systems could provide very good strengths, but they could also provide very serious problems unless adequate shielding from radiation or heat was provided.

D. Resin Substrate Combination

The real item of interest in the fabrication of expandable structures using this concept is how the combination of the substrate and the resin system will perform. The characteristics of the combination can be predicted if the characteristics of the substrate and the characteristics of the resin are known. Such things as the tensile strength of the fiber, the compressive strength of the resin, and the modulus of elasticity of each, which are easy to determine on the materials alone, can be used to estimate the resultant strengths. In general it can be said that tensile loads in a fiber-resin combination are taken by the fibers and that the compressive loads are taken by the resin. These ideas can be taken into account in the design of a sandwich to most efficiently provide either the amount of tensile material or the amount of resin for compression that is required in different parts of the specimen. If the design criteria of a particular structure is one of tension only, such as in a pressure containing vessel, the sandwich type material is not as efficient as filament winding for instance. However, as soon as the design criteria is one of bending, it has been determined that sandwich type material weighs only approximately 1/5 as much as a filament wound structure.

An example of the properties obtainable with various materials are as shown below in psi:

<u>Material</u>	<u>Tensile Strength</u>	<u>Flex Strength</u>	<u>Modulus of Elasticity</u>
181 Fiberglass Cloth	40,000		$6 \times 10^6^*$
Urethane Film	10,000		3×10^6
Gelatin Film	13,000		1×10^6
Urethane - Glass	60,000	30,000	$8 \times 10^6^*$
Gelatin - Glass	60,000	40,000	$10 \times 10^6^*$

* Based on area of glass fibers only.

V. EXPERIMENTAL DEVELOPMENT

A. General

This expandable honeycomb concept has been experimentally developed for a number of different configurations. They can generally be classed as shelters or solar collectors. These two items present completely different problems in fabrication and design. The solar collectors are a problem in creating a light weight structure with a high degree of accuracy and the shelters study is more of a problem in obtaining a high strength-to-weight ratio structure in a compact package. These two completely different problems demonstrate the flexibility of design that is available with this concept.

B. Solar Collectors

1. Concept

The solar collector concept, as it has been developed to date, utilizes a sandwich type fabric structural material in combination with a rigidizable plastic resin system to maintain a plastic reflective surface in the shape desired. The structural material is bonded to the reflective plastic surface. That bonding layer also helps to eliminate fabric show-through and orange peel effects. After the composite is formed into the paraboloidal shape it could then be attached to a pressure containing spherical balloon which would be inflated to "shape" the collector. The whole system would be packaged in a canister for transportation into space. After being placed into the desired position, the canister would be opened and the assembly deployed. Inflation into the proper shape would be effected by releasing predetermined quantities of subliming materials in the balloon.

If the rigidizing resin used were a plasticizer boil-off type, that would be the final step in the deployment and rigidization of the structure. If a vapor cured resin system were chosen, the catalyst container and a manifolding system to direct the vapor to the resin impregnated structural material would be required. After deployment and rigidization of the solar energy concentrator, the pressure container would be removed by means of a hot wire or pyrofuze technique. The subliming materials contained on the plastic material would provide thrusting action to push the thin material away from the solar energy concentrator.

The total assembly consists of the solar collector composite itself, a plastic pressure retaining balloon, the inflation gases required, and a canister. Based on present state-of-the-art, the total assembly weight is estimated to be approximately 1/2 lb per sq ft of projected area in addition to the weight of the required canister.

2. Small Models

Early experimental efforts were devoted to assembly of the complete composite as eight inch model collectors. This series of models was used to develop assembly techniques, investigate resin impregnation approaches, screening for applicable materials, and learning the most appropriate cure approaches. Variables such as different plastic reflective surfaces, different flexible adhesive layers, different sandwich type structural materials, different rigidizing resins, and different cure conditions were investigated in this series.

3. Two and One-Half Foot Diameter Models

This experimental size was the main tool in further developing fabrication, assembly, impregnation, and curing techniques which were used. Again, various plastic reflective surfaces, adhesive layers, structural materials, and rigidizing resins were experimentally tested. It appears that either the vapor cured urethane or the solvent release gelatin system offers the most promise and can be applied to this type structure interchangeably with only minor variations in the construction. Figure 4 shows a rigidized 2½ ft diameter solar collector model.

4. Five Foot Diameter Models

Several five foot diameter solar collector models were assembled, using the concept outlined above, and were vacuum cured using a polyurethane vapor cured resin system. The structures were sufficiently flexible for packaging, cured in about two hours, and had sufficient rigidity to retain their shape. Figure 5 shows a cured five foot diameter solar collector model.

5. Ten Foot Diameter Solar Collector Models

A ten foot diameter solar collector was assembled from one mil, aluminized Mylar, a flexible epoxy adhesive layer, and approximately one inch deep nylon drop thread material. The structural material was impregnated with a polyurethane resin system and cured in a stratospheric vacuum chamber at WPAFB. The internal pressure which retained the paraboloidal shape was not maintained throughout the seven hour cure cycle and major distortions resulted in the reflective surface. The structural material had sufficient rigidity to retain the overall shape after cure. Figure 6 shows the reflective surface of that 10 ft diameter collector.

C. Shelters

1. Concept

Heavier, more rigid structures which have been studied have included various cylinders, space type man shelters, and terrestrial quonset type structures. In general, the procedure is to arrive at a best design and fabricate the structure into the desired shape using dry sandwich type structural material. After complete assembly the structure can be impregnated with the liquid resin system and still be completely flexible for packaging. This structure is then ready for deployment, inflation, and cure of the plastic resin system.

An inflatable structure always tends toward a spherical shape, therefore, it appears that flat surfaces should be avoided if possible. Restraining lines could be used to force the inflated structure into semi-flat shapes. The actual inflation of these structures into their desired shapes can be accomplished in several ways. In a vacuum environment, the catalyst vapor pressure or the pressure which is developed by the plasticizer is usually sufficient to inflate the structures into the desired shape. The porosity of the structural material must be kept sufficiently low so that a pressure differential can be maintained across the face of the structural material. An impermeable bladder could be used to force inflation of the overall structure. The high strength advantages that are inherent in a sandwich type material can only be obtained if the sandwich itself is fully expanded. This sandwich expansion can be incorporated directly into the design and fabrication. For instance, a cylinder with a known radius of curvature can be fabricated with the outer face of the sandwich material longer than the inner face by the differences in the circumferences.

2. Small Models

Early experimental development of fabrication, impregnation, deployment, cure, and testing techniques which were applicable to the production of shelter type structures were conducted on small sandwich material cubes. The cube was very simple to fabricate and provided a quick and cheap experimental program. Various sandwich materials, resin systems, and cure conditions were investigated. A number of eight inch shelter models were also fabricated and rigidized using different materials and resin systems. These models provided a basis for investigation with larger sizes. Figure 7 shows a vacuum cured eight inch model shelter which was cured with a vapor cured polyurethane.

3. Cylinders and Shelters

A number of cylinders and shelters approximately $3\frac{1}{2}$ ft in diameter and 4 ft long were the next experimental development step. Different sandwich type materials and resin systems were used during the phase. This series covered a pressure range from atmospheric down to approximately 10^{-6} mm Hg and used both a vapor cured urethane and a gelatin resin system. Figure 8 shows a 3 ft diameter cylinder which was vacuum cured with a gelatin resin system in approximately 6 hours. The flat section was not intentional, it resulted from the weight of the structure during cure. Figure 9 shows a 7 ft diameter by 8 ft high

space shelter that was cured in a vacuum environment with a vapor cured urethane resin system. That cure required approximately seven hours. Inflation was with residual gases and catalyst vapors.

4. Aerospace Maintenance Dock

A 13 by 15 ft quonset type structure (semi-cylinder) was fabricated from expandable honeycomb material. The especially designed sandwich material included in that structure was fiberglass. That structure was completely assembled as dry fabric sandwich material, impregnated with a polyurethane resin, inflated with an axial flow blower, and cured with the water vapor present in the atmospheric air. The 400 lb structure was designed to withstand 100 mph winds and a 30 lb per sq ft snow load with a safety factor of $1\frac{1}{2}$. A 2 inch deep sandwich was chosen for the roof section with flutes running in the circumferential direction. The structure initially packaged in approximately 3 cubic feet for an expansion ratio of about 330 to 1. Figure 11 shows the deployed and rigidized structure.

5. Cylindrical Space Structure

A current study is developing a 10 by 25 ft cylinder from expandable honeycomb. It will incorporate an internal bladder for pressure retention, an integrally connected floor, it will be packaged between canister-half bulkheads, it will be remotely deployed in a 10^{-6} mm Hg environment, and will contain a buffering layer to protect the internal bladder both from meteoroids and from internal damage.

The fiberglass-plastic bulkheads were prepared by the WPAFB Experimental Fabrication Division by multiple layup of fiberglass and epoxy resin over a mold. They were then sanded and machined to provide the smooth surfaces necessary to form the "10 ft diameter vacuum chamber".

Several 1/6 size models have been fabricated and rigidized. Complete impregnation of the structural material and rigidization within $1\frac{1}{2}$ hours have been accomplished. This program is utilizing a vapor cured urethane system.

Figure 12 shows an artists concept of the packaged, deployed, and rigidized configuration, Figure 13 shows a 1/6 size model packaged within the canister-half bulkheads, Figure 14 shows the deployed 1/6 size model during cure, and Figure 15 shows the structural material with the bulkheads removed.

VI. CONCLUSIONS

- A. The expandable honeycomb concept has been shown to be a feasible and desirable approach to providing expandable structures for space and remote area use. Large load carrying structures and solar collectors which require a great degree of accuracy are all within the fabrication and rigidization realm of possibility.
- B. A number of plastic resin systems have been developed which are satisfactory for space application. The most promising appear to be a vapor cured urethane system and a gelatin plasticizer boil-off system.



FIGURE 4 - VACUUM CURED 2 FT SOLAR COLLECTOR MODEL



FIGURE 5 - VACUUM CURED 5 FT DIAMETER SOLAR COLLECTOR MODEL
64

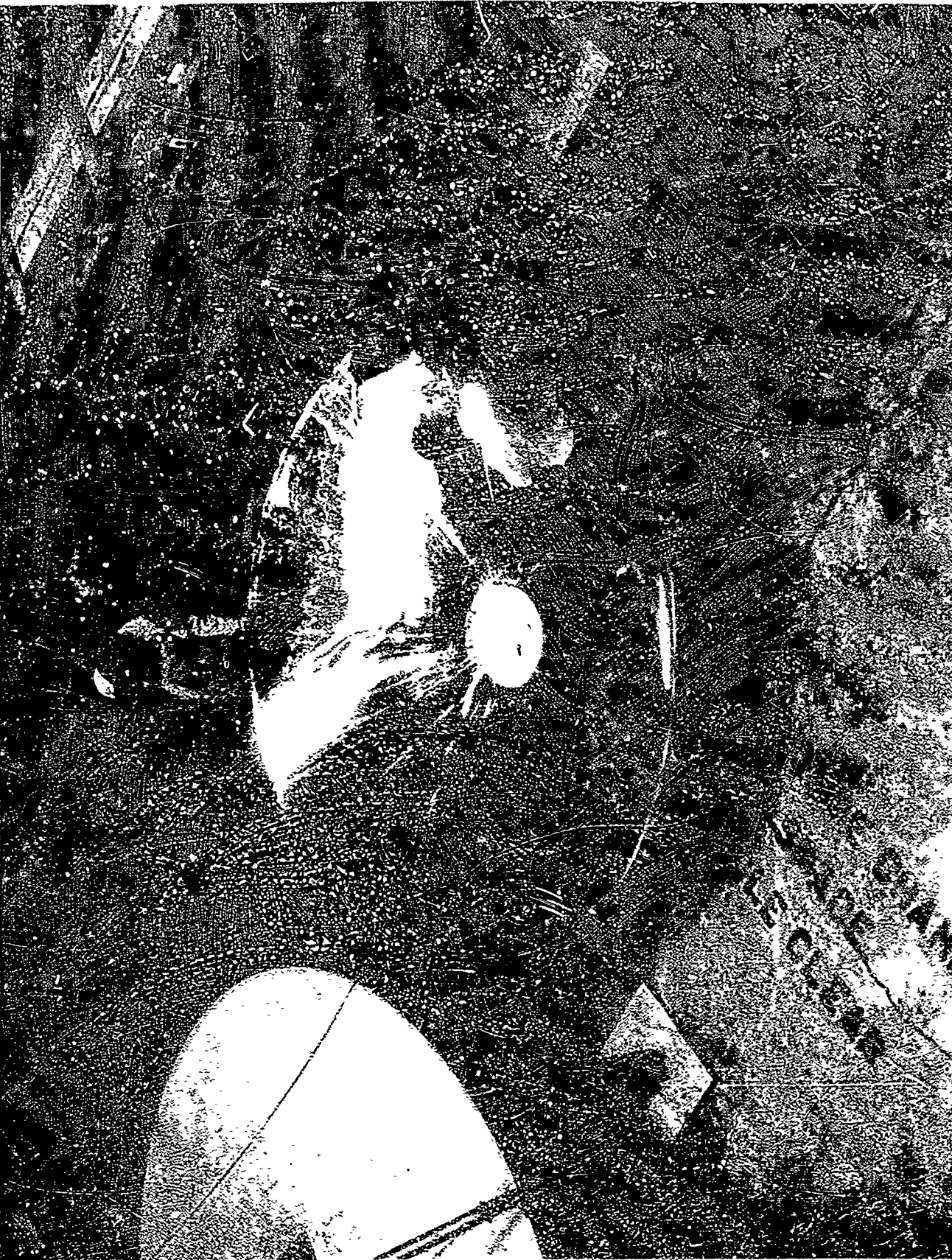


FIGURE 6 - VACUUM CURED 10 FT DIAMETER SOLAR COLLECTOR MODEL

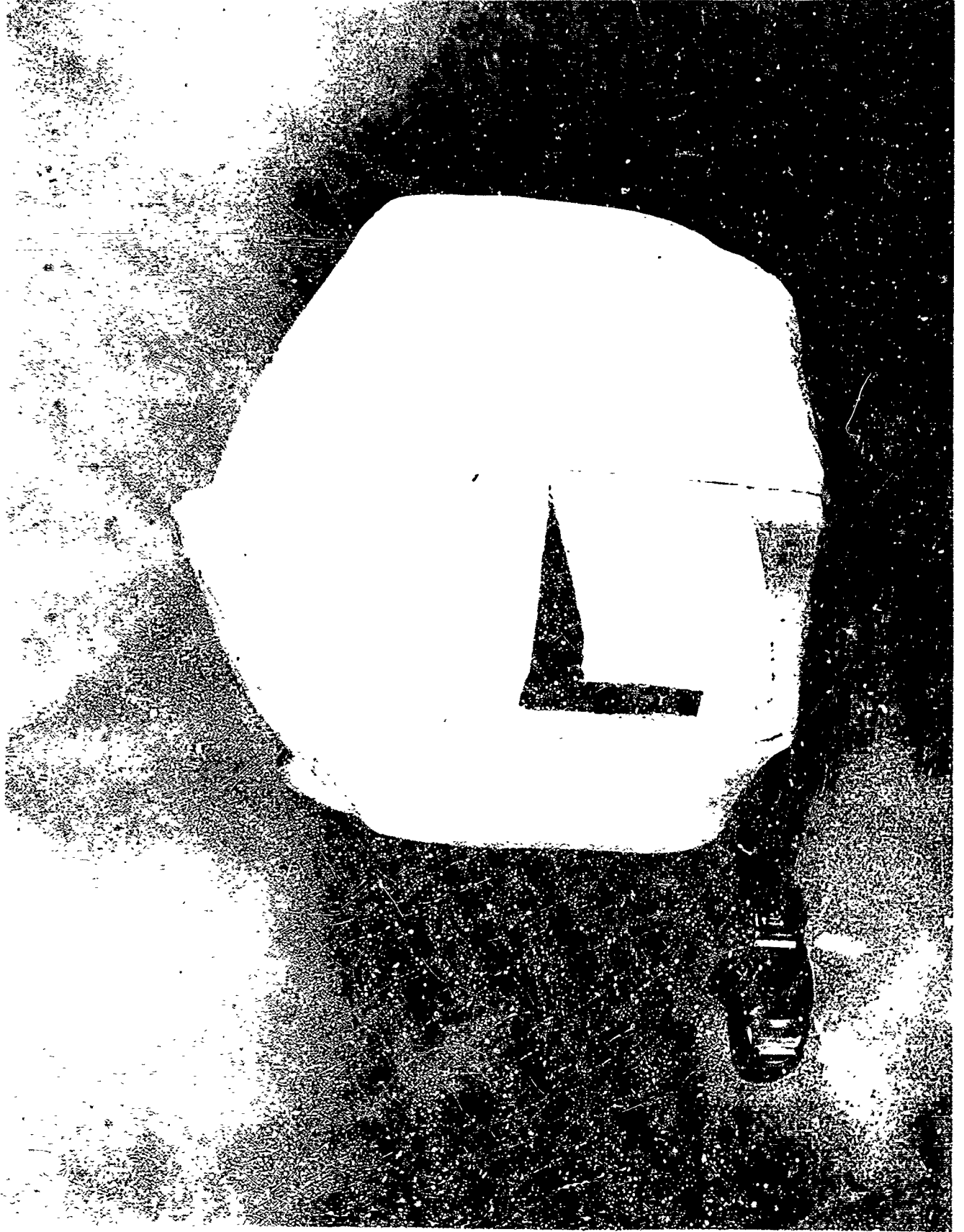


FIGURE 7 - NYLON SHELTER MODEL, 1/10 SCALE VAPOR CURED EPOXY



FIGURE 8 - GELATIN CURED 3 FT DIAMETER CYLINDER



FIGURE 9 - URETHANE CURED 7 FT DIAMETER SPACE SHELTER



FIGURE 11 - DEPLOYED AND RIGIDIZED 13 x 15 FT AEROSPACE MAINTENANCE DOCK

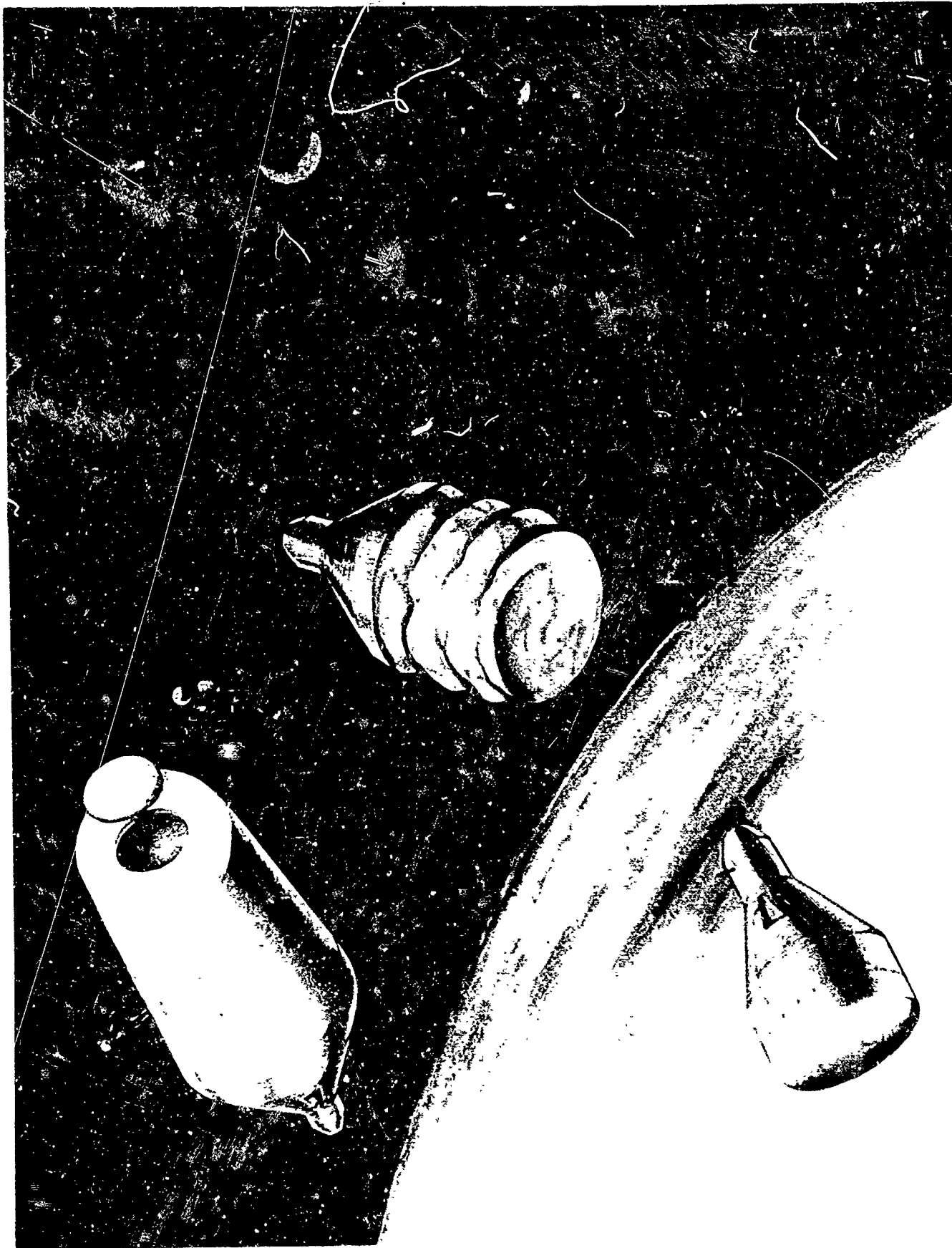


FIGURE 12 - ARTISTS CONCEPT OF AN EXPANDABLE CYLINDRICAL SPACE STRUCTURE

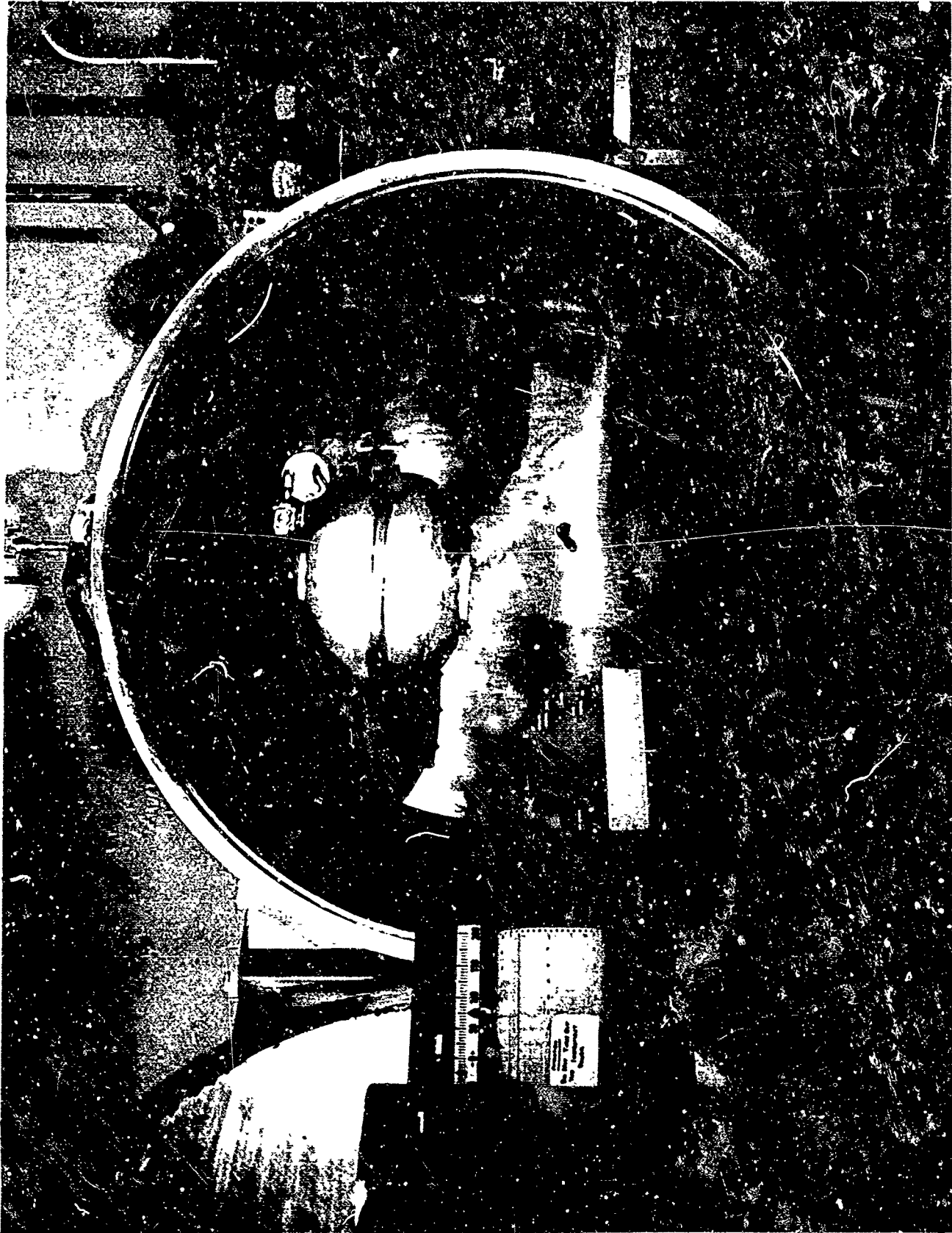


FIGURE 13 - MODEL SIZE CYLINDRICAL SPACE STRUCTURE WITHIN THE CANISTER

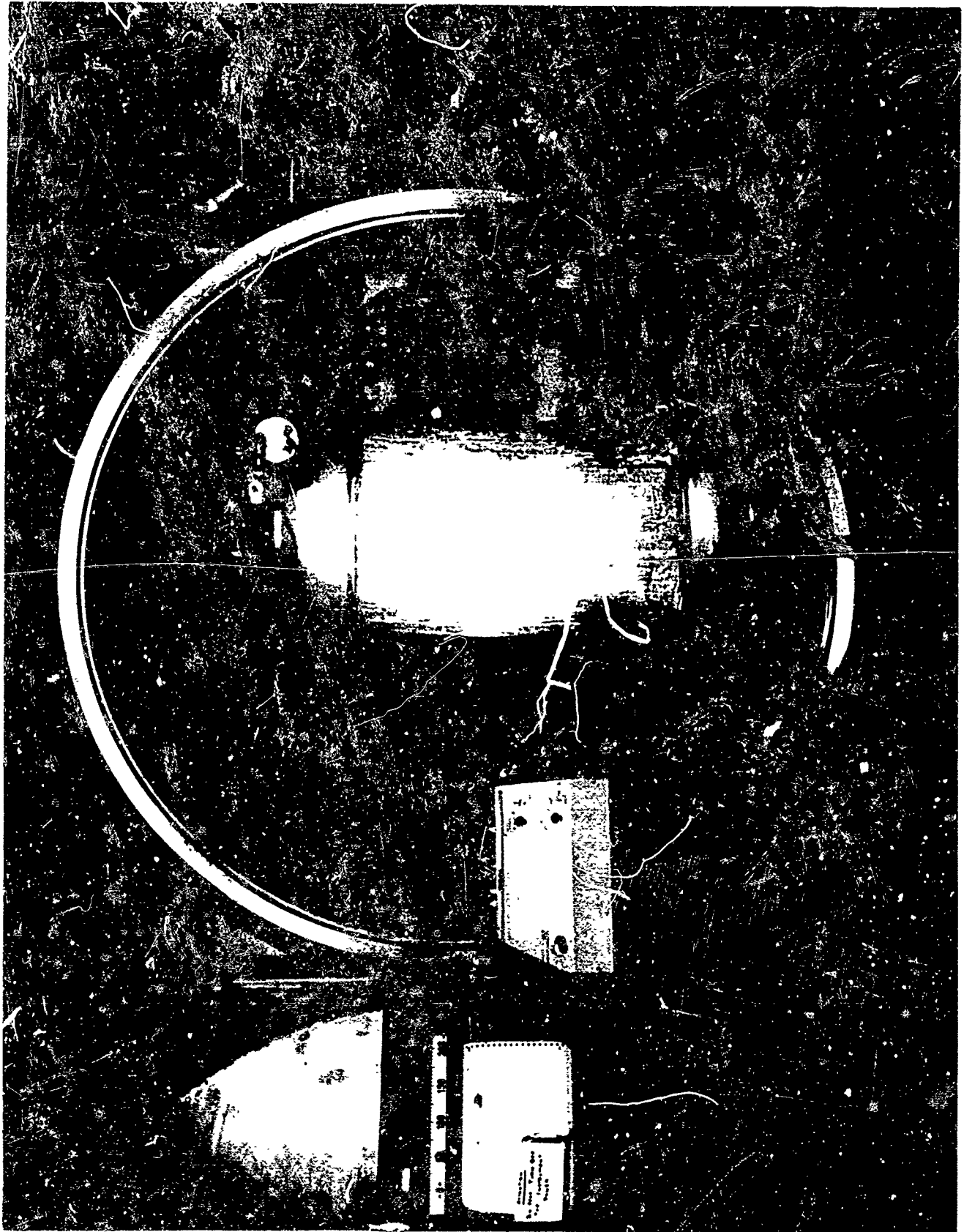


FIGURE 14 - DEPLOYED 1/6 SIZE CYLINDRICAL SPACE STRUCTURE



FIGURE 15 - CYLINDER WALLS IN 1/6 SIZE CYLINDRICAL SPACE STRUCTURE

SESSION II

LIGHTWEIGHT, EXPANDABLE SUPPORT SHELTER SYSTEMS

James M. Alexander

College of Design, Architecture, and Art
University of Cincinnati
Cincinnati, Ohio

BACKGROUND

The period of the "cold war," characterized as it has been by limited warfare situations and counter-insurgency actions, has given rise to new thinking on the part of the armed services in the area of supporting actions in hot spots of activity by means of utilizing unconventional warfare tactics.

New and radical techniques and methods of supporting limited war are needed. This is especially true as this activity frequently occurs in remote areas of the earth that are usually inaccessible by normal transportation methods. Climatic situations encountered may vary from desert conditions to those found in tropical jungle or wet delta.

The supporting of troop operations in these extremes of climate becomes a very important consideration. The problems of support are in the areas of functional support shelters, resupply techniques, and overall logistics.

INTRODUCTION

Under the sponsorship of the Support Techniques Branch, Aero Propulsion Laboratory, Wright-Patterson Air Force Base, a group of researchers at the University of Cincinnati is engaged in a program seeking to establish new and unique design concepts for lightweight expandable shelters to be utilized in limited warfare actions. (Contract # AF 33 (615) 1285)

The members of the group are, from the Department of Industrial Design: Professors James M. Alexander (principal project leader) and Joseph M. Ballay and, from the Department of Architecture: Professors Karl H. Merkel (associate project leader), Bruce E. Goetzman, and Richard H. Stevens. A full-time research assistant, Lawrence Fabbro (Industrial Design 1964), and several upper class co-op students have also participated.

The work under the contract was to develop concepts for two types of structures: (1) small general purpose shelters and (2) large (50' span) shelters capable of housing fighter aircraft.

The work has progressed along the following lines:

1. further definition of problem
2. concept studies on both large and small shelters
3. construction and testing of full-size small shelter # 1 (under amendment to the contract)
4. further studies of small shelter concepts
5. construction and testing of full-size small shelter # 2 (under amendment to the contract)
6. resumption of concept studies for large shelter (stage of work at time of writing of this paper).

This paper will follow the above outline except that all discussion of studies for the large shelter shall be deferred to the end of the paper.

DEFINITION OF PROBLEM

To further determine the detailed needs of the Air Force, trips were made to Eglin Air Force Base, Florida and Langley Field, Virginia. Conferences at Eglin acquainted the group members with capabilities of transport aircraft, extraction techniques, and needs for low-cost - possibly disposable - shelters in limited warfare situations.

At Headquarters, Tactical Air Command, Langley Air Force Base briefing on Base Base operations and use of the Gray Eagle package was held. It was recommended that the small shelter should fill an existing gap between (1) existing tentage and (2) panelized prefabricated structures of conventional materials. Design criteria established that the shelter (1) should be designed for approximately five erection and disassembly cycles, (2) should, with moderate maintenance, have a useful erected life of up to two years, (3) should withstand winds to 60 knots, (4) should support a live load of 5 to 8 pounds per square foot, and (5) should be capable of being insulated.

An inside width of sixteen feet was considered optimal and the structure should be capable of being expanded in length. Lightness of weight, low package volume, short erection time, and simplicity of erection process were major design goals.

The large shelter has as its design objectives: (1) size: approximately 50'x80'x25' high, (2) live load: 20 PSF, (3) wind load: 30 mph, (4) temperature range -25° to +125°F., (5) as low total weight, package cubage, and erection time as possible.

SMALL SHELTER CONCEPTS

INITIAL CONCEPTS

Initially considered concepts included air-inflated or air-supported structures and structures employing fixed in place structural elements. The former were not pursued largely because of duplicate efforts by other services and the latter was not followed because of the still-developing state of the art in this sophisticated concept.

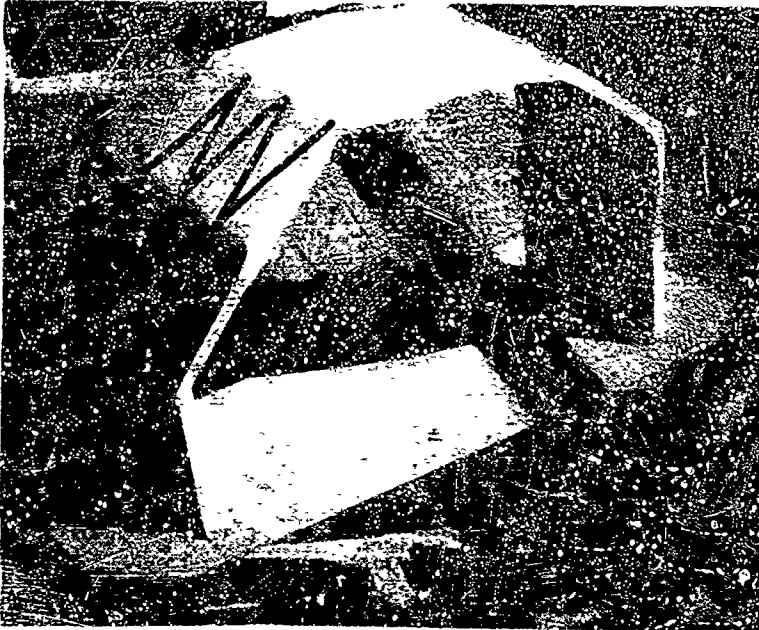


FIGURE 1. Scale Model - "bow-tie" concept.



FIGURE 2. Scale Model - modified "bow-tie" concept.

The general area of modular panelized concepts utilizing inexpensive light-weight sheet material was settled on.

"BOW-TIE" MODULAR CONCEPT

Preliminary studies of various geometric configurations led to a "bow-tie" shaped module (Figure 1) that seemed to offer great rigidity through ribs formed by turning down the edges of the modules. A variation (Figure 2) suggested a reduction of number of modules required but gave less rigidity because of the lack of continuity of the diagonal ribs.

The "bow-tie" concept offered many advantages:

1. Only two basic modules are necessary, full panels and half-panels (exclusive of treatment of ends of shelter).
2. Triangulated structure of the panels and continuity of the arched structure stress lines of the combined panels both indicated adequate rigidity in small scale model studies.
3. Assembly can be made from the ground and from inside the structure.
4. Ribs are formed by turning panel edges inward thus protecting edges of material from exposure to weather.
5. Ribs on the interior provide opportunities for attachment of equipment, utilities, furniture, interior partitions, etc.
6. Unlimited linear expansion.
7. The triangulated system permits limited openings to be developed in

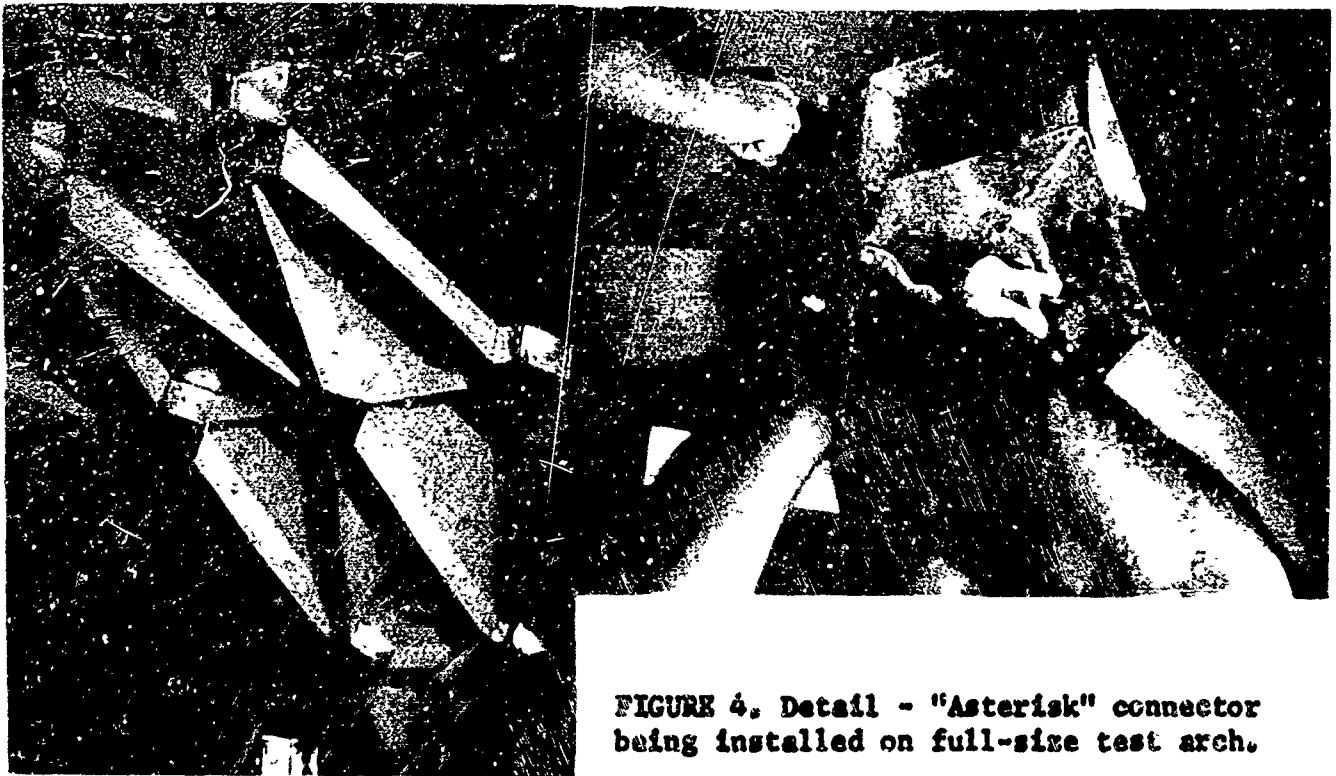


FIGURE 3. Test arches of corrugated fiberboard. "Bow-ties" attached by (left) cherry rivets and (right) sheetmetal "asterisk" connectors.

the side walls for ventilation, windows, doors, etc. Removal of several modules and half-modules could make possible attachment of passageways to adjacent shelters.

8. The units could be easily disassembled and repackaged flat for easy reshipment.

Test arch using cherry rivet connectors

The "bow-tie" approach offered prospect of success sufficient to warrant construction of one or more full-size arches. The first one constructed had an inside width of 16', an inside height of 8', and was 2 modules "long" (4' at base). The material used was Container Corporation of America W5C (B flute) corrugated fiberboard. Though not seriously considered for eventual adoption, cherry rivets with washers were used to secure adjacent modules to each other as shown in the left arch in Figure 3.

While the constructed arch sustained its own weight, serious deficiencies were noted: (1). Progressive tension failure at the "waist" of the "bow-tie" (parallel to the corrugations of the fiberboard, (2). slight compression bowing of folded ribs near base of arch, (3). considerable side sway and opening up of six-way intersections.

The low cost of the material used suggested the possibility of throw-away structures permanently joined with adhesive. As this was not within the scope of our problem, no further study in this direction was made.

It was recognized that use of other materials that did not have the directional qualities of corrugated board should overcome some of the difficulties. Tape reinforcement was experimented with as tensile reinforcement at critical points of stress.

The construction of the first series of arches was undertaken basically to determine the structural feasibility of the concept, the geometric configuration of the components, and possible methods of attachment. The necessary research in the areas of weather-resistant surface treatment and the weather-peeling of joints was deferred until this structural feasibility was established.

Test arch using sheetmetal "asterisks"

In order to further rigidize the structure a star-shaped slip-on fastener was designed and several of these "asterisks" were fabricated for testing. The "asterisk" did succeed in rigidizing the intersections by eliminating the opening-up noted on the first arch and by taking much of the tensile stress off the waistline folds of the bow-tie modules. These connectors featured metal plates that fitted snugly over the flanges at the vertices of the triangular panels, holding the flanges together and being locked to the flanges with bolts. This test arch is shown on the right in Figure 3, and the connector is shown being installed in Figure 4.

Counteracting the advantage of achieving greater rigidity were several apparent shortcomings: (1) The connectors were complicated, heavy, and bulky for storage and (2) they were much stronger than the sheet material being used. Also, the weight of these connectors increased the tendency of the folded ribs of the panels to buckle in compression at the base of the test arch.

Test arch using sheetmetal rib reinforcement

The next experimental arch differed from the previous ones in that a different sheet material was used: Union Carbide Techni-Foam. This material is a sandwich material consisting of two layers of 69# Kraft paper and a filler material of urethane foam. Board thicknesses obtained were $\frac{1}{4}$ inch and $\frac{3}{8}$ inch.

For this arch $\frac{3}{8}$ " thick Techni-Foam was used. The folded ribs of the "bow-tie" modules were reinforced with 28 ga. galvanized iron strips having a "J" section ($2 \times \frac{3}{8} \times 5\frac{1}{2}$ "). The connectors used were Simmons spring-loaded type #W7. The assembled test arch is shown in Figure 5, and the Simmons connector is shown in Figure 6.

The waists of the "bow-tie" panels had a tendency to spread under tensile loading of the arch, indicating a need for a connector to hold the waist together in the finished structure and also to make the panel easier to handle during the folding up of the box prior to erection. A "hair pin" type device was designed and used for this purpose.



FIGURE 5. Test arch - TECHNI-FOAM with sheet-metal reinforcement and SIMMONS connectors.



FIGURE 6. Detail - SIMMONS connector.

Though the Simmons connectors proved a quick means of connecting if alignment was perfect, hand methods of fabrication made it impossible to achieve this degree of perfection in all cases. The structure provided fair resistance to lateral sway and good resistance to longitudinal movement.

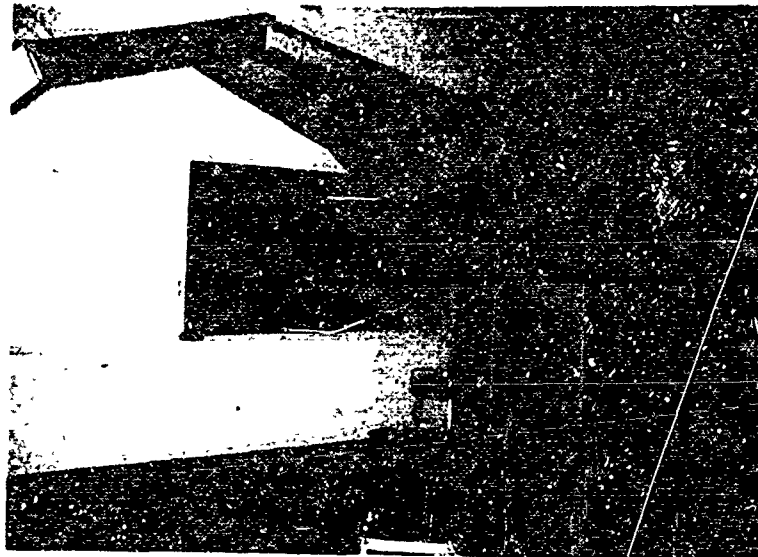
It was decided that the design was too conservative in the amount and weight of metal added. The metal in effect took over the structural function of the folded ribs and added weight to the structure. The weight of this metal was approximately twice the weight of the Techni-foam board required! The need for the 3/8 inch thick board was also questioned.

A further complication arising from the use of the Simmons connector, with the female half of each connector fabricated in place, was the complicated numbering of modules for erection in proper sequence.



FIGURES 7 and 8. Construction of test arch shown in Figure 5.

FIGURE 9.
Test Arches - Fome-Cor
(left), Techni-Foam (right)
with minimal sheetmetal re-
inforcement and thumbscrew/
wingnut connectors.



Final "bow-tie" concept test arches

In line with the conclusions reached on the previous test arch, the following modifications were made on the next arch: (1). 1/4 inch thick Techni-Foam was substituted for the 3/8 inch material, (2). A simple thumbscrew/wingnut connector was substituted for the Simmons connector, (3). Metal reinforcement was changed from galvanized steel to .020 inch aluminum and consisted of a 1"x1/2"x1" channel edge strip, a chevron shaped gusset plate on each flange at the waist of the "bow-tie", and 3" square load-spreading washers at the thumbscrew locations, and (4). a 1/8"x1" steel strap stirrup with washers and thumbscrew was designed to secure the waist of the module in its folded position. These refinements were evolved in a series of test modules and arches, the details of the refinements being worked out in conjunction with a series of static load tests.

While this work was in progress, it was learned that Techni-Foam was being withdrawn from the market and another material had to be substituted. The material chosen was FOME-COR, a Kraft paper and styrene foam sandwich board. This material was available in 1/4 inch thickness with a 42 lb. liner (as compared with the 69 lb. liner on the Techni-Foam). A comparison of the two materials showed the following:

	<u>1/4" Techni-Foam</u>	<u>1/4" Fome-Cor</u>
1. weight per sq. ft.202 lb.	.155 lb.
2. adhesion liner to foam	-	superior
3. surface smoothness	-	superior
4. resistance to chemical action.	superior	-
5. resistance to intense heat	superior	(melted at 180°F)
6. resistance to indenting	superior	-

To secure comparative structural data identical "bow-tie" modules and test arches were constructed and subjected to static load tests. Test arches in Fome-Cor and in Techni-Foam are shown in Figure 9.



FIGURE 10. Concentrated load test - "bow-tie" module.



FIGURE 11. Concentrated load test - inverted "bow-tie" module.



FIGURE 12. Uniform load test on Arch shown in Figure 9.

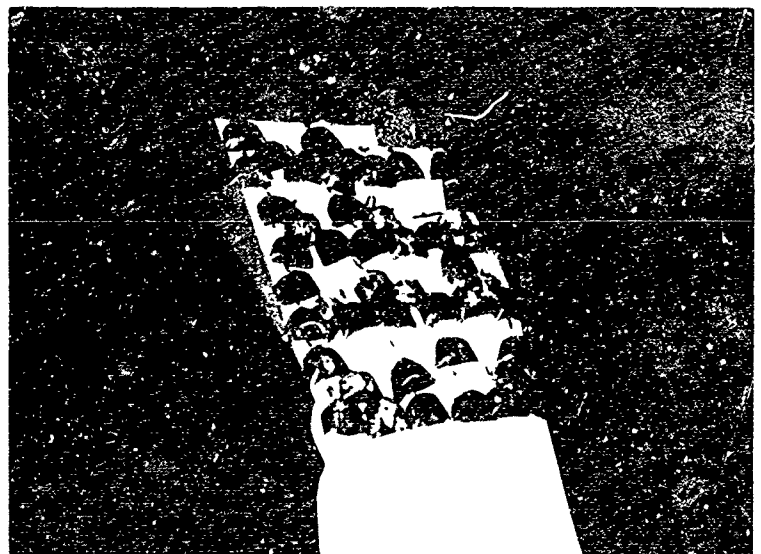


FIGURE 13. Uniform load test - "bow-tie" module

Tests on individual "bow-tie" modules produced the following data. Reinforcement in line with changes outlined on preceding page was found most effective in this series of tests.

Type of test	Figure #	Techni-Foam module	Fome-Cor module
1. Center load, module upright	10	Failure at 44 #	Failure at 60#
2. Center load, module inverted	11	Not tested	No failure 60#*
3. Uniformly distributed load (8½ sq.ft.)	12	No failure at 100#*	Failure at 160#

* not tested to destruction

Two complete modular arches (one using Techni-Foam, one using Fome-Cor) were tested by the application of gradually increasing uniformly distributed loads as shown in Figure 13. Failure occurred in the Techni-Foam arch as the load approached 10 lb./sq.ft. and in the Fome-Cor arch as the load approached 8 lb./sq.ft. Vertical deflection on the Techni-Foam arch was 1-13/16" at the ridge at 8 lb./sq.ft. load. On the Fome-Cor arch it was 1-13/16" at the ridge at 6 lb./sq.ft. load. It was felt that the testing of just one arch rather than a completed structure was an unfair test. (Note: Construction of Shelter #1 proved that this was true.)

CONSTRUCTION OF SHELTER # 1.

At the conclusion of the structural tests described above, the research group (under an amendment to the contract) was directed to construct a full-size shelter employing the modular "bow-tie" concept as developed in the preceding studies.

The structure was to be designed, constructed, test-erected, packaged and shipped to an Air Force base for field test in less than eight weeks after the directive was received.

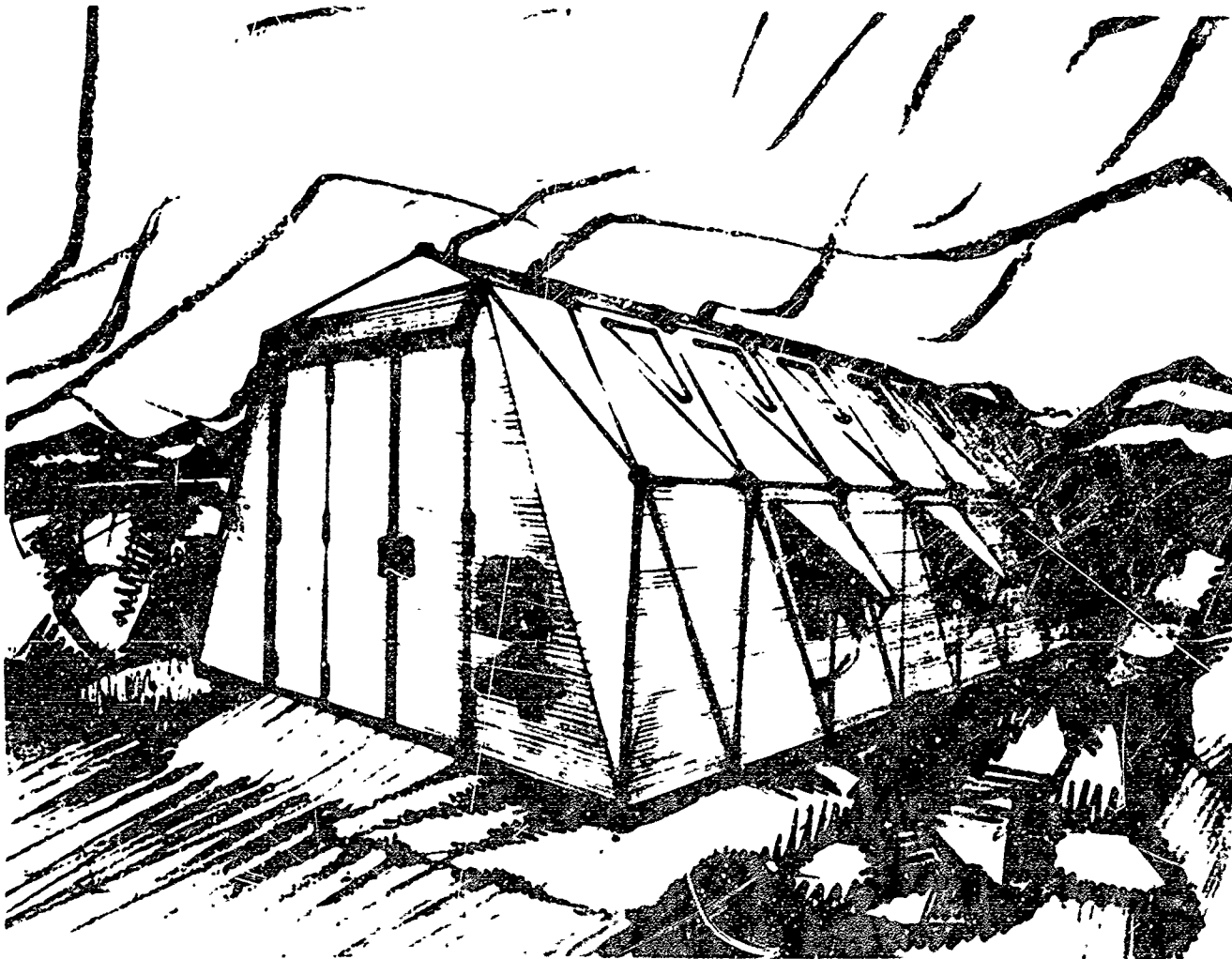


FIGURE 14. Rendering-Shelter using "bow-tie" concept.

Dimensions specified for Shelter # 1 were 38' long x 16' wide. A large 8' door was called for in one end, a small one at the other end, and ventilating windows were to be provided in ten modules. Grade beams and a flooring material were to be supplied.

All components for Shelter # 1 were built, fabricated, and/or assembled by the research group at the College during the months of July and August. It was delivered for field testing on 1 September. Following is an abbreviated description of the various components and elements of the design:

Structure: folded "bow-tie" modules of 1/4" Fome-Cor reinforced with .020 aluminum edge channel. "chevron" reinforcement at waist, washers at connectors.

Connectors: thumbscrews, wingnuts, and washers; strap steel and wingnut stirrups and washers at bow-tie waists.

End treatment: identical folded Fome-Cor side panels and gable pieces at each end framing 8' wide x 6'-10" high opening.

End opening options: (a) 1 double door filling 8'x6'-10" opening, door material: 1 1/2" thick Urecomb (Union Bag-Camp Paper), door frame: wood head and jambs (shipped K.D.). (b) three interchangeable units to fit within 8'x6'-10" opening: single 2'-10" x 6'-10" x 1 1/2" thick Urecomb door preassembled in wood frame, 2'-10" x 6'-10" Fome-Cor blank filler panel, and 2'-10" x 6'-10" Fome-Cor panel containing screened ventilating openings with top-hinged protective shutter.

Exterior and interior protective finish: two coats epoxy-type aroflint 505 paint (Archer-Daniels-Midland). Exterior color: light olive, interior color: off-white.

Weather seal between modules: 1/4" x 1 1/2" strips closed-cell neoprene sponge attached to ribs below fold line on "bow-tie" modules, 3/8" neoprene "doughnuts" on strap stirrups at joint intersections.

Windows: triangular cut outs in Fome-Cor, screened on inside, top hinged protective shutter, operating rod.

Grade beams: 4 1/2" x 7" hollow wood sections made of plywood and 2 x 4's connected by 4 x 4 "tongues" locked into place by 1/2" carriage bolts dropped into prepared holes.

Floor covering: Neoprene coated nylon-mesh tarpaulin.

In three areas the pressure of schedule forced adoption of details that should, time permitting, have been developed further: (1) grade beam could have been much lighter in weight - probably aluminum, (2) neoprene weatherseal gave indications of not being completely effective, (3) thumbscrew/wingnut connector installation was time-consuming. Weight of the 16' x 38' shelter (less wood grade beams, stakes and tarpaulin) was 837 lbs. Figure 15 shows basic drawings and Figures 16, 17, and 18 views during production and test-erecting at the University.

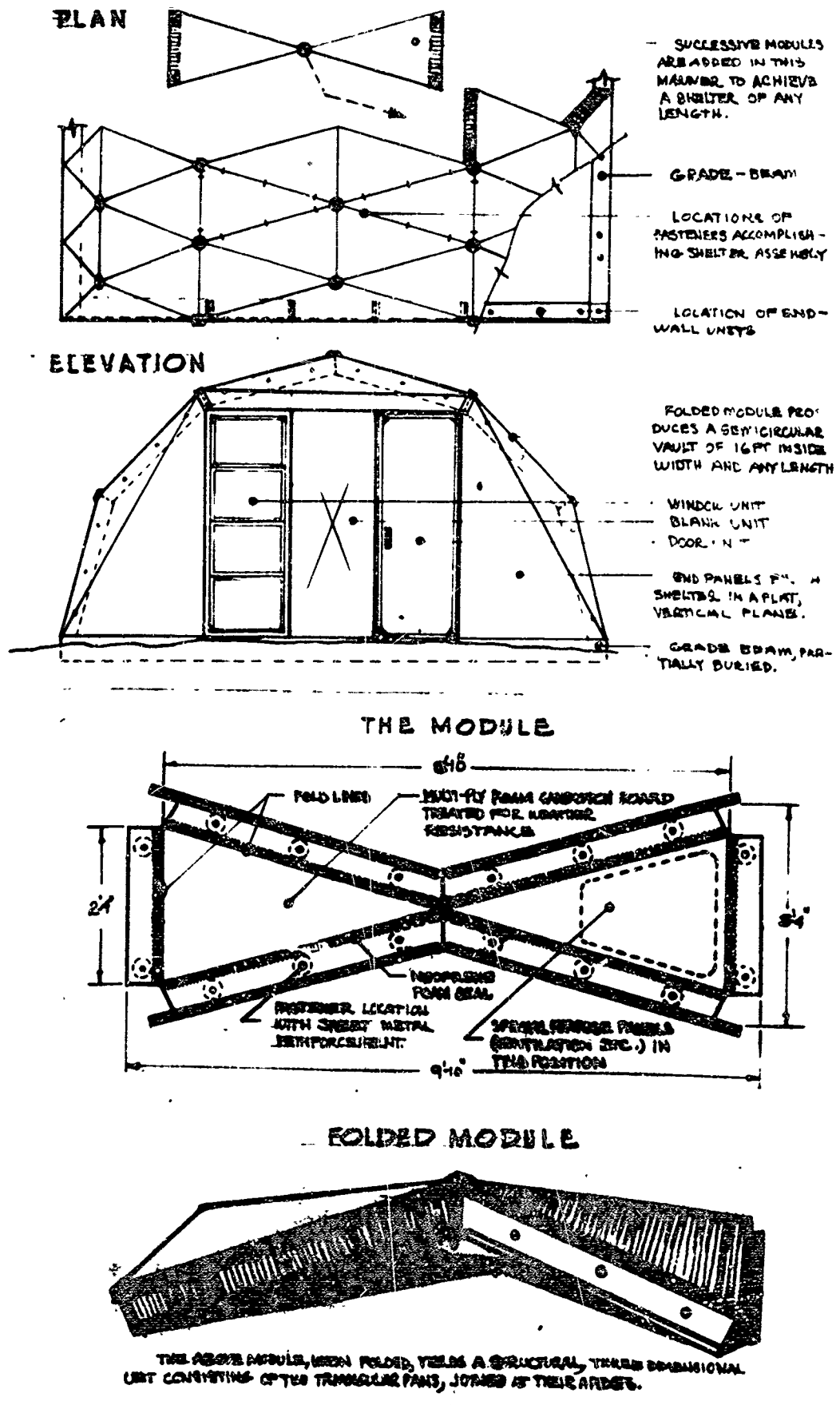


FIGURE 15. Plan, elevation, and module drawings, "bow-tie" concept. Shelter # 1.

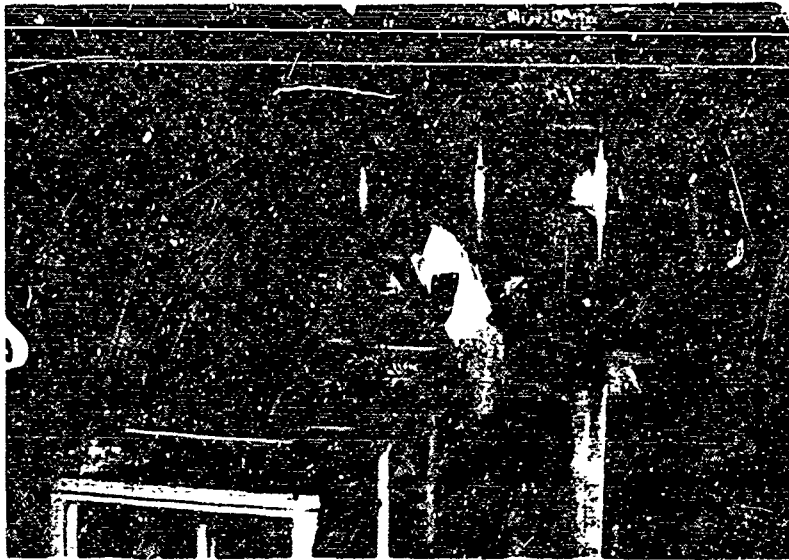


FIGURE 16. Production of Shelter #1. Application of epoxy-type coating.

FIGURE 17. Shelter # 1 (16'x38') test-erected in University of Cincinnati fieldhouse.

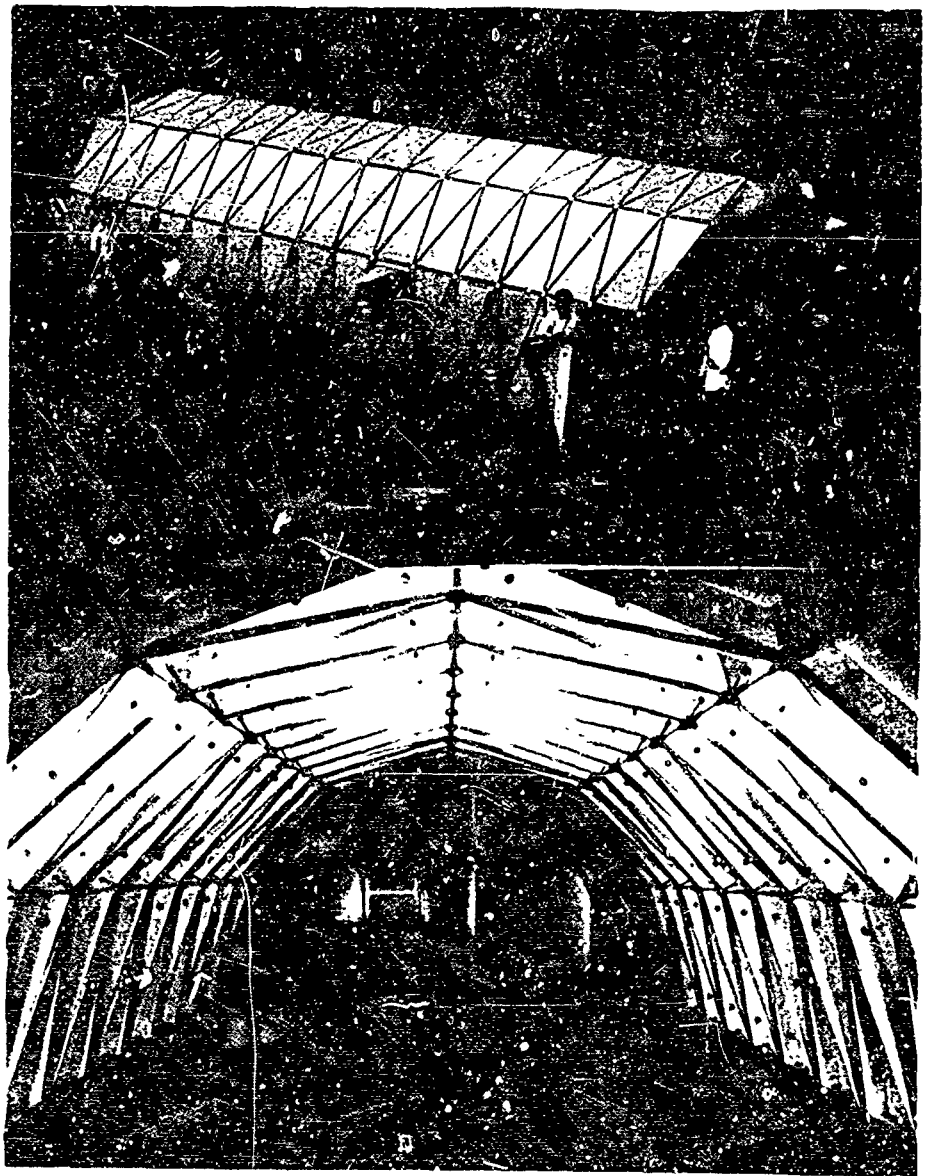
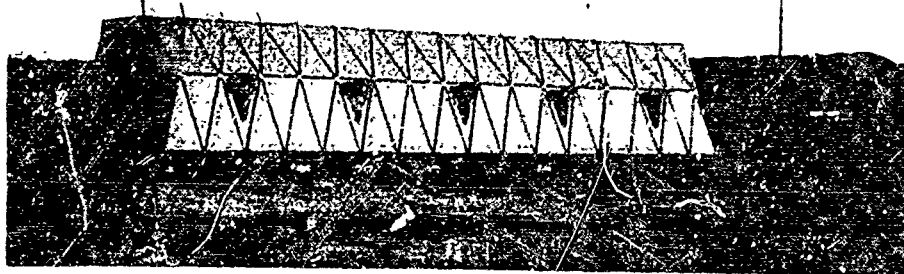


FIGURE 18. Shelter # 1 interior view.

**FIGURE 19. Shelter #1
Field test-Indian River
III exercise, Eglin Air
Force Base, Fla.
September, 1964**

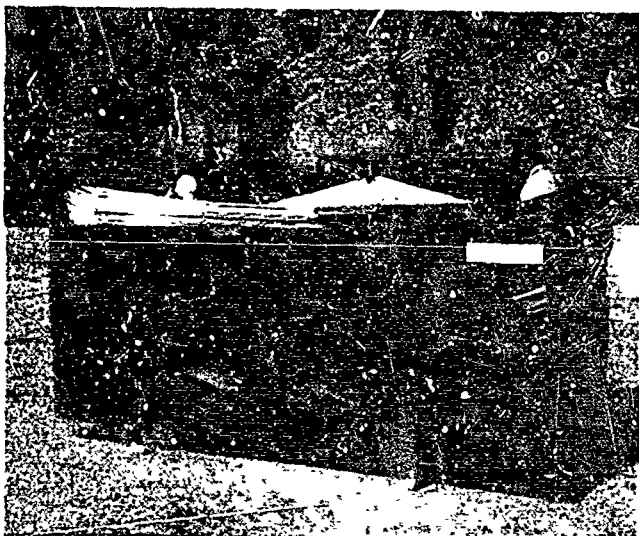


FIELD TESTING OF SHELTER #1

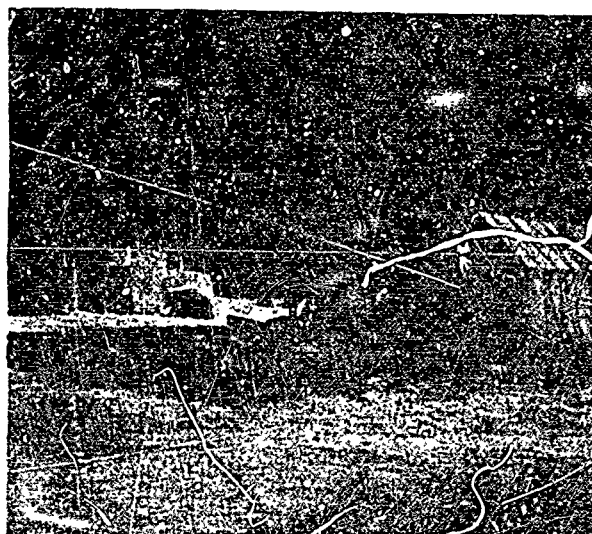
On 2 September, 1964 Shelter #1 was shipped by air to Eglin AF Base for erection, testing and use as a command post briefing room at Indian River III exercise. Erection was accomplished by a five-man University team in approximately five hours (25 man hours) in 103° f. temperature. Sixteen days later it was dismantled, repackaged, and air-lifted to Wright-Patterson AF Base and then returned by truck to the University of Cincinnati.

During the test the structure performed satisfactorily from a structural standpoint. At one time it withstood winds of approximately 45 mph with no significant vibration or deflection of components. Auxiliary tie down ropes and stakes provided for such contingencies were employed during this storm.

As anticipated, considerable leakage was encountered in heavy rain. Joints were taped, as an expedient, for the remainder of the test to assure its being waterproof.



**FIGURE 20. Shelter #1 - Unpacking
basic package.**



**FIGURE 21. Shelter #1 - Erection at
Eglin AF Base, Florida**

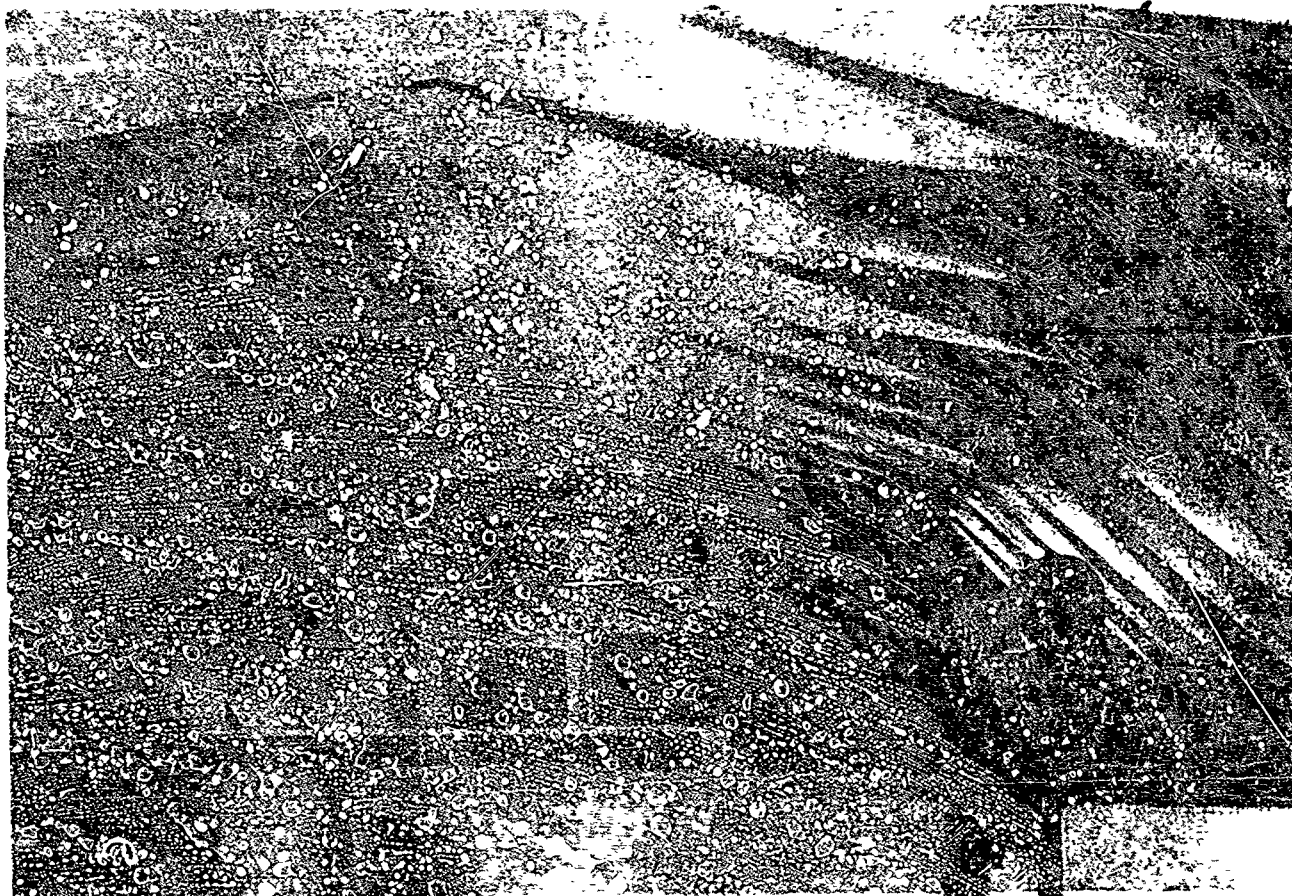


FIGURE 22. Shelter # 1 in use at Indian River III exercise.

For this exercise the Air Force at Eglin provided standard 4' x 8' plywood floor sections which fit within the 16' interior dimension between grade beams.

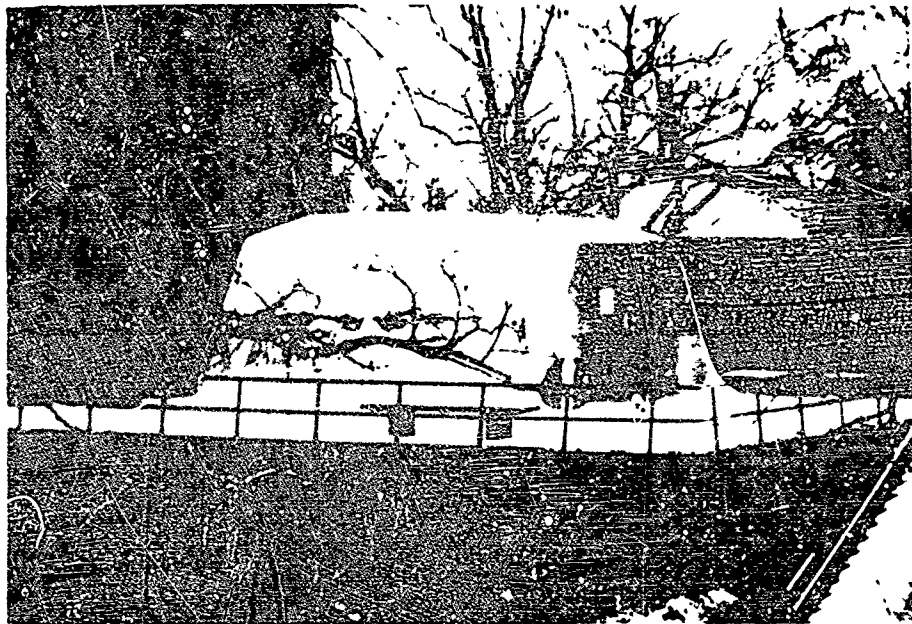
The surface coating of the modules proved satisfactory as did the foam sandwich material employed.

Design goals for further studies were: (1) more effective sealing against leakage, (2) reduction of weight by use of lighter weight grade beam, and (3) more rapid erection time by employing a less time-consuming connecting device than the thumbscrew/wingnut one.



FIGURE 23. Shelter # 1 interior view during erection.

FIGURE 24. Shelter #1
Snow-load test at
University of Cincinnati. February, 1965



PROPOSED IMPROVEMENTS

After the return of Shelter #1 to the campus, a shortened 16'x20' section was erected and, to date, has stood in all kinds of weather for eight months (See Figure 24). No deterioration of material or finish can be detected.

Studies have been made in order to improve weather seal and reduce erection time by reducing time required to install connectors. Figure 25 shows the proposed change featuring continuous aluminum strips (to assure even pressure along length of joints) and an adaptation of a Simmons cam-activated fastener.

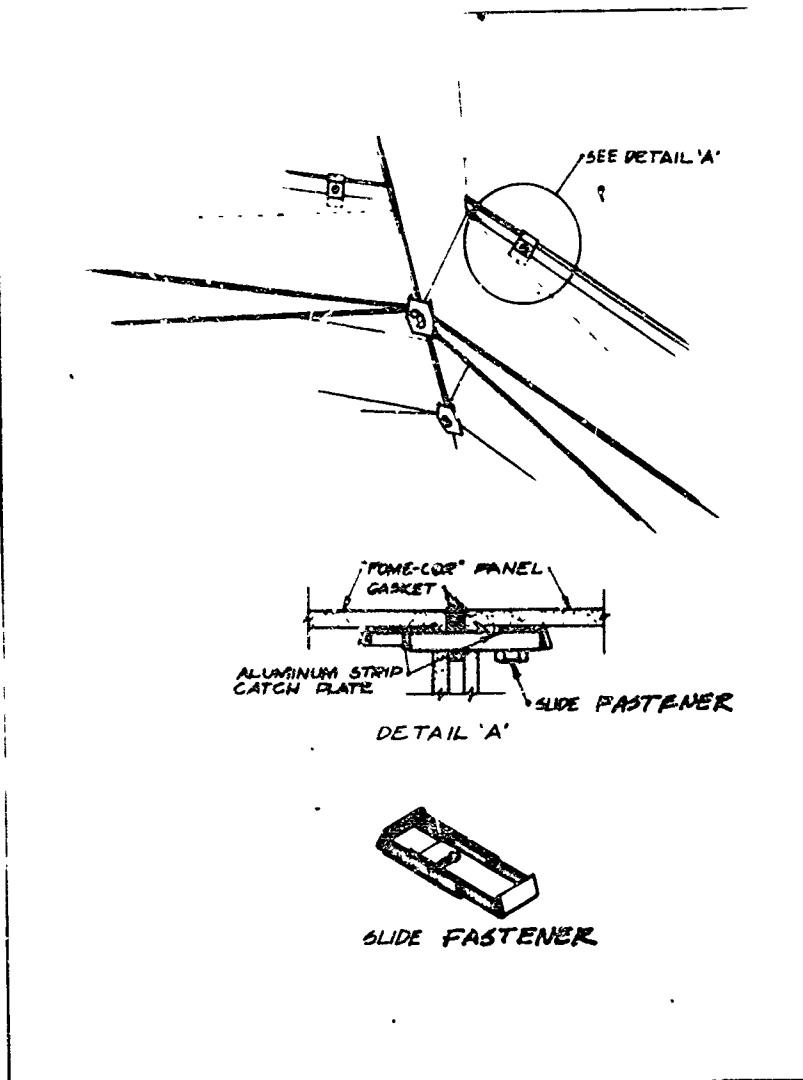


FIGURE 25. Shelter #1. Proposed improved connector concept.

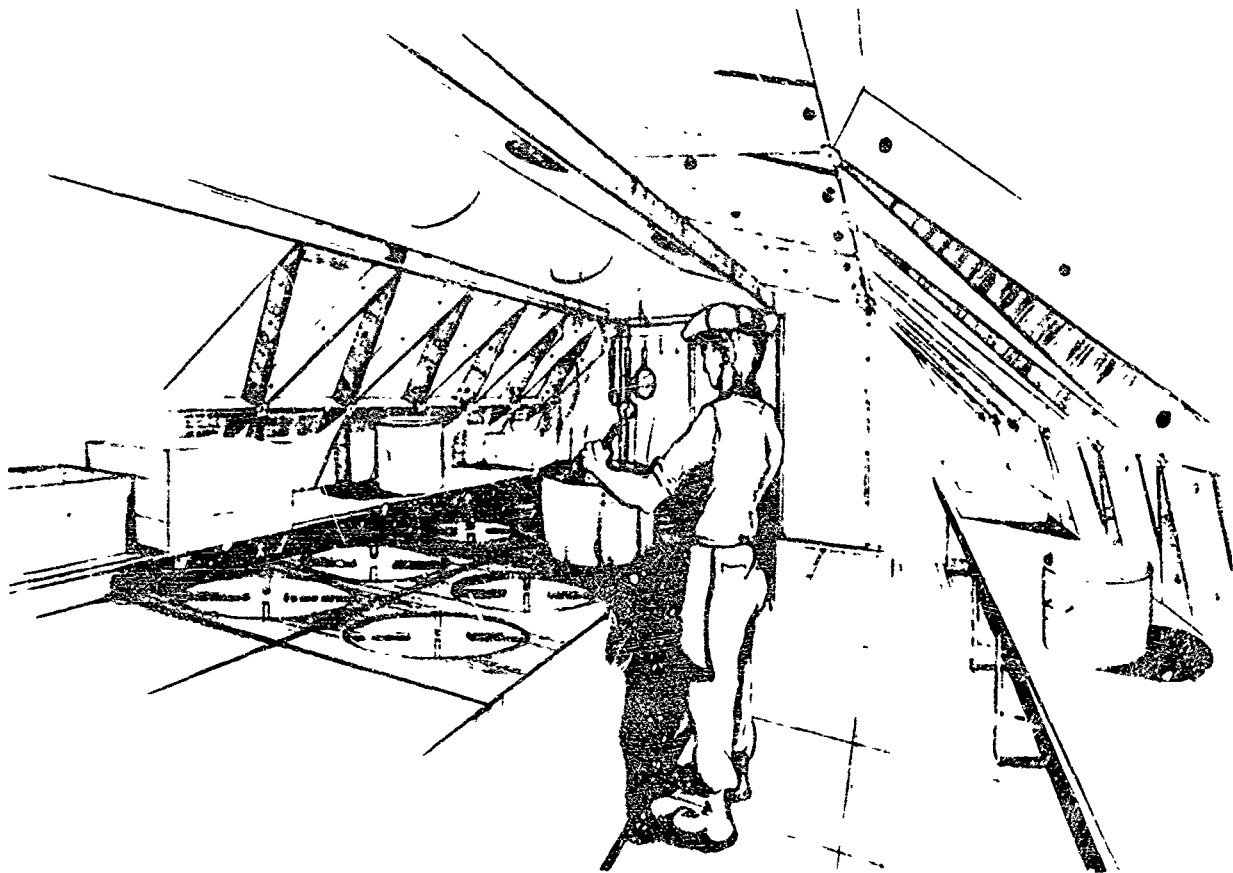


FIGURE 26. Shelter # 1 - Rendering showing possible use as a field kitchen.

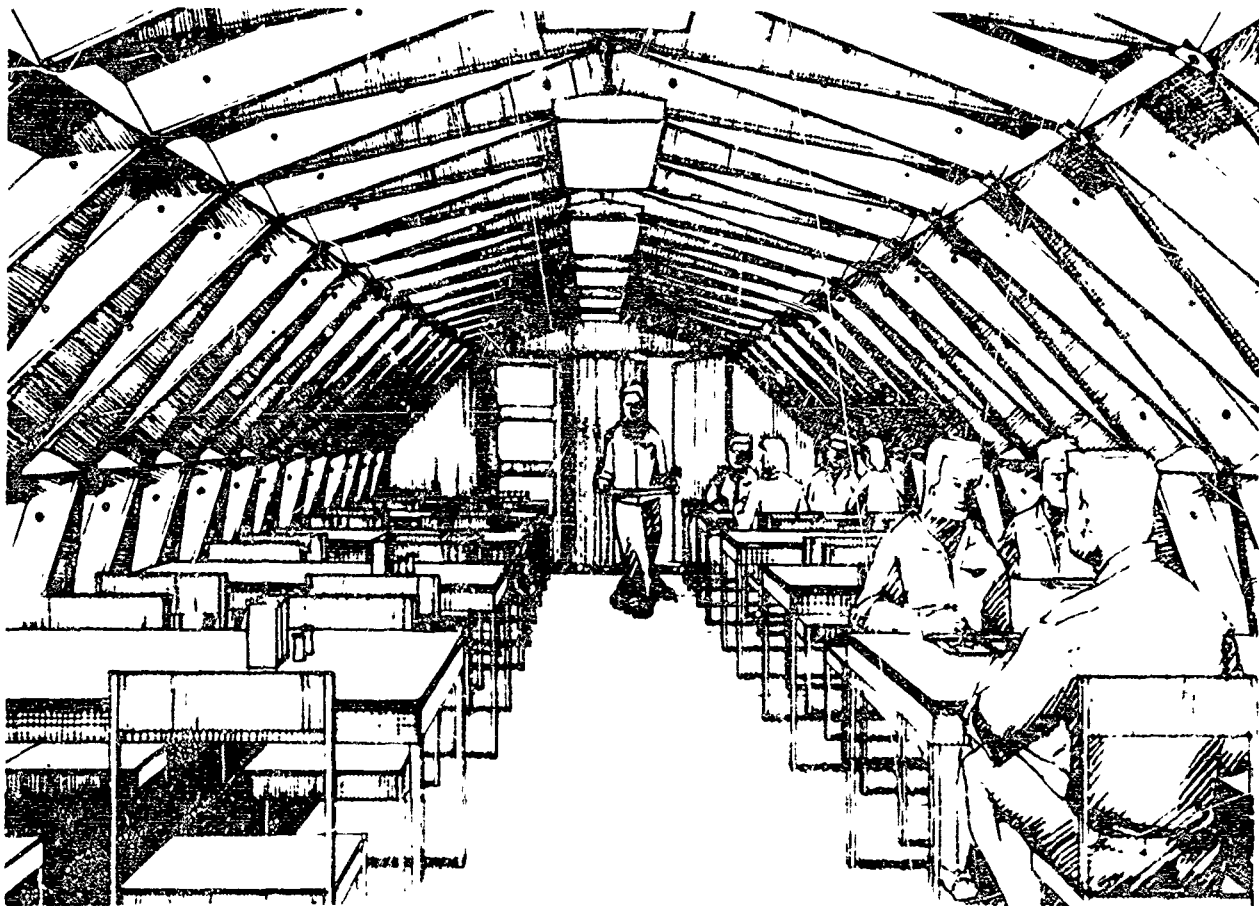


FIGURE 27. Shelter # 1 - Rendering showing possible use as a mess hall.

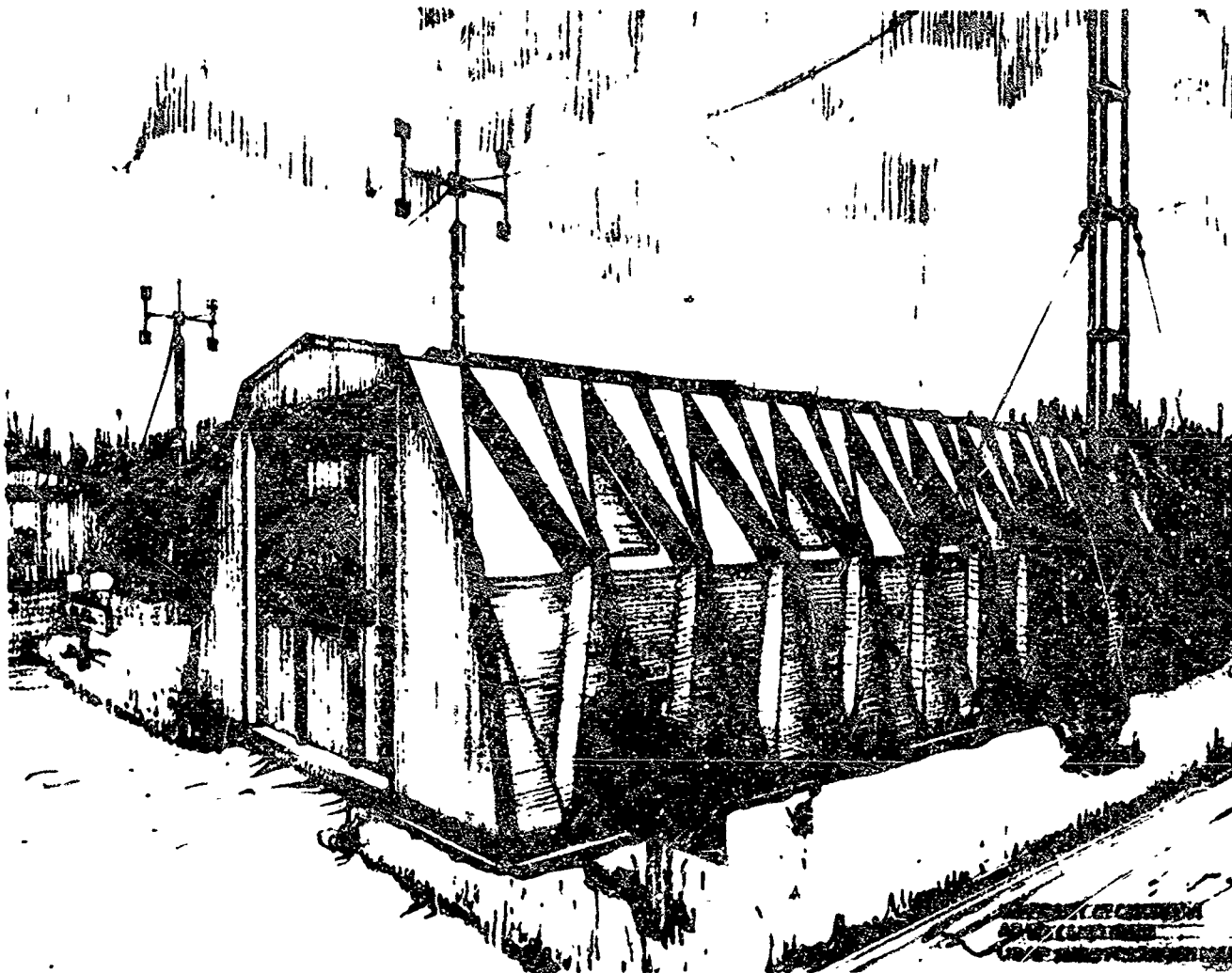


FIGURE 28. Rendering - Shelter using "folded-diamond" concept.

"FOLDED-DIAMOND" CONCEPT

Orders were placed for a number of specially fabricated modified Simmons slide fasteners (Figure 25) and certain gasket sections for adaptation to the "bow-tie" shelter. While delivery of these items was awaited, another concept was evolved.

This concept was based on a folded plate formed from a rectangular flat sheet of Fome-Cor. Less waste of the sheet material resulted from the adoption of a rectangular module. Three of these rectangular modules were taped together so that, when unfolded and formed along previously scored lines, one complete arch could be created. In terms of numbers of separate pieces to be handled in erection, this approach meant that fifteen such arches would cover the same area as the ninety-six "bow-tie" modules (in a 38' long shelter).

Strength is obtained by scoring "bow-tie" shapes on the rectangular modules and folding them during erection so as to form triangular prisms resulting, when assembled into a shelter, in a series of diamond shapes in two planes.

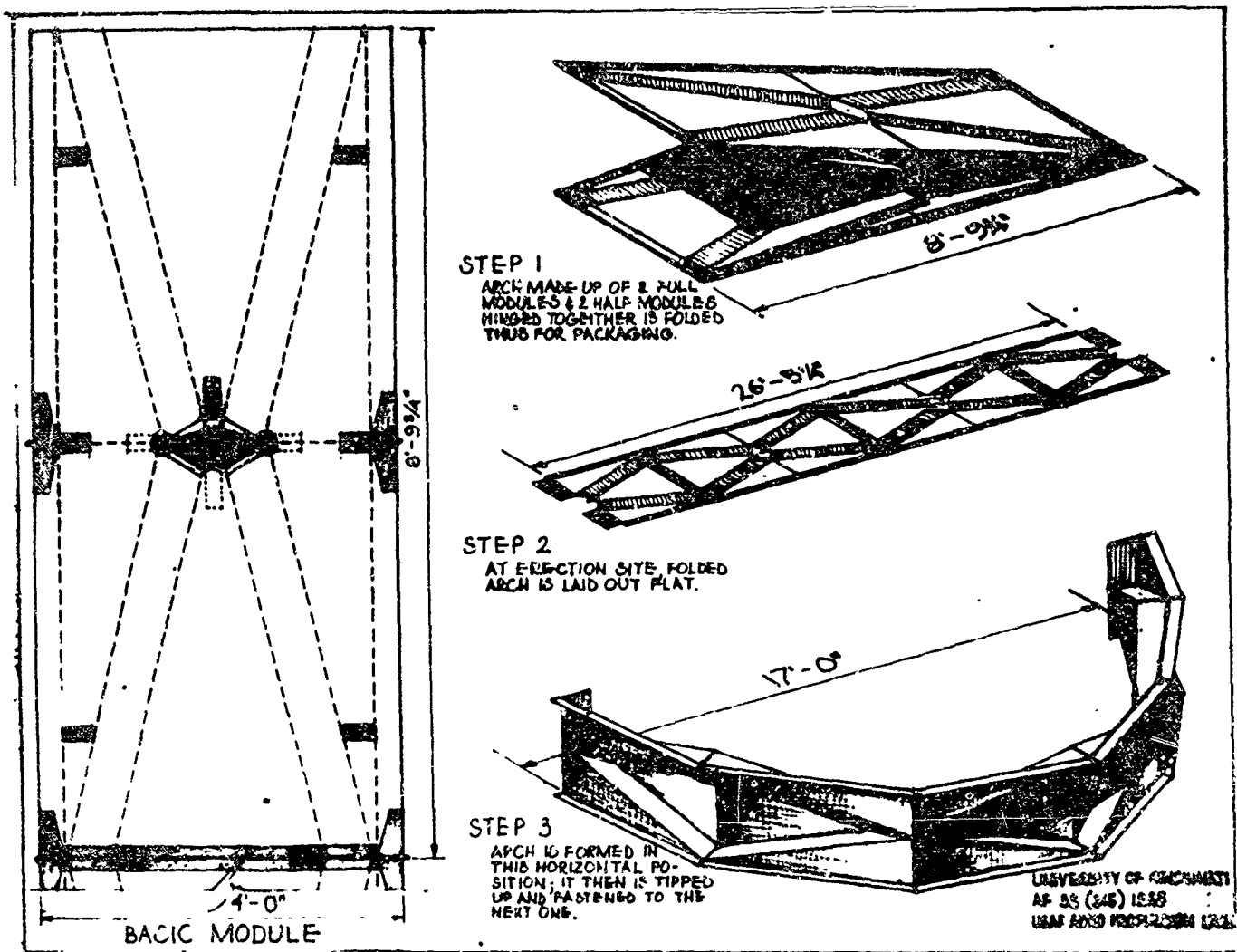
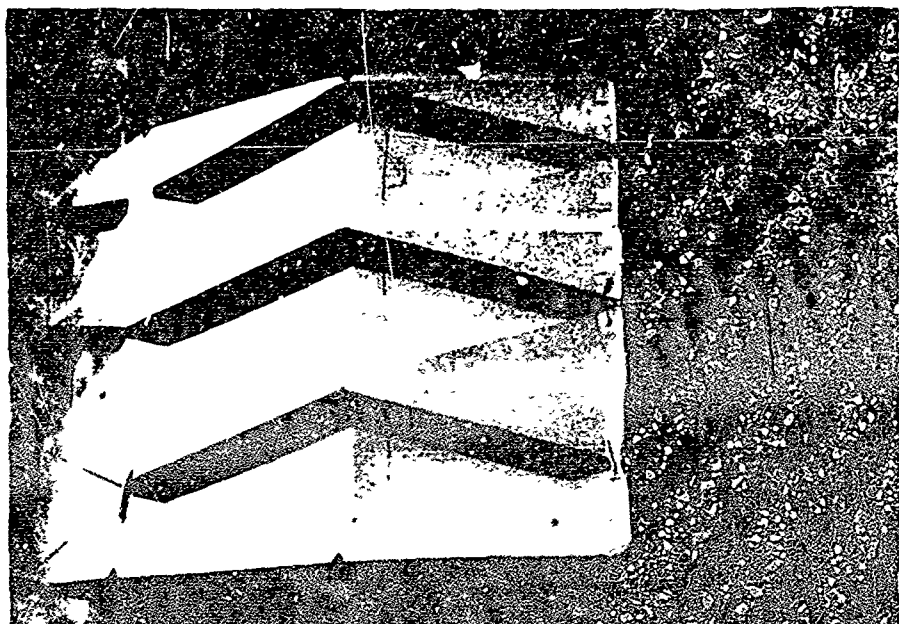


FIGURE 29. Drawing - Basic Module and Typical Arch-"folded diamond" concept.

A preliminary full-size triple arch in corrugated fiberboard was constructed to verify the basic geometry (See Figure 30). Figure 29 shows a further refinement involving stand-up ribs at joints, metal-reinforced and treated-fabric diaphragm-covered orifice at the center of the module, and fabric tie-straps utilizing Velcro nylon fasteners. The folds are so arranged that the inward folded prisms overlap to form self-flashing gutters. Continuous connector-flashing tape fits snugly over the standing ribs.

FIGURE 30. Test Arch in corrugated fiber board. "Folded diamond" concept view from above



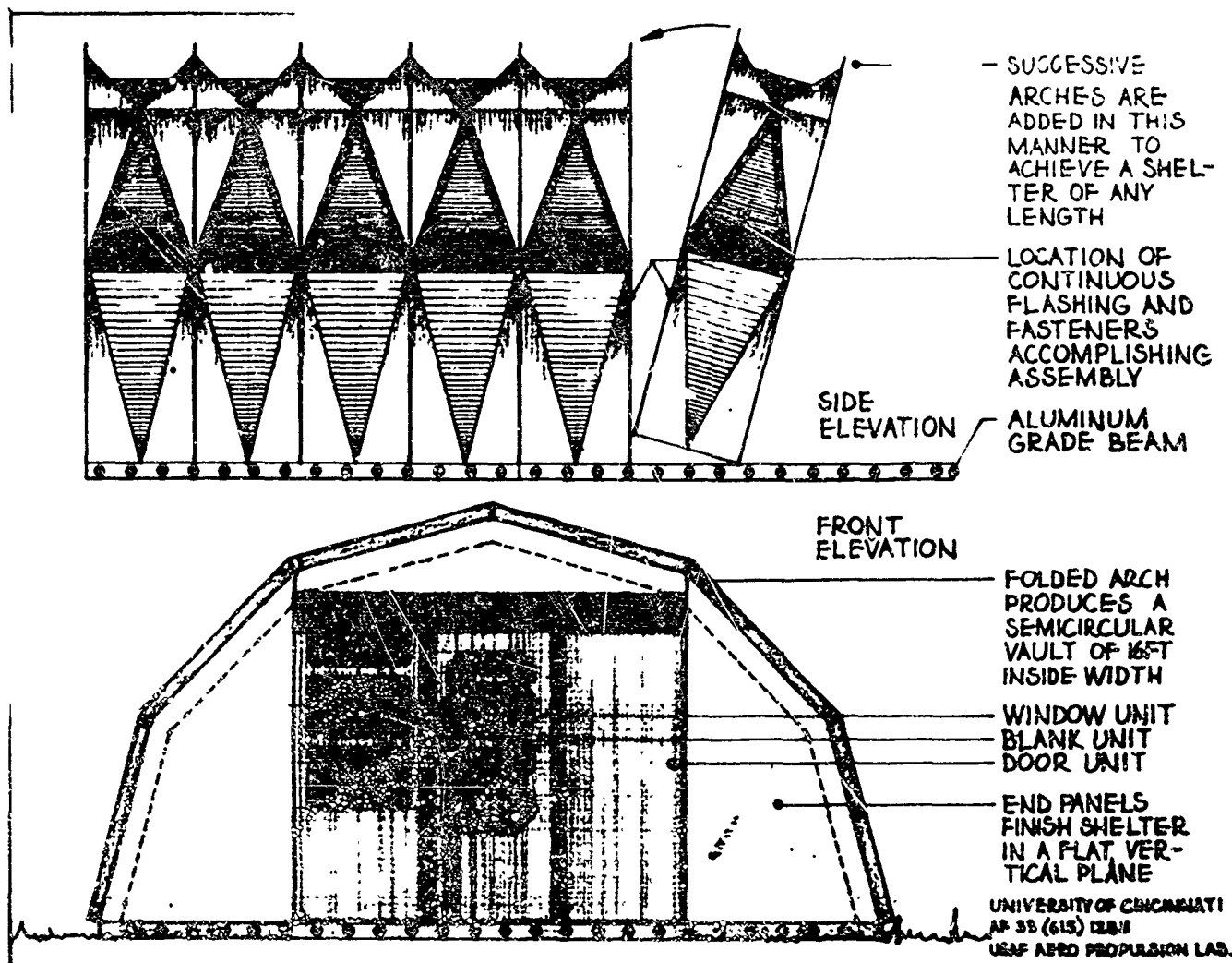


FIGURE 31. Drawing - Elevations of "folded diamond" concept shelter

A three-arch section test vault was constructed next. One-quarter inch Fome-Cor was used for the panels with hinges made of Tedlar tape. An improved light-weight aluminum grade beam was designed but was not available for this test. The test arch was loaded to 8 lbs. per square foot. Failure occurred at this loading. This was deemed encouraging considering the saving of material of this concept over the "bow-tie" concept. It was noted however that, prior to failure, deflection at the ridge was $4 \frac{3}{4}$ " as compared with the $1 \frac{13}{16}$ " deflection on the "bow-tie" arch under the same loading. Failure occurred when the upright ribs buckled at the first hinge point above the grade beam.



FIGURE 32. Test arch Fome-Cor "folded diamond" concept.

One drawback to an approach characterized by upstanding ribs and the alternating planes of the folded prisms is the difficulty of applying additional insulation when needed. Although this concept represented a step forward in the areas of economy of material and reduction of numbers of components, it needed further stiffening of the ribs and did present a fairly complex on-the-site folding operation for an untrained erection crew.

"FOLDED BEAM" CONCEPT

The "folded diamond" approach had led the team into considerable research in the areas of adhesives, flexible attachment devices, and coated fabrics. Rather than pursue modifications of the "folded diamond" approach a different direction was charted based largely on this aforementioned research. From this study evolved the "folded beam" concept. In this concept all diagonal folds or rib patterns were abandoned and a straight-forward parallel rib pattern was adopted.

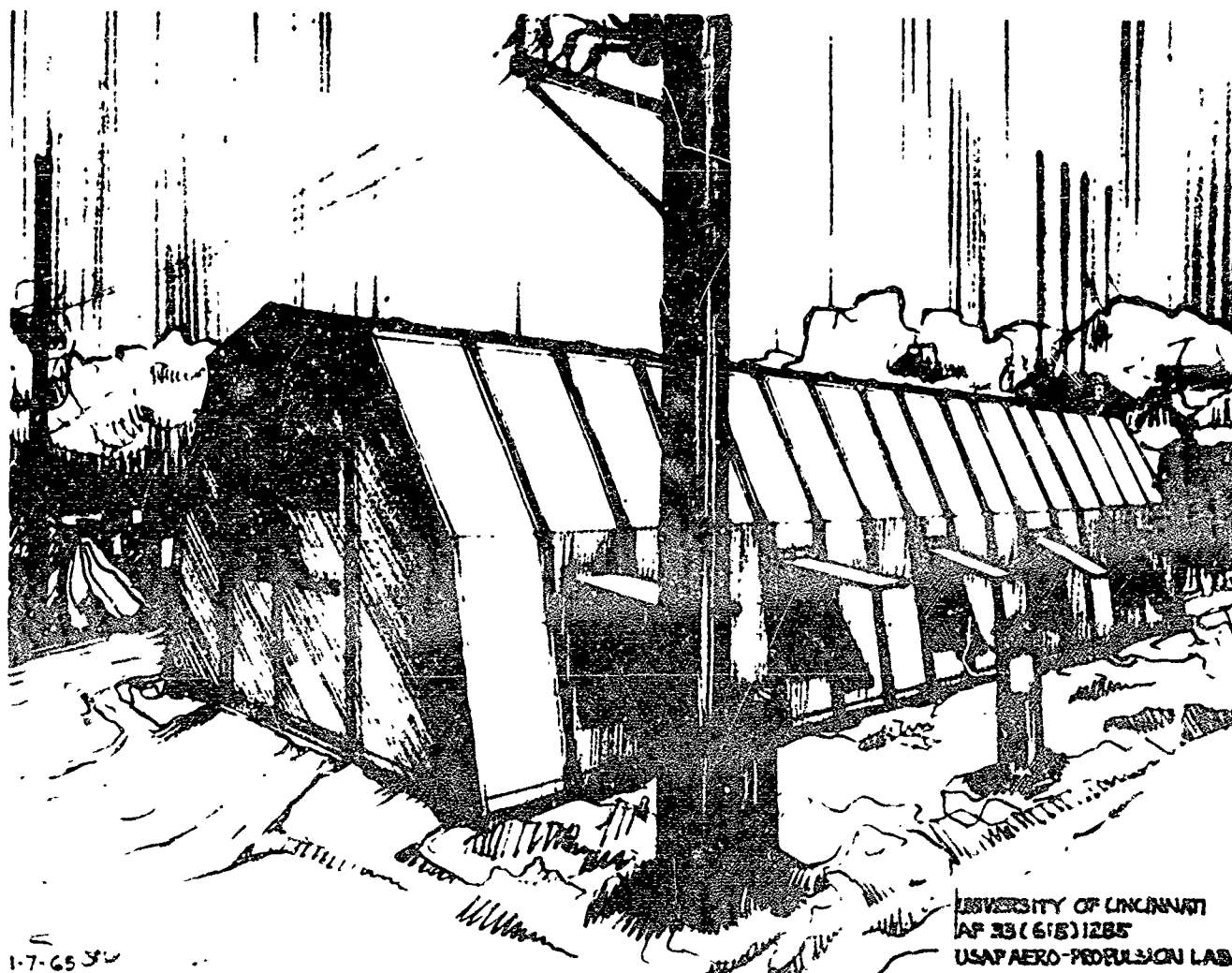


FIGURE 33. Rendering - Shelter using "folded beam" concept.

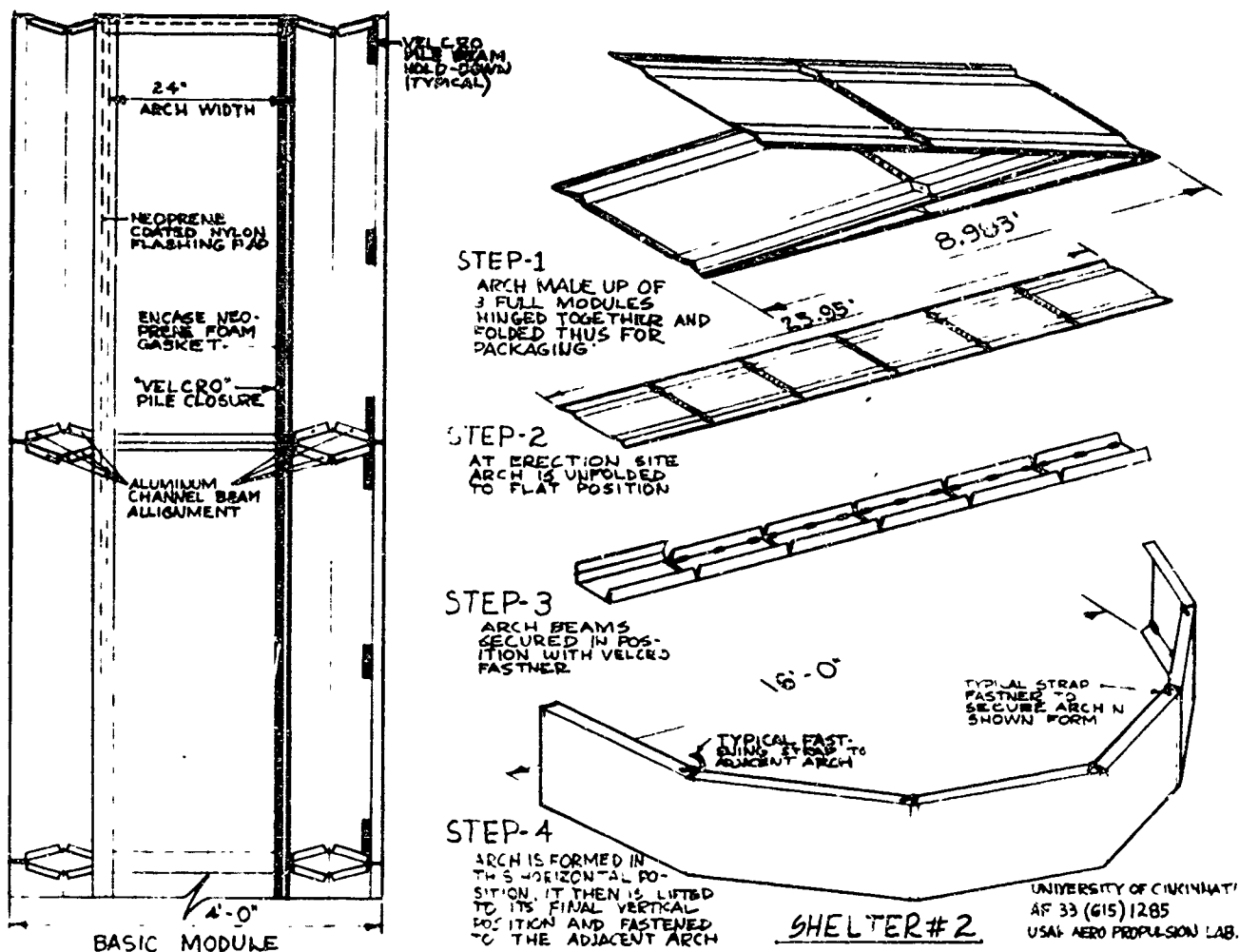


FIGURE 34. Drawing - Basic module and typical arch "folded beam" concept.

As in the previous concept, a typical arch was formed by Tedlar hinging together three rectangular panels each 4 ft. wide by approximately 9 ft. long. The outboard 12 inch strip on each side of the 4 ft. wide module was scored so that, when folded, a rigid triangular-section beam was formed. The beam is held in its folded position by means of previously attached strips of Velcro, aligned so that hook engaged pile when the beam was folded.

A typical arch is formed by following the four steps shown in Figure 34. For reinforcement in compression and for alignment in folding the segments into the arch, tongue and grooved light-weight aluminum channels cover the edges of the diamond-shaped openings in the module (See Figure 34). Tensile strength at these angles is obtained by cross-over webbing straps with Velcro "hook" patches that attach to properly placed "pile" patches on the appropriate beam face surfaces.

Velcro is also used in attaching adjacent arches to each other. This is done both internally and externally. Inside the shelter cross-over straps with Velcro patches lace adjacent beams together. Externally a broad band of neoprene-coated nylon is permanently glued to one edge of the arch and is secured in erection to the adjacent arch by means of continuous Velcro "hook"



FIGURE 35. Uniform load test single "folded beam" arch.

strip on the flashing being pressed into a continuous strip of "pile" Velcro on the mating edge of the adjacent arch. The flashing also spans a compressible foam-filled neoprene gasket strip that parallels the Velcro "pile" strip. This assures a leakproof joint in use.

The details described above and in Figure 34. were worked out in full size typical sections and in two full size arch tests. Though it was realized that, as in Shelter #1, a complete shelter would have greater strength than a test of a single arch would show, a single arch was constructed and loaded to failure. This occurred after a uniform load of 6 lbs. per sq. ft. was applied. (See Figure 35)

In the second test the middle 2 ft. of a double 4 ft. arch was loaded. It carried a load of 10 lbs. per sq. ft. At this loading vertical deflection at the ridge was 1 3/4". It was left loaded overnight and failed sometime during the night. Figure 36 shows the second test. 3 M Scotch filament tape gives added tensile strength at joints.



FIGURE 36. Uniform load test two attached "folded beam" arches.

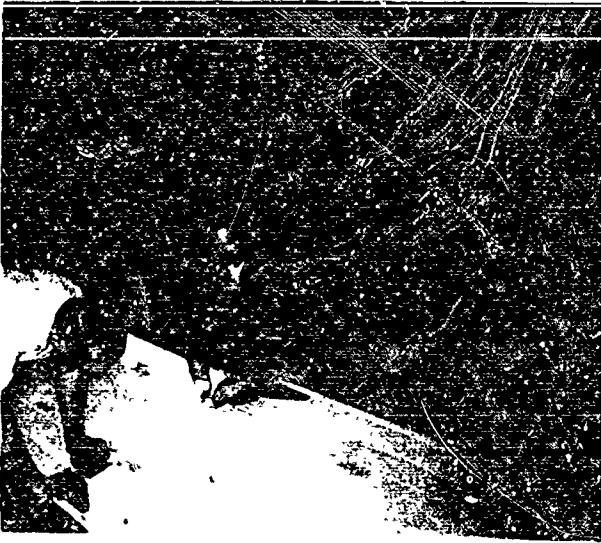


FIGURE 37. Shelter # 2 Folding beams in test erection.

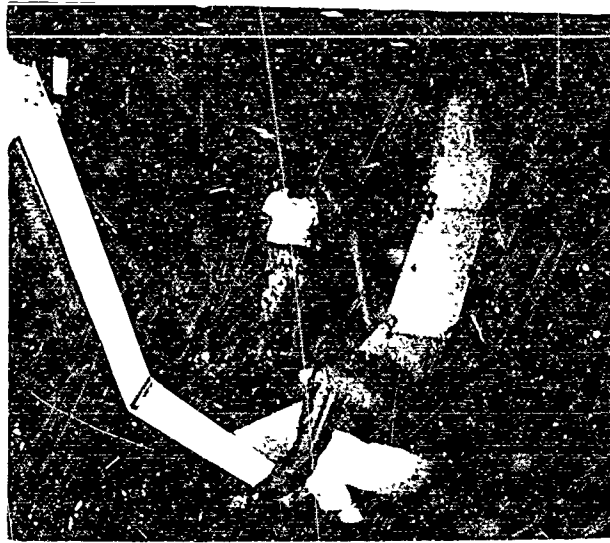


FIGURE 38. Shelter # 2 Test erection at University of Cincinnati.

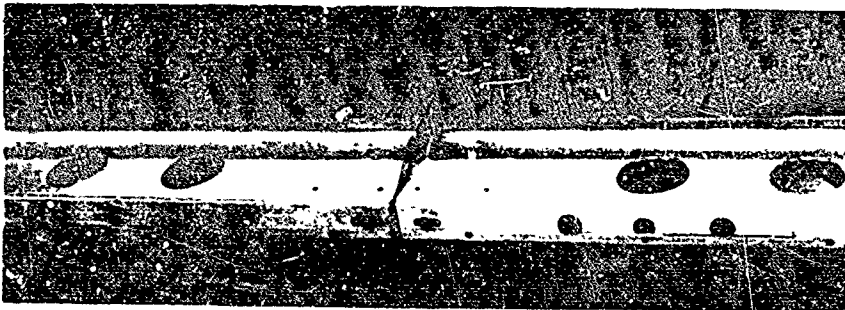


FIGURE 39. Shelter # 2 Aluminum grade beam typical joint.

CONSTRUCTION OF SHELTER # 2.

The "folded beam" approach was selected for the second of two shelters to be constructed under the Amendment to the Contract. This structure was to be 32' long x 16' wide. End panel requirements were similar to those for Shelter # 1.

As constructed and erected at the University, Shelter # 2 had the following features and materials:

Structure: "folded beam" arches of 1/4" Fome-Cor with Velcro attachment to each other and to grade beam, Neoprene-coated nylon arch and grade beam flashing, Tedlar panel hinges.

End treatment: Similar to Shelter # 1 but with folded Fome-Cor door heads and jambs (no wood) and heavy fabric door hinges.

Grade beam: fabricated aluminum (See Figure 39).

Exterior and interior protective finish (after extensive trade-off tests): ADM aroflint 505 - Exterior 2 coats olive drab, Interior 2 coats off-white.

Adhesives (in appropriate applications): 3M Fast Bond 30, Fuller # 915, Velcro # 45, Elmer's casein.

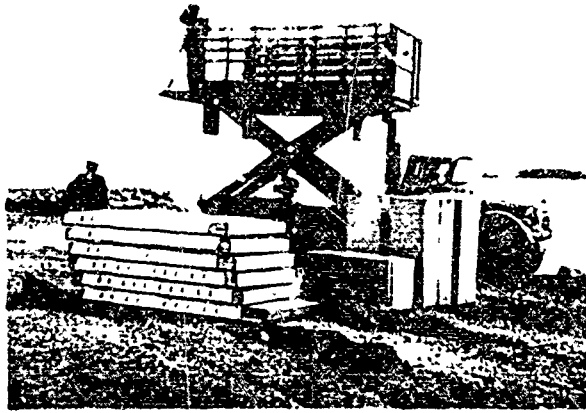


FIGURE 40. Shelter # 2. Langley AF Base, Va. Packaged Shelter left: basic shelter, right: insulation kit.



FIGURE 41. Shelter # 2. erection of "folded beam" arches, Langley AF Base, March 1965.

Insulation (optional): 1st thick panels of gold Bond Zero-Cel polyurethane foam board attached with Velcro.

Windows: rectangular Tedlar hinged cut outs in Fome-Cor, screened inside, bi-fold grommetted shutters riding on Venetian blind operating cords.

Skylights: fixed 1/4" thick clear acrylic sheets.

FIELD TESTING OF SHELTER # 2

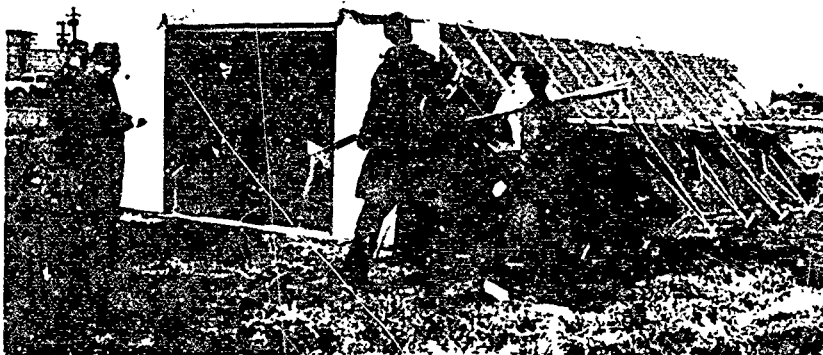
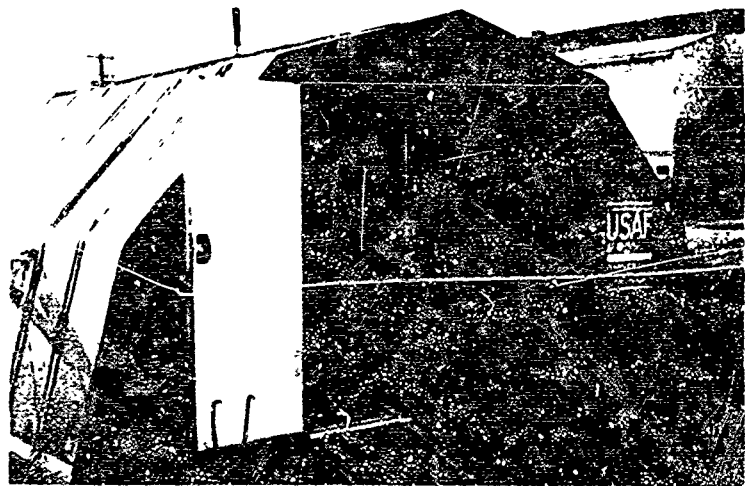


FIGURE 42. Shelter # 2 Erected shelter showing end with large doors.

On 18 March, 1965 Shelter #2 was shipped by air to Langley Field AF Base for erection and testing. A five-man University team erected the Shelter in approximately three hours (15 man hours).

FIGURE 43. Shelter # 2 Erected shelter showing end with small door, filler panels.



The Shelter was packaged for shipment in six packages each approximately 4'-4" x 9'-0" x 7" thick. Total weight of the shelter (including aluminum grade beams but not including stakes or tarpaulin) was 630 lbs. Insulation was packaged separately. Packaged shelter and insulation kit are shown in Figure 40. Erection time could have been reduced considerably had the site been more level thus making unnecessary some realignment of end treatment components on one end. Erection was accomplished in gusty weather so care was exercised in folding and carrying the lightweight arches.

Shelter # 2 remained in position at Langley for a period of one month showing no evidence of structural failure, leakage, or deterioration of materials or finish. During this period high winds and considerable rainfall provided a good weatherability test.

At time of writing the shelter is being returned to the University in anticipation of its being shipped to and exhibited at the Second Expandable Shelter Conference.

LARGE SHELTER CONCEPTS

As stated in the Introduction, the work under the contract includes developing of concepts for large shelters capable of housing fighter aircraft. Exploration of concepts for the large shelter were carried on concurrently with the preliminary studies of the small general purpose shelters. Work on the large shelter concepts was set aside during the period of construction of small shelters # 1 and # 2 and have been resumed only during the month following completion of tests of shelter #2.

INITIAL CONCEPT

The major approach followed in initial studies involved the use of trussed arches with a coated fabric (or lightweight sheet) covering. The concept is explained in renderings (Figures 44 and 45) which show the completed structure and a possible erection procedure.

The material used for the trussed arches would most likely be aluminum (or possibly magnesium) tubing although all preliminary models have utilized light rod stock.

The basic element in the arch in this concept is a "keystone" shaped element formed by rotating two trapezoidal shaped frames up from a rectangular frame until a triangular section is formed. The keystone units would then be joined together to form the trussed arch. This sequence is illustrated in Figures 46, 47, and 48. Figure 49 shows a complete arch constructed at one-third scale.

The depth of the triangular section is determined as required for bending as an arched beam. The base width of the triangular section is determined as required for lateral stiffness. The rotating of the trapezoidal frames would bring together at the apex of the triangular section two tubes thus giving a double compression member at this point.

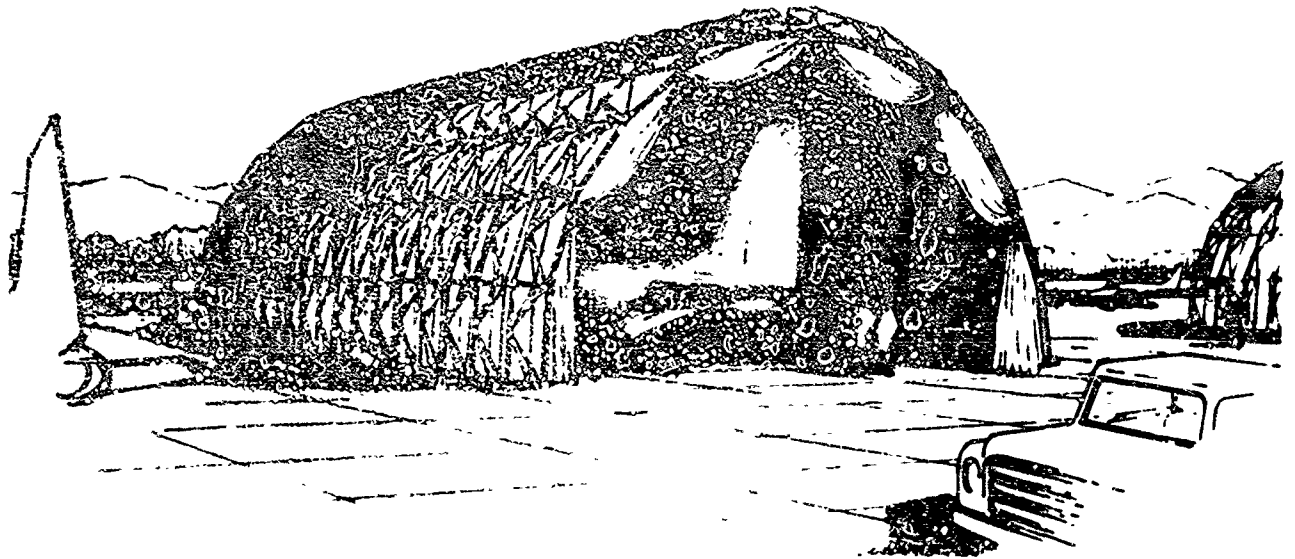


FIGURE 44. Rendering - hangar concept (50' span)

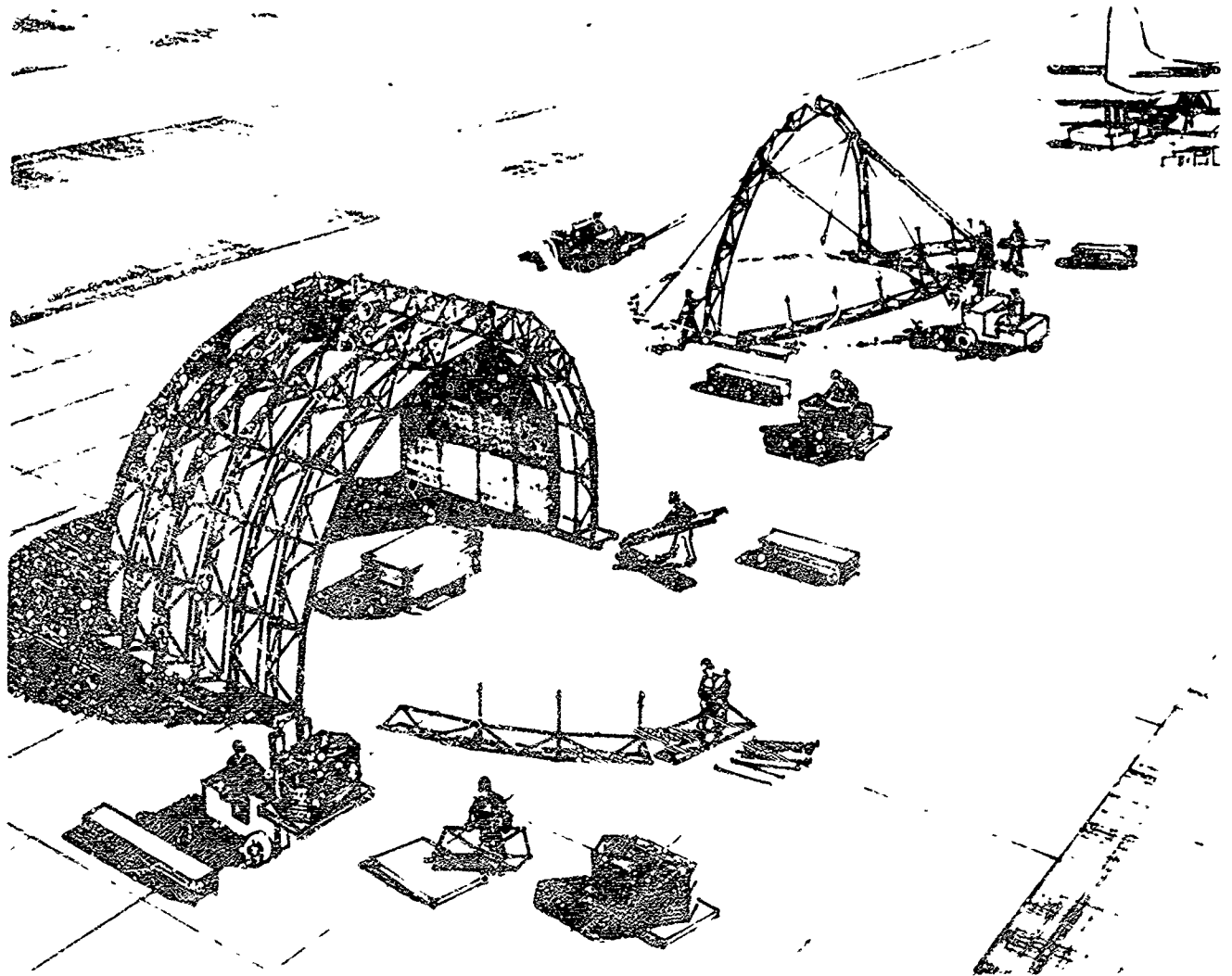


FIGURE 45. Rendering - hangar concept (erection procedure)

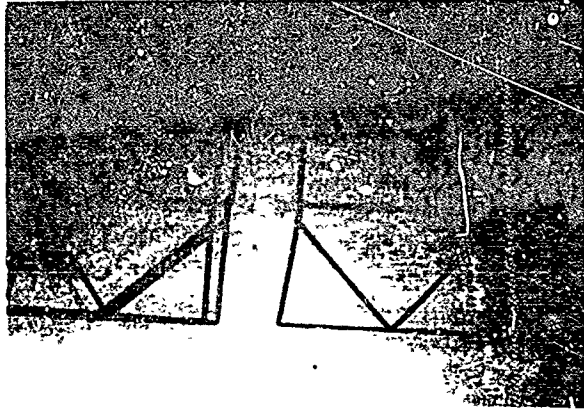


FIGURE 46: Welded rod hinged trapezoidal frames in flat position.



FIGURE 47: Frame being rotated into triangular "keystone" section.

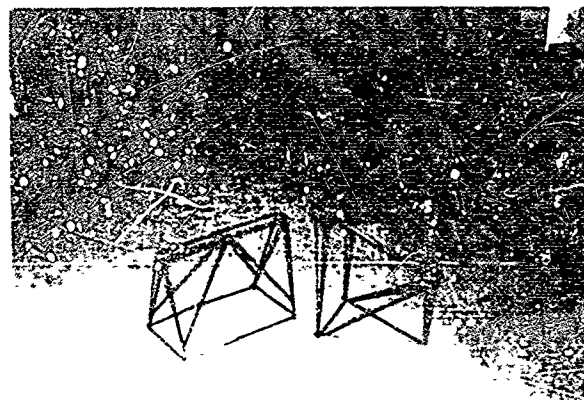


FIGURE 48: Left: "keystone" unit. Right: two units joined.

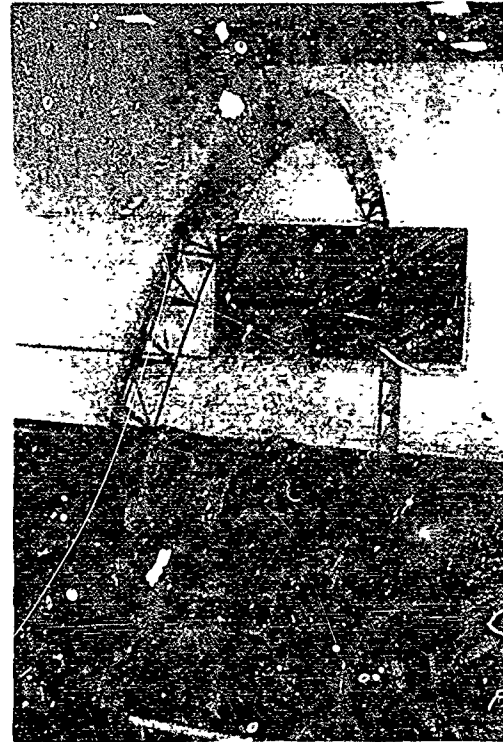


FIGURE 49: Hangar concept - one third scale trussed arch formed from welded rod "keystone" units.

This approach has the following features:

- (1) Structural members can be shipped flat.
- (2) Arches may be set up adjacent to each other or spaced apart with purlins and wind braces.
- (3) Power winches would probably be the only erection equipment necessary.
- (4) The erected trussed arch would form a built-in ladder for the erection crew.

Under study at present are attachment devices for the arch components, purlin and cross bracing design, types of covering material and attachment methods for same, ground anchoring and grade beam design. Detailed structural design and material specification will follow.

ALTERNATE CONCEPTS

Return to study of the large shelter after construction of small shelters #1 and #2 has been featured by a reexamination of alternate concepts that may be worthy of further investigation. Among these approaches are ones featuring:

- (1) Three hinged arches in which arches are shipped K.D., fastened together with center hinge point blocked up, anchored securely at left hinge point, then winched upward by pulling cable between left and right hinge point (with right hinge point sliding in track toward left hinge point).
- (2) Tension structure of hexagonal plan (or three sided ends on long structure) featuring compression masts and tension lines supporting fabric skin.
- (3) Compression arch consisting of shell made of corrugated sheet plastic overlapped at ends and sides, bolted together with spring-loaded thumbscrew-type connectors, and erected by rigidly fixing one side of structure and winching other side's grade beam toward the fixed side until desired configuration achieved.
- (4) Combination segmented trussed arch and rigid insulation panel construction.
- (5) Space frame.

SUMMARY

The author and other members of the team have concluded:

1. A valid area for significant design exists between the category of fabric tentage on one hand and heavier rigid buildings of conventional materials requiring permanent footings on the other hand.
2. In order to keep down cubage, total weight, and package size, it is just as important to give as careful attention to design of packaging techniques and accessory items (floor coverings, doors, mechanical equipment) as to the shelter proper.
3. As in any modular or expandable structure, the method of connection of components is of vital importance. The design of the fastening system oftentimes holds the key to satisfactory performance in the areas of weathertightness, structural unity, total package weight, and man hours consumed in the erection process.
4. While it may be relatively simple to design a satisfactory structure in a laboratory situation, the real validity of the design is largely determined by how it performs in the environment in which it is to be used (i.e., (1) A lightweight shelter is only as good as the anchorage to the terrain that can be provided. (2) A system of connectors must, on one hand, be positive enough to provide weathertight seals but, on the other hand, must have enough flexibility and/or tolerances to accommodate the inevitably encountered minor variations in terrain surface).

5. Simplicity of erection process is vital in recognition of the likelihood that, in use, the shelter will be erected by untrained personnel who are not familiar with the intricacies of a complex system.
6. As well as meeting the needs of the Air Force in the limited war situations outlined, expandable structures of the types being developed under this contract have a real potential use in such areas as (1) Civil Defense, and disaster relief applications (2) use in underdeveloped nations (3) migrant worker temporary housing, and (4) recreational uses.

BARE BASE DEVELOPMENT CONCEPTS

A collaborative design project
accomplished by Junior Architecture
and Industrial Design students,
College of Design, Architecture, and Art
University of Cincinnati
in cooperation with Tactical Air Command

Instructors:

J. M. Alexander
G. C. Born
K. H. Merkel

Sponsored by:

Support Techniques Branch
Air Force Aero Propulsion Laboratory, RTD
F. W. Forbes, Project Advisor
A. J. Zappanti, 1/Lt

BARE BASE DEVELOPMENT CONCEPTS

Karl H. Merkel, Professor of Architecture

James M. Alexander, Professor of Industrial Design

Gilbert C. Born, Instructor of Industrial Design

University of Cincinnati, Cincinnati, Ohio 45221

INTRODUCTION

The research and development papers presented at this conference deal primarily with expandable structures and their application as shelters, boats, antennas, solar collectors, aerospace crafts, space stations, etc. etc.. The project described in this paper, however, will include several other items not necessarily in the expandable structures classification.

The research projects here described are some of the results of an unfunded collaborative exercise in creative problem solving by nineteen students of the College of Design, Architecture, and Art of the University of Cincinnati. The students worked under the direction of James M. Alexander, Professor of Industrial Design, Gilbert C. Born, Instructor in Industrial Design, and Karl H. Merkel, Professor of Architecture, with the cooperation and assistance of the U.S.A.F. Aero Propulsion Laboratory, RTD, and Headquarters, Tactical Air Command.

BACKGROUND FOR THE PROJECT

Students of the DAA College in 1962 prepared a number of design concepts for lunar shelters* with the cooperation of the Flight Accessories Laboratory, ASD, USAF. Personnel of the Aero Propulsion Laboratory were impressed by the performance of the students and believed they were capable of attempting another unfunded short term design research project for the Air Force.

The subject suggested for the project was the "Development of Bare Bases" for the Tactical Air Command; a Bare Base being defined as an airfield having one or more runways, taxiways, and a ramp, but no support facilities. In most cases, the bare base is a commercial airport or an abandoned airfield. It is assumed that facilities such as maintenance, housing, administration, and hospital buildings, etc., are not available. However, any existing facilities are used to whatever extent possible. Facilities and equipment, when not available at the bare base, must be flown in by cargo planes on short notice.

The development of a Bare Base involves problems of town planning, design of buildings and equipment, packaging, and shipping. Problems such as these are typical for the architect and industrial designer. Architectural designers and industrial designers are trained to apply their knowledge of Art and Science toward satisfying the complex physical and psychological environments and facilities which modern man uses and needs. Many recently developed materials, methods, and knowledge have opened new perspectives for the designers in their search for solutions to problems of satisfying these needs.

*Lunar Shelter Concepts Univ. of Cin., F.A.L. A.S.D. 1962.

The Bare Base and its facilities and equipment were proposed as being in need of some re-examination in light of some of the recent developments. Preliminary re-examination indicated a number of problems which as design exercises would stimulate the creative efforts of the student architects and industrial designers.

Nineteen selected fourth year students (ten architects and nine industrial designers) were organized into five design teams, each having two architects and industrial designers (except one team having only one industrial designer).

The DAA College conducts a Co-operative School-Work program in which the architectural and industrial design students are enrolled. The design project was scheduled for a seven week Co-operative school term. The problem was introduced to the students at the beginning of the first week when they received the "Bare Base Development Program.* The students were then briefed by personnel from Headquarters TAC on TAC's mission in limited warfare and on relative successes and/or failures of recent Bare Base exercises. Some items or operations needing improvement were pointed out during the briefing with the suggestion that the students make some proposals for more satisfactory solutions.

The design teams then researched the Bare Base operations and the various required subjects with the assistance of information and manuals furnished by TAC, and by personnel from A.P.L.. The teams developed statements of their philosophy of Bare Base Approach and prepared design proposals for the specified items.

At the end of the seventh week of work each team submitted a twenty-minute slide presentation of their concepts at Wright-Patterson Air Force Base. This paper presents several illustrations and proposals selected from the students' work.

*Bare Base Development Concepts Univ. of Cin., A.P.L., RTD, U.S.A.F.
1965, pp. 3-8.

REQUIREMENTS OF THE "PROGRAM"

Personnel from Headquarters TAC, the Aero Propulsion Laboratory and faculty at U.C. prepared a Program outlining the requirements for the design projects, a brief summary of which follows.

TAC operations around the world depend upon suitable operating bases known as "Bare Bases". These bases must be equipped quickly from a rear Main Operating Base with all weapons systems and support facilities appropriate to meet a particular threat. To facilitate quick mobility the material and personnel have been arranged into "packages" of various items.

When the need arises, a bare base is selected in the critical area and a survey team inspects the site. The survey team recommends which "packages" are needed to make the base operational. These "packages" are flown in to the base in rapid succession according to a prearranged sequence of priorities of need. Units of the Combat Support Group arrive at the same time to begin development of the site and to ready the field for arrival of tactical forces.

Bare base operations are planned for a minimum of 30 days occupancy. The development of the bare base must be accomplished within certain prescribed time limits and according to predetermined sequences of events.

The base which the students were to develop was to provide for a total complement of 1100 men (including Tactical, Maintenance, and Support personnel and a Provisional Headquarters) together with necessary aircraft, shelters, and full support facilities and equipment.

Each team of students was assigned a site map chosen from a selection of TAC and SAC airfields in various parts of the world. The site maps were previously altered to eliminate certain existing facilities in order to simulate typical Bare Bases.

The students were required to research Bare Base operations and to propose a list of priorities for air lift items and erection of operational and support facilities, as well as to solve design problems in four specific categories.

The four design problems were:

1. A site development plan, in model form with movable components, showing shelters, vehicles, and equipment. A photographic record was

to be made showing the sequential development of the base at meaningful stages and calibrated to a time schedule of events.

2. The design of a shelter system, showing in model form or drawings the procedures of packaging, handling, erecting and demounting the shelters.

3. The design of a multipurpose land vehicle to accomplish normal transportation and other functions around an airfield, and to present a model and drawings to demonstrate flexibility of use.

4. Survey equipment needs, and present drawings of new ideas for one or more items such as airstrip lighting, fuel handling equipment, personal equipment, etc..

RESULTS OF THE DESIGN RESEARCH PROJECT

The students recognized a number of items or procedures which appeared to be in need of restudy and new design proposals. Technology has moved so rapidly that it has made obsolete many of the items in present use which have not changed their design or materials of construction for years. Some of the concepts proposed by the students and presented in this paper are entirely within practical limits of today's materials and methods. Some of the proposals are based on predicting possible applications for ideas and materials which are still in the early experimental stages, or perhaps are just dreams of what may be.

The concepts which the students presented were published in February 1965 by the Air Force Aero Propulsion Laboratory in a booklet entitled "Bare Base Concepts". The publication does not necessarily indicate Air Force approval of the concepts. Whatever actual use any of the concepts may have, might be open for question, but it is hoped that the ideas presented in the following pages by a few illustrations and portions of the text from the booklet, may disseminate some of the information the students collected and may stimulate further research in these areas.

TEAM 1

Duane Gordon	Arch. '66
Dale Harris	I.D. '65
John McKnight	Arch. '66
John Plut	I.D. '65

SHELTER CONCEPT

The shelter is a suspended structure with three basic units on a single fiberglass member in the center of the three-cluster unit. (Fig. 1)

Time required to erect this thirty-man shelter is forty minutes for six men.....

The exterior skin of the structure is fabricated from 1/4 inch polyurethane foam of the flexible type. Laminated on both sides of the polyurethane foam will be a layer of mylar and woven nylon fiber. It was found that the "k" (insulating) factor of this material was as low as .22 thus demonstrating the ability of this shelter material to be used in a variety of climates. It is also worth-while to note that the tent skin weighs approximately 0.1 pound per square foot.

One tent unit complete with a floor can be folded down and rolled into a package of thirteen (13) feet long by eighteen (18) inches in diameter with its mylar flooring rolled around the outside to protect the unit in shipping.

A conservative estimate of the weight per one ten man unit is approximately four hundred and fifty pounds.....

HANGAR

.....We decided that the most efficient way to support a hangar structure is to suspend the enclosing material with relatively light tension cables.....

The structure consists of six pylons and six tension cables from which is suspended the wall and roof of the hangar (Fig. 2). The pylons would be made from high strength fiberglass.....

This hangar has six sides forty-five (45) feet long. It will accommodate two F-4-C jet fighters (Fig. 3).....

The hangar has two doors for plane access located on opposite sides of the hangar. These doors are made of the same material as the walls

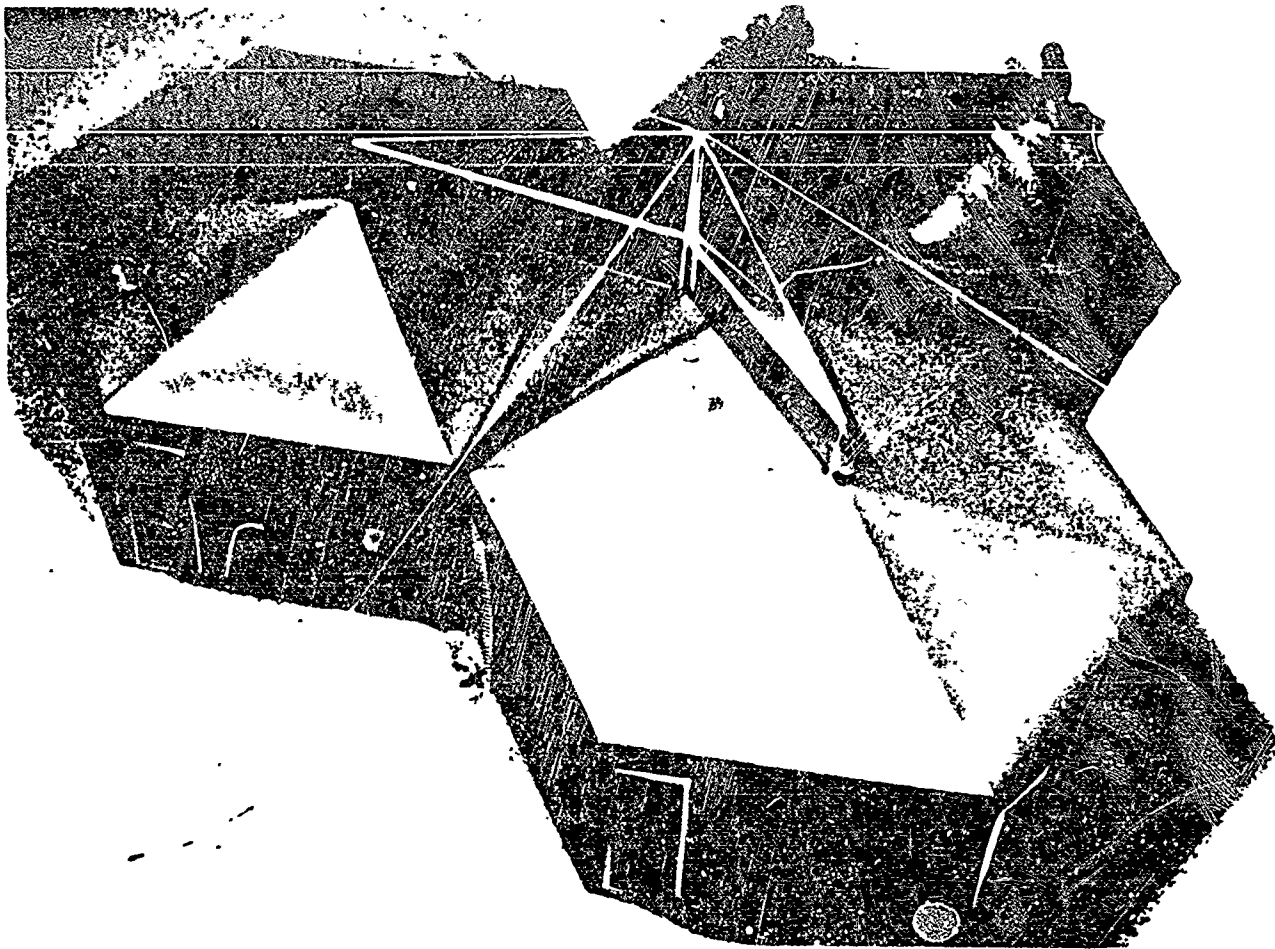


Fig. 1: Aerial View, placing last unit of shelter in place.

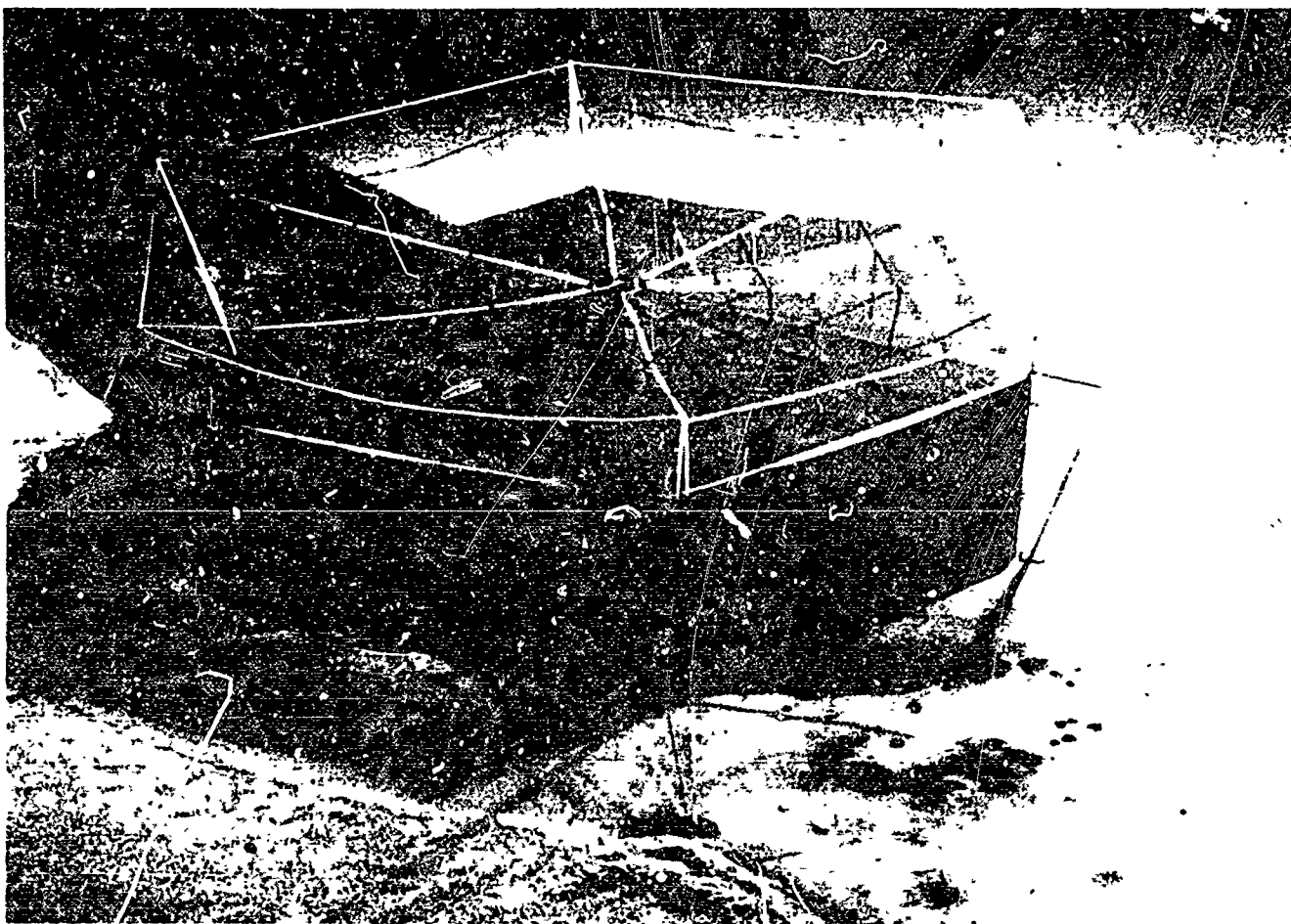


Fig. 2: Aerial view of hangar.

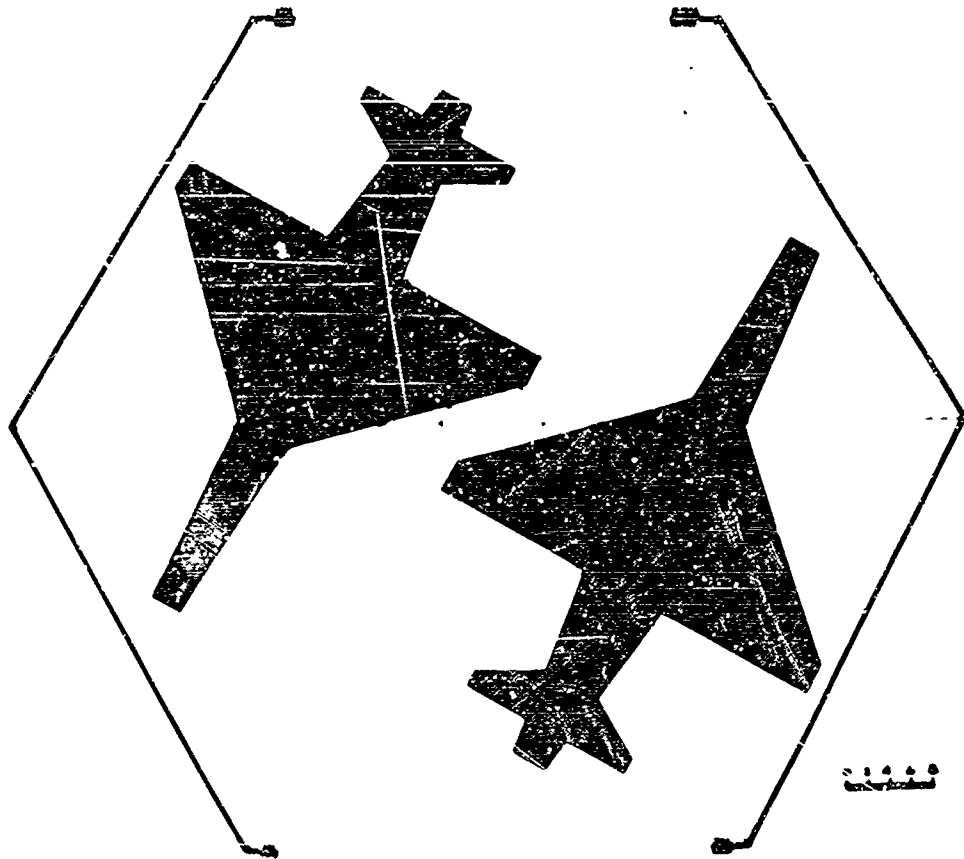


Fig. 3: Hangar plan, housing for two F-4C aircraft.

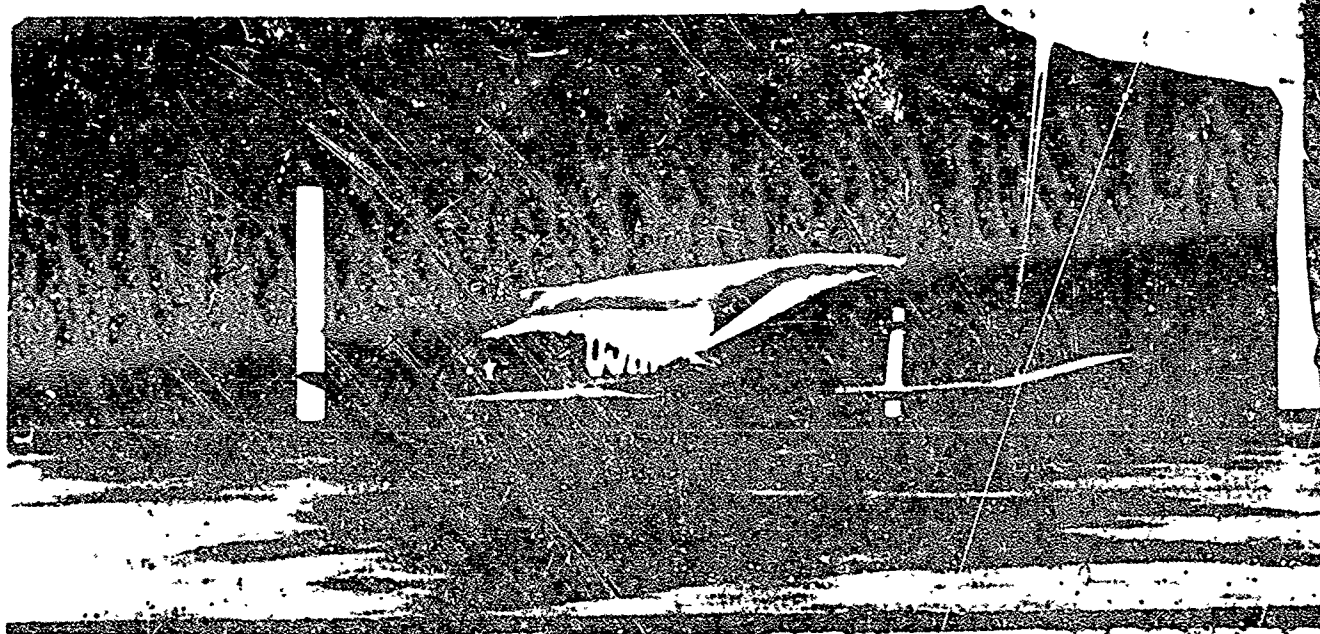


Fig. 4: F-4C fighter at hangar door.

and ceiling which is the same as the smaller shelter. They fold (on overhead rollers) to the sides giving a forty-five foot clear opening. (Fig. 4).....

UTILITY VEHICLE SURVEY

.....According to TAC Manual #00-12 there are eighty-eight (88) vehicles allotted in the average base support group. These vehicles may be broken down into three categories: light, medium, and heavy duty in accordance with their own specific weight and the functions they perform.....It is felt that the light and medium duty function could be performed by a single vehicle type located somewhere between the two classes.....

VEHICULAR CONCEPT

In order to fulfill the required functions, the new vehicle must be flexible to adapt to the various situations which would include variations in terrain and climate (Fig. 5). A vehicle which would perform well on the hard, even surface of the runway system would not do well if the off-runway terrain was sand or mud.....A fluid-drive system was used to reduce moving and complex parts and transmit power from the engine to the wheels through flexible tubes rather than rigid drive shafts, universal joints, gear boxes, differentials, etc. Now that there are no rigid connections to the wheels, they can be made to rotate 360 degrees to allow the vehicle more flexibility. (Fig. 6)

The engine should be light for its power output, efficient in terms of fuel input, easy to maintain, and reliable. An engine has been developed which is particularly well suited to our fluid drive concept. The engine (Fig. 7) was designed by Harold Kosoff and consists of a tube with two pistons which come together in the center of the tube to form the combustion chamber.

Since the vehicle has the ability to raise or lower itself on its own suspension, the ground equipment for the fighter aircraft could be designed to allow the vehicle to back under the equipment, raise itself and the load, and carry the equipment to the job. (Fig.8)

The vehicle has the ability to operate at the same speed and with the same amount of maneuverability in any direction. This concept necessitates giving the driver seating and controlling facilities which will accommodate the multi-directional movements.....

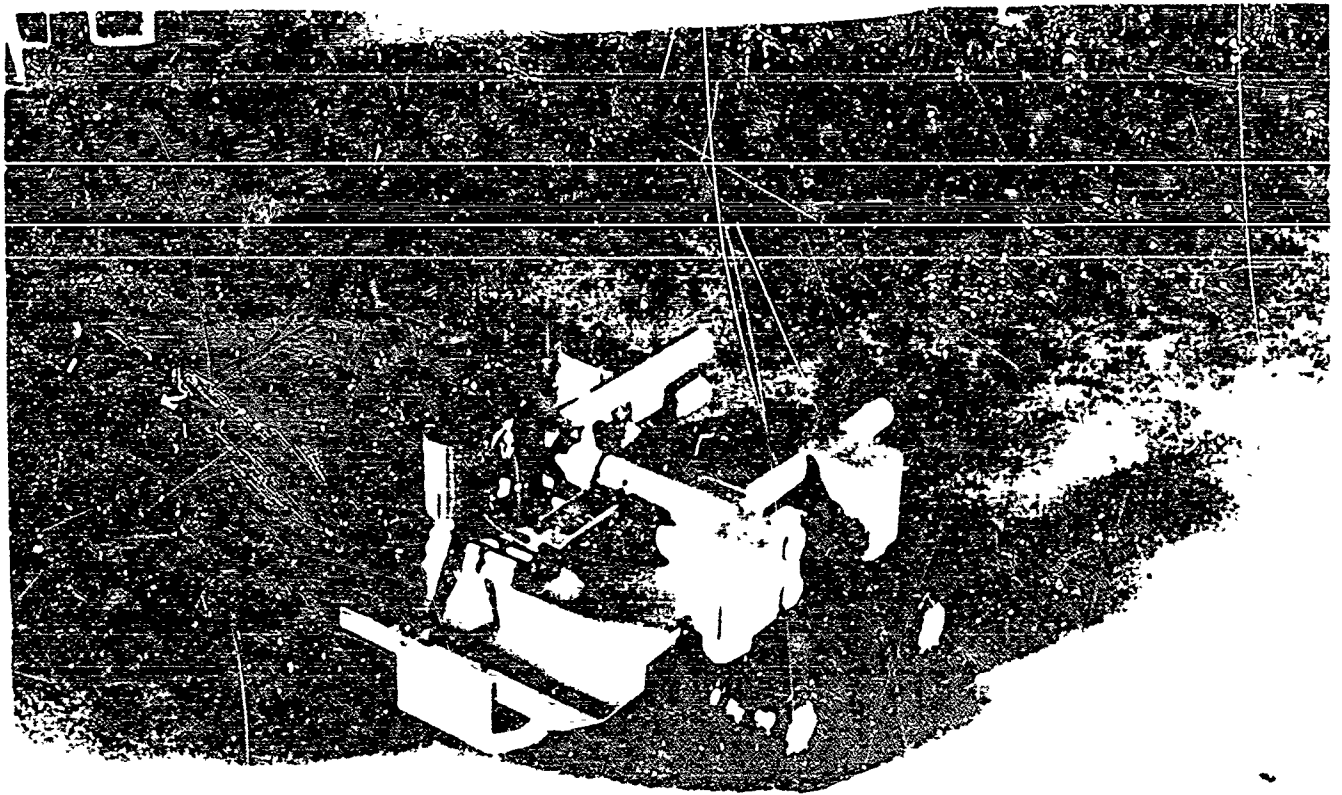


Fig. 5: Vehicle, showing open V-shaped frame.



Fig. 6: Vehicle showing wheel rotation.

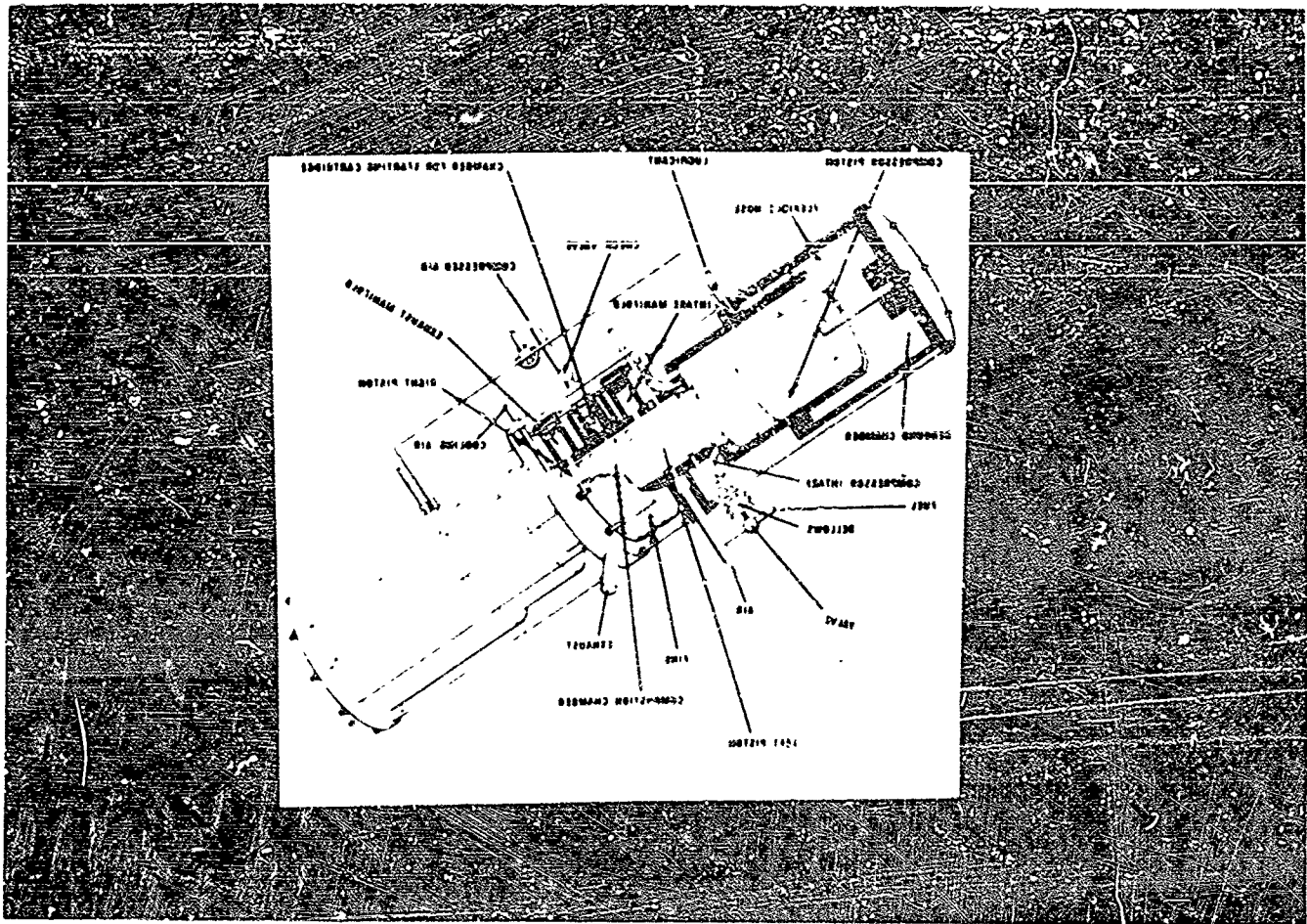


Fig. 7: Drawing of Kosloff engine.

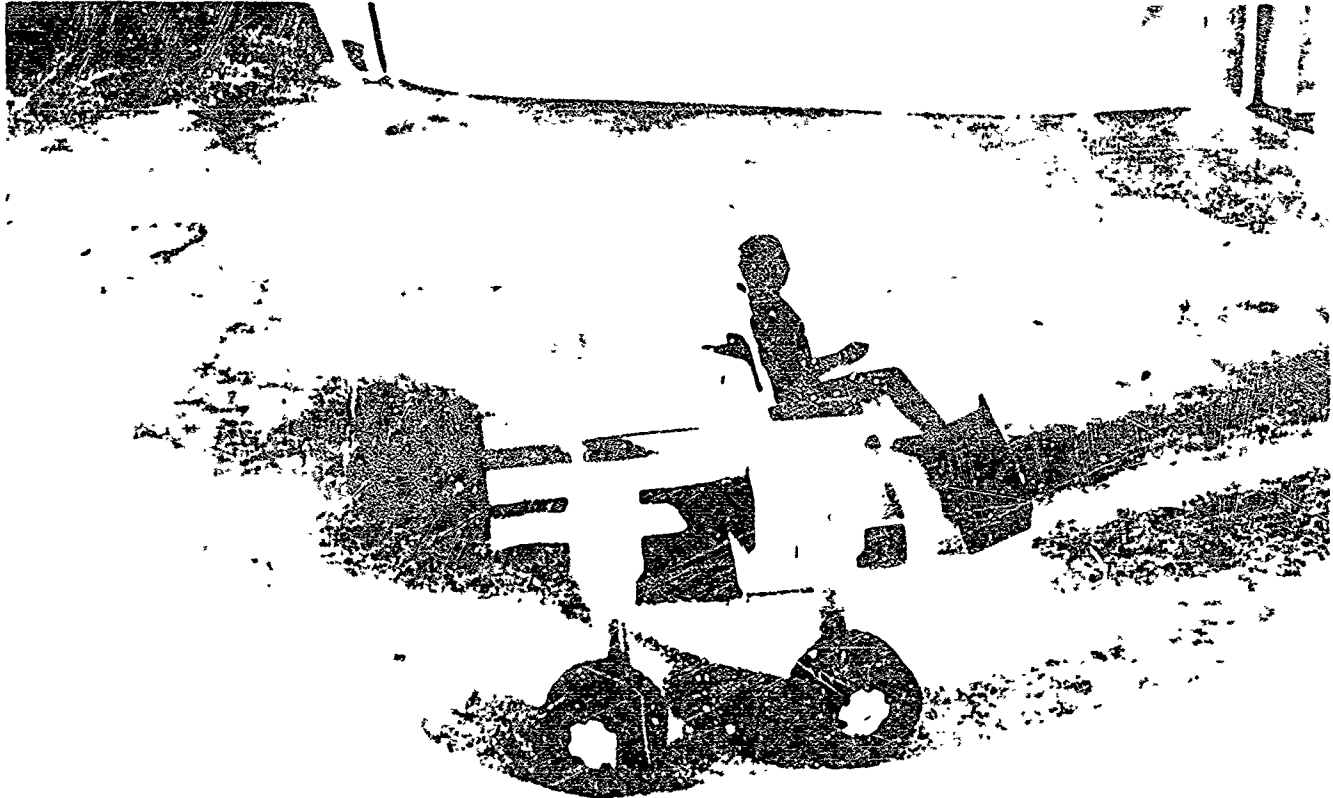


Fig.8: Vehicle in raised position.

TEAM 2

Ruth H. Grad I.D. '65
Thomas C. McMullen Arch. '66
David K. Oldham Arch. '66
John W. Wissinger I.D. '65

TENTS

The billeting structures are sixteen by thirty-two foot inflatables each of which houses twelve men. This tent is made up of four individual sections (Fig. 9) which make the one large one. (Fig. 10)..... The package itself is the Royalite floor with the inflatable part of the structure already attached to it.

In shipping, four of these packages are strapped together to make a larger package two feet by four and one-half feet by eight feet.....The inflatable parts are zipped together, and the end panels are then zipped in.

A three-man team would most likely be used to erect this structure, and four of these teams could erect billeting for eleven hundred men in five hours.....

The messing structure and hospital are the same type of unit as our billeting structures. The difference is that the erected units are twenty-four feet by forty feet because of the need for extra space in both.....

HANGAR

Our hangar structure is also made of inflatable material but, due to its larger size, it is constructed in a somewhat different manner. It consists of a double layer of tubes with double zippers so that its three vaults can be supported properly. (Fig. 11)

The three vaults are twenty-five feet across and are twenty-eight feet above ground level at the highest point. The sides have sixteen foot vaulted openings to which can be attached smaller tents for utility or for light or ventilation (Fig. 12). The end panels are not inflated but are flat and roll up and down.....



Fig. 9: Shelter in process of inflating section #2.

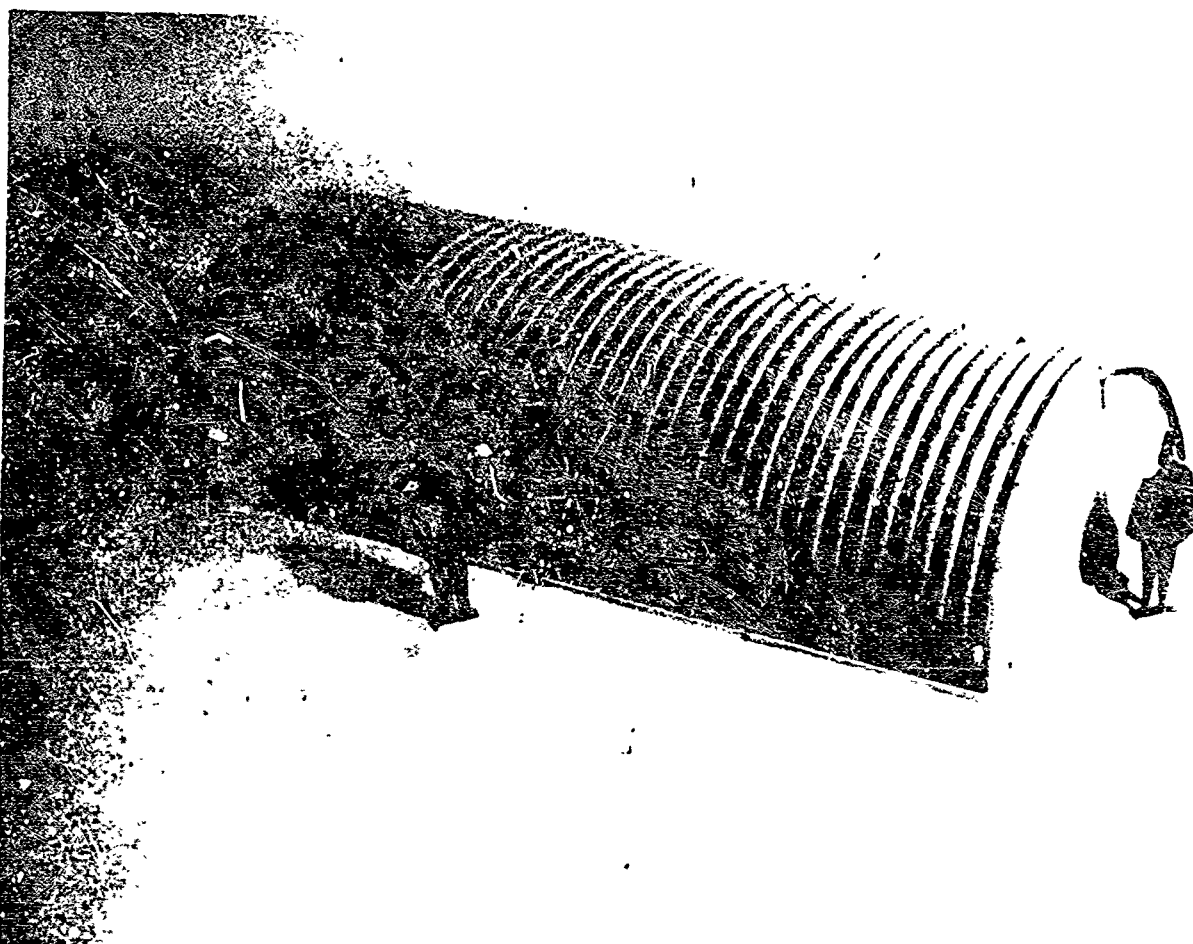


Fig. 10: Twelve-man inflatable shelter.

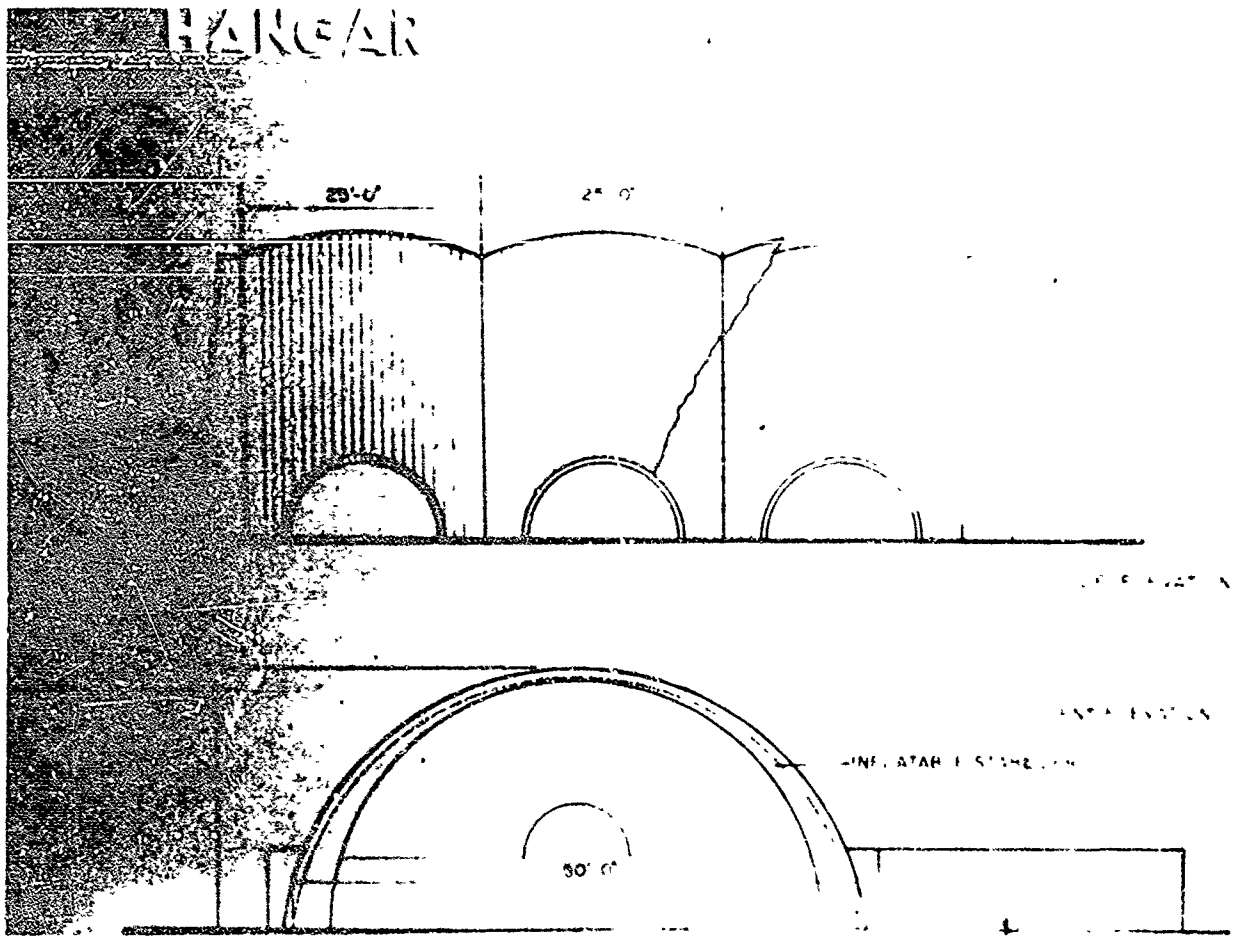


Fig. 11: Drawing of hangar.



Fig. 12: View of hangar with attached wings.

VEHICULAR CONCEPT

.....The standard trucks now in use have too much dead weight. These trucks were designed for road use and are too general for this specific project. Also, the cabs have much unused space.

Our vehicle should be specifically for a Bare Base. We cut down on the unusable weight and have a cab to carry only the driver...
...

The two cabs we plan to use attach to a basic trailer with a posilock (Fig. 13).....

Both the cab and trailer use lightweight materials in their construction to lighten their shipping weight. The trailer has an expanded Royalite base floor over molded ribs to give it additional strength. The frame is made of lightweight aluminum alloy. The tires under the trailer are of the "air-sack" type and required very low pressure (7 psi). These provide an easy ride without regular suspension.....

A power take off at both front and rear operates many of the other attachments for the cab. A crane attachment on the front utilizes this as well as the same weight counter-balance that the fork lift uses. Other parts that can be worked in this manner include: grader blade, weed cutter, runway sweeper, ditch diggers and crane (Fig. 14).....

RUNWAY LIGHTING

Runway Lighting is to have radio operated lights which need no generator and wires along the airstrip.....

The individual light is a gas cylinder in a tubular housing which contains a pilot light and a radio control box. When the radio control receives its signal, the valve is opened to emit the gas which is then lighted by the pilot light. (Fig. 15)

The top has directional mirrors which receive the light from the parabolic mirror around the light. These directional mirrors cause the light to be at its strongest when looking directly down the runway.....The fuel would last approximately thirty hours. This is based on the theory that the lights are on for only about one hour per night. Thus, a unit would be a thirty day lighting supply. At one hundred fifty to two hundred foot spacing of the lights, the runway should be sufficiently illuminated.

FUEL

Our plan for storing and transporting fuel is a semi-rigid plastic tank in a frame on wheels (Fig. 16). The tank has a thirty-six hundred gallon capacity. This enables it to fuel three F4C's.

The tanks would be stored until needed and then, with the same posi-lock our other vehicles have, would be driven from the storage area to the airstrip by one of the cabs.

The tank would be filled at the Main Operating Base and shipped to the Base Base. As the fuel is used, the semi-rigid plastic tank begins to deflate down into the frame structure which is braced with steel ribs to hold the tank.

When the entire tank is emptied, it lies on this steel base. The side pieces, which are made of telescoping tubular metal, are then collapsed so as to make a compact unit to ship back to the starting base to receive more fuel.....

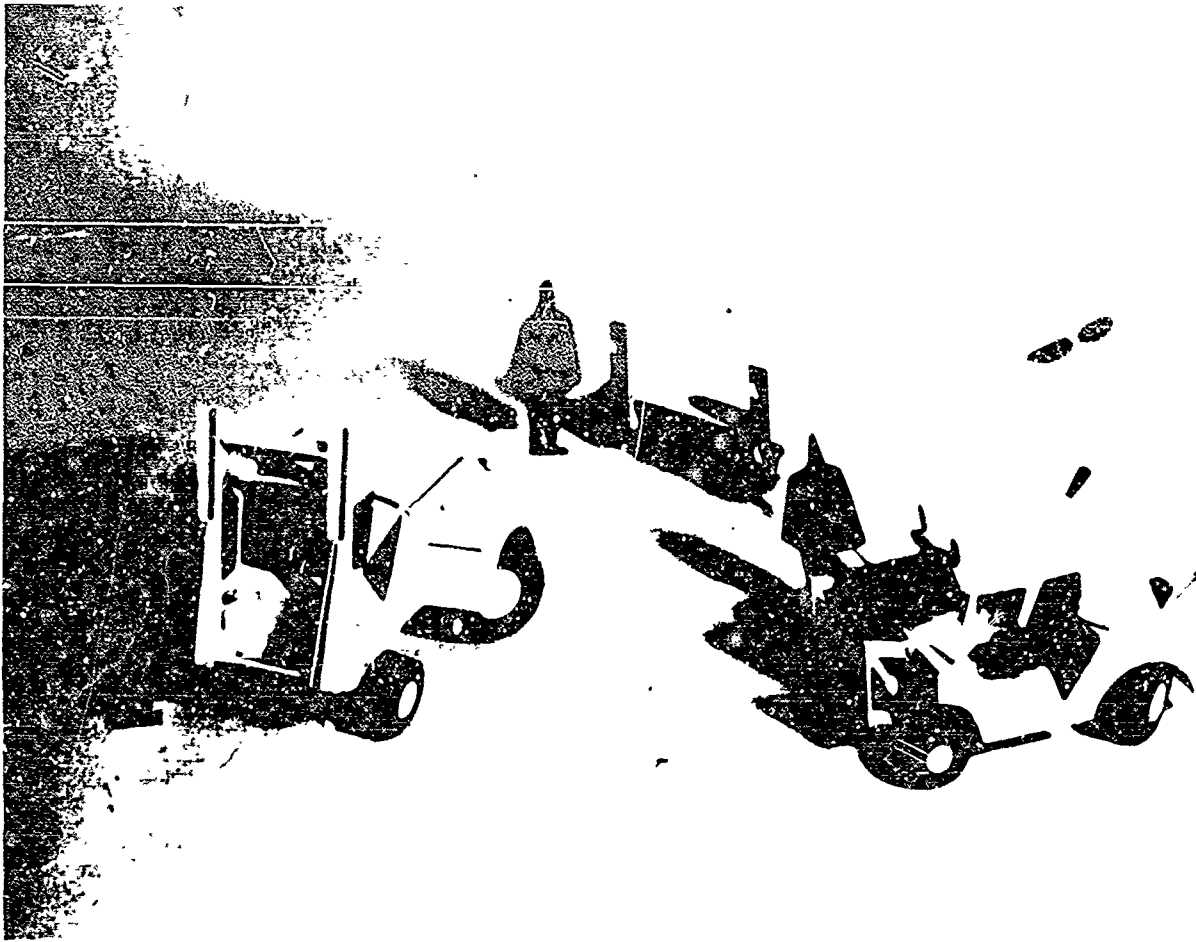


Fig. 13: Vehicle components (two cab units, one trailer).

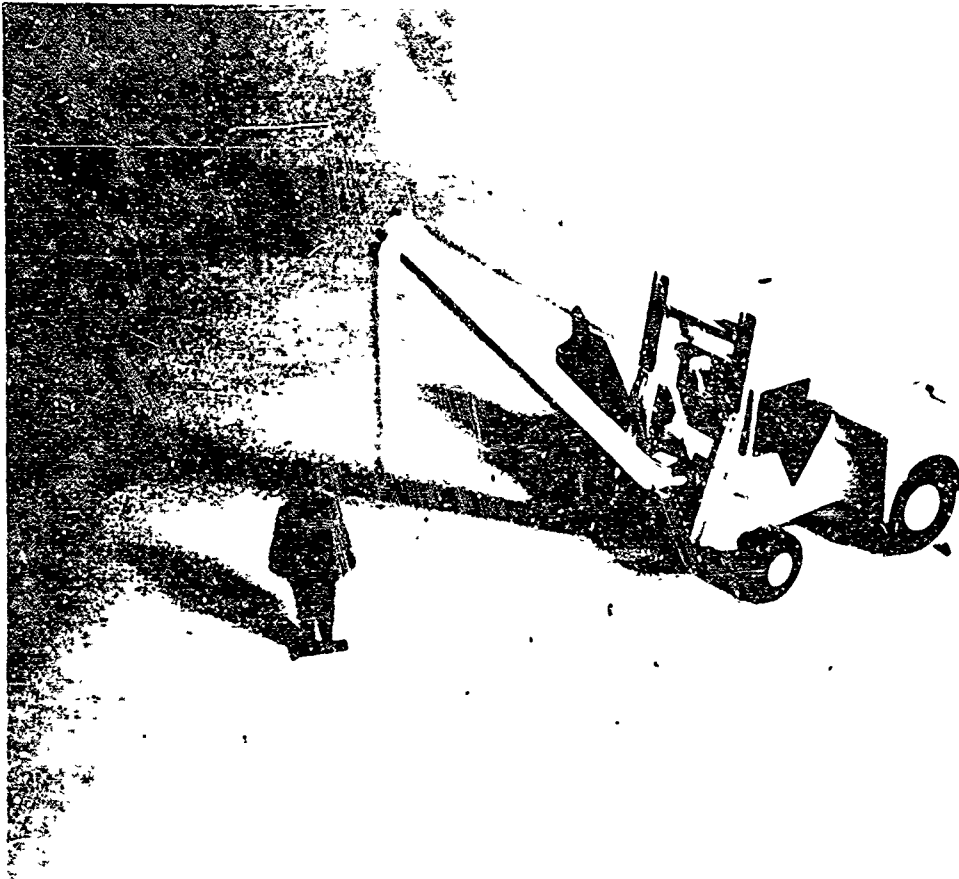


Fig. 14: Crane attached to cab unit.

RUNWAY LIGHTING...

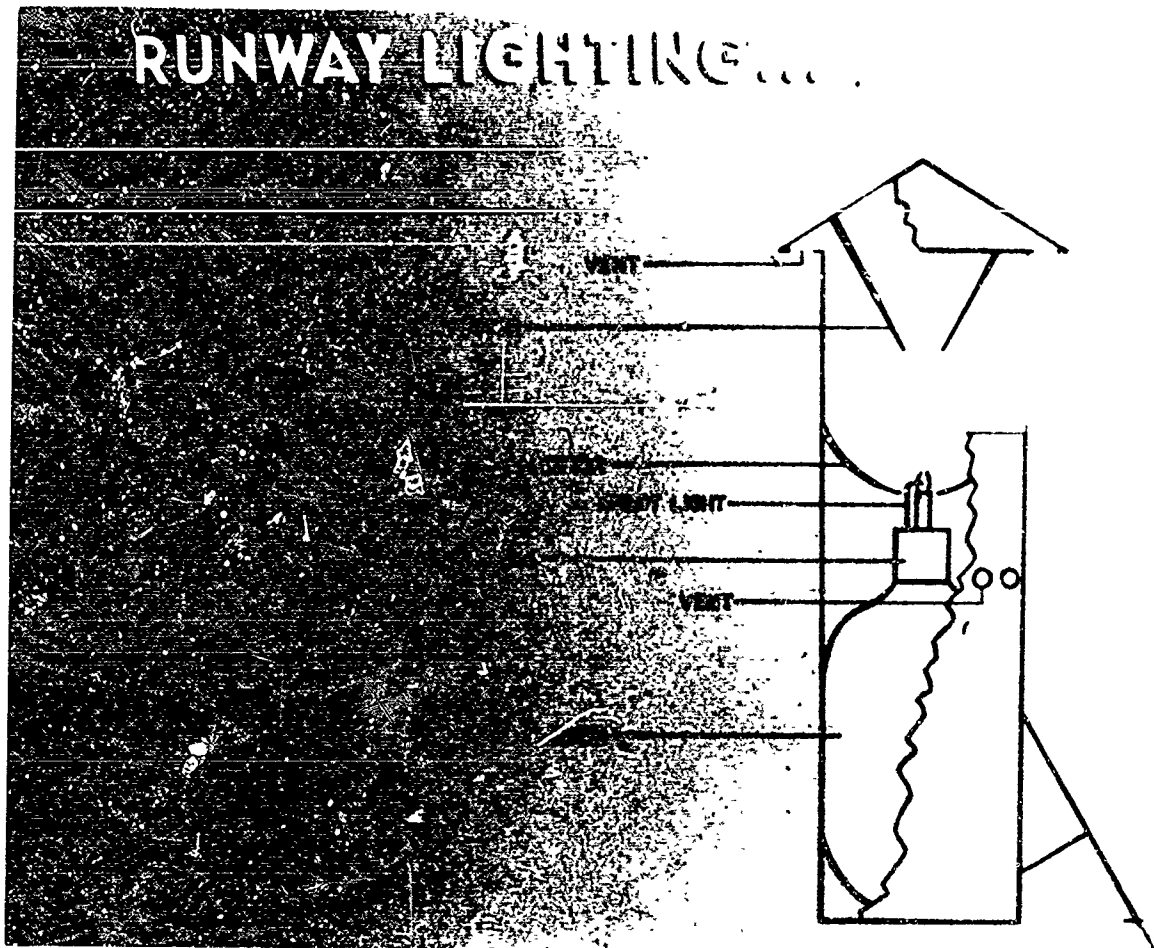


Fig. 15: Drawing of Runway Lighting Unit.

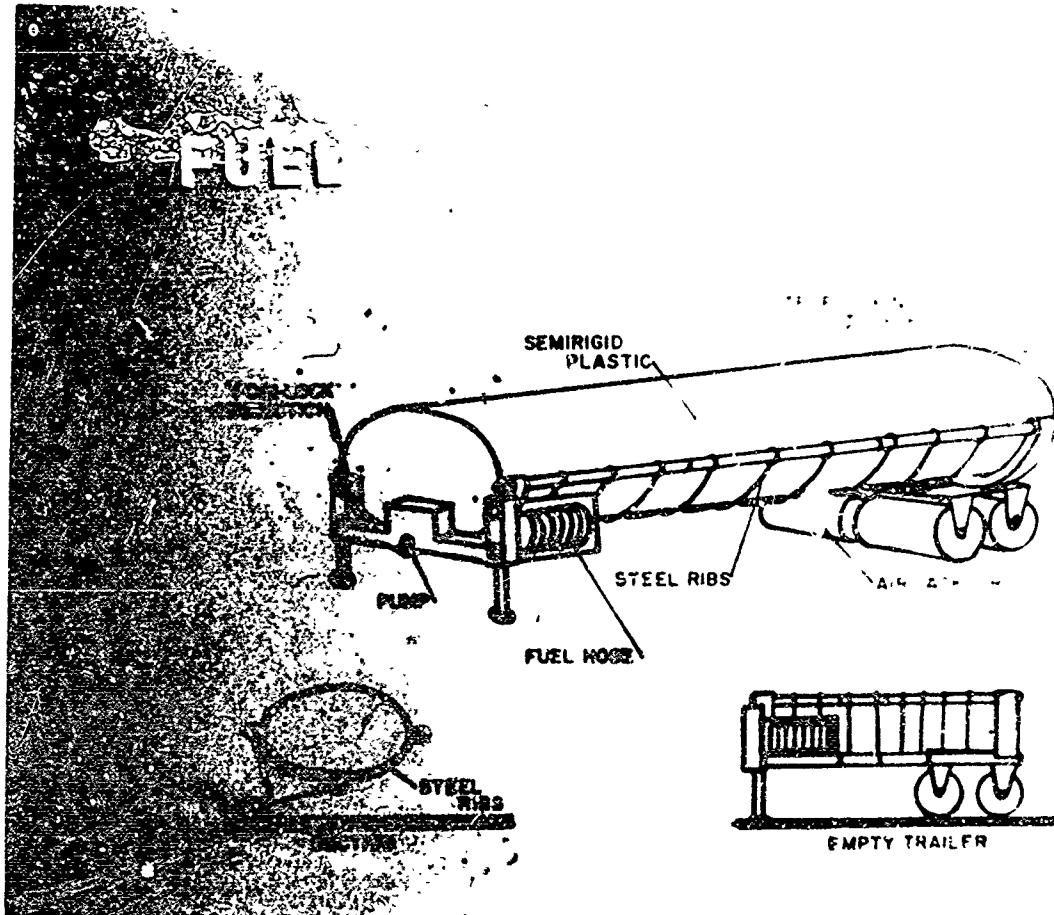


Fig. 16: Fuel Trailer.

TEAM 3

Hans Bleiker	Arch. '66
Jerry Chuck	I.D. '65
Philip Joehnk	Arch. '66
Robert Wiesman	I.D. '65

SITE ANALYSIS

Our site is an elaborate airfield on the Atlantic Coast. In analysing the airfield we find that it would be best to use one major runway, one alternate and one for take off of TAC alert aircraft only. We would set aside 3 aircraft from each of the two squadrons to be designated and placed on an alert status at the northern end of the field.

The terrain of our site is very advantageous to the security of our base. Along the western coast there is a cliff rising 200 feet above the water. From the cliff running easterly there is a 2% slope. In locating the fuel storage areas, we use natural drainage to our advantage. In the event of fuel leakage it will not drain across the base. We designate two areas for fuel storage, thereby reducing the vulnerability of attack. In the same manner we designate two munitions dumps.

Special features of the site are a large, unbroken apron space and a small mound located centrally within the airfield complex. The latter lends itself quite readily for an air control center. The former will be used for a terminal area, TAC ready area, motor pool, run-up, hangars and maintenance of aircraft and vehicles. This allows all of the units to be located within close proximity of each other.

There is a main road running North and South to the east of the field with branches leading to the apron space, a taxi way and the southern fuel storage and munitions area. Access to the northern fuel storage area will require a minimum amount of paving. The northern munitions dump and liquid oxygen production and storage will be along the main road. Air police will set up check points at all intersections with main offices located at the junction of the branch that approaches the terminal area. Fire and Rescue units would be located between the main runway and the alert runway with easy access to both. Initial utilities for the entire base would be located just east of the terminal area. Billeting, messing, administration, the hospital and all special housing will be sited east of the main road away from the main operating areas. Larger support utilities will be located in this area. A small amount of grading and paving will be necessary in preparing this camp area (Fig. 17).

PRIORITIES

In setting up priorities we vary from the Gray Eagle system by a different break down and sometimes by a different sequence. This system, like the present one, will work except when special circumstances prevail.

FIRST PRIORITY

- A. Air Police to set up security immediately for the base.
- B. Establish Terminal Area, Fire and Rescue, and Air Control to take care of the arrival of initial flights.

SECOND PRIORITY

- A. Initial utilities for operation of the airfield only.
- B. Motor Pool and Ground Equipment.
- C. Support utilities to be established for the arrival of additional personnel.
- D. Billeting and Messing.

THIRD PRIORITY

- A. Maintenance and Run-up Area.
- B. Initial fuel storage, munitions and liquid oxygen.
- C. Operations.
- D. Increased Billeting and Messing.

From the loading of the C-130's at the rear main operating base to the end of our Third Priority presently takes 72 to 96 hours. With the use of the equipment we have designed we believe this time will be cut down considerably.

FOURTH PRIORITY

- A. Arrival of Tactical Air Craft.

FIFTH PRIORITY

- A. Administration Building.
- B. Hospital.
- C. Special Housing.

SIXTH PRIORITY

- A. Hangars
- B. Erection of remainder of base and camp.

SEVENTH PRIORITY

- A. Improvements based on projected length of tenancy.

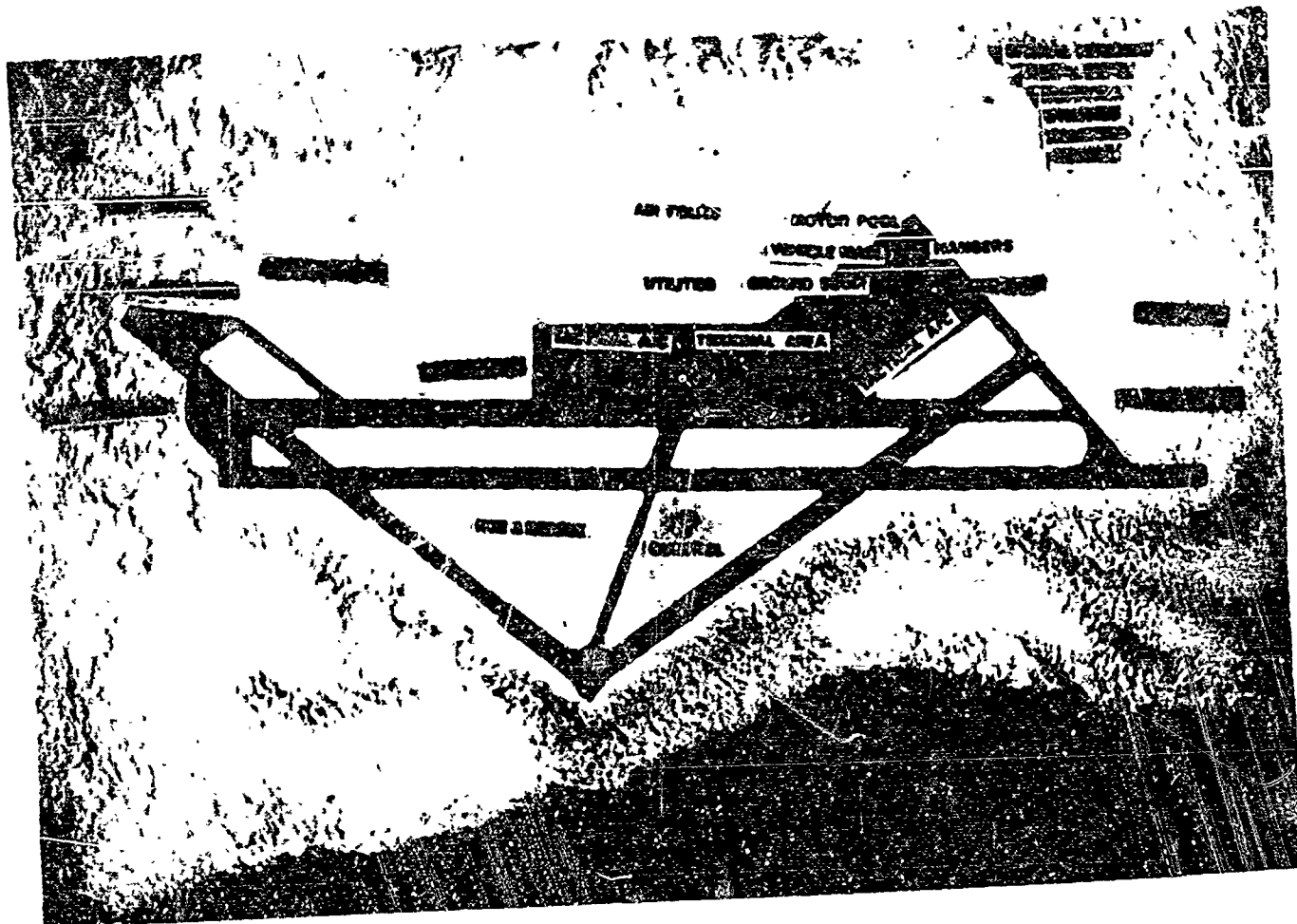


Fig. 17: Aerial view of Developed Site.

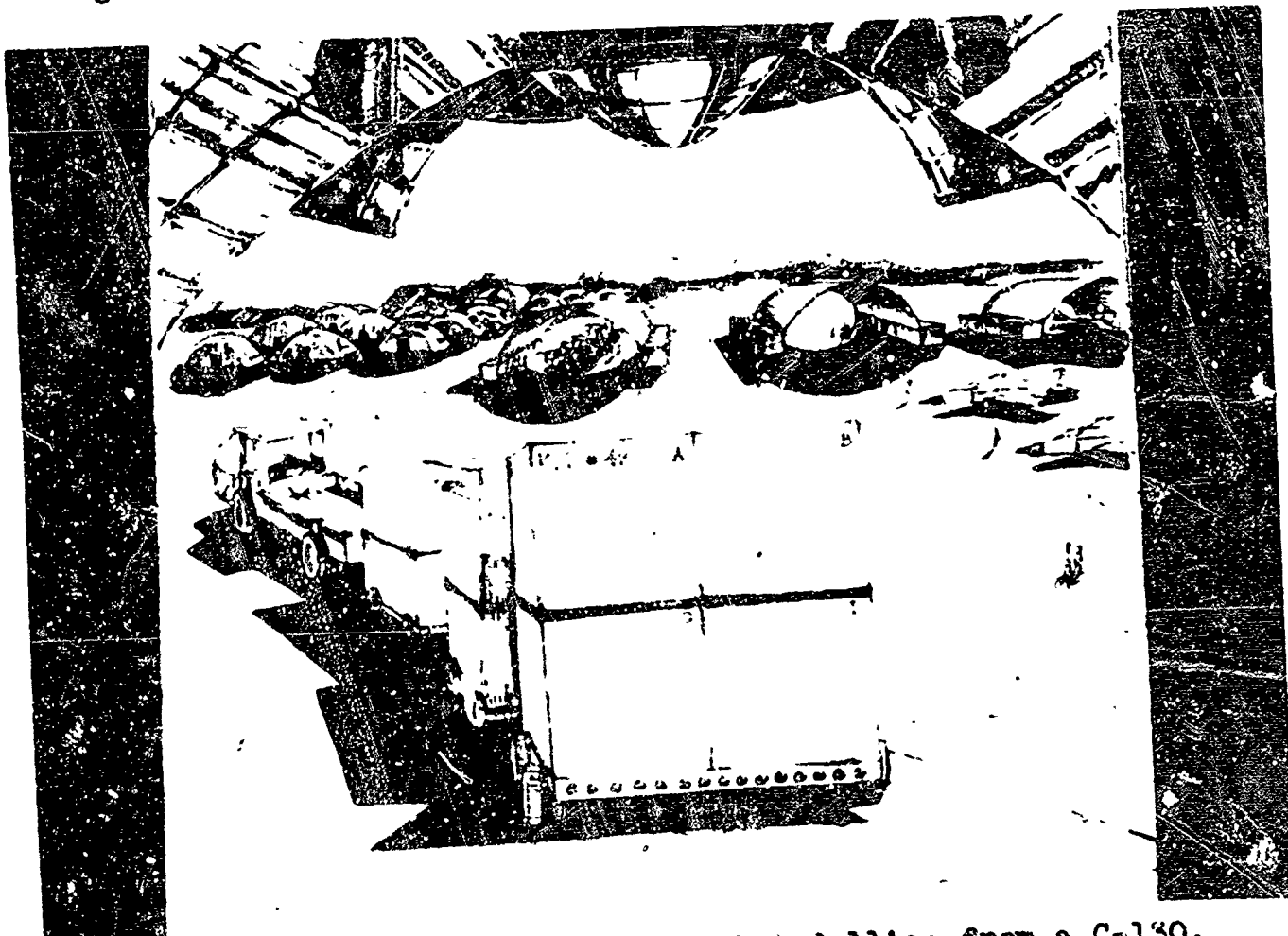


Fig. 18: Unloading a train of pallet-dollies from a C-130.

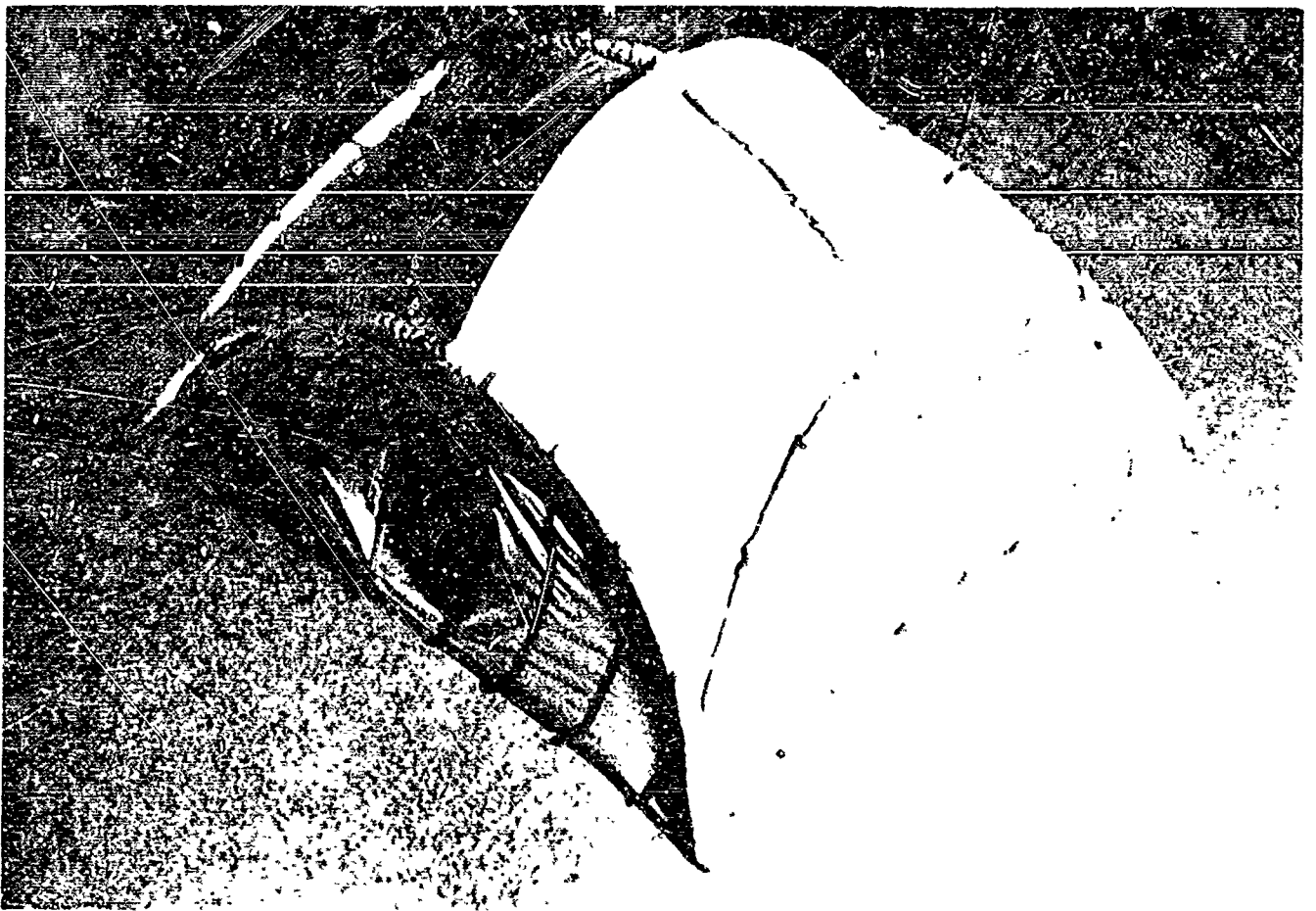


Fig. 19: Aerial view of erected shelter.

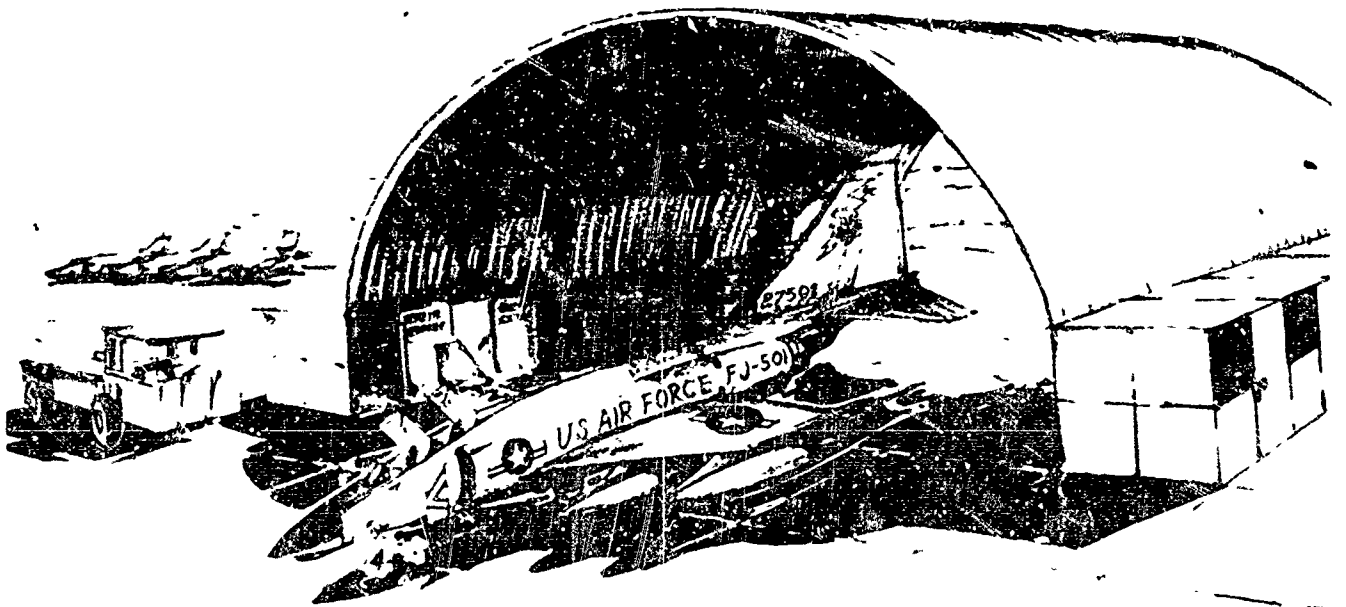


Fig. 20: Hangar with flanking service cubicles.

INTERPRETATION

We interpret this problem to consist of reducing the effort of making a bare base operational. This we have accomplished by pursuing the problem in two areas.

The first area of attention is aimed at reducing the number of required support flights; the second area of attention eliminates much of the labor on the base. Some of our designs are successful in one of the two areas, others in both.

The number of C-130 support flights can be reduced by making the required equipment lighter and/or making more than one use of that equipment.....

PALLET-DOLLY SYSTEM

To accomplish the unloading of the C-130's faster and with less effort than the present method, we have designed a pallet-dolly system (Fig. 18). All equipment is loaded on wheeled pallets of 8' - 0" x 8' - 0", and in the case of longer items on wheeled pallets of multiples of this module. Rather than having a forklift unit carry equipment from the plane, our dollies are pulled out of the aircraft either one by one by a small vehicle or en masse, depending on the weight of the contents. A C-130 will hold five dollies.

PERSONNEL SHELTER

The 26' - 0" x 26' - 0" tent, housing twelve men, is supported by four pneumatic main arches (Fig. 19). These arches are in turn braced from each other by two flatter pneumatic arches. One-cubic-foot compressed air bottle (4000 psi) is used to inflate the arches simultaneously to approximately 5 psi. The fabric skin is attached to the ribs and is self erecting when the structure is inflated.....

HANGARS, ETC.

.....The one-foot diameter hose from the fuel containers are purged with nitrogen and then used as structural members. The 400 feet of hose on one reel is made up of five 80' - 0" sections connected by 2-1/2" unions. Each of the sections becomes a pneumatic arch with a 50' - 0" span. As these arches stand side by side, one fuel rack accounts for five feet of the total 50' - 0" hangar space, one C-130 load--or five racks make 25 lineal feet of hangar. A 100' - 0" x 50' - 0" hangar would require the hose of four C-130 loads. Only a portion of the fuel containers are used in this way, the majority remaining in circulation.....

The hangar arches rest on the welded-pipe fuel racks rather than on the ground. A waterproof membrane is pulled over the entire arch system (Fig. 20). As this system does not use up hose and racks at the same rate, different combinations are illustrated for the messhall complex (Fig. 21).

MULTI-PURPOSE VEHICLE

In an effort to reduce the inventory of vehicles, we have designed a light multi-purpose vehicle which is capable of performing several of the less critical tasks. With attachment parts, it can be used for carrying personnel, light hauling, forklifting, heavy carrying, grading, and runway sweeping (Fig. 22).

A small turbine power plant located under the bed, drives the wheels and all other systems via hydraulic transfer of energy. The wheels are attached to the bottoms of four large hydraulic actuators which are capable of supporting the chassis at variable heights from two to six feet off the ground.....

FUEL CONTAINERS

Instead of shipping the fuel in 500 gallon rubber tanks, which have to be largely manhandled, we transport our fuel in 8' - 0" high rack which contains 2250 gallons and is carried on one of the 8' - 0" x 8' - 0" dollies. The rack holds a 400-foot spool of 1' - 0" diameter hose containing the JP-4 (Fig. 23).

COOK'S STOVE

The cook's stove (Fig. 24) takes advantage of the facts that heat can be reflected effectively and that JP-4, a high temperature fuel, is available on the base.

Individual burners provide direct heat for the hot plates and the griddle. A large vertical parabolic reflector directs the heat to the oven at the far end of the stove. This oven is based on the camper's reflector oven. The heat is thrown evenly, from the top and the bottom, onto the baking shelf by the two flat reflectors.....

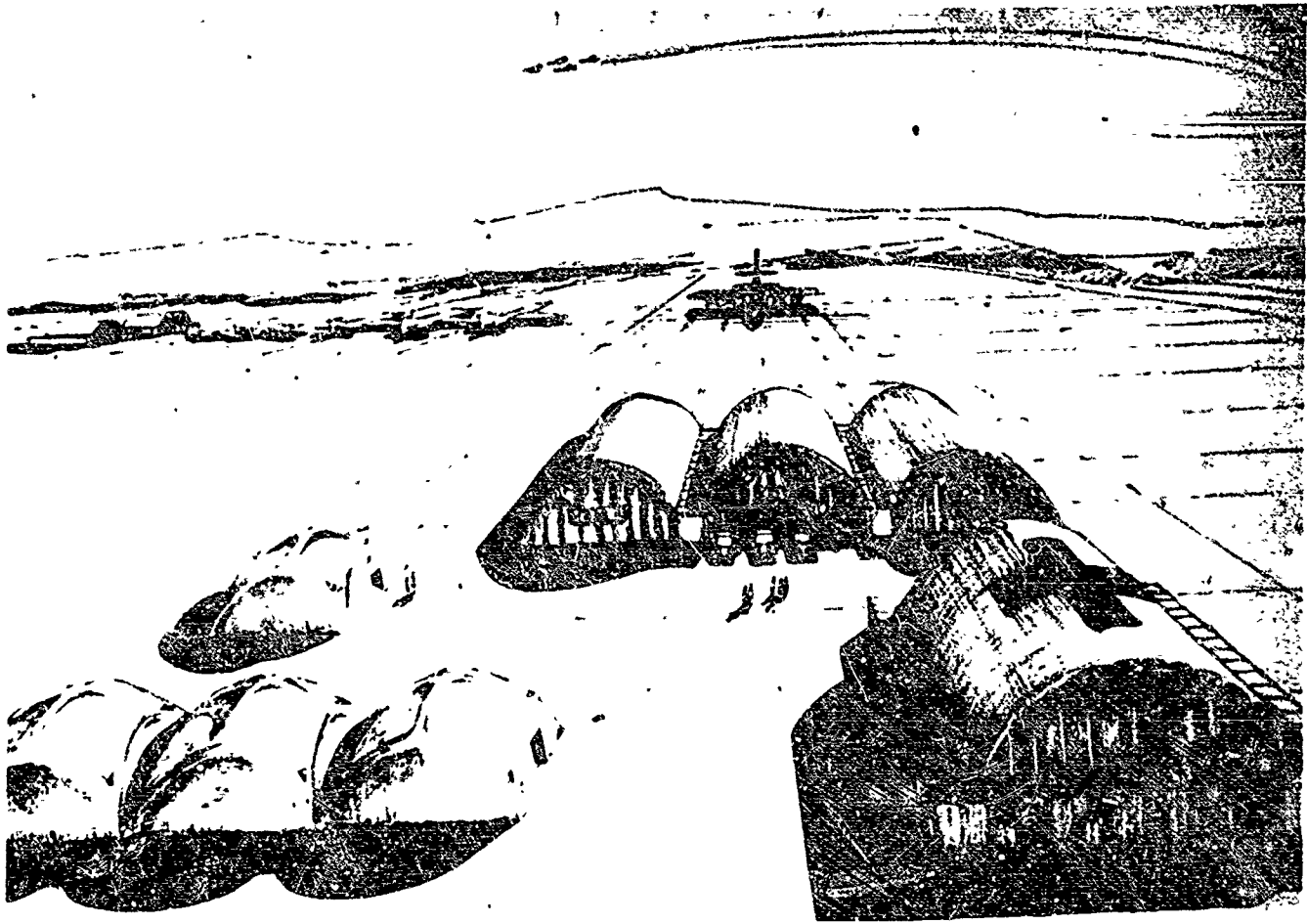


Fig. 21: Adaptations of shelters for billeting, mess halls, and hospital.

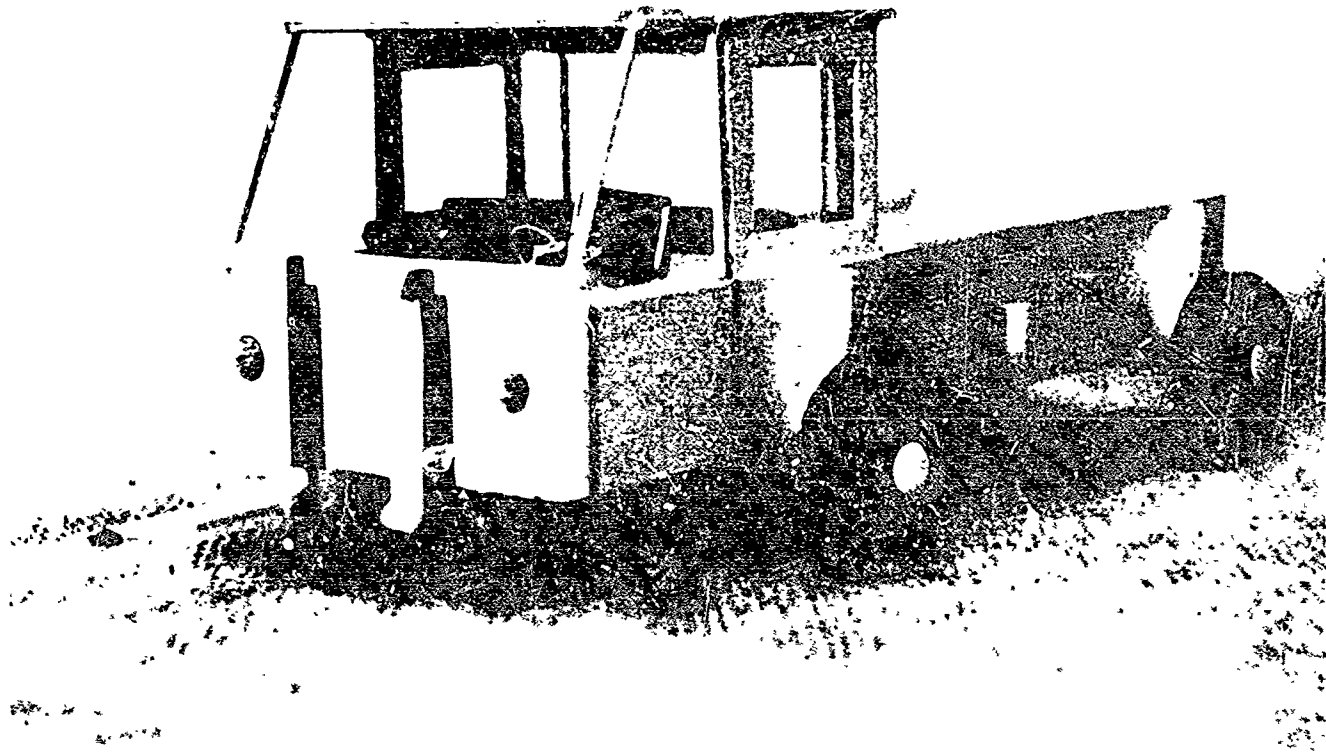


Fig. 22: Multi-purpose vehicle.

COOK'S STOVE

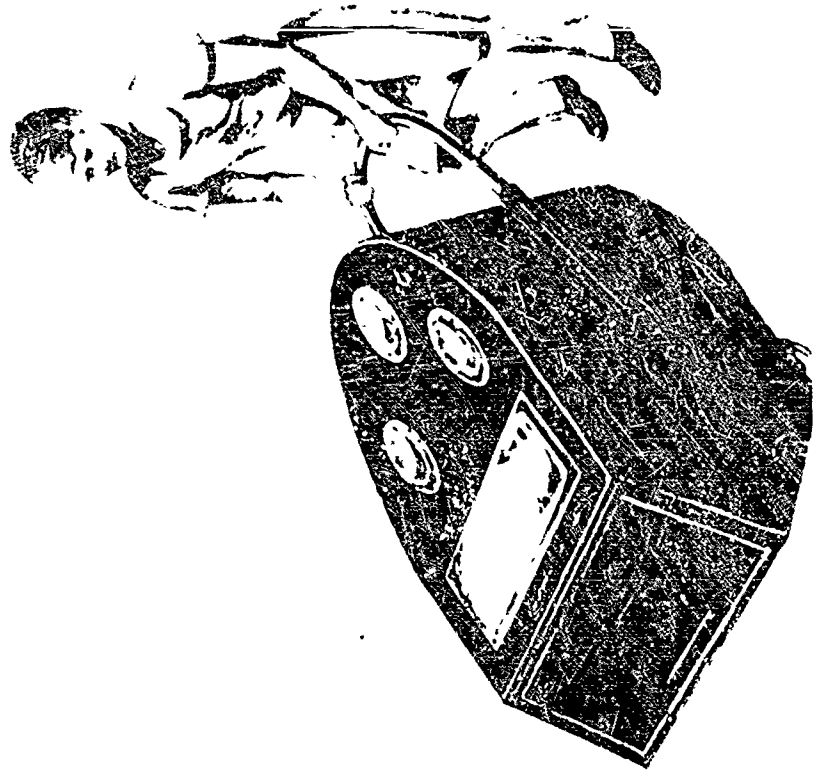


Fig. 24: Cook's Stove.



FUEL CARRIER

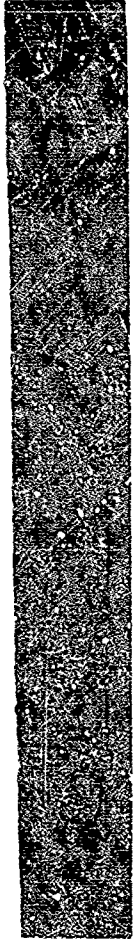
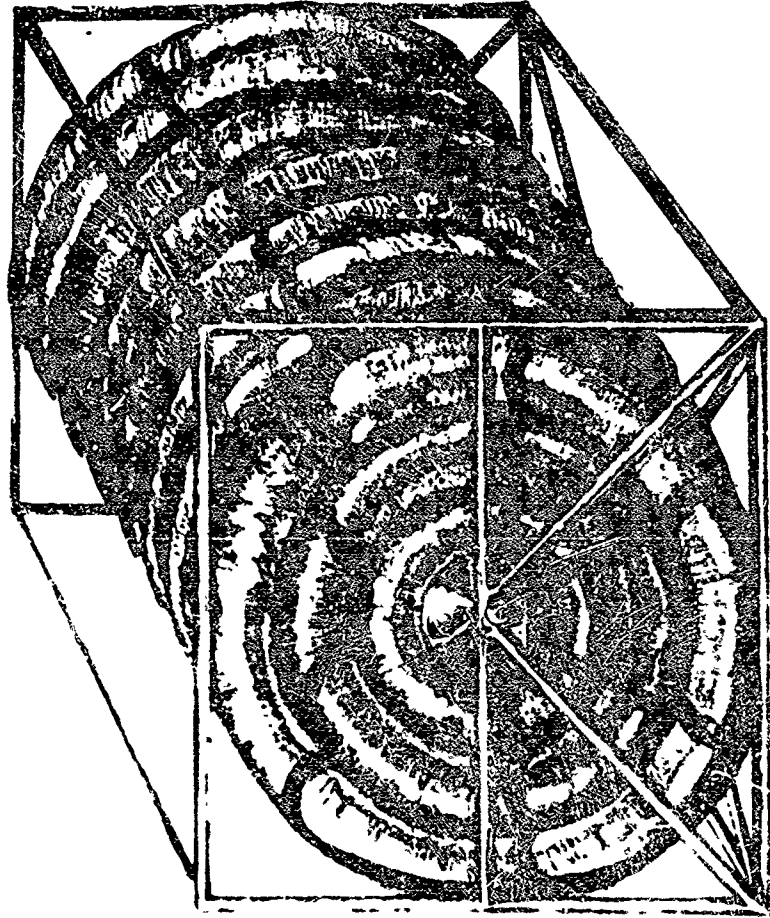


Fig. 23: Fuel Carrier.

TEAM 4

Jeffrey Chambers	I.D. '65
John Coons	I.D. '65
Ronald Miller	Arch. '66
Rodney Lane	Arch. '66

SHELTER SYSTEM

Our concept makes use of a pallet in two ways. First, it is a carrying platform for materials brought to the Bare Base site. Second, it is used as a shelter system for Bare Base site.....

The pallet is made of honeycomb sandwich panels. The honeycomb material is aluminum with aluminum faces.

A housing unit designed for sixteen men is made up of two pallets and one end panel package.

The floor of the unit is brought together by tie rods mounted in the honeycomb (Fig. 25). At this point, one pallet would be unfolded into position and an end panel placed into it (Fig. 26). This would make the unit rigid. The second pallet which unfolds in the opposite direction is raised into position and connected to the first section, the second end panel is put into position. The unit is now complete (Fig. 27). Time allowed for one unit using three trained men for erection is 15 minutes.....

FLEXIBILITY-HANGAR

The hangar is constructed of the same pallets used for the smaller shelters. Their construction differs in that one joint is unhinged and the panels are extended to their full length (8' x 48'). Two pallets are butted end to end, making up one bay..... Structural ribs of honeycomb also stiffen the structure at interior points and on the ends (Figs. 28,29).....

TRANSPORTATION CONCEPT

The multi-purpose vehicle is a modular system consisting of a power unit and a trailer unit (Fig. 30). The unit is based on a tricycle arrangement, the larger wheels being used for power transfer and the smaller set, rigged to the steering mechanism. The unit is capable of working several take-off power units required for the operation of attachments such as the forklift (Fig. 31), runway sweeper, winch, bull dozer, and others. The vehicle is also adaptable for use as a passenger car (Fig. 32). Extreme maneuverability is facilitated

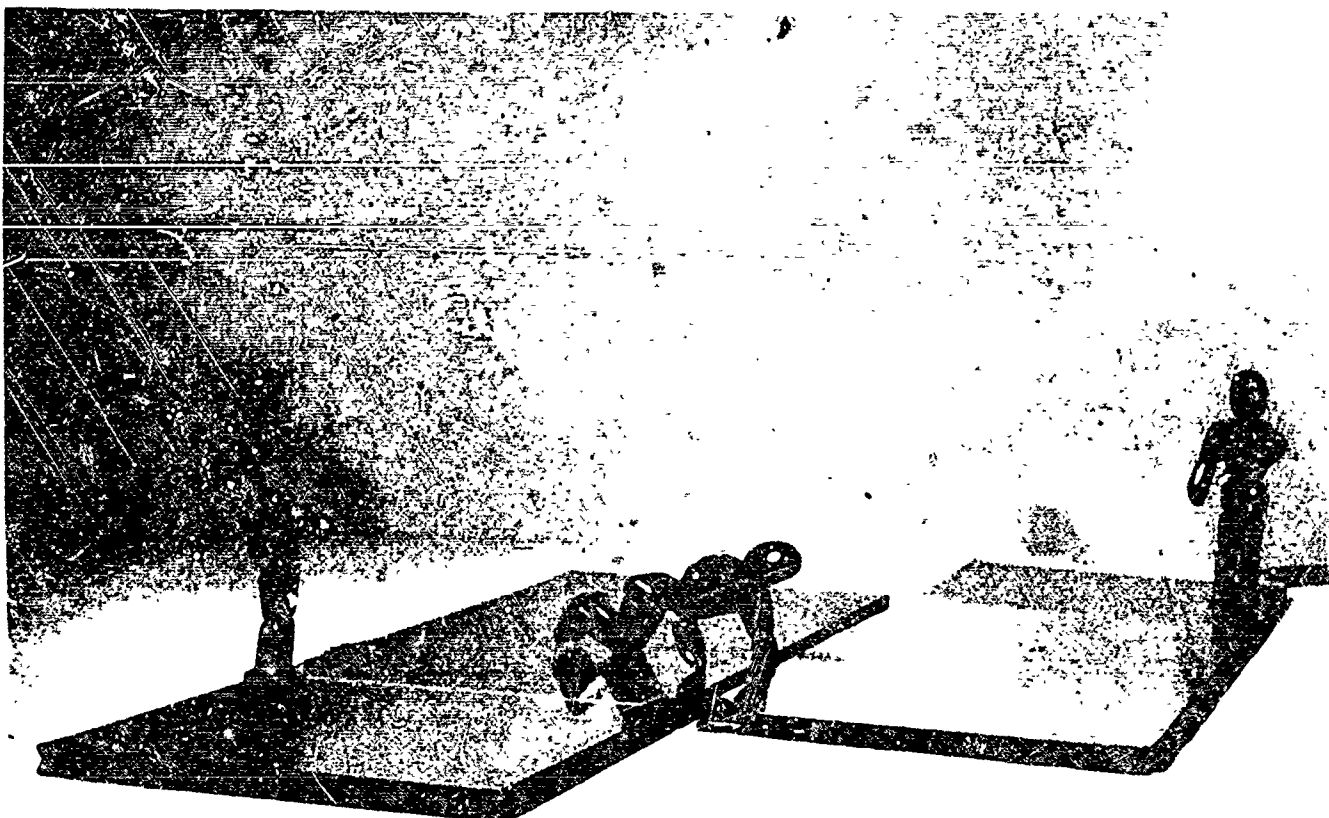


Fig. 25: Pallets laid alternately, floor panels tied together.



Fig. 26: First pallet unfolded, end panel being installed.

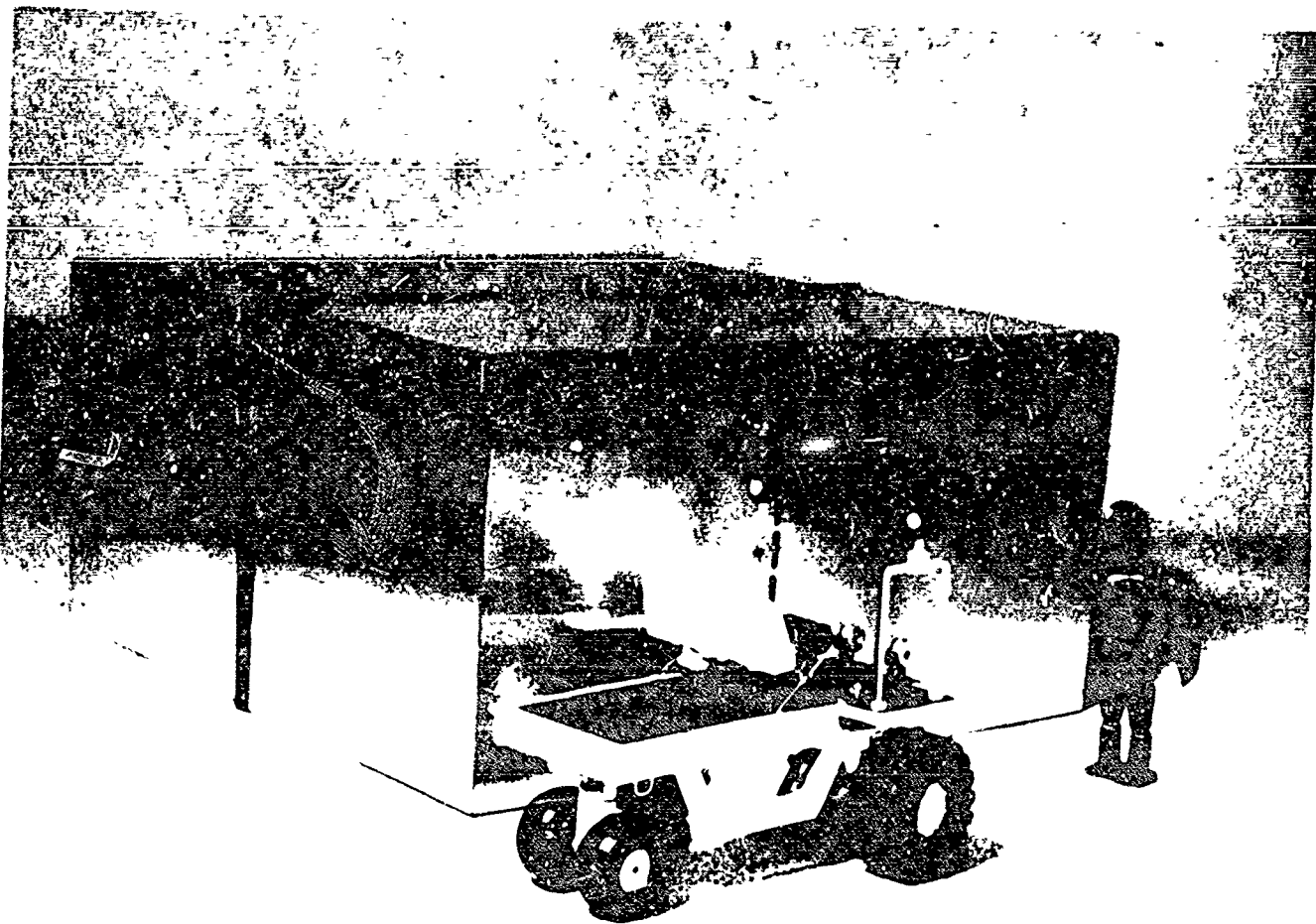


Fig. 27: Completed personnel shelter.

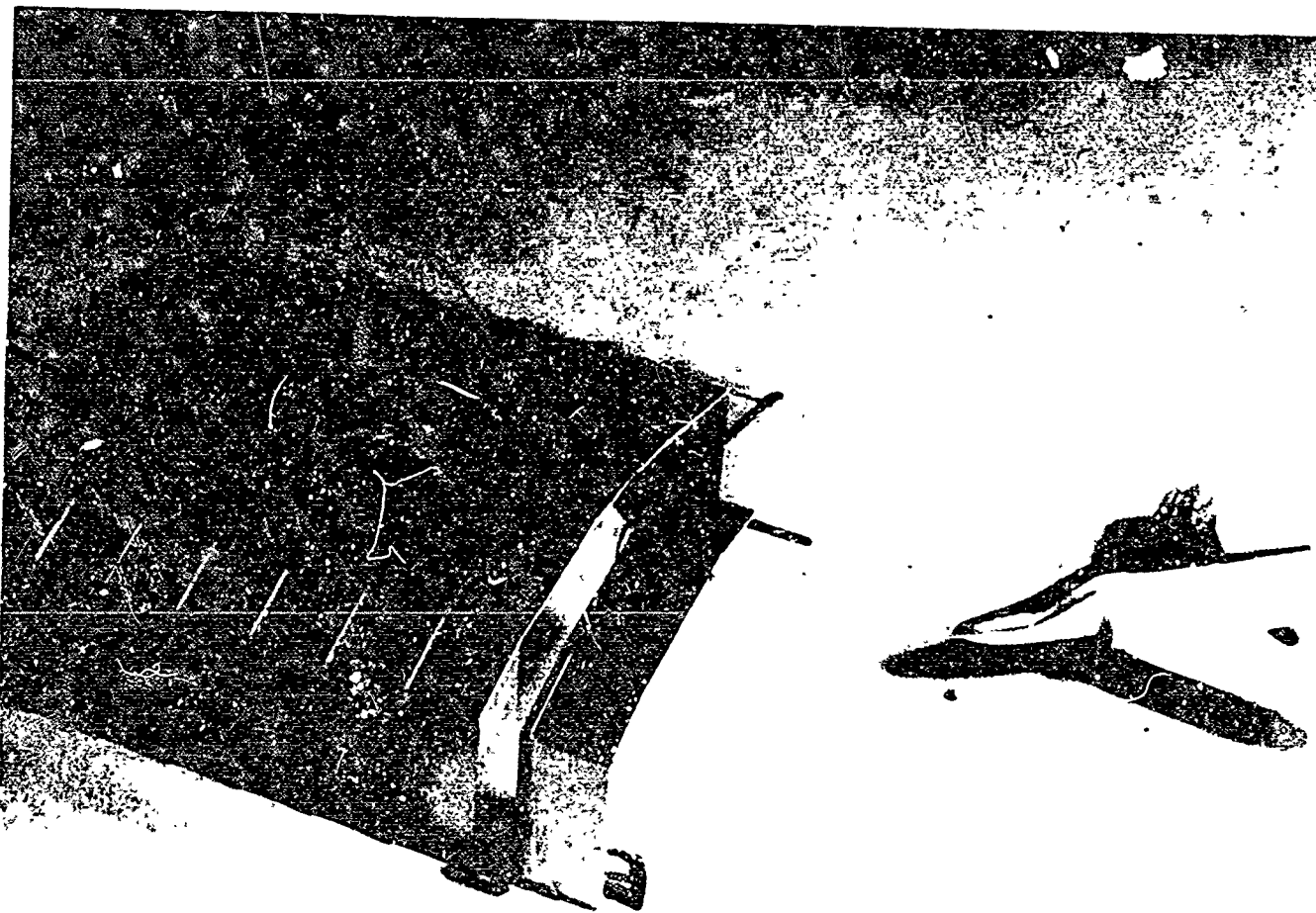


Fig. 28: Erecting panels and ribs of Hangar.

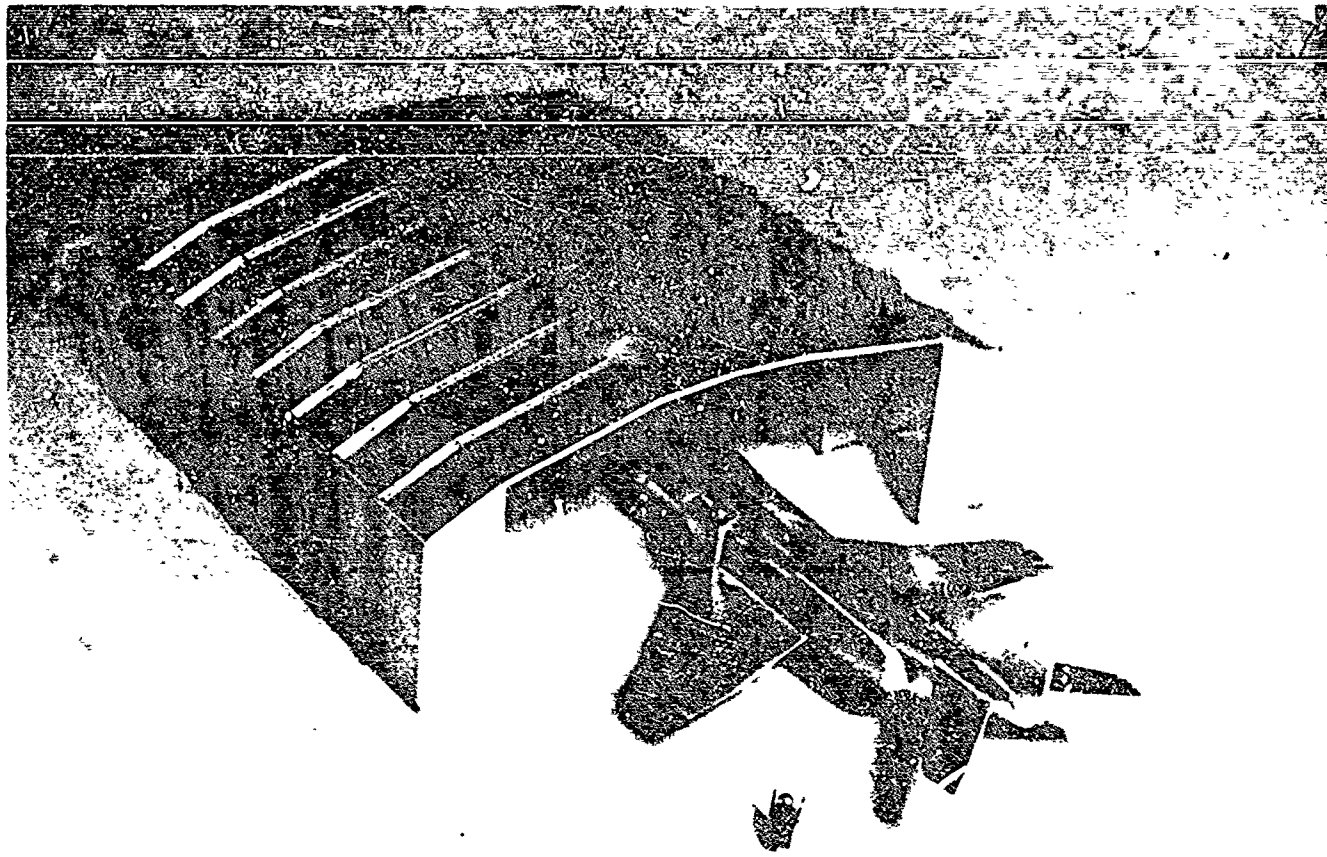


Fig. 29: Hangar showing stabilizing panels.

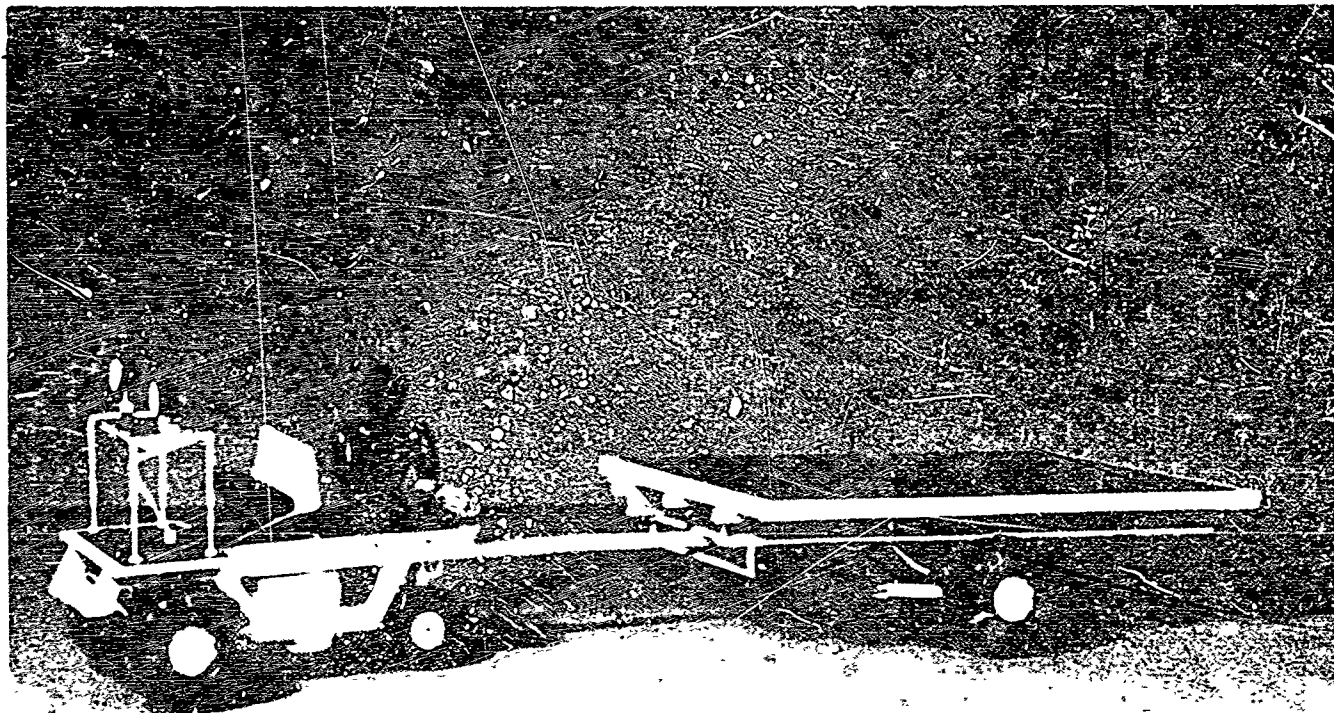


Fig. 30: Multi-purpose vehicle with trailer.

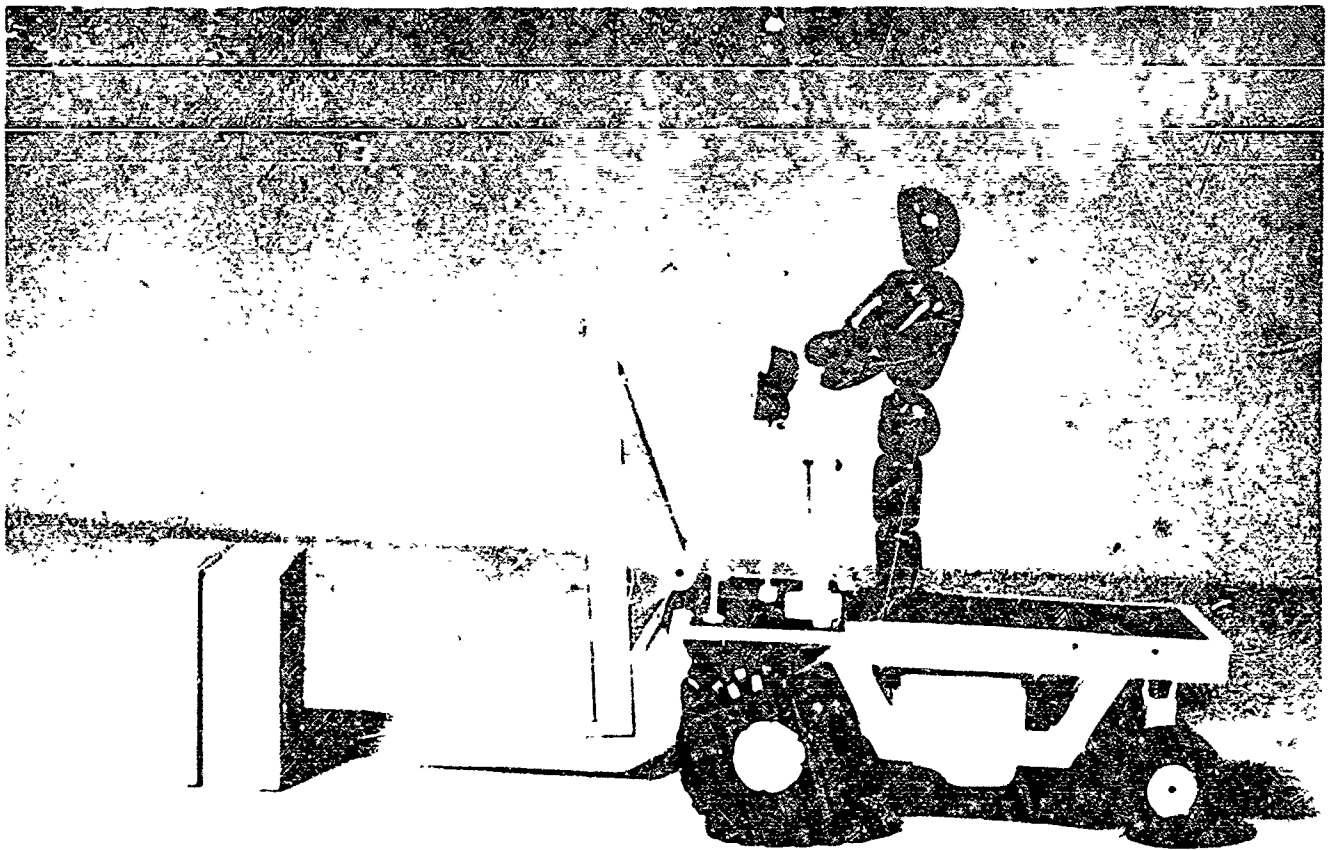


Fig. 31: Vehicle with fork-lift attachment.



Fig. 32: Vehicle equipped as a personnel carrier.

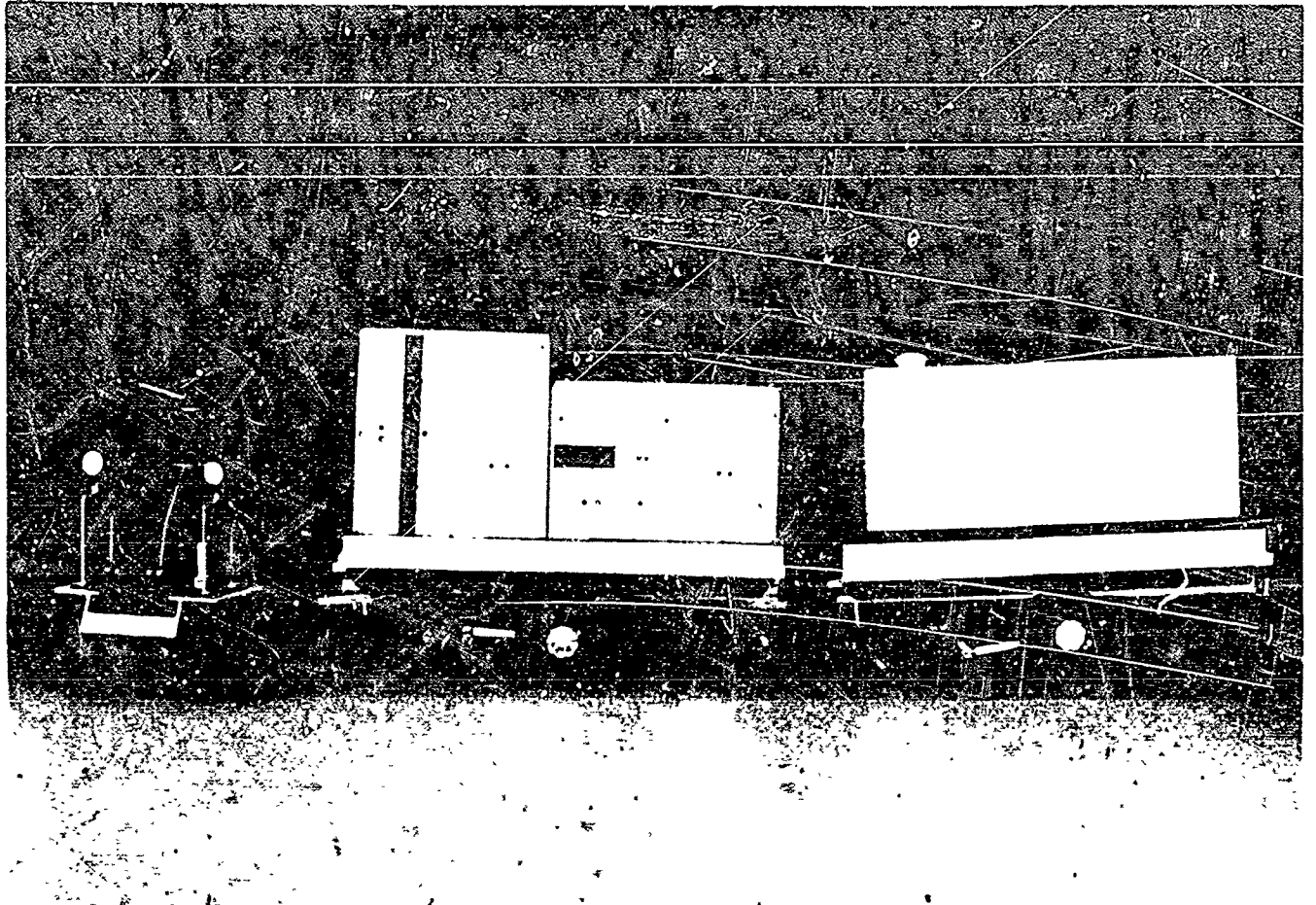


Fig. 33: Single trailers in tandem.

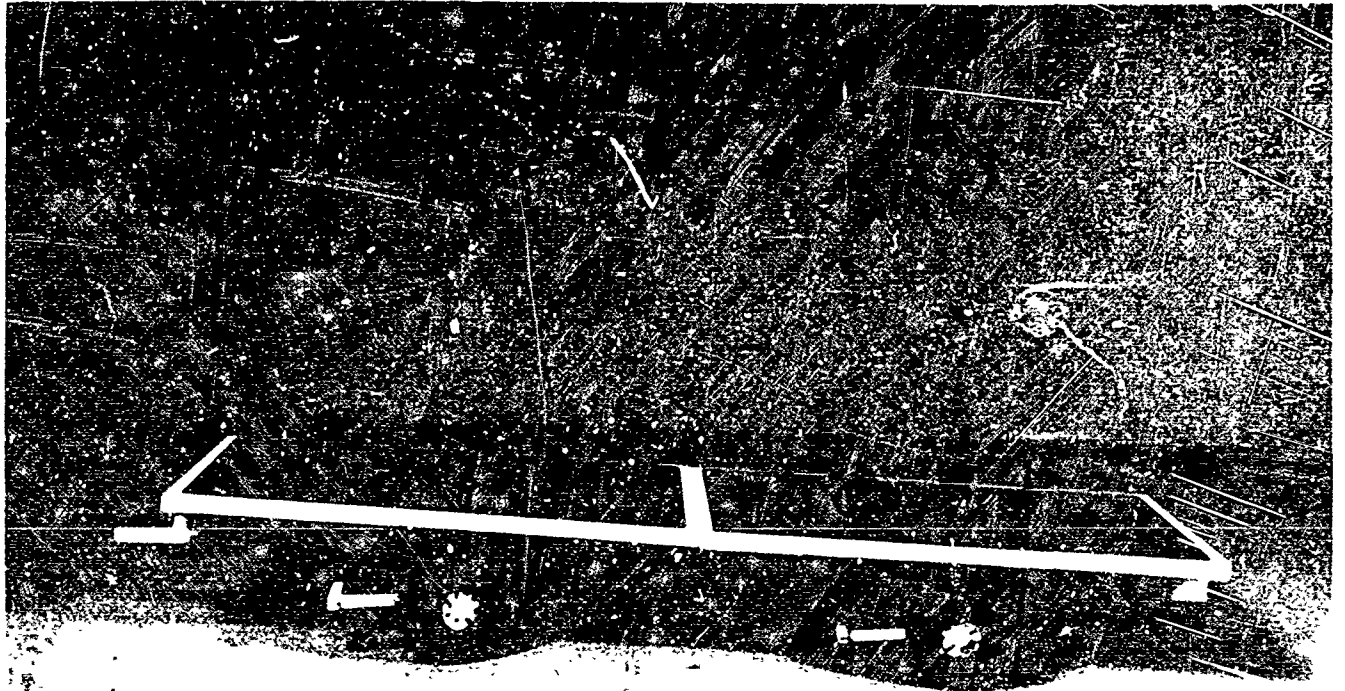


Fig. 34: Units joined to form large trailer.

by enabling the vehicle to be driven in either direction at comparable speeds. Also, tiller steering has been included to allow driver to sit or stand and face either direction.

The trailers are designed as lightweight modular units. Each is basically a flat cargo bed mounted on a two-wheel suspension unit (Fig. 30). Each unit is equipped with tongue steering and a modular coupling system (Fig. 33). Its first application is as a hauling unit used to unload the C-130's. For this duty two units are joined rigidly to form a single four wheeled trailer (Fig. 34). The dimensions of this double cargo bed match those of the pallet.

TEAM 5

Stanley Hoelle Arch. '66
Raimonds Maculans Arch. '66
Robert Coulter I.D. '65

BASIC SHELTER

The shelter is an arched structure of light canvas over a skeleton frame. "Delrin" plastic rods form the frame structure for the shelter. These rods have a compressive stress of 18,000 psi and a tensile stress of 10,000 psi. They are resistive to heat, cold, acids and mildew. They can be painted, pigmented, cut or welded (Fig. 35).....

The rods are set in grade beams and are held in the arched form by cables under the removable canvas flooring.....

VEHICLE DESCRIPTION

The basic body shell of the vehicle is of unitbody construction, and.....has four-wheel drive and four-wheel steering to make it quite agile and maneuverable.....

Many standard jeep attachments can be used on this vehicle, which is equipped with a Power Take-Off front and rear..... A large vehicle of same basic lines but with caterpillar drive would be used for heavier jobs at the base. This vehicle could be fitted with grader blades, cranes, or other body units for specific work (Fig. 36).

RUNWAY LIGHTING

A very efficient type of lighting is neon. A single strip of light on both sides of the runway is sufficient for its location by the pilot.

The portable quality of the lighting is achieved by pumping the neon gas into flexible clear plastic tubing which can be wound onto reels that are mounted on a vehicle.

This single wire, cold cathode system can be powered by portable generators as needed.

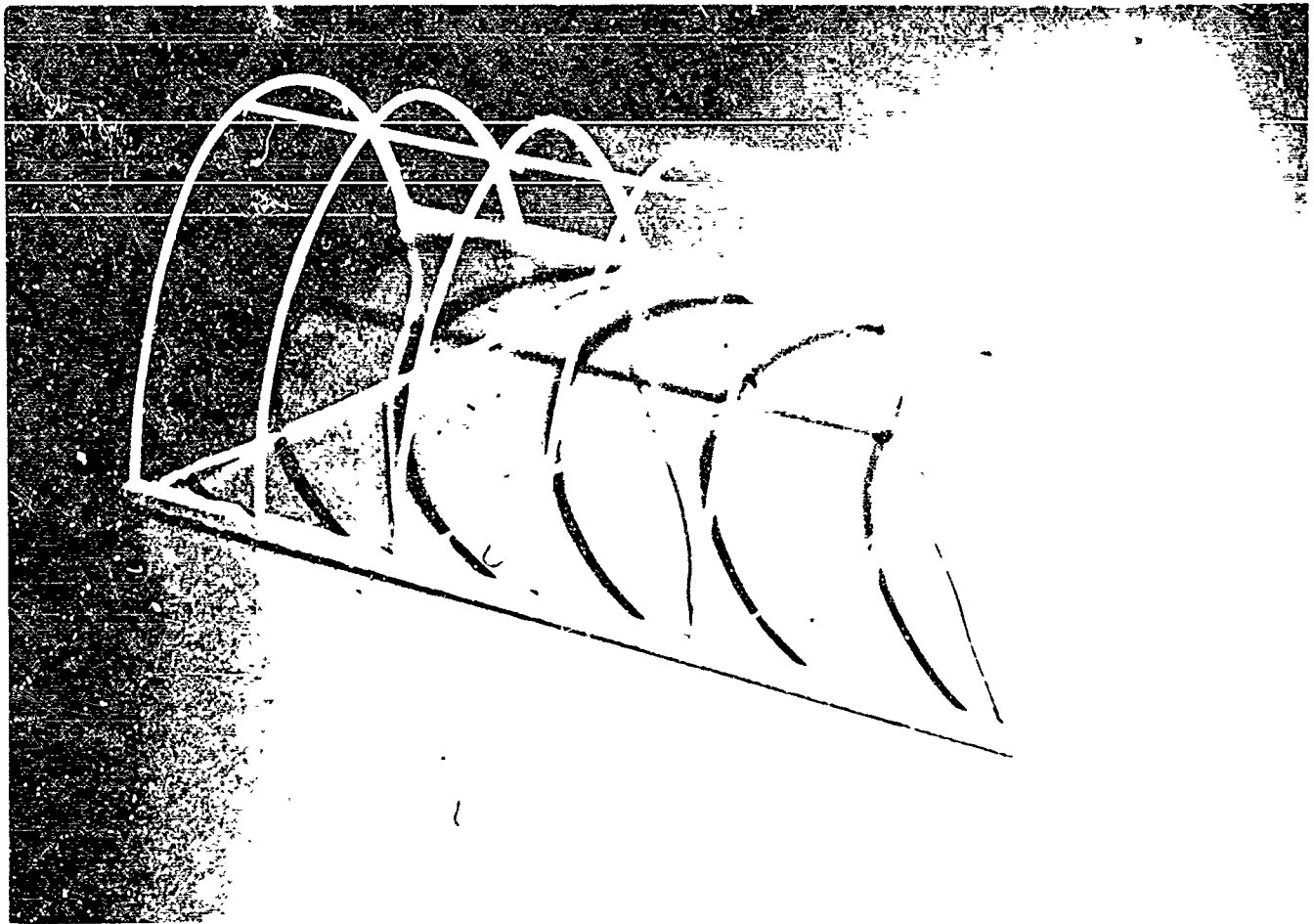


Fig. 35: Skeleton of shelter, showing ribs in place.

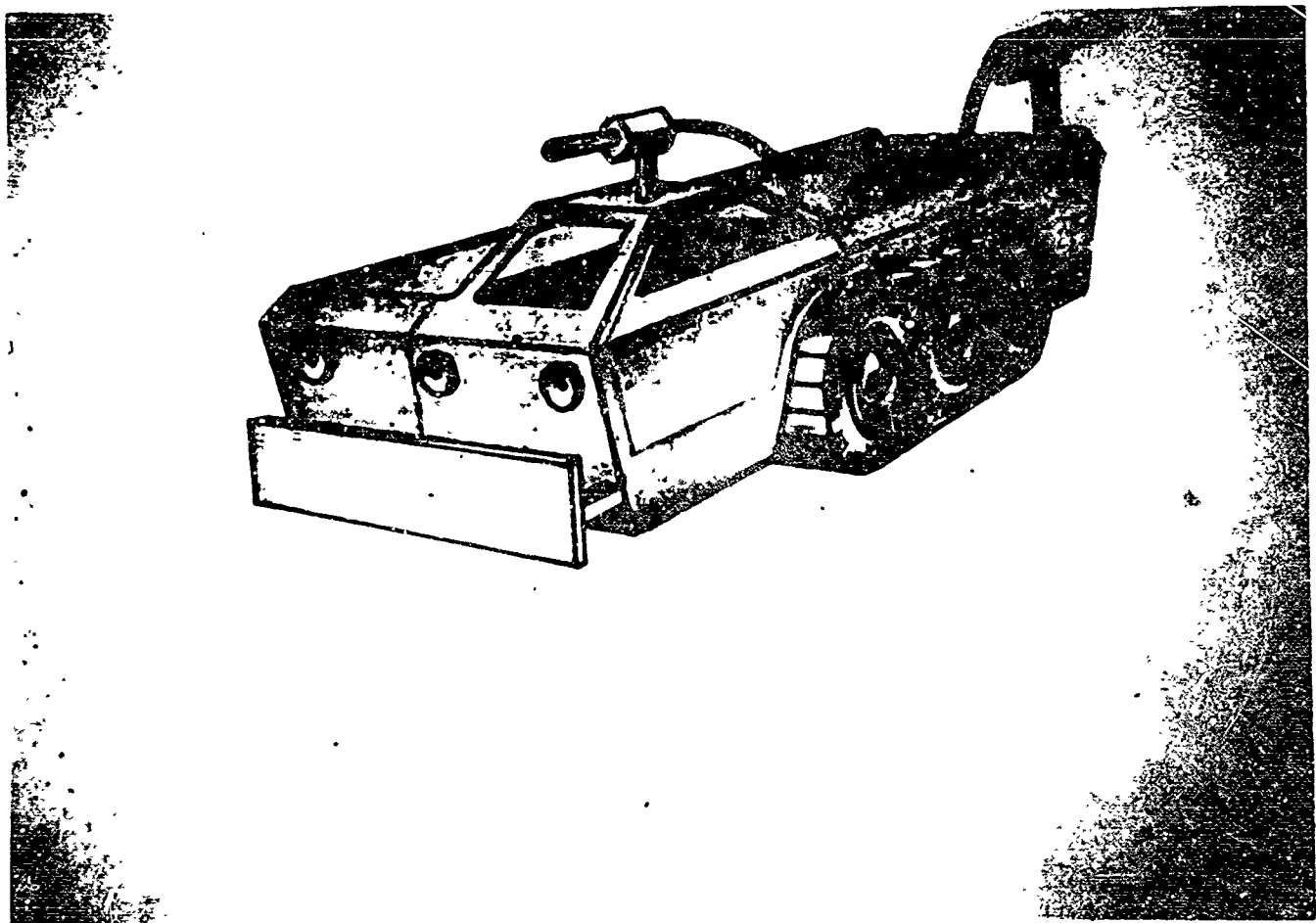


Fig. 36: Large vehicle with fire-fighting equipment.

**"RATIO" AUTOMATED ASSEMBLY TECHNIQUE
FOR SPACE STRUCTURES**

Paul Slysh, General Dynamics/Convair

1. INTRODUCTION

RATIO* is a technique for implementing the automatic or semiautomatic assembly of large space structures. Work on this technique has received GD/C and NASA** sponsorship.

The technique includes sectionalizing the structure into structural modules capable of being nested, and of configuring mechanisms for the automatic or semiautomatic assembly of the modules. The modules and mechanisms may themselves be rigid or expandable structures.

The technique is applicable to deploying such structures as reflectors for antennas and solar concentrators, booms, extended-area solar panels, as well as cylindrical, lenticular and toroidal space stations and re-entry bodies.

The RATIO technique is illustrated in this paper by describing its application to the deployment of a paraboloidal reflector for an antenna.

* This technique is proprietary with the General Dynamics Corporation.

**NAS7-228, Study of RATIO Automatically Assembled Structures, Final Report GDA-DDG64-017, dated 1 July 1964.

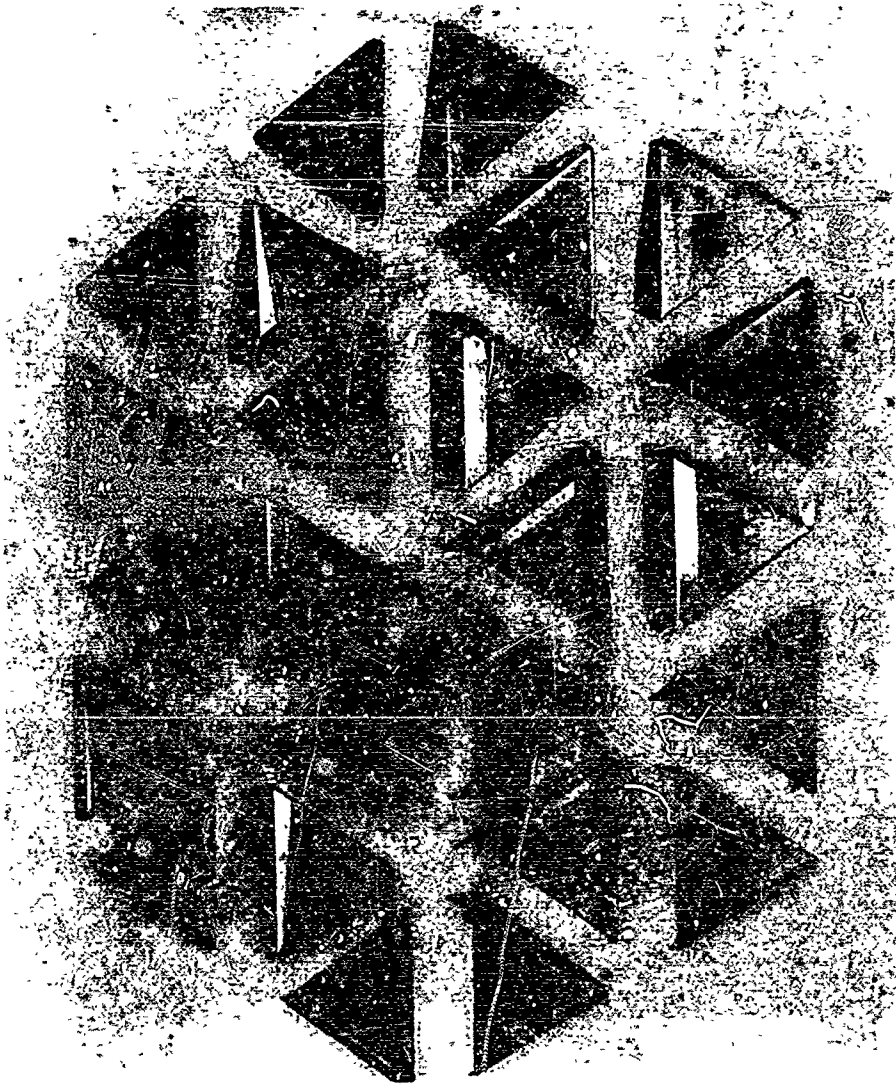
2. REFLECTOR CONFIGURATION AND ASSEMBLY SEQUENCE

The chosen reflector has a hexagonal contour and is sectionalized into 24 triangular panels. Using a planar model Fig. 1 shows how the reflector is (a) sectionalized, (b) stacked, and (c) assembled.

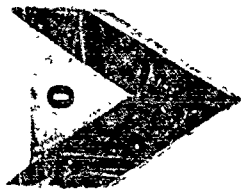
It is seen in Fig. 1 that the assembly of the panels takes place according to a systematic sequence of relative motions between successive panels. Panel 1 is assembled to panel 0 by a counterclockwise rotation and linear displacement of panel 1 with respect to panel 0. The same rotation and linear displacement takes place between panel 2 and 1, 3 and 2, 4 and 3, and 5 and 4. Panel 6, however, is assembled to panel 5 by a clockwise rotation of the stack with respect to panel 5. Further examination of Fig. 2 indicates that panels 7, 8, 9, 11, 12, 14, 15, 17, 18, 20, 21, 23, are assembled by counterclockwise rotations and panels 10, 13, 16, 19, 22, are assembled by clockwise rotations. As will be explained, these assembly motions are variations of a single set of assembly motions.

A view of the reflector as part of a space station casegrain antenna is shown in Fig. 2. In this example, panel 0 is used for pedestal mounting the antenna with respect to the space station and for mounting the subreflector with respect to the reflector.

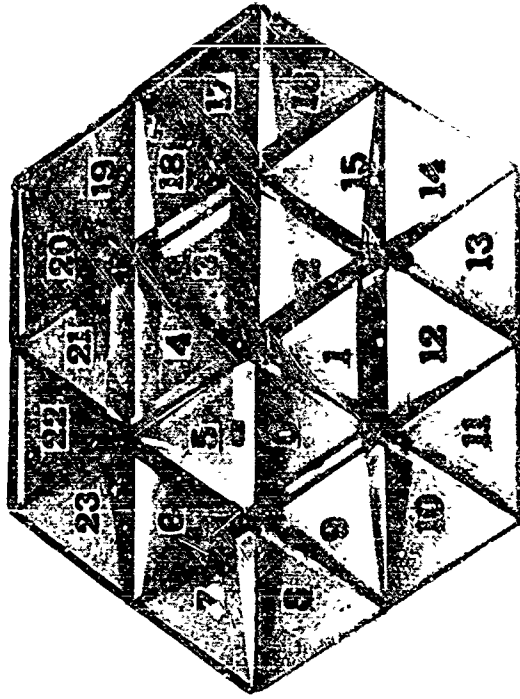
The subreflector support may be a RATIO, stretch formed wire mesh or other expandable structure. In this case, the support and subreflector are stored between panels 0 and 1 and are deployed after panel 1 is assembled to panel 0. The pedestal remains fixed to panel 0 at all times (i.e. when the antenna is in both the stowed and deployed states).



(a)



(b)



(c)

Figure 1. Reflector Structure - Planar Model

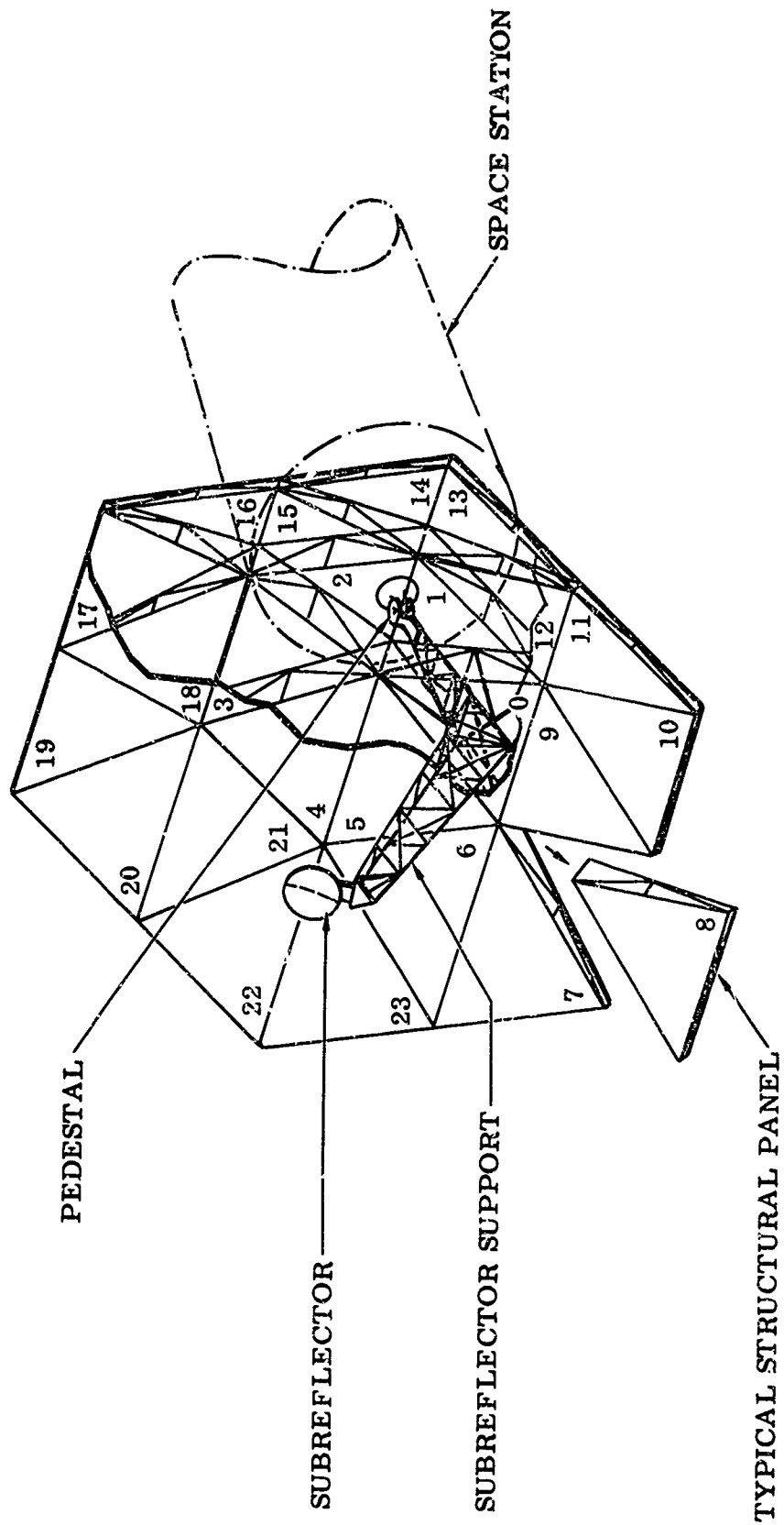


Figure 2. Assembled Antenna

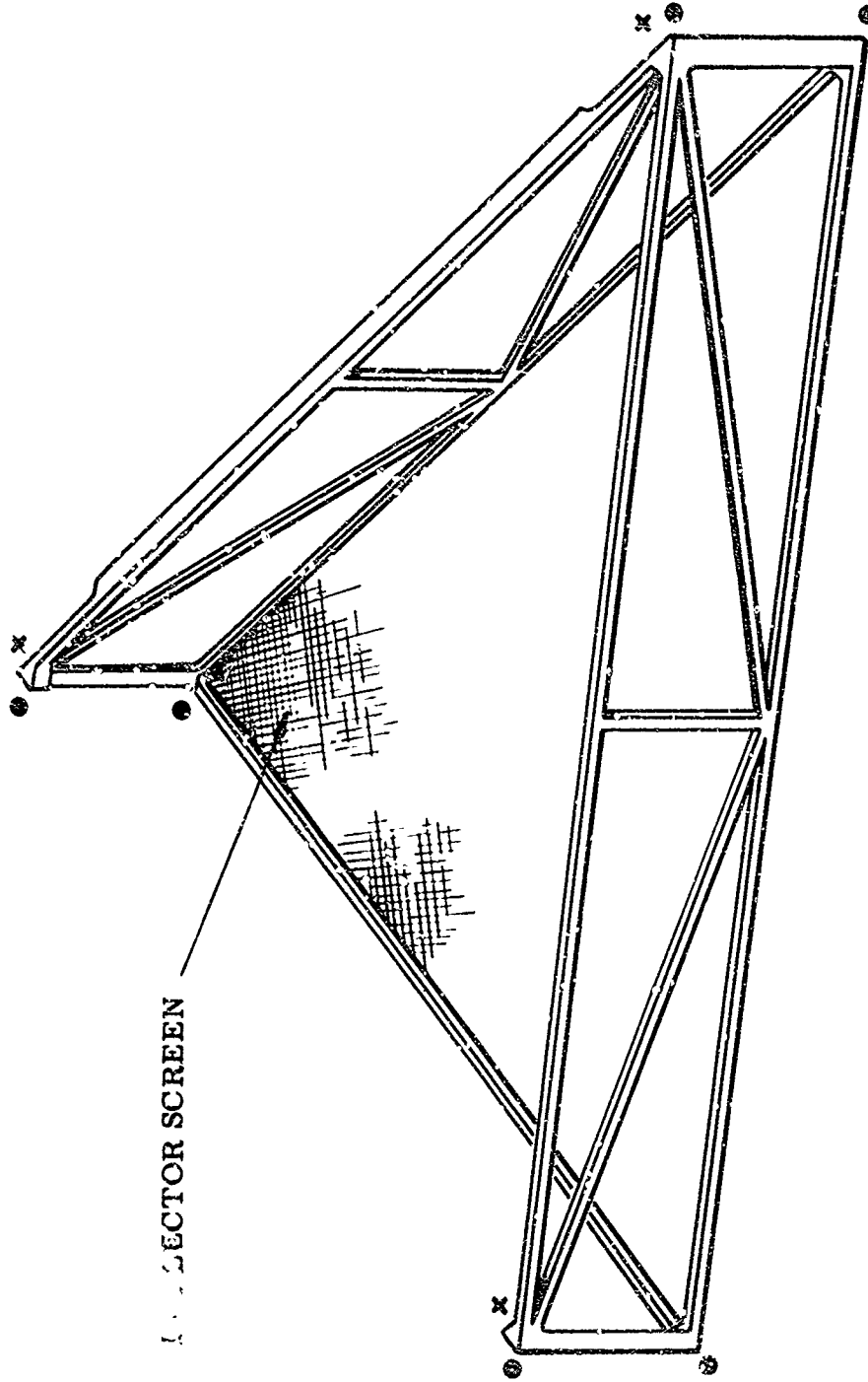
3. PANEL CONSTRUCTION AND FASTENERS

A chosen thin-wall, tubular, cross-frame panel is shown in Fig. 3 together with the corner locations of the panel-to-panel structural fasteners. The corner locations for the assembled-state fasteners provide structural continuity. A typical structural corner and the assembled-state fasteners are illustrated in Fig. 4. The stowed-state fasteners (explained later) are actuated latches located along the edges of the back rib structure.

In the chosen model the ribs along the reflector periphery are only fastened to each other in the assembled-state by fasteners in the structure directly behind the reflector surface.

The width of one of the truss members on the panel rib edge (see Fig. 3) is shown having a width $(2T)$ in the plane of the reflective surface which is twice the width of the other members. This increased width is used to equalize the effective length-to-radius-of-gyration ratios of the rib-edges members in the planes parallel and normal to the reflective surface.

The need for tight machining tolerances is minimized and stress free mating between the assembled panels is enhanced by fabricating the panels by a join-at-assembly method. Typically this method consists of: (1) fastening (screwing) together all the mating structural corners, (2) fixturing the fastened-together corners in their proper space relation to each other, (3) fitting the precut and preformed truss members to the structural corners, and (4) pinning or riveting the truss members to the structural corners at assembly. Fabricated in this way, with precautions for avoiding built-in stresses, the panels may be separated and reassembled within the reassembly tolerances of the (screw) fasteners.



REFLECTOR SCREEN

- LOCATIONS OF FASTENERS FOR FASTENING PANELS TO EACH OTHER IN ASSEMBLED STATE
- * LOCATIONS OF FASTENERS FOR FASTENING PANELS TO EACH OTHER IN STOWED STATE

Figure 3. Typical Reflector Panel

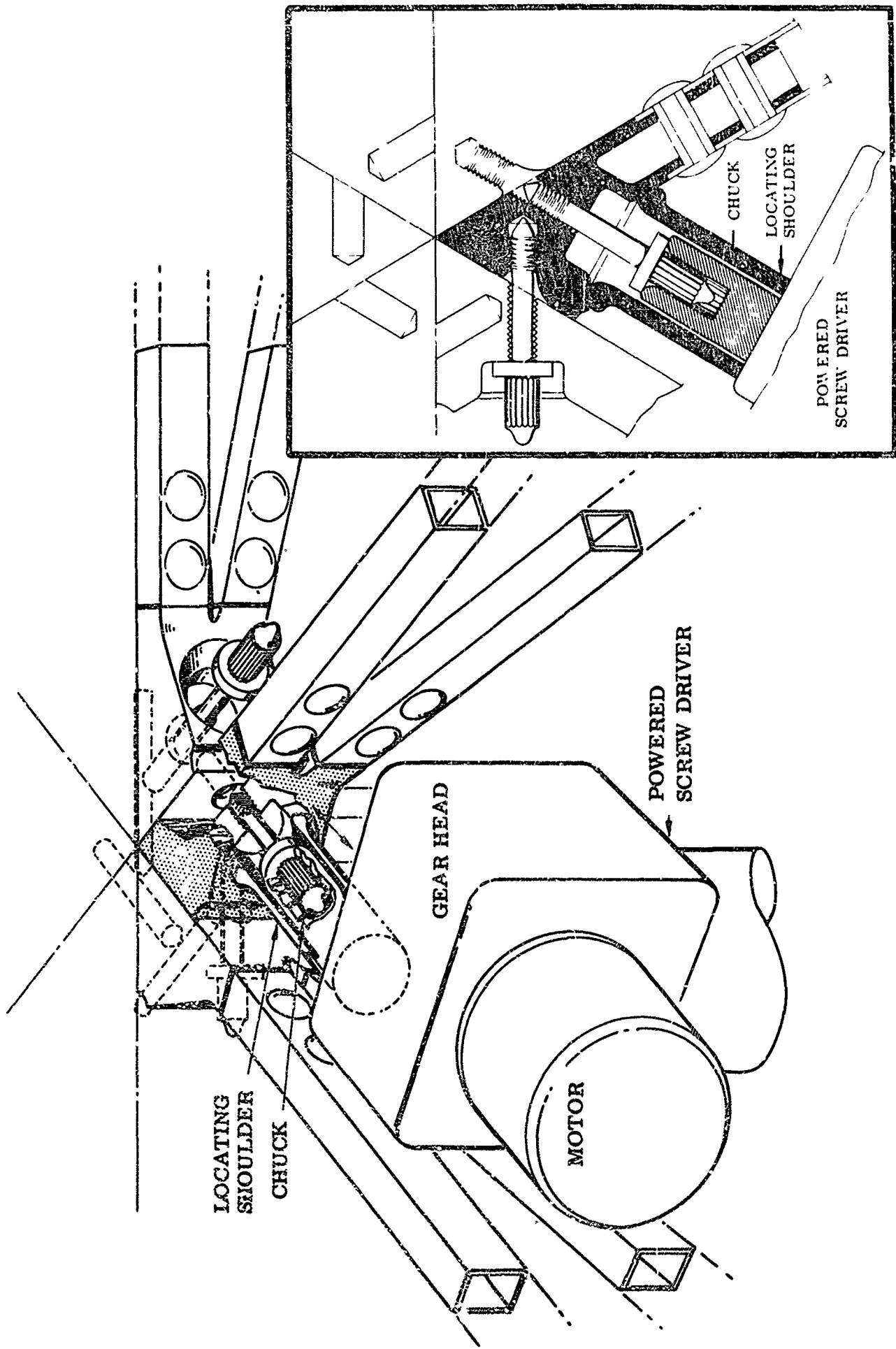


Figure 4. Typical Structural Junction and Fasteners

The reflective surface, in the form of a screen wire mesh, is added after the frame structure fabrication is complete.

4. ASSEMBLY EQUIPMENT

A powered screw driver for actuating the screw fasteners is depicted in Fig. 4. Four single chuck and two double (tandem) chuck powered screw drivers are carried on a V-shaped (lower) gripper frame, as shown in Fig. 5a. The two double chuck drivers are at the apex of the V, and the four single chuck drivers are at the other corners. The relative positions of the drivers on the frame are compatible with the relative positions of the screws on the panels.

The screws held captive in the structural corners, as in Fig. 4, are engaged by the telescoping shoulders and chucks. The lead-in sections on the screws, shoulders and chucks cooperate to align the drivers and structural corners. In this way the entire panel is aligned with the lower gripper. Then, through the action (to be described) of the assembly equipment a set of mating structural corners are brought into alignment (within the available panel-to-panel screw lead-in tolerances). The chuck-engaged screws are driven to achieve the final alignment and lock-in between the corners. The telescoping shoulder and chuck are finally withdrawn into the gear head disengaging the driver from the panel.

Figs. 5a,b,c, picture the automatic assembly equipment with respect to stowed and deployed reflector. It is seen in these pictures that the panels are manipulated by three V-shaped grippers. The upper gripper acts as a dummy panel to which the unassembled stack of panels are attached. The middle gripper is shown engaged, in Fig. 5b, to the

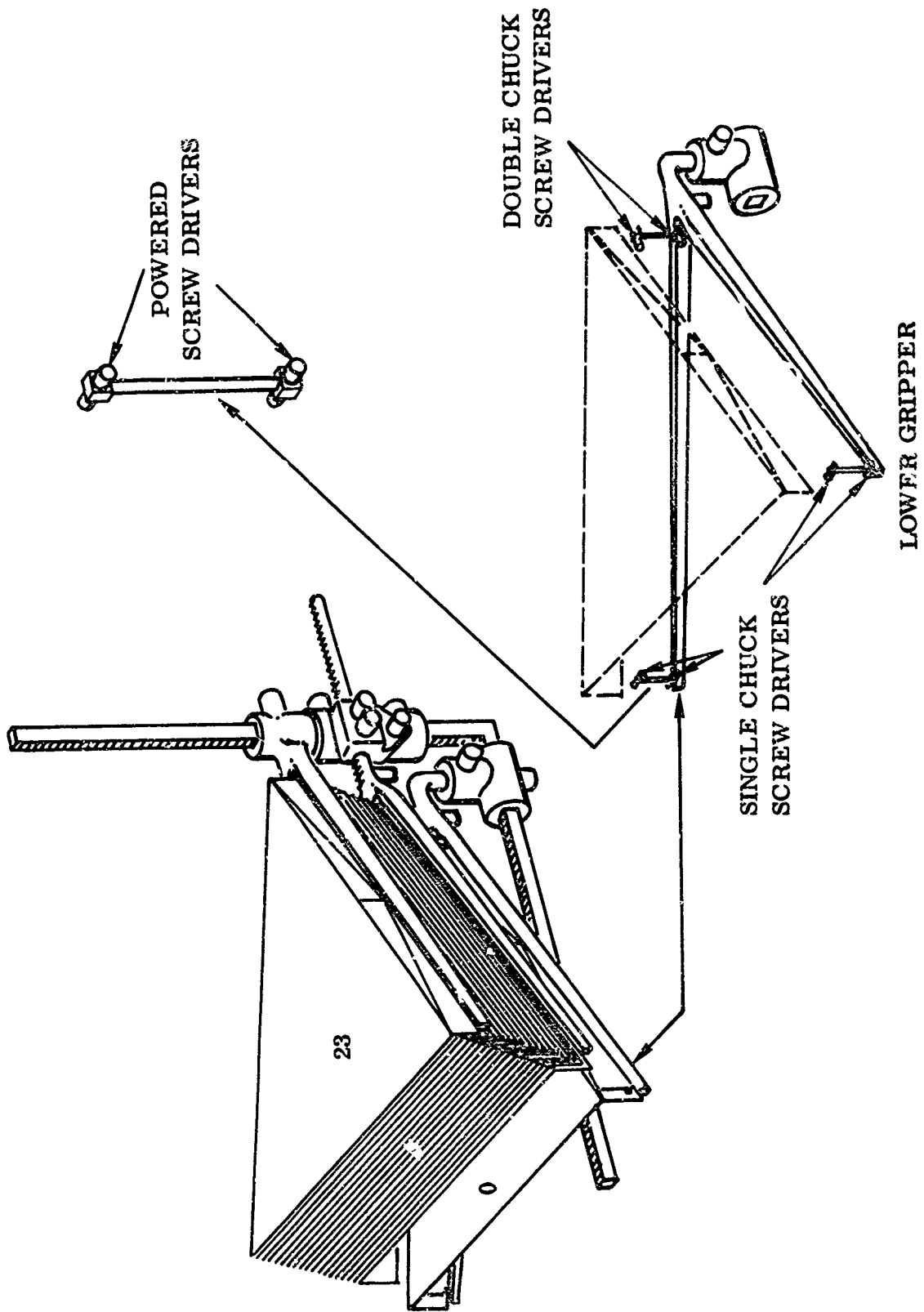
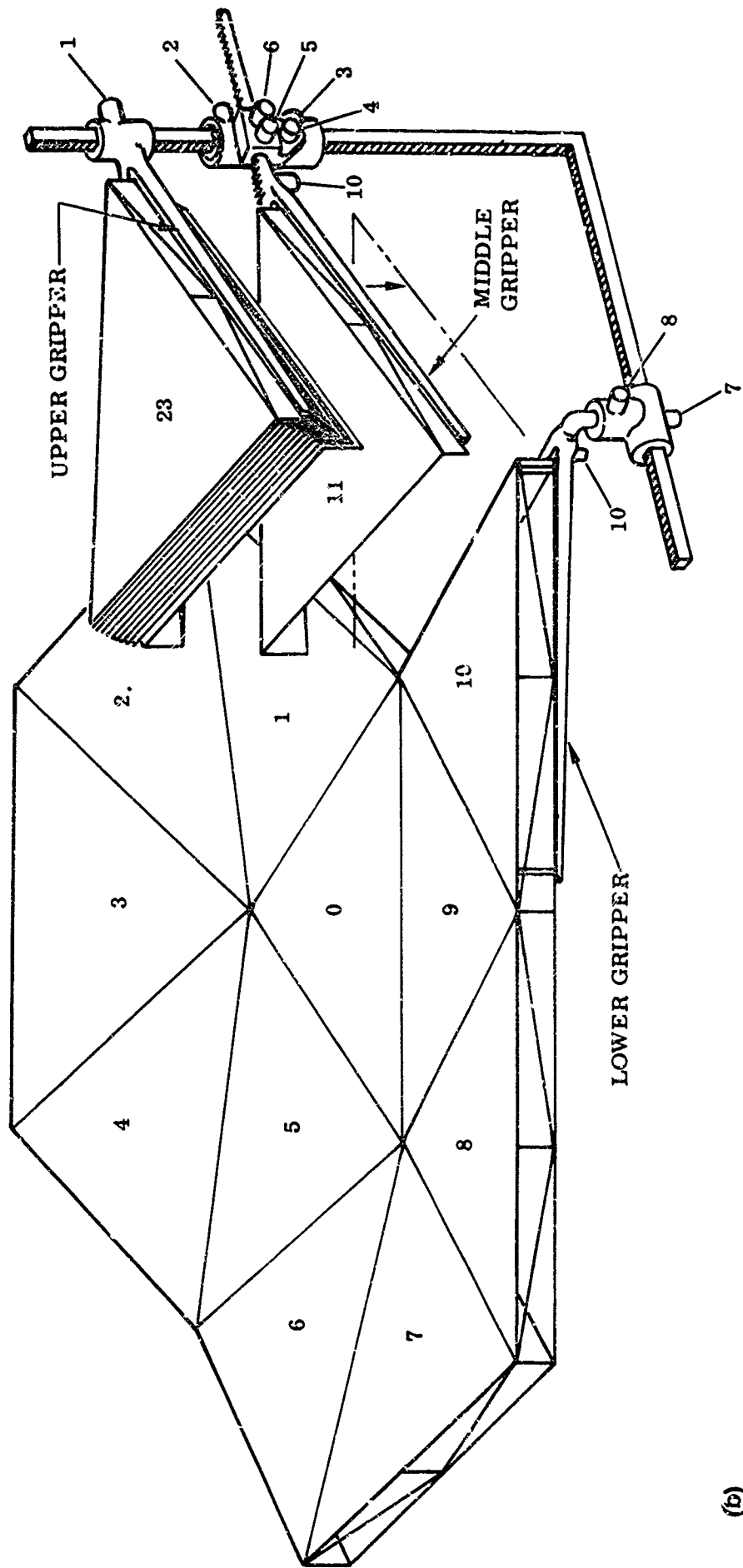
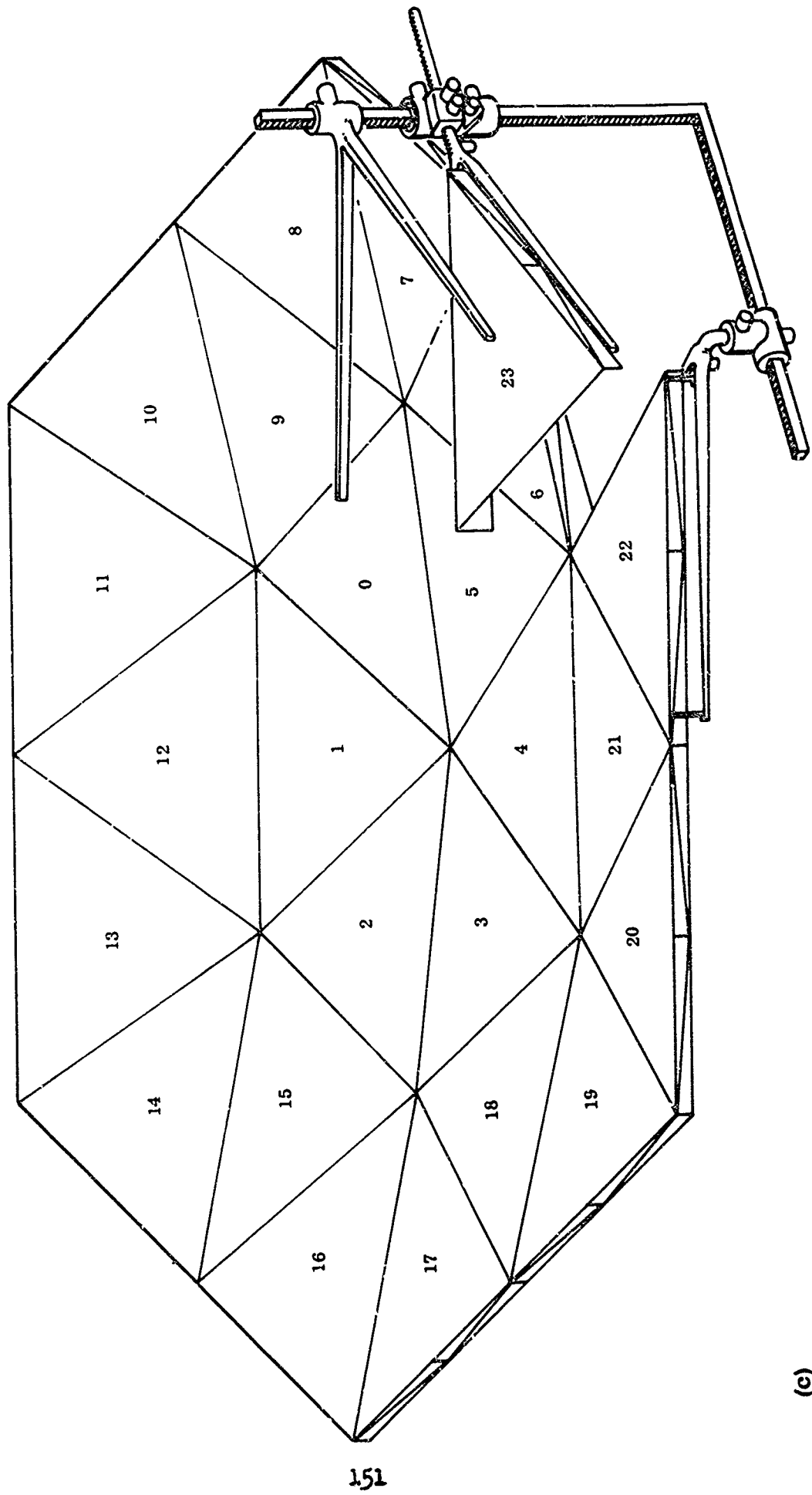


Figure 5. Assembly Equipment

(a)



(b)



(c)

bottom (rib side) of a panel which has been removed from the bottom of the stack and is in transport to an assembly position. The lower gripper is attached to the last assembled panel (panel 10 in Fig. 5b) which acts as an anchor between the assembled and unassembled panels.

The middle gripper fork, which has a cross-sectional width equal to the width of the panel ribs, engages and grips the panel along the lower edge of its rib. This gripper can also grip a panel along the upper (reflector-face) edge of the ribs.

5. DRIVE FUNCTIONS

Fig. 6 is a schematic showing the drive functions of the assembly equipment. The drive functions called out in Fig. 6 correspond to the numbered drives in Fig. 5b.

Drive functions 1, 2, and 7, are linear translations of the upper, middle, and lower grippers respectively, in the indicated directions along the floating rack frame. Drive function 5 linearly translates the middle gripper parallel to the plane of the middle gripper. The drive functions 3, 4, 6, and 8, are angular displacements of the middle and lower grippers.

Functions 9a,b,c,d, by using separate two-directional drives, produce linear displacements and rotations in the powered screw drivers. One direction of rotation of these drives for a controlled time period produces the forward displacement of the shoulders and chucks. Continuation of this rotation produces rotation of the chucks. Reversing the drives withdraws the shoulders and chucks without rotating the chucks. Drive functions 9a,b,c,d, therefore have three states.

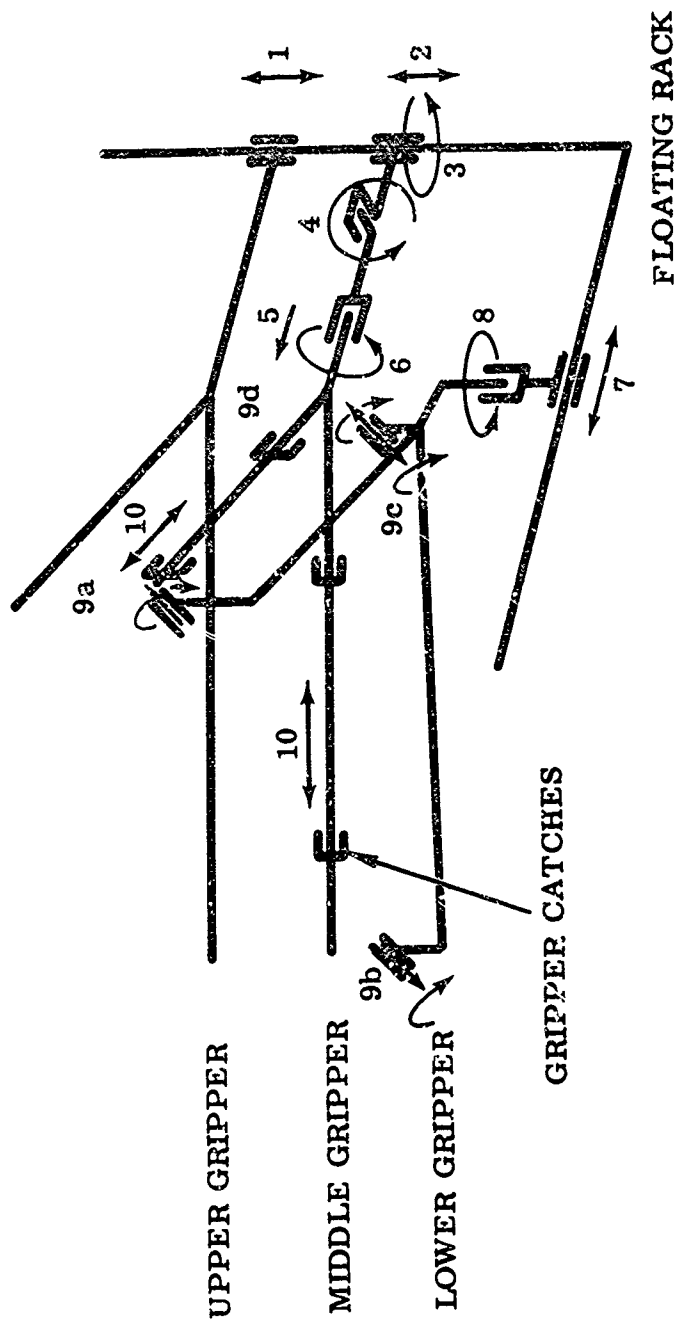


Figure 6. Assembly Equipment Mechanism Functions - Schematic

Drive function 10 is a single linear actuation for simultaneously operating the latches on the middle gripper. Fig. 7 shows a schematic of the middle gripper and panel latches. When the gripper and panel are aligned, operation of actuator 10 produces gripper-panel engagement and the unfastening of the structural stow-state latches. The panel, attached to the gripper and detached from the stack, is now free to be transported by the gripper.

A set of latches integral with the latches on the top side of the middle gripper protrude from the bottom side of the gripper. When the gripper is positioned on top of a panel the latches engage the panel.

The actuators 1 to 8 may typically be powered by step motors, actuators 9 and 10 by continuous running motors, or actuator 10 by a solenoid.

6. MECHANISM FUNCTIONS

The mechanism functions for the assembly of panel 1 to panel 0 are outlined in Fig. 8. The operations cycle diagram in Fig. 9 indicates the drive function actions according to the sequence of events 1 to 15 required for the assembly of panel 1 to panel 0. The corresponding events depicted in Fig. 8 are also called out in Fig. 9. The events to achieve the assembly of panel 1 are summarized with reference to events 1 to 15 in Fig. 9:

1. The stack of panels, fastened to each other, are initially held by all three grippers. The lower and middle grippers are attached to panel 0, and the upper gripper is attached to panel 23 (at the top of the stack in Fig. 5) - Release panel 0 from the stack and raise the stack

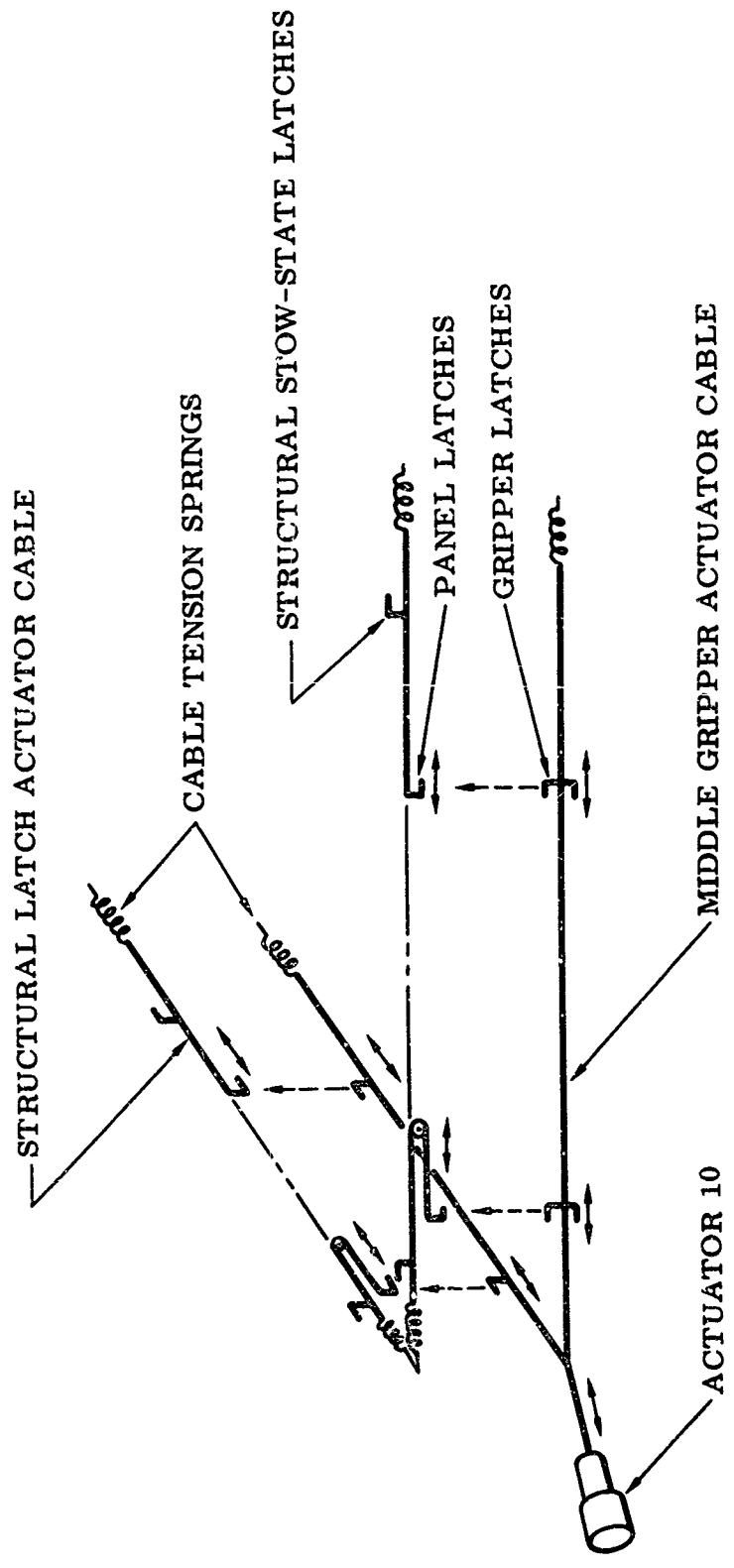


Figure 7. Latch Actuators - Schematic

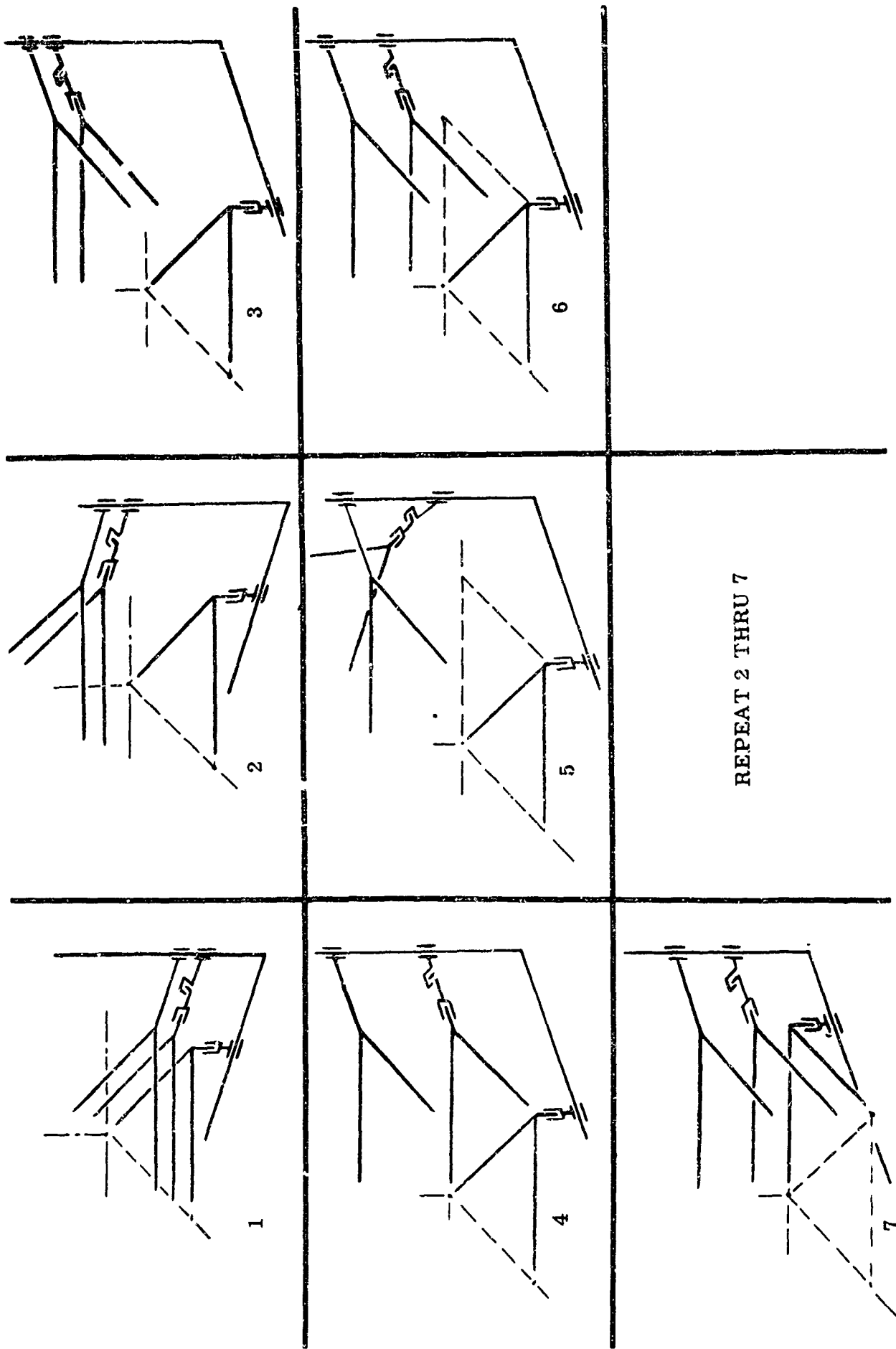


Figure 8. Mechanism Functions for the Assembly of Panel 1 - Schematic

EVENTS
(FIG. 8)

DRIVE FUNCTIONS

	10	9	8	7	6	5	4	3	2	1	EVENTS
ASSEMBLY OF PANEL 1	●									●	1 (2)
	●					●			●		2 (2)
	●										3 (2)
			●	●	●	●	●	●	●	●	
MOVE MIDDLE GRIPPER FROM BOTTOM TO TOP OF PANEL 1	●										5 (4)
										●	6 (4)
			●	●				●			7 (5)
					●	●	●	●	●	●	
MOVE LOWER GRIPPER FROM BOTTOM PANEL TO PANEL 1	●										9 (6)
											10 (6)
		●									11 (6)
										●	12 (6)
											13 (7)
										●	14 (7)
											15 (7)
		●									

Figure 9. Operations Cycle Diagram

from panel 0 - These events are brought about by exercising function 10 to unfasten panel 0 from the stack, and function 1 to raise the upper gripper. The dots along the event-1 row in Fig. 9 indicate that the drive functions 1 and 10 are exercised as described.

2. Release middle gripper from panel 0 and move to a position of engagement with panel 1 - Exercise of function 10 releases panel 0. Exercise of functions 2 and 5 transports the middle gripper to the engagement position.

3. Operate function 10 to grip panel 1 and release it from the bottom of the stack.

4. Translate panel 1 to its assembly position with respect to panel 0. To accomplish this, functions 2, 4, 6, 7, 8, and 3, are used. Because the upper gripper rides on the same leg of the floating rack frame as does the middle rack carrying panel 1, the stack is also moved by the use of the 7,8 functions; the stack follows along above panel 1.

5. Fasten panel 1 to panel 0 and release the middle gripper from panel 1, by exercising functions 9 and 10.

6. When panel 1 is fastened to panel 0 the assembly mechanism is repositioned on the structure to approximately the same gripper-panel relation which existed at the start of panel 1 assembly. This is started by event 6 in which the middle gripper is disengaged (lowered) from the bottom of panel 1.

7. Here the middle gripper is swung parallel to its face to clear the bottom of panel 1.

8,9,10. Now the middle gripper is located on and fastened to the top of panel 1 leaving the bottom of panel free for the attachment of the lower gripper.

11 to 15. The lower gripper is released from panel 0 and transported for attachment to the bottom of panel 1.

With the completion of event 15 the assembly equipment, except for the middle gripper, is in the same position relative to panel 1 as it was relative to panel 0 at the completion of event 1. It is therefore necessary, with some small modifications, to repeat events 2 through 7 to achieve the assembly of panel 2 to panel 1 as well as 3 to 2 and all subsequent panels.

The modifications in the panel-2-to-panel-1 and all subsequent assembly motions are due to: (1) the decreasing height of the stack as the assembly progresses and panels are removed from the stack, and (2) changes in relative positions or assembly angles between different panels depending on their location on the reflector.

The decrease in stack height (1) is systematic requiring a systematic biasing in the 1 and 5 drive functions with the progress of the assembly.

The changes in relative panel assembly positions (2) take place only three times: the assembly positions are the same for panels 1 to 5, for panels 6, 9, 12, 15, 18, 21, and for panels 10, 11, 13, 14, 16, 17, 19, 20, 22, 23. These changes in assembly position are achieved by modifications in the 4 and 6 drive functions as required.

It follows from the above that one basic motion, or sequence of events, together with the indicated systematic variations in drive functions

1, 5, 4, and 6, are necessary to achieve the overall reflector assembly.

The control logic needed to control the assembly equipment is rather simple by most computer standards. In this example the estimate control logic would weigh under three pounds.

7. FEATURES OF THE RATIO TECHNIQUE

1. It is generally possible to design space structures such that they can be sectionalized into panels which nest in each other to minimize storage volume and susceptibility to damage by boost loads. The panel shapes can be chosen to satisfy available storage volume requirements. In the deployed state the structures are ribbed, and have structural continuity.

2. The assembly equipment can be manually or automatically controlled.

3. For deployment of a structure such as an antenna from a space station it is possible to choose panel assembly sequences in which:

(1) The first panel in the stack of panels is attached to the station and the assembly equipment carrying the stack moves away from the station as it assembles the rest of the structure. (This is the assembly sequence described in this paper.)

(2) The assembly equipment and stack of panels are attached to the station and the structure as it is assembled moves with respect to the station. In this case the last panel of the assembled structure is attached to the station. This assembly sequence facilitates access to the assembly equipment for control, repair, or maintenance by the station personnel, and reduces the instrumentation complexity

for checking the alignment of each assembled panel. This sequence also introduces the possibility of having the assembly equipment available, attached to the last assembled panel, to serve as the antenna altitude control pedestal.

A variation of (1) above is to attach the station to any of the panels to be assembled. As in (1), at the completion of assembly, the assembly equipment is on the last assembled panel. If the chosen panel to which the station is attached is the last panel, then the conditions in (2) exist.

4. Typical preliminary design estimates indicate that for 30 to 200 foot reflector structures having structural weights on the order of 0.05 lbs. per square foot the automatic assembly equipment weight ranges from 50-to-100% of the structural weight for the smaller structures to 10-to-20% for the larger structures. Actual structural and assembly equipment weights depend upon such parameters as: the number of panels into which the structure is sectionalized, structural tolerances, structural rigidity, assembly time, storage volume, etc.

5. The size of the structures that can be assembled is mainly limited by the number and sizes of panels which can be orbited. The same assembly equipment having assembled one stack of panels can be shifted to a new stack to continue the assembly operations.

6. The fasteners used to hold the panels together in the assembled state may be of the reversible or irreversible screw, latch, explosive rivet, magnetic, chemical, or metal forming types. In the stowed state the panels may be held together by similar, reversible fasteners, or by a separate mechanism or manual device which releases one panel at a time from the stack. The fasteners may be

actuated through the action of the transport mechanism or by a separate fastener actuating mechanism. The fastener systems generally perform panel-to-panel lead-in, alignment, and lock-in functions.

7. The slow deployment speeds of the structure make it possible to test and evaluate flight-weight hardware in a gravity compensated (underwater) environment.

8. The assembly equipment is generally significantly more rigid than the structure it is assembling. This makes it possible for the equipment to pull the structure into alignment in the event of small misalignments as caused by reassembly tolerances (thermal gradients, etc.). The fastening action is therefore limited to between panels held by gripper frames. (Referring to Fig. 1, panel 5 is fastened to panel 4 when the middle gripper is holding panel 4. Then the possible misalignments between panels 0 and 5, which may result from the sequential assembly of panels 1 to 5, are pulled out by the assembly equipment. If for some reason the misalignments are excessive, the assembly process may be reversed to look for or eliminate the cause of the misalignment.)

9. It is generally possible to sectionalize the structure such that the effective relative positions of the structural fasteners are the same for each panel while (as in the case of a paraboloidal reflector) the surfaces or geometry of the panels are not the same. Variable extensions in the panel gripper functions can be used to extend the allowable variation in the relative positions of the fasteners.

10. Assembly equipments consisting of two or any number of gripper or manipulator arms are theoretically possible. The equipments may (1) be extended to handle separate structural corners for implementing panel-to-panel fastening, (2) providing articulation at the joints for adjusting panel-to-panel alignment, and (3) for serving other station material handling functions when the structural assembly is complete.

11. The assembly equipment can carry a panel-to-panel position register system. This system may use optical or mechanical devices for sensing the alignment or successful completion of a panel assembly.

12. Fixed or variably adjusted dummy panels (depending on the structure) may be substituted for damaged panels. The assembly equipment may be used for separate handling of these panels.

CHEMICAL RIGIDIZATION OF PREFORMED FLEXIBLE FOAMS

J. F. HANNY, J. W. JONES, G. H. PETERS, AND J. C. SCOTT

CAPSULAR RESEARCH AND PRODUCT DEVELOPMENT DEPARTMENT

THE NATIONAL CASH REGISTER COMPANY

In order for man to continue to expand his knowledge of space, it is essential that he develop materials and structural concept that can be used to erect, support, and maintain large space laboratories. The materials and structural designs selected must be compatible with the payload capabilities of current launch vehicles.

At the present time, there are definite weight and volume limitations imposed on the space structure designer if he only considers the conventional stay-as-they-are structures. However, if he can extend his material reservoir to include expandable structures, his design goals can be achieved without sacrificing valuable space or equipment.

The Aero Propulsion Laboratory, Wright-Patterson Air Force Base, Ohio, has recently awarded NCR a research and development contract to develop and optimize a chemical rigidization system for expandable structures. The NCR chemical rigidization system utilizes a pre-formed, flexible polyurethane foam, of a high porosity grade, as a matrix phase for a vinyl-type monomer. The impregnated foam system is then adhered to the surface of the expandable structure. When desired, the structure may be expanded, and an on-command polymerization of the monomer is initiated, thereby producing a rigid structure.

The anticipated application for this rigidization system dictates a set of rigorous conditions, under which it must operate, as well as a number of design requirements that must be met. The system must be stable in an aerospace environment, as well as under terrestrial conditions. However, when exposed to

an aerospace environment, the rigidization reaction must be amenable to a low energy initiation mechanism, and once initiated, it must be fast and effective. The rigidized material should possess a high strength-to-weight ratio and a low density.

With these conditions and requirements in mind, NCR remains confident that this rigidization system is quite adaptable to its anticipated application.

The rigidization of the flexible foam is primarily dependent upon the polymerization of the absorbed monomer. The vinyl-type monomer is a clear liquid, having the following physical properties:

Boiling Point	-	200° C at 1 Torr
Color	-	Colorless to pale amber
Specific Gravity	-	1.076
Refractive Index	-	1.4620
Water Solubility	-	Insoluble

The polymer is obtained by a free radical polymerization mechanism and is a clear, glass-like, completely thermoset material. Some of the polymer's physical properties are as follows:

Tensile Strength at 25° C.	-	4000 PSI
Refractive Index	-	1.5024
Dielectric Constant (60 CPS)	-	5.5
Thermal Conductivity - (BTU/hr., 1 ft. ² /°F/in)	-	2.4
Light Transmission (% at 4500 Å)	-	92

To effect polymerization of the monomer, it is necessary to dissolve therein a free radical generator or initiator. The decomposition of this initiator into free

radicals is hastened by the presence of a reducing agent. Studies indicate the initiator has a slight tendency to decompose when dissolved in the monomer, and permitted to stand at room temperature. If the solution is allowed to stand long enough, the free radical concentration may increase to a critical level, thereby initiating polymerization. It is this gradual build up of polymer chains that limits the stability of the system. However, by introducing into the system some free-radical scavenger or polymerization inhibitor, these free radicals are "tied up" and rendered inactive. During the course of this study, it was observed that oxygen is a very effective inhibitor for this system, and that exposing the impregnated foam to atmospheric oxygen gave a shelf life in excess of six (6) months. Permitting the impregnated foam to stand for this length of time had no adverse effects on its normal rigidization characteristics.

Rigidization Rate

The rate at which the flexible foam can be rigidized is dependent upon: (1) the polymerization rate; (2) the number of initiation sites and; (3) the impregnated foam's density. The effect of monomer concentration on the flexible foam rigidization rate has been determined by maintaining a constant polymerization rate and number of initiation sites, and altering the concentration of monomer in the impregnated foam.

The samples were prepared by impregnating the flexible foam matrix with various amounts of monomer initiator solution to obtain different rigidized foam densities. The polymerization reaction was initiated by introducing a catalyst into the monomer-impregnated foam. This was accomplished by adhering NCR microcapsules containing the catalyst to the surface of a nichrome heater strip and bringing this into contact with the foam surface. Initiation was achieved by passing an

electrical current through the heater strip.

Figure 1, is a graph of the rigidization time versus density of the rigidized foam, and indicates the range of monomer concentration that can be used without appreciably changing the time required to rigidize a given volume of flexible foam. This indicates that foam impregnation is not a very critical area, unless the strength properties of the rigidized structure are affected. (All foam sections had the same initial volume (5" x 5" x 1") and were rigidized at 0.05 Torr.)

Rigidization Exotherm

The rigidization exotherm is the result of heat energy being generated by the rapid bond formations in the free radical polymerization of the monomeric foam impregnant. The maximum exotherm obtained from the rigidization process is a function of the quantity of foam impregnant. The greater the quantity, the higher the exotherm.

Studies were conducted to determine the relationship between rigidization exotherm and the density of the impregnated foam. Samples of impregnated foam were prepared having densities in the range of 4.8 lbs/cu. ft. to 31.5 lbs/cu. ft. A thermocouple was inserted into the sample, and the assembly placed in a vacuum chamber. After the pressure was reduced to 0.075 Torr, the rigidization was initiated by releasing the encapsulated polymerization catalyst. The peak temperature was observed and recorded as the rigidization exotherm. Figure 2, is a graph of the rigidization exotherm versus the density of the impregnated foam. By varying the density of the impregnated foam from 2.5 gms/in³ to 5.0 gms/in³, the rigidization exotherm is increased by approximately 60°F.

Strength of Rigidized Foam

Previous studies indicated the overall rate of rigidization and the rigidization

exotherm are dependent upon the density of the monomer-impregnated, flexible foam. The following study was initiated to determine the effect of the varying of the density of the impregnated foam on the strength properties of the rigidized foam. The samples rigidized during the exotherm study were used to determine the tensile and compressive strengths. One-inch cube sections were cut from the rigid samples and adhered to specially-designed, stainless steel fixtures for tensile strength evaluation. Figure 3, is a graph of the tensile and compressive strengths of the rigidized foam as a function of the density of the impregnated foam.

Composite Adhesive

NCR's expandable and rigidizable solar collectors are based on a structural composite, made up of aluminized Mylar and flexible foam. The composites' structural integrity and packaging capability is dependent upon the development and/or selection of flexible adhesives that will effectively adhere to the composite materials.

A number of adhesives of various types are being investigated:

- 1) Silicones
- 2) Urethanes
- 3) Polyesters
- 4) Polyamides
- 5) Polysulfides
- 6) Epoxies
- 7) And combinations thereof.

Some of the properties and requirements that must be inherent in the adhesive systems are listed below:

- 1) Good adhesion to the Mylar and the impregnated foam before and after rigidization.

- 2) Flexibility upon curing
- 3) Minimum shrinkage upon curing
- 4) Good flexural strength
- 5) No adverse effects on composite materials or the rigidizing system.
- 6) Adaptability to space environments, as well as terrestrial environments without adverse effects on the system, and
- 7) Adaptable to various methods of application - casting, spraying, etc.

The most promising adhesives evaluated to date are the silicones and polyurethanes. Many of the adhesives being investigated will bond to Mylar and the dry foam, but when the monomer is introduced into the foam, a delamination occurs at the Mylar interface. It is most desirable to obtain an adhesive that will bond to both the Mylar and impregnated flexible foam, thus allowing the foam to be impregnated before the solar collector is assembled. By impregnating the foam first, it is possible to obtain a more uniform distribution of the monomer in the foam.

A second problem area related to the adhesive system is the quality of the reflective surface. The reflective surface of most of the collectors has been good, but there is need for improvement. There appears to be a correlation between the quality of the reflective surface and the composite adhesive. It is anticipated that once a functional adhesive is developed and/or selected that meets the bonding requirements, the problem of obtaining excellent mirror surfaces will also be solved.

Rigidization of Solar Collectors

A number of fifteen (15) and eighteen (18)-inch diameter solar collectors have been rigidized under vacuum conditions, 10^{-3} Torr. These preliminary experiments were designed to evaluate the rigidization system's functionality, reproducibility,

triggering mechanism, and the geometric tolerances that could be maintained during rigidization. To date, the rigidization system has functioned very effectively and reproducibly, giving consistent structural properties, rigidizates, and geometric tolerances. The collectors also possessed very good reflective surfaces.

Figures 4 and 5, are cross-sectional diagrams of the fabricated collectors, and Figures 6 and 7, are photographs of the eighteen (18)-inch and three (3)-foot diameter solar collectors that were rigidized in the high vacuum facilities at Wright-Patterson AFB.

Additional collectors, ten (10) feet in diameter, will be fabricated, rigidized, and evaluated in the near future to determine the scaling effects induced by the presently used materials and fabrication techniques.

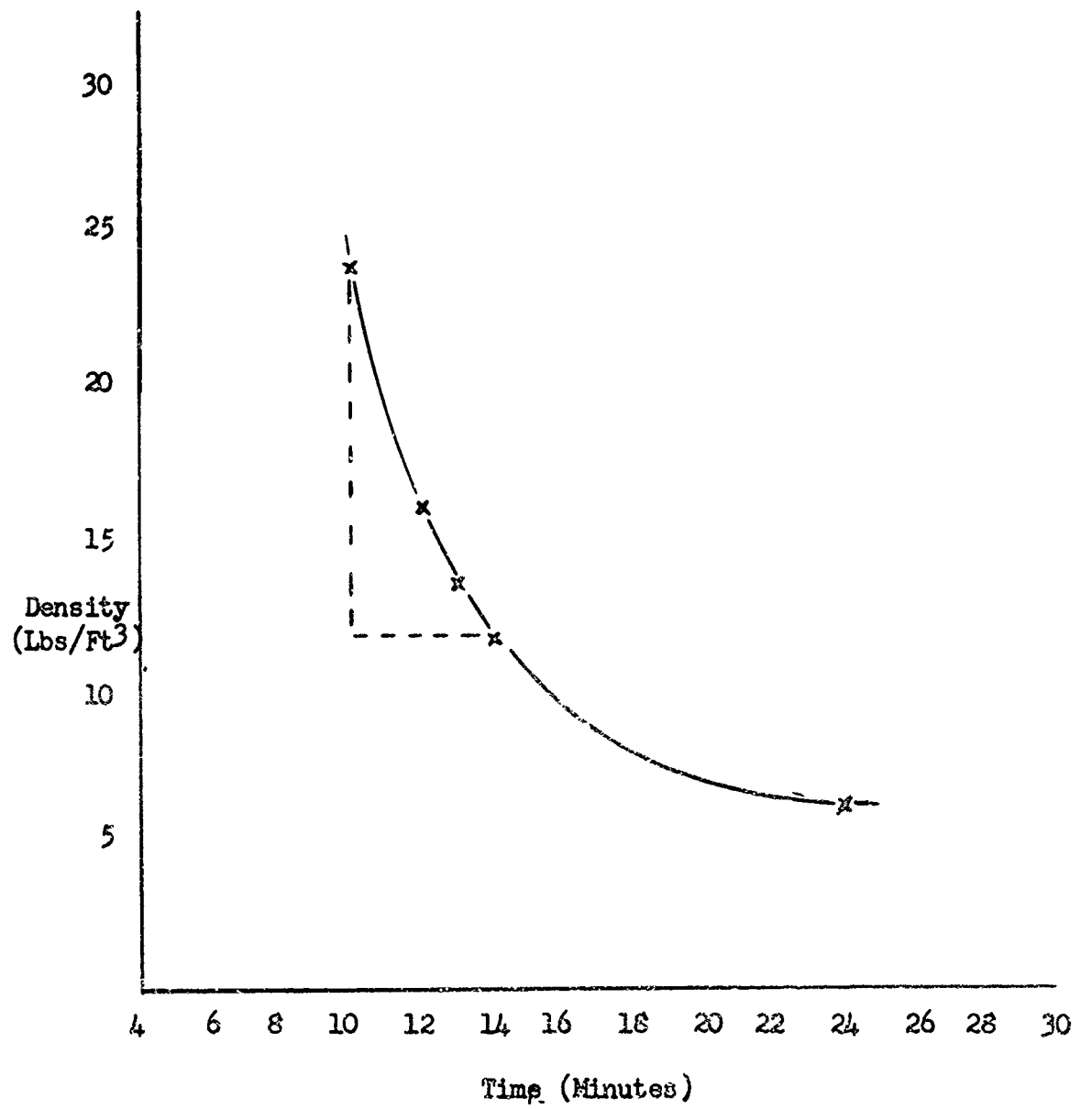


FIGURE 1
Rigidization Rate Vs. Density
of Impregnated Foam

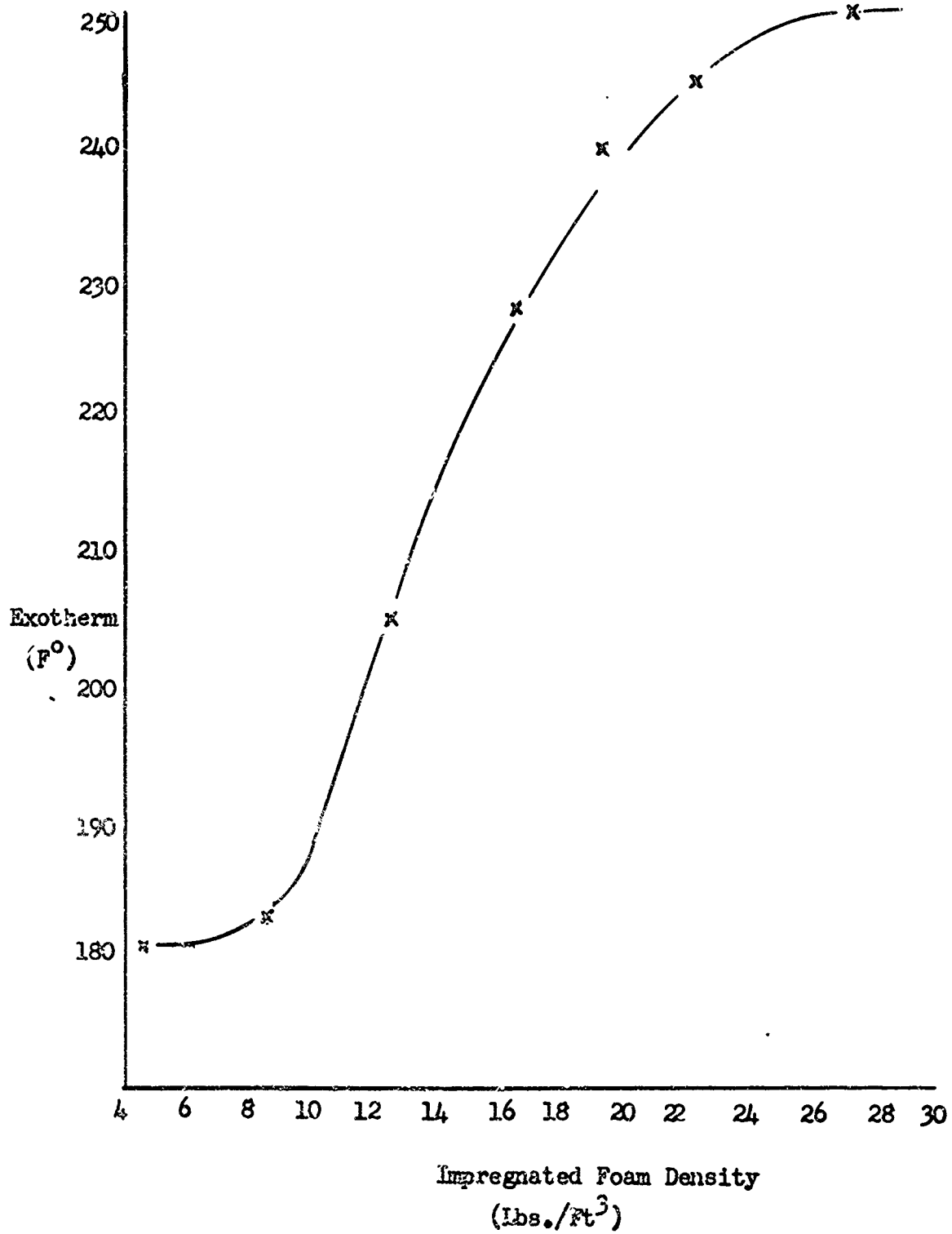


FIGURE 2
Rigidization Exotherm Versus
Impregnated Foam Density

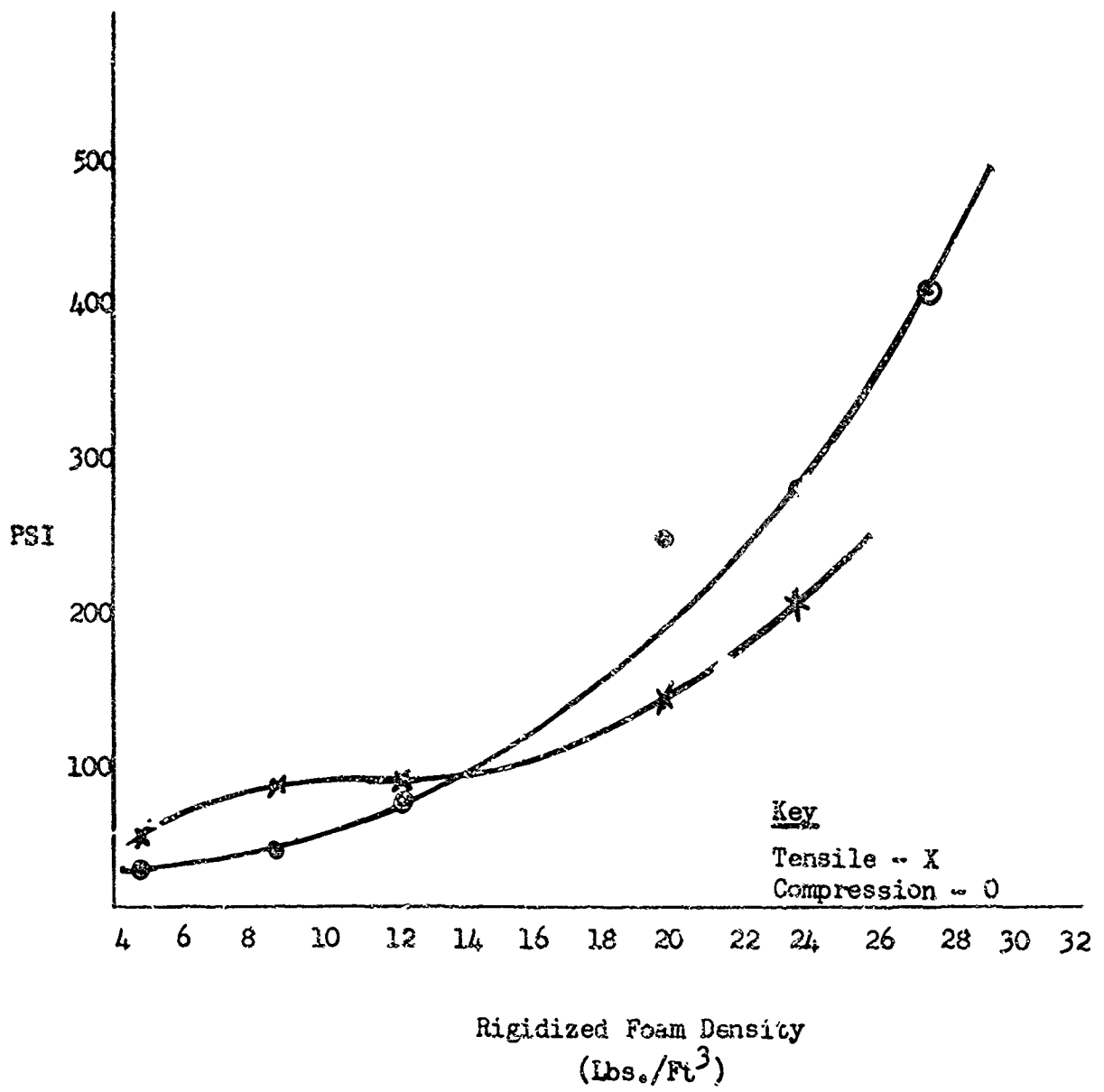


FIGURE 3

Strength Properties of Rigidized
Foam Vs. Rigidized Foam Density

NOT DRAWN TO SCALE

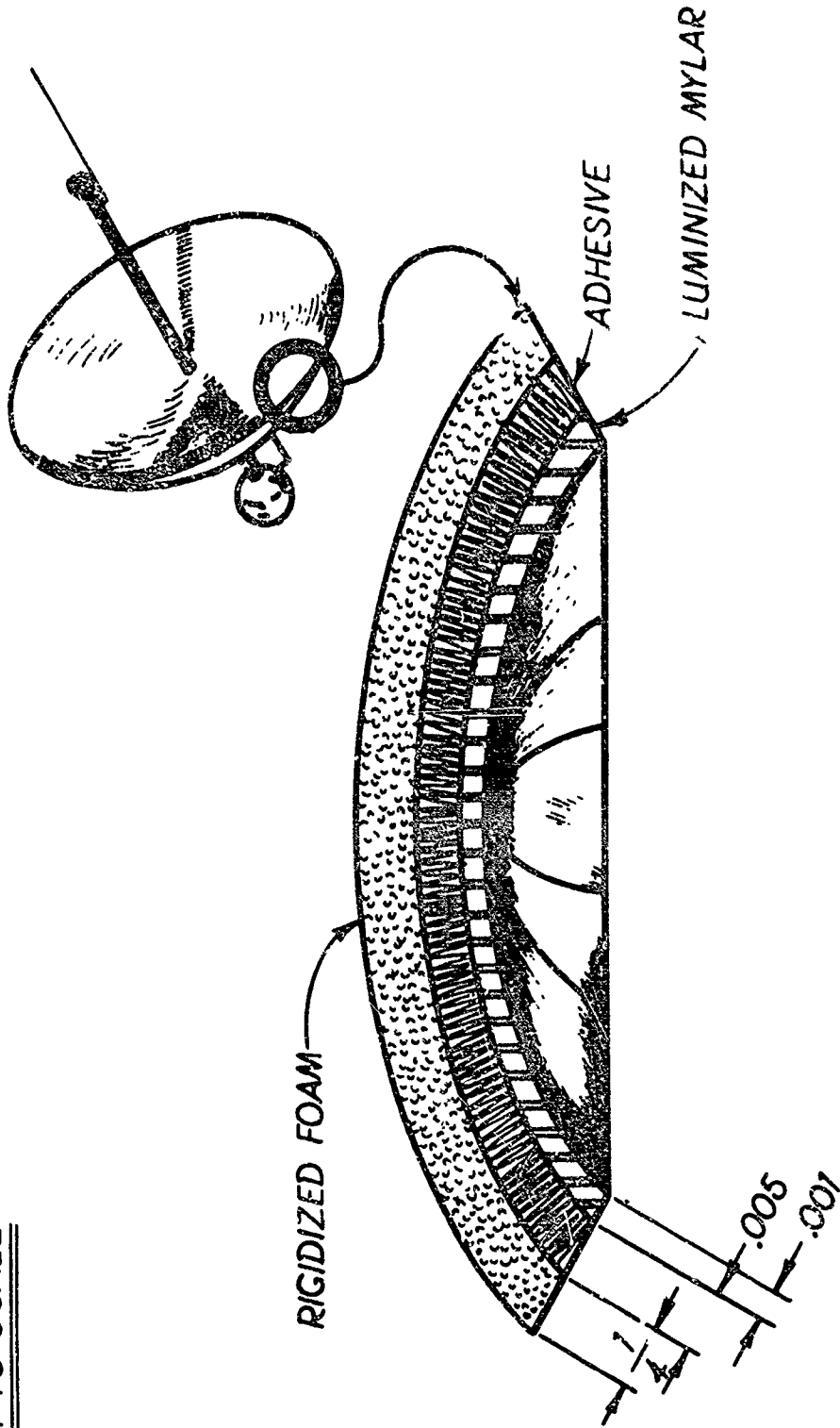


FIGURE 4
RIGIDIZED SOLAR COLLECTOR WITHOUT STIFFENER RING (SECTION SHOWN)

NOT DRAWN TO SCALE

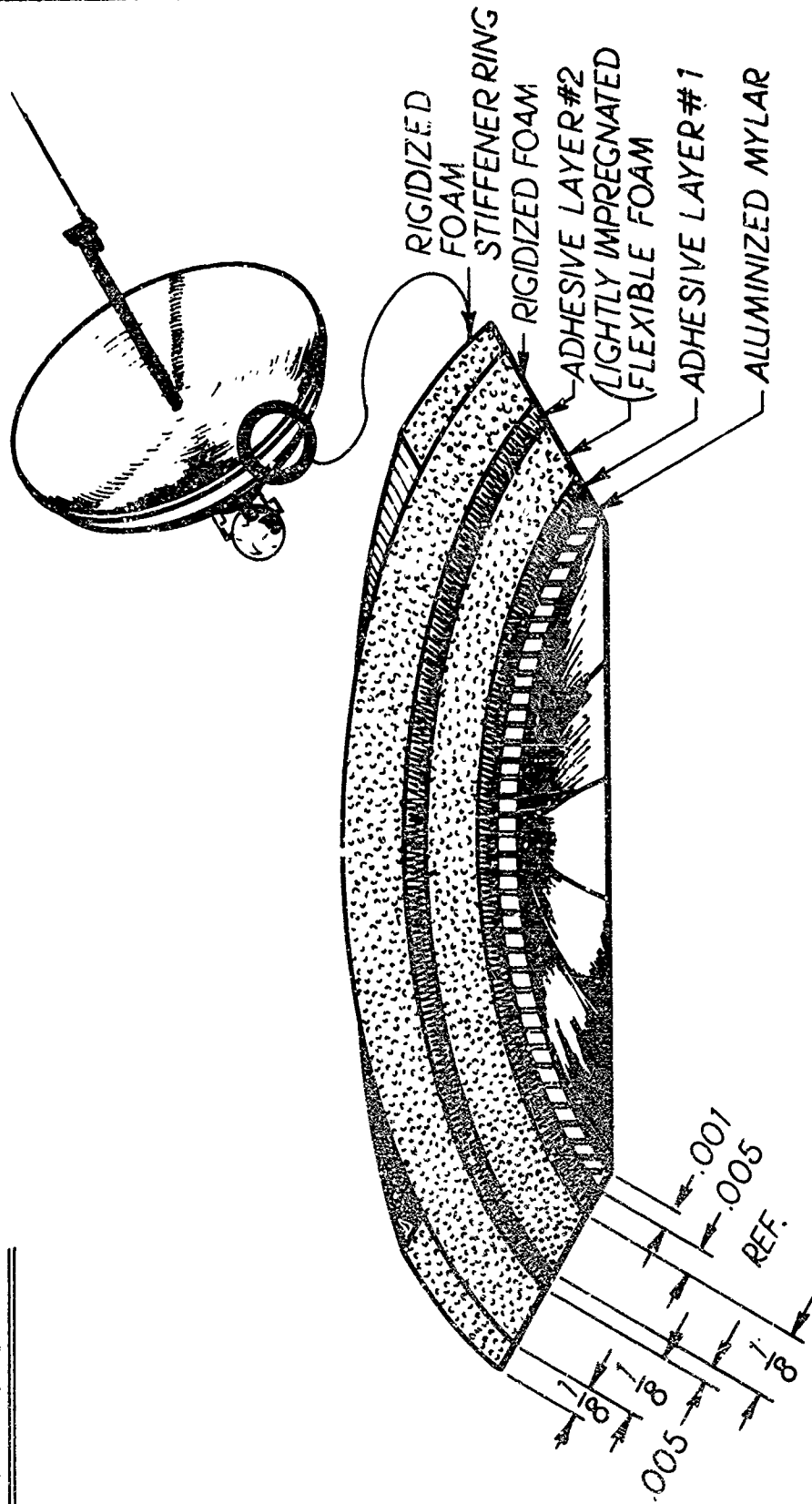


FIGURE 5
RIGIDIZED SOLAR COLLECTOR WITH STIFFENER RING (SECTION SHOWN)

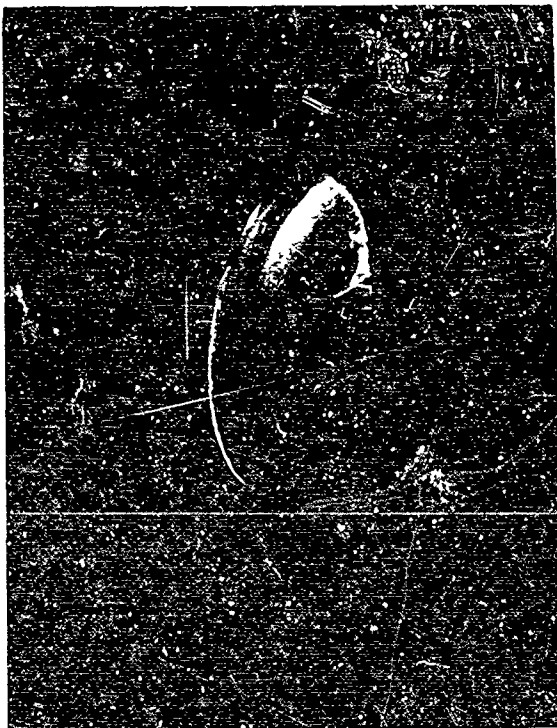
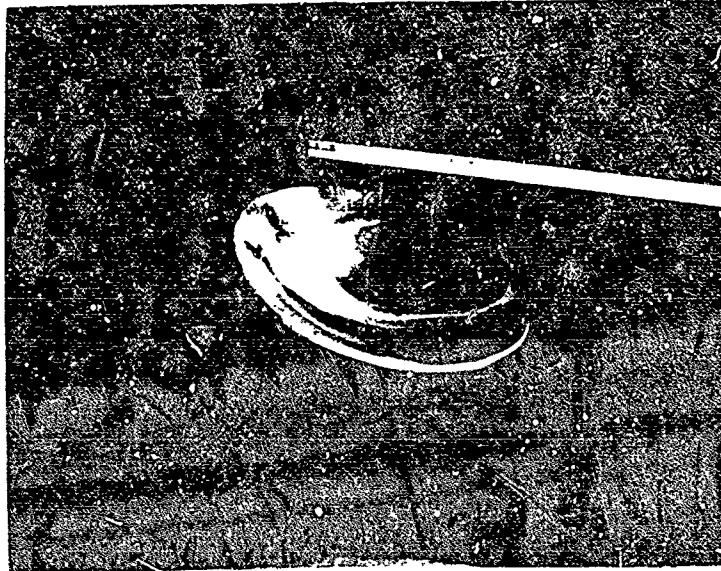
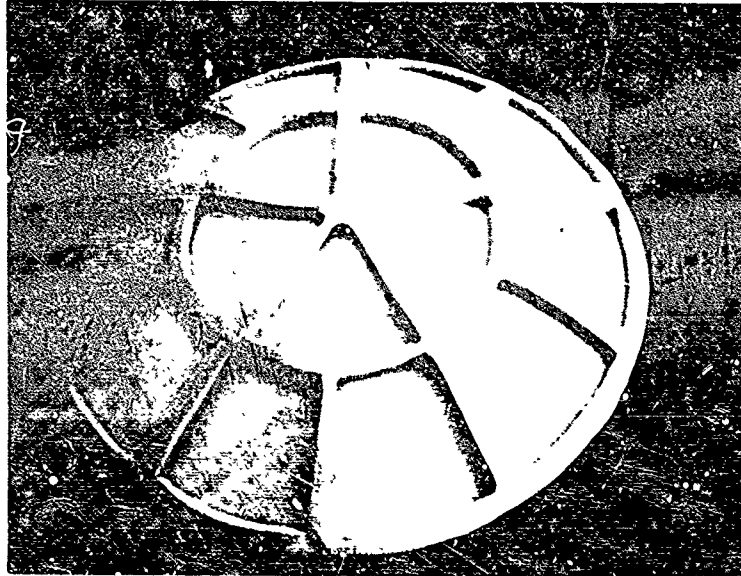


FIGURE 6
Rigidized $1\frac{1}{2}$ Foot Diameter
Solar Collectors



BACK



FRONT

FIGURE 7

Rigidized 3 Foot Diameter Solar Collector

MAINTENANCE TECHNOLOGY FOR SPACE SYSTEMS

Chester B. May
Air Force Aero Propulsion Laboratory

INTRODUCTION

Early assessment of man's actual capability and utility in performing maintenance tasks in the hazardous environment of space is necessary as the results could significantly affect the space maintenance concepts and the role that man will play in maintaining future space systems.

The first manned American space program established that man can contribute significantly to the success of space missions with the proper design consideration in the system. This recognition has led to the establishment of experiments for the two manned American space program that will explore the ability and utility of man in maintaining his vehicle in a space environment.

This paper will attempt to define the technology that presently exists in the various disciplines with respect to their utilization for establishing design criteria to maintain vehicles in a space environment. The areas to be discussed are; joining techniques, maintenance operations, assembly techniques, electrical repairs, and utilization of abstract models.

Maintenance Objective

The objective of the space maintenance experimentation is to obtain the capability to maintain, assemble, and repair vehicles in a space environment. To accomplish this mission the following approach is being used.

1. Develop the tools and techniques to enable the accomplishment of maintenance on a vehicle in a space environment.
2. To develop the design criteria necessary for the fabrication of systems to be maintainable in a space environment.
3. To develop and utilize abstract models for the maintenance planning of space systems.
4. To design and fabricate the necessary test models that will enable verification and establishment of man's ability to perform repairs in the various disciplines of maintenance for space.

There is a definite need for an organized space maintenance program to bring together all of the work that has and is being done by both in-

dustry and the government in the area of space maintenance. Proper organization of the technology in the various disciplines (required to accomplish maintenance on a total system) would insure the design and fabrication of test models that could be utilized to effectively obtain design criteria to be used in designing future space systems for longer and more extended missions.

MAINTENANCE TECHNOLOGY

General: The exploration of the space frontier for effective utilization by man will require him to live in this new environment for long periods of time. Some of the common subsystems required to make up the environment man must take with him to survive in this new frontier are: structures, propulsion, electronics, environmental control system, power supply and fluid system. In order to operate a system containing these subsystems a detailed maintenance analysis of each subsystem must be performed along with the necessary research to investigate the constraints placed on the orbital worker by space suits, weightlessness, available tools, and phenomena such as micrometeorites and radiations.

There are certain tools, techniques, and concepts that can be established from a research point of view to accomplish maintenance on representative subsystems in space without designing to maintain a particular system. However, the research would probably prove worthless if no plan were formulated to implement the research into a practical maintenance program for maintaining vehicles in space. The following discussion will be on concepts, tools, and maintenance techniques and how they can be utilized to establish design criteria for future systems.

Joining Systems

Whether one is familiar with maintenance requirements or not, it is not hard to visualize the need to establish methods of joining materials in space. Some of the basic requirements of a joining technique for space would be; (a) must operate in a vacuum of 10^{-12} torrs, (b) must operate with materials over the temperature range of -150°F to $+250^{\circ}\text{F}$, (c) must be capable of bonding to various types of materials used to fabricate space vehicles and (d) must be safe and capable of being accomplished with man in the loop both inside and outside of a space vehicle. There are four areas presently being explored for establishing techniques that can be utilized by man in a space environment to join materials or objects together. These are adhesives, soldering, brazing, welding and mechanical fasteners. The temperature range for the operation of these systems are shown in Figure 1.

Adhesives - The programs to date directed toward developing adhesives systems for the space environment have been concerned with bonding problems such as; astronauts to work sites, equipment to work site, etc. Basic requirements for this type of system are; short cure times (10 to 15 seconds), small power requirements (e.g. D-cell nickel cadmium range) for

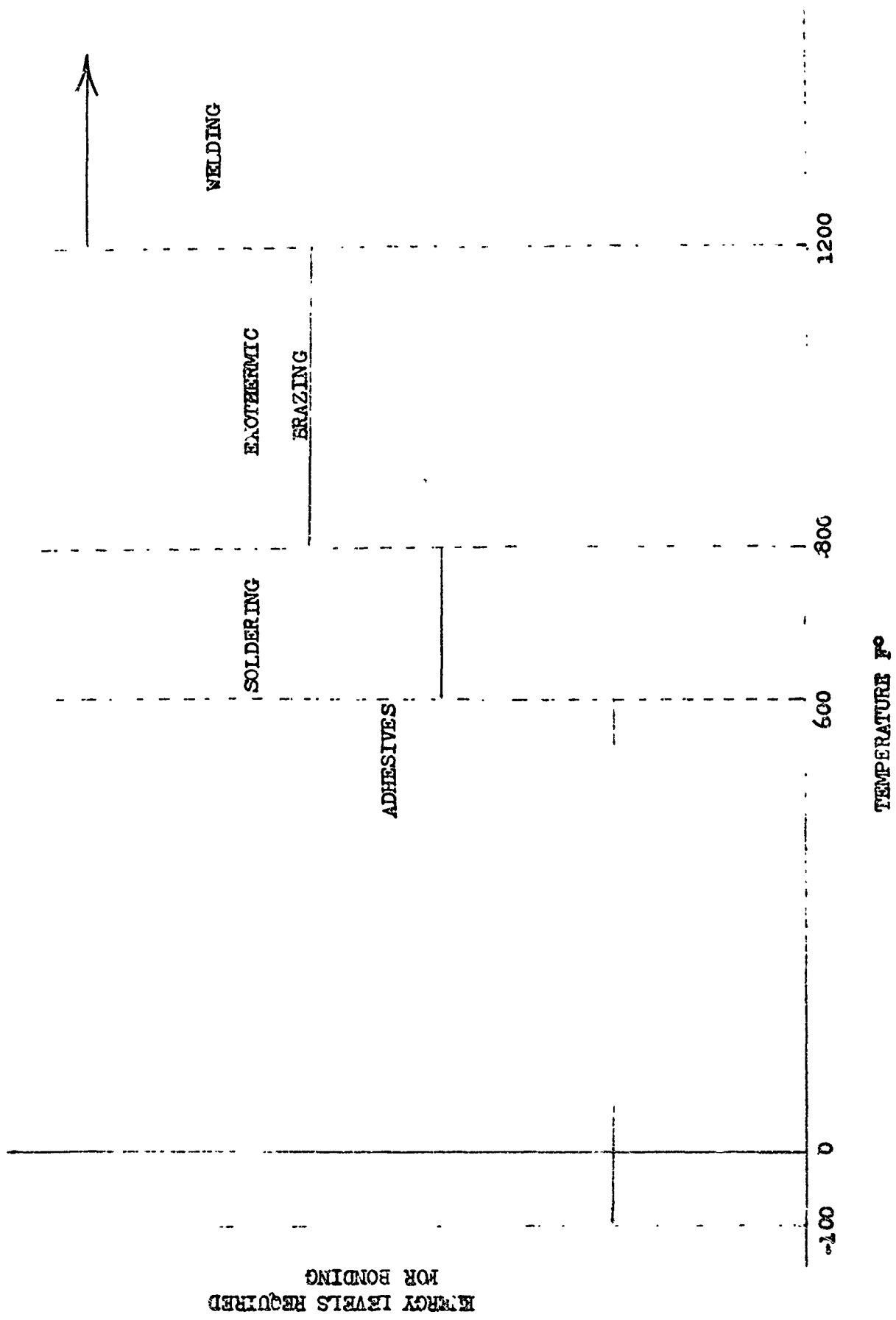


Figure #1

ease of protability, be able to function in a dispenser mechanism for reusability, and strengths of at least 100 psi in tension and shear.

The initial program directed toward developing an adhesive system to satisfy the above requirement was performed by the Archer Daniels Midland Co. (ADM) under an Air Force Contract. The austerity of the program limited the scope to developing an adhesive pad that could be utilized by the Air Force to prove feasibility of the astronaut adhesive/mechanical bonding concept. The system accomplished this and also defined the problem areas that would have to be solved if off-the-shelf adhesives were to be modified for use in space (See Reference 1).

Based upon the problems defined in the ADM effort, two areas were defined for immediate work; (a) the encapsulation of an epoxy resin adhesive system, and (b) the development of a surface pre-heat pad utilizing an exothermic chemical reaction system (See Figure 2). Efforts in these areas are under contract for development by the Air Force. The adhesives systems being studied in these research programs are; epoxy resins systems, hot melt system, and thermal plastic systems. The application of this work for space structural adhesive system will be discussed at the end of the above efforts.

Adhesives are now available for bonding practically all solid materials (organic or inorganic) in the earth environment. Extending this technology for use in the space environment will require considerable study and definition of the joining problem to be accomplished. It is expected that as man becomes more active in the space role the advantages provided by adhesives system in the areas of; assembling structures, bonding objects to work site, electrical insulation, and electrical conductors will in the near future emphasize the importance of developing adhesives for use by man in the space environment.

Soldering

Soldering is one of the most common methods of joining electrical wires to terminals for all types of equipment in the earth environment. However, in considering the various techniques of joining electrical wires in space it probably commands the least amount of attention at this time. Some of the limitations of the soldering techniques justifying this are; (a) The requirement for alignment of the joint while the joint is being made, (b) the problem of pieces of the joining material floating out of control, and (c) the lack of analysis of performing the operation in an oxygen rich environment.

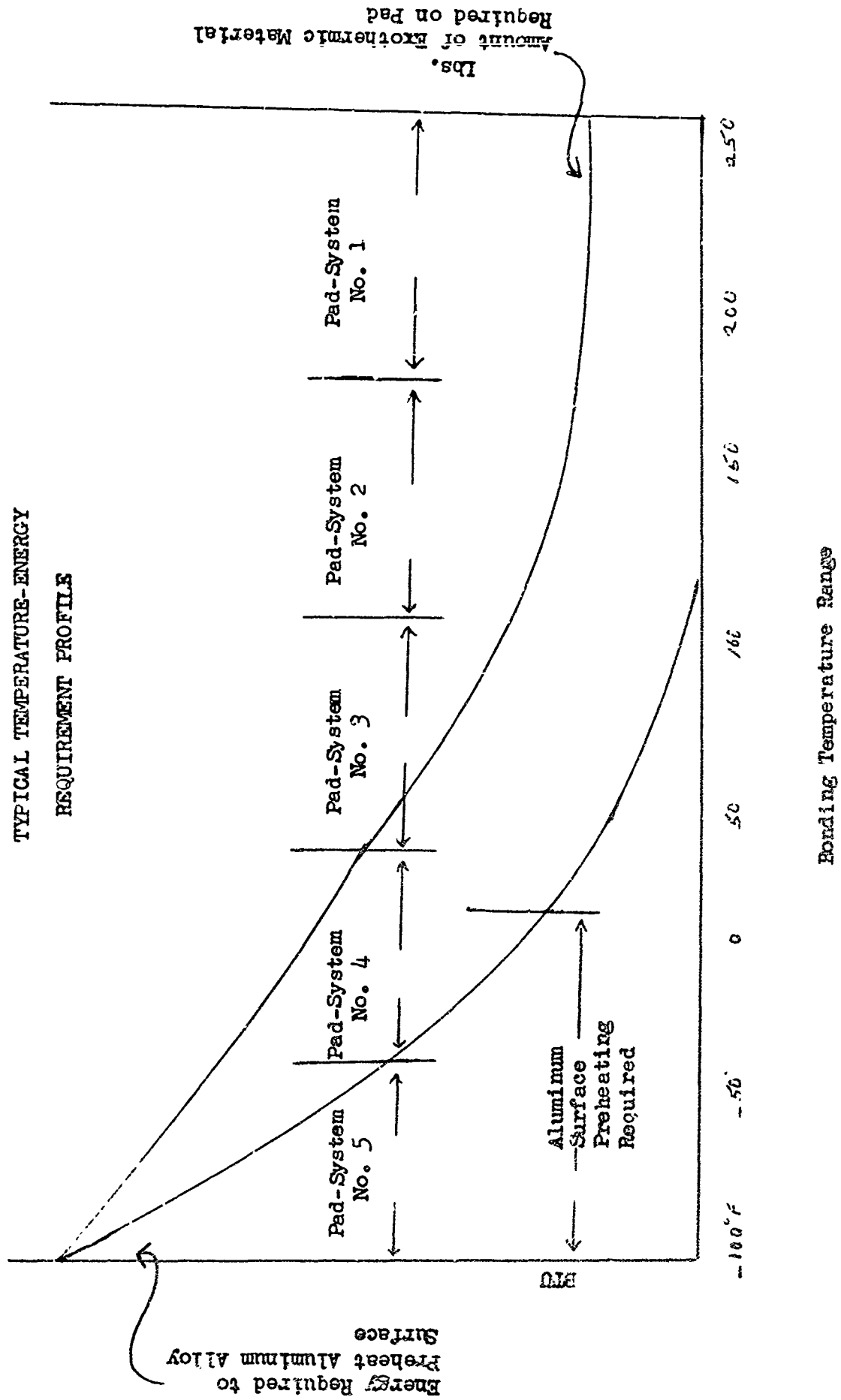
Brazing

Most of the work accomplished in the area of brazing as a technique for joining materials in space has been accomplished under an Air Force contract (Reference 2). The effort developed and brazed in a vacuum exothermically brazed joints of stainless steel and titanium alloy, capable of withstanding structural loads.

Exothermic chemical reaction was the heating concept developed that provided heat pulses to the base metal and braze alloy to accomplish the

FIGURE 2

TYPICAL TEMPERATURE-ENERGY
REQUIREMENT PROFILE



joining of the materials. The concept provides the following advantages; (a) controlled heating times, (b) remote control capabilities, (c) module bonding units and (d) lightweight module bonding unit.

The work accomplished under the above effort has provided technology that could be explored now on an actual space test bed for application to joining problems in a space environment.

Welding

The exploration of welding techniques that can be utilized by man in a space environment has been limited to the electron beam technique (Reference 9). There has been considerable discussion on the advantages and disadvantages of various welding techniques (e.g. ultrasonic, friction, explosive, arc, and coldwelding) for space application, but the only welding technique where representative hardware has been designed for feasibility testing in space is the electron beam welding technique.

The Air Force has established the basic requirements for the design of an electron beam gun type welder that could be utilized by a suited astronaut in a space environment. This was accomplished for the purpose of establishing feasibility of welding joints in space. A physical model representing the concept has been fabricated for demonstration purposes. The actual development of operating hardware remains to be accomplished.

Welding techniques that take advantage of the space environment (e.g. friction welding, coldwelding) are definite candidates for future research along with explosive welding. It is the author's belief that in order to develop an effective welding technique for joining materials (with man in the loop) tests will have to be accomplished using a vehicle in space.

Mechanical Fasteners

The area of mechanical fasteners for utilization in space has not as yet experienced many changes or new innovation. No one to date has made a comprehensive analysis of the mechanical fastener area for the specific purpose of designing a fastener with the following factors as constraints; operation by a suited astronaut, space environment, structural loads and space assembly operations.

Fasteners such as Allen's Aeroscrew/Aeromut fastener technique exemplify a more efficient type of fastener but it was not designed for use by a suited astronaut in a space environment. Unique fasteners and rivet concepts are needed for the space assembly task that man will be required to accomplish during the next several decades of manned spaceflight.

Electrical Repair

The magnitude of electrical equipment aboard space systems will require that man have the capability to accomplish electrical maintenance in space. This capability will consist of; detection, isolation, special

tools, and positive control over the component parts. The philosophy of electrical maintenance for space will not be discussed in this paper, but rather the efforts directed toward establishing design requirements for tools to be used in electrical repairs.

One of the efforts being pursued at the present time by the Air Force is directed toward the development of a manual device for locating electrical arc-producing faults (Reference 4). The tool designed and fabricated under the above effort operates by sensing the radiation emitted by the sensing elements. The tool permits fault isolation by manual scanning techniques and detects signal levels as a function of probe location. The tool was designed to locate and isolate an RF disturbance within a two square inch area. The readout is visual and is located within the hand-held unit (total unit housed in two separate units).

An in-house study has been conducted by the Air Force to establish the requirements for the design of a wire joining tool that can be used by a suited astronaut. The function that such a tool should be able to accomplish are; wire wrap with built-in insulation capabilities, wire joining (e.g. fusion) with insulation capabilities and insulation of wires (e.g. epoxy coatings).

Fluid System Repairs

The research to date for maintaining fluid systems suffers from a lack of definition as to what is really needed for maintaining fluid systems in space. Maintenance engineers have only to take a look at systems such as; attitude control, propellant storage, equipment and station environmental control, space suit environmental control and electrical power (fuel cells) to realize the importance of being able to accomplish maintenance on systems containing fluids in space.

The approach being followed for fluid maintenance is to recommend simple experiments (using a space test bed to define the problem areas). These recommendations are based on detail analysis of fluid system repairs and the observation that there are many functions required to be accomplished in a fluid system maintenance task would be common to other requirements. Examples of this are; brazing a pipe coupling or brazing a structural patch, removing the shaft of an hydraulic actuator or removing the shaft of an electrical actuator, tightening a fluid line connector or tightening a structural fastener, etc.

The design, fabrication and testing of representative fluids tasks on simulators within the earth environment will provide valuable information concerning the repair technique for valves, pumps or similar assemblies without the loss of fluid. However, the data spectrum will not be complete for design criteria until end to end testing can be accomplished aboard a test vehicle in the actual space environment.

Tools

The utilization of motion simulators providing 6 degrees of freedom, and aircraft flying the Keplerian trajectory to provide approximately 30

seconds of zero gravity has provided invaluable information for the design of space tools. The maintenance concept that has evolved from studies accomplished on the above simulators has proven to highly effective in providing man with the capability to perform maintenance under weightless conditions.

The concept being pursued in the tools and techniques area for maintenance operations is to: (a) provide minimum reaction power tools with the necessary adapters to accomplish functions such as impacting, shearing, drilling, tapping, sawing, etc. (b) provide modified hand tools, (c) provide rigid and flexible work site attachment techniques for the astronaut, and (d) provide a special multi-high power (5-10 horsepower) tool for emergency tasks.

Power Tools - High output torque with low reaction was the basic requirement established for multipurpose power tools. The exploded drawing shown in Figure 3 illustrates the design of a multi-purpose minimum reaction electrical power tool. Operating with an unrestrained field and armature, this tool can produce a torque output of 15 to 50 ft. lb. with less than 0.016 ft. lb. being transmitted back to the operator. The multipurpose tool can be used to perform the functions of a wrench, drill, thread tapper, and screwdriver.

The multi-purpose minimum reaction power tool, commonly denoted the "Space Power Tool (SPT)", consists of a counter rotating mechanism and the tool handle which stores the batteries. The only torque that can be transmitted back to the operator is that caused by the friction in the bearings which support the counter rotating mechanism in the tool handle. By using the frictional force inherent in a fastened object that resists other forces until it is overcome, a controlled internal restraint mechanism transfers the reaction torque to the object being fastened.

The natural characteristics of a fastener which permits this transfer of the reaction torque are illustrated by the semilinear curve in Figure 4. As a tightening torque is applied, the fastener will not rotate; no motion in the cw direction will occur, until the torque exceeds the $\pm A$ level. As the tool turns in the counterclockwise direction during the tightening process, it will by design not exceed the $-A$ level; again by design, no torque will exceed the $+A$ level as the tool turns clockwise.

Tested under weightless conditions at Wright-Patterson Air Force Base, the SPT demonstrated its capability to torque a fastener satisfactorily while a negligible force was transmitted back to the operator. The success of these tests led to another study to evaluate and define the relationship between the SPT and fastener types and to determine design criteria which would ensure that the torque delivered by future tools would not be appreciably transferred back to the operator. The SPT has the capability to accept adapters developed to perform other functions such as cutting, sawing, hammering, riveting, and hole punching.

ELECTRIC MINIMUM REACTION SPACE TOOL

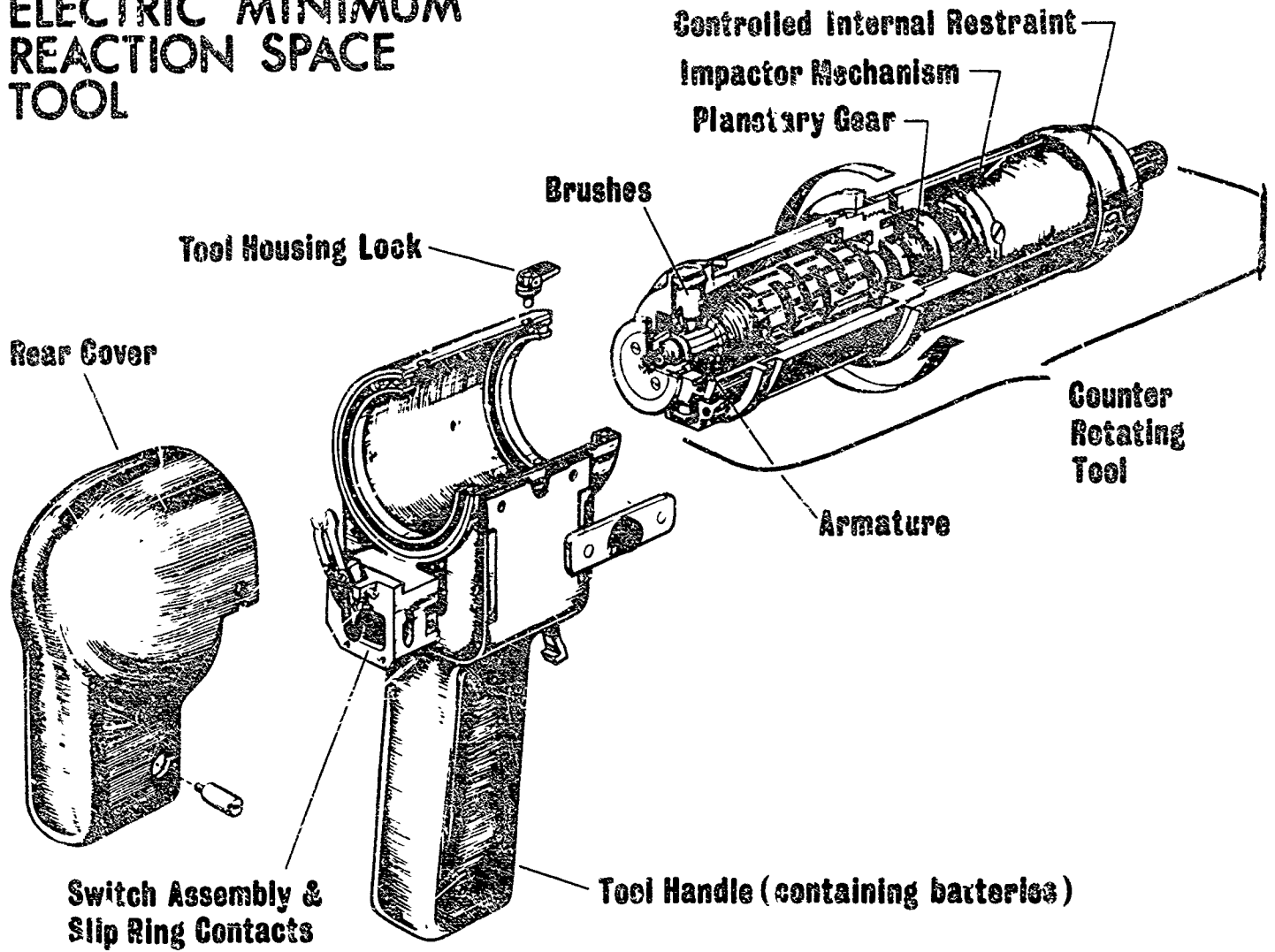


Figure 3

Minimum Reaction Power Tool

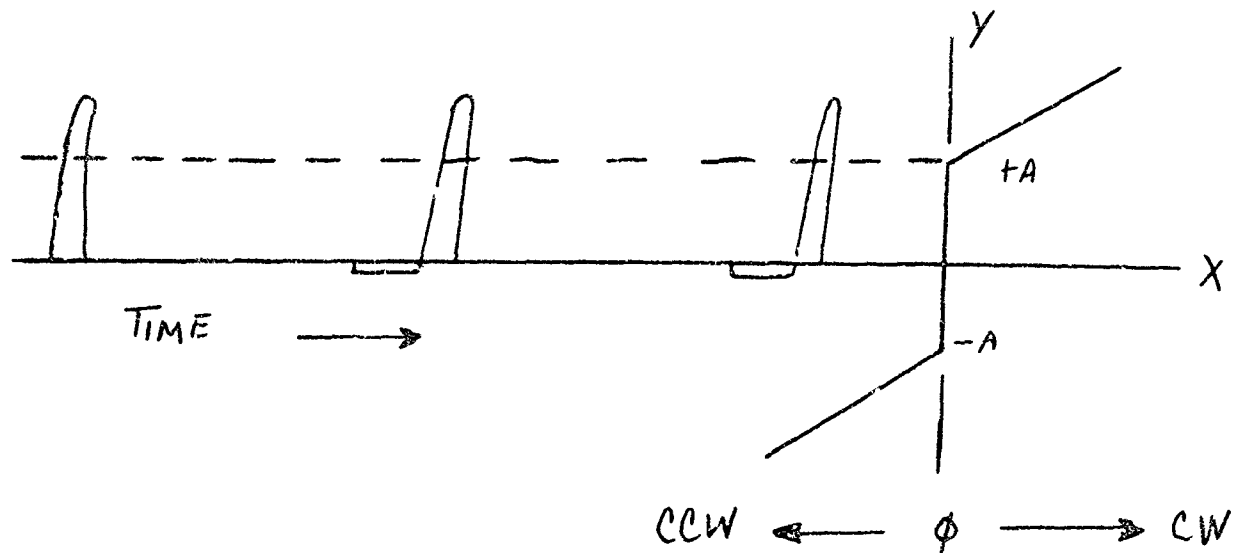


Figure 4

Natural Characteristic
Of A Fastener

Hand Tool - To obtain data relative to the magnitudes of torques and forces that a man could produce under weightless conditions, test subjects applied conventional tools to various tasks conducted during early tests in the simulated zero-g environments. Rather than being representative of work which could be performed in a weightless environment, the tests indicated the motions attendant with the work efforts which would prevent an astronaut from accomplishing useful work in space.

The Air Force has evaluated several unique tools developed by various companies to enable the in-house duplication of tasks performed by conventional tools in a normal earth environment. Many of these tools require special adapters at every bolt and a hand squeezing motion. Among the hand tools tested was a torque cancelling unit which uses two pins to transfer the torque to the structure and requires a squeezing motion to apply the torque. A summary of its evaluation is as follows:

The arrangement of the handles parallel to the plane of the work site or perpendicular to the axis of the fastener proved unsatisfactory because (a) the position required for the operator's hand was both inconvenient and tiring, (b) the particular squeezing action required was too arduous, and (c) the distance between the handles was excessive for the average hand. The use of pins to effect an attachment actually increases the complexity of the system since the removal of each nut would require drilling two holes

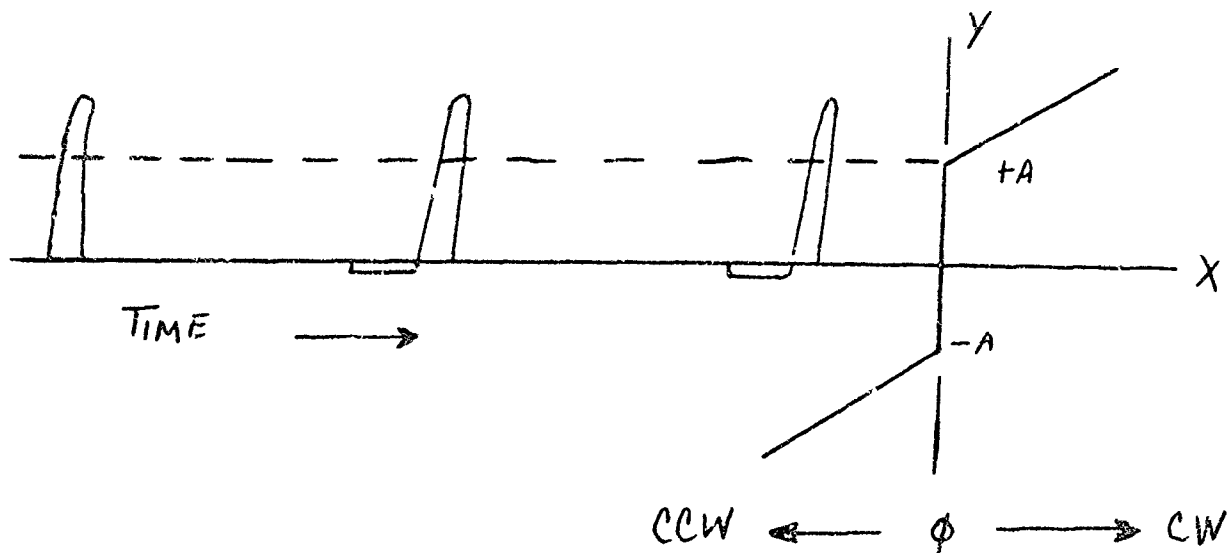


Figure 4

Natural Characteristic
Of A Fastener

Hand Tool - To obtain data relative to the magnitudes of torques and forces that a man could produce under weightless conditions, test subjects applied conventional tools to various tasks conducted during early tests in the simulated zero-g environments. Rather than being representative of work which could be performed in a weightless environment, the tests indicated the motions attendant with the work efforts which would prevent an astronaut from accomplishing useful work in space.

The Air Force has evaluated several unique tools developed by various companies to enable the in-house duplication of tasks performed by conventional tools in a normal earth environment. Many of these tools require special adapters at every bolt and a hand squeezing motion. Among the hand tools tested was a torque cancelling unit which uses two pins to transfer the torque to the structure and requires a squeezing motion to apply the torque. A summary of its evaluation is as follows:

The arrangement of the handles parallel to the planes of the work site or perpendicular to the axis of the fastener proved unsatisfactory because (a) the position required for the operator's hand was both inconvenient and tiring, (b) the particular squeezing action required was too arduous, and (c) the distance between the handles was excessive for the average hand. The use of pins to effect an attachment actually increases the complexity of the system since the removal of each nut would require drilling two holes

for the pins; furthermore, the pin type of attachment is correcting only for pure torque does not allow for the application of other types of forces.

An in-house study involving operators using conventional tools strove to determine whether a man can use the friction characteristic inherent in a fastener to control his stability. This characteristic was discussed above illustrated in Figure 4. The study indicated that the use of the friction characteristic does facilitate an operator's maintenance of his position. However, to use both hands in performing a maintenance task on a spacecraft exterior, an astronaut would have to be rigidly attached to the exterior. This requires a versatile (ability to attach to a prepared or unprepared surface) attachment system borne by the astronaut.

Attachments to Couple Astronaut to the Spacecraft Exterior - Tests conducted at Wright-Patterson Air Force Base firmly evidenced that in - space maintenance man will need an attachment system to couple himself to the spacecraft exterior to effectively perform a maintenance task while weightless. This requirement prompted the investigation of techniques that would be useful in an attachment system. Such techniques included the use of mechanical connectors, toe holds, flexible lines, rigid rods, telescoping arms, unfurlable structures, magnets, and adhesives. Requirements for the prototype attachment system prescribed that the system (a) provide a stable platform, (b) be sufficiently rigid to prevent pendulum motion (c) be simple to operate, (d) be capable of becoming attached to a prepared or unprepared surface of the various types of metals incorporated in spacecraft exteriors, (e) operate on surfaces with temperatures ranging from -150° to $+250^{\circ}$ F, (f) have a bonding system capable of operating in a vacuum, (g) provide 100 psi in tension, compression, and shear, and (h) be lightweight.

Based on the above requirements, the designs selected for further investigation were a single knee attachment and a three-point rigid attachment system consisting of three components; (a) a tripod linkage formed by either telescoping or unfurlable rods, (b) a dispenser to contain several adhesive pads (the present unit holds three pads), and (c) an adhesive system to bond the tripod to the spacecraft. Figure 5 illustrates the coupling of the attachment system to a spacecraft exterior. The blowup in the lower right corner of Figure 5 depicts the basic configuration of dispenser mechanism. The functions of this mechanism are four fold: (a) storing the adhesive pads, (b) dispensing them one at a time to the spacecraft surface, (c) actuating the firing of a pyrofuze foil or exothermic material on the adhesive to melt the adhesive and applying a force to the pad to cause its adherence to the surface and (d) releasing the pads from the coupling device to permit the astronaut's leaving the work site. The prototype adhesive system consists of a hot-melt layer of adhesive whose contact side is covered by a pyrofuze foil with the other side attached to a foam which, in turn, is mounted to a backing disc.

for the pins; furthermore, the pin type of attachment is correcting only for pure torque does not allow for the application of other types of forces.

An in-house study involving operators using conventional tools strove to determine whether a man can use the friction characteristic inherent in a fastener to control his stability. This characteristic was discussed above illustrated in Figure 4. The study indicated that the use of the friction characteristic does facilitate an operator's maintenance of his position. However, to use both hands in performing a maintenance task on a spacecraft exterior, an astronaut would have to be rigidly attached to the exterior. This requires a versatile (ability to attach to a prepared or unprepared surface) attachment system borne by the astronaut.

Attachments to Couple Astronaut to the Spacecraft Exterior - Tests conducted at Wright-Patterson Air Force Base firmly evidenced that in-space maintenance man will need an attachment system to couple himself to the spacecraft exterior to effectively perform a maintenance task while weightless. This requirement prompted the investigation of techniques that would be useful in an attachment system. Such techniques included the use of mechanical connectors, toe holds, flexible lines, rigid rods, telescoping arms, unfurlable structures, magnets, and adhesives. Requirements for the prototype attachment system prescribed that the system (a) provide a stable platform, (b) be sufficiently rigid to prevent pendulum motion (c) be simple to operate, (d) be capable of becoming attached to a prepared or unprepared surface of the various types of metals incorporated in spacecraft exteriors, (e) operate on surfaces with temperatures ranging from -150° to $+250^{\circ}$ F, (f) have a bonding system capable of operating in a vacuum, (g) provide 100 psi in tension, compression, and shear, and (h) be lightweight.

Based on the above requirements, the designs selected for further investigation were a single knee attachment and a three-point rigid attachment system consisting of three components; (a) a tripod linkage formed by either telescoping or unfurlable rods, (b) a dispenser to contain several adhesive pads (the present unit holds three pads), and (c) an adhesive system to bond the tripod to the spacecraft. Figure 5 illustrates the coupling of the attachment system to a spacecraft exterior. The blowup in the lower right corner of Figure 5 depicts the basic configuration of dispenser mechanism. The functions of this mechanism are four fold: (a) storing the adhesive pads, (b) dispensing them one at a time to the spacecraft surface, (c) actuating the firing of a pyrofuze foil or exothermic material on the adhesive to melt the adhesive and applying a force to the pad to cause its adherence to the surface and (d) releasing the pads from the coupling device to permit the astronaut's leaving the work site. The prototype adhesive system consists of a hot-melt layer of adhesive whose contact side is covered by a pyrofuze foil with the other side attached to a foam which, in turn, is mounted to a backing disc.

ADHESIVE ATTACHMENT TECHNIQUE

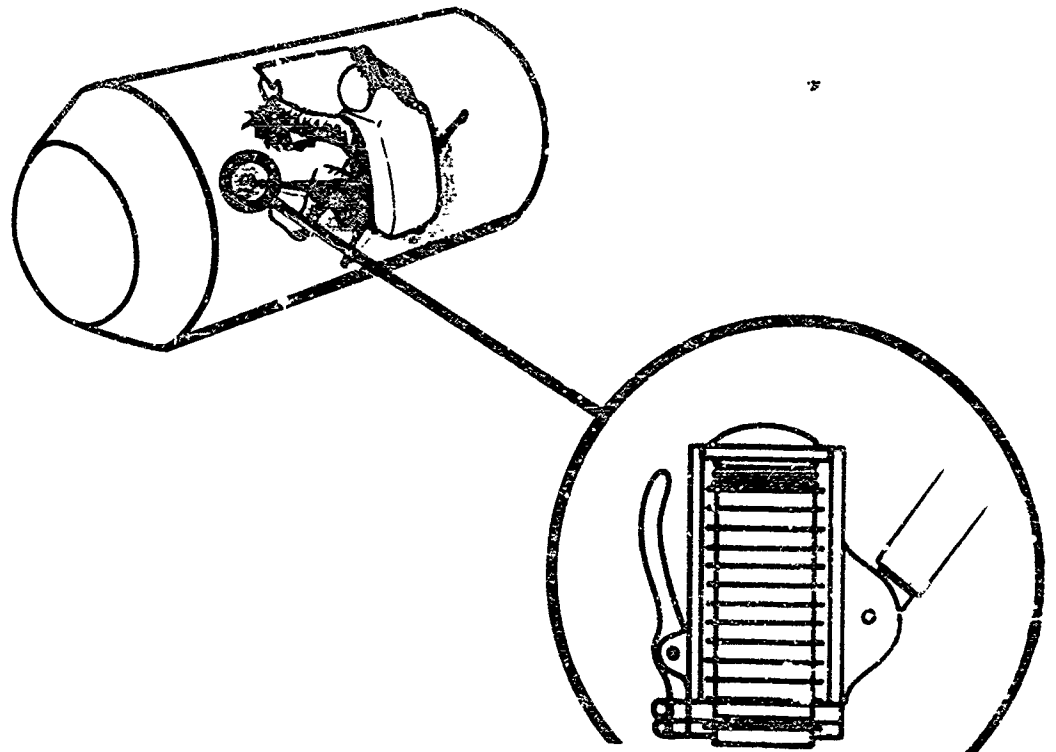


Figure 5

Adhesive Attachment Technique

Two braids at opposite sides of the adhesive pad connect the foil so that the adhesive may wet the surface as it melts. Upon solidifying, the adhesive forms a bond between the adhesive pad and the surface. The adhesive system used two types of adhesives, one for low-temperature (-150°F) and the other for high-temperature (+250°F) conditions. The former is a mixture of Versamid 100 and Versamid 940, their distribution by weight being 75 and 25 percent, respectively, and the latter is a mixture of Versalon 1112 and Versamid 100, their distribution by weight being 85 and 15 percent, respectively.

In-house tests of the prototype adhesive system indicated that the heat generated was insufficient to properly melt the adhesive. Much of the heat for melting was lost because of the heat-conduction properties of the bonding surfaces.

Because of the insufficient heating to effect adequate bonds with the adhesive pads (and other deficiencies such as those found in the foam backing) the Air Force is now considering the use of a pressure-sensitive encapsulated epoxy resin system to produce the bond or the use of an exothermic material to supply the required heat for a system using a thermal plastic system. Another potential modification to the attachment system is the incorporation of unfurlable arms, based on the concept of the carpenter's tape, to improve the tripod linkage.

Gyroscopic Stabilization for Space Maintenance Workers - The problem of stabilizing a space worker when he is applying forces required for maintenance tasks is easily accomplished by attaching the worker to the work site. However, in some cases, such as space station assembly, the attachment technique is not practical. Therefore, the worker must be stabilized by some other system. One such system is the AMU back pack. The problem here is that using the AMU to stabilize the worker while performing tasks requires a large fuel expenditure.

A suggested stabilization system would be a gyroscopic platform that could absorb the momentum, required for the worker to perform the task, by precession of the gyroscopic element and permitting the astronaut to remain stationary.

The major problem associated with this concept is the phenomenon known as "gyro lock." This phenomenon can be explained briefly as follows. When a torque is applied to the spin axis of a gyroscope, the gyroscope will resist this torque and precess in a plane that contains the torque vector orientation such that it is parallel to the torque vector. When this occurs the gyroscope is in the condition of "gyro lock" and loses all ability to resist the applied torque. In other words it can be said that a gyroscope will resist an applied torque as long as the torque vector and spin vector are not parallel.

Therefore, to develop a passive gyro stabilization system it is necessary to devise a scheme of coupling gyroscopic elements such that the lock condition can be avoided. To this end, several techniques have been evalu-

ated with a small mock-up using inexpensive gyroscopes. The results of these have all been negative, however, additional concepts are being tested. It is possible that electromechanical concepts could be incorporated to achieve the desired characteristics.

Remote Maintenance Techniques - From the start of the nuclear age man has been concerned with performing maintenance in hazardous environments. The success of the development and utilization of remote manipulators in the nuclear area has given prominence to the possibility of integrating remote maintenance capabilities with man's capability for accomplishing certain types of maintenance in space.

It has been demonstrated on air bearing and aircraft simulators that man can operate a remote vehicle away from his mother ship. The next logical step is to design manipulators that can be attached to the remote unit which contains propulsion, stabilization, television, and power supply for determining the types of tasks that man can best accomplish with this type of system. The development of minimum reaction power tools over the past few years is expected to greatly reduce the weight of a man/machine system for maintenance.

Summary

Tool Repair Kits - The types of tools and equipment that represent the basic maintenance requirement for space are:

1. Tools, both hand and power, to perform a wide variety of required maintenance tasks.
2. Astronaut attachments single, two and three points depending on complexity of tasks.
3. Spare parts to replace failed items.
4. Repair kits for the purpose of effecting repairs not practical through normal component or blackbox replacement techniques. Included are: (a) leak repair kits for skin and radiators, (b) electrical malfunctions detection and repair tool for general wire joining kit, (c) fluid maintenance repair kits to effect repair of on-board fluid systems, (d) damage control kit to provide general material to effect emergency repairs (including a high power multi-purpose tool) of the station, (e) joining kit including: adhesives, brazing and welding capabilities, (f) development of Ancillary equipment to support crew maintenance operation, example of equipment required for work within the station, include, extension lights for viewing, vacuum mechanism for removal of filings from a pressurized cabin, etc. For work outside a maneuvering unit for attitude control and translation purposes will be required, (h) maintenance techniques and plans describing in detail the procedures and processes by which space maintenance operations will be performed.

Design Criteria

The purpose of this section is to present an approach for establishing design criteria for space systems.

Mock-Ups - The breaking down of a complete space system into the various subsystems for purposes of maintenance analysis enables the establishment of function common to all and the ones that are unique to a particular type of subsystem. The performance of subsystem analysis provides a guide for the design and fabrication of representative models (e.g. structural repair, joining experiment, fluids experiment, etc.) that can be used on earth simulators and space test beds to acquire comparative data. This data can then be used to establish design requirements for future systems that are to be maintained in space.

Tests - The acquisition of data to establish design criteria will have to be carefully planned in order to obtain data that can be realistically compared using the various types of simulation (6 degree of freedom, zero-g aircraft, space test bed). Each type of simulation has constraints that will have to be taken into consideration for purpose of selecting the type of data to collect for comparison. Some of these limitations are:

1. **Air Bearing** - Use of the 6-degree-of-freedom simulator to evaluate the torques and motions produced by man along under weightless conditions requires knowledge of the simulator effects. The motion of a rigid body with a fixed coordinate system through the center of its mass and moving with it can be expressed by using the Euler equations of motions. These expressions give a torque equation relating rotational motion, a force equation relating translational motion, and a direction cosine equation relating angular displacement. These equations along with a detailed analysis of their application to the 6-degree-of-freedom simulator are presented in another paper. (Reference 5)

The study of the applicability of the Euler equations to the data obtained from the 6-degree-of-freedom simulator demonstrated that the torque effects caused by the simulator cannot be mathematically calculated to permit their extraction from the total torque output to reveal the torque produced by man alone. Since the simulator system consists of not one but three rigid bodies, that is, the man with his back pack, the yaw ring, and the roll frame, the Euler equations would have to be applied to the coordinate systems for each of the bodies. But the use of three different coordinate systems would be of no avail since there is no transfer function to relate the systems. Still, as discussed in this study, the 6-degree-of-freedom simulator may be used to determine man's ability to perform maintenance tasks by measuring his motions up to the levels where he loses control to perform any further useful work. Another revelation pertinent to the use of the 6-degree-of-freedom simulator was the observation during tests in the zero-g aircraft that man's actions in a torque application comprised, for the most part, three motions in one plane; one was rotational, and the other two were translational. Should the 6-degree-of-freedom simi-

lator be restricted to permit only these three degrees of freedom, the simulator could function as a single rigid body. This restriction would then allow the application of the Euler equations to torque measurements and the subsequent extraction of the simulator effects to yield the torque caused by man alone. Consequently, future test phases with the 6-degree-of-freedom simulator intend to study man's motions in the six-degree-of-freedom mode and to measure both man's motions and the torque delivered to a fastener in the 3-degree-of-freedom mode. The simulator will also be used to establish base line data with the constraints of the Euler equations removed and then correlated with data from the zero-g aircraft.

2. Water Simulation - The author believes this type of simulation will be valuable in learning how to construct large structures under simulated weightless conditions. The simulation of performing large structure assembly type tasks forces one to use water simulation. The size and gravity problems encountered using a 6-degree-of-freedom simulator and the zero-g aircraft will not enable the performance of these types of tasks. The problems that must be overcome to use water simulation (e.g. data is qualitative) for other types of tasks are many with practically no real advantages other than the one mentioned above.

Human Factors - The inclusion of man in the maintenance loop requires one to consider the following:

1. A preliminary evaluation of problems imposed on the man by the pressurized suit or hard shell enclosure, micrometeorite protection, heat exchange, time required by task, radiation protection, gravity conditions, safety conditions, warning devices, vision problem, communication, illumination, physiological comfort, mechanical requirements, and efficiency input/output.

2. Human performance evaluation of space requirements and manual dexterity capability and how these might be effected by protective equipment.

3. Training requirements for space maintenance tasks will involve time in simulators (6 degree of freedom and aircraft) and space chambers in preparation for the task to be performed.

The development of a truly flexible space suit is still considered to be the number one problem for the orbital worker to successfully carry out his maintenance mission.

Computer Models for Maintenance

The two types of computer models (physical and abstract) both have application in the area of maintenance planning for space. The following are possible application of an analog model for a space worker:

1. It is possible that a space worker can use the tool he is working to apply reaction forces for stability. The feasibility of this has been demonstrated for planar motion and is reported in "Manual Application of

Impulses While Tractionless." The problem is more complex for torques applied in a six degree of freedom environment. In this case, the reaction torques may induce rotation about other axes. An analog program could be used for investigation of this problem.

2. An analog model can be used to evaluate the effectiveness of applying short duration impulse forces for space maintenance. This type of force application may leave the worker relatively stable. Typical examples of this type of loading would be manually impacting a common wrench or using a hammer.

3. During extra vehicular assembly the space worker may have to perform some tasks when attachment is not possible or practical. Under these conditions the worker may be able to use an Astronaut Maneuvering Unit (AMU) for the stability as well as mobility. An analog could be used to determine if the required tasks can be performed with the assistance of the AMU.

4. In connection with the above application an analog model can be used to determine the fuel consumed when the AMU is used for stability while the worker is performing such tasks.

5. Also in the same light, an analog model can be used to determine if the AMU thrust levels are sufficient to stabilize the worker while performing maintenance tasks.

6. The use of minimum reaction tools require small stabilization forces. If the space worker is equipped with a battery of these tools the AMU could be used for stabilization with a minimum fuel consumption. An analog program could be used to evaluate the feasibility of this concept.

7. It is possible that an analog model can be used to simulate the use of simple short tethers. Such tethers can be used for providing the small stabilization forces required while working with minimum reaction tools.

8. An analog model can be used to study the mobility of a space worker by self-propulsion while confined in a spacecraft.

9. An analog model can also be used to evaluate the maneuverability of an astronaut with the AMU. A typical example would be the evaluation of various emergency procedures.

10. An analog model can be used as a prototype for a similar program for the AMU.

Abstract Model - Abstract models are predictive devices which may be utilized as; (a) an evaluation tool of either existant or proposed maintenance and support systems by simulating real world conditions, (b) a comparison device which will generate a relative evaluation of the predicted performance among competing concepts of a maintenance system,

(c) a design tool to formulate an optimum maintenance system through a trial and error or iterative procedure.

In order for computers to play an active role in the maintenance planning for space systems, it is important to keep their role in mind throughout the testing phase so that data can be logged for easy accessibility when the time comes for its use.

SUMMARY AND CONCLUSION

Summary

The objective of this paper has been to; (a) bring to the attention of those interested in space maintenance some of the things that have occurred over the past several years to enhance man's ability to accomplish maintenance in space and (b) present an approach to get from maintenance concept, to test hardware that can be utilized for obtaining design criteria required for the fabrication of maintainable vehicles for future space missions.

Conclusion

Man has progressed considerably in the past several years in his drive to obtain unique tools, maintenance devices and abstract models. All directed toward obtaining the technology that will enable him to design space maintainable systems. Considerable testing and evaluation of man-machine relationship in air bearing simulators and the KC-135 aircraft under zero-g conditions has been accomplished. However, none of this data establishes how effectively maintenance can be performed considering the combined effects of extended time in space, the space environment, and weightlessness. Until this is accomplished the design criteria necessary for obtaining the technology to design space maintainable systems can not be obtained. Tests to date have indicated that man can in general with the proper tools and techniques accomplish maintenance in the space environment.

REFERENCES

1. Space Maintenance Adhesives - AFAPL TR-65-40, Vol II
2. Exothermic Joining in a Vacuum - ML-TDR 64-7, Narmco Research & Development Co.
3. Electron Beam Welding in Variable Environment - ASD Nr 8-243
4. A Manual Device for Locating Electrical ARC - Producing Faults AFAPL TR 65-25.
5. Maintenance in a Weightless Environment, C. B. May, AIAA Conference April 1965.
6. Development of an Abstract Model for Aerospace Maintenance Systems AFAPL TR 64-150, March 1965

SESSION III

STRUCTURAL CONSIDERATIONS FOR AN EXPANDABLE

LENTICULAR SATELLITE

By Jerry L. Humble

NASA Langley Research Center

INTRODUCTION

Communications systems in general, as with practically anything of potential commercial value, must ultimately be evaluated from an economic standpoint. In a space oriented communications system, the satellites themselves, as the orbital subsystems, must likewise be economically evaluated. Several factors enter into this evaluation. Passive communications satellites inherently have a long effective life and their bandwidth capability allows a great many communications channels per satellite. But aside from the advantages inherent to one type satellite or the other, two basic parameters always appear. The satellite subsystem's weight affects the launch cost and the signal return which the satellite is capable of reflecting or retransmitting affects the ground station cost. Thus, the efforts in passive communications satellites are oriented toward achieving a better microwave return signal for a minimum of satellite weight.

The NASA Langley Research Center has made a continuing effort in the area of passive communications satellites and in very lightweight expandable structures in general. The gravity-gradient stabilized lenticular passive communications satellite with an orbital position control capability is the latest of the devices to be considered in this effort.* Langley Research Center directed studies dealing with the lenticular satellite have been preliminary in nature to this point, with very little emphasis on optimization but they clearly indicate the feasibility of the concept. It has been shown that the lenticular concept can produce a satellite with communications capabilities superior to the passive spheres for a given satellite weight.

PART I

LENTICULAR CONCEPTUAL PHILOSOPHY

To indicate the basic lenticular conceptual philosophy, first consider a spherical passive communications satellite in Earth orbit (fig. 1). One

*This paper is based on work performed by the NASA Langley Research Center and by the Goodyear Aerospace Corporation, Akron, Ohio, and the Radio Electric Corporation, Aerospace Division, Baltimore, Maryland, under contracts directed by the Langley Research Center.

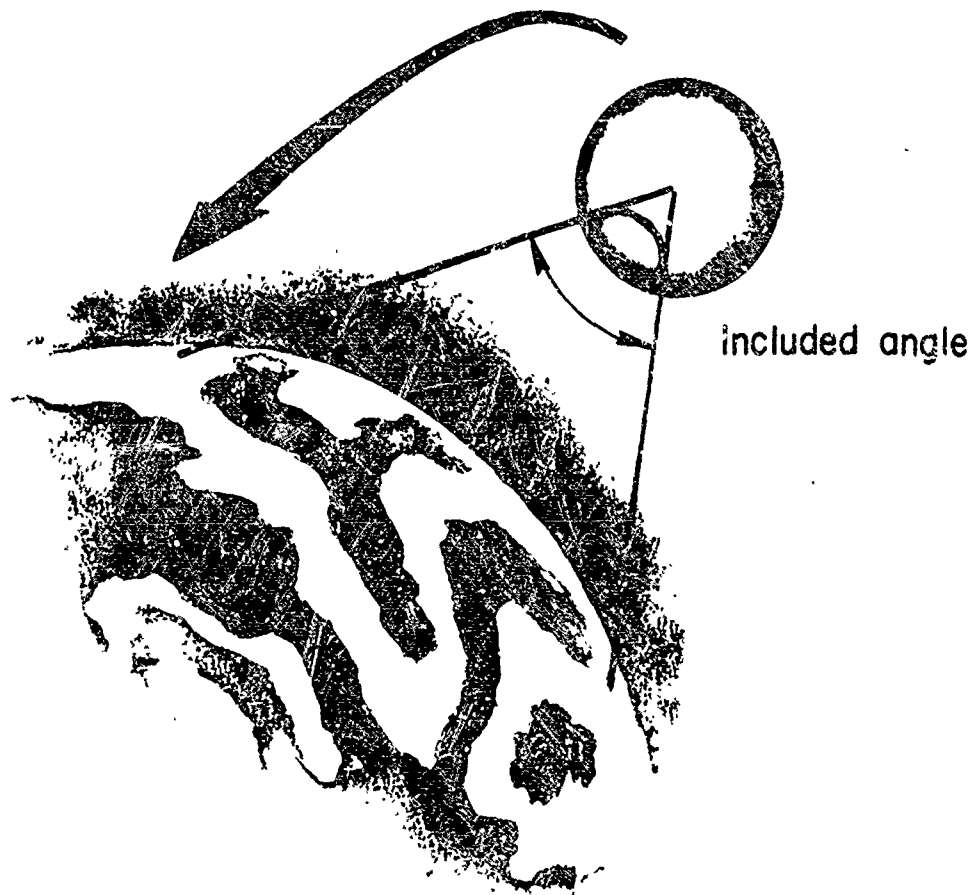


Figure 1.- Basic lenticular concept.

might note that the only part of the spherical surface which is necessary for communications between two ground stations is that segment defined by an angle from station to station, through the center of the sphere. This included angle is then, at a maximum, slightly more than that from horizon to horizon. Any point on the spherical surface outside that segment can contribute very little to a microwave return signal. One could maintain essentially the same communications capability and realize a great deal of savings in satellite weight (and consequently launch cost) if only this spherical segment were placed in orbit. The radar reflection cross-section-to-weight ratio of the satellite could increase tremendously.* For example, at a 2000 n.mi. orbital altitude, the nominal horizon-to-horizon included angle is 8° , and approximately 87 percent of a spherical satellite weight is attributed to surface areas unnecessary for communications. The restriction to this train of thought is, of course, that the spherical segment must be Earth oriented to achieve this savings.

*No great deal of elaboration on microwave theory will be made for purposes of this paper except to say that the radar reflection cross section may be considered to be a measure of the communications capability of the satellite. The microwave return signal is stronger with higher reflection cross sections. The value of this cross section is essentially $\pi\rho^2$ for a reflecting spherical surface, where ρ is the radius of curvature.

A very attractive orientation/stabilization technique, also passive, is that of gravity gradient. A more thorough delineation of gravity-gradient methods and theory will be dealt with later, but for now let it suffice to say that gravity-gradient techniques supply a local vertical orientation and a means of close tolerance stabilization around that reference. More simply, the spherical segment's axis of revolution always points toward the Earth's center.

In order to effectively utilize satellites in a communications system, it is desirable to provide some means of accurately positioning the satellites in an orbit relative to each other or to some point on the Earth's surface. The feasibility of solar sailing a lenticular satellite has been established in studies under the direction of the Langley Research Center. Briefly, this technique involves, in principle at least, providing a sail surface on the satellite, oriented along the local vertical and perpendicular to the orbital plane. One might note then (fig. 2), that as the satellite moves around in its orbit, opposite sides of the sail face the sun at any two points in the orbit 180° apart. By applying coatings with different thermal characteristics to the two sides of the sail, one could attain different forces, a combination of direct solar and reradiation forces, at two points 180° apart in the orbit (fig. 2).

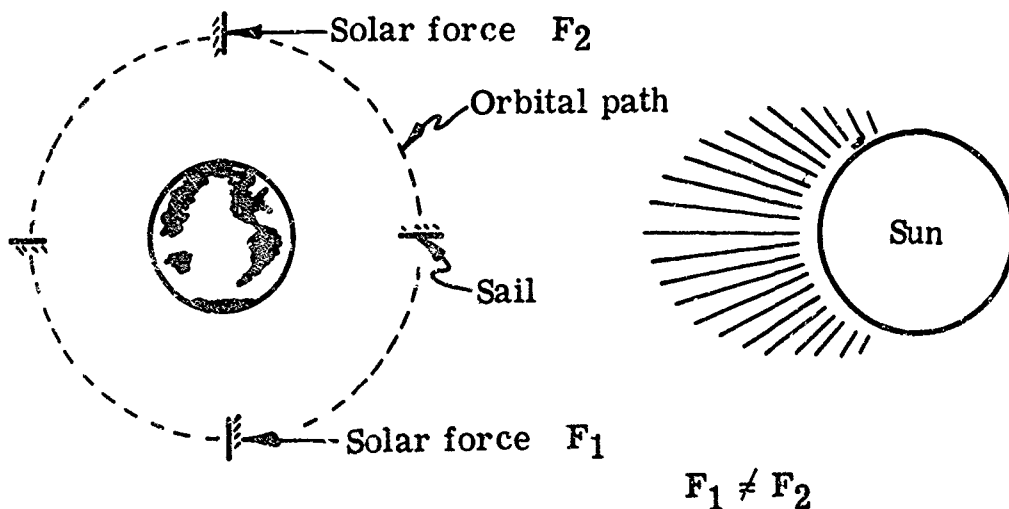


Figure 2.- Orbital solar sailing.

The net effect of these forces is that the satellite's orbital rate will either increase or decrease, depending on what thermal characteristics are provided and which side of the sail is oriented down the satellite's tangential velocity vector. Thus, the satellites have the capability of varying the separation angle between them (fig. 3).

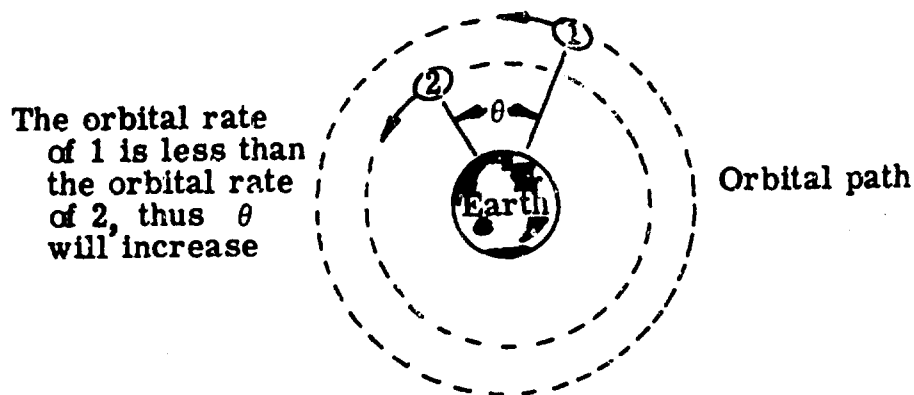


Figure 3.- Orbital position control.

PART II

CONFIGURATIONAL DEVELOPMENT - MATERIALS AND LOADS

One might now proceed with the configurational development of a gravity-gradient stabilized lenticular passive communications satellite.

The spherical segment itself is of primary interest as the microwave reflector and its shape is of utmost importance. Any technique, within the state of the art, for the deployment of a good microwave reflecting spherical surface requires straining the surface material, either to form the spherical shape or to remove wrinkles left from package folds. The inflation and strain-rigidization technique of membrane deployment is compatible with this requirement, and has received intensive research. For this inflation/rigidization procedure, a diaphragm or another spherical segment must be attached to the reflector segment around its periphery to form a gas enclosure (fig. 4). Inflation gas pressures then stretch the membranous material beyond its yield point to form the spherical segment surface. Some peripheral restraint must be added to prevent the reflector/diaphragm combination, or lens, from attempting to assume a complete sphere under inflation pressures. The edge restraint can be supplied by an inflatable torus (fig. 4).

Assuming two identical spherical segments for the lens, one might note that the loads placed on the torus are dependent on two factors (fig. 5), the lens included angle and the lens material yield strength. The in-plane components are the only loads considered in the torus design as the out-of-plane components cancel each other. The included angle is a communications system consideration and is not a variable for structural design purposes. Thus the lens material must have a very low tensile yield strength for minimization of torus loads. The lens material on the other hand, must be capable of withstanding solar pressure (i.e., 13.6×10^{-10} psi for specular reflection) without buckling. The need for a lens material with a low yield strength and some value of skin section area moment of inertia, for a given radius of curvature, is established.

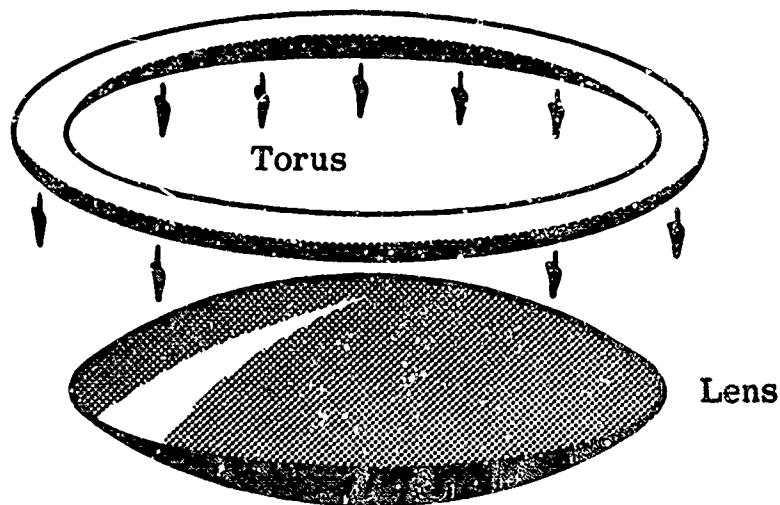


Figure 4.- Lens/torus.

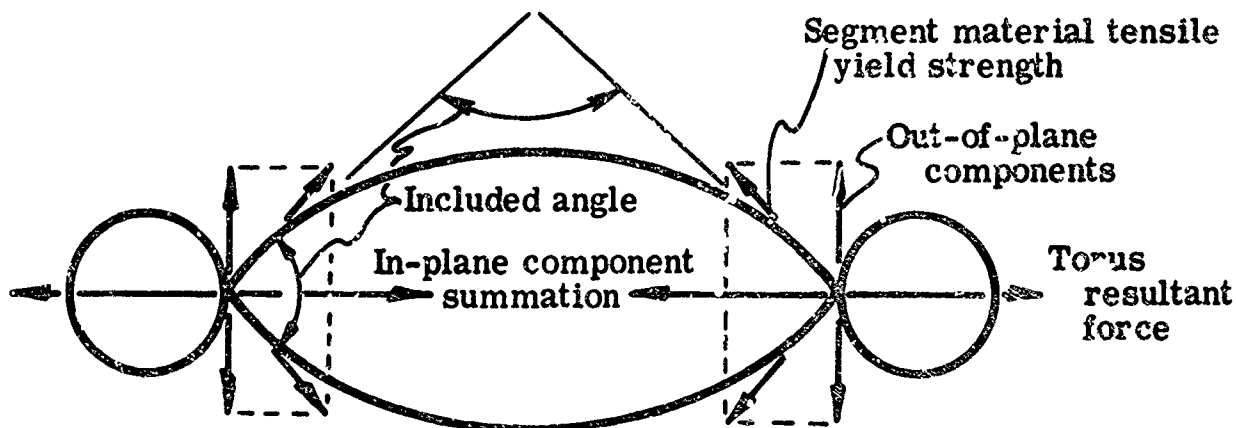


Figure 5.- Torus loads.

Several possibilities for a lens material do exist which provide a low area to area moment of inertia ratio cross section desirable for this application. The grid materials (fig. 6), such as the wire mesh and chemically milled metallic sheet, simulate the rings and stringers of more conventional semi-monocoque structures, in principle at least. The lens' function as a microwave reflector is only nominally impaired by the use of the grid materials, and preliminary studies have indicated their potential in this application.

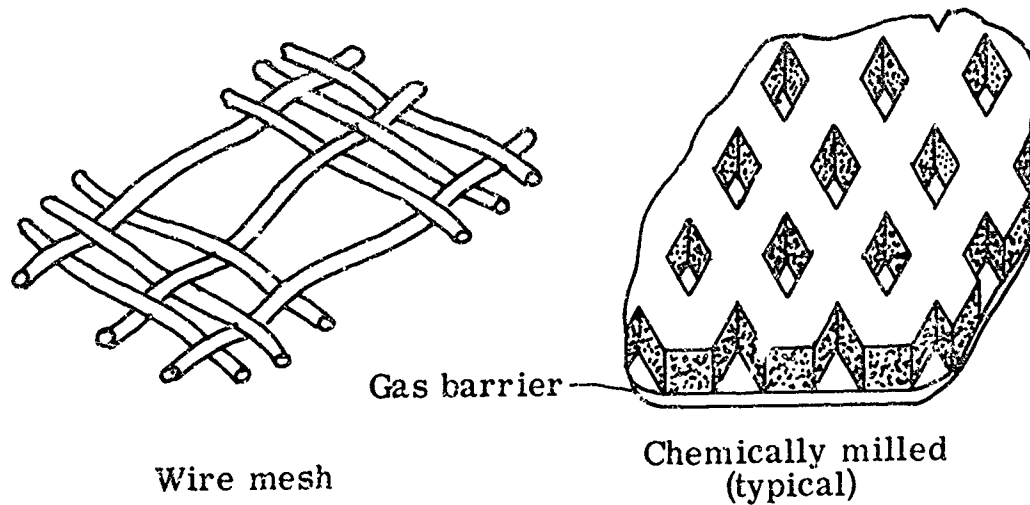


Figure 6.- Representative grid materials.

The gas barrier to be utilized on a metallic grid material is largely determined by orbital position control and gravity-gradient stabilization considerations. If the lens is not to be used as the solar-sail, one might choose a "photolyzable" film as the gas barrier. The gas barrier film is not needed in this case after inflation, its mass distribution is actually detrimental to the gravity-gradient stabilization system, as will be discussed later, and it provides a greater surface area exposed to solar pressure. Solar pressure acting on the lens surface could produce a torque large enough to appreciably affect the gravity-gradient stabilization system, and it could contribute to an orbital eccentricity which also decreases the effectiveness of the stabilization system. Studies have indicated that low-strength photolyzable films, suitable for use as a gas barrier, can be made available.

"Photolyzable" film "evaporates" when simultaneously exposed to ultraviolet radiation and an increased film temperature. The film temperature may be increased to the desirable level passively by using various dyes to provide the proper film thermal characteristics. Heat inputs and ultraviolet radiation are, of course, very easily acquired in an orbital environment.

If the lens is to be used as the solar sail, one can choose one of the many very thin plastic films, vacuum deposited and coated to the proper thermal characteristics, as the gas barrier for the grid materials. A continuous surface is desirable in this case to provide more sail area.

"Solid" laminate materials (fig. 7) have also been produced which are very lightweight. In principle, these materials simulate conventional monocoque structures. The use of these materials for the lens is limited to the case where the lens is utilized as the solar sail.

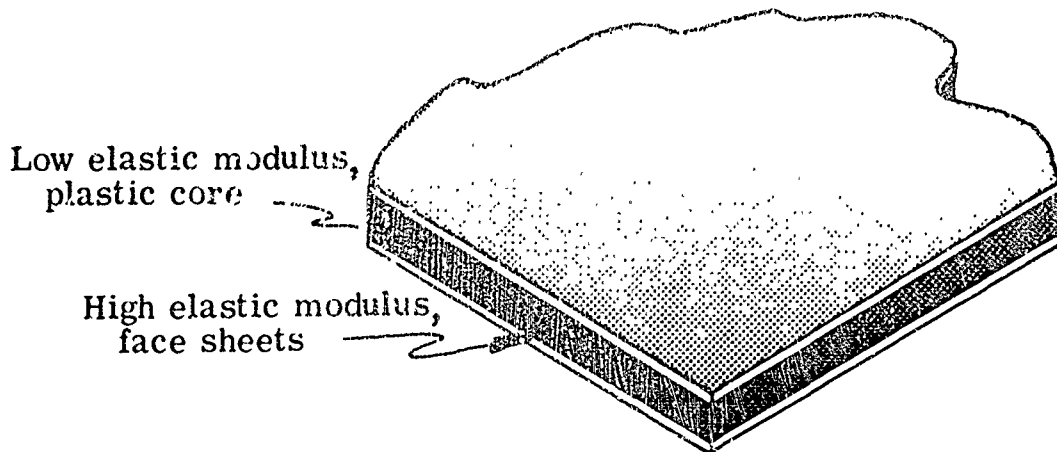


Figure 7.- "Solid" laminate material.

The importance of an optimized lens material can hardly be overemphasized. The loads placed on the torus and the weight of the lens are minimized by proper lens material selection. The lens and torus constitute a very large percentage of the total satellite weight. An optimum lens material is not readily defined, however, as some uncertainty exists concerning the true buckling pressure such a very large radius of curvature to skin thickness ratio spherical structure can withstand. Ground tests are generally inconclusive due to the appreciable effects of a one "g" environment on the very light-weight material. Consequently, lens material designs generally tend to be conservative.

The torus, as previously mentioned, is intended to maintain an accurate lens constraint during inflation, and the loads placed on it for a given included angle, are directly proportional to the tensile yield strength of the lens material. After completion of the inflation process, the torus serves no further purpose and in fact makes the job of acquiring the mass distribution desirable for gravity-gradient stabilization more difficult. Ideally, one would prefer that the torus simply evaporate after completion of the inflation cycle. A high-strength photolyzable film could do just that. However, in their present state of development, these films are far too brittle to allow packaging. If the high-strength films are not further developed, the major materials requirement for the torus would be that it be light-weight, high strength, and, to avoid communications interference, microwave transparent. The design criteria for the torus can be shown to be wrinkling, which requires only that the torus skin remain in tension at all times during lens inflation, and strength to withstand inflation pressures.

To apply a gravity-gradient stabilization technique to the lens or lens-torus combination, one must closely examine a few basic physical phenomena.

First, acceleration placed on the satellite due to gravity must be considered vectorially in a three-dimensional geocentric coordinate system, in spherical coordinates if one chooses. On the other hand, orbital centrifugal accelerations placed on the satellite may be considered, vectorially, in a

two-dimensional coordinate system with the origin at any appropriate point along an axis through the Earth's center and perpendicular to the orbital plane, or in cylindrical coordinates (figs. 8 and 10). The point of this rudimentary dissertation is that the difference in direction cosines of the gravity and centrifugal related acceleration vectors, acting on some incremental mass particle away from the satellite mass centroid, is one contributing factor to the gravity-gradient stabilization torques. Further, one must

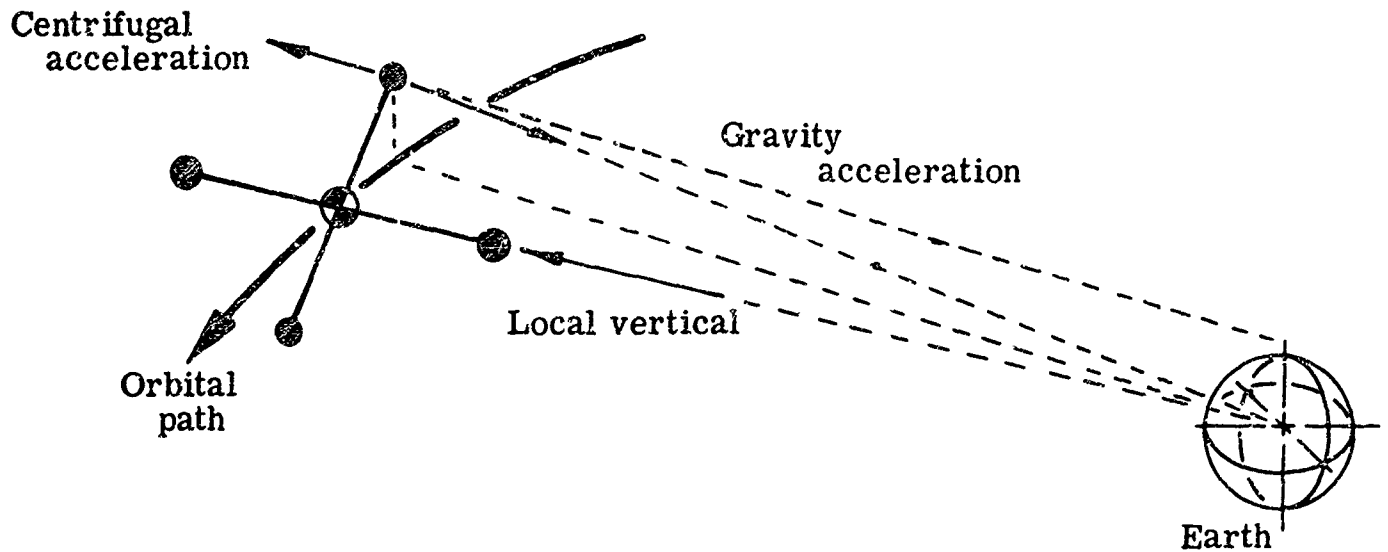


Figure 8.- Yaw accelerations.

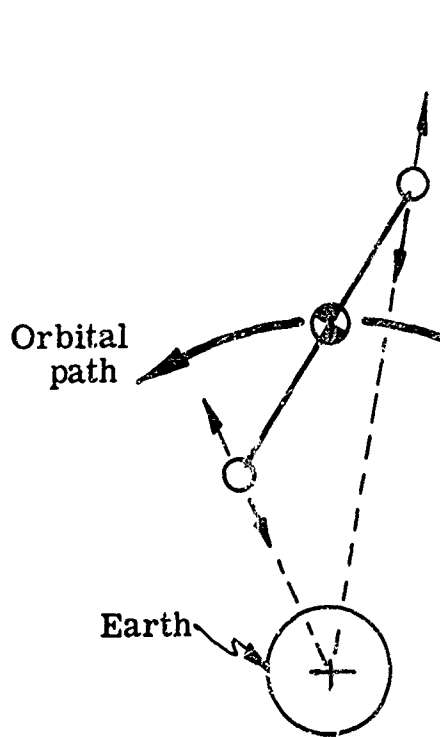


Figure 9.- Pitch accelerations.

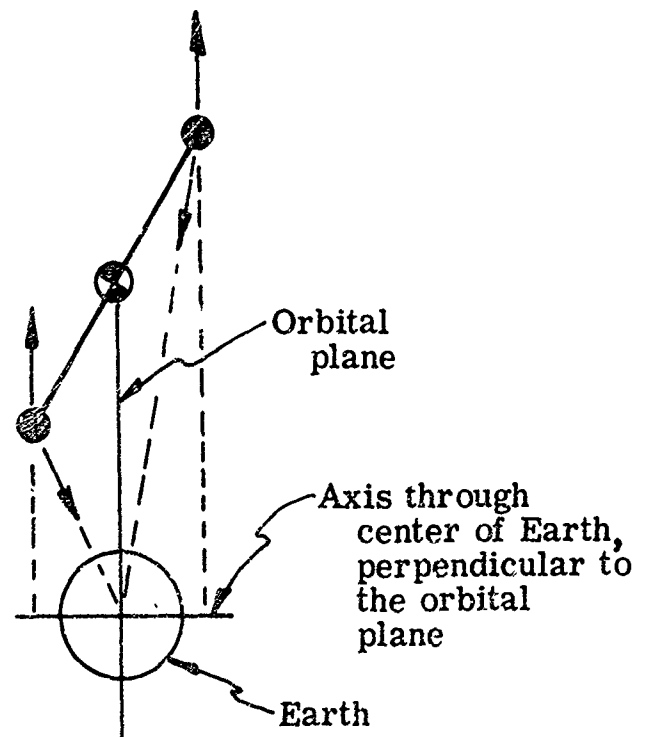


Figure 10.- Roll accelerations.

realize that only the mass centroid of any satellite is truly at zero "g" (i.e., net centrifugal acceleration equals net gravity acceleration). The gravitational attraction term is essentially compatible with the well-known inverse square law of Newtonian origin and the centrifugal accelerations ideally vary directly as the geocentric orbital altitude. The gravity acceleration is greater than the centrifugal acceleration acting on a mass particle closer to the Earth than the satellite mass centroid. The opposite is true of a mass particle farther from the Earth than the mass centroid (figs. 9 and 10). Gravity-gradient stabilization techniques require that the satellite mass be distributed in such a manner as to effectively utilize these small differential accelerations (fig. 11). The result is that the satellite is capable of sensing the local vertical and the orbital plane, and a restoring torque exists any time there is an angular displacement of the satellite from these two references.

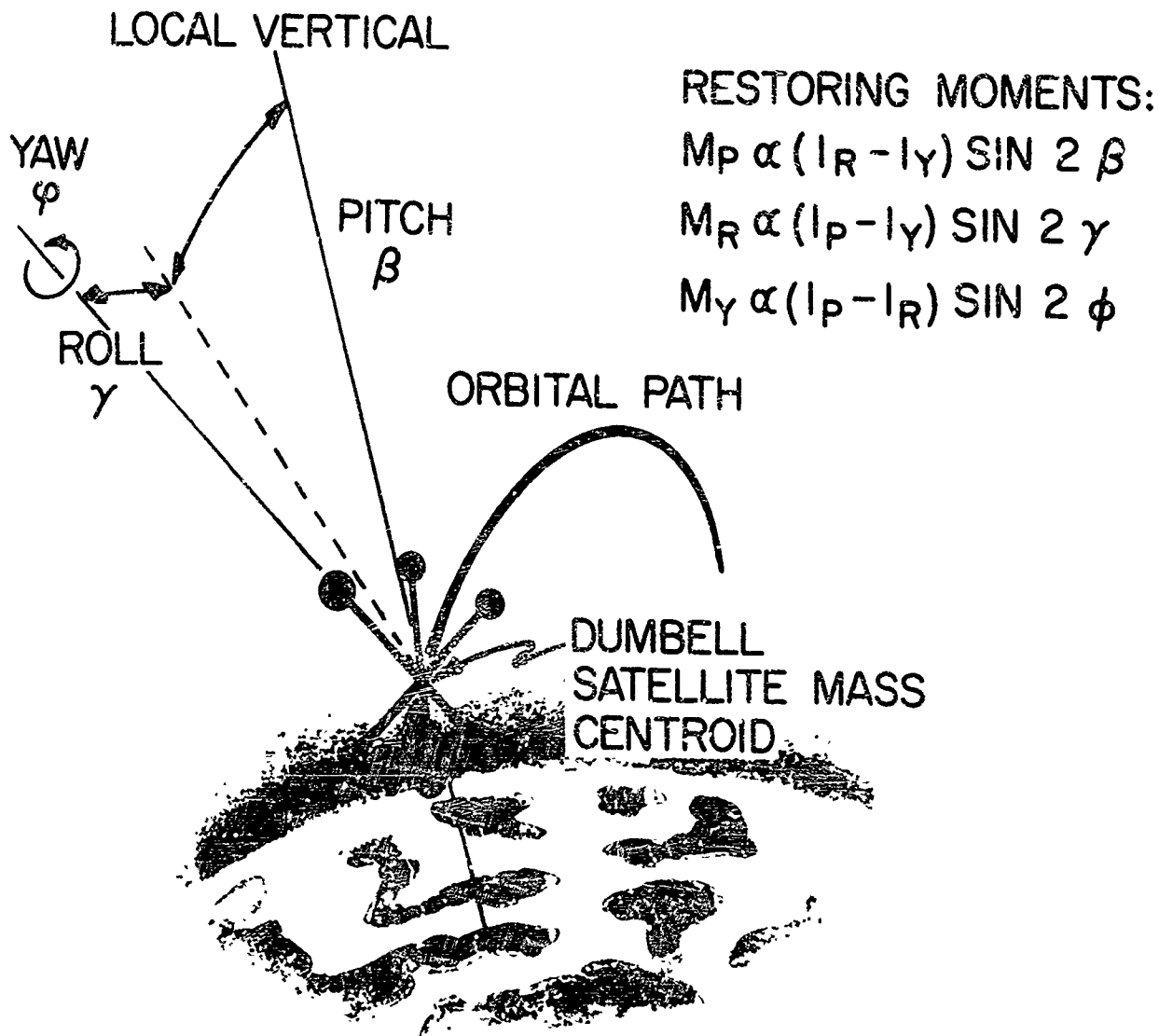


Figure 11.- Gravity-gradient restoring moments.

For the particular application of the lenticular satellite, the mass distribution is achieved basically by attaching the canister halves, in which the satellite is packaged for launch, the inflation system and controls to the lens by long boom arrangements. One can now clearly see the detrimental effects on gravity-gradient stabilization of the torus and lens gas barrier mass distribution (fig. 11). It is desirable to keep the yaw inertia as small as possible so that the pitch and roll inertias may remain small, thus requiring shorter booms. A lighter damping device may also be utilized as the energy which it must dissipate, being proportional to the absolute mass moment of inertia of the satellite, is kept to a minimum.

To gain some insight into the loads placed on the satellite by this mass/boom arrangement, one might observe a simple two-dimensional case of a pitch pointing error (fig. 12).

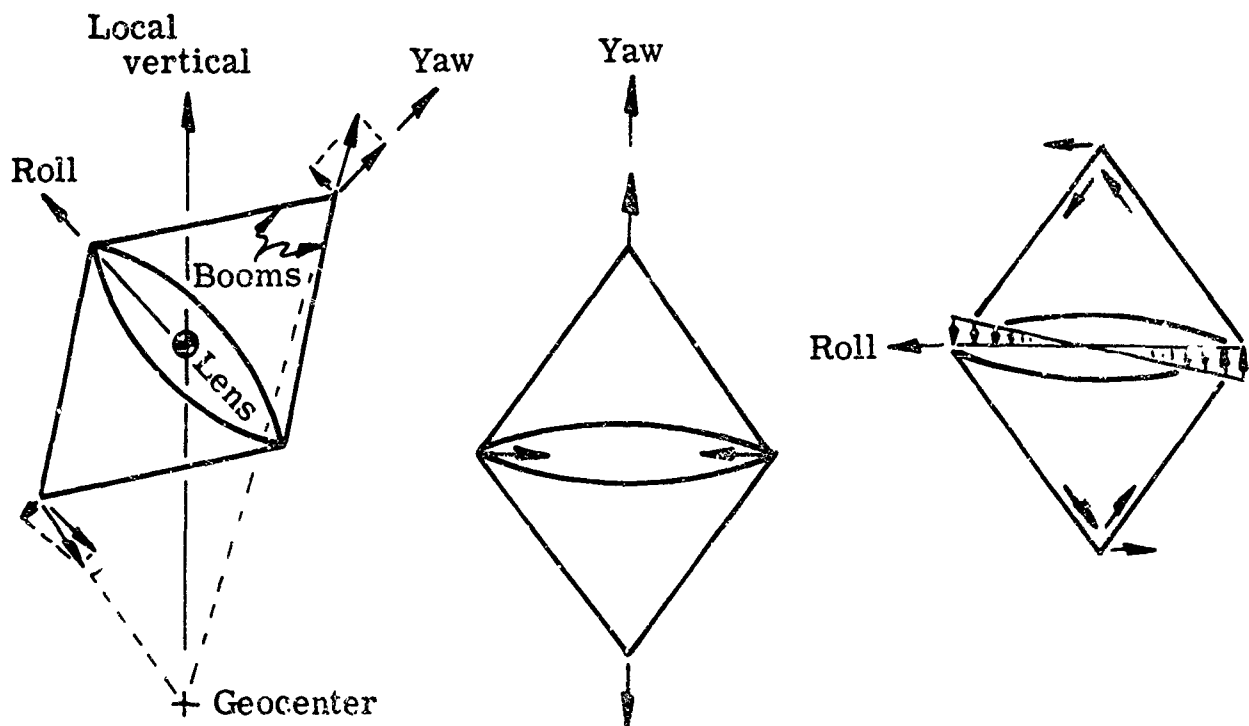
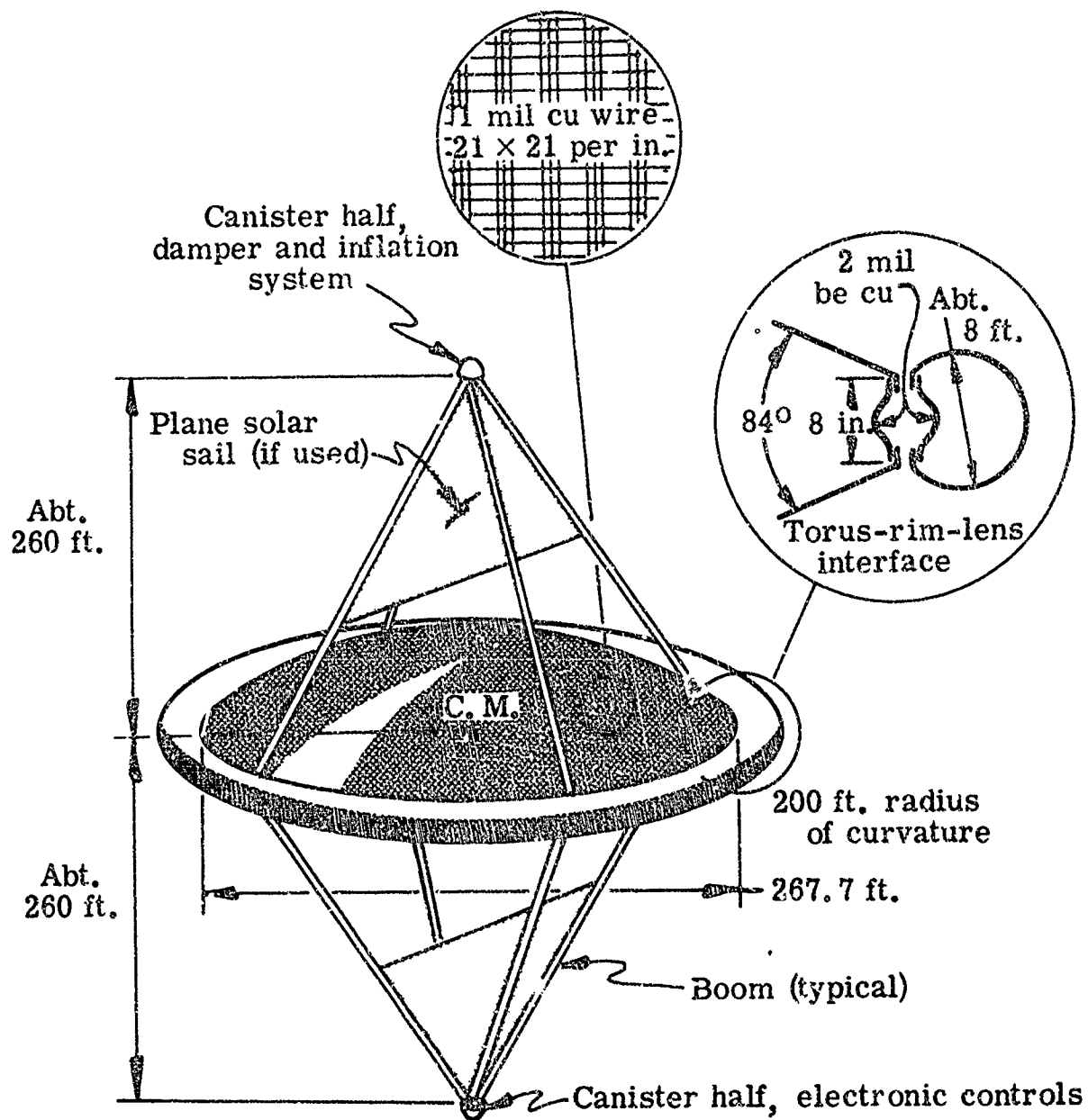


Figure 12.- Rim/boom loads.

Consider only the gravity-gradient resultant forces placed on the canister halves and the components of these forces in a satellite oriented coordinate system. The components along the yaw axis apply a tensile force to the booms and consequently a load around and in the plane of the lens periphery. The roll axis components apply a compressive load to one boom and a tensile load to the other. The roll axis loads which rotate the satellite in pitch are resisted by the inertial mass of the lens. The combination of these resultant loads placed on the lens and its periphery would certainly distort it, reducing its effectiveness as a microwave reflector, if some additional structural member were not provided to absorb them. A relatively rigid rim with a collapsible cross section around the lens periphery could absorb the loads; it could also serve as a "solid" attachment point for the booms and as



Total weight, 1450 lb. launch

Lens inflation pressure, 3.16×10^{-4} psi

Lens material tensile yield strength, 3.8×10^{-1} lb/in.

Torus inflation pressure, 1.678×10^{-1} psi

Figure 13.- General features, baseline configuration.

a convenient interface between the torus and lens. The major design consideration for the rim is to keep its deflections small, thus avoiding lens distortion. The booms themselves are designed to a conservative compressive load and are not allowed to have large transverse deflections due to solar pressures.

However, unless some means of energy dissipation is provided, the perturbed satellite would continue to oscillate indefinitely, much like a frictionless pendulum. Therefore, some damping system must be added. Several damping systems, primarily passive, can be utilized in this application.

Figure 13 shows the general dimensions and features of the completed configuration. This particular configuration is designed for a 2000-nautical-mile orbital altitude with an 84° included angle.

A wire mesh grid, although not necessarily optimum, was chosen in the preliminary studies as being reasonably representative of probable lens materials characteristics. Copper wire was a compromise selection based on the many characteristics desirable in this application, including small thermal expansions, low yield strength, the ability to be woven in very small diameters, and preferably nonmagnetic.

PART III

PACKAGING AND DEPLOYMENT

Very little has been said to this point concerning the packaging and deployment of the lenticular satellite. This area is, in fact, one of the primary design considerations. Structural members such as the rim do not have a specific shape purely by chance. Packaging and deployment analyses of such an inflatable satellite are however, at best, a qualitative affair. The packaging procedure is illustrated in figure 14. Note that the rim is of a collapsible cross section with two hinges nearly 180° apart. For packaging, the hinges are used to fold the rim and torus back on themselves. The rim and torus are then rolled up, leaving the lens in a cone shape. Accordion folding the lens completes the packaging procedure.

After the package is placed inside the canister, the canister is evacuated. This is done so that very close control and monitoring of the canister and package internal pressures can be maintained. Air trapped inside the package folds is a contributing factor to what are called residual gases. Since such very low pressures are required for inflation, residual gases have previously contributed to deployment and inflation problems with very light inflatables. One might intuitively expect a residual gas problem with this packaging technique since it leaves an open space inside the package, but this does not seem to be the case. A programmed number of holes in the satellite skin and a perforated "basket" inside the canister assist in the canister and package evacuation.

Packaging efficiency (i.e., actual volume of expandable material as compared to the internal volume of the canister), for the lenticular satellite is

probably low with the packaging procedure shown in figure 14. How low it will be after the detailed satellite design is not known, but the studies to this point indicate that compatibility of the canister with available launch vehicles is no serious problem.

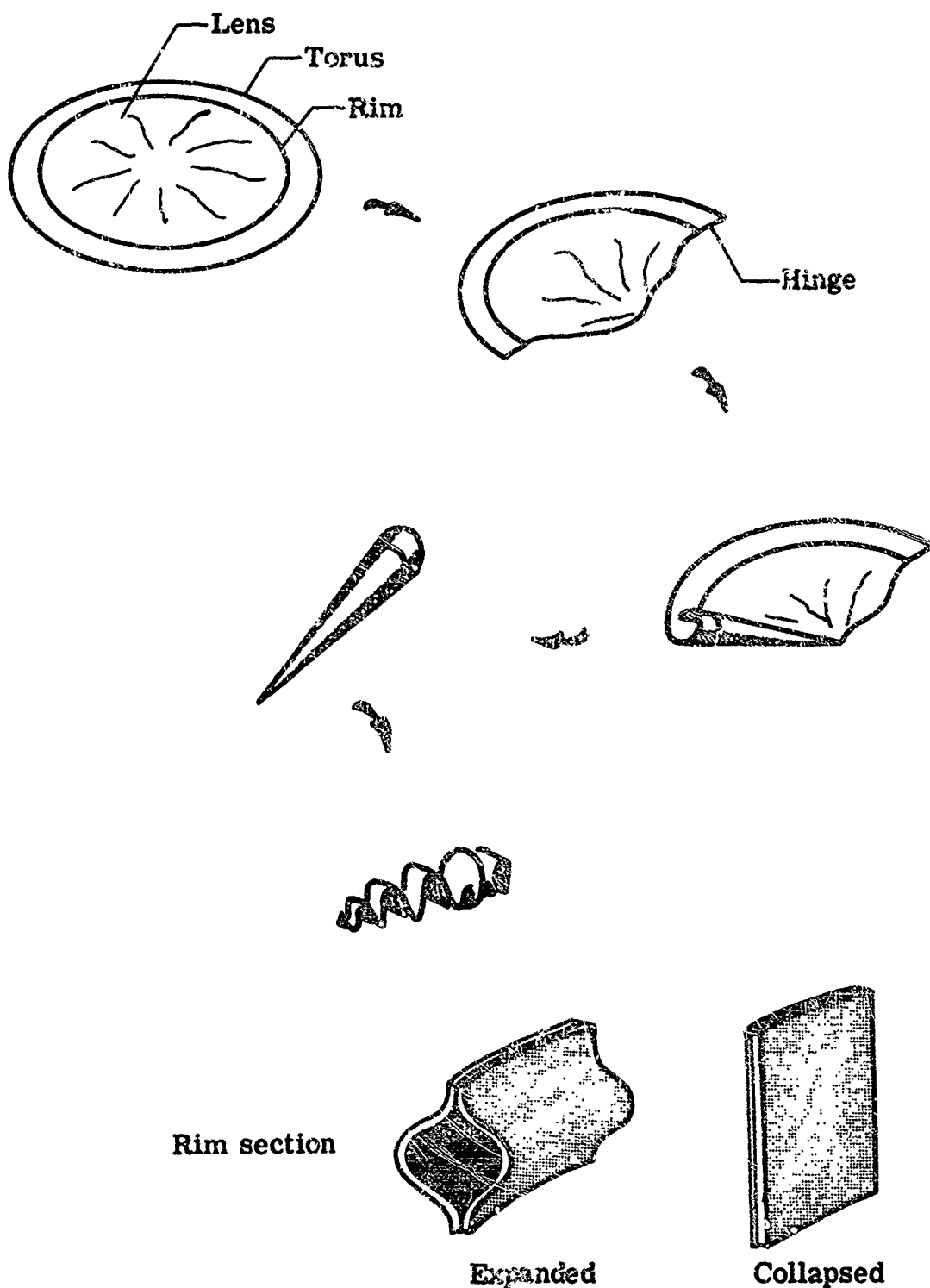


Figure 14.- Packaging sequence.

Deployment is accomplished by inflating the torus (fig. 15). The outside torus section is first inflated, and the remaining torus inflation is controlled by diaphragms with orifices built into the torus. Thus the deployment rate and direction are controlled. The rim cross section expands to its rigid condition after torus inflation. Only after the torus is fully deployed and

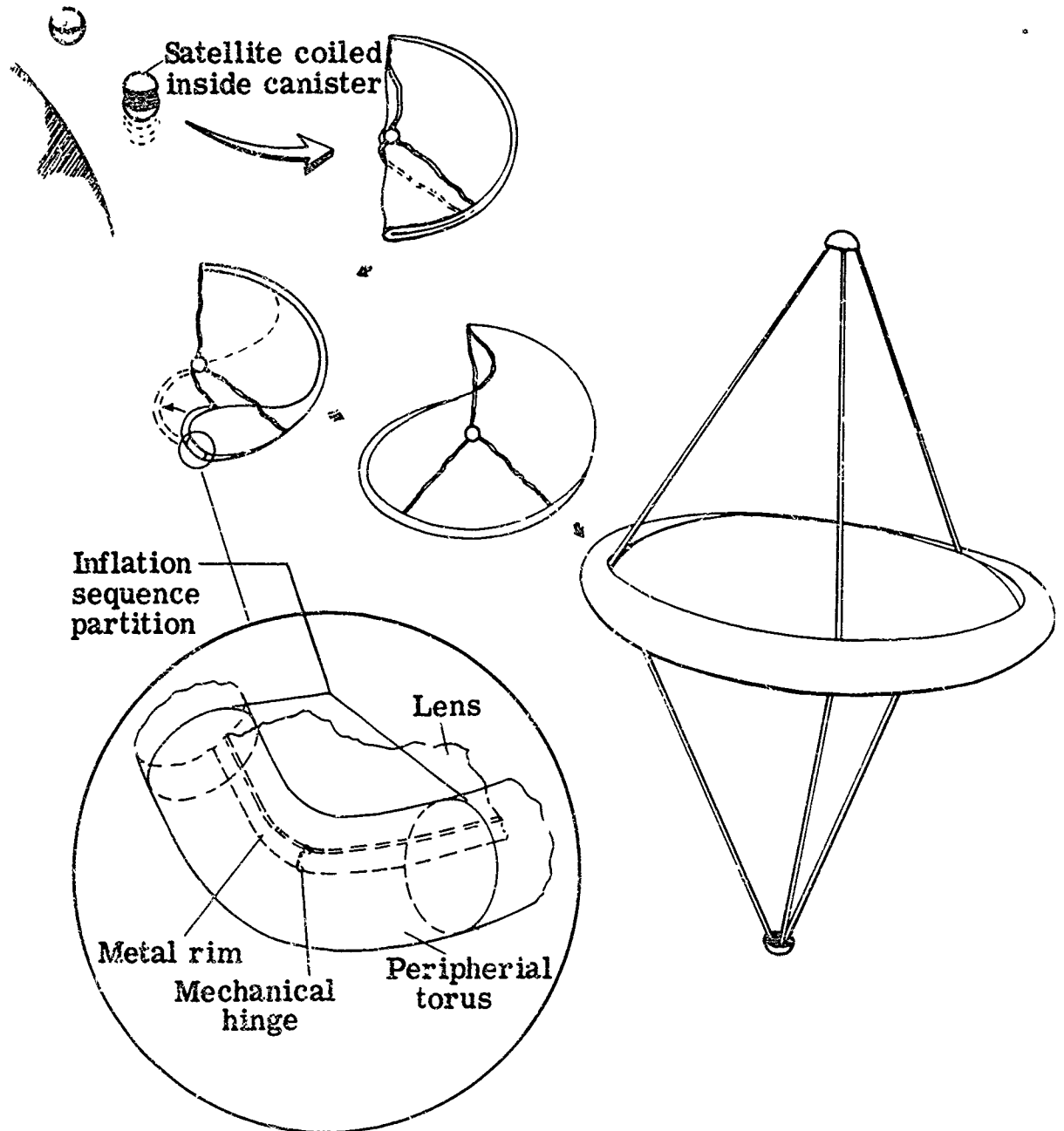


Figure 15.- Deployment sequence.

inflated does the lens pressurization/rigidization process begin. All inflation is done through the booms. Deflation is accomplished by permeation of the inflation gas, helium, through the materials and through a programmed number of holes in the satellite skin.

A series of deployment tests have been conducted at Langley Research Center using 20-foot-diameter lens models. The models were packaged in the canisters and evacuated, and were then successfully deployed in a 60-foot vacuum sphere.

PART IV

LENTICULAR POTENTIAL

The major effort on the lenticular satellite has been, to this point, concerned with the satellite design for a 2000 n.mi. orbital altitude, horizon-to-horizon included angle and a 400-foot sphere equivalent lens. An effort is now under way to expand on this presently available data to determine the effects of variations in these three basic parameters on the satellite's performance and physical characteristics. It should be iterated here also that very little effort has been directed toward optimization of a lenticular satellite, and its potential should not be overlooked. Preliminary studies indicate that the weight of the 2000 n.mi. configuration shown in figure 15 may be reduced by more than 50 percent, still without damaging its communications capabilities.

APPLICATION OF INFLATABLE STRUCTURES TO STATION KEEPING
OF PASSIVE COMMUNICATIONS SATELLITES

By John E. Cooper

NASA Langley Research Center

INTRODUCTION

To accomplish future goals of the nation's communications program, it will be necessary to establish a network of communication satellites. Regardless of whether the network consists of either active or passive communications satellites, a suitable method of station keeping must be employed in order to minimize the number of satellites required in a world-wide continuous communication satellite system. Results of previous NASA statistical studies (refs. 1 and 2), illustrated in Figure 1, have shown that the required number of randomly spaced communication satellites increases rapidly as the requirement for 100-percent continuous service is approached for various communication links. However, this number of required satellites can be significantly reduced and the 100-percent continuous service attained if suitable initial placement and station keeping techniques can be accomplished.

The term "station keeping" is used in different ways depending on whether one is considering synchronous or nonsynchronous orbits. For synchronous orbits, station keeping refers to maintaining the satellite at an apparent fixed position in space with respect to viewing it from fixed ground stations. The apparent fixed position is attained by placing the satellite in a circular equatorial orbit at approximately 22,300 statute miles altitude so that the orbital period of the satellite matches the period of the earth's rotation. Under these conditions the satellite appears to remain fixed in the sky when viewed from a fixed position on earth and the problem of station keeping lies in maintaining the orbital period equal to the earth's rotational period. However, when considering nonsynchronous orbits; station keeping refers to maintaining constant altitude, near circular orbits, and equal spacing, as measured from the center of the earth, between a group of satellites in a common orbital plane as illustrated in Figure 2. This can be achieved by initially spacing the satellites around the orbit and then keeping their orbital periods equal to one another. It is this latter definition of station keeping that is meant when referred to further in this paper.

From the tracking data (ref. 3) of the NASA Echo I experimental passive communication satellite, launched August 12, 1960, it is seen that such a satellite, when put into a near circular orbit, can experience significant variations in apogee and perigee due to differential perturbation effects on the orbit. Such variations in altitude cause large unwanted fluctuations

in the radio signal strength received at the ground station from the communication satellite. The solar perturbation is the dominant contributor of these differential orbit perturbation effects. Even though the solar photon flux imparts a small force per unit area on the satellite, its effect is significant on the low-density large area-to-mass-ratio satellites, such as Echo I, required for efficient passive communication satellites. One can see (ref. 4) that even if a group of low-density passive communication satellites were initially spaced in orbital patterns, that due to the inherent differential orbit perturbation effects and the initial orbit injection errors between satellites the spaced system would eventually randomize and discontinuities in service would occur between ground stations. Therefore, some method of station keeping to initially place and maintain constant altitude and angular spacing of satellites is needed in order to reduce the number of satellites required in a practical and economical continuous communications satellites system.

A method of attaining the orbit position control necessary to accomplish station keeping of low-density passive communications satellites was originally proposed by Westinghouse Electric Corporation. The purpose of this paper is to present the concepts and results of the investigations of the proposed method performed both in-house and on contract, with Westinghouse Electric Corporation, under the direction of the Langley Research Center of the National Aeronautics and Space Administration.

ORBIT POSITION CONTROL METHOD FOR STATION KEEPING

The orbit positioning control methods that have been utilized or proposed in the past have generally been limited to mass dispensing techniques such as thrusting jets. In addition to having limited lifetime dependent on the quantity of mass carried onboard the satellites, the techniques of using point sources such as jets are not consistent with the structural capabilities of large inflatable passive communication satellites. Therefore, investigations were made into the controlled variation of unsymmetrical passive forces on inflatable Echo type low-density satellites throughout the satellite's orbital period so as to develop a passive control force for positioning a group of satellites with respect to each other in similar orbital planes. The control force is derived from the reaction on the satellite's surface of direct solar photon flux (both incident and reflective components), earth's radiation, and the satellite's reradiation (thermal emission). The forces are passive by nature since they do not depend on moving parts or mass expenditure but on the solar reflectance, absorptance, and emittance properties of the materials and are small values per unit area and therefore consistent with the structural characteristics of thin film materials. The total control force is compiled of small components distributed over the surface area of the satellite and therefore its magnitude and orbit positioning capability are directly dependent on large area-to-mass-ratio satellites which, due to booster and launching requirements, are applicable to the utilization of inflatable, expandable, or erectable structures in space.

As illustrated in Figure 3, this passive control force is used to control the orbital energy of the satellite. For simplicity let us assume a flat plate of unit area in a circular orbit about the earth with the sun in the orbital plane. One side of the plate is assumed to be a perfect absorber and the other side a perfect specular reflector. When considering the plate normal to the incident solar radiation pressure, the force per unit area when the reflective side faces the sun will be twice the value of the force when the absorptive side faces the sun. If the reflective side is oriented toward the sun during that half of the orbit when the satellite is receding from the sun and the absorptive side is oriented toward the sun during that half of the orbit when the satellite approaches the sun, then the energy of the orbit is increased and the satellite will seek a higher altitude thereby causing the period of the orbit to become longer and the angular rate about the center of the earth to decrease. The satellite will seem to fall back in orbit with respect to other unaltered satellites and is considered in the "Slow Mode" of operation. If the procedure is reversed and the absorptive and reflective sides are oriented toward the sun during the receding and approaching halves of the orbit, respectively, then the orbital energy is decreased and the satellite seeks a lower altitude causing the orbital period to decrease and orbital angular rate about the earth to increase. The satellite will then speed up in orbit with respect to other unaltered satellites and is considered in the "Fast Mode" of operation.

Therefore, orbit position control can be attained to accomplish station keeping by orienting different surface areas, which have different solar reflectance and absorptance characteristics, toward the sun throughout different intervals of the orbital period. Since this technique utilizes the solar radiation pressure, normally considered a perturbing force, its usable lifetime is unlimited and the force is available everywhere in space, except in the earth's shadow where a satellite remains for only a small fraction of its lifetime.

SPHERICAL SATELLITES

Initial studies were performed to apply this orbit position control technique to Echo type inflatable spherical satellites. Satellite sizes from 100 to 400 feet in diameter were investigated in the altitude ranges of 500 to 3500 statute miles. Various coating patterns and characteristics were investigated in order to determine the best configuration with respect to obtaining large force differentials on opposite sides of the satellite in addition to minimizing the torques on the satellite due to radiation. Naturally, coatings possessing the properties of the ideal perfect absorber or reflector are hypothetical, and therefore a literature search was performed to determine realistic coating characteristics. Based on these considerations, a two hemispherical pattern coating scheme was chosen to be most suitable for orbit positioning control, where one side of the satellite is an absorber and the other side predominantly a diffuse reflector.

Attitude Maneuver Systems

Two different attitude maneuver systems, illustrated in Figure 4, were studied with regard to their capability of controlling the orbital energy. For the Dual Flip or Solar Oriented case, the axis of symmetry with respect to the surface coatings is aligned toward the sun and two 180° flips about either the yaw or pitch axis are performed near points A and B of the orbital path so as to present the opposite hemispherical surfaces towards the sun during the approaching and receding halves of the orbit. For the Vertically Oriented case, the axis of symmetry is aligned along the velocity vector so that the satellite rotates in pitch once per orbit and thereby varies the surface coatings facing the sun over the orbital period. For this case, the 180° flip about the yaw axis is required only when it is desired to change the mode of operation from Fast to Slow or vice versa.

Each system requires some method of attitude control for the desired alignment in addition to a torquing system for the required flips. The initial concept was to utilize magnetic torquing by equipping the satellite with three mutually orthogonal current-carrying coils to react against the geomagnetic field and produce the desired three-axis control. This system (ref. 5) requires continuous sensing throughout the orbit of the sun's direction and the earth's magnetic field vector with respect to the satellite's symmetry axis. In addition, it requires solar and geomagnetic ephemeris information, expressed in orbital coordinates, stored onboard the satellite and supplied to the control system on a continuous basis. From these data, the attitude control system determines the attitude error of the satellite and programs the required currents in the coils necessary to make the desired attitude corrections. Therefore, in addition to the coils, there is required onboard the satellite solar cells for power and sun sensing, magnetometers, storage devices, and logic and computer circuitry for orientation and damping.

Although the Dual Flip system yielded slightly greater orbital energy changes per orbit, it was found to be inconsistent with the structural capabilities on the thin film Echo materials due to the large torquing requirements in performing the two 180° flips per orbit in short periods of time. Since the flips required for the Vertically Oriented system are needed only when changing modes, the torquing effects on the structure are greatly reduced by performing the flipping maneuver slowly over the period of several orbits. Also, the power requirements for the Vertically Oriented system are approximately only one-fourth the requirements of the Dual Flip system. Therefore, the Vertically Oriented system was chosen to be pursued in the studies.

Mobility

A measure of the capability of this orbit position control technique to accomplish station keeping is termed "mobility" and is defined as the change in angular separation as a function of time between two identical satellites started from the same point in a common orbit with one in the Fast Mode and the other in the Slow Mode of operation. A sample mobility curve is shown in Figure 5 which is derived from the effect of the direct

solar incident and reflective forces upon 200-foot-diameter, 2000-pound spherical satellites in 45° inclination, 1500-mile-altitude orbits with realizable surface coating characteristics as illustrated. The curve indicates a constant angular acceleration rate of separation between the two satellites and shows that after 30 days the total angular separation would be 100° and the satellites would be in different orbits and still separating as the altitude and periods of the satellite would differ slightly. However, if after 15 days the mode of operation of each satellite were reversed so that the one in the Fast Mode was put in the Slow Mode and vice versa, then the curve from 15 days to 30 days would indicate a constant angular deceleration rate of separation equal to the acceleration rate of the curve for the first 15 days and is shown as the dotted curve in Figure 5. For this situation the two satellites would be back into the same common orbit as they started from after 30 days with an angular separation of 50° between them. The satellites could then be put into the same mode or neutral mode and would remain separated 50° as they orbit the earth except for slight deviations due to possible small differences in other orbital perturbations. Should the procedures of orbit positioning control be performed on one satellite with respect to a neutral satellite, the curve would resemble that of Figure 5 but the separation rates and total angular separation with time would be one-half those shown for corresponding time intervals.

In addition to the incident and reflective direct solar radiation, the effects of earth's radiation, albedo, and the satellite's own reradiation (thermal emission) on mobility or change in orbital energy were investigated as a function of the coating characteristics of various inside and outside surface areas of the satellite. The mobility of the satellite is largely dependent on the differential tangential forces along the orbital path rather than differential radial forces. Therefore, the effect of earth's radiation and albedo is insignificant compared to the direct solar radiation. However, the effect of the satellite reradiation force can be significant with different emissivity characteristics for the two hemispherical outside surface areas, especially since the temperature differentials diametrically across the spherical balloon are significant due to the large distances in separation of the surface areas involved. When considering the Vertically Oriented case, the reradiation forces, while an order of magnitude smaller than the direct solar force, is almost continually aligned to the velocity vector of the satellite while the direct solar force varies with respect to the velocity vector sinusoidally throughout the orbit.

Figure 6 shows a comparison of mobility curves for the various coating patterns illustrated. Curve 1 indicates the mobility when considering just the direct solar force effect on Configurations A or B, where the absorptivity is 0.85 and corresponding reflectivity is 0.15 on one hemispherical side and the diffuse reflectivity is 0.65 and corresponding absorptivity is 0.35 on the other side. Curve 2, representing mobility of Configuration A when considering the total forces on the satellite, is considerably less than curve 1 and therefore indicates that the effect of the differential reradiation forces available from realizable emissivity values is in opposition to the direct solar forces. This is more apparent in curve 3 where the mobility from the total forces on Configuration B is plotted. The curve is dotted to represent a negative or reverse mobility, where the Fast

Mode when considering direct forces now becomes the Slow Mode when considering total forces and the Slow Mode becomes the Fast Mode, etc. For this case the reradiation forces are dominant due to the large difference in emissivity values for the two hemispherical coatings. Since the effects of the direct solar and reradiation forces were in opposition, it was believed that by eliminating the differential direct solar effect over the orbit, an even greater mobility could be obtained. Curve 4 confirms this belief by utilizing Configuration C which has uniform outside absorptivity and reflectivity and therefore also minimizes the solar torques on the spherical satellite. Investigations into the variations of the emissivity values on the inside surfaces resulted in little effect on the mobility and were therefore chosen as 0.9 to maintain the temperature distribution over the satellite within tolerable limits.

All of these mobility curves were computed with the sun in the plane of the orbit. Actually the sunline moves out of the plane of the orbit as the earth orbits around the sun. The inclination of the sun, defined as the angle between the sunline and the orbital plane of the satellite, varies periodically over a yearly cycle and its amplitude will reach 90° for orbital inclinations between 67° and 157° . Accordingly, the mobility will be reduced when the sun moves out of the orbital plane. However, the resulting Configuration C will have sufficient mobility even when the sun is normal to the orbital plane since the differential reradiation forces are mainly dependent on the energy received from the sun rather than the incoming direction.

Resonance

This technique of orbit position control depends solely on controlling the orbital energy and thereby the orbital period of the satellite. However, the effect of orbital eccentricity on the system is an important consideration. Normally the eccentricity varies in a cyclic manner throughout the lifetime of the satellite as experienced by Echo I (ref. 3). The period and amplitude of this oscillation are dependent on the area-to-mass ratio of the satellite as well as the orbital inclination and altitude. The solar radiation pressure is the dominant perturbing factor on low-density satellites causing the eccentricity variations, and its effect on spherical satellites has been widely investigated (refs. 6, 7, and 8). However, there are certain critical combinations of orbital inclinations and altitude where the eccentricity does not vary periodically but continues to build up as a direct or staircase function. These conditions (ref. 8) are termed "resonance" and must be avoided as they would eventually destroy the orbit if continued over a long period of time.

Computer studies were performed to predict the maximum limit on eccentricity buildup for various orbits and satellite sizes. A sample case is shown in Figure 7, where the maximum eccentricity buildup is plotted against orbital inclination for a 200-foot-diameter, 2000-pound spherical satellite in a 1500-mile-altitude orbit. The peaks on the curve indicate areas of resonance which must be avoided. However, these inclinations can be used at other altitudes, where the resonance conditions will then occur at different inclinations. Since the maximum eccentricity is directly proportional

to the area-to-mass ratio of the satellite, it can be easily computed for all satellite sizes for any given curve of constant altitude.

LENTICULAR SATELLITE

As a spherical passive communications satellite, such as Echo I, orbits the earth only that segment of the sphere which faces the earth at any given time contributes significantly to the reflected communication signals back toward the earth. Therefore, a considerable portion of the sphere, which reflects the radio signal received outward into space, may be eliminated, and thereby achieve a considerable reduction in weight, by utilizing an earth-oriented passive segment of the sphere. This concept, illustrated in Figure 8, consists of using a similar segment on the top half of the satellite to form a membrane for inflation techniques and is termed a "lenticular" satellite. As illustrated, the angular extent of such a satellite should be approximately 84° in a 2000-nautical-mile-altitude orbit in order to reflect communication signals back to any point on the earth that can be seen when viewed from the satellite. Subsequent studies are being performed under the direction of NASA Langley Research Center into the feasibility and design of this lenticular satellite concept utilizing gravity gradient stabilization for the vertical earth pointing requirement. The communication advantages of the lenticular satellite and the structural and stabilization concepts involved are discussed in another paper (ref. 9) to be presented at this Conference and therefore will not be dealt with further in this paper. However, the application of the solar sailing orbit position control technique to the gravity gradient stabilized lenticular satellite is discussed in the following paragraphs.

Since the results of the station keeping studies on spherical satellites indicate a preference for vertical orientation, the technique readily applies to the lenticular satellite which also has the vertical orientation requirement based on its use as a passive communications reflector. Also the use of the passive gravity gradient stabilization for two-axis control eliminates the need for the complex and active magnetic three-axis attitude control system presented earlier for the spherical satellite. However, some additional method of control and flipping is required about the yaw (vertical) axis in order to accomplish station keeping.

Various lenticular configurations with corresponding orbit position control schemes were investigated, and the two most feasible concepts are presented in Figure 9 with the resulting dimensions and weights as shown. The configuration on the right obtains its mobility in the same manner as the spherical satellites, as it consists of a solid lens having two different surface areas with different emissivities. The line of symmetry through the patterns, indicated by the x-axis, is aligned along the velocity vector and flipped 180° about the yaw axis when changes in mode of operation are desired. The configuration on the left obtains its mobility through the use of flat sails attached between the stabilization booms of one plane and having different reflective properties on either side, by aligning the plane of the sails normal to the velocity vector. This method also requires the same 180° flipping about the yaw axis for mode changes. The total required

sail area is split equally above and below the lens so as to assist in distributing the mass symmetrically and thereby minimize the solar torquing disturbances on the stabilization systems. This configuration uses a photolyzable material on the lens as a gas barrier for the inflation system (ref. 9). The material then disappears in the space environment leaving behind a wire grid mesh lens which is suitable as a microwave reflector for passive communications.

Advantages of using the mesh lens with flat sails over the solid lens are as follows: First, a neutral orbit positioning control mode can be obtained by aligning the plane of the sail parallel to the orbital plane. Second, the maximum eccentricity limit can be decreased by reducing the projected area-to-mass ratio of the satellite towards the sun during critical eccentricity buildup periods by aligning the plane of sail parallel to the sunline, since the mesh lens projects a considerably smaller area towards the sun than the solid opaque lens. However, the photolyzable mesh material is still in the development stages as well as a sail material yielding the required optical properties for station keeping and still being microwave transparent so as to avoid communications interference. A mobility in the range of 100° per 30 days is feasible with either configuration at 2000 miles.

Two concepts of obtaining the required three-axis damping and yaw control are also indicated in Figure 9. The Ames-X principle (ref. 10) of using inertial coupling for three-axis damping of gravity gradient stabilized satellites is schematically shown on the configuration on the right. DeHavilland type extendable yaw and damper booms with tip masses provide the satellite with the necessary moments of inertia distribution and are skewed to the satellite body axis in such a way (ref. 10) as to align the x-axis in the orbital plane. By utilizing either magnetic hysteresis or eddy current dampers with this Ames-X concept, three-axis damping can be achieved. The yaw flipping for mode changes, etc., is accomplished through the use of a step-servo motor and hermetically sealed harmonic drive which rotates the satellite beneath this stabilized boom structure to the desired positions for performing station keeping. In the configuration on the left is illustrated the Rice/Wilberforce damper concept, investigated by Goodyear Aerospace Corporation, consisting of a lossy spring and viscous damper. The required moment-of-inertia distribution between the x-axis and the y-axis is obtained by placing weights around the rim of the lens and the required yaw torquing obtained by use of a reaction wheel. Either system could possibly be utilized with either configuration; however, the feasibility studies so far indicate a preference for the Ames-X concept.

CONCLUDING REMARKS

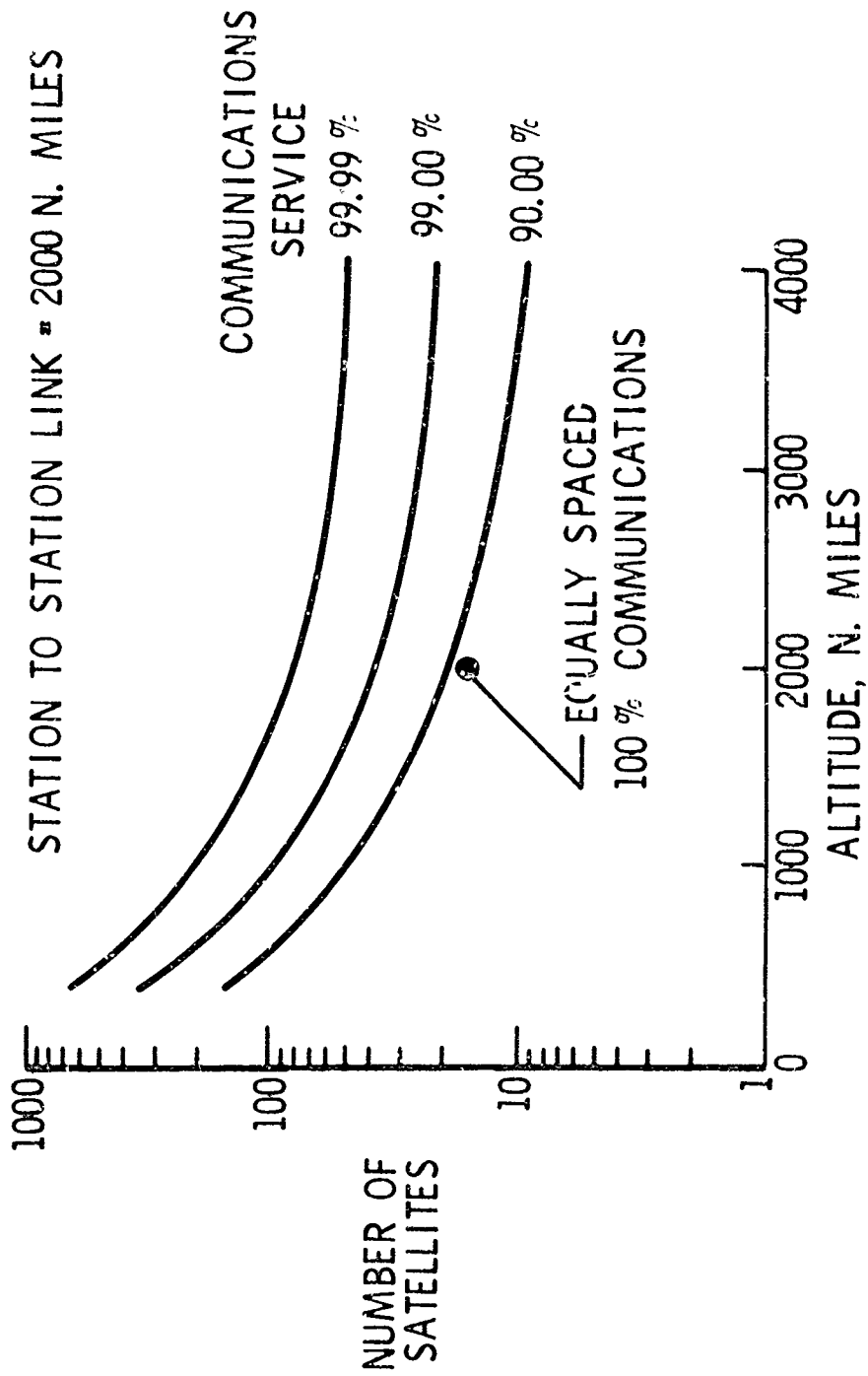
The results of the studies have demonstrated feasibility in utilizing the passive solar radiation force and the satellite's reradiated thermal emission force to perform orbit position control to accomplish station keeping of low-density Echo type spherical and lenticular passive communication satellites by controlling the orbital energy and thereby controlling the orbital period of the satellites. The studies have shown that the technique depends on large area-to-mass-ratio satellites and therefore due to launching requirements are directly applicable to inflatable, expandable, and erectable structures in

space. The amount of mobility available is dependent on the differences in solar reflectance, absorptance, and thermal emittance that can be achieved through the use of realizable lightweight coatings. In addition, semipassive attitude stabilization and damping systems have been shown feasible for the lenticular satellite.

The resulting data so far have been limited to low-altitude 2000-nautical-mile range. However, studies are being initiated under the direction of Langley Research Center to extrapolate the mobility results of the lenticular satellite parametrically from the existing data with respect to variations in inclinations, shapes, and altitudes up to and including synchronous orbit. In addition, subsequent overall trade-off studies are being planned to determine the most economical satellite communication system feasible now and in the near future utilizing orbit position controlled lenticular passive communication satellites.

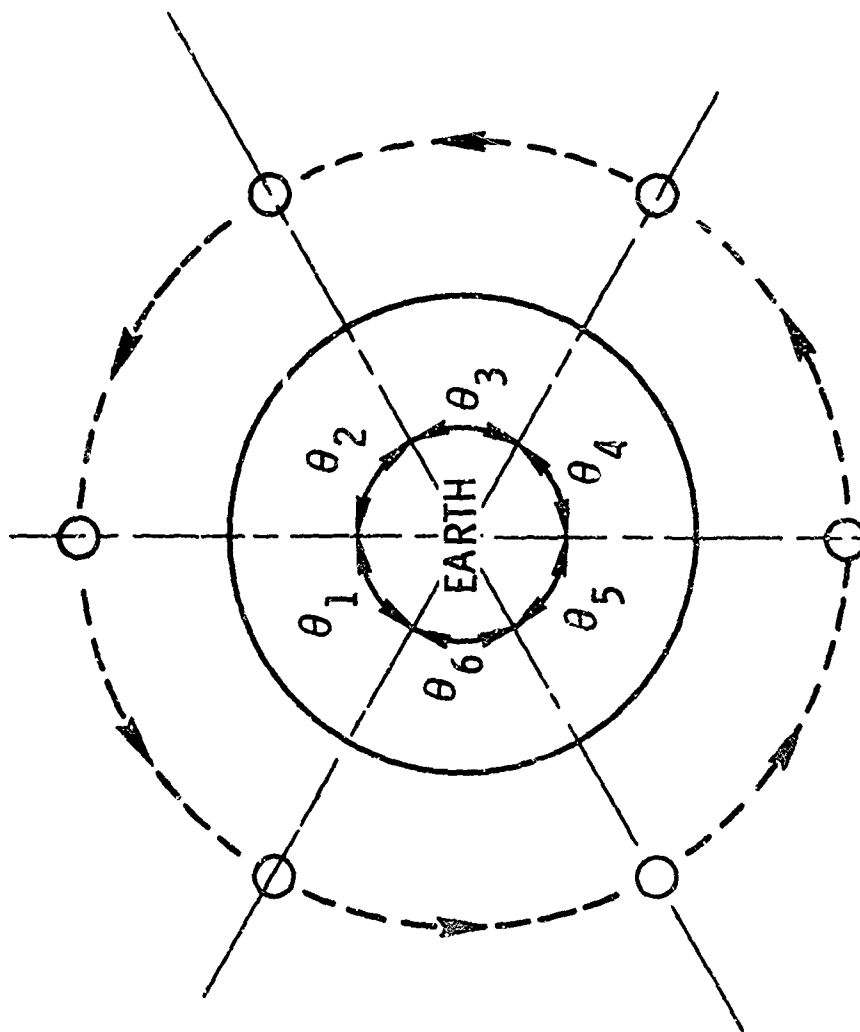
REFERENCES

1. Bennett, Floyd V., Coleman, Thomas L., and Houbolt, John E.: Determination of the Required Number of Randomly Spaced Communication Satellites. NASA TN D-619, 1961.
2. Bennett, Floyd V.: Further Developments On the Required Number of Randomly Spaced Communication and Navigational Satellites. NASA TN D-1020, 1962.
3. Westrick, Gertrude C., and Johnson, Katherine G.: The Orbital Behavior of the Echo I Satellite and Its Rocket Casing During the First 500 Days. NASA TN D-1366, 1962.
4. Reiger, S. H.: A Study of Passive Communications Satellites. R-415-NASA (NASr-20(02)), The Rand Corporation, February 1963.
5. Buckingham, A. G., Lim, Y. C., and Miller, J. A.: A New Technique of Orbit Position Control Using Solar Pressure as the Linear Propulsion Means and the Earth's Gravitational and Magnetic Field as the Attitude Control Means. AIAA Paper No. 64-661, August 1964.
6. Musen, Peter: The Influence of the Solar Radiation Pressure on the Motion of an Artificial Satellite. J. Geophys. Res., vol. 65, no. 5, May 1960.
7. Bryant, Robert W.: The Effect of Solar Radiation Pressure on the Motion of an Artificial Satellite. NASA TN D-1063, 1961.
8. Polyakhova, Ye. N.: Solar Radiation Pressure on the Motion of Earth Satellites. AIAA J. (Russian Suppl.), vol. 1, no. 12, December 1963.
9. Humble, Jerry L.: Structural Considerations for Expandable Lenticular Satellite. Proceedings of the Second Aerospace Expandable Structures Conference, May 1965.
10. Tinling, Bruce E., and Merrick, Vernon K.: The Exploitation of Inertial Coupling in Passive Gravity-Gradient Stabilized Satellites. AIAA Paper, August 1963.



NASA

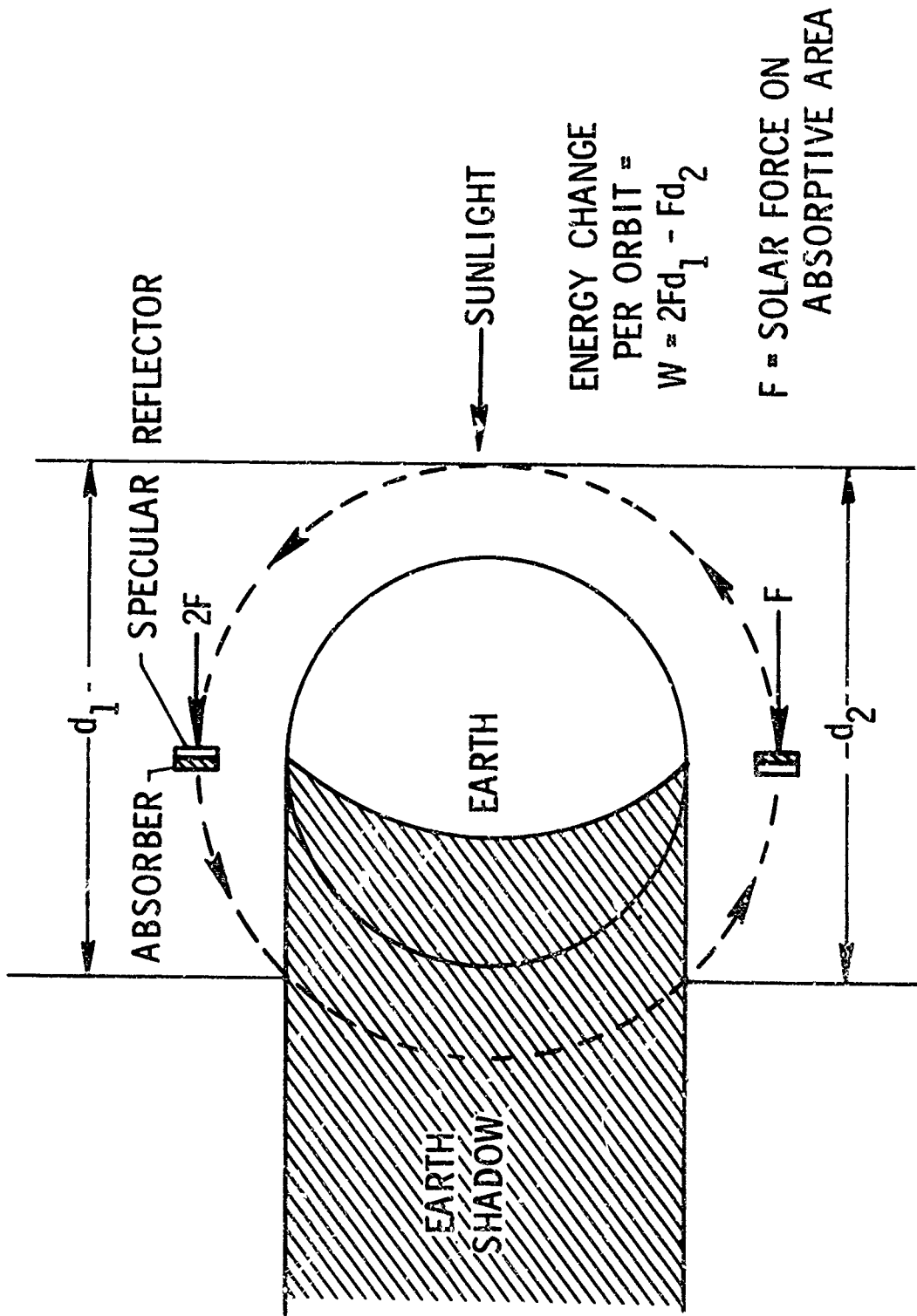
Figure 1.-- Random system.



MAINTAIN $\theta_1 = \theta_2 = \theta_3 = \theta_4 = \theta_5 = \theta_6$

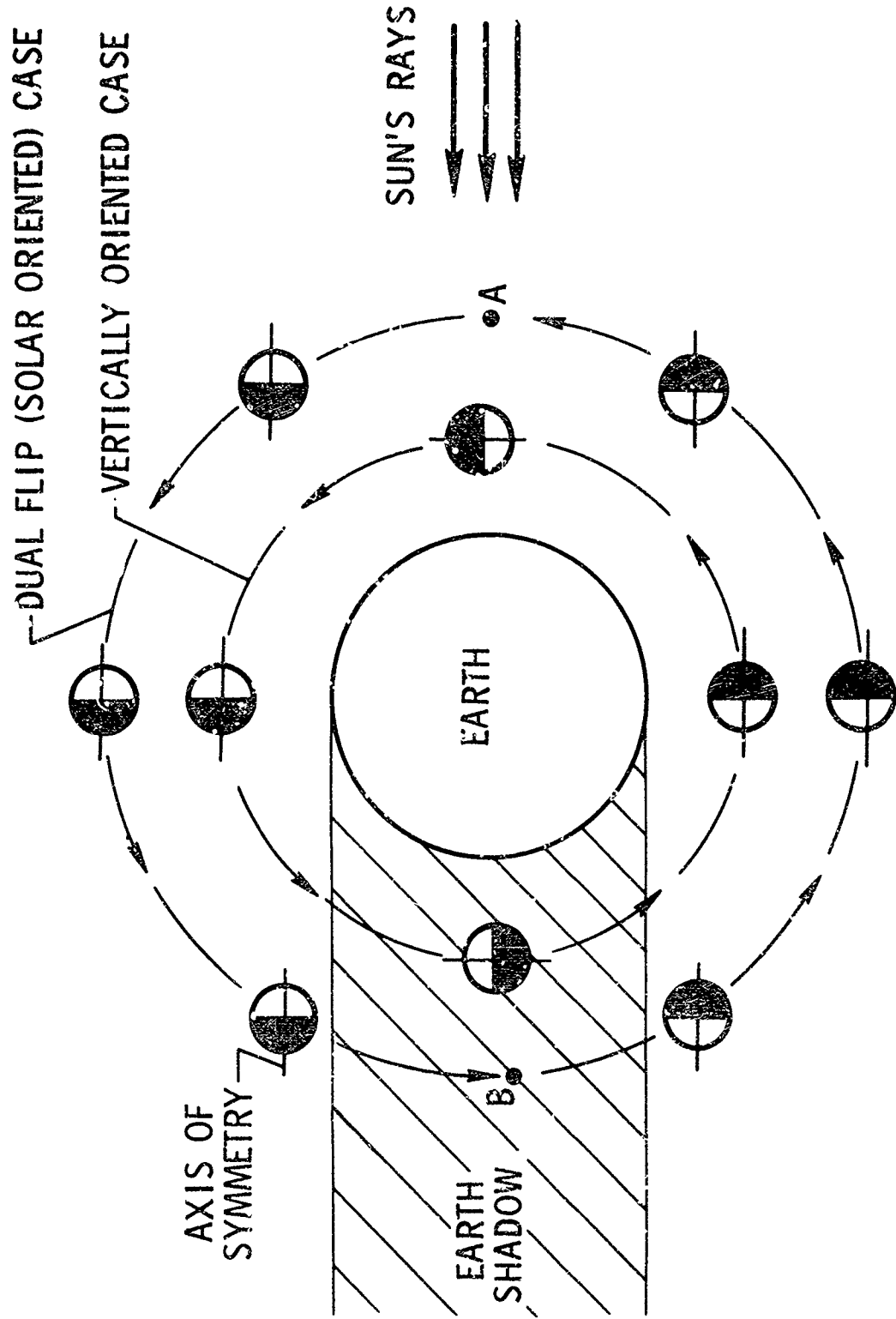
NASA

Figure 2.- Station keeping concept.



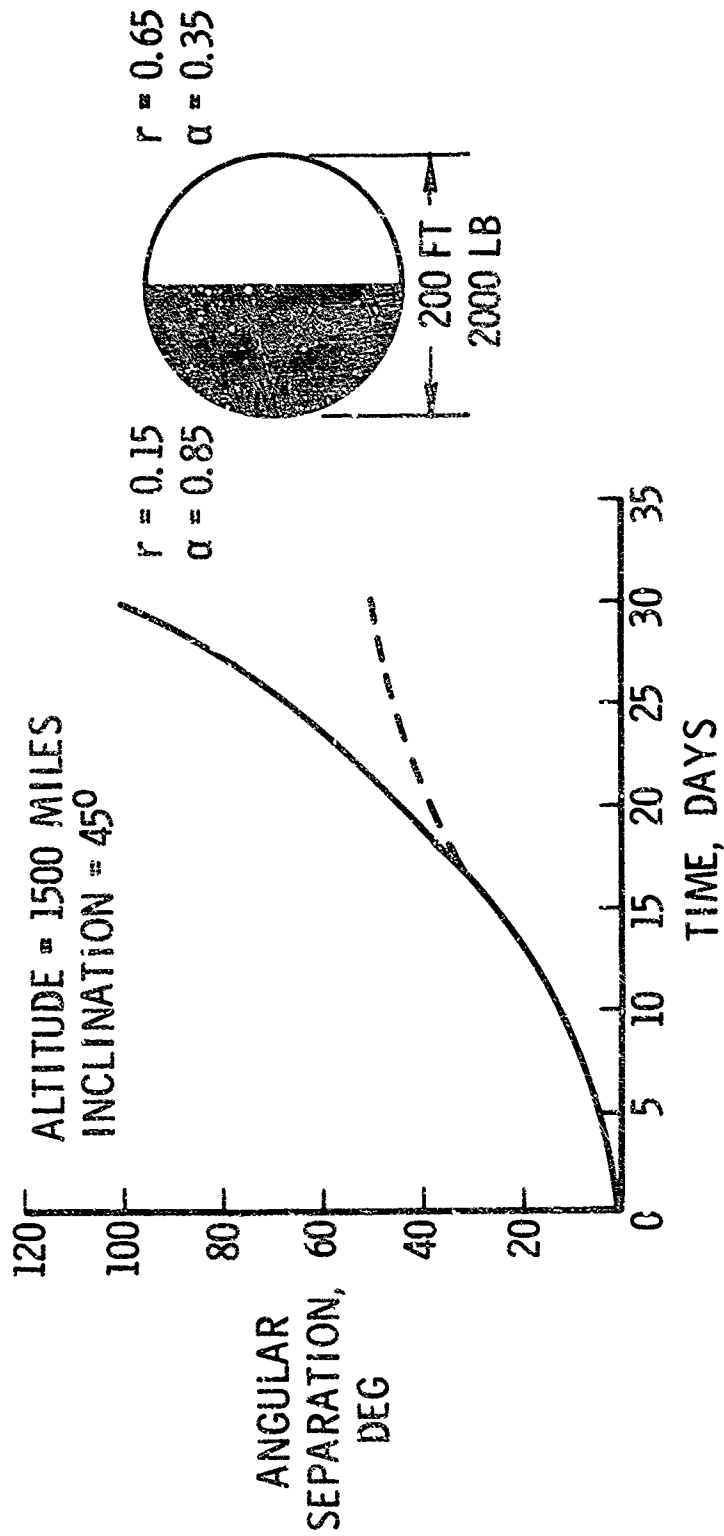
NASA

Figure 3.- Orbit position control method.



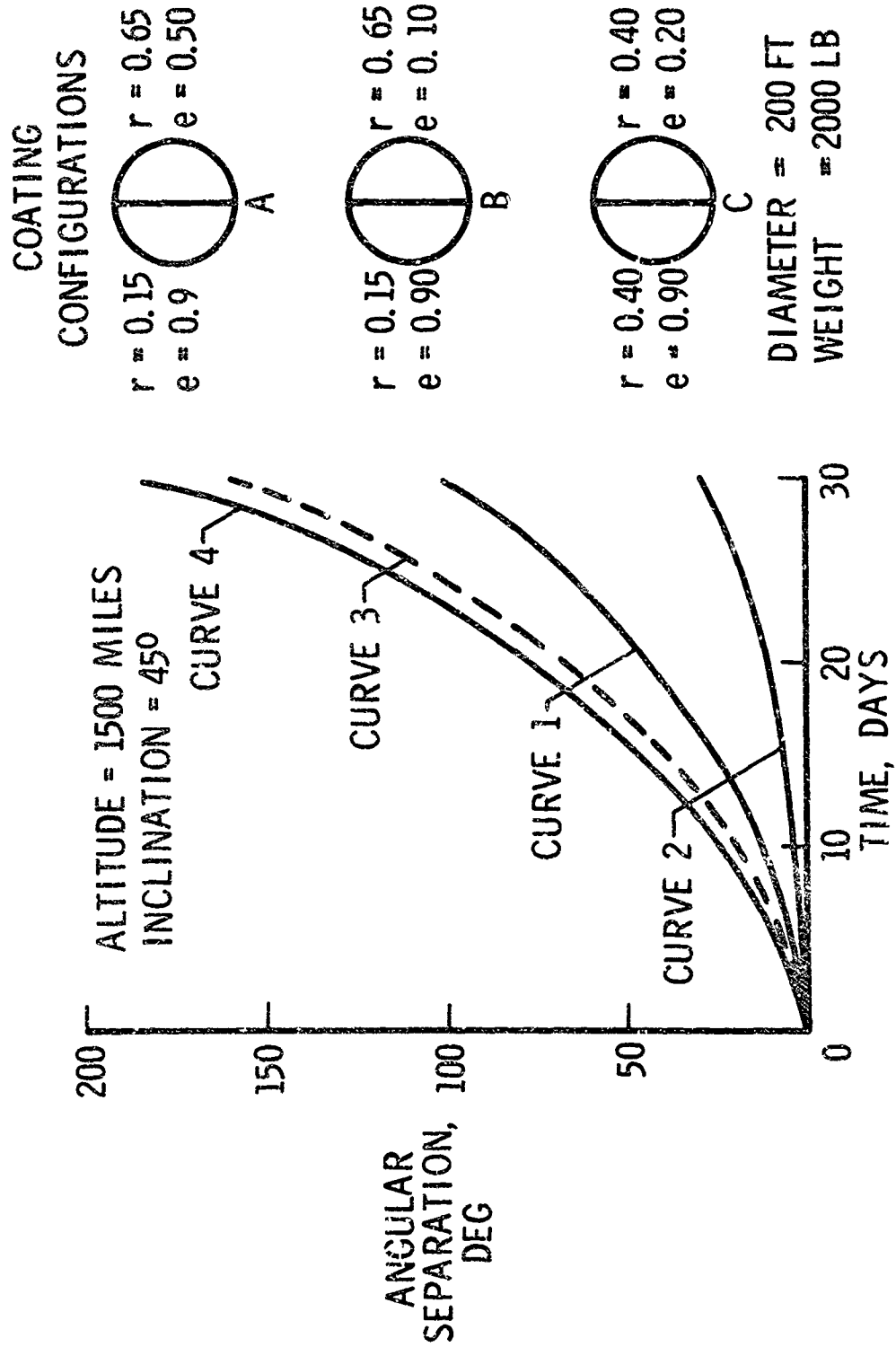
NASA

Figure 4.- Attitude maneuver systems.



NASA

Figure 5.-- Mobility.



NASA

Figure 6.- Mobility comparisons.

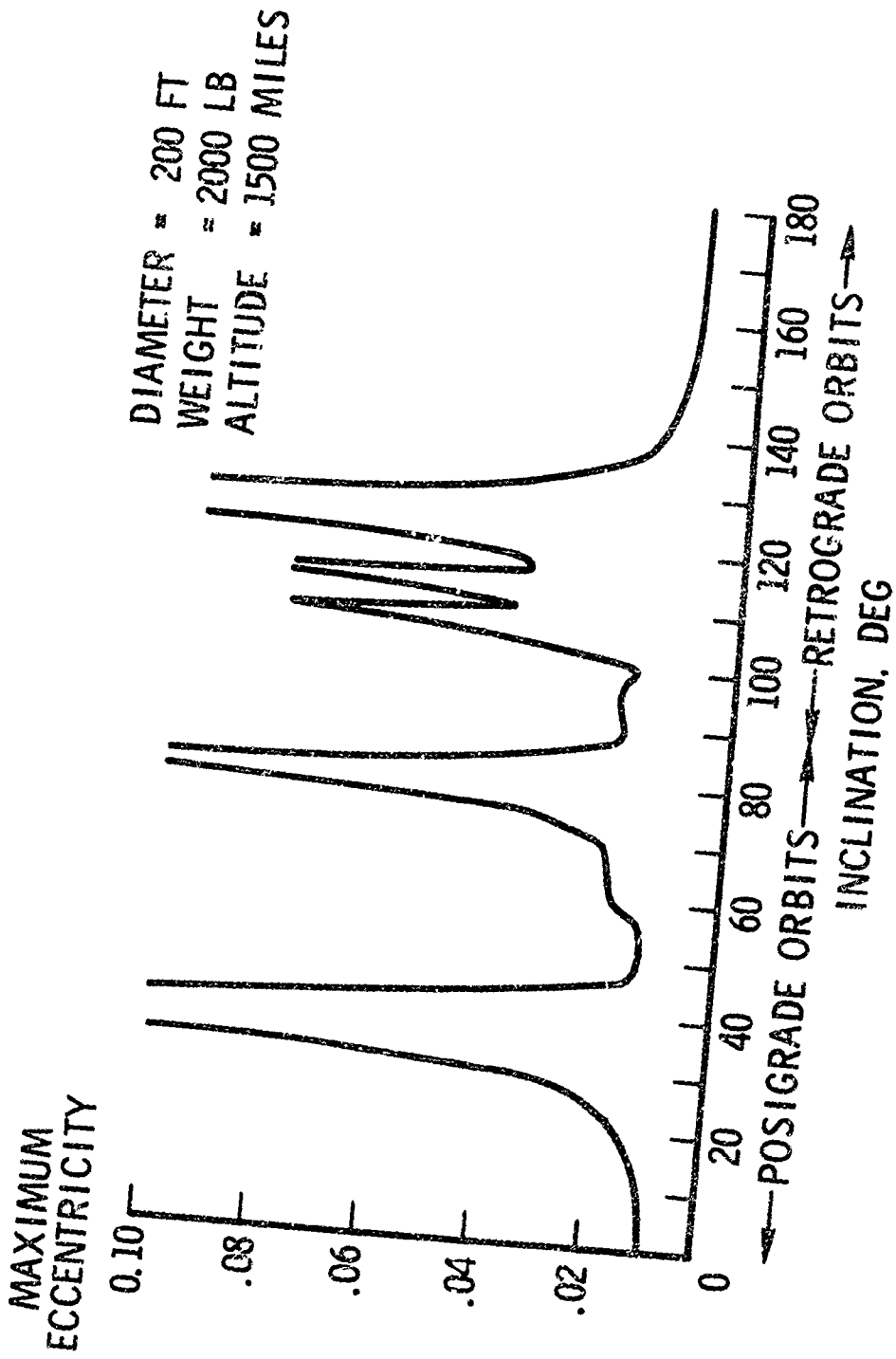


Figure 7.- Resonance conditions.

NASA

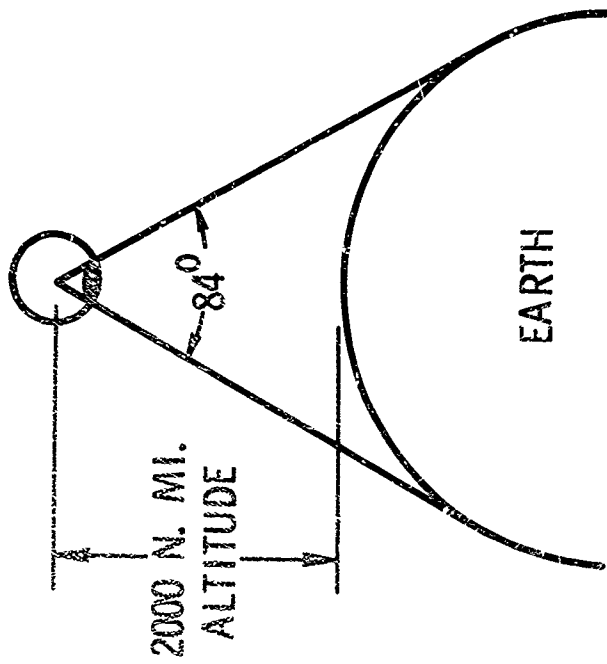
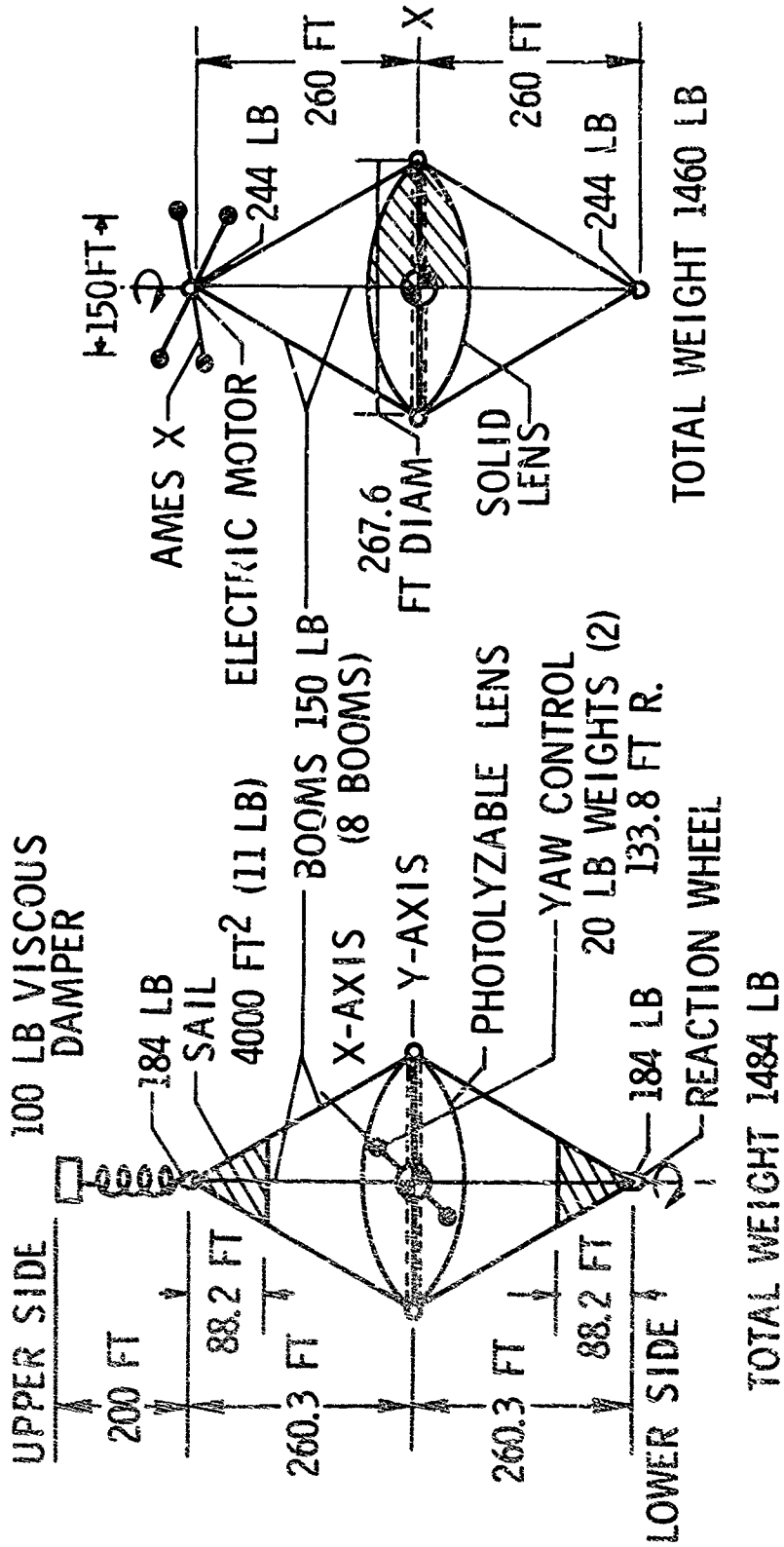


Figure 8.- Lenticular concept.

NASA



NASA

Figure 9.- Station kept lenticular satellite.

DEVELOPMENT OF MANUFACTURING TECHNIQUES FOR A
METAL FABRIC REINFORCED RE-ENTRY PARAGLIDER

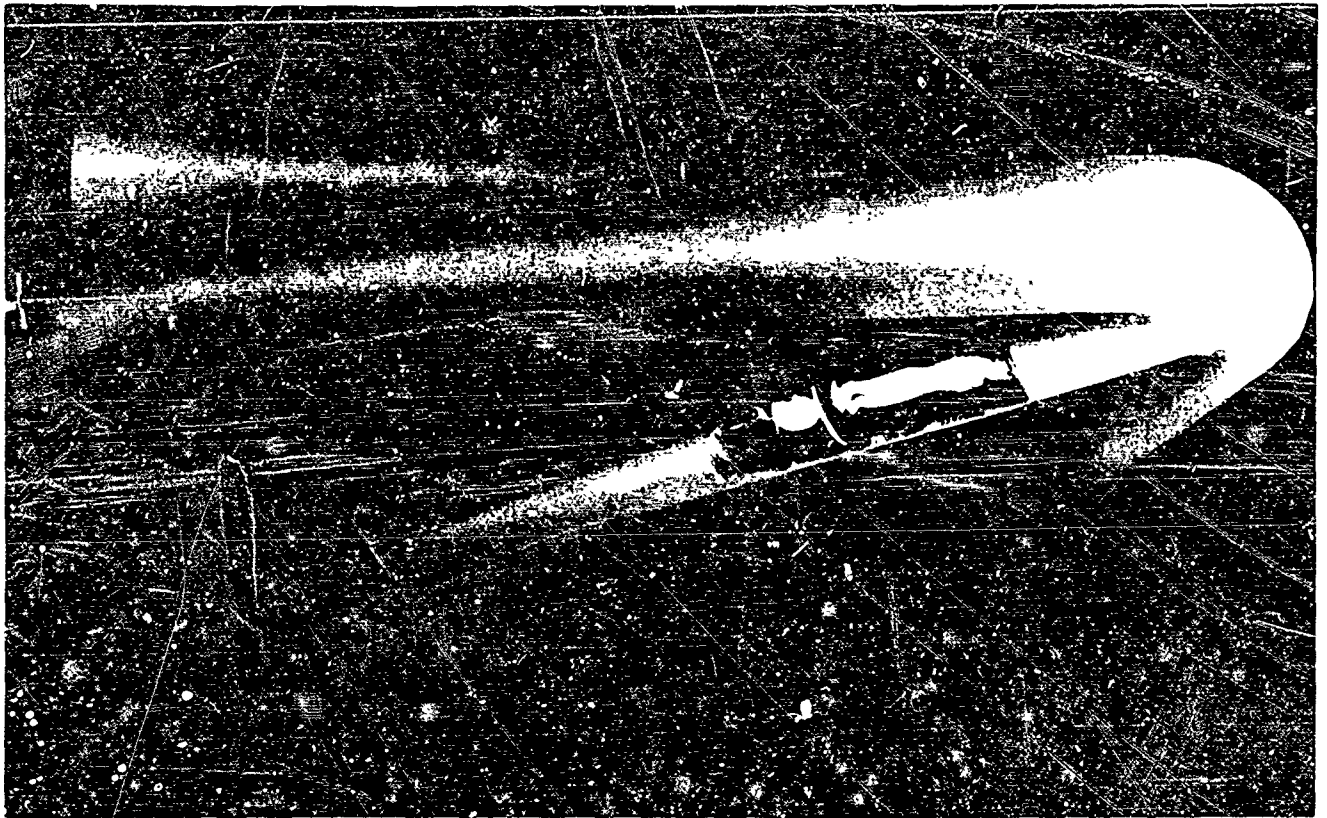
J. F. Keville

Space-General Corporation
El Monte, California

Early in 1963 a contract for the development, fabrication, and test of re-entry paraglider components was awarded to Space-General Corporation by the Manufacturing Technology Division of the Air Force Materials Laboratory. The first phase of the project included optimization of the vehicle configuration, selection of the proper trajectory with emphasis on the aero-thermodynamic aspects of the re-entry regime, materials evaluation and selection to meet the environmental and inherent structural objectives, and design of the actual critical components of the vehicle. The results of this work during the first year were presented at the First Aerospace Expandable Structures Conference in October 1963.

In order to summarize the program objectives and the earlier work, reference is made to Figure 1 showing a photograph of a model of the proposed paraglider with a cutaway showing the position of the man and life support system. This completely flexible, inflated vehicle would be capable of returning a human being from orbit by re-entering the earth's atmosphere at hypersonic velocity and decelerating to effect a subsonic controlled landing on earth. The vehicle consists of an inflated body made up of three tapered booms attached to a common toroidal apex. Attached between the center boom or keel and each leading edge boom is a thin flexible wing membrane which assumes an approximately semi-conical shape during flight. The booms taper from 32 inches in diameter at the forward end to 13 inches at the aft tip with an overall vehicle length of approximately 23 feet. The jets at the boom tips are used for attitude control in space while the aft edge of the flexible wing can be gathered and pulled downward or let out by use of a trailing edge cable for aerodynamic flight control.

An artist's concept of the deployment of the paraglider is shown in Figure 2. The vehicle is packaged similar to a life raft and attached to the space station such that a man can enter the crew compartment section of the paraglider from within the space station; the vehicle is then ejected away and subsequently inflated. Having been aligned at the proper attitude, the vehicle is retro-fired from orbit and re-enters sensible atmosphere at about Mach 30. It is expected that the vehicle can be controlled remotely from the space station or the ground, by self contained auto pilot, or manually by the man on board. Since this is to be used as an escape vehicle it must be assumed that the occupant may be incapacitated due to injury or illness and the vehicle must return him to the ground without manual control in as short a time as possible.



05-051

FIGURE 1. RE-ENTRY PARAGLIDER



FIGURE 2. DEPLOYMENT OF ESCAPE VEHICLE

The total flight time from a position 200 miles above the earth to a controlled landing location would be under 2 hours. The trajectory characteristics during the re-entry heating regime are depicted in Figure 3. It may be seen that the vehicle encounters the first significant dynamic pressure below 400,000 feet altitude. Its velocity begins to rapidly decay below 300,000 feet altitude while the dynamic pressure increases to a maximum of about 5.3 psi, then rapidly falls off as subsonic velocities are approached.

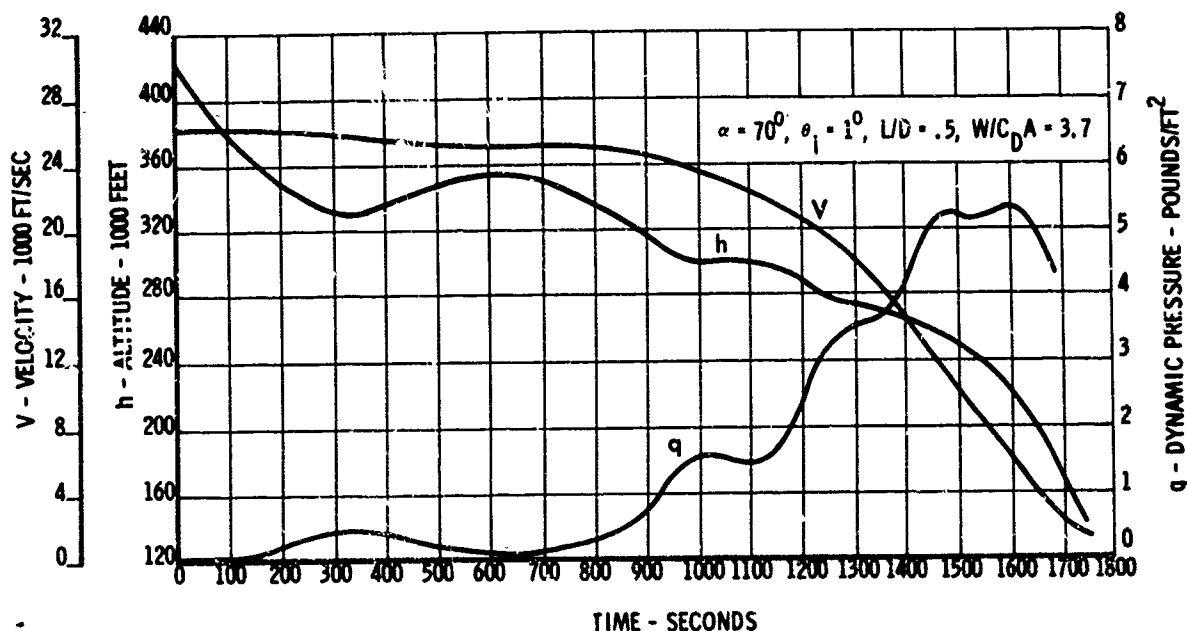


FIGURE 3. TRAJECTORY CHARACTERISTICS

The thermodynamic data presented at the previous meeting has been refined by further computer studies based on more recent air-arc plasma-jet evaluation of the silicone rubber coating that was selected, and the final temperature, heat-flux history during the re-entry period is shown in Figure 4. The vehicle re-enters at an angle of attack of 70 degrees and the data is for the aft tip of the boom which is the hottest point created by re-entry heating due to its reduced diameter.

The materials selected after considerable research are a nickel-chromium metal fabric woven from fine filaments in the form of a textile resembling a lightweight canvas, and two kinds of silicone rubber, one for impregnating or saturating the two plies of metal fabric, and the other for exterior coating as an ablative and heat resisting material. The two plies of metal fabric made up in bias relationship total approximately 27 mils thickness with a maximum silicone rubber coating of an additional 123 mils, making a total maximum thickness in the hottest areas of 150 mils.

Although the exterior char surface of the ablative silicone rubber reaches about 2000° F, the surface of the underlying interface between parent elastomer and char does not exceed approximately 1100° F, as shown by curve T₁ in Figure 4. There is only a small variation between the inside metal fabric surface and the outer surface of the outer metal fabric ply. Curve T₂ shows the average temperature of the metal fabric as predicted by computer analysis. The heat

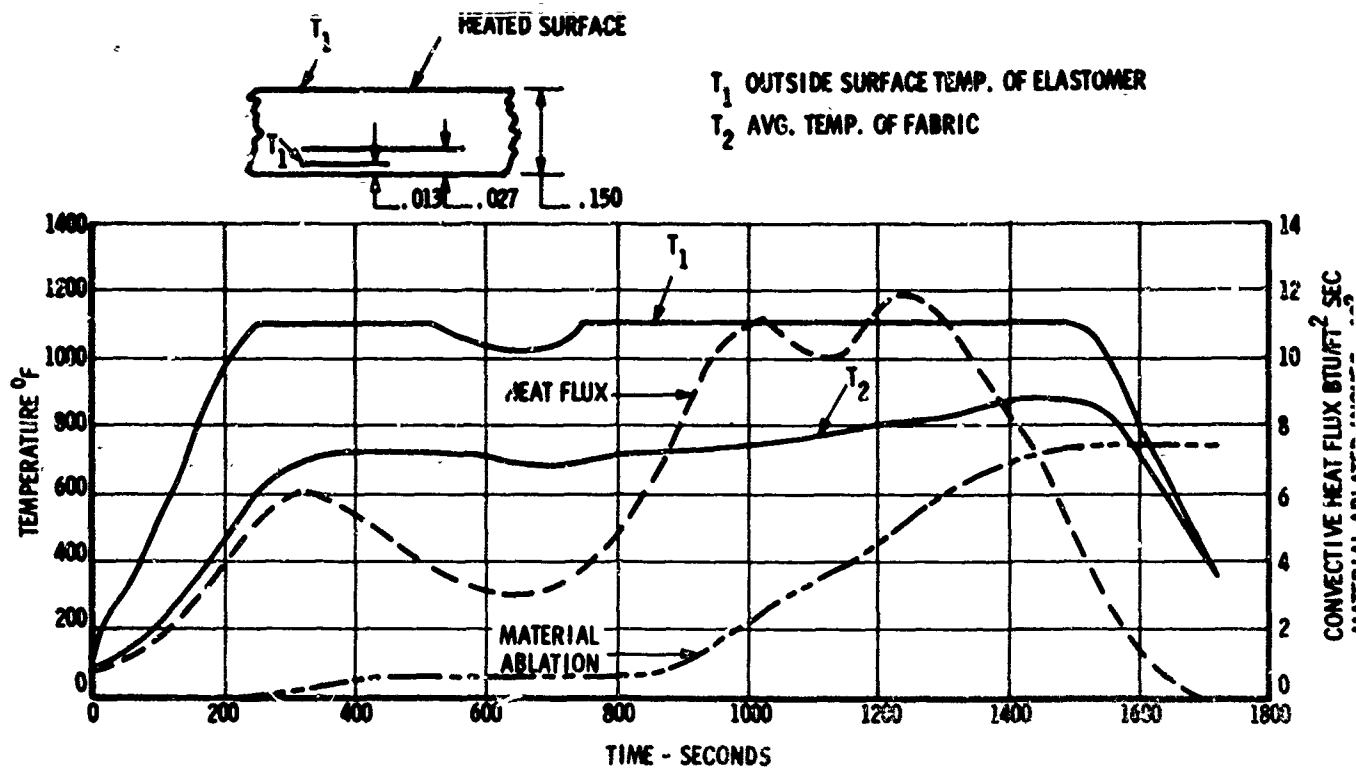


FIGURE 4. PARAGLIDER HEATING EFFECTS AT TIP OF BOOM

flux reaches a maximum of about 12 BTU/ft² sec. Consistent with our desire for the use of flexible materials, the dynamic pressure, deceleration forces, and heat flux are relatively low for a re-entry body because of the utilization of a vehicle configuration and corresponding flight attitude to maximize the lift coefficient. The amount of material ablated is predicted to be 75 mils, leaving a residual coating of about 50 mils of high temperature silicone rubber as a heat barrier contingency to assure that the ablation will not reach the metal fabric reinforcement even in the most critical areas.

The reinforcing fabric was manufactured from metal yarns consisting of 49 one mil filaments, plied and cabled by textile twisting methods. The fabric was woven of 58 yarns per inch in each direction using a 2x2 basket weave. An enlarged photograph of this fabric is shown in Figure 5. Each of the apparent strands consists of two yarns. Due to the low textile twist in these yarns, they tend to flatten, giving the fabric a rather smooth surface and also preventing large transverse openings. The 2x2 basket weave was selected after evaluation of numerous weaves because it allows close grouping of yarns (i.e. high pick and end count) with nominal crimping of yarns while retaining reasonable in-plane sturdiness (i.e. it is not "sleazy"). The one mil wire is actually a potentiometer type resistance wire consisting of 73% nickel and 20% chromium which displays approximately 20% greater tensile strength for a given weight and weave than the more common 80-20 alloy. More flexibility for the desired strength could have been obtained using a smaller diameter wire, but the selection was one of economics, the cost of 0.5 mil wire being about 6 times that of the 1.0 mil wire at the time of procurement. Future work should employ the finest possible diameter of filament consistent with the

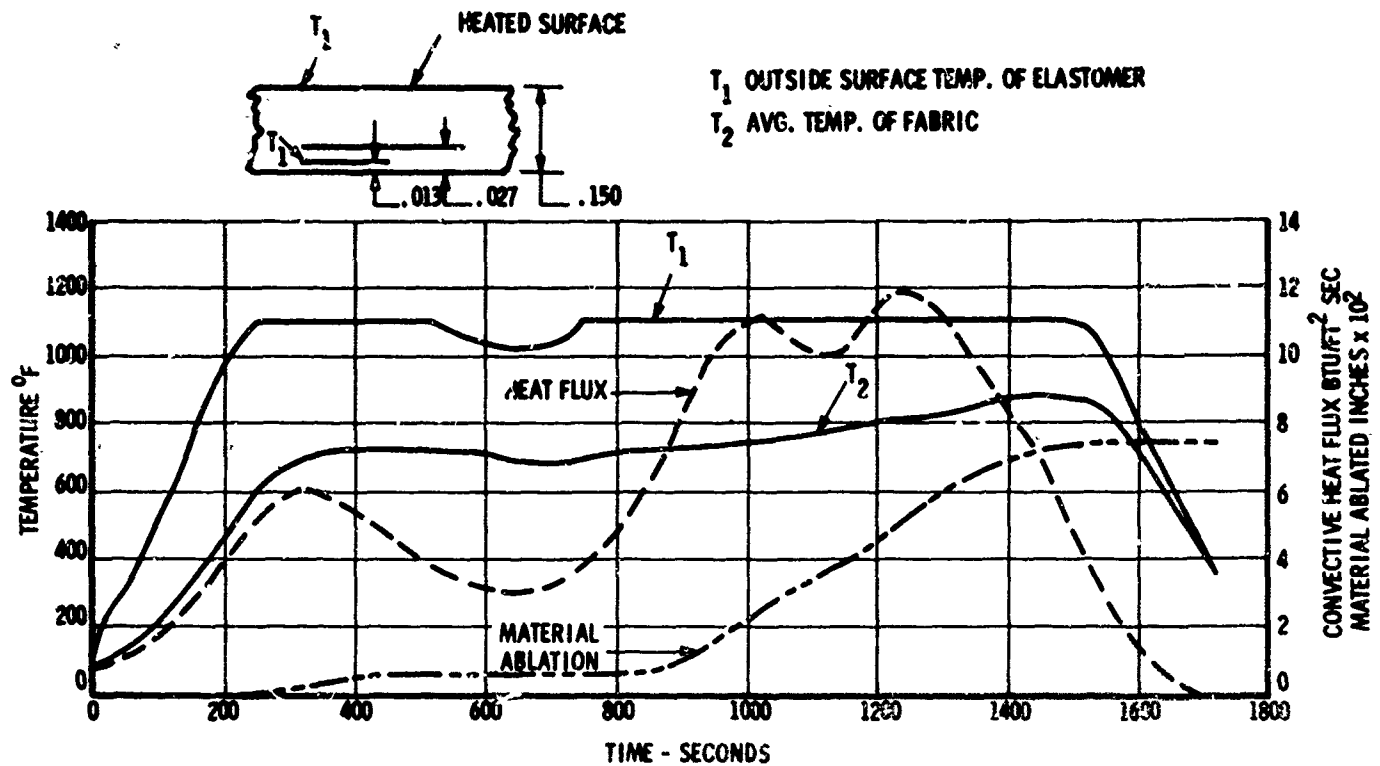


FIGURE 4. PARAGLIDER HEATING EFFECTS AT TIP OF BOOM

flux reaches a maximum of about 12 BTU/ft² sec. Consistent with our desire for the use of flexible materials, the dynamic pressure, deceleration forces, and heat flux are relatively low for a re-entry body because of the utilization of a vehicle configuration and corresponding flight attitude to maximize the lift coefficient. The amount of material ablated is predicted to be 75 mils, leaving a residual coating of about 50 mils of high temperature silicone rubber as a heat barrier contingency to assure that the ablation will not reach the metal fabric reinforcement even in the most critical areas.

The reinforcing fabric was manufactured from metal yarns consisting of 49 one mil filaments, plied and cabled by textile twisting methods. The fabric was woven of 58 yarns per inch in each direction using a 2x2 basket weave. An enlarged photograph of this fabric is shown in Figure 5. Each of the apparent strands consists of two yarns. Due to the low textile twist in these yarns, they tend to flatten, giving the fabric a rather smooth surface and also preventing large transverse openings. The 2x2 basket weave was selected after evaluation of numerous weaves because it allows close grouping of yarns (i.e. high pick and end count) with nominal crimping of yarns while retaining reasonable in-plane sturdiness (i.e. it is not "sleazy"). The one mil wire is actually a potentiometer type resistance wire consisting of 73% nickel and 20% chromium which displays approximately 20% greater tensile strength for a given weight and weave than the more common 80-20 alloy. More flexibility for the desired strength could have been obtained using a smaller diameter wire, but the selection was one of economics, the cost of 0.5 mil wire being about 6 times that of the 1.0 mil wire at the time of procurement. Future work should employ the finest possible diameter of filament consistent with the

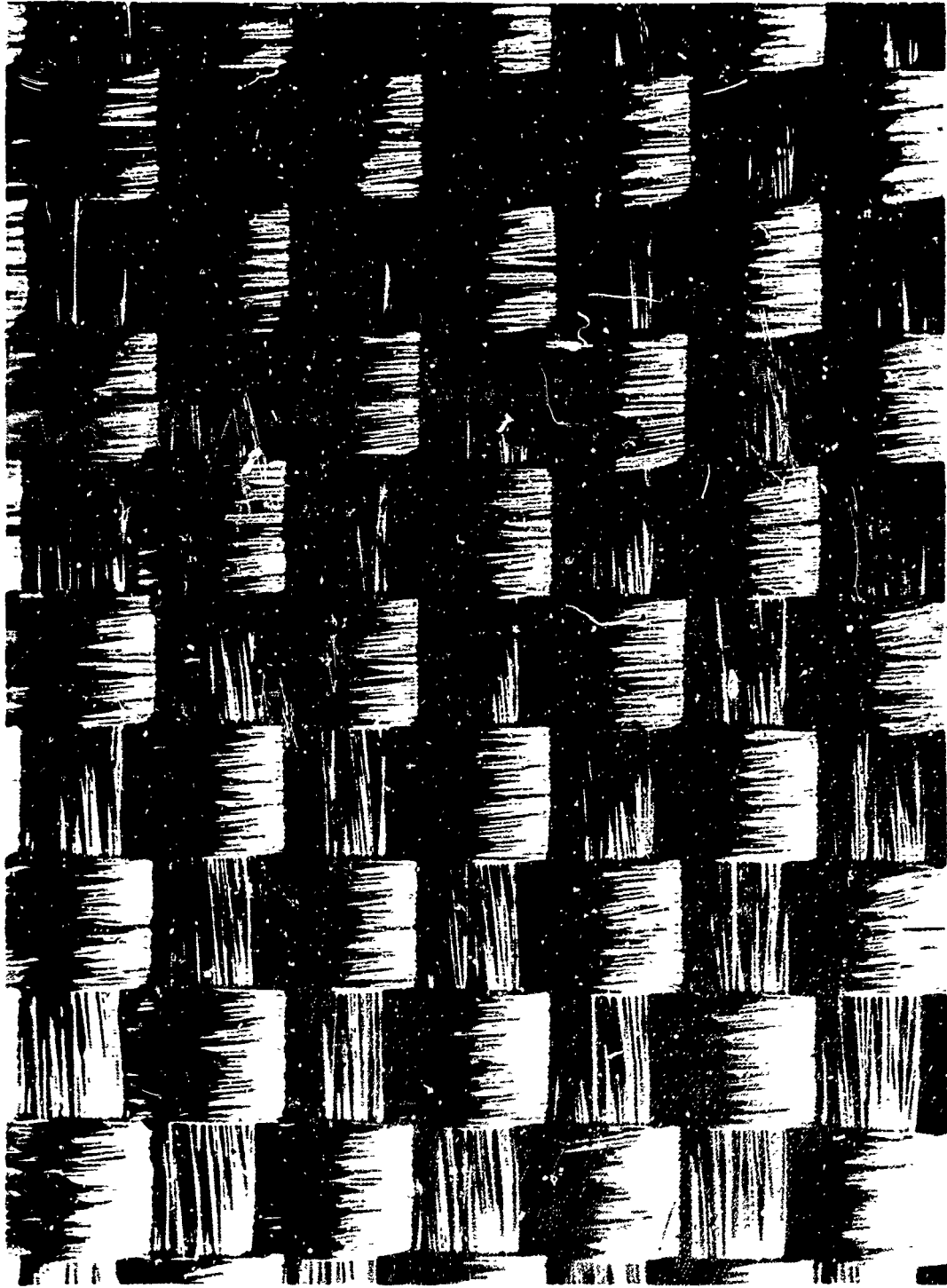


FIGURE 5. TWO BY TWO BASKET WEAVE (58 x 58), 1.0 MIL WIRE

WARP

FILL

budget considerations, type of fabric desired, and the filament strength required for the fabric manufacturing operations.

A pilot run of about 80 square feet of 26 inch wide fabric provided considerable background in the twisting of the yarn, warping and weaving on the loom and scouring or cleaning of the fabric. The final production run of the fabric was over 5 feet wide and nearly 80 yards long, being, perhaps, the largest quantity of such fabric produced as of that time. Over 400 yards of 1.6 inch wide metal fabric tape with 80 ends and 40 picks per inch were also woven using the same yarn. This tape is used in wrapping and strengthening the highly loaded areas of the apex, as will be shown later. One of the innovations resulting from the development work in the pilot run was the spooling of 7 filaments of wire on one spool to facilitate the twisting of a 7x7 or 49 filament balanced yarn. This resulted in a saving of about \$6000 worth of wire which would otherwise have been wasted due to unequal runout of monofilament spools. The manufacture of the wire, the twisting into yarn, and the weaving were subcontracted separately so that each operation could be monitored directly from the Project Office. All work was done on the basis of formal specifications. The average direct cost of the fabric woven to date is \$64 per square foot, not including administration and coordination expense. Most of this cost is due to the wire. Improvements in multiple fine wire drawing as well as in the twisting and weaving operations would bring today's cost of this fabric below the cost experienced last year.

Two plies of this fabric will be bonded together in 45° bias relationship to give maximum in-plane shear strength in torsion and shear loading. The combined matrix will exceed the required maximum design hoop strength of 176 pounds per inch at 1000^oF provided a seam or minimum joint efficiency of 70% relative to parent fabric strength can be obtained in the numerous joints required in the construction.

Typical load elongation curves are shown in Figure 6 for the production run fabric. Approximately 5 weeks were spent in attempting to adjust the loom to obtain equal crimp in fill and warp yarns, however the best that could be obtained was about a 6 to 1 ratio. This is reflected in the two curves shown. It is desirable to obtain equivalent crimp or elongation in both warp and fill in order to have a balanced fabric which will distribute the loads uniformly and predictably. Better balance than this was obtained with some loom settings but at the sacrifice of fabric quality in that warp breakage occurred due to high loading of the warp in an attempt to reduce its crimp. A tabular summary of the physical properties is shown in Table I. The percent crimp was determined by measuring the length of a straightened segment of yarn from a known length of fabric. It will be noted that the yield elongation in warp and fill differ by only 2.8%, however, so that it is unlikely that gross distortion of the vehicle will occur due to this lack of crimp balance. The ultimate strength of the one mil wire was 184,000 psi which converted to a fabric strength of 339 to 375 pounds per inch, a calculated strength translation of 90-97%.

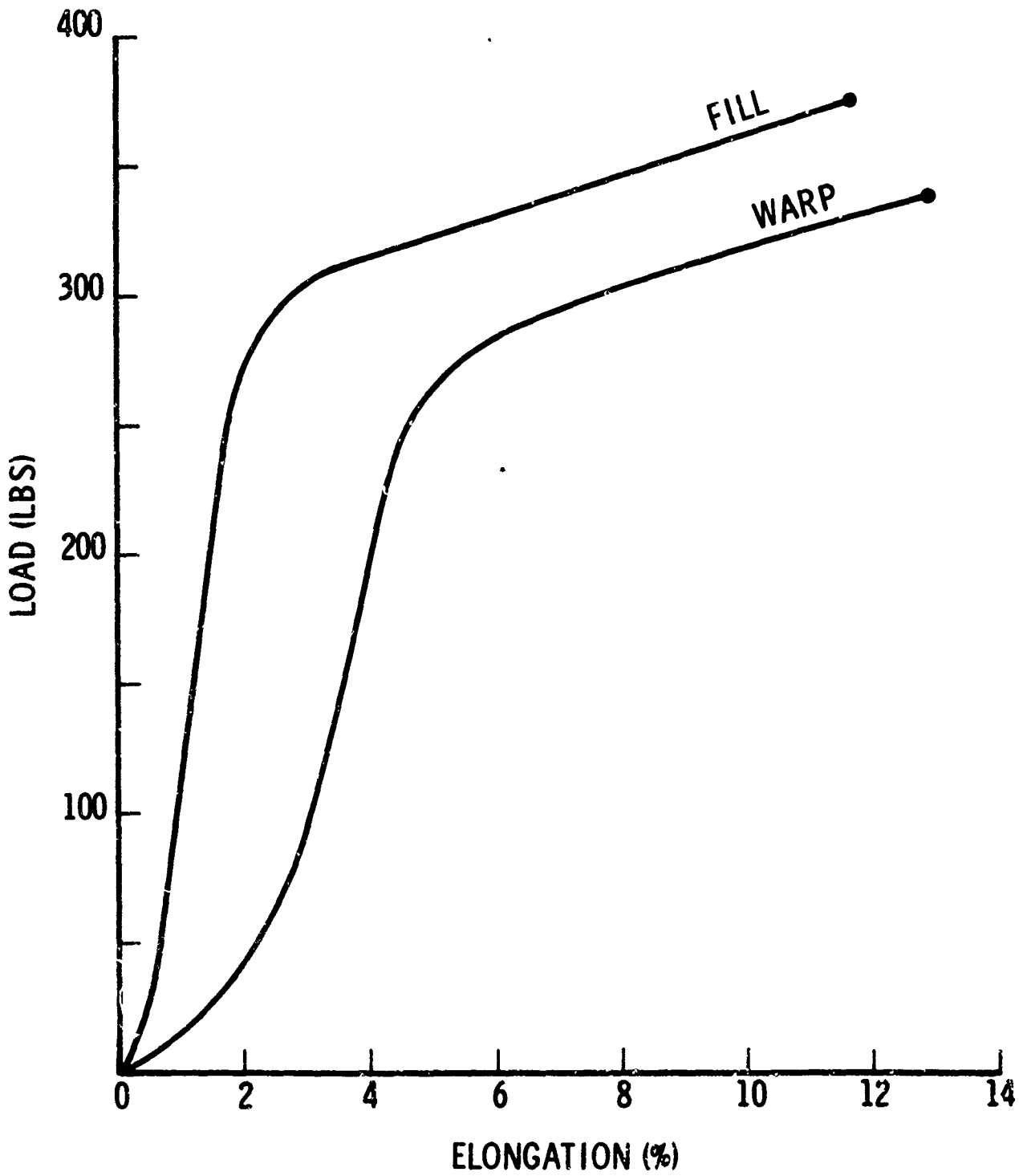


FIGURE 6. TYPICAL FABRIC LOAD VS ELONGATION AT 70°C

TABLE I

RESULTS OF TESTS ON MULTIFILAMENT METAL FABRIC AT 70°F

	<u>Warp</u>	<u>Fill</u>
Yield Elongation, %	4.83	2.05
Yield Load, lbs	278	300
Rupture Elongation, %	12.94	11.67
Rupture Load, lbs	339	375
Modulus of Elasticity, lbs x 10 ⁻²	105	205
Crimp, %	1.84	0.29

The fabric was scoured or cleaned of the wax applied during the twisting and weaving operation by transferring it to a motor driven jig which passed the fabric through a spray of hot non-ionic detergent solution four times, followed by two rinses with hot clear water. The fabric was then dried with forced air and infrared lamps prior to final inspection.

Conclusions and recommendations based on experience in the manufacture of this unusual fabric include the following:

- a. Yarns made from fine diameter wire filaments can be handled on normal textile handling equipment provided the guide surfaces and tensions are carefully prepared and monitored.
- b. Because of the high modulus of elasticity of the wire yarn, standard weaving techniques to achieve certain fabric characteristics with textiles do not have the same effect in the weaving of metal fabrics.
- c. The loom should have a small shed opening and positive let-off with maintenance of constant warp tension by hydraulic dash-pot or similar means. This may also help absorb beat-up shock and vibration and improve crimp balance.
- d. Improved techniques of holding out the selvage rather than the usual selvage temples or "crow-pickers" should be studied to permit high warp tensions without breakage due to angulation of the yarns leaving the reed. High warp tensions would improve crimp balance.
- e. The warp should be rolled on the beam with special caution to maintain uniform tension during weaving.
- f. Jig scouring of wide metal fabrics requires more care and special handling than normal textile fabrics and special jig fixtures with

crowned rolls should be provided to prevent wrinkling and skewing of the fabric during this operation.

Joining techniques for metal fabric have been studied in depth. Much research has been conducted on methods of sewing and stitching, adhesive bonding, integral weaving, arc welding, exothermic brazing and welding, gold and silver alloy brazing using infrared heating sources, as well as electric heating, etc., spot brazing, and spot welding. The latter method was selected as being the most satisfactory due to its inherent flexibility without severely damaging the fabric and without the absolute need of an inert atmosphere. The joining technique which has been developed for the purpose of this project consists of 2 rows of spot welds with spots in each row being approximately 0.025 inches apart and the rows spaced approximately 1/8 inch apart with a 1/2 inch overlap of the fabric layers. As many as five layers of fabric have been successfully joined by this technique. A square pulse, capacitance discharge power supply is used with a deep throated welder producing "through" welds by virtue of small diameter electrodes being alternately reciprocated up and down. A schematic of this welder is shown in Figure 7. The expected induction losses with high rate of rise current discharge have been largely overcome through the use of wide, thin, flat conductors supported by the upper and lower arms of the welder frame. Several arm arrangements are being constructed to permit the welding of all of the intricately located seams, especially those in the toroidal apex. The lower arms can be attached at two possible locations on the main frame.

A close-up schematic of the upper welder head is shown in Figure 8 showing the reciprocating probe electrodes and the silicone rubber tired driving wheel. The timing of the raising and lowering of the probes, intermittent action of the driving wheel (so that the fabric is not moving while a probe is in the down position performing the welding of one spot), and the signal to the power supply to pulse the weld current are synchronized by an adjustable timing device. The speed of welding will be variable from 0 to approximately 25 inches per minute. Welds typical of those shown in the photomicrograph, Figure 9, are produced.

Earlier attempts at welding with two electrode wheels in parallel on one side of the fabric joint with a backup conductive strip were found to be unsatisfactory for the purposes of this project because of the high wheel loading which was required. This would have resulted in heavy backup forms and strong but accurately aligned fixturing to move the welding head or/and part in relationship to one another, while proceeding down a seam of compound curvature.

The procedure planned for the welding machine shown in Figures 7 and 8 is to weld the material "soft" without backup forms using more conventional "through" welding with an electrode on each side of the fabric. This will prevent the serious difficulty previously encountered with the two electrodes on one side wherein a large proportion of the current shunted through the fabric layers without actually contributing to the weld fusion process. Thus, current consumption had to be increased with increase in number of fabric layers, and attendant burning of the fabric between the electrodes was encountered with the former method.

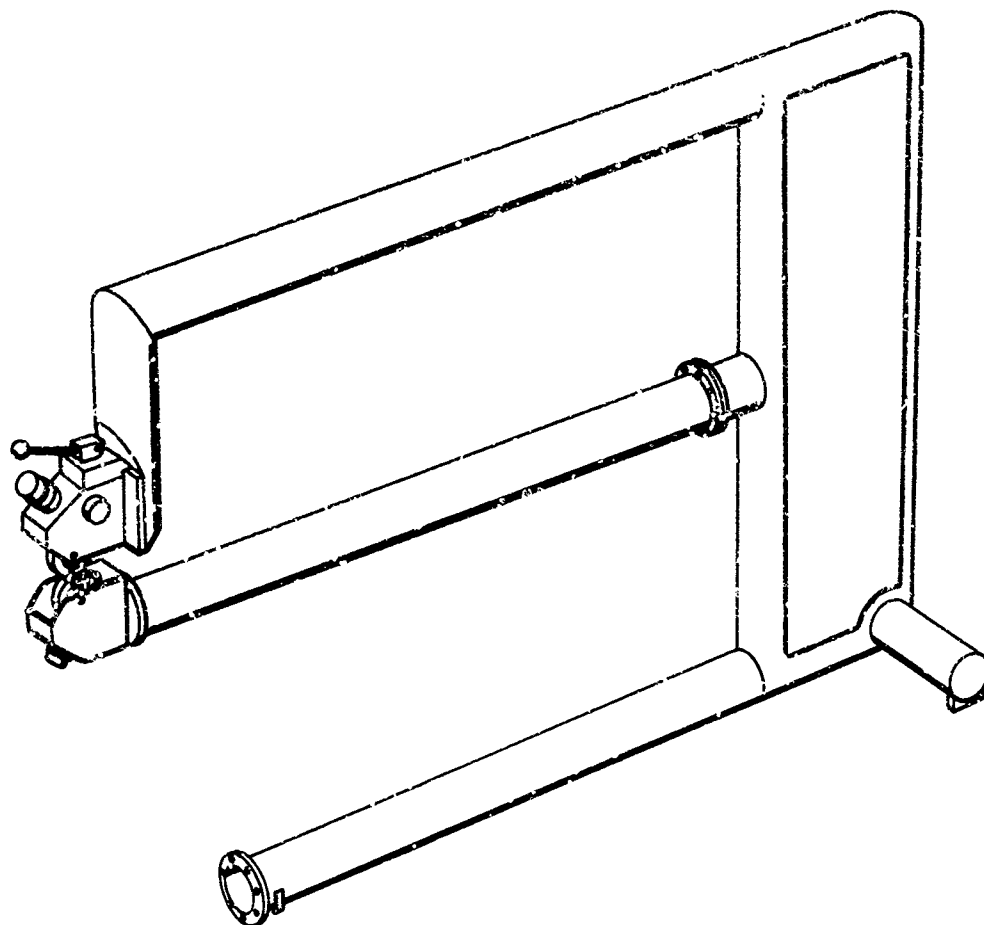


FIGURE 7. FABRIC WELDER

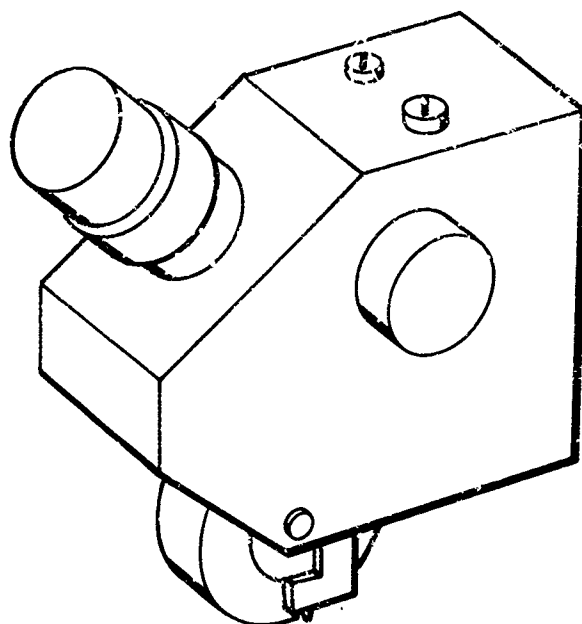


FIGURE 8. WELDER HEAD



FIGURE 9. PHOTOMICROGRAPH OF SPOT WELDED JOINT

The objectives of this program include not only the development of the manufacturing techniques but the testing of a number of components of the paraglider using simulated re-entry loads and temperatures to prove out the design technology as well as the fabrication methods. Originally in the program, sub-scale components were to be built and tested, but scaling and similarity studies indicated that extrapolation of the results from sub-scale components to predict the performance of full scale components would require many assumptions difficult to firmly justify and result in unreliable design parameters for a full scale vehicle. This is true, in part, due to the fact that although the overall size of a component can be scaled, the fabric can not be scaled proportionately, and where high temperature testing is to be performed on a surface by heating in an intentional non-uniform manner, scale-up of test results becomes impossible.

The program has therefore been modified from that reported at the last Expandable Structures Meeting. Fifteen small 7 to 10 inch diameter, open ended frustums will be fabricated including impregnation and coating, and tested with end closures in place at internal pressures producing the proper reinforcing fabric loading while torsion, shear, and bending loads are applied both at room temperature and temperatures simulating those of the re-entry regime. Subsequently, a full scale boom tapering from 32 inches to 13 inches and 17 feet long will be built and tested throughout the full realm of loading and temperature environments that it would encounter in actual flight. After this experience has been gained, a full scale apex which will be nearly 12 feet wide and 7 feet long with a 32 inch diameter cross section will be similarly tested. These tests will be carried out in a relatively inert atmosphere simulating the low oxygen content of the re-entry altitude. Quartz infrared

heating lamps with gold plated, parabolic reflectors have been procured for the purpose of heating these components from one side to simulate the re-entry heating effect during the appropriate tests.

The complexity of construction of the apex is illustrated in Figure 10, which schematically indicates the layup of two plies of fabric with the individual pattern pieces cut small enough so that gross compound curvature can be avoided in any given piece. Finally the structure is "mummy" wrapped with two layers, at the outer periphery, of tape to carry the circumferential loads through the small crotch area. The load concentration in this area is obvious due to the interruption of the basic toroidal surface by the intersection of the keel boom. It has been elected not to use internal supporting drop yarns or fabrics in this area due to design, structural, and fabrication complexities which it is believed would be introduced.

Having reviewed the nature of the components to be built and the reinforcing fabric to be used, the fabrication process will be summarized so that a better understanding of the stepwise fabrication procedures including the impregnation and coating can be portrayed.

The flat metal fabric is cut both in longitudinal patterns as well as bias patterns for the outer and inner plies respectively. The bias patterns are first laid up on a hard surface forming tool identical in shape to the desired part (e.g. frustum, boom or apex). The individual pieces of fabric are basted together using a stitching technique with the same metal yarn from which the fabric was manufactured. The stitching will be done by hand using a curved needle and will be the most time consuming step in the fabrication process. Tests of welded specimens with and without this metal yarn basting show no degradation due to the basting. The stitches are fairly long and can be put through slowly with a sharp needle causing negligible damage to the fabric. It should be noted that machine sewing of seams as a final method of joining the fabric (without welding) has been shown in previous Air Force contract efforts to be comparatively unsatisfactory, yielding seams in most cases not greater than 60% efficiency.

After basting of the first ply, the form is removed. In the case of the apex, the form will be separable by unclamping flanges from within and removing individual segments of the form. The basted part is then taken to the welding machine, properly supported by tubing racks or other devices to prevent wrinkling, and the seams are welded. The other outer ply is similarly fabricated. In the case of the apex the form is reinserted and the tapes basted in place followed by subsequent removal of the form and welding of these members in place. When all parts have been welded, the inner ply is placed inside of the outer ply and the forming tool again inserted. The forming tool is constructed such that it is vacuum tight. A plastic bleeder screen is placed over the fabric surface and the entire assembly is vacuum bagged. A minimum vacuum of 28 inches of mercury has been found to be satisfactory for impregnation (although impregnation cannot be performed at atmospheric pressure) and degassed high temperature, phenyl base, liquid silicone rubber is introduced into the evacuated vacuum bagged assembly.

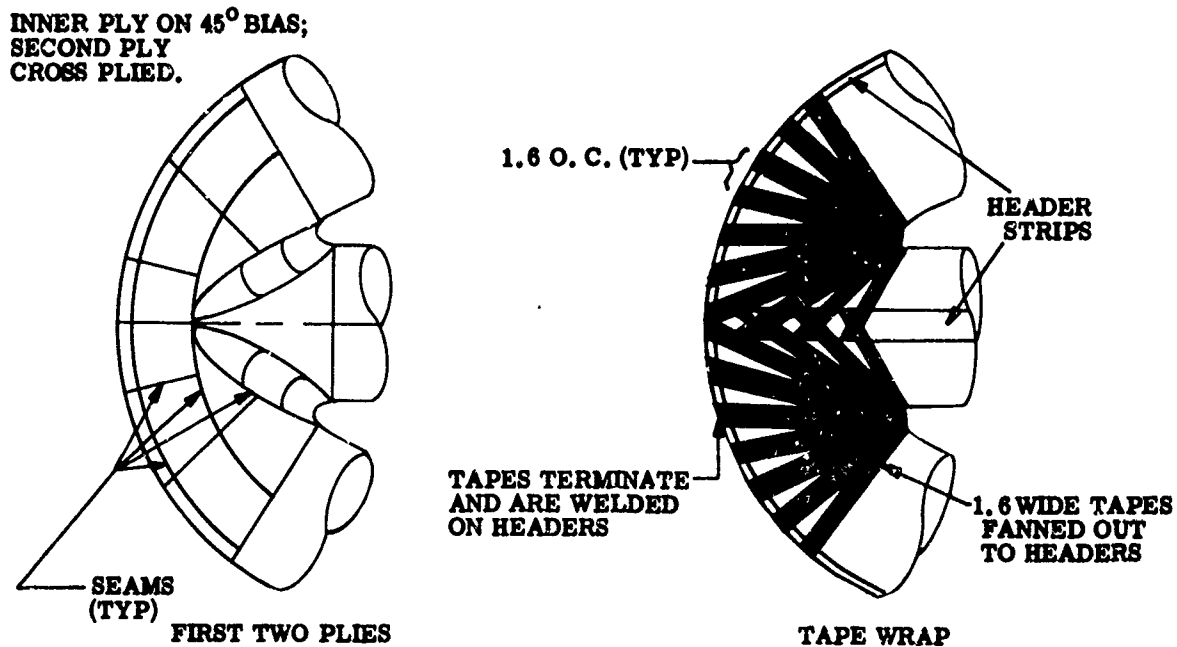


FIGURE 10. APEX CONSTRUCTION

After partial curing at room temperature, the vacuum bag and bleeder screen can be removed and the excess silicone rubber wiped off the surface of the metal fabric. The impregnated fabric is allowed to completely cure. An adhesive layer of the liquid RTV rubber is applied and the high temperature silicone rubber is overlaid using a calendered thickness of 0.025 inches. The adhesive is allowed to room temperature cure and subsequent layers of the high temperature silicone rubber are applied to build the contour to the maximum matrix thickness of 0.150 inches along the stagnation line at the bottom of the apex and boom tapering to a minimum of 0.025 inches at the top of these components where no ablation occurs. These calendered sheets are stitched in place so as to remove all entrapped air and the entire assembly vacuumed bagged to permit autoclave curing of the high temperature, ablative, silicone rubber coating. The forms and vacuum bags can be removed before the high temperature post-cure with the components supported on pipe racks or similar structures if necessary. The components are now complete and ready for environmental testing.

Considerable development effort has been applied to the technique of properly cleaning the cloth, and application of the impregnation primer in addition to the impregnation, coating and vacuum bagging techniques. These processes have been recently qualified to the point of issuance of final specifications. With the final qualification of the welding system the entire fabrication process will be released for manufacture of the major test components.

It is hoped that the techniques described will contribute measurably to the field of expandable structures particularly where metal fabrics may be employed.

BENDING OF UNFURLABLE TUBULAR STRUCTURES IN SPACE

by

Dr. George G. Herzl
Senior Engineering Specialist
Philco Corporation
WDL Division
Palo Alto, California

1. INTRODUCTION

Recent developments in spacecraft technology have led to the requirement for lightweight, long tubular booms that can be launched in compact containers and unfurled in space. Typical applications are booms for gravity-gradient stabilization (1), for separation of delicate instruments from the main spacecraft, and booms for erection of very long antennas (2). The construction of these booms is such that the unsupported structure would collapse from its own weight in ground environments; consequently, the associated design problems are quite different from those encountered in conventional structural design.

The proper functioning of spacecraft utilizing such booms depends on the straightness of the unfurled boom in space. The major causes of boom bending are listed in Table 1. The items are divided into two groups, depending on whether bending is localized in a small portion of the boom, or whether bending is gradually distributed along the entire length of the boom. Items listed under "Localized Bending" may cause total failure of the boom, but they are preventable in all cases; items listed under "Gradual Bending" cannot be totally eliminated, but proper design can keep them within acceptable tolerances. The following discussion will explore in detail the various causes of boom bending.

2. LOCALIZED BOOM BENDING

2.1 Inertial and Coriolis Forces During Boom Deployment

Some residual rotation of the spacecraft is inevitably present when boom deployment is initiated. The radial deployment of the boom in this rotating frame of reference causes boom bending and shear due to: (a) inertial forces, and (b) Coriolis forces. The inertial forces result from the de-spin of the spacecraft caused by the increase in moment of inertia. Boom loading is in the direction of the initial rotation. Coriolis forces are those which, for example, are experienced by a person walking on a rotating turntable. In this instance, boom loading is in a direction opposite to loading caused by inertial forces. The combined effect of the inertial and Coriolis accelerations may

TABLE 1
MAJOR CAUSES OF BOOM BENDING

Localized Bending						
Type of Bending	Cause	Predictability	Remedy	Preventable	Relative Importance*	Reference Section
Elastic deformation during deployment	Inertial and Coriolis Forces during deployment.	Yes	Limiting deployment velocity and initial angular rate.	Yes	1	2.1
Elastic deformation during deployment	Rebound at the end of deployment.	Yes	Regulate deployment velocity. Provide energy dissipation mechanism.	Yes	1	2.2
Due to space environment	Localized cold welding of boom sections due to defects of material or coating.	Yes	Quality control in production. Limit amount of testing.	Yes	1	2.3
Gradual Bending						
Permanent deformation during deployment	Non-homogeneous material properties.	Yes	Quality control and sample testing.	No	2	3.1
Permanent deformation during deployment	Tolerances (dimensional, heat treatment, etc.)	Yes	Quality control and sample testing.	No	2	3.1
Permanent deformation during deployment	Induced by deployment mechanism.	Yes	Quality control and sample testing.	No	2	3.1

*Relative worst-case system performance, if cause is not eliminated: 1. Total failure
2. Marginal
3. Acceptable

TABLE 1 (Continued)

Type of Bending	Cause	Predictability	Remedy	Preventable	Relative Importance*	Reference Section
Gradual Bending (Continued)						
Orbit dependent deformation	Uneven heating due to solar radiation.	Yes	Optimize thermal properties of boom. Minimize projected area.	No	3	3.2.1
Orbit dependent deformation	Heating due to earth albedo	Yes	Optimize thermal properties of boom. Minimize project area.	No	3	3.2.1
Orbit dependent deformation	Thermally-induced impulse	Yes	Optimize thermal properties of boom. Minimize projected area. Twilight orbit.	No	2	3.2.2
Orbit dependent deformation	Gravity gradient	Yes	Minimize weight and length	No	3	3.2.3
Orbit dependent deformation	Variation of gravity gradient due to orbit eccentricity (inhomogeneous earth).	Yes	Optimize orbit	No	3	3.2.3
Orbit dependent deformation	Solar pressure	Yes	Minimize projected area	No	3	3.2.4

*Relative worst-case system performance, if cause is not eliminated: 1. Total failure
 2. Marginal
 3. Acceptable

TABLE 1 (Continued)

Type of Bending	Cause	Predictability	Remedy	Preventable	Relative Importance*	Reference Section
Gradual Bending (Continued)						
Orbit dependent deformation	Micrometeorites	No	None. Damage probability small.	No	3	3.2.5
Orbit dependent deformation	Electromagnetic effects.	Yes	Equatorial orbit. Use nonmagnetic material.	Yes	3	3.2.6
Orbit dependent deformation	Active control	Yes	Minimize components producing buckling.	No	3	3.2.7
Orbit dependent deformation	Atmospheric drag.	Yes	Select higher orbit.	No	3	3.2.8
Environmentally induced.	Material degradation due to sublimation.	Yes	Proper selection of materials and coating.	No	3	3.3
Environmentally induced.	Radiation erosion.	No	None	No	3	3.3
Environmentally induced.	Solid particles erosion	No	None	No	3	3.3

*Relative worst-case system performance, if cause is not eliminated: 1. Total failure
2. Marginal
3. Acceptable

cause total failure (e.g., buckling) of the boom if the load exceeds the permissible bending moment or shear. During the retraction of the boom, both inertial and Coriolis forces act in the opposite directions.

Figure 1 shows the results of a study (3) of this problem. Figure 1-a shows the configuration of a two-body system separated by a boom that adequately describes the entire spectrum of systems from a dumbbell having equal end-masses to an antenna having no end-masses in a fully deployed configuration. Figures 1-b and 1-c show the relations of parameters for a range that includes most systems of practical importance. Maximum loading occurs shortly after deployment is initiated, and total loading is kept within a safe range by limiting the deployment velocity and initial angular rate.

2.2 Rebound at the End of Deployment

The fully extended boom is a long, slender column that cannot support any appreciable amount of compression loading; therefore, the deployment mechanism must include some provision to minimize rebound. This is accomplished by using a regulator to program the extension velocity so that it is very small at the end of extension. Defective performance of the regulator may lead to total failure (buckling) of the boom.

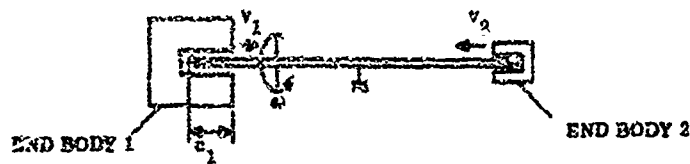
3. GRADUAL BOOM DEFORMATION

3.1 Deformation During Deployment

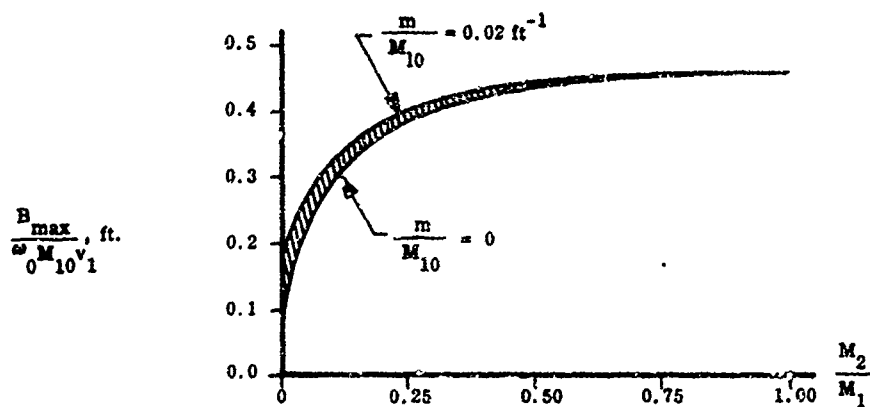
Permanent deformation that occurs during the extension of the boom is, at the present state-of-the-art, the most important limiting factor in boom performance. Deformation is due to: (a) manufacturing tolerances and (b) deployment mechanism. Manufacturing tolerances include non-homogeneous material properties, dimensional tolerances, uneven heat treatment, finishing, etc. Careful selection of materials and production control help minimize boom deformation. Permanent bending induced by the deployment mechanism can be minimized by increasing the length and smoothness of deployment-guiding elements. The total deformation effect from both sources can be reduced by compensatory bending of the boom in a direction opposite to that observed during ground-testing in a simulated 0-g environment. The ultimate direction of bending (or spiraling) of the boom in space is unpredictable and, therefore, cannot be corrected by a system compensation.

3.2 Orbit-Dependent Deformation

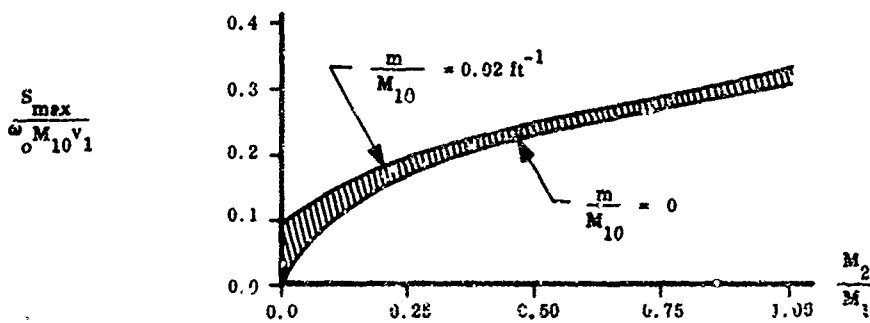
Boom bending due to orbit-dependent causes is generally small for short booms, but becomes significant for very long booms. For example, tip deflection for a 1000-foot-long boom (4) due to the combined effect of uneven heating, solar pressure, and gravity gradient effect is 400 feet. In contrast, the tip deflection of a similar 100-foot boom is less than 2 feet. However, as system performance requirements are becoming more stringent, considerable effort is being undertaken to reduce the tip deflection -- even for shorter



a. TWO BODY SYSTEM SEPARATED BY BOOM



b. BENDING MOMENT



c. SHEAR

NOMENCLATURE:

- B bending moment
- I moment of inertia
- M initial mass of end body
- S shear
- c length of boom in end body
- m mass of boom per unit length
- v velocity of ejection from end body
- ω angular velocity

SUBSCRIPTS:

- 0 initial
- 1 refers to end body 1
- 2 refers to end body 2

RANGE OF PARAMETERS:

- $1.0 \leq M_{10} \leq 100$ slug
- $0 \leq m \leq 0.020$ slug/ft
- $1.0 \leq v_1 \leq 10.0$ ft/sec
- $v_2 = 0$
- $c_1 = c_2 = 1.5$ ft

$$\frac{I_{10}}{M_{10}} = \frac{I_{20}}{M_{20}} = 1 \text{ ft}^2$$

Figure 1 Maximum Bending Moment and Shear for Representative Range of Parameters of Two Body System Separated by Boom

booms. In the following sections, we will discuss the various orbit-dependent causes in more detail.

3.2.1 Uneven Heating Due to Solar Radiation and Earth Albedo

When the boom is exposed to solar radiation, the side facing the sun heats up more than the far side, causing it to bend away from the sun. Steady-state temperature distribution and bending takes place when the heat received is equal to the amount re-radiated into space. The distribution is determined by the thermal properties of the internal and external surfaces of the boom, the conductivity of the material, and the geometry of the configuration.

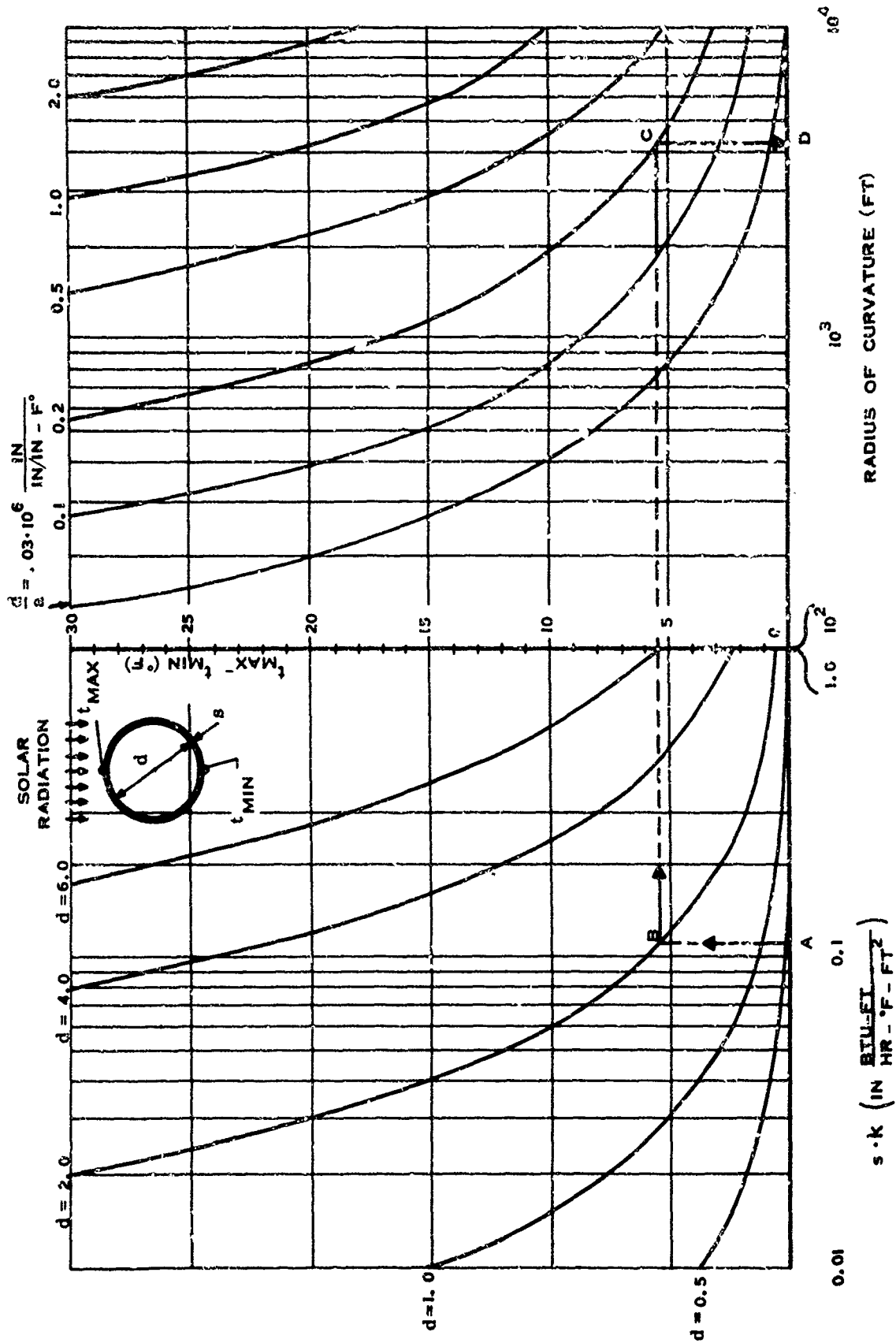
Figure 2 shows the results of a study made on pointing-error problems for passively stabilized spacecraft (5). The radius of curvature is calculated by following the path A, B, C, D of the sample calculation of a 2-inch diameter, beryllium copper boom 0.002-inch thick, having a highly-polished, silver-coated external surface covered by a coating to regulate emissivity. The resulting maximum temperature differential is 5.5°F, and the corresponding radius of curvature is 4,200 feet. If the boom were made of stainless steel, the corresponding figures would be 27°F and 600 feet. For angles of incidence other than 90 degrees, the difference between the temperature at any point on the periphery of the boom and the average temperature diminishes proportionately with the 1/4-power of the cosine of the angle of incidence of the solar radiation. An increase in the angle of incidence also reduces the average temperature, but this in itself does not influence boom bending since it does not induce differential elongation. Bending radius is independent of the modulus of elasticity and thickness of the material of the boom; curvature can be minimized by making the boom diameter small and by selecting boom materials having a small coefficient of expansion and good thermal conductivity.

Earth albedo radiation has the same effect as solar radiation, except to a much lesser degree. This effect can be neglected for practical calculations for all except for very low orbits.

3.2.2 Thermally-Induced Impulse

An abrupt change in the temperature distribution at the periphery of the boom occurs each time the satellite moves from the earth's shadow into sunlight, causing a rapid heating of the boom. The effect of the sudden extension of parts of the boom is equivalent to an impulse excitation, resulting in free oscillation of the boom-satellite system. (These oscillations were detected from telemetry data received from the satellite 1963 22A (1)). If the system has no special provisions for damping out these oscillations, this motion is damped only by internal losses of the material. If the boom is made of beryllium copper having a low hysteresis coefficient, the oscillations will last several hours.

Thermally-induced impulses can be eliminated by selecting an orbit that is entirely in sunlight. If this is not possible, the amplitude of the oscillations can be reduced by suitably plating and coating the boom surface to minimize the absorption of solar energy and provide increased hysteresis damping.



NOMENCLATURE:
 a absorptivity k conductivity
 e emissivity s boom thickness a = 0.05; e = 0.15
 d boom diameter t temperature

Figure 2 Radius of Curvature of Booms Exposed To Perpendicular Solar Radiation

3.2.3 Gravity-Gradient Effect

The "gravity-gradient effect" is a misnomer for the combined effects of the gravitational and centrifugal gradients on spacecraft. It was demonstrated (1) that this effect can be utilized for passively stabilizing satellites to point at all times toward the center of the earth, just as the moon always presents its same side towards the earth. The effects also produce boom bending that is particularly pronounced for very long booms.

Each particle of the orbiting satellite is attracted towards the center of the earth by a force that is inversely proportional to the square of the distance and proportional to the radius of the instantaneous orbital path. Figure 3-a shows, schematically, the relationship of the forces with altitude for various boom elements. In the following discussion it is assumed that: (a) the entire spacecraft is in the orbital plane, (b) the spacecraft is symmetrical, (c) earth is a homogeneous sphere, (d) the orbit is circular, and (e) centrifugal forces due to spacecraft rotation about its own center of gravity are negligible. The dashed lines in Figure 3-b show boom bending due to the gravity-gradient effect. The elementary force acting on an elementary particle (Δm) is $\Delta F = 3\omega^2 \times (\Delta m) \cos \theta$. By taking the components of the forces perpendicular to the boom and multiplying by the corresponding distances from the center of gravity of the system and integrating, we obtain the bending moment:

$$M = 0.5 A \omega^2 l^3 \sin 2\theta$$

where:

- A = boom cross-sectional area, feet square
- M = bending moment, foot-pounds
- l = boom length, feet
- ω = orbital rate, radians per second
- θ = included half-angle, radians
- ρ = boom density, slugs

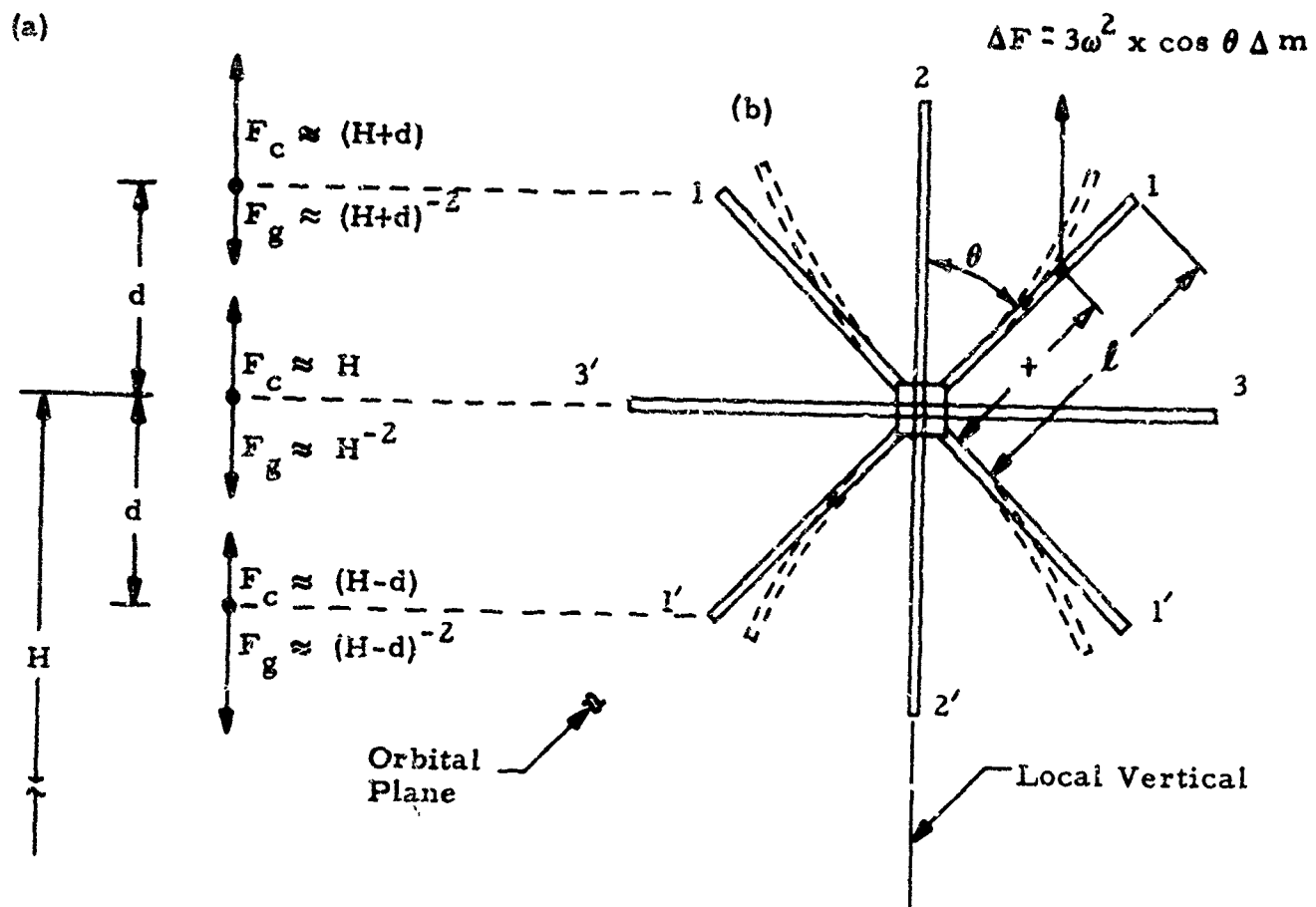
This equation indicates that the bending moment is maximum for $\theta = 45$ degrees (booms 1 and 1') and is equal to zero for $\theta = 0$ (booms 2 and 2') and $\theta = 90$ degrees (booms 3 and 3'). This gravity gradient effect is an important design consideration for systems that contain long booms since bending is proportional to the cube of boom length.

Maximum tensile stress is obtained by considering the sum of the axial components of the forces per unit area:

$$\sigma_{\max} = 3\omega^2 \rho l \cos^2 \theta$$

Stress is linearly proportional to the length and density of the boom material and the square of orbital rate. It is maximum for $\theta = 0$ (booms 2 and 2') and equal to zero for $\theta = 90$ degrees (boom 3 and 3').

Variations of the gravity-gradient forces due to orbit eccentricity and the non-homogeneous earth induce additional bending moments which become significant only for very eccentric orbits.



- a) Relation of gravitational and centrifugal forces per unit mass with altitude for various boom elements.
- b) General configuration of symmetrical satellite with three long booms.

Figure 3 Boom Bending Due to Gradient of Gravitational and Centrifugal Forces

3.2.4 Solar Pressure

Solar pressure on the boom is produced by the momentum of the photon stream from solar radiation. Its magnitude depends on the angle of incidence and the reflectivity of the surface. For perpendicular incidence in earth orbit, it is equal to $N \times 4.53 \times 10^{-5}$ dynes per square centimeter, where $1 \leq N \leq 2$; the low limit applies to an ideal absorber and the high limit to an ideal reflector of photons. The sun also emits other particles, such as protons and electrons; however, the produced pressures are insignificant in comparison because they have low linear momenta.

The maximum bending moment and the corresponding tip deflection, for any set of booms, such as shown in Figure 3-b, exposed to perpendicular solar radiation, is given by:

$$M_{\max} = 0.5 S d l^2$$

$$f = S d l^4 / 8 E I$$

where:

M_{\max} = maximum bending moment, in-lbs

f = tip deflection, in.

$S = N \times 6.56 \times 10^{-10}$, lbs per in²

d = boom diameter, in.

l = boom length, in.

E = modulus of elasticity, lbs per in²

I = inertia, in⁴

These equations were developed on the basis of small-angle approximation and are sufficiently accurate only for short booms having a uniform cross-section. For large deflections, we must consider additional terms in the equations and take into account the variation of angle of incidence. The calculations are best performed numerically, since there is no closed-form solution.

3.2.5 Micrometeorites

Depending on the properties of the impinging micrometeorites (composition, shape, linear momentum, angle of incidence, etc.), and the properties of the boom (material, thickness, etc.), these particles will have one of the following effects:

- a. Coalesce with the boom and deliver the entire momentum.
- b. Splash some material backwards (cratering effect) delivering more than the corresponding momentum discussed in case a.
- c. Penetrate through the boom and deliver only part of its momentum to the boom.

The effect of the impact is in all cases similar to the thermally induced impact discussed in Section 2.2.2, except that the force acts only upon a very small area instead of being distributed over the entire length of the boom. A grazing impact may cause torsional loading of the boom. The probability of a direct hit of the extremity of the boom (where the moment arm is large) is small as confirmed by the impact data from the Explorer-16 satellite.

3.2.6 Electromagnetic Effects

Hysteresis currents are generated in a boom made of conductive material when it moves in the earth's magnetic field. The energy for generating the currents is derived from the kinetic energy of the system; consequently, the vehicle is decelerated. The associated inertial forces depend on the magnetic field which is cyclic in position and time and is influenced by sources other than the earth (e.g., sun spots). The resulting bending moment is minimized by selecting an equatorial orbit that is nearly a path of constant field strength or by using nonconductive materials.

If the material of the boom is magnetic, it tends to align itself with the earth's magnetic field. The generated torques also produce inertial forces and bending moments.

3.2.7 Active Control

Following are the two principal categories of active spacecraft actuation methods:

- a. Propulsion, such as gas jets, vapor pressure, ion engines, activation of coils for alignment with magnetic field, etc.
- b. Internal moving parts, such as reaction wheels, rate gyros, etc.

Boom-bending moments are induced by the inertial forces resulting from the methods used for active control. They depend on many parameters and no general relations can be developed, but they can be held within safe limits by good dynamic systems design.

3.2.8 Atmospheric Drag

Atmospheric drag is the largest source of boom bending at orbital heights below 400 miles. A dynamic pressure of about 6×10^5 dyne per cm^2 (D - 8.7 lbs per in^2) is typical. The equations for maximum bending moment and tip deflection given in Section 2.2.4 are applicable by substituting the value D for S. The same restrictions on validity of the equations are applicable.

3.3 Environmentally Induced Bending

Of the principal characteristics of space environment, radiation, hard vacuum, meteorites of various sizes, and temperature extremes cause material

and surface degradation and, indirectly, boom bending. Zero gravity, on the other hand, enables us to erect long, lightweight booms that would collapse under their own weight on the earth.

Hard vacuum in space (10^{-10} torr at an altitude of 500 miles, 10^{-12} torr at 1,000 miles) greatly accelerates sublimation of boom surfaces, i.e., boom material particles leave the surface. The impact of small, solid particles and radiation from various sources (solar flares, radiation due to protons and electrons trapped in Van Allen belt, cosmic and auroral radiation) also cause boom surface degradation. Consequently thermal absorptivity and emissivity change, resulting in increased boom bending due to uneven heating of the boom periphery, thermally-induced impact, and solar pressure, as discussed in Sections 3.2.1, 3.2.2, and 3.2.4.

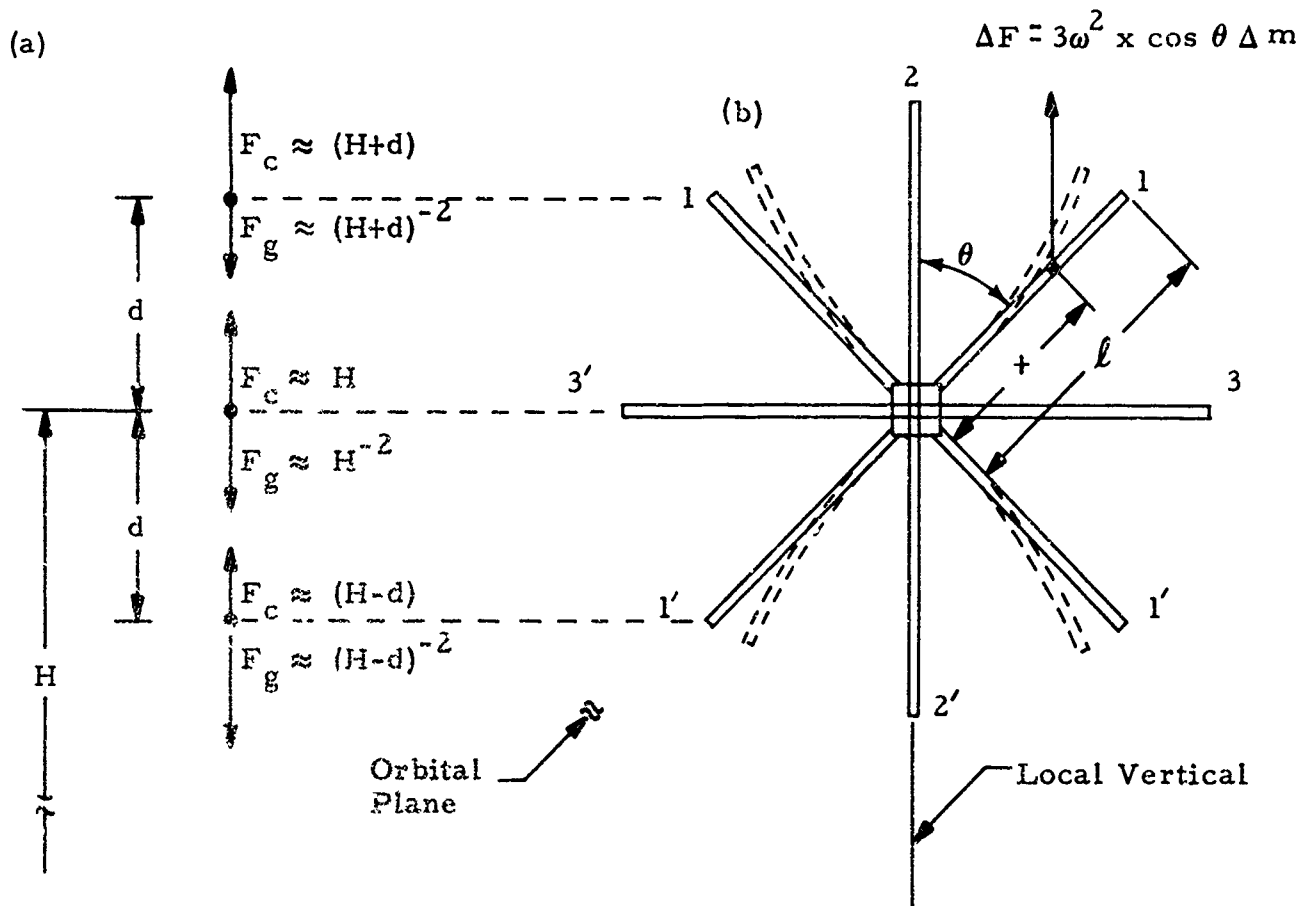
4. CONCLUSIONS

Boom bending can be either localized or gradually distributed over the entire length of the boom. Localized bending occurs during boom deployment and is due to inertial and Coriolis forces, rebound at the end of deployment, and localized cold welding. The deformation may in the worst case lead to total failure of the boom, but is in all cases predictable and preventable. Three classes of gradual boom bending are discussed: (a) initial distortion, (b) orbit dependent distortion, and (c) slowly induced distortion due to space exposure. Gradual bending cannot be entirely eliminated, and the object of the design is to keep it within tolerable limits. Results of calculations and diagrams are presented for various cases of practical importance.

A great deal of experimental and theoretical work is presently being conducted on the subject discussed in this paper. Means for minimizing some problems are contrary to the means for minimizing others, but fortunately, not all problems are encountered on all missions. Therefore, the task of the design engineer is to determine the dominant factor and to optimize the system accordingly. The never-ending desire to further improve system performance will impose more stringent requirements and will stimulate much more work in this field in the near future.

REFERENCES

1. Fischell, R.E. and Mobley, F.F.: "A System for Passive Gravity-Gradient Stabilization of Earth Satellites," Paper No. 63-326, AIAA Guidance and Control Conference, August 1963.
2. Samuelc, R.L.: "The Extension, Profile and Stability of Very Long Booms in Spacecraft Experimentation."
3. Herzl, G.G. and Walton, R.R.: "Boom Deployment Problems for Passively-Stabilized Spacecraft," Philco Corporation Technical Note MW-009.
4. Stone, R.G.: "RAE-1,500-Ft. Antenna Satellite," *Astronautics and Aeronautics*, March 1965.
5. Herzl, G.G.: "Pointing Error in Passively-Stabilized Spacecraft Caused by Thermal Bending," *Journal of Spacecraft and Rockets*, AIAA, July/August 1965.
6. Personal Communication by William C. Triplett.



- a) Relation of gravitational and centrifugal forces per unit mass with altitude for various boom elements.
- b) General configuration of symmetrical satellite with three long booms.

Figure 3 Boom Bending Due to Gradient of Gravitational and Centrifugal Forces

DEVELOPMENT AND EVALUATION OF A
RIGIDIZED INFLATABLE MICROWAVE REFLECTOR

K.F. Gibson

Computing Devices of Canada Ltd.

G.M. Peace

Bendix Corporation Research Laboratories

INTRODUCTION

The Aerophysics Division of Computing Devices of Canada has recently completed the development of a rigidized inflatable microwave reflector for possible application in space. The reflector is prepackaged in a small container and automatically unfolds forming a rigid reflecting surface.

The parabolic reflector surface is achieved by means of a proprietary forming technique that eliminates the use of accurate jigs or patterns for the preparation of the reflecting surface.

This paper presents a discussion of the materials and the method used to produce a number of experimental reflectors. The results of a microwave evaluation test program are presented.

Figure (1) illustrates the proposed microwave reflector in its inflated and rigidized condition. A container for the rigidizing agent, mixing, storage, and flow control system is shown attached to the rim of the microwave reflector. This is only one means of providing rigidization to the reflector and in subsequent studies predistribution or storage in a premixed form will be considered. In its simplest form the reflector is made by bonding a polyester film to the top and bottom surfaces of a flexible support rim. The inner surface of one of these films is coated with a metallic reflecting material. Provision is made for feeding a rigidizing agent into the support rim and then into the space between the two membranes which form the front and back surfaces of the reflector. Low density foaming plastics have been the main rigidizing agents considered to date. Numerous other configurations are possible with this technique and some of these are mentioned later. However, the main objective of the present study has been to demonstrate the feasibility of forming the curved reflecting surface by this simple technique which would be useful as a microwave reflector.

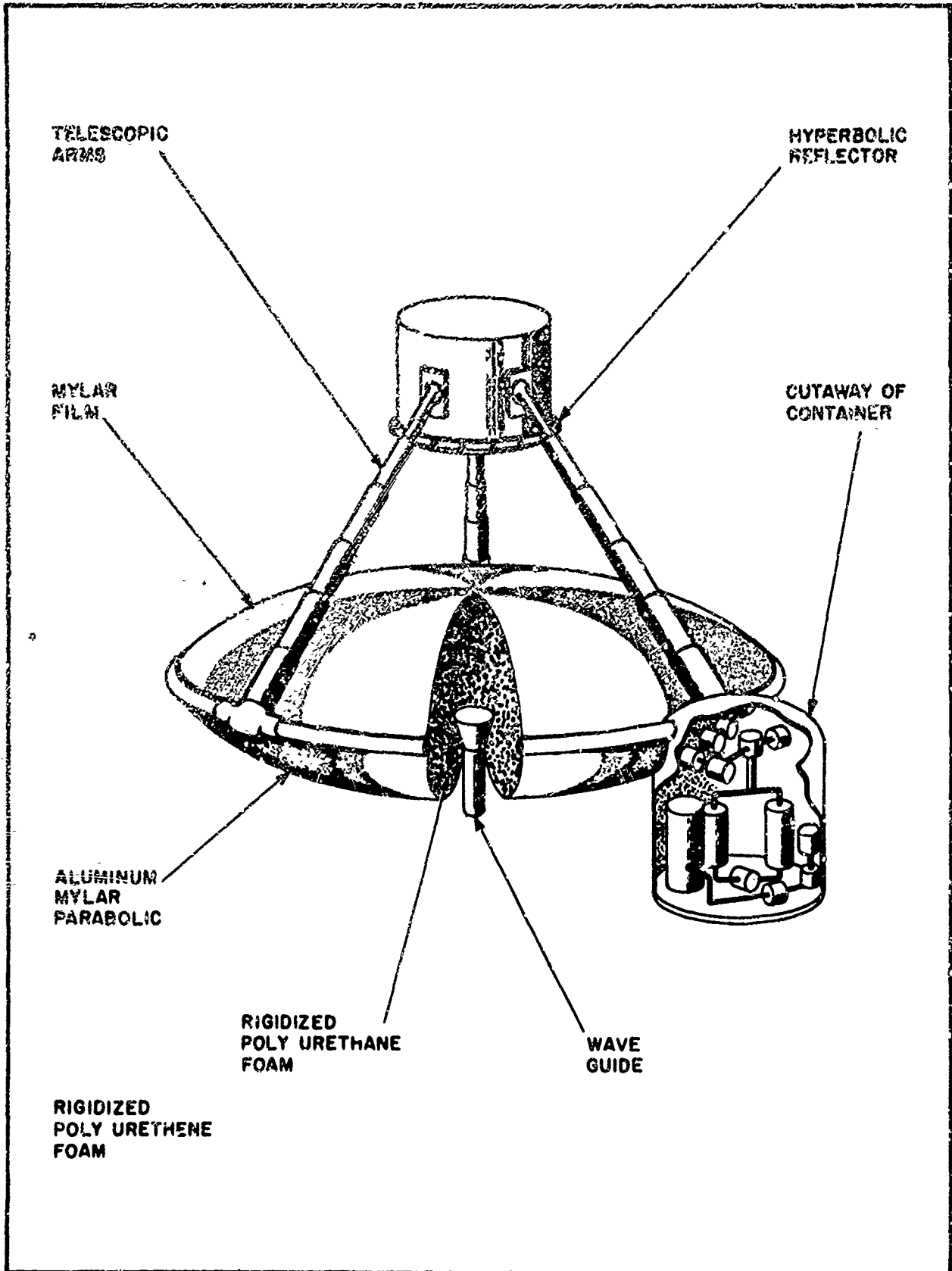


Figure 1
 The Microwave Reflector in Space

THEORY

Consider a membrane of negligible weight and flexural rigidity suspended with a uniform edge tension over a closed circular boundary and dilated by a pressure P over one surface. The characteristic differential equation of the membrane surface is obtained by the equations for static equilibrium of an infinitesimal surface element. As the overall deflection is relatively small ($\frac{z}{D}$ is approximately 0.1) there is justification in assuming that the surface tension is uniform in magnitude in all positions on the surface. In this case with small deflections, the edge forces on the element are Tds and Tdy where T is the constant tensile force per unit width of the membrane.

Figure (2) illustrates the following equations -

The downward vertical component of Tdy on the left hand edge is

$$F_1 = T dy \sin \theta \quad (1)$$

and the upward vertical component of the Tdy on the right hand side is

$$F_2 = T dy \sin \gamma \quad (2)$$

now θ and γ differ by the change in slope between X and $X + dx$, this change may be written

$$\gamma = \theta - \left(\frac{\delta^2 z}{\delta x^2} \right) dx \quad (3)$$

In a typical reflector produced in Computing Devices' Laboratory the diameter is 3-feet and the depth is approximately 4.5-inches. Using this depth then $\tan(\text{angle}) = .25$ and for this value there is a negligible difference between the angle and its sine. Therefore the sines in equations (1) and (2) may be replaced by the angles.

Similarly the vertical components of the forces at the remaining edges are

$$F_3 = T dx \theta' \quad (4)$$

$$F_4 = T dx \gamma' \quad (5)$$

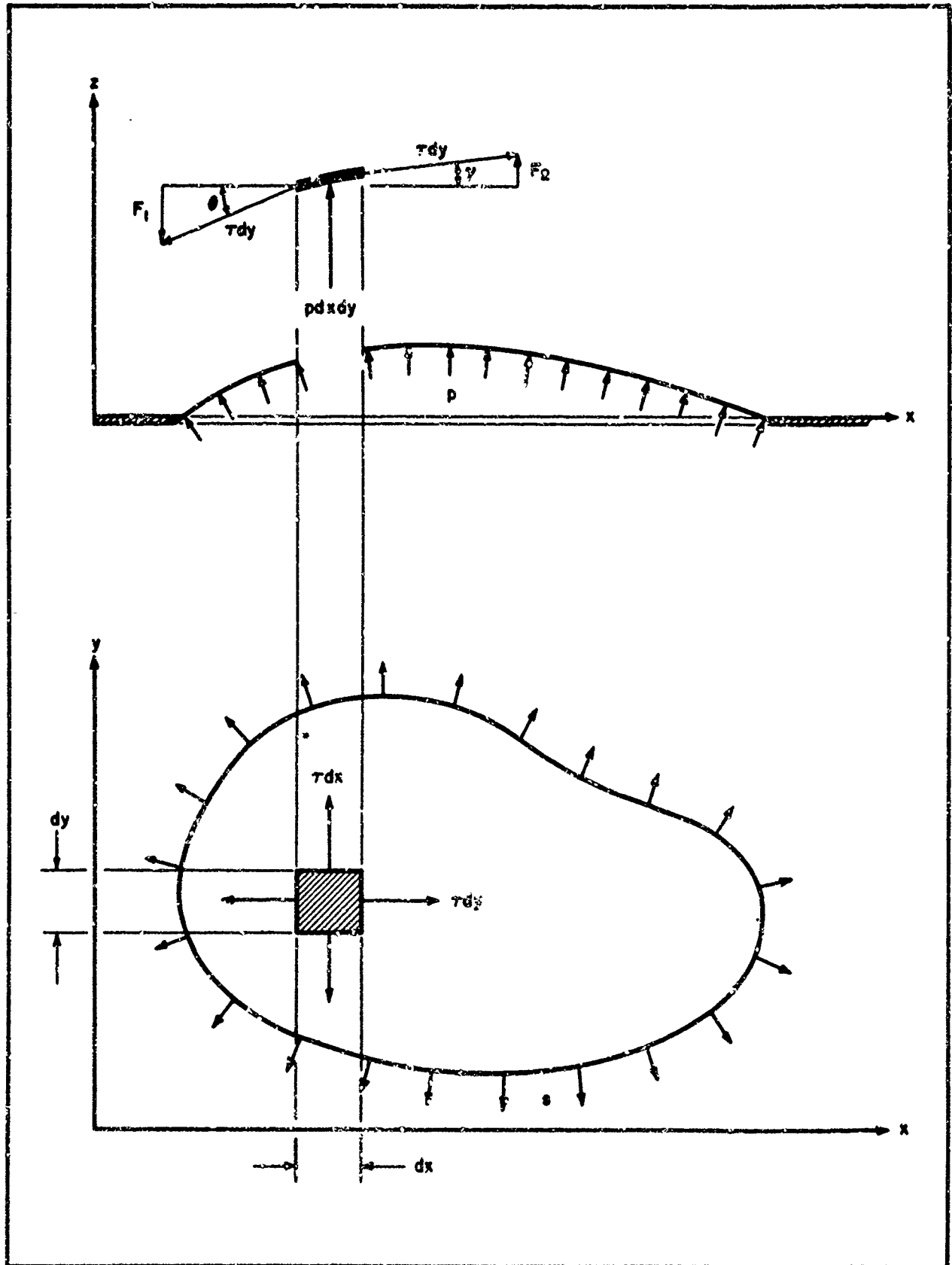


Figure 2

Dilated Membrane on a Closed Boundary

Equating the sum of these forces to the pressure force and imposing the conditions for static equilibrium

$$T dy \theta - T dy \left(\theta - \frac{\delta^2 z}{\delta x^2} dx \right) + T dx \theta' - T dx \left(\theta' - \frac{\delta^2 z}{\delta y^2} dy \right) + p dx dy = 0 \quad (6)$$

which reduces to

$$\frac{\delta^2 z}{\delta x^2} + \frac{\delta^2 z}{\delta y^2} + \frac{p}{T} = 0 \quad (7)$$

Transforming equation (7) to cylindrical coordinates gives

$$\frac{d^2 z}{dr^2} + \frac{1}{r} \frac{dz}{dr} + \frac{p}{T} = 0 \quad (8)$$

The solution to equation (8) is a parabola

$$z = \frac{1}{4} \frac{p}{T} (r_0^2 - r^2) \quad (9)$$

This theory is applicable only for very small deflections and uniform stress at all points in the membrane surface, including edges. The theory also ignores the elastic properties of the membrane and it is not surprising to find some deviation from the parabolic form in actual reflectors. Control over edge conditions and elastic properties of the membrane leads to a method of controlling the surface shape. No attempt has been made at such control in the experiments described in this paper but it is hoped these effects can be investigated in future work.

MATERIALS

The principal materials required for construction of the proposed reflector may be divided into the following categories:

- (a) Rigidizing material
- (b) Reflector material

Any rigidizing material for the reflector must satisfy the following requirements:

- (a) Dimensional stability after cure
- (b) Compatibility with space environment
- (c) Sufficient rigidity and strength
- (d) Small package volume and reliable deployment

- (e) Low density
- (f) Low microwave absorption

The following requirements are desirable but not essential:

- (g) Ambient temperature cure
- (h) Minimum exotherm during rigidization
- (i) Non-corrosive and non-toxic
- (j) Readily available
- (k) Low Cost.

It was evident that one of the new foaming plastics would have to be used as a rigidizing agent. These foaming plastics have various characteristics but most of them have the property of low density.

The following foaming plastics were examined:

- (a) Urethanes
- (b) Polystyrenes
- (c) Epoxy Foams
- (d) Polyvinyl chloride foams
- (e) Phenolic resin foams
- (f) Silicon foams.

Indications were that the urethane foams were superior in that they had low exotherm and also the ability to be foamed in place. Alteration of foam properties within certain limits to suit various requirements is also practical by varying the formulation of the foam constituents. Although much work remains to be done on urethane foams, the state of the art of this foam relative to the others mentioned is well advanced.

There are two main methods of producing the foam; the first is called the prepolymer system in which the isocyanate and resin are mixed anhydrously and no foaming occurs. The foaming can be accomplished at some future date by the addition of a catalyst. In the other method (one shot) all the additives are mixed directly and the foam is produced immediately. A one shot system would not have been practical for this application due to the control which would have to be exercised (temperature and pressure etc) over a number of ingredients at the same time. The experiments have been restricted to the prepolymer system.¹

The final physical properties of the foam may be varied greatly according to the mix. Rigid foams may have densities between 1.3 and 30 lbs per cu ft with corresponding changes in their compressive strengths. Urethane foams are excellent thermal insulators with exceedingly low coefficients of thermal conductivity. Difficulties have been experienced in closed molding of urethane foams, but the introduction of polyether foams aided by the development of new catalysts have alleviated most of these problems. The relatively high vapor pressure of the constituents in urethane foam rule out the possibility of curing at the ambient pressure encountered in space; therefore a relatively high pressure environment must be provided by artificial means.

A polyether urethane foam which was blown with a halohydrocarbon was chosen. According to the manufacturer this foam was very stable after rigidization and had a 90 to 95% closed cell structure. It is self-bonding to most surfaces and the bond exceeds the tensile strength of the foam. Its chemical resistance is excellent and it will withstand a temperature variation of -200°F to $+250^{\circ}\text{F}$ with little effect on dimensional stability. The foam has good elongation and is capable of moving with the surface to which they are bonded without affecting the cell structure or cell properties. The densities of these foams in an unrestricted mold is 2 lbs per cu ft. Tensile strengths are from 50-55 psi, compressive strengths at yield of 30-35 psi.

The foam proved to be suitable as far as rigidity is concerned, although problems were encountered in its dimensional stability with variations of temperatures. The density of the foams proved to be in the region of 2 lbs per cu ft and the cell structure was acceptable at the end of the series of experiments.

To keep the weight of the reflector as low as possible it is desirable that the metallic reflecting surface be a thin film. This is readily available in the form of polyester films with a metallic coating of very high reflectivity. The main consideration is that if the reflector material surface has irregularities then they must be smaller than the wave length of the incident radiation.

The particular film chosen to contain the foaming urethane was polyethylene terephthalate, commercially known as Mylar. This film is readily obtainable in an aluminum coated condition of various thicknesses. The aluminized Mylar proved to be an excellent microwave reflector, although a wrinkling problem was encountered and is mentioned later.

SPACE ENVIRONMENT

The space environment is characterized by:

- (a) Zero gravity
- (b) Vacuum-thermal effect

(c) Solar energy flux

(d) Meteorite Hazard

ZERO GRAVITY

The absence of gravity is, generally speaking, an asset to the construction of a space device due to the elimination of the major source of mounting loads and stresses. This lack of gravity introduces a minor problem in the storage and transfer of liquid rigidizing materials but should be readily solved.

VACUUM THERMAL EFFECTS

It is estimated that at an altitude of 600 miles (the start of the Van Allen Belt) the pressure would be about 10^{-10} torr, and rates of volatilization and sublimation become appreciable at these low pressures for materials of relatively high vapor pressure such as organic compounds. In general, the vapor pressure of the basic molecular polymer constituting a plastic is not likely to be high enough to cause a significant loss of material, except for the short terminal molecules found at the surface. However plasticizers found in many plastics have relatively high vapor pressures which may cause the loss of large amounts of material. The rate of diffusion of the plasticizer within the plastic thus plays an important part in the overall loss. Improperly compounded or incorrectly cured composites will experience critical losses. This emphasizes that the utmost care and the best techniques must be used when adopting plastics for use in space.

The classic equations used for quantitative studies on the evaporation rate of materials in space are generally not applicable to plastics due to their complex molecular structures. Recently much experimental work has been done in this field and the results would indicate that the decomposition rates are radically altered by the addition of small amounts of impurities. In general, loss rates tend to decrease exponentially with time when surface temperature is constant. The mass loss rate for plastics is controlled by temperature and is primarily a surface phenomena - weight losses increase significantly with decreasing material thickness.

In summarizing, it may be said that the effects of high vacuum on structural plastics are not as serious as was previously supposed and may be minimized by careful compounding of the plastic constituents.²

SOLAR ENERGY FLUX

Deterioration may be produced in polymers by ultra-violet radiation in the 0.2 - 0.4 micron band acting under a high vacuum. Other degrading sources are ionization induced by gamma rays up to .001 microns in wave length and bombardment by heavy

ions. The effects of high level radiation on plastics have been thoroughly investigated. Polymers are subject to damage depending on temperature and pressure, and the presence of any reinforcing fillers. Plastics are damaged by scission of bonds and subsequent reorientation of molecular structure. This reorientation consists of the formation of new bonds between chains, breaking of chains,³ evolution of gases and reaction with the ambient environment.

Test data on polyethylene terephthalate (Mylar) when exposed to a combination of radiation in the range 2000 - 6000 Angstroms and pressures in the neighborhood of 10^{-6} torr for periods of up to 500 hours produced weight losses of approximately 1%. The polyester shows a significant increase in flexural rigidity up to 200 hours exposure which is attributed to cross linking. After 500 hours, ultimate flexural strength decreases but is slightly greater than the original strength.³

Significant quantities of heat may be absorbed by the reflecting structure and the attendant thermal stresses and structural deterioration may cause the reflector to warp and become useless. It is therefore desirable that a low absorptivity be accompanied by a reasonably high emissivity.

METEORITE HAZARD

Vehicles operating in space will collide with meteoroids and other celestial matter of varying size, mass and velocity, with resultant damage varying from minor surface pitting to total destruction. The probability of meteoroid puncture is far less than the probability of erosion from dust. The reflecting surface would be well protected against meteoroid dust by the urethane foam.

LABORATORY EXPERIMENTS

The major emphasis in these tests was to demonstrate that a surface suitable for microwave reflection could be developed by simply forming a thin diaphragm with a foaming plastic. Less emphasis was placed on operational aspects and the system design considerations. However the following problem areas were recognized:

- (a) Rigidizing material assessment and selection -
 - (i) rigidity
 - (ii) dimensional stability
 - (iii) density
 - (iv) elevated temperature resistance tests.

- (b) Support structure materials assessment -
 - (i) flexibility
 - (ii) dimensional stability
 - (iii) density
 - (iv) elevated temperature resistance tests.
- (c) Reflector assessment -
 - (i) microwave reflectivity
 - (ii) temperature control characteristics.
- (d) Structure developments -
 - (i) bonding techniques
 - (ii) fabrication techniques
 - (iii) method of inflation
 - (iv) methods of rigidization
- (e) Rigidizing agent handling systems -
 - (i) storage
 - (ii) mixing
 - (iii) flow control
 - (iv) injection
 - (v) predistribution methods
- (f) Packaging -
 - (i) collapsing technique
 - (ii) folding methods
 - (iii) storage container

It is not proposed here to tabulate all our laboratory experiments, but more to discuss the results and the paths which were indicated by successful experiments.

It was obvious from the beginning of the foam handling that great care had to be taken when the constituents were mixed. The constituents had to be held at closely defined temperatures, e.g. the blowing agent between 65 and 75 deg. F. and the mixing had to

be closely controlled as far as time, temperature, and the efficiency of mixing were concerned. Various sophisticated mixing methods were tried but in the end the simplest possible mixing device was used, that is an electric motor driving a mixing paddle. Experiments were carried out with various mixing paddles and mixing techniques and it was found that the resultant foam structure depended upon:

- (a) the shape of the paddle
- (b) the mixing speed
- (c) the mixing technique

These parameters dictated the flow pattern of the fluids during the excitation period.

When it was thought that a reasonable foam could be produced, an apparatus was set up which clamped two sheets of mylar along the circumference of an 8-inch diameter ring. The two sheets of mylar were separated by a nominal distance of .5-inch. The foam was injected into this mold using a hand operated piston device and the resulting deformation of the Mylar indicated that there was a reasonable hope of duplicating this experiment on a larger scale. Numerous experiments were carried out on this 8-inch jig and the reflectors were sectioned and foam structures examined. It was found that the foam, when injected into the circumference of the mold, seemed to travel in a front across the mold. This front was generally of a larger cell structure and higher density than the remaining foam.

Identical experiments were carried out on a 3-foot diameter clamping ring, the foam being manually injected at the circumference. A reflector produced using this rig is shown in Figure (3). In some of these experiments the foam was injected at three separate parts of the circumference, but this resulted in the wave fronts meeting at the center of the reflector causing a bad foam structure at this point. All the experiments were carried out in a laboratory where fine temperature control was not possible, and it was noticed that after the foam had fully rigidized the temperature changes during the few days after rigidization caused crinkling of the Mylar surface. The program continued with the rigidizing of an outer plastic tube. Various materials were tried but the most suitable of them seemed to be a cloth reinforced polyvinyl tube. Eventually a technique was perfected so that the ring could be unfolded to a circular configuration by the injection of air and then foam rigidized.

The next step in the program was to bond the Mylar to the ring and to rigidize both the outer ring and the reflector in one operation. Figure (4) shows a section of one of these reflectors. A rough dimensional check was made on the reflector surface and it was found that the inner area of approximately two feet diameter was close to parabolic while the outer edges had a lower focal length. The support ring imposed edge conditions on the Mylar which further distorted the final shape of the reflector.



FIGURE 3
THREE FOOT DIAMETER REFLECTOR
WITH ALUMINUM RIM



FIGURE 4
SECTION OF THREE FOOT DIAMETER
RIGIDIZED RIM REFLECTOR

It was noted that this distortion was not constant on all surfaces produced, but changed as the focal length of the reflector changed. Various packaging and folding techniques were studied and eventually a package for a three foot diameter reflector could be folded into a 3-inch x 5-inch x 1½-inch package. This is not an optimum and with the use of more suitable circumferential material it is estimated that this volume could be reduced to 1/4 of the present package volume.

During the laboratory experiments, a three foot diameter foam rigidized reflector weighing 4 lbs was produced. This weight is by no means an optimum and a 3-foot reflector was foreseen with more development work, weighing approximately 1½ lbs. In this reflector the Mylar surface would have a narrow urethane foam backing. To produce such a reflector a triple diaphragm type of rig would have to be used. The first void between the aluminized Mylar would be foam filled and the next void, backing the clear Mylar, would be gas filled during rigidization. At the moment, polyurethane foams of 2 lbs per cu ft of rigidized density have volume expansion ratios between 30-35. But as the state of the art improves this ratio will increase and should provide for lower mass reflectors.

MICROWAVE EVALUATION

Electrical characteristics of the first developmental 3-foot diameter reflector were measured to determine how effective it would be as a collimating device at microwave frequencies. The experimental tests were conducted in the X and C band frequency ranges.

X-BAND PROPERTIES

X-band radiation characteristics of the inflated reflector were obtained by employing a feed horn with a primary pattern which closely approximated a rotationally symmetric Gaussian power pattern.⁴

This feed was chosen for purposes of determining the electrical symmetry of the foamed parabola since the feed pattern is nearly identical in all planes over a 25 db dynamic range. The feed provided an approximate edge illumination of -10 db which is specified by the 3-foot diameter and the 28-inch focal length of the reflector. Figures (6) and (7) illustrate the radiation pattern characteristics of the reflector with the aforementioned feed. Inspection of the radiation patterns indicate non-symmetry in the collimated parabola in that the side lobe structure for both radiation planes is not identical. This non-symmetry, although not severe for most practical applications, is related to phase errors produced by mechanical non-uniformities and properties of the foamed dielectric. The side lobe level indicated in Figures (6) and (7) is approximately 10 db higher than that obtainable with an ideal parabolic reflector with the same aperture illumination and is an indication of the presence of phase error.

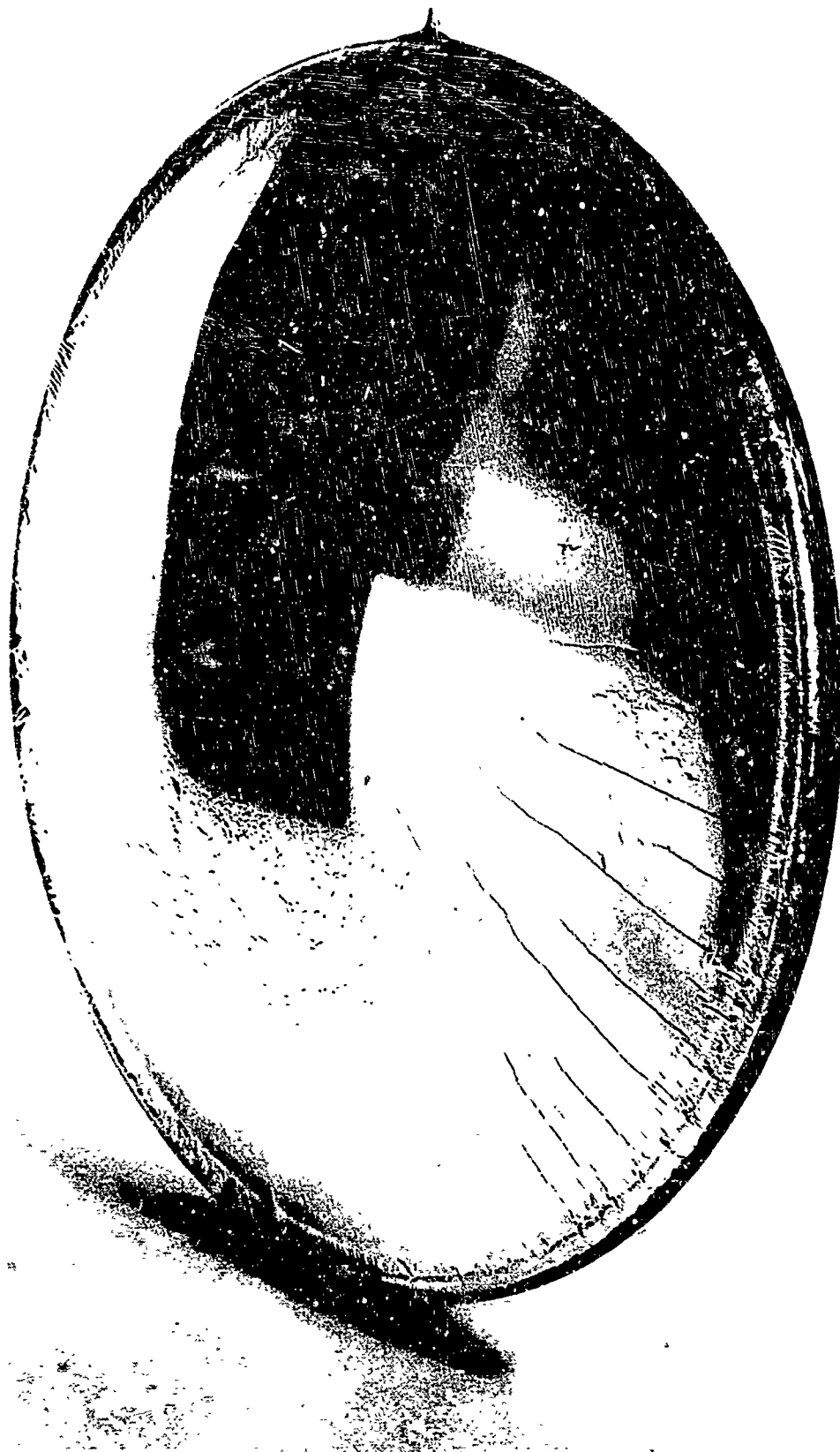


FIGURE 5
A THREE FOOT DIAMETER RIGIDIZED
RIM REFLECTOR

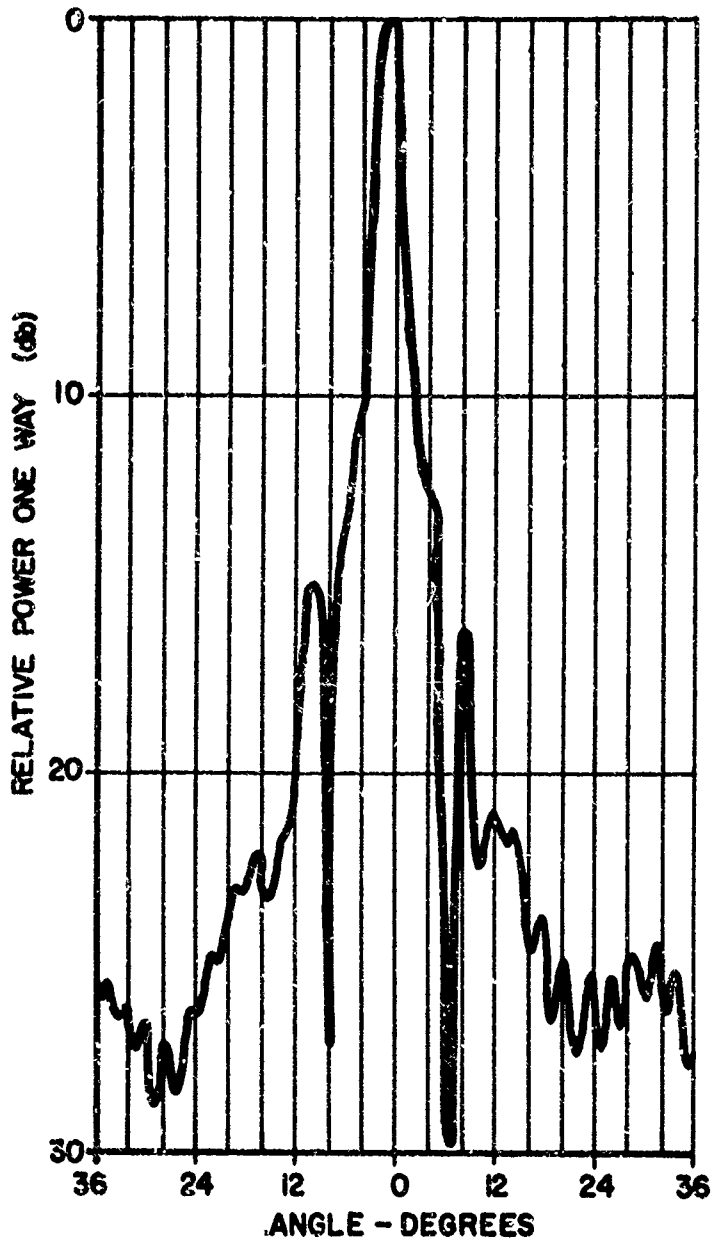


Figure 6
X-Band, Parabolic Antenna Pattern, H Plane,
at 0 Degrees
280

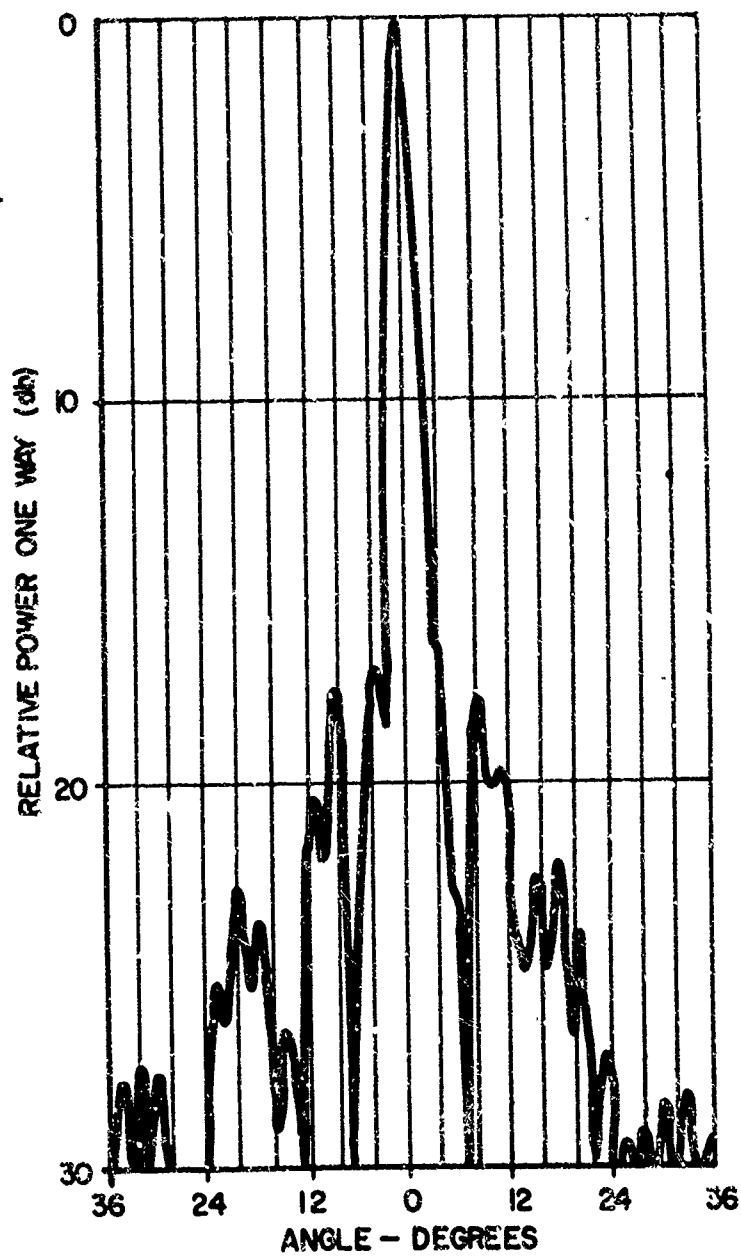


Figure 7

X-Band, Parabolic Antenna Pattern, E Plane

Measured values of gain obtained with the experimental reflector are indicated in Figure (8).

PHASE ERROR EFFECTS

Phase errors produced over a collimating aperture normally increase the side lobe level of the secondary radiation pattern and cause a reduction in gain.

In order to accurately predict the effect of phase error for parabolic reflectors one must consider the two dimensional phase distribution over the perturbed aperture. Given the resulting phase distribution and assuming a Gaussian shaped pattern one can calculate the secondary pattern characteristics and compare the result to that obtained from an ideal parabolic surface and thus predict any increase in side lobes and reduction in gain. No attempt has been made at present to accurately correlate the phase errors of the inflated parabola with its radiation characteristics. However a brief investigation has been conducted to determine first order effects of the mechanical properties of the reflector. Several sources of phase error observed from mechanical properties of the experimental reflector are discussed below.

(1) Surface wrinkle of the reflector was measured and found to be less than 10 mils from the average surface. The total phase error produced from this perturbation is less than 6° in the X-band frequency range.

(2) The surface error of the reflector was measured with a depth micrometer. The measured results are shown in Figure (9) as a function of displacement from the focal axis. The x-dimension was measured along either side of each orthogonal plane (0° , 90° , 180° , 270°) with the focal axis as the origin.

A theoretical parabolic curve fitted through the coordinate values $x = 1.25$ and $y = 12$, was used as a reference. The average error obtained was 40 mils with a maximum to minimum variation of 80 to 0 mils. This mechanical error produces a phase variation from 0° to 40° at X-band frequency. One would anticipate a 10-15 db increase in side lobe level, with respect to an ideal parabolic surface for such a phase error. A side lobe of this magnitude (approximately 17 db below the main beam) was obtained experimentally as previously discussed.

(3) The dielectric foam also effects the phase property of the radiating system to some degree. The aperture phase differential as produced by the presence of the foamed dielectric is also dependent on aperture illumination. For a highly tapered illumination the phase error produced by the foamed dielectric is minimum. The insertion phase of the foamed material used in these experiments is approximately 3.7° per inch at X-band frequency.

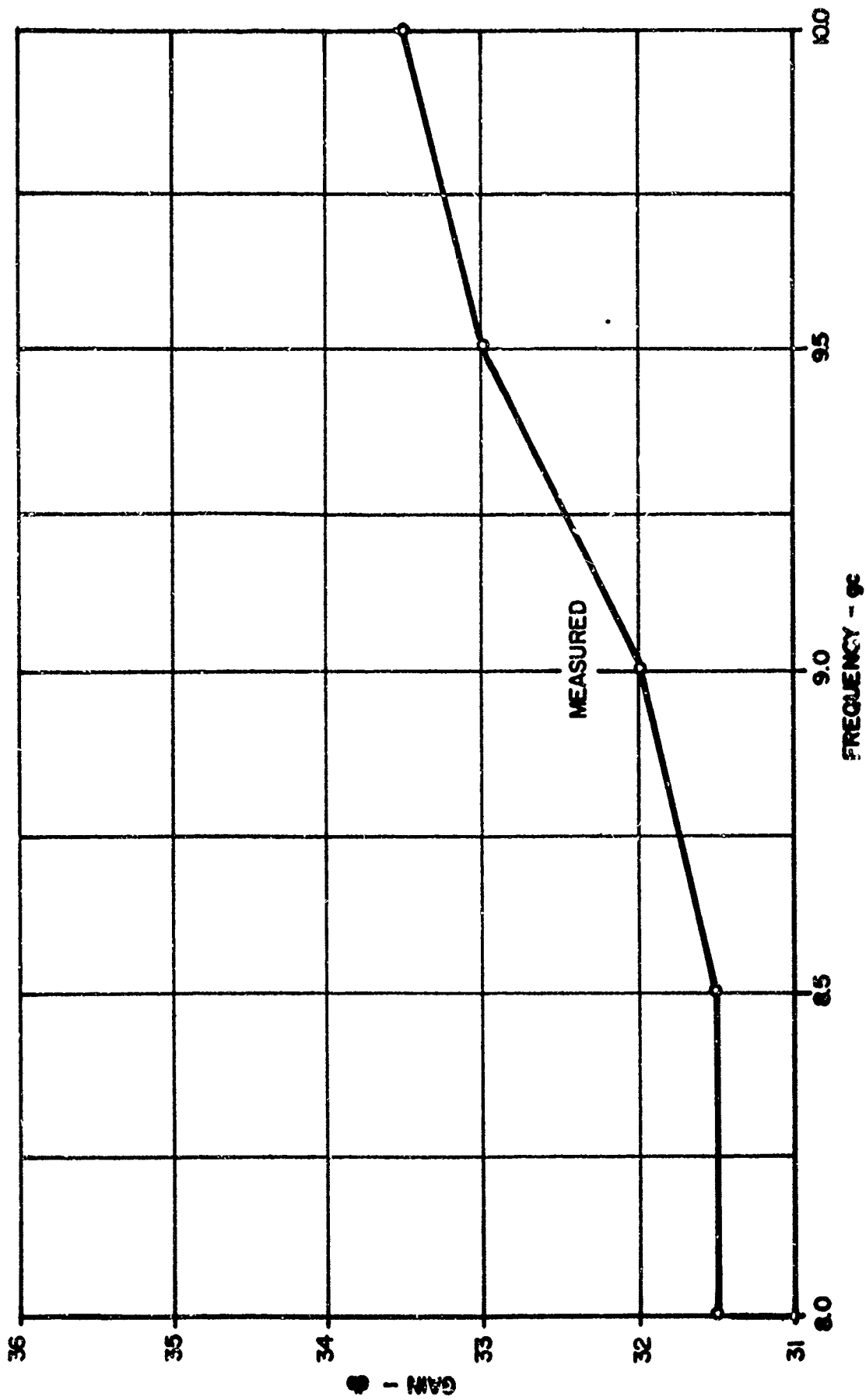


Figure 8. X-Band Gain Measurement as a Function of Frequency.

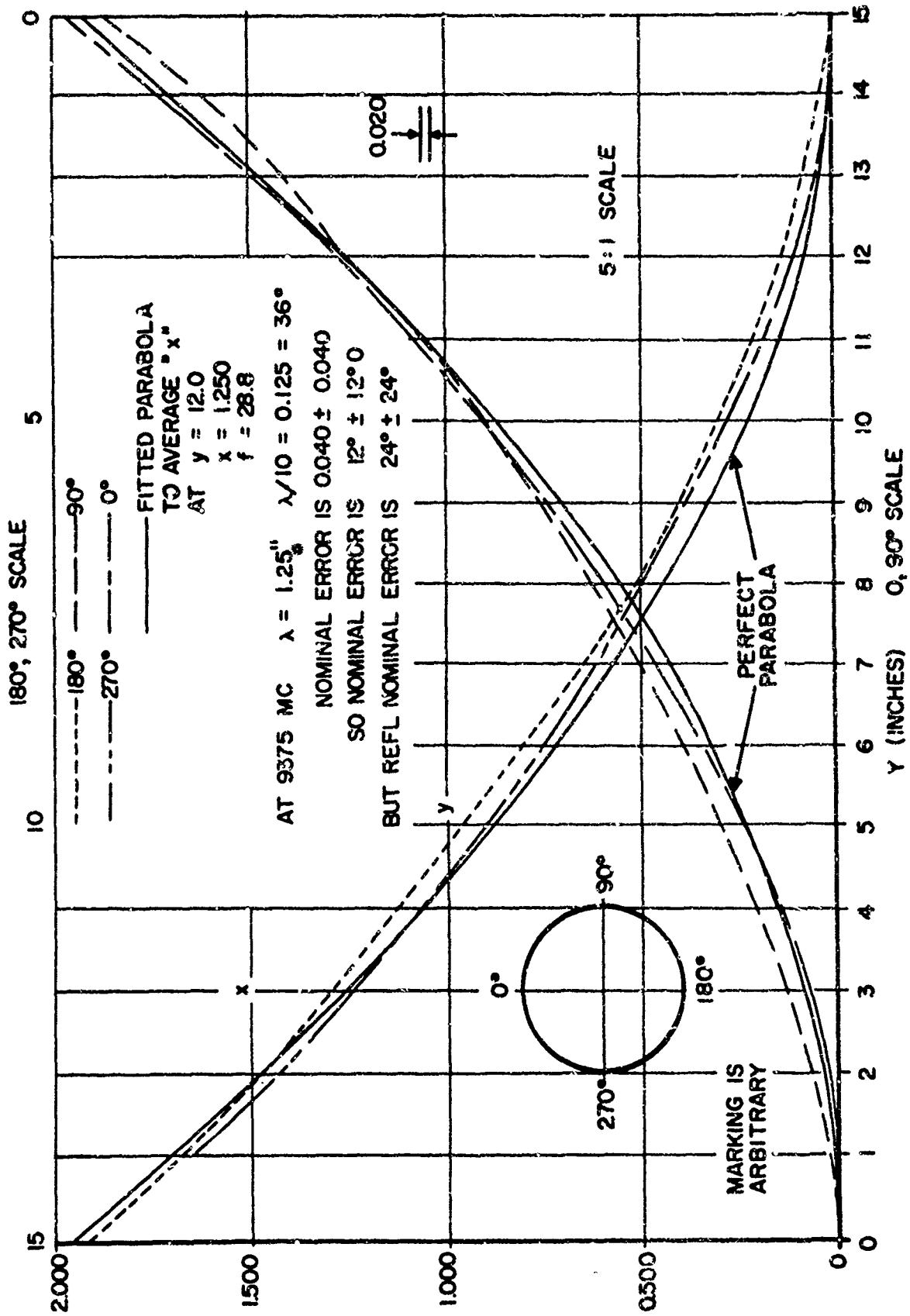


Figure 9. Measured Parabolic Reflector Dimensions.

C-BAND PROPERTIES

A C-band sectoral horn that produced a parabolic aperture edge illumination of -2.5 db and -7.5 db for H and E planes respectively, was used to observe the effect of a lower frequency. The measured patterns were as predicted. The -2.5 db aperture gave -12 db side lobes with a 4.5 degree main beam. The -7.5 db aperture had -15 db side lobes and had a 5 degree beamwidth.

Figure (10) shows the antenna as tested on the outdoor range.

CONCLUSIONS

The application of the proprietary forming technique in the development of a Rigidized Inflatable Microwave Reflector and the subsequent microwave tests performed, indicate that the present surface characteristics, resulting from the fabrication process used, permit the reflector to be used satisfactorily at X-band microwave frequencies or lower. Further refinements in the process, or smaller dish dimensions, could permit the useful extension of the method to K-band frequencies.

The investigation of the described techniques as applied to the manufacture of a much larger reflector and the application of predistributed rigidizing agents are also foreseen as being necessary in future development activities.

Figure 7. Measured Parabolic Reflector Dimensions.

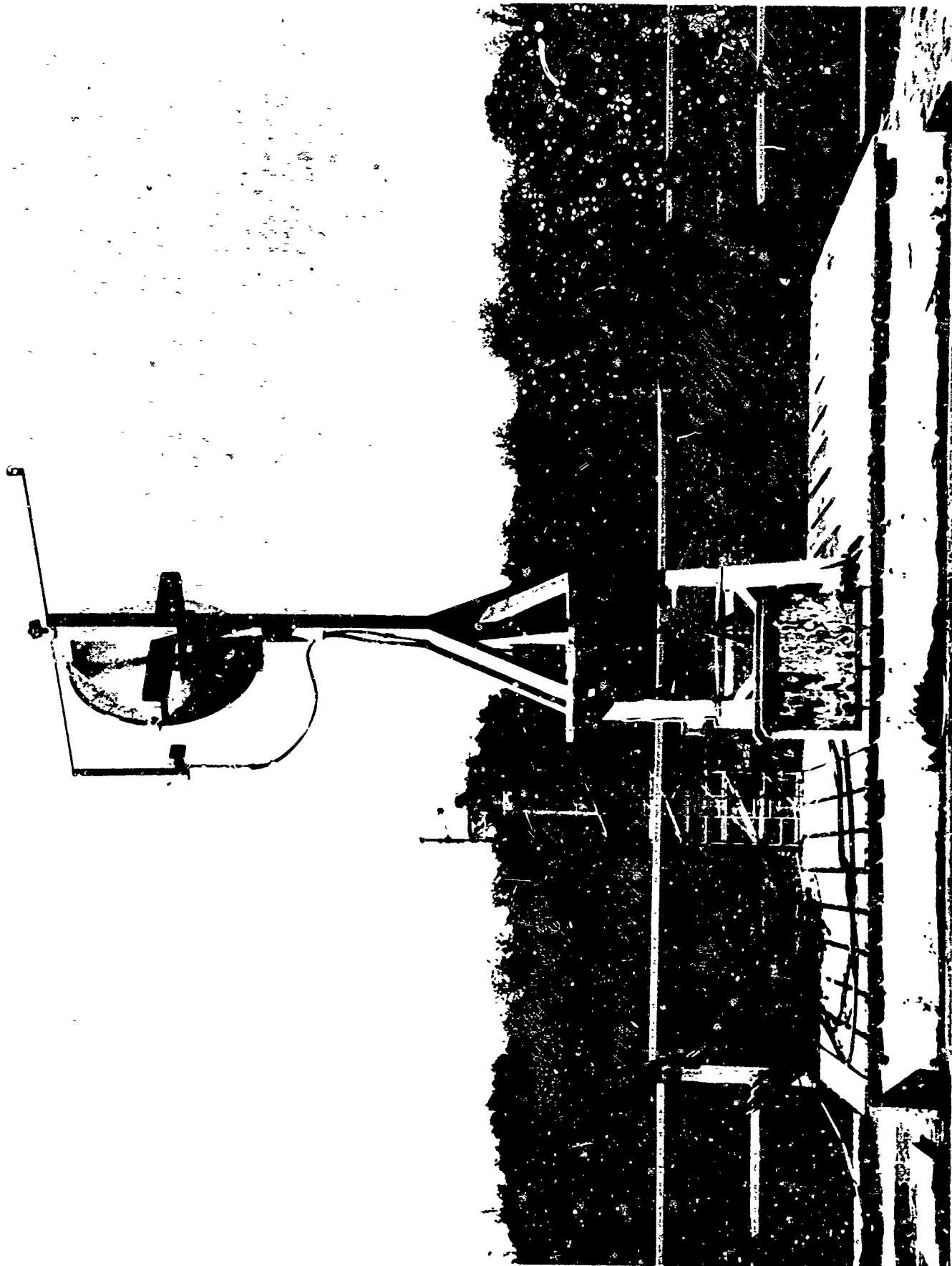


FIGURE 10

185 Foot Antenna Range Test Equipment

REFERENCES AND BIBLIOGRAPHY

- 1 Ferrigno, T.H. Rigid Plastic Foams. Reinhold Press.
- 2 Gatzek, L.G., Isenberg, L. The Space Environment as related to Materials Engineering for Space Power Systems

Materials and Processes for Space Power and Primary Propulsion Symposium. January 2-5, 1963, Philadelphia.
- 3 Mauri, R.E., Fugger, J. Structural Materials-Organic

Space Materials Handbook, Lockheed Missiles & Space Company.
- 4 Peace, G.M., Swartz, E.E. Amplitude Compensated Horn Antenna. Microwave Journal March 1964.

BIBLIOGRAPHY

- Saylor, W.P. et al Space Radiation Guide - Aerospace Medical Division USAF.
- Houck, O.K. Effects of Fabrication Materials and Processes on Solar Energy Collection Performance - Wright Patterson A.F.B. 1963.
- Clark, D.R. Solar Reflector Testing in Combined Vacuum and Ultra Violet-Boeing Co. 1963
- Hildreth Press Inc Modern Plastics Encyclopedia 1964.
- Computing Devices of Canada Solar Energy Concentrator - Proposal No. 4048/TP1, May 1963.
- Gibson, K.F. A Report on a Preliminary Study of a Rigidized Inflatable Space Reflector, Computing Devices of Canada, April 1964.

SESSION IV

SODIUM SILICATE AS A VERSATILE STRUCTURAL MATERIAL

Herbert I. Hoffman, Senior Research Engineer

Department of Mechanical Sciences
Southwest Research Institute, San Antonio, Texas

INTRODUCTION

The family of soluble silicates includes the well-known, inexpensive sodium silicate, commonly called water glass. Soluble silicates are produced by reacting silica sand with appropriate alkalies, resulting in opalescent, viscous liquids in solution with water. Partly dehydrated, they are also available in various powder forms. Rapid boiling of the solutions or of the hydrated solids causes an intumescence or foaming, which is the characteristic that is of special interest in this paper. As an industrial chemical selling for under 3 cents per lb in bulk, the soluble silicates are used directly in adhesives, detergents, specialized paints and fire retardants. Beginning with an 1883 patent, there is an evolution of industrial applications based upon using the foamed material for its insulation value, both thermally and acoustically.

While using sodium silicate solution as a high temperature adhesive, the foaming resulting from thermal exposure with high temperature applications became of interest. Foamed samples were then prepared by simple boiling and by more complex methods of heat input. Sections of two laboratory-produced foams are shown in Figure 1. The larger disc was foamed under reduced pressure in a bell jar; the significance of ambient pressure versus heating rate is of major interest. It became evident that 10 lb per cu ft foams of structural quality could be produced for approximately 9 cents per lb, contrasted with a minimum of about 55 cents per lb for plastic foams with similar physical properties (1).

Aside from unusual performance possibilities, the potential cost savings are enough to encourage interest in applications where mass production of expendable components is desirable. For example, quickly erected insulated shelters and inexpensive, expendable air drop cushion packages are two possibilities of special interest. In space applications, other qualities of sodium silicate offer advantages over present chemical rigidizing and foaming systems. Furthermore, it offers an excellent potential for an

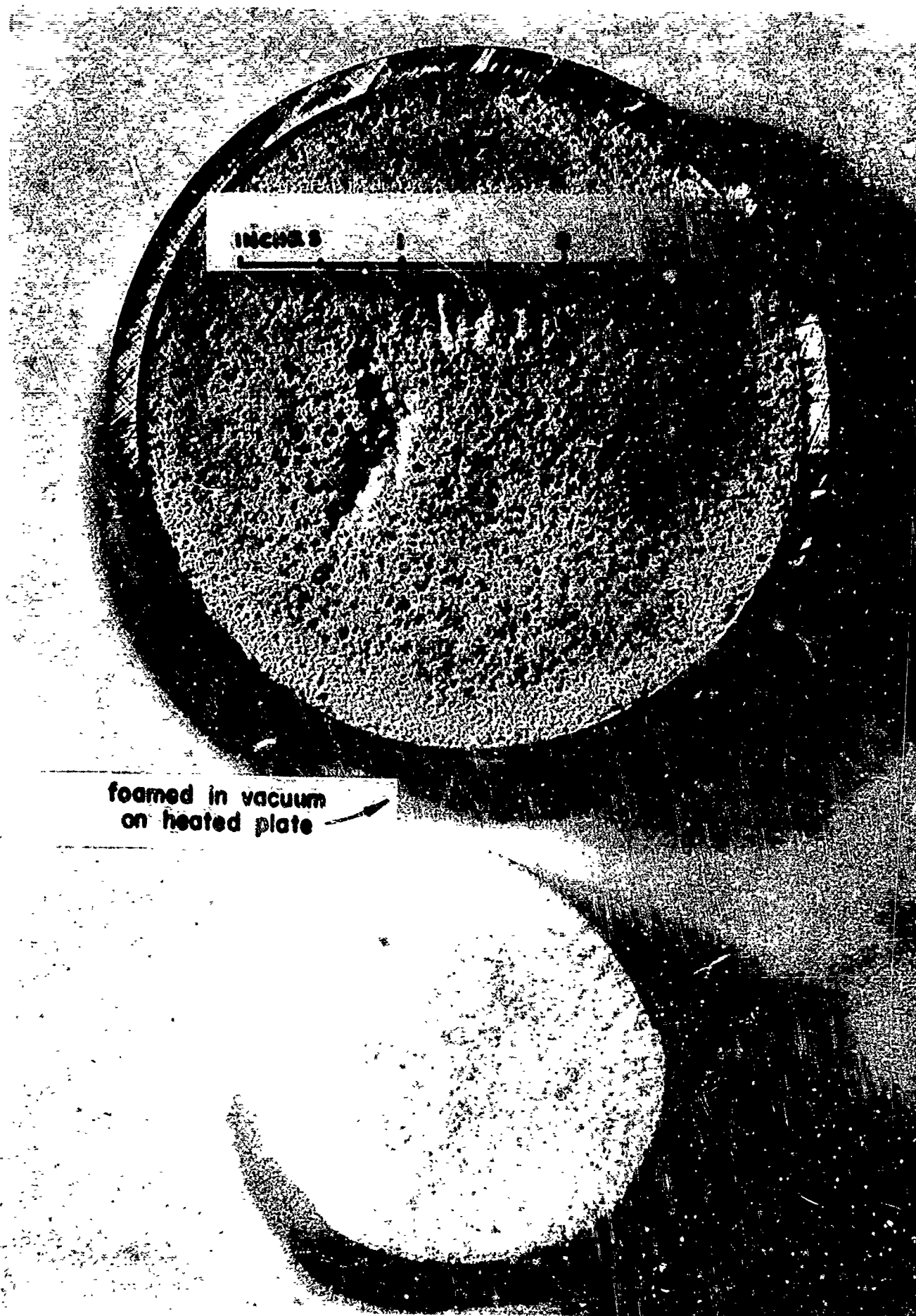


FIGURE 1. RIGID SODIUM SILICATE FOAM

inorganic, thermal insulation and heat sink which could be shaped in space.

TECHNICAL BACKGROUND

Sodium silicate is widely used in industry as an agent to control the physical properties of solutions. It is used as a wetting agent, as a heavy-duty cleaning compound, and as an emulsifying agent. Its properties as a binder, sealer, and adhesive are among its major commercial attributes. In soil stabilization, the reaction between sodium silicate and clay soils has become a technology of its own. Sodium and potassium silicate compositions are very well accepted as binders in the manufacture of heat resistant paint and coatings. Some coatings with silicates will perform well at temperatures approaching the melting points of the protected metal parts (2). Fire retardance continues to be one of the major fields for soluble silicates. Their bonding strength and thermal resistance are useful in the manufacture of refractory materials, including blocks and cement. Figure 2 tabulates the chemical compositions and physical properties of soluble silicates.

Perusing through the complex chemistry of silicates, a designer is sharply reminded that the exact composition of the material can be identified only from the crystalline form. The composition of sodium silicate is readily modified by common contaminants and additives; fortunately, this has not been a problem in foaming experiments.

In developing design concepts, it should be noted that the boiling point of silicate solutions is slightly above that of water at normal pressure, while a typical freezing point is approximately 2° below that of water. Dense solutions of sodium silicate suffer little from freeze separation which might be anticipated due to exposure in the vacuum of space.

Densities of commercially available sodium silicate solutions vary from 11 to over 14 lb per gallon. In solid forms, it is available in sizes from lumps through fine powders. Their densities range from approximately 55 to about 88 lb per cubic foot, covering hydrous and anhydrous forms.

The discussions in this paper are based upon experiments with sodium silicate, which is the most common and least expensive of that family of soluble silicates. Potassium silicate, also commonly available, is somewhat more expensive and has not been considered in the preliminary experiments.

Physical Forms and Their Uses

As suggested by the traditional applications mentioned previously, sodium silicate has many forms. Figure 3 illustrates some of the "solid" forms which can be generated by heat and vacuum. The two paths indicate

HYDRATED SODIUM SILICATES

$\text{Na}_2\text{O} : \text{X} \cdot \text{SiO}_2 : \text{H}_2\text{O}$ -----indicates oxide proportions in typical water glass
ratio 2.5 to 3.5 of interest $\left\{ \begin{array}{l} \text{various \%} \end{array} \right.$

Example: $3 \text{Na}_2\text{O} \cdot 13 \text{SiO}_2 \cdot 11 \text{H}_2\text{O}$; specific gravity 1.13

ANHYDROUS SODIUM SILICATES

- $\text{Na}_2\text{O} \cdot \text{SiO}_2$ - sodium metasilicate: melting point 1089°C
- $\text{Na}_2\text{O} \cdot 2 \text{SiO}_2$ - sodium disilicate: m. p. of various crystal forms: 678° , 707° , 874°C
- $\text{Na}_2\text{O} \cdot 3 \text{SiO}_2$ - polysilicate: m. p. 820°C . When dissolved in 15% of H_2O and heat foamed, results in 30 to 100 expansion; thermal conductivity about .029 Btu/hr-ft²-deg F.

FIGURE 2. PROPERTIES OF SOLUBLE SILICATES

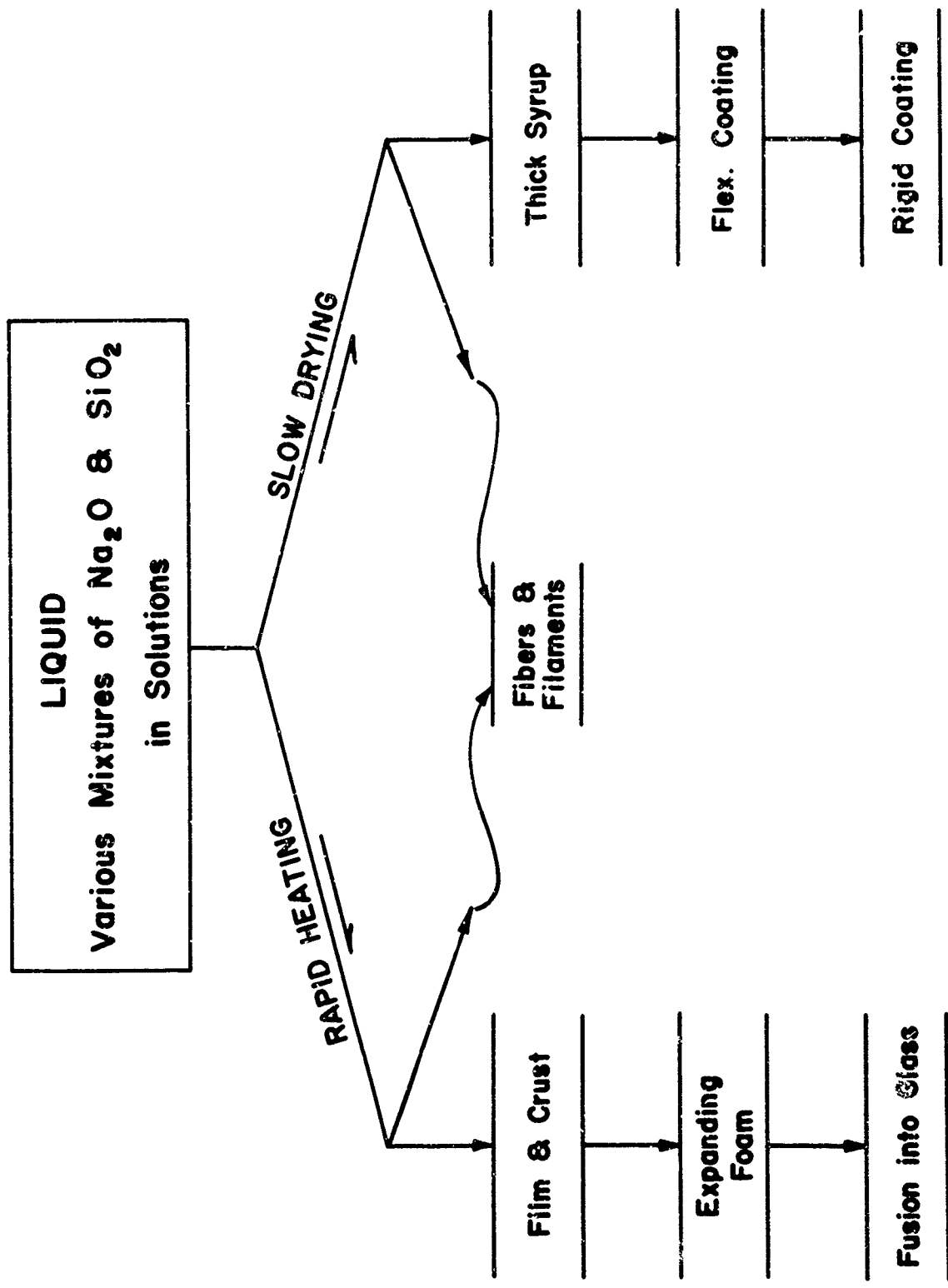


FIGURE 3. FORMS GENERATED BY DEHYDRATION

the successive effects of rapid heating, including exposure to flame, vs. the effects of slow dehydration. Preliminary experiments conducted in a vacuum bell jar indicate that the same forms indicated here can be achieved in vacuum, perhaps with supplemental heat in some cases. This suggests the possible values of self-activation in space. It will be noted that the silicates can be drawn into fibers and filaments which can be solidified by heat or vacuum. This suggests possibilities of building or winding structures in place. Slightly more conventional is the concept that fabric ribbons saturated in liquid sodium silicate could be used for repair or construction in space, resulting in an immediate curing of the coating into a reinforced glass structure capable of foaming under intense heat.

Continuing to follow Figure 3 down the rapid heating approach, it is indicated that rapid heating of the solution will form crusts of glass which in turn will finally generate into a rigid, coarse foam as heating continues. Exposure to still higher temperatures in excess of 600°F at atmospheric pressure, the rigid foam continues to expand into fine, white rigid foam. When this material is further exposed to flame or other extreme heating, the rigid foam enters into the molten state. The slow dehydration path indicated on Figure 3 perhaps is not as immediately thought provoking from a design point of view. However, this process carries the solution through a thickening into the glass state. Under vacuum exposure, it is likely that freezing and drying would continue unless supplemental heat were provided to cause foaming.

The compressive strength of a laboratory sample of foam is illustrated in Figure 4. After initial crushing, the load for continued crushing leveled off at about 40 and 50 psi for the two relatively slow loading rates. Impact loads would run higher. Additives would probably increase those values significantly.

Application Problems

Conduction heating and gas foaming methods of generating silicate foams and procedures for foaming in place are described in the literature. The generation of silicate foams by boiling or rapidly heating the liquid solution has been used to manufacture refractory blocks and insulating boards; however, this heating method has not been appropriate for generating foam in place except where the walls of the cavity to be foam-filled can withstand the required heat of conversion. Some of the documented uses of silicate foams involved prefoaming pellets of the material and, in turn, bonding those together in place with resorting to further heating.

One question faced by a designer is the solubility of the rigid foamed silicates. Fortunately, the solubility of sodium silicate foam in boiling water can be brought to a negligible value either by exposure of the foam to

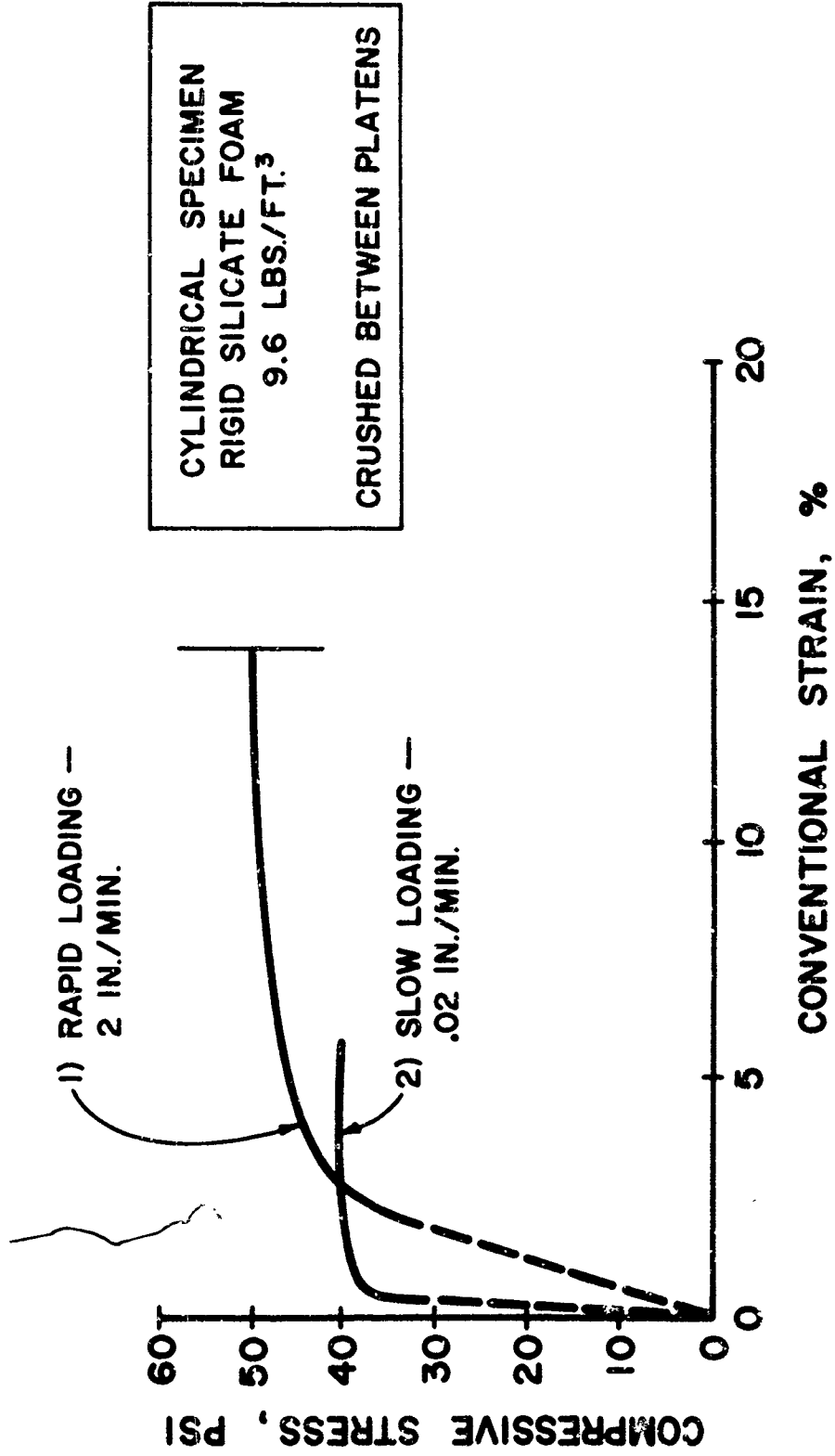


FIGURE 4. CRUSHING STRENGTH OF RIGID FOAM

an acid gas or by proper composition of the solution from which the foam is made.

It is with this background of the chemistry, the mechanics, and economics of sodium silicate that the demands of expanding and rigidizing structures for space applications and for limited war applications must be considered. Methods of heating (beyond conventional conduction) must be considered. For expandable structures which might require flexible skins of plastic or fabrics, it might be necessary to place the foams or to rigidize these structures without endangering the skins by extreme heating. At the same time, space applications offer an obvious and unique possibility for rigidizing; the hard vacuum can promote dehydration and freeze drying of the material. Where rigidizing alone is of interest, a rigid crust resulting from vacuum drying may be sufficient. The generation of rigid silicate foam in space would require heat to supplement the dehydration effect of vacuum.

Having set the stage, we now enter upon another portion of this subject.

CHOICES IN PROCEDURE

Mechanical Features

Thus far, we have generalized on the physical forms which might be useful in expanding and rigidizing of collapsible structures. Summarizing, we can choose 1) the relatively simple step of rigidizing a flexible matrix by vacuum and/or heat dehydration of its coating, or 2) the more complex applications going beyond the rigid coating into expansion of rigid foam. In evolving conceptual designs, it is necessary to assume not only the properties of the expandable and/or rigidizing medium, but the means for accomplishing that change of properties.

Conversion Methods

There is always the choice of using expansion methods based on gas generation, which is inherent in many foaming processes. Gas generation due to chemical reaction, instead of vapor or steam generation from rapid boiling, poses a different set of problems, but should be considered. The fact that a rigid foam can be generated from an inexpensive solution by simply boiling the material, offers advantages for many terrestrial applications where economics and low shipping volumes are important.

To face the numerous expandable structure problems which have been evidenced by our discussion today, we are forced to consider more than the simple boiling or conduction heating of the solution to generate rigid coatings and foams. For example, it is to be considered that for some

space applications, such as a solar collector to be rigidized, it may prove reasonable to pigment the material so that radiated energy absorbed by the structure will be sufficient to harden it quickly.

For generating foam samples for laboratory study, excellent results have been obtained using a radar oven or microwave oven to produce internal heating and subsequent boiling and foaming of sodium silicate solutions. By microwave, samples have been foamed inside Plexiglas shells and in Mylar bags. Microwave or radar heating suggests a possible tie-in between this method of heat application and the communication microwave systems and radar which might be available at a site where foaming is required.

Other foams were expanded from solution poured over molten lead for a heat source.

Electrolytic heating of the sodium silicate solution appears to be an interesting, practical way to achieve foaming. To develop a uniform structure, it would seem reasonable to submerge a series of alternate cathodes and anodes in the solution which, in turn, would be confined in a hollow chamber or cavity which is to be foam-filled. Input of electrical energy through the electrodes would cause resistance heating and result in a foaming of the silicate. A similar approach would be the direct use of resistance wires in a solution. Another class of heating and foaming method is the use of pyrotechnic materials mixed with or laminated to the sodium silicate to be foamed. It is conceived that mixtures such as thermites, including magnesium powder, would burn throughout the solution, causing enough heating to result in a rigid foam. It is likely, of course, that such a process would generate sufficient combustion gases that the gases would have a major effect on the foam structure. Chemically similar would be the common additives of an acid plus a metal in order to generate heat and gas, causing foaming of the material. The electrolytic and pyrotechnic methods have not been attempted on this project.

Flexible Packaging

Packaging films are available which are flexible enough at low temperatures for space applications and still would withstand upper temperatures which would be involved in foaming of sodium silicate solutions. Many of the applications for rigidizing in space with sodium silicate would involve distributing a quantity of the solution between plastic films so that the solution is sealed and protected from the vacuum dehydration which otherwise would occur in space. A flattened storage pouch could be prefolded and would later serve as the skin of an expanded structure.

APPLICATIONS

Limited War Requirements

The perennial problem of air drop cushioning seems to be a natural area in which to consider inexpensive, rigid foams of silicates. Figure 5 suggests collapsed containers, filled with hydrated silicate, to be expanded into rigid, energy-absorbing foam. This can be accomplished in a foaming oven. The foam may be cast monolithically within the cushions, or the container may be filled with pellets or chunks of foam. Where salvage of a flexible cushion or collapsed container is reasonable, the foam may be removed by water or by steam, or by simple mechanical crushing and shaking in the event that insoluble foam has been used. Thus, the cushion containers may be reused when convenient; however, it is believed that the greatest gain might be made by selecting the option in the field of saving shipping cubage through the use of foam generating units at depot level.

A similar operation would use the inexpensive foam for field-expanded shelters. Sealed, compressed, flexible packets containing sodium silicate could be readily transported and stockpiled, together with a fuel-fired oven for expanding them into rigid, molded panels. One advantage of this system is that once panels or building components were expanded and rigidized, they would not require air compressors or blowers in the field to maintain their shape. For economy in shipping weight and volume, it is suggested that a collapsed and packaged component would contain a solid form of hydrated sodium silicate. At a behind-the-lines depot, individual panels or sections could be placed in suitable molds and perhaps heated by conventional military fuels. These panels would thus be heated and expanded into rigid building sections, complete with plastic or coated fabric skins. This has been done for building boards in the past! It could be convenient to use skin materials of camouflaged coloration and to mold contours which would be suitable for camouflaged covering of gun emplacements and vehicles. In other words, artificial boulders or hummocks could be molded in the field for movement by helicopter or other vehicles to the area where concealment is required. An interesting sidelight to this camouflage device is that radar reflectivity, as well as optical appearance, could be tailored into the foam to the extent and pattern desired by the addition of metal powder.

Space Applications

In space system structures, one may consider several types of duties which sodium silicate might serve either as rigid film or as expanded film. For example, a deployed flexible surface can be rigidized by allowing a film of liquid sodium silicate to dehydrate on its surface. This is, of course, similar to the previously demonstrated use of gelatins in rigidizing structures.

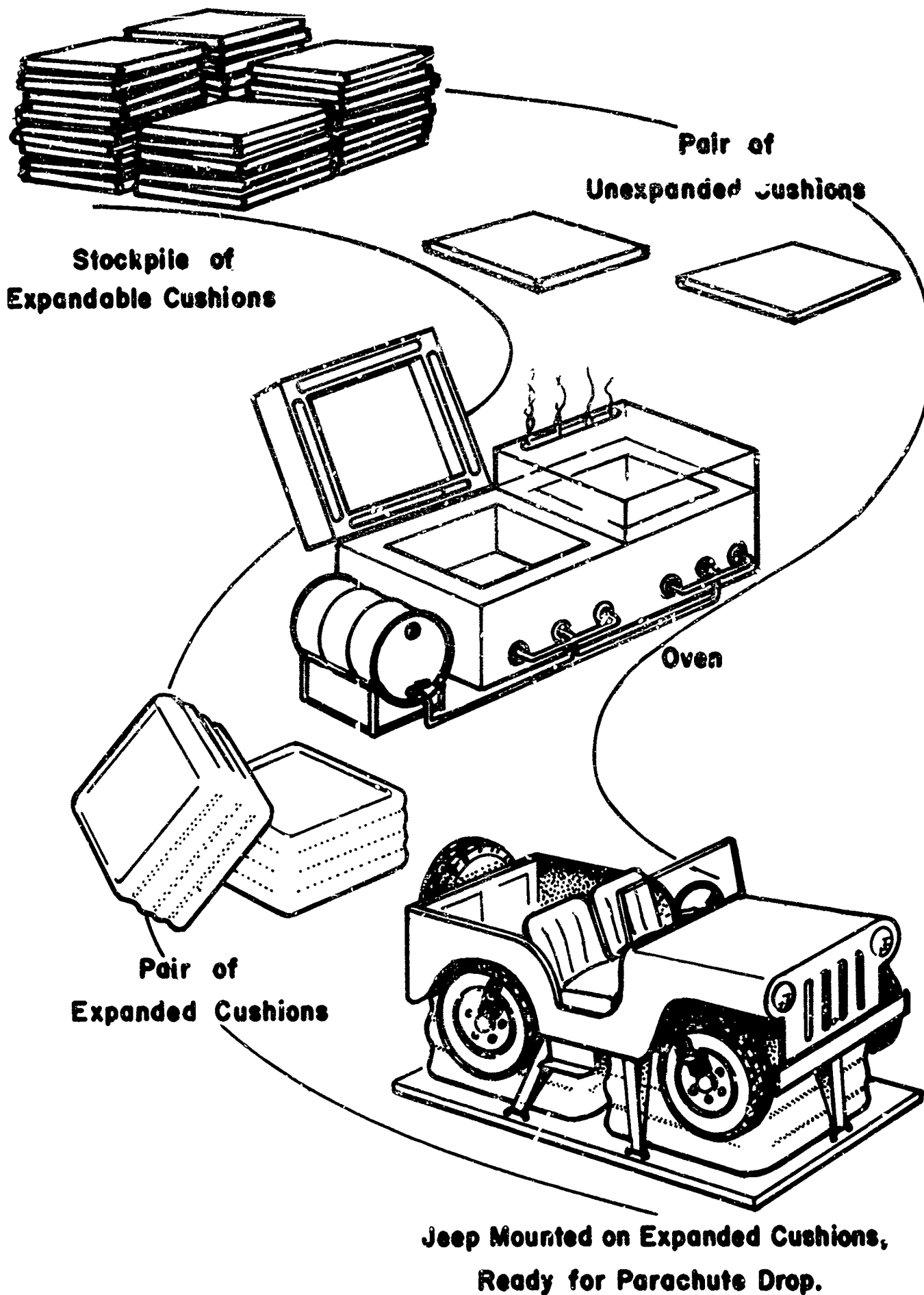


FIGURE 5. SILICATE FOAMING FOR AIR DROP CUSHIONING

Under extreme thermal exposure, the silicate film would expand into a rigid foam.

Now going a step beyond rigidizing, but not necessarily separate from it, are applications based on expanding the sodium silicate from either a viscous solution, a gel, or a hydrated solid into a rigid insulating foam. The relative merits of expanding in space from the liquid or from the solid hydrate could be evaluated only in terms of a specific application. Either form can be foamed within a vented hollow panel or on an exposed surface. The choices of energy to provide heat of vaporization for foaming in space could include radiated thermal energy, packaged electrical energy, and sheet pyrotechnic. In some applications, stored heat from adjacent surfaces would foam the silicate in vacuum. (3, 4)

Expendable Thermal Protection

Sodium and potassium silicates have maintained places as binders in the modern technology of high temperature coatings. A one-time thermal protection is common in many fields, including fire protection in structures. In that field, the intumescence of boric acid, soluble silicates and other hydrates is widely used for its one-time effective heat absorption and insulation. Studies of retention of water and of gelatin for one-time cooling of protected airframe skins have been previously reported.

The properties of soluble silicates indicate that a reinforced layer would serve as a hydrated "plaster" and would, upon exposure to high temperature (for example, during re-entry), foam into an insulating layer while releasing the bound moisture. An example of this application is illustrated in Figure 6.

Many adaptations are plausible, including the combining of an ablative surface with the foaming silicate.

CONCLUSIONS

It would appear that the heat absorption technique of allowing a hydrated coating to calcine can be developed into several useful channels to meet the missions of military and space activities.

Using hydrates which would harden under heat or vacuum exposure would provide a rigidizing technique similar to that accomplished with gels. This is a direct way to capitalize on vacuum-activated rigidization. The next step which may follow in combination with the first is the expansion, in place, of a liquid or solid hydrate into a rigid foam suitable for providing mechanical properties in expandable structures such as those under discussion.

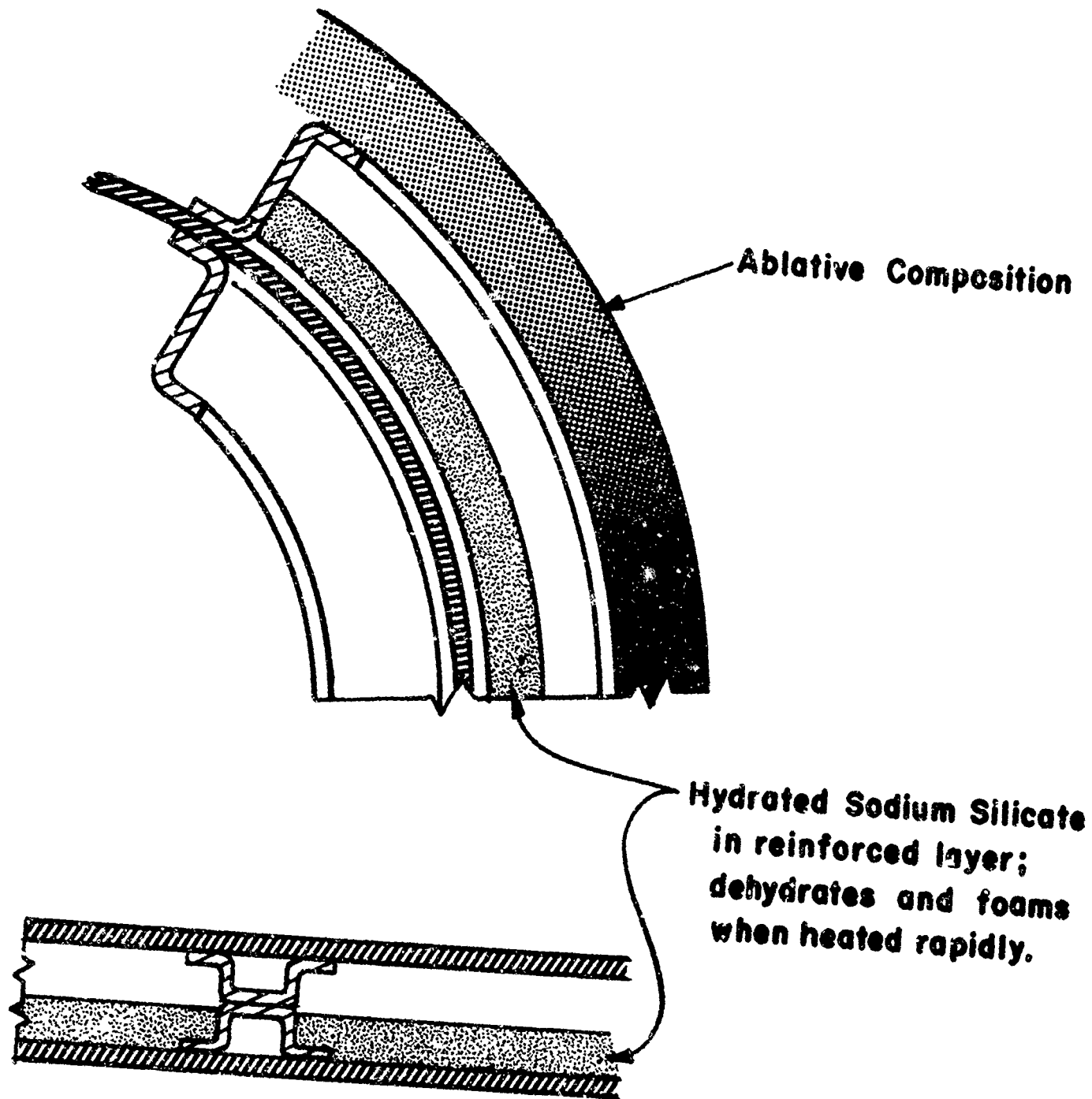


FIGURE 6. THERMAL PROTECTION OF VEHICLE WALL

In the laboratory, foaming expansion ratios range from 3 to 5 times the original liquid volume with good foam properties.

For aerospace applications, rigidizing and/or foaming from mineral hydrates such as sodium silicate probably would offer bonus advantages in thermal properties and long term stabilization compared with organic materials currently studied.

For terrestrial military missions requiring temporary shelters and air drop cushioning, the bonus advantages over reported methods are inherent environmental durability, low cost, and the simplicity of salvaging and later refilling foam-stiffened components in the field.

One of the next tasks in evaluating this material for space applications will be thermal effects in vacuum; this study would be accomplished largely in the SwRI Arc-Image Facility which can provide a sustained flux up to $3,690 \text{ Btu/ft}^2\text{-sec}$.

LIST OF REFERENCES

1. Ferrigno, T. H., Rigid Plastic Foams, Reinhold Publishing Corp., N. Y., 1963.
2. Vail, James G. and Wills, John H., Soluble Silicates—Their Properties and Their Uses, Vol. 1 and Vol. 2, Reinhold Publishing Corp., N. Y., 1952.
3. NASA Contributions to the Technology of Inorganic Coatings, National Aeronautics and Space Administration, Technology Utilization Division, NASA SP-5014, 1964.
4. Hurwicz, H. and Mascola, R., "Thermal Protection of Satellites With 'Cold Wall' Ablation," Avco Corp.; American Rocket Society, Oct. 9-15, 1961.

ABSTRACT

AN INFLATABLE THERMAL RADIATION SHIELD FOR SPACE APPLICATIONS

J. E. Marshall.

General Dynamics/Fort Worth

A structural materials study and test program have been conducted in connection with an inflatable thermal radiation shield feasibility study at GD/FW. This program, sponsored by NASA/MSFC, is directed toward the development of thermal protection systems for cryogenic-fueled space vehicles.

Preliminary investigations and analyses indicated the desirability of an inflation deployed spherical shield with permanent rigidity independent of internal pressure. The spherical shape is compatible with the inflatable concept and possesses the required thermal characteristics for minimum heat transfer. Inherent shell rigidity is required to maintain shield shape and position for an extended period considering possible leaks and meteoroid penetrations. Venting is also desirable to minimize conduction heat transfer. The required rigidity is obtained by utilizing a peculiar property of the thermal shield, the extreme low temperature on its shaded surface. This surface, carrying the highest stresses due to shield inertia loads during attitude corrections, is coated with an elastomer which is flexible at normal room temperatures. When the shield is inflated and the vehicle is properly oriented in relation to the sun, the temperature of the elastomer is reduced to something below -150°F , resulting in a simple, reliable rigidizing mechanism; the stiffening of the elastomer into a rigid hemispherical cap.

Determination of material properties and sphere rigidizing characteristics was accomplished through a series of tests. Elastomer specimens were exposed to vacuum and low temperature and tested in tension and bending at low temperature to evaluate their structural properties. Model spheres were coated with elastomers, rigidized by cooling, and test-loaded on a centrifuge to determine their load carrying capability. Extrapolations were made to estimate mass penalties required for full scale radiation shields. Results indicated that a 27-1/2 foot diameter shield, roughly that required for the earth braking stage of a proposed Mars vehicle, could withstand accelerations of at least .03 g, a reasonable value based on attitude control requirements. The mass penalty for such a sphere would be approximately 45 LBM.

AN INFLATABLE THERMAL RADIATION SHIELD

FOR SPACE APPLICATIONS*

J. E. Marshall

General Dynamics/Fort Worth

SUMMARY

A test program has been conducted to determine the structural feasibility of a low-temperature rigidized inflatable thermal radiation shield for cryogenic fueled space vehicles. Some elastomers have been evaluated for use as rigidizing coatings. Model spherical shields coated with a vinyl-base lacquer have been rigidized by cooling and centrifuge tested to determine allowable loading. These data are extrapolated for estimation of mass penalty and allowable loading of full scale shields. Results indicate that a 330-inch diameter inflatable spherical shield utilizing the low-temperature rigidizing concept would weigh approximately 45 pounds and endure lateral accelerations of about .03 g's.

INTRODUCTION

Efforts to improve the performance of space propulsion systems have resulted in much interest in and some utilization of high energy cryogenic fuels. In order to successfully incorporate a cryogenic fueled propulsion system in any extended mission space vehicle, extremely high fuel storage efficiency must be achieved. Fuel boil-off losses due to solar radiation heating become increasingly important as the mission length increases. Tank insulation, both conventional and "super-insulation", while decreasing losses, cannot approach the efficiency of a separate thermal radiation shield, standing off from the tank structure and greatly reducing tank incident energy.

For such a stand-off shield to be structurally efficient, and thus of minimum weight, it must be designed for its specific operational environment. For certain missions of interest, this operational environment is one which is almost entirely free of significant inertia or aerodynamic loading. For a Mars mission, for instance, a shield would be subjected only to loads due to solar

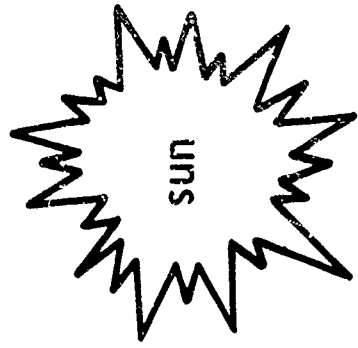
* This work was supported by NASA Contract NAS8-11317 and monitored by R. D. Wegrich, Propulsion and Vehicle Engineering Laboratory, NASA/MSFC, Huntsville, Alabama

pressure, micrometeoroid impact, and attitude control impulses; for periods of several months. Designing for the high aerodynamic and/or inertia loadings of boost or other high thrust mission phases will result in an unnecessarily heavy structure. Therefore, in order to minimize shield weight through avoiding these extreme loadings, it is necessary to investigate the possibilities of variable geometry or expandable structure. This concept will permit the design of a compact structural configuration suited to the extreme loading of the high thrust periods and yet efficient in its primary application, when it may be expanded to attain its required size, shape, and position.

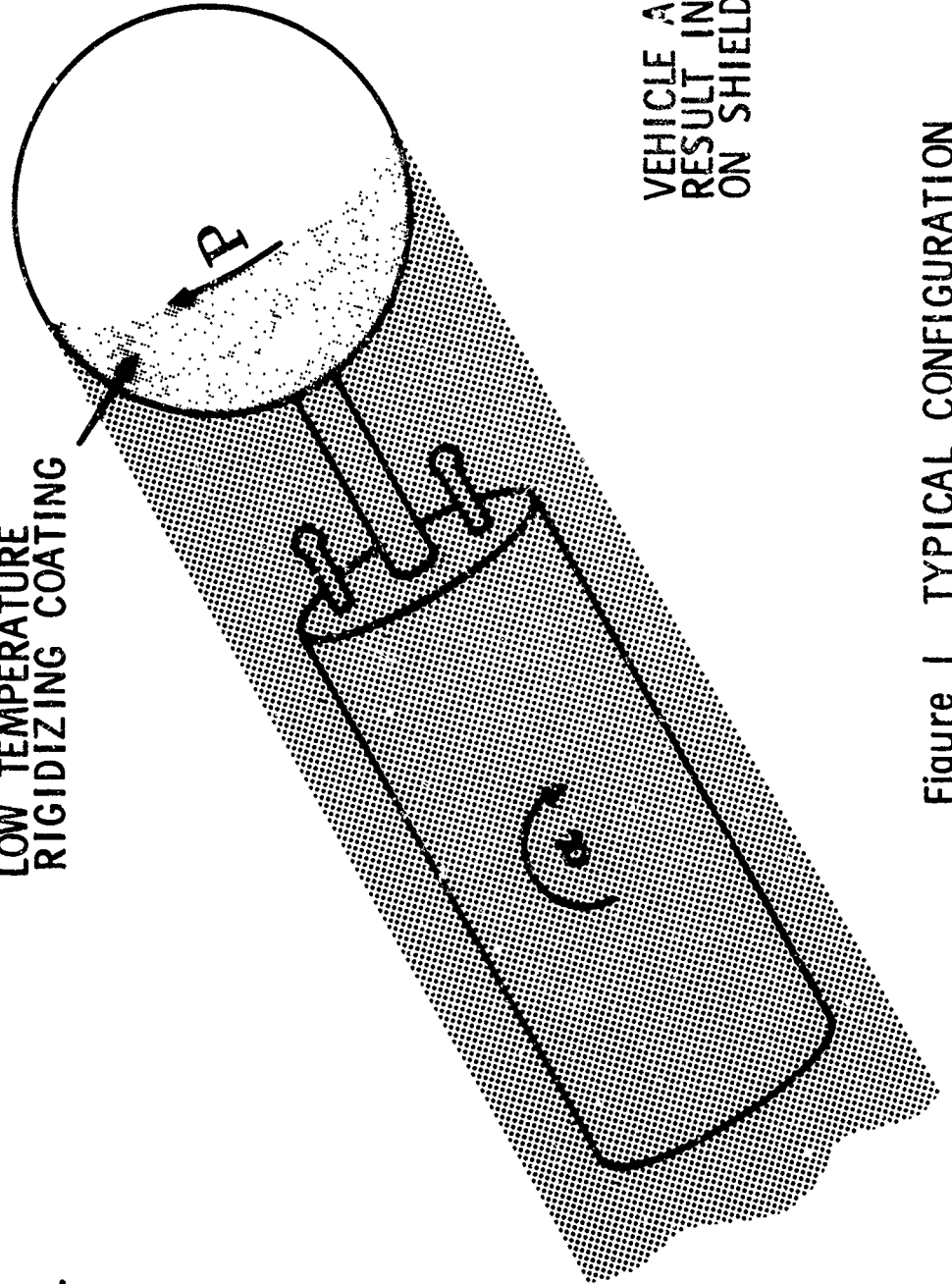
From thermal considerations, a spherical shield is desirable. This configuration is also suitable for the design of a minimum weight inflatable structure. For the very lightly loaded shields, a reinforced or stiffened inflatable sphere and circular cylinder support appear feasible. Minimum weight and stored volume, flexibility of shape of storage container, simplicity, and reliability are some of the features of such a system. To minimize heat transfer across the shield, the inflating gas will be allowed to escape following complete inflation. This venting removes the shell's stabilizing pressure and makes it necessary to supply, by other means, rigidity sufficient to resist excessive shield deflections or deformation. After reviewing several possible rigidization methods, it was decided to investigate a system utilizing a peculiar property of the shield; the low temperature existing on its shaded side. This low temperature would be used to rigidize a coating of a normally flexible elastomer applied to the spherical surface. Solar orientation of the vehicle would insure the maintenance of this low temperature on the support side of the spherical shield. This temperature is estimated to be from -100 to -300°F.

Figure 1 shows a typical configuration, with the spherical shield mounted on the aft end of a vehicle along the longitudinal centerline. The vehicle attitude control system maintains the necessary solar orientation. Attitude control system pulses generate vehicle angular accelerations causing lateral inertia loads on the shield structure. These are the principal shield loads.

The preliminary investigation of this self-rigidizing system required evaluation testing of possible coating materials to determine their relative value as low temperature structural reinforcement. The basic sphere was to be constructed of an aluminum-mylar-aluminum sandwich material. This material, used in the Echo II balloon satellite and designated by the manufacturer (G. T. Schjeldahl Co., Northfield, Minn.) as X-15 laminate, has a total thickness of .00075 in. Due to the lack of an adequate analytical technique for the design of a spherical shell under the expected loading, further testing was necessary to determine the degree and extent of reinforcement required to rigidize a given shield.



LOW TEMPERATURE
RIGIDIZING COATING



VEHICLE ACCELERATIONS, α ,
RESULT IN INERTIA LOADS, P,
ON SHIELD.

Figure 1 TYPICAL CONFIGURATION

DESCRIPTION OF TEST PROGRAM, PROCEDURE, AND RESULTS

The test program was conducted in three parts:

- (1) Determination of structural properties of possible reinforcing materials.
- (2) Evaluation of the relative abilities of these materials to rigidize the spherical shield configuration.
- (3) Determination of the degree and extent of rigidization required to maintain shape and position of the shield under predicted loading conditions.

The rigidizing materials included in the test program were:

- (1) Polyurethane Foam
- (2) Neoprene
- (3) Natural Rubber
- (4) Latex
- (5) Silicone Rubber (Dow Corning X-3-0902 RTV)
- (6) Viton "A" (DuPont Fluorocarbon)
- (7) EC776 (Minnesota Mining and Manufacturing)
- (8) Polysulfide Rubber (Thiokol)
- (9) Vinyl Base Lacquer (Brolite DC-25)

DETERMINATION OF STRUCTURAL PROPERTIES OF ELASTOMERS

Test specimens were prepared by applying a coating of the candidate materials to six-inch squares of the X-15 material. These nine squares were then cured completely and cut into strips, one inch by six inches. Two strips of each material were set aside as controls. The remaining four strips of each material were exposed to an environment of 4×10^{-7} mmHg, and -124°F for a period of 48 hours. Typical test specimens are shown in Figure 2. The environmental exposure test equipment is shown in Figure 3. Following this exposure, the specimens were examined for changes in weight and appearance. No significant changes were detected in any of the specimens. Three specimens of each material were then tested in tension and three in bending as shown in Figures 4 through 6. All tests were run at -124°F . Figures 7 and 8 show typical data recorded from these tension and bending tests. With the limited number of specimens tested and the short exposure time, there was no definite indication of structural degradation or improvement due to exposure. Table 1 is a summary of some significant structural properties from these tests. An attempt has been made to evaluate the strength per unit weight and stiffness per unit weight or efficiency of the materials. The strength-weight relationship has been represented by a simple ratio of maximum measured tensile stress divided by the unit weight of the composite material in pounds per square foot. The stiffness parameter shown combines the maximum calculated bending stress, an effective modulus of elasticity, and the moment of inertia of the specimen; all divided by the unit weight of the composite material in pounds per square foot. All specimens were 1.0 inch

TYPICAL BEAM SPECIMENS AFTER TEST






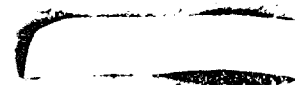

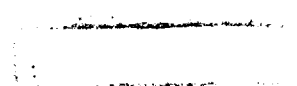

 VITON A	 EC-776	 LATEX RUBBER
 NATURAL RUBBER	 THIOKOL RUBBER	 SILICONE RUBBER
 NEOPRENE RUBBER	 POLYURETHANE FOAM	 VINYL CHLORIDE -ACETATE

Figure 2 RIGIDIZING MATERIAL TEST SPECIMENS (STRIPS)

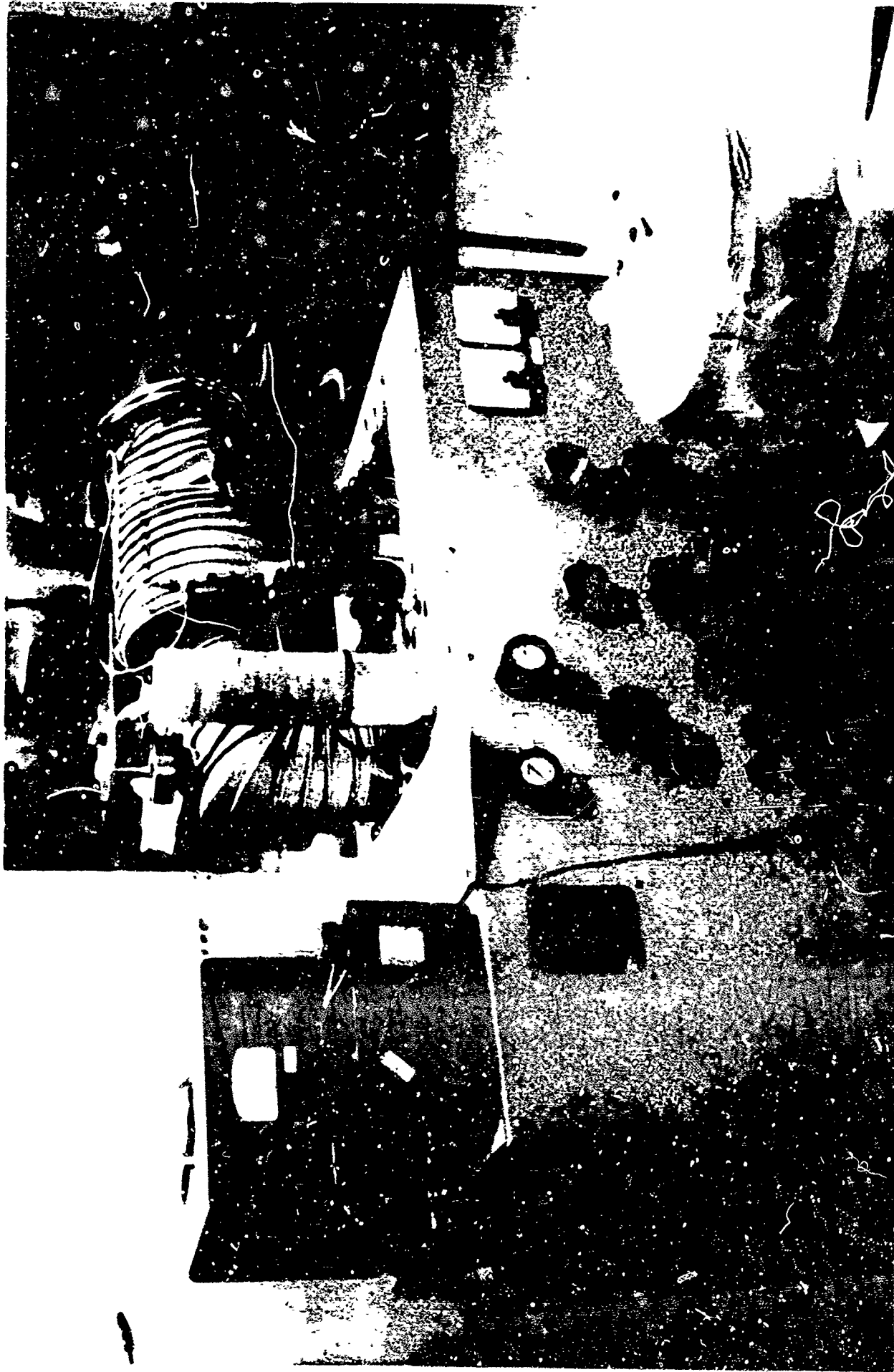


Figure 3 LOW-TEMPERATURE VACUUM EXPOSURE TEST



Figure 4 TENSILE TEST



Figure 5 BENDING TEST

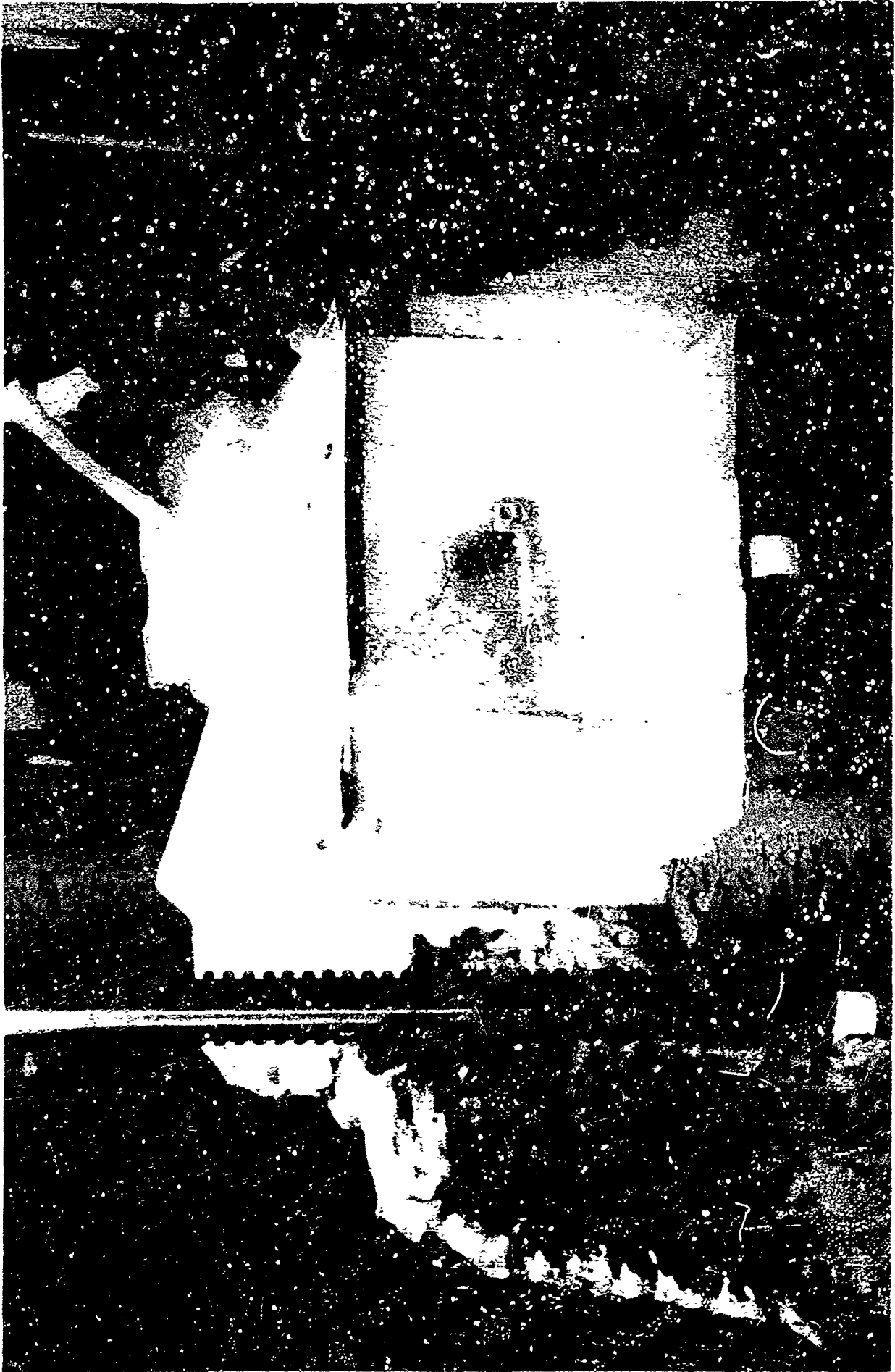


Figure 6 BENDING TEST IN OPERATION

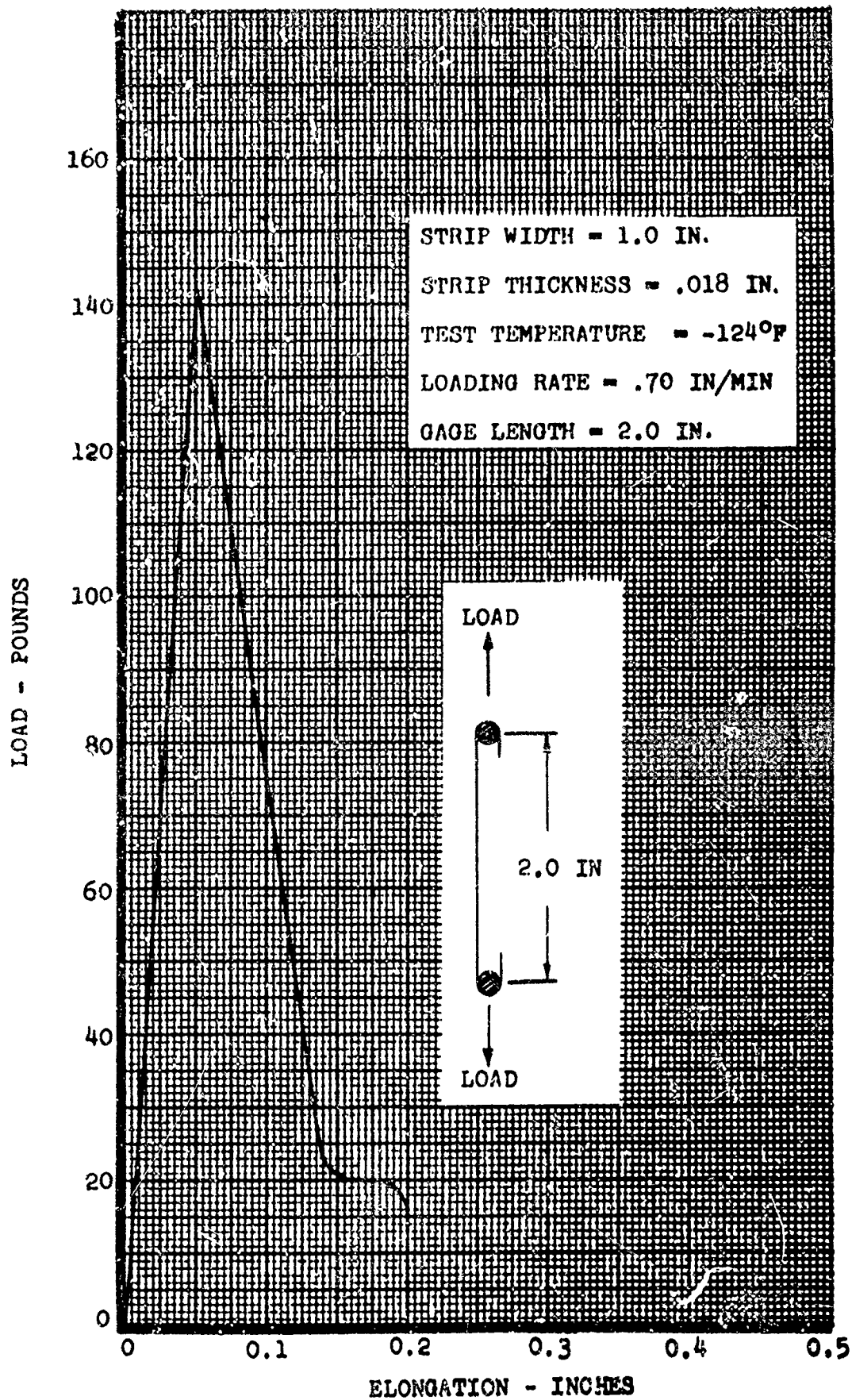


Figure 7 TENSILE TEST DATA FOR VINYL-BASE LACQUER COATING

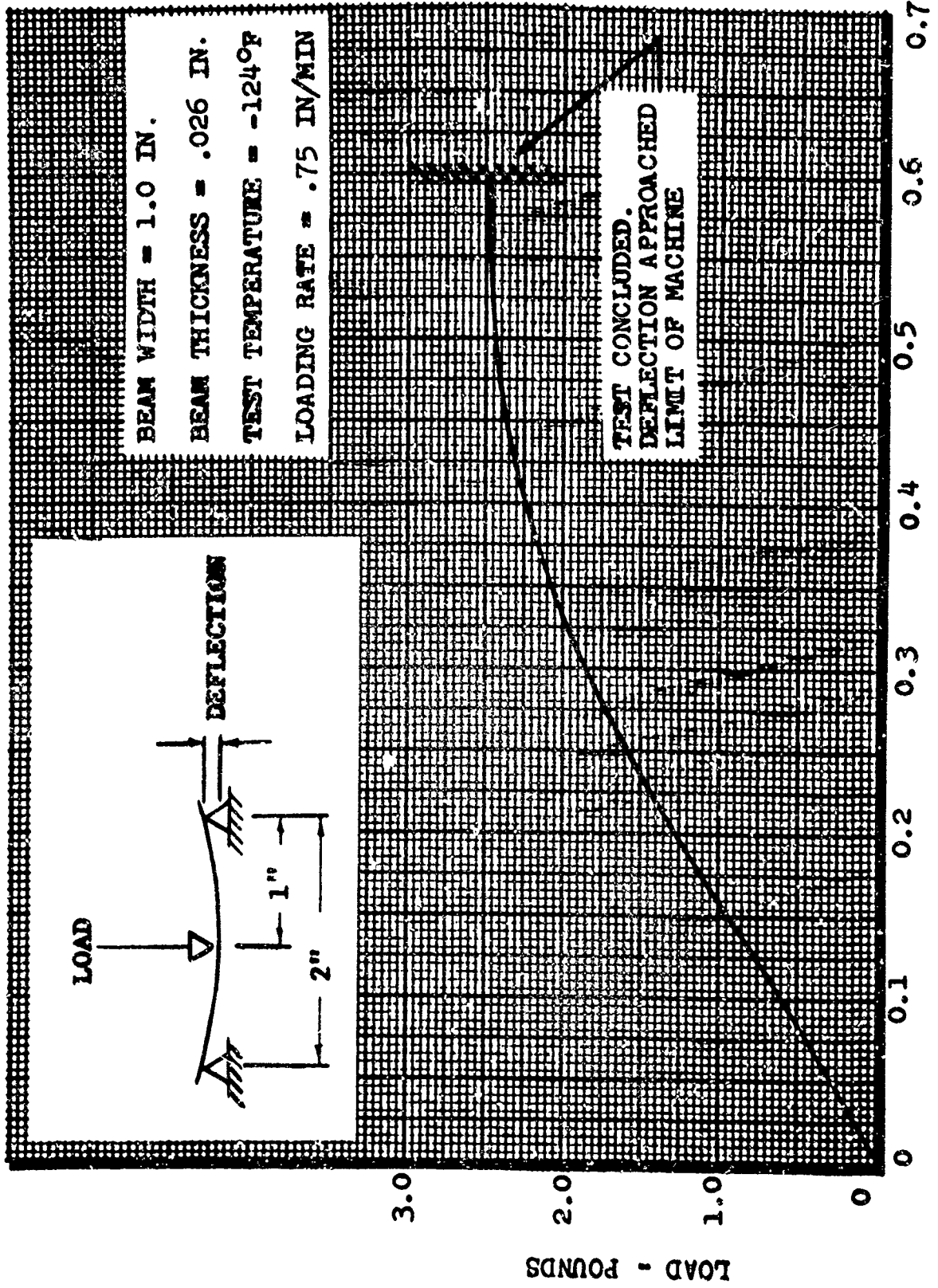


Figure 8 BENDING TEST DATA FOR VINYL-BASE LACQUER COATING

Table 1 EVALUATION OF POTENTIAL RIGIDIZING MATERIALS

SPECIMEN NO	MATERIAL	WEIGHT (LB/FT ³)	THICKNESS (IN.)	MAXIMUM TENSILE STRESS, FT. (PSI)	ELONGATION AT MAX. LOAD (%)	STRENGTH PARA-METER, METER FT. UNIT WT.	MAXIMUM BENDING STRESS, FB (PSI)	MAXIMUM BEAM DEFLECTION (IN.)	EFFECTIVE MODULUS E _{EFF} (PSI x 10 ⁶)	STIFFNESS PARAMETER E _{EFF} F _{BI} UNIT WT.
1		.06564	.25	100	16	1520				
2		.06787	.25	112	22	1650				
3	Polyurethane Foam	.07244	.25				111	.275	.00108	2125
4		.05156	.25				74	.275	.00072	1340
5 (e)*		.07523	.25				101	.275	.00098	1690
6 (e)		.07427	.25	90	12	1210				
7		.19195	.029				5700	.120	1.09	66000
8		.21445	.032	645	4	3000				
9	Neoprene	.19355	.030	564	4	2910				
10		.21998	.033				6500	.110	1.20	106400
11 (e)		.21166	.028	1275	3	5030				
12 (e)		.19670	.030				7300	.110	1.48	123700
13		.15492	.030				3200	.400	.18	8350
14		.15587	.025	1800	27	11550				
15	Natural Rubber	.16049	.025	1660	23	10000				
16		.16557	.030				4900	.56	.17	19700
17 (e)		.14993	.035	648	21	4350				
18 (e)		.14902	.027	1229	9	7840				
19		.15671	.022				11800	.32	.67	169000
20		.19857	.037				11200	.26	.70	212000
21	Latex	.21669	.044	455	16	2100				
22		.21117	.041							
23 (e)		.18926	.033	515	11	2720				
24 (e)		.20563	.030	667	19	3250				
25		.26728	.041				3500	.24	.24	18000
26		.29760	.048	509	7	1710				
27	Silicone Rubber	.30192	.044	564	7	1870				
28		.27411	.041				4000	.24	.27	22300
29 (e)		.31501	.041	552	8	1752				
30 (e)		.29124	.044	414	8	1420				
31		.24364	.035	3125	8	12850				
32		.22782	.031				9000	.51	.38	37200
33	Viscon A	.20435	.026	3510	21	19100				
34		.23082	.038	4650	36	19900				
35 (e)		.24138	.034				8600	.60	.27	46100
36 (e)		.24811	.037				11500	.48	.43	84400
37		.11047	.020	740	11	6700				
38		.11677	.021				16900	.41	.85	61000
39		.11387	.022				10100	.37	.83	64600
40	EC 6776	.10082	.021	562	6	5500				

* CONTROL SPECIMEN

Table 1 (Continued)

SPECIMEN NO.	MATERIAL	WEIGHT (LB./FT.)	THICKNESS (IN.)	MAXIMUM TENSILE STRESS, PSI (PSI)	ELONGATION AT MAX. LOAD (%)	STRENGTH PARA-METER P, UNIT WT.	MAXIMUM BENDING STRESS, PSI (PSI)	MAXIMUM BEAM DEFLECTION (IN.)	EFFECTIVE MODULUS E_{EFF} (PSI x 10 ⁴)	STIFFNESS PARAMETER $E_{EFF} \times I$ UNIT WT.
41 (c)	Vinyl-Bone Lacquer	.09551	.018	655	1	6450	7900	.41	.71	28600
42 (c)		.10153	.018	7850	3	59500				
43		.13189	.026				11000	.52	.54	58000
44		.14724	.024				10900	.52	.58	53800
45		.13472	.022	5020	15	39100				
46		.12832	.020	4000	20	30700				
47 (c)		.13027	.017				11900	.50	.80	50300
48 (c)		.12661	.012	1715	2	21900	21100	.35	2.37	150000
49		.13675	.011				11700		1.92	
50		.07845	.024	4180	8	21600				
51	.09336	.030	945	6	4600					
52	.19349	.035	1450	5	5700					
53 (c)	Polymulfide Rubber	.25426	.016	3120	14	11100				
54 (c)										
55 (c)										

wide. Thicknesses were as shown in Table 1. All bending test specimens were tested as center-loaded simple beams with a 2.0 inch span. Tension strips were 2.0 inches long. The equations defining the parameters in Table 1 are:

$$F_T = \text{Maximum Tensile Stress} = \frac{\text{Maximum Measured Tensile Load}}{(\text{Width, 1.0 in.})(\text{Specimen Thickness, } t)}$$

$$F_B = \text{Maximum Bending Stress} = \frac{Mc}{I} = \frac{3P}{t^2}$$

Where P = Maximum Beam Load From Bending Test
 t = Specimen Thickness
 c = t/2

$$E_{EFF} = \text{Effective Modulus of Elasticity} = \frac{Pl^3}{48I\delta} = \frac{P}{6I\delta}$$

Where P = Maximum Beam Load From Bending Test
 I = Specimen Moment of Inertia = $\frac{bt^3}{12}$
 l = Beam Length = 2 inches
 δ = Beam Deflection at Maximum Load
 b = Specimen Width = 1 inch

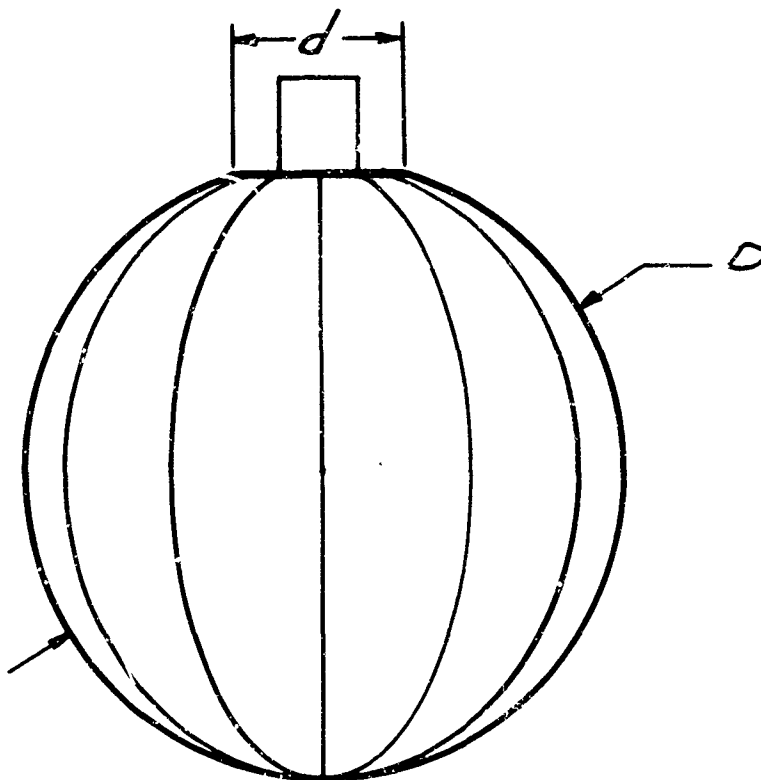
ASSESSMENT OF RELATIVE RIGIDIZATION VALUES

The results of this first phase of testing indicated which materials might be suitable rigidizers. These indications, with other considerations of ease of handling and application, determined which materials would be applied to 30-inch diameter spheres for actual rigidization tests. These materials were:

- (1) Vinyl Base Lacquer
- (2) Viton A
- (3) Latex
- (4) Neoprene
- (5) EC776

These spheres were fabricated from twelve gores of X-15 material and attached to a flanged support cylinder as shown in Figure 9. To facilitate fabrication and testing, the support cylinder was represented by a rigid metal cylinder with a rigid flange supporting the sphere. An investigation of the rigidity of the actual support cylinder was not part of this study, interest being in the stability of the "neck" of the sphere near the sphere-cylinder intersection.

Each of the selected materials was applied to one of the spheres as shown in Figures 10 and 11, covering what would be its supported or shaded hemisphere. These coatings were applied by spraying to a thickness of between .010 and .020 inch. Specimens were weighed before and after coating to determine the weight of the coating. Thicknesses were measured using a Tinsley Thickness Gage. Tabulated thicknesses are the average of several measure-



Sphere Diameter, D	Flange Diameter, d
15 in.	3.5 in.
24 in.	5.0 in.
30 in.	7.0 in.

Figure 9 TEST SPHERE GEOMETRY



Figure 10 30-INCH-DIAMETER SPHERE COATING FIXTURE

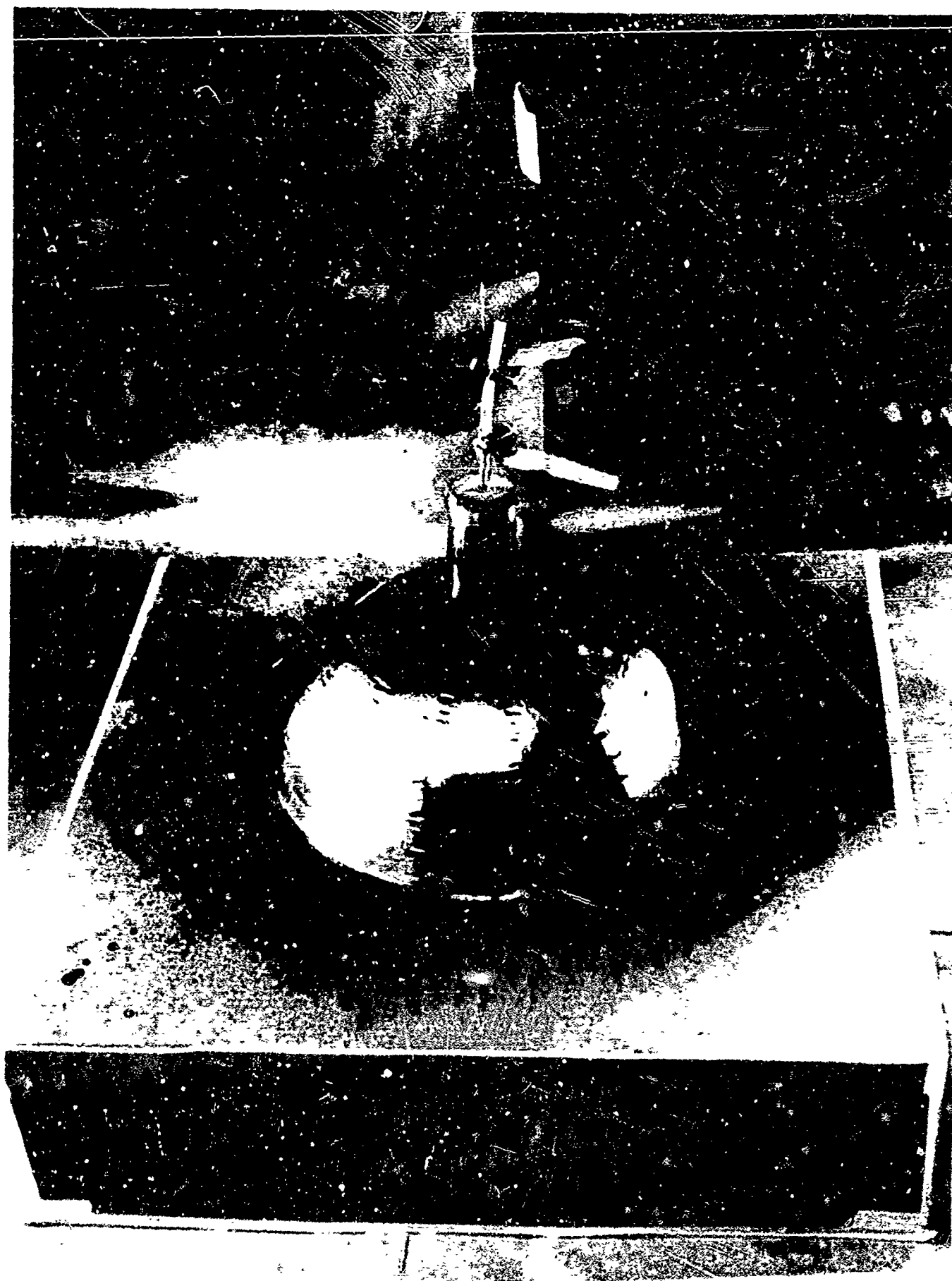


Figure 11 15-INCH-DIAMETER SPHERE COATING FIXTURE

ments taken around the critical "neck" of the sphere (see Table 2).

These spheres were tested by applying inertial loads normal to the sphere support axis using a centrifuge. To provide the desired loading, an extension arm was fitted to a Genisco Model 50159 Accelerator, giving a maximum radius of rotation of about 12 feet. A lightweight 42-inch cubic container was mounted on the end of the boom. This container was a reinforced, foam-insulated, corrugated cardboard box which protected the specimen from airloads and, after being cooled with liquid nitrogen, maintained the proper reduced temperature during testing. Wedge fairings were added to the forward and aft faces of the box for drag reduction. This test equipment is shown in Figures 12 and 13. Test spheres were suspended in the box as shown in Figures 14 and 15. A sphere surface temperature of approximately -130°F was maintained throughout the test. As the rate of rotation of the centrifuge was increased, corresponding sphere deflections were noted and points of failure were determined. Using these measured rotational rates, the specimen radius of rotation, and the specimen mass, the sphere loading could be calculated.

Sphere surface temperature near the "neck" was monitored using thermocouples taped to the surface. These thermocouple voltages were amplified by precision amplifiers mounted directly on the rotating boom. The amplified signals were then fed through slip rings on the centrifuge shaft for remote reading. Sphere deflections and failure were indicated by a wireless system to avoid noise problems inherent with the slip rings. This consisted of a battery powered electronic oscillator mounted on the specimen box. As the conducting surface of the deflecting sphere approached a coil in the oscillator circuit, a corresponding decrease in signal strength was detected by a field strength meter at the console and converted to sphere position. The components of this instrumentation are shown in Figures 16 and 17.

After installation of the test specimen in the box as shown in Figure 15, an initial pressure of about ten inches of water was held in the sphere by inflation with gaseous nitrogen. With this pressure holding the shape and position of the sphere, liquid nitrogen was pumped into the box. When the sphere had cooled sufficiently to become rigid (below about -50°F), the internal pressure was released and the box covered. The addition of liquid nitrogen was continued until the temperature of the rigidized surface reached -150°F . At this point the liquid nitrogen was shut off and the centrifuge started. For the time required for one test run, approximately two minutes, an essentially constant temperature was maintained by boiling of residual liquid nitrogen in the bottom of the box. In the event of a delayed or prolonged run, the maximum temperature rise was only 20 or 30 degrees. Such a rise had no noticeable effect on the specimen rigidity. Some runs were purposely prolonged to observe specimen behavior under constant load and increasing temperature.

Table 2 shows the results of these tests of the relative rigidizing abilities of the five elastomers. Due to the power limit of the centrifuge, maximum radial acceleration attainable

Table 2 RIGIDIZING MATERIAL EVALUATION 30-INCH SPHERES

Coating Material	Sphere Uncoated Weight (gms)	Sphere Coated Weight (gms)	Weight Of Coating (gm)	Coating Thickness (in)	Ultimate Load (g's)
Latex	257	487	230	.012	3.43
Vinyl Base Lacquer	266	540	274	.010	3.67
Neoprene	253	440	187	.015	2.76
Viton A	254	782	528	.020	>4.13
EC776	260	542	282	.020	>4.13
None			0	0	.59

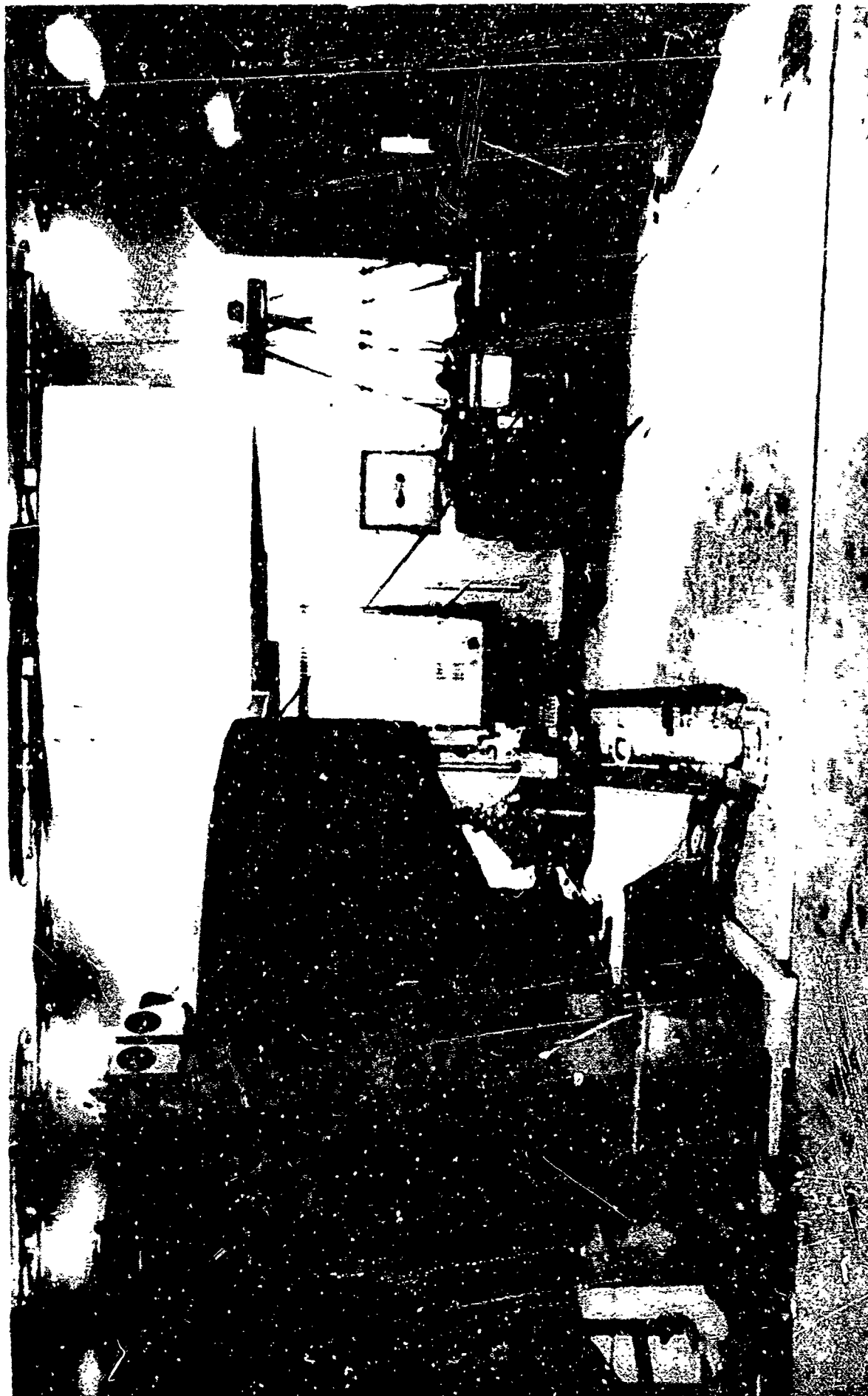


Figure 12 SPHERE LOADING TEST



Figure 13 SPHERE LOADING TEST

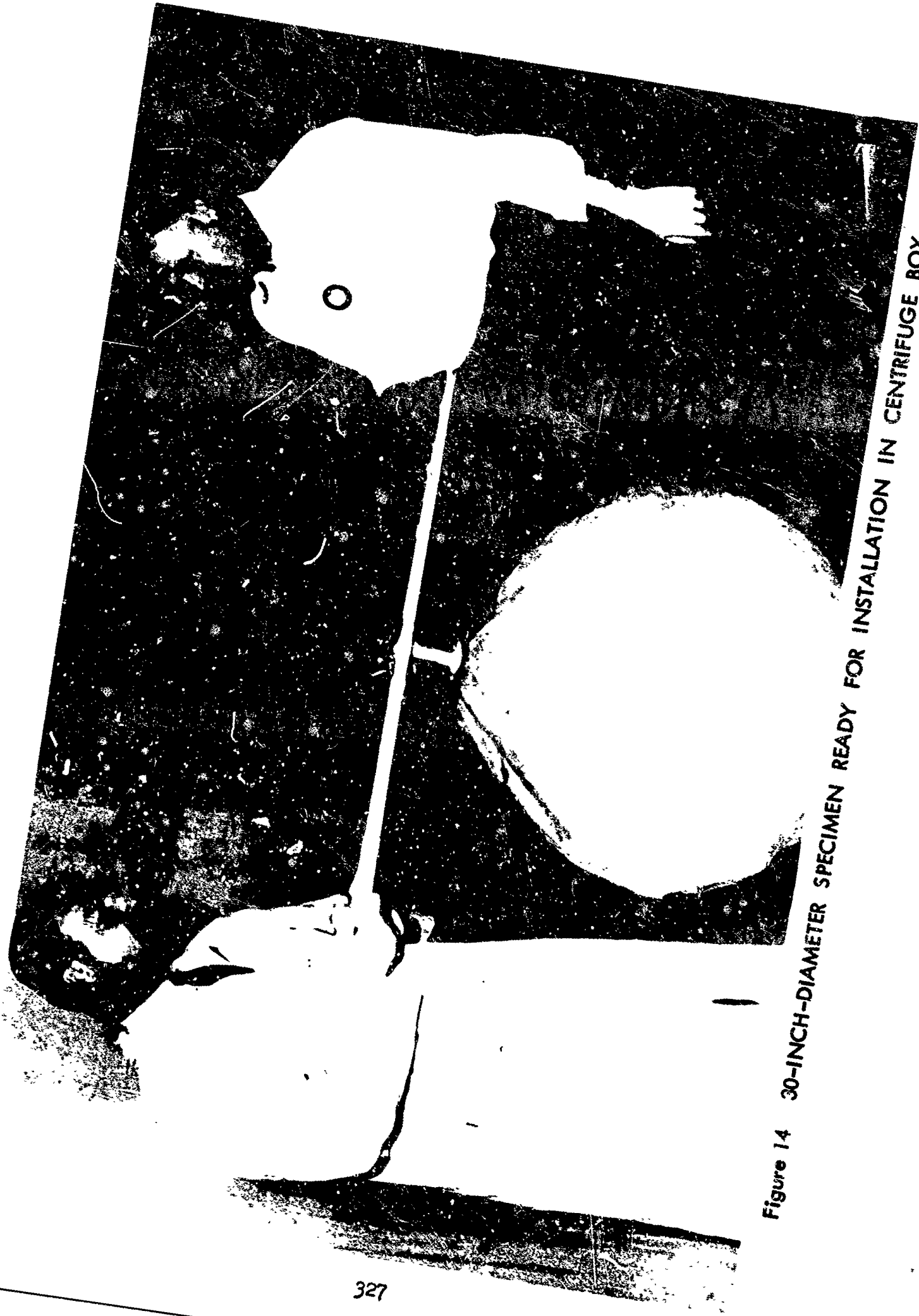


Figure 14 30-INCH-DIAMETER SPECIMEN READY FOR INSTALLATION IN CENTRIFUGE BOX

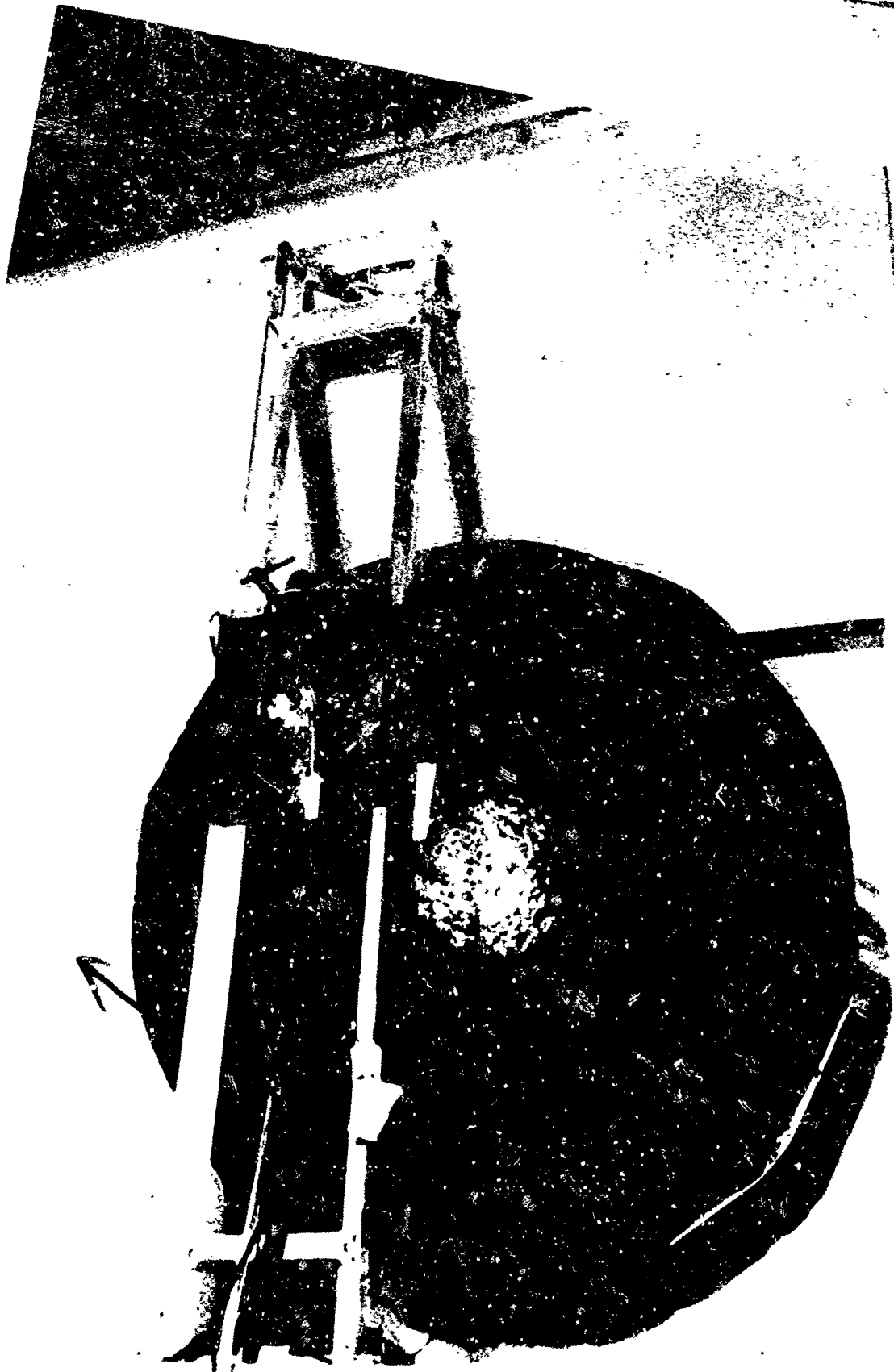


Figure 15 30-INCH-DIAMETER SPECIMEN INSTALLED IN CENTRIFUGE BOX
(TEMPORARY PRESSURE ATTACHED)

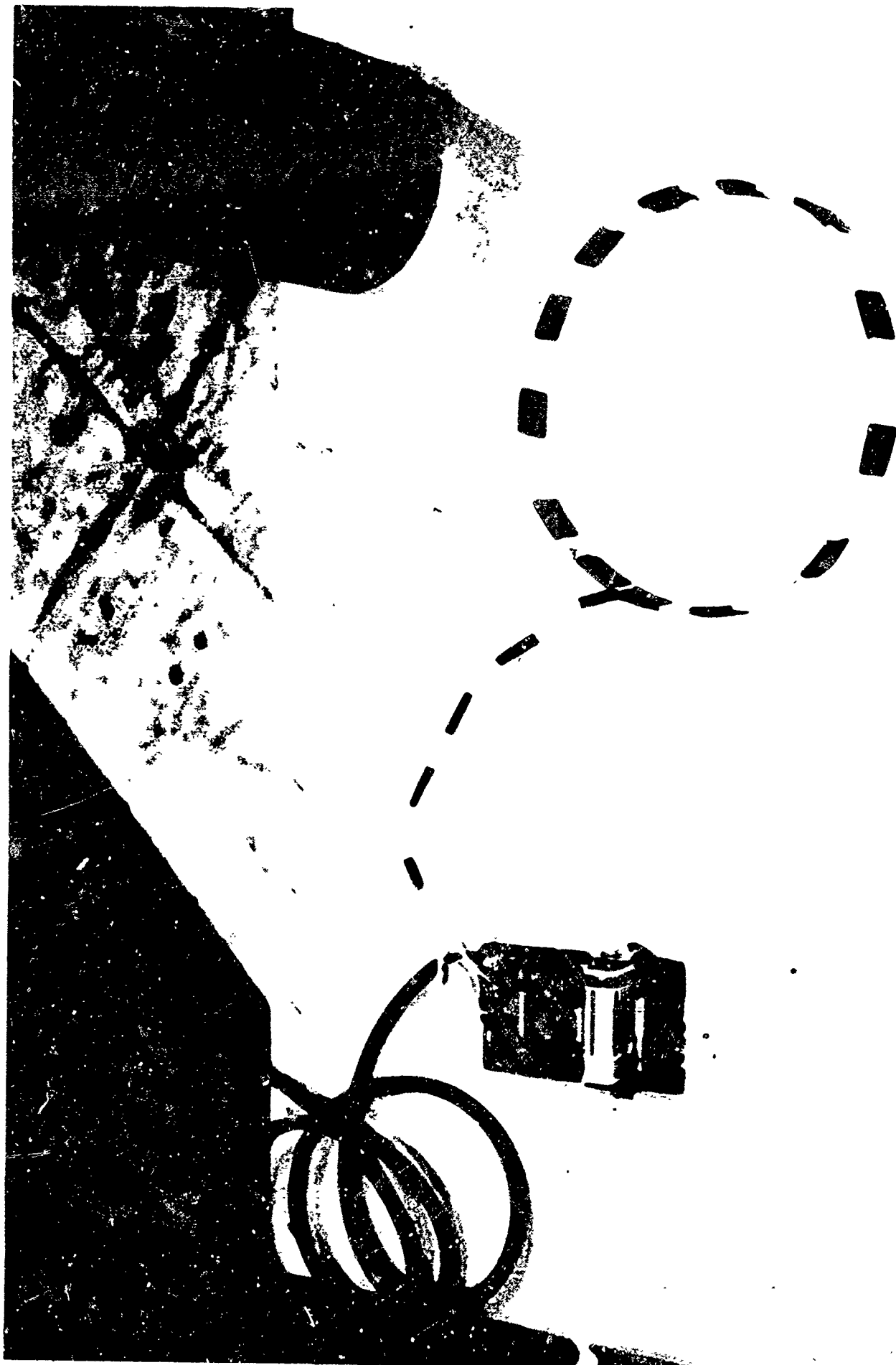


Figure 16 SPHERE POSITION SENSING SYSTEM



Figure 17 SPHERE POSITION SENSING SYSTEM INSTALLED

was 4.13 g's. At this point the "Viton A" and EC776 coated spheres had not failed. Subsequent modifications have raised this centrifuge limitation.

All sphere failures were, as expected, buckling of the material near the neck as shown in Figure 18. Most of the materials were not permanently damaged by this buckling. Only the neoprene cracked. The previous material tests had shown the neoprene to be a brittle material. The remaining materials were evaluated as follows:

- | | |
|--------------------|---|
| Viton A | - Heavy, expensive, and relatively difficult to handle. These disadvantages may ultimately be outweighed by its apparent rigidizing properties, as yet not completely evaluated. |
| EC776 | - Apparently a good rigidizing material, but the low-density coating obtained in these tests may not be reproducible. Bubbles in this coating are thought to be responsible for its efficiency. |
| Latex | - Latex has marginal flexibility for proper storage after an extended cure at room conditions. |
| Vinyl Base Lacquer | - This material is inexpensive, easy to handle and apply, and rigidizes satisfactorily. This and the Viton were the only materials which did not fail in the bending tests. |

DETERMINATION OF RIGIDIZING COATING REQUIREMENTS

On the basis of test data and other considerations, vinyl base lacquer was selected for the coating material for the remaining sphere tests. Fifteen, twenty-four, and thirty-inch diameter spheres were fabricated, coated, and tested as described previously. Both the coating thickness and extent of coverage were varied for these tests. Indications were that a coating covering the complete hemisphere is no better than an equal thickness covering one-half of the hemisphere in the polar cap area. The range of coating thicknesses was from 1.5 to 10 mils. Data from these tests are shown in Table 3. Figure 19 shows the relationship between sphere deflection and lateral load in g's obtained from the centrifuge tests. The sudden increase in slope of some of the curves is characteristic of thin shell buckling, as is the initial deflection as stiffening wrinkles are established.

The bending moment at the neck of a cylinder-supported sphere loaded by inertia normal to its support axis may be expressed as

$$M = r^3 n (\omega_2 + 3\omega_1)$$



Figure 18 TYPICAL SPHERE FAILURE

Table 3 SPHERE DATA
VINYL BASE LACQUER COATING

Specimen No	Uncoated Weight (gm)	Coated Weight (gm)	Weight Of Coating (gm)	Coating Thickness (in)	Extent Of Coverage*	Ultimate Load (g's)
1 -15 in.	106	120	14	.0045	1/4	3.55
2 -15 in.	107	124	17	.0040	1/4	4.25
3 -15 in.	106	124	18	.0055	1/2	9.15
4 -15 in.	107	125	18	.0040	1/2	4.75
II-1-15 in.	95	100	5	.0014	1/4	4.0
II-2-15 in.	95	104	9	.0027	1/4	3.8
II-3-15 in.	95	100	5	.0015	1/4	2.9
1 -24 in.	168	192	24	.0033	1/4	3.5
2 -24 in.	166	203	37	.0055	1/4	5.0
3 -24 in.	168	222	54	.0070	1/4	6.15
1 -30 in.	264	328	64	.0040	1/2	1.56
2 -30 in.	256	313	57	.0040	1/4	1.12
3 -30 in.	261	328	67	.0040	1/2	1.12
4 -30 in.	257	298	41	.0040	1/4	1.12
X -30 in.	266	540	274	.0100	1/2	3.67

* Portion of complete sphere

30 Inch Diameter Spheres
Vinyl Base Lacquer Coating
Temperature = -125°F

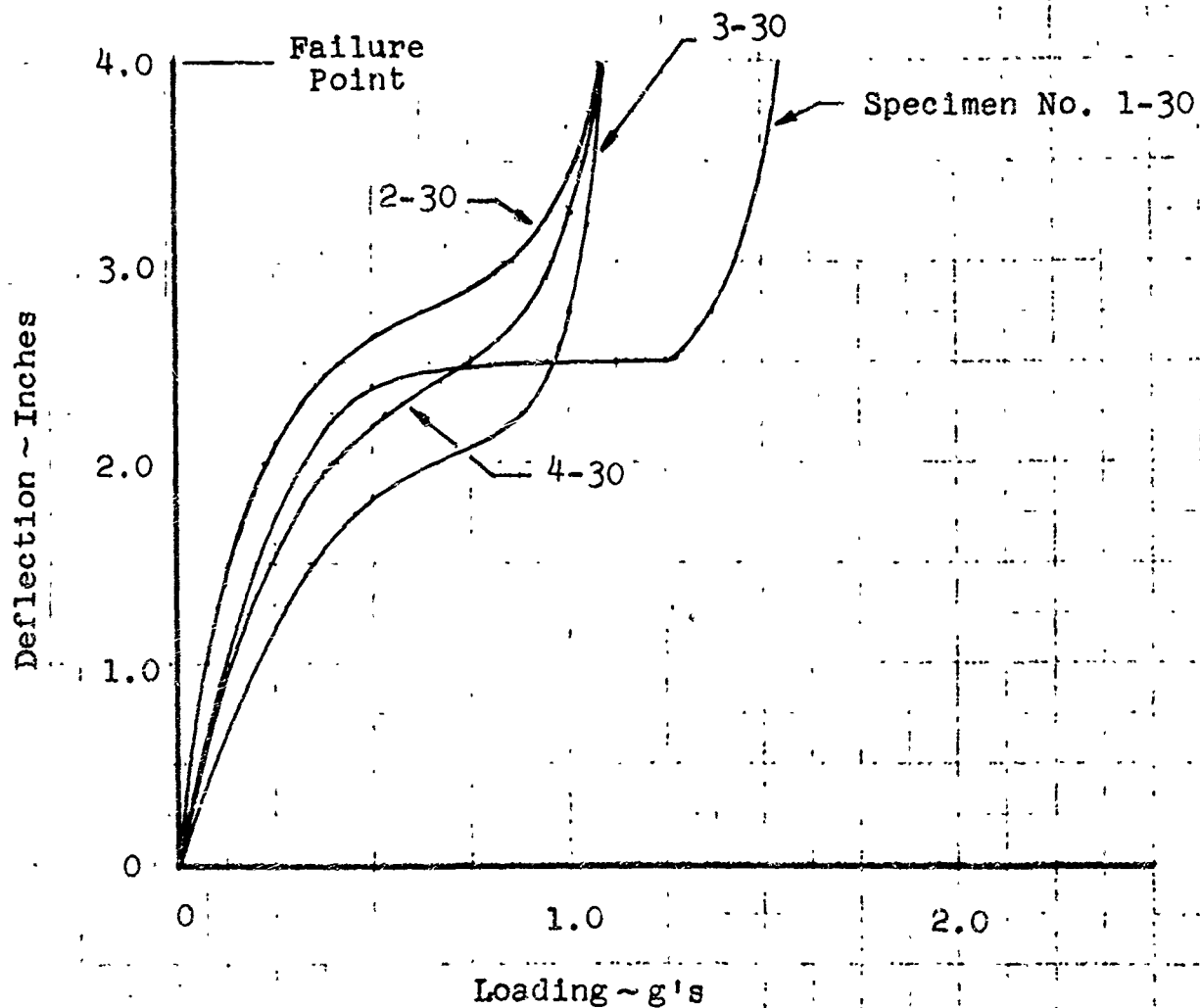


Figure 19 SPHERE DEFLECTION FOR VINYL BASE LACQUER COATED SPHERES

Where r = radius of sphere (in.)
 n = inertial loading (g's)
 ω_2 = unit weight in pounds per square inch of sphere surface on support side of sphere equator (coated hemisphere)
 ω_1 = unit weight in pounds per square inch of sphere surface on far (uncoated) hemisphere
 M = bending moment (in-lbs)

Therefore, for spheres of similar unit weights (i.e., the same thickness of coating, t_c), the loading at the critical area can be seen to be proportional to r^3n . The critical buckling load on a thin shell elastic structure is assumed to be a function of the ratio of shell radius to thickness, r/t . Table 4 summarizes these loading and geometric parameters for the test specimens.

EXTRAPOLATION OF TEST DATA TO FULL SCALE SHIELD GEOMETRY

The results of the sphere rigidization tests were extrapolated to estimate the suitability of the low temperature rigidizing concept for application to a proposed Mars Mission Vehicle. Figure 20 shows data from Table 4 with extrapolation to a 330-inch diameter sphere with vinyl base lacquer coating thicknesses of 4 and 10 mils (total thicknesses of .00475 and .01075 inches, respectively). The estimated masses and load carrying capabilities from this extrapolation are shown in Table 5. For the 330-inch diameter shield with a 10 mil coating the allowable lateral load is estimated to be .0356 g's. For a hypothetical vehicle whose center of gravity is 50 feet from the shield center, this allowable shield load corresponds to an attitude control angular acceleration of $1.31 \text{ }^\circ/\text{sec}^2$.

Table 4 SPHERE TEST SUMMARY

VINYL BASE LACQUER COATING

Specimen	Radius "r" (in)	Coating Thickness "t _c " (in)	Total Thickness "t" (in)	r/t	Loading At Failure "n" (g's)	r ³ n
1 -15 in.	7.5	.0045	.00525	1430	3.55	1490
2 -15 in.	7.5	.0040	.00475	1580	4.25	1780
3 -15 in.	7.5	.0055	.00625	1200	9.15	3840
4 -15 in.	7.5	.0040	.00475	1580	4.75	1975
II-1-15 in.	7.5	.0014	.00215	3480	4.0	1680
II-2-15 in.	7.5	.0027	.00345	2170	3.8	1595
II-3-15 in.	7.5	.0015	.00225	3330	2.9	1220
1 -24 in.	12	.0033	.00405	2960	3.5	6040
2 -24 in.	12	.0055	.00625	1920	5.0	8620
3 -24 in.	12	.0070	.00775	1550	6.15	10600
1 -30 in.	15	.0040	.00475	3160	1.56	5290
2 -30 in.	15	.0040	.00475	3160	1.12	3800
3 -30 in.	15	.0040	.00475	3160	1.12	3800
4 -30 in.	15	.0040	.00475	3160	1.12	3800
X -30 in.	15	.0100	.01075	1394	3.67	12420

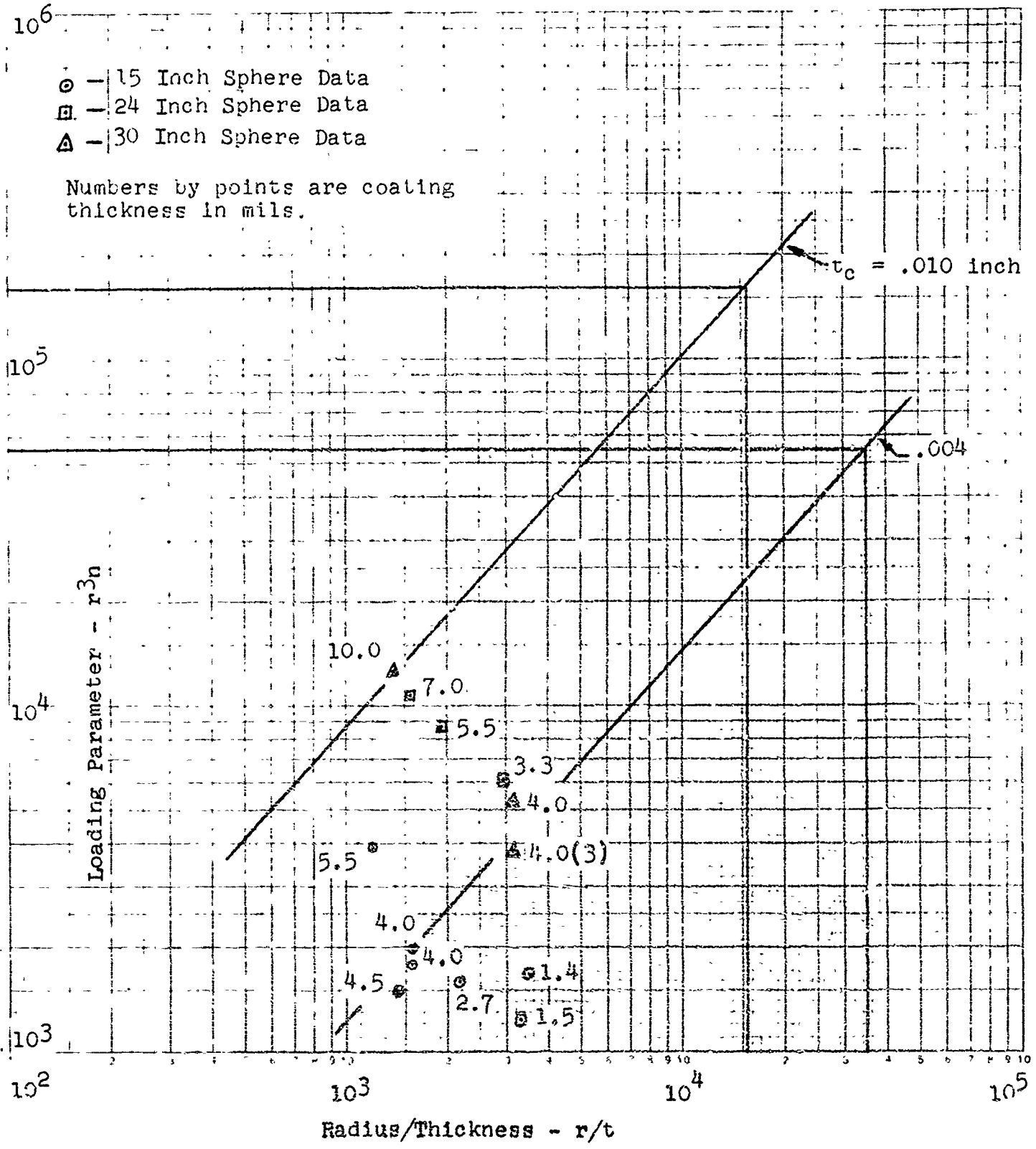


Figure 20 EXTRAPOLATION OF TEST DATA FOR VINYL BASE LACQUER COATING

Table 5 MASS ESTIMATION - FULL SCALE SPHERICAL SHIELD

Diameter (Inches)	Basic Sphere Mass (LBM)	Coating Thickness (in)	Coating Mass -25% Of Surface Coated (LBM)	Total Sphere Mass (LBM)	Ultimate Lateral Load (g's)
330	23	0.004	9	32	0.0123
330	23	0.010	22	45	0.0356

A PREDISTRIBUTED FOAM FOR RIGIDIZING MEMBRANE STRUCTURES IN SPACE

N. Jouriles

Goodyear Aerospace Corporation

INTRODUCTION

Early concepts of rigidizing membrane structures involved the generation of the rigidizing material in space and its distribution over the membrane structure in space. The rigidizing material was a urethane foam. This method is illustrated in Figure 1, which shows an egg-shaped membrane structure. The portion attached to the hub is a paraboloid (or solar concentrator); the opposite portion is a hemisphere that completes the pressure envelope. A film jacket attached to the paraboloid forms a space between the paraboloid and the film.

When the structure is inflated to a specific pressure, it takes on a specific contour. Then the rigidizing material is generated and injected into the space between the solar concentrator and the jacket. After the foam has set and cured, the spherical portion is cut away, leaving a rigid paraboloid in space (Figure 2).

A problem exists, however, in the even distribution of the rigidizing material. Because distribution problems have occurred in ground applications, it is not unreasonable to presume a low probability of accurate distribution with large structures in space. Such structures in this instance are the size of the Echo I satellite, with a paraboloid of 40 to 50 ft in diameter.

The objective of a program sponsored by NASA-Langley* was to develop and analyze a material that could be predistributed over the surface to be rigidized in space. The resulting material was an azide-base polyurethane foam, which was used in rigidization experiments performed in vacuum chambers on solar concentrators up to 2 ft in diameter.

A thermally activated urethane foam system was selected because it did not require an auxiliary blowing agent and because the urethane technology had already been developed to a high degree. The urethane system also offered flexibility in the selection of a foam formulation that would produce the desired physical characteristics.

In this program, various azide structures were investigated, and an optimum one selected for use in this application; a foam formulation was developed

*Contract No. NAS 1-3301 from the National Aeronautics and Space Administration, Langley Research Center, Hampton, Va.

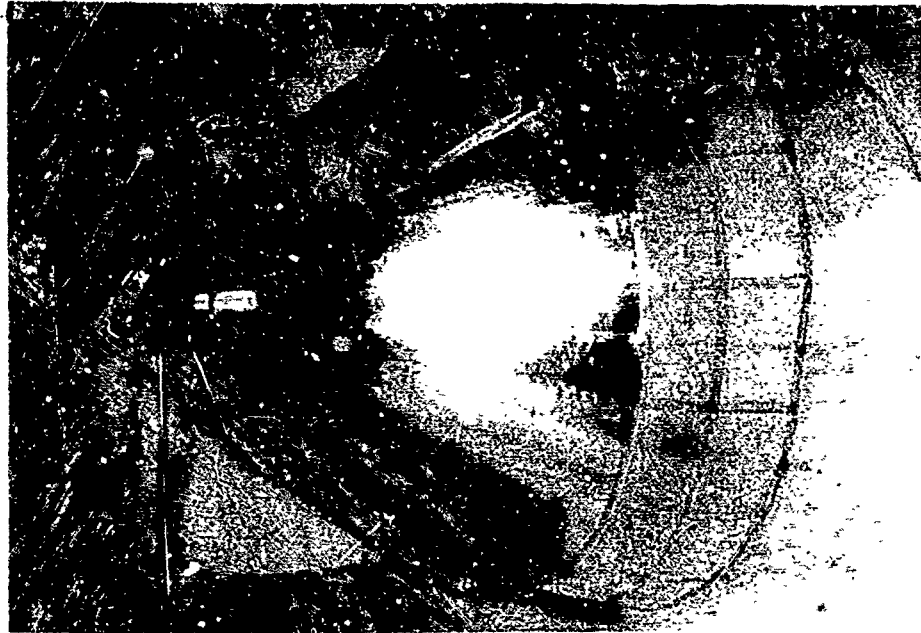


Figure 1 - Inflatable Solar-Concentrator Model



Figure 2 - Rigidized Inflatable Solar-Concentrator Model

and made adaptable to the space-rigidizing of solar concentrators; the physical properties of the foam product were determined and their effectiveness in space was established; and the effects of this rigidizing process on the paraboloidal contour were determined.

The azide-base polyurethane foam offered promise, because it could be produced in vacuum with only the application of heat and because it offered a solution to the problem of distributing foam in space. But additional work is needed to advance the state of the art of this new pre-distributed foam.

This paper discusses the development of the process conditions, the production and testing of the foam product, the rigidizing of 2-ft models in vacuum, and contour measurements of the models.

FOAM PRODUCT AND PROCESS DEVELOPMENT

In the development of the foam product, a number of goals were set up for the production of a foam that will rigidize in the space environment. A hypothetical 300-naut-mi orbit was selected. Some of these goals are:

1. Triggering temperature: 175 F (the temperature should be high enough to prevent an inadvertent reaction and low enough to require a minimum heat input)
2. Sublimation tendency: 10 percent after 100 hr in vacuum (should be 10 percent or less after exposure to a vacuum of 10^{-5} torr so that the rigidizing process can react after a delayed period in orbit)
3. Rate of azide rearrangement: 50 min or less (this goal was set so that the rigidizing process would be completed in one orbit)
4. Reaction rate of isocyanate: set in 30 min; cure in 1 hr (this goal was set for the same reason as that in No. 4 to complete the rigidizing process in one orbit)
5. Heat release: 15 cal per square inch (this goal was set to minimize adiabatic temperature rise and to prevent distortion of a smooth mirror surface)

Figure 3 shows the foam processing sequence. The basic material applied to the space structure is shown in the dotted rectangle. A few catalysts and surfactants complete the formulation. As heat is applied, the first reaction is the triggering of the azide at 175 F in Step 1. Upon decomposition of the azide, or by Curtius's rearrangement, an isocyanate, additional heat, and some nitrogen are produced. The heat produced by the azide plus the heat supplied originally are now sufficient to release the blocked isocyanate in Step 2. The isocyanate then combines with the polyol resin in Step 3 to produce the polyurethane foam. This foam is of the rigid open-cell variety, which enables it to be removed from the vacuum chamber without damage.

Figure 4 shows the temperature history of the rigidizing process (in the change in scale on the abscissa, the shaded area represents 1 min of time). Heat is applied at the rate of approximately 12 F per minute. At 175 F, the azide is triggered. Its exotherm causes a temperature spurt to 350 F. At this point, the blocked isocyanate is released and combines with the polyol resin to produce the foam. The foam sets in less than 1 min and gradually cools to the environmental temperature.

Figure 4 is a typical temperature-history curve showing flexibility in the heating rate. A 100-percent "go" probability is obtained when the triggering temperature is reached in from 4 to perhaps 30 min. Slower heating periods are possible, and some have been tried with somewhat less than a 100-percent go probability.

How can this required heat be applied to a large surface? One approach could be by the use of selected surfaces. If the space vehicle can be presumed

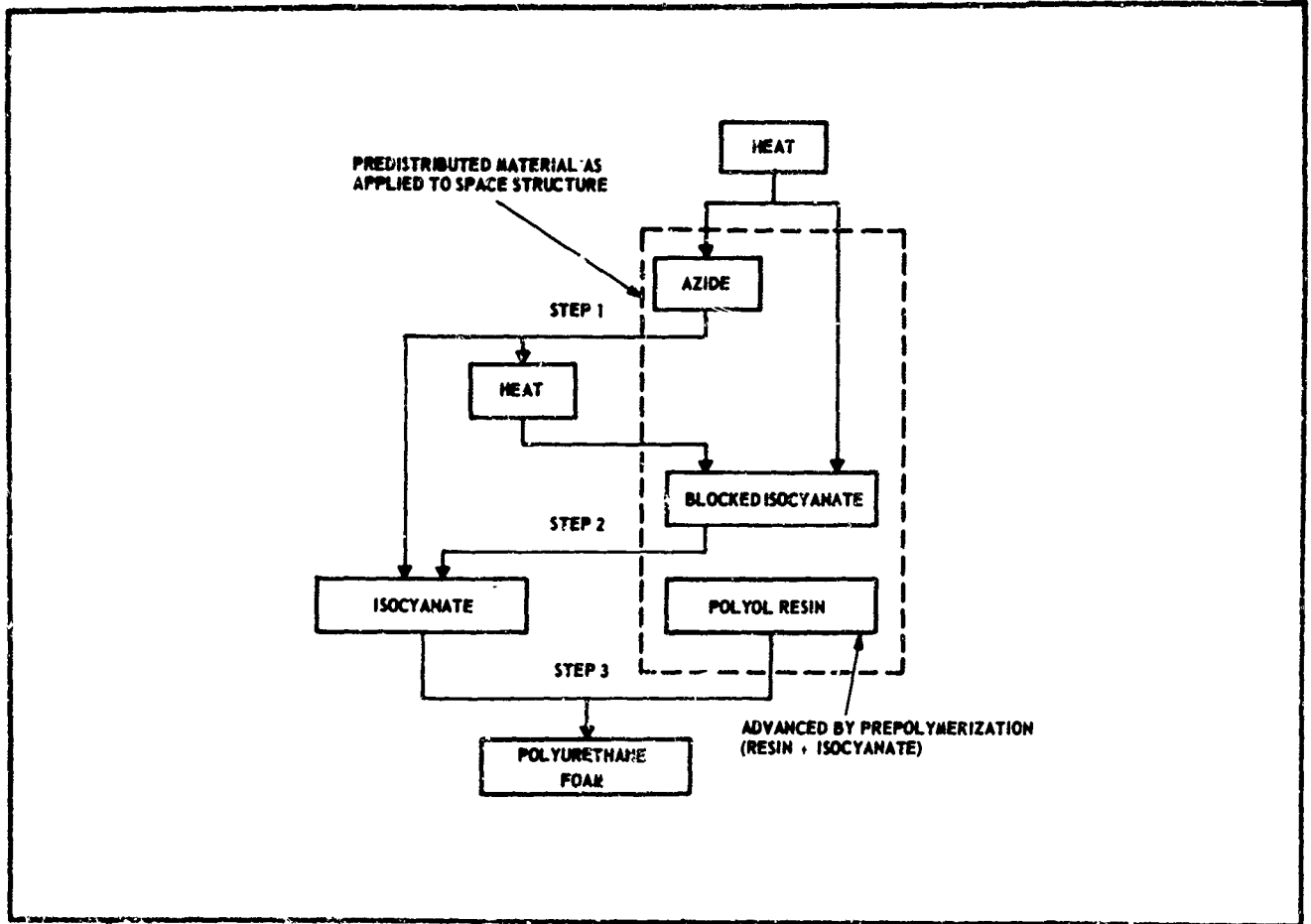


Figure 3 - Block Diagram of Rigidizing Process

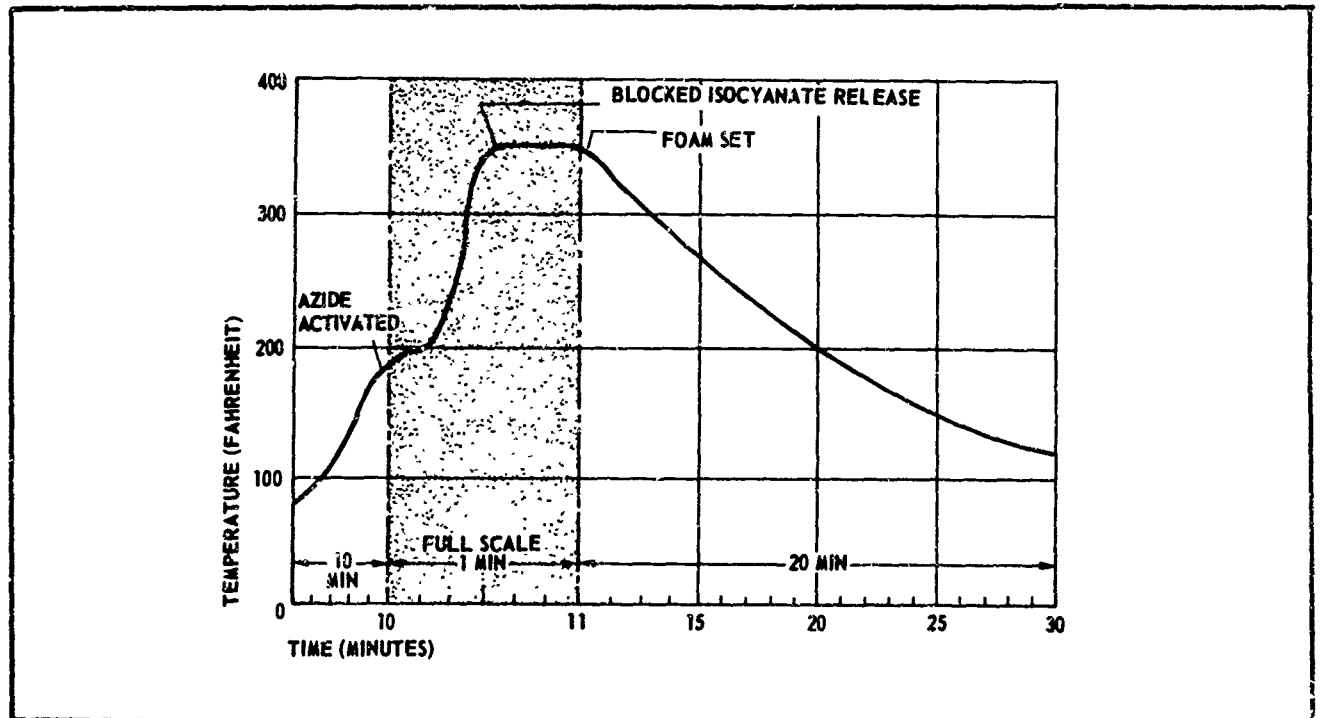


Figure 4 - Temperature History of Rigidizing Process

to have the capability of orientating the solar concentrator, so that the back side faces the sun, then a selected surface can absorb the required heat. The surface materials that were investigated are given in Table I.

TABLE I - SELECTED SURFACE MATERIALS FOR
BACK SIDE OF SOLAR CONCENTRATOR

Surface	Absorp- tance, α	Emit- tance,
Aluminized Mylar	0.12	0.05
Black surface	0.9	0.9
Cr-Ni-V*	0.94	0.40
Cobalt oxide	0.93	0.24

*Chromium-nickel-vanadium.

Again, at a hypothetical orbit of 100 naut mi and a period of 100 min, the calculated surface temperatures shown in Figure 5 can be obtained by the selected surfaces. With aluminized Mylar, the temperature buildup is not rapid enough to assure a go condition. The cobalt oxide reaches 175 F in about 3 min and continues on past 220 F without leveling off. The Cr-Ni-V coating reacts in a manner similar to that of the cobalt oxide. A black surface, however, builds up to 175 F in 5 min and begins to level off at 215 F, a very desirable temperature history for this material.

As shown in Figure 4, the azide is triggered at 175 F, and the exotherm causes the material temperature to spurt to 350 F where it lingers for a minute or so and begins to cool down. Figure 6 shows the cooldown rates of those same selective surfaces, starting at 350 F. The cobalt oxide levels off at about 460 F; the Cr-Ni-V at 380 F. The aluminized Mylar with its low emit-tance cools down at a slow rate. The black surface, however, cools down in a highly acceptable manner.

On the basis of this brief thermal analysis, the heat requirement can probably be met by painting the surface black and orienting the solar concen-trator so that the back side would face the sun for the rigidizing process.

PREPARATION OF PHYSICAL TEST SPECIMENS

The predistributed material can be applied to a membrane as either a paste or as sheets, like tile. With the latter, a ball of the material (resem-bling a ball of dough or clay) is placed in a hydraulic press and formed into a sheet of the desired thickness. This can then be cut and formed in patterns for almost any desired configuration.

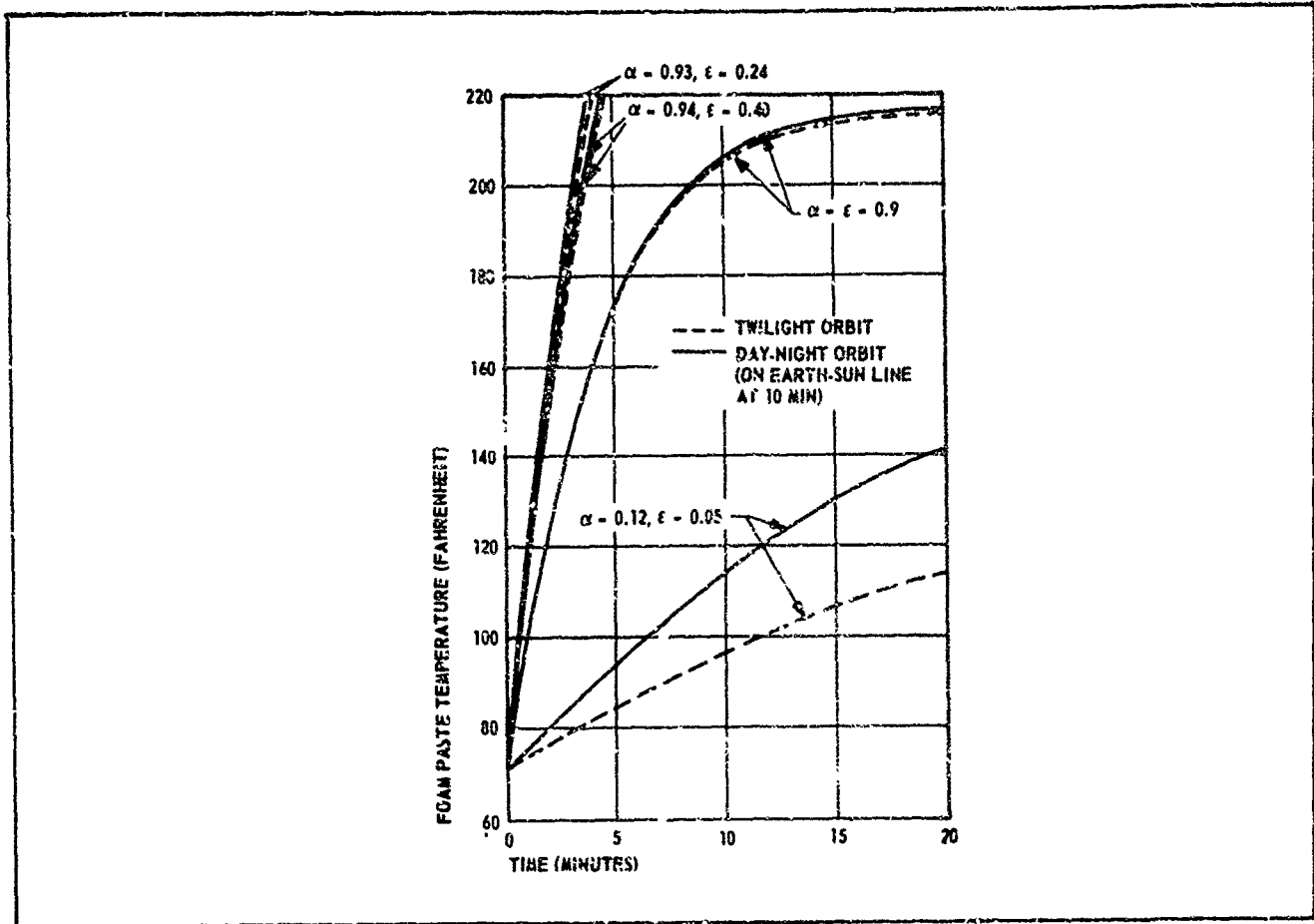


Figure 5 - Surface Temperatures versus Time (Reversed Orientation)

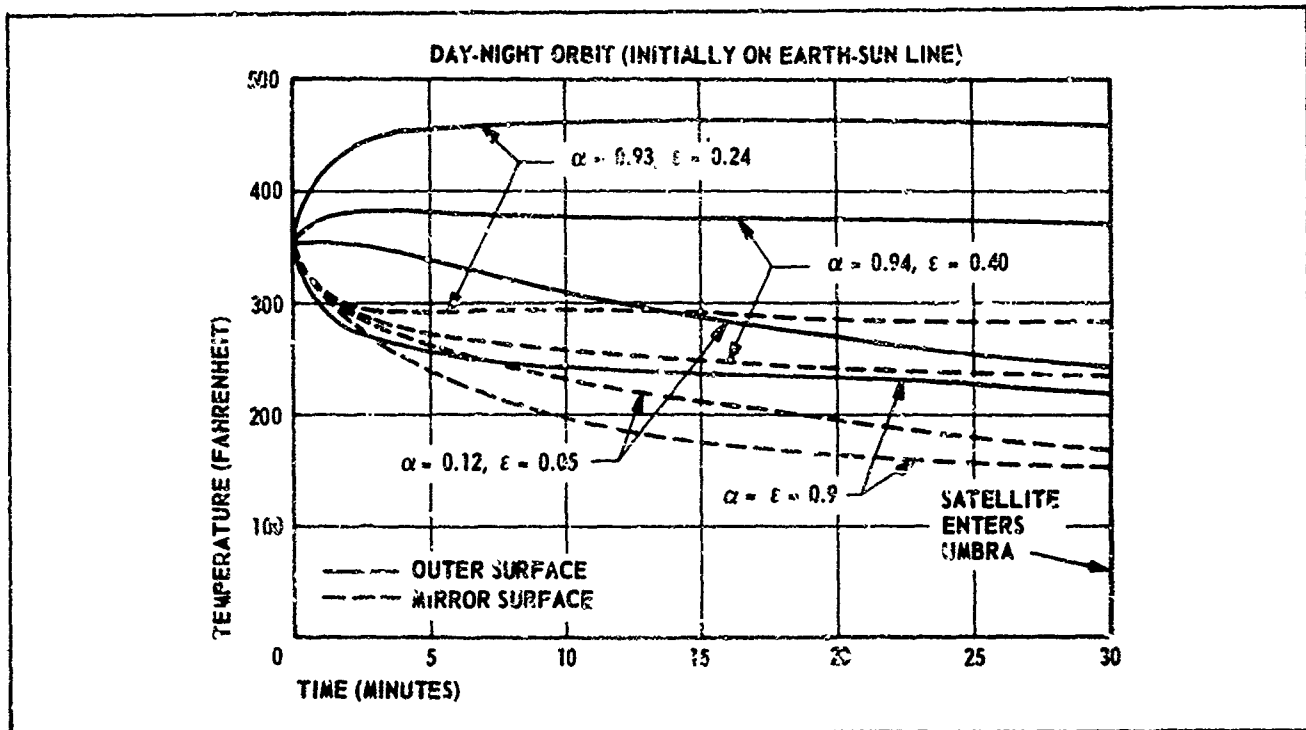


Figure 6 - Foam Temperatures versus Time (Reversed Orientation)

As a paste, the predistributed material can be troweled on, as shown in Figure 7. The membrane is then clamped to a metal ring (Figure 8), which then is inserted in a bell jar (Figure 9). The bell jar is sealed and pumped down to a pressure of 10^{-5} torr. The quartz lamps are then turned on, and heat is applied at a rate of 12.5 F per minute. Figure 10 shows a typical foam mass as removed from the bell jar. (Since the foam is of the rigid open-cell variety, it can be removed from vacuum without damage. Figure 11 shows a typical foam-mass section.) Test specimens are cut from the foam mass.

Bars of foam 1 by 1 by 4 in. have been used as test specimens for thermal expansion and stress-strain tests; 2-in. cubes have been used for density and dimensional stability measurements.

PHYSICAL PROPERTIES

Tests to determine the physical properties of the foam product were conducted in an evacuated environment of 10^{-5} torr. There is some information in the literature on the physical properties of foam material produced at atmosphere, but very little on those generated and tested in vacuum. However, the scope of this test program was to yield only sufficient physical property data to determine whether the rigidizing foam material has the basic capabilities for application to space solar concentrators.



Figure 7 - Preparation of Test Sample

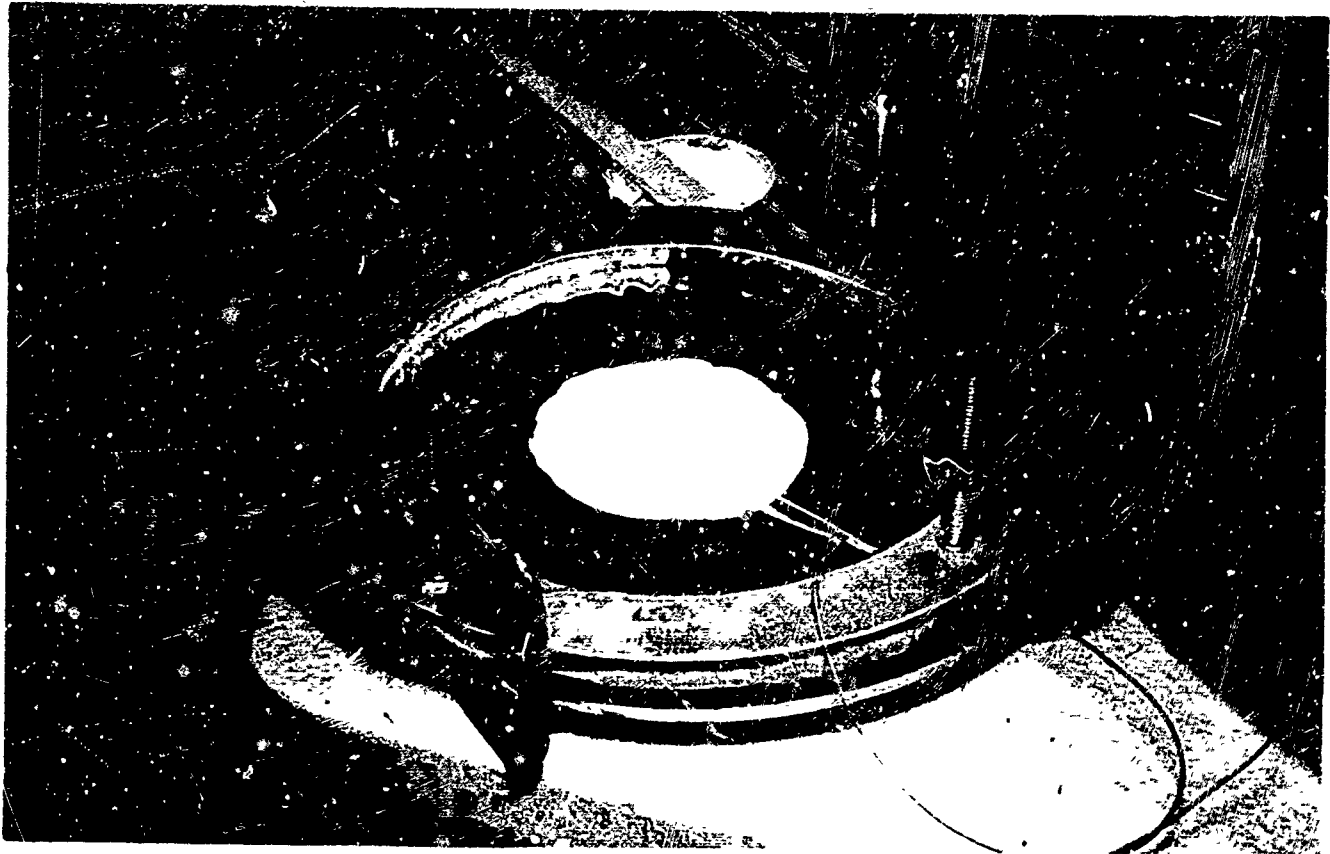


Figure 8 - Test Sample in Ring Fixture

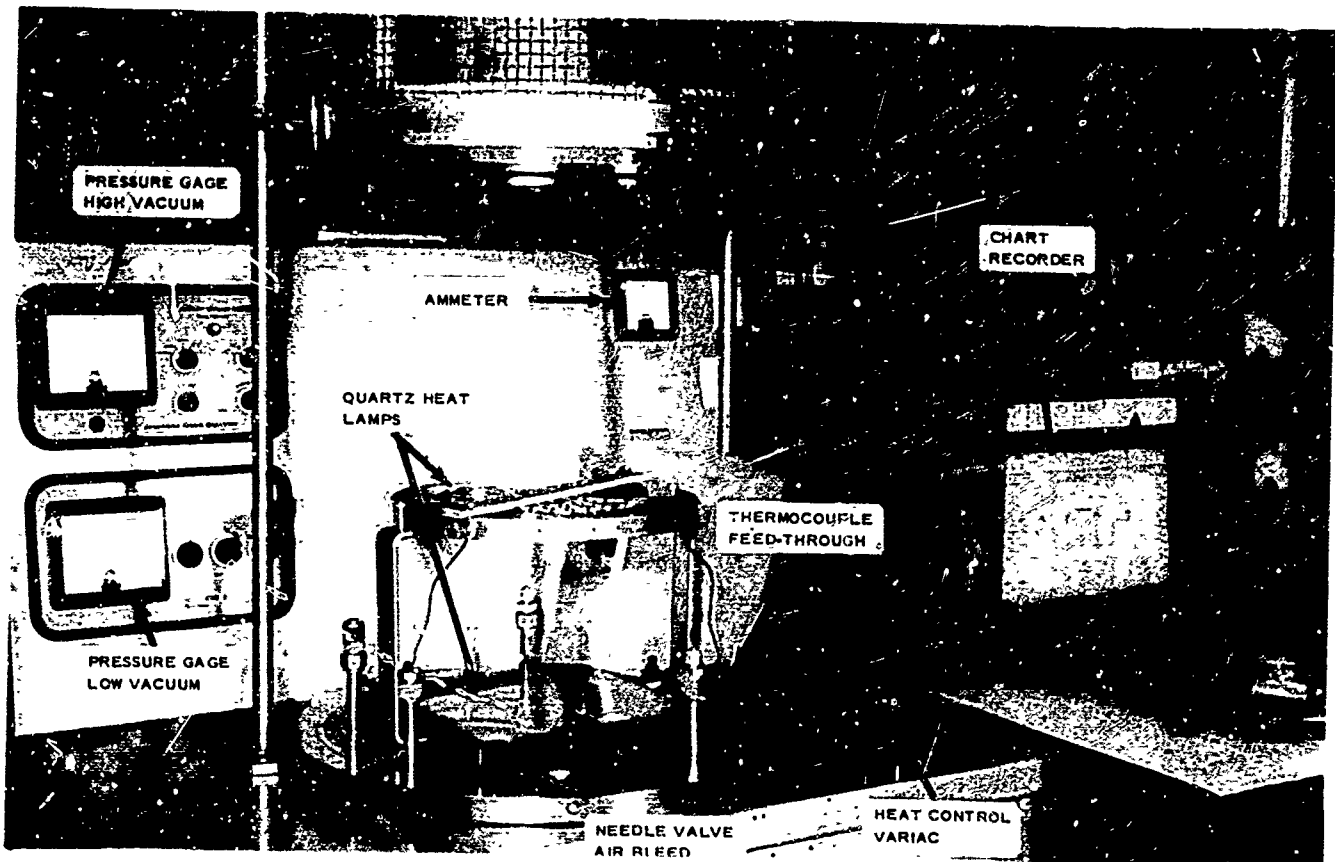


Figure 9 - Bell-Jar Test Facility

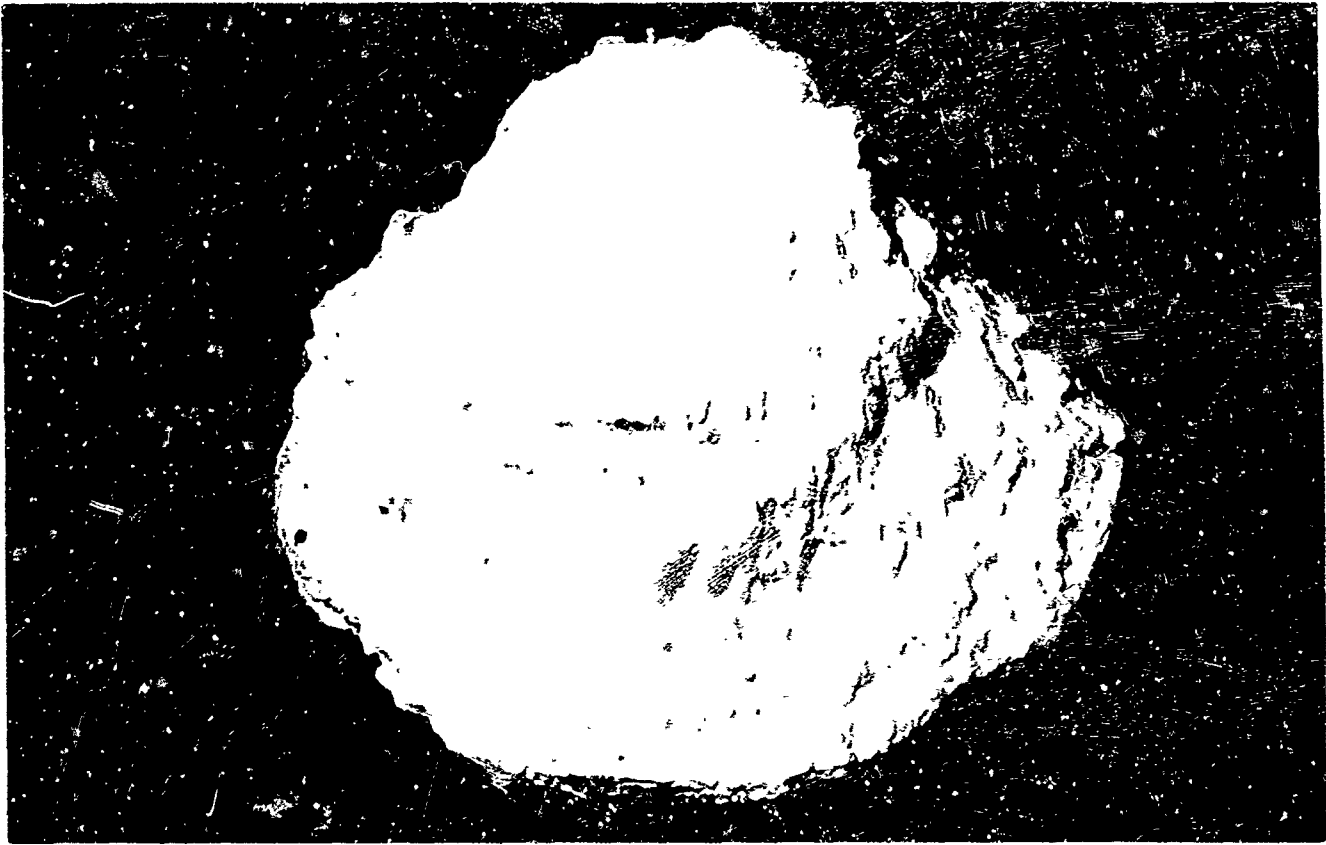


Figure 10 - Typical Foam Mass

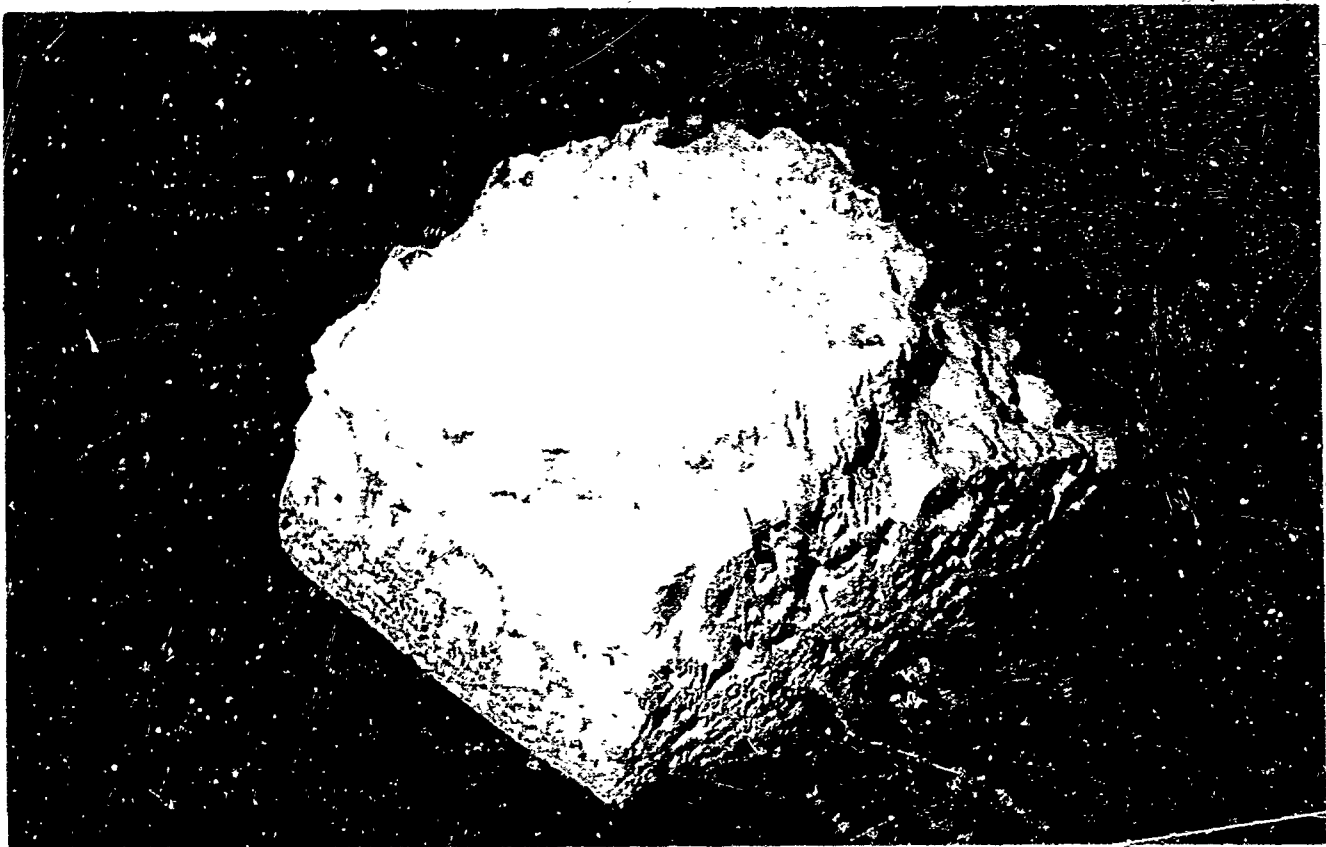


Figure 11 - Typical Foam-Mass Section

The foam product of the predistributed material with densities ranging from 3 to 4.5 pcf were vacuum tested to determine their basic physical properties within the temperature range expected on an orbiting solar concentrator (-200 to +240 F). The following test data are obtained from a formulation having a microquartz filler of 2 percent.

In Figure 12, the tensile ultimate stress is plotted against temperature for the density range of the material tested. At room temperature, a 3-pcf-density material has a tensile ultimate stress of 3.5 psi; at -200 F, it increases to about 4. At the other extreme, it approaches zero at approximately 235 F. With a material of slightly higher density (4.6 pcf), the tensile ultimate stress is 22 psi at room temperature; at -200 F, it is up to 27 psi. At 250 F, it falls to 14 psi and continues on to zero at or about 300 F.

When the tensile yield stress is plotted against temperature for the various densities of the foam, the curves follow a very similar pattern.

In Figure 13, the tensile modulus stress is plotted against temperature for the various densities of foam. At room temperature, the 3.2-pcf foam has a tensile modulus of 300 psi; at -200 F, it increases to almost 600 psi; and at 240 F, it approaches zero. The 4.6-pcf foam has a tensile modulus of just over 1000 psi at room temperature; it rises to 1700 psi at -200 F and falls to less than 500 psi at 250 F.

In Figure 14, the compression yield stress is plotted against temperature for foam at the various densities. The general trend is for the values to rise at the lower temperatures and to fall off at the high temperatures, approaching zero at or about 300 F.

In Figure 15, the compression modulus is plotted against temperature for foam of the various densities noted. The values increase slightly from room temperature to -200 F, and fall off to values approaching zero at or about 250 F.

In Figure 16, the shear modulus is plotted against temperature for the various densities noted. The values given are from room temperature to 240 F. Note the series of straight lines with a very slight negative slope. The values vary less than 10 percent with the increase from room temperature to 240 F.

In Figure 17, the elongation of a bar of foam 1 by 1 by 4 in. is plotted against temperature. Once again, these measurements were performed in a vacuum of 10^{-5} torr. The "knee" of the curve is at 250 F. This curve was for one of the lower-density foams. With higher-density foams, the knee appears at slightly higher values. A 3-pcf foam has the knee at about 260 F, and a 3.5-pcf foam has the knee at about 280 F.

Figure 18 shows the creep curves for two samples exposed to a temperature of 135 F and a vacuum of 10^{-5} torr while at a 50-percent tensile yield stress. The creep becomes somewhat negligible after 75 hr. However, one of the samples did exhibit a primary creep strain of 0.011 in. per inch during the first 75 hr as compared to an elastic strain of 0.007 in. per inch.

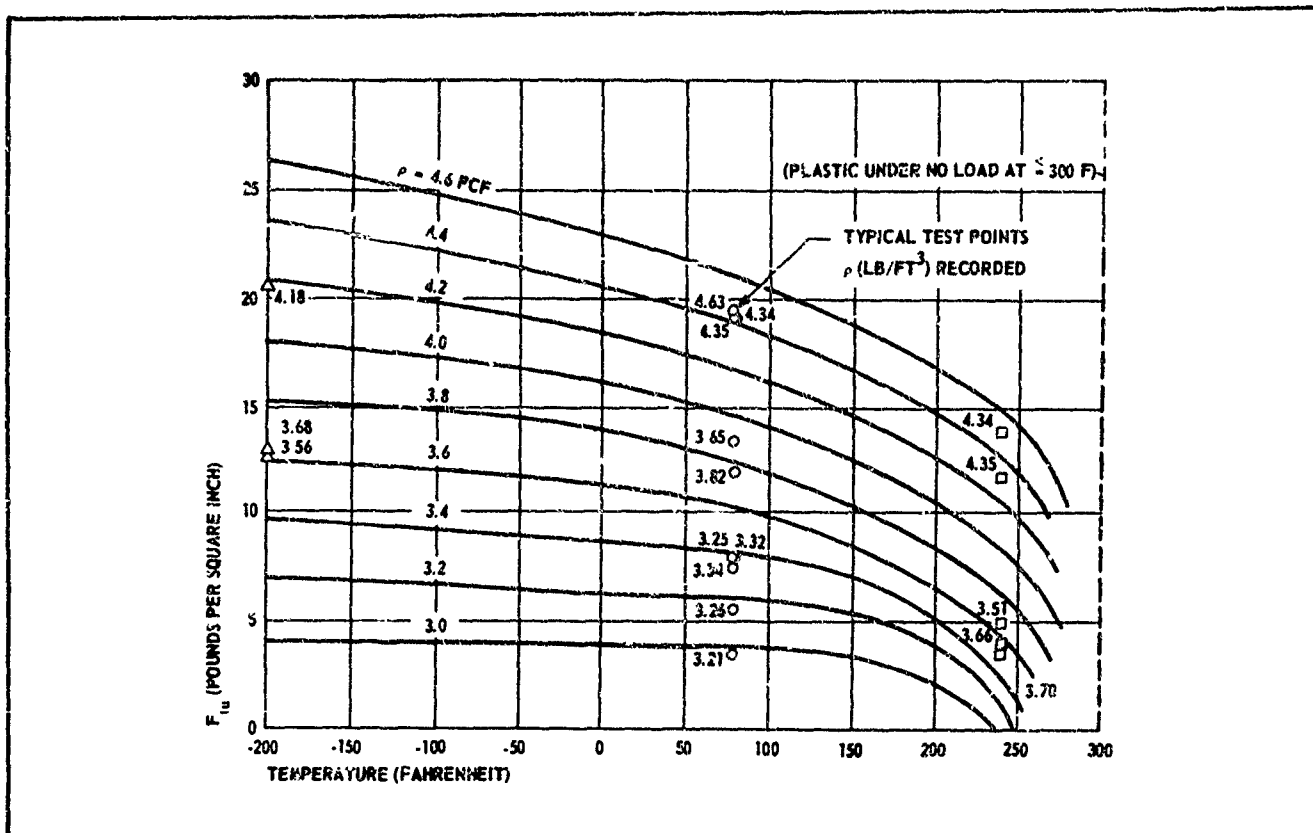


Figure 12 - Tensile Ultimate Stress versus Temperature

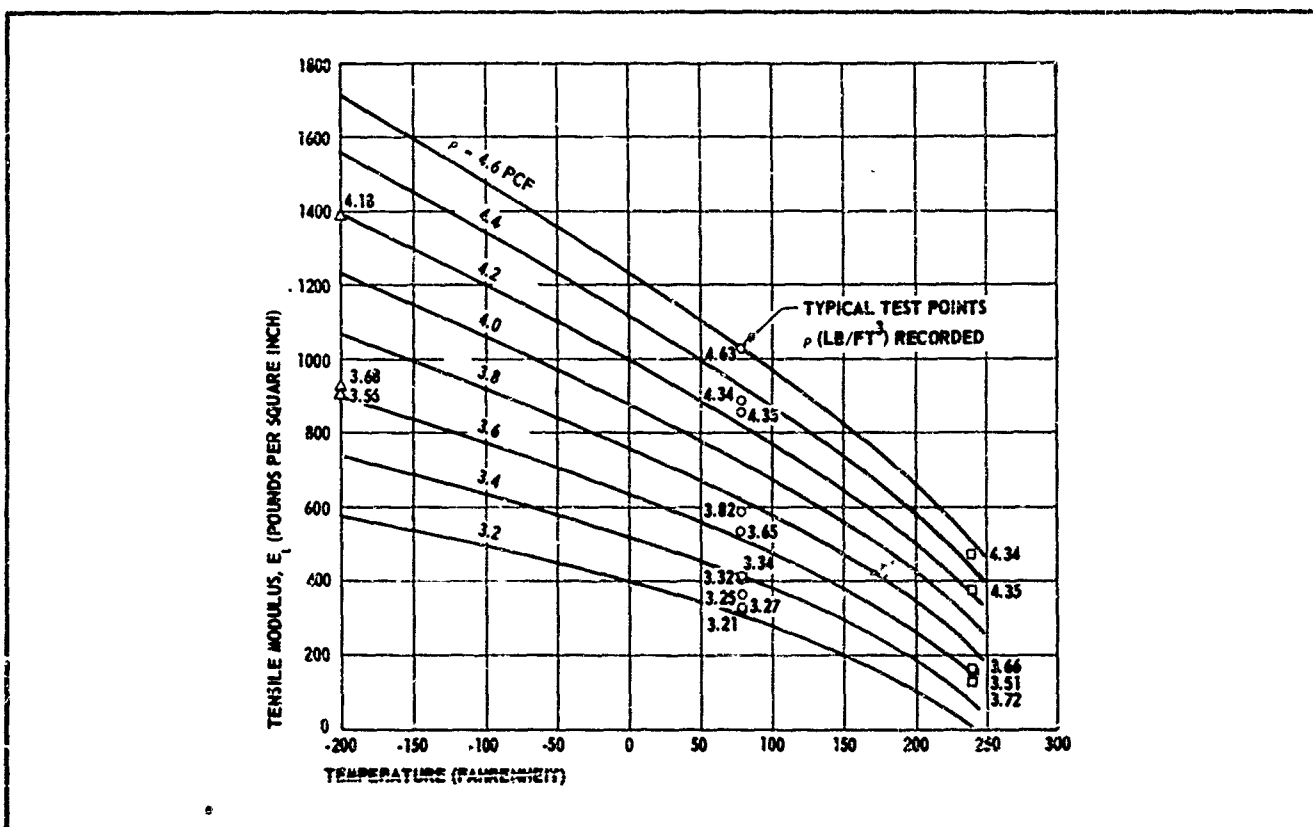


Figure 13 - Tensile Modulus Stress versus Temperature

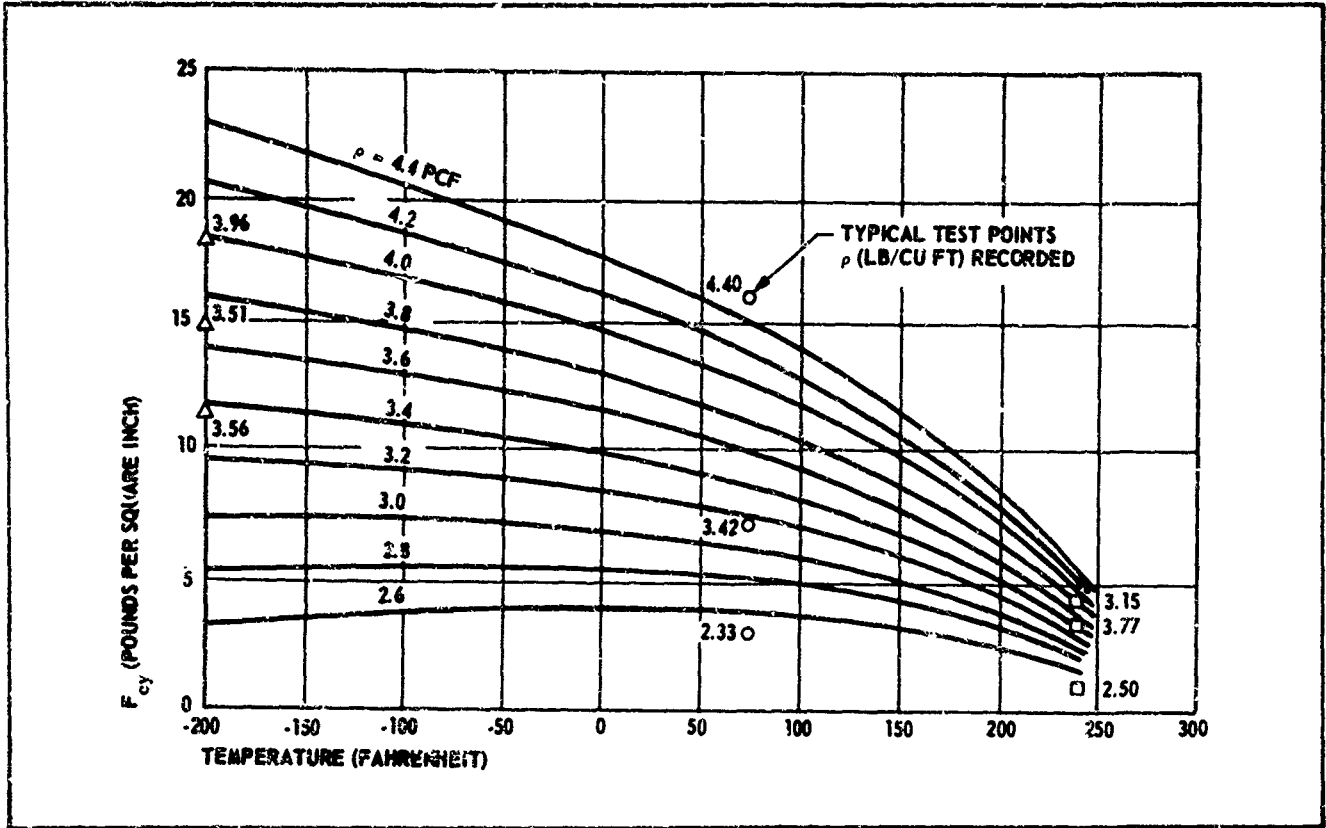


Figure 14 - Compression Yield Stress versus Temperature

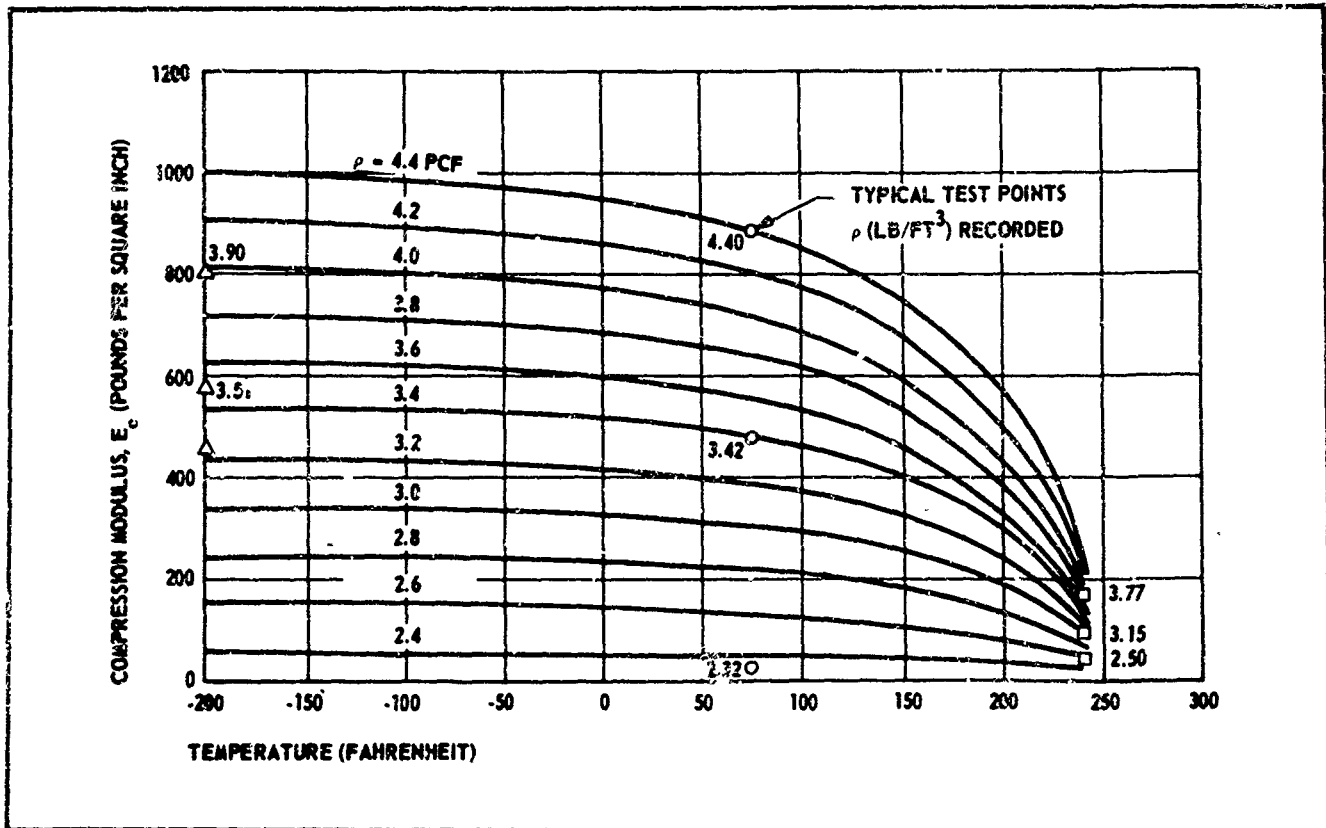


Figure 15 - Compression Modulus versus Temperature

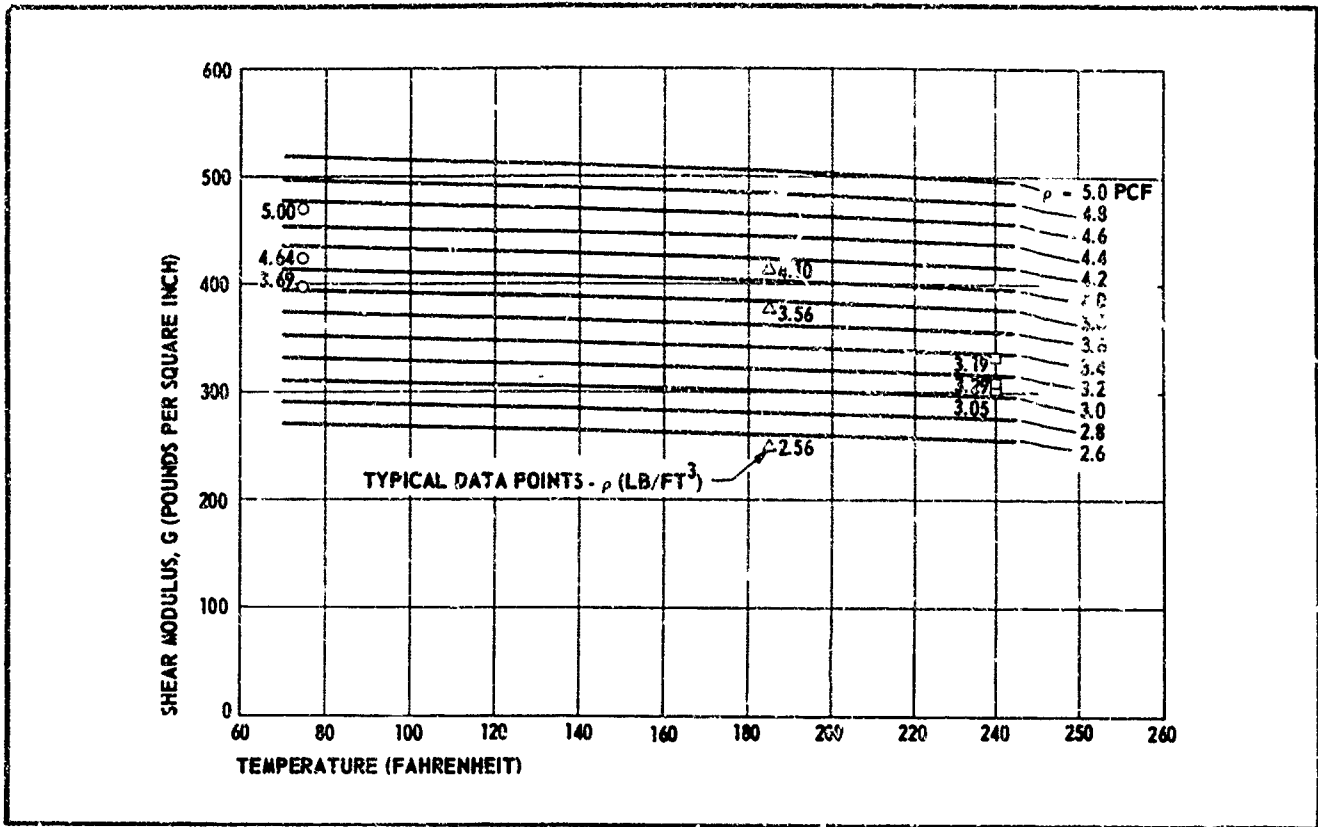


Figure 16 - Shear Modulus versus Temperature

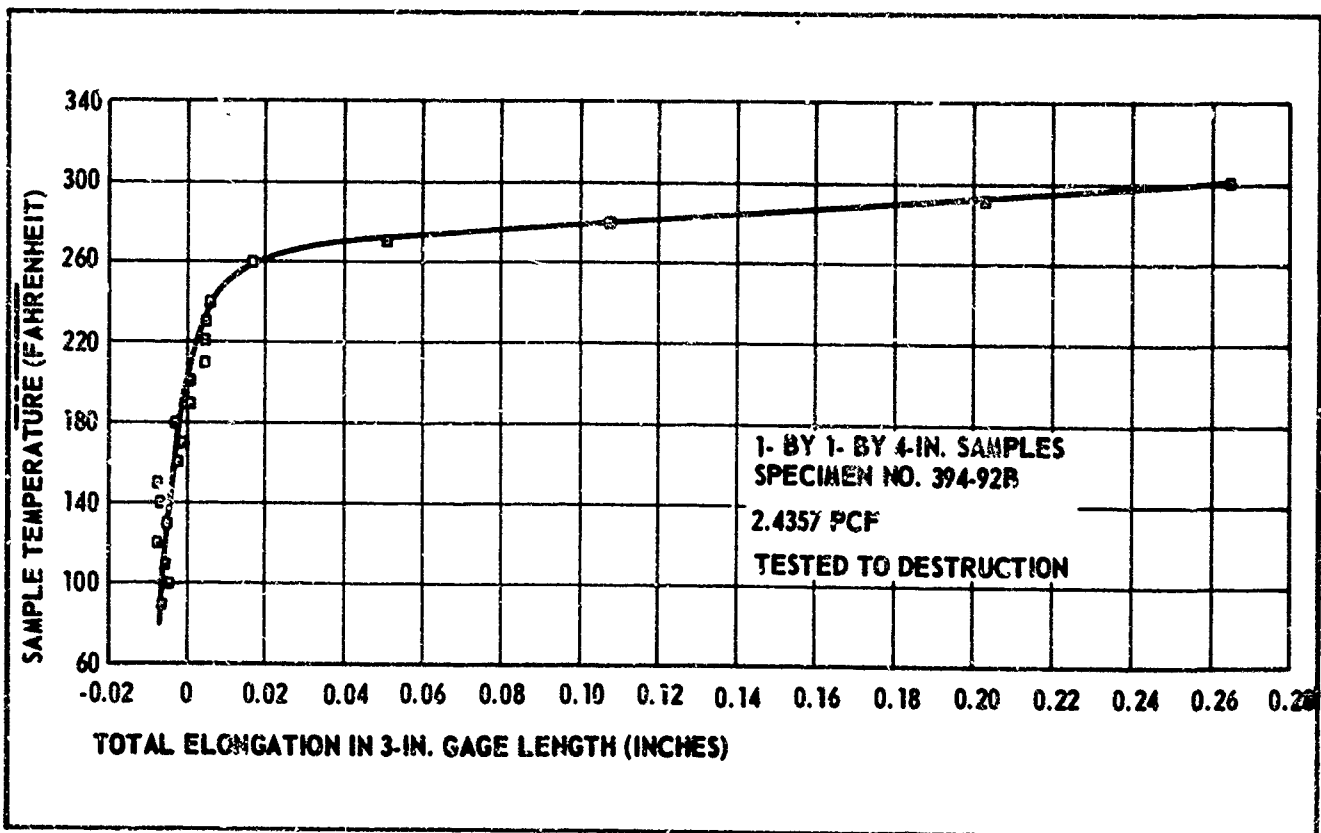


Figure 17 - Linear Thermal Expansion

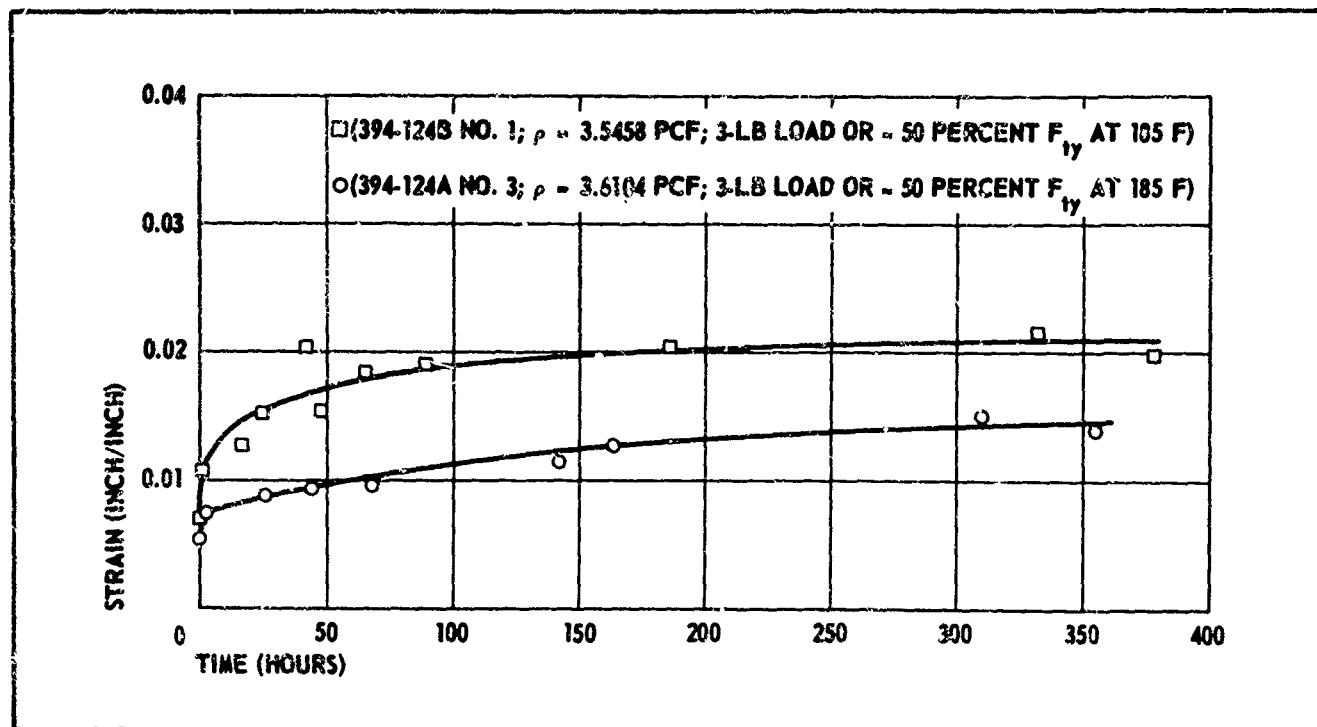


Figure 18 - Predistributed Foam Creep Curves for Two Samples

Dimensional stability measurements were made on 2-in-cube samples that were exposed to vacuum at room temperature. Dimensional changes over approximately 1000-hr periods amounted to less than one percent.

The foam is self-bonding to the film substrate. Peel tests have been run at room temperature and up to 240 F. Also, after exposure to vacuum and ultraviolet radiation for periods of up to 1000 hr, there was some reduction of peel strength with increased temperature and ultraviolet exposure; however, even the minimum values obtained are considered more than adequate for solar concentrator applications.

This foam should be tested immediately after its production in vacuum, but this is impossible. However, since the material is open-celled, its removal from the production vacuum chamber for shaping into test samples and its reinstallation in a vacuum chamber for test are believed to have had little effect on its physical properties. Under these circumstances, this procedure was about the best that could be done. It could not be accomplished with closed-cell material.

TWO-FOOT MODELS

Several two-foot models of solar concentrators have been fabricated. These concentrators were rigidized in a vacuum chamber, where the predistributed foam was activated by heat.

Figure 19 shows a hemispherical assembly of an inflated solar concentrator. The paraboloidal portion is aluminized Mylar; the remaining portion, transparent Mylar. The rim of the hemisphere is attached to a plexiglass plate. The internal pressure is maintained at 7 in. of water. A back flap on the back of the mirror serves as a separator when the concentrator is packaged.

Figure 20 shows the model with the back flap taken up and the predistributed material applied to one-half the mirror area, which runs to the line. The hub area shown will have twice the thickness of foam over the rim area. The purpose of the aluminum-foil heat shield was to keep as much heat as possible off the plexiglass baseplate. After rigidization, a nichrome hot wire burns off the pressure envelope.

Figure 21 shows the membrane mirror with the double and single thickness of predistributed material applied to the mirror area.

Figure 22 shows the back flap spread in position over the predistributed material.

Figure 23 shows the mirror assembly placed in the vacuum chamber. The plexiglass plate is balanced on three screw jacks. The spiral above the mirror is an infrared heating element.

Figure 24 shows the chamber door closed and the heating unit in position.

Figure 25 shows a view of the surface in the vacuum chamber with the heating initiated.

Figure 26 shows the foaming action just beginning.

Figure 27 shows the foaming action progressing.

Figure 28 shows the foaming action completed.

Figure 29 shows the hot-wire burn-off.

Figure 30 shows the chamber door open and the rigidized mirror portion with the balloon limp.

Figure 31 shows the face of the rigidized mirror (not trimmed) and the plexiglass plate. The instrument in the foreground is a contour-measuring apparatus that is attached at the hub. The instrument makes a 360-deg sweep. Its fingers are set at different radii and are calibrated with a template to the contour of a perfect parabola.

Figure 32 shows the temperature and pressure curves during the rigidizing process. There were 14 thermocouples embedded in the predistributed material in 14 locations. They all traced out a temperature curve that was very much the same. The internal pressure of the balloon was retained at 7.5 in. of water \pm 0.5 in. The pressure was released just before burn-off. The chamber pressure seemed to follow the temperature pattern. It rose slightly with the increase in temperature; as the azide activated and gave off some nitrogen, there was a sudden rise in chamber pressure. After the

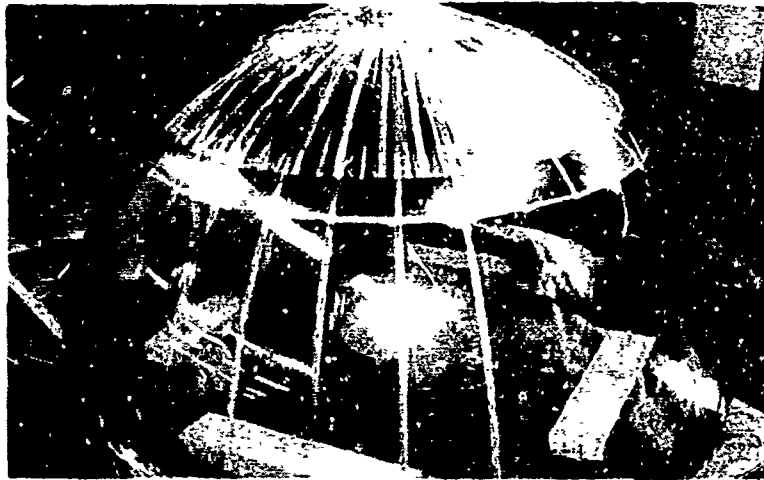


Figure 19 - Hemispherical Assembly of Inflated Solar Concentrator

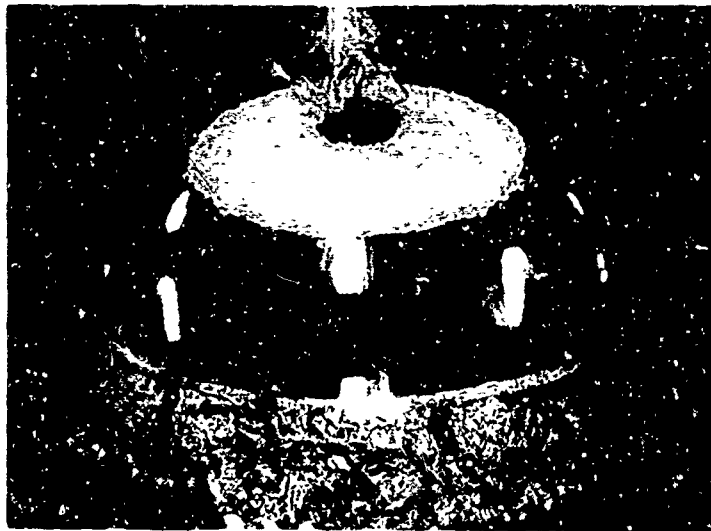


Figure 20 - Predistributed Foam Applied to One-Half of Mirror Area



Figure 21 - Mirror with Double- and Single- Thickness Predistributed Foam

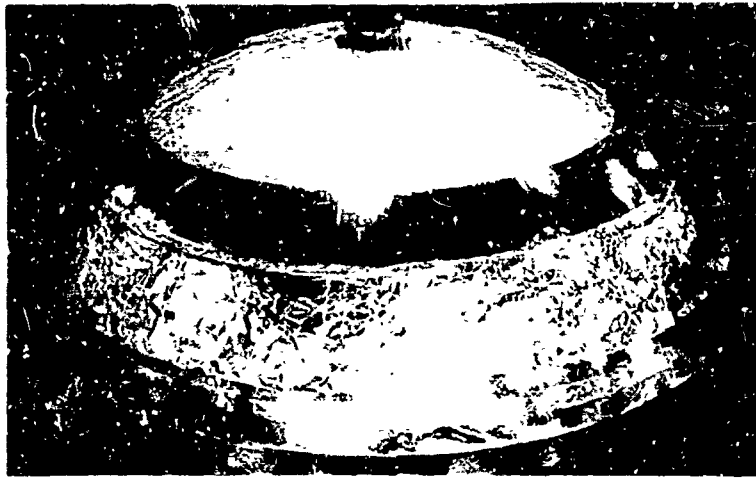


Figure 22 - Mirror with Back Flap

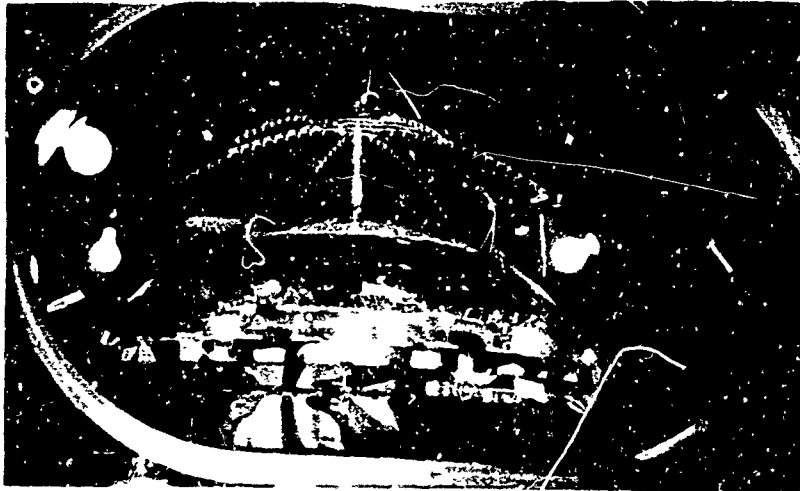


Figure 23 - Mirror in Vacuum Chamber



Figure 24 - Heating Unit in Vacuum Chamber

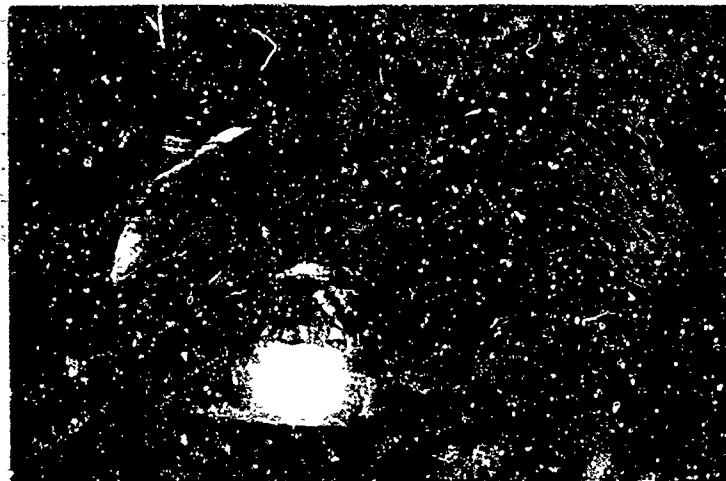


Figure 25 - Heating Started

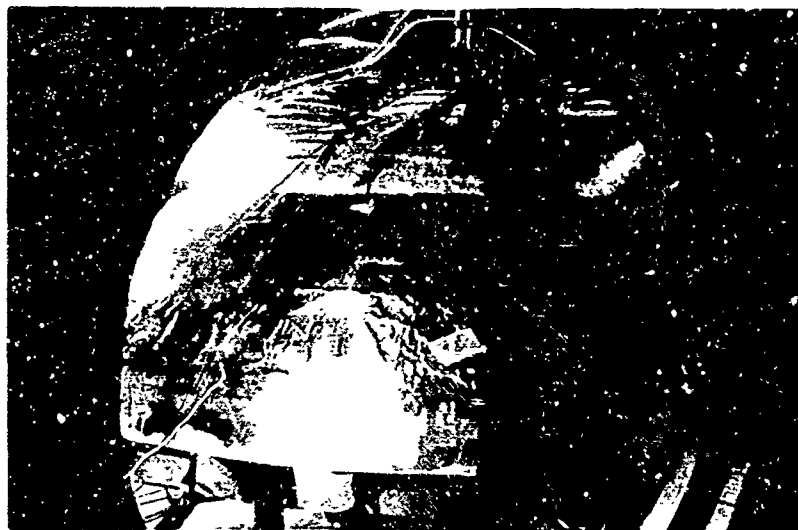


Figure 26 - Foaming Action Started

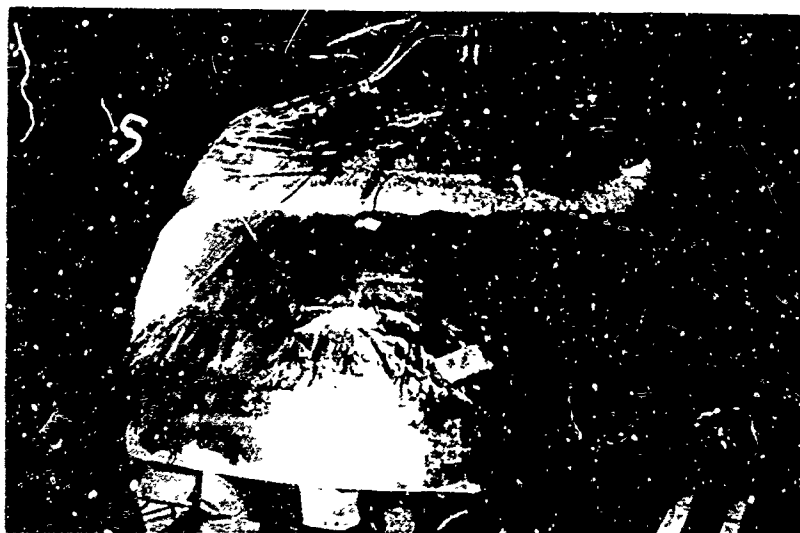


Figure 27 - Foaming Action Progressing

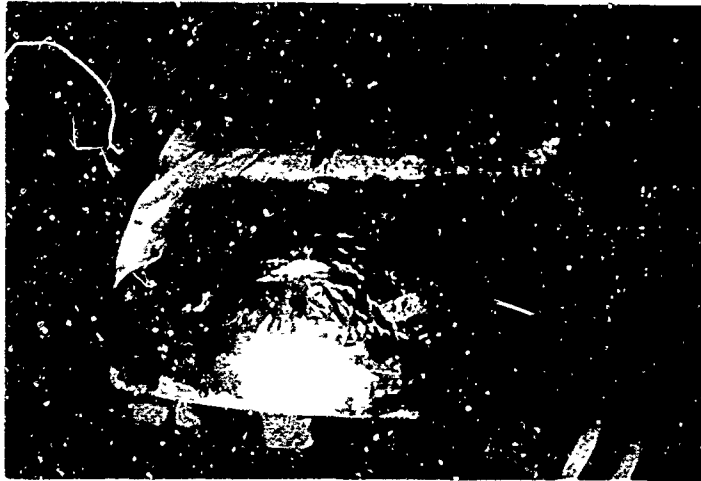


Figure 28 - Foaming Action Completed



Figure 29 - Hot-Wire Burn-Off Completed

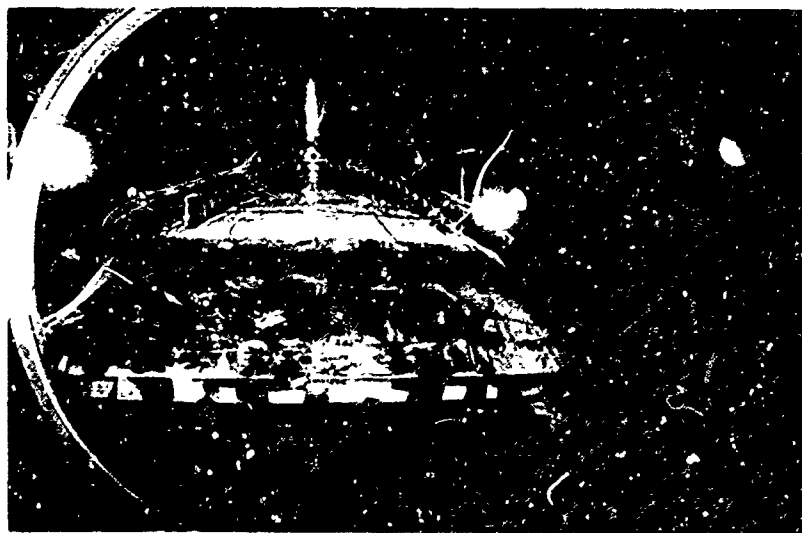


Figure 30 - Vacuum Released - Chamber Open



Figure 31 - Rigidized Mirror (Untrimmed) and Plexiglass Plate

foaming was completed, the pumping system caught up and again began evacuating the chamber. A slight rise in pressure occurred during the balloon burn-off, when some gas was generated and some internal pressure was released.

Figure 33 is a polar plot of the mirror contour. The fingers on the contour measuring apparatus are spaced at radii of 4, 6, 8, 10, and 12 in., respectively. The solid line represents the contour of a geometrically perfect parabola. The dotted line is the contour deviation of the pressurized membrane in the evacuated environment, and the dot-dash line represents the contour deviation after rigidization and after burn-off of the balloon, but still in vacuum.

Figure 34 shows a quarter view of the front surface of this solar-concentrator model. This photo was taken in a small photographic studio with a spotlight projecting on the mirror surface from a distance of 10 ft. The diverging rays of the spotlight caused the hyperbolic pattern at the focal point. Smoke was generated to capture the concentrating rays.

CONCLUSIONS

On the basis of the work accomplished in this program, the following conclusions were reached:

1. A workable predistributed foam material capable of rigidizing solar concentrators and other membrane structures in space has been developed.
2. The predistributed foam can be heated to initiate the foaming action in space with selective surfaces to control the absorption of sunlight.
3. The foam product has useful structural strength and

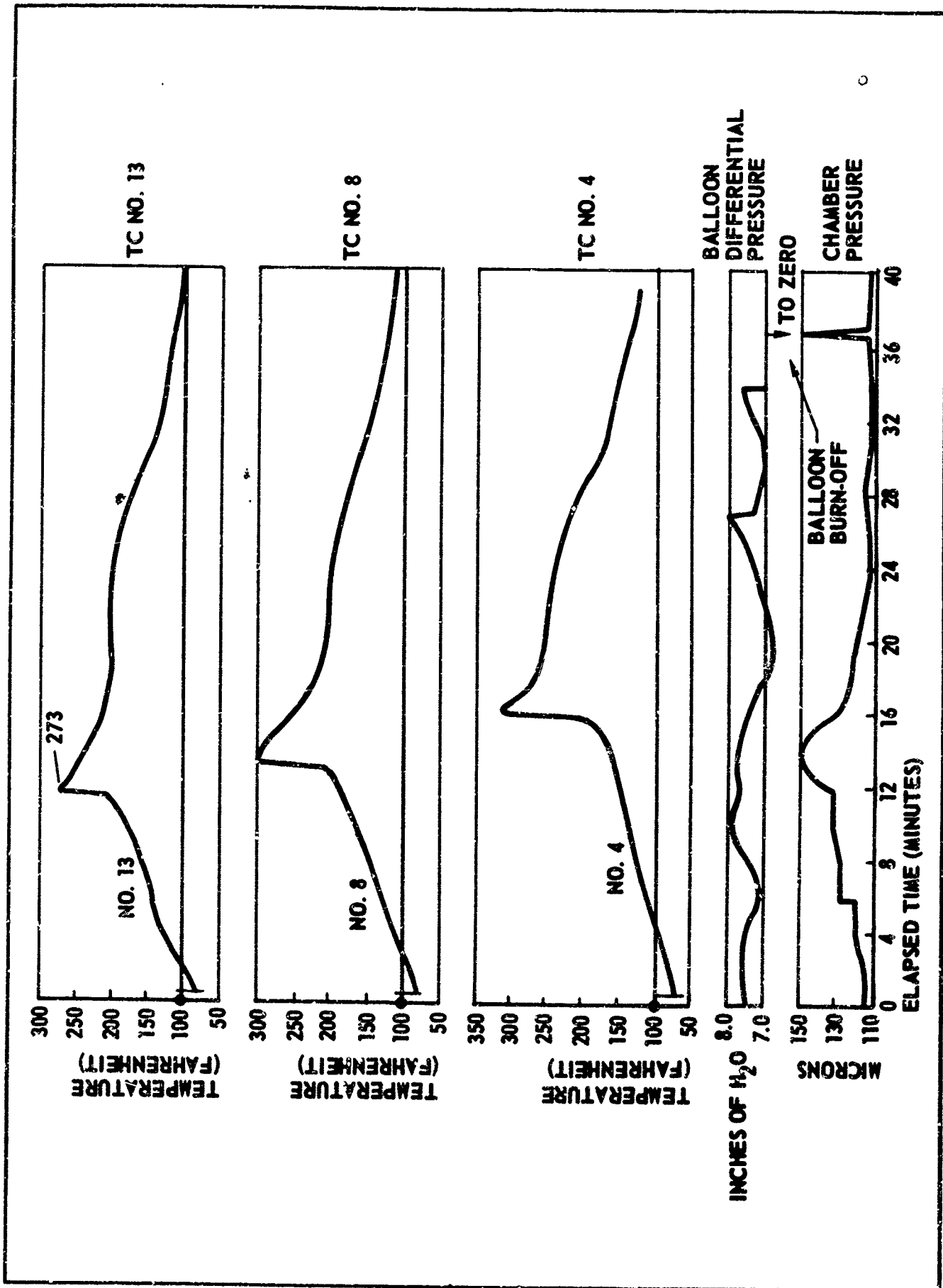


Figure 32 - Temperature and Pressure versus Time during Rigidization

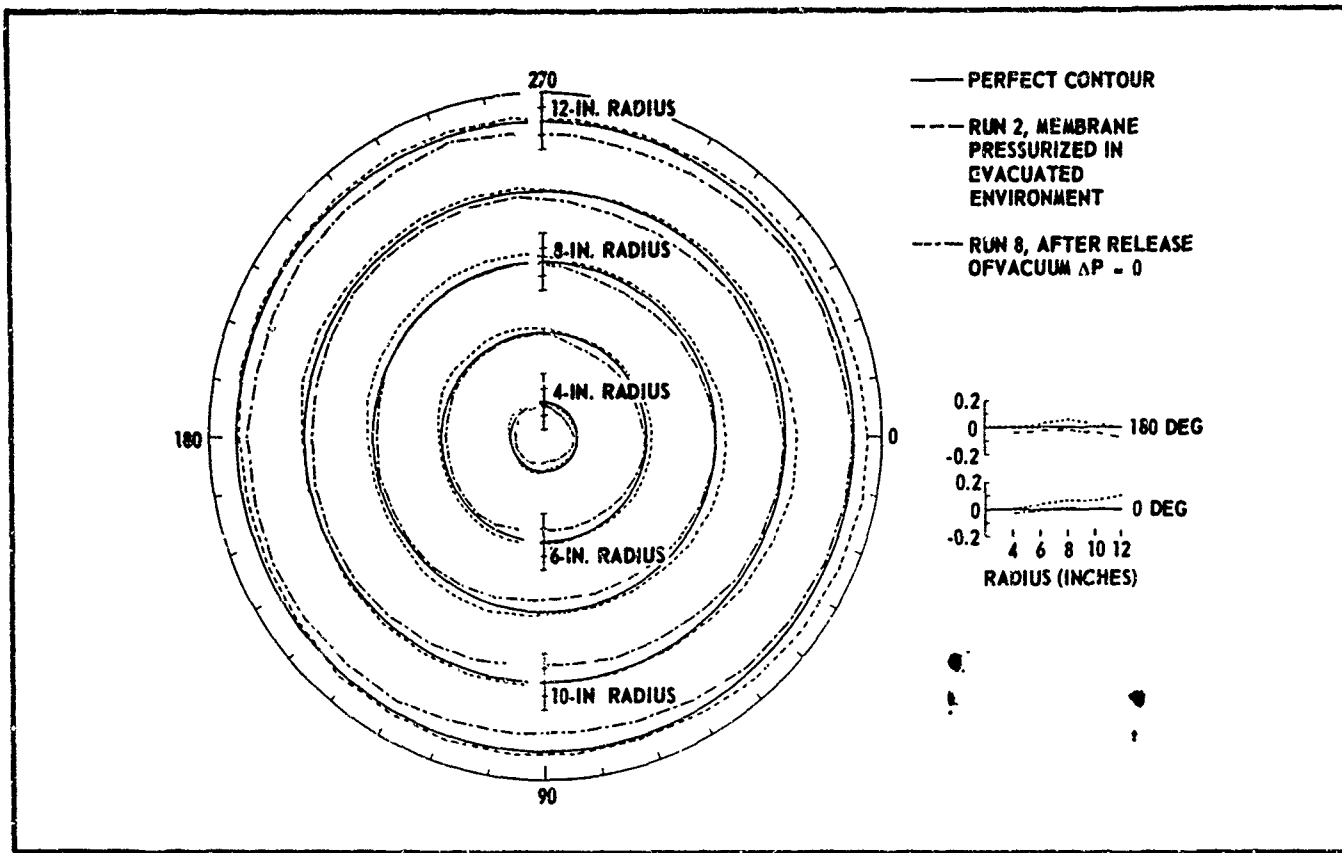


Figure 33 - Polar Plot of Mirror Contour



Figure 34 - Quarter view of Front Surface of Concentrator

stiffness in a vacuum up to temperatures approaching 240 F for densities greater than 3 lb per cubic foot. This material is primarily brittle, but a small amount of ductility is present at temperatures in excess of 100 F.

4. The limited amount of test data indicates that the tensile, compression, and shear properties increase with increasing density and decrease with increasing temperature, as is typical for urethane foams.
5. The thermal-coefficient-of-expansion tests of the foam indicate a small value, and thermal expansion decreases with an increase in density.

SEMI-RIGID STRUCTURES FOR SPACE APPLICATIONS

EXPANDABLE SPACE STRUCTURE

P. M. Knox, Jr.
R. O. Moses

MARTIN COMPANY

INTRODUCTION

This development program was initiated by the Manufacturing Technology Division of the Air Force Materials Laboratory and the Air Force Flight Dynamics Laboratory, Wright-Patterson Air Force Base, to determine and develop the manufacturing methods, processes, and related design data required for the efficient and practical use of available materials for expandable space structures under Contract AF 33(657)-9733.

Future operational mission requirements for space vehicles or stations will necessitate a substantial increase in payload size and weight, and therefore increased booster requirements. Abolvement of these booster requirements can be aided by the design of efficient space structures. One such structural concept is the expandable semirigid or telescoping structure. The effort covered by this contract is to develop the manufacturing knowhow for a telescoping space structure and establish its feasibility by evaluation and test for use as a manned space station.

The predominating considerations for the conventional space structure are:

- 1) Sealing and control of air leakage due to meteoroid penetration;
- 2) Environmental control;
- 3) Systems integration;
- 4) Compatibility of materials with natural and induced environments;
- 5) Structural and mechanical considerations.

The concept of Expandable Space Structures (ESS) introduces several new problems:

- 1) Structural integrity of telescoping structures;
- 2) Mechanical feasibility of stowage and deployment in a space environment;
- 3) Tooling and manufacturing problems associated with stowage and deployment requirements.

Design, fabrication, and ground testing of a semirigid telescoping expandable space structure (ESS) is covered in this paper. The work was performed in three phases: Phase I, design; Phase II, manufacturing; and Phase III, testing.

VEHICLE CONCEPT

The expandable space structure (ESS) program is oriented around a telescoping semirigid structure concept. This concept provides a collapsible structure for minimum size when required, and yet provides a rigid, metallic, large-volume structure after expansion to full length. The structural concept can be used for a complete space vehicle structure or for portions of the complete structure. An expandable space structure provides a low-length, reduced-volume payload to minimize boost phase flight problems and permit maximum use of the payload booster capability. Once in orbit it may be expanded to produce a useful volume for astronaut occupancy, equipment relocation, or numerous other applications discussed below.

The design concept provides a leak tight vehicle capable of maintaining an atmosphere for its occupants. It is of double-wall construction for maximum protection against meteoroids, and can maintain a livable temperature environment by passive thermal control using paint coatings or by an active radiator system. An R&D structure designed around this concept is seen in Fig. 1. This design may be varied in size, number of telescoping segments, and in various details for different applications.

DESIGN CRITERIA

The basic philosophy governing vehicle design is to develop an expanding structure that will prove concept feasibility. Design of the expandable sections considered the requirements of a manned space station. Portions of the vehicle not pertinent to proving concept feasibility, such as end closures, are designed for proper functioning of the telescoping structure, but need not be of the configuration proposed for space flight.

1. Functional Requirements

The following requirements were considered in vehicle design:

- a. Performance in low-earth orbits (maximum 500 mi.);
- b. Maintain internal pressurization of 7 to 15 psi and loads resulting from same;
- c. Radiation shielding of occupants and equipment (5 to 30 days);
- d. Structural life expectancy of 1 year;
- e. Minimum weight construction;
- f. Material shielding and self-sealing characteristics;
- g. Thermal control - external surface temperature of -150 to 400°F;

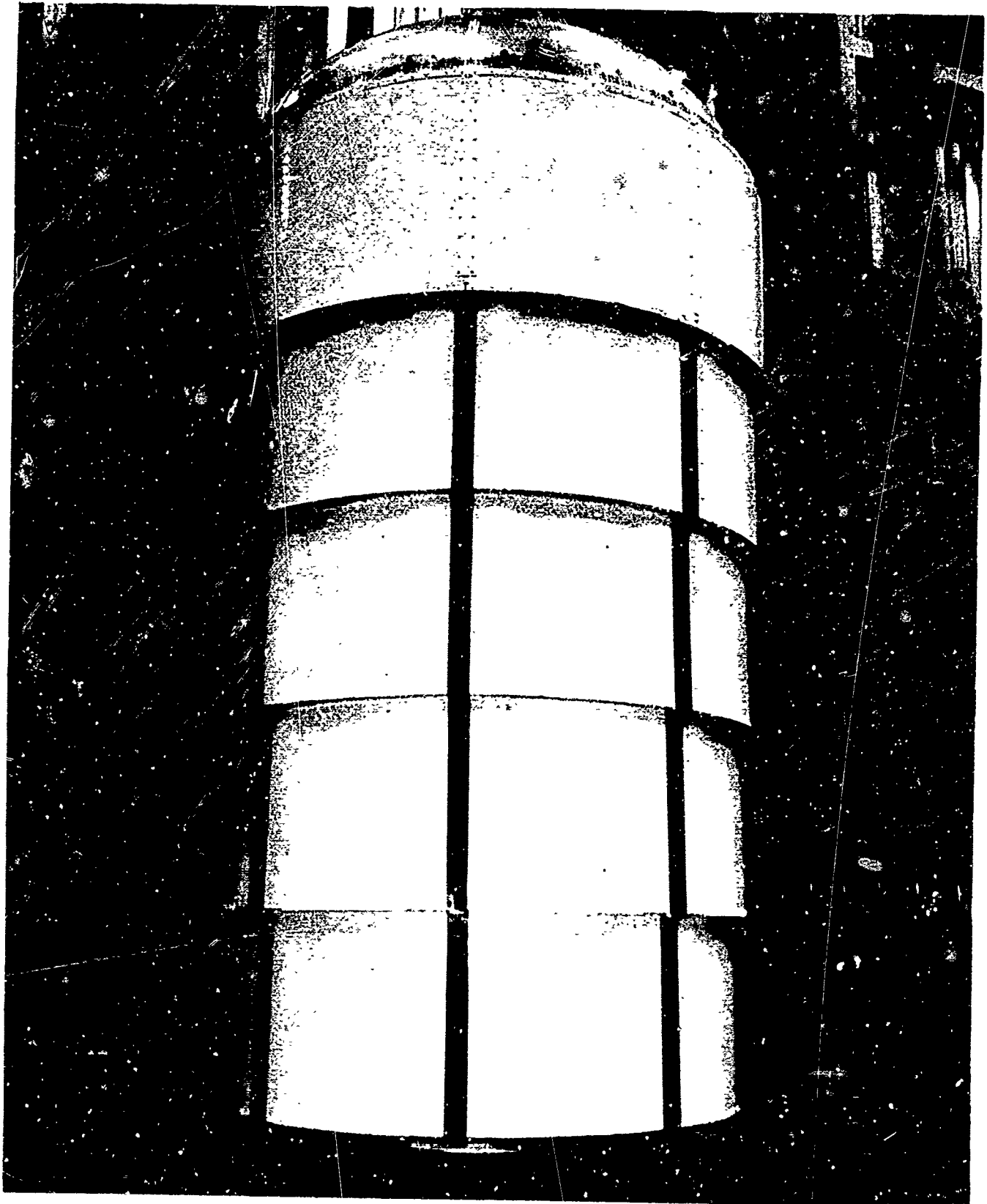


Fig. 1 ESS Vehicle Fully Extended

- h. Methods and reliability of deployment;
- i. Vibration and dynamic loading during launch and boost trajectory;
- j. Loads imposed on structure during deployment;
- k. Ratio of deployed volume to packaged volume of 5 to 1 or more;
- l. Packageability and ease of ground handling;
- m. Interaction of above stresses;
- n. Ease of fabrication;
- o. Modular concept so two similar modules, if made to rendezvous in space, would have easy and quick connection capability to each other;
- p. A structural component of a size equivalent to a cylinder 8 ft. in diameter and 15 ft. long;
- q. A semirigid structural concept that considers the telescoping rigid section configuration.

VEHICLE DEVELOPMENTAL STUDIES

During vehicle development, studies were performed to assist in the actual design of the expandable space structure (ESS) vehicle. From these, some of the actual design parameters evolved. The more significant studies performed are listed below.

1. Thermal Control Studies

Two thermal analyses were performed of the ESS vehicle in orbit. The first analysis is considered most significant since it investigates a more likely orbit for a manned space vehicle. This orbit represents an east launch from AMR into an orbit inclination of 33.3 deg, at an altitude of 257 n.mi. In this orbit, the longitudinal axis of the vehicle was oriented perpendicular to the orbit velocity vector with one side constantly facing the earth. Vehicle temperatures were computed for this orbit. With the air temperature maintained at 70°F internally, thermal analyses showed the inner skin temperature stayed 50° ± 10°F throughout the orbit. The outer skins varied from as low as -80°F to as high as +40°F.

A second thermal analysis was performed for a northward launch into a twilight orbit. For this analysis, the vehicle had one face oriented constantly toward the earth and another face toward the sun. The longitudinal axis of the vehicle was parallel to the orbital velocity vector. There is no roll about the longitudinal axis. Thermally, this orbit condition is more severe than that described first, and represents a steady-state heat flux condition to the vehicle. This orbit was chosen for environmental chamber testing of the vehicle

because of its test simplicity. Steady-state heat fluxes can be simulated in the chamber rather than transient rotating fluxes. Vehicle skin temperatures were computed for this orbit condition with the internal air temperature again maintained at 70°F. The inner skin temperatures varied from +62°F on the hottest side to +33°F on the coldest side. The external skin temperature varied from +38°F on the hottest side to -80°F on the coldest side.

2. Space Radiation Studies

The aluminum structure of the ESS vehicle has a unit shielding weight of 0.411 gm/cm². The rubberized fabric bladder in the vehicle has a unit weight of 0.071 gm/cm² and is equivalent to at least that much aluminum, giving a total effect shielding weight of 0.482 gm/cm². The total dose rates were computed, assuming the permissible dose to the crew to be 50 rad. The results are shown in Fig. 2. The orbit inclination chosen for the ESS vehicle proved to be a poor choice from a radiation dosage standpoint and would permit less than two days in orbit for the maximum permissible dosage to the crew. Orbital inclinations of less than 10 deg, however, would permit flight durations longer than a year for the selected altitude and maximum dosage. The rubber bladder should be good for about 40 years assuming a damage threshold of 10⁶ rad. The aluminum structure would be sound for at least 10¹⁰ years.

3. Puncture Pressure Loss

Analyses were performed of vehicle leakdown rates to determine how much time an astronaut would have to find a puncture leak and repair it. Fig. 3 shows the results of this analysis. For an extremely small hole of 0.003-in. diameter, which would be very difficult to find, it would take approximately 90 days for the pressure to leak down from 11 psi to 8 psi. For a considerably larger hole of 0.10-in. diameter, that can probably be found by sound, approximately two hours are required for the same pressure decay. The study has shown that an astronaut should have adequate time to find and plug a leak before the cabin pressure leaks down to a dangerous level.

VEHICLE DEVELOPMENT TESTS

Developmental tests were performed in support of the expandable space structure (ESS) program for design areas that were in doubt, or where data were not available.

1. Panel Sealing Tests

In the interest of program economy the ESS vehicle was designed of conventional riveted structure rather than welded structure. Welded structure would provide a lower leak rate than riveted structure, but it was thought that the difference in leakage rates would be negligible. Welding the structure would result in structural distortions detrimental to demonstration of the telescoping principle, and would require development of special costly welding fixtures. Test panels of typical joints and splices were tested to determine

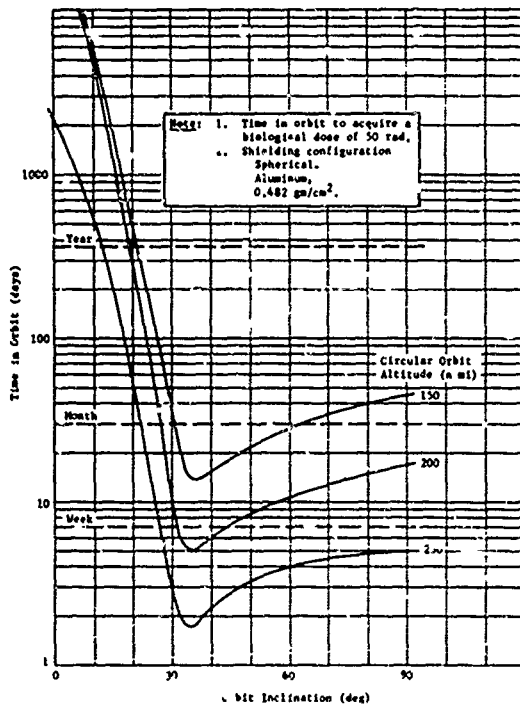


Fig. 2 Nuclear Radiation Biological Limits

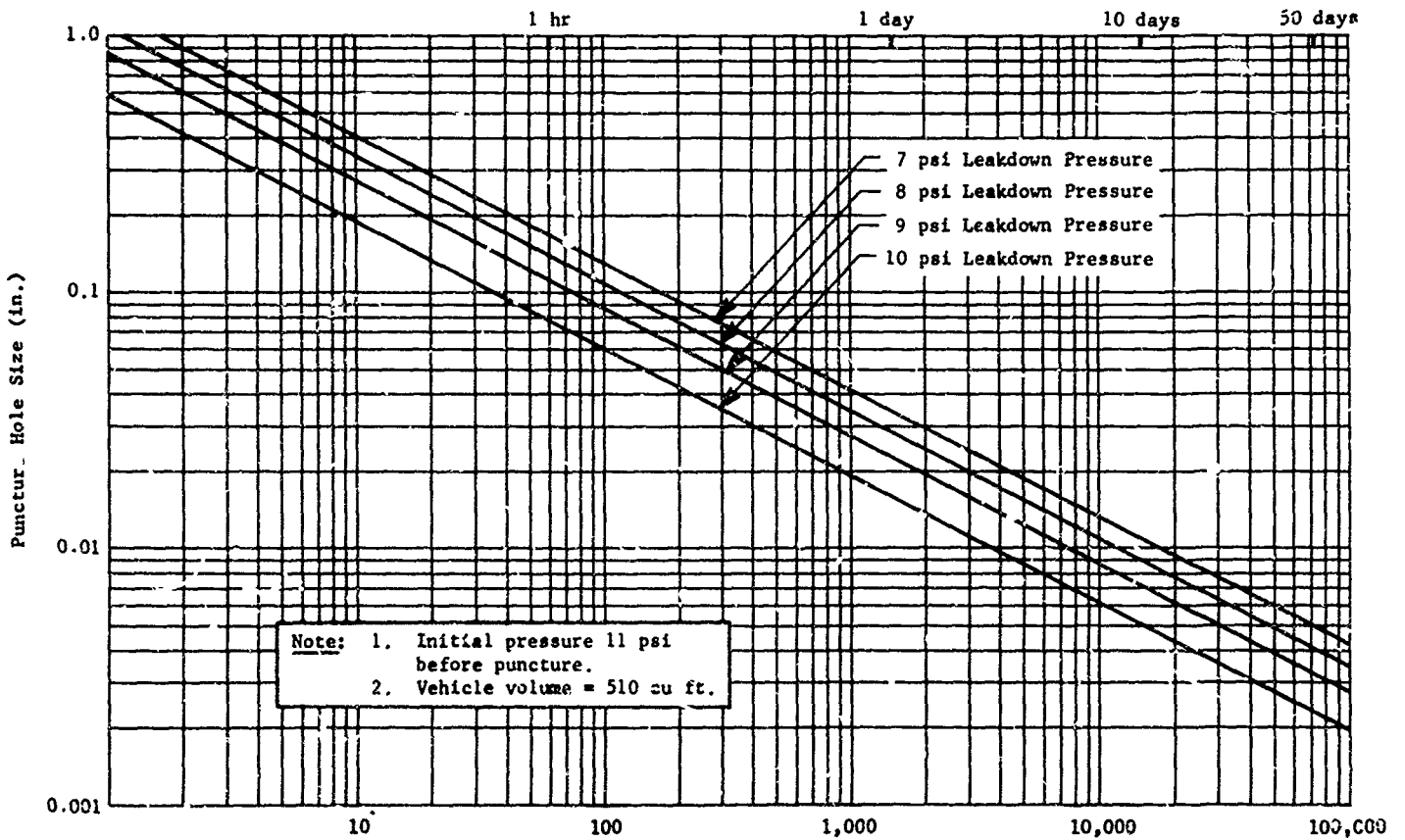


Fig. 3 Time in Minutes to Leak Down to Pressure

the adequacy of the seal-riveted structure. The panels simulated the joint used in vehicle fabrication and the kind of sealing used for that joint. The panels were mounted in a pressure vessel and leak-tested by applying a differential pressure across them. The pressure vessel test fixture is seen in Fig. 4. A typical sealant test panel is shown in Fig. 5. Only one panel indicated a leak, and this leak was attributed to the test setup rather than the panel.

2. Meteoroid Penetration Tests

A survey of meteoroid testing data was performed in support of the Expandable Space Structure Program. In addition, meteoroid penetration testing of the structure was performed by Martin using the two-stage light-gas gun facility at Denver Research Institute.

The Martin generated single-wall data reflect the testing technique of firing as many as five different sizes of glass balls at a shot. By this means, several brackets on critical ball size at a velocity near 17,000 ft/sec were obtained. Because of occasional breakup of a glass ball, some shots produced only one end of a bracket. On two occasions, a produced puncture was marginal, and it could be plotted as a point. The highest single-wall data point was obtained from a 3-mm ball at 24,000 fps. A typical test panel is shown in Fig. 7. Puncture data from single-wall penetrations are shown in Fig. 6.

The double-wall shots were fired using groups of three glass balls of nearly identical size, at velocities from 17,000 to 24,000 fps. At the higher velocities, it was found that so little separation between balls and sabot occurred, and so many balls broke up, that this multiple bead technique was necessary to produce identifiable data. Thus, each shot could give only one end of a bracket, and many produced no usable data.

The open points in Fig. 6 indicate double-wall targets with 0.020 2024 T3 bumpers spaced 1.0 in. away from 2024 T3 walls. Arrows indicate the directions of the brackets bounded by each data point. Solid points indicate targets identical to the open ones, except that the space between bumper and wall was filled with 3-pcf polyurethane foam.

Although data are inconclusive so far, it appears that on a weight basis (Fig. 6) the foam does not produce the large increase in stopping efficiency that was anticipated. The foam appears to channel the fragments of a shattered bead rather than to increase their spread, although absorbing much of their energy. Bead penetrations, with and without foam, were very similar, characterized by a thin spall off the back of the inner wall.

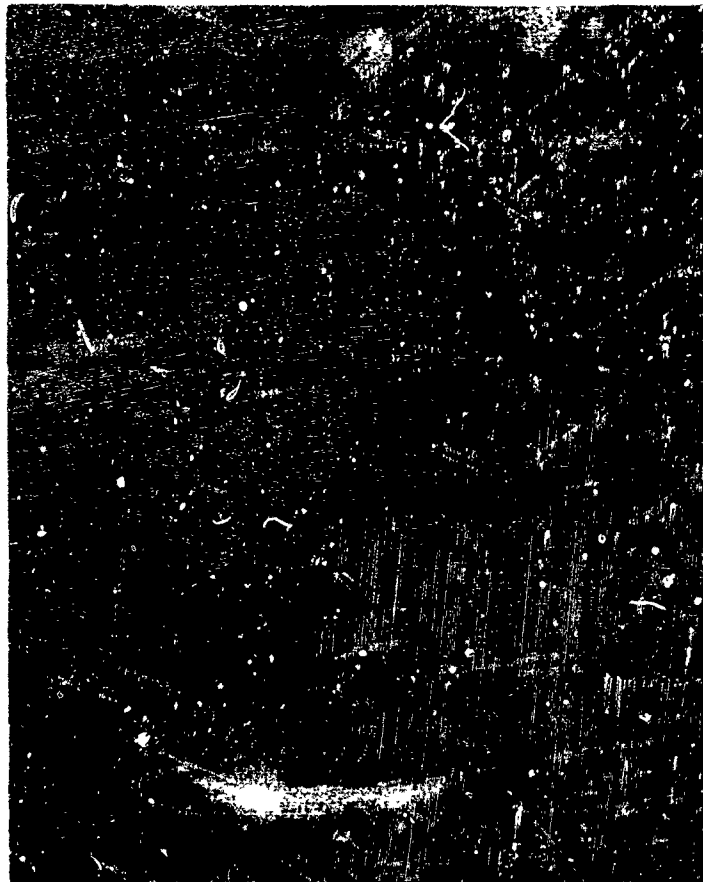


Fig. 4 Pressure Test Fixture for Panel Sealing, Leak Test

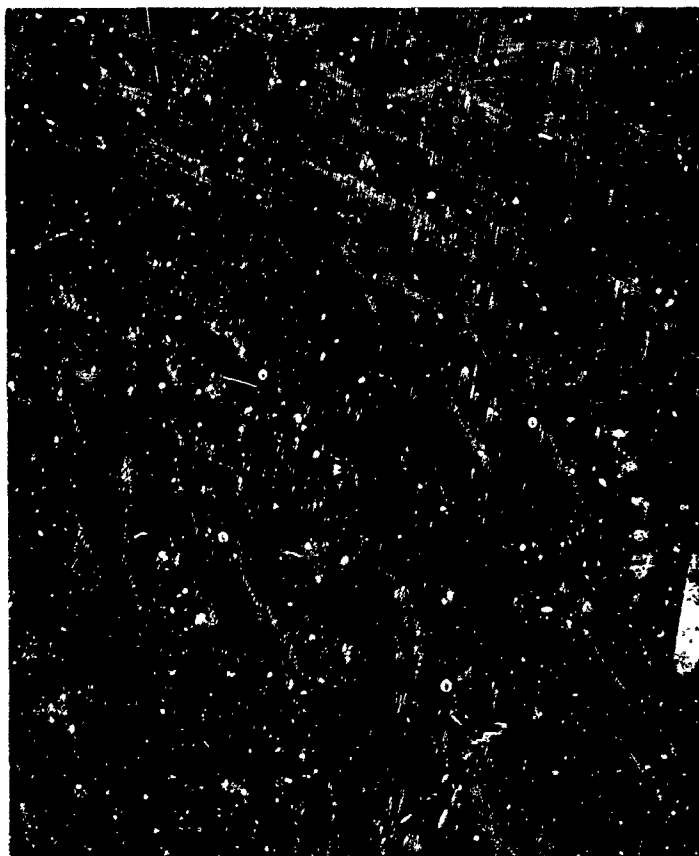


Fig. 5 Typical Test Panel

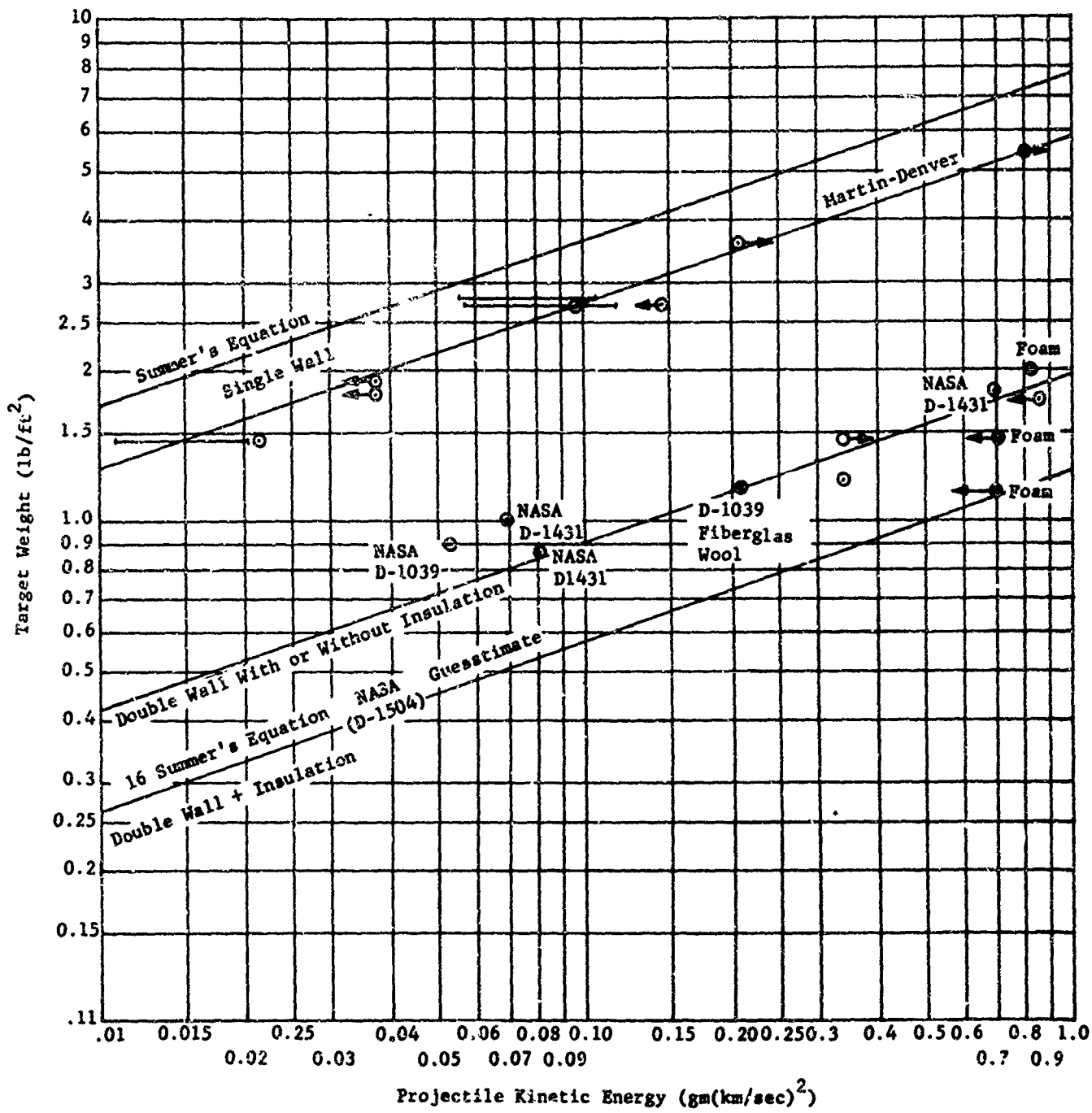


Fig. 6 Penetration Correlations, Glass Balls, Aluminum Targets



Fig. 7 Meteoroid Protection Test Panel Single Wall

3. Hypervelocity Penetration Stressed-Panel Test

Hypervelocity penetration tests of stressed panels were performed at puncture velocities slightly supersonic in the test panel material. For these tests glass beads were fired at the targets in the velocity range of 17,500 to 18,000 fps. The speed of sound in aluminum is approximately 16,740 fps.

A special pressure vessel test fixture (Fig. 8) was designed for the hypervelocity gun target chamber. This fixture provided a pressure differential across the test panel to achieve the desired stress level. An aluminum meteoroid bumper sheet was placed about 1-in. in front of the panel to simulate double-wall structure. Figure 9 shows a panel that ruptured at a stress of 28,000 psi.

Only five shots were fired in this test series. The tests were started at a stress level of 43,000 psi (yield stress) and carried downward to 28,000 psi. Since the results were somewhat erratic, much more testing is needed to pin down accurate stress levels of catastrophic rupture. However, it appears that large diameter punctures, say 1-in. diameter, will produce catastrophic rupture below 28,000 psi.

VEHICLE DESIGN

A prototype expandable space structure (ESS) design meeting design criteria requirements and incorporating design features resulting from developmental studies and tests is shown in Fig. 1. Major dimensions are given in Fig. 10. The vehicle design represents an 8-ft. diameter vehicle, 15-ft. long in the extended configuration and 5½-ft. long in the retracted configuration. The telescoping portion that demonstrates the expandable principle has five sections, is 32-in. long in the retracted configuration and slightly over 12-ft. long when extended. It has a ratio of expanded to retracted internal volume of 5.45.

A. Structural Configuration

Each telescoping section is identical in construction to other sections with the exception of top and bottom end closure provisions. Each section consists of a double-wall, sheet metal barrel with machined ring frames at each end for structural load transfer from one section to the next. Longitudinal "hat-section" stringers provide for separation of inner structural and outer meteoroid skins. The structural configuration is shown in Fig. 11. Riveted construction is used for joining all sheet metal and for joining inner structural skins to the end frames. The structural components are discussed below.

1. Machined End Frames

The end frames are designed from 7079-T652 rolled-ring forgings. This is a heat-treated and compression-stress-relieved material possessing excellent strength properties, and is dimensionally stable for machining. The cross



Fig. 8 Pressure Test Fixture for Hypervelocity Meteoroid Penetration of Stressed Panels



Fig. 9 Ruptured Panel Hypervelocity Penetration Test

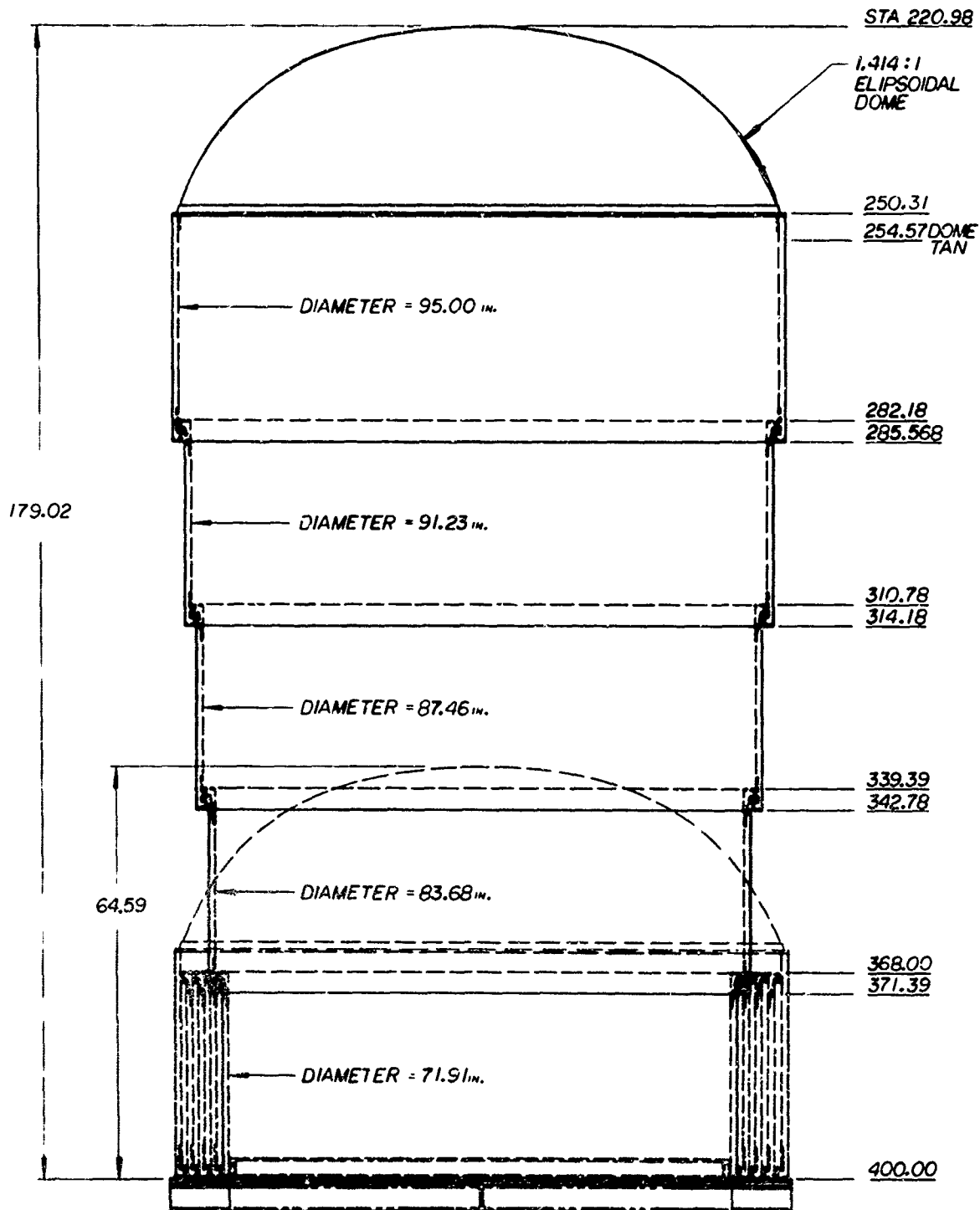


Fig. 10 Longitudinal Section of Vehicle

section of a pair of mating frames is shown in Fig. 12, depicting the forward frame of one telescoping section mated with the aft frame of the adjacent section.

In all cases the inner skin is the structural skin. Local moments produced by axial pressure loads are reacted within the frames themselves.

2. Floating Skins

To prevent severe thermal stresses within the vehicle structure the outer skins are free floating with respect to the inner skins. Analyses show that considerably greater thermal fluctuations occur in the outer skins than in the inner skins in a space environment. The free-floating characteristics permit the outer skin to expand or contract without loading the sub-structure. The free-floating feature is accomplished by oversize holes in the outer skins.

3. Forward Closure

For program economy, the forward closure of the vehicle uses a surplus Titan I dome. The attachment frame which joins the dome to the vehicle was designed of 7079-T652 aluminum alloy.

The aft bulkhead, a noncritical item for feasibility demonstration of the telescoping system, is a structural component with strength capability and reliability greater than that of the telescoping portion of the vehicle. Consequently, a machined-from-plate waffle bulkhead was designed for this application weighing about 100 pounds more than the honeycomb bulkhead.

B. Vehicle Telescoping Control

Orbital flight forces involved in deployment of the vehicle would be small, consisting of friction only. For ground testing, however, gravity produces substantial resisting forces. A problem is presented by the tendency of the vehicle to tilt during deployment, thus producing a bending moment on the vehicle. To cope with this bending moment, deployment control devices are used consisting of a guide-shoe-and-track assembly and a rub strip (Fig. 13). The bending moment is reacted by a force couple acting at the shoe and rub strip as shown in Fig. 13. The distance between these two forces decreases as the vehicle extends. At full deployment these forces are only three inches apart. Therefore, a small amount of tilt can produce fairly high loads at these points. Due to these anticipated high loads a total of eight guide rails were designed into the vehicle configuration. Subsequent testing, however, proved that the guide rails were over-designed and four rails would be sufficient. It is probable that no guides would be required for deployment in a gravity-free field, but this is difficult to prove. In any event ground testing requirements will undoubtedly govern the design, and some guide rails will be provided.

Torsional resistance is provided by the guide shoes in the tracks. Any two opposite shoes acting to produce a couple will resist the minute torsional loads.

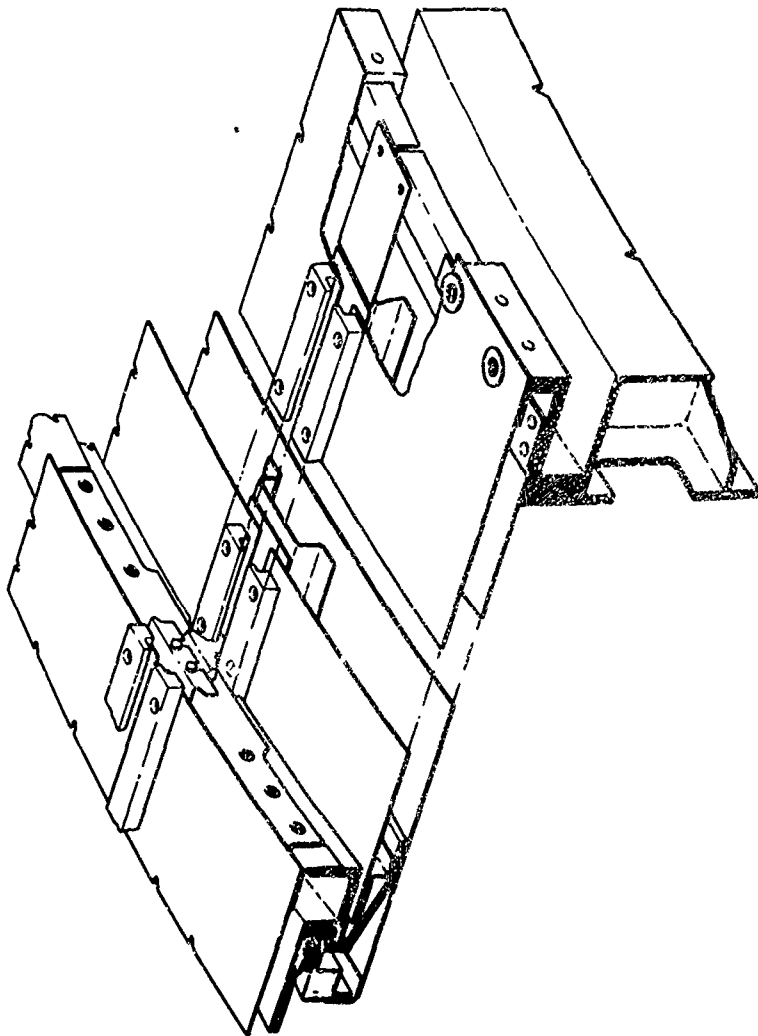


Fig. 11 Structural Configuration Expandable Space Structure Vehicle

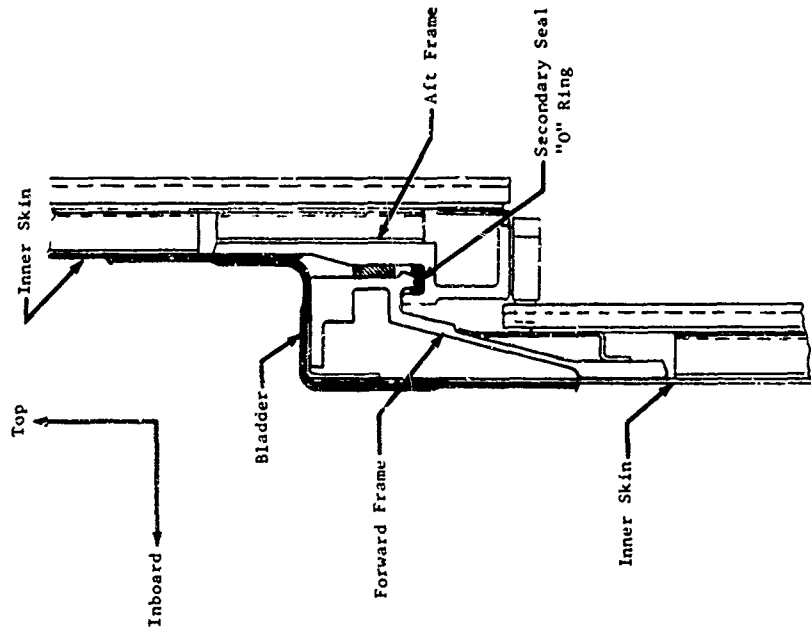


Fig. 12 Expandable Space Structure Mached Mating Frames

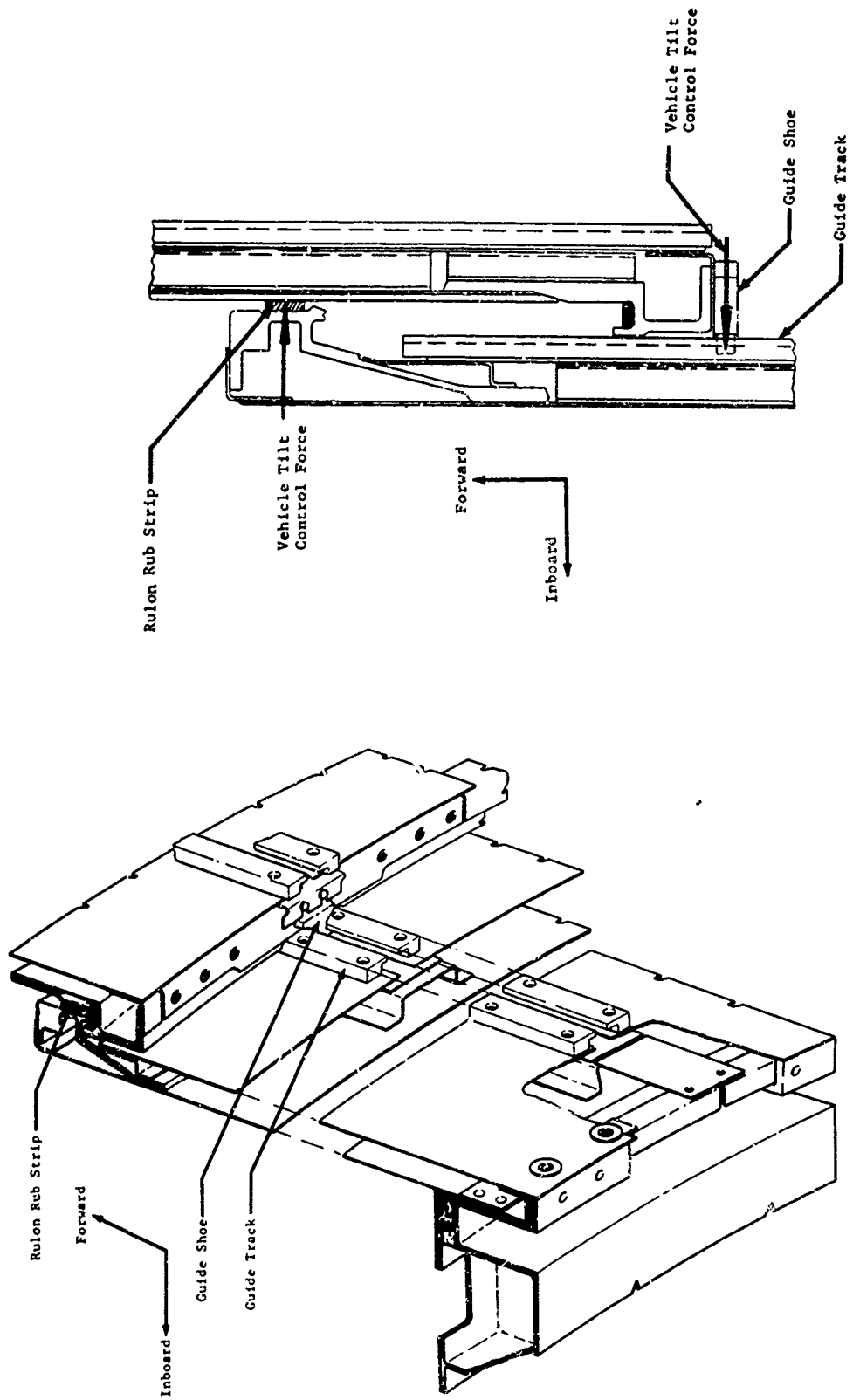


Fig. 13 Tilt Control Moment Reactions

The vehicle is designed to be deployed in orbit and in ground test by admitting low pressure air into the vehicle. A primary seal provides for pressure retention during the deployment. A secondary seal does not function until full deployment is reached.

C. Vehicle Pressurization Control

Two methods of pressure retention are included in the vehicle design. A bladder of Dacron fabric coated on both sides with Hycar rubber provides the primary pressure seal. This consists of an 0.040-in. thick cylindrical sleeve extending the full length of telescoping sections and incorporates a thickened integral "O" ring at each end. The "O" rings are clamped by a retaining ring at each end to hold the bag in place and provide the necessary pressure seal. The bladder is also fastened at the top of each telescoping section by tabs. Rubber bungee cords are also incorporated in the bladder design for testing requirements where the vehicle must be retracted. They physically pull the bladder away from the vehicle walls during retraction and force the bladder to fold compactly. Pictures of the bladder installed in the vehicle are shown in Fig. 14 and 15.

The second method of vehicle pressure retention is provided by a secondary sealing system consisting of the basic vehicle structure plus flattened "O" ring seals at the ends of the telescoping sections. The riveted structure is sealed with sealant between all faying surfaces, and rivets are dipped in sealant prior to driving. The "O" rings consist of a semi-rectangular cross-section shape of neoprene rubber cemented in place in a seal groove as shown in Fig. 12. The two interlocking frames slide together and engage during vehicle deployment, forcing a lip on one frame to compress the seal and prevent leakage (Fig. 12). A second lip, adjacent to the first, bottoms out to carry the structural load to prevent excessive seal compression.

D. Meteoroid Puncture Control

Meteoroid protection is provided by a double-wall structure. A 0.040-gage inner structural skin and a 0.020-gage outer meteoroid bumper, both of 2024 T3 aluminum, are spaced 0.75-in. apart for the desired meteoroid protection.

For 30 days in orbit, and a total length times diameter of 113 sq. ft., the probability of no puncture for this structure is .98 as shown in Fig. 16.

MATERIALS EVALUATION

A test program was initiated to test candidate construction materials for fabrication of the expandable space structure (ESS) vehicle. Testing performed under this program included:

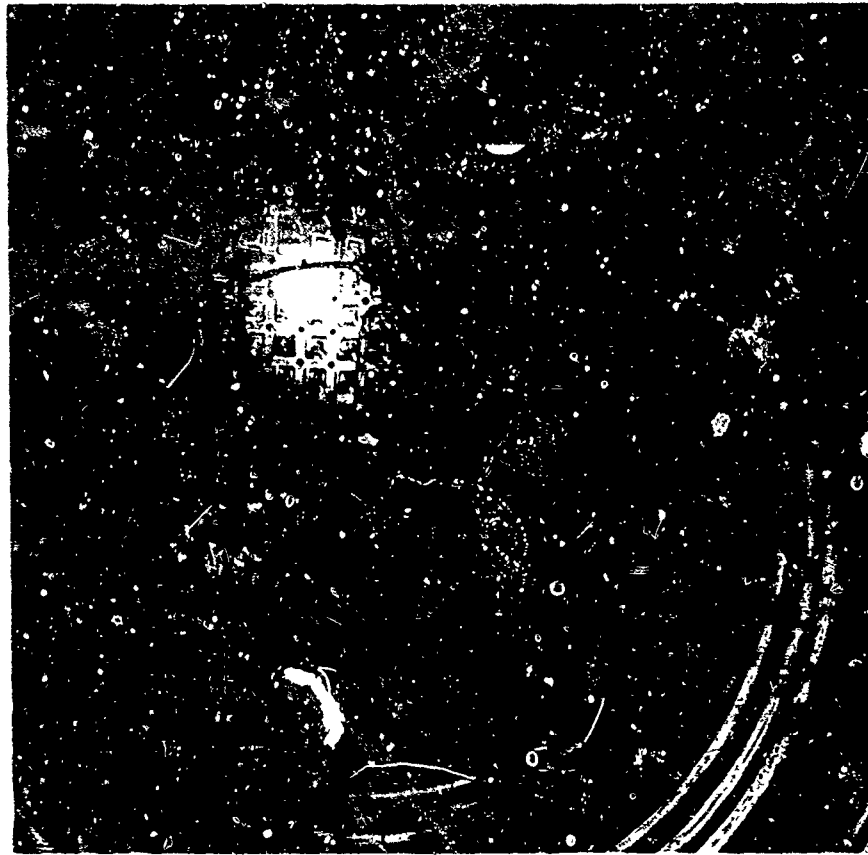


Fig. 14 Internal View, Retracted Position



Fig. 15 Internal View, Extended Position

- 1) Short-term materials outgassing tests;
- 2) Thermal coatings evaluation tests;
- 3) Self-sealing bladder materials testing;
- 4) Long-term space environment materials testing.

The short-term outgassing tests were performed to determine the problems created by outgassing of polymeric materials as it pertained to space environmental testing of the ESS vehicle. The purpose of thermal coating tests was two-fold. Thermal characteristics were determined for vehicle thermal control analyses, and materials degradation tests determined the changes in properties as a result of space environment exposure. Typical outgassing rates are shown in Fig. 17.

Self-sealing bladder materials testing was performed to determine feasibility of self-sealing bladders and not particularly in support of the ESS vehicle design. Results are shown in Table 1.

Material Test Code Number	Puncture Hole Diameter (in.)				
	0.010	0.013	0.020	0.050	0.080
JB-600	0	0	0.007	0.0122	0.085
JB-601	0	0	0	0.0061	0.025
5	0	0	0	0	0.034
6	0	0	0.003	0.006	0.370

Leakage rate is in ml/sec.

TABLE 1

Long-term materials testing exposed polymeric materials to hard vacuum for periods up to one year and evaluated material properties changes at intervals during this period. Typical results for gasket materials after one year exposure are summarized in Table 2.

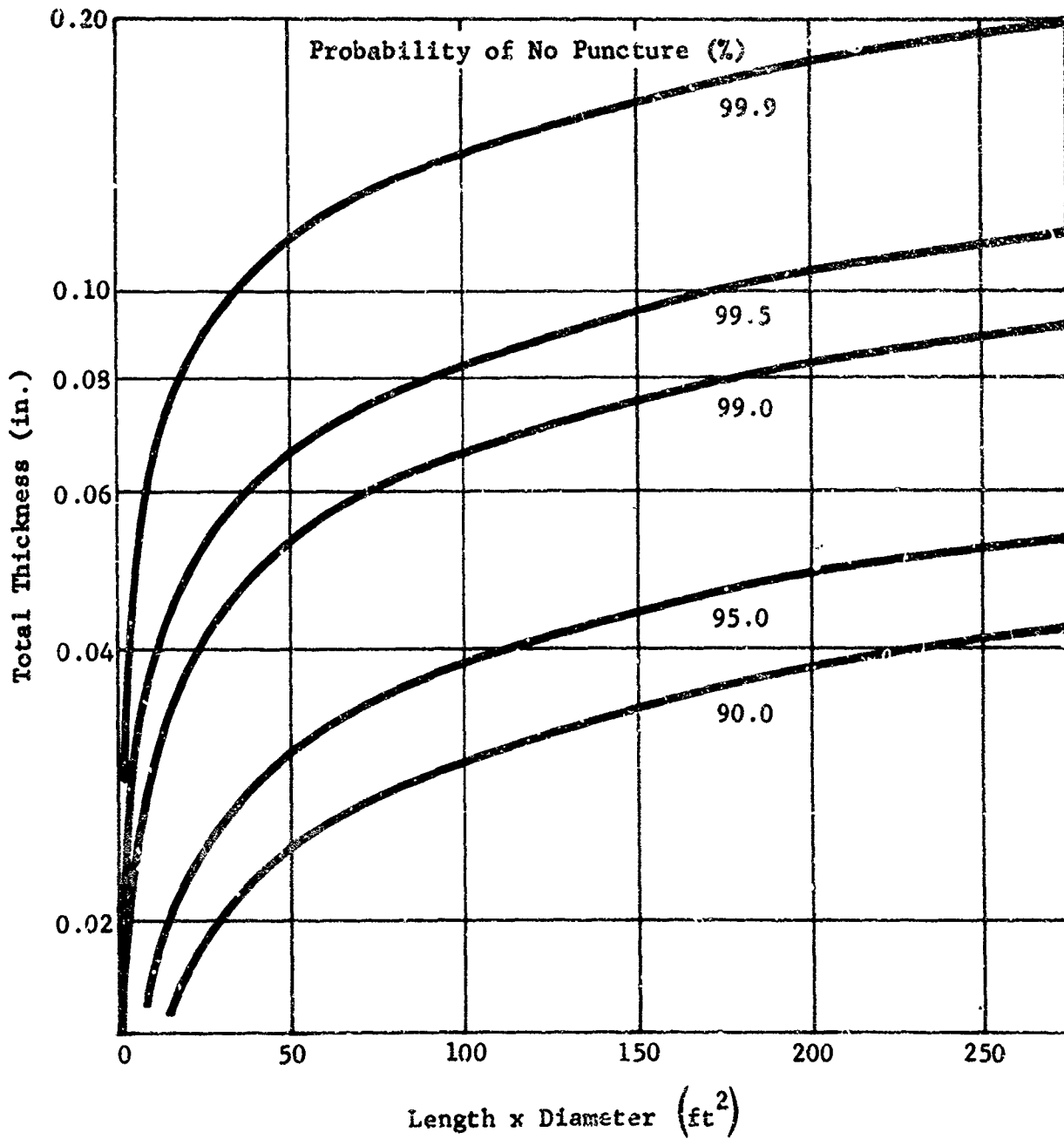


Fig. 16 Effect of Acceptable Probability of No Punctures on the Total Thickness of Aluminum Double-Walled Shell Required for Protection from Meteorites for 30 Days

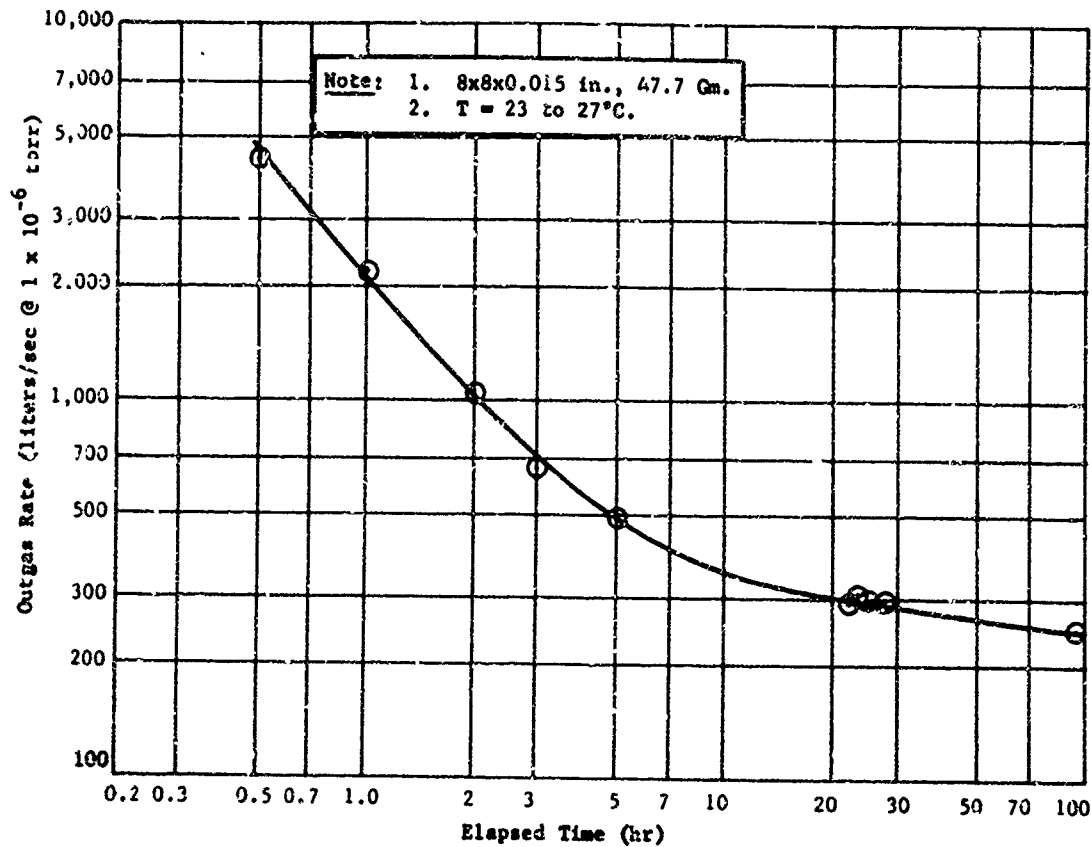


Fig. 17 Outgas Rate vs Time for BF Goodrich 139 KP-509.

Table 2 Test Results of Elastomers (Gasket Materials)

Material Condition	EE 2055 (Bryperon)	Percentage Change	Bryolon 200 (Nihylum Zepylon)	Percentage Change	L-601-2 (Bryperon)	Percentage Change	121-KP-55 (Bryperon)	Percentage Change	139-KP-9 (Bryar)	Percentage Change
As Recd and Conditioned										
Ultimate Tensile Strength (psi)	1762		2160		1925		1671		1961	
Ultimate Percentage Elongation (%)	507		425		298		363		503	
Tensile Stress, 300% E (psi)	921		1013		776		1290		1066	
Shore A Hardness (pts)	56		66		70		69		70	
Compression Set (%)	48		55		50		59		25	
Heat-Aged (100 hr at 150°C)										
Ultimate Tensile Strength (psi)	1800	+2	2160	+22	2225	+16	1776	+6	2176	+10
Ultimate Percentage Elongation (%)	468	-7	350	-17	200	-33	396	+11	550	+16
Tensile Stress, 300% E (psi)	1220	+22	1787	+11	1215	-1	1215	07	1233	+16
Shore A Hardness (pts)	55	-2	66	0	73	+3	73	06	70	0
Compression Set (%)	39	-19	46	+11	41	-26	52	+12	12	-52
Weight Change (%)	+0.1		+0.1		-0.1		-0.1		0	
Heat-Vacuum Exposure (2 mo, 2x10⁻⁵ torr)										
Ultimate Tensile Strength (psi)	1605	-9	2060	+20	2000	+6	1600	+6	2116	+6
Ultimate Percentage Elongation (%)	442	-12	511	+28	183	-12	373	+3	492	+16
Tensile Stress, 300% E (psi)	1214	+22	1920	+6	152	-12	1562	+3	1333	+25
Shore A Hardness (pts)	55	-7	70	+6	75	+7	71	+3	55	+2
Compression Set (%)	55	+27	56	+26	21	+96	50	+15	17	-11
Weight Change (%)	0		-22		-3.2		+1.6		-5.0	
Heat-Vacuum Exposure (6 mo, 1x10⁻⁵ torr)										
Ultimate Tensile Strength (psi)	1820	+4	2060	+20	1993	-	1822	+11.0	2044	+10.0
Ultimate Percentage Elongation (%)	421	-14	493	+18	322	-	390	+38	350	-10
Tensile Stress, 300% E (psi)	1260	+40	2067	+13	152	-	1323	+17	1007	+66
Shore A Hardness (pts)	55	-7	70	+6	75	+7	70	+3	57	+2
Compression Set (%)	10	-21	15	-23	0	-53	19	+66	5	-80
Weight Change (%)										
Heat-Vacuum Exposure (12 mo, 1x10⁻⁵ torr)										
Ultimate Tensile Strength (psi)	1820	+4	2217	+2	2125	+10	1767	+5	2111	+9
Ultimate Percentage Elongation (%)	467	-7	497	+10	306	-6	350	+1	500	+15
Tensile Stress, 300% E (psi)	1182	+26	1811	+1	152	-	1671	+5	1000	+22
Shore A Hardness (pts)	51	-8	65	+2	70	+6	69	0	60	+11
Compression Set (%)	13.2	-73	13.0	-76	10.0	-29	23.8	-36	6.6	-72

TESTING

Testing of the completed expandable space structure (ESS) vehicle was accomplished under Phase III of the program. The tests performed are as follows:

A. Proof Pressure Test

This test was performed to prepare the vehicle for subsequent activities with the vehicle pressurized. The internal bladder was deleted, and the pressure was retained by the secondary "O" ring seals on each telescoping section. The vehicle was subjected to proof pressure, and it sustained this pressure with no evidence of structural malfunction. The proof pressure was 12.1 psi, which is 10% over the design limit pressure of 11 psi.

B. Functional Test, Pressure-Actuated Deployment

The purpose of this test is to demonstrate expansion of the ESS vehicle using internal air pressure for deployment.

The first pressure-actuated deployment test was performed with the bladder installed unlubricated and required .7 psi to extend the vehicle to full length. To evaluate the effects of friction on deployment, the bladder was removed from the vehicle and lubricated with Dow Corning high vacuum grease. A cloth was lightly dampened with the grease and rubbed on the outside surface of the bladder. Only enough grease to leave an invisible film was used. The same thin coating was applied to the inside of the aluminum skin in contact with the bladder. The bladder was then reinstalled in the ESS vehicle. Subsequent testing of the vehicle showed the deployment pressure to be 0.25 psi. Figure 14 shows the folded bladder in the retracted position. Figure 15 shows the bladder with vehicle in the extended and pressurized condition. Note the three bungee cords per section that assist in bladder folding during retraction.

C. Combined Seal Leak Test

Two tests of the combined seals were performed in an atmospheric environment. For this test, the vehicle was placed in a temperature-stabilized room and pressurized to 11.25 psi. The vehicle pressure was adjusted again to 11.25 psi pressure after the internal temperature had stabilized at room temperature. The valves were then sealed shut and the pressurized vehicle allowed to stand for 54 hr. At the end of this period, the pressure had dropped only 0.05 psi, a leakage rate of 0.001 psi/hr. This amounts to a loss of 0.045 cu. ft./hr. of air at standard conditions, or 0.0034 lb./hr.

D. Secondary Seal Leak Test

This test was accomplished immediately after the combined seal leak test, and without removing the bladder from the vehicle. The bladder was unsealed and unfastened at the bottom end and tied back to admit internal air pressure between the bladder and the vehicle structure.

For this test, the vehicle was pressurized to 11.0 psi and allowed to stand for a period of 7 hr. The pressure during this period decayed approximately 0.7 psi, leakage rate of 0.1 psi/hr. This leakage rate is adequate to permit an astronaut to locate and make repairs to the primary pressure seal without losing an excessive amount of vehicle pressure.

E. Environmental Chamber Test

Environmental chamber testing of the ESS vehicle was performed by Lockheed Missiles and Space Company in its high vacuum orbital simulator (HIVOS) test chamber. For this test, the necessary instrumentation was installed at Martin-Denver, and the ESS vehicle was shipped to Lockheed at Sunnyvale, California.

1. Heat Flux Simulator

A solar heating simulator was designed and fabricated by Lockheed. General Electric 1600 T3 infrared heat lamps were installed on the simulator in vertical rows to provide simulated solar, earth emitted, and earth reflected heating to the vehicle.

2. HIVOS Testing

Deployment Test - The ESS was mounted on the door of the HIVOS environmental chamber and the heat flux simulator lowered over it and fastened in place. The door, which is the bottom of the chamber, was raised with the ESS in place, and closed. The HIVOS was pumped down to a pressure level of 3×10^{-6} torr. After 2 hr. in this vacuum, vehicle deployment was started. Deployment motion was monitored by TV. The cannistered TV camera is seen in Fig. 18. For this testing, the camera was pointed upward. Deployment was smooth with a slight tilting and subsequent straightening action near the end of travel of each section. The maximum pressure during deployment was 0.28 psi to full extension. This compares with a pressure of 0.25 psi for deployment in the atmosphere.

Leakage Test - Leakage tests were made using the 0 to 15 psi absolute pressure gage transducer within the vehicle. Compensating for temperature changes, the pressure in the ESS dropped from 10.95 to 10.90 psi in 8 hr., a loss of 0.00625 psi/hr., or 0.03 cu. ft./hr. of gas (at standard conditions). This leakage rate is approximately six times as great as that measured in the atmosphere but is probably not as accurate. This number may be somewhat in error because of the short test duration and temperature fluctuations.

Thermal Test - The space thermal environment was simulated during this test. Only the cylindrical portions of the vehicle were under test. The top and bottom were thermally isolated by a multilayer radiative type super-insulation covering these areas.

The vehicle test configuration had multilayer insulation installed between the inner and outer skins. The outer skin had been previously painted with Dow Corning Q-9-0090 (white) dimethyl silicone paint. The heat flux was provided by the heat flux simulator gage shown in Fig. 18, which had previously

been placed over the ESS vehicle. The solar, earth-emitted, and earth-reflected heat was simulated by vertical rows of 3/8 in. diameter by 18 in. long tungsten quartz heat lamps. These are General Electric 1600 T3 infrared lamps seen in Fig. 18.

During the thermal test, the HIVOS chamber remained evacuated and the chamber walls were cooled to liquid nitrogen temperatures to simulate outer space. The heat lamps were turned on, with the voltage in each vertical lamp row controlled to give the proper heat flux in that area. The actual heat flux that the vehicle would see in flight is shown in Fig. 19. Note that the absorptance (α) of the vehicle coating is 0.16 for the solar radiation spectrum and 0.90 for the long wavelength of the earth-emitted radiation. The actual heat flux values used for tests are shown in Fig. 20. These values compensate for a quoted absorptance (α) of 0.20 for the thermal coating in the heat lamp infrared spectrum in place of the solar absorptance of 0.16.

To simulate this heat flux curve, the heat lamp voltage varied from 44 volts to a maximum of 135 and then down to 50 around the periphery of the ESS vehicle producing the proper input heat distribution.

The raw data from the thermal test instrumentation was reduced and corrected for the following factors:

- a. Variation in coating properties;
- b. Variation of absorptance with infrared wave lengths;
- c. Unpainted guide rails;
- d. Internal blower temperature.

The temperatures from this analysis are shown in Fig. 21 and show fair correlation with test results for outer skin temperatures, shown in Fig. 22. Although there is not exact agreement between test temperature data and computed values, the agreement is satisfactory and indicates that the original computed values of temperature for the vehicle in earth orbit flight are applicable.

F. Cycle Test, Ground Environment

The cycle test was to demonstrate reliability and repeatability of deployment of the ESS vehicle in an atmospheric environment. The test plans called for 20 cycles of extension and retraction. Many unplanned extensions, retractions, and pressurization cycles were performed before the formal cycle test. Consequently, it was decided that the full 20 cycles would not be performed during this test. The vehicle now has accomplished over 30 tabulated cycles, including those performed in the cycle test.

G. Structural Tests

The structural confirmation of the ESS vehicle consisted of two tests, a boost phase load test and an ultimate pressure test.

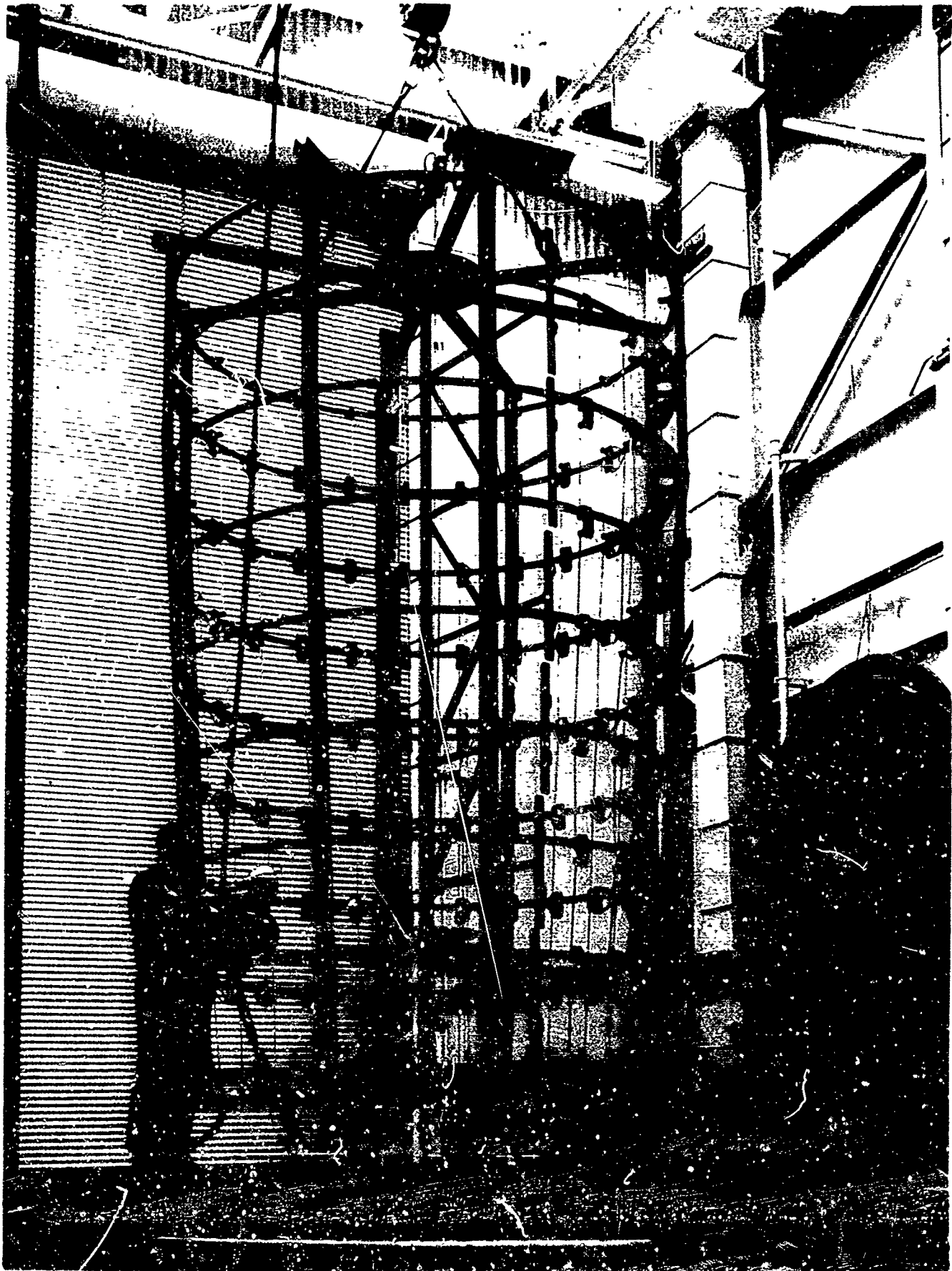


Fig. 18 Heat Flux Simulator Cage

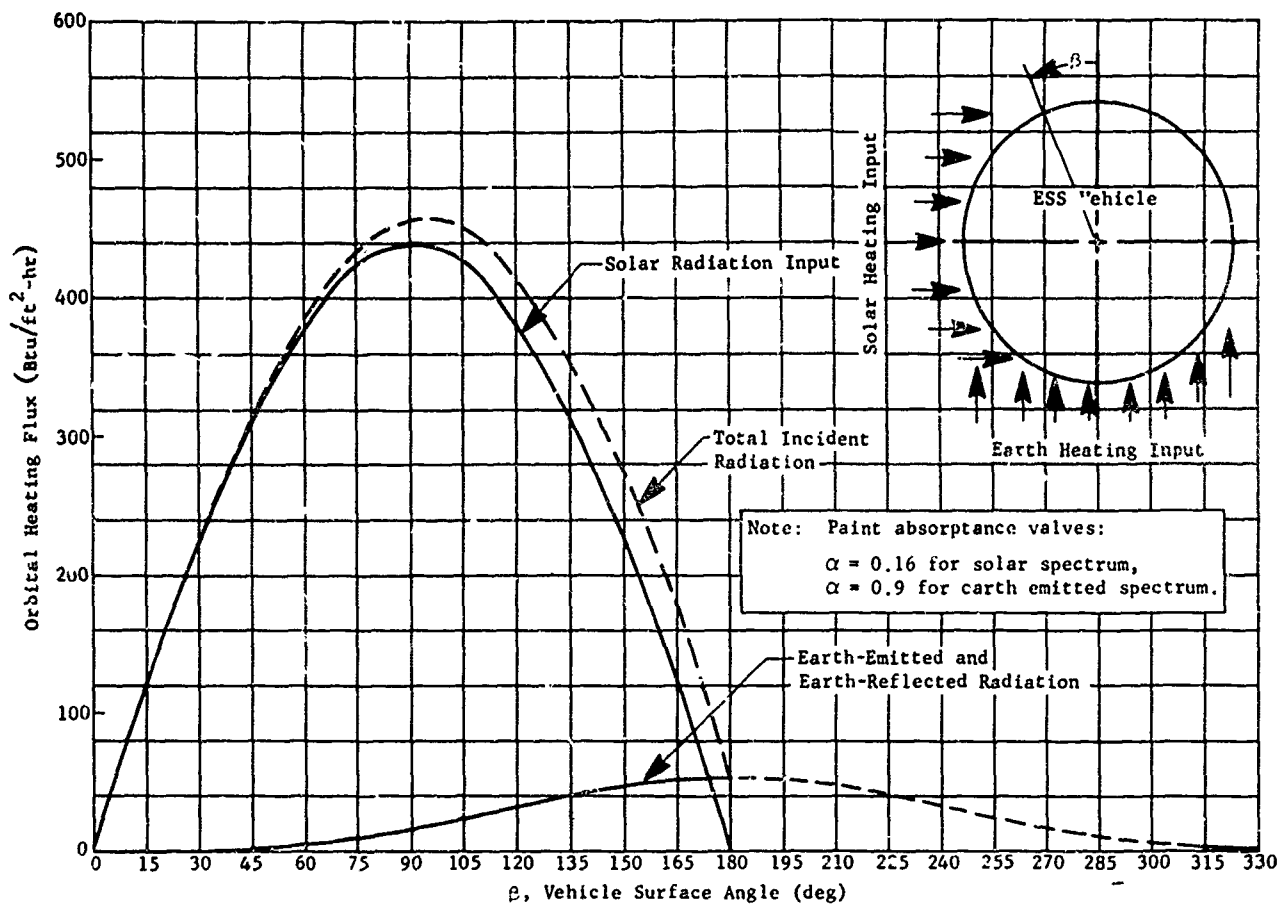


Fig. 19 Space Flight Heat Flux (Polar Orbit)

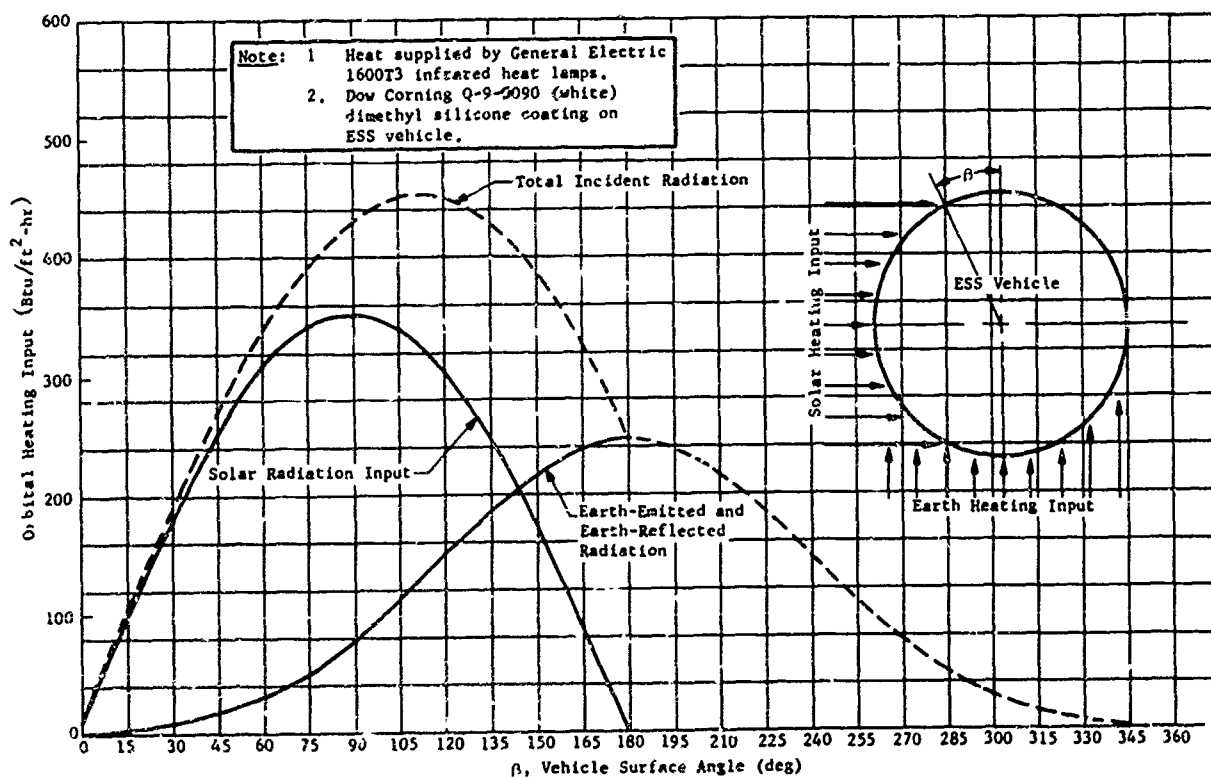


Fig. 20 Heat Flux Input for Thermal Test

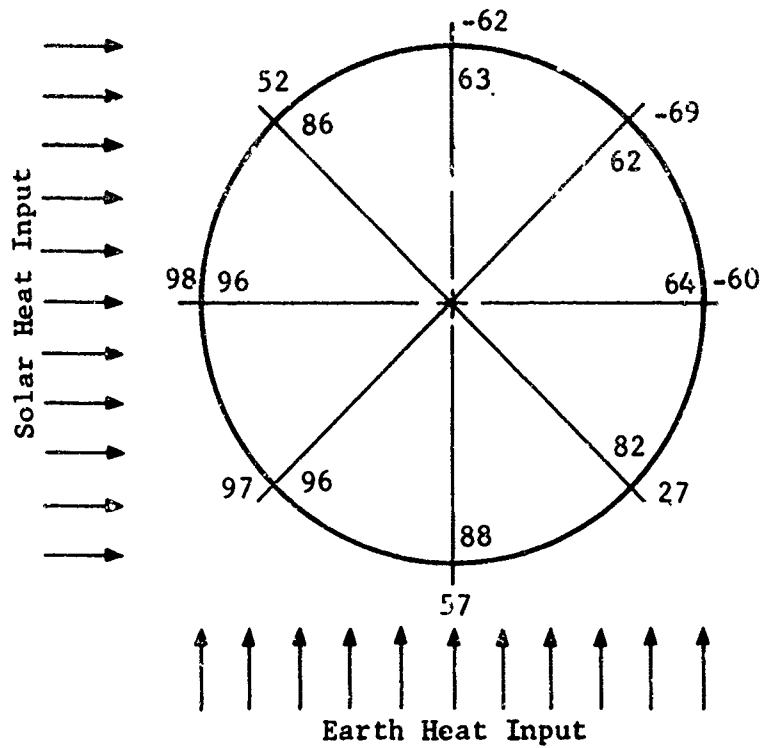


Fig. 21 Calculated Temperatures using Revised Input Data

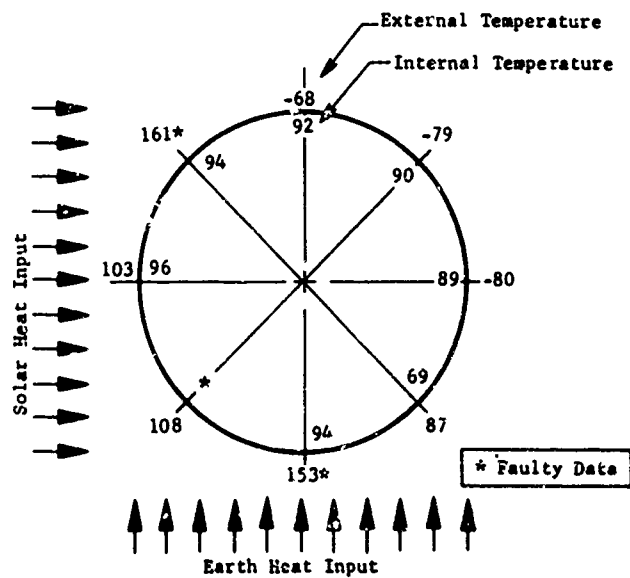


Fig. 22 Thermal Test Recorded Temperatures (°F)

1. Boost Phase Load Test

The objective of this test was to demonstrate the capability of the expandable space structure to withstand maximum loads imposed during boost. The critical loading condition occurs during maximum dynamic pressure when critical shear, moment, and compressive loads are imposed on the outer section with the vehicle in the collapsed position. At the same time, burst and collapse pressures are imposed on the outer skin panels.

The vehicle was mounted to a base loading fixture in the collapsed position, and the outer section was bolted down. All applied loads were reacted in the base fixture. The vehicle was filled with water to minimize the hazard. It was then pressurized at the crown of the dome to 5.8 psig. Axial and side loads were applied through a loading head attached to the forward adapter skirt. Side load was also applied directly into the skirt. Burst pressure load was simulated on the leeward stringers by applying load directly through load beams. Collapse pressure was simulated on the wind-ward external skin panel with pressurized air bags.

2. Ultimate Pressure Test

The objective of the ultimate pressure test was to demonstrate capability of the space station structure to withstand 150% operating pressure (16.5 psig) internally without failure. The vehicle was complete including internal bladder.

During the ultimate pressure test the vehicle retained pressure with no apparent leakage, although a precise leakage test was not performed in conjunction with this test. A routine check of the vehicle after the ultimate pressure test showed no evidence of structural failure. This was to be expected since most of the pressure structure was designed to criteria other than strength requirements.

POTENTIAL USES

Potential uses of ESS vehicles are shown in Fig. 23 through 27. Figure 23 shows the ESS used in artificial gravity simulation vehicles. In this concept two space capsules are joined together by a telescoping tube. The whole unit is retracted for launch and the telescoping tube is expanded in orbit to provide a rigid joining structure for the two end capsules. The tube would provide the necessary structure for centrifugal loads (artificial gravity) produced by spinning and provide a meteoroid protection passageway between capsules for personnel traffic. The tube could be pressurized to provide a shirt-sleeve environment if desired. Advantages of this approach over a cable system joining the two end capsules include bending and torsional rigidity. This eliminates the boat-rocking sensation in the end capsule due to personnel movement and the torsional windup which results with a cable system. In addition, cable tangling during deployment is eliminated as a potential hazard.

Figure 24 shows a space station using an expandable space structure tube to provide physical separation of the personnel capsule on one end and a nuclear power package on the other end.

Figure 25 shows a manned space vehicle using the telescoping structure as a partial garage for a personnel re-entry vehicle. Such a garage could provide a pressurized shirt-sleeve environment around the vehicle for making repairs, inspections, etc., and would prevent loss of tools in space. The garage could be large enough to accept the entire re-entry vehicle and have a closure door if desired.

Figure 26 shows a space vehicle with a portion of the vehicle designed of an expandable space structure. This vehicle illustrates a concept that could be used to circumvent boost-imposed payload length limitations.

Figure 27 shows the entire vehicle fabricated as an expandable space structure.

CONCLUSIONS AND RECOMMENDATIONS

The expandable space structure program has been successfully completed. In retrospect, the following observations can be made concerning expandable structure:

- Large size telescoping structure fabricated of individual rigid segments is quite feasible.
- Short coupling of rigid cylinders (small engaged length/diameter) at full extension does not necessarily produce binding if properly designed.
- Telescoping structure is somewhat heavier than nontelelescoping structure, but not prohibitively so.
- Deployment of semirigid telescoping structure by internal pressure is feasible and is an acceptable means of extension.
- Leakage rates of telescoping structure can be kept low enough that long-term internal pressurization is feasible and practical.

The weight of the present ESS vehicle is approximately 40% heavier than that of a comparable nontelelescoping structure. The majority of this weight difference is due to the large eccentricity in longitudinal load in the inner skins in stepping down from one telescoping segment to the next. The ring frames are heavy to react this resulting moment. The large eccentricity is due in turn to the double-wall structure for meteoroid protection. If the outer skins were designed to package against the inner skin in the retracted vehicle position and be spring loaded to move away from the inner skin after vehicle extension, the eccentricity can be reduced and a considerable weight savings achieved. The telescoping structure weight would then be much closer

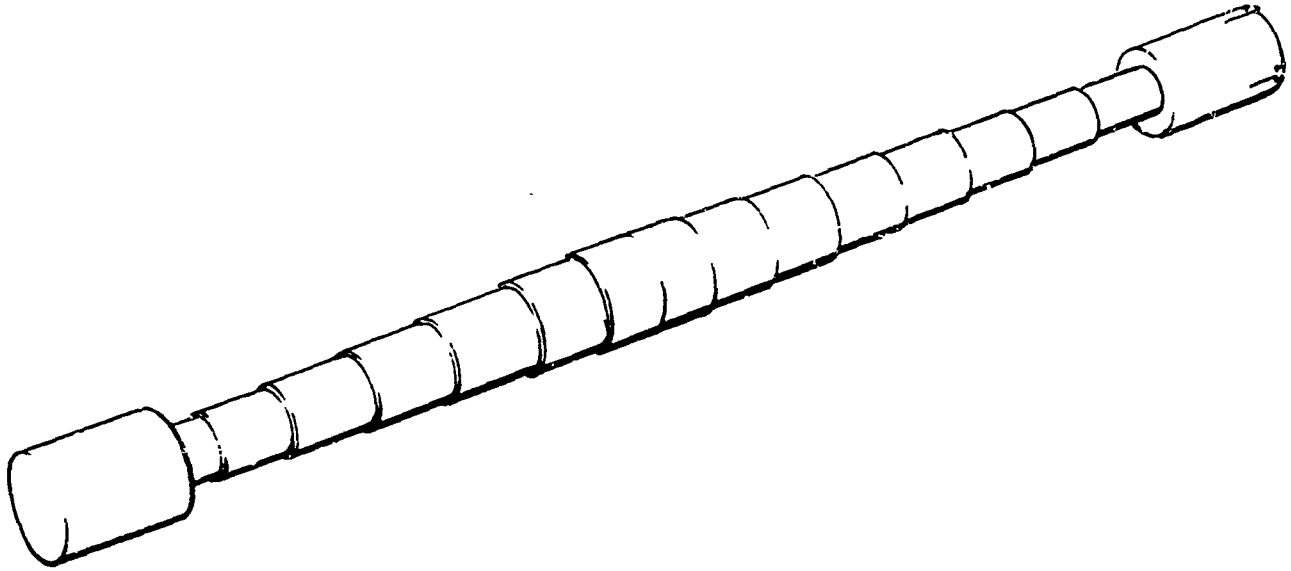


Fig. 23 Artificial Gravity Simulation Space Vehicle
using Expandable Space Structure

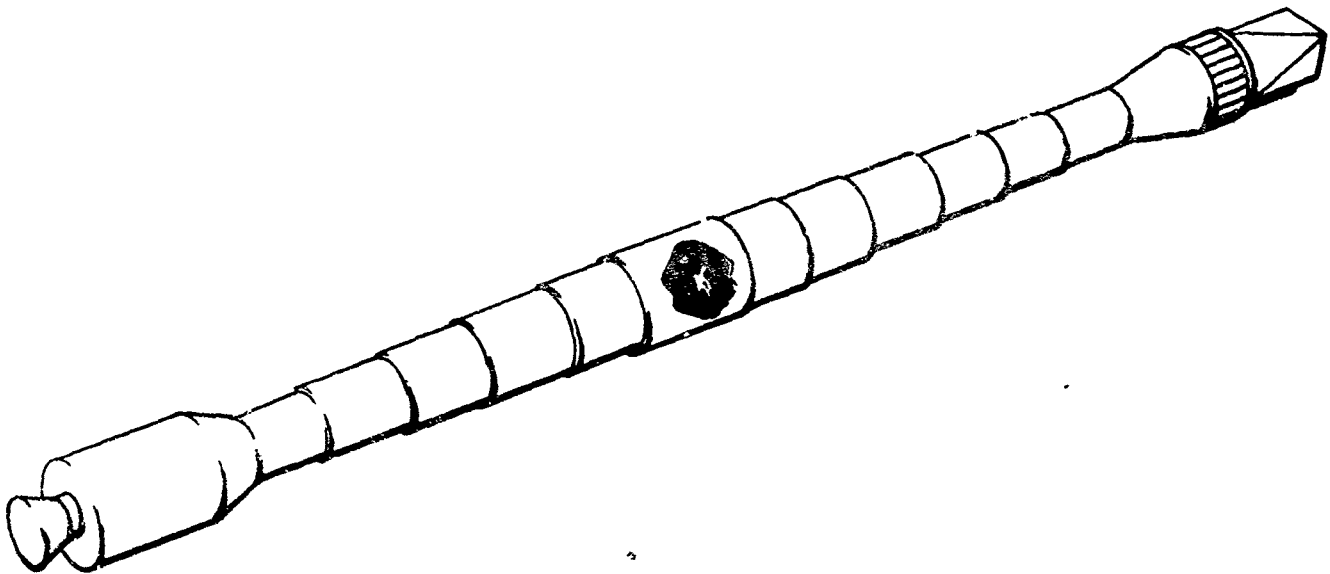


Fig. 24 Space Station Manned Module Separated from Nuclear Power Supply by
Expandable Space Structure

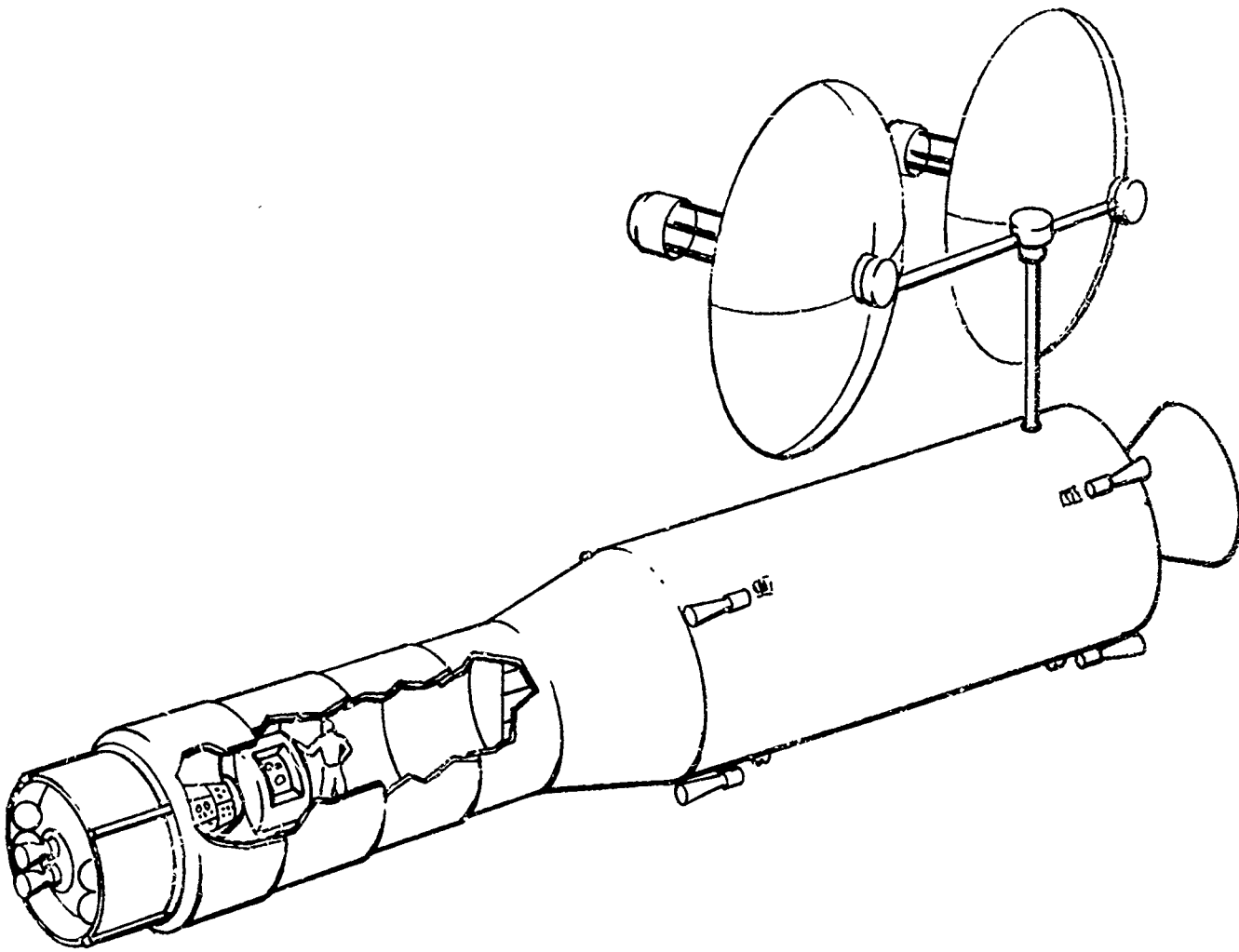


Fig. 25 Expandable Space Structure used as Partial Garage for Re-Entry Vehicles

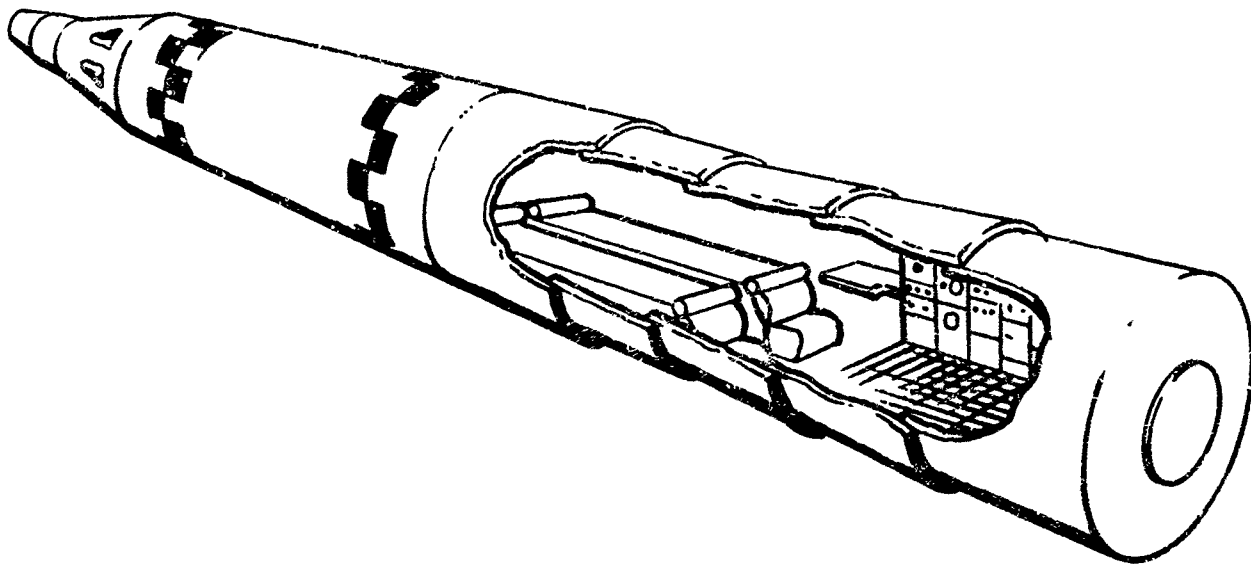


Fig. 26 Space Vehicle using Partial Construction of Expandable Space Structure for Living Quarters

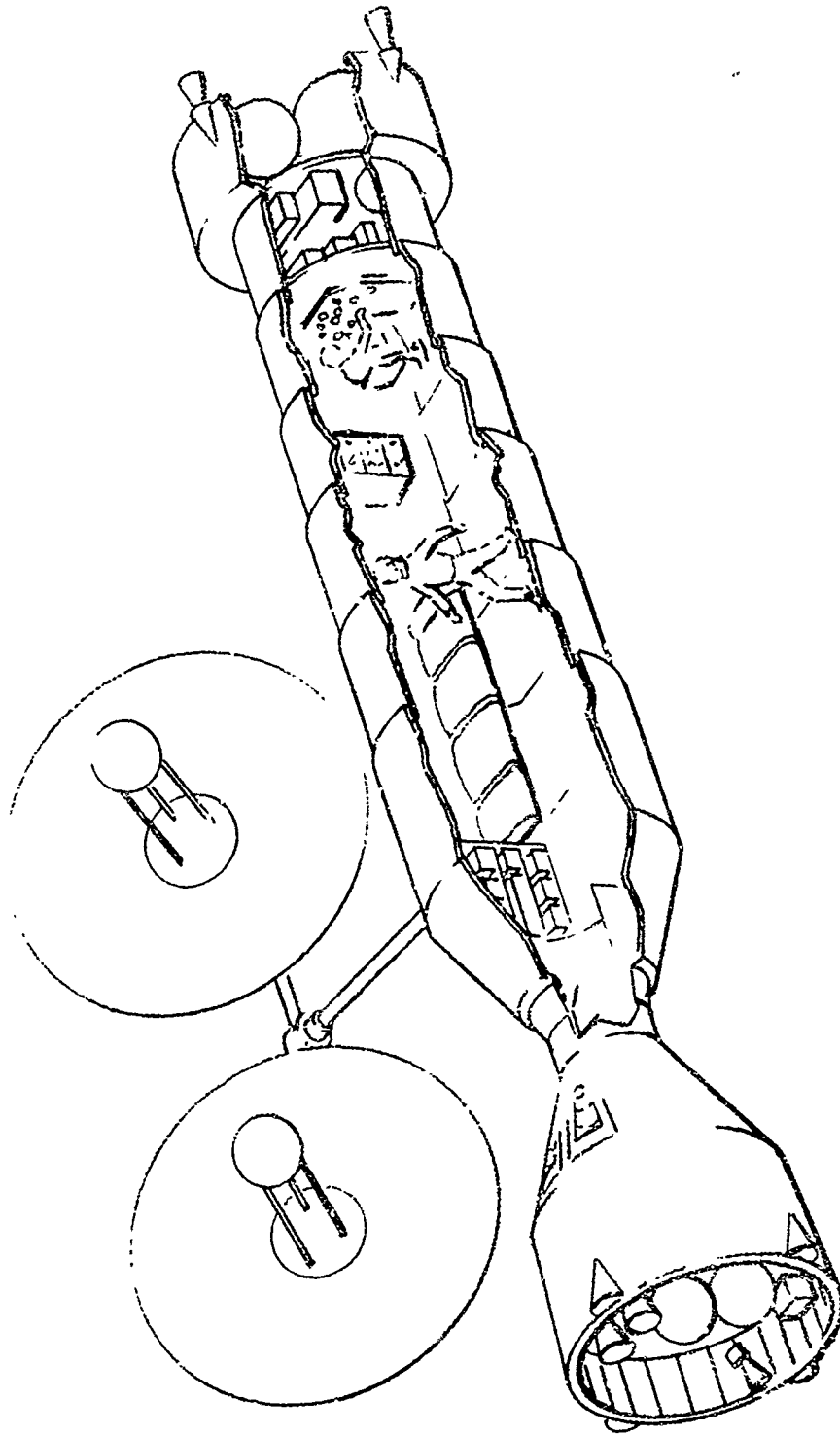


Fig. 27 Space Vehicle Designed Entirely of Expandable Space Structure shown
Rendezvoused with Re-Entry Vehicle

6

to that of a nontelelescoping structure and possibly equal it. An advantage of the telescoping structure is that most of the outer skin can be light. It does not have to be heavy gage to resist aerodynamic heating and panel flutter.

It is recommended that telescoping expandable space structure be seriously considered for the following applications:

1. Structural applications for manned or unmanned space vehicles where vehicle length proves to be restricted by booster considerations or other problems;
2. Structural applications for joining multiple space units, such as joining two or more space capsules in an artificial gravity configuration. The tubular telescoping components provide a structure that is rigid in bending, in torsion, and axially, once extended. It provides protected passageway for personnel moving from one vehicle to another;
3. Space vehicles, either manned or unmanned, where a large amount of relatively empty space is desired.

Expandable space structures of the type described in this report can provide a long-term pressurized environment for human occupants and when painted with suitable coatings can provide tolerable occupancy temperatures by passive thermal control. This is desirable for passageway, etc., as well as for basic space vehicle modules.

BUILDINGS IN BARRELS, PART III

S. B. Swenson

U. S. Army Engineer Research and Development Laboratories

Fort Belvoir, Virginia

INTRODUCTION

First thinking and origin of the principles utilizing low bulk materials for rapid fabrication of structures in remote areas dates back many years and the origin is obscure; however, records of these Laboratories indicate some investigations were conducted as early as 1959, utilizing inflated structures, reinforced plastics and foam insulation. Lack of funds prevented any significant research and it remained for the Climatic Research and Test Branch of the Laboratories to place the impetus which finally accelerated the program with its presentation of the concept as the "Buildings in Barrels" approach to military structures.

In rapid order after this, a first building was designed, fabricated and exhibited in Puerto Rico in February 1961, and a second building was exhibited at the Pentagon in the same year.

Concurrently, plans were under way for participation in the Arctic Housing program during the 1961 summer season. For this the USAERDL rushed the construction of molds of improved design. During July, August and September of that year, the Task Group constructed two buildings in the Arctic: one, 16 feet x 30 feet located in an ice tunnel, and another, 16 feet by 70 feet located in a snow trench. This application of plastics in building construction drew wide attention and captured top honors at the Society of the Plastics Industry Conference Exhibit in 1962.

These original structures still stand as excellent examples from the standpoint of utility and after four years no new design has evolved which offers more simplicity of erection or better insulation or livability. It has been necessary, however, to sacrifice some of these advantages in favor of more important considerations, such as the reduction of man-hours and support equipment required.

We now entertain the possibility that many of the considerations in the concept which attract the earth-bound user also pertain to space applications. The following report is presented as a possible contribution toward advancement in that field.

DESCRIPTION OF ARCTIC BUILDING

The Arctic building was of modular design utilizing stressed skin panels of reinforced glass fiber with polyurethane foam core. Each module consisted of three distinct sections: Wall, ceiling and floor components. The modules were keyed to each other through the use of a tapered tongue and groove system and held together at the base by a clip angle and pressure sensitive tape over the wall and ceiling or roof joints. These basic modules were so designed that

a combination of 4 wall panels, 4 floor panels and 2 ceiling panels would produce six linear feet of building. The end walls were fabricated in one piece. The equipment required to field fabricate these panels included: (a) Glass fiber-polyester spray equipment. (b) Polyurethane metering and mixing machine. (c) Molds (6 sets floor molds, 3 sets each ceiling and wall molds and 1 end wall mold). (d) Materials such as polyurethane foaming resins, polyester resins, and glass fiber roving.

The fabricating process was essentially as follows: (a) Disassembled molds were treated with parting compounds to facilitate casting release. (b) The mold faces were then sprayed with polyester resin and chopped glass fiber compacted by rolling with paint rollers. (c) The prepared molds were then assembled and predetermined amounts of foam were introduced into the mold cavity through charging holes. (d) After the foam had expanded to fill the cavity, the completed structural unit was removed from the mold and post cured for 24 hours prior to assembly.

TESTS, EVALUATION AND CONCLUSION (ARCTIC STRUCTURE)

The photographs, charts and notes, Figures 1 thru 12, following the text present a comprehensive test report on the Arctic Structures.

In evaluating the Arctic operation, the following conclusions were set forth:

Problems:

a. **Rate of Production:** It has been determined that the military target for acceptable field production rate should not be less than one 16 foot x 48 foot building in 8 hours with 8 men. The Arctic test proved, however, that considerable research and development in field fabrication technique was necessary to acquire the rate of production desired.

b. **Equipment:** A considerable amount of unnecessary and inefficient equipment was shipped to the Arctic for use in fabrication of the two buildings, most of which would have to be eliminated or reduced in bulk.

1. **Polyurethane foam metering and mixing equipment:** The mixing and metering machine used in the Arctic had a working capacity of approximately 10 pounds per minute. Complications arising from the low capacity of the machine considerably extended the pour time for each casting and was the cause of an excessive amount of reject panels.

2. **Glass fiber-polyester spray laminating equipment:** This equipment performed very well but in the final analysis, the spray process requires complicated equipment in the field, demands considerable time (mixing resins, spraying, rolling, cure time, trimming, and cleaning molds, applying wax and other mold release agents, etc.) and presents toxicity and waste problems. Since there is no logistic advantage in spray laminating in the field, methods or designs utilizing commercially available sheet stock are more attractive.

c. **Complexity of Molds:** The costs of polyurethane foam materials in the early stages of the program dictated that designs should observe maximum conservation of material consistent with good structural value. The final panel design had a nominal thickness of 2" and utilized a moulded in rib section around the perimeter as a load supporting member. This design increased the bulk of the mold and complicated fabrication. The number of molds required to fabricate the Arctic buildings also increased the amount of material shipped. A total of four different type molds was required i.e., end wall, side wall,

roof panel and floor panel. To minimize the bulk of material shipped to the field for fabrication, it is desirable to design the building so that one mold can be utilized to fabricate several different components.

d. Snow and wind load requirements: Army regulations for the operation of material under extreme conditions of environment requires that such structures withstand a maximum of 40 pfs snow load and 80 mph winds with gusts to 120 mph. However, the configuration or slope of the elliptical arch design is such that snow will accumulate on no more than the middle two thirds of the roof. Also, because of their light weight, these plastics buildings will require tiedown arrangements to withstand lifting forces present under high wind conditions. Therefore, it is believed that snow and wind load requirements for the shaped arch building need not exceed 30 psf (uniform over entire building) and 80 mph, respectively.

SUMMARY OF FINDINGS (ARCTIC STRUCTURES)

In the statement under rate of production, the acceptable rate of production was indicated to be approximately 64 man-hours per 16 ft. x 48 ft. building. The 100 feet of building that was fabricated and erected in the Arctic consumed some 6000 man-hours. Even considering the experimental nature of the project, it is very evident that other designs or methods would have to be developed. Also, even though material shipping bulk coincided with the original logistic concept, the bulk of the support equipment assumed such large proportions as to far outweigh the original advantage, especially for low production requirements.

Continuing research was programmed to:

- a. Evaluate other methods:
 1. Sprayed Shelters.
 2. Honeycomb Structures.
- b. Modify design and techniques of the Arctic structures.

Two sprayed shelters, (Figures 13 and 14) were constructed at USAERDL, Fort Belvoir, neither of which offered enough advantages to warrant further study. The effort to spray glass fiber laminates and polyurethane foam on the interior of inflated shelters was beset by so many difficulties that the program was terminated.

A more lengthy study was made utilizing both plastics faced and aluminum faced paper honeycomb core panels, (Figures 15 and 16) as a building material. Shipping unexpanded paper honeycomb and processing in the field offers approximately the same logistic advantage as polyurethane foam as a core material. Moreover, equipment and techniques required for fabricating panels are very simple, and shaped panels utilizing honeycomb paper core develop tremendous strengths. There is however one major disadvantage in that the insulation value of this type of panel is low, and no practical field method has been found to improve it. Limited research continues along this line, but maximum effort has been concentrated on simplification of design and fabrication techniques of the original shaped panel building. The happy circumstance of declining cost of foaming materials (approximately \$1.25 per lb. in 1960 to 40¢ - 50¢ per lb. for some that are available today) permitted a new look at the original approach and afforded greater extravagance in the use of material and increased design freedom. Whereas, ribs and buttresses had been necessary to attain desired strength, it was now possible to achieve the same results utilizing panels with flat skins and varying core thicknesses.

The finalized modular design, (Figure 17) permitted the use of a two-piece flat skinned arch thus eliminating the separate roof arch and doing away with

the requirements for laminating equipment. Flat prefabricated skins can be shipped to the site in less space than an equivalent amount of laminating material, at the same time leaving equipment and waste at home. Another venture toward simplification was to revert to hand mixing (Figure 18) of the foaming material, thus eliminating the last bit of complicated machinery. This turned out to be highly successful and had become S.O.P. until recent developments in froth foaming, (Figure 19) projected a brighter picture. The adoption of flat skins or facing materials also opened the way for use of a variety of facing materials such as aluminum, steel, plywood, fiberboard, etc.

Further streamlining of the system was hampered by the cumbersome method of utilizing unit molds. The necessary bulk and handling of molds reduced productivity in the Arctic venture and much of this problem still existed.

To eliminate as much as possible the complexity and handling problem, a system of gang molds was devised whereby a practically continuous production line could be maintained, with minimum manipulation of mold components. Figure 20 shows a line drawing of the mold design together with building assembly diagrams.

This was the status of the project at the end of the second phase (Part II).

The system was checked out using a near prototype mold; a 3-man crew consistently produced satisfactory panels by this method, and there was therefore sufficient reason to maintain the assumption that a practical building and a method to produce it in the field is a feasible military objective.

In early 1964, a contract was awarded for the fabrication of a six cavity gang mold capable of producing 6 - 4 ft. wide half modules per production cycle with provisions for increasing this capacity if practicable. Molds for the end walls were fabricated at the USAERDL shops.

In the meantime, studies continued using a variety of skin materials other than glass reinforced plastics, including plywood, steel and aluminum. Variations of foam formulae and foam casting techniques were also studied in anticipation of ultimate application in the production molds. For practical reasons in present development, .032 aluminum sheet has been selected as surfacing material.

Although it does not necessarily follow that previous observations on the hand mixing and pouring of foaming materials should be modified, investigations of recent advances in froth foaming techniques have suggested an alternate procedure along these lines might be practicable: The complexity of metering machines is fast disappearing; the present system in use at the laboratories utilizes nitrogen pressurized supply tanks piped to metering pumps which discharge the chemical components into a labyrinth mixing chamber. Despite simplicity of design, results with this equipment are very satisfactory. Foam quality is consistently good, capacity is relatively high (22 lb/min) and molds can be charged without risk of excessive pressure build-up.

The Contractor-supplied gang molds were set up for production in July 1964 and several experimental panels were made using both of the aforementioned charging techniques. It was found that with the use of conventional foaming techniques the risk of bursting the molds was extremely high, in fact, during one attempt to introduce a complete charge in one shot, several cheek pieces were ruptured and had to be repaired. Conversion to froth foaming techniques obviated this problem and in the first full cycle operation of the gang molds six panel cavities were charged with froth foam, averaging 90 seconds charging time each or 9 minutes for the group.

The end wall design consisted of 4 vertical panels 4 ft. wide. The molds were designed so that each production cycle would produce a right and left hand component. The end wall production cycle also coincided with the module production rate so that two end walls would be produced for each 24 feet of building.

Although floor panel molds were designed that could be used in the same manner as the module gang molds, there seemed to be many situations where this type of floor would not be required. There was also some indication that a system could be devised that would permit the floors to be poured in place. Further work on the development of the floor system has been held up pending the results of research presently in progress.

Sub-surface Lunar installations, among others visualized in some space engineering concepts, bear remarkable similarity to present installations in the Arctic and Antarctic. In such applications where structures are isolated from exterior forces, whether it be snow, wind, rain or other phenomena, designs, techniques and materials would have to be developed which are compatible with the circumstances. It is conceivable that the inherent structural strength of polyurethane or other foam material developed for space application could obviate the requirement for core facing materials. Several prototype all-foam panels have been produced. Weighing only one half as much as the faced-foam core panels and possessing otherwise favorable characteristics, they are specially adaptable to low load applications.

FABRICATION

In October of 1964, a detail of six Army enlisted men were assigned to the USAERDL to be trained in the operation of the molds and equipment and to test the kit under near-field-conditions. By mid December, these six men had erected a 28 foot structure at Camp A.P. Hill in Virginia.

The process as now set up is as devoid of sophistication as our four years of research has been able to attain; aluminum skins are supplied on pallets, pre-cut, prime-ciated and ready for placement in the molds. After being placed in the molds, the cover plates are positioned and draw bars are inserted through the cover plates and mold cavity and engaged in threaded inserts in the base. These bars hold the whole assembly in alignment and contain the pressure of the expanding foam in the molds. The raceway, or hole, left in the casting when the bars are withdrawn is later used to hold the modules and end walls together in assembly by passing steel tie rods through the holes from end wall to end wall and drawing the entire structure together. To obviate the necessity of handling overly long tie rods, the rods are made up in sections with threaded ends that can be coupled together as they are passed through the panels. Taping the joints with pressure sensitive tape and cutting doors and windows, as required, completes the job.

Since the Camp A.P. Hill operation, several other structures have been fabricated. Another building, under construction as of this writing, is a special purpose structure for electronic testing, it is being fabricated with glass fiber laminate facings and will be entirely devoid of metallic parts except for screws fastening the building to the anchor sills.

With experience gained from experimental and test production studies, it has been possible to project an estimate of personnel and equipment requirements, and material and man-hour cost for producing a 16' x 32' structure in the field.

NOTE: Although the time studies were conducted as accurately as possible, emphasis should be placed on the fact that the man-hour figures indicated in the following outline are based on prototype production. Factual figures will not be available unless or until a production run of several units are fabricated under field conditions.

OUTLINE OF REQUIREMENTS

EQUIPMENT:

- 1 set each-gang molds for walls.
- 1 set each-gang molds for end walls.
- Polyurethane froth foam dispenser.
- Portable air compressor - approximately 1/4 H.P.
- Electric power for dispenser, portable tools and for heating molds, if necessary.
- Minimum shelter for initial operation, 16' x 24' heated structure in low temperature applications. (In tropics or temperate environment, minimal shelter can be fabricated on site).

MATERIAL:

- a. Foam - (2.2 lbs per cu. ft. density)
- | | | |
|---|---|-------------------------------------|
| Eight 4 ft. Modules @ 100 lbs. per module | - | 800 lbs. |
| Two End Walls @ 100 lbs. per end wall | - | <u>200 lbs.</u> |
| Total Requirements, Foam | | - 1000 lbs. @ \$0.60/lb. = \$600.00 |
- b. Aluminum Sheet (Alloy 3105-H25 .032 in. thick)
- | | | |
|--|---|---|
| Eight 4 ft. Modules @ 104 lbs per module | - | 832 lbs. |
| Two End Walls @ 124 lbs. per end wall | - | <u>248 lbs.</u> |
| Total Requirements, Aluminum Sheet | | - 1080 lbs. @ \$0.443/lb. = <u>478.00</u> |
| Total Material Cost, basic 16' x 32' w/o Floor | | = <u>\$1078.00</u> |

LABOR:

(8-man team with minimum training of 100 hrs. per man)

a. Fabrication:

- | | | |
|---|---|----------------|
| 1. Modules - One gang mold casting cycle per 24 M.H.
yields 6 panels (3 Modules) at an average of
4 man-hours per module. | | |
| Eight 4 ft. Modules @ 4 M.H. per module | - | 32 M.H. |
| 2. End Walls - One gang mold casting cycle per 6 M.H.
yields 4 panels (1 end wall) | | |
| Two End Walls @ 6 M.H. per end wall | - | <u>12 M.H.</u> |
| Total Fabrication time | - | 44 M.H. |

b. Assembly:

- | | | |
|---|---|---------|
| One 16' x 32' structure can be field erected
on a prepared base or level ground in 40 man
hours. An additional 8 man hours may be required
to provide doors and windows. | - | 48 M.H. |
|---|---|---------|

TOTALS:

Labor as calculated	-	<u>92 M.H.</u>
Labor incidental to operations (average)	-	<u>8 M.H.</u>
Total Labor	-	100 M.H.

Labor Cost, Basic structure w/o Floor (@ \$5.00/M.H.)		= \$500.00
Material Cost, basic structure w/o Floor		= <u>1078.00</u>

Total Cost per 16' x 32' Basic Unit		= \$1578.00
-------------------------------------	--	-------------

(Each additional 4' module: Material - \$106.00; Labor - \$20.00 = \$126.00)

SUMMARY

The concentrated research into the uses of expandable materials in field fabrication of military structures is bearing fruit. Buildings are presently in service and seemingly doing a good job and individual panels and modules are undergoing test. Modifications on the mold design are now underway and final tests are being programmed.

CONCLUSIONS

Our conclusions should be tempered by the fact that the research program "Buildings in Barrels" is not completed. We can, however, make certain observations on the basis of experience to date. We have witnessed the practicability of special purpose buildings in the Arctic and have fabricated and tested many shapes and designs which exceed requirements. There are many avenues of research still to be explored; design criteria must be stabilized, fabrication technology broadened and foaming equipment and materials can be improved.

The development of this concept at the laboratories has been viewed with interest by both the military and civilian. The desirability of exploring its potential for civilian application is evident. Easily heated, structurally sound and insect and vermin proof, such structures should find an attractive market for farm buildings, grain storage, etc. Emergency housing and Civil Defense are also a consideration.

Now, with the rapid mastery of space travel and exploration, the requirement for materials and methods for space fabrication of structures becomes more pressing. Expandable materials and collapsible molds, modified for operation in space atmospheres could be a solution. The past research of the plastics industry has developed polyurethane foam materials to the present state in little more than a decade. It should be logical to assume that with comparable diligence the next decade could turn up a material applicable to space structures. Progress and achievement is largely dependent upon the continued interest and participation of the plastics industry and various research organizations, both Government sponsored and commercial. Continued collaboration among these groups is essential for achievement of our goals.

REFERENCES

1. Ray H. Anderson, USAERDL, Ft. Belvoir, Va., Memorandum Report, Rigid Foam Plastic Shelters, Arctic Field Tests, 16 April 1962.
2. Robert K. Hedrick, and Abraham Perez, USAERDL, Ft. Belvoir, Va., Memorandum Report, Rigid Foam Plastics Shelters, Structural Tests of Reinforced Plastic Beams, Honeycomb Panels, and Experimental Arctic Building, 15 October 1962.
3. Abraham Perez and S. B. Swenson, USAERDL, Ft. Belvoir, Va., Memorandum Report, Rigid Foam Plastics Shelter by Spray Application to an Air Supported Mold, 30 July 1963.
4. S. B. Swenson, USAERDL, Ft. Belvoir, Va., "Buildings in Barrels" - Part II, Paper report to the Society of the Plastics Industry, Reinforced Plastics Division, 6 February 1964.



Figure 1. Glass Fiber, Polyurethane Plastics Building Located in a Snow Tunnel.

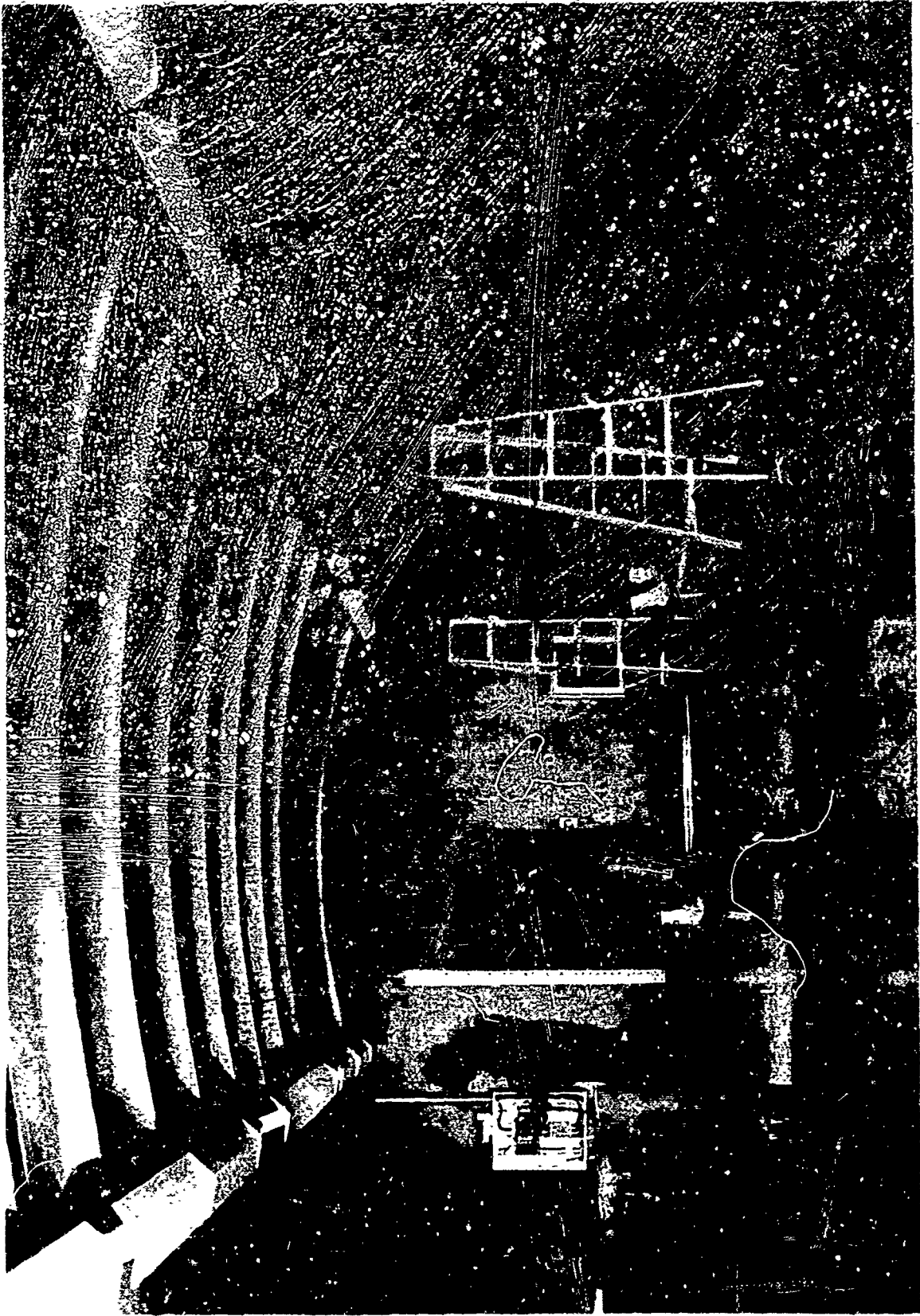


Figure 2. Interior of Plastics Building Illustrated in Figure 1

DESIGN WIND PRESSURES

WIND VEL. MPH	q PSF	C	WINDWARD WALL	C	LEEWARD WALL	C	WINDWARD ¼ ROOF	C	CENTER ½ ROOF	C	LEEWARD ¼ ROOF
40	4.1	0.70	2.9	-0.50	-2.0	-0.51	-2.1	-0.95	-3.9	-0.58	-2.4
50	6.4		4.5		-3.2		-3.3		-6.1		-3.7
60	9.2		6.4		-4.6		-4.7		-8.7		-5.3
70	12.5		8.8		-6.3		-6.4		-11.9		-7.3
80	16.4		11.5		-8.2		-8.4		-15.6		-9.5
90	20.7		14.5		-10.4		-10.6		-19.7		-12.0
100	25.6		17.9		-12.8		-13.0		-24.3		-14.9

NEGATIVE VALUES INDICATE EXTERNAL SUCTION ON BUILDING SURFACE.

V=WIND VELOCITY IN MILES PER HOUR

q=VELOCITY PRESSURE = $0.00256V^2$

C= SHAPE COEFFICIENT

p=DESIGN WIND PRESSURE NORMAL TO SURFACE (ACTING RADIALLY ON ROOF)

p=Cq IN LBS. PER SQ. FT.

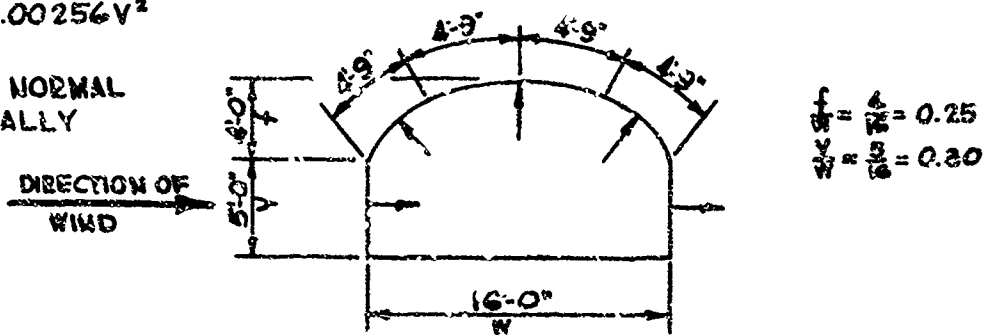
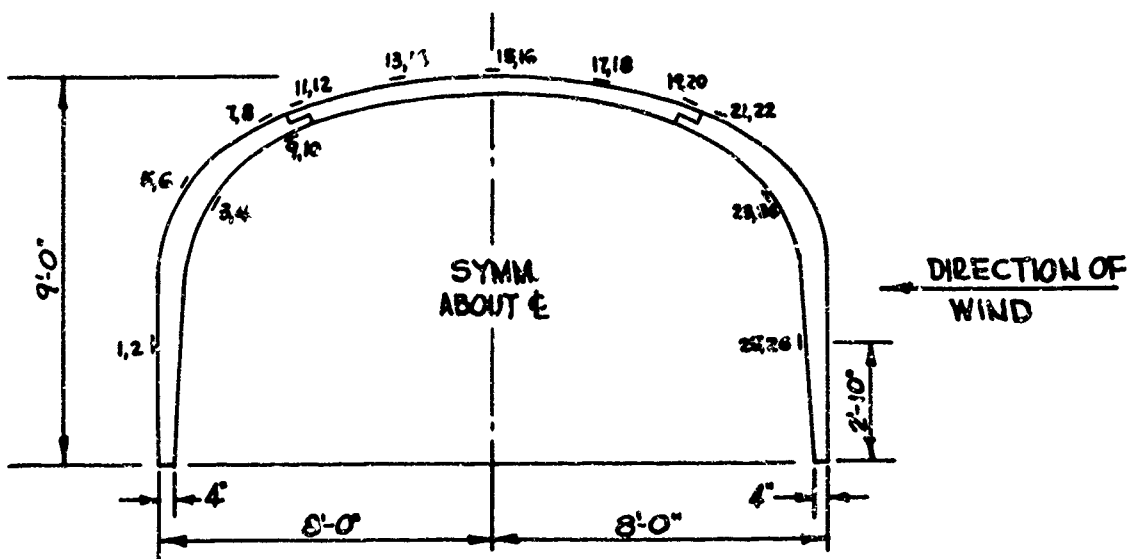


FIG. 3

WIND PRESSURE DISTRIBUTION

TOTAL APPLIED WIND LOAD ON 9'-0" SECTION OF BUILDING										
VELOCITY MPH	WINDWARD WALL		LEEWARD WALL		WINDWARD ¼ ROOF		CENTER ½ ROOF		LEEWARD ¼ ROOF	
	AREA-SF	P-LBS.	AREA-SF	P-LBS.	AREA-SF	P-LBS.	AREA-SF	P-LBS.	AREA-SF	P-LBS.
40	45	130.5	45	-90.0	42.75	-89.7	85.5	-333.3	42.75	-102.6
50		202.5		-144.0		-141.0		-521.4		-158.1
60		288.0		-207.0		-201.0		-743.7		-226.5
70		396.0		-283.5		-273.6		-1017.3		-312.0
80		517.5		-369.0		-359.1		-1,333.8		-406.2
90		652.5		-468.0		-453.0		-1,684.2		-513.0
100	↓	805.5	↓	-576.0	↓	-555.6	↓	-2,077.5	↓	-636.9

FIG. 4



LOCATION OF STRAIN GAGES
WIND LOAD TEST

NOTE:
1. STRAIN GAGES LOCATED ON BOTH
SIDES OF LONGITUDINAL JOINT, ALONG
RIB PORTION OF PANEL.

FIG. 5

E=0.80×10 ⁶ psi. STRESSES: KSI.		WIND LOAD STRESSES PLASTIC BUILDING - 16'-0"× 9'-0"			
Wind Velocity - MPH.		50	70	90	100
GAGES	1	0.088	-0.016	0.184	FAILURE
	2	0.084	-0.020	0.176	
	3	-0.088	-0.440	-0.616	
	4	-0.092	-0.428	-0.616	
	5	—	—	—	NO
	6	0.116	0.572	0.828	
	7	-0.108	-0.204	-0.008	NO READINGS
	8	-0.020	-0.108	-0.008	
	9	0.088	0.288	0.268	
	10	0.068	0.212	0.240	
	11	0.004	-0.028	0.060	FAILURE
	12	-0.004	-0.036	0.052	
	13	0.080	0.344	0.664	
	14	0.088	0.384	0.760	
	15	0.188	0.780	1.380	FAILURE
	16	0.188	0.796	1.400	
	17	0.060	0.300	0.520	NO READINGS
	18	0.064	0.296	0.500	
	19	-0.024	-0.144	-0.264	
	20	-0.020	-0.132	-0.248	
	21	-0.044	-0.276	-0.516	FAILURE
	22	-0.060	-0.324	-0.604	
	23	0.116	0.452	0.928	
	24	0.136	0.512	1.000	
	25	0.132	0.372	0.944	FAILURE
	26	0.140	0.388	0.904	
Deflections - ins.	VERT.	0.125	0.5625	1.125	
	HOR.	0.000	0.3125	1.3125	

FIG. 6.

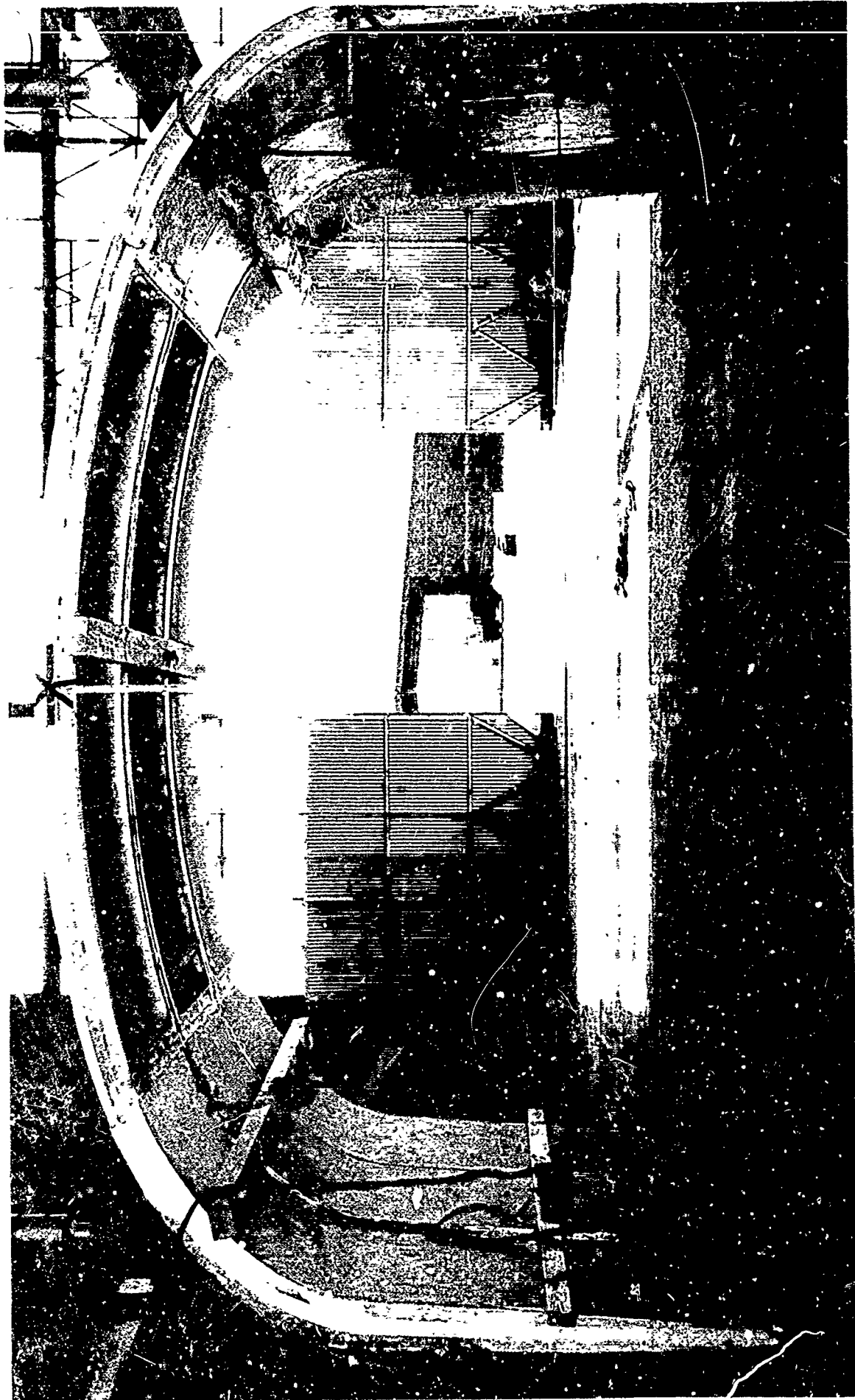


Figure 7. Test Setup for Application of Simulated Wind Forces on Shelter Test Module

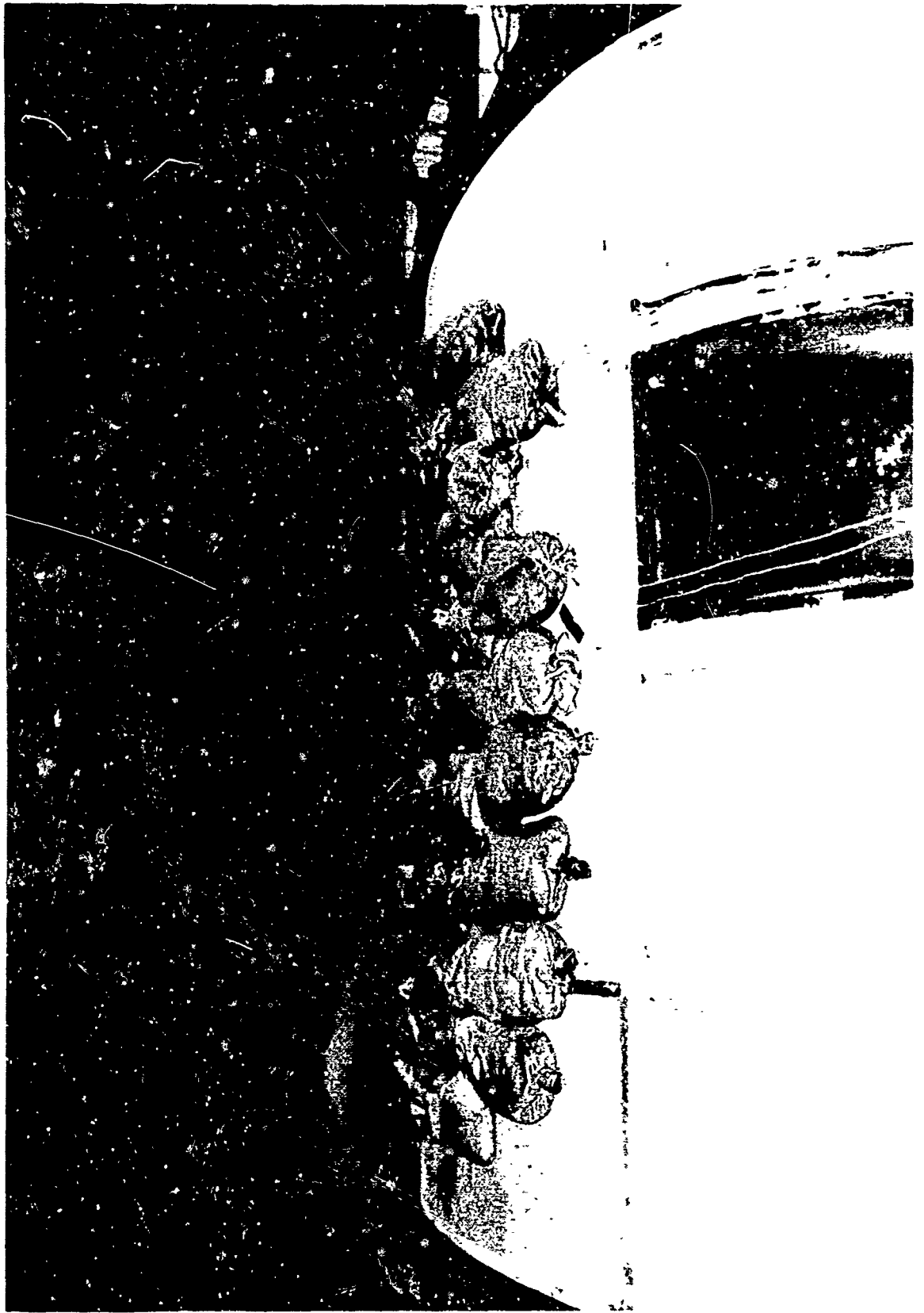


Figure 8. Test Setup for Application of Simulated Snow Load on Shelter Test Module

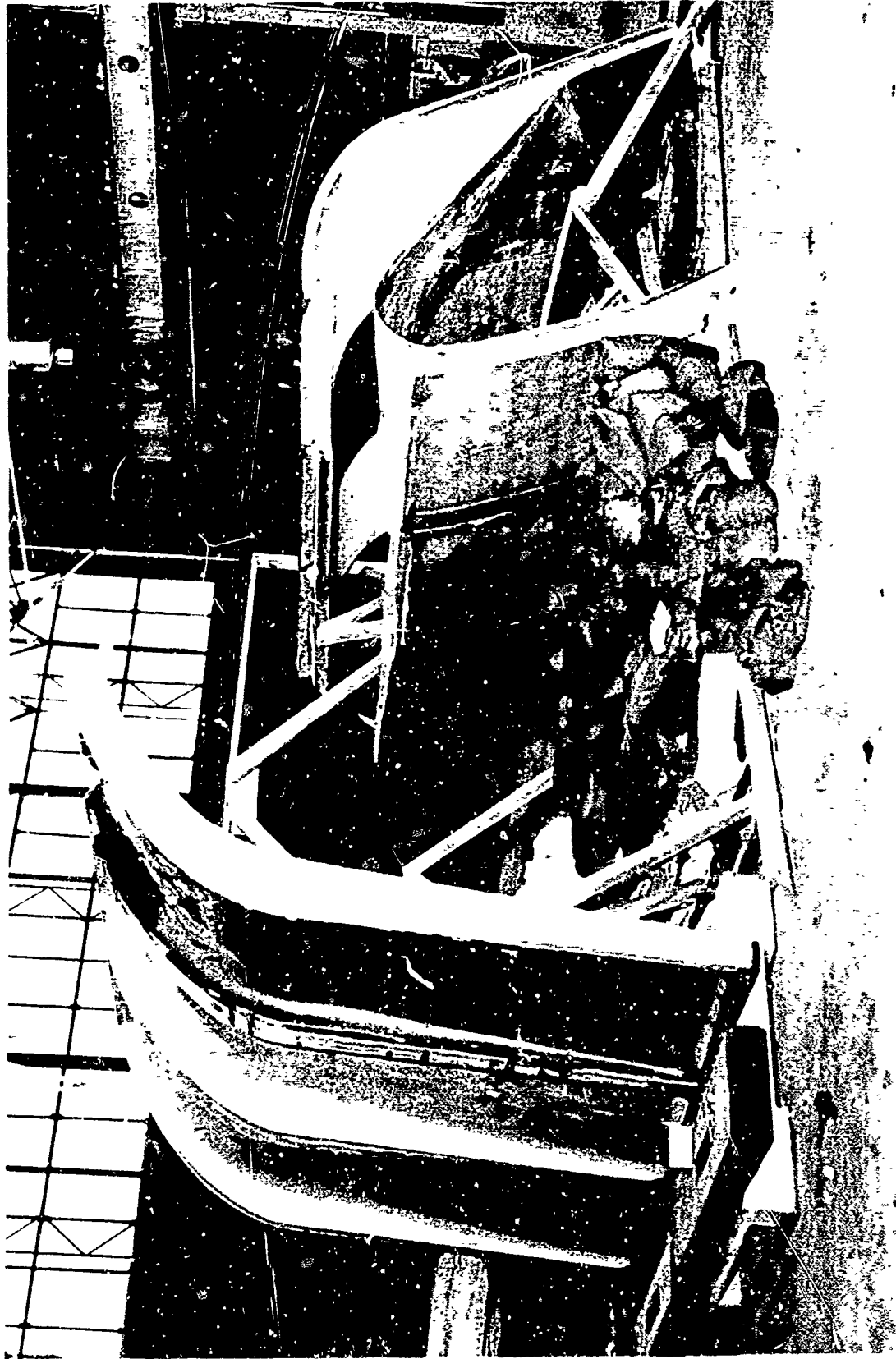
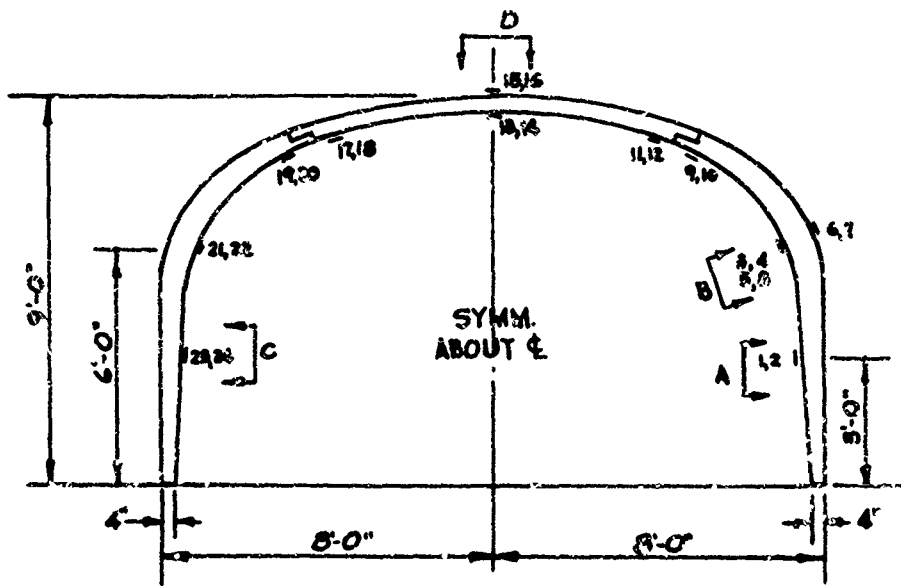
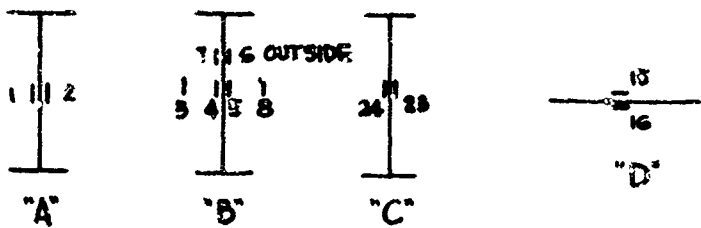


Figure 9. Failure of Shelter Test Module Under 50 PSF Sustained Simulated Snow Load



LOCATION OF STRAIN GAGES
SNOW LOAD TEST



NOTES:

1. STRAIN GAGES LOCATED ON BOTH SIDES OF LONGITUDINAL JOINT, ALONG RIB PORTION OF PANEL, EXCEPT FOR GAGES 3 + 8 THAT WERE POSITIONED MIDWAY ON THE PANEL FACE.

2. GAGES 6, 7, 15 + 16 WERE LOCATED ON THE OUTSIDE SURFACE OF SHELTER, THE REST, ON THE INTERIOR SURFACE OF IT.

FIG. 10

SNOW LOAD TEST
PLASTIC BUILDING - 16'-12"

LOAD	2000		2500		3000		3500		4000		4500	
	STRESS	MOMENT	STRESS	MOMENT	STRESS	MOMENT	STRESS	MOMENT	STRESS	MOMENT	STRESS	MOMENT
1	-124	55.8	-124	55.8	-124	55.8	-124	55.8	-124	55.8	-124	55.8
2	-124	55.8	-124	55.8	-124	55.8	-124	55.8	-124	55.8	-124	55.8
3	-124	55.8	-124	55.8	-124	55.8	-124	55.8	-124	55.8	-124	55.8
4	-124	55.8	-124	55.8	-124	55.8	-124	55.8	-124	55.8	-124	55.8
5	-124	55.8	-124	55.8	-124	55.8	-124	55.8	-124	55.8	-124	55.8
6	-124	55.8	-124	55.8	-124	55.8	-124	55.8	-124	55.8	-124	55.8
7	-124	55.8	-124	55.8	-124	55.8	-124	55.8	-124	55.8	-124	55.8
8	-124	55.8	-124	55.8	-124	55.8	-124	55.8	-124	55.8	-124	55.8
9	-124	55.8	-124	55.8	-124	55.8	-124	55.8	-124	55.8	-124	55.8
10	-124	55.8	-124	55.8	-124	55.8	-124	55.8	-124	55.8	-124	55.8
11	-124	55.8	-124	55.8	-124	55.8	-124	55.8	-124	55.8	-124	55.8
12	-124	55.8	-124	55.8	-124	55.8	-124	55.8	-124	55.8	-124	55.8
13	-124	55.8	-124	55.8	-124	55.8	-124	55.8	-124	55.8	-124	55.8
14	-124	55.8	-124	55.8	-124	55.8	-124	55.8	-124	55.8	-124	55.8
15	-124	55.8	-124	55.8	-124	55.8	-124	55.8	-124	55.8	-124	55.8
16	-124	55.8	-124	55.8	-124	55.8	-124	55.8	-124	55.8	-124	55.8
17	-124	55.8	-124	55.8	-124	55.8	-124	55.8	-124	55.8	-124	55.8
18	-124	55.8	-124	55.8	-124	55.8	-124	55.8	-124	55.8	-124	55.8
19	-124	55.8	-124	55.8	-124	55.8	-124	55.8	-124	55.8	-124	55.8
20	-124	55.8	-124	55.8	-124	55.8	-124	55.8	-124	55.8	-124	55.8
21	-124	55.8	-124	55.8	-124	55.8	-124	55.8	-124	55.8	-124	55.8
22	-124	55.8	-124	55.8	-124	55.8	-124	55.8	-124	55.8	-124	55.8
23	-124	55.8	-124	55.8	-124	55.8	-124	55.8	-124	55.8	-124	55.8
24	-124	55.8	-124	55.8	-124	55.8	-124	55.8	-124	55.8	-124	55.8
25	-124	55.8	-124	55.8	-124	55.8	-124	55.8	-124	55.8	-124	55.8

FIG. 11.

SNOW LOAD TEST LONG RANGE LOADING			
LOAD PSF	DATE	DEFLECTIONS- INS.	
		FRONT	BACK
0	3/9/62	0	0
20	3/9/62	1.125	1.250
20	3/12/62	1.250	1.1875
0	3/12/62	0.125	0.250
30	3/12/62	1.500	1.3125
30	3/13/62	1.750	1.5625
0	3/13/62	0.375	0.3125
40	3/13/62	2.125	2.000
40	3/14/62	2.375	2.375
0	3/14/62	0.625	0.4375
50	3/14/62	3.250	3.000
50	3/14/62	FAILURE	

FIG. 12.



Figure 13. Spraying Glass Fiber Laminate on Interior of Inflated Structure



Figure 14. Exterior of Sprayed Shelter. The Structure Consists of A 3" Foam Core with Interior and Exterior Skin of Reinforced Plastic

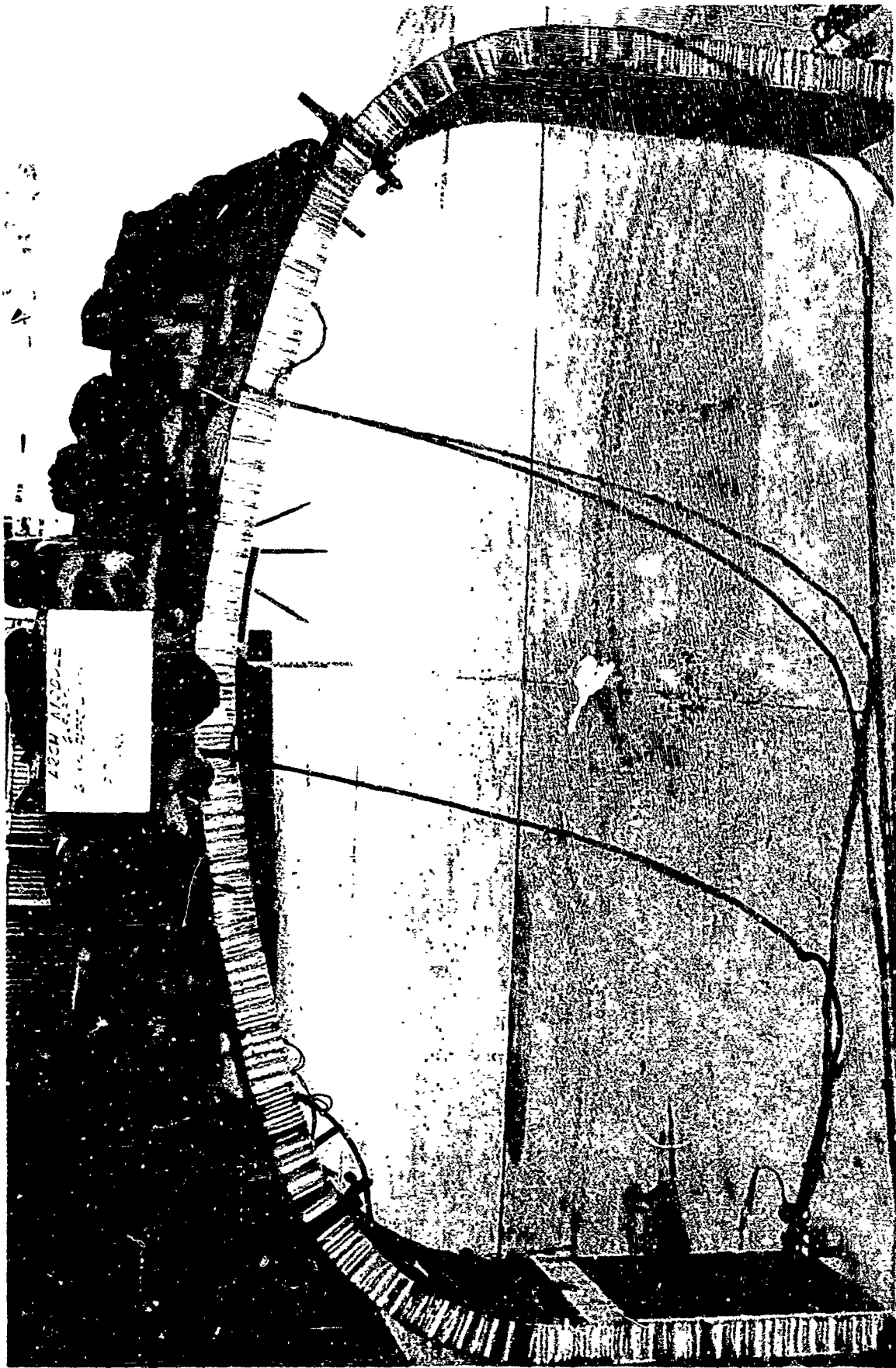


Figure 15. One of the Several Paper Honeycomb Shaped Panels Designed and Tested at Usardi. Note the Extreme Loading of 120 lb./sqx ft.



Figure 16. Aluminum Faced Paper Honeycomb Core Structure. Excessive Fabrication Time Caused Abandonment of this Design



Figure 17. Present Module Design -----Taking Observations of Deflections and Creep under 50 P.S.F. Loading

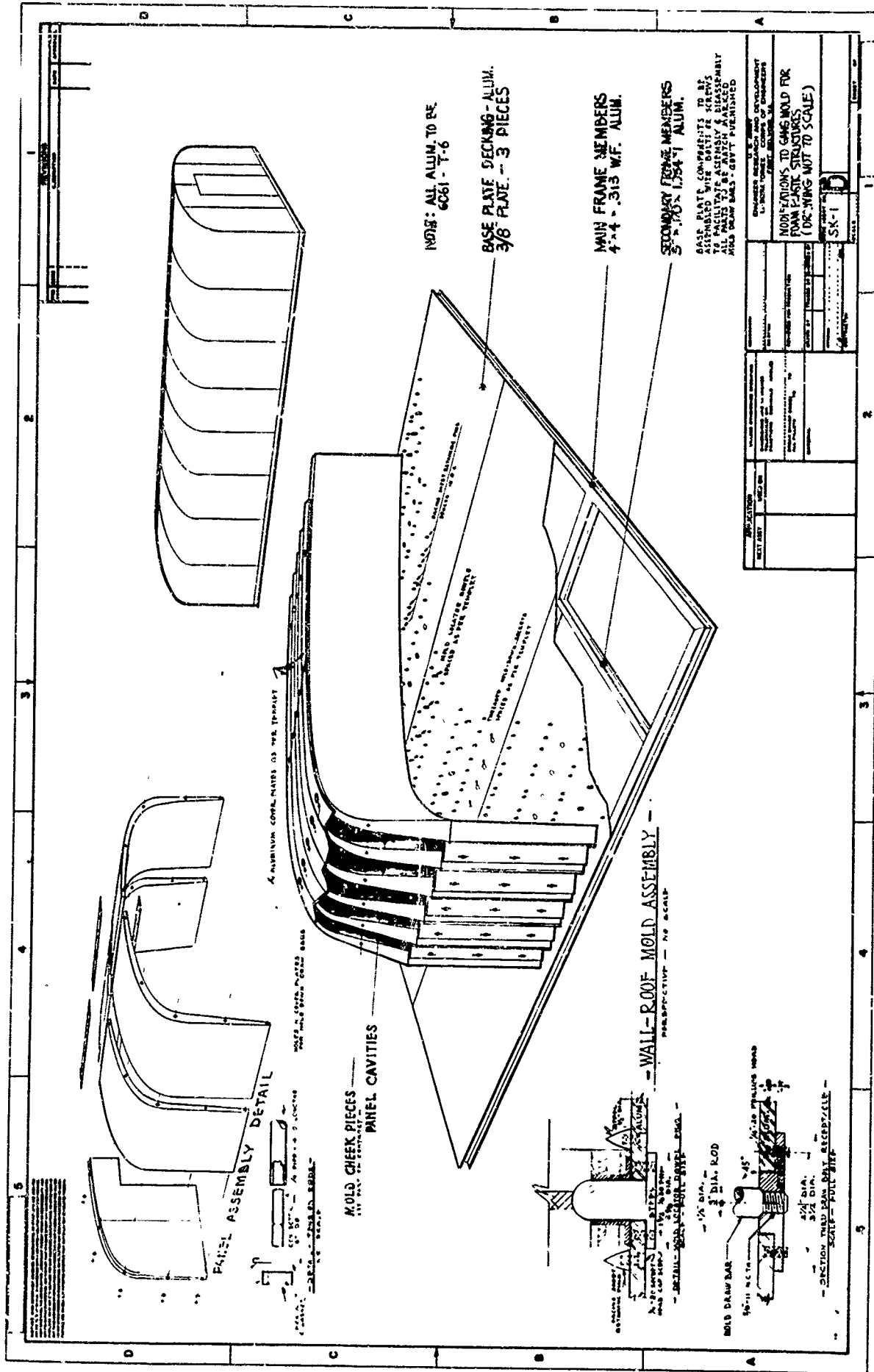


Figure 18. Line Drawing of Molds and Building. A Similar System of Molds is used for Producing End Wall Units

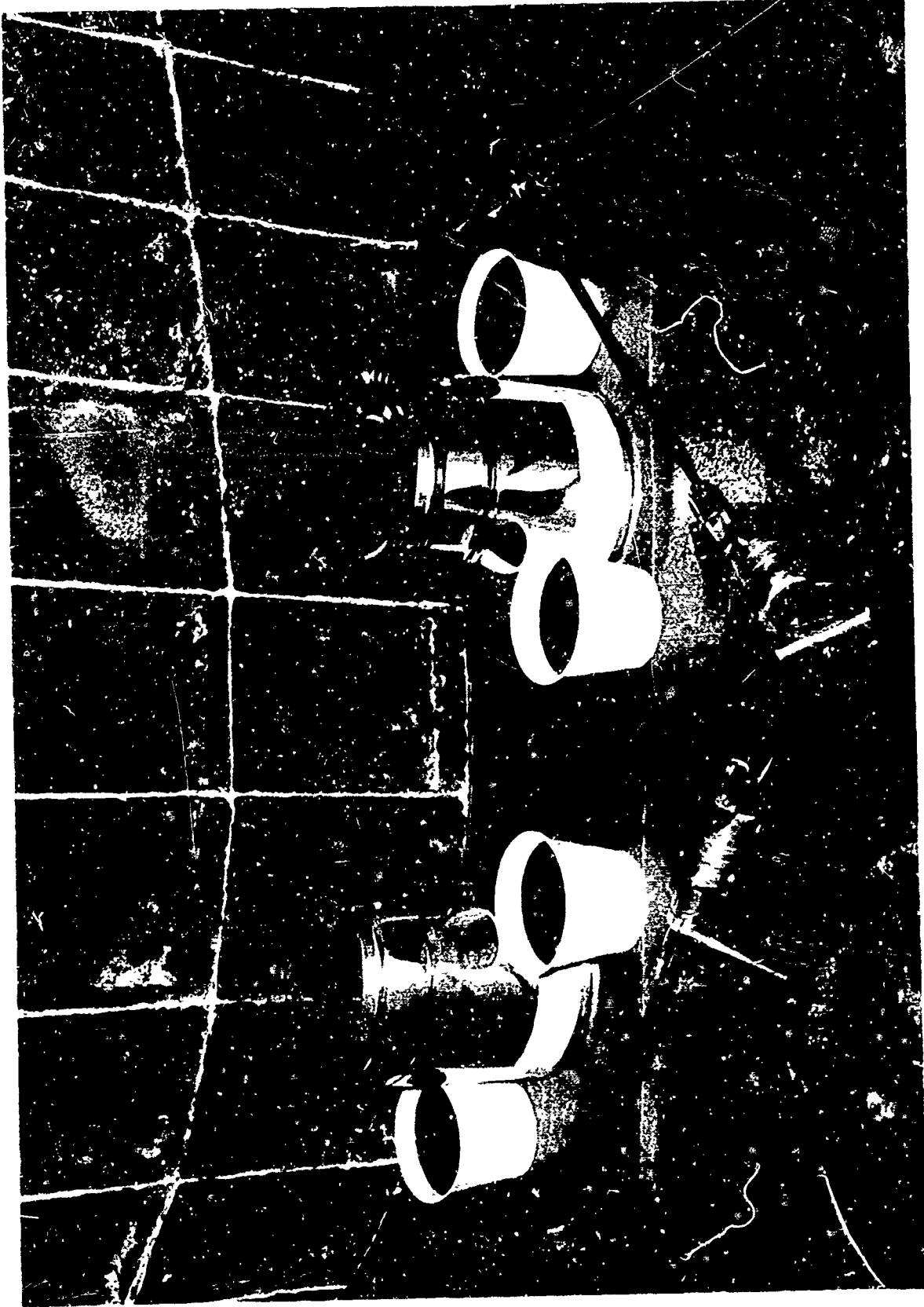


Figure 19. The Materials and Equipment used in the Process that Preceded the Froth Foam System. It is all that is Necessary to Fill a Half Module with Foam of 2 lb/cu.ft. Density

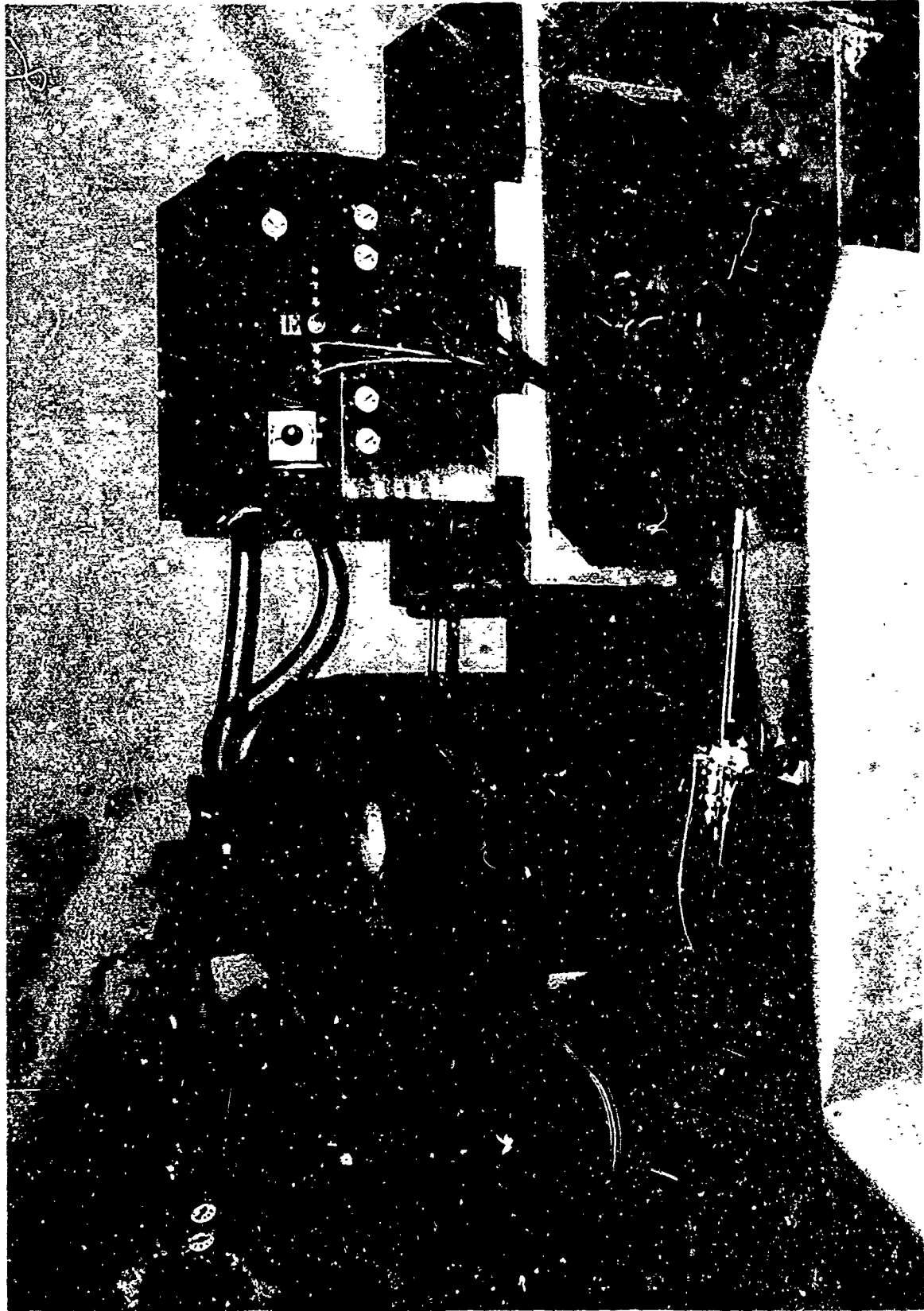


Figure 20. The Polyurethane Froth Foam Dispenser Presently Used in the System



Figure 21. Placing Aluminum Facing Sheet in Mold Preparatory to Casting



Figure 22. Injecting 2 lb. per cu. ft. Froth Foam into the Six Cavity Mold



Figure 23. One of Six Completed Panels Removed from Mold

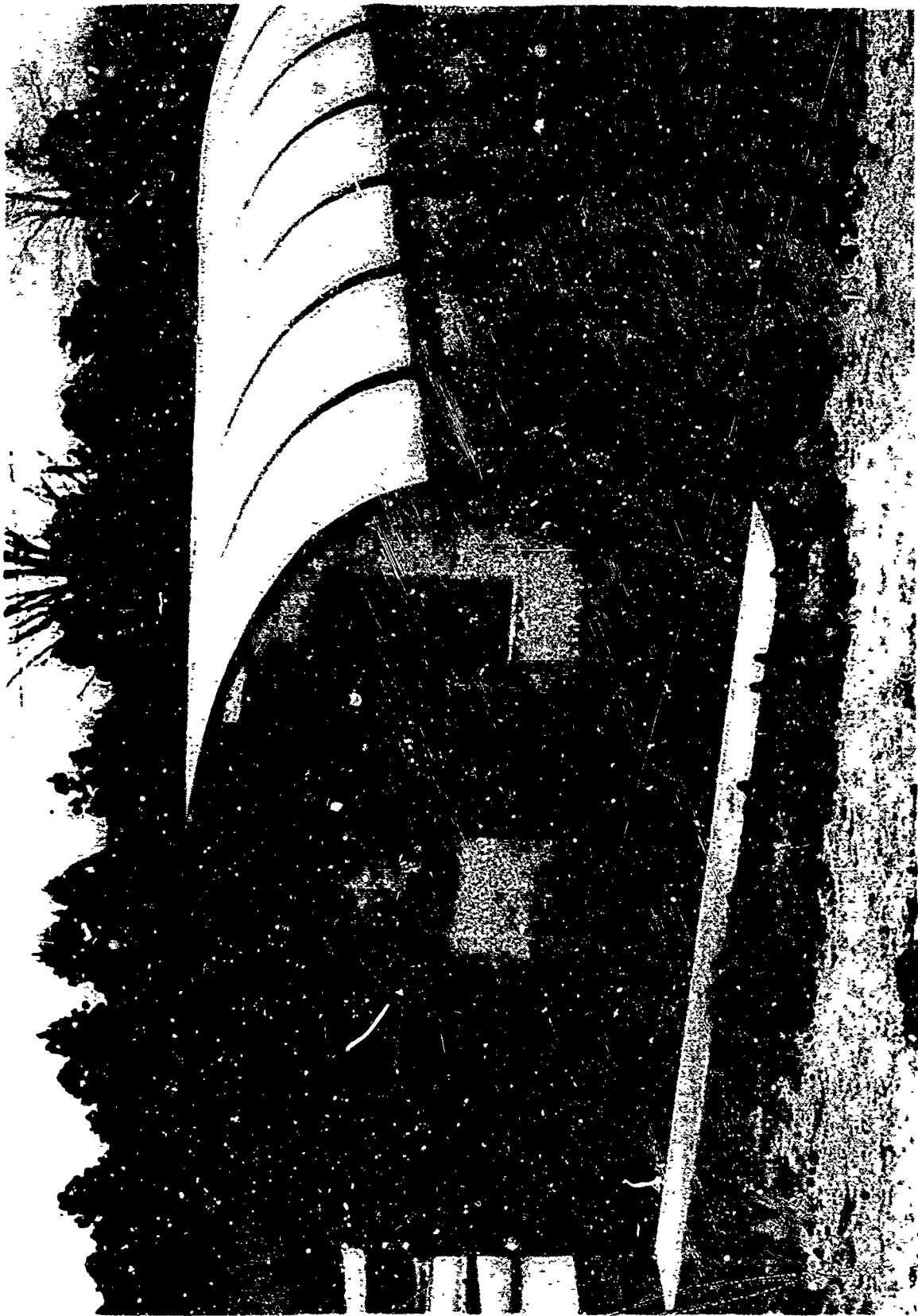


Figure 24. The Typical 16' Wide Aluminum Faced Foam Plastics Structure
Installed at Camp A.P. Hill, Va.

U S G O U S A R M Y E N G I N E E R I N G C O R P S

METAL FABRICS FOR AEROSPACE EXPANDABLE STRUCTURES

W. D. Freeston, Jr.
Fabric Research Laboratories, Inc.
Dedham, Massachusetts

Many aerospace structures under current development require utilization of flexible, textile-like fabrics having high strength at elevated temperatures. To minimize form-drag during launch, these aerospace structures must have a small pre-deployment volume. Thus, the fabric must be capable of being folded, packaged, and subsequently deployed without suffering damage.

The most suitable candidate materials available in filament form at the present time are the superalloys and the refractory metals and their alloys. Under the sponsorship of the Fibrous Materials Branch of the Air Force Materials Laboratory, the feasibility of weaving fabric from multifilament yarns, composed of metal filaments as fine as 0.0005 inch in diameter, on modified, power textile equipment has been demonstrated.

The properties of the fabrics are compared to those of a typical, equally strong, commercial fabric woven from single wires. The superior flexibility, crease recovery, fold endurance and tear strength of multifilament metallic-yarn fabrics are shown.

The tensile properties, tear strength, creep and fold endurance of a multifilament-yarn fabric in air at temperatures to 2000°F are given.

Joining panels of metal fabric by conventional sewing with threads composed of a large number of fine metal filaments is discussed.

INTRODUCTION

Many aerospace structures under current development, such as re-entry drag and lift-drag vehicles, require utilization of flexible, textile-like fabrics having high strength at elevated temperatures. To minimize form-drag during launch, these aerospace structures must have a small pre-deployment volume. Thus, a fabric used in these structures must be capable of being folded, packaged, and subsequently deployed without suffering damage.

The temperature and tensile load that the fabric in a particular aerospace application will experience depends on the design and mission of the structure. For instance, it is estimated that the temperature of the fabric in a paraglider returning from an orbiting space station with a launch weight of 1000 pounds can be kept below 1000°F by utilizing a "skip-glide" re-entry and an ablative fabric coating, such as silicone rubber. The required fabric strength would be over 200 lbs/inch at the 1000°F temperature level⁽¹⁰⁾. Systems of greater weight intended for other missions may encounter temperatures in the 1500°F to 2500°F range.

Trailing, aerodynamic, decelerator systems capable of stabilizing and decelerating supersonic and hypersonic airplanes, aerospace vehicles and ejected payloads are also under development. One of the designs being evaluated by the Air Force at the present time is the Hyperflo canopy. It has a conical-frustrum shaped, canopy configuration, some portions of which may be exposed to temperatures of 600°F to 1800°F.

The textile-like materials potentially useful in these aerospace structures, i.e., the materials available in fiber form that are flexible and exhibit high strength at elevated temperatures, are the superalloy and refractory metals, ceramics (oxide fibers, including glass) and carbonaceous residues. Considerable research effort is being expended on fibers in all three classifications. Noteworthy progress has recently been made in the carbonaceous-fiber area. However, the most suitable candidate materials available at the present time for use at 1000°F, and above, are the superalloy metal filaments.

Metal filaments are, inherently, many times stiffer in tension than organic filaments. Therefore, in order to obtain a metal fabric whose bending flexibility approaches that of an organic-fiber fabric, the metal fabric must be woven from yarns composed of a large number of very fine metal filaments.

Assuming complete freedom of filaments to bend individually, yarn rigidity is proportional to the square of the filament diameter for equally strong yarns. Since metal filaments, as a class, are ten to twenty times stiffer in bending than organic filaments, metal filaments have to be drawn to less than one-quarter the diameter of organic filaments to achieve equal yarn rigidity at equal yarn strength.

The diameter of typical organic filaments is approximately 1.0 - 1.5 mils. The diameter of metallic filaments necessary to achieve equal yarn rigidity at equal strength would, therefore, be on the order of 0.3 mil. And there must be about 600 - 2400 metal filaments per yarn compared to 50 - 150 organic filaments⁽²⁾.

The finest wires commercially available in quantity are 0.5 mil (0.0005 inch) in diameter. This wire is not supplied by the manufacturers in multifilament-yarn form since high-strength wire cannot be melt-extruded, as can polymeric fibers, but must be drawn through diamond dies with only a small area reduction on each pass. The fine wire must be twisted into a yarn in a subsequent operation.

However, during the past year limited quantities of metal yarns composed of a large number of fine wires and produced by a multifilament drawing process have become available. This is of considerable economic importance. Singly-drawn, 0.5-mil diameter, superalloy wire costs from roughly \$1,000 (Chromel R) to \$3,000 (René 41) per pound. However, the price of multi-drawn wire yarn (composed of 0.5-mil wires) is \$25 (stainless steel) to \$210 (Chromel R) per pound.

Hoskins Manufacturing Company has produced multifilament yarns composed of fine, nickel-base alloy, metal filaments by placing large-diameter metal filaments in a formed-up ribbon of iron and drawing the composite to a small diameter. The iron sheath is then dissolved and the yarn twisted⁽⁷⁾.

Brunswick Corp. produces a similar product by imbedding large metal filaments in a metal matrix and drawing the composite to a small diameter. The matrix is subsequently dissolved(11).

Multi-drawn, metal yarn can be drawn such that the individual filament size is smaller than 0.5 mil and, undoubtedly, yarn can be produced with 600 to 2400 filaments. Thus, it should be possible in the near future to produce a metal fabric having the same flexibility for the same fabric strength as conventional, synthetic-fiber fabrics.

MULTIFILAMENT FINE-WIRE YARN FABRIC

The technology required to wind and twist fine wire into yarn and weave the yarn into fabric has been developed using modified textile equipment(3,5). A ring-twister specifically modified to twist, ply, and cable wires having diameters from less than 0.5 mil to 1.5 mils into yarns with 0.1 to 50 turns per inch twist was recently constructed. The design incorporates the necessary-type creel and guides, and an electronic stop motion that detects the rupture of a single, 0.5-mil diameter, metal filament(6).

The fine-wire, multifilament-yarn, metal fabrics woven to date have been designed for maximum translation of filament and yarn strength into fabric strength, and for maximum fabric flexibility, crease recovery, fold endurance and tear strength. The success of these efforts is demonstrated by comparing the fine-wire, multifilament-yarn fabric to a typical, monofilament wire screen. The above-mentioned properties of the multifilament-yarn fabric are considerably superior to those exhibited by wire screen and approach those of conventional organic-fiber textiles(5).

The averages of the warp and filling properties of a series of multifilament-yarn, fine-wire fabrics are summarized in Table 1. The properties of a typical commercial fabric of equal strength woven from single wires are also given. As shown, the multifilament-yarn fabrics weigh approximately the same, yet have air permeabilities approaching one one-hundredth that of the monofilament-fabric. The multifilament yarn fabrics also have tear strengths from two to four times, and fold endurances from twenty to one hundred times those of the typical monofilament fabric. The monofilament fabric exhibits essentially no wrinkle recovery, while the multifilament yarn fabrics exhibit recoveries up to 33%. (The methods used to measure the permeability, tensile properties, tear strength, fold endurance and wrinkle recovery are outlined below.)

As also shown in Table 1, a 50% decrease in fabric air permeability, a five-fold increase in fold endurance and a two-fold increase in wrinkle recovery can be realized by weaving a fabric from multifilament yarns composed of 0.5-mil diameter wires rather than from equally strong yarns composed of 1.0-mil diameter wires.

TABLE 1

FABRIC PROPERTIES

Wire Diameter (mils)	Material	Filaments per Yarn	Weave Pattern	Ends per Inch	Picks per Inch	Weight (oz/yd ²)	Permeability (ft ³ /min/ft ²)	Tear Strength (lbs) average	Folding Endurance (cycles) average	Tensile Rupture Load (lbs/inch) average	Wrinkle Recovery (%)
0.5	Chromel A*	100	two-by-two basket	81	81	21.2	16-21	12.7	999	216	32
0.5	Chromel A	100	three-by-four twill	81	82	21.2	21-22	17.5	1201	215	33
0.7	Chromel A	49	two-by-two basket	82	119	23.9	8-11	8.7	437	213	13
1.0	Chromel A	25	two-by-two basket	81	81	20.1	47-57	8.3	232	205	16
1.0	Chromel A	25	three-by-five twill	81	81	20.0	54-57	14.7	265	199	25
5.0	304 Stainless	Mono-filament	plain	90	92	20.7	828	3.5	11.5	181	~0

432

*Registered trademark, Hoskins Manufacturing Co., Detroit, Michigan; 80 Ni, 20 Cr.

CHROMEL R WIRE FABRIC

Seven yards of eighteen-inch wide fabric were woven from a twisted, multi-filament yarn containing fully annealed, 0.5-mil diameter, superalloy, Chromel R[®] wire(3). The fabric was woven from Chromel R wire because it is readily available in 0.5-mil diameter filaments and because it has excellent high-temperature properties(8,9). The construction, weight, air permeability, wrinkle recovery, tensile properties, tear strength, and fold endurance of the fabric at 70°F are given below. The tensile properties of the fabric at temperatures from 70°F to 2000°F, and at jaw speeds of 0.5 inch/minute and 5.0 inches/minute are also given, as are the tensile strength of creased fabric samples, and the fabric tear strength and fold endurance. The fabric creep at 50% of the at-temperature rupture load at temperatures from 1000°F to 2000°F is also given(4). In addition, the fabric tensile properties at -110°F and -320°F are noted.

The tensile properties of the 0.5-mil, Chromel R wire at ambient temperatures are given in Table 2. These properties were determined with an Instron tensile-testing machine using a ten-inch gauge length and a jaw speed of 0.5 inch/minute. The wires were mounted in standard fiber jaws faced with masking tape. A typical, although not necessarily average, stress-strain diagram is given in Figure 1.

TABLE 2

TENSILE PROPERTIES OF 0.5-MIL CHROMEL R WIRE

Yield Load (gm)	Yield Elongation (%)	Rupture Elongation (%)	Rupture Load (gm)
11.4	0.57	6.97	13.5

The 0.5-mil, Chromel R wire was twisted and plied into a one-hundred filament yarn. Ten ends of the individual strands of wire were twisted 3.0 Z turns per inch and ten ends of the twisted yarn were then plied 3.0 S turns per inch. (This yarn construction is denoted by: 10/10/0.5 mil/3.0 S/3.0 Z.) The yarn is balanced, i.e., torque free.

The yarn was woven into a two-by-two basket-weave fabric. The pick-and-end count, weight, thickness and air permeability of the fabric are given in Table 3. The fabric permeability was measured with a Frazier Permeometer, using 0.5 inch of water-pressure drop across the fabric.

TABLE 3

PROPERTIES OF 0.5-MIL CHROMEL R WIRE FABRIC

<u>Weave Pattern</u>	<u>Ends per Inch</u>	<u>Picks per Inch</u>	<u>Weight (oz/yd²)</u>	<u>Thickness (inch)</u>	<u>Permeability (ft²/min/ft²)</u>
Two-by-two basket	80-81	80-81	19.9	0.0077	2.1

*Registered trademark, Hoskins Manufacturing Co., Detroit, Michigan;
73 Ni, 20 Cr, 3 Al, 3 Fe, 0.5 Si, <0.05 C.

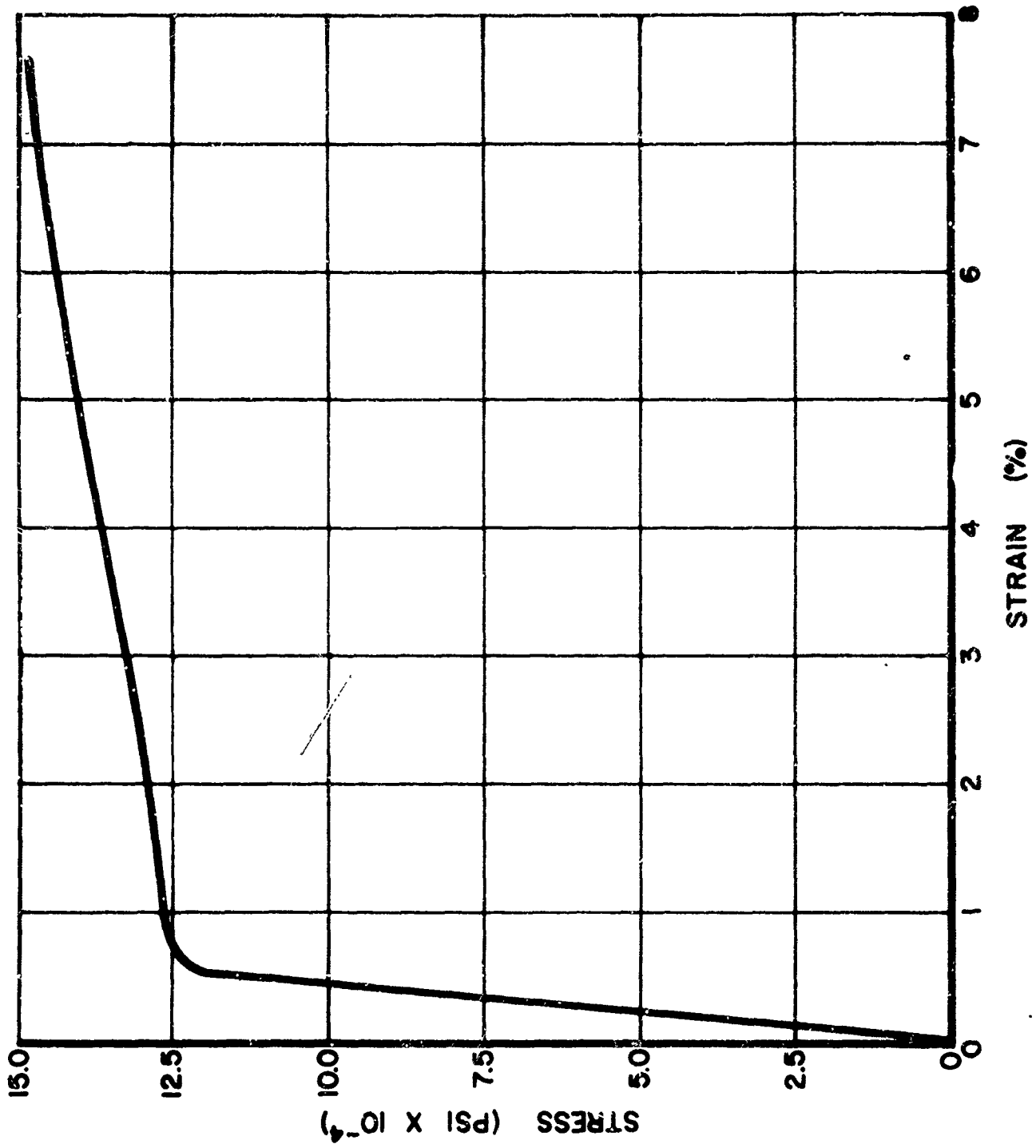


FIGURE 1. STRESS - STRAIN DIAGRAM OF 0.5-MIL CHROMEL R WIRE.

The average tensile properties of the multifilament-yarn, 0.5-mil Chromel R wire fabric are given in Table 4. Specimens in both the warp and filling directions were tested on an Instron tensile tester. One-inch wide, ravel-strip specimens, 3.5-inches gauge length, 0.5 inch per minute jaw speed, and flat, leather-lined, serrated jaws were used. The tensile moduli values given represent the slope of the initial linear portion of the fabric load-elongation curves in pounds per inch width of fabric per unit strain.

TABLE 4

TENSILE PROPERTIES OF 0.5-MIL CHROMEL R WIRE FABRIC

Yield Elongation (%)		Yield Load (lbs/inch)		Rupture Elongation (%)		Rupture Load (lbs/inch)		Modulus (lbs/inch x 10 ⁻³)	
Warp	Fill	Warp	Fill	Warp	Fill	Warp	Fill	Warp	Fill
4.0	1.4	198	213	9.5	7.2	226	245	109	210

The tongue tear strength of the Chromel R wire fabric in the warp and filling directions (breaking filling and warp yarns respectively) is given in Table 5. Specimens 3-inches wide and 4.5-inches long were used. They were cut lengthwise along their center-line for a distance of approximately 2 inches. A one-inch length of each cut end was placed into Instron jaws, one in the upper jaw and one in the lower. The specimens were subjected to a constant rate of extension of 2 inches/minute for approximately 2 inches of tear, and the load recorded.

The load-elongation curve obtained in a tear test is sawtoothed, each peak representing one or several yarn breaks. The tear-strength values given in Table 5 are the visual averages of the peak values of the tests.

TABLE 5

TEAR STRENGTH, WRINKLE RECOVERY AND FOLD ENDURANCE OF 0.5-MIL CHROMEL R WIRE FABRIC

Tear Strength (lbs)		Monsanto Wrinkle Recovery (%)		MIT Fold Endurance (cycles)	
Warp	Filling	Warp	Filling	Warp	Filling
17.7	14.5	33.3	30.0	968	992

The wrinkle recovery of the Chromel R wire fabric in the warp and filling directions is given in Table 5. It was measured with the Monsanto Wrinkle Recovery Tester (ASTM D1295-53T). In this test 1.5 by 4.0-centimeter test specimens are folded 180° with a 0.01-inch thick, metal shim between the two fabric surfaces. A load of 1.5 pounds applied for five minutes is used to crease the specimens(3). The recovered angle is measured after a five-minute free-recovery time and its percentage of 180° is calculated, i.e., the percent wrinkle recovery equals Recovered Angle/180° x 100. Specimens in both the warp and filling directions, bent against the direction of curl and with the direction of curl, were tested and the results averaged.

The fold endurance of the Chromel R wire fabric in both the warp and filling directions is also given in Table 5. It was measured with the MIT Folding Endurance Tester (ASTM D643-43, Method B). In this test both ends of the fabric are clamped in jaws. The lower jaw is subjected to a rotary, oscillating, bending movement such that the fabric is folded through an angle of 135 ± 5 degrees to both the right and left of the center-line position, 180 times per minute. The folding surfaces of the jaw have a radius of curvature of approximately 0.015 inch. A tension of 1.5 kg was applied to the test specimens at the upper jaw. The opening width of the jaw was 0.01 inch.

Test specimens 0.59-inch wide and 4.5-inches long were used. The results given in Table 5 are the averages of the tests.

The elevated-temperature tensile tests of the Chromel R wire fabric were performed on an Instron tensile tester using a resistance-heated, clam-shell oven. The test specimens were gripped with jaws fabricated from Inconel '702'. The jaws extended into the heated zone of the clam-shell oven thereby enabling material elongations to be recorded directly on the Instron chart.

Jaw breaks and jaw slippage were prevented by lining the serrated jaw faces with two layers of 181 quartz fabric. New linings were used for each test.

Test specimens 1-1/8-inches wide and 6-inches long were cut from the fabric in both the warp and filling directions. These strips were ravelled to a 1.0-inch width immediately prior to testing. A gauge length of approximately 3.5 inches was used.

In all elevated-temperature tests the test specimens were held at temperature for 15 minutes prior to testing. Since the oven cools down somewhat as the jaws and sample are being inserted, the time between insertion of the test specimen and the test was roughly 17 minutes at 1000°F and 20 minutes at 2000°F.

The length of the fabric between the jaws in each test was only approximately 3.5 inches due to the lack of precision of the clamping procedure. In a 70°F tensile test, the jaws are set a fixed distance apart, namely 3.25 inches, at the start of the test. The exact gauge length is then determined by adding to this fixed distance the amount of jaw travel, as given on the Instron chart, from the start of the jaw travel until a load rise is indicated.

This procedure cannot be used for the tests performed at elevated temperatures due to the thermal expansion of the jaw assembly. Also, this thermal expansion is difficult to either measure or calculate accurately. Therefore, in all elevated-temperature tests, the gauge length GL used to calculate percent elongation and modulus values was taken as the average sample gauge length of the 70°F tests, 3.52 inches, plus the calculated thermal expansion of the fabric, i.e.,

$$GL = 3.52 (1 + \alpha \Delta T)$$

where $\Delta T = T - T_0$, T is the test temperature, $T_0 = 70^\circ\text{F}$, and α is the coefficient of thermal expansion of the material being tested. This expression assumes that the percent crimp in the fabric is the same at all temperatures. At 2000°F, the gauge-length correction is less than 2%.

The rupture loads of the Chromel R wire fabric are plotted in Figure 2 as a function of test temperature and testing speed.

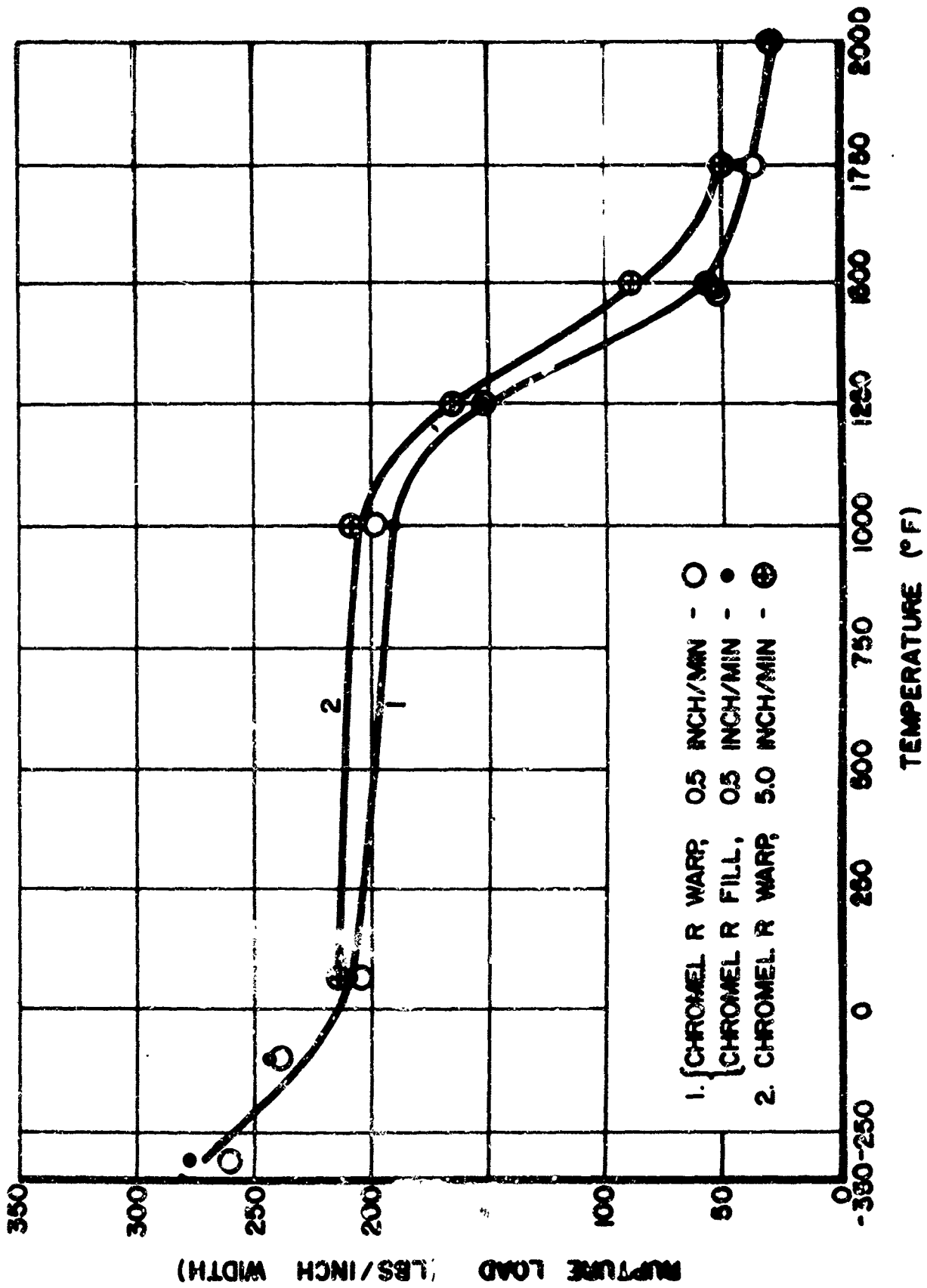


FIGURE 2. CHROMEL R WIRE FABRIC RUPTURE LOAD AS A FUNCTION OF TEMPERATURE.

The tensile strength of the Chromel R fabric decreases rapidly in the 1100°F to 1700°F temperature range. The strength of the fabric at 2000°F is 15% of the strengths at 70°F in the warp and filling directions. Also, the strength of the fabric increases with increasing testing speed, particularly at the elevated temperatures.

The rupture elongation of the Chromel R fabric is plotted in Figure 3 as a function of test temperature. As shown, the elongation remains roughly constant over the temperature range of 70°F to 1250°F, increases sharply near 1500°F and then decreases rapidly beyond 1500°F. The fabric rupture elongation at 1500°F is greater than at 70°F. This is probably a result of the wire being annealed, the work-hardening caused by twisting and weaving being removed. The decrease in fabric elongation beyond 1500°F evidently results from oxidation hardening of the wire. The 0.5-mil wire is particularly susceptible to this because of its large surface-to-volume ratio.

Typical, warp load-elongation diagrams of the Chromel R wire fabric at a jaw speed of 0.5 inch/minute and test temperatures from 70°F to 2000°F are given in Figure 4. Similar diagrams for the filling direction are given in Figure 5.

The creep, extension under a constant load, of the Chromel R wire fabric in the warp direction was measured on the Instron at elevated temperatures. The loads used were one-half of the average, at-temperature, fabric-warp, rupture loads, i.e., 100 lbs at 1000°F, 77 lbs at 1250°F, 28 lbs at 1500°F and 15 lbs at 2000°F. The test specimens were exposed to the desired temperature for 15 minutes prior to the start of the test and the creep was measured for 15 minutes. A jaw speed of 0.1 inch/minute was used to maintain the desired specimen loading. The results were corrected for the jaw creep. However, this was a small correction.

The fabric creep at 1000°F and 2000°F is low, less than 2% in 15 minutes. At temperatures between 1000°F and 2000°F the creep increases to about 10% in 15 minutes. The low creep at 2000°F is probably due to oxidation hardening of the fine wire.

The tensile properties in the warp direction of Chromel R wire-fabric test specimens creased at 70°F were measured at temperatures from 70°F to 1750°F. The following procedure was used to crease the fabric (Standard Method for Static Fold Resistance of Fiberglass Decorative Fabrics, OCF Test No. DF 505). Fabric test specimens 1-1/8-inches wide by 6-inches long were folded in half and placed under a 10-lb weight for 10 minutes. One square inch of folded fabric was placed under the weight. The face of the weight in contact with the fabric measured 2 inches by 4-3/8 inches. The specimens were unravelled to a one-inch width prior to testing. As in previous tests, the specimens were held at temperature for 15 minutes before testing.

The tests showed that creasing the fabric decreases the strength by only a small amount up to 1500°F. However, at 1750°F the tensile strength of the creased fabric is only two-thirds that of the uncreased fabric.

The tongue-tear strength of the Chromel R wire fabric was measured in the warp direction (breaking filling yarns) at temperatures from 70°F to 2000°F. The specimens were held at temperature for 15 minutes prior to testing. Specimens 3-inches wide by 4-inches long were used. They were cut lengthwise along

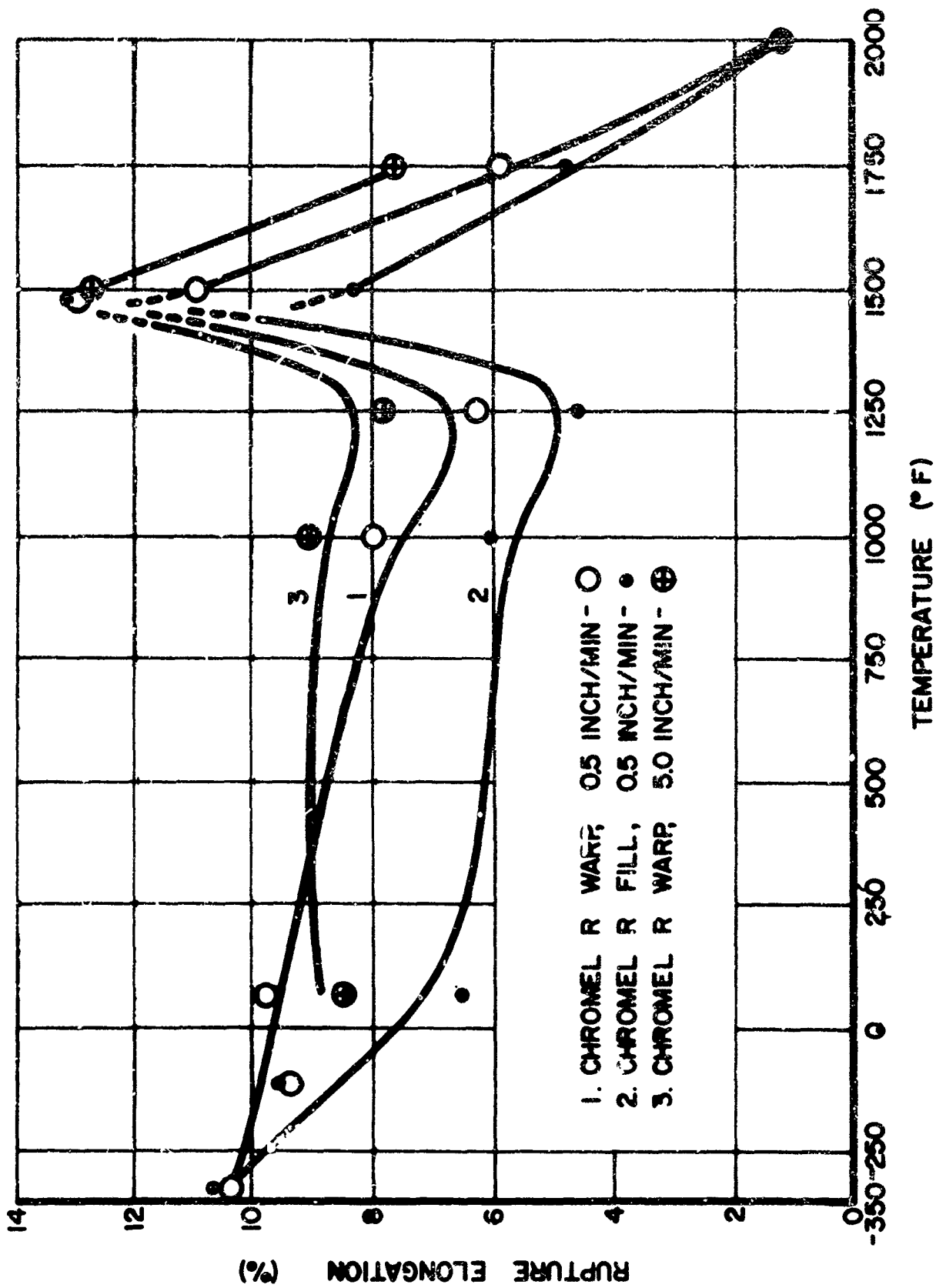


FIGURE 3. CHROMEL R WIRE FABRIC RUPTURE ELONGATION AS A FUNCTION OF TEMPERATURE.

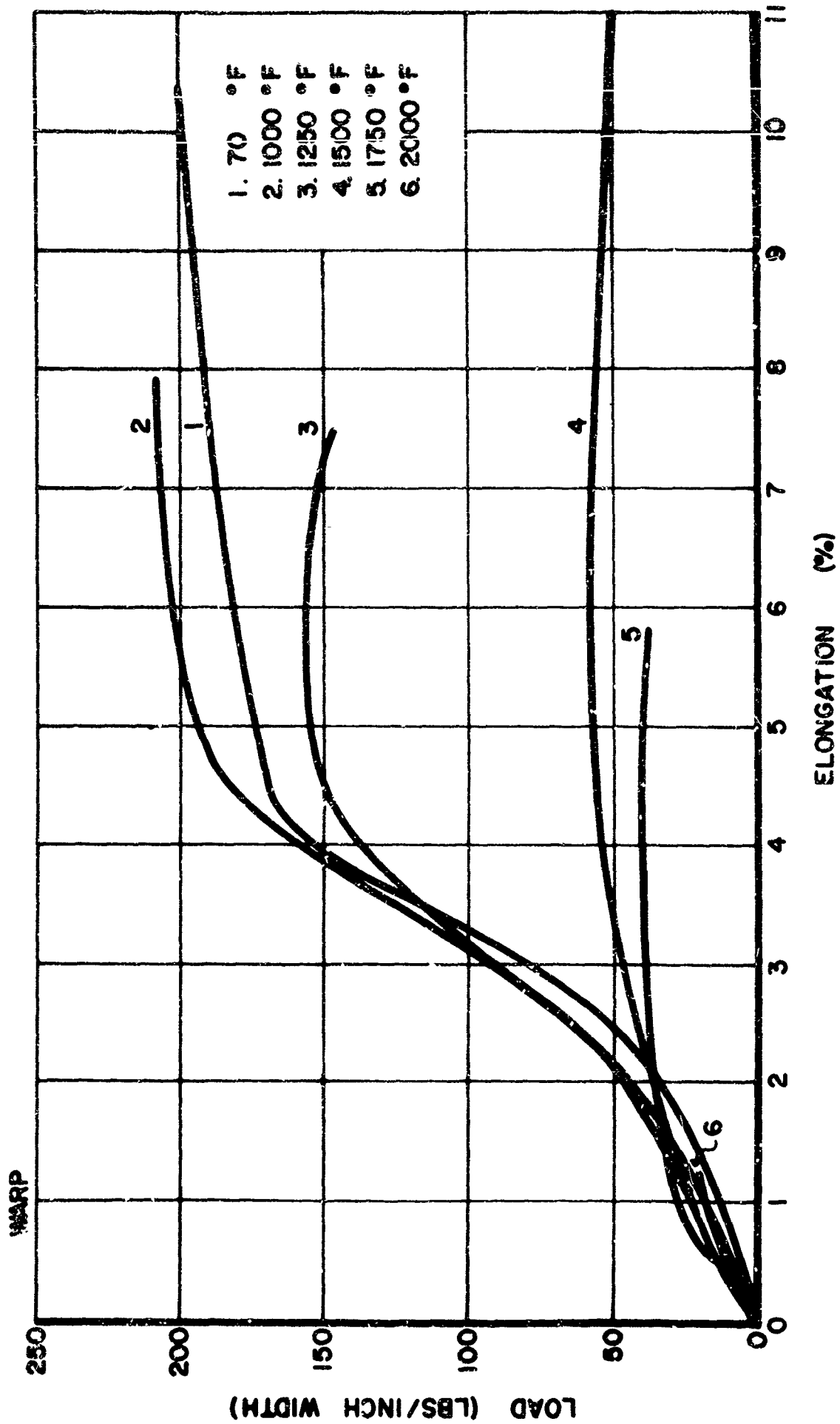


FIGURE 4. TYPICAL WARP LOAD-ELONGATION DIAGRAMS OF CHROMEL R WIRE FABRIC AT A JAW SPEED OF 0.5 INCH/MIN AND TEMPERATURES FROM 70°F TO 2000°F

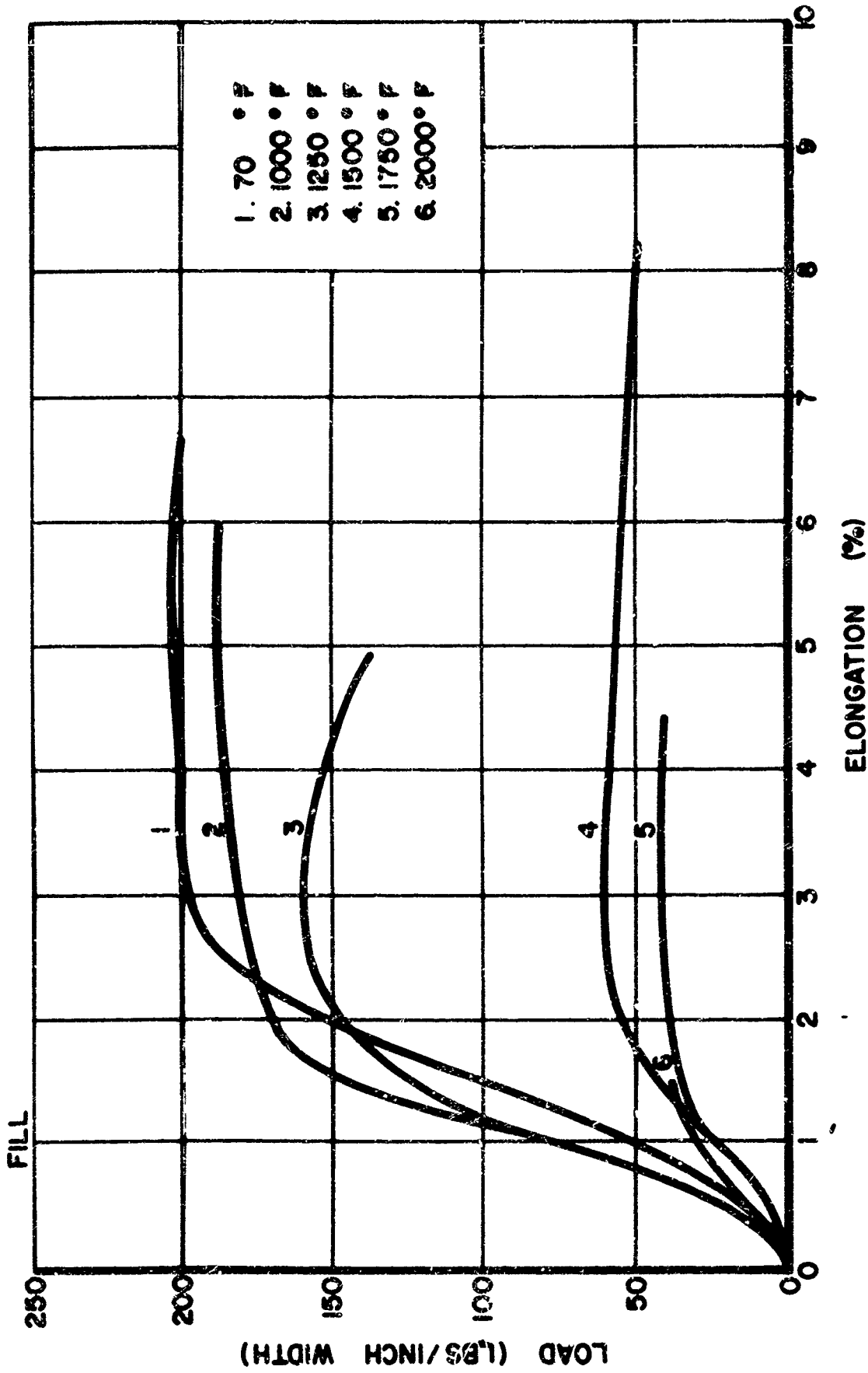


FIGURE 5. TYPICAL FILLING LOAD-ELONGATION DIAGRAMS OF CHROMEL R WIRE FABRIC AT A JAW SPEED OF 0.5 INCH/MIN AND TEMPERATURES FROM 70°F TO 2000°F.

their center-line for a distance of approximately 2 inches. One inch of each of the two portions of the cut end were placed into the Inconel jaws, one in the upper jaw and one in the lower jaw. The specimens were subjected to a constant rate of extension of 2 inches/minute for approximately 1-1/2 inches of tear.

The tear strength of the fabric is plotted in Figure 6 as a function of test temperature. The values plotted are the visual averages of the peak values.

The fold endurance of the Chromel R wire fabric was measured at elevated temperatures in a kiln. The results are plotted in Figure 7 as a function of test temperature. As shown, the fold endurance of the fabric is almost zero at 1750°F to 2000°F.

CORELESS CORD

The designs of some aerospace systems require that one component of the system be attached to another component by a flexible line or cable with high-temperature durability, for instance, the joining of the payload to the canopy of the Hyperflo parachute. Therefore, the feasibility of braiding fine wire into coreless cord was investigated. The cord was braided from a metal yarn composed of 75 ends of 1.0-mil, Chromel A wire on a #1 New England Butt Braider with Mossberg carriers. The cord construction and weight are given in Table 6(3). The cord is very flexible, indicating that 0.5-mil wire is not necessary in such structures.

TABLE 6

CORELESS METAL CORD

Number of Carriers	Type of Stitch	Wire Diameter (mils)	Filaments per Yarn	Picks per Inch	Ends per Carrier	Total Ends	Weight (yds/lb)
16	regular (two over and two under)	1.0	75	10.0	6	96	13.5

The average breaking strengths of the cord at 70°F, 1000°F and 1500°F are given in Table 7(4). Two-inch diameter capstan jaws and a jaw speed of 2.0 inches/minute were used. The strength of the cord at 1000°F and 1500°F was measured using a clam-shell oven with the jaws outside the oven. The cord elongation to rupture at 70°F is approximately 16 percent.

TABLE 7

BREAKING STRENGTH OF 1.0-MIL, CHROMEEL A WIRE, CORELESS CORD AT ELEVATED TEMPERATURES

Temperature (°F)	Rupture Load (lbs)
70	677
1000	530
1500	164

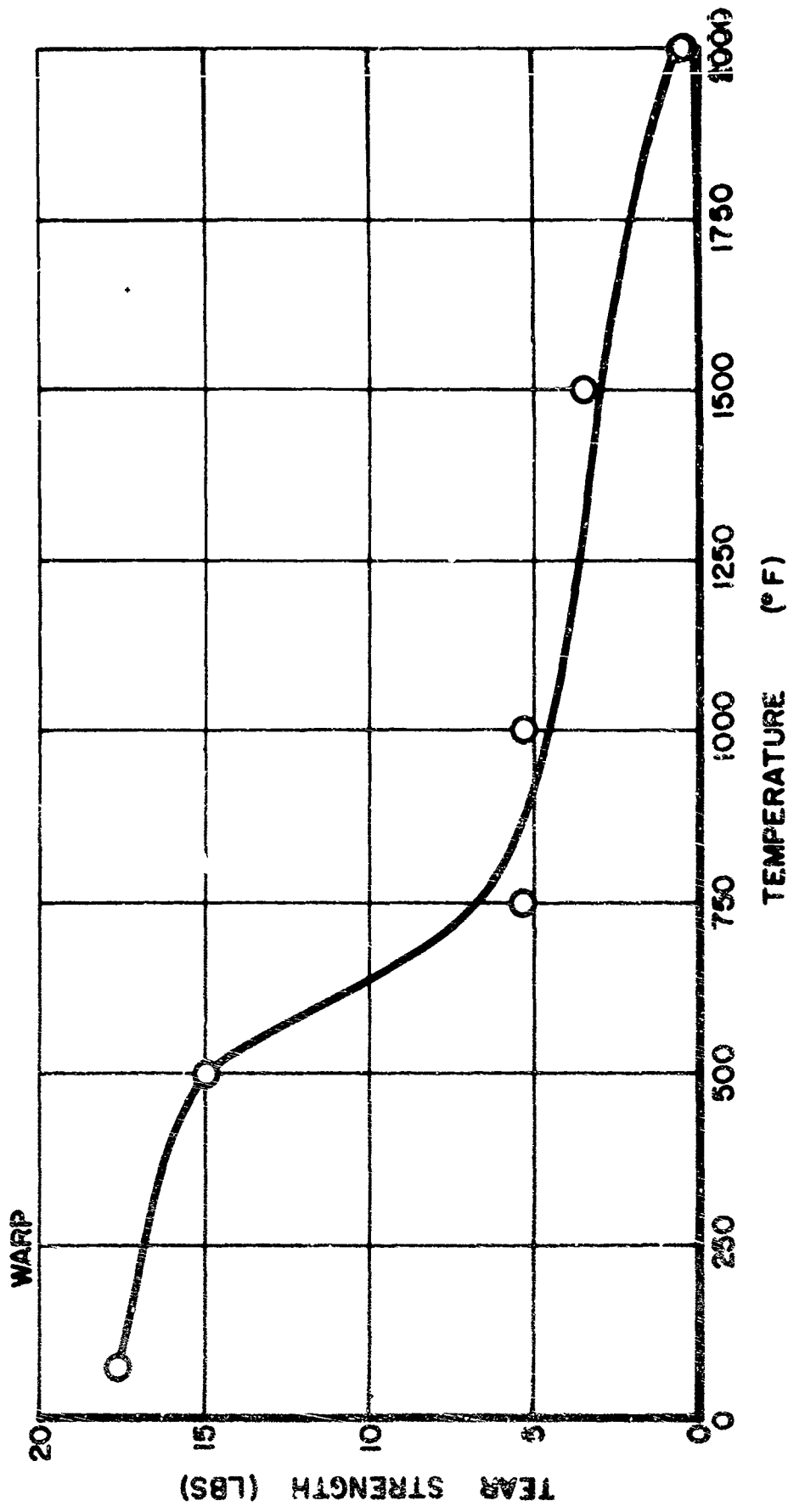


FIGURE 6. CHROMEL R WIRE FABRIC TEAR STRENGTH AS A FUNCTION OF TEMPERATURE

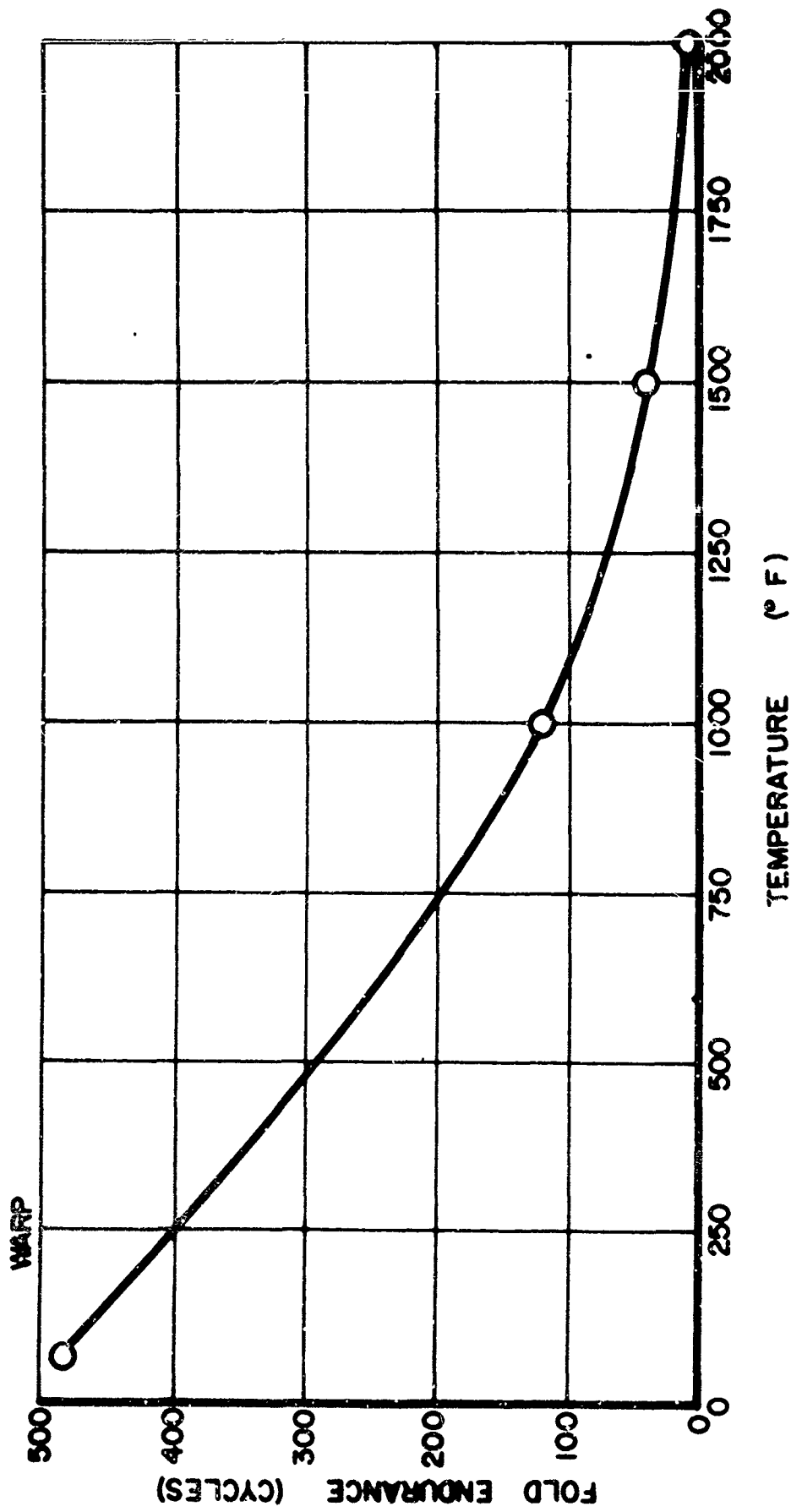


FIGURE 7. CHROMEL R WIRE FABRIC F_{LD} ENDURANCE AS A FUNCTION OF TEMPERATURE.

SEAMING OF METAL FABRIC

The development and evaluation of flexible, high-strength, thermo-durable, fibrous structures are only the first steps toward the utilization of such materials in an aerospace system. The fibrous structures, fabrics, must be tailored into the required configuration and the mechanical properties of the resulting configuration must be determined. An investigation of the joining of panels of multifilament-yarn, fine-wire, metal fabrics by sewing was, therefore, undertaken.

A metal sewing thread was designed⁽¹⁾ and twisted from five hundred, 0.5-mil, Chromel R wires for the study. To prevent the occurrence of broken filaments during the sewing operation, the thread was coated with Teflon.

No difficulties were encountered in the sewing operation itself. A standard, industrial sewing machine was used. Various combinations of seam types, stitches per inch, rows of stitches, gauge, and sewing-thread tension have been tried^(3,4). Seam efficiencies of 65% have been obtained consistently using an integral IS-2 seam and four rows of stitches. Work in this area is continuing and it is anticipated that higher seam efficiencies are possible.

CONCLUSION

Flexible, high-strength, thermally durable, textile-like fabrics have been developed. They are capable of being folded, packaged and subsequently deployed without suffering damage. These multifilament, fine-wire yarn fabrics are being considered for several aerospace structures at the present time and undoubtedly will find application in many more in the next few years.

The major shortcomings of a fine-wire, multifilament-yarn, metal fabric for aerospace applications is its weight. The Chromel R wire fabric discussed herein weighs 20 oz/yd². However, even on a strength-to-weight basis, these metal fabrics are superior to fabrics woven from other fibrous materials at the present time, including glass and quartz, at temperatures of 1000°F and above.

LIST OF REFERENCES

1. Coplan, M. J. and Block, M. G., WADC-TR-56-313, Part I (1956).
2. Coplan, M. J., Powers, D. H., Jr., Barish, L., and Valko, E. I., WADD-TR-60-9 (1960).
3. Coplan, M. J., Freeston, W. D., Jr., and Platt, M. M., ML-TDR-64-102 (1964).
4. Freeston, W. D., Jr., AFML-TR-65-118 (1965).
5. Freeston, W. D., Jr., and Gardella, J. W., ASD-TDR-63-542, Part II (1963).
6. Freeston, W. D., Jr., Sebring, R. E. and Swanson, A. K., AFML-TR-64-342 (1964).
7. Gorton, C. A. and McMahon, C. C., ML-TDR-64-48 (1964).
8. Johnson, D. E. and Newton, E. H., ASD-TDR-62-180, Part II (1963).
9. Johnson, D. E., et al; ASD-TR-62-180 (1962).
10. Keville, J. F., Interim Engineering Progress Reports on Contract Number AF 33(657)-10252 (1963-1964).
11. Newton, E. H. and Johnson, D. E., ML-TDR-64-92 (1964).

Simulation of Meteoroid Impact Effects

on

Expandable Structures

1/Lt. Andre J. Holten

INTRODUCTION

The micrometeoroid simulation facility, located at WPAFB, was developed to fulfill the needs for materials testing within the AF Materials Laboratory as well as a support to other organizations with requirements for hypervelocity impact data. The technique used for the acceleration of the milligram size particles is the exploding foil device.

The AFML hypervelocity⁽¹⁾ facility consists of an electronically-triggered, high-energy storage system together with high-speed streak and framing photographic instrumentation for measuring particle velocity, size, shape, and momentum. Electronic instrumentation is provided for measuring capacitor bank discharge characteristics and the energy input to the exploding-foil gun.

Since the gun disintegrates when it is fired, a special room houses the evacuated gun chamber and exploding-foil gun to protect equipment and operating personnel. Also provided is a shielded control room, a dark room, and a data analysis area.

THE AIR FORCE MATERIALS LABORATORY EXPLODING FOIL FACILITY

Energy Storage System

The energy storage system consists of four banks of capacitors (Cornell-Cublier Type NRG 381), with each bank

composed of ten 1- μ F, 100-kV capacitors connected in parallel. At full rated voltage, the capacitors store 5000 J each, providing a total stored energy of 2000,000 J. At this energy level, however, the manufacturer guarantees the capacitors for only 1000 shots. If the capacitors are charged to no more than 50 kV, the guarantee is extended to 10,000 shots or 1 year. Because many more than 1000 shots are to be fired, it was agreed that the bank be given a rating of 50 kV maximum with a corresponding stored energy of 50,000 J.

The radial arrangement of the banks (Figure 1) was chosen to minimize the length of the discharge cables connecting the banks to the exploding-foil gun. Each bank is discharged through a three electrode reduced pressure trigger gap switch. The pressure is chosen such that jitter is minimized on firing at a particular voltage. At the correct pressure all four switches fire within 0.05 μ sec. of each other. The total circuit inductance is 92.1 nanohenries. The total circuit ring frequency is 80 kc. The gun contributes nominal inductance to the circuit with the result that the circuit firing conditions are rather independent of the gun design. The discharge conditions at the full rated voltage of 50,000 V are:

Peak current 7×10^5 amps
Energy delivered during first half
cycle 15,000 J
Time to peak current 3 μ sec.
Half width of initial power pulse 2 μ sec.

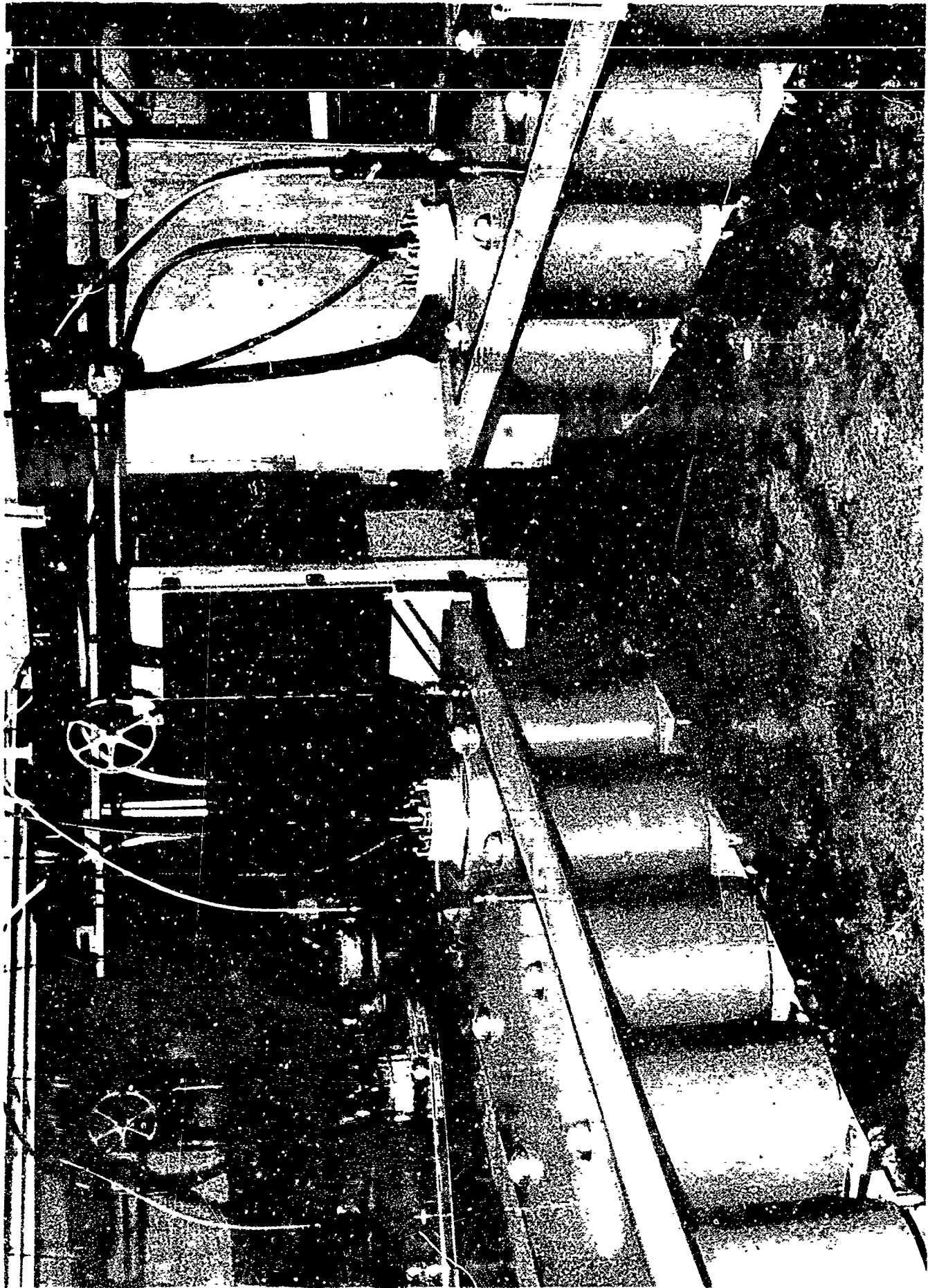


Figure 1. Overall View of the AFML Facility

Gun Chamber

The gun chamber (Figure 2) is constructed from a standard 3-in. cast bronze "cross" pipe fitting to which special brass flanges have been added for supporting the optical ports, target holder, and gun mount. Because of high-voltage insulation problems, the gun breech is maintained at atmospheric pressure and only the gun barrel, free-flight region, and target are evacuated. Optical flats are used in the viewing ports and are held in place against "O" rings by a quick-change flange. The diameter of the viewing ports is 6 cm.

The chamber provides a maximum free-flight distance of 25 cm. A modified Kinney KPW-4 vacuum system, capable of maintaining a vacuum better than 10^{-3} torr, is used to evacuate the gun chamber. A 4-in. high-vacuum line extends from the diffusion pump to a point a few inches from the gun chamber. A pneumatically-operated, high-vacuum valve protects the diffusion pump from debris and exposure to atmospheric pressure. The fore pump is protected from all but very small particles by a fine wire screen located below the roughing line.

With the attachment shown in Figure 3, circular samples up to 7" in diameter and up to 3" thick can be tested. 3" x 3" samples with a 1" lip on each side can be tested in the stressed condition. Calibration of the attachment in the stressing mode is not complete yet, pending the acquisition of strain gauges.

Shadowgraph Photography

Photographing small particles from the exploding-foil gun is complicated by the dense radiating plasma surrounding the

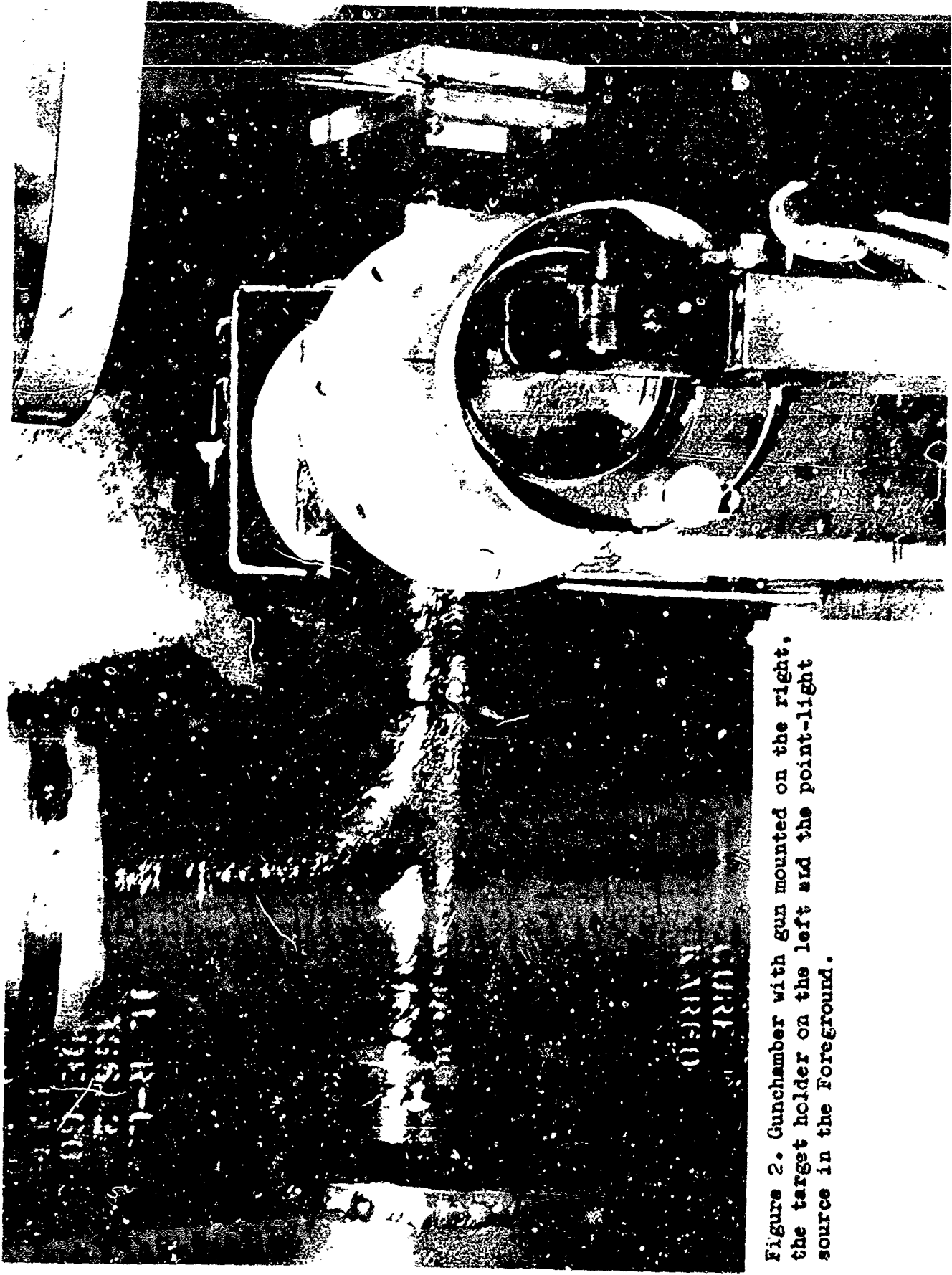


Figure 2. Gunchamber with gun mounted on the right, the target holder on the left and the point-light source in the Foreground.

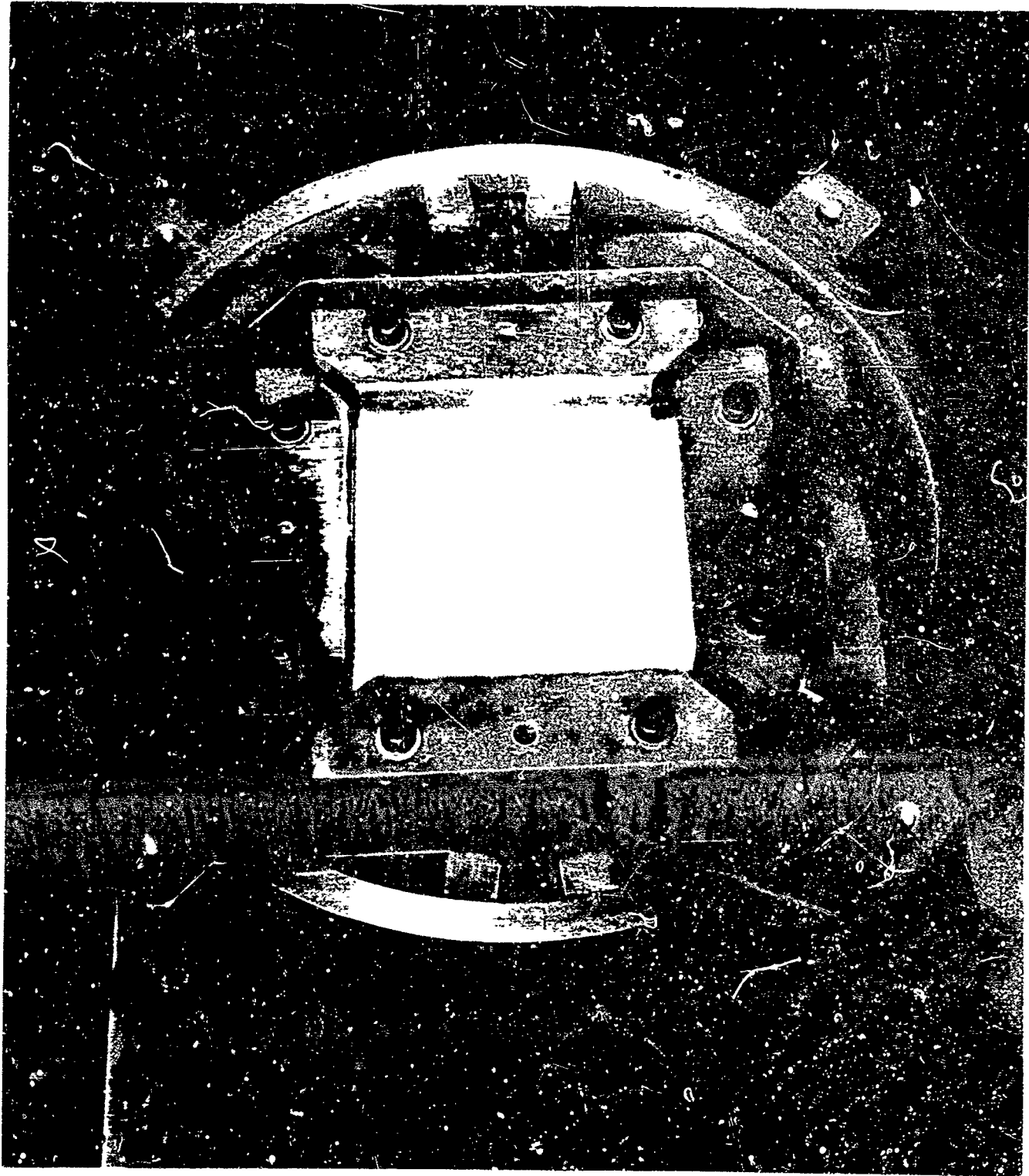


Figure 3. Target Holder. Shown is 3"x3" Target in Clamping Frame

particle in the free-flight region. We have found that we can discriminate against this plasma, however, by using an intense pulsed backlighting source to penetrate the plasma and illuminate the solid particle.

Diagnostic Equipment

The diagnostic equipment associated with the AFML facility consists of a streak camera and a double-pulsed Kerr cell camera for determining particle in-flight parameters; a framing camera for target recoil studies; high intensity pulsed light source for shadowgraph photography; and high-speed oscilloscopes for measuring bank discharge characteristics and photomultiplier signals.

Backlighting Sources

The high-intensity pulsed backlighting source was developed for use in the AFML facility. The unit, with a maximum stored energy of 7200 J, is used with a confined air arc. By proper choice of capacitance and inductance, the light pulse duration meets the requirements of the high-speed streak camera (15-30 μ sec.).

Framing Camera

The Beckman & Whitley 339B camera is used in a unique way so as to allow for a framing as well as a streak record of the same event. Information on the particle shape and velocity can be obtained in this manner.

Double-Pulsed Kerr Cell Camera

This camera uses a single Kerr cell shutter to take two pictures superimposed on the same film. The Kerr cell is

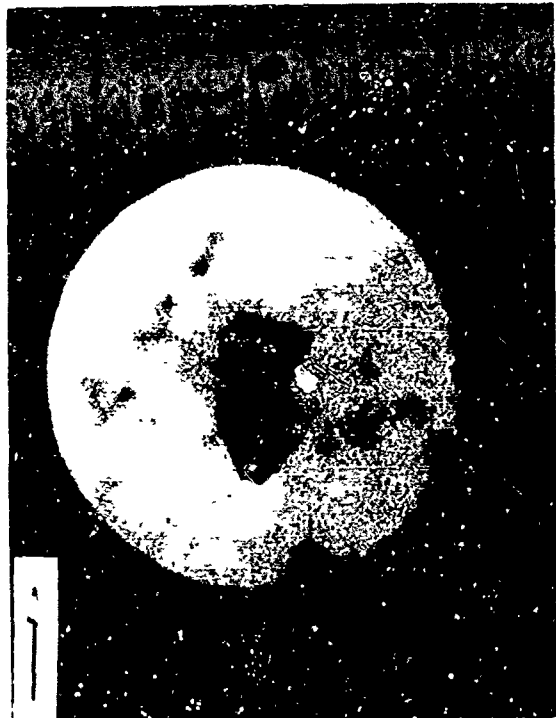
subjected to two voltage pulses with a variable time interval between pulses.

With this camera two 20-nsec exposures are obtained at precise interframe times of 1 through 5μ sec in 1μ sec steps. At the present we are using the same optical configuration for both cameras and using a beam splitter to divide the optics. In this manner we photograph the projectile from the same port with two different camera systems. Velocities measured by both cameras correlate to within 5%.

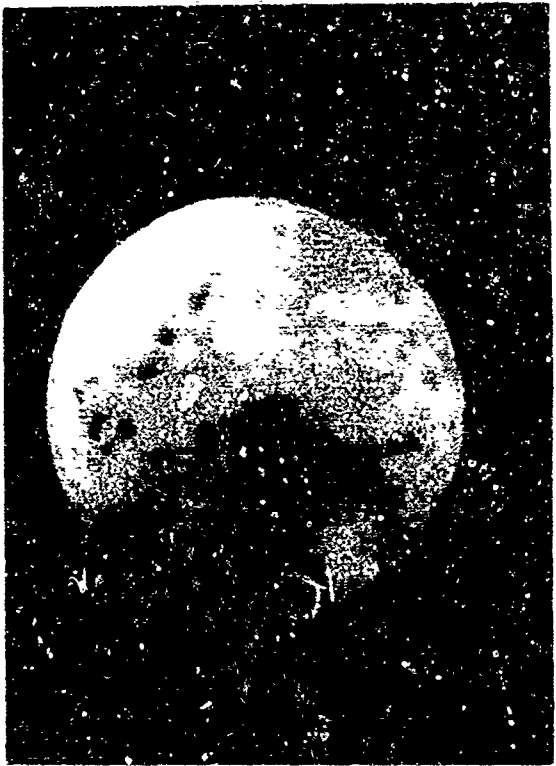
The Kerr-cell photographs in Figure 4 are an example of the information that can be obtained. The plasma surrounding the particle can be seen, as well as the poorly defined shape of the projectile itself. No. 570 shows a shattered particle.

DESCRIPTION OF OPERATION OF THE EXPLODING FOIL GUN

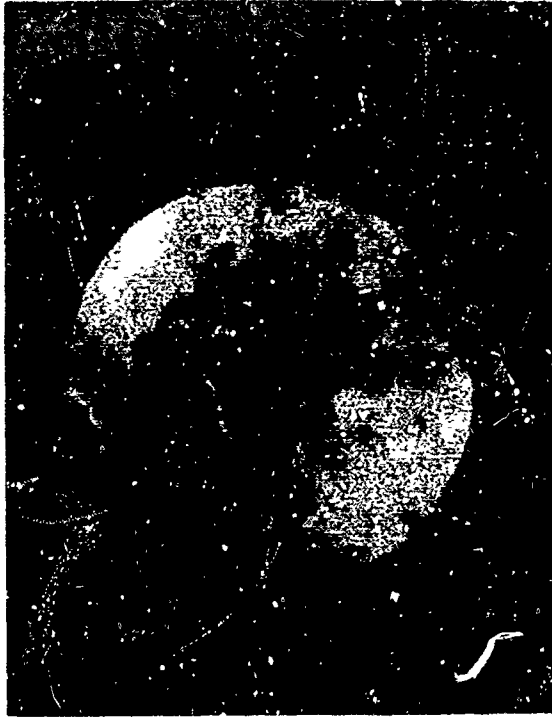
The gun is made up of three conductors electrically connected in series (Figure 5), with the one in the middle being the exploding aluminum foil. The electrical explosion is separated from the gun barrel and vacuum chamber by a mylar diaphragm (rupture disc) which confines the explosion for a short time interval during which the foil melts, vaporizes and begins to expand. In approximately 2μ sec. the diaphragm ruptures forming the disc-shaped particle. At the time of impact this particle weighs roughly 5 milligrams and travels at velocities between 7.5 and 9 kilometers per second. Single



566



567



568



570

Figure 4. Examples of Double-pulsed Derr-cell Records. Arrow Indicates Direction of Travel

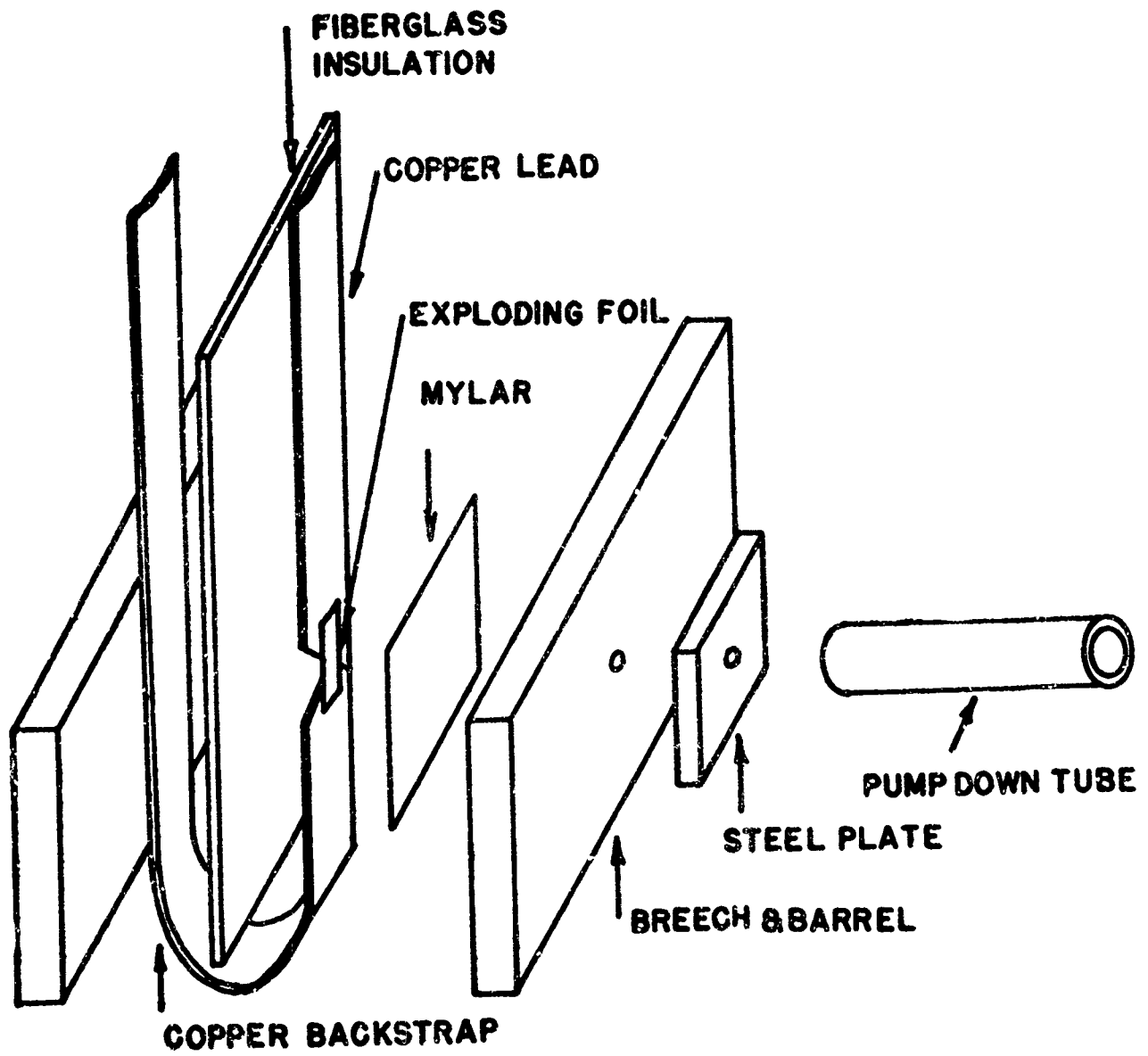


Figure 5. Exploding Foil Backstrap Gun

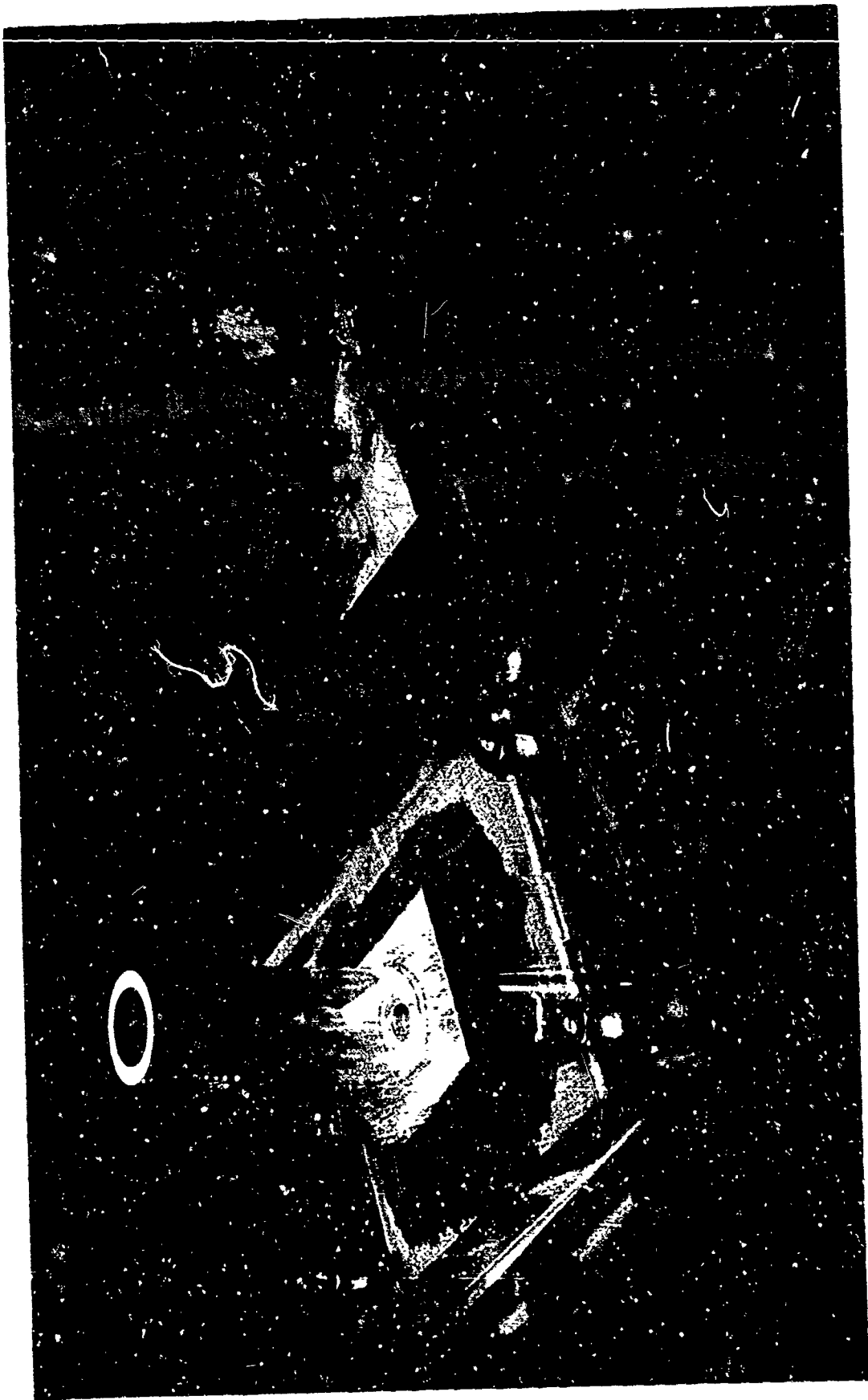


Figure 6. Exploding Foil Backstrap Gun

particle impacts at these velocities are achievable on approximately 50% of the shots fired, i.e. up to 5 impact data points per day. Figure 6 shows the gun in the assembled condition.

We are continuing the development of a gun that will enable us to accelerate spheres, between 50-100 μ in size, to speeds of around 20 kms. The gun designs studied include the coaxial gun, which has shown promise in free expansion studies conducted in the past, and the electrothermal gun, with which North American Aviation has been very successful.

Projectile Mass Measurements

The projectile mass is determined from penetration equations. The use of these equations is valid because the data points or targets selected for mass determinations have nearly hemispherical craters (within 10%). The equation chosen was the following⁽²⁾

$$\frac{V_c}{V_p} = 0.12 \left(\frac{\rho_p}{\rho_t} \right)^{\frac{1}{2}} \left(\frac{\rho_p v^2}{S_T} \right)^{.845}$$

where V_c = crater volume
 V_p = projectile volume
 ρ_p = projectile density
 ρ_t = target density
 v = velocity
 S_T = target shear strength

Transposing this equation for mass calculations with lead

targets one obtains: $m_p = .63 \times \frac{V_c}{\sqrt{1.69}}$ (v in Km/sec, V_c in cm^3)

We proceeded to calculate the projectile mass from selected single particle impacts which produced hemispherical craters.

The projectiles in each case were Mylar $\frac{1}{4}$ " diameter discs 0.010" thick having an initial weight of ~ 11 mg. The average particle mass we obtained was 4.8 ng with a RMS error of 25%.

TESTING OF EXPANDABLE STRUCTURES

The materials tested on the AFML facility are all described in more detail in other papers included in these proceedings. (3,4,5,6)

The Goodyear Aerospace specimens (3) were tested in the stressed as well as in the unstressed condition. With the 2" layer of 1 pcf foam the back surface was never damaged (Figure 7). It was then assumed that in certain applications the foam might be compressed to a fraction of its normal thickness (2 inches). In subsequent tests a typical 5 mg. mylar projectile travelling at 8 kms barely penetrated a sample compressed to 1" (rendering 2 pcf foam), while a similar particle travelling at a speed of 7.9 kms completely penetrated a sample compressed to $\frac{1}{2}$ inch, i.e. 4 pcf foam (Figure 8).

The material developed by Whittaker Co. (4) showed similar effects. In the fully expanded state penetration was not possible, while in the compressed condition either serious damage or complete penetration of the back surface occurred (Figure 9). Since the dacron back surface is rigidized the damage observed usually was some form of spallation or delamination.

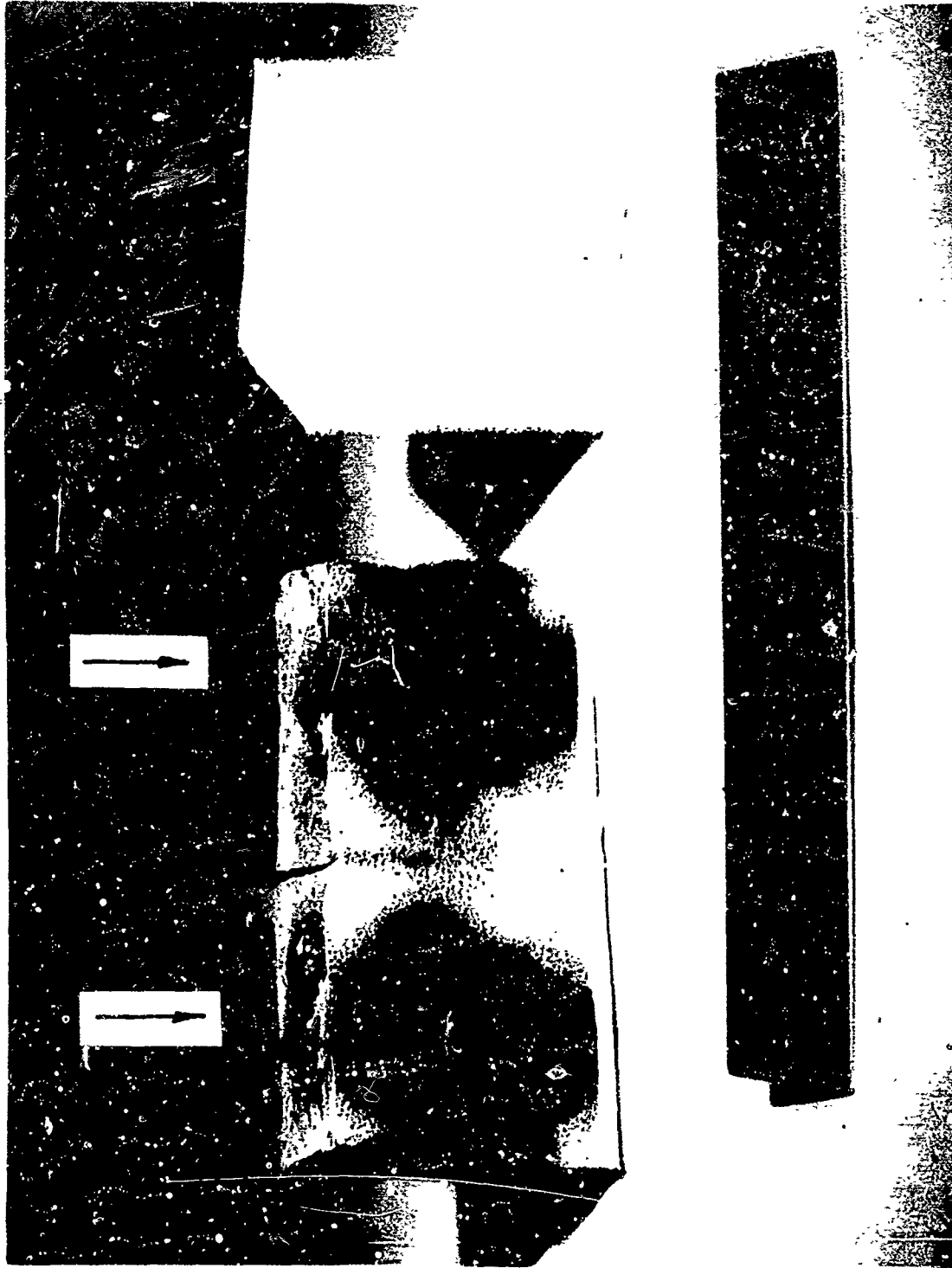


Figure 7. Goodyear Structure. Cutaway Shows Extent of Damage

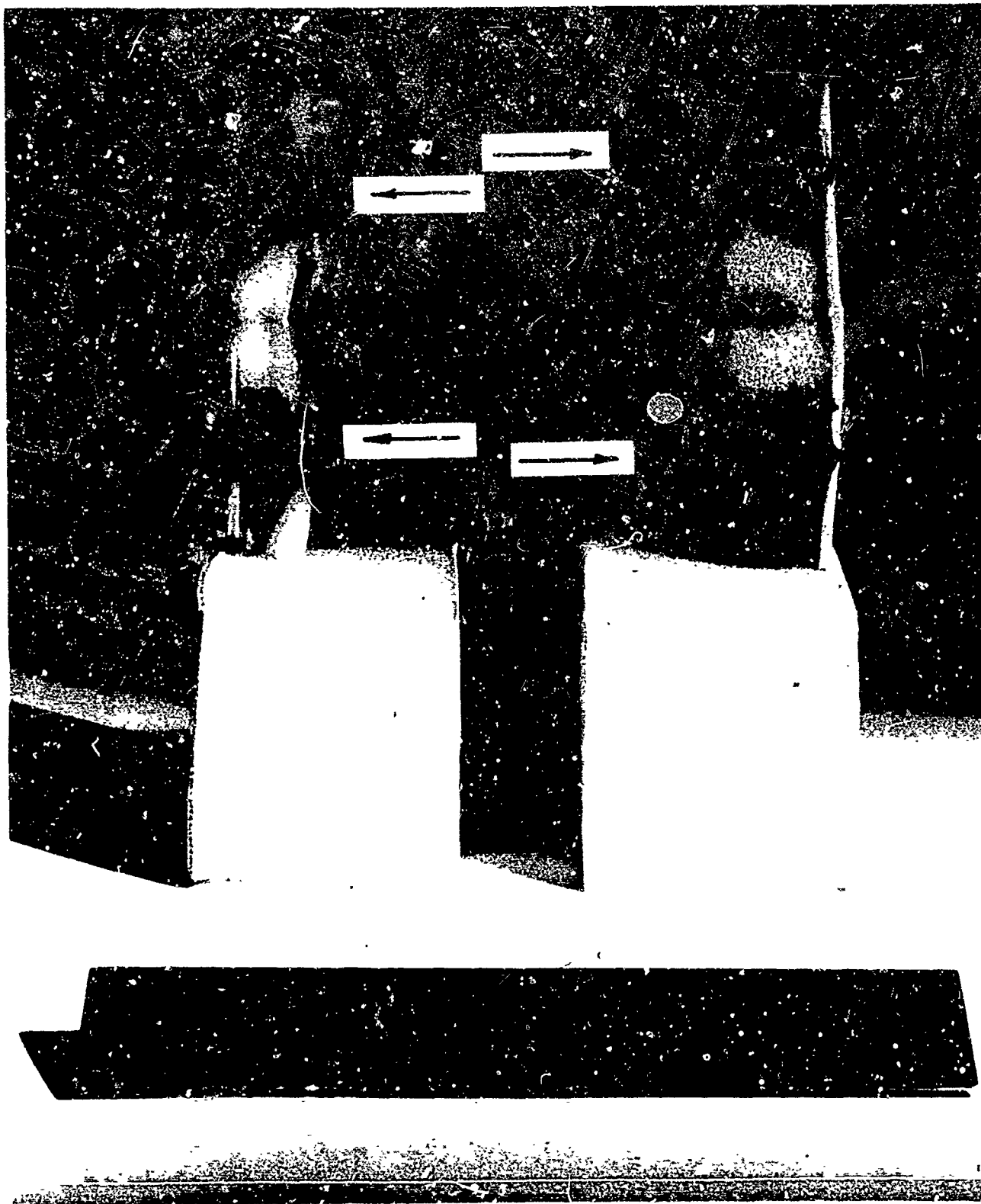


Figure 8. Goodyear Structure. Samples Compressed to $1/2''$ and $1''$.
Arrows Indicate Direction of Particle Impact

Another material tested was that made by National Cash Register.⁽⁵⁾ The $\frac{1}{2}$ inch layer of flexible 1- $\frac{1}{2}$ pcf foam is backed by a layer of 15 pcf rigidized foam. A typical mylar projectile could not penetrate a specimen with a 1 inch layer of rigidized foam while it completely penetrated a sample with a $\frac{1}{2}$ inch layer of rigidized foam (Figure 10).

A structure tested was the one developed by the Viron division of GCA.⁽⁶⁾ The foams, used for each of the specimens impacted, differed. However, none were completely penetrated. It was discovered, however, that particle penetration was affected by the location of the point of impact (Figure 11). Deepest penetration was obtained if the impact occurred at a seam at the front surface; essentially the particle sees only two surfaces in this case. Relatively deep penetration occurs if the particle impacts at a point close to a seam of the second and third layer of material. In this case the spray created by the second layer does not sufficiently diverge to reduce the impact energy per unit surface area of the third layer.

Ballistic Limit of Bumper Structures

Comparison studies were conducted looking at the ballistic limit of several bumper structures. Table I gives a list of the materials and arrangements that were studied.

Acknowledgements

The author wishes to thank Alan K. Hopkins for his assistance in the preparation of this paper and John E. Myrberg for the preparation of the photographs.

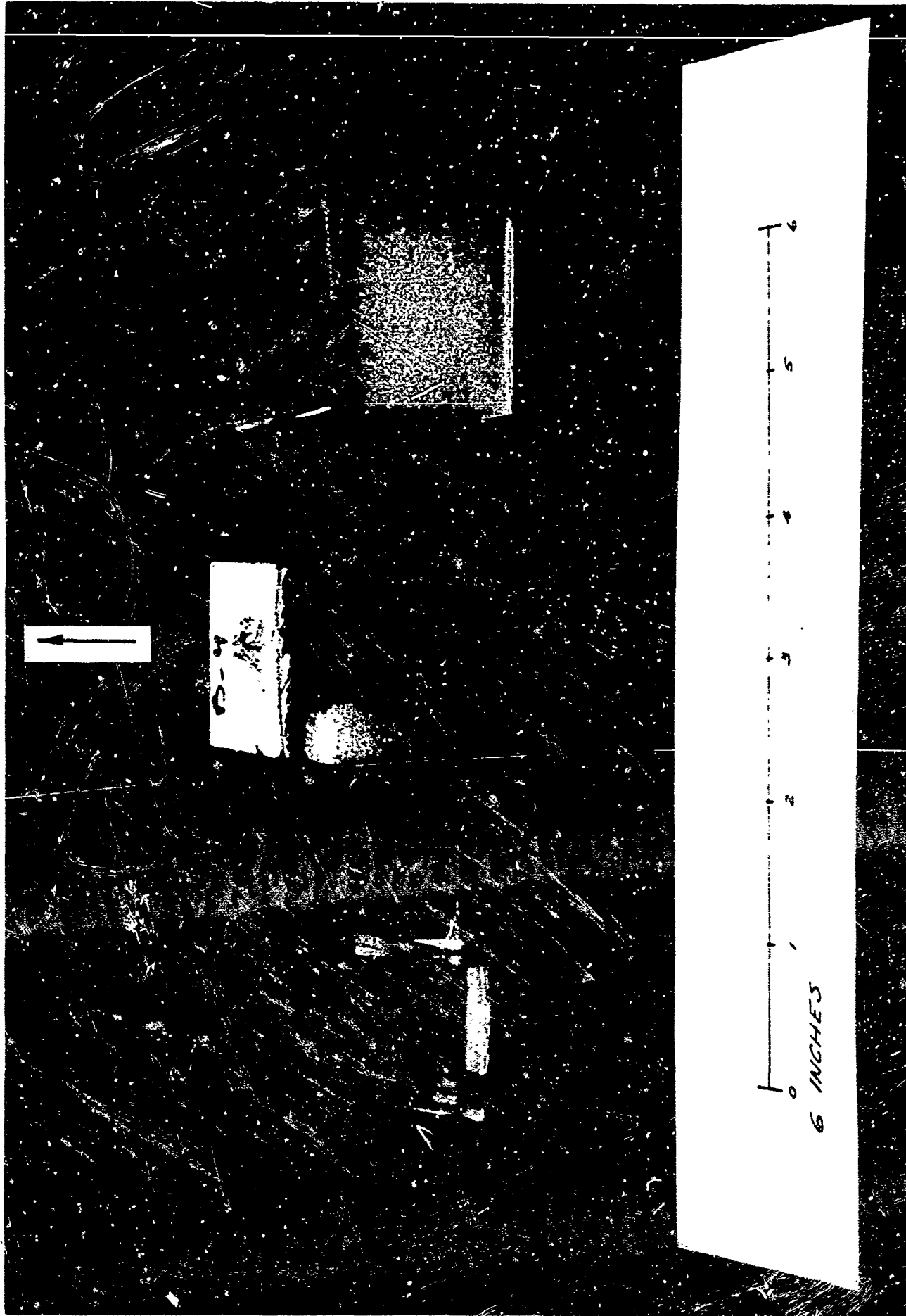


Figure 9. Whittaker Structure. Sample was Compressed as Shown on the Left. Damage to Back Surface can be seen on Sample in the Center

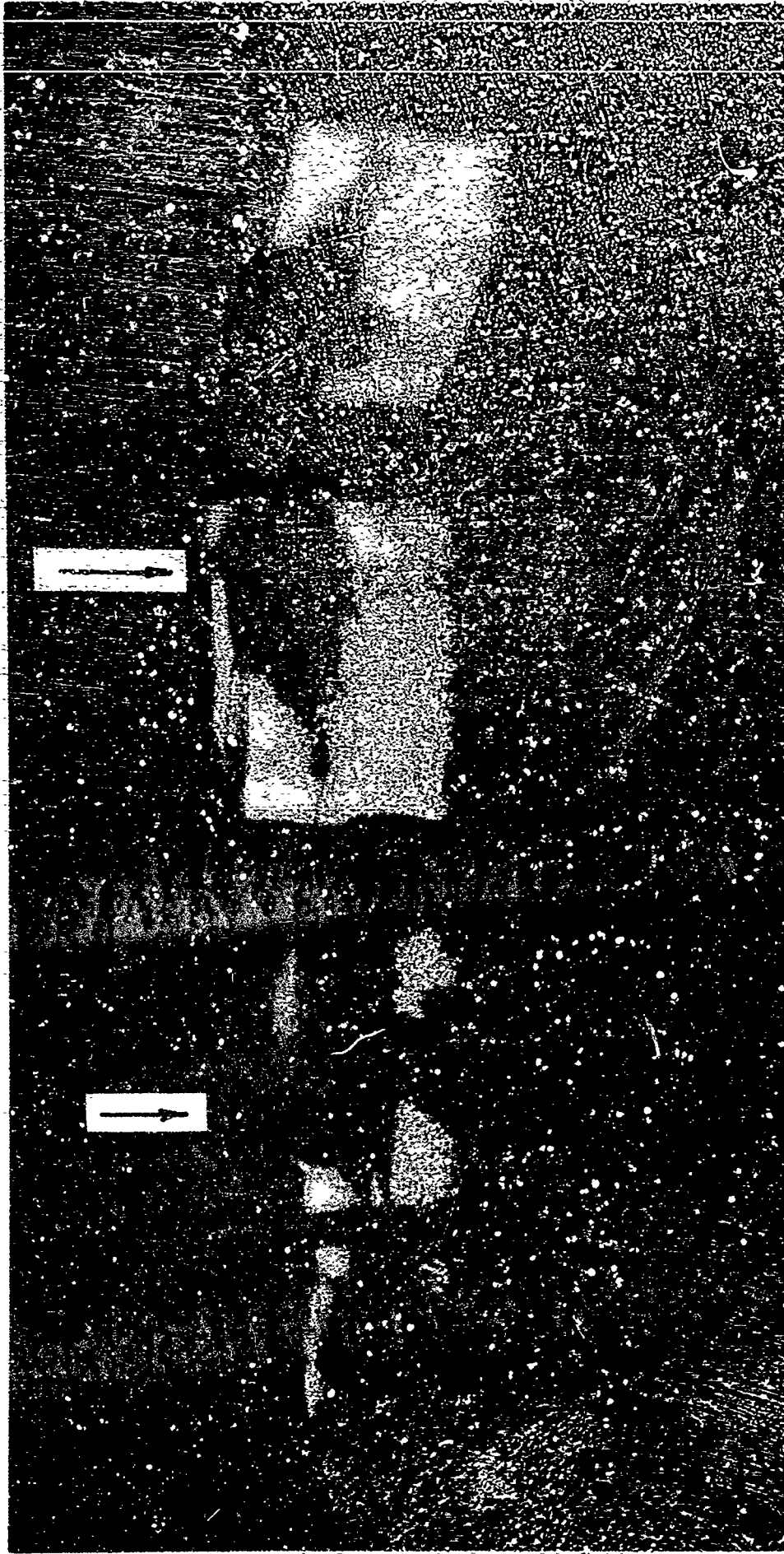


Figure 10. National Cash Register Structure. Samples have 1/2" (on the left) and 1" (on the right) layer of Rigidized Foam

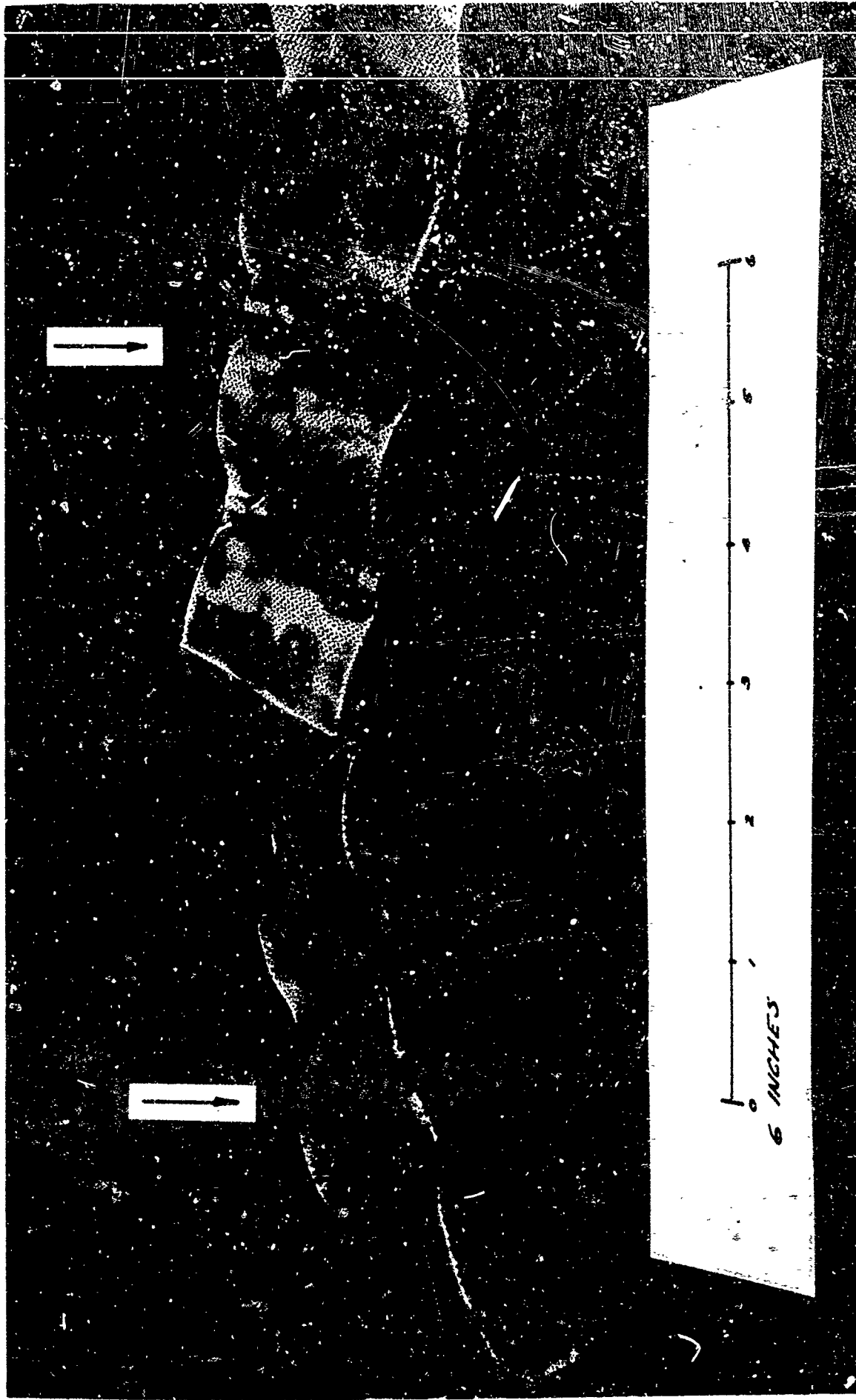


Figure 11. Viron-Geophysics Corp. of America Structure. Foam Type in Sample on the left is Vinyl (Firm, Closed Cell, 6.7 pcf) and in Sample on the right is Neoprene (Medium, Closed Cell, 18.3 pcf)

TABLE I

Ballistic Limit of Bumper Structures

for 5 mg mylar projectiles travelling between 7.5 and 9 kms.

Material	Total Thickness(inch)	Bal. Lim. (lb/ft ²)
Al 2024 T3	1/4	3.60
Al (.010" and .090")	1	1.42
NCR (3/4" rigid foam)	1 1/4	2.3
Goodyear (11b/ft ³ foam)	1 1/2	.60
GCA (.015" riterglass truss)	1 1/4	.43

REFERENCES

1. W. H. Clark et al. Proc of 7th Hypervelocity Impact Symposium. (1965) Vol. I - p. 207
2. Neil R. Sorenson. Proc. of 7th Hypervelocity Impact Symposium (1965) Vol. VI. - p. 281
3. Leo Jurich et al. Proc of 2nd Aerospace Expandable Structures Conference. 1965
4. Jerry Williams, Norman O. Brink. Proc of 2nd Aerospace Expandable Structures Conference. 1965
5. John F. Hanny. Proc of 2nd Aerospace Expandable Structures Conference. 1965
6. I. W. Russell, Charles Koons, Proc of 2nd Aerospace Expandable Structures Conference. 1965

SESSION V

DEVELOPMENT OF AN EXPANDABLE AIRLOCK UTILIZING

THE ELASTIC RECOVERY PRINCIPLE

By Jerry G. Williams

NASA Langley Research Center

INTRODUCTION

Recent studies of expandable structures have been centered around several manned space mission applications. Some of these applications as shown in figure 1 include: lunar shelters, space hangar, access tunnels, and expandable airlocks. The purpose of this paper is to discuss research on the latter application, namely, the expandable airlock.

The basic function of an airlock in a space vehicle is to permit crew and cargo transfer between the pressurized space vehicle and the vacuum of space. The principal advantages of a flexible expandable airlock as opposed to rigid internal concepts are reduced weight and increased useable volume. An expandable airlock is lightweight since it is constructed of high-strength filaments or fibers in an isotensoid design. Deployment in a favorable pressure differential (usually a vacuum) allows the airlock to be designed for internal pressure loads only. The absence of the requirement for resisting external loads is thus another weight reduction factor. An expandable airlock provides increased useable spacecraft volume because it is deployed external to the space vehicle when required and is compactly packaged during the launch phase of the mission, or when its extension would adversely affect extravehicular operations or experiments. Rigid internal airlock concepts, on the other hand, sacrifice valuable internal volume. If the airlock must be used internally, however, the expandable airlock has the advantage of being able to be stored in a minimum volume and erected only when actually needed.

Expandable airlock applications for advanced space station concepts such as the proposed MORL are shown in figure 2. Airlock A is an external airlock application which could be packaged in a recessed port in the wall of the space station during launch and later externally deployed as required. This airlock could be retracted, if necessary, either to meet operational requirements or to better protect the airlock. This airlock requires a protective wall system to make it compatible with the space vacuum, thermal, micrometeoroid, and radiation environment. A flexible transparent composite wall material located at eye level in the expanded airlock could serve as a viewing station for external experiments, thus reducing extravehicular activity.

Airlock B is what might be classified as an internal expandable airlock since it is located in the interior of the space station in the experiment and docking hangar compartment. The airlock is not exposed directly to the space environment and thus does not require the environmental protective wall required for external application (airlock A). Here again a flexible

transparent window section in the airlock would permit direct viewing of experiments in the unpressurized hangar compartment without space exposure of the astronaut. The airlock would be collapsed for storage when not in use.

The access tunnel shown connected to the resupply or crew ferry spacecraft would be an expandable structure similar in design to the expandable airlock. The tunnel would provide direct transfer from the space station living compartment to the stored ferry vehicle, either as the primary supply or astronaut transfer tunnel, or as an emergency escape tunnel. Its flexible and expandable characteristics would provide easy alignment. It is, of course, exposed to the space environment and would require a protective wall system.

EXPANDABLE AIRLOCK COMPONENTS

An expandable airlock is basically composed of three-component systems: (1) structural pressure vessel, (2) environmental protective wall, and (3) a deployment system. The structural pressure vessel is that part of the airlock wall which resists the applied pressure loads. It includes both the structural wall and end enclosures. It must be impervious to leakage and for most flexible composite materials requires the use of a bladder. The optimum design of a filamentary structure requires isotensoid fiber orientation, i.e., the fibers lie along geodesic paths and transfer loads in tension only. In the case of a structure that folds, the fibers must retain the designed orientation in the expanded configuration. A matrix is usually required to perform this function.

The environmental protective wall is that part of the airlock which shields and protects the airlock's integrity against the environmental hazards of space. It includes micrometeoroid protection, radiation shielding, and a thermal insulating wall and surface coating. The desirability or necessity for all or some of this protection is related to the function of the airlock. For example, an internal airlock application does not require micrometeoroid protection; whereas, reliability demands that a permanent cargo transfer tunnel have this protection. In general, the protection required for the airlock is for airlock materials protection rather than for the protection of the astronaut, since in most transfer operations the astronaut will have his own independent life support and space environment protection system and will be in the airlock for only short periods of time.

The airlock deployment system is that part of the airlock which deploys the airlock from the packaged configuration and stabilizes it in both the pressurized and unpressurized modes of operation. It is important that the airlock remain deployed in the unpressurized mode to insure that the astronaut's movements are not restricted by the airlock's collapsed walls. A reliable deployment system is, of course, essential to the successful operation of any expandable airlock. There are numerous possible systems for performing the deployment operation. Most systems, however, can be classified by one or combinations of the three categories shown in figure 3: (1) air pressurization, (2) mechanical actuation, or (3) elastic recovery.

Air pressurization of the airlock chamber is possibly the simplest method of deployment. It, however, does not provide a stable configuration in the unpressurized mode of operation. A second concept of deployment by air pressurization is pressurization of a spiral annulus located in the airlock wall. A stable configuration is then achieved even for the unpressurized mode. A modification of the spiral annulus is the pressurization of several straight tubes located symmetrically about the airlock circumference.

Mechanical deployment systems include various ingenious concepts. Among these are telescoping tubes which essentially jack the airlock into place, and concentric cylinders which telescope to form the airlock structure. The hemispherical configuration is included to illustrate that expandable airlocks are not necessarily limited to cylindrical configurations. This airlock could be hand deployed and has merit for internal auxiliary, or emergency, airlock application. The success of a mechanical deployment system depends on the successful solution of problems associated with mechanical operations in the space environment. Vacuum welding and vacuum lubrication are technical areas which require thorough investigation.

The elastic recovery concept utilizes the stored potential energy of a strained elastic material for deployment. Elastic recovery concepts include the use of stress memory materials, springs encased in the airlock wall, and thick-walled structures constructed of resilient open-cell foam.

For external airlock application, a thick-walled structure constructed of a resilient foam material is a promising approach. The foam, in addition to providing deployment actuation, also affords micrometeoroid protection and insulation for thermal control. It maintains a stable configuration in the deployed mode of operation and it is well suited for multiple deployment.

A typical compression stress-strain curve for a polyester open-cell foam is shown in figure 4. For this plot, a constant compression strain rate of 1 inch per minute was experienced by a 4-inch cube of polyester foam with a density of 1.30 lb/ft³. Curve A is the initial loading and unloading curve. The area under the loading portion of the curve is a measure of the work required to compress the sample, and the area under the unloading portion is a measure of the energy available for restoring the material to its original configuration. The area between the curve is, of course, a measure of the energy lost in the compression cycle, either through heat, viscous flow, or plastic deformation. A compression set in the foam is indicated by the offset from zero on the abscissa corresponding to zero load. For this viscoelastic material the compression set decreases with time.

Curve B is a plot of the fifth cycle of a continuous cyclic load on the material. The loading portion of this curve is lower than that for the initial curve, indicating that less energy was required to compress the foam for this cycle than for the initial cycle. The unloading curves, however, are almost identical, indicating that the potential energy available for restoring the material to its original configuration is not severely affected by continuous cyclic loading.

Curve C is a plot of the sixth hysteresis cycle on the foam. A time interval of $27\frac{1}{4}$ days elapsed between cycles number 5 and number 6. This plot

shows a tendency for the material to recover, with time, some of its original characteristics as indicated by the upward shift of the loading portion of the plot.

Curve D is the stress-strain curve for a second 4-inch cube of the same material. This sample was loaded to the same maximum load as was the first sample, and then left compressed for a period of 7 days. After this period the load had relaxed to approximately 54 percent of its initial value. The difference in the loading portion of the two samples (curves A and D) is probably due to the nonhomogeneous property of the foam material. The significantly lower position of the unloading curve, however, indicates that long-term storage in the packaged configuration of an elastic recovery expandable structure will cause the structure to lose some of the energy available for deployment. The time required for deployment is also related to the length of time compressed as indicated by the larger compression set of curve D. These various characteristics of the foam material must be considered in the design of an elastic recovery deployment mechanism.

ELASTIC RECOVERY AIRLOCK DESIGN*

Guidelines

The remainder of this paper will discuss the design of an expandable airlock which utilizes the elastic recovery principle for deployment; specifically, a resilient foam. Guidelines for this design are shown in table 1. These guidelines specified a cylindrical configuration with sufficient volume for the transfer of a pressure-suited astronaut (approximately 4 feet in diameter and 7 feet in length). Deployment from the packaged mode was to be achieved through utilization of the stored potential energy of a compressed foam. Provision for multiple deployment was required since this offers additional environmental protection to the airlock and allows an unobstructed spacecraft exterior. The airlock was assumed to operate in a 200 n. mi. circular orbit with a 28.7° inclination. Passive thermal control was required to hold the internal temperature of the airlock within 50° F to 80° F. A 10-psi operating pressure was assumed for structural design with a safety factor of 5. A 30-inch-diameter hatch which could be opened with a force of 40 pounds or less was required. A maximum leakage of 0.01 lb/day with 1 atmosphere pressure differential was the allowable leakage rate. A requirement of 0.995 probability of zero penetration was specified for micrometeoroid protection. Radiation protection was not specified since the astronaut would be in the airlock for only short periods of time and since he has his own independent space suit protection. Some radiation protection is, of course, inherently afforded by the airlock wall.

*The elastic recovery concept was studied by the Whittaker Corporation, Narmco Research & Development Division under contract NAS7-283, entitled "Research On An Expandable Airlock Utilizing the Elastic Recovery Principle." Mr. N. O. Brink was project engineer.

Materials

The materials which comprise the airlock wall may be divided into four major functional categories as shown in figure 5: (1) the outer thermal control surface, (2) layers for micrometeoroid protection and thermal insulation, (3) the structural fabric, and (4) an inner impervious liner. The composite wall must also incorporate in its design sufficient foam thickness to actuate deployment by the elastic recovery principle. In addition, the resulting composite wall must maintain flexibility to insure that it can be packaged and deployed.

Thermal Control

The use of polymeric composite structure materials presents very definite temperature limitations on the airlock. The maximum allowable temperature of the foam material in a space vacuum environment is approximately 250° F. Above this temperature, the foam will lose its elastic recovery properties and above 300° F will lose its structural integrity. The necessity for maintaining the temperature within the airlock between 50° F to 80° F further required an extensive and accurate thermal analysis.

The passive thermal control capability of the airlock was determined from a parametric study of temperature levels as a function of surface optical properties and insulation thickness. The thermal environment of an orbiting vehicle is established by radiation heat influx on the external surfaces. In a low earth orbit, solar radiation, earth-reflected solar radiation, and earth-emitted thermal radiation are the contributing factors to the total heat influx. In the case of an airlock structure which is not an independent vehicle, the effects of reflected and emitted radiation from the surfaces of the space vehicle on the airlock must also be included. The heat influx to an orbiting vehicle varies greatly from point to point around the orbit because of the dependence on the vehicle's altitude, its attitude with respect to the sun and the earth, and whether it is in sunlight or shadow.

The complexity of an accurate analysis of the thermal environment as influenced by all of these variables necessitated the use of a computer program. For this calculation, the cylindrical airlock was divided into an octagonal body having eight flat surfaces and an end plate as shown in figure 6. The bottom surface in contact with the space vehicle was assumed to be a nonheat-transfer surface. The computer program then determined the geometric shape factors between each surface of the orbiting airlock and the heat sources, and solved the pertinent finite difference heat-transfer equation at 50 intervals around the orbit. The heat influx to each surface included reflected solar radiation and thermal radiation from a 260-inch-diameter circular base. Two extreme heating conditions were assumed for the analysis: (1) a maximum heating condition in which the airlock was considered to be constantly orientated toward the sun during an orbit of maximum time in sunlight exposure, and (2) a minimum heating condition in which the airlock was considered to be constantly in the shadow of the space vehicle for an orbit of minimum time in sunlight exposure. The condition for maximum heating was found to be when the axis of the airlock was oriented at an angle of approximately 30° with the sun vector.

Results for the maximum heating condition indicated that a surface coating with an absorptivity of 0.19 and an emissivity of 0.25 combined with a 2-inch-thick foam layer would maintain the internal temperature of the airlock within the specified limits of 50° F to 80° F for the condition of maximum heating. In addition, the external surface temperatures would be maintained within the allowable limits for the composite materials. However, for the minimum heating condition, the internal airlock air temperature for this same design would drop rapidly. The internal air temperature would drop to 50° F in approximately 35 minutes and after several orbits would stabilize around -40° F. The corresponding lowest external surface temperature would be approximately -85° F. These extreme temperatures were considered to be within reason of feasibility since they would not adversely affect the airlock materials and would be tolerable for a pressure-suited astronaut.

Micrometeoroid Protection

Micrometeoroid protection is provided by an outer cloth bumper which acts to break and fragment the hypervelocity micrometeoroid particles, a layer of foam which retards the fragmented particles, and an inner cloth main wall (see fig. 7a). An analysis showed a requirement for: a bumper laminate weight of approximately 0.27 lb/ft², a 1.35 lb/ft³ density foam thickness of approximately 2.0 inches, and a main wall weight of approximately 0.12 lb/ft². Preliminary hypervelocity impact tests in which 10-milligram polyethylene terephthalate disks struck composite wall samples at velocities of approximately 7,000 and 18,000 feet per second indicate that a lower bumper weight may be sufficient. A typical cross-sectional view of a sample taken from these tests is shown in figure 7b.

Structural Design

Since the airlock was a cylindrical configuration with a relatively thick composite wall, improved folding and packaging characteristics were provided by designing a corrugated bellows-shape configuration in the cylindrical airlock section. The deployed and packaged configurations are illustrated in figure 8.

Two design approaches were considered for the airlock load-carrying structure: (1) a filament wound structure and (2) a filament reinforced knitted structure. The filament wound approach initially appeared attractive since a helically wound cylinder constitutes one of the most efficient structures; i.e., the lightest weight for a given internal pressure load. However, filament winding a corrugated cylinder requires elaborate fabrication techniques. In addition, the matrix required to maintain filament orientation tends to stiffen the structure.

A filament reinforced knitted structure is shown in figure 9. Axial loads are carried by continuous fibers woven back and forth in the knit with the knitted material used simply as a matrix to position the load-carrying fibers. Circumferential loads are carried by circumferential hoop bands located at the points of corrugation and spaced uniformly along the length of the cylinder. The advantages of this approach are: (1) the knitted

matrix is easy to fabricate, lightweight, and extremely flexible and (2) the loops formed by the longitudinal fibers as they traverse back and forth form a natural and efficient means of attaching the airlock to the space vehicle and to the end hatch. For this purpose, the longitudinal fibers can be woven around a rigid mounting ring during the knitting process or later threaded by a rigid ring. For these reasons, the filament reinforced knitted structure was the selected structure.

An inner liner was designed to retain the air within the airlock. Desirable characteristics for the liner material included flexibility, toughness, low permeability, and low toxicity. A review of candidate materials showed polyvinylidene chloride film to possess the best properties. The thickness of film required to prevent extrusion through the structural fabric was determined experimentally. The results of this test indicated a $3/4$ -mil thickness would sufficiently prevent extrusion through the structural fabric mesh under a pressure differential of 45 psi. To provide additional safety, a liner thickness of 2 mils was recommended. A scuff pad may also be desirable to resist abrasion and puncture from abusive treatment by the astronaut's equipment. The liner attachment was so designed that the liner could be removed and replaced if punctured or for preventative maintenance.

Packaging Study

The requirement of flexibility of the composite wall of an expandable structure cannot be overemphasized. It is absolutely necessary for successful packaging and deployment of such a structure. A wall structure built up of several flexible components and bonded together to form a composite structure can so easily turn out stiff and inflexible. Several basic principles, however, if followed can give the desired flexible characteristic. These principles include: (1) prevent binder impregnation of the laminate materials, (2) use a low modulus binder, (3) use a minimum of adhesive material, and (4) reduce the number of plies to a minimum. Limiting the binder impregnation of the foam and cloth proved to be the key factor to improved flexibility in this study. A successful technique which was developed for this purpose is a transfer technique. This technique is a two-step procedure, whereby the resin (in this case a polyurethane) is first spread out in a thin film, and allowed to advance to a tacky state. The cloth or foam material is then laid on the resin to pick up enough to cover the surface. The laminate materials are then bonded together with contact pressure and cured at room temperature. A sample of composite flexibility achieved by this technique is shown in figure 10. The cloth and foam layers represent the thickness required for micrometeoroid protection.

Folding and packaging characteristics of the airlock were studied through the use of scale models. Complete scaling of a composite structure is problematical because of a difference in scaling laws. Geometric scaling is a linear function of the airlock dimensions and wall stiffness is a cubic function of the wall thickness. For this study, the airlock dimensions were scaled geometrically by one-quarter and the wall thicknesses by one-half.

This produced a model which was 1 foot in diameter and $1\frac{3}{4}$ feet in length with a 1-inch wall thickness. The folding model study began with simple

cylinders and progressed to more complex configuration including models with flexible or rigid hoop bands and simulated convolutions.

A simple cylindrical model is shown in the deployed and packaged configurations in figure 11. The large major folds or buckles visible under the shroud are typical for this type of cylinder. This type of fold is not optimum from a deployment standpoint, since the best recovery characteristics for a flexible composite structure are exhibited when the resilient form is uniformly compressed. This suggests, to insure that large portions of the foam do not remain uncompressed, the use of many minor folds in the composite wall rather than a few major folds. The use of many minor folds also provides faster deployment, since shallow creases "pop out" more readily than deep creases.

The approach taken for improving the folding pattern of the composite wall was to restrict the folding pattern through the use of hoop bands uniformly spaced along the length of the cylinder. (See fig. 12.) Both flexible and rigid hoop bands were evaluated. It was found that flexible bands had little effect on decreasing the number of large folds. (See fig. 13.) These major folds or buckles are essentially the same as those observed for a cylinder without hoop bands.

Rigid hoop bands, however, constructed of filament wound impregnated glass rovings were found to be effective in restricting folding to the desired pattern. This model is shown in figure 14 in the deployed and packaged configurations. The use of rigid rings is also compatible with structural requirements for the airlock since hoop rings are required to resist the circumferential loads.

A full-scale cylindrical section of the airlock was constructed to determine the packaging ratio and the load required for packaging. This section as seen in figure 15 was 4 feet in diameter and 3 feet in length. The thickness of the walls was 2 inches, approximately that required for the airlock. Loads were applied to the cylinder by means of weights suspended from the center of the top end plate. A load deformation curve for the cylinder is seen in figure 16. Since this cylinder did not have rigid hoop bands to restrict the folding pattern, a major circumferential buckle occurred at a load of approximately 130 pounds. When the load was removed this major buckle was not completely relieved; consequently, the cylinder returned to only 66 percent of its original height. It is anticipated, however, on the basis of the one-quarter scale tests, that a cylinder constructed with a corrugated surface and rigid hoop rings would fully deploy. However, even if the airlock did not completely deploy, air pressurization would complete the deployment. Once deployed it would maintain the expanded configuration. On the basis of the packaging tests, an $8\frac{1}{2}$ to 9 expanded volume to packaged volume ratio is considered feasible.

Assembled Airlock

An artist's concept of the assembled airlock is seen in figure 17. A cutaway section exposes the inner liner, the corrugated structural fabric,

and the protective outer wall. The cover cap serves as a shroud for the airlock during launch and as protection when the airlock is not deployed.

Retraction cables are designed to provide multiple deployment capability. These cables are attached to the hatch flange and separated from the flexible walls by a spacer. Torque applied to a winding ring at the base provides equal displacement of the cables, thus insuring uniform retraction of the airlock. The airlock in its retracted configuration is shown above.

The end closure hatch is a rigid structure held in place by three spring-loaded bullet-type catches. The top of the hatch is covered with foam and a cloth bumper to provide micrometeoroid protection equivalent to that afforded the flexible walls. It is designed for inward opening thus providing a positive pressure seal. Underwater zero gravity simulation studies have shown an inward opening hatch to be a feasible approach. A detail of the hatch components is shown in figure 18.

A weight estimate for the expandable airlock system is shown in table 2. The total weight is 101 pounds. Not included in this weight estimate are the valving system, retraction ring drive unit, and base closure plate. The material weight for the airlock of 43.4 pounds is based upon an assumed area of 95 square feet and upon the weights of actual composite samples. The end rings, hatch, hoop rings, and inner liner accounted for 41.8 pounds. The remainder of the 101-pound airlock system weight consists of the retraction mechanism.

CONCLUSIONS

In conclusion, an expandable airlock which utilizes the stored potential energy of a compressed foam for deployment appears to be a feasible approach for manned space mission applications. It will maintain a stable configuration in the deployed mode of operation and it is well suited for multiple deployment. The foam in addition to providing deployment actuation, also provides micrometeoroid protection and insulation for thermal control. Adequate packaging characteristics can be achieved through the use of a corrugated bellows-shape configuration supplemented with rigid hoop rings designed to restrict the folding to the desired pattern. A filament reinforced knitted structure is not only lightweight and extremely flexible, but provides a natural and efficient means for attaching the airlock to the space vehicle and to the end hatch.

REFERENCES

1. Brink, N. O.: Research On An Expandable Airlock Utilizing the Elastic Recovery Principle. Final Rept. (Contract NAS7-223), Whittaker Corporation, Narmco Research & Development Division, April 1965.
2. Brink, N. O.: Development and Evaluation of the Elastic Recovery Concept for Expandable Space Structures. NASA CR-121, 1964.
3. Loisch, J. A.: Design of Inner Pressure Shell for Airlock Structure Astro Research Corporation Report 159, Aug. 1964.
4. Olson, M. W.: A Research Study To Investigate the Application of Filament Winding for Sections of an Erectable Space Station. Final Rept. (Contract NAS1-2317), U.S. Rubber Co., April 1963.
5. Schuerch, H.; and Eyer, A.: Structural and Folding Analysis of the Airlock. Astro Research Corporation Report 169, Oct. 1964.

TABLE 1.- EXPANDABLE AIRLOCK DESIGN CRITERIA

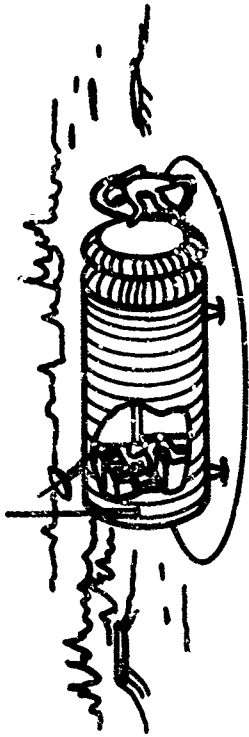
Configuration	Cylindrical, 4-foot diameter, 7 feet long
Deployment	Elastic recovery, multiple
Orbit parameters	200 n. mi. circular orbit 28.7° inclination
Thermal control	Passive system
Internal temperature range	50° F to 80° F with a design temperature of 64° F
Structural design	10-psi design pressure with a safety factor of 5
Hatch design	30-inch diameter opening with an opening force of 40 lb or less
Leakage	Maximum of 0.01 lb/day at 1 atmos- phere pressure differential and 60° F temperature
Meteoroid protection	99.5 percent probability of zero penetration
Radiation protection	Not designed into the airlock wall due to the short period of time astronaut is in the airlock

TABLE 2.- AIRLOCK WEIGHT ESTIMATE

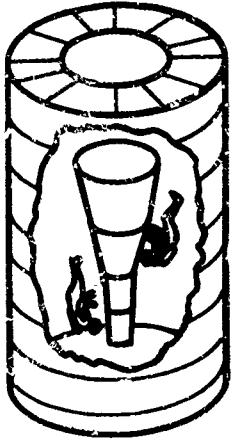
Item*	Materials	Weight, lb
1. Hatch	Laminate, ring and foam	10.5
2. Upper end ring	Aluminum	18.9
3. Cap	Laminate	3.0
4. Composite wall**		
a. Protection layers	Foam and cloth 38 lb	
b. Structural fabric	Dacron and monofilament 5.4 lb	43.4 (total)
5. Hoop rings and drawstrings (2)	Wound fiberglass	6.5
6. Airtight liner	Polyvinylidene chloride	2.5
7. Bottom end ring	Aluminum	3.4
8. Retraction mechanism	Various	
a. Cable hanger (4)		4.0
b. Cables and eyes (4)		1.0
c. Pulleys (8)		.8
d. Winding ring		4.0
e. Winding ring retaining assembly (4)		1.0
f. Shield assembly	Laminate	2.0
Total weight		101.0

*Valves, tubing, retraction drive unit, or attachment plate not considered.

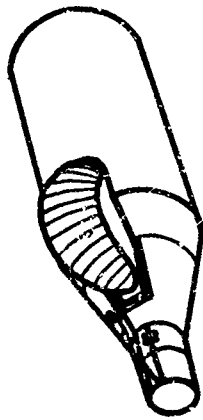
**Composite wall weight based on a surface area of 95 ft².



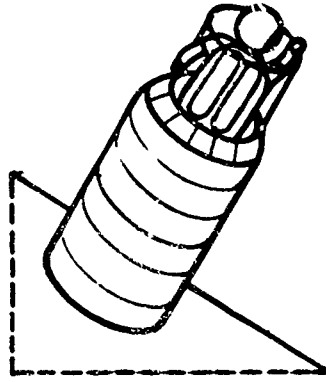
(a) LUNAR SHELTER



(b) SPACE HANGAR



(c) ACCESS TUNNEL



(d) EXPANDABLE AIRLOCK

NASA

Figure 1.- Space applications for flexible expandable structures.

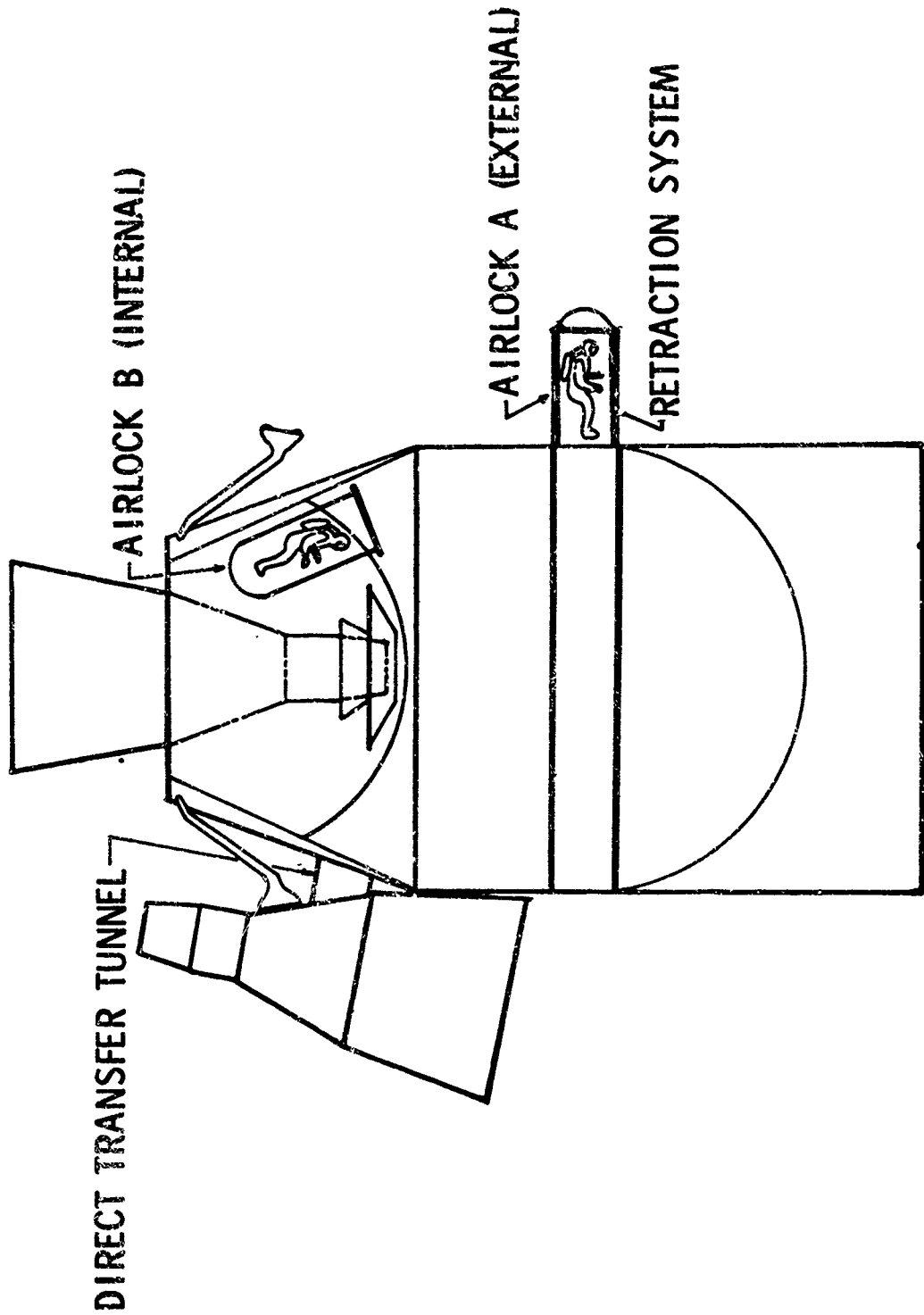
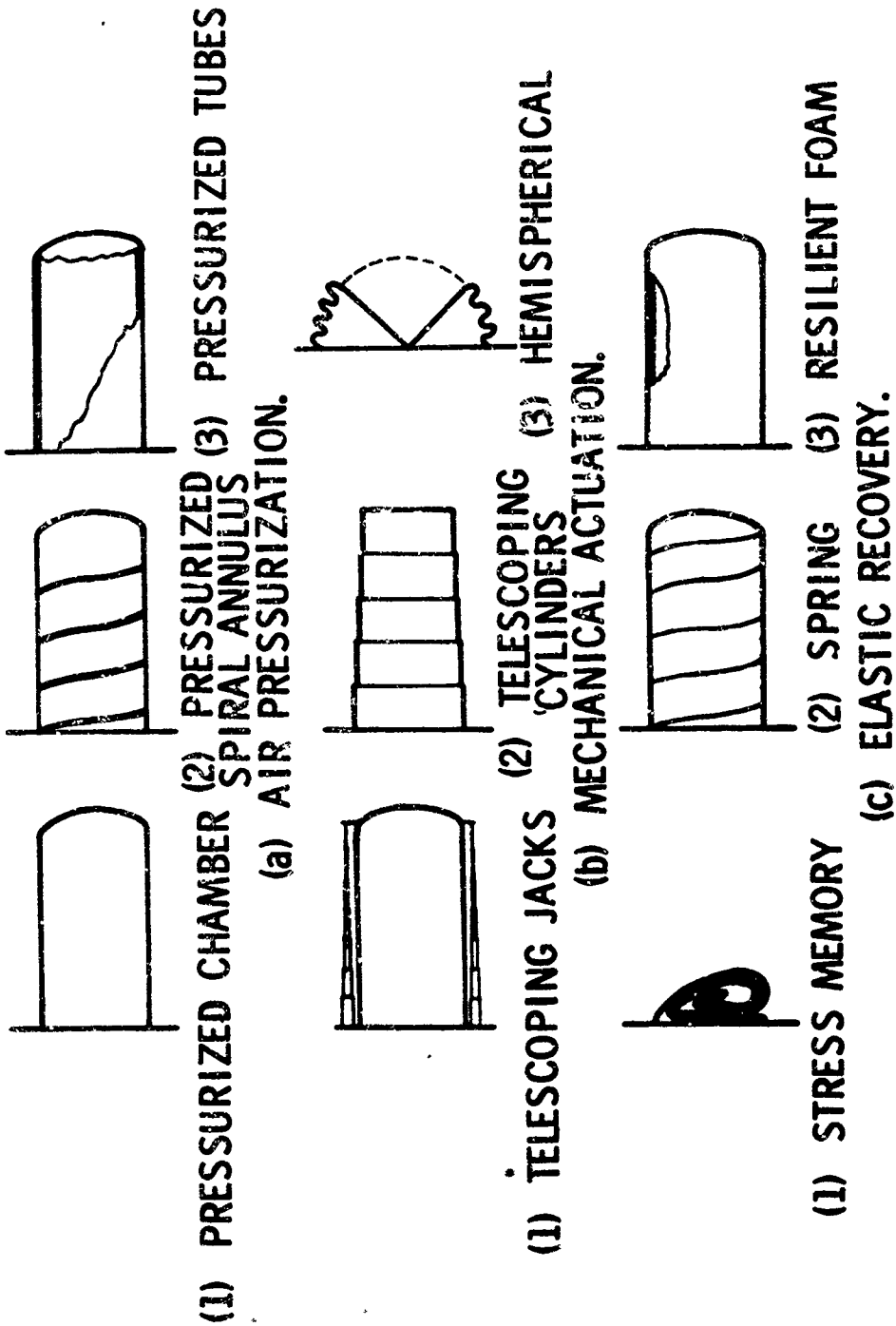
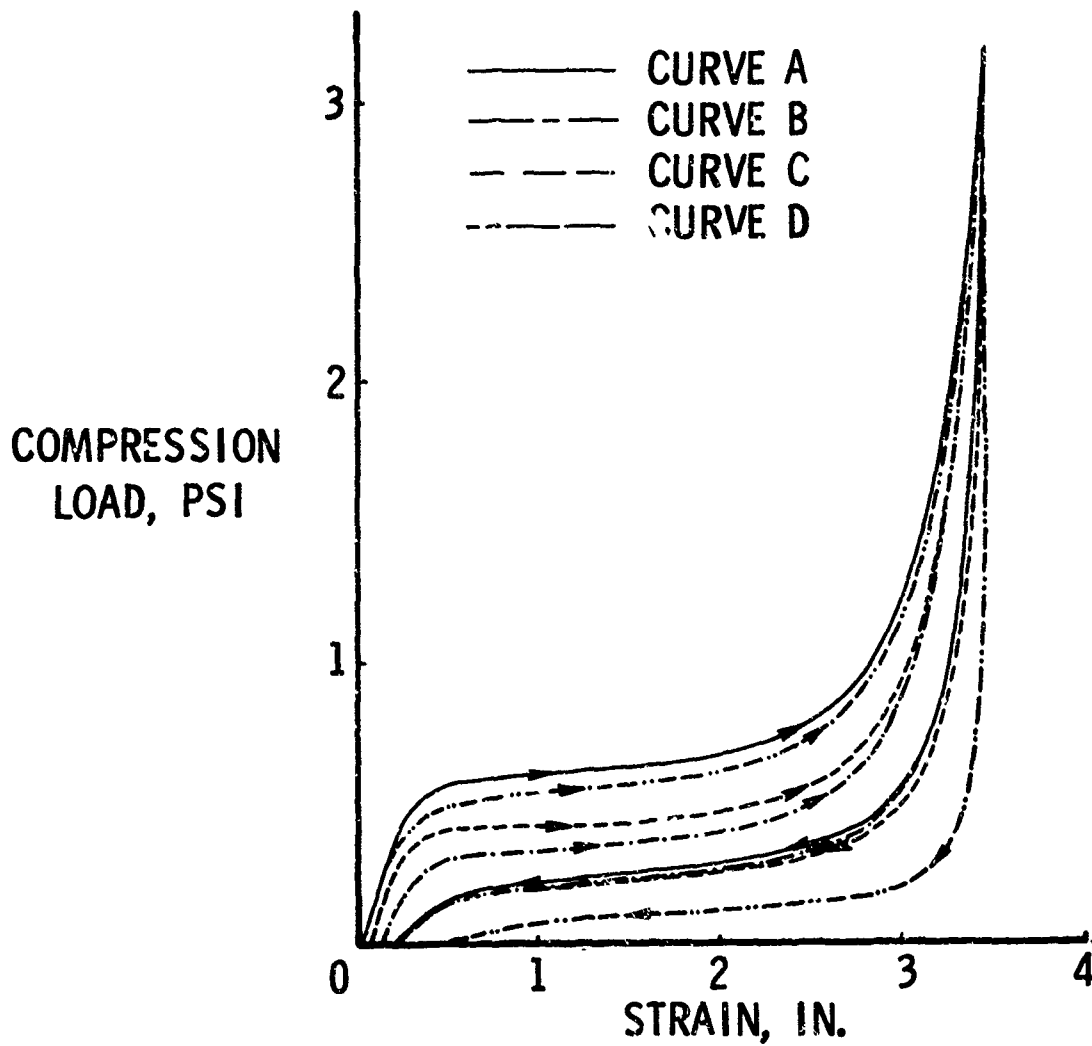


Figure 2.- MORL expandable airlock application.



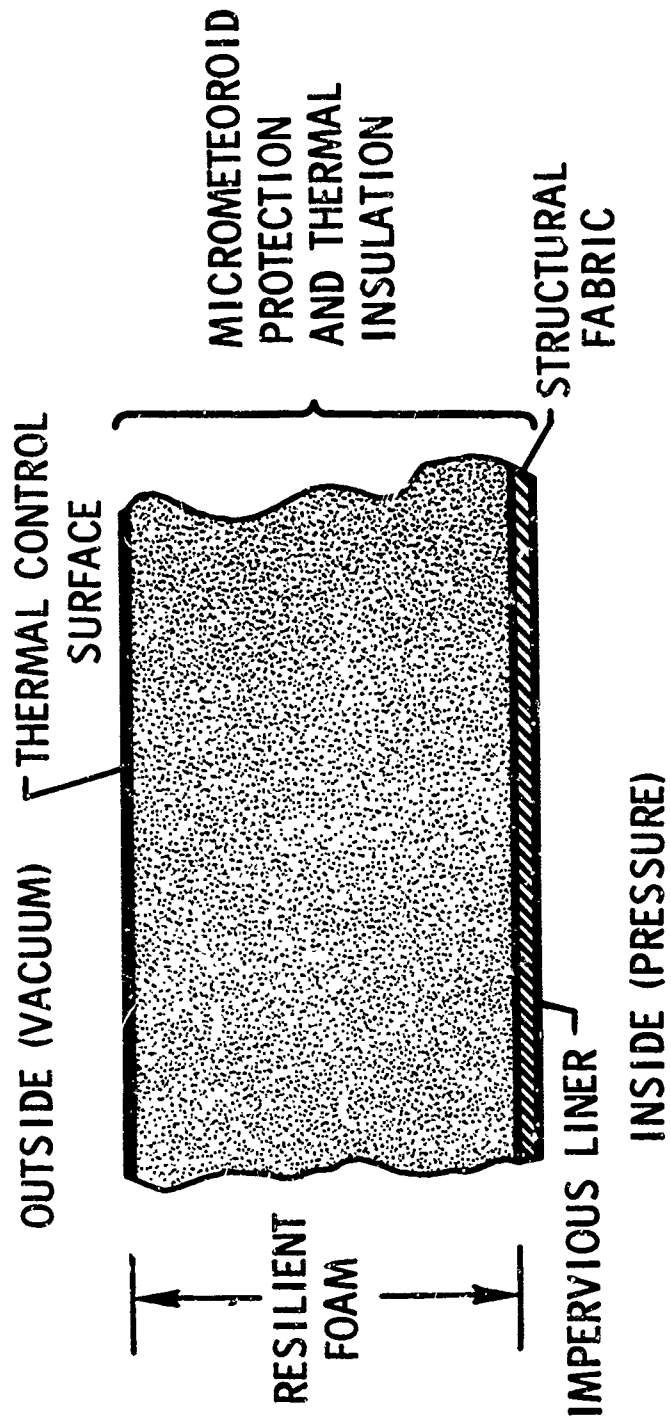
NASA

Figure 3.- Deployment system.



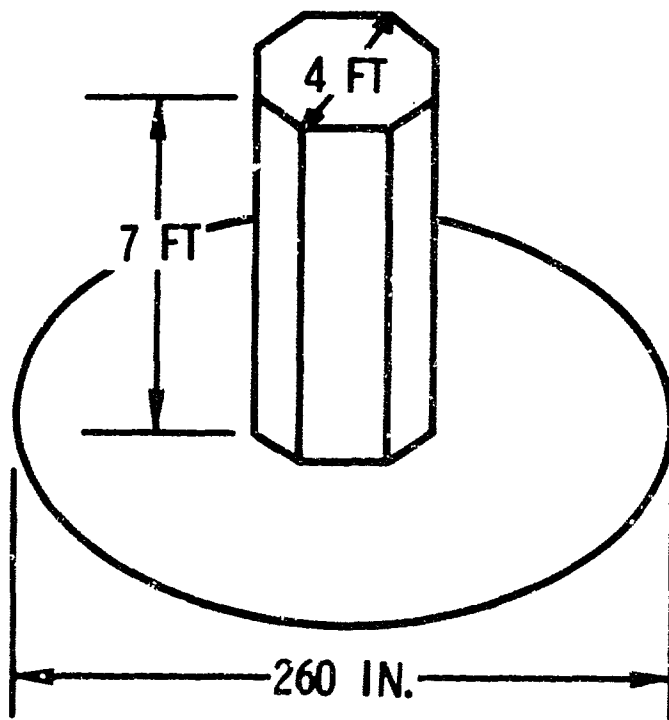
NASA

Figure 4.- Compression stress-strain curve for 4-inch cube of polyether open-cell foam.



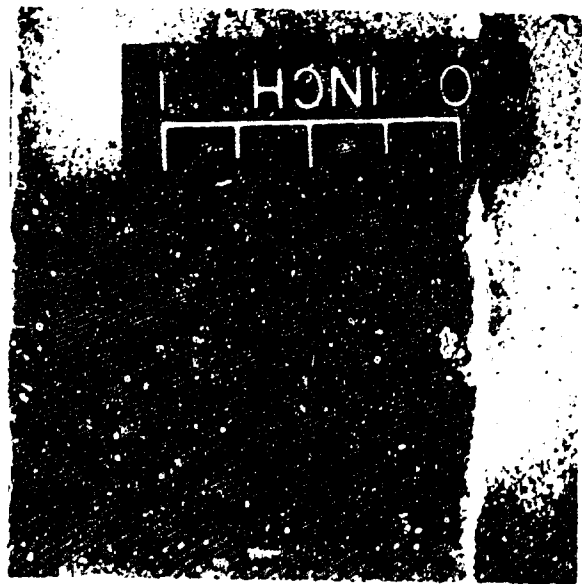
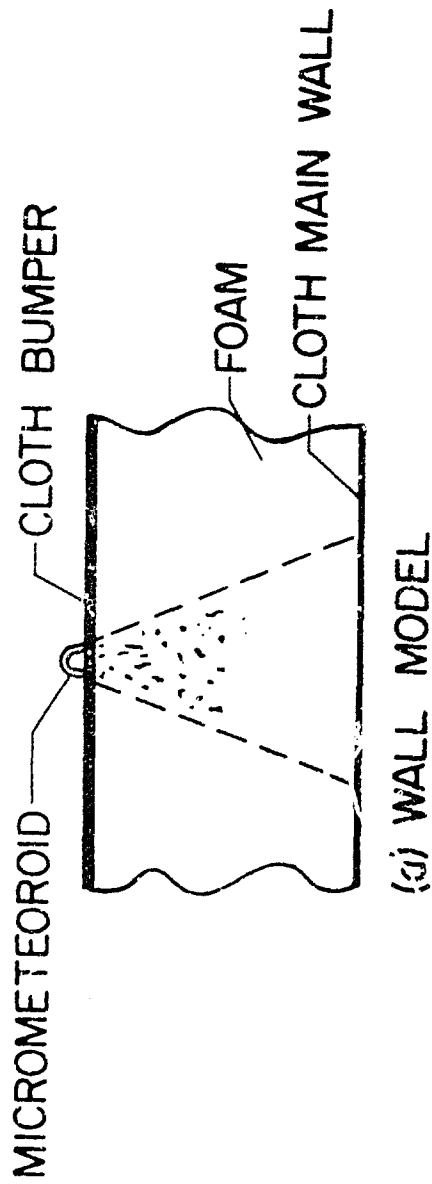
NASA

Figure 5.- Typical wall section.



NASA

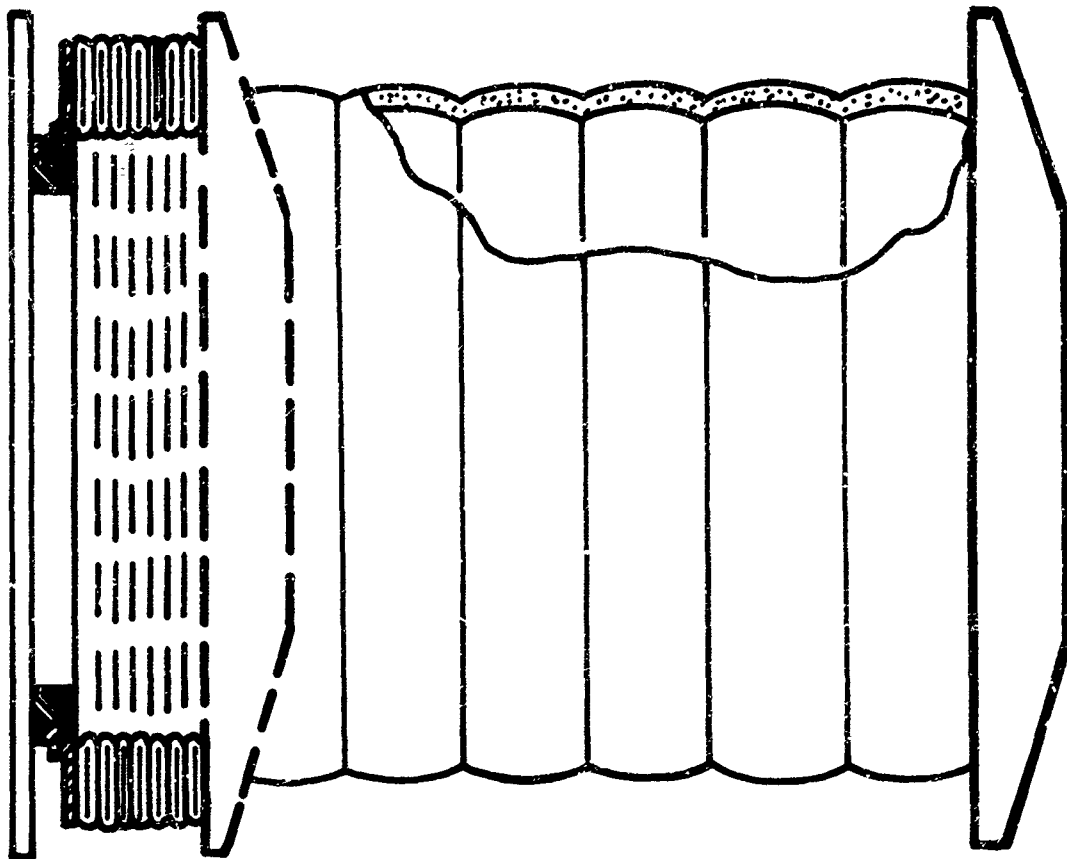
Figure 6.- Octagonal thermal model of airlock.



(b) HYPERVELOCITY IMPACT TEST SAMPLE

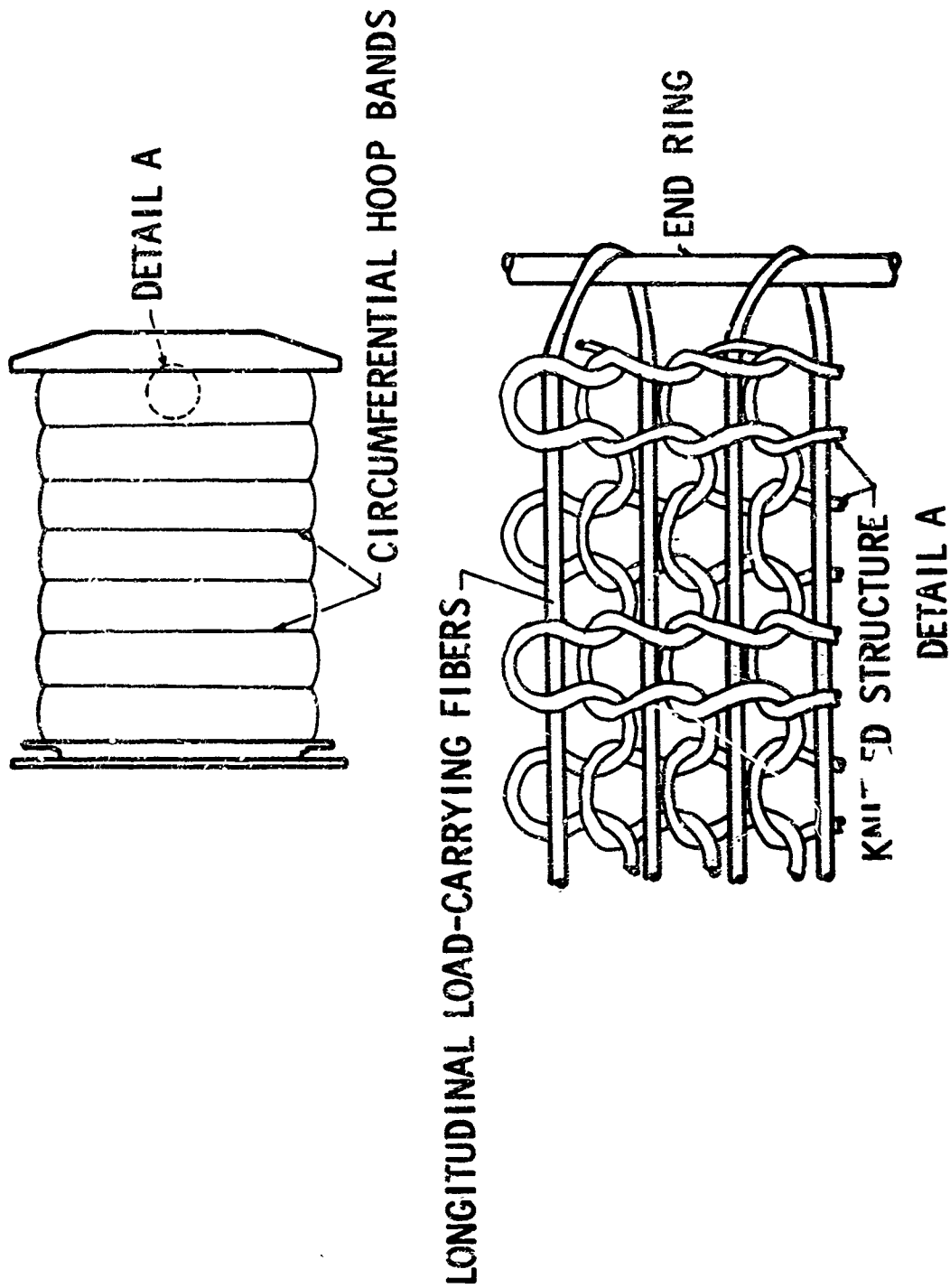
NASA

Figure 7.- Micrometeoroid protective wall.



NASA

Figure 8.- Corrugated bellows configuration.

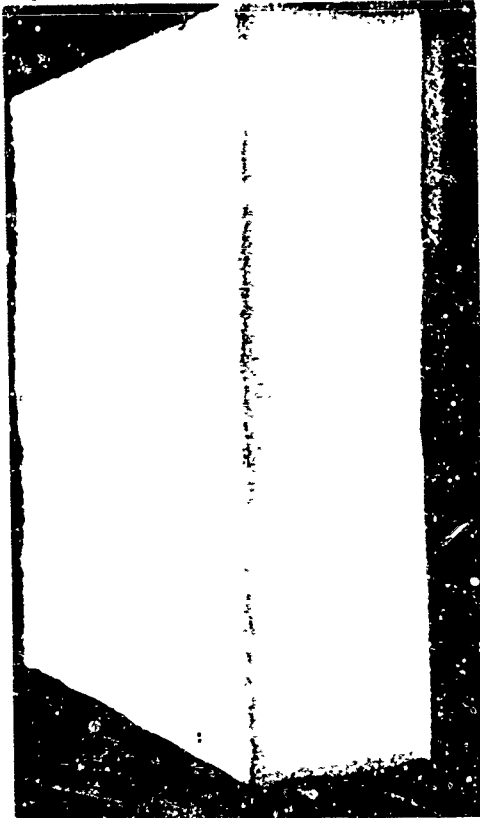


NASA

Figure 9.- Structural filament reinforced knitted fabric.



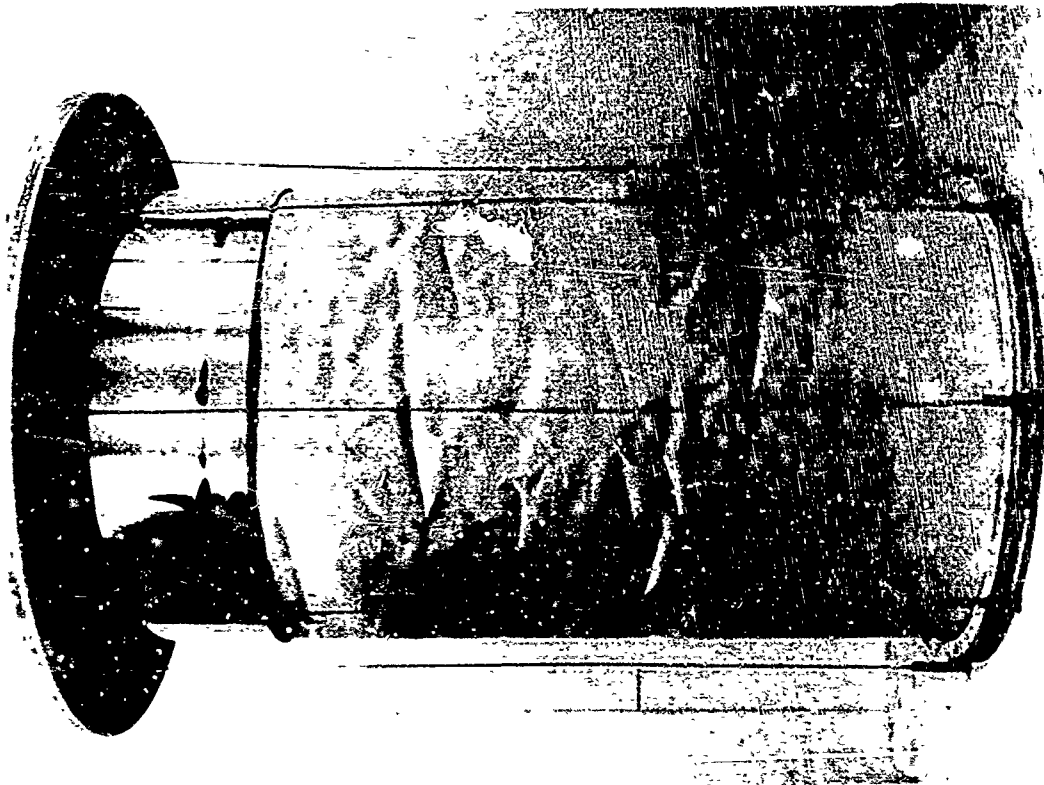
(a) FOLDED



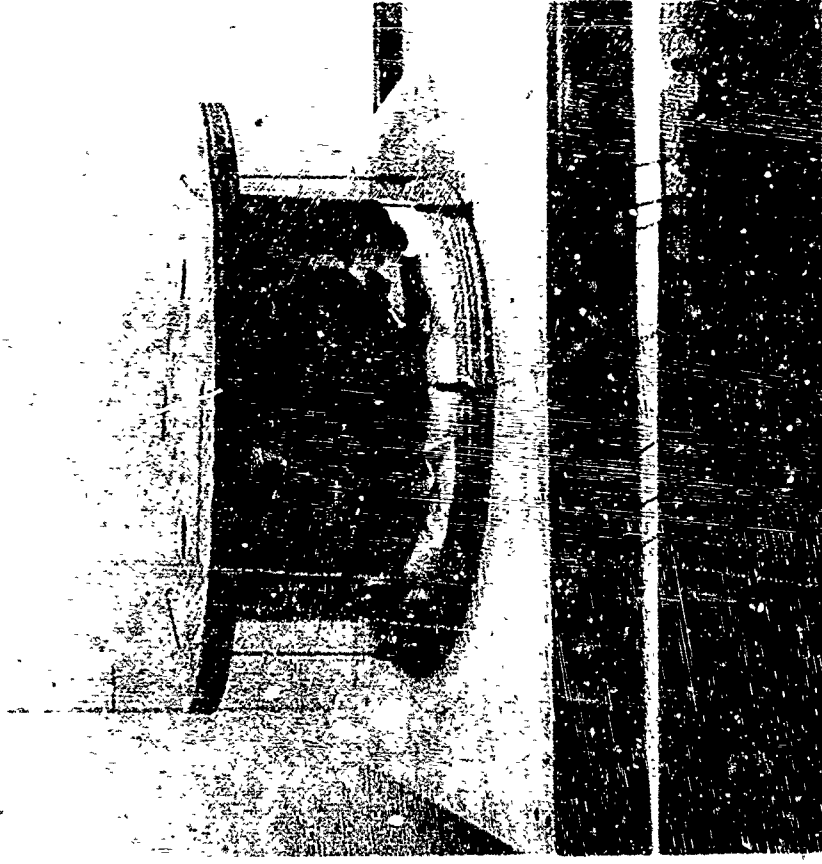
(b) UNFOLDED

NASA

Figure 10. - Flexible elastic recovery composite.



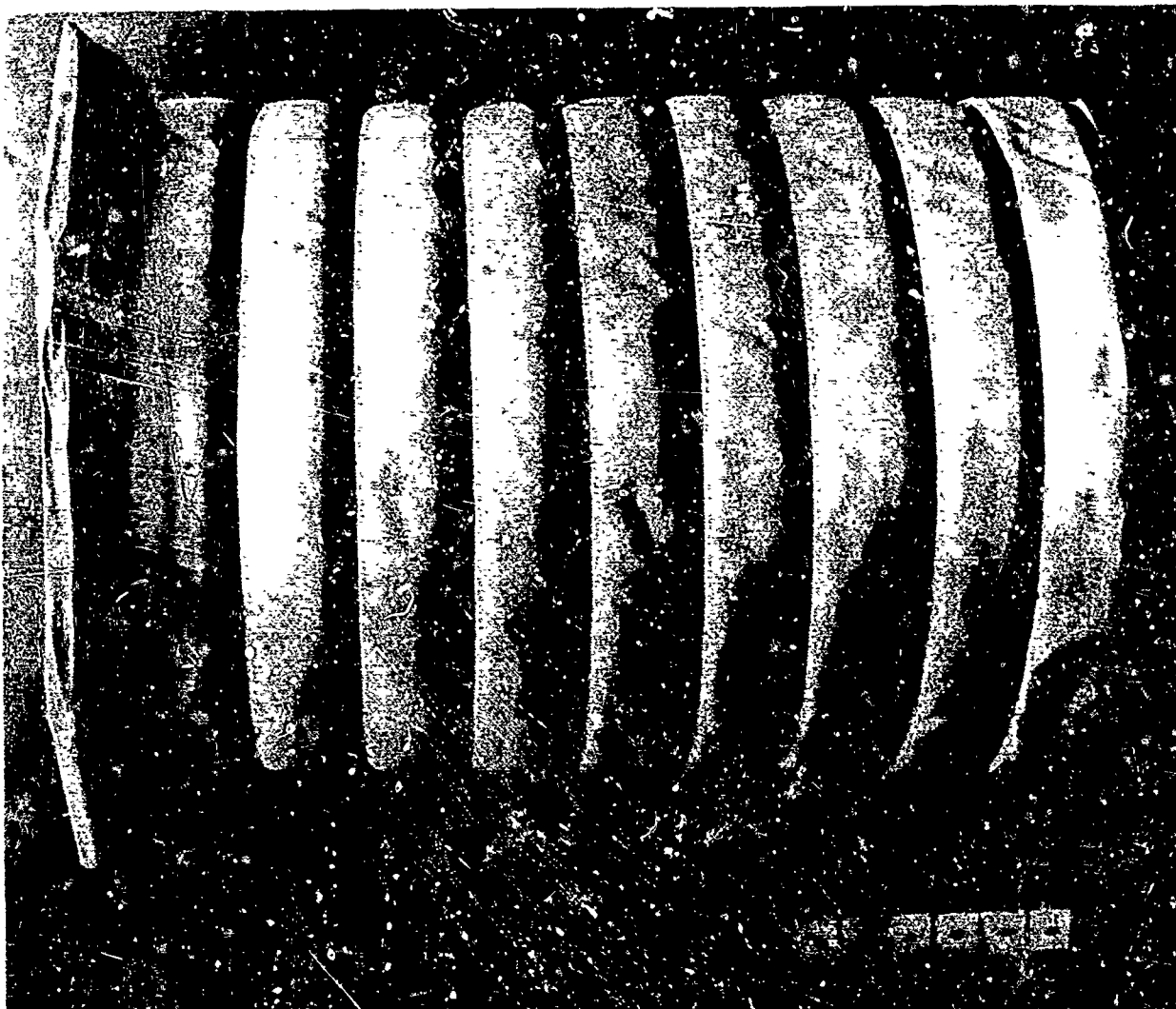
(a) DEPLOYED



(b) PACKAGED

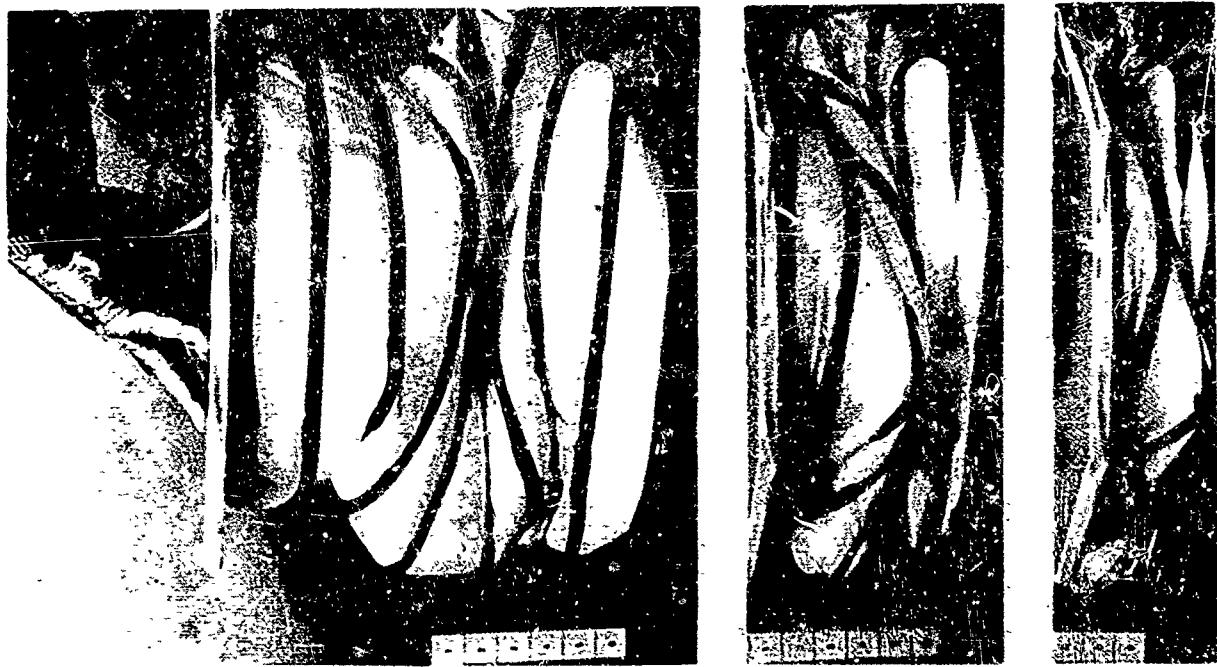
NASA

Figure 11. - Cylindrical model.



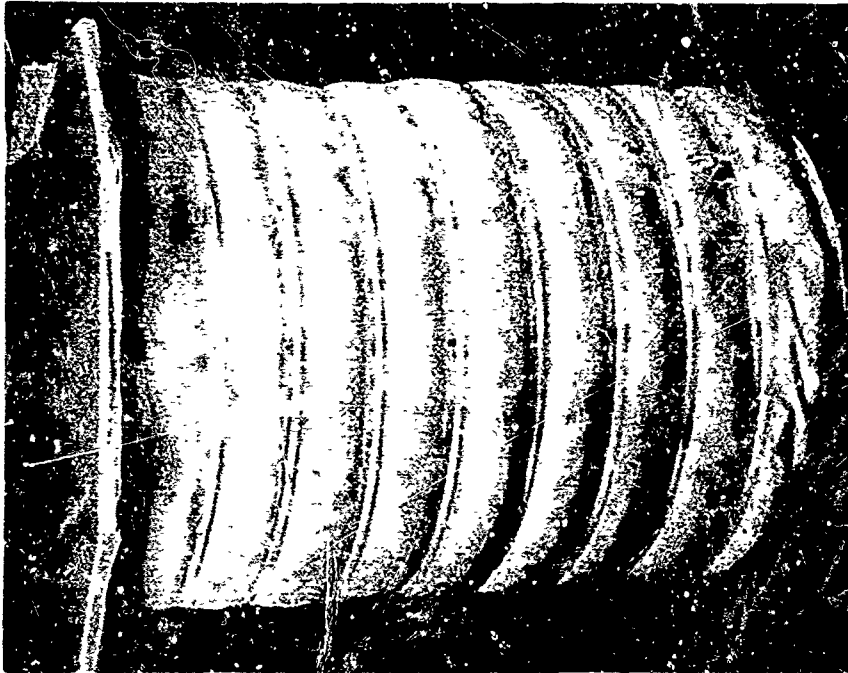
NASA

Figure 12.- Cylinder with hoop bands.



NASA

Figure 13.- Folding sequence for cylinder with flexible hoop bands.



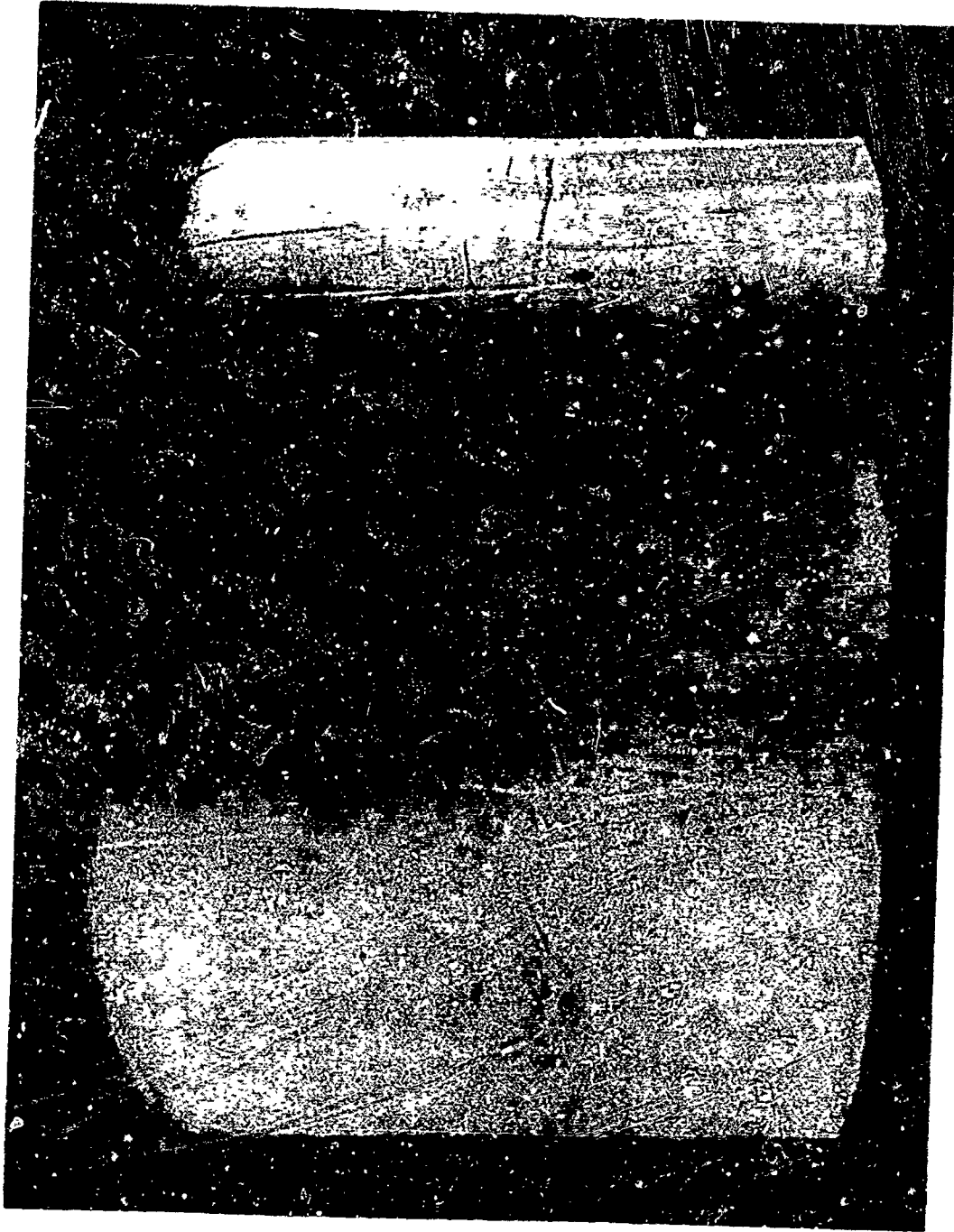
(a) DEPLOYED



(b) PACKAGED

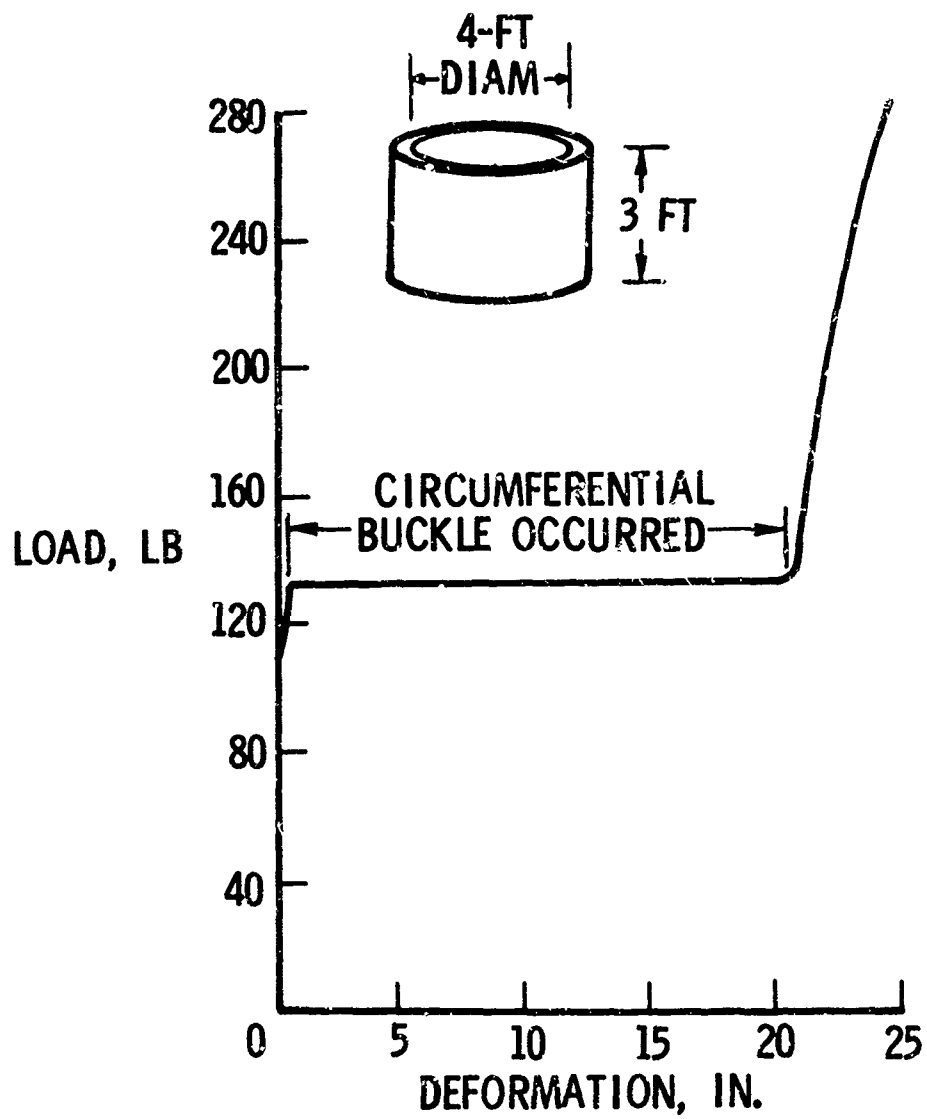
NASA

Figure 14.- Cylindrical model with rigid hoop bands.



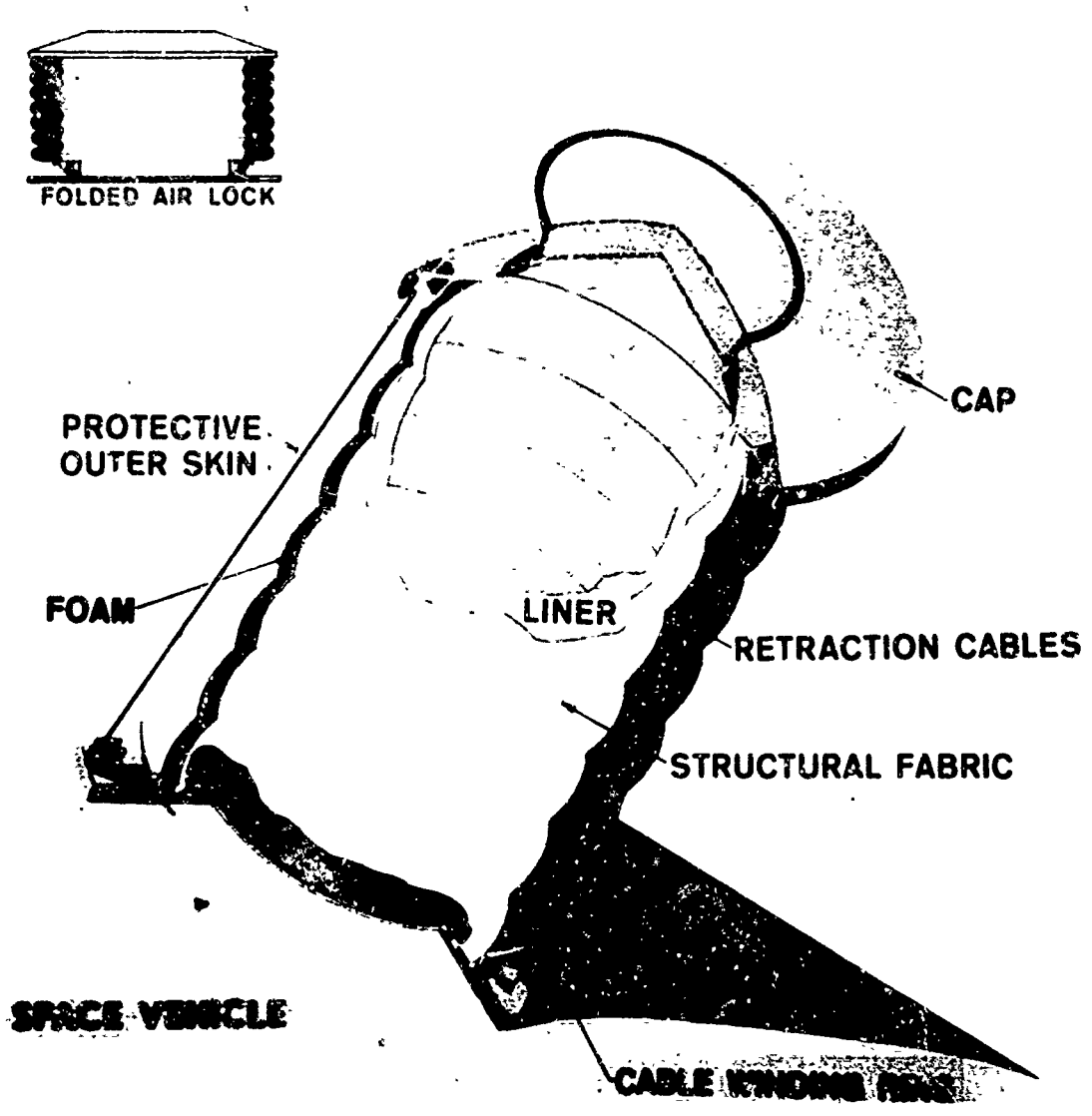
NASA

Figure 15.- Large test cylinder, 4 feet in diameter and 3 feet long.



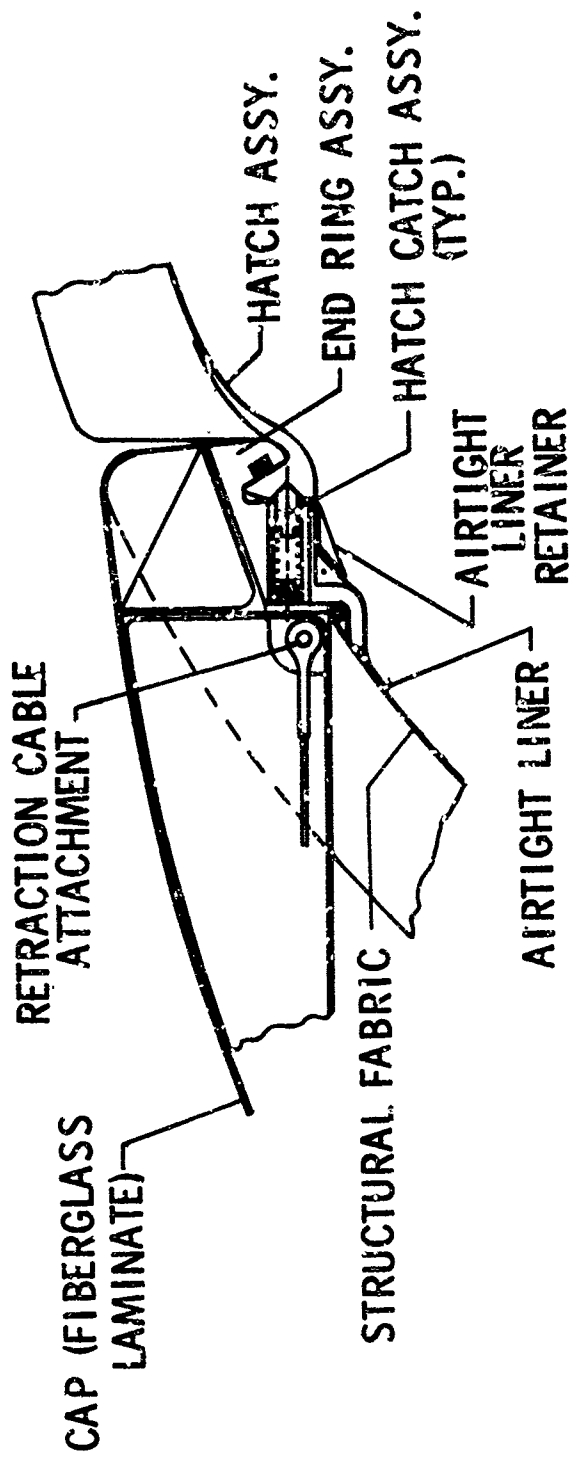
NASA

Figure 16.- Load-deformation curve for 4-foot-diameter cylinder.



NASA

Figure 17.- Expandable airlock.



NASA

Figure 18.- Hatch detail.

POTENTIAL APPLICATIONS FOR EXPANDABLE AND INFLATABLE STRUCTURES
FOR RE-ENTRY VEHICLES

R. P. Wykes

North American Aviation, Inc,
Los Angeles Division

LIST OF SYMBOLS

V	flight velocity (ft/sec)
ALT	altitude (ft)
W	gross weight of vehicle (lb)
S_B	basic body planform area (ft ²)
S_{Total}	basic body planform area plus added area (ft ²)
A	projected area of drag unit (ft ²)
D	diameter (ft)
F_D	drag force (lb)
C_D	drag coefficient
Q	stagnation point heating rate (BTU/ft ² -sec)
q	dynamic pressure $1/2 \rho v^2$ (lb ft ²)
G	acceleration of gravity (ft/sec ²)
CG	center of gravity
CP	center of pressure
l/D	trailing cable length/drag unit diameter ratio
L/D	lift/drag ratio

INTRODUCTION

At present, space exploration is essentially still in its initial phases. Most re-entry vehicle designs have been approached with relatively unsophisticated structural concepts that require extensive recovery operations. Parachute deceleration and brute force of the structure are relied upon to reduce potential damage to test data and equipment.

Future vehicles (figure 1) will be manned, and expected to fulfill varying missions such as service for ferry vehicles, to supply and maintain unmanned orbiting reconnaissance and military command posts, as well as commercial missions. These vehicles will be required to land more or less conventionally, be reserviced, and re-used without extensive rebuilding of the airframe. They will have the potential which will give the crews adequate capability to correct re-entry errors, select any of several landing sites, and change flight paths from long-range glide to short-range glide after re-entry. These are features that the lifting body re-entry vehicle with stowable variable geometry lifting surfaces and expendable or inflatable structures can provide. Figure 2 illustrates typical optional vehicle re-entry and terminal phases.

The conception of these vehicles that meet future mission requirements will present unforeseen new challenges for research and development in numerous unexplored areas of technology and structural design. The application of inflatable and expandable structures will play a major role in space exploration, and shows much promise in terms of space and re-entry vehicle structures.

POTENTIAL MISSIONS FOR RE-ENTRY VEHICLES

Figure 3 is a mission profile for a typical lifting body re-entry vehicle. As studies have indicated, the re-entry phase of the mission is the most severe. The environment imposed upon the vehicle largely determines its overall design in terms of aerodynamic performance and structural requirements. It is noted that the velocity and angle of attack at re-entry creates severe aerodynamic heating problems. Coupled with this is the restriction of a bank roll maneuver required to prohibit the vehicle from skipping back into orbit. The remainder of the mission is now limited by more or less aerodynamic characteristics of a nonvariable geometry configuration. This limits maneuverability into the terminal footprint area. Figure 4 shows the potential mission profile and advantages of a typical lifting body re-entry vehicle mission utilizing a remote drag device and variable geometry lifting surfaces. If deployed prior to re-entry the trailing drag device aids in the re-entry phase by decreasing the severe heating problem resulting from the velocity, and required high angle of attack. A more gradual re-entry is possible which eliminates the necessity for the pullout bank roll maneuver. A drag device that has the capability of modulating its force will result in variable descent times. The forces acting upon this device can also be exploited for the power to extend variable geometry lifting surfaces for improvement of terminal phase characteristics.

VEHICLE DESIGN CONCEPTS

GENERAL DESIGN CRITERIA FOR RE-ENTRY VEHICLES

Listed in the following are some of the items to be considered in the proposed design of re-entry space vehicles that land conventionally and have variable aerodynamic characteristics induced by the use of trailing, and extendable, expandable, and inflatable aerodynamic surfaces and devices.

1. Location of inflatable devices
2. Allowable weight and space available for deployable surfaces, devices, and inflation units

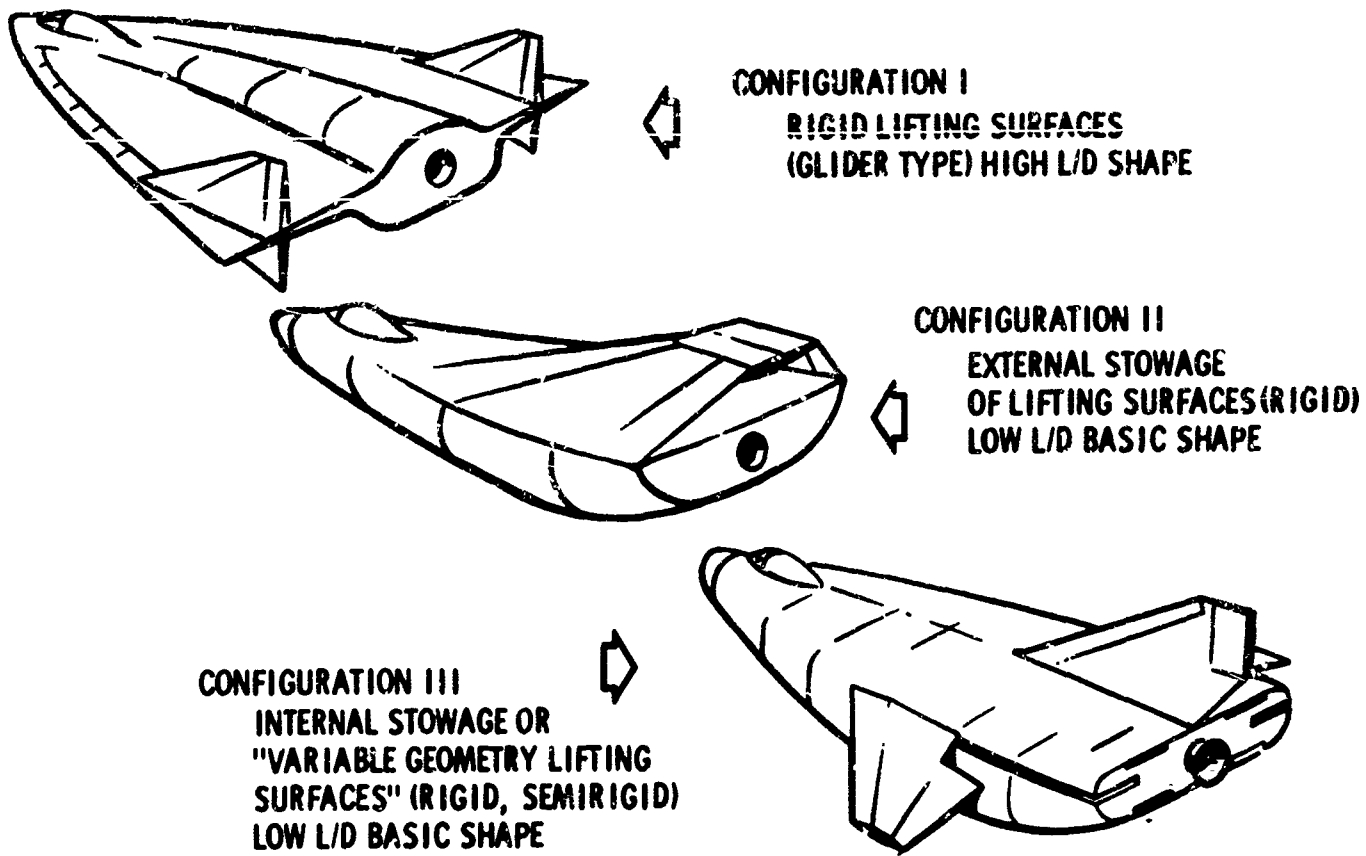


Figure 1. Typical Re-entry Vehicle Lifting Body Configuration

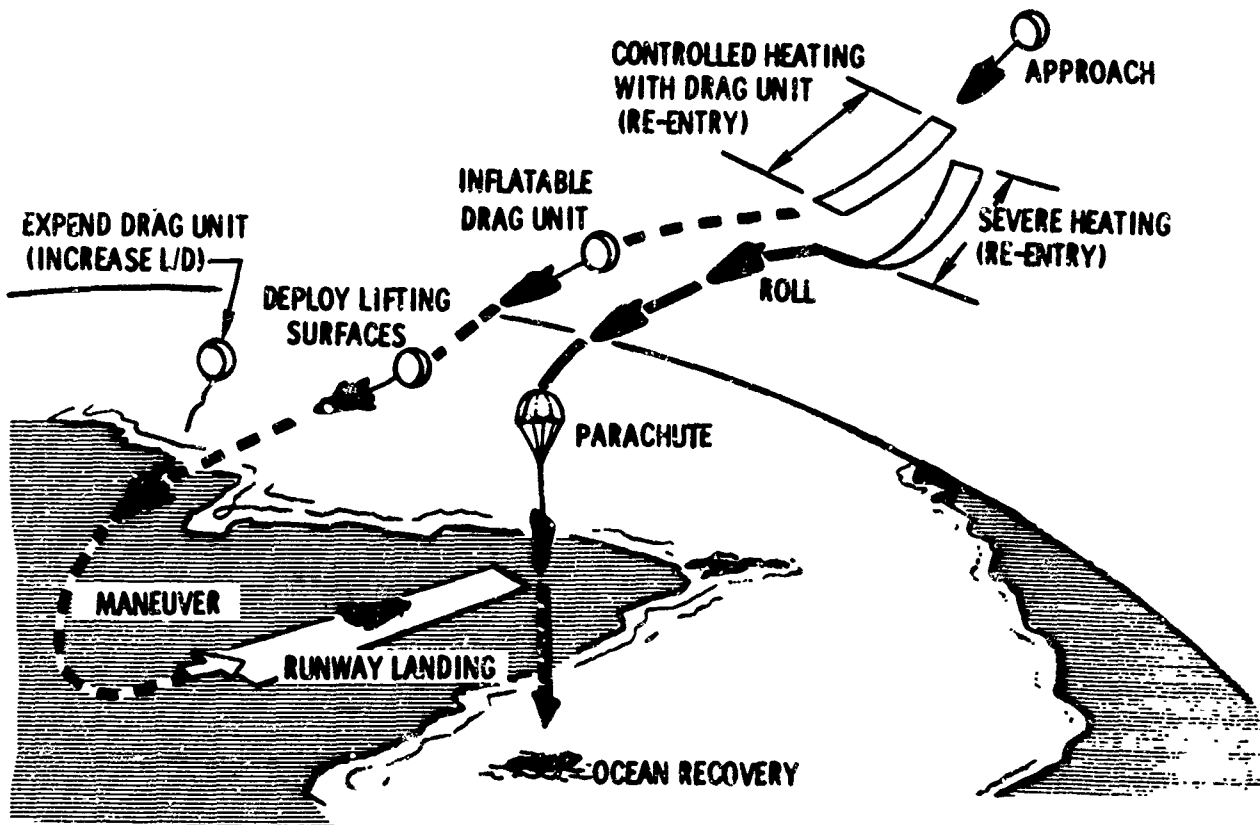


Figure 2. Missions and Terminal Phases for Existing and Potential Re-entry Vehicles

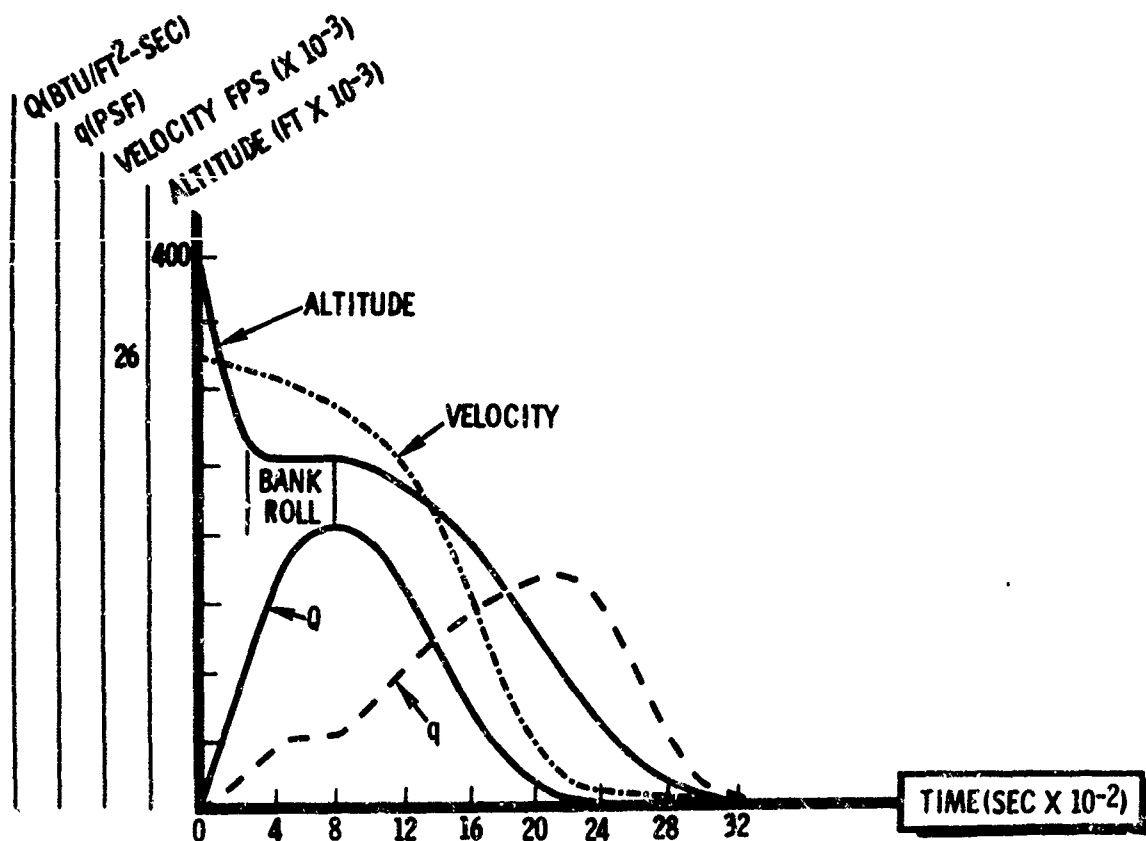


Figure 3. Typical Lifting Body Re-entry Mission Profile
L/D 1.2 (No Drag Unit - No Wing Extension)

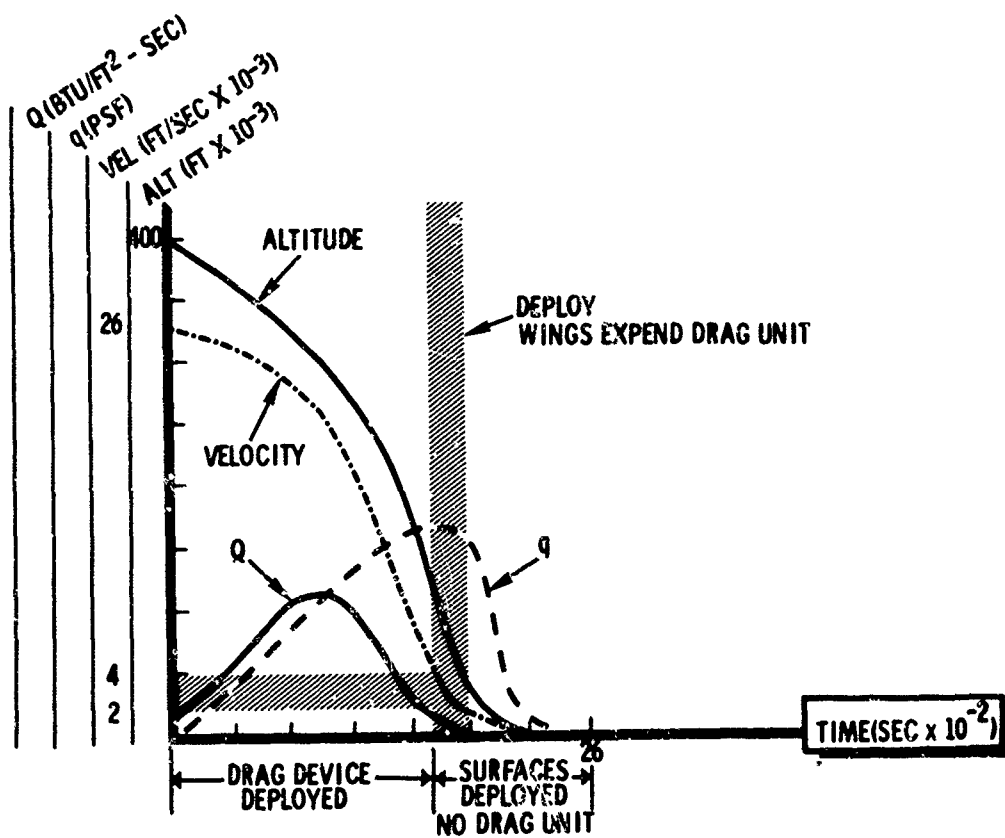


Figure 4. Mission, Using Drag Device and Extension of Lifting Surfaces
500

3. Provision for sufficient reliable power sources and mechanisms for deployment of lifting surfaces
4. Retention of aerodynamic smoothness of vehicle after surface extension and device deployment
5. Total vehicle configuration (stable or unstable) throughout the entire mission
6. Aerodynamic heating during re-entry phase
7. Possible range, speed, and altitude at initial deployment of surfaces and devices
8. Maximum G-tolerances of vehicle and rate of G-onset
9. Desirable stability, angle of approach and rate of descent on impact
10. Weight of vehicle at terminal phase
11. High L/D, low wing loading, and low terminal velocity.

Expandable and inflatable structures have the desired potential for solving the major problems related to the preceding design criteria. Future development and reliability of expandable and inflatable structures are inevitable, and their potential applications are now being intensively explored. The design of space and re-entry vehicles presents a rewarding area of unlimited scope for conceptual applications of inflated, rigid, and semirigid expandable structures.

The following presents the possible evolution of a typical lifting body re-entry vehicle configuration utilizing expandable and inflatable structures.

For illustrative purposes, configuration III, figure 1, is selected for this basic body shape of the typical re-entry vehicle. This vehicle will have an assumed L/D of approximately 1.2 for re-entry and a desired L/D of 5.0 plus for supersonic and subsonic flight.

To obtain this relatively large increase in L/D, it is necessary to increase the vehicle's planform area. This can be accomplished by means of extendable surfaces stowed in the main body of the vehicle. The stowage and actuation of these surfaces present problems that require unique innovations to conventional design concepts that will result in a total vehicle configuration that is feasible for required re-entry missions.

APPLICATIONS FOR INFLATABLE AND EXPANDABLE STRUCTURE AND BALLUTE-TYPE DRAG DEVICES

As previously mentioned, existing studies have indicated that the environment created by aerodynamic heating during the re-entry phase is a critical problem. The high velocities and high angles of attack encountered during the hypersonic phase of current re-entry vehicles produce aerodynamic heating, thermal protection, material, structural stability, and dynamic problems. These problems can be mitigated over a large portion of the re-entry phase of

the mission by the deployment of an inflatable, or expandable aerodynamically stable, high-drag device. The spherical segment type (AVCO drag brake), figure 5, appears to be best suited for the re-entry phase, as it lends itself to drag modulation plus having a fairly constant C_D at high Mach numbers. An added advantage to this concept is that the energy is dissipated remotely from the basic vehicle structure. The large radius of the device reduces the aerodynamic heating problems. An analysis should be made for each desired vehicle mission to realize the trade-offs between thermal protection weight and controlled remote aerodynamic drag and energy dissipating unit.

Another outstanding problem inherent to existing hypersonic lifting body re-entry vehicle configurations is the low L/D ratio (1.2 to 3.0). This limits the maneuverability of the vehicle, and results in a decreased terminal footprint area. The variable geometry lifting surface concept is a relatively new approach to achieving substantial increase in L/D ratios when most desired. Heretofore, heavy on-board power sources have been proposed as the actuation units for the extension of rigid or semirigid lifting surfaces. This investigation proposes concepts exploring the use of high-drag, aerodynamically stable, expandable or inflatable units as the power source for associated mechanisms used for the deployment or extension of lifting surfaces during the flight regime of supersonic velocities.

DESIRED DESIGN REQUIREMENTS FOR INFLATABLE OR EXPANDABLE DRAG DEVICES

1. High drag, low weight, low bulk
2. High degree of stability
3. High degree of reliability (over-all system)
4. Reliable means for inflation
5. Adequate strength for applied loadings
6. Ability to withstand environmental conditions (space and deployment)
7. Feasibility of fabrication

CONFIGURATIONS FOR DEPLOYABLE AND INFLATABLE AND EXPANDABLE AERODYNAMIC DECELERATORS AND POWER SOURCE

The requirement for inflatable-balloon-type decelerators was originated as a result of the problems inherent with the operation of parachutes at supersonic speeds. The erratic inflation and poor stability characteristics of conventional parachutes at these speeds necessitated investigation of other methods of deceleration.

Various shapes and configurations have been tested to arrive at maximum stability and drag at a minimum weight and bulk cost. Initial investigations of unit shapes ranging from conical to spherical, and intermediate combinations of both (figure 5) have been performed by forced inflation and subjecting them to simulated flight conditions corresponding to typical re-entry and aerodynamic environments.

80-DEGREE CONICAL BALLUTE (FIGURE 5, CONFIGURATION I)

Inflatable conical drag devices have been investigated for supersonic flight conditions (Mach No. 2.0 to 5.0). Various design configuration concepts have been tested to determine the most feasible and reliable methods for inflation. Some were preinflated, pressurized models, while others relied upon ram air. It was found that the preinflated, pressurized models performed satisfactorily, but difficulty with air mass pulsation at the air inlets required screen and reed type inlets. A side inlet screen valved 80-degree conical ballute showed the most promise as an optimum conical configuration. Drag coefficients (C_D) ranged from 0.8 to 1.0. (See figure 6.)

SPHERICAL-TYPE BALLUTE (FIGURE 5, CONFIGURATION II)

Test results reveal that the spherical shape is highly efficient with respect to high-drag and stability characteristics at high altitudes and Mach numbers. However, this configuration did show instability in the subsonic flow regimes, due to an unbalance of forces generated from the nonuniform pressure distribution variation caused by the unsteady release of vortices into the wake of the device. To relieve this problem, a burble fence was introduced to positively trip the flow over the spherical body from laminar to turbulent flow. The net effect of this was that in the supercritical regime (at subsonic and transonic speeds), the flow separates evenly and aft of the sphere, resulting in balanced forces and aerodynamic stability. Drag coefficient C_D ranges from 0.8 to 1.0. (See figure 6.)

SPHERICAL SEGMENT TYPE (FIGURE 5, CONFIGURATION III)

The spherical segment type configuration has been extensively investigated, both analytically and in wind tunnel tests under the direction of the Retardation and Recovery Branch of the Flight Accessories Laboratory. It has become known as the AVCO drag brake. This device differs from the previously mentioned devices in that it is a mechanically expandable structure, and in appearance is very similar to an inverted umbrella. This allows for the protection of the actuation container by placing it behind the expanded structure and shielding it from the extremely high re-entry temperatures.

The analytical investigations show that the use of such a device permits controlling of the maximum re-entry temperature and deceleration, and affords landing-point control within the orbital plane.

The drag coefficient (C_D) is slightly above unity in the supersonic and above regimes. However, it drops off in the subsonic region. This decelerator body can be utilized in all flight regimes from orbital velocities to touchdown, and is aerodynamically stable with self-aligning aerodynamic moments.

MATERIALS

The success of these proposed expandable and inflatable drag structures depends upon flexible, impermeable, thermally stable, high-strength, fibrous materials. A distinct advantage that these structures (formed with coated, woven materials) have over rigid structures are deployment control, compactibility, and reduced weight. In instances where aerodynamic heating may occur,

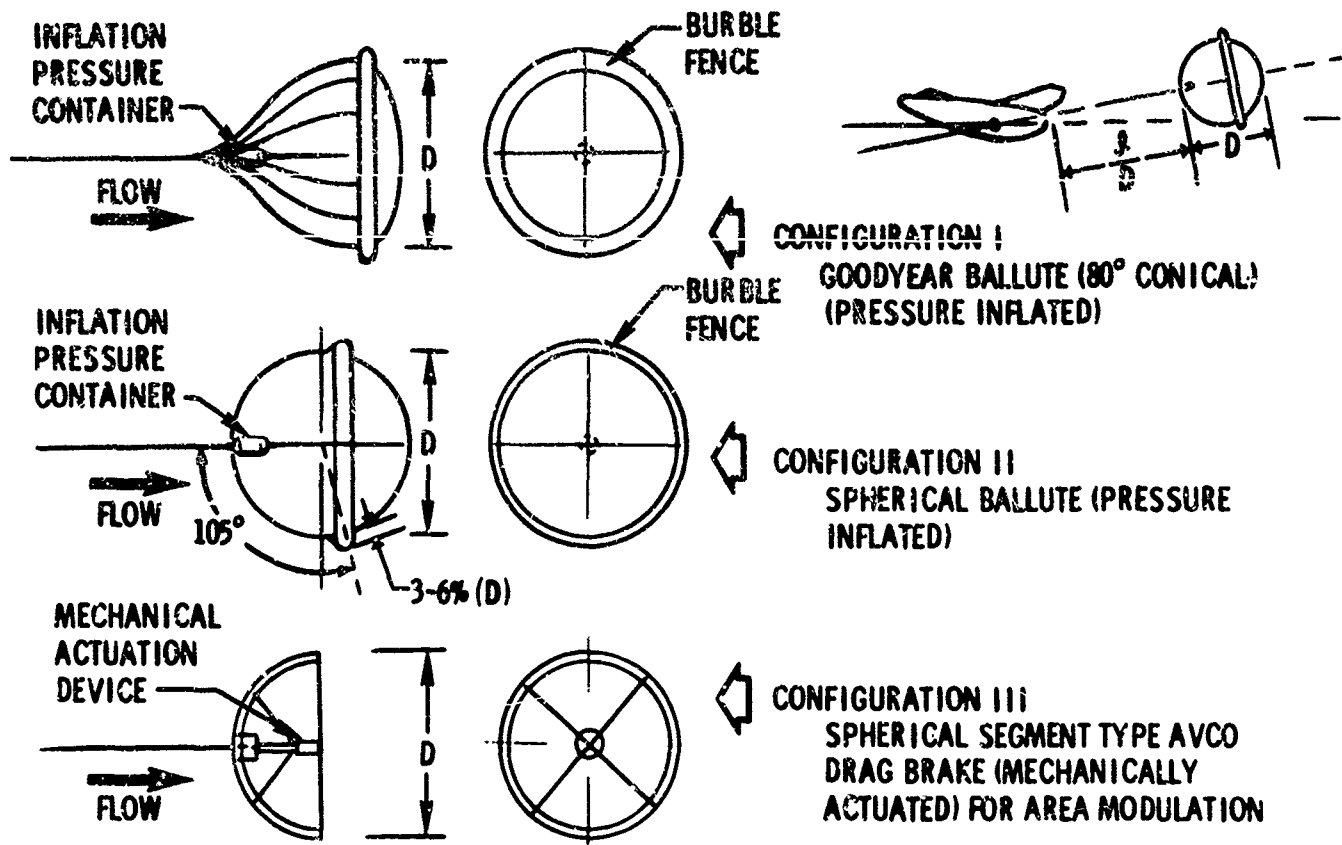
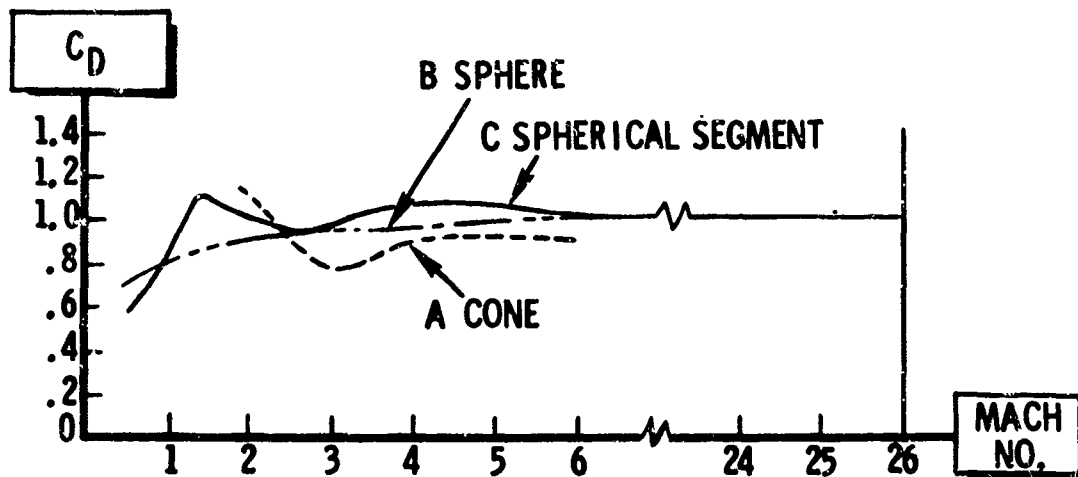


Figure 5. Typical Inflatable and Expandable Drag Units

BASED ON
PROJECTED AREA



- A. 75% CONE BALLOON 6.3% FENCE (WIND TUNNEL TEST DATA)
REF. ASP-TR-61-579
- B. SPHERICAL
REF. WADC TR 59-324
- C. AVCO DRAG BRAKE (SPHERICAL SEGMENT)
WIND TUNNEL TEST DATA REF. ASD TR-61-579

Figure 6. Drag Coefficient Versus Mach Number for Typical Drag Devices

thermal stability can become a major problem with expandable structures, since re-entry temperatures range from 1500°F to 2500°F, depending upon the configuration. This criteria restricts the use of present-day textile fibers unless they are prohibitively thick or have a matrix of inflexible material. These requirements would seriously impair their potential compactibility and recoverability.

Boron-based fibers and nickel-based superalloys in ultrafine filament-form woven into a mesh appear to be the most suitable candidate materials. Seam welding is used to join segments to form desired configurations. The matrix (or coating) material, which restricts leakage and loss of internal pressure, is an area requiring extensive research and development. Coatings have been developed to withstand the temperature, but the results of cooling, shrinkage, or bending creates adverse effects on permeability.

LOCATION AND DEPLOYMENT OF DRAG DEVICE

The inflatable drag device compartment should be located at the extreme tail of the vehicle. While deployed, the developed force should pass through the vehicle's CG at the flight-path angle. This is to minimize induced moments imposed on the vehicle after deployment. If possible, the aft wall of the compartment should have a considerable slope, so as to aid in the expulsion or extraction of the unit. In general, the motion of the deploying device will be straight aft in relation to the flight path of the vehicle.

INFLATION OF BALLUTE OR DRAG DEVICE

Several methods of inflation are available which are light, reliable, and easily packaged. The most familiar and most readily available method is to inflate the device by means of pressurized gas contained in either a metal or filament-wound, glass-fiber container. Various gases may be utilized such as helium, carbon dioxide, etc, for low-altitude - high q (dynamic pressure) inflations. Inflation time can be kept to a minimum by using a properly designed nozzle and valve arrangement. If a high-altitude inflation is desired, it can be achieved by means of a nonpressurized container filled with alcohol. Since temperatures will be relatively low until the actual re-entry occurs, the drag device can be lined with a very thin (separate unit) rubber or plastic bladder. Because of the low ambient pressure, the vapor pressure developed by vaporization of the alcohol will be sufficient to allow inflation to take place. The liquid volume and temperature will govern the resulting internal pressure of the inflated drag device. Inflated with the pressure developed by the vaporizing liquid, the device will be deployed and in a trailing position for re-entry. When re-entry occurs, and the dynamic ambient pressure increases, a ram air or bottled pressure inflation can take over. As the ram or container pressure increases sufficiently above the low initial inflation pressure, a collapsing of the internal bladder will occur, and it will be compressed to the rear portion of the ballute.

Mechanically actuated drag units can be deployed and modulated independent of the ambient pressure, and present no problems in this respect.

SOME POTENTIAL APPLICATIONS FOR INFLATABLE OR EXPANDABLE DRAG UNITS

The developed drag can be utilized twofold. The initial deployment will provide a decelerating force for the reduction of re-entry velocity and

required angle of attack. The unit is deployed prior to, or during, the re-entry phase, and the trailing cable is extended until the optimum l/D (length of cable to drag unit diameter ratio) is reached. At this point, a stop on the cable introduces the drag load into the vehicle's primary structure. It is possible to modulate the developed drag by increasing or decreasing the projected area of the unit.

When sufficient energy has been dissipated by means of the drag device and the programmed velocity and altitude for wing deployment has been reached, the cable stop is released. This allows the drag force to continue through the vehicle, and is equally divided and introduced into the lifting surface extension mechanism. Up to the present, hydraulic actuators and electric motors have been considered as the only means for providing the required forces to overcome the developed aerodynamic drag, inertia, and friction forces resulting from the extension of these surfaces. Each surface was provided with a heavy, on-board actuating unit and a common hydraulic pressure reservoir and associated accessories that ensured symmetrical surface extension.

A proposed solution to this problem is to exploit and control the existing aerodynamic drag forces that can be developed during or after re-entry of the vehicle. The controlled use of a remote, aerodynamically stable drag unit with a sufficient C_D during the entire flight regime can provide this required energy source. The deployment of a stowable, expandable or inflatable, lightweight, drag unit such as those previously mentioned appears to fulfill these requirements.

The release of this drag force and resulting moments must be programmed so that they will equal or exceed those developed by combined forces resulting from the extension of the lifting surfaces into the airstream. (See figures 7 and 8.) As shown in the typical mission profiles, the desired force is required at lower altitudes and Mach numbers to alleviate aerodynamic heating of small radius leading edges, and to obtain a sufficient dynamic pressure (q).

Using a specific deployment location on the mission profile just prior to the terminal phase, we can roughly compute the potential drag force of the unit. Using values derived from the known mission profile

C_D = Coefficient of drag for unit

q = Dynamic pressure

A = Projected area of drag unit

we can roughly compute the potential drag developed at this point.

$$F_D = C_D q A$$

Figure 9 shows typical potential drag forces developed for units of varying diameters and dynamic pressures.

After the actuation cycle has been completed, the surfaces are locked into position, and an explosive charge is initiated at a point on the cable beyond the basic vehicle. Thusly, the drag unit is severed and leaves the vehicle

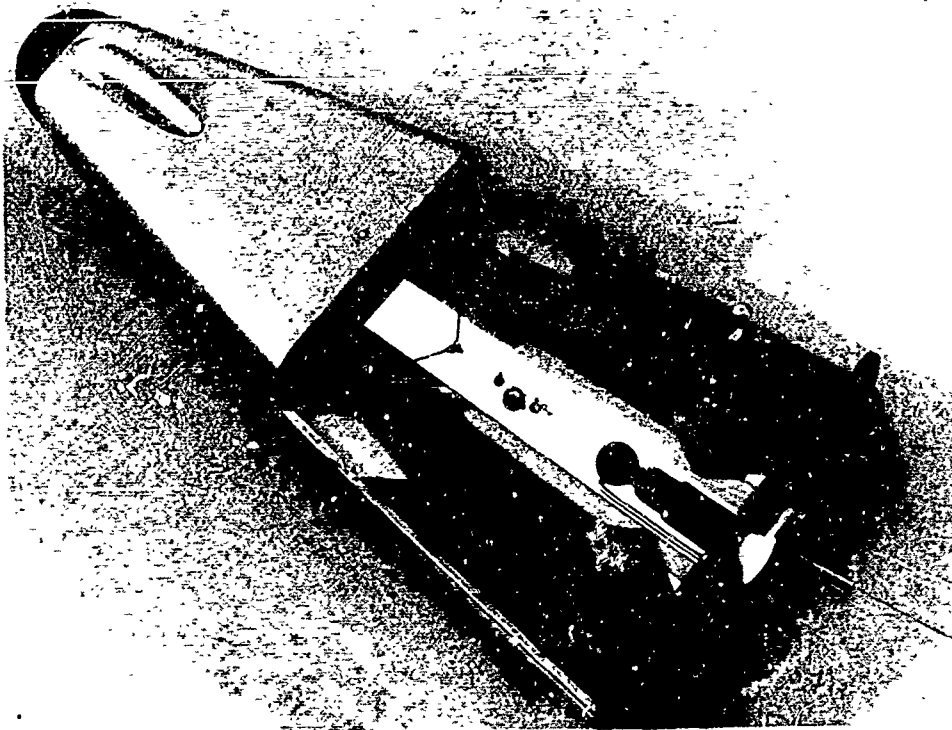


Figure 7. Lifting Surfaces Stowed

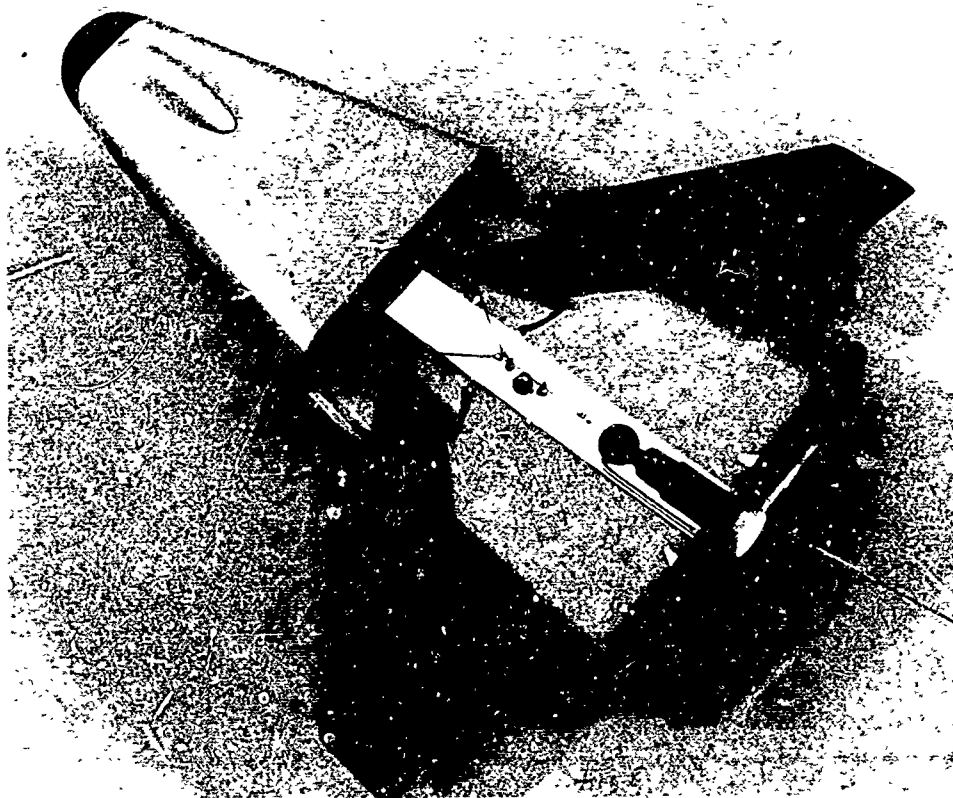


Figure 8. Lifting Surfaces Extended

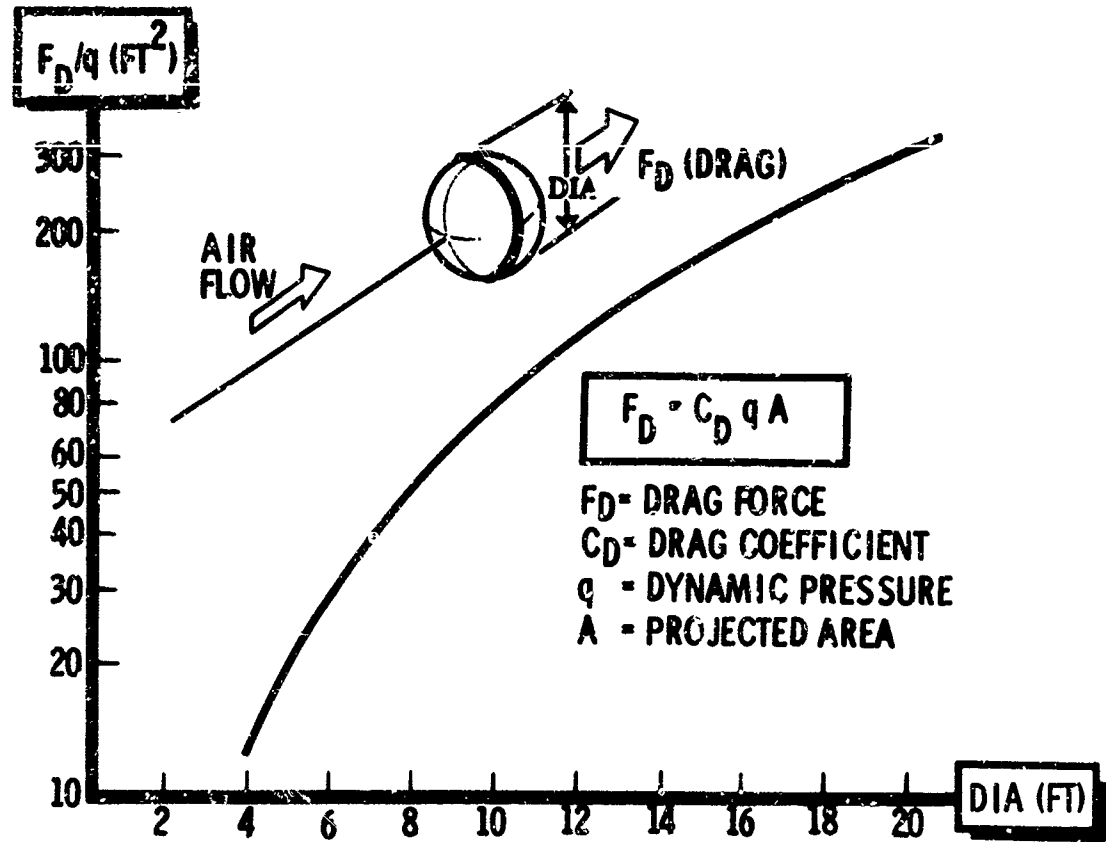


Figure 9. Drag Versus Diameter for Typical Drag Units

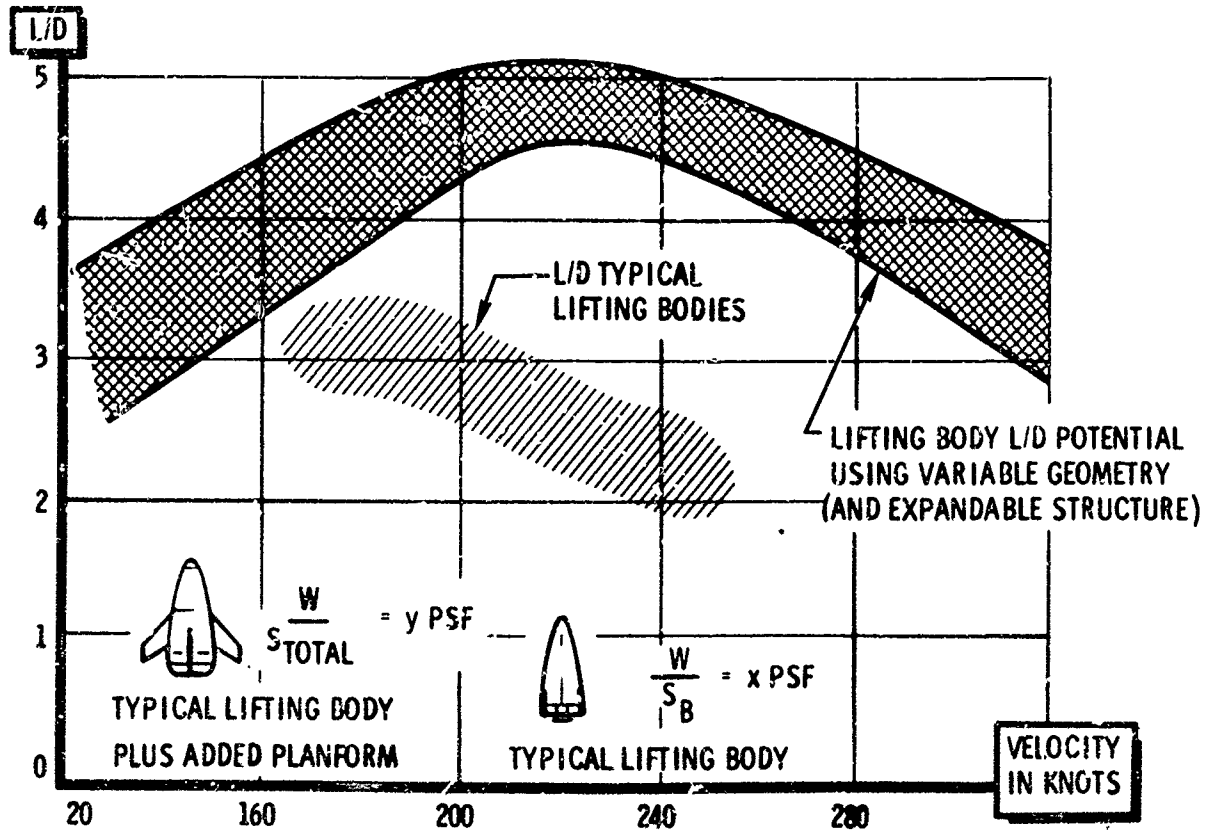


Figure 10. Lifting Body L/D Comparison

clean with an increased L/D and improved maneuverability at supersonic and terminal velocities. (See figure 10.)

Another added potential feature of utilizing a remote drag device is that of directional stability at hypersonic and supersonic velocities. This eliminates the necessity of large verticals having large angles of flare to produce the desired directional stability.

OPTIONAL DEPLOYMENTS OF DRAG UNIT TO VARY RE-ENTRY MISSIONS

1. Entire mission
2. During re-entry phase (only)
3. During re-entry phase and deployment of lifting surfaces (only)
4. During deployment of lifting surfaces (only)

SOME PROBLEM AREAS RELATED TO DEPLOYMENT OF TRAILING DRAG UNITS

All deployments of trailing aerodynamic decelerators or drag units create a force known as "snatch force," which arises from the differential deceleration rates of the basic vehicle load and the deploying drag unit. The rapid deceleration of the drag unit, in relation to the relatively slow deceleration of the basic vehicle, creates a sizable differential velocity which must be reduced to zero. The maximum deceleration force of the vehicle created by the drag device deployment should be programmed so as not to exceed the limits of human and structural tolerances.

A proposed solution to this problem is to absorb this shock force into an energy-absorbing reeling device that is used to gradually extend the trailing cable to its first-phase terminal length.

Optimum force vectors located at the cable juncture and cable-wing attachments and the cushioning effect of the aerodynamic drag and inertia forces will have a dampening effect on the initial shock imposed upon the actuating system by the release of the remote drag force into the wing actuation cycle.

Because of the differential in moments created by the associated forces of aerodynamic drag and inertia, the wing extension will have to be limited by a snubbing device before the locking mechanism can be initiated and the trailing drag unit is severed.

OTHER EXPANDABLE STRUCTURE

"Air Mat," a double-walled, inflatable structure, developed by Goodyear, has interesting possibilities for use as a drag device. Two layers of flexible material tied together with a large number of threads (30 to 60 per square inch) of the same material form a semirigid shape when inflated with low pressure. "Air Mat" can also be made from wire-cloth material such as Rene' 41 and other superalloys. Advantages gained through the use of such construction methods would be the possibility of lightweight, large-surface area devices. Its foldability results in the ability to package the deflated device into

about 3 percent to 5 percent of its inflated volume (figure 11) and to readily vary its inflated drag area. This concept has been developed to the point whereby these materials now can be woven into curved shapes, such as spheres and other symmetrical body shapes applicable to the previously proposed drag devices. This type of construction would eliminate the necessity of gores and joints and results in a lighter than conventionally constructed device of similar shape.

Another concept that may be utilized for lightweight, high-volume expandable filler is the variable geometry elastic recovery one. This concept is based upon the use of the recovery properties of a flexible polyurethane foam as the core material. The basic load-carrying outer skin can be either a woven fabric or a superalloy filament woven cloth. If rigidity is required, the skin may be lined with a nonpermeable bladder to eliminate porosity and internal gas pressure used for increased stabilization of the structure.

POSSIBLE APPLICATIONS FOR "AIR MAT" AND ELASTIC RECOVERY CORE

FILLER FOR AERODYNAMIC SMOOTHNESS (FIGURES 12 AND 13)

The location of extendable rigid or semirigid lifting surfaces sometimes present the problem of leaving voids in the basic vehicle structure that would have adverse effects on the aerodynamic characteristics of the over-all vehicle. This void is usually a considerable volume. "Air Mat" is an ideal filler. Figures 12 and 13 illustrate typical applications for upper- or lower-winged vehicle configurations that utilize it as an inflatable sandwich that pushes secondary structure to the original mold line. Midwing configurations (figure 12) result in smaller voids, but again "Air Mat" qualifies as the ideal lightweight, expandable filler.

AFTERBODY (FIGURE 14)

A basic lifting body shape and planform configuration sometimes results in a stability problem, due to CP and CG locations at subsonic speeds. The addition of an inflatable afterbody, using "Air Mat," shifts the CP and center of volume aft. This inflated structure also aids in the reduction of the basic aft-body aerodynamic drag when it is desirable.

SUBSONIC CONTROL AND STABILIZING SURFACES

After re-entry and the deployment of the variable geometry lifting surfaces (supersonic-subsonic velocities) an aerodynamic stability problem may arise for certain re-entry shapes or configurations. The addition of a forward canard or augmented vertical stabilizer surface area may be required. The "Air Mat" concept merged with a rigid expandable structure again can qualify to meet these requirements.

Figures 15, 16, 17, 18, and 19 illustrate each critical mission phase of a typical lifting body re-entry vehicle utilizing expandable and inflatable structures.

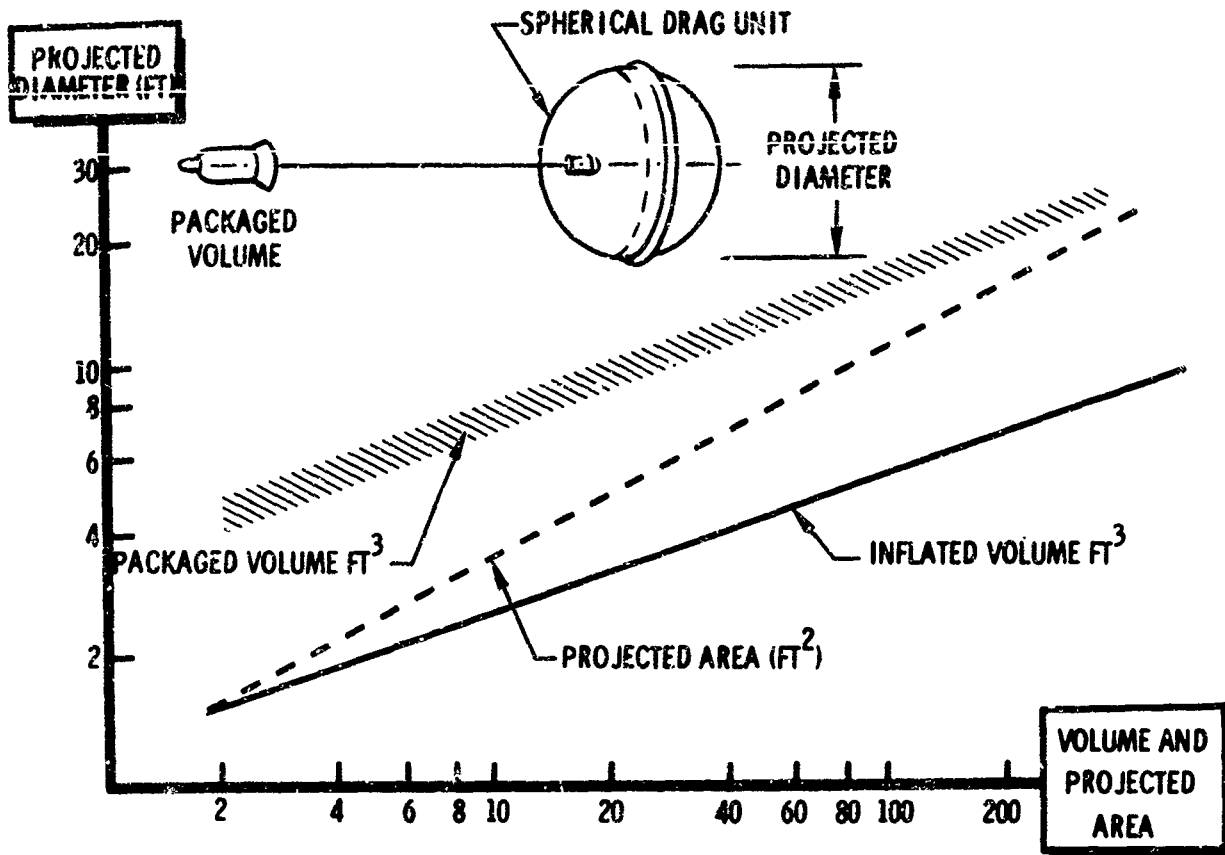


Figure 11. Geometry Versus Projected Area for Spherical Drag Unit

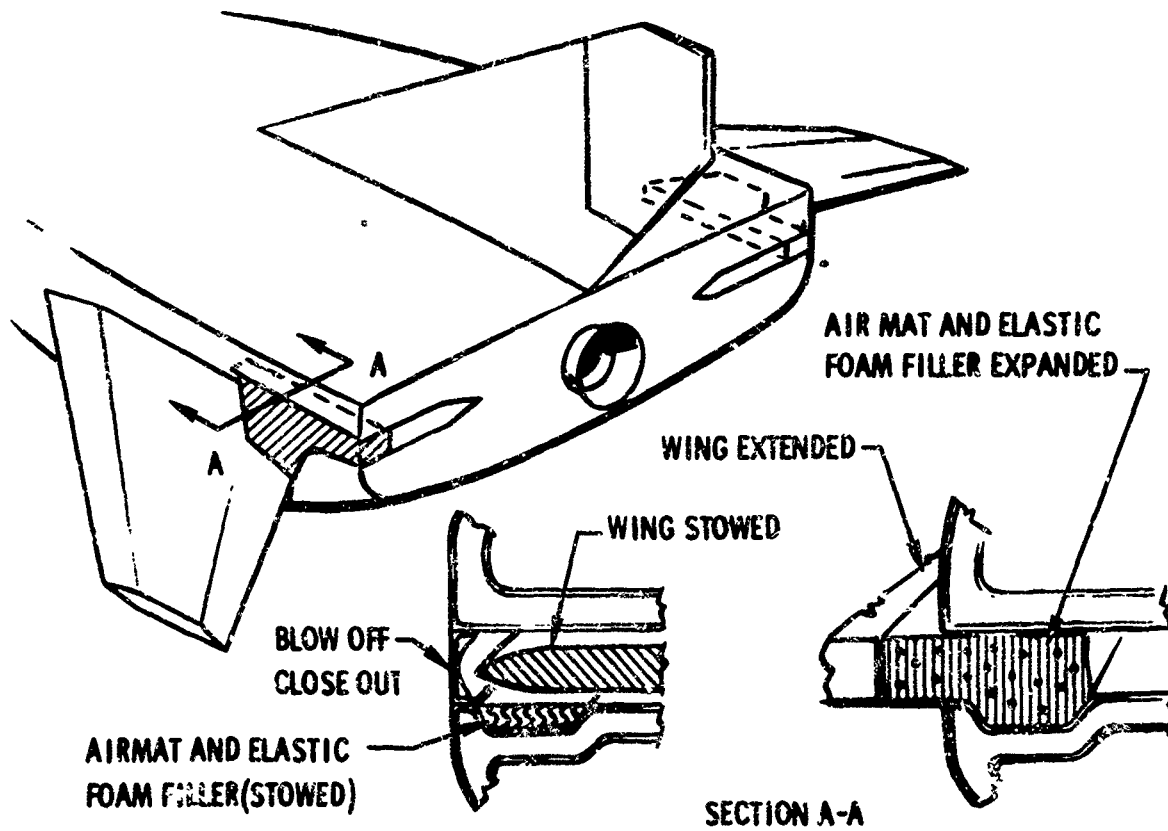


Figure 12. Aerodynamic Filler

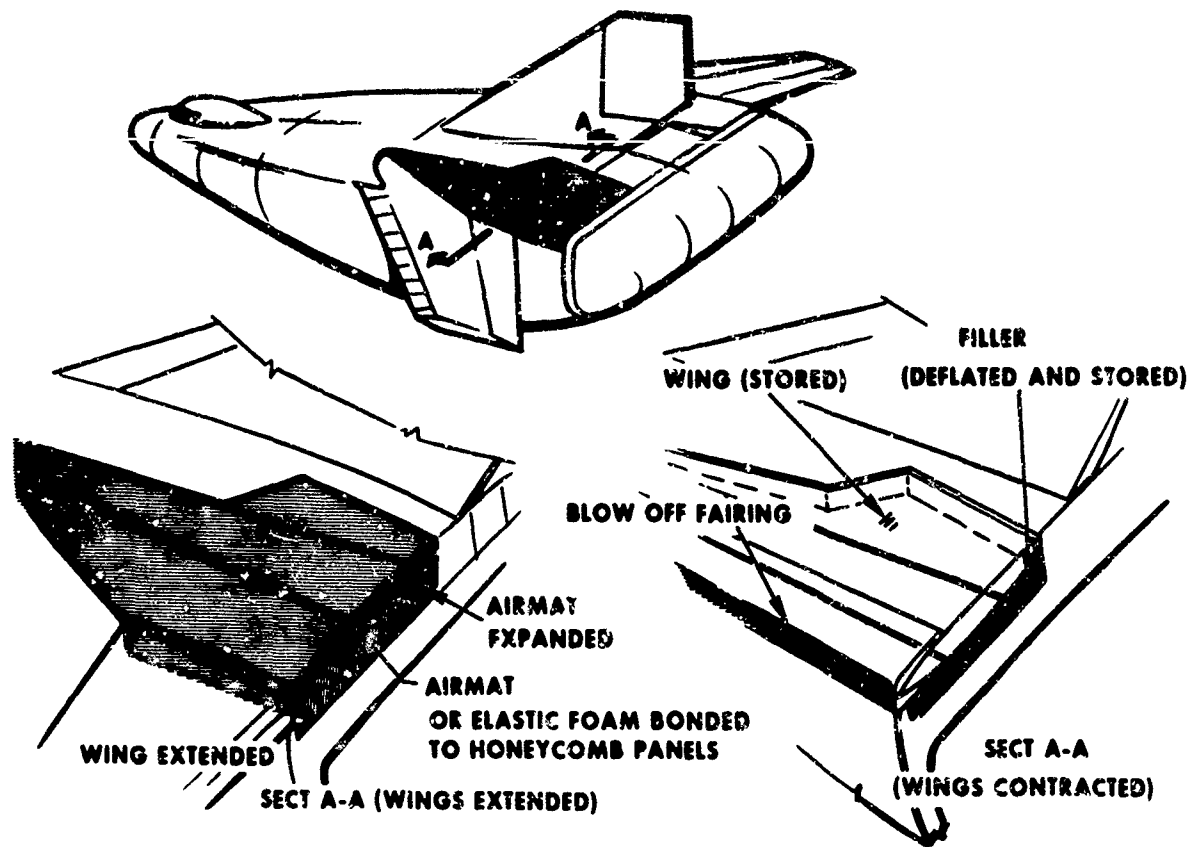


Figure 13. Filler for Aerodynamic Smoothness

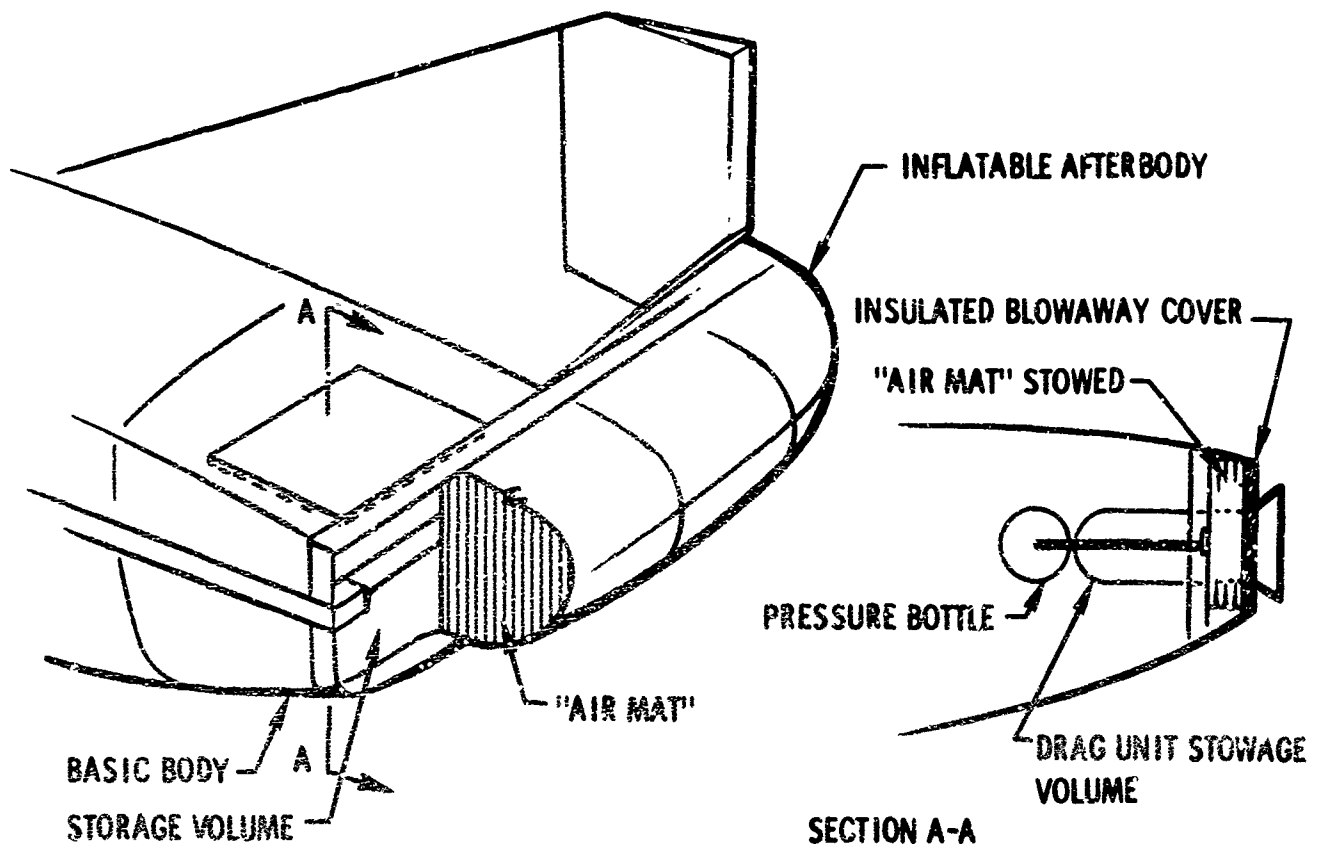


Figure 14. Inflatable Afterbody

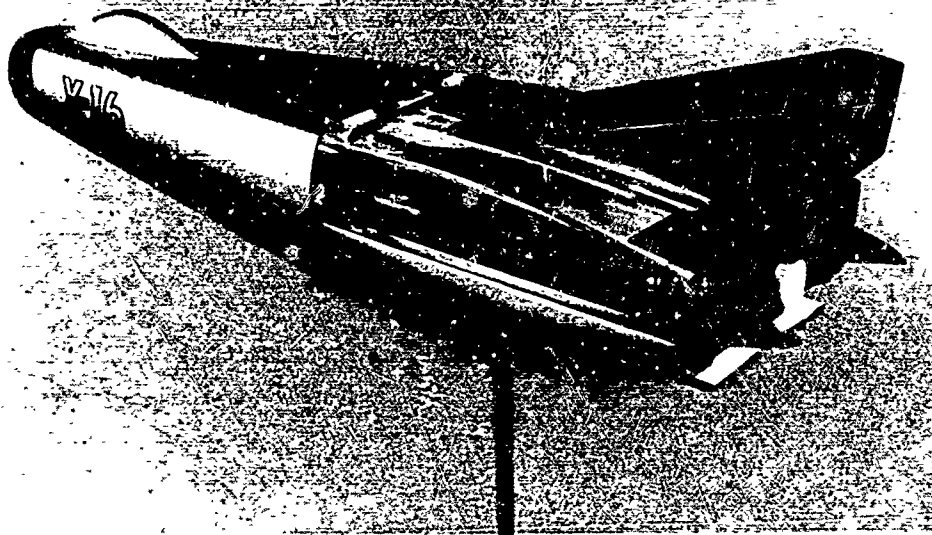


Figure 15. Vehicle Re-entry Approach Phase

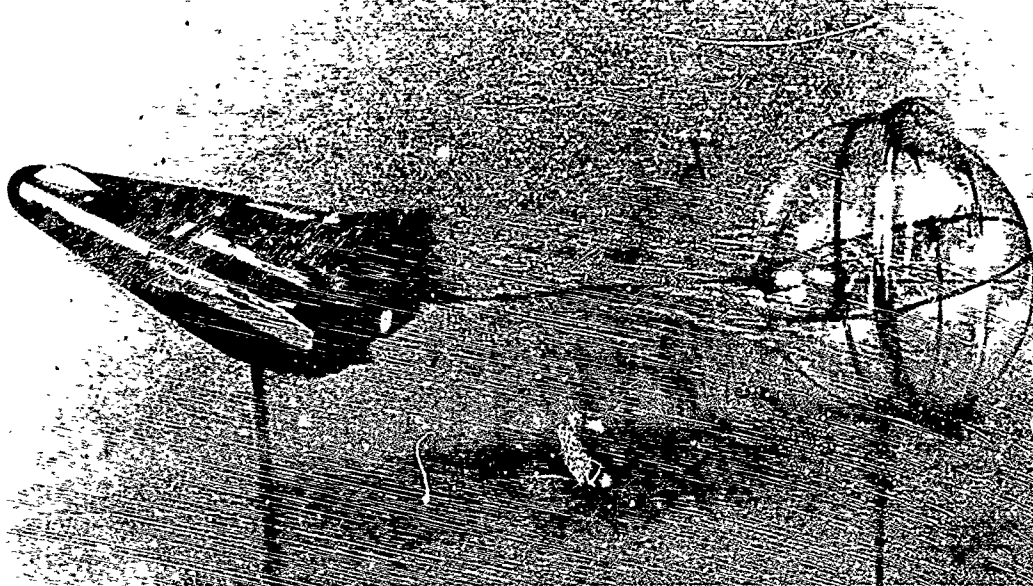


Figure 16. Vehicle Re-entry (Drag Unit Deployed)



Figure 17. Vehicle Terminal Phase (Drag Force Extending Lifting Surfaces)

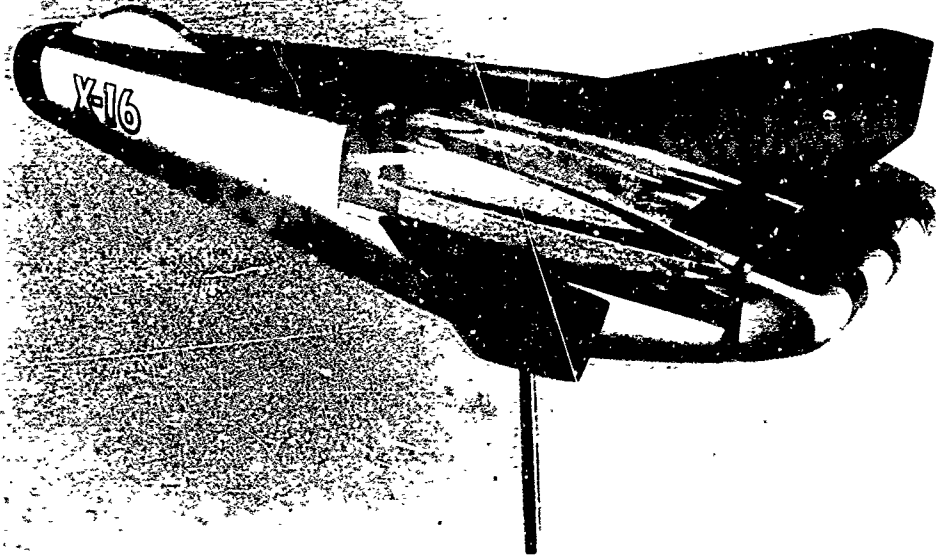


Figure 18. Vehicle With Surfaces Extended, Drag Unit Severed,
and Afterbody Inflated



Figure 19. Vehicle Landing Approach

SUMMARY AND CONCLUSIONS

Listed in the following are some of the potential advantages of the presented concepts:

1. The deployment of a trailing inflatable or expandable drag device provides remote aerodynamic drag during re-entry of the vehicle. This results in a potential decrease in required vehicle re-entry angle of attack and a controlled reduction of vehicle aerodynamic heating problems.
2. The remote inflatable or expandable drag device increases the directional stability of the vehicle (reduces required vertical stabilizer area and locates it on the C_L of the vehicle).
3. These concepts remove the requirement for heavy on-board power sources and provide a single, remote, compact, lightweight, concentrated and efficient power source unit for lifting surface extension. This device and associated actuation mechanisms provide a counteracting and self-dissipating energy system that can be initiated at any time during or after re-entry of the vehicle.
4. After completion of the actuation cycle, the inflatable trailing drag unit (ballute, etc) is expendable through severing the cable with an explosive charge, thus increasing the L/D and maneuverability of the vehicle for the remainder of the flight mission.
5. The use of these concepts presents the possibilities for optional re-entry glide paths encountered in variable military or nonmilitary missions that require short- or long-duration descents and combinations of both.
6. The use of the drag device and the resulting L/D increase introduces the possibility of lower terminal velocity, lower approach angle of attack, lower wing loading, and increased maneuverability for conventional airstrip landings. It replaces the elaborate on-board recovery equipment formerly used to reduce potential structure and equipment damage on test and manned re-entry vehicles.
7. They provide booster launch capability of the vehicle, e.g., because of initial shape (with wings contracted it can be mounted on staged booster such as Atlas, etc).
8. Inflatable and expandable structures can be utilized to enhance the aerodynamic and structural design of existing and projected lifting body re-entry vehicle configurations.

Figure 20 points out the stepping stones that have been placed and the goals to be attained. Figure 21 again categorizes the major challenge areas and questions to be answered in the search for mastery of space and space travel.

As in any state-of-the-art advancement, many unsolved problems and undiscovered areas for improvements become evident. These concepts, using inflatable and expandable structures are but a sample of the potential that remain to be developed and expanded.

REFERENCES

1. Aerospace Expandable Structures Conference Transactions, AF Aero Propulsion Laboratory, AF Flight Dynamics Laboratory, Oct 23-25, 1963, Dayton, Ohio.
2. Performance of and Design Criteria for Deployable Aerodynamic Decelerators, TR No. ASD-TR-61-579, Dec 1963.
3. A Study of Hypersonic Aerodynamic Drag Devices Interim Technical Report, W. B. Champney and B. Engel, Cornell Aeronautical Laboratory, Inc, April 1960, Wright Air Development Division, TR 59-324.
4. An Investigation of the Deployment Characteristics and Drag Effectiveness of the Gemini Personnel Decelerator at Subsonic and Supersonic Speeds, Phase II, Warren E. White and Charles D. Riddle, Propulsion Wind Tunnel Facility, ARO, Inc, TR No. AEDC-TDR-63-255, Dec 1963.

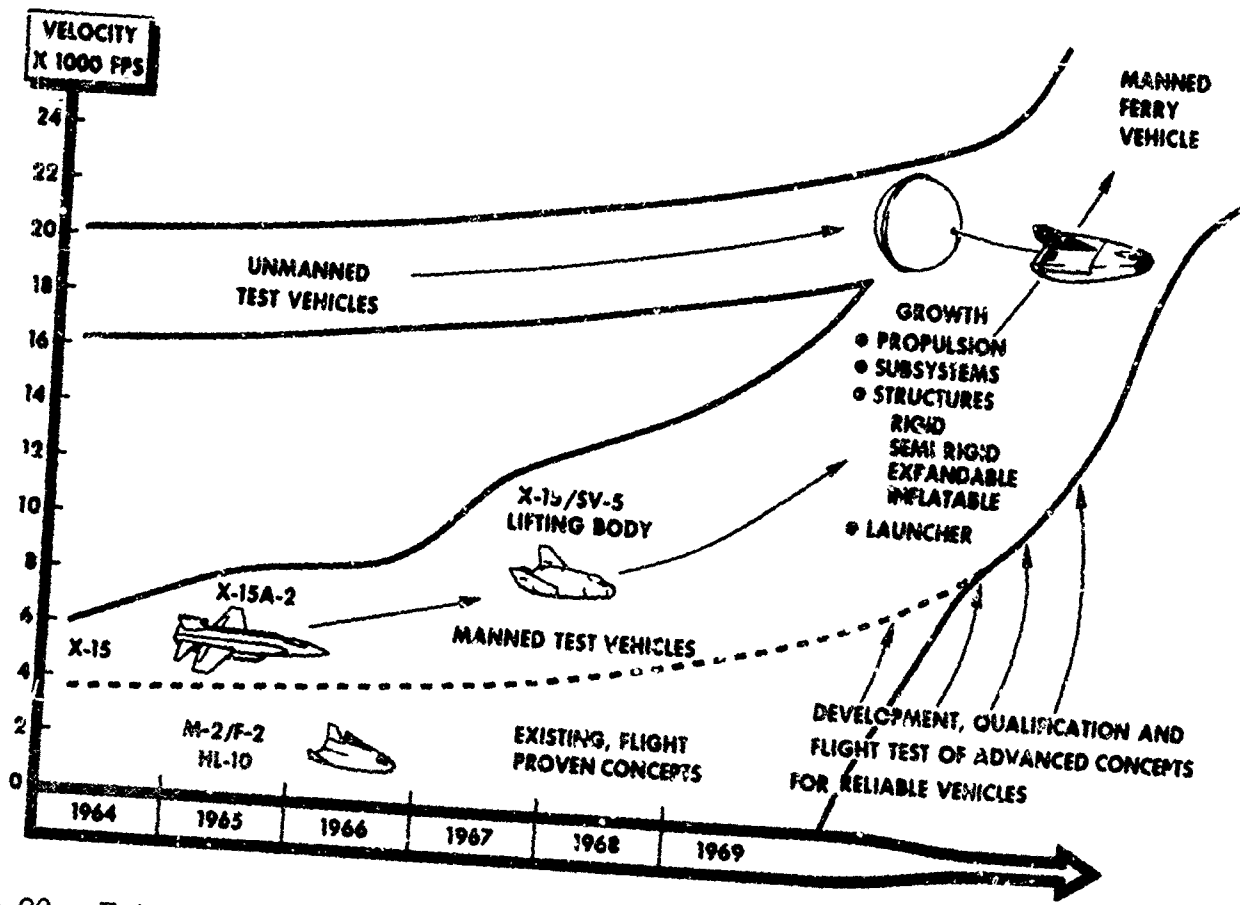


Figure 20. Future Re-entry Vehicle Flight Research and Technology Development

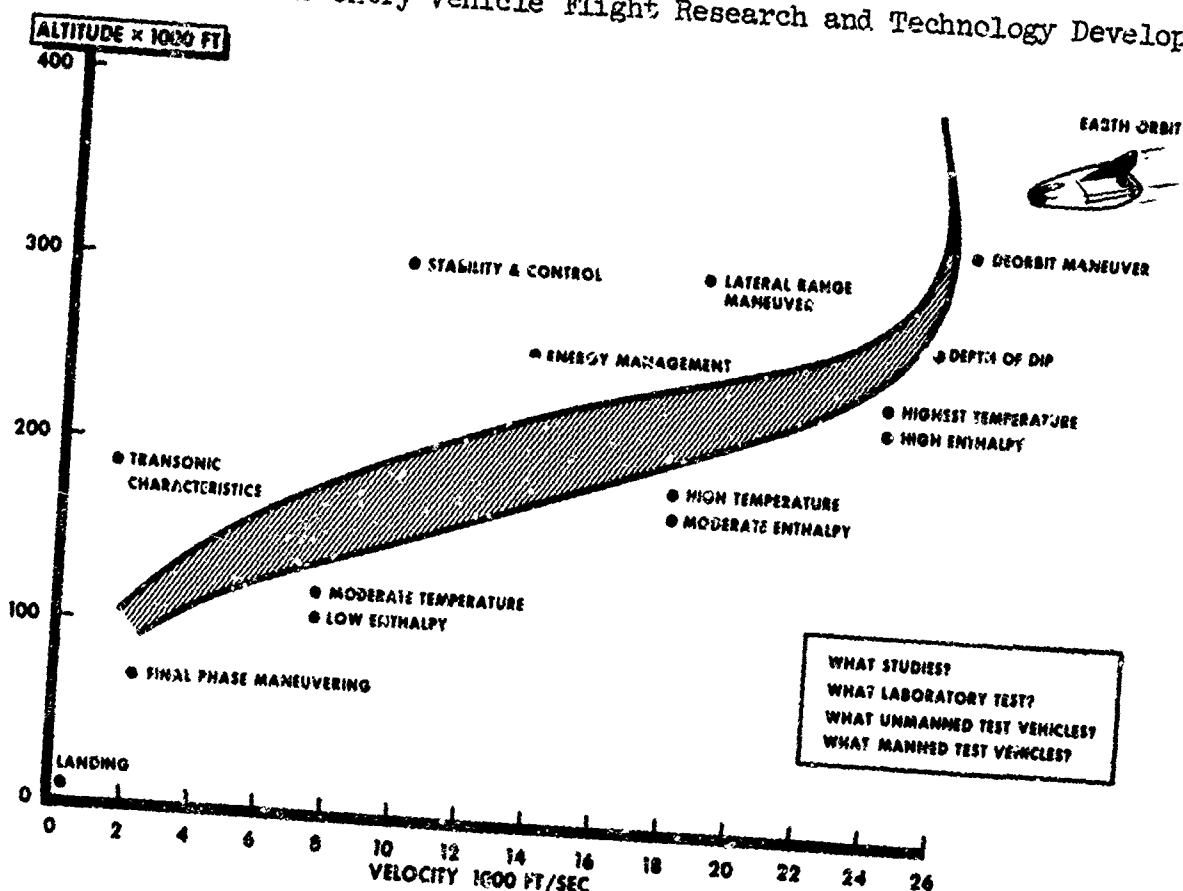


Figure 21. Re-entry Vehicle Hypersonic Environment Major Problems to Solve

COMPRESSION TESTS OF WIRE-FILM CYLINDERS

by Earl Rottmayer, staff engineer
Goodyear Aerospace Corporation, Akron, Ohio

INTRODUCTION

Wire-film composites have many features that make them particularly attractive as a structural material for space applications. They can be fabricated into a variety of strong, extremely lightweight shapes and sizes that can be packaged into a small volume for launch. In space the material can be erected easily by inflating to the rigidification pressure. After the inflatant escapes, the rigidified unpressurized structure maintains its design shape. Among the potential applications of wire-film materials are passive communications satellites, decoys, and space vehicle camouflage systems.

One efficient structural element that can be made from wire-film material is a circular tube. A single tube could be used as a beam or a strut, or a number of tubes could be combined to make a truss. Preliminary analyses and in-house test programs at Goodyear Aerospace Corporation have demonstrated that extremely lightweight wire-film tubes with significant structural strength are practical. This paper offers information for the design of wire-film cylinders in compression by reporting a test program with the following objectives:

1. To establish the rigidification pressure that gives wire-film tubes the best structural characteristics
2. To determine the buckling coefficient for tubes loaded in compression
3. To determine the axial stiffness for tubes loaded in compression
4. To investigate the effects of packaging on the above properties

TEST SPECIMEN

A typical wire-film cylinder tested is shown in Figure 1. It consisted of a film to contain the pressure required for rigidification, equally spaced wires

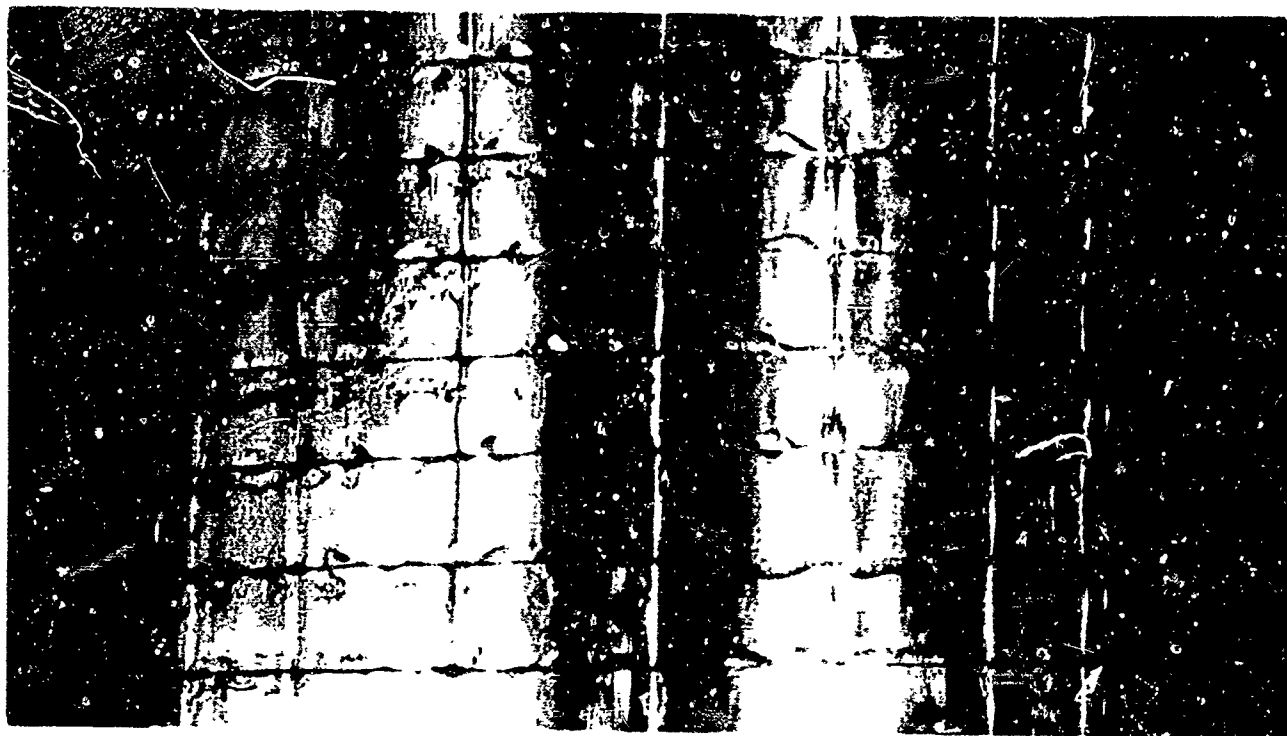


Figure 1 - Typical Wire-Film Cylinder

in the longitudinal direction, and wires wrapped continuously in the hoop direction. The diameters of the longitudinal and hoop wires were kept the same for a particular specimen, and the spacing of the hoop wires was one-half of the spacing of the longitudinal wires. The nomenclature used to describe the specimen is shown in Figure 2. Twenty eight specimens were fabricated, four each of seven types. In all cases the film was 1/4-mil Mylar, a practical minimum, to reduce the contribution of the film as much as possible. The other and more important variables were selected to cover as wide a range as practical. These included three wire materials (aluminum, stainless steel, and copper), three wire diameters (3, 5, and 10 mils), two spacings of the longitudinal wires (1/4 and 1/2 in.), and two cylinder diameters (3.000 and 1.273 in.). The data for the seven types of specimens are given in Table I.

The specimens were made in pairs on a mandrel using filament-winding techniques (see Figure 3). At each end of the mandrel was a special aluminum end cap containing a fitting to attach the pressure source and a micromanometer to measure the pressure. The fabrication procedure for the specimens was as follows.

1. A flat sheet of 1/4-mil Mylar lined with longitudinal wires was fabricated on a large-diameter mandrel.

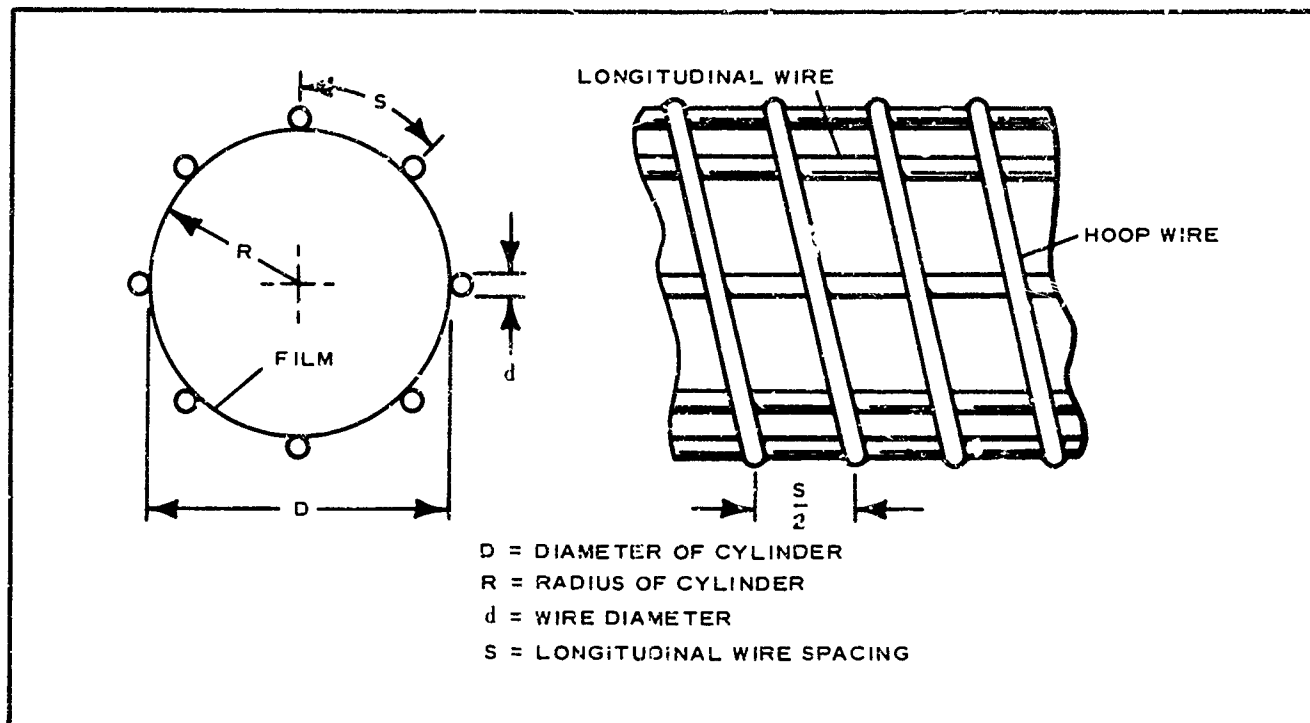


Figure 2 - Wire-Film Nomenclature

TABLE I - DESCRIPTION OF TEST CYLINDERS

Specimen type	Cylinder		Wire		S, from Figure 2 (in.)	Film
	Length (in.)	Diameter (in.)	Material	Diameter (mils)		
1	24.0	3.000	Stainless steel	3.1	0.500	1/4-mil Mylar
2	10.2	1.273	Stainless steel	3.1	0.250	1/4-mil Mylar
3	10.2	1.273	Stainless steel	5.1	0.250	1/4-mil Mylar
4	10.2	1.273	Aluminum	5.0	0.250	1/4-mil Mylar
5	10.2	1.273	Aluminum	10.5	0.250	1/4-mil Mylar
6	10.2	1.273	Aluminum	10.5	0.500	1/4-mil Mylar
7	10.2	1.273	Copper	2.9	0.250	1/4-mil Mylar

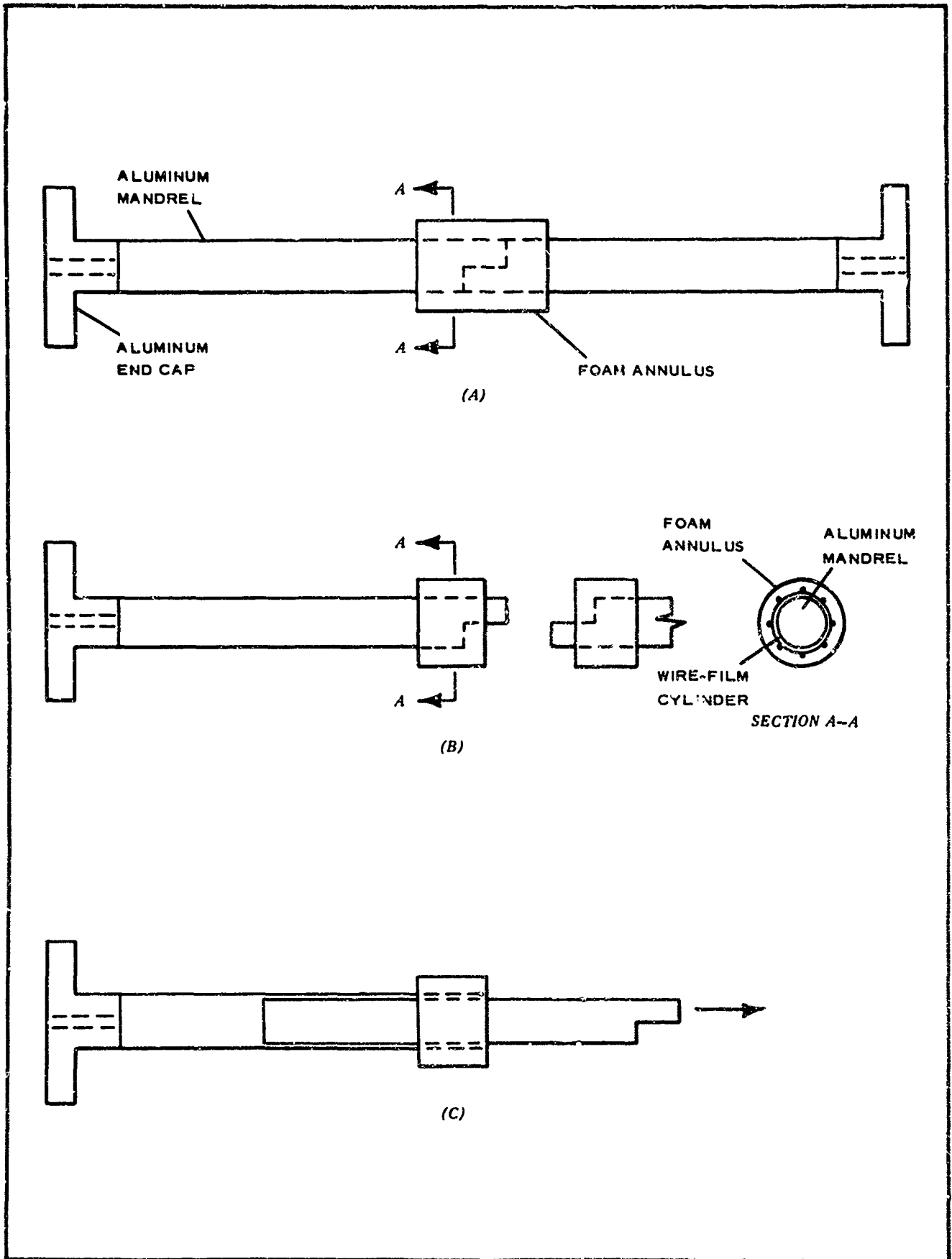


Figure 3 - Fabrication of Wire-Film Cylinders

2. The flat sheet was removed and wrapped around a mandrel and end caps of the desired cylinder diameter, with the longitudinal wires parallel to the mandrel axis. A longitudinal seam was made in the Mylar film, and the film was cemented to the end caps.
3. The hoop wires were wound on the wire-film cylinder while it was still on the mandrel.
4. A foam annulus was foamed around the cylinder at its midpoint (Figure 3A).
5. The annulus was machined to a specified diameter, thus making it concentric with the mandrel and cylinder center line.
6. The foam annulus and wire-film cylinder were diametrically cut at the midpoint of the cylinder's length. The mandrel had been made in two halves, and the halves were separated (Figure 3B).
7. The mandrel was removed from the cylinder halves with the aid of forced air, which was circulated between the mandrel and cylinder through small holes in the mandrel. (Figure 3C)
8. A foam plug was inserted and glued to the foam annulus.

TEST PROCEDURE

Compression was tested in an Instron machine, which automatically recorded the load-deflection curve. The aluminum end cap was attached to the crosshead of the Instron machine, as shown in Figure 4. A pressure differential, small compared to that required to develop the yield strength of the wires, was applied to the specimen. Then, the pressure differential was reduced to zero, the crosshead was run down, and the centering disk was located. This disk contained a centrally located button to ensure that the compression load was applied concentrically to the axis of the cylinder. A compression load-deflection curve was then obtained. By observing the record it was always possible to tell when the maximum load was attained.

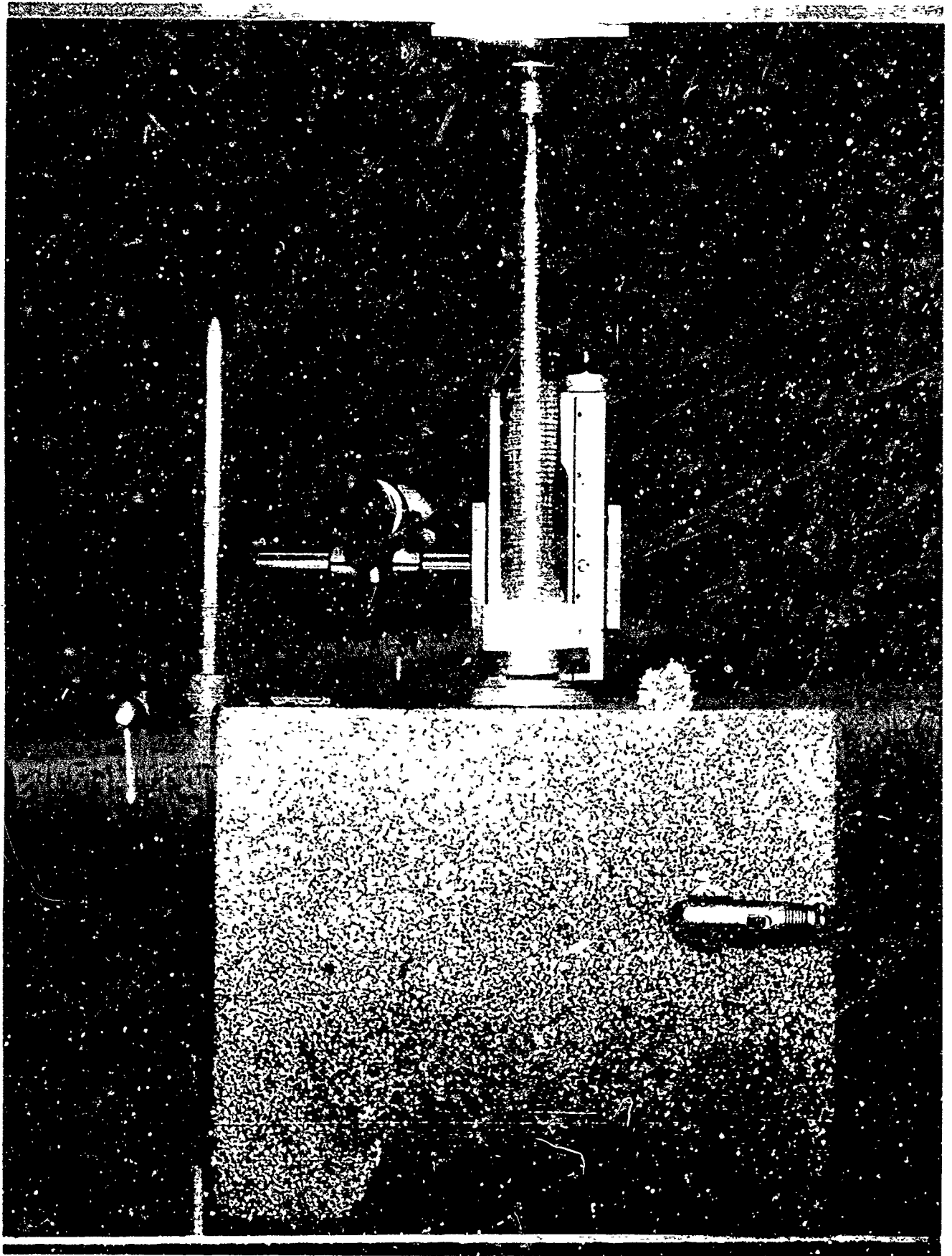


Figure 4 - Wire-Film Specimen Installed in Instron Machine

After the maximum compression load was reached, the crosshead was run up and the above procedure was repeated at successively higher inflation pressures until the maximum load began to decrease.

After the tests were completed, the same specimens were packaged. A double fold about one inch long was made at the center of the specimen, and a load was applied for 18 hours. This load was selected to give an average pressure on the fold of 5 psi. These specimens were then tested in the same manner as described above for the unpackaged cylinders.

RIGIDIFICATION PRESSURE

One of the objectives of the test was to determine the best rigidification pressure. To correlate this pressure with the specimen design, several key pressures were computed using methods developed at Goodyear Aerospace^a and the stress-strain characteristics of the wire-film material. Stress-strain curves for the wire used to make the specimen were obtained (see Table II for the principal properties). The key pressures considered were:

- p_p - the pressure at which the proportional limit stress of the longitudinal wires is attained under pressure,
- p_y - the pressure at which the yield stress of the longitudinal wires is attained under pressure, and

TABLE II - WIRE PROPERTIES

Material	Diameter (mils)	Proportional limit (psi)	Yield stress (psi)	Modulus (psi)
Stainless steel	3.1	48,000	80,000	28×10^6
Stainless steel	5.1	28,000	41,000	28×10^6
Aluminum	5.0	3,000	5,500	10×10^6
Aluminum	10.5	3,000	6,000	10×10^6
Copper	2.9	12,100	24,000	16×10^6

^aRottmayer, F : Rigidization Analysis of Wire Film Materials. GER-11117. Akron, Ohio, Goodyear Aerospace Corporation, 20 May 1964.

p_L - the pressure at which the residual compressive stress of the longitudinal wire is equal to the buckling stress. The buckling stress is computed as if the longitudinal wires were a pin-ended column with a length equal to the spacing of the hoop wires

The effect of the rigidification pressure on both the buckling strength and the axial stiffness of the cylinders was similar. In general, both these properties increased with increasing pressure to a maximum value and then began to decrease. A curve of the buckling load versus rigidification pressure for the four Type 1 specimens is shown in Figure 5. Spotted along the abscissa are the three key calculated rigidification pressures. In this instance it is apparent that maximum load is obtained at a rigidification pressure slightly lower than key pressure p_y .

A rigidification pressure summary is given in Table III. In addition to listing the calculated key pressures for the seven types of cylinders, the table gives the rigidification pressure at which the maximum load and maximum stiffness were obtained. It is evident from Table III that the rigidification pressure should be greater than p_p . Comparing p_y and p_L to the optimum test pressures, it is concluded that the rigidification pressure should be either p_y or p_L , whichever is smaller.

BUCKLING STRESS

The buckling stress considered here is not one of general column instability but one of local instability involving both the longitudinal and hoop wires. A typical failure is shown in Figure 6. The problem of buckling of wire-film cylinders is similar to that of circular cylinders stiffened by ring-stringer combinations (a problem treated in Becker's Handbook of Structural Stability^a). This problem is similar to that of the wire-film cylinder, where the hoop wires can be considered the rings and the longitudinal wires as the stringers. Using this approach and rewriting the equation in terms of the wire-film cylinder, the buckling stress (σ_{cr}) is given by

^aBecker, H.: Handbook of Structural Stability, Part VI - Strength of Stiffened Curved Plates and Shells. T.N. No. 3786, NACA, July 1958.

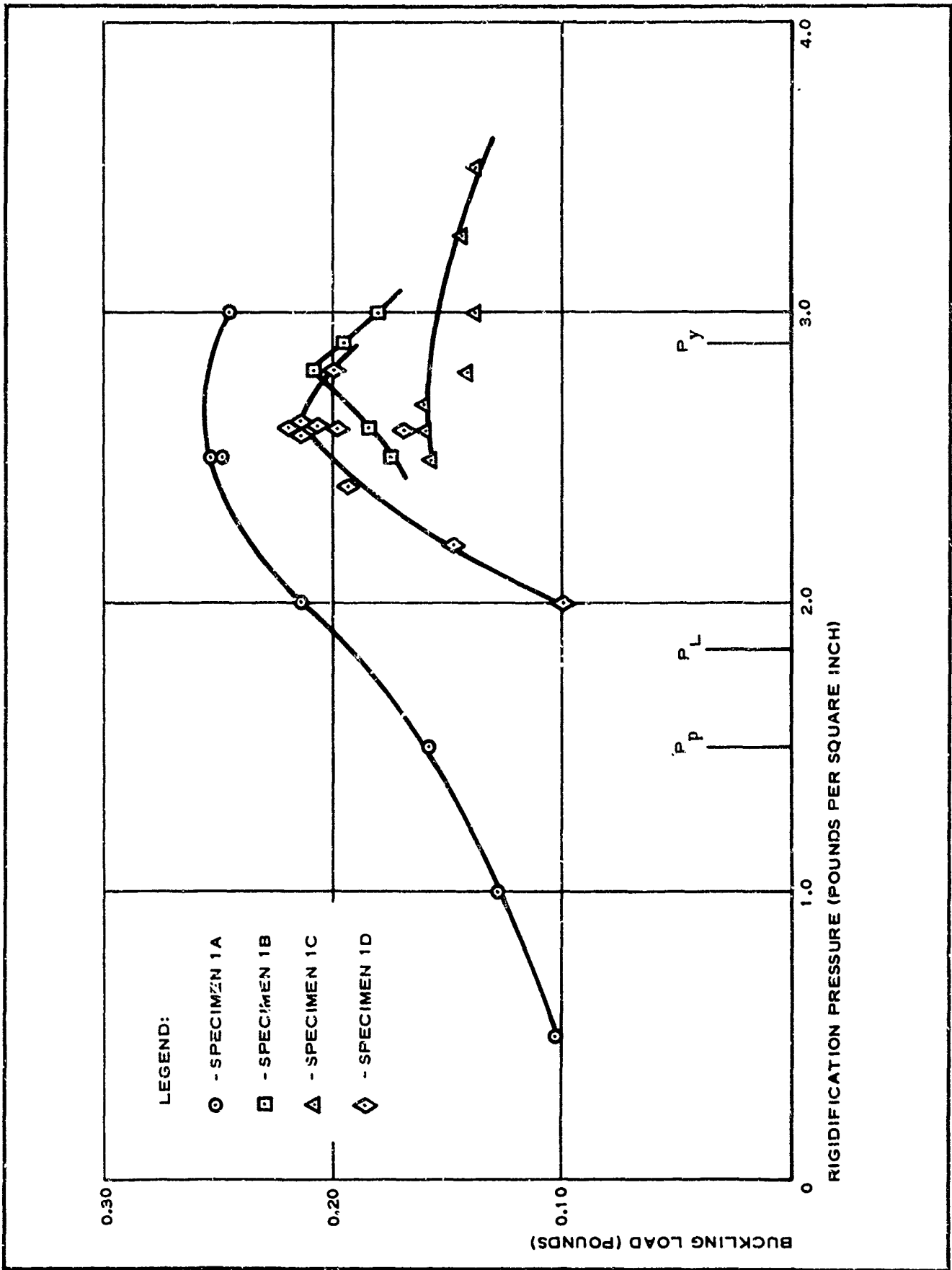


Figure 5 - Buckling Load versus Rigidification Pressure

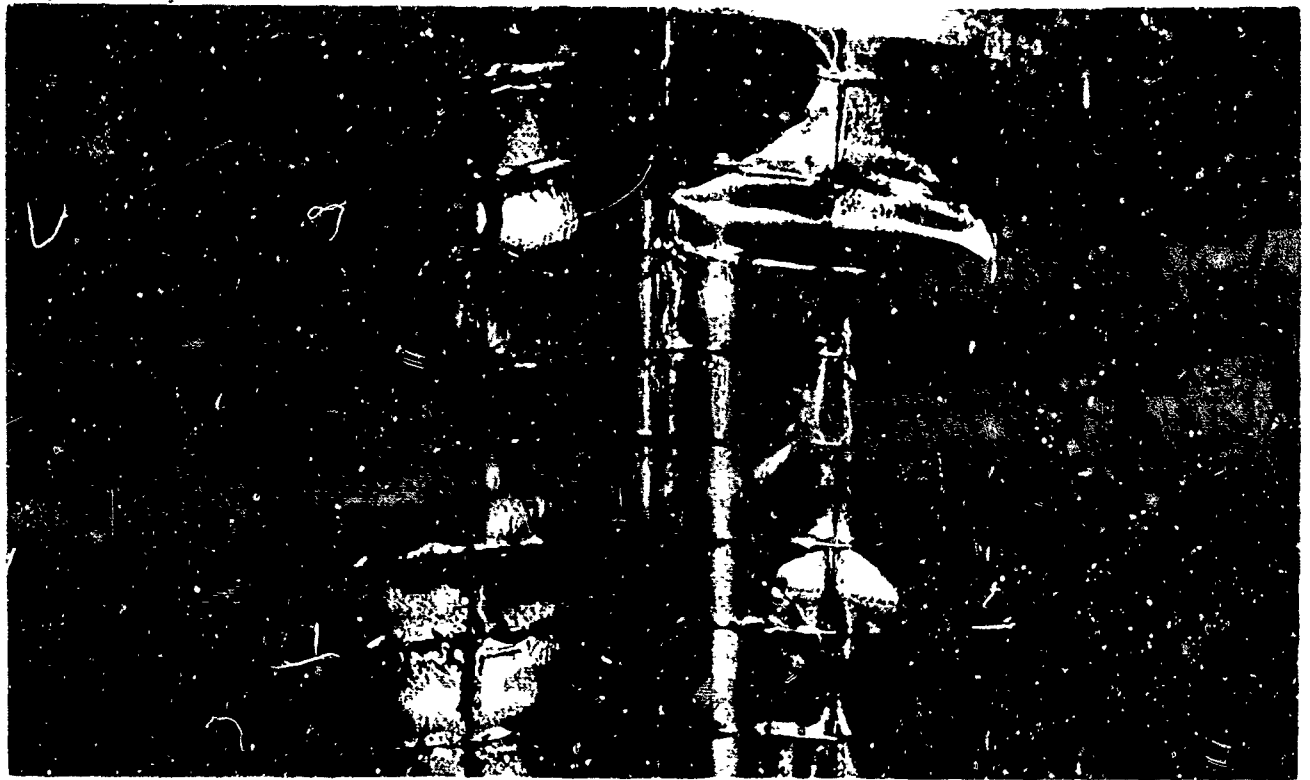


Figure 6 - Typical Compression Buckling Failure

TABLE III - RIGIDIFICATION PRESSURE SUMMARY

Specimen type	Key calculated pressures (psi)			Optimum test pressures (psi)	
	P_p	P_y	P_L	Maximum load	Maximum stiffness
1	1.5	2.9	1.9	2.6	2.0
2	5.9	12.0	10.1	7.0	7.0
3	7.9	13.4	19.0	14.0	13.0
4	1.0	3.5	4.5	4.0	3.0
5	3.5	8.4	High	8.0	9.0
6	1.8	5.3	10.0	8.5	8.0
7	1.5	6.0	3.1	3.0	2.5

$$\sigma_{cr} = C\eta EQ, \quad (1)$$

where

C = empirical constant to be determined,

η = plasticity reduction factor,

E = modulus of elasticity of wires, and

$$Q = \frac{d^{3/2}}{6.72 RS^{1/2}}, \quad (2)$$

where d, R, and S are defined in Figure 2.

The cross-sectional area of the longitudinal wires is given by

$$\begin{aligned} A &= (2\pi R) \frac{\pi d^2}{4S} \\ &= \frac{\pi^2 R d^2}{2S}. \end{aligned} \quad (3)$$

The selection of the specimen types was based primarily on the desire to cover a wide range of the parameter Q, in order to establish the empirical constant C in Equation 1. The range covered was from 0.242×10^{-4} to 5.031×10^{-4} . The values of Q for each specimen are given in Table IV, along with the cross-sectional area A and the maximum load obtained on each specimen.

TABLE IV - SPECIMEN DATA

Specimen type	Q × 10 ⁴	A × 10 ⁴ (sq in.)	Maximum compression load (lb)			
			A	B	C	D
1	0.242	1.42	0.255	0.218	0.161	0.219
2	0.807	1.21	0.642	0.488	0.456	0.540
3	1.703	3.27	1.76	2.33	3.22	1.88
4	1.653	3.15	0.550	0.580	0.750	0.710
5	5.031	13.86	6.16	6.24	5.42	6.80
6	3.557	6.93	1.32	2.25	0.845	0.960
7	0.730	1.06	0.244	0.182	0.264	0.236

C was determined by plotting $\sigma_{cr}/\eta E$ against C. The value of σ_{cr} was determined by dividing the maximum load on each specimen by the cross-sectional area of the longitudinal wires. All specimens except those of Type 5 failed in the elastic range, so the plasticity relation factor was unity, with the one exception. For Type 5 specimens the secant modulus of the wire material was used (see Figure 7). The three straight lines in the figure correspond to values of C of 1.0, 1.5, and 2.0 (shown for reference).

The data are consistent for all specimens, except for those of Type 6. This type had a large wire spacing, in relation to cylinder diameter, which resulted in a large helical angle for the hoop wires. Such a large helical angle is apparently undesirable and should be avoided. For this reason these points should be ignored in selecting C. The remaining points have a fair amount of scatter, but this is to be expected in any buckling test of thin cylinders. A value of C equal to 1 is certainly conservative because all data points are above this line. A value of 1.5 is more realistic, however, and is recommended for design purposes at this time.

AXIAL STIFFNESS

The axial stiffness (EA) is defined by

$$EA = \frac{Pl}{\delta}, \quad (4)$$

where

l = length of member,

P = applied axial load, and

δ = deflection associated with load P .

Usually, the axial stiffness can be predicted accurately by multiplying the modulus of elasticity by the cross-sectional area of the member, which in this case would be the area of the longitudinal wires. If the member is not straight, the axial stiffness is considerably reduced, depending on the amount of initial eccentricity. The axial stiffness can be computed in this case if the deviation of the member from a straight line is known.

During rigidification the longitudinal wires are subjected to a combination of

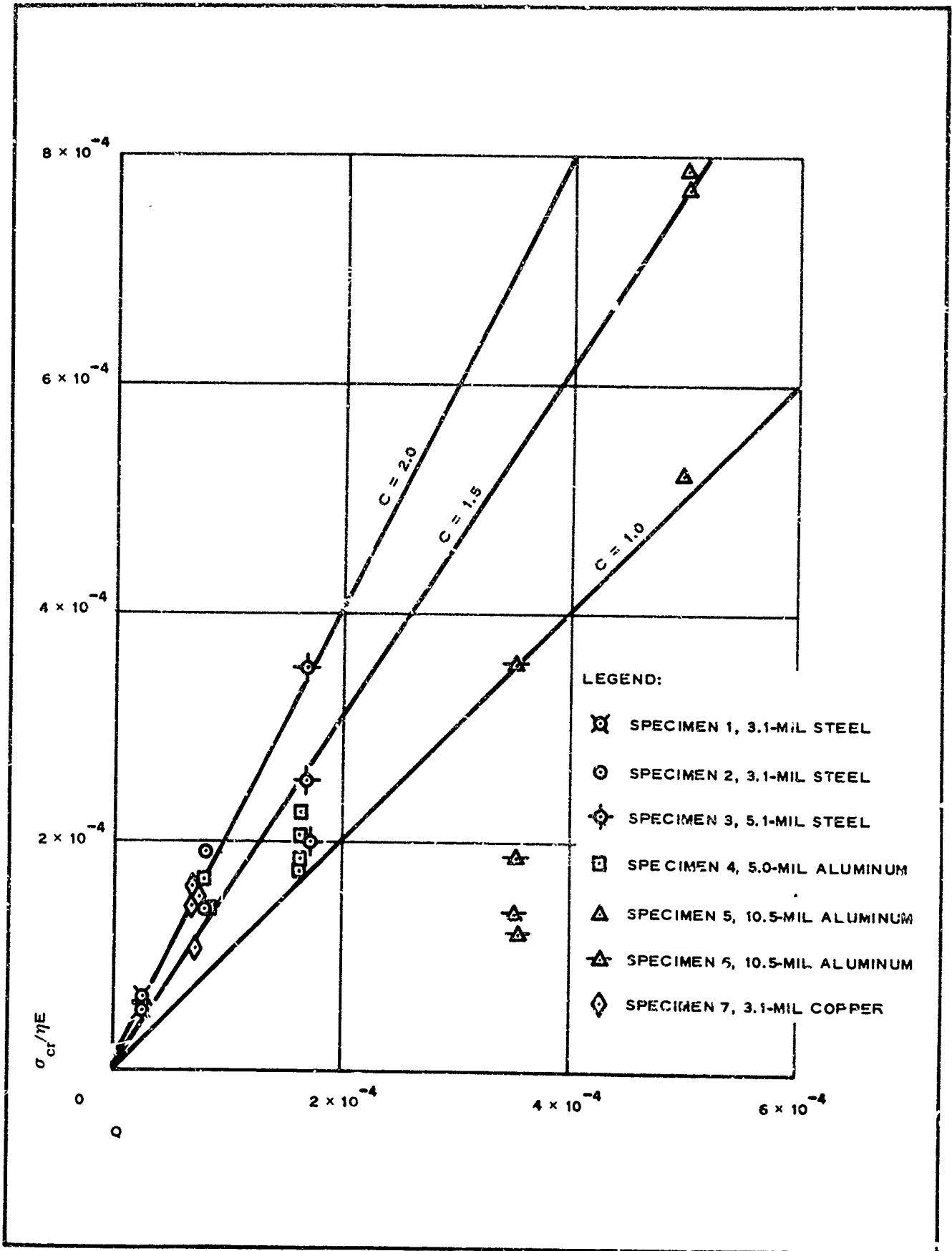


Figure 7 - $\sigma_{cr}/\eta E$ versus Q

tension and bending stresses, and permanent deformations are to be expected at the higher inflation pressures. It was beyond the scope of this program to attempt to predict the deformation of the longitudinal wires as a function of pressure.

The axial stiffness of the specimen was obtained by test. The initial slope of the load-deflection curve automatically recorded by the Instron machine established the ratio P/δ required in Equation 4 to compute the axial stiffness. This was found to be a function of pressure, just as the maximum load was.

The maximum values of EA determined by test are given in Table V. Also given for comparison is a basic calculated value determined simply by multiplying the modulus of elasticity of the longitudinal wire by its cross-sectional area. The ratios of the test values to the theoretical values are listed in the last column.

It is evident that the effective stiffness of the wire-film cylinder is considerably less than the calculated value. The minimum value (21.1 percent) was obtained on Type 1 specimens; the maximum (52.5 percent), on those of Type 3. No attempt is being made at this time to predict the stiffness, so a detailed discussion of the results is not warranted. The most important point, perhaps, is that if stiffness is the governing criterion, an effective stiffness of 50 percent of the basic calculated stiffness can probably be attained.

TABLE V - AXIAL STIFFNESS

Specimen type	EA _w (calculated)	EA _w (test)	Calculated/ - test
1	3,980	840	0.211
2	3,390	928	0.273
3	9,150	4810	0.525
4	3,150	1400	0.445
5	13,860	6530	0.475
6	6,930	2320	0.333
7	1,700	611	0.360

PACKAGING

The effects of packaging are illustrated by plotting unpackaged data against packaged data. The buckling loads are shown in Figure 8; the effective modulus, in Figure 9. In both figures the packaged values are less than the unpackaged values. The test points scatter about the line labeled 0.8, which corresponds to a 20-percent reduction.

It should be emphasized that the packaged specimens were the same specimens that were tested originally as unpackaged specimens. While unpackaged, they were tested many times and subjected to inflation pressures greater than the optimum pressure. Therefore, it is reasonable to anticipate that the packaged values would be less than the unpackaged values. For these reasons it is concluded that packaging has little or no effect on the properties of the cylinder.

CONCLUSIONS

The following conclusions have been reached:

1. The optimum rigidification pressure is the one that produces yield stress of the wire or buckling of the wire, whichever is smaller.
2. The value of the local buckling constant is 1.5.
3. An effective axial stiffness of 50 percent of the basic calculated value can be achieved.
4. Packaging has little effect on the axial stiffness or buckling load.

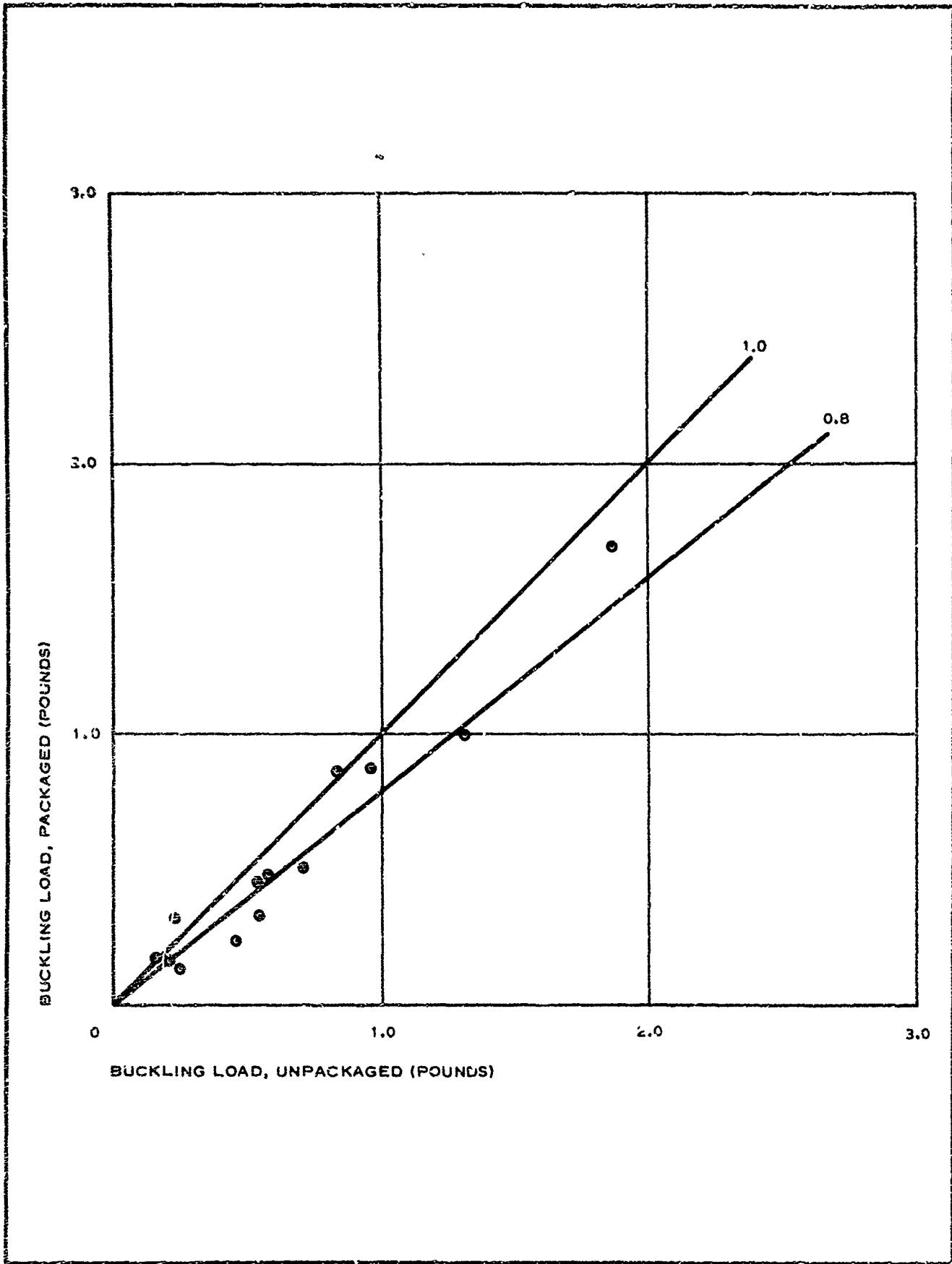


Figure 8 - Buckling Loads; Packaged versus Unpackaged

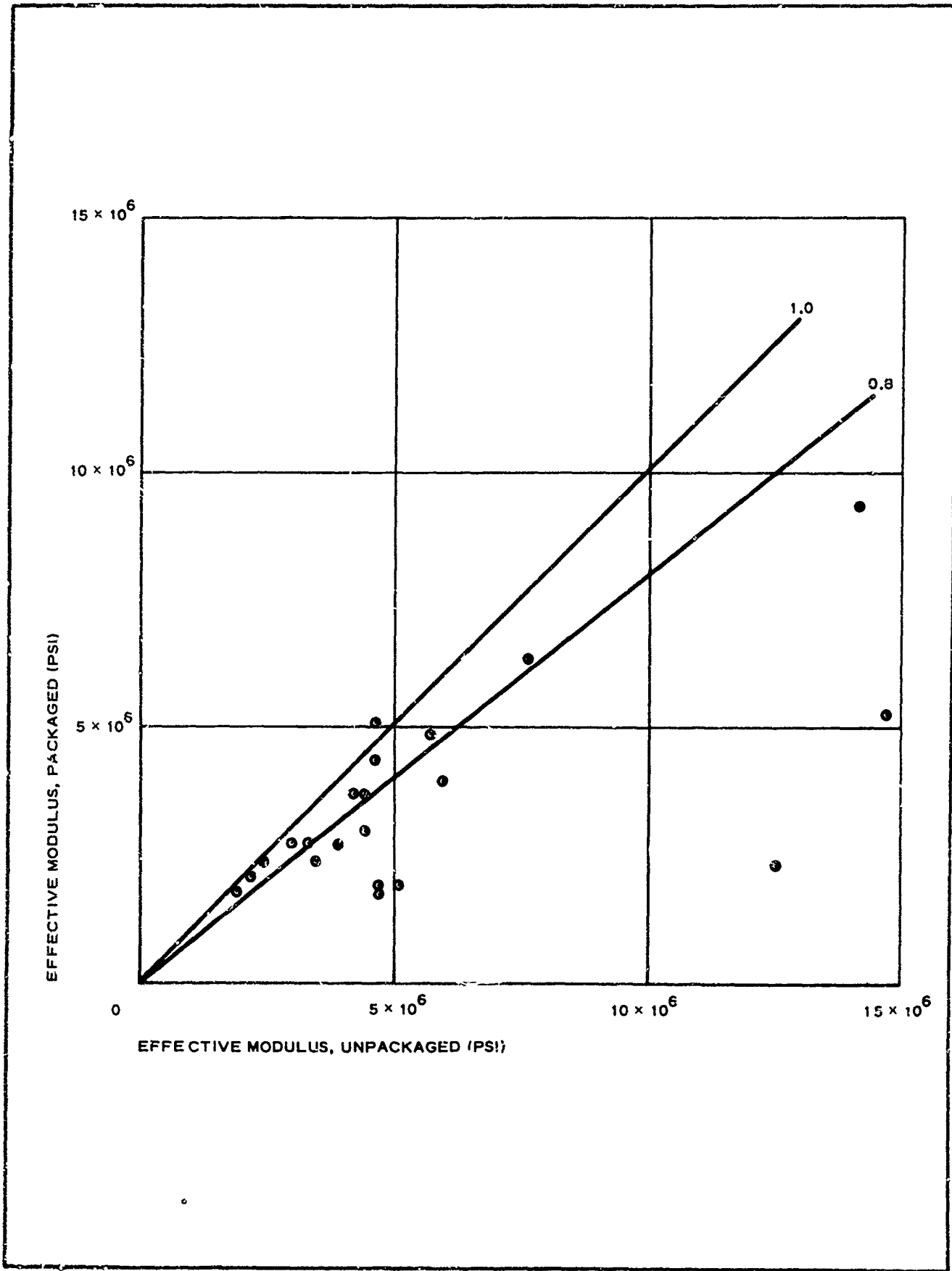


Figure 9 - Effective Modulus; Packaged versus Unpackaged

DESIGN CRITERIA FOR INFLATED, EXPANDABLE BEAMS USED AS
STRUCTURAL MEMBERS IN AN ADVANCED CONCEPT PARAGLIDER

By Royce A. Toni and James F. McNulty

NASA Langley Research Center

INTRODUCTION

As a result of the interest shown in an inflatable paraglider for possible application as a device for suitable payload recovery, it has been necessary to develop the engineering tools to perform a structural design of the inflated members associated with the load transfer from the aerodynamic membrane to the shroud lines. The basic problem is to provide a minimum weight design while still assuring that the members will not buckle or burst under load.

Design procedures have been developed which allow inflated curved beams to be designed with due consideration being given to concentrated and distributed loads acting in arbitrary planes. Paragliders designed by methods outlined herein have been tested in wind tunnels under varying aerodynamic loading conditions and have been found to exhibit buckling tendencies near the load condition predicted analytically.

This paper concerns itself primarily with the analytical design procedures to be utilized after the loading condition has been established. The determination of the loading conditions on the structural members, either experimentally or analytically, is an interesting but separate problem.

SYMBOLS

- A leading-edge and keel cross-sectional area equal to $2\pi r$, in.
- A_e leading-edge axial compression depicted in figure 2 under section A-A as accumulative effects along member's length and shown vectorially according to right-hand rule in figure 4, lb
- A_k keel axial compression depicted in figure 2 under section C-C as accumulative effects along member's length and shown vectorially according to right-hand rule in figure 5, lb
- E Young's modulus of elasticity for fabric, lb/in.
- F fabric breaking strength, lb/in.
- I leading-edge and keel cross-section moment of inertia, in.³

I_x	leading-edge and keel cross-section moment of inertia with respect to x axis, in. ³
I_y	leading-edge and keel cross-section moment of inertia with respect to y axis, in. ³
J	leading-edge and keel cross-section polar moment of inertia, in. ³
K	strength-to-weight ratio of fabric, lb/in./oz/yd ²
M_e	leading-edge vertical bending moment depicted in figure 2 under section A-A, and shown vectorally according to right-hand rule in figure 4, ft-lb
$(M_e)_I$	leading-edge inboard bending moment depicted in figure 2 under section B-B, and shown vectorally according to right-hand rule in figure 4, ft-lb
(M_k)	keel vertical bending moment depicted in figure 2 under section C-C, and shown vectorally according to right-hand rule in figure 5, ft-lb
M_R	leading-edge resultant bending moment equal to $\sqrt{(M_e)^2 + [(M_e)_I]^2}$ shown vectorally according to right-hand rule in figure 4, ft-lb
n_0	burst preventive safety factor, unitless
"O"	that point on structural member's cross section where stress is critical due to bending (refer to figs. 4 and 5)
p	inflation pressure, lb/in. ²
Q	static moment of inertia of arc, in. ²
r	structural member inflated radius, in.
r_f	fabricated radius for an inflated beam, in.
S	length along arc of a circle, in.
V_e	leading-edge vertical shear depicted in figure 2 under section A-A, and also shown in figure 4, lb
$(V_e)_I$	leading-edge inboard shear depicted in figure 2 under section B-B, and also shown in figure 4, lb
V_k	keel vertical shear depicted in figure 2 under section C-C, and also shown in figure 5, lb
W	fabric weight, oz/yd ²

x,y	Cartesian coordinate system for a structural member's cross section with a positive sense shown in figure 3
Z	torque, ft-lb
Z _e	leading-edge torque, ft-lb
ε	strain for an inflated material, in./in.
ρ	perpendicular distance from centroid of an area to its axis of inertia, in.
σ _H	hoop stress, lb/in.
σ _L	longitudinal stress, lb/in.
τ _O	resulting shear stress at point "O," lb/in.
τ _V	shear stress, lb/in.
τ _Z	torsional stress, lb/in.
τ _{cr}	critical shear stress equal to $\sqrt{\sigma_H \sigma_L}$, lb/in.
θ	angular direction along circumference of structural member's cross section with a positive sense as shown in figure 3, deg
θ ₁	angle locating some arbitrary point on structural member's cross section (refer to fig. 3), deg
ω	angle defined as $\tan^{-1} \frac{M_e}{(M_e)_I}$ (refer to fig. 4), deg

DESCRIPTION OF AN ADVANCED CONCEPT PARAGLIDER

A paraglider, simply speaking, is a flying wing which has glide and maneuver capability through adjustment of the shroud line lengths which locates the payload relative to the resultant aerodynamic lift vector; this, in turn, determines the glide and sideslip angle. According to reference 1, an inflatable paraglider would be classified as that type expandable structure which employs the use of internal gas pressurization to provide the energy for deployment and then is dependent upon the same pressurization to maintain the paraglider in its deployed shape.

Once deployed and pressurized the advanced concept paraglider takes on the shape illustrated in figure 1. The leading edges and keel serve as the structural members and are joined at the apex; thus, in effect they represent a structural frame composed of inflated fabric beams. The space vehicle is slung beneath the paraglider and connected to it by shroud lines, or

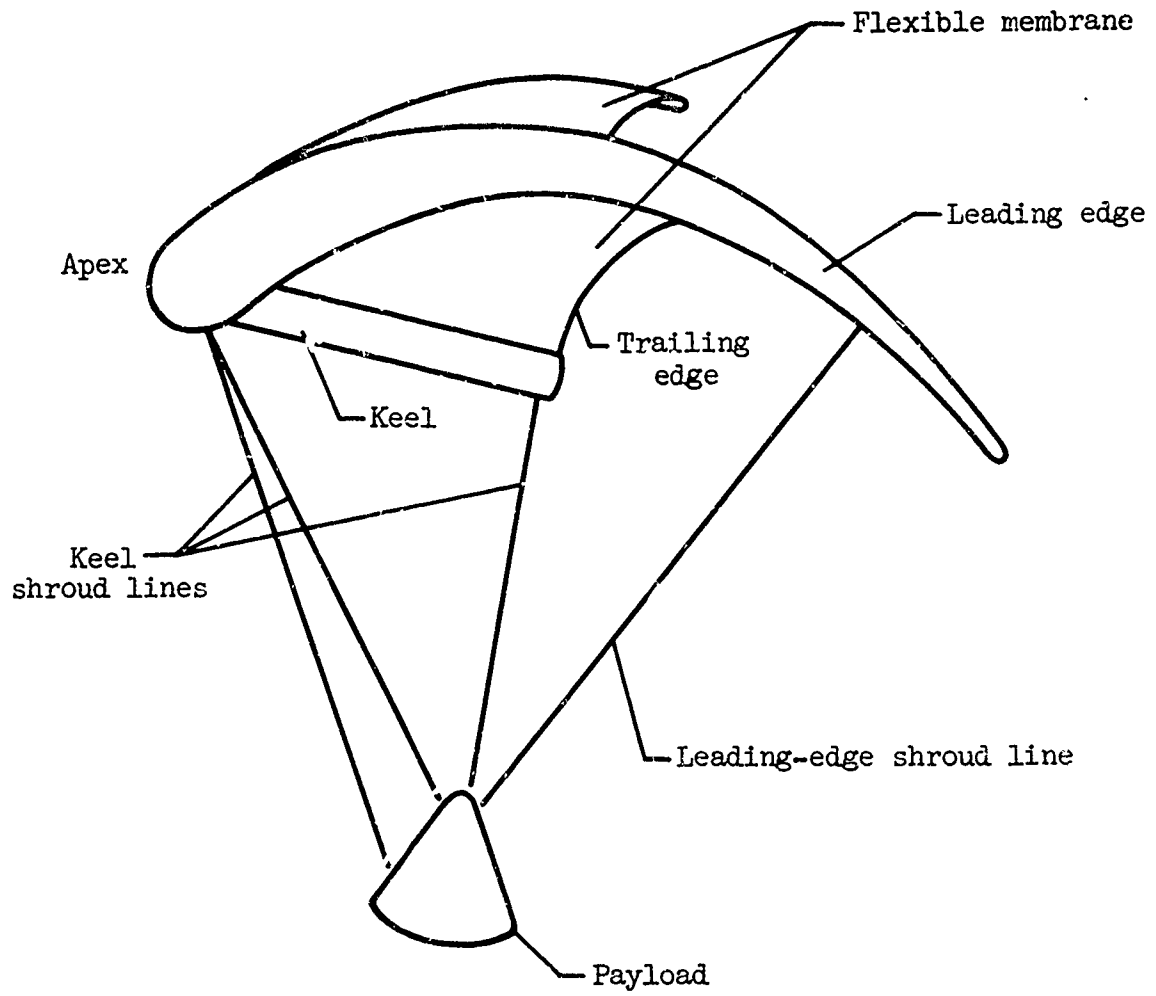


Figure 1.- A deployed advanced concept paraglider.

cables. The number of cables directly affects the imposed loads acting upon the structural members. The more cables, the less critical become the effect of the loads; however, at the same time the expectancy for successful deployment is reduced. Thus, a trade-off must be made. It was felt that the arrangement of three cables from the keel (two at the apex and one at the aft end) and one cable from each of the leading edges (at the three-quarter points) provided sufficient stability and structural integrity while keeping the complexities of the deployment to a minimum.

In the advanced concept, high-aspect-ratio paraglider, the longitudinal shape of the leading-edge center line is curved, approximating an arc of a circle while its circular cross section varies linearly from a relatively large diameter at the apex to a small diameter at the tip. The keel is considerably shorter in length and maintains a constant-diameter circular cross section. Physically the advanced concept paraglider differs from the conventional concept in that the latter has three structural members of constant circular cross section, equal in length and lying in the same plane.

Attached between the leading edges and keel is the membrane. That part of the membrane running from tip to tip of each structural member is termed the trailing edge. The membrane is entirely flexible and assumes a shape governed by the aerodynamic pressure.

The primary advantage of the advanced concept paraglider is that it offers a relatively marked increase in glide characteristics over the conventional concept by reducing the drag; thus, the advanced concept would have the flexibility to glide to more distant landing sites.

LOAD AND MOMENT DEFINITION

Paraglider design is hindered by an inability to define theoretically the load distributed to the leading edges and keel due to aerodynamic pressure acting on the membrane. This difficulty is created by both the flexibility of the membrane (it changes its shape with every maneuver as does the magnitude of the load distribution) and the difficulty of defining the direct aerodynamic load on the structural members themselves.

In an attempt to circumvent the aforementioned difficulty, Langley Research Center initiated a program that incorporated the use of a high-aspect-ratio, rigid paraglider model fitted with load and moment measuring balances. The model was wind-tunnel tested over a range of angles of attack. The resulting load and moment coefficients were recorded and plotted for each structural member for various stations along its length. Since the balances were multicomponent it was possible to record any desired force at these stations in three perpendicular planes. The same loads model configuration was compatible with models investigated for aerodynamic performance at various angles of attack. From the aerodynamic study, the paraglider's glide and flare angles of attack were selected; the data from the loads model for these angles of attack were then used as design inputs.

The resulting loads for the glide angle of attack served as the design criteria for the structural members in dictating member deflections so as to

achieve the desired in-flight shape. Those loads for the flare angle of attack, corrected for a conservatively assumed 1.5g load factor, dictated the leading-edge internal pressure requirements to resist wrinkling. The pressure was then selected for the entire vehicle and served as the basis for arriving at a keel radius.

The inertia loads were taken into consideration by initially assuming the weights of the structural members and distributing them along the member's length to a second-order approximation for the leading edge (since its cross section tapers with length) and a uniform distribution for the keel (since its cross section is constant with length).

The shroud line loads were distributed in accordance with elastic bending theory (the actual mechanics are beyond the scope of this paper). Thus, the aerodynamic, inertia, and shroud line loads all contributed to the total effective imposed loads acting upon the structural members.

For the advanced concept paraglider considered herein the leading-edge geometry was governed by aerodynamic considerations. The design loads and moments shown in figure 2 were determined in the manner outlined above.

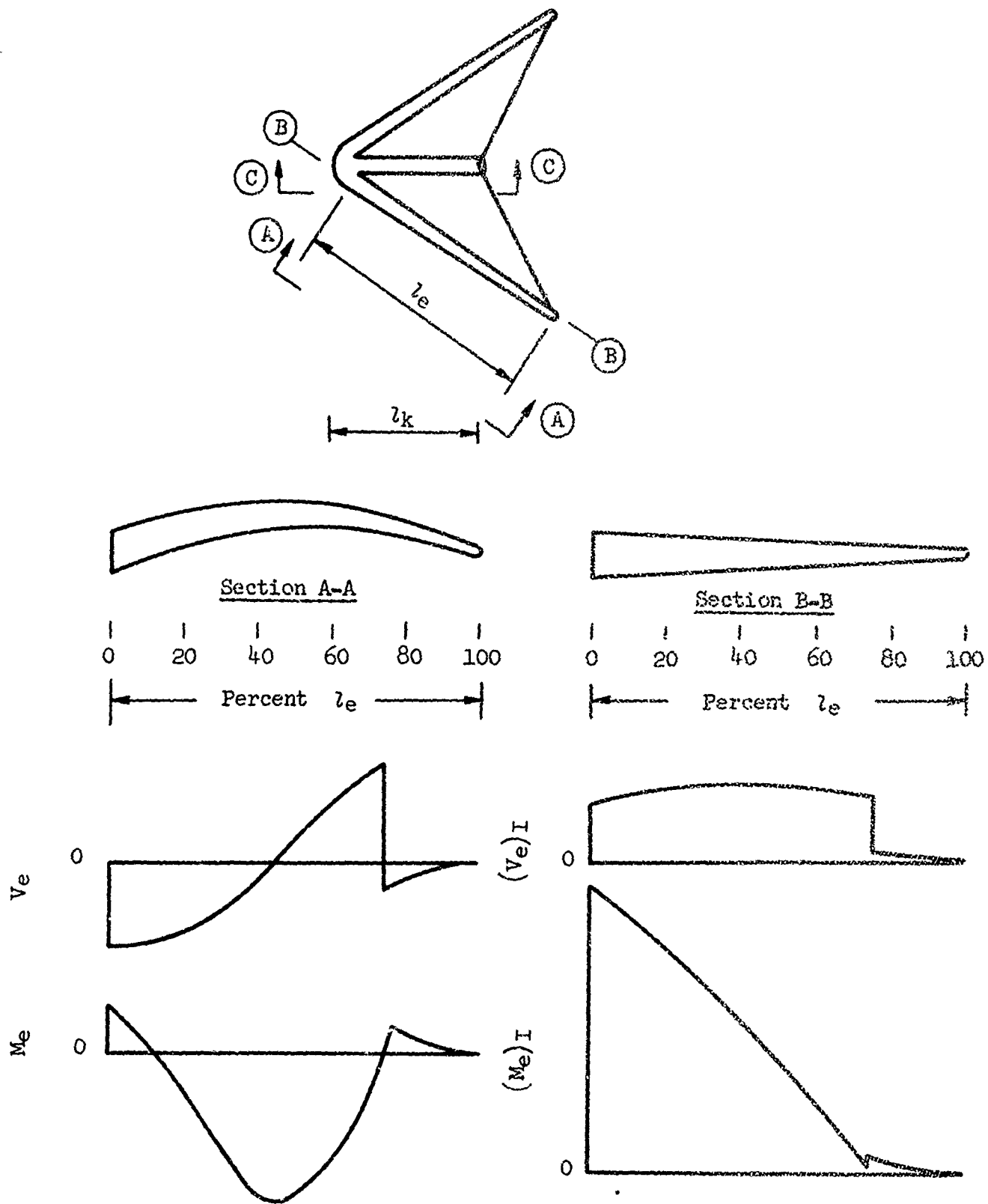
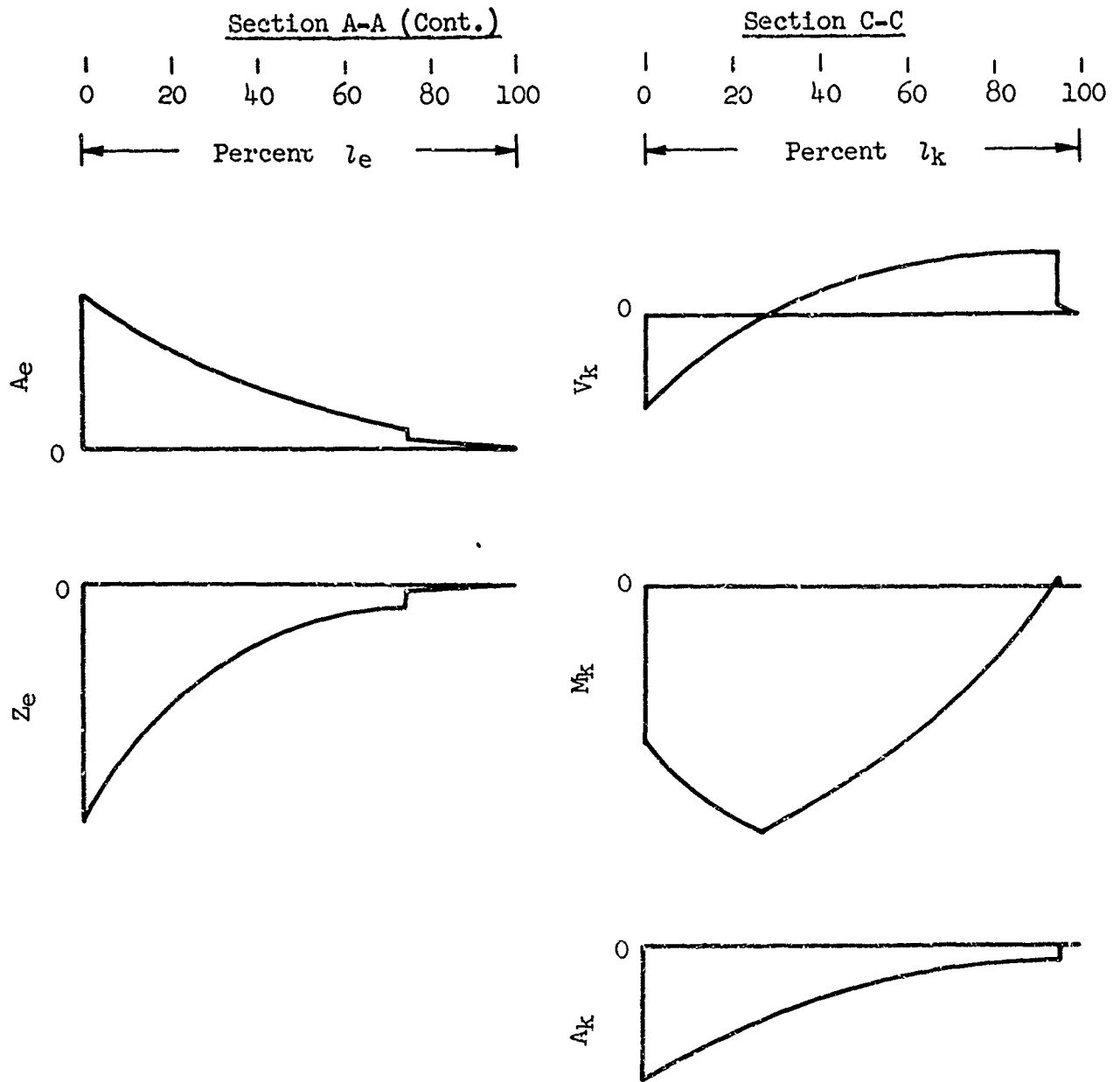


Figure 2.- The resulting imposed load shapes on the structural members of a prototype advanced concept paraglider of aspect ratio 5.4 with a flare angle of attack of 23° and a 1.5 load correction factor.



NOTE: A_e and A_k are the leading-edge compression and the keel tension, respectively, and are shown as accumulative effects along the member's length.

Z_e is the leading-edge torque and is positive in direction when looking down leading edge from tip to apex.

Section B-B is a plan view of the leading edge.

Figure 2.- Concluded.

BASIC EQUATIONS USED IN INFLATABLE BEAM DESIGN

This section pertains to the derivation of equations applicable for design of a circular cross section, inflated fabric beam. Figure 3 shows the typical cross section for such a beam and will be referred to in deriving the expressions for area, moment of inertia, static moment of inertia of arc, and torsional shear stress. The cross section is considered a ring with a thickness t negligible in comparison with radius r . As is customary with fabric design procedures, stress is expressed as lb/in. of fabric, I as in.³, and A as inches; thus, t is omitted as a parameter.

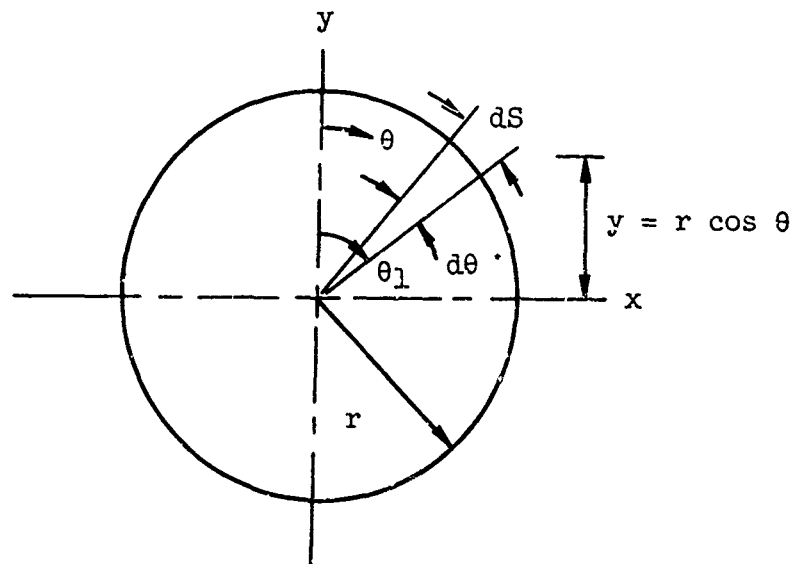


Figure 3.- Cross section of inflated fabric beam.

1. Area

$$A = \int dA \quad (1)$$

For the area associated with $d\theta$ in figure 3

$$A = \int_{\theta_1 - d\theta}^{\theta_1} r d\theta \quad (2)$$

Integrating for the complete ring results in:

$$A = 2\pi r \quad (3)$$

2. Moment of Inertia

The mathematical definition of moment of inertia is stated in the following expression:

$$I = \int \rho^2 dA \quad (4)$$

where ρ is the perpendicular distance from the differential area dA , to the axis of inertia. For the case illustrated in figure 3 the following is true

$$I_x = I_y \quad (5)$$

and considering the x axis as the axis of inertia yields

$$I_x = \int_{\theta_1 - d\theta}^{\theta_1} y^2 dA \quad (6)$$

By substituting an expression for y , in terms of r and θ , into equation (6) along with the assumption

$$dS = r d\theta = dA \quad (7)$$

and integrating over the entire cross section, the following expression is arrived at

$$I_x = 4r^3 \int_0^{\pi/2} \cos^2 \theta d\theta \quad (8)$$

Performing the indicated definite integration yields the equation for the moment of inertia. Thus,

$$I_x = \pi r^3 \quad (9)$$

3. Static Moment of Inertia of Arc

By definition the static moment of inertia of an area is the product of that area and its perpendicular distance from the neutral axis. Thus, for the differential area illustrated in figure 3,

$$dQ = \int_{\theta_1 - d\theta}^{\theta_1} y dA \quad (10)$$

Substituting the expression for y and dA into the above, and expressing the integral for that part of the arc above the neutral axis yields

$$Q = 2r^2 \int_0^{\pi/2} \cos \theta \, d\theta \quad (11)$$

Performing the indicated definite integration results in the expression for the static moment of inertia of arc or,

$$Q = 2r^2 \quad (12)$$

4. Torsional Shear Stress

Torsional shear stress for a circular cross section in the form of an equation is simply stated as

$$\tau_z = \frac{Zr}{J} \quad (13)$$

where Z is the torque and J the polar moment of inertia. The polar moment of inertia is defined as

$$J = I_x + I_y \quad (14)$$

and substituting equation (5) into the above yields the polar moment of inertia for a circular cross section.

$$J = 2I_x \quad (15)$$

Now replacing I_x by equation (9) results with J ,

$$J = 2\pi r^3 \quad (16)$$

Substituting the above into equation (13) yields an expression for the torsional shear. Thus,

$$\tau_z = \frac{Z}{2\pi r^2} \quad (17)$$

DESIGN OF STRUCTURAL FRAME MEMBERS

Once the imposed loads are established for the structural members it is possible to arrive at the inflation pressure for the leading edge followed by determining the radius for the keel. The engineering concept employed was

developed by the authors in collaboration with Goodyear Aerospace engineers* under NASA Contract NAS1-3020.**

1. The Leading-Edge Structural Member

In considering the leading edge a cross section subjected to the imposed loads is shown in figure 4. From figure 4 it can be seen that,

$$\omega = \tan^{-1} \frac{M_e}{(M_e)_I} \quad (18)$$

$$M_R = \sqrt{M_e^2 + (M_e)_I^2} \quad (19)$$

$$V_2 = V_e \cos \omega - (V_e)_I \sin \omega \quad (20)$$

$$V_1 = (V_e)_I \cos \omega + V_e \sin \omega \quad (21)$$

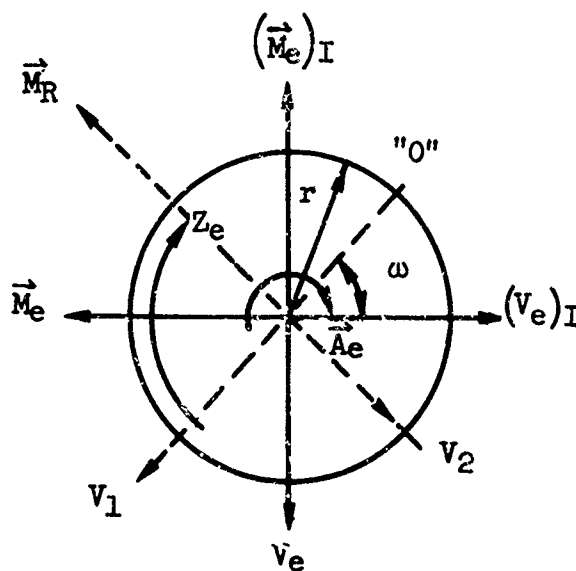


Figure 4.- Leading-edge cross section under imposed loads (looking from tip toward apex).

*B. W. Raff and T. L. Hoffman.

**This contract represents one phase of the research currently under investigation by Langley Research Center concerning inflatable paragliders, and it pertains primarily to a recovery system for manned space vehicles using an Apollo-type capsule. Goodyear Aerospace Corporation of Akron, Ohio, was the contractor.

The point "0" represents that point on the cross section where the stress is critical for buckling due to the resultant bending moment M_R . Also at that point the value of the shear stress is zero due to V_1 and maximum due to V_2 . The shear stress due to torsion is constant around the ring.

If the inflation pressure is symbolized by p , then the normal stresses are given by

$$\sigma_H = pr \quad (22)$$

$$\sigma_L = p \frac{r}{2} - \frac{A_e}{A} - \frac{M_R r}{I} \quad (23)$$

(The above equation takes into consideration the effect of combined stresses, including the influence of inflation pressure. It is in this respect that the design concept differs from the more conventional practice which deals with noninflation type structures.)

Making substitutions for A and I into equation (23) results with

$$\sigma_L = \frac{\pi p r^3}{2\pi r^2} - A_e r - \frac{2M_R}{I} \quad (24)$$

The shear stress due directly to V_2 for a ring can be stated as

$$\tau_V = \frac{V_2 Q}{2I} \quad (25)$$

and making the proper substitutions for Q and I yields

$$\tau_V = \frac{2V_2 r}{2\pi r^2} \quad (26)$$

The shear stress due to torsion was derived in the previous section as

$$\tau_Z = \frac{Z_e}{2\pi r^2} \quad (27)$$

The resulting shear stress at point "0" is the difference between the shear stress due to V_2 and the shear stress due to torsion, or stated in the form of an equation,

$$\tau_0 = \frac{2V_2 r - Z_e}{2\pi r^2} \quad (28)$$

Reference 2, page 21, shows the expression for critical shear stress in terms of the normal stresses as being

$$\tau_{cr} = \sqrt{\sigma_H \sigma_L} \quad (29)$$

The critical shear stress is defined as the shear stress which causes one principal stress to go to zero (i.e., causes wrinkling in the members). Thus, if the shear stress in equation (28) is made equal to the critical shear stress, the state of incipient buckling at point "0" is defined. From squaring both sides of equation (29) comes the expression

$$(\tau_{cr})^2 = \sigma_H \sigma_L \quad (30)$$

Substituting equations (22), (24), and (28) into equation (30) yields

$$\left(\frac{2V_2r - Z_e}{2\pi r^2} \right)^2 = \frac{pr(\pi pr^3 - A_e r - 2M_R)}{2\pi r^2} \quad (31)$$

Simplification of the above equation and use of the quadratic formula yields a workable expression for determining p.

$$p = \frac{A_e r + 2M_R \pm \sqrt{(A_e r + 2M_R)^2 + (2V_2r - Z_e)^2}}{2\pi r^3} \quad (32)$$

Thus, p is determined based upon the interactional effects of shear, bending moment, axial forces, and torque. Values of the aforementioned forces at various increments along the beam can be substituted into equation (32) yielding a range of inflation pressures. The maximum yielded inflation pressure from this range is selected as the inflation pressure for the structural system and assures that no point on the structural members will wrinkle due to a compressive stress since this was postulated by use of equation (29). It now readily follows that a fabric can be selected which assures that burst will not occur by applying a safety factor to the hoop load (pr).

2. The Keel Structural Member

In considering the keel the problem is altered somewhat in that the inflation pressure is known and emphasis is placed upon determining the radius, which in this case is constant throughout the member's length. A keel cross section subjected to the imposed loads is shown in figure 5.

The point "0" is that point on the keel cross section where the stress is critical for buckling due to the bending moment M_k . It can be seen that the shear stress at "0" due to V_k is zero, and also, that there is no torsional stress.

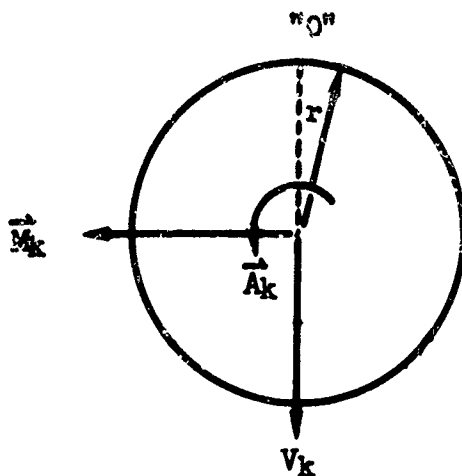


Figure 5.- Keel cross section under imposed loads (looking from tip toward apex).

The normal stresses are given by

$$\sigma_H = pr \quad (33)$$

$$\sigma_L = \frac{pr}{2} + \frac{A_k}{A} - \frac{M_k r}{I} \quad (34)$$

It should be noted that equation (33) differs from equation (22) in that the involved radii are not the same. Also in equation (34) the direction of the axial load A_k is opposite to that of the leading edge. When substitutions are made for A and I in equation (34) the expression becomes

$$\sigma_L = \frac{\pi pr^3 + A_k r - 2M_k}{2\pi r^2} \quad (35)$$

Since the point "O" is critical and there are no shear stresses at this point, the critical shear stress is zero and equation (29) yields

$$\sigma_H \sigma_L = 0 \quad (36)$$

Substituting equation (35) into the above gives a third-order expression from which r can be solved.

$$\pi r^3 + A_k r - 2M_k = 0 \quad (37)$$

It can be seen that the radius of the keel is a function of the inflation pressure, bending moment, and axial forces. Knowing the inflation pressure, and substituting values of the involved forces at various increments along the beam into equation (37) yields a range of radii. The maximum radius from this range is selected as the radius of the keel structural member.

EFFECT OF INFLATIVE GROWTH AND BURST ON FABRICATED RADIUS

Since the structural member will "grow" in size when inflated owing to the hoop strain, it is therefore essential the member be fabricated to a lesser diameter so that, at operating conditions, the configuration will accurately depict the desired aerodynamic geometry.

In accordance with fabric terminology the modulus of elasticity E is measured in pounds/inch. If r_f represents the fabricated radius, then from Hooke's Law,

$$\text{Growth in circumference} = \frac{2\pi r_f p r_f}{E} \quad (38)$$

If the desired aerodynamic radius (the radius the structural member achieves once inflated) is designated r then equation (38) can be rewritten as

$$2\pi r - 2\pi r_f = \frac{2\pi r_f p r_f}{E} \quad (39)$$

from which

$$r = r_f \left(\frac{p r_f}{E} + 1 \right) \quad (40)$$

But

$$\epsilon = \frac{p r_f}{E} \quad (41)$$

and substituting equation (41) into (40) results in

$$r_f = \frac{r}{1 + \epsilon} \quad (42)$$

Thus the member should be fabricated to the radius given by equation (42).

It now readily follows that a fabric can be selected which assures that burst will not occur by applying a safety factor n_0 to the hoop load $p r_f$. That is to say, the required material strength is defined as

$$F = n_0 p r_f \quad (43)$$

Replacing r_f in the above expression with equation (42) gives

$$F = n_0 p \left(\frac{r}{1 + \epsilon} \right) \quad (44)$$

If the strength-to-weight ratio of the material is designated K , then

$$K = \frac{F}{W} \quad (45)$$

and

$$F = KW \quad (46)$$

Substituting the above expression into equation (44) yields an expression for the desired material weight.

$$W = \frac{n_0 p r}{K(1 + \epsilon)} \quad (47)$$

Thus equation (47) represents the governing equation for the selection of material based upon weight requirements, where the weight is expressed as a function of the burst safety factor, inflation pressure, strength-to-weight ratio, strain, and inflated radius. In addition, it is noted that the selected fabric should have equal strength in the hoop and meridional directions since, at the point of maximum stress in the meridional direction the pressure stress and tension bending stress combine to equal the stress in the hoop direction.

CONCLUDING REMARKS

For an advanced concept paraglider whose inflatable structural frame is composed of curved tapered leading edges and a cylindrical keel, analytical formulas are presented in the paper which will allow, for defined load conditions, the determination of:

(1) The required pressurization to assure that the leading edges will not buckle under load.

(2) The diameter required for the keel, compatible with the internal pressurization, which assures that the keel will not buckle under load.

In addition to the above, methods are included on selecting fabric strengths to safeguard the frame against burst and on defining the frame's fabricating size so that, under pressurization growth, the frame will assume the desired aerodynamic size.

REFERENCES

1. Forbes, F. W.: Expandable Structures. Space/Aeronautics, Dec. 1964, pp. 62-68.
2. Introduction to Structural Analysis of Expandable Structures. GER-9870.
3. Hoffman, T. L.; and Raff, B. W.: Advanced Concept Inflatable Paraglider Prototype and Model Design. Contract No. NAS1-3020, GER-11520.
4. Singer, Ferdinand L.: Strength of Materials. Harper and Brothers Publishers, New York, 1951, ch. 5.
5. Singer, Ferdinand L.: Engineering Mechanics. Harper and Brothers Publishers, New York, 1954, Second Edition, ch. 8.

DEVELOPMENT OF SPACE EXPANDED AND RIGIDIZED SOLAR
ENERGY COLLECTORS

By

Seymour Schwartz

Materials Technology Department

Hughes Aircraft Company

Culver City, California

INTRODUCTION

The largest problem in the use of inflatable solar concentrators in space programs is the development of a feasible technique for their fabrication. This technique must produce concentrators that are light in weight and easily packaged in a small volume. More important, it must be possible to inflate and rigidize them in a space environment and the rigidized concentrator must have a specified form suitable for its function.

The Hughes Aircraft Company, under NASA Contract 1-3244, undertook to develop the techniques and produce concentrators that would meet the following general requirements. The concentrator should be packageable in a small volume and be automatically inflated in space to form a rigid paraboloid. The reflecting surface of the concentrator was to be aluminized polyester film formed by the Hughes "no master stress-relaxation" process. The back surface of the aluminized film was to be covered with a flexible reinforcement coating that would become rigid after the concentrator was inflated in the space environment.

Originally it was planned that the reinforcement would be a polyester-resin-fiberglass laminate, activated by ultraviolet radiation. After a number of tests had been made, however, it was decided that this reinforcement system possibly would not result in the highest quality optics. Therefore a coincident investigation was also made into the use of an epoxy syntactic foam as a reinforcement. With either type of reinforcement it was planned that the final assembly weight would be approximately 0.4 lb per sq foot.

This report covers the experimentation and testing which led to the production of concentrators able to meet the contract requirements. Three major problems were involved. First, techniques had to be optimized for inflating the paraboloid assembly to the specified form. A second problem was the development of a suitable rigidizing layer, one which would also produce an acceptable optical surface on the polyester film. The third problem concerned a method for bonding the rigidizable layer to the film,

which normally acts as a parting agent. Complicating all these problems was the requirement for inflation and rigidization in the high vacuum of a space environment. This was a particularly difficult requirement for the chemical rigidizing process, since such processes normally occur in a pressurized, terrestrial environment.

CONCENTRATOR DESIGN

The general design and configuration of the paraboloid fabricated is illustrated in Figure 1. The paraboloid is five feet in diameter and is encircled by a torus six inches in cross section. The reflective surface of the paraboloid is 2-mil aluminized polyester film and the outer, clear pressure retaining membrane is 2-mil clear polyester film.

As shown in Figure 1, both film surfaces are formed of a series of hexagonals, joined by a heat-sealing technique. This mosaic surface eliminates the gored construction usually employed for such structures and has several other advantages. First, most proposed space collectors are very large, with diameters of from 30 to 100 feet. Since aluminized polyester film is currently not available in widths greater than five feet, the mosaic technique provides a means of making uniform surfaces of unlimited size.

A second advantage of the mosaic construction lies in its suitability for the technique developed to form the paraboloid. This technique is a Hughes proprietary process, in which a film is formed to the desired parabolic curvature by a combination of stretch and relaxation techniques, without using a costly master form. When using this technique with conventional pie-shaped gore construction, the unequal stresses throughout the surface, due to the concentration of seals at the center, prevent attainment of the correct curvature. Use of the mosaic surface, with its equally distributed seals, eliminates this difficulty.

The five-foot diameter paraboloids and torus assemblies were ordered from an outside vendor. The torus assemblies attached to the paraboloids were also made of 2-mil polyester film, since preliminary 2.5 psi would not buckle when acted upon by the internal pressure of 0.5 psi needed to form the paraboloid.

It was planned then, after receipt of the assemblies from the vendor, to inflate them to the required shape, then apply the rigidizing layer. On subsequent curing, in a vacuum environment, the part should assume the correct shape permanently.

In previous, Company funded efforts, Reference 1, a technique had been developed to form polyester film materials to a paraboloidal shape without a master form tool. This technique consists, in brief, of overstretching a film by pressurization, or vacuum. Then on relaxation, the film in returning to its original shape goes through a number of curves, including a paraboloid. Establishing the correct pressure to result in a paraboloid was then a relatively simple task. The paraboloidal shaped film could then be used as a master for subsequent layup of the rigidizing layers. However, after layup of the first few trial parts it was found that the paraboloid had to be formed, in the relaxed state, with an absolute minimum of residual stresses, or gross, physical distortion would result as soon as the cured part was removed from the fixture.

POLYESTER RIGIDIZATION

The rigidizing technique initially utilized was an ultraviolet activated polyester resin system originally developed on a NASA contract, as a possible successor to the Echo II balloon, Reference 2. After making a few sample parts, however, it was found that the use of this technique gave rise to several problems. First the polyester resin, as is characteristic of most polyesters, showed very poor adhesion to the underlying film. This adhesion was so poor that the initial samples delaminated partially due to the stresses in the film. More serious than the delamination, however, was the fact that wherever the film did adhere to the fiberglass laminate the optical surface was quite poor. This degraded optical surface had two forms, a patternless, uneven, distortion and a uniform, regular distortion in which the fabric weave was visible on the optical surface.

Polyester resins, when impregnated into a fabric, inherently do not result in a good surface, because of the relatively high volumetric shrinkage. Since fabric "show-through" is a well known phenomena with polyester resins, it is common commercial practice to utilize a heavily filled gel coat between the mold and the fiberglass laminate. An investigation was therefore made into materials which could act as a gel coat to help hide the fabric pattern.

The gel coat to be useful for the particular paraboloid fabrication problem would have to be more than a heavily filled material to which the polyester resin would adhere. It would also have to have good adhesion to the polyester film, normally a parting agent, and would have to be flexible in the cured state. A number of materials were tested which appeared to meet the requirements. These include several urethane coatings, a silicone RTV and a Butyl rubber cement, a flexible polyester and a flexible epoxy coating and several types of polysulfide coatings. These latter materials were found to give the best combination of properties, and so were selected as the intermediate coating between the polyester film and the polyester rigidizing layer.

TOOLING

Even with the use of the polysulfide gel coat, a great deal of irregular, patternless distortion occurred in the small, one-foot diameter, rigidized samples which were made initially. These first samples were all made at normal room pressures, in order to first develop an optically satisfactory technique. The type of fixture used for these first test samples was a simple metal fixture in which the film was inflated as a diaphragm. With this fixture, obviously the reflective surface could not be examined until the part was removed. It was therefore impossible to determine if the distortions in the reflective surface were due to the gel coat application or occurred with the application of the final polyester rigidizing laminate, or on cure of this laminate. In order to determine at what stage the distortion commenced, then, the original fixture was modified to include a transparent window, Figure 2. This worked so well that a number of smaller, (6 in. diameter) solid acrylic fixtures were also made, Figure 3.

OPTICAL TESTS

With the use of the transparent fixtures it was possible to observe the effect of each coating on the aluminized polyester film. No discernable

distortion was found on application of the gel coat. Distortion, however, did become noticeable with the onset of polyester gelation. A number of types of polyester resins, and fabric combinations were tested. In general, it was found that materials known to have low shrink characteristics, such as the diallyl phthalate based materials, combined with the finest, practicable weaves of cloth, resulted in the best surfaces. Non-woven reinforcements such as felts, mats and overlay veils were also tried without, however, any noticeable improvement. In each case, of course, the resin was one which was ultraviolet catalyzed, so it could be automatically set up in space.

After preparing a great number of samples using the various polyester combinations, several samples were prepared using room temperature cured epoxy resins. An immediate improvement was noted, Figure 5. It was therefore concluded that the inherently large shrinkage of the polyester system would always act as a barrier to attainment of the highest optics. Tests were therefore made to determine if an epoxy system could be developed to result in both rigidity and satisfactory optics.

EPOXY RIGIDIZATION

The first tests made with an epoxy system utilized an epoxy resin and a finely powdered silica filler. Excellent optical results were secured. However, the resulting cured structure, approximately 0.1 inch thick, was both too heavy and much too brittle. Further tests, made to develop a more satisfactory coating, resulted in a syntactic foam utilizing an epoxy resin, and phenolic microballoons as the filler. A special catalyst system was developed which cured in several hours at 240° F, but gave a room temperature shelf life of approximately two months. The use of syntactic foam gave much improved optical results, Figure 5. Because of the success of the epoxy syntactic foam some tests were also made to develop an ultraviolet cured polyester syntactic foam. However, because of the opacity the phenolic microballoons could not be used with this system. Glass microballoons were tried, but were also too opaque if used in the thickness required.

FILM HEAT TREATMENT

With the advent of the heat cured epoxy system another problem arose; that of shrinkage of the polyester film after heating. It was found that the film, as received from the vendor, shrank as much as 1 1/2 percent on heating for a short period at 325° F. This shrinkage, during cure of the rigidizing coat, could then interfere with obtaining optimum curvature in the heat cured epoxy rigidized parabola or might cause distortion, in service, of the polyester cured parabola.

A series of tests were made on the aluminized film and it was found that 16 hours at 250° F caused the shrinkage rate to be reduced to an almost asymptotic value. The 16 hour treatment at 250° F was therefore used to "pre-shrink" all the film used for later fabrication tests.

For maximum results, the pre-shrinking should take place at 325°F. However, visual examination of the aluminized film heat treated at this temperature indicated a slight decrease in the brilliant luster, so the 250° F temperature was chosen for use.

VACUUM TESTS

All of the above tests of the polyester and epoxy rigidization systems were made with the rigidizing layer maintained at normal room pressure conditions. (The reflective film of course, was pressurized as required to obtain the parabolic shape). With the development of the syntactic foam system a series of tests were made to determine the behavior of each system under vacuum conditions.

The first tests made with either system indicated that, under vacuum conditions, the optical results would be considerably degraded. When rigidization was attempted in the vacuum with the polyester system the volatiles in the resin, plus dissolved air, caused considerable delamination, with resultant degradation of the optical surface. Tests of a syntactic foam covered surface gave approximately the same results, since dissolved air and other volatiles in the foam caused considerable bubbling of the foam. (The foam was de-aerated as much as possible prior to application on the paraboloid).

A number of inflation-pressurization techniques were tried in an effort to impose a back pressure on the laminate or the foam during the cure cycle. None were particularly effective or automatic, until a mechanical back-pressure system was developed. In this system two perforated, non stretched, 1/2 mil polyester film diaphragms were placed over the reinforcing layer when the assembly was in the deflated position. Later, on inflation, the perforated diaphragms acted as mechanical restraints on the laminate at the same time the perforations allowed the volatiles to escape, thus preventing bubbling or delamination. In addition to acting as a back-pressure media the diaphragms were used as parting agents to prevent sticking and/or delamination when the entire structure was packaged. Figure 6 illustrates the back pressure membrane technique.

Another problem brought out when vacuum tests were initiated was the difficulty in maintaining the required curvature during the cure cycle. This was particularly true with the epoxy syntactic foam paraboloid since, as heat was applied, the internal pressure increased and at the same time all the components in the structure softened slightly. Control of the curvature therefore could not be done simply by pressure control. A system was finally developed in which movement of the paraboloid surface actuated solenoid valves which in turn either admitted pressurizing air or vented the paraboloid interior to the vacuum. This control system was based on the use of fixed reference wires, attached to a ring holding the structure, and a sensor contacting the paraboloid's apex. In actual service, of course, another system would probably be used, possibly based on variation of focal length.

With the development of the back pressure membrane and the electrical position sensor it was then possible to prepare the five foot diameter paraboloids of either type and to demonstrate their packaging abilities and the automatic expansion and rigidization techniques.

PACKAGING

The packaging demonstration was made using the syntactic foam reinforced paraboloid, since it was the stiffest and the bulkiest of the two paraboloids. The paraboloid was rolled into an approximately 8 inch diameter roll, 5 1/2

feet long. The rolled up structure had a hollow space 4 inches in diameter into which could be placed air bottles, valves, etc. In the demonstration, illustrated in Figure 7, plant air lines were used, instead of independent air bottles, however. As shown the structure automatically released itself from the container and inflated to full size. The torus pressure used was 2 1/2 psi and the paraboloid pressure was .1 psi (note: as shown in the illustration this was not enough to cause full inflation, since it was desired not to stretch the structure).

PARABOLOID FABRICATION

Two demonstrations were made of the expansion and rigidization capabilities of each system. The first paraboloid demonstrated consisted of the preformed two mil aluminized polyester film and was reinforced with a laminate consisting of seven fiberglass layers and a diallyl phthalate resin. In addition the two unstretched, 1/2 mil perforated back pressure diaphragms were installed. The structure was placed in the altitude chamber, unpressurized, and brought to the correct curvature automatically and maintained at that curvature during the cure period. To cure the polyester laminate eight 40 watt tubular ultraviolet lamps were preinstalled in the chamber. Despite the relatively low powered radiation source the parabola appeared fully cured after a four hour period, at a simulated altitude of 113,000 feet.

The second demonstration paraboloid was a pre-coated epoxy syntactic foam paraboloid. The rigidizing layer of syntactic foam was 0.1 inch thick, and included two 1/2 mil perforated diaphragms. Because the heat could not be applied evenly on this structure it was cured very slowly, the curing cycle was 24 hours during which time the edges of the apt were gradually raised to 200° F while the center reached 248° F. During this period the curvature also was continually monitored.

In both the demonstrations a good paraboloid was obtained, and as in previous tests, the optical surface of the syntactic foam reinforced paraboloid appeared to be somewhat the better. Figure 8 shows an informal test of the syntactic foam reinforced paraboloid. The weight of the five foot diameter polyester paraboloid was 7.88 lb, with a unit weight of 0.40 lb per sq ft. The epoxy paraboloid weighed 8.11 lb, with a unit weight of 0.42 lb per sq ft.

After removal of the paraboloids from the forming fixture it was found that neither type was rigid enough for mounting on an optical test fixture at the three specified points, without gross distortions in curvature. The lack of rigidity in each case was due to the weight of the structure, since when the paraboloid was uniformly supported on the edges, by being placed on a table, each structure appeared uniformly curved. To correct this weakness, a light ring of epoxy impregnated glass braid was bonded to each structure. This produced the necessary rigidity.

In addition to preparation of the required five foot diameter paraboloids, several other paraboloids were prepared during the course of checking out the equipment, determining the cure procedure, etc. From these test paraboloids, physical test specimens were cut so that a quantitative measure of the physical properties might be obtained. The results of these tests are shown below in Table 1.

Physical Properties of Residization Layers

Test Type	Temp. of	Epoxy Str., psi	Foam Mod., psi	Polyester Str., psi	Laminate Mod., psi
Tensile	72	593	336,000	13,300	655,000
Tensile	240	282	143,000	4,460	156,000
Flexural	72	721	-	17,000	-
Flexural	240	518	-	299	-
Edgewise	72	625	-	593	189,000
Compression	240	140	89,600	335	-

TABLE 1

The values shown in Table 1 are very low in comparison to laminates made under normal pressurization conditions. For the purpose intended, however, the strengths appear to be adequate.

Two specimens approximately 2 1/2 x 4 inches of each material were placed in quartz vacuum chambers to determine the effects of high vacuum and infrared and ultraviolet radiation. Each specimen had a small thermocouple mounted on the rear (non-aluminized surface) with the junction imbedded in the specimen, in contact with the aluminized surface.

The samples were maintained at a vacuum of approximately 10^{-6} mm Hg for 240 hours. The surface temperatures were maintained at 180° F using five infrared heating lamps. (This was the maximum temperature which could be obtained.) The ultraviolet lamp (in the housing) maintained one solar equivalent radiation on the samples for the duration of the test. After the exposure period the samples were tested for loss of weight and change in physical appearance. The loss in weight amounted to approximately 4 1/2 percent for the epoxy and 7.0 percent for the polyester samples. There was no apparent change in the appearance of the epoxy reinforced samples. The polyester samples, however, showed a small amount of surface wrinkling, due no doubt to degradation of the polysulfide gel coat.

A number of tests were also made to determine the optical characteristics of the completed paraboloids. The reflectivity of the polyester paraboloids averaged 79.3 percent while that of the epoxy foam paraboloids averaged 82.0 percent. Surface angular deviations and axis intercepts were also determined on the paraboloids made at the simulated 113,000 ft altitude. The results indicated that the surfaces were generally parabolic, but with some astigmatism present. The surface angular deviation from a true paraboloid was within $\pm 1.0^\circ$ for both structures.

Calorimeter tests were also made to determine the efficiency of the completed paraboloids. A water cooled calorimeter with various sized asbestos aperture plates was used. The ambient solar flux was monitored with an Eppley pyrliometer. Figure 9 illustrates the test setup. The results of the tests indicated that the epoxy paraboloid had an efficiency of 45 percent at an area ratio of 900 and an efficiency of 19 percent at an area ratio of approximately 6500. The polyester reinforced paraboloid had an efficiency of 41 percent at an area ratio of 900 and an efficiency of 27 percent at an area ratio of 3600.

REFERENCES

1. J. P. Bagby, "Report on Solar Concentrator Work During 1962," Hughes Aircraft Company, Rept. TM-739, Jan 1963
2. "Final Report - Space Structure Rigidization," Hughes Aircraft Company, Report P 61-13, Sept. 1961
3. S. Schwartz and J. P. Bagby "Rigidized Inflatable Solar Energy Concentrators," Hughes Aircraft Company Report P 64-123, Dec 64

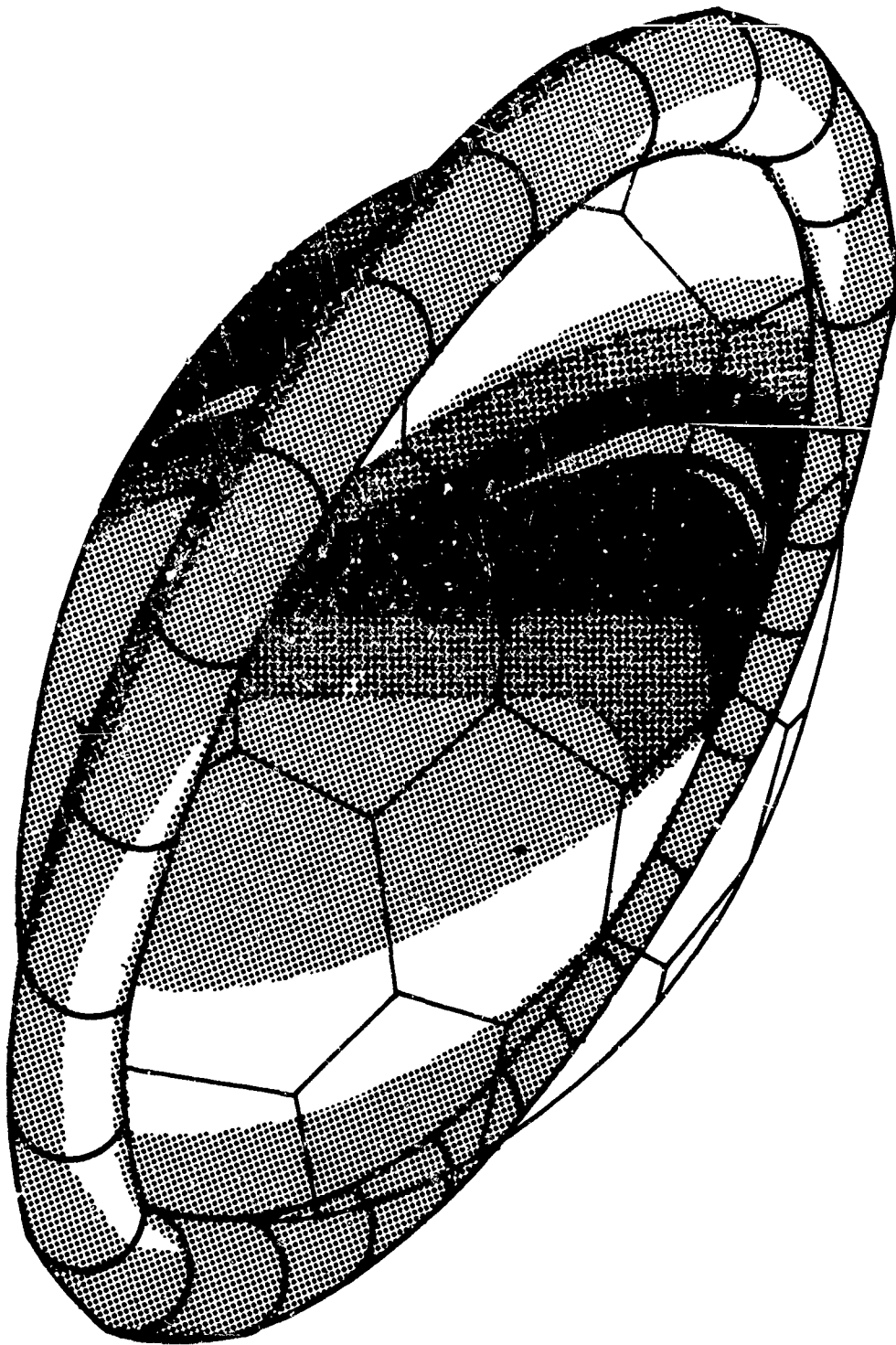


Figure 1. General Configuration of Solar Concentrator

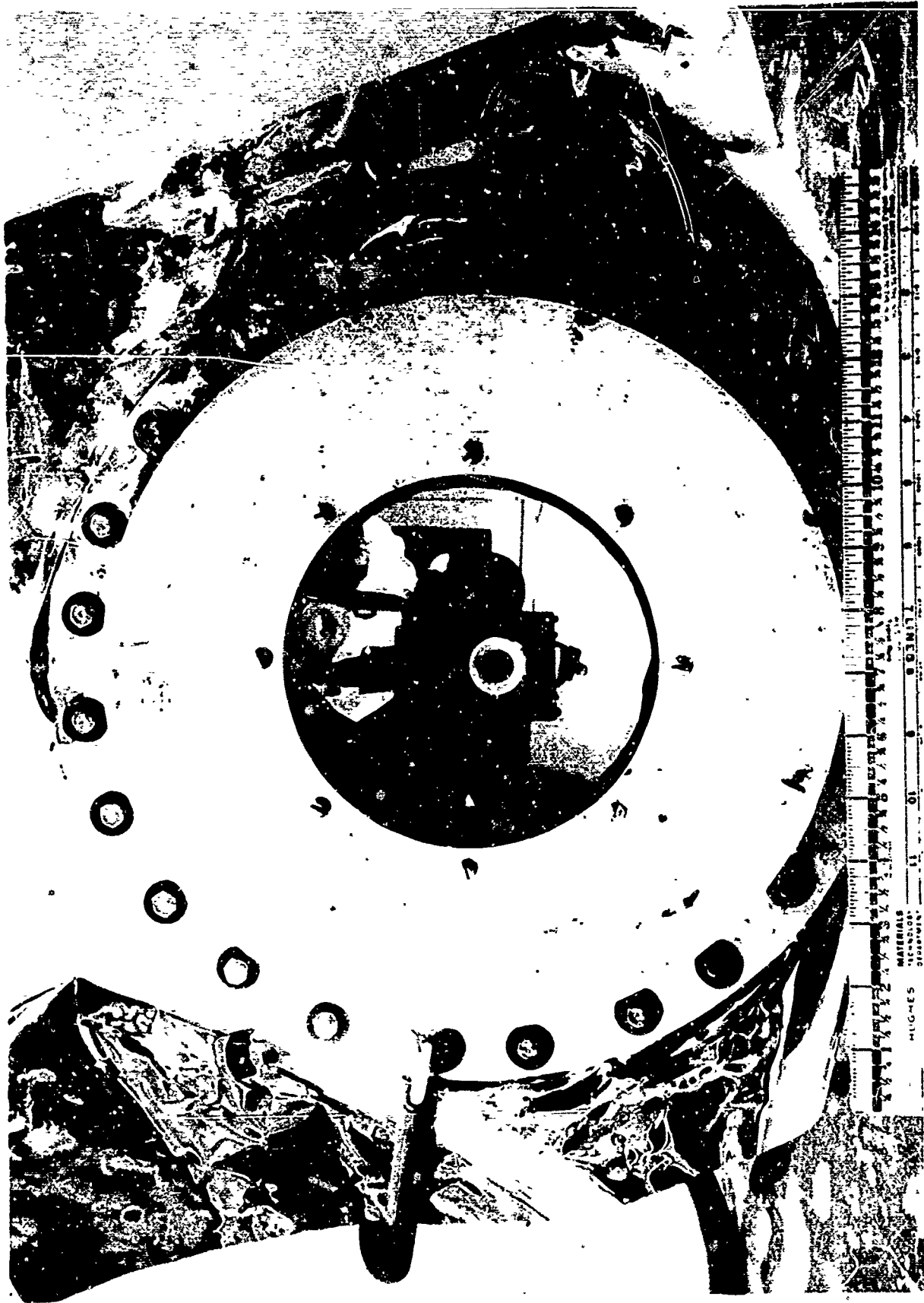


Figure 2. Reflectivity of Inflated Aluminumized Film

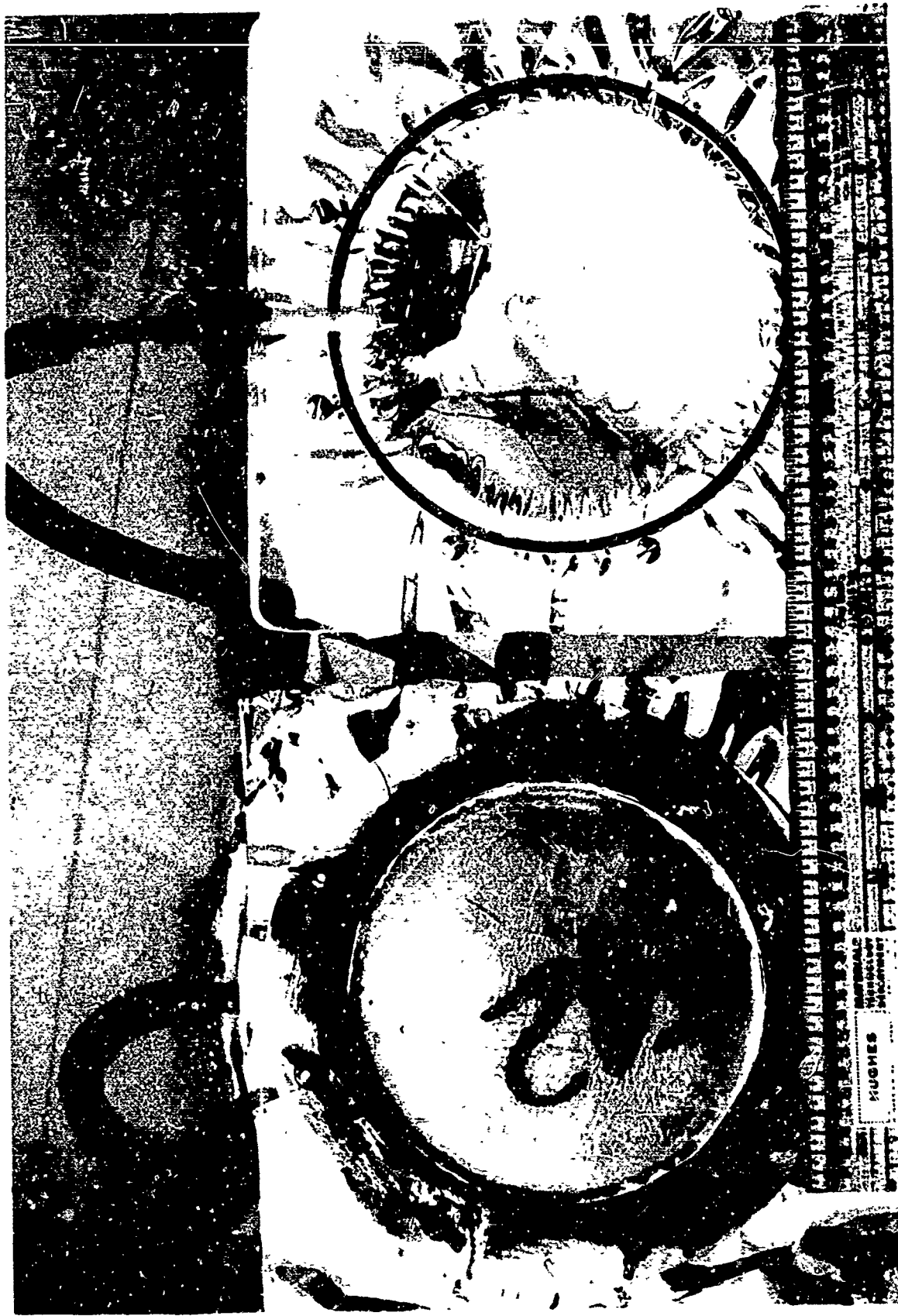


Figure 3. Small, Transparent Acrylic Forming Fixtures



Figure 4. Comparisons of Optical Quality of Polyester vs Epoxy Rigidized Paraboloids

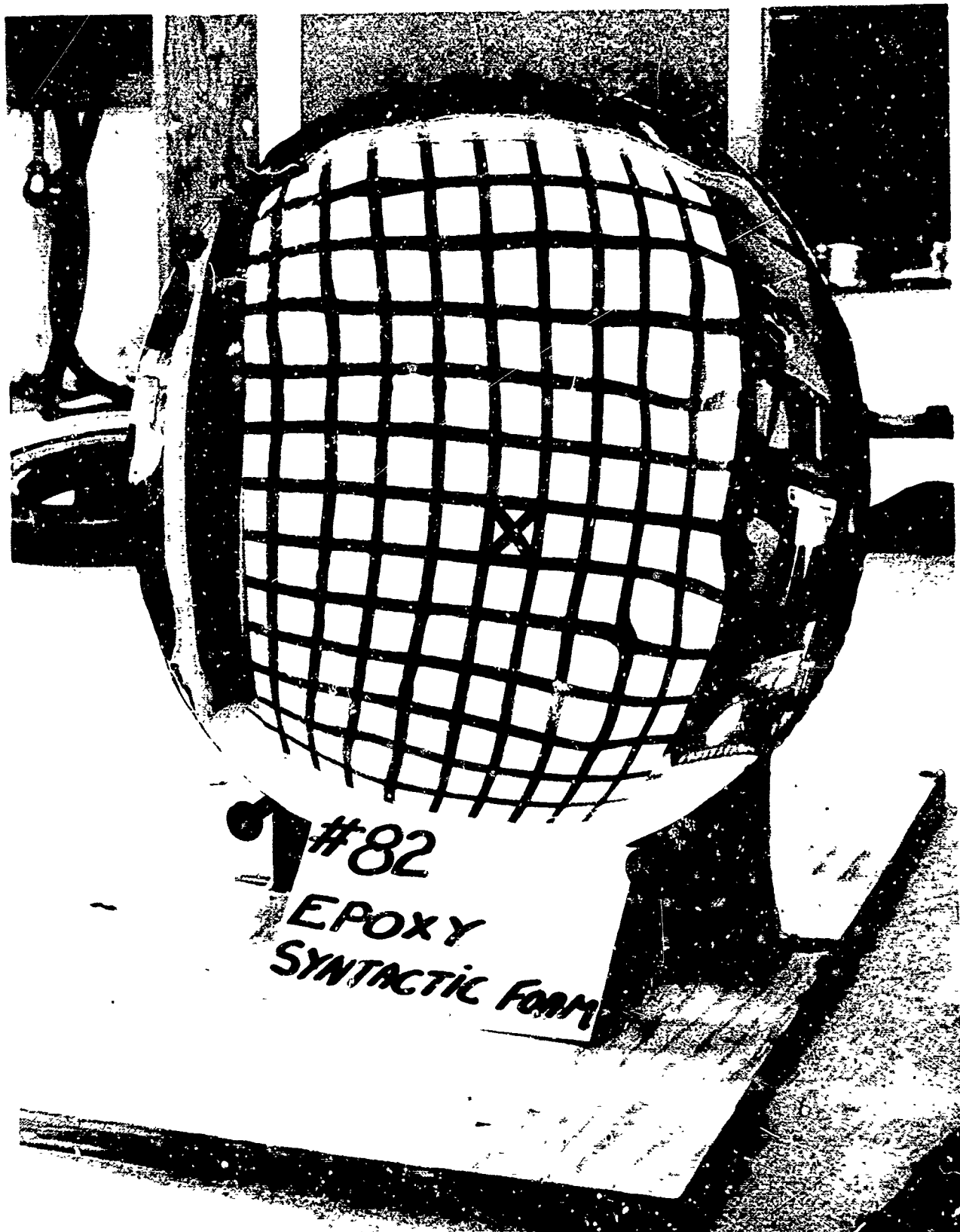


Figure 5. Two-Foot Diameter Parabola Rigidized with Epoxy Syntactic Foam

TWO 1-MIL PERFORATED
DIAPHRAGMS

2-MIL ALUMINIZED FILM

REINFORCEMENT

PRESSURIZED AS
REQUIRED TO
MAINTAIN SAGITTA

Figure 6. "Back Pressure" Membranes

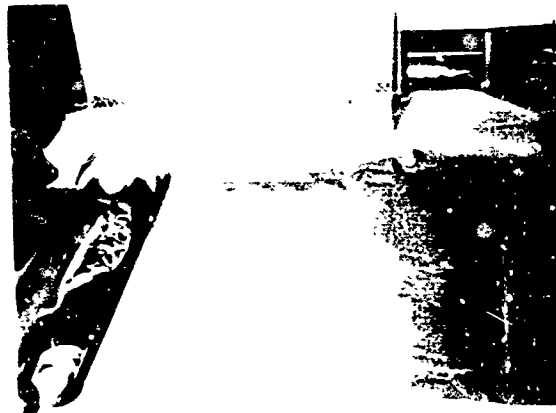


Figure 7 Packaging Sequence



Figure 8 Foam Reinforced Paraboloid

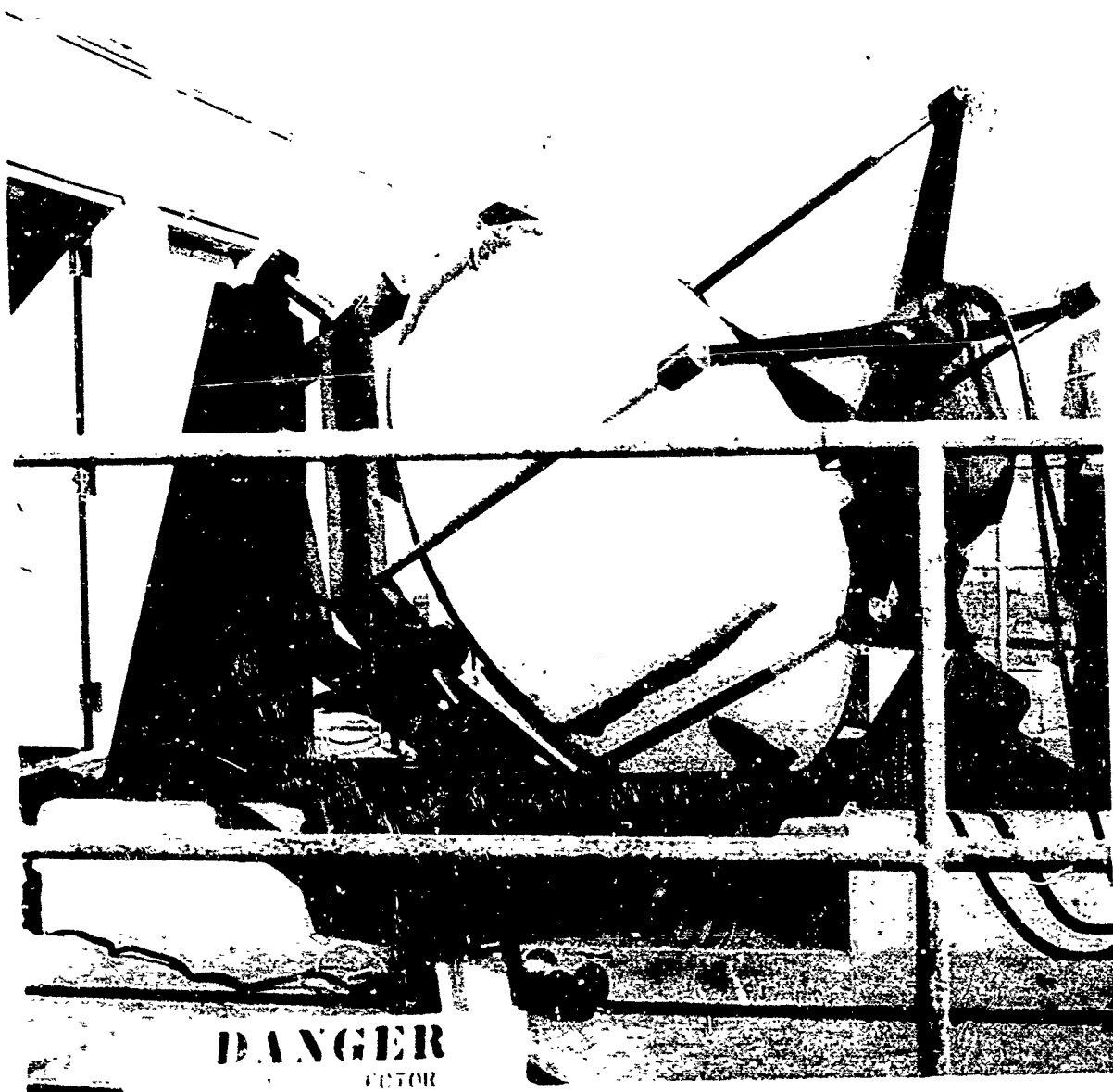


Figure 9 Test Set-up for Determining Calorimetric Efficiency

SESSION VI

ALUMINUM FOIL EXPANDABLE STRUCTURES

BY S. MOTTA
Sr. Consulting Engineer
Research Directorate

RESEARCH AND ADVANCED DEVELOPMENT DIVISION
AVCO CORPORATION
WILMINGTON, MASSACHUSETTS

ALUMINUM FOIL EXPANDABLE STRUCTURE

INTRODUCTION

The work presented in this paper is the result of an investigation conducted by the Research Directorate of Avco RAD, largely company sponsored, to determine the feasibility of using aluminum foil to fabricate expandable space structures.

The choice of a metallic foil, over the more pliable plastic counterpart, was dictated by the two goals we set out to reach:

- (1) Automatic rigidization of our deployed shapes
- (2) The highest possible reliability index of our structures to survive space environment.

A survey of the field indicated that most of today's expandable structures fall into one of the following categories: (a) pressure dependent structures, (b) structures achieving rigidization through the medium of additives such as resins, permanently bonded to the expandable material, and finally (c) foamed in place double wall structures. Each category does justice to a particular set of structural requirements and, I am sure, is not meant to be offered as an optimum solution to all inflatable structural problem.

Our structure is not pressure dependent, does not use resins or foam for its rigidization, and therefore, does not fall in any of the aforementioned categories nor does it necessarily attempt to solve the same type of problems.

Our entire approach to the general problem of inflatables stems from the very basic fact that if you stretch a piece of aluminum foil so as to induce a membrane stress of 5,000 to 6,000 psi, depending on its thickness, you have caused the foil to reach a state of permanent set, allowing it to retain its inflated shape even after complete depressurization.

Briefly stated, we set out to achieve rigidity as a by-product of controlled stretching, and thereby substantiate our first goal of automatic rigidization.

It was reasoned that if this state of metallic "rigor mortis" so to speak, could be achieved by using dead soft aluminum foil as bought from the producer, without any special treatment, we would be well on our way to substantiating our second goal, i.e. a high reliability index. The rest of this paper will offer documentary proof of the feasibility of the concept. Before getting into the more technical aspects of the problem, however, and in order to provide a ready visual reference to some of the facts and figures to follow, I should first like to show a movie of the erection of a corner reflector which was our first piece of hardware following a thorough study of the physical properties of our medium: 99% pure dead soft aluminum foil.

It consists of six arms deploying in the x,y,z directions from a central pressure source located at the origin of the axis. The first frames show a two foot model with triangular mylar sails going through the expansion three times. This is followed by the erection of one of the six arms full size. It is a column 16 ft. high, 6 inch diameter, $\frac{1}{2}$ mil thick. (3 minutes of movie follows).

The fabrication of this corner reflector was, of course, preceded by a thorough study of the foil itself. Several foils were screened for mechanical and chemical properties before it was decided to work with aluminum foil 1145 H2E4. This is Alcoa's designation for a foil with a nominal purity of 99.5% aluminum. Although this foil is usually annealed before final inspection, Alcoa chose the term H2E4 to denote the residual temper due to cold work generated by the rollers. Several thicknesses of foil were analyzed for chemical composition. The following table shows the results of our chemical study.

TABLE I

Nominal Thickness of Sheet (inches)	Alcoa Lot No.	Element %							
		Fe	Cu	Ti	Mn	Mg	Zn	Si	Al
0.0005	966-874	0.1	0.05	0.01	0.01	0.01	ND*	0.01	99.72
0.0010	966-878	0.1	0.05	0.01	0.01	0.01	ND*	0.01	99.72
0.0015	966-875	0.1	0.05	0.01	0.02	0.01	ND*	0.01	99.71

* not detected

Variations in thickness were another problem. Alcoa reports the commercial tolerance of thickness control is $\pm 10\%$ of nominal. This appears to be generally true although very accurate measurements with a Van Kewren light wave micrometer revealed deviations as great as 14%.

TABLE II

VARIATION OF FOIL GAGE WITHIN A GIVEN LOT

Nominal Thickness (inches)	No. of Observations	Range of True Thickness (inches)	Max. Deviation From Nominal (%) Thickness
0.0015	48	0.0015 - 0.00160	+6.6
0.001	42	0.00109 - 0.00114	+14
0.0005	51	0.00052 - 0.00057	+14

Aluminum foil is likely to contain tiny perforations commonly referred to as "pin holes" which seem to be the inevitable result of rolling metal to very thin gages. The following table summarizes the results of microscopic examination conducted by Alcoa, where 100 sheets were examined for each gauge.

TABLE III
TYPICAL VARIATION OF PINHOLES WITH GAGE

Nominal Thickness of Foil (inches)	Number of Sheets With Pinholes	Number of Sheets with no Pinholes
0.00035	100	none
0.0005	100	none
0.0007	15	35
0.001	8	92

Exhaustive stress-strain studies were made. The specimens measured approximately 6" in length and 0.50" in width, the edges being parallel throughout the length. Because of the thinness of the foil accurate determination of cross sectional area was critical. Hence, all measurements were made by Avco's measurements section. The width was measured to ± 0.001 by a "Sip" machine and the thickness ± 0.000010 " by a Van Keuren light wave micrometer. Tables IV to VII show the results.

Figure 1, page 7, shows typical stress strain curves for the range of thicknesses used in our work. Both yield and ultimate stresses increase with the thickness of the foil. This effect is believed to be the result of nicks, severed edges, non uniformity and the wrinkles which could work the material all of which are most likely to occur in specimens of smaller gauges.

Figure 2 plots this effect, as well as the percentage elongation for the various thicknesses. The results reported for elongation were determined by fitting the fractured specimens together and measuring the distance between gauge marks.

Armed with this information, we started fabricating our column test samples. Seam bonding of the edges, required for the fabrication of a tubular member, was one of

TABLE IV

TYPICAL STRESS-STRAIN PROPERTIES OF 1145-H2E4 ALUMINUM FOIL, 0.005 IN. GAGE

With Respect To Rolling Direction	Yield Stress .2% Offset PSI	Ultimate Tensile Stress, PSI	Young's Modulus $E \times 10^{10}$ PSI	Elongation (%)
	4260 4140 3900 3940	6240 6450 5840 6090	10.0 10.1 10.0 9.9	0.9 1.1 1.0 1.4
	4060 170	6155 260	10.0 0.08	1.1 0.22
	3990 4180 4080 4040	5800 6080 5950 5510	10.0 9.8 9.9 10.0	1.1 1.1 1.2 0.86
	4073 80	5835 250	10.0 0.15	1.1 0.14

TABLE V

TYPICAL STRESS-STRAIN PROPERTIES OF 1145-H2E4 ALUMINUM FOIL, 0.01 IN. GAGE

With Respect To Rolling Direction	Yield Stress .2% Offset PSI	Ultimate Tensile Stress, PSI	Young's Modulus $E \times 10^{10}$ PSI	Elongation (%)
	3760 4310 4120 4200 3980 4030	6890 6820 6980 6800 6390 6280	9.9 9.9 10.1 10.2 10.0	2.3 2.3 2.3 2.3 1.6 1.6
	4067 190	6693 290	10.0 0.13	2.07 0.36
	4250 3920 3900 3760 4170 4090 4030	6370 6240 6410 5990 6570 6480 6280	9.6 10.1 10.4 9.9 9.8	1.6 2.3 2.0 1.6 1.6 2.0 1.6
	4017 170	6334 190	10.0 0.31	1.81 0.29

TABLE VI

TYPICAL STRESS-STRAIN PROPERTIES OF 1145-H2E4 ALUMINUM FOIL, 0.0015 IN. GAGE

With Respect To Rolling Direction	Yield Stress .2% Offset PSI	Ultimate Tensile Stress, PSI	Young's Modulus $E \times 10^{10-6}$ PSI	Elongation (%)
	3970 4070 4040 4560 4190	7930 8350 8530 8040 8140	9.6 10.2 9.9 9.9 10.0	3.1 3.9 4.7 3.3 4.7
	4166 230	8198 240	9.9 0.22	3.94 0.76
	4070 4100 3910 4070 4120	7730 7810 7460 7440 7570	9.4 10.1 10.0 9.8 10.2	4.5 4.7 3.9 3.9 3.9
	4054 80	7602 160	9.9 0.32	4.18 0.39

= sample arithmetic mean

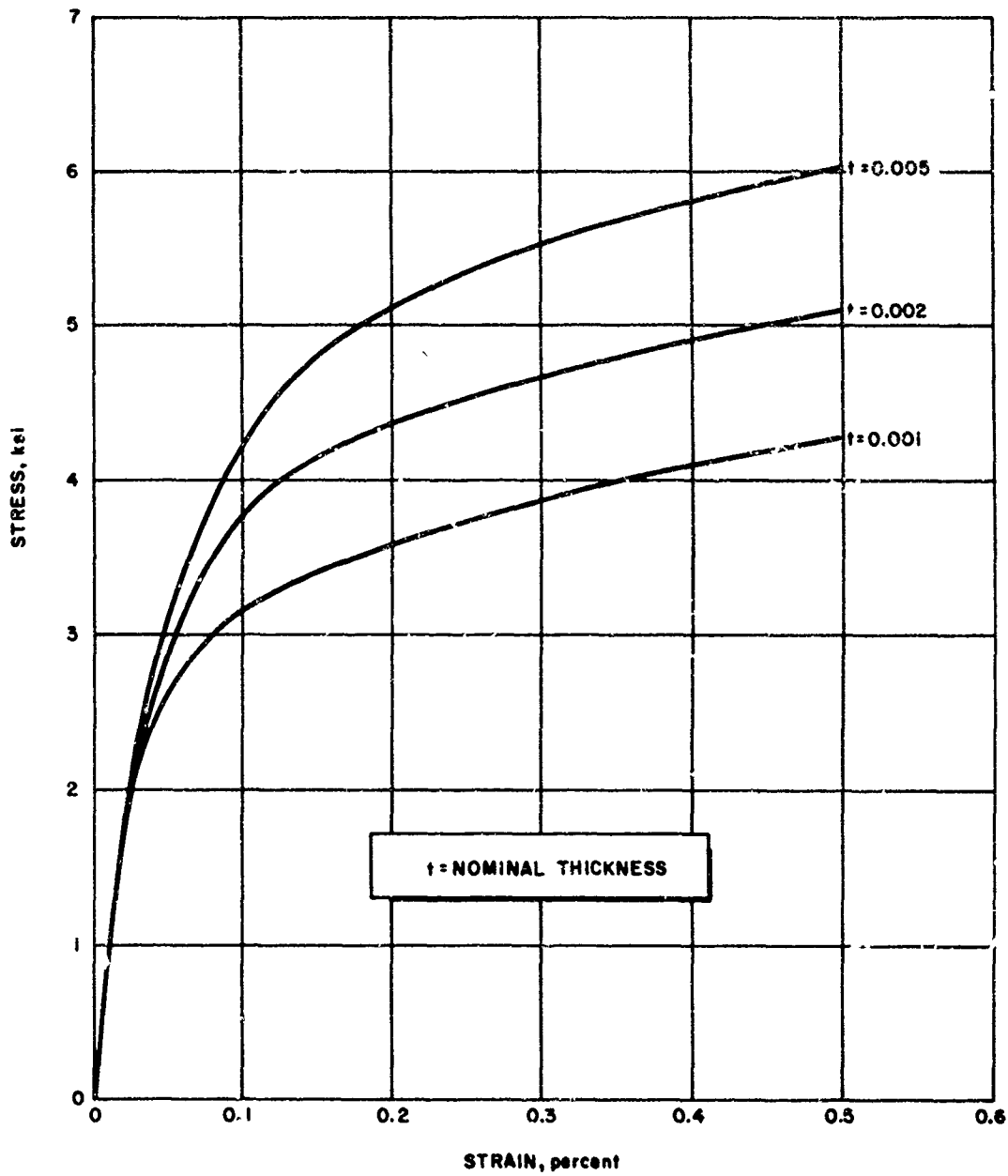
= standard deviation

Identical tests for $t = 0.002$ and $t = 0.005$ yielded the following results:

TABLE VII

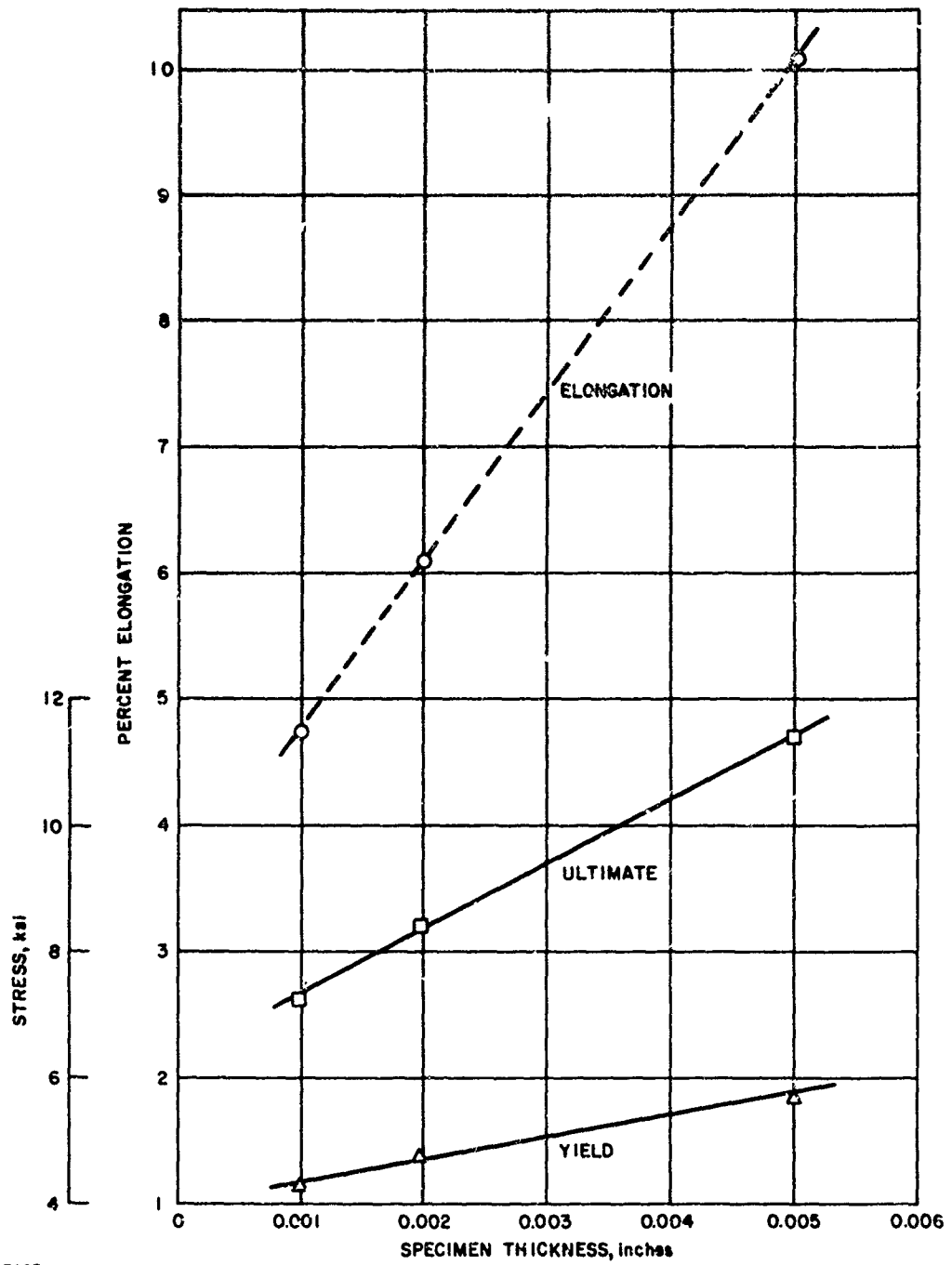
RAD FGT TESTING MACHINE

Spec. No.	Nominal Thickness (inches)	Ultimate Stress (psi)	Yield Stress (0.2% offset) (psi)	Elongation %	Young's Modulus $E \times 10^6$ (psi)
2-1	0.002	8290	4370	6.3	10.0
2-3	0.002	8590	4570	6.2	10.1
5-1	0.005	12000	5360	7.8	10.1
5-3	0.005	11900	5700	12.5	--



65-3824

FIGURE 1 TYPICAL STRESS-STRAIN CURVES



65-3665

FIGURE 2 VARIATION OF ULTIMATE STRESS, YIELD STRESS AND ELONGATION vs. THICKNESS

the first hurdles. The modern advances in electron beam welding have made the edge welding of two aluminum foils a matter of routine. An adapter kit was designed for installation on a Hamilton Standard electron beam welder, which would allow the wrapping of two identical aluminum foil ribbons on a round reel. The free ends of the ribbon are made to pass through two copper chill plates and on to the driver reel. The electron gun aims directly at the free edges of the ribbons and starts welding as soon as the chill plates have locked on to the foils. The operation is repeated until the full length of one edge of the foil is welded. To weld the other edge, you reverse your reels and proceed as before. This is a recent development and was not available at the time we were ready to run the tests.

For the purpose of our tests, however, where life expectancy was not the important problem, ordinary cellophane tape was found adequate to carry the hoop stresses caused by internal pressure. Figure 3 shows a typical test setup for the tubes thus fabricated. A gravity loading system was used in the test, allowing a positive determination of collapse of the tube. Each tube was inflated to a pressure corresponding to a calculated hoop stress equal to its yield. The pressure was measured with a manometer connected to the air supply hose. By using a plump bob for guiding and shims under the base, the tube was aligned vertically. Loading was accomplished by slowly adding lead shot to the receptacle until collapse occurred; at this time, the funnel took up its initial slack and became suspended by the ropes as shown. This, of course, was done to prevent scattering of the lead shots. Failure under column load occurred by local crippling at a section where some imperfections existed or one near the fixed end. Table VIII shows the size of the tube tested and the crippling stresses at failure. The results are plotted on Figure 4. The r/t ratio is plotted against the ratio of the crippling stress versus the yield allowable (σ_c / σ_y). Curves were drawn to fit the test points. There is an obvious

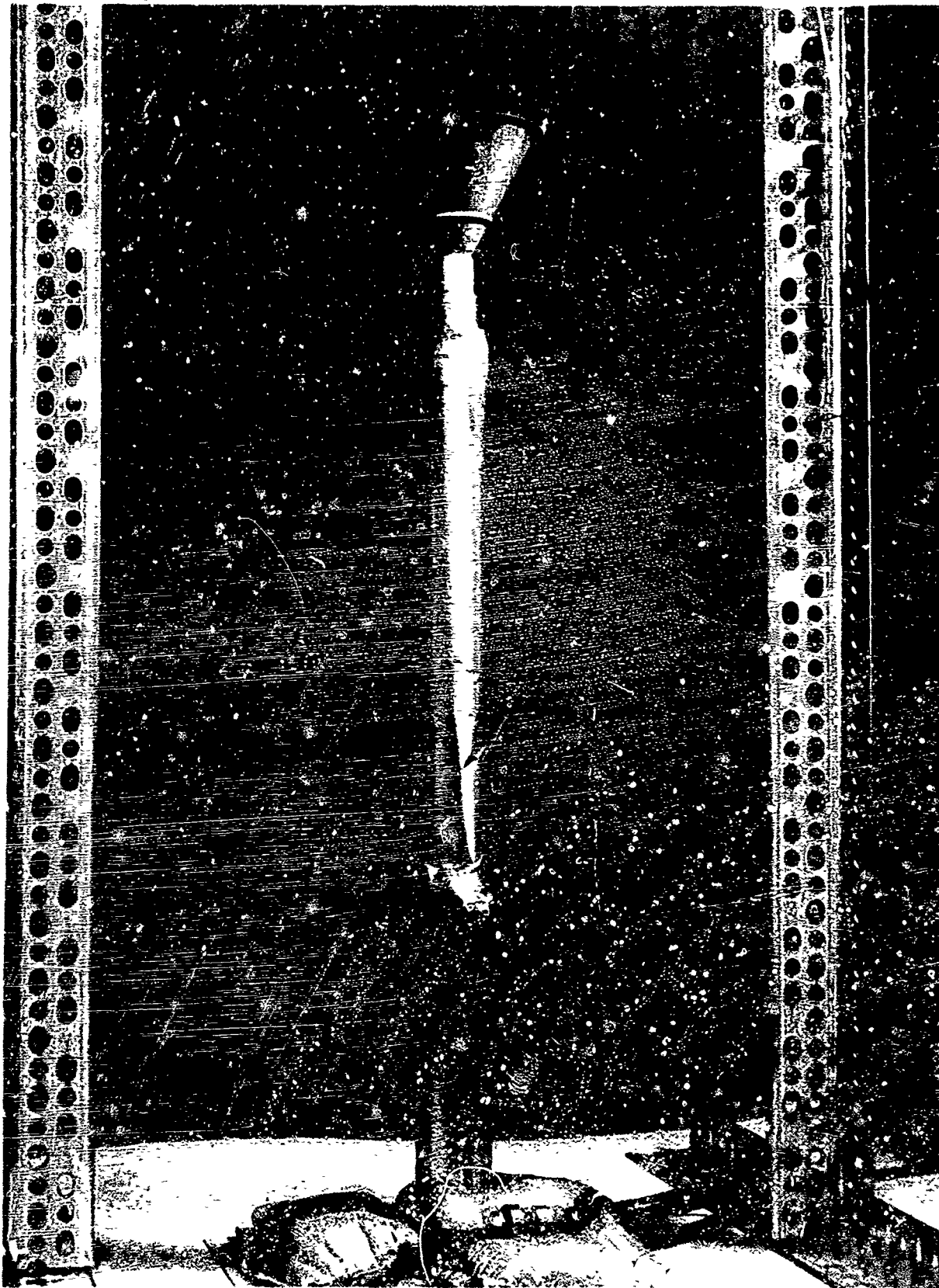
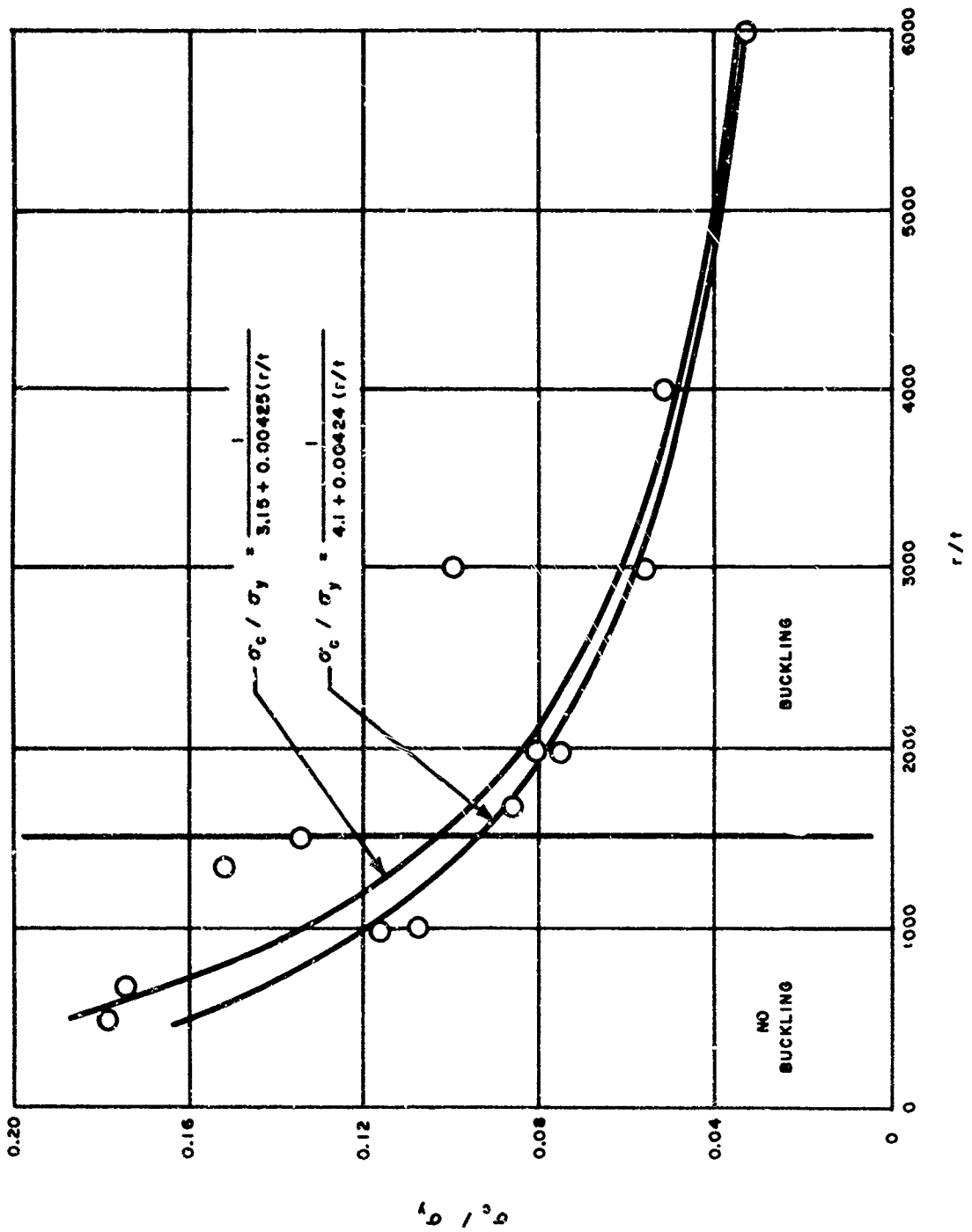


FIGURE 3 TYPICAL TEST SETUP

TABLE VIII
TEST DATA--ALUMINUM TUBES

Tube Size D x t	Test 1		
	p Inflation Pressure	Collapsing P _c Load	Collapsing c Stress
1.5 x 0.0015	14.0 psi	5.03 lbs.	711 psi
2.0 x 0.0015	10.5	6.55	695
3.0 x 0.0015	7.0	6.59	467
4.0 x 0.0015	5.2	11.5	610
5.0 x 0.0015	4.2	8.19	347
6.0 x 0.0015	3.5	9.12	322
12.0 x 0.0015	1.75	11.46	203
2.0 x 0.0010	7.0	2.69	428
3.0 x 0.0010	4.6	5.10	541
6.0 x 0.0010	2.3	7.54	400
12.0 x 0.0010	1.17	5.08	134
2.0 x 0.0005	3.5	0.94	299
3.0 x 0.0005	2.3	1.06	225
6.0 x 0.0005	1.17	1.29	137
12.0 x 0.0005	0.58	---	---



65-3866

FIGURE 4 TEST RESULTS AND EMPIRICAL CURVES

trend of decreasing stress with increasing and the nature of the trend suggests an expression of the following type to fit the data

$$\frac{\sqrt{\sigma}}{r} = \frac{1}{a + b \left(\frac{r}{t}\right)}$$

The numerical values for a and b that best suited the curves are given in Figure 4. As previously stated, the corner reflector was our first piece of tangible hardware.

This was followed by a series of conceptual studies in connection with several proposal programs. Some experimental work was done on isolated ideas but none of them reached hardware stage. As all creative designers well realize, many details require imagination, intuition, skill and some tests to assess their true value. Nevertheless, a few of these conceptual studies are presented here with the full conviction borne out of our experience that they are plausible and in many cases state-of-the-art.

1. Structures Suited for Solar Reflectors and Circular Antennas

A series of 36 gores are seam-bonded to each other over a spherical master mandrel. The outer edges of the gores are draped over a toroid of circular cross section and the inner edges are tucked in between two rigid plates forming the base of a central pylon. The entire assembly is covered by a hemispherical balloon to entrap the gas pressure that will be used to stretch the gores beyond their yield point. The toroid will be inflated first by a self-contained gas generator. This will be followed by the inflation of the balloon. The rigidity of the individual gores is enhanced by treating them with a film of glycerine on the non-reflecting face which will boil off in the presence of vacuum, leaving a hard crust. The central pylon can be used to support a thermionic converter for the generation of electricity or a reflecting horn in the case of a space foldable antenna. Figure 5 shows a schematic of the concept and Figure 6 shows a 6' foot collector with a partial vacuum maintained on the underside. The gores are aluminum foil, 0.001" thick.

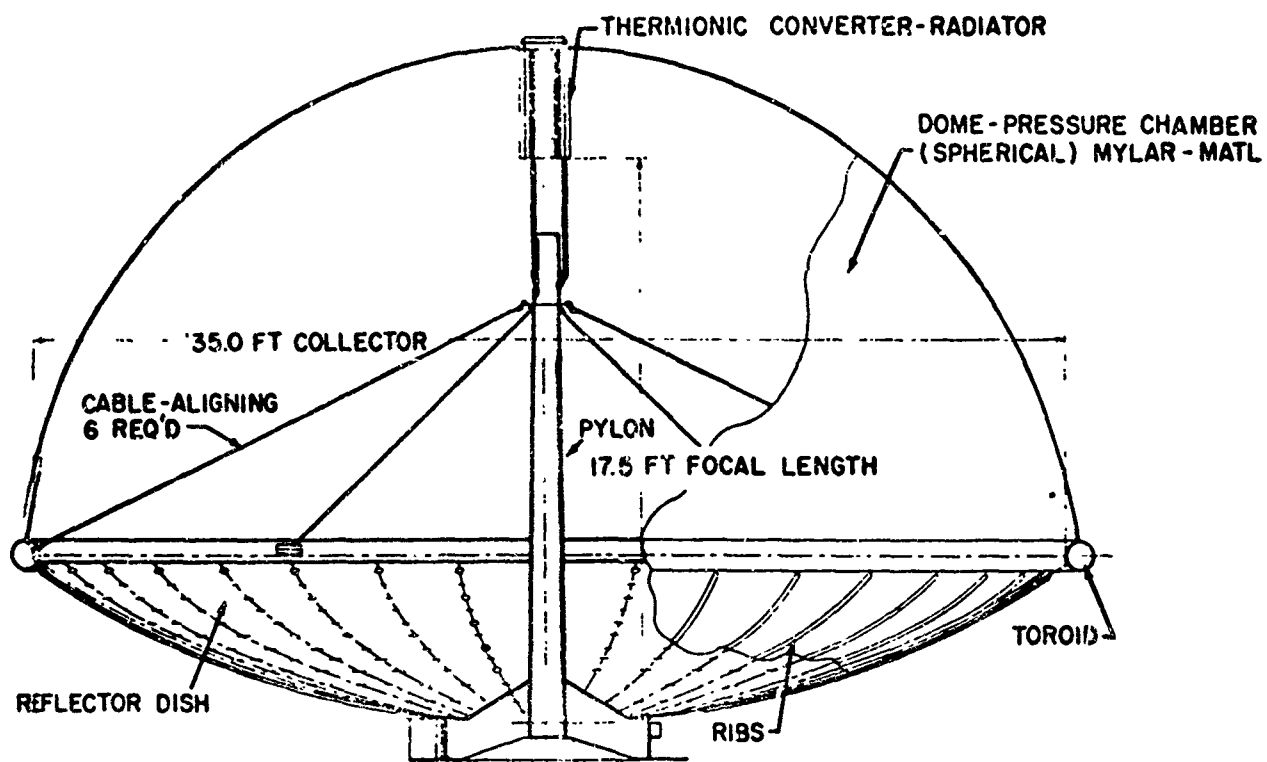


FIGURE 5 POWER PLANT SYSTEM WITH EXPANDED TUBE-SUPPORTED COLLECTOR

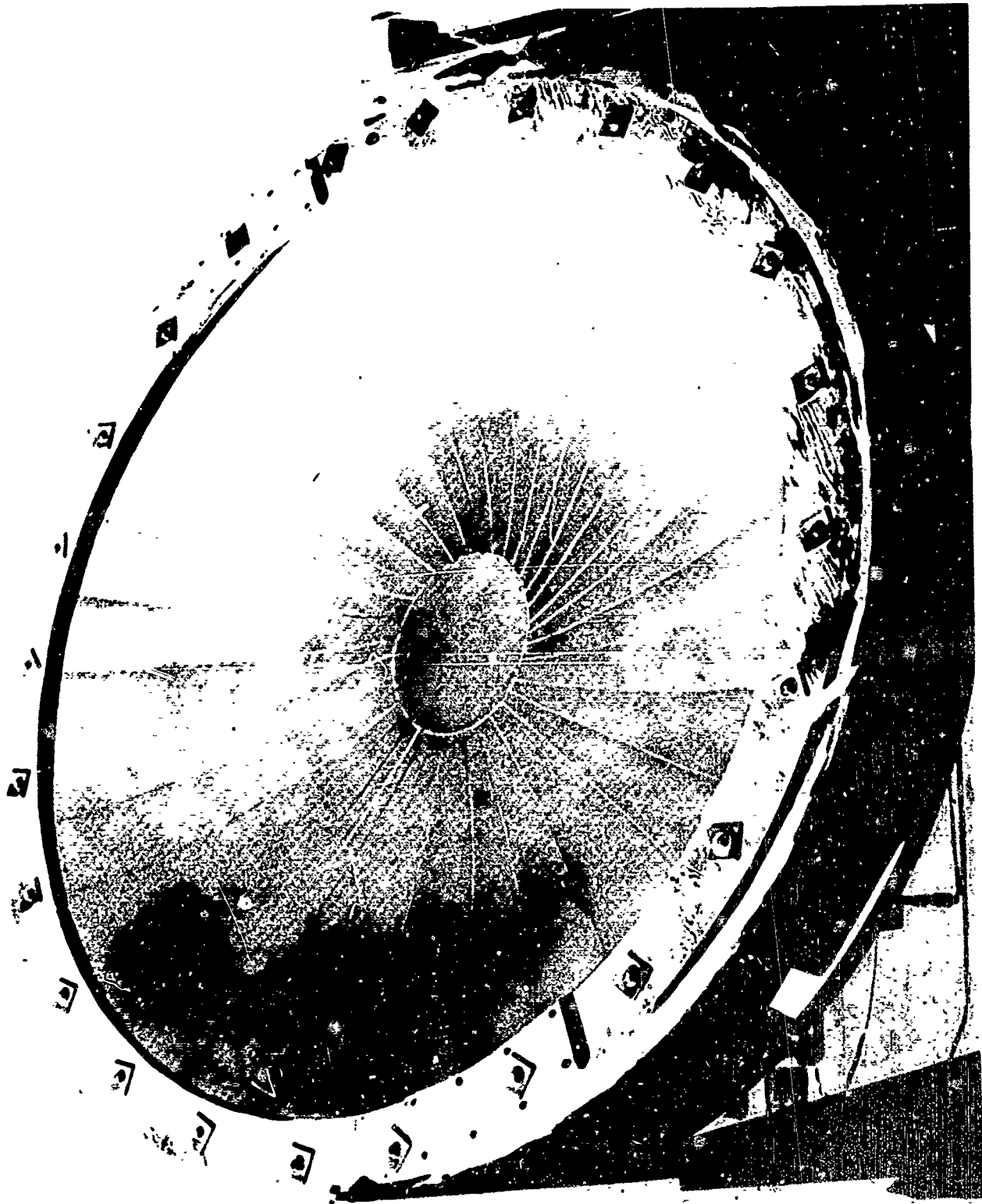


FIGURE 6 SIX-FOOT SOLAR REFLECTOR UNDER NEGATIVE PRESSURE
P5677B

2. Soft Lunar Landing Problem

The uncertainty surrounding the nature of the lunar terrain makes it desirable to originate a system of obtaining the maximum possible contact surface on the landing vehicle to retard or hopefully eliminate any possible sinking below the lunar surface. Figure 7 shows a simple way of multiplying the square footage of contact surface by stretching a mylar tent prior to impact. The extension of the tent is accomplished by ten expandable tubular trusses originally folded close to the periphery of the vehicular structure. Each truss consists of two aluminum foil tubes, 0.003 wall thickness, connected at the apex by a rigid elbow. All elbows are connected by a wire which, upon expansion, will drag out the tent material.

3. Anti-Contamination Pylon

All S.N.A.P. Reactor Programs required a considerable weight of shielding material (250 lbs. according to one estimate) to protect their electronic assemblies from radiation contamination. An expandable pylon with foldable bays was designed. Each bay was defined by two triangular end frames made of flat fiberglass plate, separated by three expandable tubes at the apices. In the stowed condition the tubes were folded ribbons, allowing the triangular plates to be stacked up close to each other accordion fashion. Upon inflation the electronic tray, mounted on the outer end frame, would be displaced a distance of 90' from the source of contamination. See Figure 8

Many other applications limited only by the imagination of the designer can be conceived. The resulting structure in every case has the important property of retaining its deployed shape, without relying on internal pressure or hard to control chemical reactions.

ASSISTED DEPLOYMENT OF INFLATABLE STRUCTURES

All of the ideas presented so far are based on aluminum foil whose thickness varies from 0.0005 to 0.003.

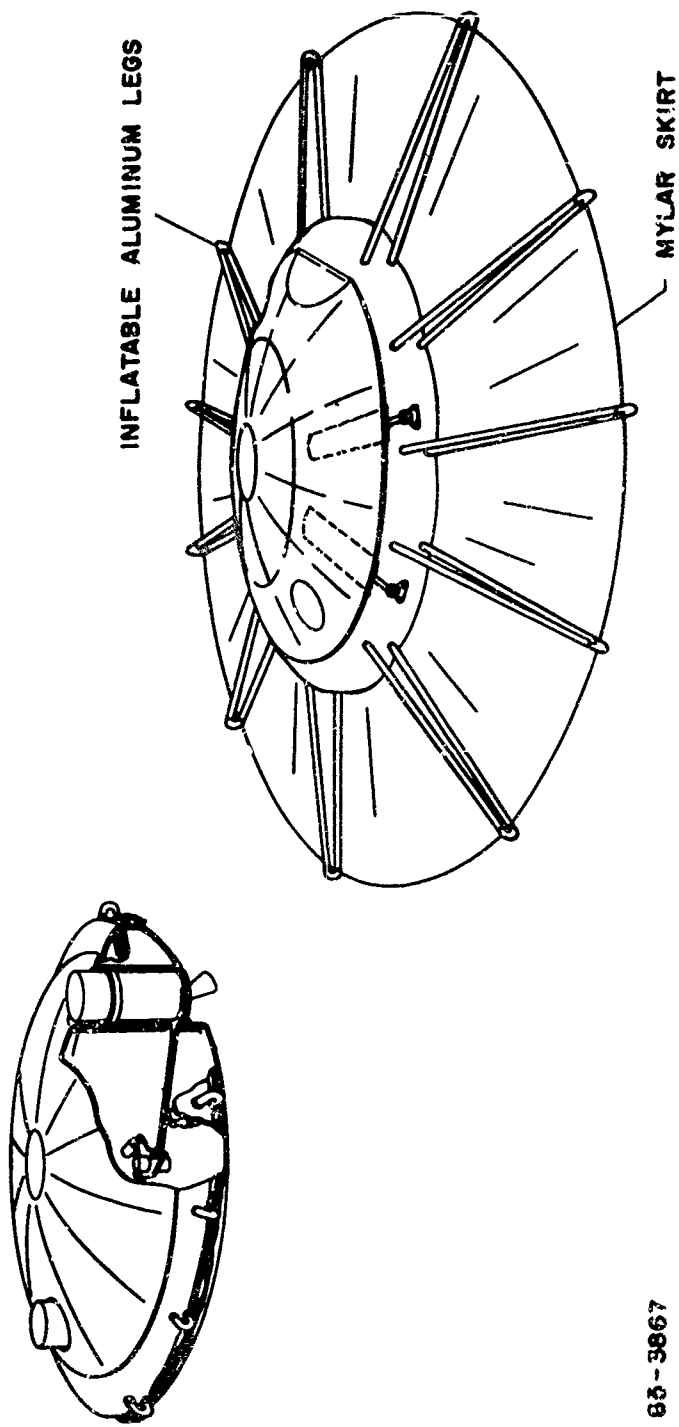
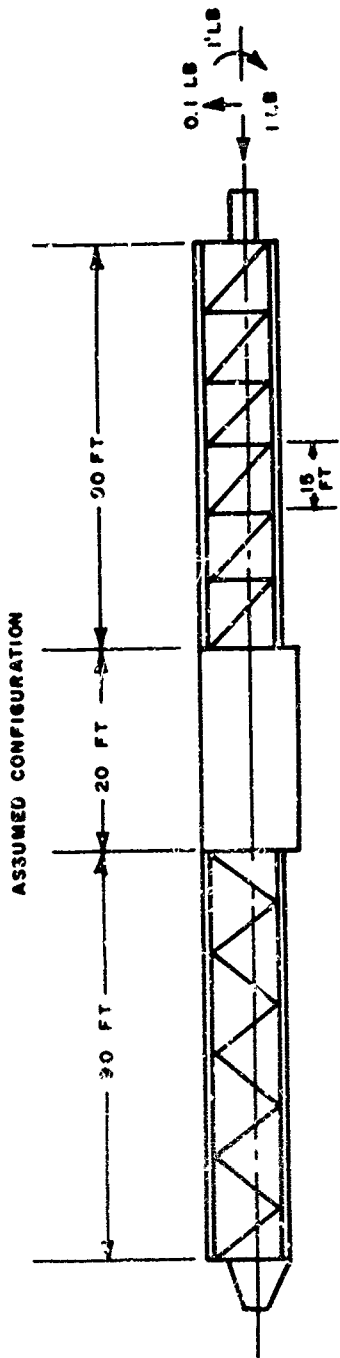
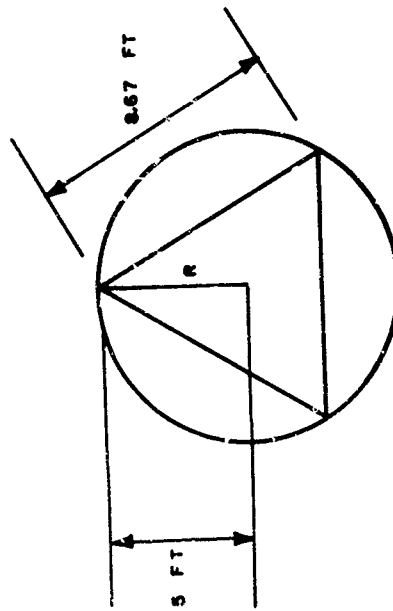


FIGURE 7 WEBBED MAT--HOVERING AND LANDING CONFIGURATION

65-3867



ASSUMED LIMIT LOADS
 THRUST = 1.0 LB
 SIDE LOAD = 0.1 LB
 ROLL MOMENT = 12.0 IN./LB



68-3868

FIGURE 3 EXPANDABLE PYLON

The hardware we will present at this point deals with thicknesses from 0.003 to 0.015. The basic operational difference between these two types of structures is to be found in the method of deployment.

The thinner structures will pass from their stowed configuration to their final geometry by means of internal pressure only, as shown by the movie. The thicker structures, when similarly pressurized, never quite make it. They need an assist. A tube 1" O.D., for example, and 0.005" wall thickness will rigidize into a perfect tube when inflated from a straight flat ribbon. However, if it is folded first, carefully avoiding any sharp corners, and then pressurized from its folded geometry, it will not straighten out into an acceptable strut. Re-annealing after folding offers a partial remedy, but results are not structurally acceptable. We had reached an impasse. The question was, Shall we see what results we get by providing the assistance needed? Is it worth this new complication? or, Should we forget about it? It was decided to go ahead with the experiment. An external force was used to pick up the folded structure at some convenient point and hold it up in its stretched shape long enough to pressurize the tubes. The force required is minimal. It could be a buoyancy force, such as a balloon or a float, or it could be a micro-thruster for space work. Its only function is to allow pressurization to occur at or near final configuration.

The first legitimate basis we had to run this experiment was in connection with the Navy ASW Program. I am not at liberty to go into details for security reasons. The only object in mentioning it is to explain why in the next movie you will see the forming of a tube underwater by utilizing the buoyancy force of a float. Obviously, the same objective can be achieved in air or space. (2½ minutes of movie follow)

The resulting tube was cut in various lengths to cover a slenderness ratio from 20 to 180, and the specimens thus obtained were subjected to a typical column test (Ref. pg. 20 Figure 9).



FIGURE 9 TYPICAL COLUMN TEST

The solid line on Figure 10 shows a plot of test points, and the dotted line shows results calculated on the basis of a simple Euler type formula.

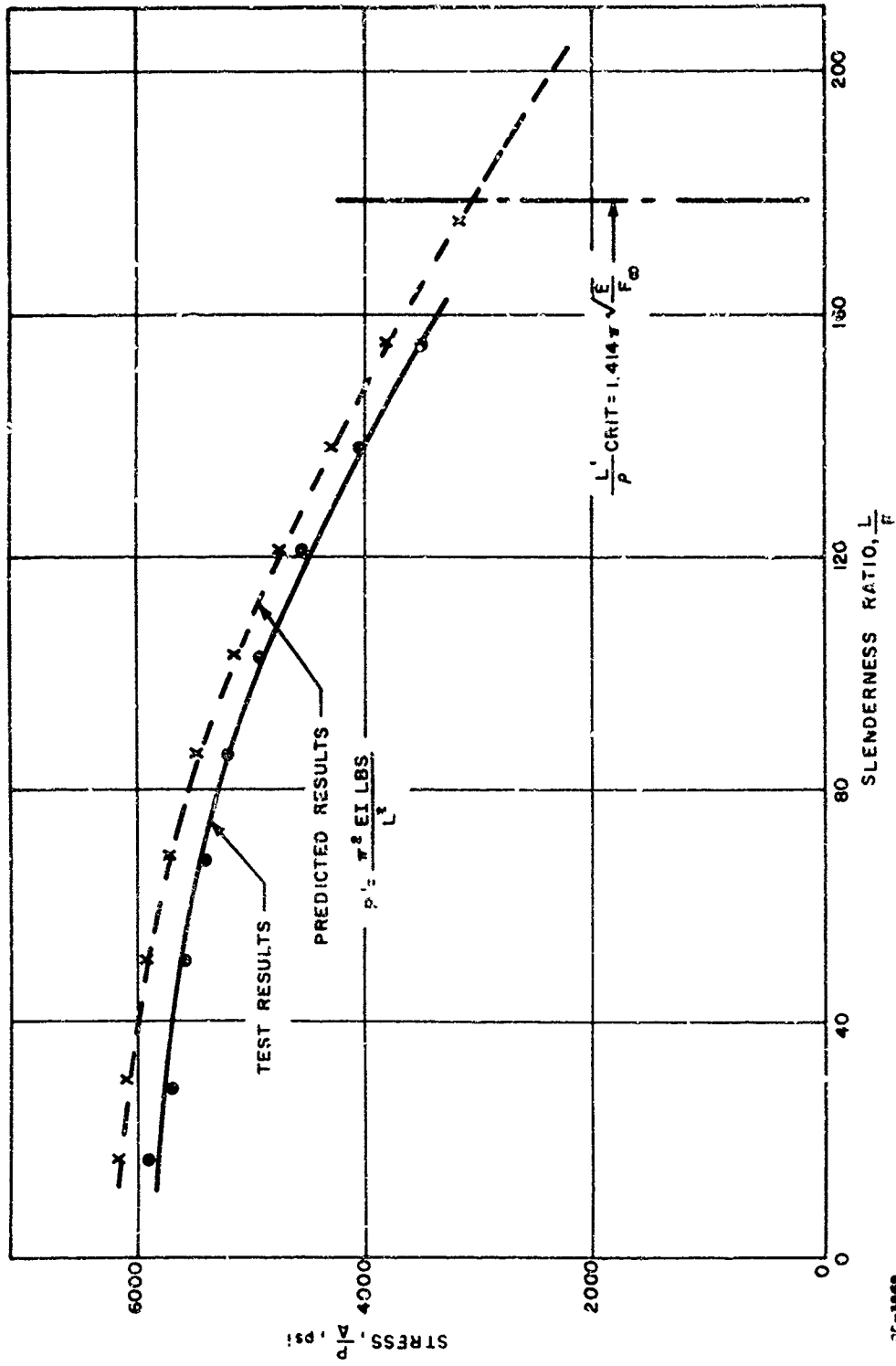
$$P_{\text{column}} = \frac{\pi^2 EI}{L^2} \quad \text{lbs.}$$

The agreement is very satisfactory. The structural behavior of these tubes has proven to be very predictable. It was demonstrated again in the construction and testing of the equilateral tripod shown on Page 23. The following movie shows the erection and inflation of this space truss in water. (3 minutes of movie)

After draining the water out of the tubes, this truss was tested for the loading condition shown in Figure 12 to assess its strength against a vertical load. Figure 13 plots load increments versus deflections to a failure load of 147 lbs. The weight of the tubes and fitting is approximately $\frac{1}{2}$ lb., exclusive of the anchoring device.

Another problem whose solution eluded us for a long time, is the fabrication of a toroid of circular cross-section starting from a flat ribbon. The basic problem here is that the circumferential length of an element of a toroid is proportional to its distance from the center line of symmetry. The outer fibers are obviously longer than the inner ones. Starting with a ribbon made up of two flat strips, seam welded at the long sides, it was necessary to find a way of stretching the outer ribbon without disturbing the inner one. Also, the amount of stretching for each fiber had to be proportional to that fiber's distance from the center of the toroid. The answer is illustrated by Figure 14.

The ribbon is draped over the periphery of a solid wooden mold and tightened against it with a nominal tension load. Upon introducing pressure the ribbon is forced to expand outwardly, thus inducing a variable tension stress on all fibers of the cross section: zero at the inner fiber and 6000 psi. approximately at the outermost one.



05-3889

FIGURE 10 TEST RESULTS: SLENDER RATIO VERSUS CRITICAL STRESS AT FAILURE

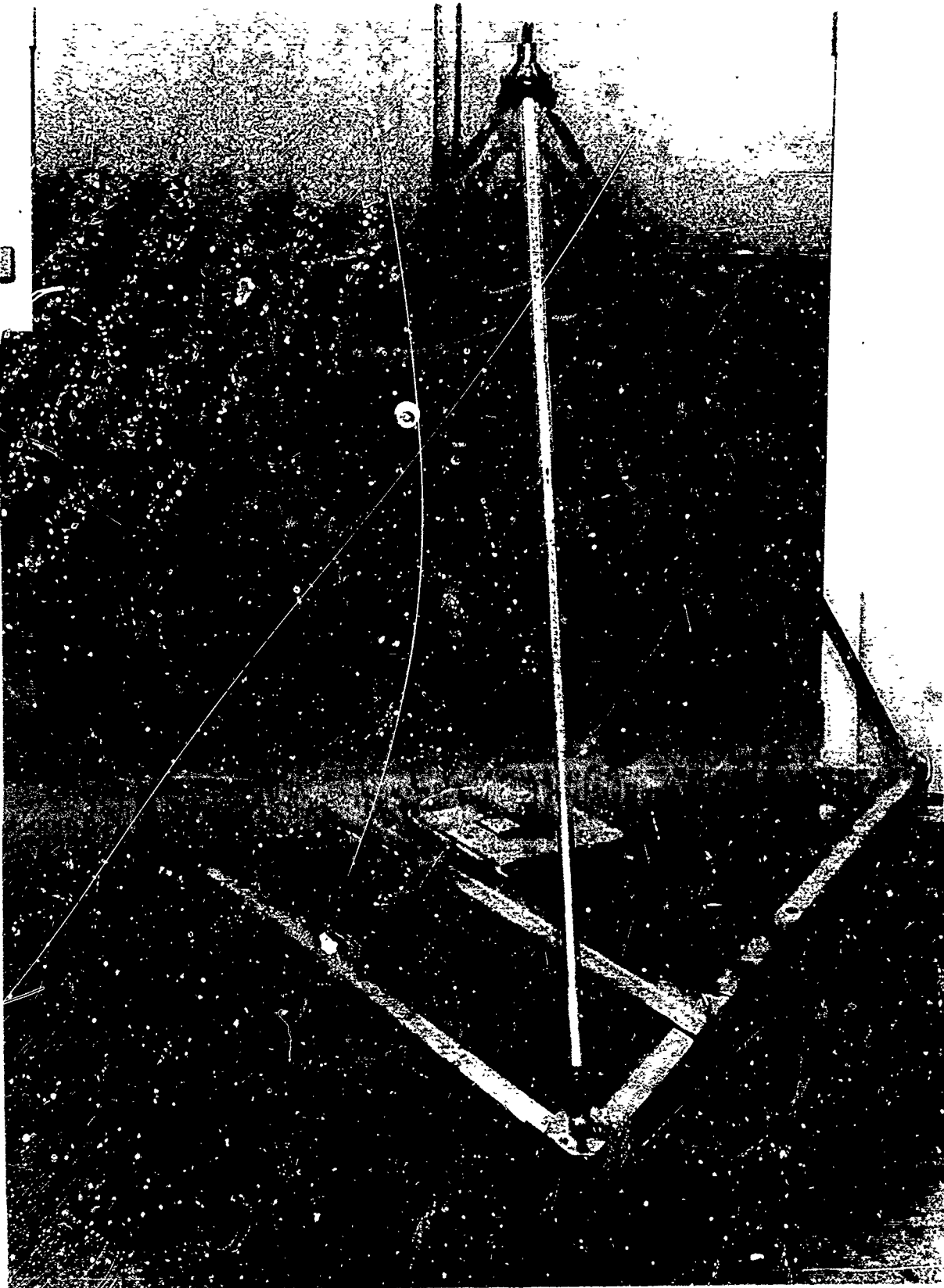


FIGURE 11 EQUILATERAL TRIPOD

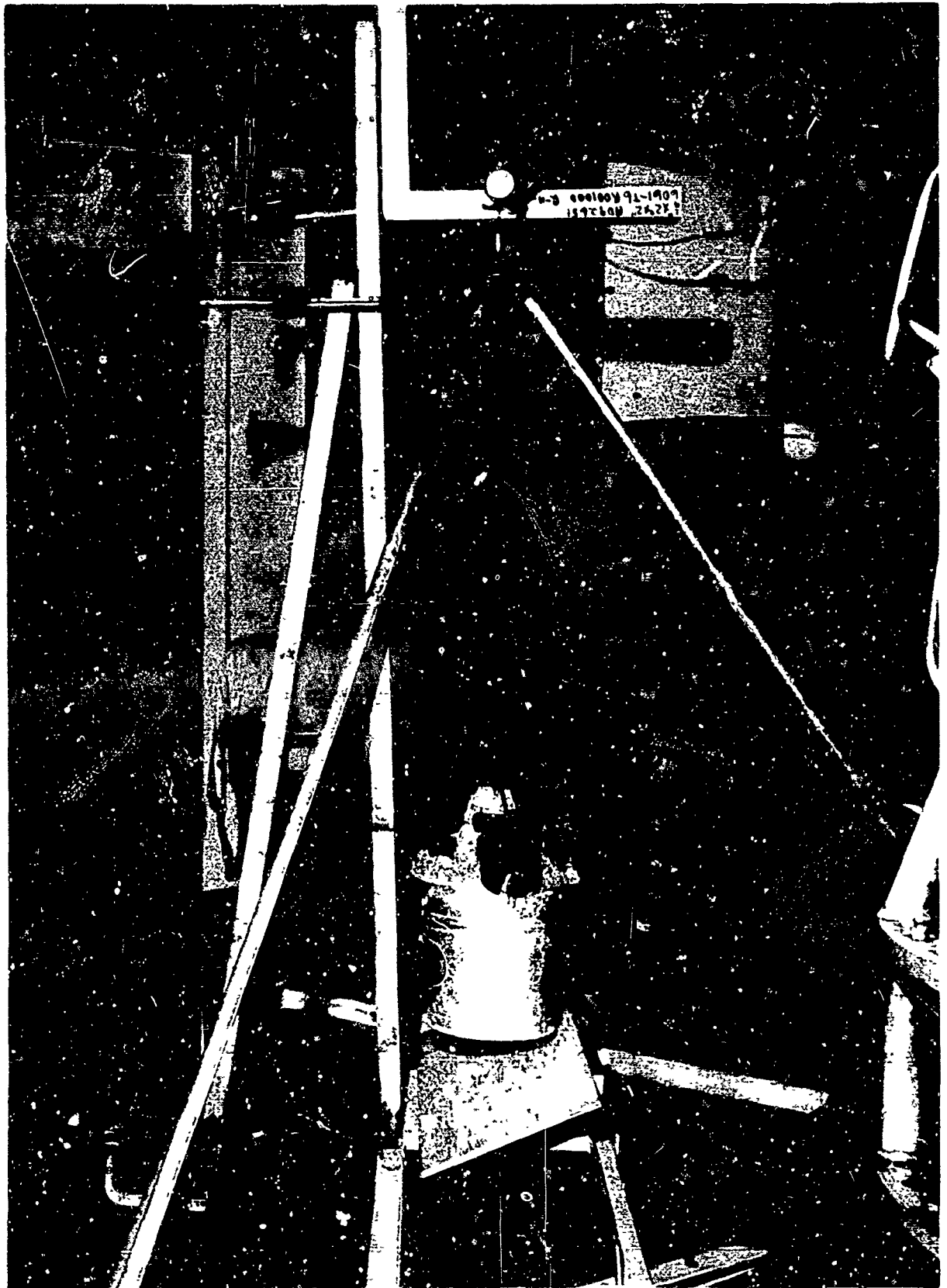
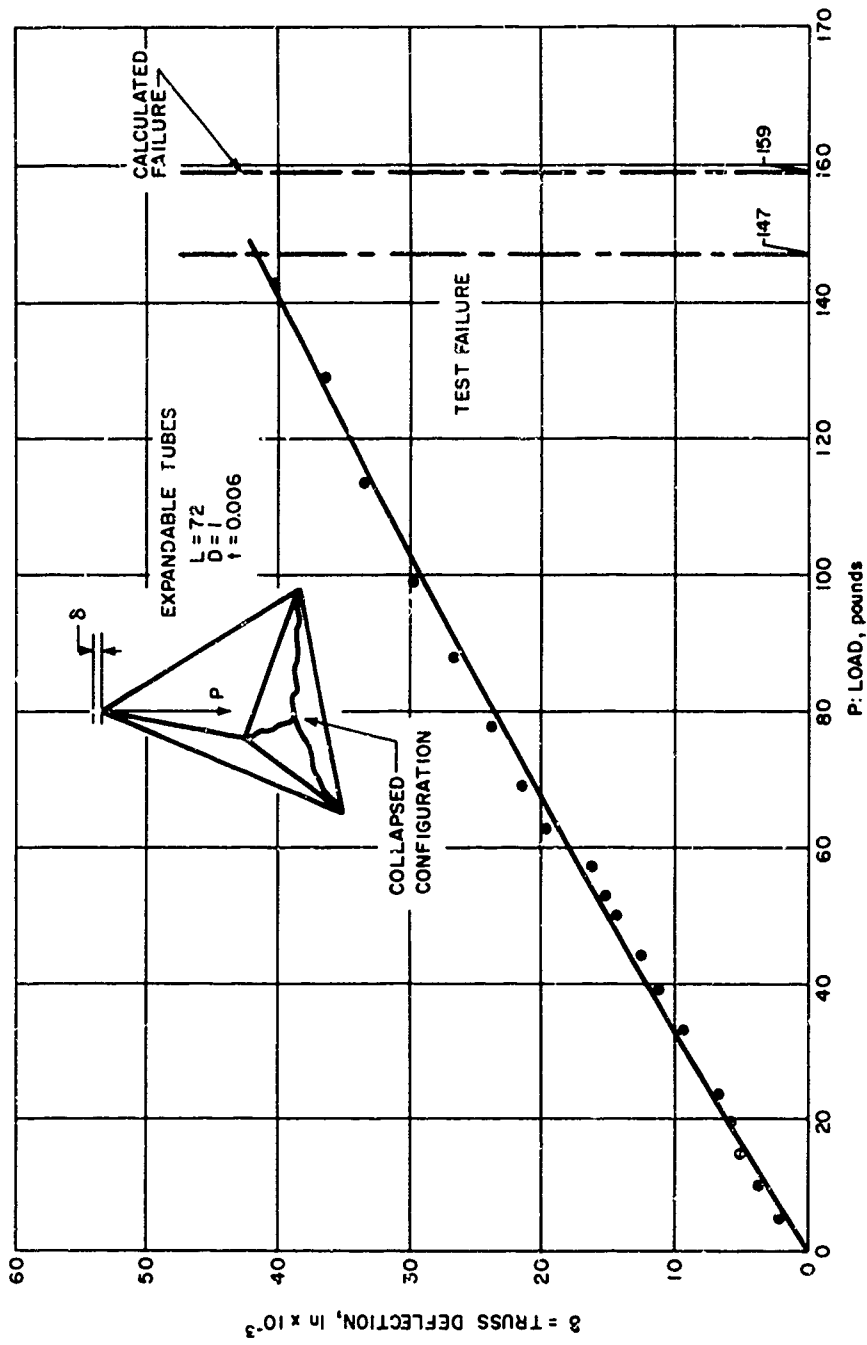


FIGURE 12 TESTING JIG FOR SYMMETRICAL VERTICAL LOADING



65-3870

FIGURE 13 DEFLECTION OF TRUSS VERSUS VERTICAL LOADING

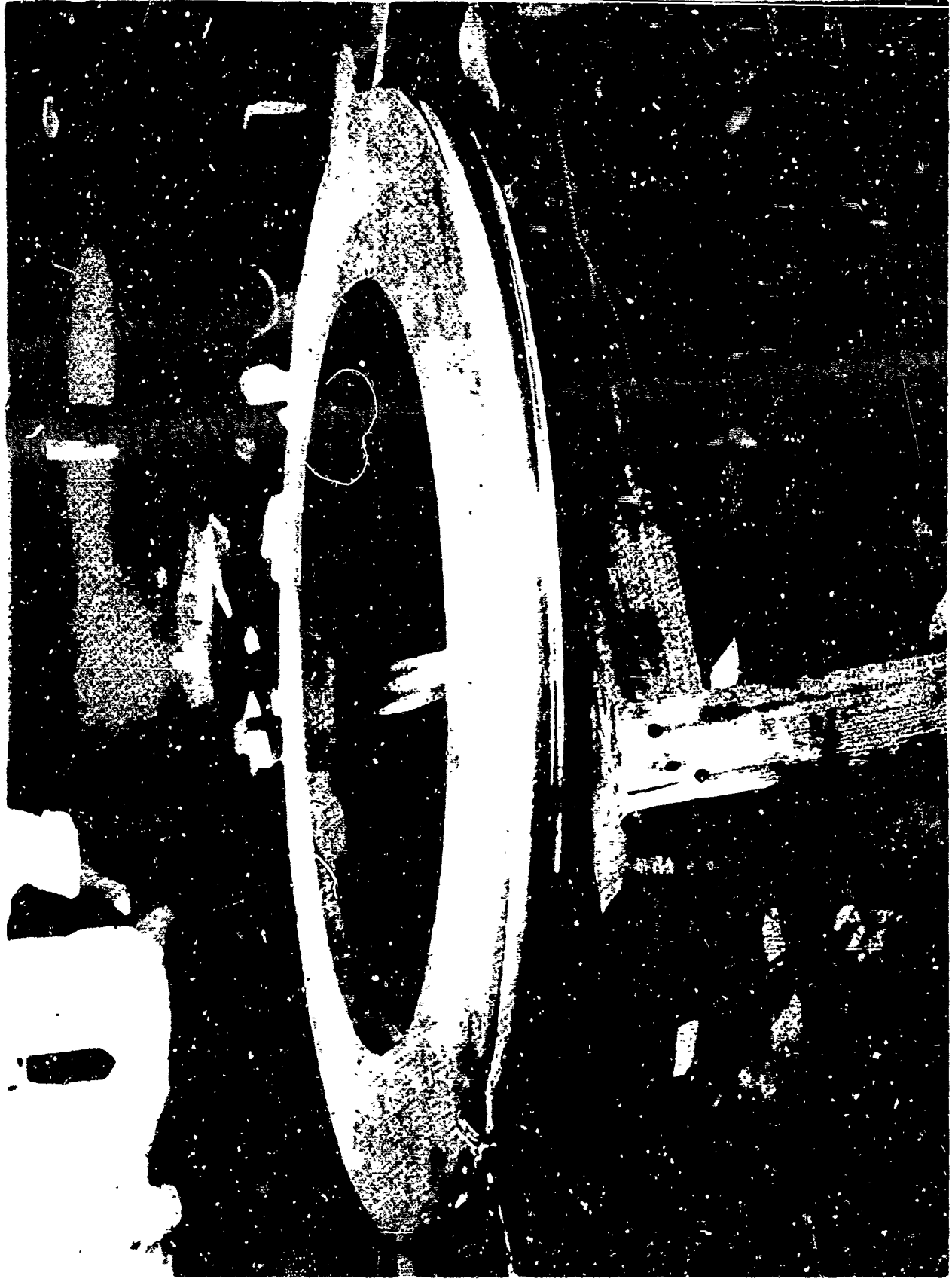


FIGURE 1.4 FABRICATION METHOD FOR A CIRCULAR TORUS



FIGURE 15 TORUS TEST SETUP

ESTIMATED WEIGHT: 1.912 POUNDS
INFLATING PRESSURE: 60 P.S.I.

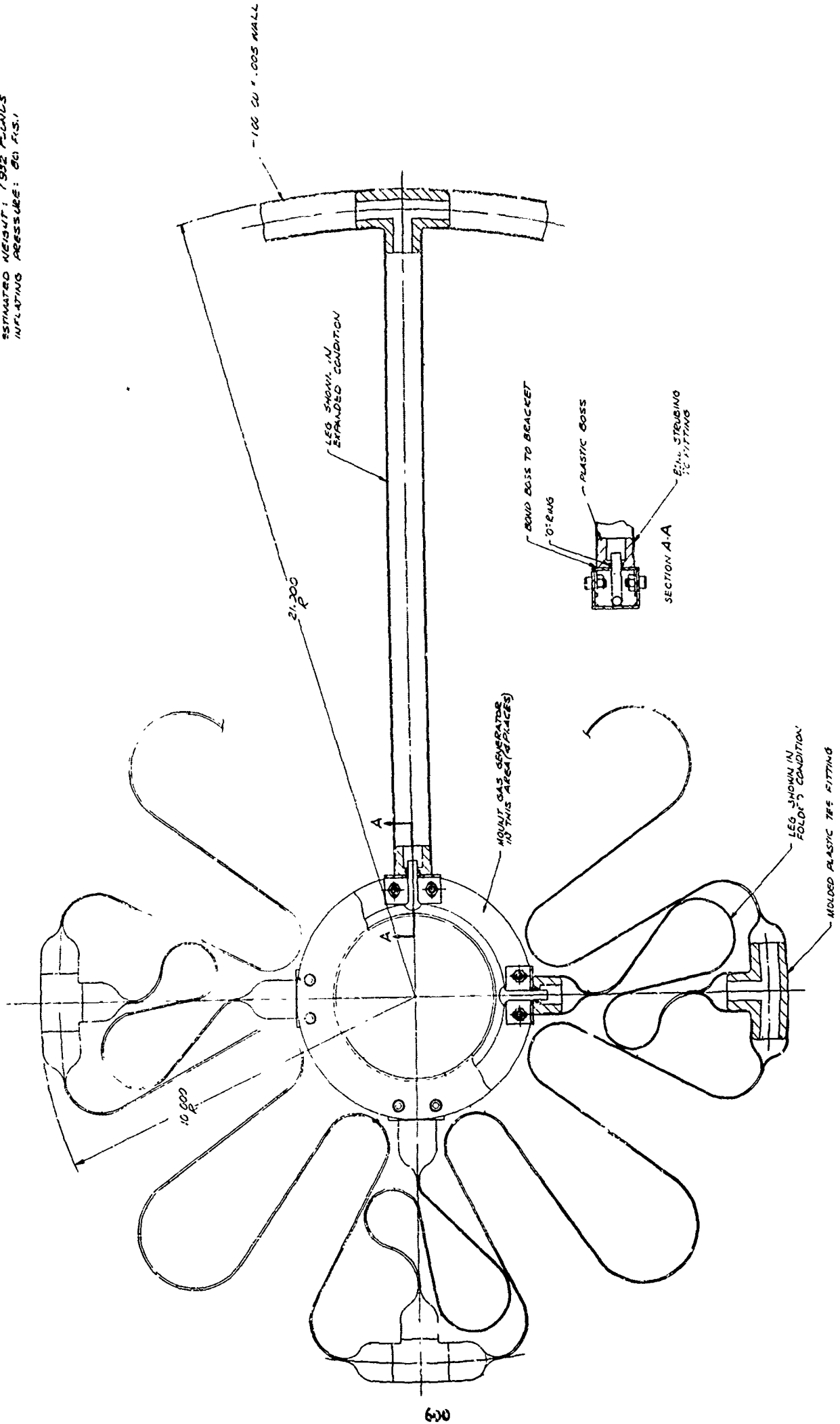
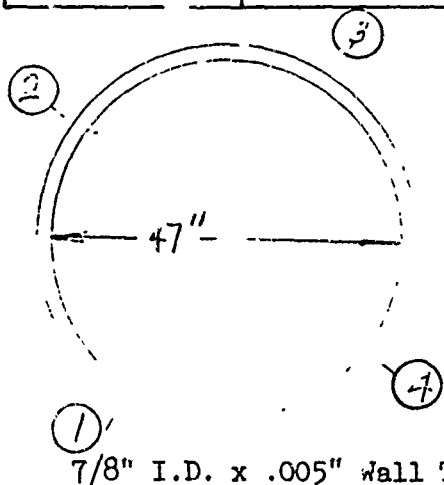


FIGURE 16 EXPANDABLE TOROIDAL FRAME

TABLE VIII
TORUS TRUSS DATA

LOAD	GUAGE 1	GUAGE 2	GUAGE 3	GUAGE 4
4 lb. 1 oz.	0	0	0	0
40 lb.	+0.006	+0.002	+0	+0.0012
60 lb.	+0.009	+0.0032	+0.001	+0.0037
80 lb.	+0.0108	+0.0031	+0.0011	+0.0037
100 lb.	+0.0147	+0.0040	+0.0039	+0.006
120 lb.	+0.014	+0.0041	+0.0025	+0.0071
140 lb.	+0.0134	+0.0042	-0.0005	+0.0075
160 lb.	+0.0145	+0.0049	-0.0015	+0.0075
180 lb.	+0.0137	+0.005	-0.0028	+0.0079
200 lb.	---	---	---	---
220 lb.	+0.0169	+0.0061	-0.0049	+0.006
240 lb.	+0.0169	+0.0068	-0.0062	+0.0062
260 lb.	+0.017	+0.0078	-0.0078	+0.0072
280 lb.	+0.0179	+0.0081	-0.009	+0.0074
300 lb.	+0.0189	+0.0184	-0.0207	+0.0201
320 lb.	+0.024	+0.0176	-0.0219	+0.020
340 lb.	+0.0258	+0.0163	-0.022	+0.0215
360 lb.	FAILURE			



7/8" I.D. x .005" Wall Thickness

Failed at #1 Guage where there were several local buckles initially and where pressure line was connected.

Minus readings indicate change in direction of guage travel.

The strain resulting from these stresses accomplishes the proportional stretching required for a toroid. After annealing to remove work hardening, the tube can be reflattened and folded in any geometry; it will always inflate into a circular configuration. Figure 15 shows the setup to test this torus for a uniformly distributed radial load. Table VIII shows the load increment and deflections at four diametrically opposite points. Failure load was 360 lbs. Total weight of toroid was 0.203 lbs. A direct application of this principle was provided by a design problem dealing with precision decoys. It was required to provide radial support to a fabric shell of a given diameter. The support had to be concentric with the ϕ of thrust within close limits. Figure 16 on page 29 shows how this was done with the help of four radial arms and a toroidal structure.

Our plastic division is presently tackling the problem of foaming in vacuum. There is little doubt in our minds that foam filled aluminum shells would generate a new family of structures with an exceptionally high strength/weight ratio.

CONCLUSION

Our investigation has proved that foldable structures of appreciable strength and rigidity can be achieved with a metallic foil, aluminum for example.

Though considerable analytical work remains to be done and manufacturing processes must be streamlined. The results obtained so far from the efforts of a few people gives ample justification for further experimentation.

REFERENCES

Page 10, 11, 12 are extracted from: "RAD-TM-61-4" Collapse of Erectable Al Foil Tubes Under Axial Compression by Victor W. Miselis.

FABRICATION AND PRESSURIZATIONS TECHNOLOGY FOR IMPROVEMENT
OF SURFACE ACCURACY OF PASSIVE COMMUNICATIONS SATELLITES

By David C. Grana and Walter E. Bressette

NASA Langley Research Center

INTRODUCTION

Since the successful demonstration of the Echo I satellite for the purpose of communication by means of passive reflecting of radio waves, the NASA Langley Research Center through both in-house and contractual studies by the G. T. Schjeldahl Company of Northfield, Minnesota, has been actively engaged in a research program to improve the RF reflecting surface of the passive communication satellite.

The objectives of the program are first to investigate and document the state-of-the-art fabrication technique used for the Echo satellites in order to establish the source and magnitude of the inherent errors during forming, cutting, sealing, and handling; second, to evaluate improved manufacturing procedures by constructions of small-scale 12-foot spheres using such devices as mandrels and molds; and, third, to determine the effects of the number of gores and the manufacturing process on the surface conditions and radius of curvature accuracy before, during, and after internal 12-foot-diameter-sphere pressurization using a photogrammetry technique. This paper will present the highlights of this program.

CONCEPT AND THEORY

The Echo concept illustrated in figure 1 is, in fact, an approximate sphere consisting of a number of flat gores, fastened together by 1-inch-wide adhesive-coated tapes, with spherically shaped caps located at both ends of the gores. The shape and size of the gore are determined by a geometric projection (ref. 1) with the edges of the gores representing great circles on the flat-sided approximate sphere. The greater the number of gores the closer the flat-sided figure will approximate a sphere. The entire structure is made of a pliable material, which, after deployment in space, is presumed permanently strained by an inflatable to form a rigid spherical shape with the center line of the gore L permanently yielded to equal the gore edge line C . The degree of permanent strain required is illustrated in figure 2. The plot shows that the permanent strain required to strain a gore-constructed approximate sphere to spherical shape is only dependent upon the number of gores in the sphere and is reduced as the number of gores is increased. The curve was calculated from the equation shown on the right side of the figure.

$$\epsilon_p = \frac{\frac{\pi}{N} - \sin \frac{\pi}{N}}{\sin \frac{\pi}{N}} \quad (1)$$

where

ϵ_p permanent strain required to obtain a perfect sphere

N number of gores in approximate sphere

The equation was derived from the concept illustrated in the sketch representing a cross section of one of the gores in the approximate sphere where the objective in pressurizing the balloon is to yield the material from the flat chord section, as shown by the dotted line, to a spherical arc contour, as shown by the curved line.

The permanent strain may next be related to the skin stress by means of the stress-strain curve for the material under consideration. For the present application, Echo II material was used, mainly because of material availability and the possibility of comparing the final 12-foot-diameter test spheres with much larger sphere data. An Instron stress-strain curve for the Echo II material is presented on the left in figure 3. In order to be sure if the uniaxial Instron data would be realistic for predicting the stress required for the approximate spheres, additional stress-strain information was obtained by a diaphragm technique that stressed the material biaxially. As can be seen, the diaphragm data agree quite well with the continuous and much easier to obtain Instron data. From the Instron stress-strain curve the permanent strain was analytically determined and is presented on the right side of the figure. Because of the difficulty of locating multilaminate material yield points necessary for determining the permanent strain from an Instron stress-strain curve, an optical comparator was used to measure the Instron sample before and after stressing to determine the actual permanent strain obtained. These data are also presented in the right-hand plot and compare very well with the analytical data taken from the Instron stress-strain curve. It is now possible, by use of figures 2 and 3 and the thin-wall homogeneous sphere equation, to calculate the internal pressure required to strain an approximate sphere constructed of a specified number of gores to spherical shape. It is conceivable that, even though the sphere is nonhomogeneous, the thin-wall homogeneous sphere equation is valid to predict the point where the flat gore will reach a spherical shape, because the double-thick material at the tapes should not yield appreciably compared to the gore material.

If the perfect sphericity point, at any point on the approximate sphere, is exceeded, then use of the thin-wall sphere equation cannot hope to be valid because of the variation in material thickness throughout the sphere. It also seems realistic that any manufacturing imperfection that must be removed by strain has to be such that will require strains less than the strain necessary to remove the flat gores. In light of this thought, it next became important to determine the manufacturing tolerance for the Echo method of construction. The inherent errors during forming, cutting, and sealing were summed and equated to the gore method of construction as percent of width of gore. Because the calculated errors remained constant and the gore width varied, it became apparent at this point, as shown in figure 4 that the strain required

to remove the maximum expected fabrication errors would vary from pole to equator by as much as a factor of 10 with the pole area requiring the greatest amount of correction. Figure 4 shows the maximum percent error, which is equivalent to maximum strain required to remove the error, for Echo II material and the 12-foot spheres used in this program. The curves were calculated from the equation to the right of the figure.

Equation (1) of figure 4 is the equation for the curve:

$$\text{Percent error} = \frac{k \Sigma(\text{errors})}{\sin \theta} = \frac{100 \Sigma \text{ errors}}{W}$$

where

$$k = \frac{100 \sin \theta}{W}$$

Equation (2) determines the width of the gore

$$W = \frac{2\pi R \sin \theta}{N}$$

where

R radius of sphere

N number of gores

It is interesting to note that the 24-gore mandrel-constructed 12-foot-sphere maximum-error curve is very similar to the Echo II 135 sphere curve. It is also evident from the magnitude of the percent error, especially in the sphere pole-cap area, that the actual errors will have to be much less than predicted in order to avoid exceeding the required strain for removal of the flat gores.

EXPERIMENTAL APPROACH

Since the strain theory was not related to the size of the sphere and the strain requirements for correcting the manufacturing tolerances could not be optimized by theory, a 12-foot sphere was selected for the program test size because it was the largest sphere that could be built practically, handled, and photographed in the numbers required. Nine spheres were built, one or more 32, 48, and 64 flat-gore spheres by the Echo II method which, as shown in figure 5, consisted of seaming together with 1/2-inch-tape, pre-cut gores on a curved rail; three 48 flat-gore spheres where adjacent gores were cut and sealed without gore position change on the mandrel shown in figure 6; and one 48 flat-gore sphere which was constructed on a hemispherical mold. The mold-type construction would not be practical for the large spheres, but

it was included in this program in order to compare manufacturing errors. Photogrammetry measurements of the spheres were made by Ohio State University at low and high pressure for all the spheres, first at a very low pressure to determine the manufactured condition, and, in sequential order, as shown in figure 7, in order to determine the effect pressurization had on the sphericity of the originally constructed sphere. From the initial low value the pressure was increased to one-half the value calculated as the perfect sphericity pressure depending upon the number of gores, back to the low value, next up to the design and back to the low pressure, and then to $1\frac{1}{2}$ design

before returning to the low pressure again. The photogrammetry plates were then converted to contour plots by a wild A-7 autograph. In figure 8 is shown a typical contour map which covers approximately $1/4$ the area of the 12-foot-diameter sphere. From contour plots such as this, cross sections along the gore center line, parallel to the gore at the equator and through the pole caps were obtained from which overall changes in sphericity with pressurization could be observed. The wild A-7 autograph is also capable of magnifying local areas of the contour plots for the purpose of observing manufacturing imperfections from which the various techniques of manufacturing will be compared.

RESULTS AND DISCUSSION

At the present time all of the spheres have been photographed and much of the photogrammetric data is still being analyzed. The detailed manufacturing imperfections from the various methods of manufacturing will be published at a later date. Enough information on the sphericity of the approximate spheres with increasing pressure is available to clearly make some preliminary conclusions.

Presented in figure 9 is the ratio of measured to design radius of curvature along a gore center line and across the gores at the balloon equator before and after pressurization to both design and $1\frac{1}{2}$ times design for the 32-gore approximate sphere. It can be seen at the initial low pressure that in general the balloon is constructed from 0 to 60 inches from the equator nearly as designed but is poorly constructed from 60 inches to 72 inches from the equator. This is not too surprising since this area, as shown in figure 4, is the same area where the manufacturing errors are increasing very rapidly and also where the gores terminate in a solid one-piece spherical pole cap. It cannot be expected that every balloon constructed of gores would be out of design near the pole cap as much as this one but it is reasonable to say that the pole-cap area is the most critical construction area and as seen from the data at the initial low pressure could be the limiting factor for the overall tolerance on sphericity of the inflatable sphere. In general, the sphericity of the sphere both along a gore and across the gores improves with increasing pressure. However, the pole area fault remained even after the approximate sphere had been stressed to an average pressure of $1\frac{1}{2}$ times that required to theoretically strain the gores to spherical shape.

CONCLUDING REMARKS

In summary, from theoretical consideration and experimental data taken by means of photogrammetry on 12-foot-diameter gore-constructed approximate spheres, the following concluding remarks can be made:

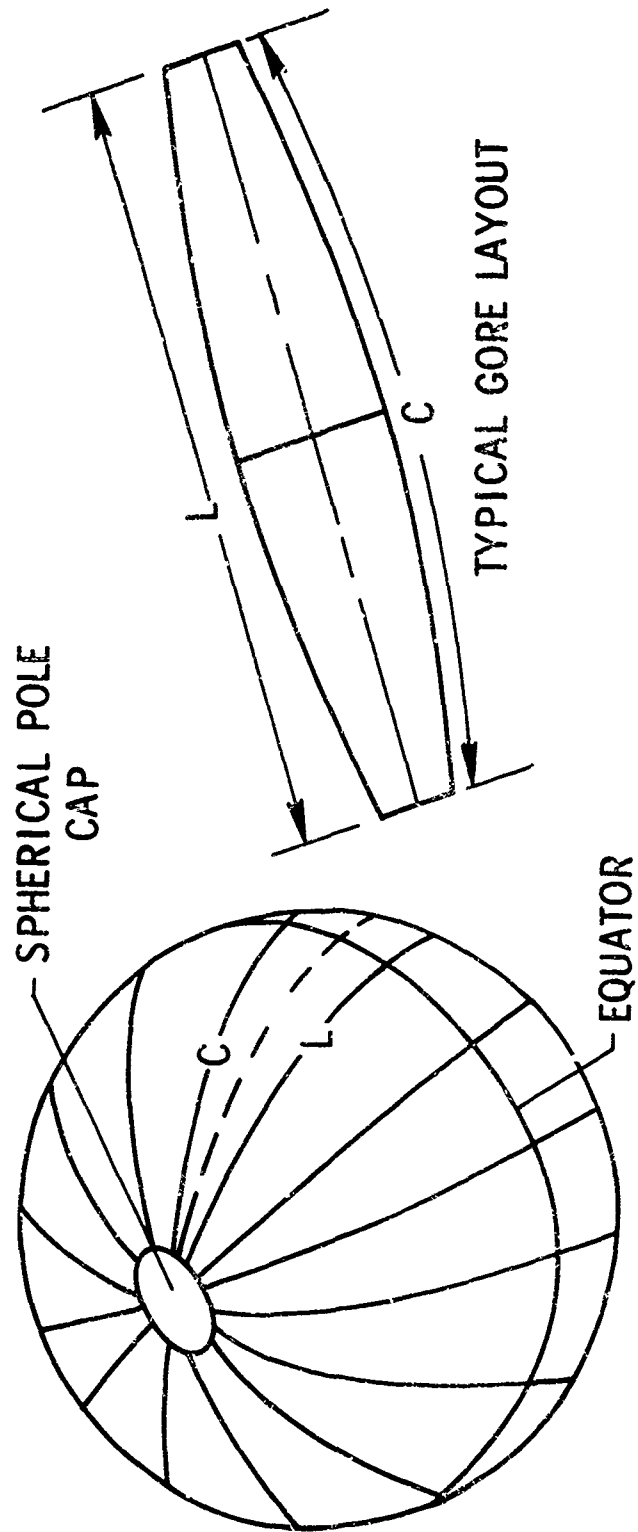
1. The permanent strain required to strain a gore-constructed approximate sphere to spherical shape is only dependent upon the number of gores in the sphere.

2. The greater the number of gores in a gore-constructed approximate sphere, the lower the strain required to strain the approximate configuration to spherical shape by an inflatable system.

3. Stress-strain data obtained by a biaxial diaphragm technique agreed with the continuous and much easier to obtain Instron data.

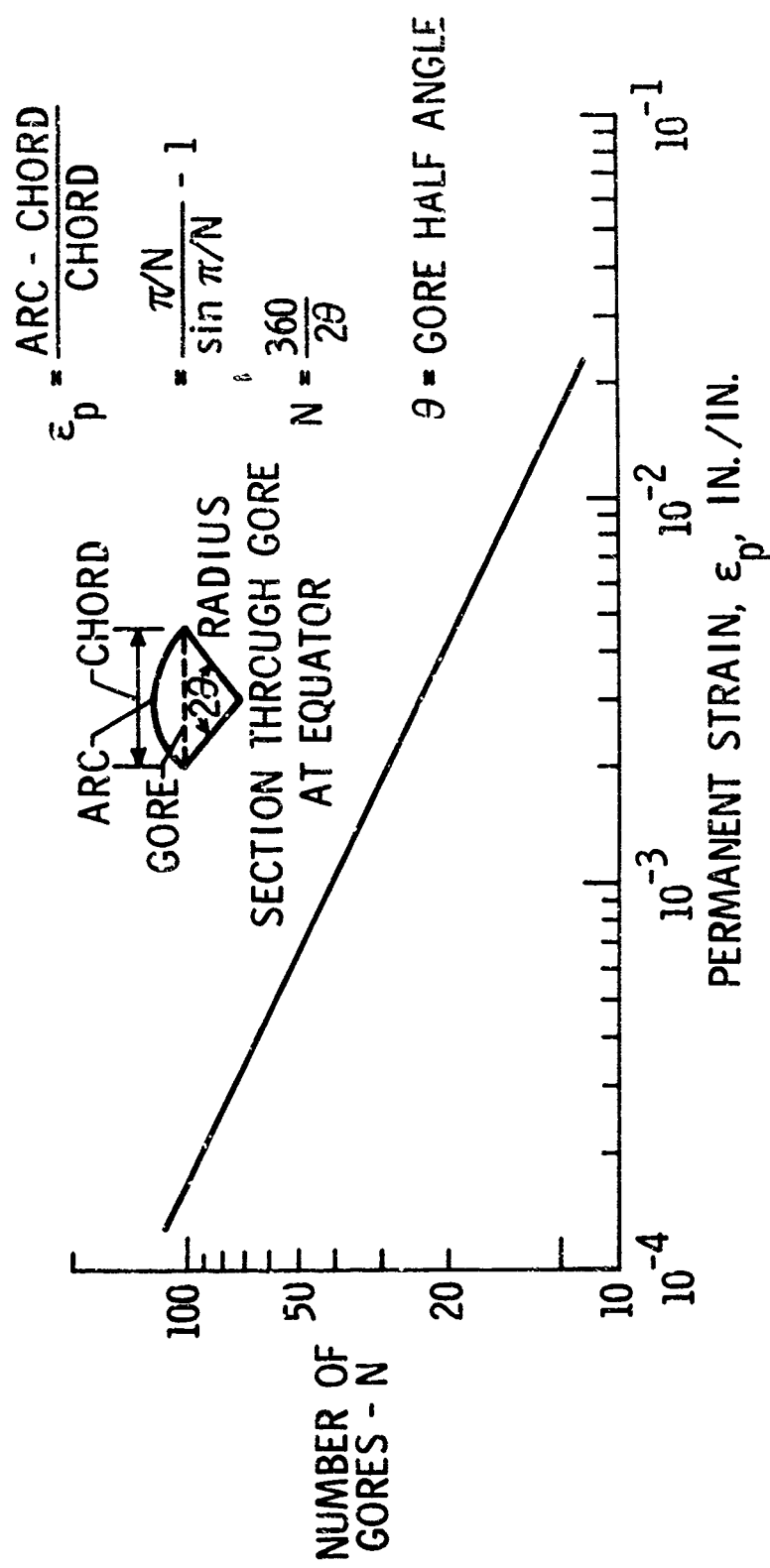
4. The strain required to remove the maximum expected fabrication errors varied from pole to equator by as much as a factor of 10 with the pole area requiring the greatest amount of correction.

5. In general, the sphericity of the 32-gore approximate sphere improved with increasing pressure, but it was not possible to remove a faulty pole-cap area by stressing the balloon to $1\frac{1}{2}$ times the theoretical pressure required to strain the gores to spherical shape.



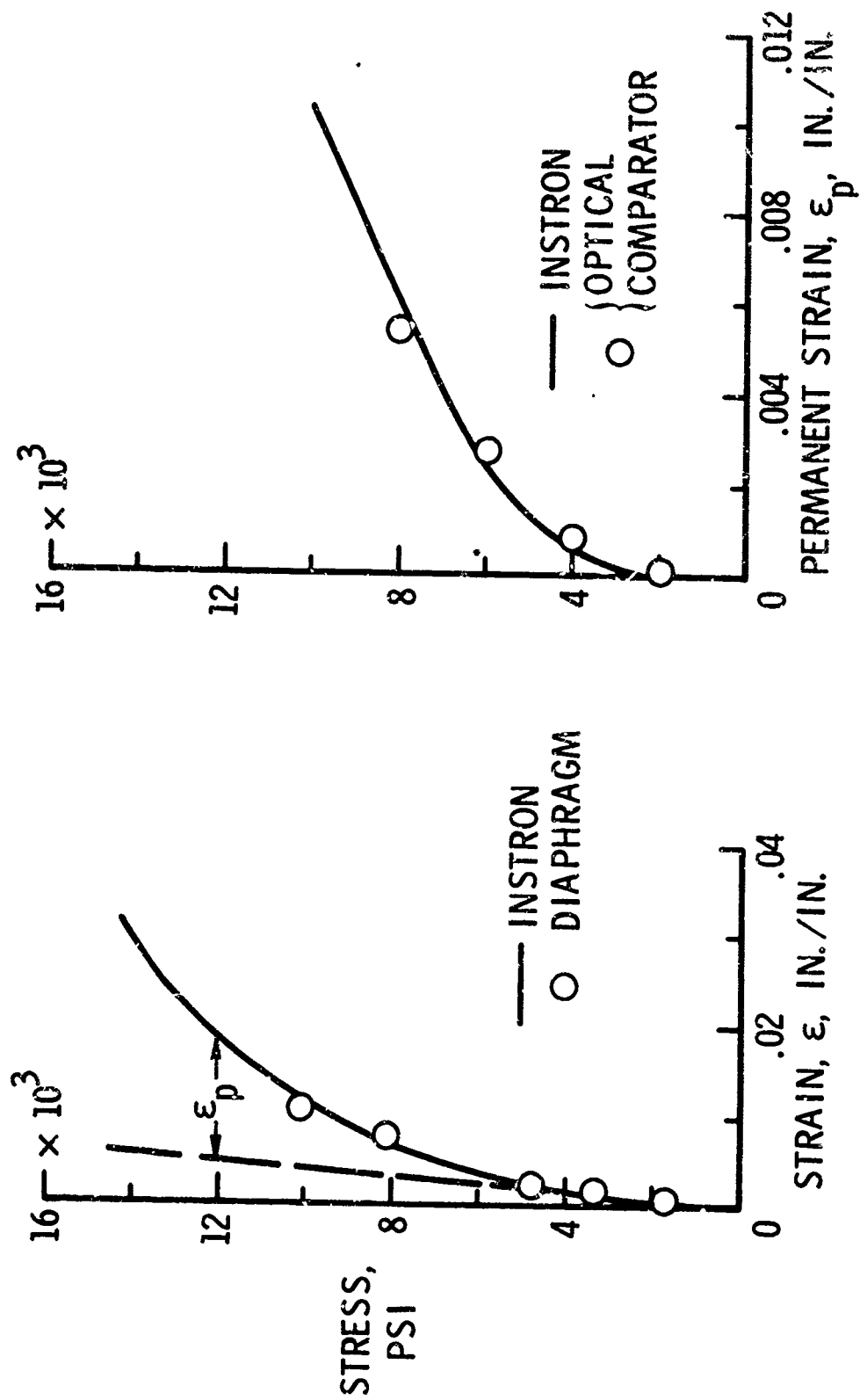
NASA

Figure 1.- Gore construction technique.



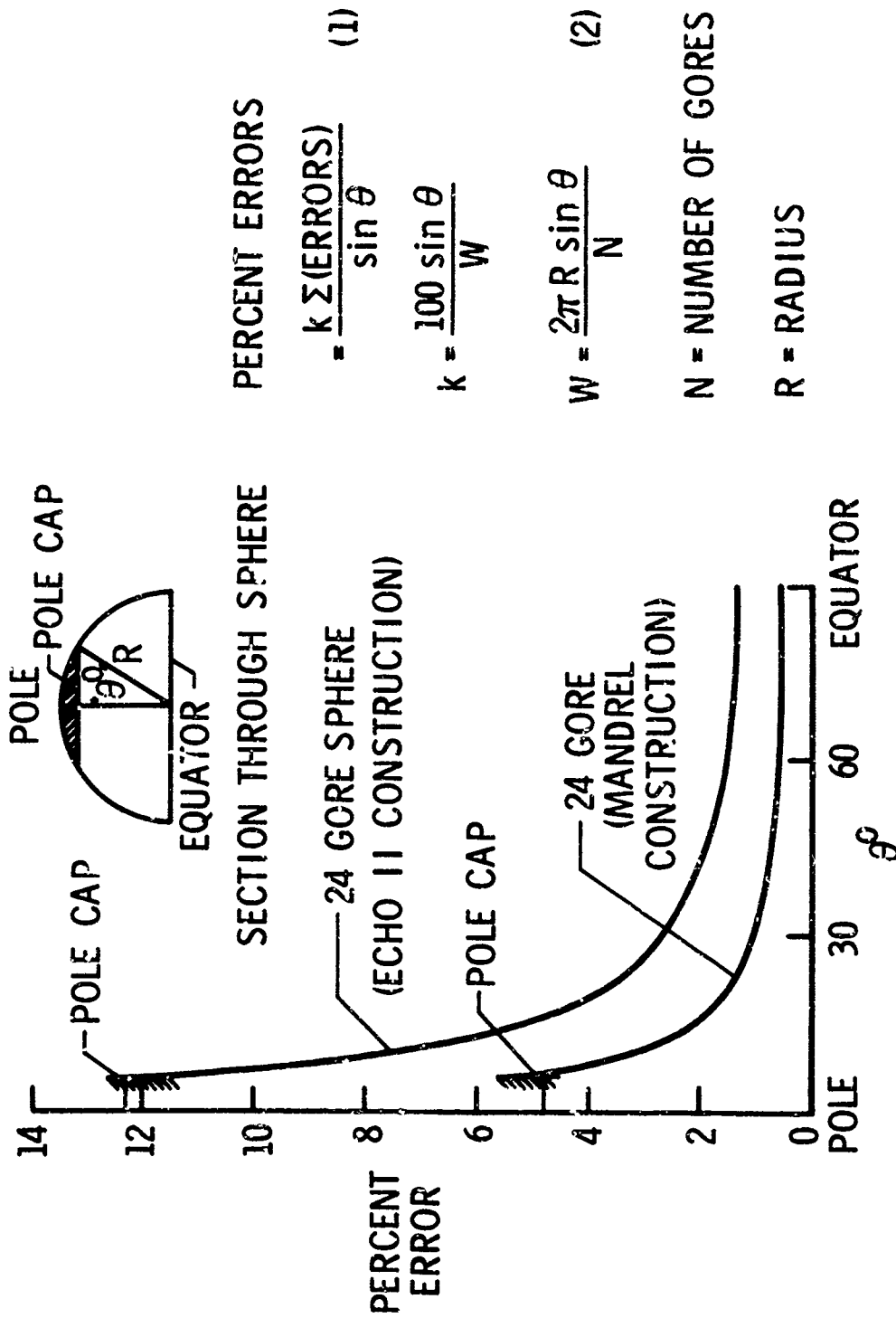
NASA

Figure 2.- Permanent strain requirements as a function of number of gores.



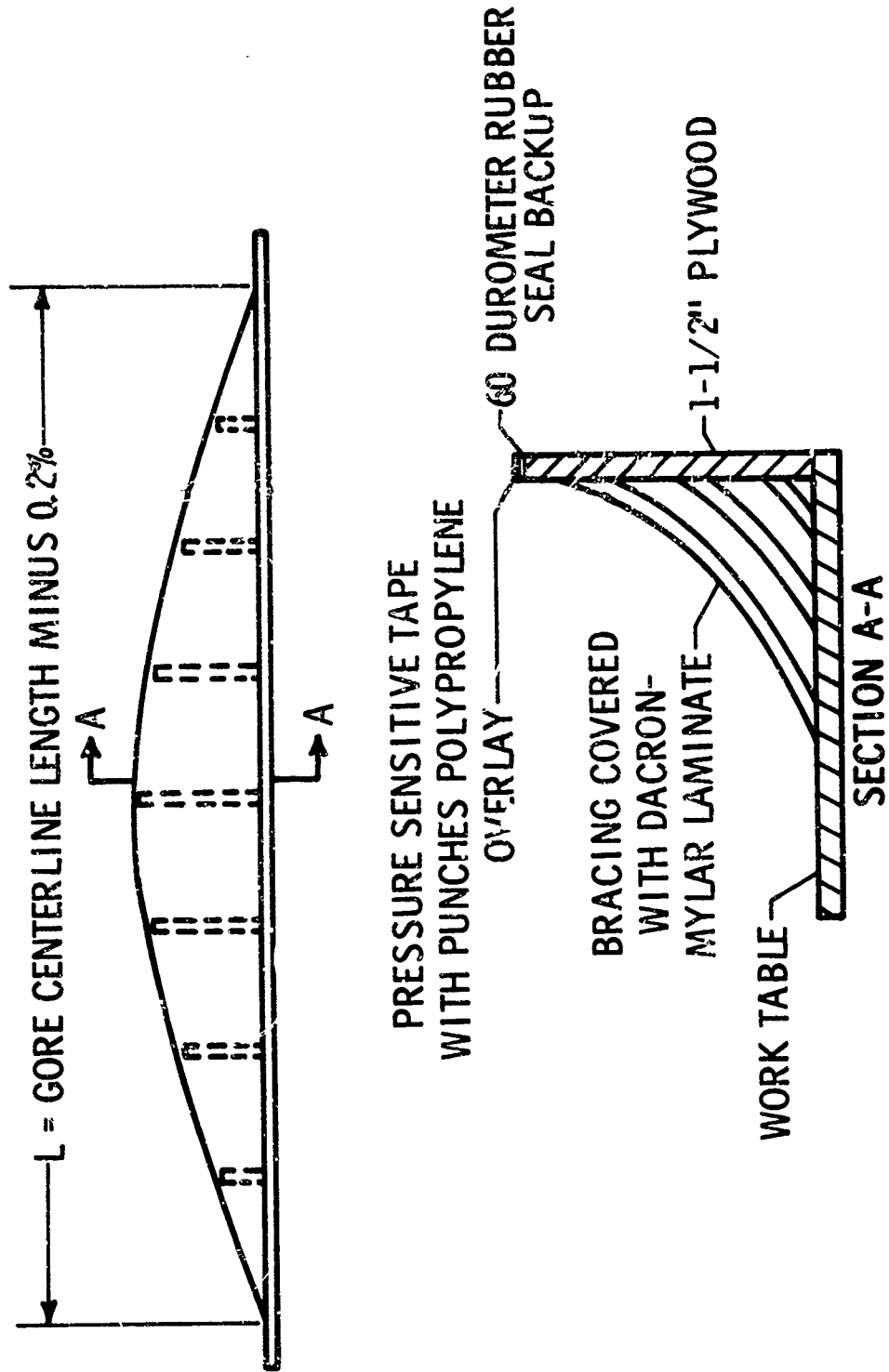
NASA

Figure 3.- Stress/strain data for Echo II material.



NASA

Figure 4.- Variation in maximum error due to fabrication imperfections as a function of angular location on sphere.



NASA

Figure 5.- Typical sealing rail - 12-foot spheres.



NASA

Figure 6.- Mandrel technique for fabrication of gores.

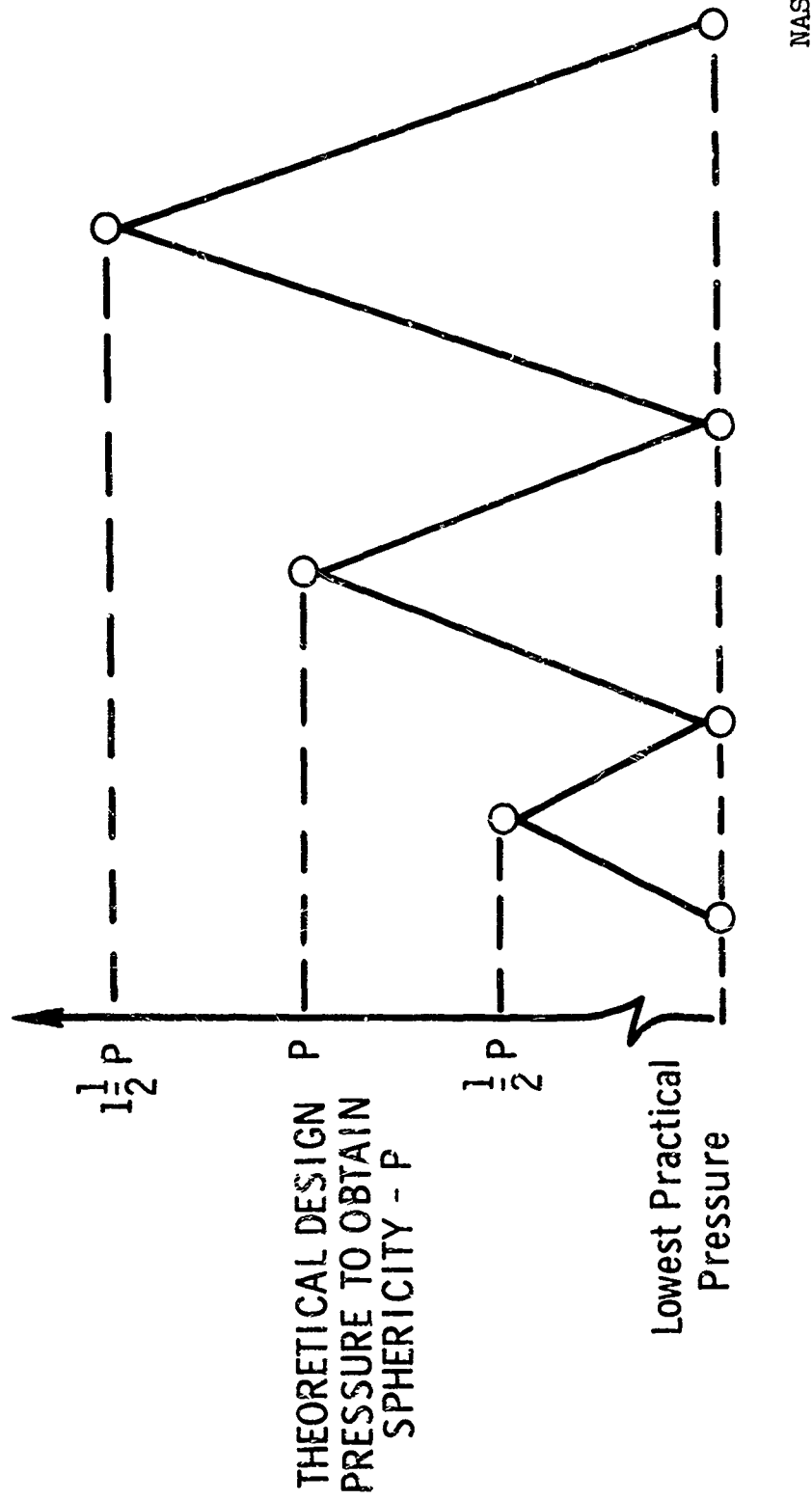


Figure 7.- Techniques used to inflate and measure test spheres.

NASA

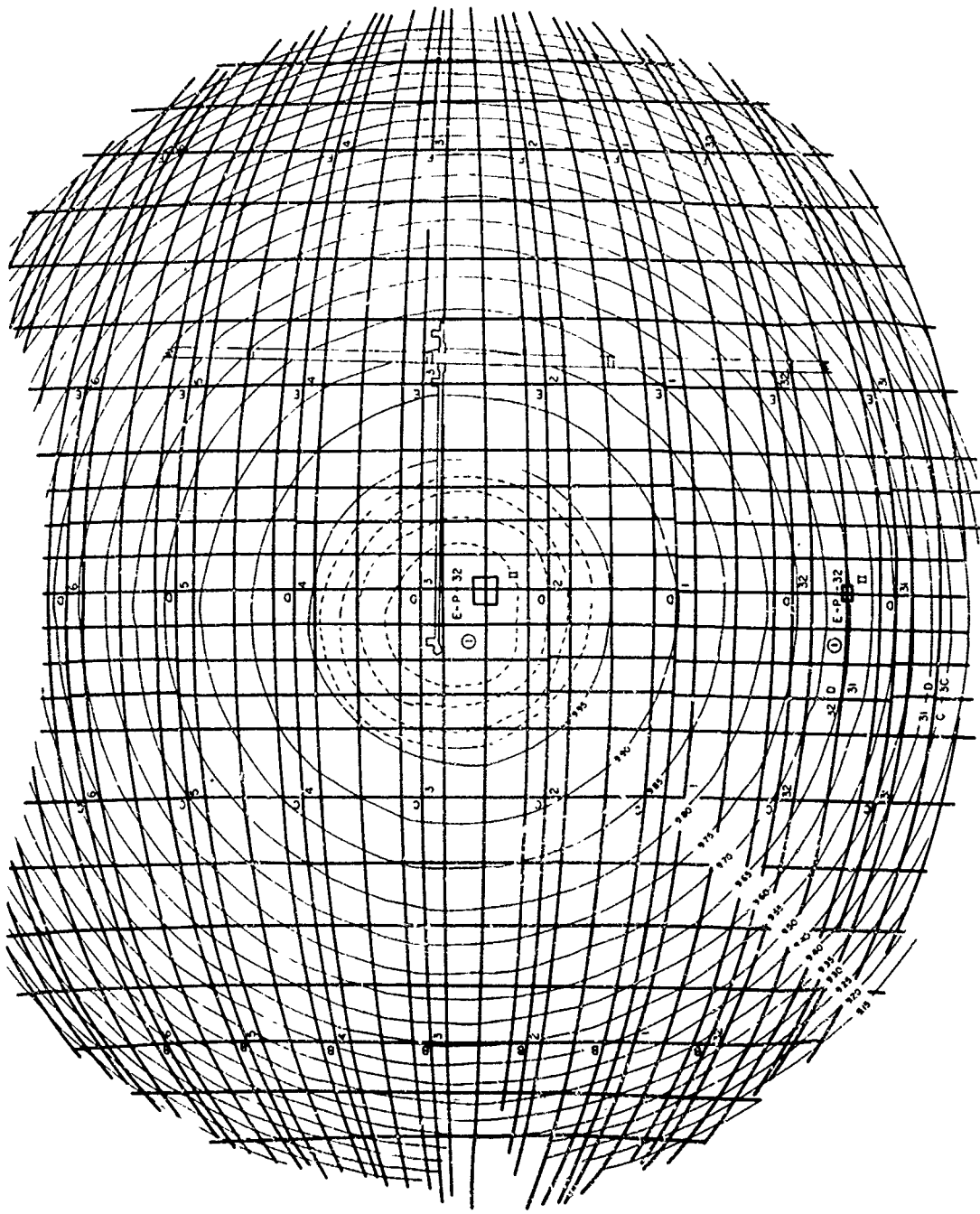
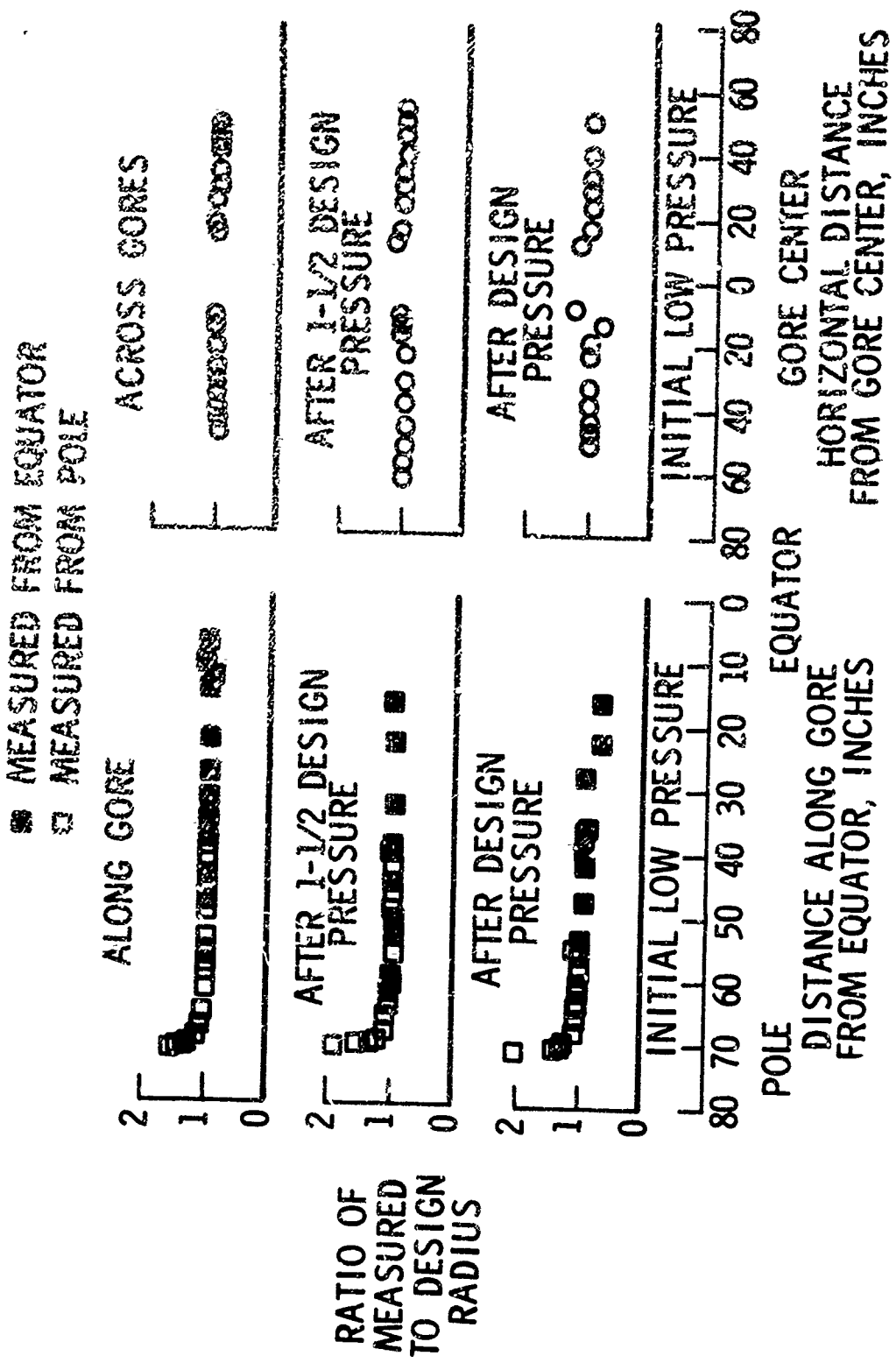


Figure 8.- Typical contour measurement plot.



NASA

Figure 9.- Ratio of measured to design radius of curvature before and after pressurization for 32-gore approximate sphere.

MEMBRANE ANALYSIS OF PRESSURIZED THIN SPHEROID SHELLS
COMPOSED OF FLAT GORES,
AND ITS APPLICATION TO ECHO II

by

Hossein Bahiman
and
John M. Thole

INTRODUCTION

Computation of the shape of a pressurized thin spheroid shell composed of a large number of identical flat gores requires solution of five nonlinear partial differential equations of equilibrium and boundary conditions for three displacements of a gore. The position of each point on the gore could be determined as a function of two independent variables, namely, the distance of the point from the center line of the gore and the latitude of the point with respect to the equatorial plane of the spheroid. For an approximate solution to these nonlinear partial differential equations each displacement is expanded into a power series of the distance of the point from the gore center line such that the coefficients of the power series are at the most functions of the latitude. By equating to zero the terms of the lowest power in each equation, five new nonlinear differential equations for the six coefficients (two for each displacement) are obtained. The approximate solution of these equations by perturbation technique led to three displacement functions of the gore with one unknown constant. Application of variational method to the total elastic strain and potential energy of the system led to the evaluation of the above mentioned constant.

In this analysis, it is assumed that the displacement of the spheroid due to the gravity is negligible compared to the one caused by the constant internal pressure. It is also assumed that the material of the spheroid is homogeneous and isotropic and it obeys Hooke's law.

Finally this method of analysis is applied to Echo II, the 135 foot diameter passive communication satellite. Since the 3-ply aluminum-mylar-aluminum material of the satellite does not satisfy the requirements implied in the above mentioned assumptions, therefore the analytical results obtained here are expected to be only an approximation of the actual case.

THEORY

In order to determine the shape of a thin spheroid shell composed of identical flat gores it is sufficient to compute the true shape of a gore in the pressurized state. To do this, it is assumed that the material of the spheroid is homogeneous isotropic, and linear elastic. It is also assumed that the effect of gravity upon the shape of the spheroid is negligible in comparison with that of the constant internal pressure.

Let Cartesian coordinate axes be drawn in such a way that the origin O be located at the center of the balloon, y axis be along the polar axis, and Z axis be extended through the center of a gore, as shown in Figure 1. Draw $X'Y'Z$ axes from a point P of the gore in such a way that X' axis be parallel to X axis, Z' axis be in the direction OP , and Y' (or Θ) axis be tangent to the meridian at point P (Figure 1).

In the pressurized state of equilibrium, the resultant of all the forces acting on an element of the shell in the direction X' , Θ and Z'

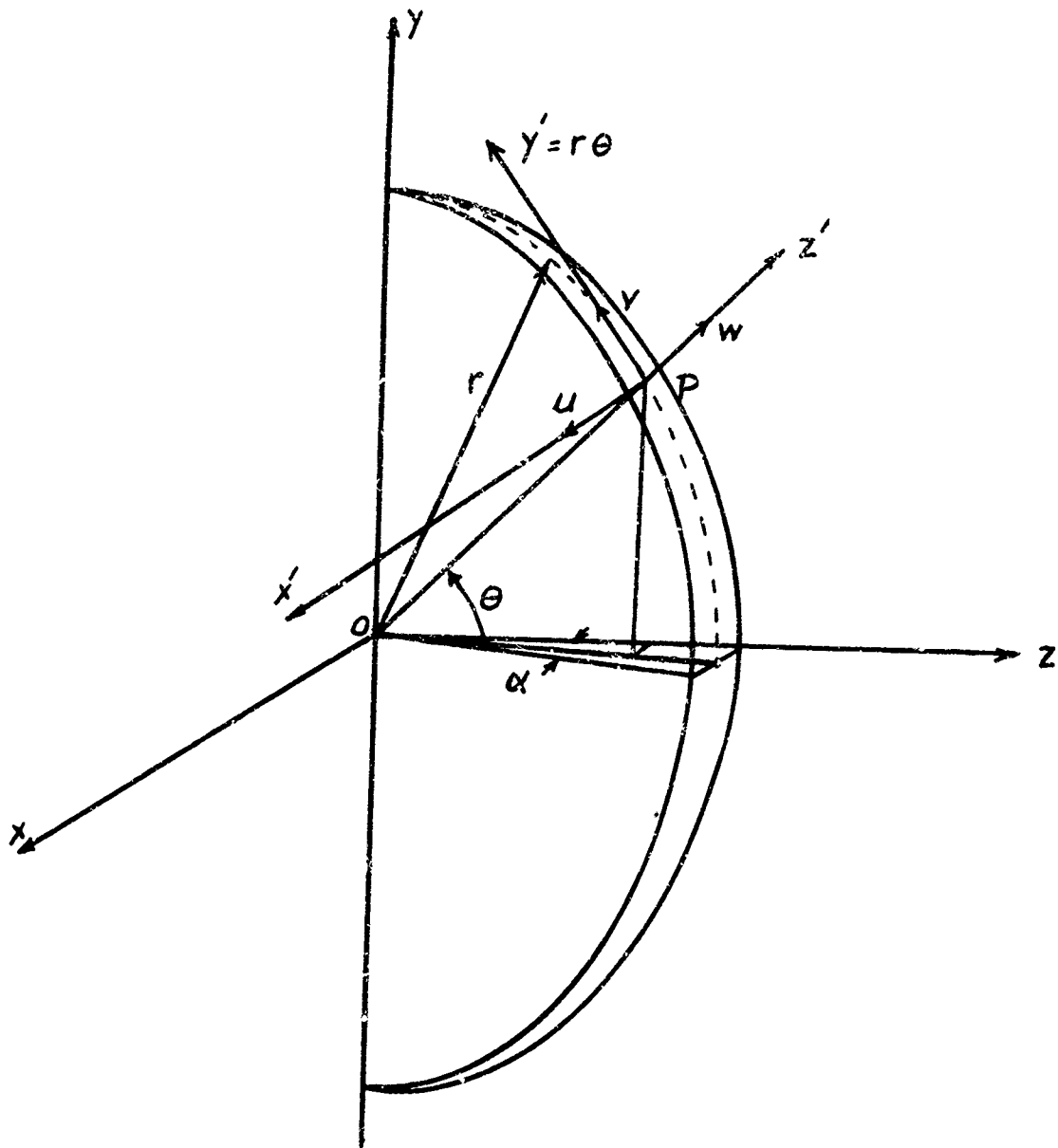


Figure 1 - Coordinate Axes and Displacement Components

vanishes. Let N_x , N_θ , and $N_{x\theta}$ be normal and shear tractions per unit length of membrane, θ be the angle between the position vector and the equatorial plane, and p be the internal pressure of the spheroid, as shown in Figure 2. Hence,

$$\begin{cases} \frac{\partial N_x}{\partial x} + \frac{\partial N_{x\theta}}{r \partial \theta} = 0 \\ \frac{\partial N_{x\theta}}{\partial x} + \frac{\partial N_\theta}{r \partial \theta} = 0 \\ \frac{N_\theta}{r} - N_\theta \frac{\partial^2 w}{r^2 \partial \theta^2} - N_x \frac{\partial^2 w}{\partial x^2} - 2 N_{x\theta} \frac{\partial^2 w}{r \partial x \partial \theta} = p \end{cases} \quad (1)$$

Let u , v , and w be displacement components at a point P in the directions X' , Y' , and Z' respectively (Figure 2). The elastic strains are given by:

$$\begin{cases} \epsilon_x = \frac{\partial u}{\partial x} + \frac{1}{2} \left(\frac{\partial w}{\partial x} \right)^2 \\ \epsilon_\theta = \frac{1}{r} \frac{\partial v}{\partial \theta} + \frac{w}{r} + \frac{1}{2r^2} \left(\frac{\partial w}{\partial \theta} \right)^2 \\ \epsilon_{x\theta} = \frac{1}{2} \left(\frac{1}{r} \frac{\partial u}{\partial \theta} + \frac{\partial v}{\partial x} + \frac{1}{r} \frac{\partial w}{\partial x} \frac{\partial w}{\partial \theta} \right) \end{cases} \quad (2)$$

Also,

$$\begin{cases} N_x = K (\epsilon_x + \mu \epsilon_\theta) \\ N_\theta = K (\epsilon_\theta + \mu \epsilon_x) \\ N_{x\theta} = K (1 - \mu) \epsilon_{x\theta} \end{cases} \quad (3)$$

where $K = \frac{Et}{1-\mu^2}$ is membrane stiffness, and E , t , and μ are Young's modulus, thickness of the shell and Poisson's ratio, respectively. Substitution of Eqs. (2) into Eqs. (3) leads to

$$\begin{cases} N_x = K \left[\frac{\partial u}{\partial x} + \frac{1}{2} \left(\frac{\partial w}{\partial x} \right)^2 + \mu \frac{\partial v}{r \partial \theta} + \mu \frac{w}{r} + \frac{\mu}{2} \left(\frac{\partial w}{r \partial \theta} \right)^2 \right] \\ N_\theta = K \left[\frac{\partial v}{r \partial \theta} + \frac{w}{r} + \frac{1}{2} \left(\frac{\partial w}{r \partial \theta} \right)^2 + \mu \frac{\partial u}{\partial x} + \frac{\mu}{2} \left(\frac{\partial w}{\partial x} \right)^2 \right] \\ N_{x\theta} = \frac{K(1-\mu)}{2} \left(\frac{\partial u}{r \partial \theta} + \frac{\partial v}{\partial x} + \frac{\partial w}{\partial x} \frac{\partial w}{r \partial \theta} \right) \end{cases} \quad (4)$$

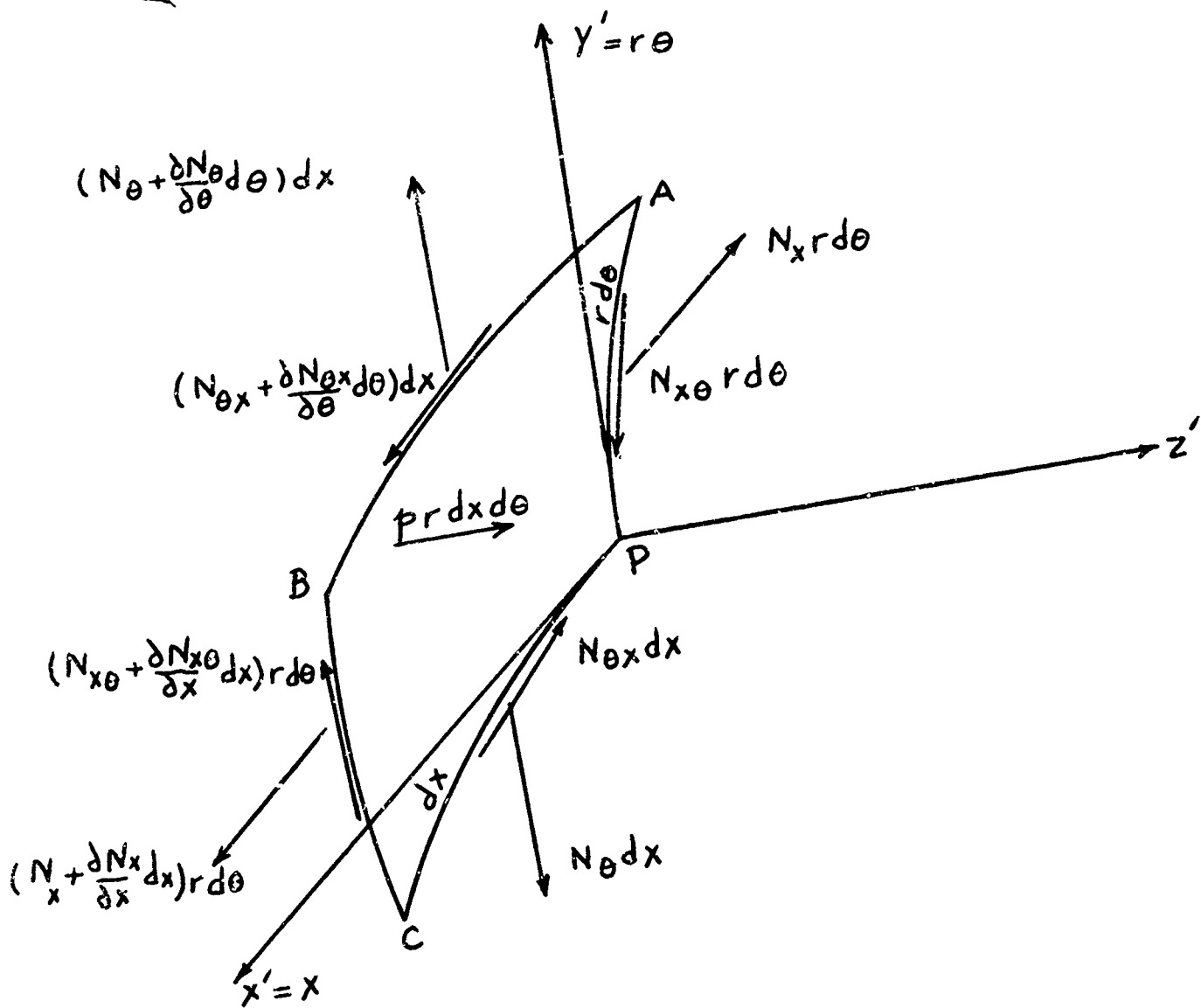


Figure 2 - Forces Acting on an Element of Gore

Substitution of Eqs. (4) into Eqs. (1) yields

$$\begin{aligned}
 & \frac{\partial^2 U}{\partial x^2} + \frac{\partial W}{\partial x} \frac{\partial^2 W}{\partial x^2} + M \frac{\partial^2 V}{r \partial x \partial \theta} + \frac{M}{r} \frac{\partial W}{\partial x} + \frac{M}{r^2} \frac{\partial^2 W}{\partial x \partial \theta} \frac{\partial W}{\partial \theta} + \\
 & \frac{1-M}{2r} \left(\frac{1}{r} \frac{\partial^2 U}{\partial \theta^2} + \frac{\partial^2 V}{\partial x \partial \theta} + \frac{1}{r} \frac{\partial W}{\partial x} \frac{\partial^2 W}{\partial \theta^2} + \frac{1}{r} \frac{\partial^2 W}{\partial x \partial \theta} \frac{\partial W}{\partial \theta} \right) = 0 \\
 & \frac{1-M}{2} \left(\frac{1}{r} \frac{\partial^2 U}{\partial x \partial \theta} + \frac{\partial^2 V}{\partial x^2} + \frac{1}{r} \frac{\partial^2 W}{\partial x^2} \frac{\partial W}{\partial \theta} + \frac{1}{r} \frac{\partial W}{\partial x} \frac{\partial^2 W}{\partial x \partial \theta} \right) + \\
 & \frac{\partial^2 V}{r^2 \partial \theta^2} + \frac{1}{r^2} \frac{\partial W}{\partial \theta} + \frac{1}{r^3} \frac{\partial W}{\partial \theta} \frac{\partial^2 W}{\partial \theta^2} + \frac{M}{r} \frac{\partial^2 U}{\partial x \partial \theta} - \frac{M}{r} W \frac{\partial^3 W}{\partial x^2 \partial \theta} \\
 & - \frac{M}{r} \frac{\partial W}{\partial \theta} \frac{\partial^2 W}{\partial x^2} + \frac{M}{r} \frac{\partial W}{\partial x} \frac{\partial^2 W}{\partial x \partial \theta} = 0 \\
 & \left[\frac{1}{r^2} \frac{\partial V}{\partial \theta} + \frac{W}{r^2} + \frac{1}{2r} \left(\frac{\partial W}{r \partial \theta} \right)^2 + \frac{M}{r} \frac{\partial U}{\partial x} - \frac{M}{r} W \frac{\partial^2 W}{\partial x^2} + \frac{M}{2r} \left(\frac{\partial W}{\partial x} \right)^2 \right] \\
 & \left(1 - \frac{1}{r} \frac{\partial^2 W}{\partial \theta^2} \right) - \frac{\partial U}{\partial x} \frac{\partial^2 W}{\partial x^2} - \frac{1}{2} \left(\frac{\partial W}{\partial x} \right)^2 \frac{\partial^2 W}{\partial x^2} - \frac{M}{r} \frac{\partial V}{\partial \theta} \frac{\partial^2 W}{\partial x^2} \\
 & - \frac{M}{r} W \frac{\partial^2 W}{\partial x^2} - \frac{M}{r^2} \frac{\partial^2 W}{\partial x^2} \left(\frac{\partial W}{\partial \theta} \right)^2 - (1-M) \left(\frac{1}{r^2} \frac{\partial U}{\partial \theta} \frac{\partial^2 W}{\partial x \partial \theta} + \frac{1}{r} \frac{\partial V}{\partial x} \frac{\partial^2 W}{\partial x \partial \theta} \right. \\
 & \left. + \frac{1}{r^2} \frac{\partial W}{\partial x} \frac{\partial W}{\partial \theta} \frac{\partial^2 W}{\partial x \partial \theta} \right) = \frac{1}{K}
 \end{aligned} \tag{5}$$

The boundary conditions are:

$$\begin{cases} N_{x\theta} = 0 & \text{on } x = r\alpha \cos \theta \\ U = \alpha W \cos \theta - \alpha V \sin \theta & \text{on } x = r\alpha \cos \theta \end{cases} \quad (6)$$

along the seam, where $\alpha = \frac{\pi}{n}$. The first expression indicates that due to symmetry shear stress vanishes along the seam where any two adjacent gores meet, and the second expression implies that the points along each seam move in the meridional plane. Since the coefficients of only the first two terms of the power series expansion of displacements will be determined by this method, continuity of slope in the plane normal to the seam cannot be used as a third boundary condition. The use of such a boundary condition would lead to an erroneous solution, namely, that the cross section of the spheroid with any plane normal to its polar axis is a true circle, no matter what the magnitude of the internal pressure. Instead, a virtual displacement is given to the pressurized spheroid in the state of equilibrium and change of the total elastic strain and potential energy of the spheroid and the load is equated to zero.

Let r be the radius of the centerline of a gore before any load is applied, and a, b, c, d, f and g be functions of variable angle θ . Displacements $W, U,$ and V may be expanded into power series as following:

$$\begin{cases} W = ar + b \frac{x^2}{r} + \dots \\ U = cx + d \frac{x^3}{r^2} + \dots \\ V = fr + g \frac{x^2}{r} + \dots \end{cases} \quad (7)$$

Substitution of Eqs. (7) and the last one of Eqs. (4) into Eqs. (5) and (6) leads to

$$\begin{cases}
 6d + (1+\mu) \frac{dg}{d\theta} + 2\mu b + (1+\mu) \frac{da}{d\theta} \frac{db}{d\theta} + \frac{1-\mu}{2} \frac{d^2c}{d\theta^2} + (1-\mu)b \frac{d^2a}{d\theta^2} + 4b^2 = 0 \\
 \frac{1+\mu}{2} \frac{dc}{d\theta} + (1-\mu)g + (1-3\mu)b \frac{da}{d\theta} + \frac{d^2f}{d\theta^2} + \frac{da}{d\theta} + \frac{da}{d\theta} \frac{d^2a}{d\theta^2} - 2\mu a \frac{db}{d\theta} = 0 \\
 \left[\frac{df}{d\theta} + a + \frac{1}{2} \left(\frac{da}{d\theta} \right)^2 + \mu c - 2\mu ab \right] \left(1 - \frac{d^2a}{d\theta^2} \right) - 2bc - 2\mu b - 2\mu ab \\
 - \mu b \left(\frac{da}{d\theta} \right)^2 = \frac{pr}{k} \\
 \frac{dc}{d\theta} + 2g + 2b \frac{da}{d\theta} = 0 \\
 c - a + f \tan \theta = (b-d) \alpha^2 \cos^2 \theta
 \end{cases}$$

(8)

Neglecting small terms of higher order in Eqs. (8) leads to

$$\begin{cases}
 6d + 2\mu b - \mu \frac{d^2c}{d\theta^2} - 2\mu b \frac{d^2a}{d\theta^2} + 4b^2 = 0 \\
 \mu \frac{dc}{d\theta} - 2\mu b \frac{da}{d\theta} + \frac{d^2f}{d\theta^2} + \frac{da}{d\theta} - 2\mu a \frac{db}{d\theta} = 0 \\
 \frac{df}{d\theta} + a + \mu c - 4\mu ab - 2bc - 2\mu b \frac{df}{d\theta} = \frac{pr}{k} \\
 c - a + f \tan \theta = (b-d) \alpha^2 \cos^2 \theta \\
 g = -\frac{1}{2} \frac{dc}{d\theta} - b \frac{da}{d\theta}
 \end{cases}$$

(9)

Since n , the number of gores, is assumed to be large therefore α^2 is very small. Thus perturbation technique can be applied to the functions a , b , c , d , f , and g in the following fashion:

$$\left\{ \begin{array}{l} a(\theta) = a_0(\theta) + \alpha^2 a_1(\theta) + \dots \\ b(\theta) = b_0(\theta) + \alpha^2 b_1(\theta) + \dots \\ c(\theta) = c_0(\theta) + \alpha^2 c_1(\theta) + \dots \\ d(\theta) = d_0(\theta) + \alpha^2 d_1(\theta) + \dots \\ f(\theta) = f_0(\theta) + \alpha^2 f_1(\theta) + \dots \\ g(\theta) = g_0(\theta) + \alpha^2 g_1(\theta) + \dots \end{array} \right. \quad (10)$$

Substitution of Eqs. (10) into Eqs. (9) yields a set of five nonlinear differential equations in terms of a_0 , b_0 , c_0 , d_0 , f_0 , g_0 , a_1 , b_1 , c_1 , d_1 , etc. containing even powers of α . Terms containing each power of α in each differential equation must independently vanish. The terms independent of α must vanish in the following way:

$$\left\{ \begin{array}{l} 6d_0 + 2\mu b_0 - \mu \frac{d^2 c_0}{d\theta^2} - 2\mu b_0 \frac{d^2 a_0}{d\theta^2} + 4b_0^2 = 0 \\ \mu \frac{dc_0}{d\theta} - 2\mu b_0 \frac{da_0}{d\theta} + \frac{d^2 f_0}{d\theta^2} + \frac{da_0}{d\theta} - 2\mu a_0 \frac{db_0}{d\theta} = 0 \\ \frac{df_0}{d\theta} + a_0 + \mu c_0 - 4\mu a_0 b_0 - 2b_0 c_0 - 2\mu b_0 \frac{df_0}{d\theta} = 0 \\ c_0 - a_0 + f_0 \tan \theta = 0 \\ g_0 = -\frac{1}{2} \frac{dc_0}{d\theta} - b_0 \frac{da_0}{d\theta} \end{array} \right. \quad (11)$$

The solution of the above equations could be given as the following:

$$\left\{ \begin{array}{l} b_0 = \text{Constant} = B \\ d_0 = -\frac{2}{3} B^2 - \frac{\mu}{2} B \\ a_0 = c_0 = f_0 = g_0 = 0 \end{array} \right. \quad (12)$$

The coefficients of α^2 in Eqs. (9) must vanish in the following fashion:

$$\left\{ \begin{aligned} 6d_1 + 2\mu b_1 - \mu \frac{d^2 c_1}{d\theta^2} - 2\mu B \frac{d^2 a_1}{d\theta^2} + 8B b_1 &= 0 \\ \mu \frac{dc_1}{d\theta} - 2\mu B \frac{da_1}{d\theta} + \frac{d^2 f_1}{d\theta^2} + \frac{da_1}{d\theta} &= 0 \\ \frac{df_1}{d\theta} + a_1 + \mu c_1 - 4\mu B a_1 - 2B c_1 - 2\mu B \frac{df_1}{d\theta} &= \frac{pr}{k\alpha^2} \\ c_1 - a_1 + f_1 \tan \theta &= \left[\frac{2}{3} B^2 + \left(1 + \frac{\mu}{3}\right) B \right] \cos^2 \theta \\ g_1 &= -\frac{1}{2} \frac{dc_1}{d\theta} - B \frac{da_1}{d\theta} \end{aligned} \right. \quad (13)$$

The solution of Eqs. (13) could be written as:

$$\left\{ \begin{aligned} a_1 &= A_1 \cos 2\theta + A_2 \\ b_1 &= 0 \\ c_1 &= C_1 \cos 2\theta + C_2 \\ d_1 &= D_1 \cos 2\theta \\ f_1 &= F_1 \sin 2\theta \\ g_1 &= G_1 \sin 2\theta \end{aligned} \right. \quad (14)$$

in which the constant coefficients are given by

$$\left\{ \begin{aligned} Y &= \frac{1}{3} B^2 + \left(\frac{1}{2} + \frac{\mu}{3}\right) B \\ F_1 &= \frac{(2\mu B + 1 + \mu^2) Y}{-4\mu^2 B - 2\mu B + \mu^2 - 1} \\ A_1 &= \frac{\mu Y + (2 + \mu) F_1}{2\mu B - \mu - 1} \\ C_1 &= Y + A_1 + F_1 \\ A_2 &= \frac{(\mu - 2B)(F_1 - Y) + \frac{pr}{k\alpha^2}}{1 + \mu - 4\mu B - 2B} \\ C_2 &= A_2 - F_1 + Y \\ D_1 &= -\frac{2\mu}{3} C_1 - \frac{4}{3} \mu B A_1 \\ G_1 &= C_1 + 2B A_1 \end{aligned} \right. \quad (15)$$

Knowing the value of Poisson's ratio, one can easily evaluate in an orderly manner γ , F_1 , A_1 , C_1 , A_2 , C_2 , D_1 , and G_1 as a function of Constant B.

To evaluate constant B, the method of virtual displacement may be utilized. The elastic strain energy of one quarter of a gore is given by

$$T = \int_{\theta=0}^{\theta=\frac{\pi}{2}} \int_{x=0}^{x=r \cos \theta} \frac{1}{2} (N_x \epsilon_x + N_\theta \epsilon_\theta + 2 N_{x\theta} \epsilon_{x\theta}) r dx d\theta \quad (16)$$

Substitution of stress and strain values in Eq. (16) yields

$$T = \int_{\theta=0}^{\theta=\frac{\pi}{2}} \int_{x=0}^{x=r \cos \theta} \left[\frac{K}{2} \left[(c + 3d \frac{x^2}{r^2} - 2ab)^2 + \left(\frac{df}{d\theta} + \frac{x^2}{r^2} \frac{dg}{d\theta} + a + b \frac{z^2}{r^2} + \frac{1}{2} \left(\frac{da}{d\theta} \right)^2 \right. \right. \right. \\ \left. \left. + \frac{1}{2} \frac{x^4}{r^4} \left(\frac{db}{d\theta} \right)^2 + \frac{x^2}{r^2} \frac{da}{d\theta} \frac{db}{d\theta} \right)^2 + 2\mu (c + 3d \frac{x^2}{r^2} - 2ab) \left(\frac{df}{d\theta} + \frac{x^2}{r^2} \frac{dg}{d\theta} + \right. \right. \\ \left. \left. a + b \frac{x^2}{r^2} + \frac{1}{2} \left(\frac{da}{d\theta} \right)^2 + \frac{1}{2} \frac{x^4}{r^4} \left(\frac{db}{d\theta} \right)^2 + \frac{x^2}{r^2} \frac{da}{d\theta} \frac{db}{d\theta} \right) \right] + \frac{1-\mu}{2} \left(\frac{x}{r} \frac{dc}{d\theta} + \frac{x^3}{r^3} \frac{dd}{d\theta} + \right. \\ \left. + \frac{2x}{r} g + \frac{2x}{r} b \frac{da}{d\theta} + 2 \frac{x^3}{r^3} b \left(\frac{db}{d\theta} \right)^2 \right] r dx d\theta \quad (17)$$

In a virtual displacement corresponding to change of B by δB the work done by the internal pressure for a quarter of a gore is given by

$$\frac{\delta \bar{W}}{\delta B} \delta B = p \int_{\theta=0}^{\theta=\frac{\pi}{2}} \int_{x=0}^{x=r \cos \theta} \frac{\delta W}{\delta B} r dx d\theta \delta B \quad (18)$$

in which \bar{W} is the total work done by the internal pressure for a quarter gore, and W is the radial displacement given by Eqs. (7). Hence, the

Constant B could be determined from

$$\frac{\delta T}{\delta B} = p \int_{\theta=0}^{\theta=\frac{\pi}{2}} \int_{x=0}^{x=r \cos \theta} \frac{\delta W}{\delta B} r dx d\theta \quad (19)$$

Thus for a given pressure p, Eq. (19) in conjunction with Eq. (17), (7), (10), (12), (14) and (15) furnishes B which upon substitution into Eq.

(15) gives coefficients A_1 , A_2 , etc. Substitution of these coefficients into Eq. (14) in conjunction with Eqs. (7), (10) and (12) gives the three displacement functions u , v , and w .

APPLICATION OF THEORY TO ECHO II

The 135 foot diameter Echo II is composed of 106 identical gores with a maximum width of 4 feet which occurs in the equatorial plane of the balloon. The 3-ply material of the balloon is composed of 0.00035 in. thick mylar sandwiched between two layers of aluminum of 0.00018 in. thickness each. The adjoining gores are located edge to edge with each other with one inch wide tape of the same material sealing the seams lengthwise. When separation of the two half-canisters takes place in the initial phase of orbiting, the residual air and water vapor inside the folded balloon which is of the order of magnitude of one millimeter inflates the satellite. While initially flat, each gore forms a narrow transverse portion of a half circular cylindrical surface of 135 feet diameter. Thus the initial shape of the balloon is a spheroid with 0.356 in. maximum deviation from a sphere which occurs in the equatorial plane.

Due to the solar radiation skin temperature increases and as a result inflation material sublimates and builds up pressure until a maximum internal pressure of 225 microns is reached. This maximum pressure corresponds to a membrane stress of 1.7 lb/in.

Although the material of the balloon is rather nonhomogeneous and anisotropic and it does not quite obey Hooke's law, nevertheless for the purpose of approximation, it is assumed that the requirements of homogeneity, isotropy and linear elasticity necessitated by this analysis are met.

The average value of K corresponding to 1.70 lb/in. skin traction (given by Tests No. 1, 3, 4, and 6 of Reference 3) is 1050 lb/in.

Since nominal Young's modulus for aluminum is 10.5×10^6 psi and for mylar is $.55 \times 10^6$ psi, therefore it is expected that aluminum should carry most of the load. The nominal value of K for aluminum layers is given by:

$$K_n = \frac{Et}{1-\mu^2} = 4240 \text{ lb/in.}$$

in which $\mu = .33$ has been inserted. This value of K_n is much larger than the experimental value $K = 1050$ lb/in. Therefore, the actual Young's modulus and perhaps Poisson's ratio for thin layers of aluminum are smaller than the nominal ones.

Following the steps suggested in the last paragraph of the previous section one could get an Eigen value equation for B whose coefficients are functions of parameter $m = \frac{pR}{K\alpha^2}$. For different values of maximum pressure the fundamental Eigen value for B is computed and listed in Table 1. Hence for $p = 225$ micron (or $.000435$ lb/in²).

$$m = \frac{.000435 \times 810}{1050 \times \left(\frac{17}{106}\right)^2} = 3.81$$

which corresponds to $B = -.319$ in Table 1. Thus, the maximum differential radial displacement at the midgore and at the seam which occurs in the equatorial plane is given by

$$w \Big|_{\substack{\theta=0 \\ x=0}} - w \Big|_{\substack{\theta=0 \\ x=24''}} = B \frac{x^2}{r} \Big|_{x=24''} = 0.227 \text{ in}$$

This corresponds to a maximum radial difference

$\Delta = 0.356 - 0.227 = 0.129$ in which 0.356 is in its initial unpressurized value.

TABLE I

Values of B versus m

m	B	m	B	m	B	m	B	m	B
0	0	2.0	-.294	4.0	-.320	6.0	-.320	8.0	-.317
.1	-.043	2.1	-.298	4.1	-.320	6.1	-.320	8.1	-.317
.2	-.079	2.2	-.300	4.2	-.320	6.2	-.320	8.2	-.317
.3	-.109	2.3	-.303	4.3	-.320	6.3	-.319	8.3	-.317
.4	-.135	2.4	-.305	4.4	-.320	6.4	-.319	8.4	-.317
.5	-.157	2.5	-.307	4.5	-.320	6.5	-.319	8.5	-.317
.6	-.176	2.6	-.309	4.6	-.320	6.6	-.319	8.6	-.316
.7	-.193	2.7	-.311	4.7	-.320	6.7	-.319	8.7	-.316
.8	-.207	2.8	-.312	4.8	-.321	6.8	-.319	8.8	-.316
.9	-.220	2.9	-.313	4.9	-.321	6.9	-.319	8.9	-.316
1.0	-.213	3.0	-.314	5.0	-.321	7.0	-.319	9.0	-.316
1.1	-.241	3.1	-.315	5.1	-.321	7.1	-.318	9.1	-.316
1.2	-.250	3.2	-.316	5.2	-.321	7.2	-.318	9.2	-.316
1.3	-.258	3.3	-.317	5.3	-.321	7.3	-.318	9.3	-.316
1.4	-.265	3.4	-.318	5.4	-.320	7.4	-.318	9.4	-.316
1.5	-.272	3.5	-.318	5.5	-.320	7.5	-.318	9.5	-.315
1.6	-.277	3.6	-.319	5.6	-.320	7.6	-.318	9.6	-.315
1.7	-.282	3.7	-.319	5.7	-.320	7.7	-.318	9.7	-.315
1.8	-.287	3.8	-.319	5.8	-.320	7.8	-.317	9.8	-.315
1.9	-.291	3.9	-.320	5.9	-.320	7.9	-.317	9.9	-.315

CONCLUSIONS

The maximum differential radial displacement of a pressurized spheroid, which is composed of identical flat gores, in a zero gravity field, computed by this technique is believed to be a very good approximation to the true one, provided that the material is homogeneous, isotropic, and linearly elastic.

REFERENCES

1. Timoshenko, S. and Woinowsky, Krieger S., "Theory of Plates and Shells," McGraw-Hill Book Co., Inc., New York, 1959.
2. Schuerch, H., "Structural Analysis of Echo II," ARC-R-91, Astro Research Corp., Santa Barbara, California, May 2, 1963.

ASTRONAUT MANEUVERING UNIT TECHNOLOGY

Peter M. Van Schaik
Air Force Aero Propulsion Laboratory

INTRODUCTION

Astronaut Maneuvering Unit (AMU) has been the title given personal propulsion systems for astronauts who will venture outside space vehicles to perform maintenance, assembly, surveillance, and repair while in orbit. The requirement for extra-vehicular activities has been derived from studies (Ref 1) of spacecraft that maintain long duration orbits. The orbital time for Project Mercury and Gemini are not of sufficient length to require extra-vehicular activities such as maintenance. In the low orbits, redundancy is the most economical method for safety of flight and mission success. If failure should occur or system degradation begin, manual take-over of the flight systems has been accomplished. In case of severe system malfunction, the spacecraft can be deorbited in one-half to one orbit period. However, as orbits become higher and longer in duration, the ability to accomplish fast retrieval decreases while the need for on the spot repairs become more urgent.

To accomplish extra-vehicular activities personal propulsion systems are required. It is not practical to use handholds or handrails over the surface of the vehicle due to weight and complexity. This complexity arises in the fact that surface protrusions are affected by aerodynamic drag during lift-off and re-entry. Individual propulsion units which are self-contained provide the capability to survey and inspect any portion of his vehicle or a second vehicle thereby increasing his capability many-fold.

There have been many poor or inadequate concepts proposed for EVA travel due to a misconception of the purpose required. Extra-vehicular activities do not involve only straight-line "flying" from point A to point B. To perform maintenance and inspect the surface, the astronaut must maneuver in various planes, curvatures, and angles. This alone defeats most hand-held and unstabilized systems. Systems which have six full degrees of freedom must have some control mode other than just open-loop.

The research systems currently undergoing development are the Modular Maneuvering Unit (MMU), Astronaut Maneuvering Unit (AMU), and Remote Maneuvering Unit (RMU). The remainder of this paper will discuss these current systems, discuss problems being encountered, and discuss design criteria and new subsystems which have great potential.

CURRENT DESIGNS

The three systems previously mentioned are concepts which have resulted from studies (Ref 2, 3), analyses, and considerable in-house

testing. In the early days of exploratory development, a design called the Self Maneuvering Unit (SMU) (Fig 1) was designed and fabricated. This unit was test flown in zero-g aircraft for over 250 Keplerian Trajectories (approx 3000 seconds of weightless time.) The data from these flights, although only qualitative in nature, did demonstrate the concept to be feasible. It showed that a back-pack is out of the way mounted on the back, that one hand can be kept free to absorb small impacts and permit carrying of tools, and that after a training period the man can control and maneuver with sufficient precision to arrive properly at worksites. Straight flights down the aircraft compartment are not sufficient to prove feasibility. Translations followed by 90° and 180° turns, then stopping properly oriented at worksites proved the best demonstration of performance.

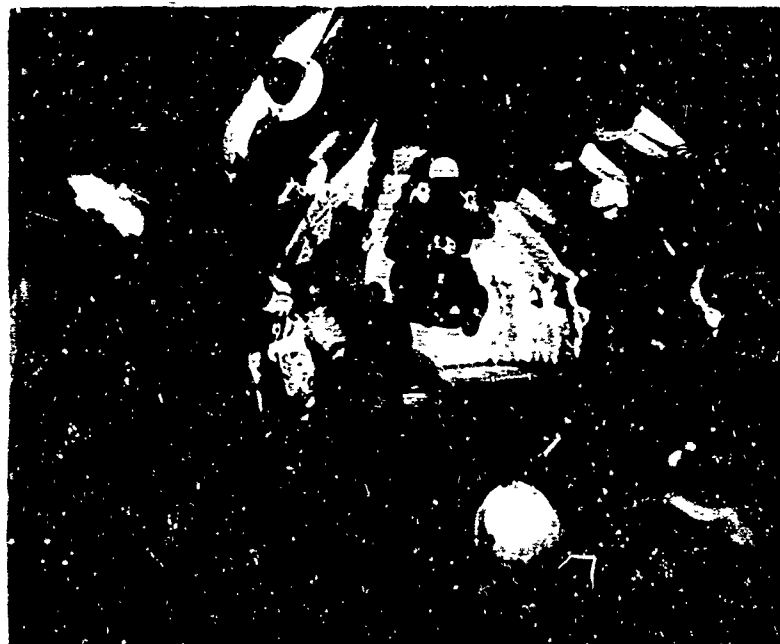


Fig 1 - Self Maneuvering Unit

Modular Maneuvering Unit

The Modular Maneuvering Unit (MMU)(Fig 2) represents a system based upon the SMU tests and modified to be compatible with the Gemini Spacecraft. The SMU was a general concept using ten (10) nozzles for maneuvering. This was accomplished by three (3) forward and three (3) aft nozzles, two (2) up and two (2) down nozzles. This crotch nozzle proved to be impractical as it provided no redundant features and introduced some cross coupling. The MMU incorporated twelve (12) nozzles which was accomplished by deleting the crotch nozzle and incorporating nozzles on each side of the hips.



Fig 2 - Modular Maneuvering Unit

The MMU was further modified by the addition of a chest pack to contain the primary ECS system hardware and emergency oxygen gas. The chest pack also provided a mounting for the status displays and abort alarm indicators. The back pack module contains all other systems for flight. It contains a hydrogen peroxide propulsion system with a total capability of about 3000 pound-seconds of propellant which is expended through the twelve (12) nozzles each having 2.4 pounds of thrust each. It contains a high pressure oxygen bottle which provides the oxygen source to the chest pack during the MMU mission. It contains a pulse modulated stabilization system utilizing three (3) rate gyros for altitude error sensing. This error signal is sent through a logic network to fire or inhibit the twelve nozzles. In addition, the back pack contains a telemetry system for transmitting biomedical data and MMU performance information. A voice transceiver is included for communication of astronaut with the spacecraft. Finally, a battery pack is included to provide self-contained power to all sub-systems. The control system will entail two side arm controllers, one for attitude and one for translation. The controls will be mounted on extendable arms to simplify the interface with the chest pack and suit.

The modifications were necessary due to space limitations which prevented storage of a back-pack in the cockpit. The chest pack, when con-

nected to the spacecraft umbilical, serves to provide ECS during egress/ingress permitting external storage of the back-pack. The chest-pack is also utilized during the MMU flight.

Astronaut Maneuvering Unit

The Astronaut Maneuvering Unit (AMU) (Fig 3) represents an integrated design based upon the old SMU design. In the AMU, the environmental control system is contained completely in the back-pack. This is obtainable through a closed ECS system of fan-battery or wet-fan types thereby eliminating the need for a chest pack. Obviously without a chest pack, the AMU must be stowed internally in the crew compartment to permit donning and checkout prior to going extra-vehicular. The control system can be obtained through a waist mounted box like the SMU or a multi-freedom control pole.

The AMU is back-mounted utilizing the 12 nozzle configuration and containing 3000-3500 pound-seconds of propellant. It contains the other subsystems such as the closed loop ECS system capable up to 3 hours of outside operation, stabilization using rate gyros, telemetry, voice transceiver, and a self contained power supply. The control was mentioned before.

CURRENT PROBLEM AREAS

In the development of the MMU and AMU, as well as testing other concepts, certain problem areas have come to light. Many of these have been fixed to satisfy the current system requirements but have not necessarily been solved for future systems. In light of tight schedules and high cost it has not been possible to redesign the system to eliminate the problem but rather the approach is to derive a solution commensurate with the schedule. Bringing these problems to light and discussing them, should permit better solutions in future applications.

Configuration

The MMU is a good example of configuration problems caused by designing the maneuvering system after the suit and spacecraft were designed. This is not the optimum design practice but it was the only configuration possible in order to even fly. One of the problems has been the suit design. The suit is designed for a semi-reclining astronaut instead of standing. This semi-reclined position causes the back to take on an egg-shaped contour making it extremely difficult to match a back-pack. The only way to circumvent this problem is to mold the pack around the astronaut to further complicate the problem each astronaut has a different back contour requiring adjustments. This molding of the pack makes the pack look bigger and results in packaging efficiency loss. This hunched-over position makes the astronaut's normal line-of-sight at approximately 45 degrees below the normal horizontal. This creates a thrust mis-alignment between the nozzle orientation and the line-of-sight. Obviously, in the weightless space the astronaut will tend to fly with forward being the normal relaxed eye position. This can be partially corrected but often solutions are possible, as we'll see later.

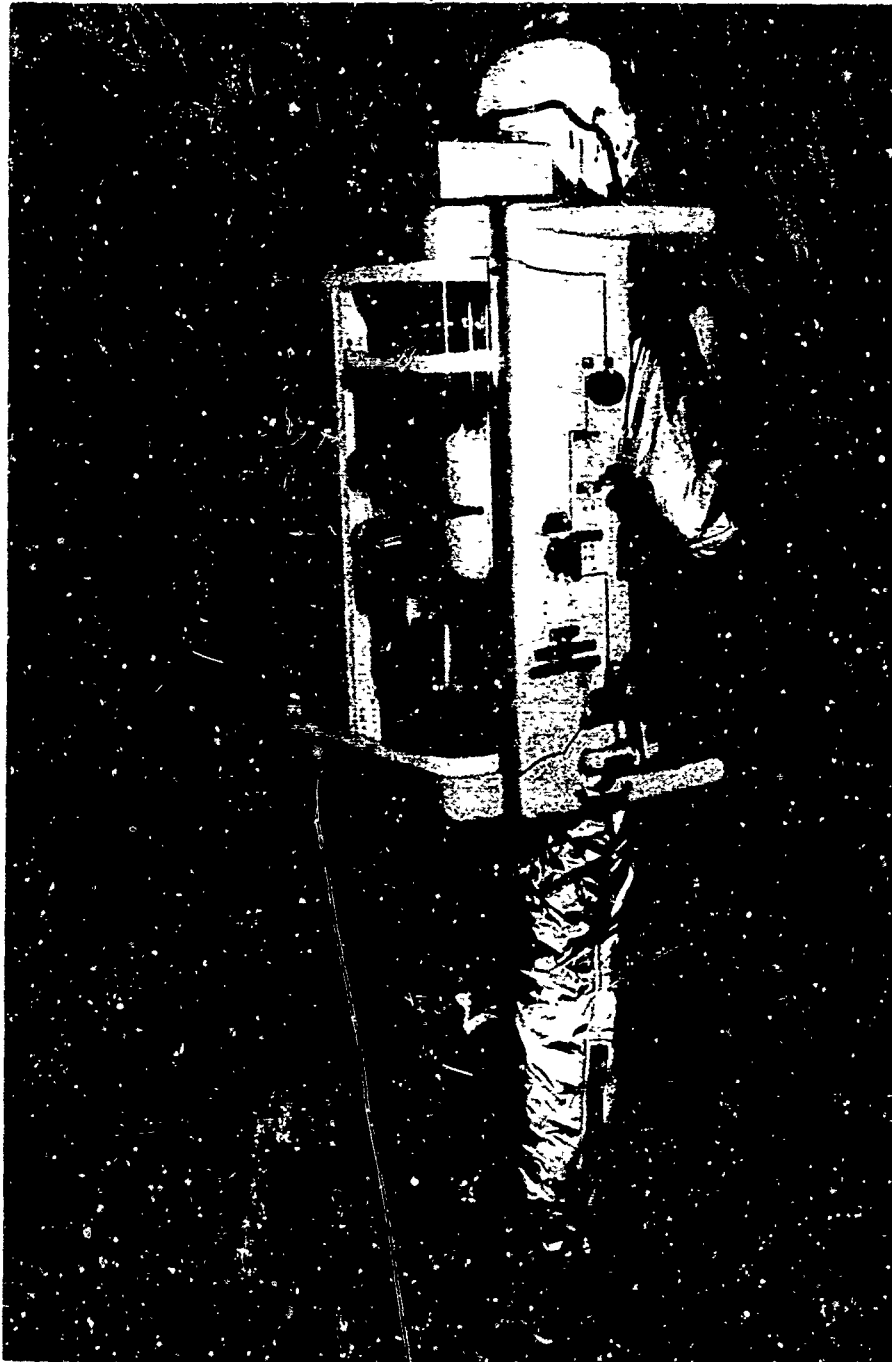


Fig 3 - Astronaut Maneuvering Unit

Another problem in the pack-suit area is the lack of mobility and dexterity. All equipment must be built strong and fool-proof since the astronaut has elephant strength when pressurized. In his attempts to overcome the suit pressure he also can deform fragile controls and cannot perform delicate control movements. Therefore, proportional controls are useless unless they are gross in nature.

Plume Heating

The surface heating of the space suit by the exhaust plume has been one area overlooked or over-simplified by many designs. It has become a serious problem in the AMU where the nozzles are anywhere from 3-12 inches from the suit. The plume expansion envelope was analyzed by both mathematical techniques and actual chamber test firings (Ref 4). As there were many unknowns at the time this study was made such as: nozzle design, nozzle locations, suit materials, and thrust levels, the impact of the study was never fully realized. However, as these parameters were defined the problem became more apparent. Many people have been misled by nozzle firings at atmospheric pressures during which the plume fails to expand as that in a vacuum. The plumes from 5 pound thrusters approach 20 inches in length and 8 inches in diameter causing serious heating problems. Most suits cannot tolerate local heating in excess of 500°F. In figures 4A and 4B typical plumes are shown. As can be seen the AMU configuration with twelve nozzles presents many heat-

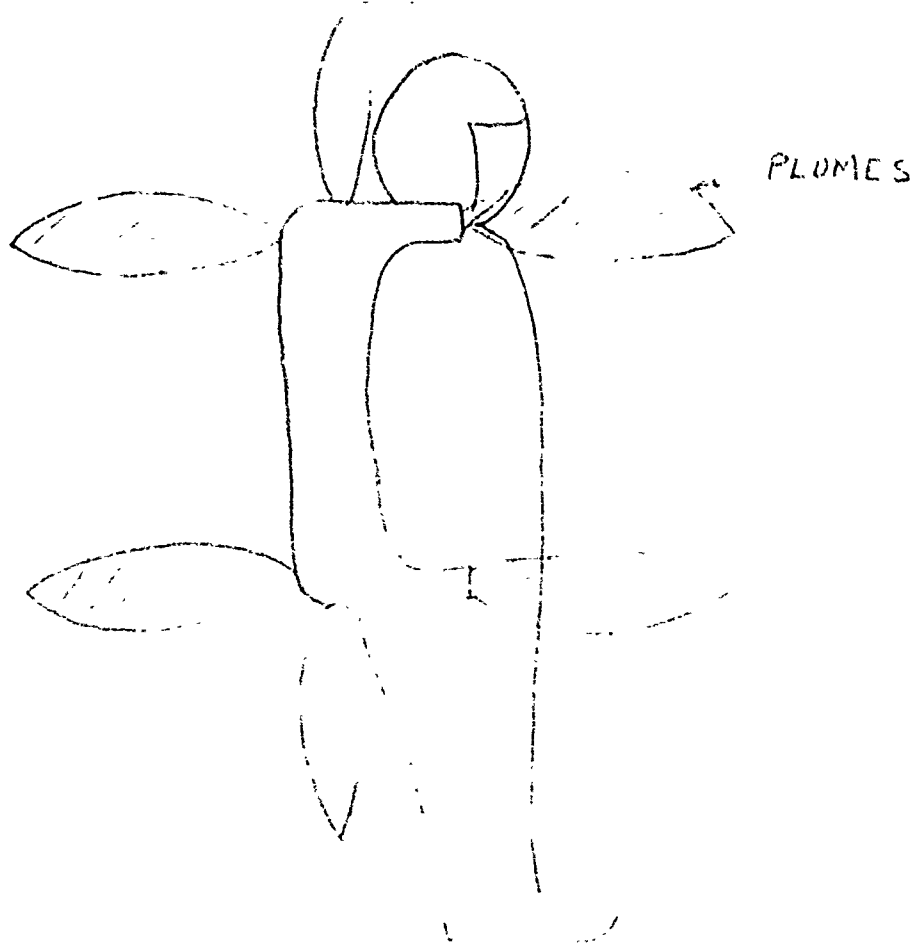
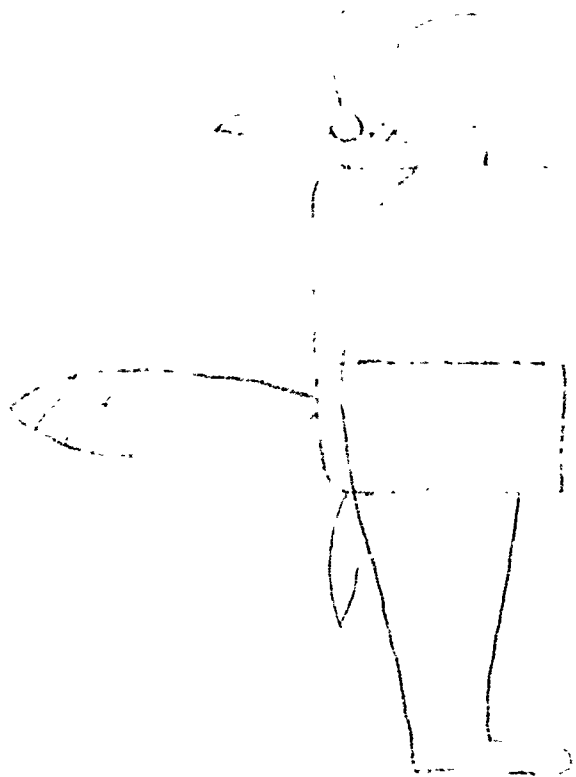


Fig 4A - Exhaust Plume Outline
(5# Nozzle, Mach 8 line shown)



**Fig 4B - Exhaust Plume Outline
(Stamp Configuration)**

ing areas, particularly on the helmet, shoulder, front and rear legs. The severity of the problem is illustrated below. This pulse is typical of the

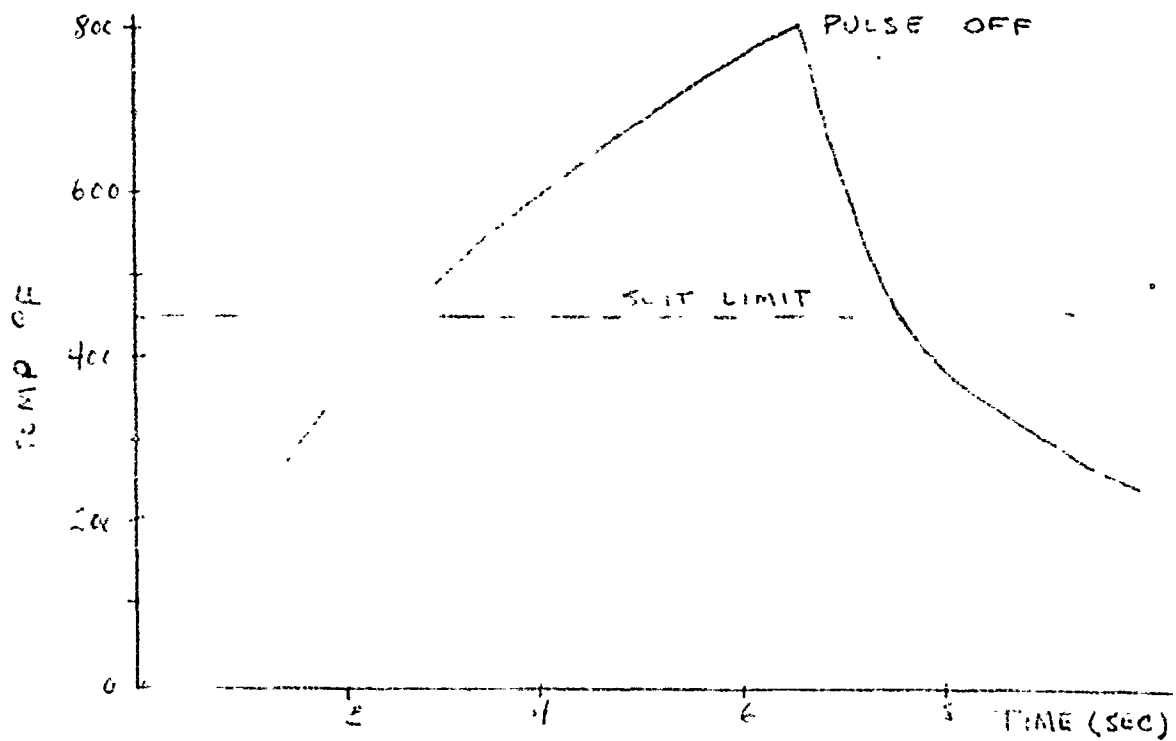


Fig 5 - Heating Rate on Suit Surface
639

Normal translation pulses although the maximum time (counting thrust on for forward and retro) may reach 12 seconds.

Stabilization

Early studies of the SMU (Ref 2) and in-house testing (Ref 3) determined that stabilization is required when complicated maneuvers, such as required during extra-vehicular maintenance, and for relatively long translations are attempted. This conclusion was primarily based on the fact that visual reference from stars were not obtainable and that once man loses the target he can no longer detect the difference between pitch motion and vertical movement. The same occurs in the other axis. Space flights that have occurred since these original studies and tests have confirmed that stars are visible and can be used as references. In addition, additional zero-g testing has shown that man after considerable training can fly most short translations in "open-loop". It may now be possible to modify the control and stabilization system from full control to a partial control system. By partial control it is meant that the stabilization system prevents the astronaut from going out of control but in normal flight does not interfere.

The SMU experimental maneuvering unit, utilized off-on jets and an amplitude type control system as shown below. This system never worked

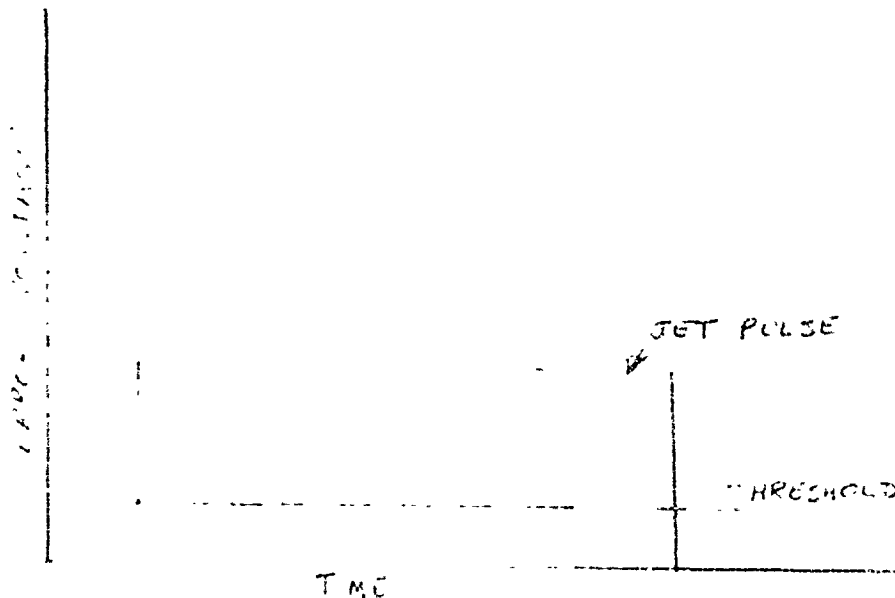


Fig 6 - Pulse Plot

properly because with the one size pulse the system went into oscillations. This was due to the large pulse still being on as the error approached the threshold which drove the SMU past zero. The new system being used in the Modular Maneuvering Unit (MMU) and Remote Maneuvering Unit (RMU) installed a pulse ratio system using a pulse modular. This is illustrated below.

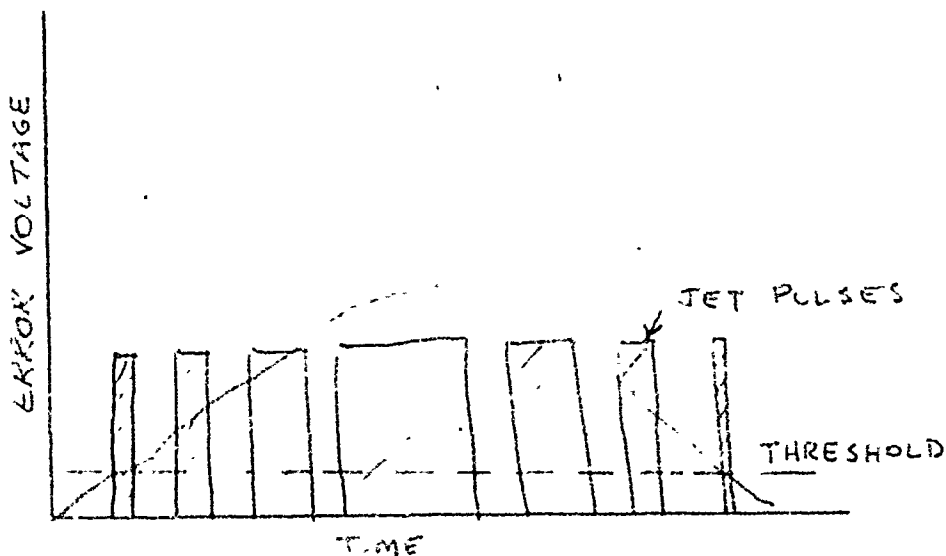


Fig 7 - Pulse Plot

This system has resulted in considerable propellant savings due to pulses being proportional to error and the elimination of oscillations. In the pulse modulation system the pulse width and frequency varies with attitude error with the limit cycling pulse being near the minimum bit size.

Both of the above systems represent full control stabilization since the control develops as limit cycling and after exceeding a 2-5 degree deadband.

Redundancy

System redundancy to an area commonly overlooked in many proposed designs. Redundancy of function is required for maneuvering units to achieve the safety of flight reliability required to fly without tether-lines. It is emphasized that the requirement is for "redundancy in function" not duplicate hardware. This is important in order to reduce weight and volume.

The current maneuvering unit design, including the MMU, has taken on the duplicate hardware approach. This came about trying to make the first "man in space" flight a complete success. The MMU essentially contains two complete propulsion systems (except for tanks), two stabilization systems, two power supplies, two electrical circuits, etc. This makes the unit quite safe but at the same time makes the unit considerably heavier and larger.

On future systems a new philosophy is required in order to reduce weight and volume and yet maintain a highly reliable, safe unit. This philosophy should comprise three basic ideas, such as

1. Redundancy by function

2. Expendables sized for moderate mission with recharging capability
3. Systems not falling into 1 above, should have redundancy to return to spacecraft only.

These will be discussed further in the paper. The main reason for this philosophy is to derive a smaller maneuvering unit that can be easier stored, weightless, be safe, and provide all function requirements.

DESIGN CRITERIA

With all the studies and tests being conducted by various Air Force agencies and NASA in the maneuvering unit area, it appears time for a review of the design criteria is in order. Many people including the Aero Propulsion Laboratory personnel are looking for a "simple, reliable, and lightweight" manned maneuvering unit. However, at the same time the unit must be capable of accomplishing a reasonable mission. Table 1 shows in condensed form the current system capability and future design which is near to state-of-the-art. It is pointed out that the future system criteria is a recommendation and any other system which provides this capability should be satisfactory. Each of these areas will now be discussed to provide a better insight into the reasoning for the parameter selection.

Configuration

Future AMU's should be a single integral pack being either a back-pack or back-waist pack. There is no need or requirement for a chest pack. The ECS is integral with the back module. Ingress/egress can be accomplished by storing the complete pack in the spacecraft where donning-doffing can occur. If for some reason this procedure is unsatisfactory a short umbilical can be used to reach the spacecraft exterior.

The primary pack shape factors should be egressing through a 34-inch diameter hatch and the exhaust plume heating problem. If solution to plume heating cannot be obtained with the back-pack, then other configurations should be considered. A third consideration for pack consideration is plume impingement on the work surface. Special provisions may have to be made to permit backing away from work areas at a very slow rate to prevent damage to the surface.

Propellant

There are approximately five propellents which will give the necessary total impulse while maintaining a reasonable size package. The first is hydrogen peroxide as being used in the MMU. Its main problems are its storability and AOL. For long missions, it will require substantial thermal control to prevent freezing or decomposition. Hydrazine is considerably better from the storage standpoint, higher specific impulse, and handling qualities. It does however have a higher plume temperature (1800°F). One promising variation is hydrazine diluted with ammonia which reduces the plume temperature and specific impulse. The final pro-

Table 1 - AMU DESIGN CRITERIA

Item	Current System	Future Systems
1. Configuration	Back-pack molded to suited astronaut. Includes chest pack. Arms used for two separate controls	Back-mounted or combination back and waist (Ref 4). No chest pack - one integral module. One or two arms free
2. Propellant	Hydrogen peroxide	Hydrazine, Hydrazine ammonia mix, solid propellents.
3. Total Impulse	3000 lb - sec plus 500 lb - sec reserve	2500 lb - sec plus 300 lb - sec reserve.
4. Nozzles	12 at 2.4 pounds thrust each. Four forward (2 fire & 2 reserve) four aft (2 fire & 2 reserve), two-up and two-down	12 at 1 pound thrust each. Four forward (all fire), four aft (all fire), two-up, two down. The back-waist unit would ease 2 forward at 2 pounds each), 2 aft at 2 pounds each, two up and two down at 1 pound each, and attitude control thrust
5. ECS	Semi-open system in chest pack, bottle supply in back-pack. Duration one hour	Closed loop fen or water transport system in back module. Duration 2 hours.
6. Stabilization	3 rate gyros, logic, and pulse modulator. Limit cycle operation Dead band ± 2 degrees, attitude rates 15°/sec	Control moment gyros and simple logic. No limit cycle. Jet actuation $\pm 2-4$ degrees, attitude rates 10-15 degrees/sec.
7. Power (Battery)	Main batteries ± 28 VDC Stab batteries ± 16 VDC	Main battery ± 28 VDC

Table 1 - CRITERIA (Cont'd)

Item	Current System	Future Systems
8. Telemetry		Same plus remote control requirements
9. Tetherline	200 foot soft line	None
10. Redundancy & Reserve		
a. Propulsion	Primary & secondary systems manual switched	Single system with electrical cut-off for on nozzle failure
b. Total Impulse	500 pound-sec	300 pound-sec
c. ECS	10 minute emergency	10 minute emergency
d. Stabilization	Back-up system	Open-loop
e. Power	Back-up batteries	Reserve battery to return to spacecraft
f. Failure	Tether	Remote control
11. Abort Alarm & Displays	Mounted on Chest Pack	Wrist mount or digital display on helmet
12. Flight Control	Side-arm controls	One-hand control or voice controller

pellents which appear attractive for this application is the solid propellant capsules (Cap Pistol) and solid charges fired into a chamber which provides gas for the system.

Total Impulse

Mission analysis and simulated flight tests have indicated that for a moderately active mission 2500 pound-seconds will suffice. The 300-pound-second reserve takes care of contingencies and provides "return to spacecraft fuel." Any additional mission requirements can be achieved by refueling.

Nozzles

Assuming for this discussion the 12 nozzle back pack is maintained, each nozzle should have one (1) pound of thrust. The forward thrust would be 4 pounds (4 nozzles x 1 lb T). This is nearly identical to the MJU which uses 2 thrusters at 2.4 pounds each for 4.8 total. Although the MJU uses the other thrusters as reserve redundancy, future systems should use all thrusters. Redundancy can be achieved by a special wiring procedure so that failed thrusters can be cut-out electrically in diagonal pairs thus accomplishing same thing as the MJU. This concept is illustrated below.

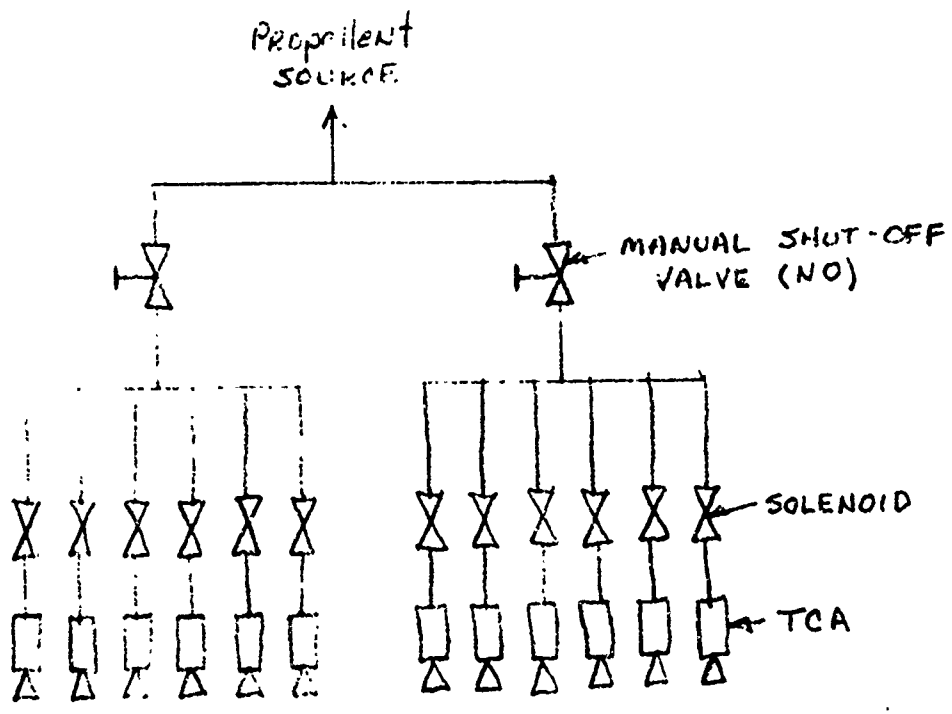


Fig 8 - Propulsion Schematic

ECS

All studies of environmental control systems for AMU's have shown either the closed loop fan system or the water transport system best for the AMU when mission time exceeds 1-2 hours. The two (2) hour time has been selected because it is compatible with mission accomplishment and the astronaut's physiological performance. Although data is considerably lacking on man's degradation per hour worked while extra-vehicular, it is reasonable to estimate that two (2) hours continuous work will be very tiring for the astronaut. It seems also reasonable to believe that there is no work requirement which requires the astronaut more than 1-2 hours at any one time. He can return to the spacecraft to reservice expendables and attain a brief rest.

Stabilization

Control moment gyros cannot be built large enough to provide complete stabilization because they will become too large and heavy. However, suppose they were only capable of 4-5 slugs of control in a 11.5 slug man-pack system. It would control small moments and act as a dampener for large moments. After exceeding a certain deadband the jets would turn on to prevent large excursions. Such a system appears advantageous and feasible but needs study and analysis.

Tetherline

The idea of using a tetherline for emergency recovery has not proven successful to date due to space dynamics which won't be discussed here. However, one concept which has not received attention to date is remote control for emergency recovery. This may not be too difficult to achieve since a telemetry system is already aboard the AMU. A trade-off study is needed to weight the feasibility and practicability of a three-body tether scheme as opposed to remote control.

Abort Alarms and Displays

The displays and alarms are still a firm requirement even though no chest pack is required. However, the displays must be limited to only those critical to EVA flight such as fuel quantity, O₂ quantity, CO₂, etc. and subsystem failure alarm. There are two possible schemes available. One is a wrist mounted display which can be read by the astronaut. A second is a modular digital light display which can be mounted to the helmet like a voice microphone. The critical parameters could be presented at some sampling rate and read by the astronaut at periodic intervals. Failure, malfunction, or low expendables could be immediately brought to his attention by flashing red. Both these methods need further analysis.

Flight Controls

A flight controller which appears attractive for the AMU is a voice controller. This is simplified from previous studies (Ref 6) where the commands are narrowed to six or eight distinct commands instead of the

whole English language. This simplified system could be made in a small package for the AMU.

CONCLUSIONS

As can be seen from the discussions in this paper, the future AMU's should contain the bare minimum in capability so that size and weight can be minimized. Added capability can be accomplished by returning to the spacecraft for resupplying and recharging.

It also can be seen that the MMU design is not recommended completely for future systems. New technology is available for improving system and subsystem design. These new items should be investigated immediately so most of them can be incorporated as soon as possible.

The discussion of current problems was discussed to bring everyone up to date and encourage new and different solutions. The MMU still will be the first manned extra-vehicular flight and will be a stepping stone to bigger and better missions in the future.

BIBLIOGRAPHY

1. Bell Aerosystems Company, Study of Space Maintenance Techniques, ASD TDR 62-931, Wright-Patterson Air Force Base, Ohio. May 1963
2. Ling-Temco-Vought, Self-Maneuvering Units for the Orbital Maintenance Worker, ASD TDR 62-278, Wright-Patterson AFB, Ohio. August 1962.
3. Van Schaik, P. N., Astronaut Maneuvering Unit Test Results, ASD TDR 63-71, Wright-Patterson AFB, Ohio. March 1963.
4. Ling-Temco-Vought, Integrated Jet-Pack Maneuvering Unit Propulsion Study and Exhaust Plume Heating Study, ASD TDR 63-729, Wright-Patterson Air Force Base, Ohio. Sept 1963
5. Van Schaik, P. N., Multi-Purpose Propulsion Units for Space Maintenance, Technical Paper presented at AIAA Conference. April 1965
6. Honeywell, Inc., Study of an Attitude Control System for the Astronaut Maneuvering Unit, NASA Report NASA CR-198. July 1964

DEPLOYMENT SYSTEM FOR THE PEGASUS METEOROID TECHNOLOGY SATELLITE

Eugene R. Gansle
Space Systems Division
Fairchild Hiller Corp.
Rockville, Maryland

MISSION DEFINITION

At the present time, a large gap exists in the statistical knowledge of meteoroid flux, composition, mass, and velocity. The primary mission of the Pegasus satellite is to narrow the range of uncertainty regarding flux and directionality of meteoroids in a near-earth orbit and to evaluate their hazard to manned spacecraft.

This is accomplished by deploying over 1000 square feet of capacitor-type meteoroid detector panels which include .016 inch, .008 inch, and .0015 inch thick aluminum target sheets. The meteoroid detectors are double sided to produce a total active area of over 2000 square feet and are deployed in a set of wings having a span of 96 feet. "Hit" data is stored for readout by ground command as well as being transmitted continuously by the beacon. Although no attitude control is provided on

Pegasus, an attitude sensing system, consisting of five solar sensors and six earth sensors, provides attitude data on the randomly oriented satellite.

Spacecraft power is provided by solar cells equally distributed on four panels which when deployed are angularly arranged like the surfaces of a tetrahedron.

The first of the three Pegasus Meteoroid Technology Satellites was successfully launched on February 16, 1965, into an orbit having an apogee of 740 km and a perigee of 500 km. The booster was a Saturn I utilizing the Apollo configuration. This consists of a boilerplate Command Module, Service Module, and Service Module Adapter located above the Instrument Unit. During launch, the Pegasus is located within the Service Module which is separated in a longitudinal direction after orbit has been achieved (see Figure 1).

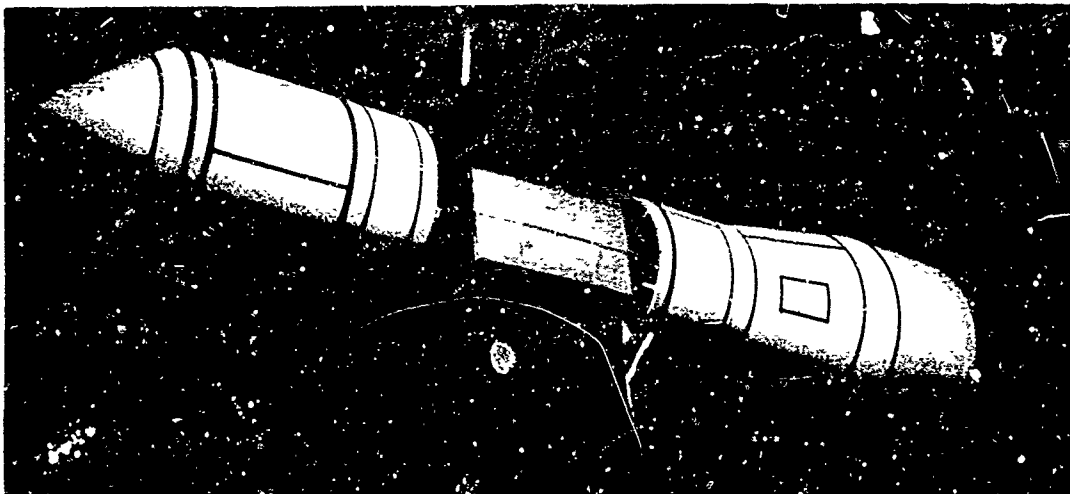


Figure 1 Apollo Service Module Separation

CONFIGURATION

The Pegasus configuration was dictated by five basic requirements:

- 2150 square feet of meteoroid detector panels
- The use of capacitor-type meteoroid detector panels
- Envelope during launch limited to nine-foot diameter and a length above the Service Module separation plane of 15 1/4 feet
- Pegasus to remain attached to the S-IV stage to insure a long-life orbit
- Pegasus weight not to exceed 3307 pounds.

Consideration of several possible configurations led to the selection of "wings" as best satisfying the requirements of the mission. The 96-foot span places much of the meteoroid detector area remote from the attached S-IV stage thereby minimizing its shadowing effect. In addition, the number of folded sections or wing frames is relatively small and the deployment system is simple and straightforward.

WING SYSTEM

The structural arrangement was governed primarily by the area requirement of the meteoroid detector panels (Figure 2). The area was distributed into 208 detector panels approximately 20 x 40 inches in area with 16 panels to a full wing frame. Twelve full wing frames and two "half" frames (eight panels each) permit the entire area to be folded within the nine-foot diameter launch envelope. Three sets of hinge fit-

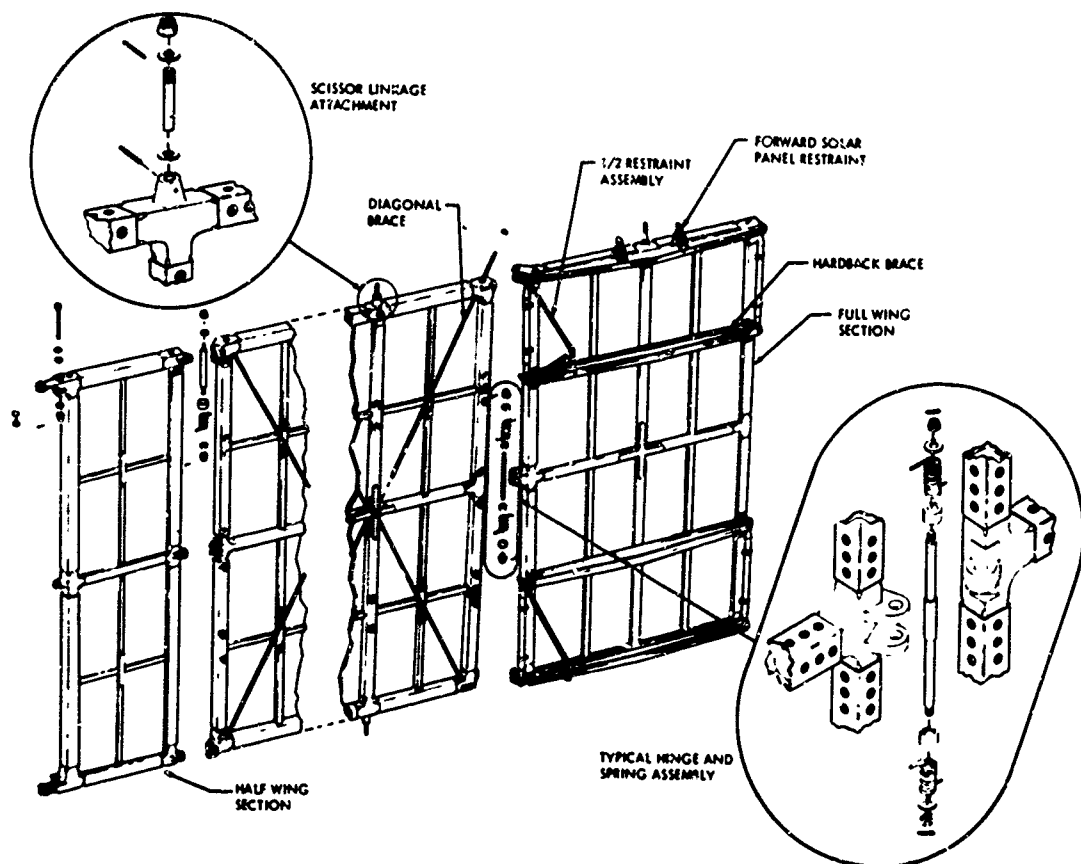


Figure 2 Wing Frames

rings join each wing frame to its neighbor and/or to the center section. The hinges alone are inadequate to support the wings during the rigors of the boost phase, so tongue-and-groove fittings were added to transmit the axial loads from wing frame to wing frame and thence to the center section. The tongues and grooves disengage immediately after initiation of wing deployment. Diagonal tension rods on each wing frame transmit shear loads across the frame and directly into the hinge fittings.

rotate apart, and the wings are then free to deploy (Figure 3).

Wing deployment geometry is controlled by a series of scissor links pivoted at the top and bottom centers of each wing frame. The inboard link and inboard wingframes are "geared" by pushrods and bellcranks to a torque shaft in the center section. Full wing deployment is accomplished with 63° rotation of the shaft. The primary deployment energy is provided by torsion springs

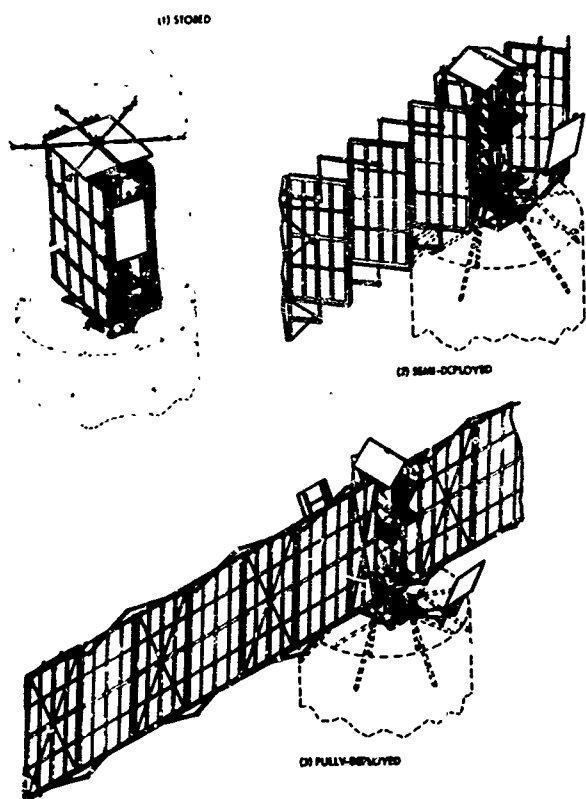


Figure 3 Deployment Sequence

The wing frames are held in a snugly stacked assembly by four sets of restraint trusses, each of which is preloaded against the center section with a load of 6000 pounds. Each pair of trusses is "hooked" together by a tongue-and-groove fitting which is held in the engaged position by a bolt and separation nut. The pretensioning is accomplished by a turnbuckle, and the load application is monitored by strain gauges on the trusses. Firing of the separation nuts allows the tongue-and-groove fittings to

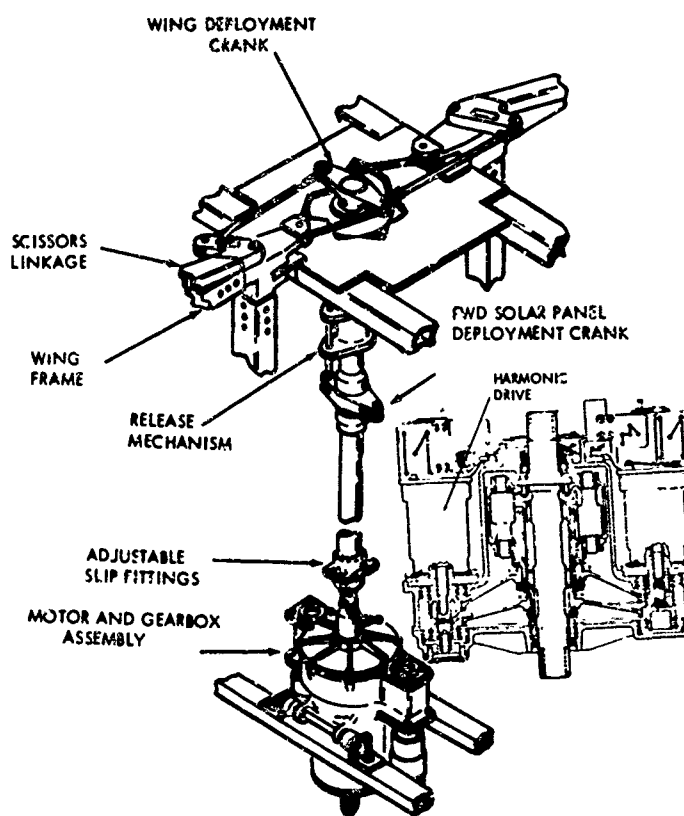


Figure 4 Deployment Drive Mechanism

located at each wing frame hinge. A back-up mode is provided by a motor-driven gearbox located at the center of the torque shaft (Figure 4). Redundant motors are coupled directly to a pair of harmonic drives which deliver the power to the double ended planetary gearbox. The harmonic drive reduction is 3400 to 1 and the gearbox reduction is 6 to 1 for a total reduction of almost 21,000 to 1. The differential action of the gearbox permits deployment even with a single jammed motor or harmon-

ic drive, and the wingspring energy is sufficient to accomplish full deployment with no motors operating. The motors contain magnetic brakes thereby providing a damping action which establishes a nominal deployment time of approximately 45 seconds.

CENTER SECTION

The function of the center section is to attach the Pegasus spacecraft to the booster and to provide a support for the wings, solar panels, and electronics (Figure 5). Its lower end is joined to the Service Module Adapter by six bolts and six shear pins equally spaced on an 80-inch diameter bolt circle. Since the Pegasus remains attached to the upper stage, no separation provisions are required at this interface.

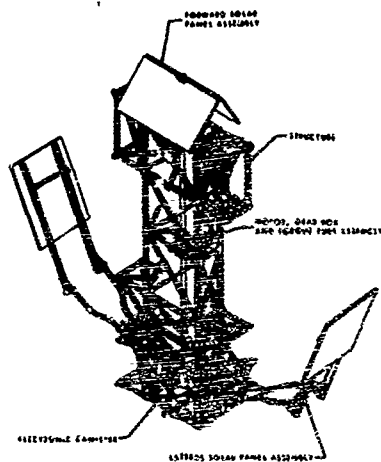


Figure 5 Center Section

The upper end of the center section requires lateral support from the Service Module. This is accomplished by six equally spaced tension rods attached to a centrally located spider fitting (Figure 6). The spider fitting has a conical lower end which engages matching fittings on the top solar panels and the center section, and is held in place by a single bolt and separation nut. Firing of this nut frees the engaged fittings and permits the tension rods and spider fitting to leave the Service Module.

SOLAR PANELS

The solar array consists of four, single faced panels which when deployed lie in the planes defined by the surfaces of a tetrahedron. They were initially intended to be deployed by linkages driven by the torque shaft thereby relating solar panel position to wing position. However, it was felt that although some degree of mission success could be achieved with partial wing deployment, full solar panel deployment is always necessary to assure adequate power. Therefore, it was determined to make the solar panel deployment as independent of the wing deployment as possible.

The top solar panels presented a special

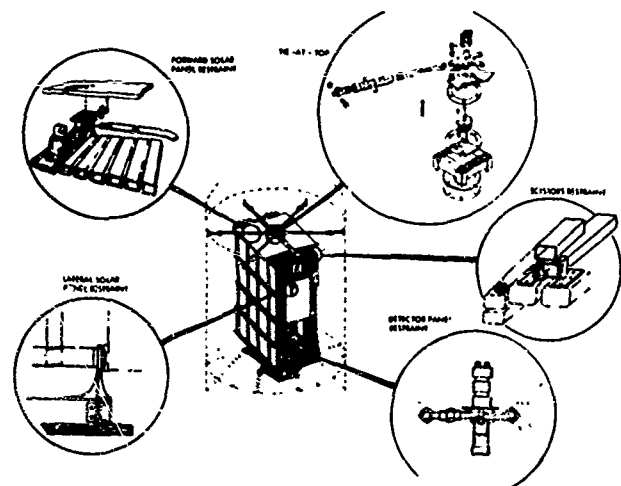


Figure 6 Restraint Systems

case because of their method of restraint and their proximity to the tension rods, which provide lateral support to the center section. During boost, these panels are restrained by the same bolt which attaches the center section to the tension rod spider fitting. Since the panels are spring-loaded at their hinges to deploy, it was necessary that their deployment be delayed after release of this bolt to preclude any possibility of a damaging impact against the tension rods. A cam-controlled locking pin

mechanism was provided to key the panel support linkage to the torque shaft for the first 10° of shaft motion (Figure 7). The cam then permits the locking pin to disengage, releasing the solar panel linkage from the torque shaft and allowing spring force alone to deploy the panels to their final position. The delay between Service Module separation and initiation of torque shaft motion allows more than ample time for safe solar panel deployment.

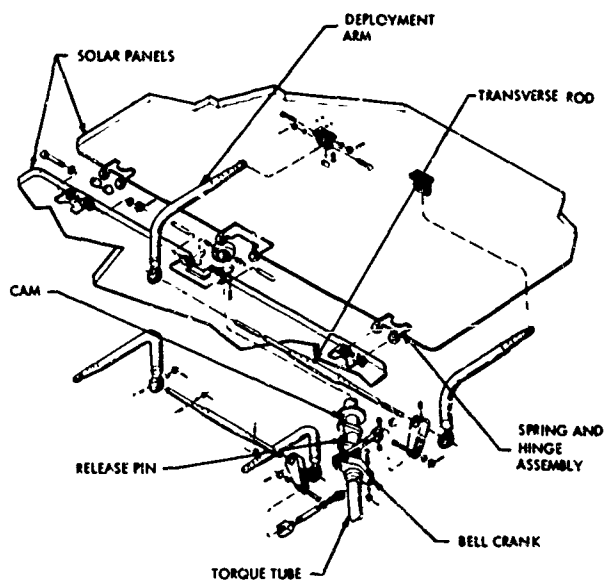


Figure 7 Top Solar Panel Assembly

Each of the lateral solar panels is restrained during the boost phase by four conical fittings which are pinched against the center section by the preloaded stack of wing frames. The initial motion of the deploying wings releases these fittings and allows the panels to be spring-driven to their final position. The panels are mounted on double-jointed arms in order to achieve the desired angular relationship and at the same time eliminate shadowing by the S-IV stage. Over-center links attached to the arms prevent the panels from rebounding and also lock them at their correct angles. The drive springs are located at these links.

SERVICE MODULE SEPARATION

Structural separation of the Service Module must occur at the plane of attachment to the Service Module Adapter and at the spider fitting which offers lateral support to the upper end of Pegasus. The Adapter attachment consists of six axial bolts and separation nuts, while the spider fitting attachment is a single bolt and separation nut as previously described. A pair of short-stroke "starter" springs surrounds each of the six bolts at the Adapter interface, but the principal ejection energy is provided by four Negator springs each having a constant load of 40 pounds and a stroke of 15 feet. Exit velocity of the Service Module is approximately five feet per second. In order to preclude any possibility of the Service Module's contacting the Pegasus during its separation, two guide rails are cantilevered from the Service Module Adapter and extend alongside the Pegasus for its full length. The rails are located to avoid subsequent deployment of wings and solar panels.

ORBITAL DEPLOYMENT SEQUENCE

The complete deployment sequence is as follows:

1. Three minutes after orbit injection, the six nuts at the base of the Service Module and the one nut tying the top of the Pegasus to the Service Module are simultaneously fired. The 12 starter springs and the four Negator springs are then free to propel the Command Module/Service Module forward on the guide rails.
2. One minute later, a signal fires the four wing restraint separation nuts and simultaneously energizes the deployment motors.

3. Almost instantaneously, the side solar panels are released by the wings and are free to fully deploy.
4. After 10° of torque shaft rotation, the top solar panels are released and are free to fully deploy.
5. Approximately 45 seconds after energizing the motors, the wings are fully deployed.

TESTING

Although the primary area of interest here is the Pegasus deployment testing, it should be mentioned that full-scale vacuum testing and vibration testing of the spacecraft in three axes was also performed. Figure 8 shows the full-scale Dynamic Test Model

(DTM) on the vertical and lateral vibration test fixtures. The inputs were applied at the lower mounting plane and the stiffness of the upper lateral support was simulated by a stationary fixture. A dual C-210 shaker system was required to deliver the inputs.

The need for performing deployment tests on a 96-foot span structure which could not sustain one g loads presented obvious difficulties. In addition, deployment capability was required at three sites, the final assembly area in Hagerstown, Maryland, the environmental testing facility in Pennsylvania, and the preparation hangar at Cape Kennedy. The early delivery required on a deployable mockup and the DTM ruled out the more exotic techniques such as air bearings, and an overhead rail system was selected (Figure 9).

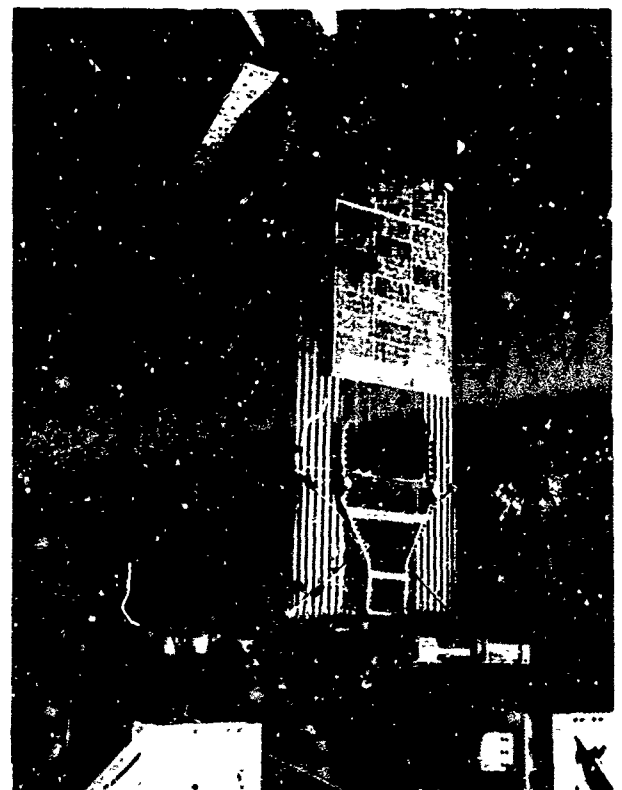


Figure 8 Dynamic Test Model on Vibration Fixture

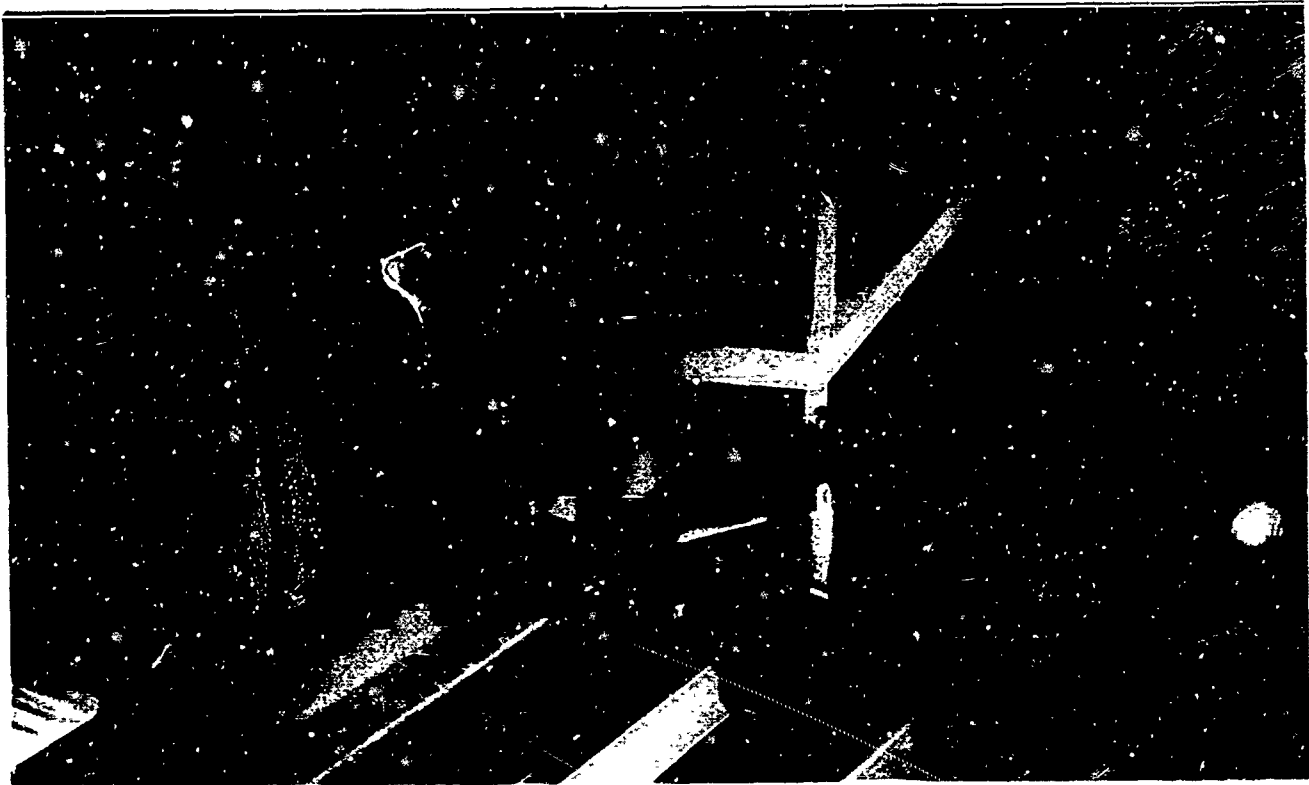


Figure 9 Photograph of Portion of Deployment Fixture - Close up of Hangers

Alternate wing frames are hung from light-weight trusses having transverse rollers at their apexes. This transverse capability is necessary because the wings do not follow a purely radial line when being deployed. The transverse roller is hung on a carriage whose rollers ride on a pair of parallel rails. Rail friction is compensated for by carefully selected weights which exert a load on the carriages in the direction of deployment by a cable/pulley system. This fixture is used for final assembly of the spacecraft as well as for deployment testing (Figures 10 and 11).

The flexibility of the Pegasus wing structure and the variations between different components call for an extensive rigging operation on the deployment fixture. The rigging includes alignment of the gearbox with the torque shaft, adjustment of the pushrods at both ends of the torque shaft, adjustment of the fixture hangers supporting the wing frames (in order to properly align the

tongue-and-groove fittings), and adjustment of the brake to achieve a properly deployed wing under the various modes of motor operation. These operations account for the several deployments required even on flight spacecraft.

The DTM was subjected to over 150 deployment tests. This was a developmental phase intended to evaluate such criteria as the

- number of wing drive springs to be used
- optimum amount of preload in the wing restraint system
- effects of varying brake settings
- effects of track condition
- performance variations under simulated motor failure conditions.



Figure 10 Pegasus Spacecraft Deploying on Zero g Fixture

Provision had been made in the design for up to four wing springs per hinge line. Deployment tests were run which included spring installations of none, one, two, three, and four springs per hinge line. Separately, and in combination with spring variation, deployments were run utilizing preloads in each of the wing restraint trusses of 0, 2000, 4000, and 6000 pounds. Hand smoothing of local rough spots in the track was required, and the technique was developed for balancing the track friction in order to more nearly simulate zero g deployment. Strain gauge monitoring of the torque shaft provided continuous values of driving and/or restraint torque in the gearbox.

Certain characteristics of the deployment system could not be determined experimentally. Response of the system to the rotational velocity of the Saturn stage could not be simulated, for example. However, analysis showed that the calculated Saturn spin rate would be a maximum of about 1.0° per second during deployment and 6.0° per second after deployment. The zero margin rates for the structure are calculated to be 3.2° and 14.15° per second, respectively. Acceleration rates show about the same safety margins.



Figure 11 Pegasus Spacecraft Deploying on Zero g Fixture

Simulated zero g deployment of the side solar array on the spacecraft structure in "normal" position could only have been simulated by the use of a very complex, very costly, and probably unreliable support and follower system. As a reasonable compromise, the panels were tested horizontally from a simulated center section.

The panels were supported in one series of tests by an air-bearing arrangement and in another by a simple follower support which effectively canceled the g effect. Since the follower support yielded essentially identical data with that of the air bearing, and since it was more reliable and simpler, it was used for the complete analysis. A series of slow motion photographs of the deployment action shows a very slight rebound and oscillation, which quickly damped out in test. This action is apparently identical with the in-space performance of the solar panel deployment system. Over-center links hold the panels in the deployed position. Since the forward solar panels form a "pup-tent" shape in opposition to gravity in normal tests, no special tests were required.

The DTM deployment test series proved its value in establishing basic criteria and techniques for subsequent testing on the prototype and flight spacecraft. The first flight spacecraft was deployed 18 times at the Fairchild Hiller plant in Hagerstown, Maryland, and 10 times at Cape Kennedy before delivery to the launch pad. Only two of these utilized live ordnance, the remainder using a solenoid-actuated release designed early in the DTM test series.

A television camera in the first flight Pegasus verified that the deployment system's behavior in space is a precise duplicate of its behavior on the wing deployment fixture. This result justifies the philosophy that any system designed for deployment in space must have a high confidence level established by extensive ground testing.

STRUCTURAL BEHAVIOR OF TAPERED INFLATED FABRIC CYLINDERS UNDER VARIOUS LOADING CONDITIONS

By L. Kovalevsky* and F. L. Rish**

*Research Specialist **Supervisor
Space and Information Systems Division
North American Aviation, Inc.

The purpose of this paper is to find approximate relations for the design of inflatable members of linearly variable (tapered) cross sections under various loadings. Considered in the analysis are axial loads (tension, compression, Euler effect), torsional moment, and internal pressure. Inflatable members are usually constructed of impregnated fabrics such as Dacron, but at the present time "exact" solutions for such materials are inadequate. Consequently, approximate procedures are needed to determine stresses in this type of member. This paper discusses not only the degree of approximation but also the procedural limitations. It includes, in addition, the effect of fiber inclination on rigidity of the member.

INTRODUCTION

Because of the rapid development of applications for inflatable structures, it is becoming increasingly important to develop a systematic theory for design work and for predicting structural behavior. The active interest in space stations, inflatable recovery vehicles, inflatable shelters, and similar structures has greatly accelerated the theoretical and experimental efforts to develop analysis methods for inflatable structures.

The theory of elasticity, which has been used with success in the analysis of conventional structures, does not adequately predict the behavior of inflatable fabric structures due to the nonlinear behavior of the composite material. Characteristic large deformations under ultimate load, composite material behavior, and hysteresis effects under cyclical loadings preclude using the conventional linear theory to accurately predict the stresses, deformations, and strength of the inflatable structure. As long as these important nonlinear effects are not well known, there is very little reason to develop an "exact" linear solution. For no matter how comprehensive the linear approach may be, the resulting equations will not adequately describe or predict the state of stresses in the inflatable structure. Consequently,

in view of the urgent need for criteria for evaluating inflatable members, simplified approaches seem to be more logical. It is for this reason that a difference of 15 percent between test results and developed theory may be considered a very satisfactory correlation at the present time.

The methods described in this paper, which is a continuation of an earlier investigation¹, are intended for preliminary design work. It is also hoped that they will suggest characteristics of inflatable structures which have not been considered previously, such as composite behavior and the effects of orientation of fibers.

CIRCULAR INFLATED CYLINDERS

The circular inflated cylinder is the most convenient model by which to study the effects of changes in the modulus of elasticity and stresses due to the orientation of the fibers at an angle to the principal directions. Such a configuration will seldom arise in practice, but from a theoretical point of view this study will lead to important conclusions which can be used in the development of an analytical procedure for tapered columns in which the fibers are not parallel to the principal directions.

Figure 1 represents the envelope of a cylinder in which the fibers are oriented at an angle α to the circumferential and longitudinal directions.

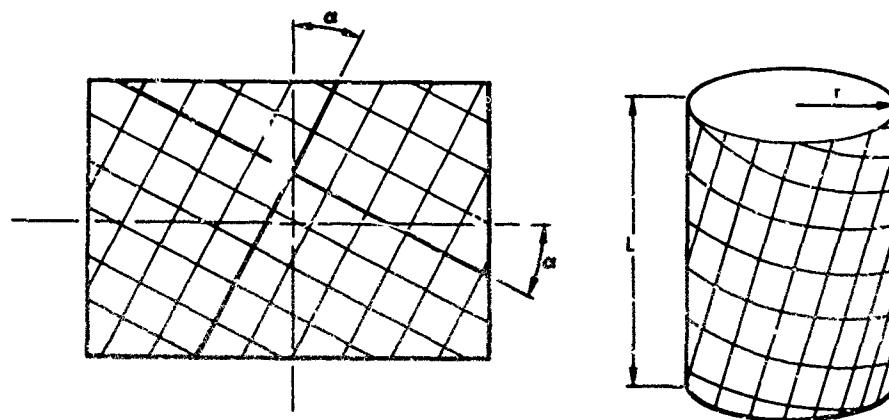


Figure 1. Cylinder With Inclined Fibers

Stresses due to internal pressure are given by the well-known relations, based on equilibrium, in the longitudinal and circumferential directions, respectively.

$$q_l = \frac{pr}{2}, \quad q_c = pr$$

If the fibers are inclined to the principal directions, the shear stress on the inclined element must be considered in the analysis.

Mohr's circle (Figure 2) is used to determine stresses in the direction of the fibers and the shear stress, yielding the following equations for the tensile and shear stresses:

$$\left. \begin{aligned} q_y &= 0.50 pr (2 - \cos^2 \alpha) \\ q_x &= 0.50 pr (1 + \cos^2 \alpha) \\ q_T &= 0.50 pr \sin \alpha \cos \alpha \end{aligned} \right\} \quad (1)$$

Generally, q_y and q_x are taken by the fibers and elastomer. The shear q_T is taken exclusively by the elastomer.

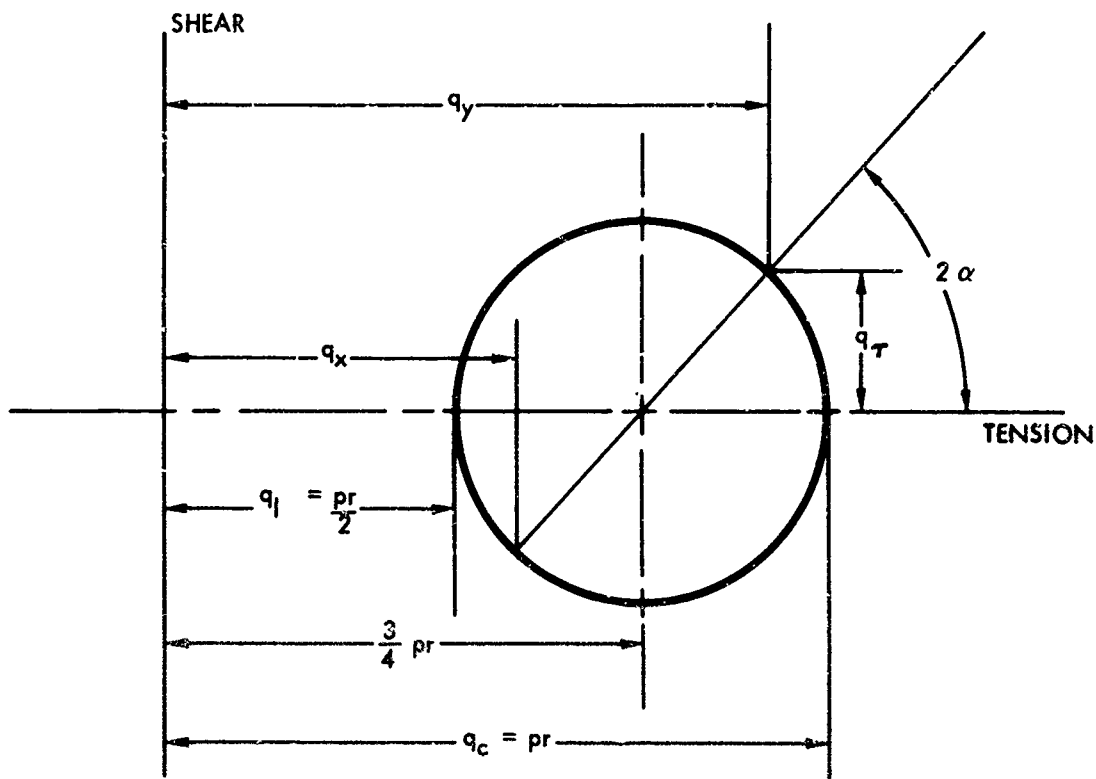


Figure 2. Mohr's Circle

The tensile stress in the elastomer is proportional to the relative stiffness of the elastomer:

$$\sigma_y = \frac{q_y}{A_r} \frac{A_r E_r}{A_r E_r + A_f E_f} = \frac{q_y}{A_r} \left(\frac{1}{1 + \frac{A_f E_f}{A_r E_r}} \right)$$

$$\sigma_x = \frac{q_x}{A_r} \frac{A_r E_r}{A_r E_r + A_f E_f} = \frac{q_x}{A_r} \left(\frac{1}{1 + \frac{A_f E_f}{A_r E_r}} \right)$$

where

A_r, A_f = cross section of elastomer and fibers, respectively

E_r, E_f = modulus of elasticity of elastomer and fibers, respectively

The equation for the shear modulus of Dacron has been derived¹, in which the elasticity of the elastomer, influence of tension on fibers (friction), and the concentration of fibers were considered. Consequently, G was the variable value, and the relation, which is used to determine deformation due to shear, depends on this variable value:

$$\gamma = \frac{T}{G} \quad (2)$$

Dacron can be considered a typical material for inflatable structures. For the material tested at S&ID¹, the following moduli of elasticity were noted:

fibers, $E_f \approx 840,000$ psi
elastomer, $E_r \approx 4,000$ psi

This leads to the conclusion that the tension stresses in the elastomer, σ_x and σ_y can be neglected and total tension may be carried by the fibers only. The shear, however, is assumed to be taken exclusively by the elastomer since the Dacron fibers behave as a mechanism under shear loads.

The shear deformation, γ , induces a rotation of the cylinder by an amount

$$\theta = \frac{\gamma L}{r}$$

Substituting for γ in Equations 1 and 2, we obtain the following expression for rotation of the cylinder:

$$\theta = \frac{0.50 pJ \sin \alpha \cos \alpha}{tG}$$

Since the shear modulus, G , is relatively small, the deformation angle (Equation 2) is significant; and angle θ can be observed visually in tests because of large cylinder length. Consequently, under internal pressure, the bulkheads rotate with respect to one another until the position of equilibrium is reached. The fibers then will not be inclined at the angle, α , but at another angle, $\alpha - \gamma$. It is assumed that the angle, γ , defined by Equation 2, is approximately equal to the angle γ determined by Equation 2a, since the inclination of fibers is relatively small.

The same phenomenon occurs if a torsional moment is applied to the end of the cylinder with the fibers parallel to the center line of the cylinder:

$$T \approx 2\pi r^2 q_T = \pi p r^3 \sin \alpha \cos \alpha$$

where q_T is taken from Equation 1, and the effects of the small inclination of q_T to the principal directions of the cylinder are neglected.

The angle of rotation of the cylinder is also of interest, since it is simple to measure during tests:

$$\theta = \frac{TL}{JG}$$

where

θ = angle of rotation of the upper bulkhead with respect to the lower

The required angle, γ , (Equation 2) can now be rewritten:

$$\gamma = \theta \frac{r}{L} \quad (2a)$$

where

$$J = 2\pi r^3 t \text{ or } J^* = 2\pi r^3, \text{ depending on dimensionality of } G^1$$

L = length of cylinder

Since γ is not too small, a change of geometry occurs and the cylinder fibers no longer intersect at 90 degrees, and the longitudinal fibers, when equilibrium is reached, are no longer inclined at the angle α , but at $\alpha - \gamma$.

Due to the change of geometry, the new values for q_x and q_y must be determined, using the new angle, $\alpha - \gamma$, rather than the inclination angle, α . Similarly, the stresses in the deformed structure are

$$\left. \begin{aligned} q_y &= \frac{1}{2} pr [2 - \cos^2 (\alpha - \gamma)] \\ q_x &= \frac{1}{2} pr [1 + \cos^2 (\alpha - \gamma)] \\ q_T &= \frac{1}{2} pr (\sin \alpha \cos \alpha) \end{aligned} \right\} \quad (3)$$

The equation for q_T is not affected by the new angle because q_T is the stress which already corresponds to the angle $\alpha - \gamma$.

If an axial load P is applied to the column, the column will rotate and α will be either increased or decreased, depending on whether the load is

one of compression or tension. Before the column can carry the load, it must be pressurized; therefore, P will always be accompanied by internal pressure. However, the effect of P can be studied separately, using Mohr's circle as before. For the case of the compression load

$$q_l = -\frac{P}{2\pi r}; q_c = 0 \quad (4)$$

In a manner similar to the preceding approach, expressions can be obtained for q_x , q_y and q_τ , $\phi = (\alpha - \gamma)$. For a compression load P

$$\left. \begin{aligned} q_y &= -\frac{P}{2\pi r} \cos^2 \phi \\ q_x &= -\frac{P}{2\pi r} \sin^2 \phi \\ q_\tau &= \mp \frac{P}{2\pi r} \sin \phi \cos \phi \end{aligned} \right\} \quad (5)$$

Again, q_τ introduces a rotation equivalent to that produced by the torsional moment:

$$T \approx 2\pi r^2 q_\tau = 2\pi r^2 \left| -\frac{P}{2\pi r} \right| \sin \phi \cos \phi = \left| -P \right| r \sin \phi \cos \phi$$

and this leads to an additional rotation of the column, θ_P , in accordance with the equation

$$\theta_P = \frac{TL}{JG}; \gamma_P = \theta_P \frac{r}{L}$$

where G is given by the equations in Reference 1.

θ_P will affect the first two stresses (Equation 5), as in the case of pressurization. Therefore, Equation 5 may be rewritten:

$$\left. \begin{aligned} q_y &= -\frac{P}{2\pi r} \cos^2 (\phi + \gamma_P) \\ q_x &= -\frac{P}{2\pi r} \sin^2 (\phi + \gamma_P) \\ q_\tau &= \mp \frac{P}{2\pi r} \sin \phi \cos \phi \end{aligned} \right\} \quad (5a)$$

Since compression is always accompanied by internal pressurization, Equations 3 and 5a can be superimposed, and

$$\left. \begin{aligned} q_y &= \frac{1}{2} pr [2 - \cos^2 (\alpha - \gamma)] - \frac{P}{2\pi r} \cos^2 (\alpha - \gamma + \gamma_P) \\ q_x &= \frac{1}{2} pr [1 + \cos^2 (\alpha - \gamma)] - \frac{P}{2\pi r} \sin^2 (\alpha - \gamma - \gamma_P) \\ q_r &= \frac{1}{2} pr \sin \alpha \cos \alpha - \frac{P}{2\pi r} \sin (\alpha - \gamma) \cos (\alpha - \gamma) \end{aligned} \right\} \quad (6)$$

If P is a tension load, the signs for P and γ_P will be reversed.

EFFECTIVE MODULUS OF ELASTICITY IN LONGITUDINAL DIRECTION

The inclination of fibers does not affect I, but may affect E. It is simpler to study the change of the elasticity modulus by assuming a tensile load on the cylinder; therefore, Equation 6 is an effective starting point. The tensile load, P, which is applied to the column and varies from an initial value of zero to the final value, tends to decrease the angle ϕ between the longitudinal fibers and the longitudinal axis of the cylinder; the angle ϕ is already a function of the following two factors:

- original inclination of fibers
- internal pressure, which will decrease α by angle γ

Therefore

$$\phi = \alpha - \gamma \quad (7)$$

To straighten the fiber, a load, P_o , must be applied, which will cancel ϕ . This means that P_o will cause a torsional moment, T_o , which will cause a rotation of the cylinder through an angle, $-\phi$:

$$-\phi = \frac{T_o L}{JG} \cdot \frac{r}{L}$$

$$T_o = \phi \frac{JG}{L} \cdot \frac{L}{r}$$

where

G = shear modulus

We also know that

$$T \approx q_{\tau} 2 \pi r^2$$

Combining the above expressions, we obtain

$$q_{\tau_0} = \frac{r \phi G t}{r} = + \frac{P_0}{2 \pi r} \sin \phi \cos \phi$$

Thus the load, P_0 , can be determined by

$$P_0 = \phi \frac{2 \pi r G t}{\sin \phi \cos \phi} \quad (8)$$

Under this load, the fibers will become parallel to the cylinder axis. If this force is increased, the cylinder will be elongated but no rotation will occur. The elongation for any $P > P_0$ will be in accordance with the known elasticity modulus, E_f , for the cylindrical skin in the longitudinal direction, if the fibers are oriented in the same direction. However, for any load $P < P_0$, longitudinal elongation will not occur at the same rate. The corresponding modulus of elasticity will be designated by E_{eff} , which depends on not only the elongation but also the cylinder rotation.

To determine E_{eff} , assume the cylinder to be loaded with a tensile load, $P' < P_0$, causing a rotation $\phi' < \phi$. Then

$$\phi' = \phi \frac{P'}{P_0}$$

In accordance with Figure 3, elongation in the principal direction can be expressed by

$$\delta = y_1 + y_2$$

where

$$y_1 = \frac{q_p t L}{E_f A} \cos (\phi - \phi') = \frac{q_p L}{E \cdot l} \cos (\phi - \phi')$$

and

$$q_p = q_y \text{ (from Equation 5a)}$$

$$y_2 = L \cos (\phi - \phi') - L \cos \phi$$

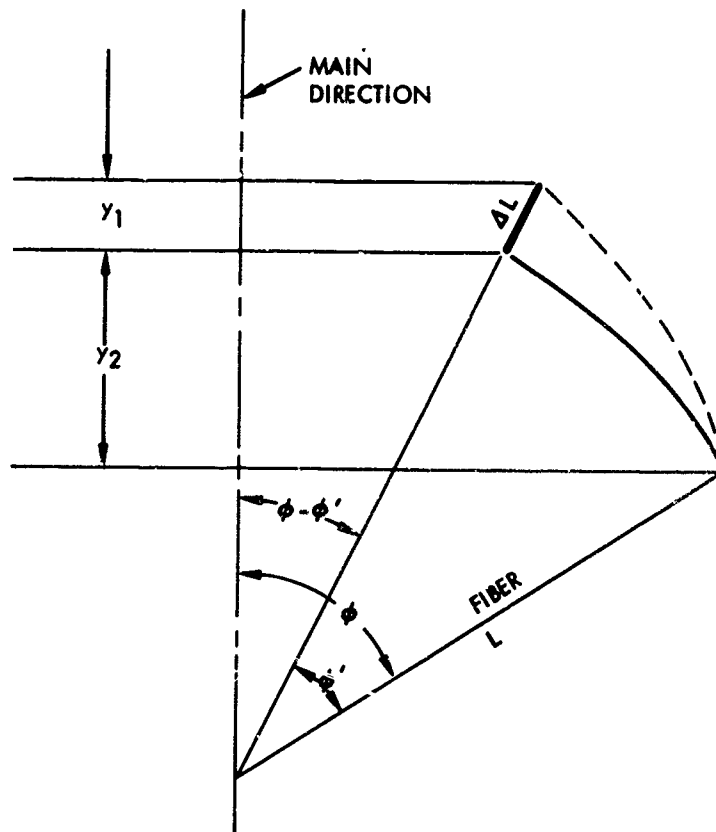


Figure 3. Nonlinear Elongation

Therefore

$$\delta = y_1 + y_2 = \frac{q_p L \cos(\phi - \phi') + \frac{E_l}{E} L [\cos(\phi - \phi') - \cos \phi]}{E_l}$$

Now consider a cylinder with the fibers oriented in the principal directions and whose length is

$$l = L \cos \phi$$

The corresponding elongation will then be

$$\delta_v = \frac{p q_1 L \cos \phi}{E}$$

where $p q_1$ is the value of q_1 in Equation 4. Since the elongation is inversely proportional to the modulus of elasticity, the effective modulus in the principal direction for the cylinder with inclined fibers will be

where

$$E_{\text{eff}} = E_l n = E_l \frac{\delta}{\delta_v} \quad \left. \vphantom{E_{\text{eff}}} \right\} \quad (9)$$

$$n = \frac{q_P \cos(\phi - \phi') + E_l [\cos(\phi - \phi') - \cos \phi]}{P^q \cos \phi}$$

TAPERED CYLINDERS

Inflatable cylinders of constant cross section usually can be made from material with fibers oriented parallel to the principal directions. Unfortunately, this is not the case with conical structures because they must be assembled from one or more sectoral pieces of material. The fibers cannot be oriented circumferentially and longitudinally. Figure 4 illustrates the typical sector, which has the following properties:

1. Only along the center line of the sector are the fibers located in the direction of the principal stresses.
2. Along any line passing through the vertex (i. e., \overline{oa}), the inclination of fibers is the same everywhere.
3. Inclination of the fibers varies along any circumferential line, \overline{bb} .
4. Maximum inclination of fibers to the principal directions is at the boundaries \overline{cc} and \overline{dd} of the sector.

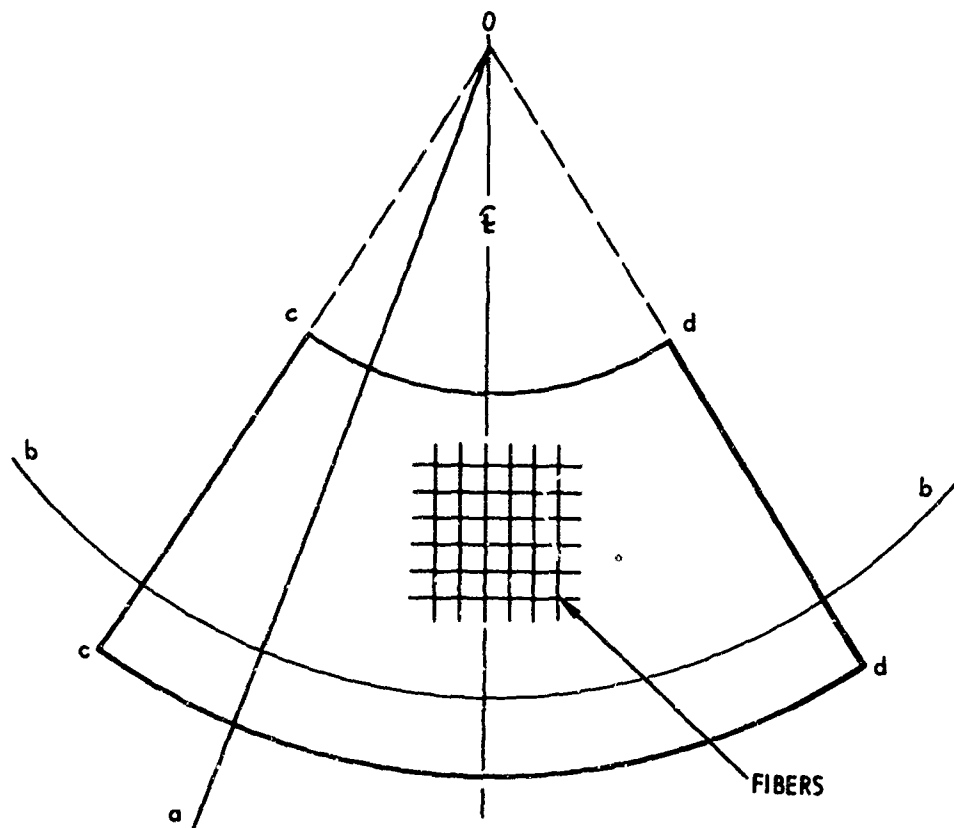


Figure 4. Typical Sector

To prevent the occurrence of too large an angle between the fibers and principal directions, the cone may be made of more than one sector. In order to fabricate the cone, a sector as shown in Figure 5 is required, with a radius of ℓ and a central angle ϕ .

$$\phi = \frac{r}{\ell} 360 \text{ (in degrees)}$$

where

r = the radius of the base of the cone

If the cone is composed of n sectors, each sector will have a radius ℓ and central angle ϕ/n (obviously, allowance must be made for joints).

If the fibers are placed so that at the center line \overline{aa} of the sector they are oriented in the principal direction, then

$$\max \alpha = \frac{\phi}{2n}$$

where

α = the inclination of the fibers from the principal directions

n = number of sectors

For any line \overline{ab} defined by angle α (Figure 5), the fibers will be inclined an angle α to the principal directions of stress.

To locate any point of interest, it is necessary to choose a system of coordinates. As a reference take \overline{aa} , the line whose fiber is in the direction of the principal stresses. Any other line \overline{ab} , relative to line \overline{aa} , can be defined by the angle α . Any point on line \overline{ab} is defined by the distances from the vertex. The angle α can be easily measured on the sector but not on the cone, and it is reasonable to replace α with the length u . Therefore, any point on the conical surface is defined by two numbers, u and S (Figure 5).

The relationship between α , u , and S is

$$u = \pi S \frac{\alpha}{180} \text{ or } = S \alpha \text{ (}\alpha \text{ in radians)}$$

$$\alpha = \frac{u 180}{\pi S} \text{ or } \alpha = \frac{u}{S}$$

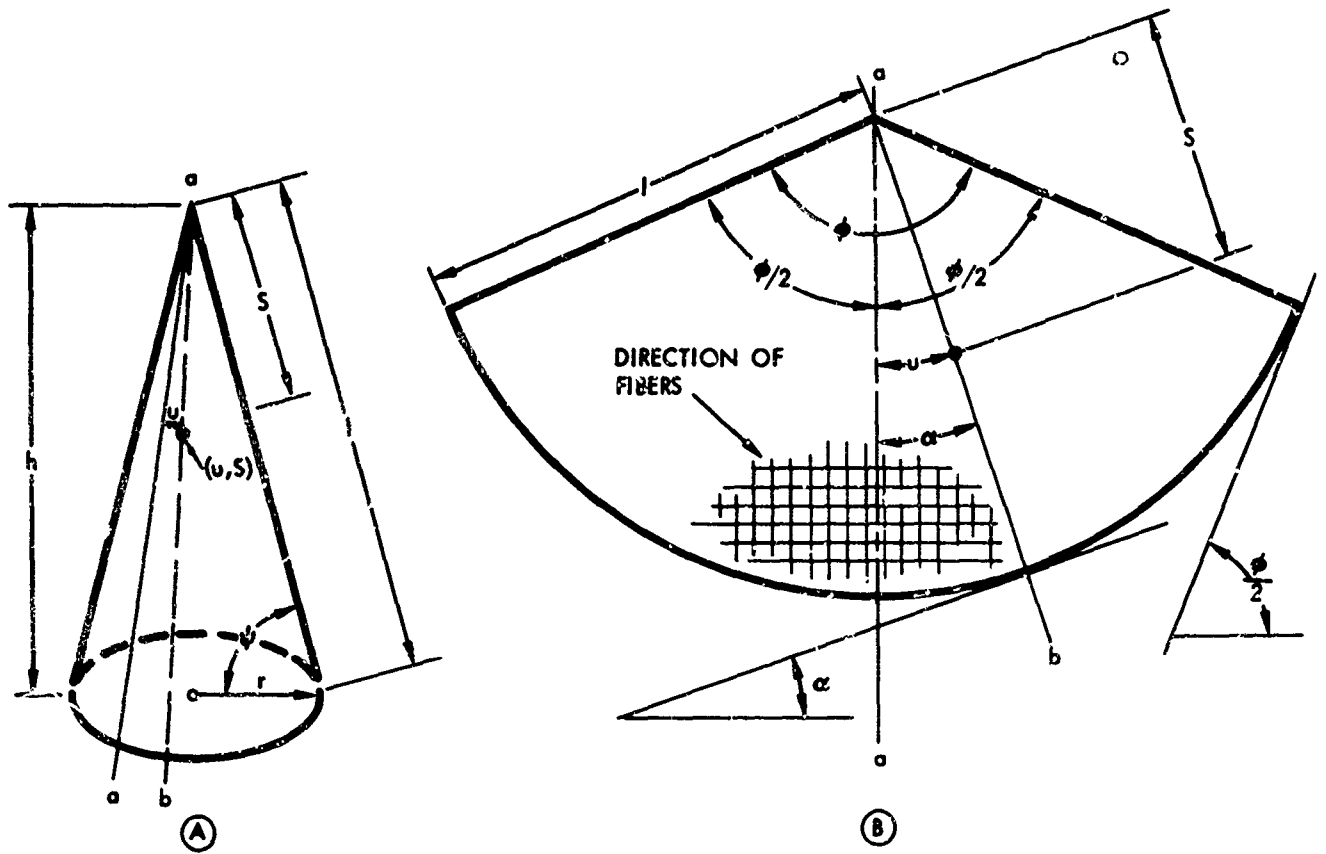


Figure 5. Inclination of Fibers From Principal Direction and Cone Nomenclature

Therefore, the point which is defined by u , S will correspond to the angle α :

$$(u, S) \rightarrow \alpha = \frac{u}{S}$$

For $\alpha_{\max} = \frac{\phi}{2}$

$$\left(S \frac{\phi}{2}, S\right) \rightarrow \alpha_{\max} = \frac{\phi}{2}$$

If the cone is made of n sectors, the above relation will be modified:

$$\left(u = S \frac{\phi}{2n}, S\right) \rightarrow \alpha_{\max} = \frac{\phi}{2n}$$

where

ϕ = the total central angle of all sectors together

SKIN STRESSES OF INFLATED CONE

Internal Pressure

The stresses in the principal direction of a cone which are due to pressurization are given by the following equations:

$$\left. \begin{aligned} q_c &= ps \cot \psi \\ q_\ell &= \frac{1}{2} ps \cot \psi \end{aligned} \right\} \quad (10)$$

where

c and ℓ subscripts indicate the circumferential and longitudinal directions

The angle ψ can be easily determined as a function of r and ℓ :

$$\psi = \arctan \frac{\sqrt{\ell^2 - r^2}}{r} \quad (11)$$

The stresses (Equation 10) can be taken by fibers only along the line \overline{aa} , where the fibers are oriented in the same directions as those stresses. At any other line \overline{ab} , the fibers are inclined at an angle α to the principal directions. Therefore, the above stresses will be split into components and the component stresses in the direction of the fibers will be determined. The induced shear will be taken in accordance with the shear modulus, G, of the material. The stress in the direction of the circumferential fiber will be denoted by q_x , and in the direction of the longitudinal fiber by q_y . The corresponding shear will be denoted by q_τ . Therefore, to known stresses q_c and q_ℓ , q_x , q_y , and q_τ will correspond at any point of the shell:

$$(q_c, q_\ell) \rightarrow (q_x, q_y, q_\tau)$$

The following expressions are based on Mohr's circle:

$$\left. \begin{aligned} q_y &= \frac{1}{2} ps \cot \psi (1 + \sin^2 \alpha) \\ q_x &= \frac{1}{2} ps \cot \psi (1 + \cos^2 \alpha) \\ q_\tau &= \pm \frac{1}{2} ps \cot \psi \sin \alpha \cos \alpha \end{aligned} \right\} \quad (12)$$

To prevent wrinkling of the skins, the following conditions must be satisfied:

$$q_x q_y \geq q_T^2$$

From this relationship can be found the limiting angle α for pressurization loading only:

$$\max q_T = \frac{1}{2} ps \cot \psi \sqrt{2 + \sin^2 \alpha \cos^2 \alpha}$$

$\sin^2 \alpha$ and $\cos^2 \alpha$ are always positive; therefore, the radical is positive too. The max q_T condition will be dictated by the maximum value of

$$y = \left[\sin^2 \alpha \cos^2 \alpha \right]_{\max}$$

The minimization process leads to the conclusion that the permissible max α is 45 degrees. Then

$$\max q_T = \frac{1}{2} ps \cot \psi \sqrt{2.25} = 0.75 ps \cot \psi$$

Axial Compression

If an inflated conical member is loaded by axial compression (Figure 6), the following stresses in the circumferential and longitudinal directions will be induced (due to compression only):

$$q_{\theta} = - \frac{P}{2\pi\xi \cos\psi}; \quad q_c = 0$$

Substituting $S \cdot \sin \psi$ for ξ , we obtain

$$\left. \begin{aligned} q_{\theta} &= - \frac{P}{2\pi S \sin \psi \cos \psi} \\ q_c &= 0 \end{aligned} \right\} \quad (13)$$

Actually, stresses due to axial loading cannot act alone and will always be accompanied by pressurization stresses. However, these two effects can be handled separately, and the results superimposed.

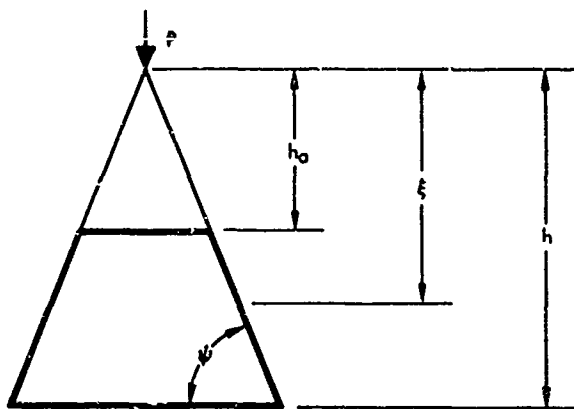


Figure 6. Section of Cone Along Axis of Rotation

Mohr's circle can again be used to determine q_x , q_y , and q_τ . And reasoning similar to that employed before will lead to similar equations. Therefore, for axial compression:

$$\left. \begin{aligned} q_y &= \frac{-P}{2\pi S \sin \psi \cos \psi} \cos^2 \phi \\ q_x &= \frac{-P}{2\pi S \sin \psi \cos \psi} \sin^2 \phi \\ q_\tau &= \pm \frac{-P}{2\pi S \sin \psi \cos \psi} \sin \phi \cos \phi \end{aligned} \right\} \quad (14)$$

To modify Equation 14 for the case of tensile load P , we have only to change the sign before P to a plus.

Now, to carry the analysis any further, we need to know the expressions for the rotational angles of the variable section. If the longitudinal fibers are parallel to the center line of each equal sector, no rotation of the cross section will occur, since the average deformation due to q_τ is zero. However, if the fibers are not parallel to the center line of the sector (arrangement of the sector fibers is not symmetrical), the rotation due to q_τ will not be zero. This type of section tends to rotate.

Torsion

Assume that an inflatable tapered cantilever (Figure 7) is loaded on the end with the torsional moment T . The distance x locates the section under consideration. The torsional moment of inertia is variable:

$$\begin{aligned} J_1 &> J_x > J_0 \\ J_x &= 2\pi r_x^3 t \end{aligned}$$

The angle of rotation at x is

$$\theta_x = \frac{C\tau}{G} \quad (15)$$

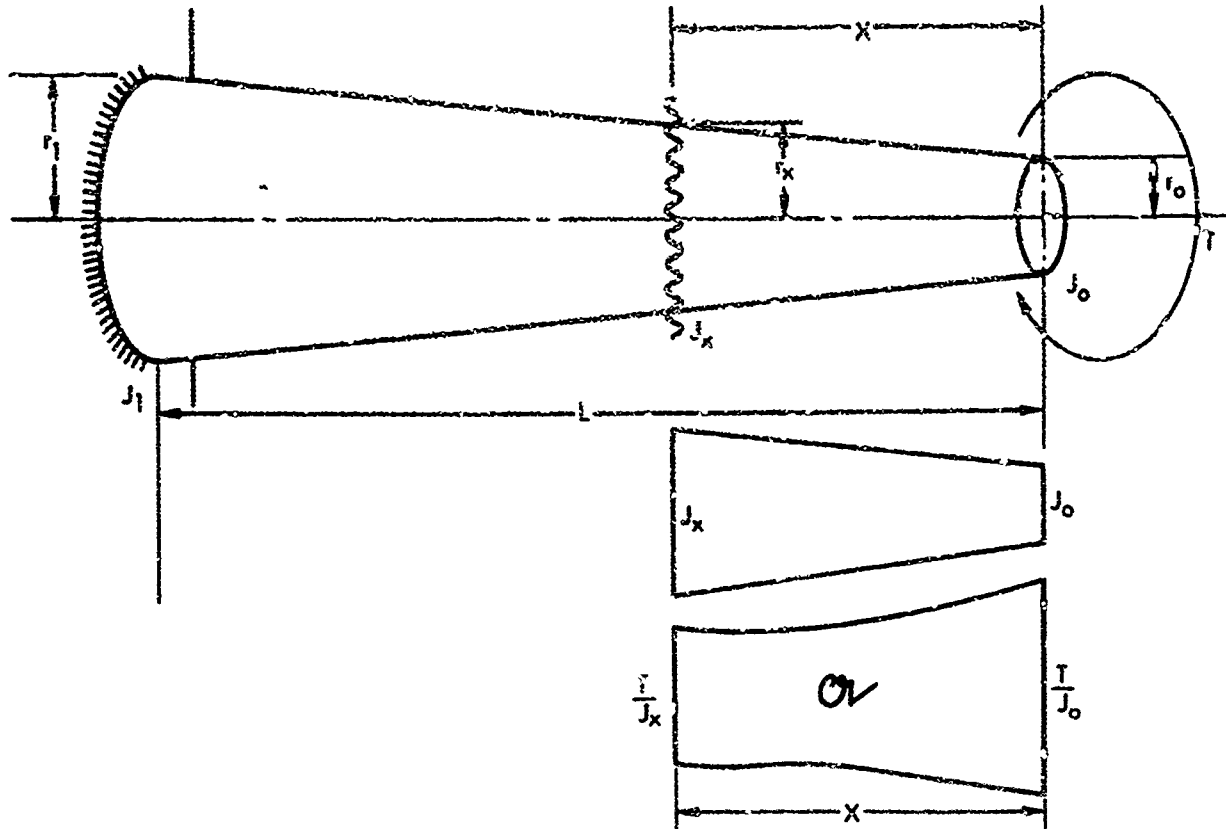


Figure 7. Inflatable Tapered Cantilever Subjected to Torsion

Some average value must be assumed for G , based on the previously derived formula for G as a function of the inclination of fibers.

$$\theta = \int_0^x \frac{T}{J_x} dx = T \int_0^x \frac{dx}{2\pi r_x^3 t} = \frac{T}{2\pi t} \int_0^x \frac{dx}{r_x^3}$$

$$r_x = x \left(\frac{r_1 - r_0}{L} \right) + r_0$$

If we let

$$\frac{r_1 - r_0}{L} = a$$

then

$$r_x = ax + r_0$$

Therefore

$$\theta = \frac{T}{2\pi t} \int_0^x \frac{dx}{(ax + r_0)^3} = \frac{-T}{4\pi t a (ax + r_0)^2}$$

$$\theta = \frac{-T}{4\pi t a (ax + r_0)^2 G} \quad (16)$$

where

$$a = \frac{r_1 - r_0}{L}$$

To obtain γ at x , we could first form the differential element and integrate along the length, which would lead to a relatively complicated equation for γ . Actually, the cone is only slightly tapered; therefore, it seems reasonable to use an approximate value for γ .

$$\gamma \approx \theta \frac{r_0}{x} \quad (17)$$

Final Expressions for Stresses

Now we can return to Equation 12. The shear stresses create a torsional moment

$$T \approx \bar{q}_\tau 2\pi r_x^2$$

where

$$\bar{q}_\tau = \frac{\int_0^{2\pi r} q_\tau dx}{2\pi r}$$

which will cause, in accordance with Equations 16 and 17, an additional twisting of the fibers:

$$\gamma = \frac{\bar{q}_\tau}{4\pi t a (ax + r_0)^2 G} \cdot \frac{r_0}{x} \quad (18)$$

Taking into account this additional change of angle, we may rewrite Equation 12:

$$\left. \begin{aligned} q_y &= \frac{1}{2} ps \cot \psi [1 + \sin^2 (\alpha - \gamma)] \\ q_x &= \frac{1}{2} ps \cot \psi [1 + \cos^2 (\alpha - \gamma)] \\ q_T &= \pm \frac{1}{2} ps \cot \psi \sin \alpha \cos \alpha \end{aligned} \right\} \quad (19)$$

Similarly, axial compression will cause an additional torsional moment, distributed locally in accordance with Equation 14:

$$T = \bar{q}_T 2\pi r_x^2$$

where

$$\bar{q}_T = \frac{\int_0^{2\pi r} q_T dx}{2\pi r}$$

which, in accordance with Equations 16 and 17, results in the angle of rotation, γ_P :

$$\gamma_P = \frac{\bar{q}_T}{4\pi t a (ax + r_o)^2 G} \cdot \frac{r_o}{x} \quad (20)$$

Now we may rewrite the expression for axial compression, Equation 14.

$$\left. \begin{aligned} q_y &= \frac{\mp P}{2\pi S \sin \psi \cos \psi} \cos^2 (\phi \pm \gamma_P) \\ q_x &= \frac{\mp P}{2\pi S \sin \psi \cos \psi} \sin^2 (\phi \pm \gamma_P) \\ q_T &= \pm \frac{\mp P}{2\pi S \sin \psi \cos \psi} \sin \phi \cos \phi \end{aligned} \right\} \quad (21)$$

The upper signs for P and γ_P are for the case of compression; the lower signs, for tension.

For cases in which an axial load acts simultaneously with pressurization loads, the stresses (Equations 12 and 14) are superimposed:

$$\left. \begin{aligned} q_y &= \frac{1}{2} ps \cot \psi [1 + \sin^2 (\alpha - \gamma)] \mp \frac{P \cos^2 (\phi \pm \gamma_P)}{2\pi S \sin \psi \cos \psi} \\ q_x &= \frac{1}{2} ps \cot \psi [1 + \cos^2 (\alpha - \gamma)] \mp \frac{P \sin^2 (\phi \pm \gamma_P)}{2\pi S \sin \psi \cos \psi} \\ q_\tau &= \frac{1}{2} ps \cot \psi \sin \alpha \cos \alpha \mp \frac{P \sin \phi \cos \phi}{2\pi S \sin \psi \cos \psi} \end{aligned} \right\} \quad (22)$$

Effect of Variable Modulus of Elasticity

Inclination of fibers was defined by the angle α , which, along the circumferential direction, varies from $\alpha = 0$ to $\alpha = \alpha_{\max}$. The modulus of elasticity E will decrease with an increasing angle α (derived in a study of an idealized cylinder with inclined fibers). Since α is constant along any line \overline{ab} , E is constant along \overline{ab} ; but it varies along the circumference.

The stiffness of the section depends on EI ; this parameter is used in bending and stability expressions.

If a section is divided into small elements, we can write

$$EI = E \sum I_i$$

where

I_i represents the moment of inertia of the i th small element. But E is variable too; therefore, the above relation can be rewritten:

$$EI = \sum E_i I_i$$

where

E_i is the reduced modulus of elasticity on the i th element to account for inclination of the fibers.

However, it is simpler to work with a constant elasticity modulus E instead of variable E_i . Therefore, let us define I_i^* :

$$I_i^* = I_i \frac{E_i}{E}$$

If y is the distance of the i th element (whose area is A) from the neutral axis, we can write

$$I_i = y^2 A \rightarrow I_i^* = (y^*)^2 A$$

which leads to

$$y^* = y \sqrt{\frac{E_i}{E}} \quad (23)$$

where

y^* = the distance of an element (corresponding to the i th element) with moment of inertia I_i^* and area A

For such a section

$$EI^* = E \Sigma (y^*)^2 A \quad (24)$$

The moment of inertia can be so written because the section is usually symmetrical about the neutral axis. This means that we are working with a transformed section which remains symmetrical about the neutral axis, which has a constant elasticity modulus E , but which is no longer circular. The group EI^* is less than EI . Such transformed sections are represented in Figure 8 for two cases; the section is composed of two and four sectors. It is usually easy to predict which directions will be most affected by the transformation; and this may be employed for determining the effective I^* to be used in calculating the Euler effect because the column will tend to be bent in the weakest direction.

The same reasoning may be used in the study of the bending of a tapered beam, and it helps one understand where to place the joints of the material in order to have a symmetrical section about the neutral axis. Generally, the transformed section will be determined at two end points of the tapered beam, because any section in between is obtained by linear interpolation.

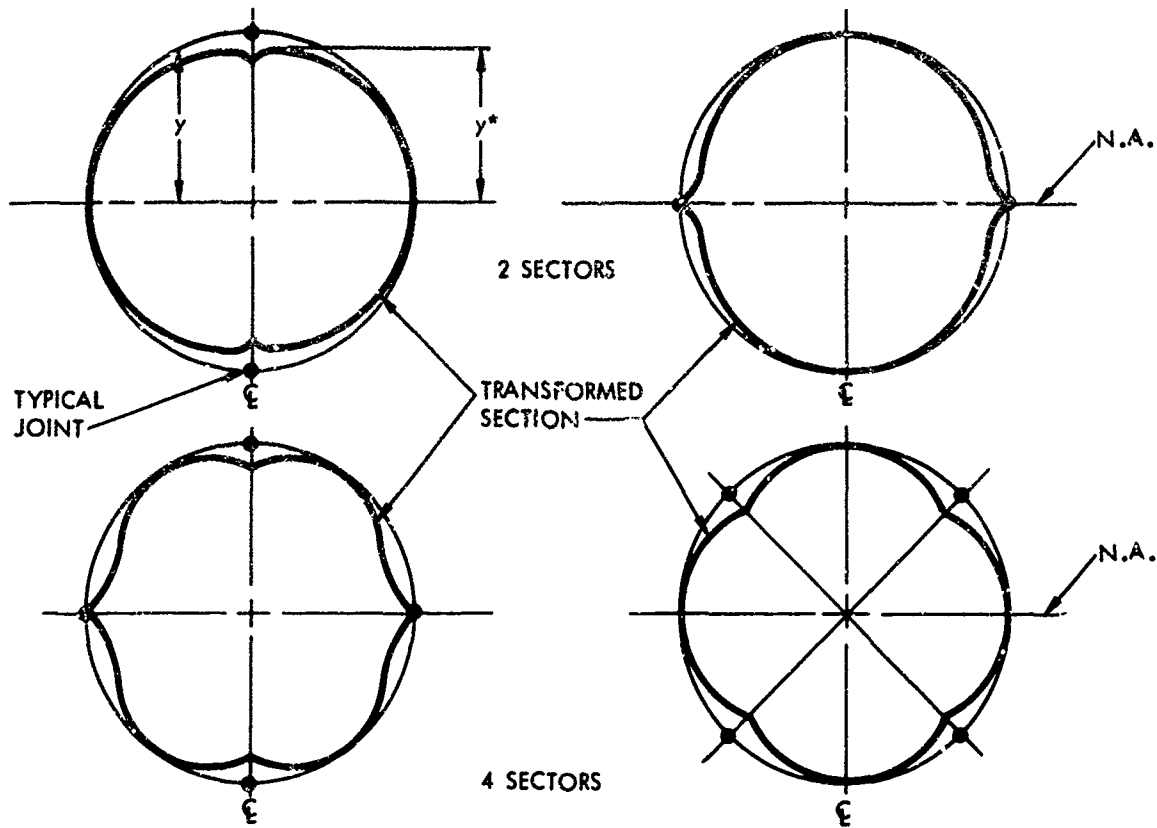


Figure 8. Transformed Sections

This is one way to determine EI . The modulus E was unchanged but the moment of inertia was modified. This is a more or less accurate way since no unjustified averaging is performed.

It is possible to approach the problem differently. Assume I to be as it is, but instead of a variable E , we use some average value. This means that the circumference is divided into segments, and the elastic modulus E_i corresponding to each segment is to be determined. Then

$$E_{\text{eff}} = \frac{\sum_{i=1}^n E_i}{n}$$

where

n = the number of segments

This approximation is less justifiable than the previous one, but it may lead to a faster determination of results.

Euler Buckling Load

In the derivation of an expression for the buckling load, the variation of the geometry along with the length must be considered. A linear relation is assumed for the variation of column depth along the length. For a circular section, the depth is the diameter; for an elliptical section, the diameter of the minor axis; and for a square section, the side. For any transformed section (described in previous paragraph), the depth is the distance between the most distant points from the neutral axis under consideration (Figure 9).

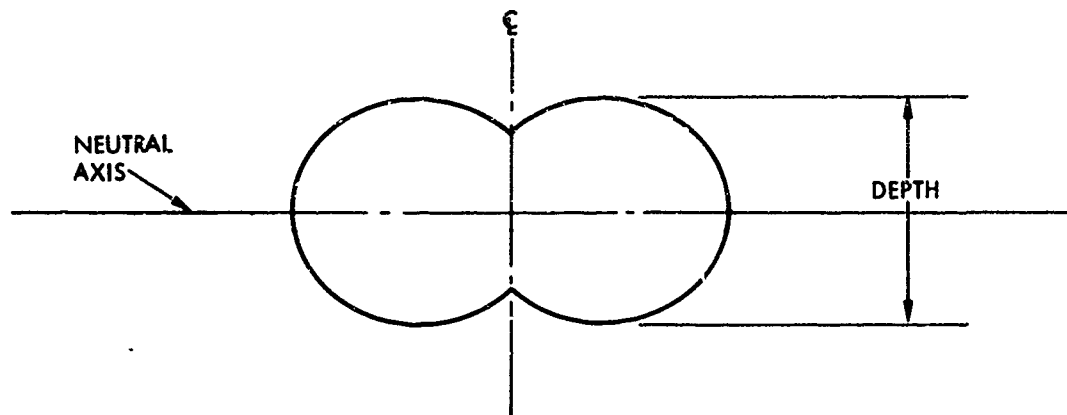


Figure 9. Depth of a Transformed Section

Consider a tapered inflated tube with rigid ends (Figure 10), where

d_A = upper, smaller depth of section

d_B = lower, larger depth of section

x = distance from upper end along the axis of the column

L = length of column

Depth of the section² corresponding to any x can be expressed by

$$d_x = d_A \left[1 + \left(\frac{d_B}{d_A} - 1 \right) \frac{x}{L} \right] \quad (25)$$

The following known equation² can be used for determining I at any point of column x :

$$I_x = I_A \left[1 + \left(\frac{d_B}{d_A} - 1 \right) \frac{x}{L} \right]^n \quad (26)$$

where

I_x = moment of inertia at distance x from upper end

I_A = moment of inertia at upper end

n = shape factor

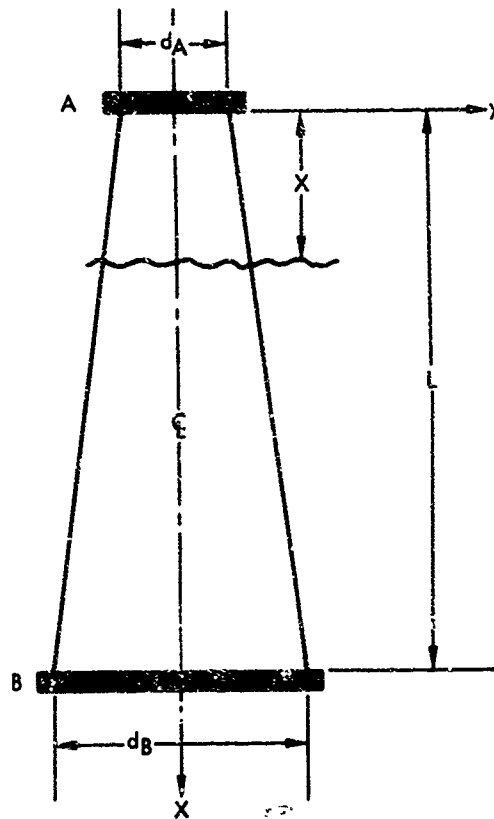


Figure 10. Tapered Inflated Cylinder

The shape factor² can be evolved by observing that Equation 26 must give $I_x = I_B$ when $x = L$. This leads to

$$n = \frac{\log \frac{I_B}{I_A}}{\log \frac{d_B}{d_A}} \quad (27)$$

For the conical case, n varies between 2 and 4.

In Reference 2 a useful equation is presented for critical loads:

$$P_{cr} = P^* \left[\frac{\pi^2 EI_A}{L^2} \right] \quad (28)$$

P^* is given in graphs for various n and d_B/d_A (Figure 11). Equation 28 corresponds to pinned supports on both ends. In the same reference similar graphs were obtained for different supporting conditions. However, for the inflatable fabric column another requirement must be considered. From a derivation of the Euler load for a cylindrical column, we know that the Euler load is limited by the limiting load (Reference 1), which is a function of the internal pressure. The limiting load will be derived in the following section.

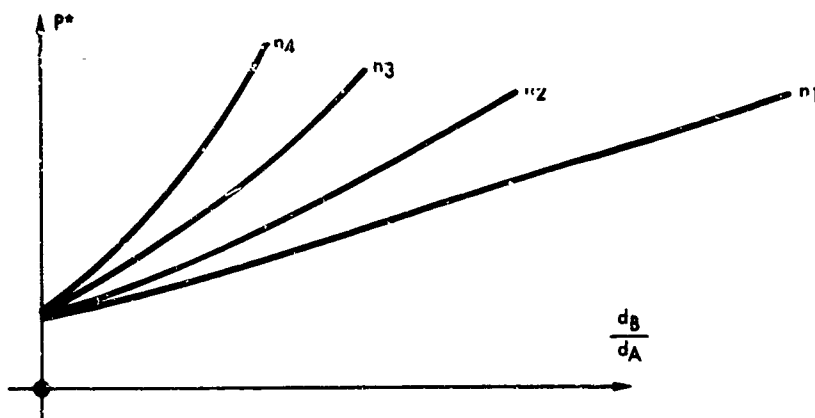


Figure 11. Determination of Critical Load

The Limiting Load P_L

The limiting load is the function of σ_ℓ or, in our case, q_y , which was presented in Equation 20. It is evident that, with reference to any section, the limiting load is variable and can be determined from the following equation:

$$q_y = \frac{1}{2} ps \cot \psi \left[1 + \sin^2 (\alpha - \gamma) \right] - \frac{P_L \cos^2 (\phi + \gamma_p)}{2\pi S \sin \psi \cos \psi} = 0$$

which leads to

$$P_L = \frac{\pi p s^2 [1 + \sin^2 (\alpha - \gamma)] \cos^2 \psi}{\cos^2 (\phi + \gamma_P)} \quad (29)$$

The weakest material will be at $\alpha = \alpha_{\max}$; consequently, if this value or some average value

$$\frac{\alpha_{\min} + \alpha_{\max}}{2} = \alpha_{\text{av}}$$

is introduced into Equation 29, there remains only one variable, S , which can be used to determine the variation of P_L along the length of the tapered beam.

CONCLUSIONS

The material presented in this paper may be regarded as a contribution to the preliminary design of inflatable structures. However, the concepts should be extended to include memory effects and hysteresis, when these phenomena have been better defined for impregnated fabric materials. Moreover, considerable research in the area of materials behavior is needed. In the meantime, it is hoped that the approaches treated here will be of use to the structural analyst.

NOMENCLATURE

q_l	Stress in l direction (lb/in.)
q_c	Stress in c direction (lb/in.)
q_x	Stress in x direction (lb/in.)
q_y	Stress in y direction (lb/in.)
q_τ	Shear stress (lb/in.)
σ_x	Stress in x direction (lb/in. ²)
σ_y	Stress in y direction (lb/in. ²)
τ	Shear stress (lb/in. ²)
E, E_r, E_f	Young's modulus in general, of elastomer, of fibers, respectively (lb/in. ²)

E_{eff}	Effective modulus of elasticity (lb/in. ²)
G, G^*	Shear modulus in lb/in. ² , lb/in., respectively
p	Internal pressure (lb/in. ²)
P	Axial load (lb)
P_E	Euler load (lb)
P_o	Load at which inclined fibers of cylinder will be straightened (lb)
P_L	Limiting load (lb)
T	Torque (lb-in.)
I	Moment of inertia (in. ⁴)
I_1	Moment of inertia of small element (in. ⁴)
J	Polar moment of inertia (in. ⁴)
J_o, J_1	Polar moment of inertia at locations o and 1
\mathcal{A}	Area of diagram of length x and ordinates $\frac{T}{J}$, which also represents reaction of fictive loading (lb/in. ²)
α	Angle of inclination of fibers
γ	Angle of distortion due to shear stress
θ	Angle of rotation of end bulkheads with respect to each other
θ_P	Rotation angle θ due to P
γ_P	Angle γ due to P
ϕ	Total inclination of fibers, $\phi = \alpha - \gamma$; also central angle of a sector of fibers
ψ	Angle between directrix of cone and radius of base
$Y_1, Y_2,$	Elongation of fibers (in.)
$\delta = y_1 + y_2$	(in.)
A, A_r, A_f	Total area, area of elastomer, area of fibers, respectively (in. ²)
t	Thickness (in.)
l, L	Length of cylinder (in.)
r	Radius of cylinder (in.)
d_A, d_B, d_x	Diameter of tapered cylinder at A, B, x locations (in.)
S	Distance from vertex of cone to any circumference (in.)
u	Circumferential coordinate (in.)
*	Modification
N. A.	Neutral axis

REFERENCES

1. Kovalevsky, L., and F. L. Rish. On the Structural Behavior of Inflated Fabric Cylinders Under Various Loading Conditions, presented at the First Symposium on Inflatable Structures (1963).
2. Gere, James M., and Winfred O. Carter. "Critical Buckling Loads for Tapered Columns," Journal of the Structural Division of ASCE, Vol. 88 (Feb. 1962).

SATELLITE APPLICATIONS FOR EXPANDABLE SPACE STRUCTURES

By H. S. Zahn
Martin Company, Baltimore, Maryland

Wherever a large pressurized volume is required in space, the advantages of a compact payload during launch and injection should be considered. Whenever repeated expansion and contraction as well as the protection afforded by a rigid, load-bearing structure is required, the particular type of space structure discussed in this paper is a prime candidate. A companion paper, "Semi-rigid Structures for Space Applications," by P. M. Knox, Jr., and R. O. Moses, Jr., describes the development and construction of this structure in detail.

Very frequently, the principal applications of this structure are for manned systems. This would include such applications as the variable extension arms of an artificial gravity space station, the expandable hangar for maintenance of vehicles in space or a combined docking and airlock system. On the other hand, unmanned applications may be of more immediate value. These include an adaptation for use as a radiator for a nuclear reactor in space or the use of this available structure as a test bed for certain space experiments. An investigation of this latter application was conducted.

Test Vehicle Features

The adaptability of the structure investigated to several experiments which would provide data for space station design appears quite feasible. The features which provide this capability are listed in Table 1. The details of construction are summarized to identify their advantages for use in a test vehicle.

- (1) The structure has been designed and tested for the environment to be encountered in a low altitude orbit launched on the ETR.
- (2) The internal expanded volume approximates the size and shape of a small manned space station. Realistic simulation without large scaling factors is possible.
- (3) The retracted dimensions of the structure fall within existing launch vehicle payload envelopes. This is critical both dimensionally (to satisfy aerodynamic criteria) and inertially (to satisfy mass distribution criteria).
- (4) Design for internal pressurization up to 11 psig permits simulation of space station environments over a wide range of pressures as well as by use of different gas mixtures.
- (5) The base bulkhead and forward dome attachment frame provide ideal locations for the attachment of equipment necessary for the vehicle

operation. The base bulkhead will withstand launch accelerations with a full load of equipment. A much lighter weight base structure can be constructed and installed if weight becomes critical.

- (6) Access to internal equipment is available through a manhole in the forward dome during checkout operations. This hatch seal has been tested with the structure.
- (7) The telescoping sections and forward dome are removable. This provides access for installation of large equipment and for any modifications necessary to conduct the tests.
- (8) The external skin panels are easily removed for reworking or for replacement by test panels. Internal panels carry the structural loads.
- (9) The structure seals and coatings have been tested for a 1-yr life. The design was established based upon this life criteria. A structure of this size and shape suitable for a 1-yr test period has not been previously available.
- (10) The passive thermal control is designed to provide an environment that will give maximum internal equipment reliability. This can be easily revised to suit test conditions by modifying the external coating and the detachable insulation between the walls of the structure.
- (11) The internal compartment may be modified to provide segments or smaller compartments if desired for test purposes. The design permits this modification to be readily accomplished.
- (12) The telescoping sections inherently provide several identical large diameter joints for test of varying seal designs. This capability would require some modification for tests requiring more than merely varying the sealant materials.
- (13) The side panels of each section protect the inner sections during launch. The outer panels of the forward section will withstand launch airloads and heating if necessary.
- (14) A mechanical lock has been designed which will permit locking the structure in the expanded position if this is deemed necessary for test or operation.

Expandable Structure Experiments

Several experiments which may be conducted through the application of this structure have been conceived. These include the following:

- (1) Tests of the expandable structure operation in space for development of actual applications.
- (2) Simulation of space station shielding for radiation environment experiments on a tissue equivalent manikin.
- (3) Micrometeoroid effects on thermal control of space stations and penetrations of a typical space station structure.
- (4) Effects of the complete environment on passive thermal control of large discontinuous structures.
- (5) Seals and sealant life tests.

TABLE 1
Test Vehicle Features

Design for Orbital Mission
 Approximation of Manned Space Station Volume
 Retraction to Within Payload Envelopes
 High Allowable Internal Pressures
 Accessible Equipment Mounting Structure
 Internal Access for Checkout
 Removable Sections and Dome for Installation
 Removable External Skin Panels
 Design for 1-yr Orbital Life
 Variable Passive Thermal Control
 Internal Segmentation Feasible
 Multiple Joints for Test
 Side Panels Protected for Launch
 Mechanically Locked Extended Sections

In addition to these tests many variations may make use of the expanded volume after orbital injection to provide operating room or a controlled, shielded exposure. Many materials tests including tests of seals and sealants may fall in this category.

Expandable Structure Operation

Operation of the Expandable Space Structure in space cannot be completely verified by ground tests. Ground tests are limited in their ability to demonstrate expansion safely, completely and without damage in the zero-gravity environment.

At first glance, this does not appear to be a significant problem. However, the weight of the telescoping sections dampens fluctuations in pressure during expansion on earth. In orbit, this mass has the opposite effect, and the inertial effects may tend to aggravate any pressure fluctuations. The relatively large pressure needed on earth (a maximum of 0.25 psig) to lift this weight and expand the structure is reduced to a very low value in orbit.

In orbit, excess pressure may have to be used to overcome any tendency of the sections to bind (Fig. 1). These pressures may establish velocities of one section with respect to another that could damage the structure or seals when the motion is stopped by the mating flanges of adjacent sections. The control of expansion pressures is expected to be more critical in orbit than on the ground, since it is anticipated that less pressure is required to expand than on earth. The only opposing forces in orbit would be the friction of the guide rails and shoes, the bladder friction on the wall and the tendency of the bungee bladder folding system to act as a retracting spring. These have been insignificant compared to gravity forces in expansion tests.

In order to verify that the expansion of the structure can be adequately controlled in orbit and that the possible uneven deployment of the telescoping sections is an insignificant factor, it is recommended that the structure be placed in orbit and expanded in an operational test. Data collected would determine any unusual problems that cannot be anticipated from ground testing.

The test would be conducted by evacuating the structure during the initial ascent and coasting period. After the payload is separated from the launch vehicle, the hold-down bolts attaching the upper section to the adapter plate would be released and the structure expanded.

The expansion would be controlled by limiting the maximum pressure to a value which could not accelerate the sections to a damaging velocity. At the onset of any slight binding tendency, the pressure buildup to this value should release the structure. Flow rates would also be controlled to a safe level. Any of several gases could be used, including dry air, O₂, N₂ or a mixture of O₂ and N₂. Gas selection would be dependent upon other tests being carried.

After complete expansion, the pressure would be automatically increased to design pressure. The high pressure source or a vibrator could be commanded to operate intermittently if complete expansion did not occur.

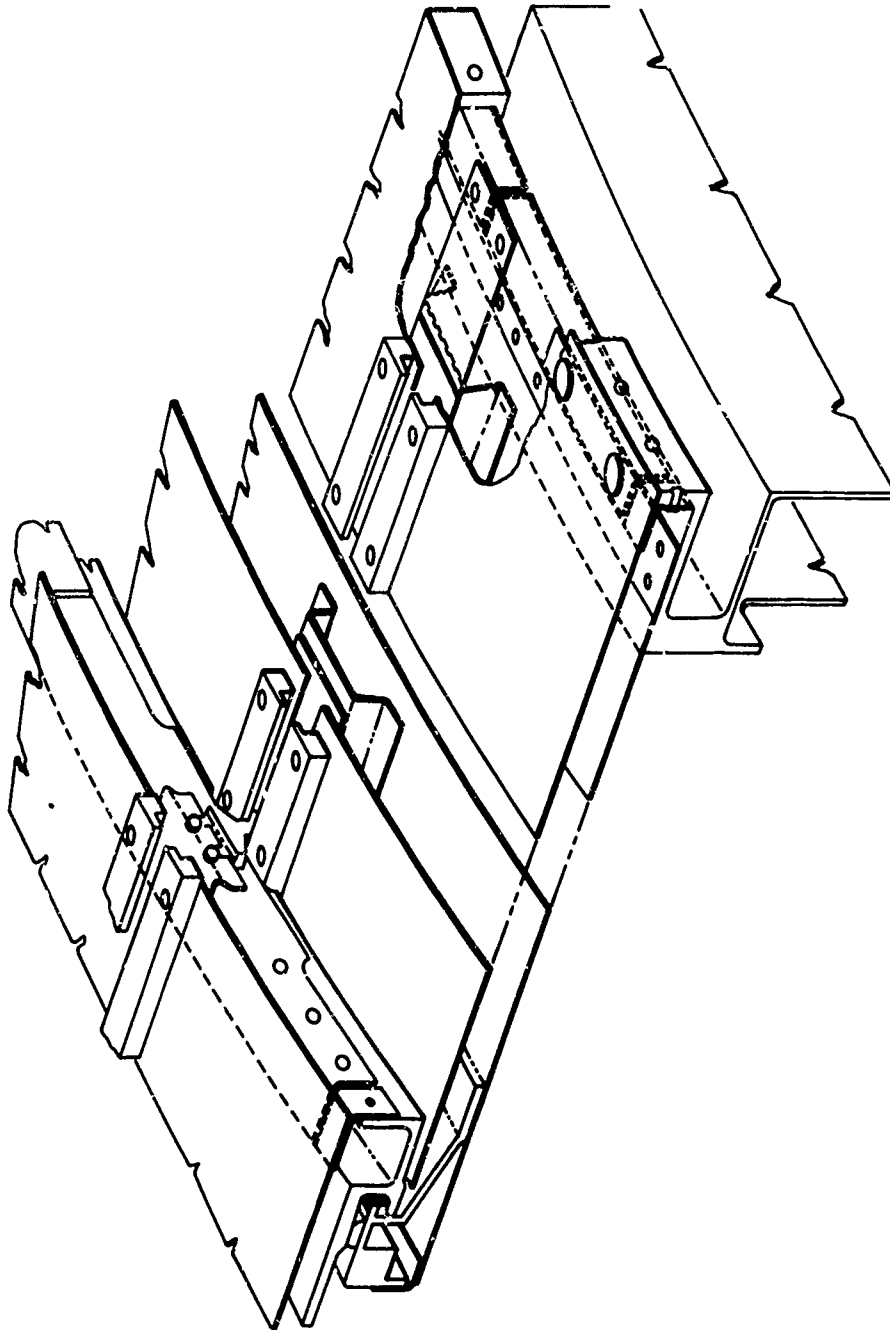


Fig. 1a. Structural Configuration, Expandable Space Structure Vehicle

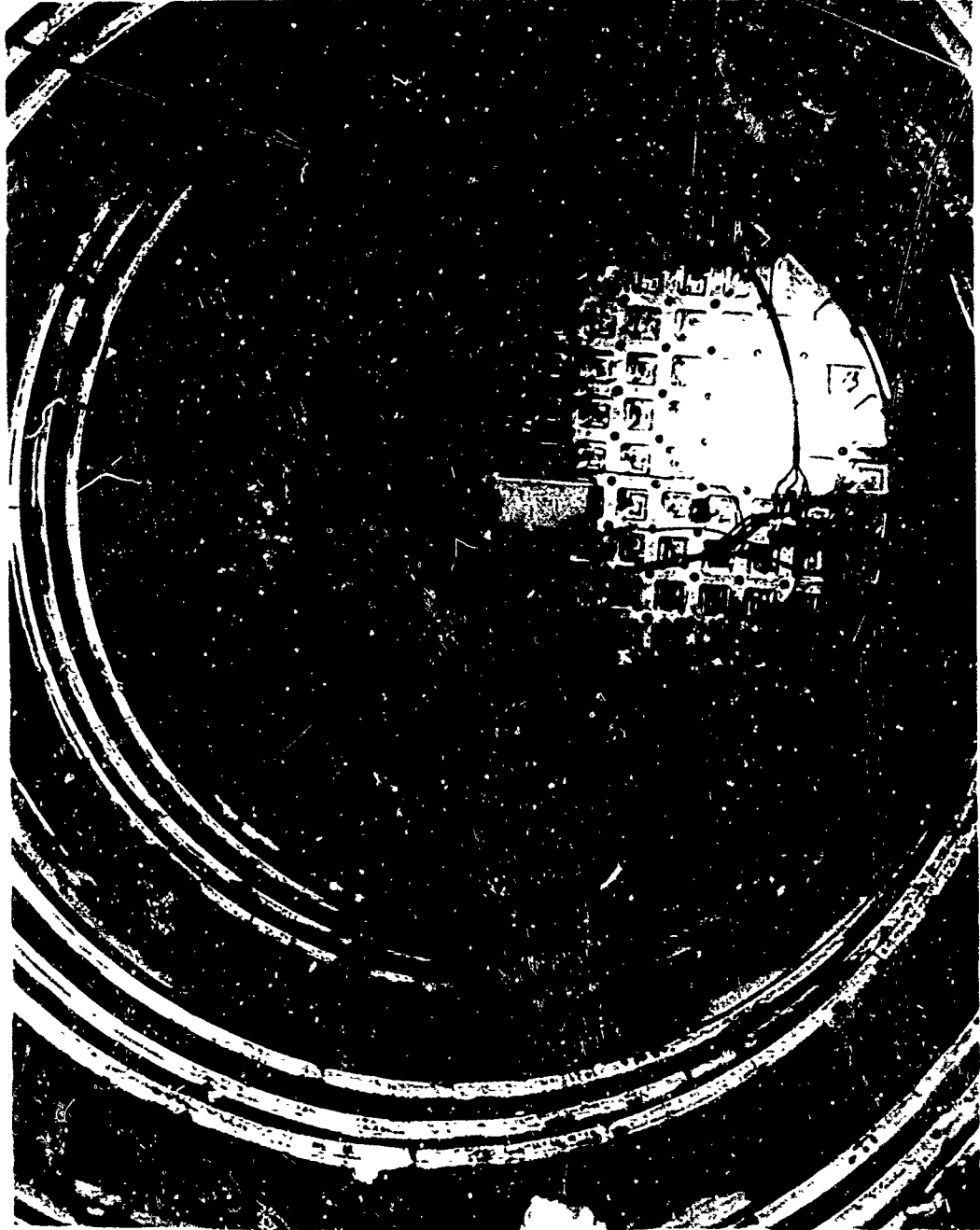


Fig. 1b. Interior View of Extended and Pressurized Vehicle Showing Bladder Extended

The foregoing test is the simplest which would provide necessary data. Additional features which may be tested could include:

- (1) The ability to retract the structure in orbit. Since this is a function required by some applications, the potential should be verified by test in the zero-gravity environment. The retraction should be conducted with and without internal pressure and would require installation of a simple positive retraction system.
- (2) A retractable structure could be easily modified to determine vacuum welding between various surfaces at the metal-to-metal contact points at each ring frame. The variation with time of contact may be a factor which is measurable through this technique.
- (3) A retractable structure could incorporate several expansion control system designs to determine which provides the most satisfactory expansion characteristics.
- (4) Other modifications require more extensive development, but could include: helical expansion and bladder folding with possible improvement of bladder stowage; intermittent bladder to provide seal at joints only and provide for installation brackets on side walls of structure; installation of additional sections to establish very long expansion arm characteristics and to study dumbbell stabilization; and installation of a large diameter rotating seal design in a special section to determine zero-gravity life and leakage characteristics in the hard vacuum.

Radiation Environment Effects

The Expandable Space Structure offers an excellent opportunity to conduct a realistic simulation experiment of the space cabin environment and to measure simultaneously the biophysical and physical parameters of space radiation. This experiment would use a tissue equivalent plastic manikin (plastinaut) and associated radiation sensors which have been developed and are available from the Air Force Weapons Laboratory, Albuquerque, New Mexico.

Considerable data are available describing the radiation environment to which a spacecraft is subjected in orbital flight. However, it is difficult to relate data which measures radiation flux with varying amounts of shielding in different spacecraft environments to the dosages that would be received by the critical organs of man. Even those attempts to measure dosage and RBE gave only the so-called "whole body values," which can be misleading. Simulation of the radiation environment on earth is unsatisfactory due to the variety of particles and energy levels encountered at various altitudes.

Consequently, it is important that a combined experiment be conducted to measure the radiation environment in a typical space cabin as well as the dosage in a simulated human body at the location of the critical organs and blood-producing centers. This dosage should be measured for sufficient time and over a wide enough range of altitudes to effectively sample the dose rates to which man may be exposed in earth orbits on possible future space missions. This requires that the experiment be highly comprehensive from the standpoint of instrumentation and time and extremely realistic as to uniformity of geometry and shielding. From such an experiment, criteria may be established for designing orbiting space vehicles over a wide range of orbital altitudes and missions.

The test would require that the astronaut be mounted in the Expandable Space Structure in a location providing uniform shielding from the structure. The location chosen was below the elliptical dome, with the astronaut mounted in a position normal to the longitudinal axis of the structure. The astronaut is supported by a couch structure which also will support some of the external environment test instrumentation. The structure will be stabilized such that, in this position, the astronaut will face in a direction opposite to the flight direction, with his feet toward the earth.

The orbit selected for test must provide a wide sampling range of the radiation environment of space vehicle. To obtain this range of dosage, and to effectively map out the orbital volume in which manned space vehicles may operate around the earth, the orbital altitude should extend to an apogee of greater than 1500 n mi with a perigee below the radiation belts.

After injection into orbit, the Expandable Space Structure is expanded. This expansion places the astronaut approximately 9 ft, 6 in. above the operating equipment attached to the aft bulkhead. Shielding from the back thus occupies only a small solid angle. It is desirable to increase the shielding provided by the elliptical dome bulkhead. Shielding would be increased by increasing the mass to approximately 2 gm/cm^2 through the insertion of a false dome within the pressure dome. Other shielding mass can be used. If additional tests of a double wall structure are performed which would require modification of the structure by addition of the double wall on the dome, then the dome shielding would be approximately 0.5 gm/sq cm .

Several variations in the test procedure may be considered.

- (1) The astronaut may be moved to another position within the structure after the initial test period. A suggested position would be along the structure longitudinal axis with feet toward the aft bulkhead (Fig. 2). In this position, shielding would be uniform completely around the astronaut and the equipment would be heavy around his feet, a situation that may exist in unmanned spacecraft. The most important feature of this test would be the ability to analyze data to determine the probable cause of any dosage anomalies that could not be explained from the

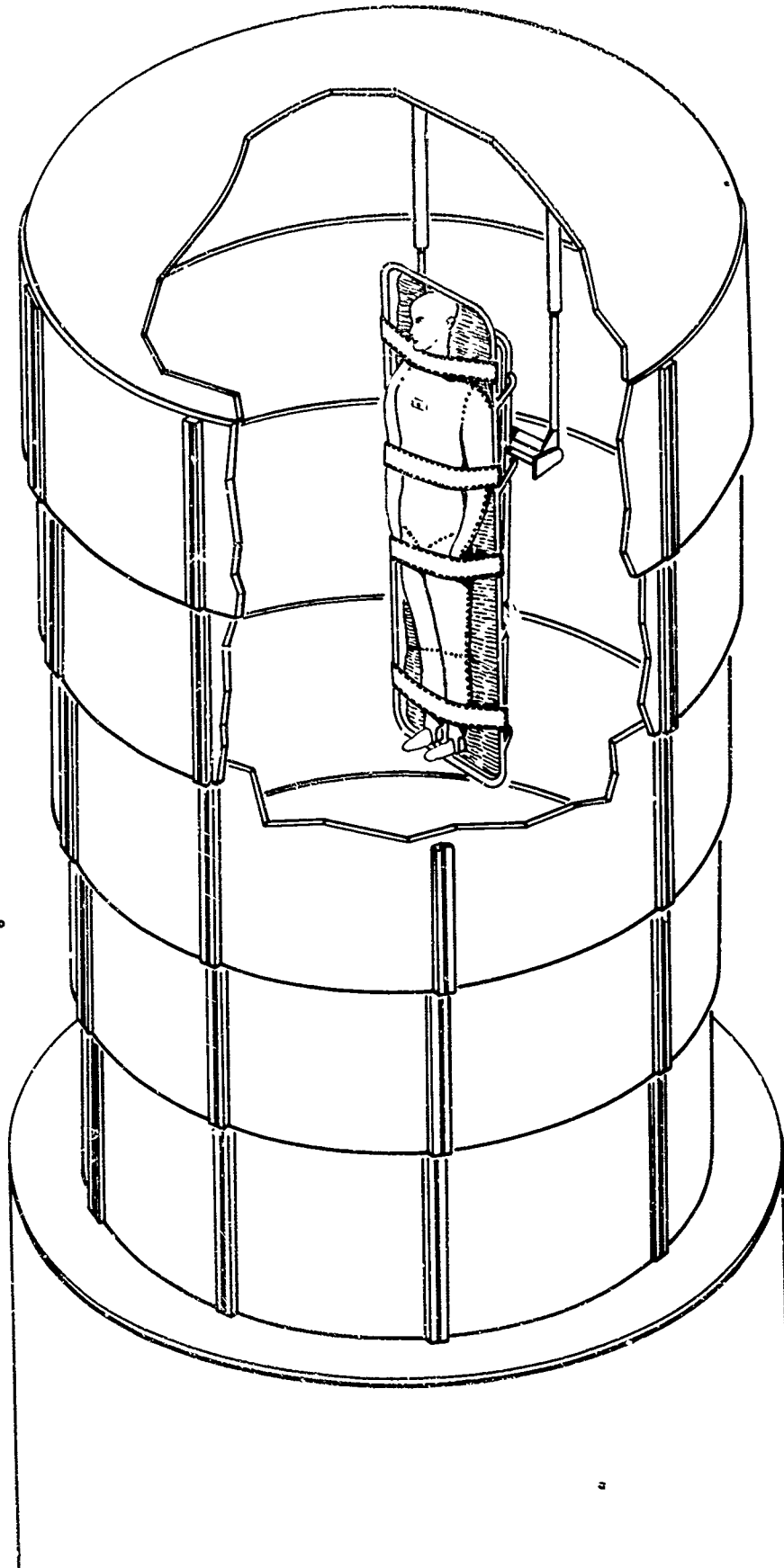


Fig. 2. Installation of Plastinaut in Structure for Test

first test. The internal volume of the structure is sufficient to perform this change in position. The astronaut may also be rotated about his longitudinal body axis. This may be desirable to obtain various exposures, since the structure may be stabilized to a predetermined attitude in orbit.

- (2) The duration of the test may be varied. The life of the space structure can be extended to 1 yr. During this life, the orbital volume may be mapped several times at extended intervals if desired. For a two-position test, an exposure of 7 days in each position is believed sufficient.
- (3) Some of the orbital tests would more suitably simulate a manned space station environment if they were conducted in a near-circular orbit. Since this would limit the radiation flux range encountered, it may be undesirable to expend a astronaut for these tests. However, data of the ambient dosage using the basic instrumentation and perhaps a section of plastic would provide a real correlation with other data provided from a astronaut test and would establish the mission duration possible in such orbits. The advantage of these orbits is the extended duration expected to be feasible during such a test because the radiation exposure to equipment is reduced.

Micrometeoroid Effects

The large surface area and volume of the structure provides an excellent large scale simulation of the probability of impact and penetration to be expected in a manned space station. With the exception of Pegasus, previous satellites have provided meteoroid data on very small scale samples. Pegasus is designed to provide data from approximately 200 sq m of instrumented thin panels during a long duration flight. The problems of converting penetrations of the Pegasus shape and thin panel to probability of no penetration of a space station of another shape and double-walled structure indicate the desirability of a better simulation.

Another gap in the field of meteoroid penetration analysis is the wide range of analytical results that may be obtained by using different data sources. This makes penetration prediction very unreliable until consistent sets of data become available. For the present, then, the better the simulation of the structure and the environment that is possible, the more confidence can be placed in the ability of the space station design to perform with the required safety.

In addition, correlation between meteoroid penetration simulation tests in ground facilities and tests in satellites can be provided. Verification of the performance of a satellite structure, designed as the result of criteria defined by ground test, would be a step forward in defining safe design criteria for this characteristic of manned space station structures.

The structure provides several features which make it extremely suitable for testing micrometeoroid penetration characteristics (Fig. 3). It is designed to withstand micrometeoroid penetrations to attain a low probability of penetration over a 1-yr period through use of a double-wall meteoroid bumper construction. Also, the external panels are easily modified to mount meteoroid impact detectors both inside and out, and the design provides protection of these detectors both during ascent and while the structure is being expanded.

Estimated penetrations of an area of this magnitude would be 13.5 per day for a 0.005-in. thick detector surface or one penetration in 69 days for a 0.025-in. detector. These periods vary with the data used as a computational base. Therefore, a significantly long period is required for the test. A life of 1 yr appears satisfactory.

To conduct the test, meteoroid foil detectors could be installed on both surfaces of all removable external panels including panels to be installed on the dome. The 0.070-in. skin of the forward section could be replaced with thinner skin if the structure were covered by a fairing. All external skin panels could be made equal in thickness to the thickest panels on the meteoroid satellite. In this way, the two tests may provide better correlation. Each panel would be separately instrumented for a total of 48 segments (including dome segments). The number of penetrations and time of penetration for each panel may be recorded over the 1-yr life.

The low probability of penetration of the double wall requires only the monitoring of internal pressure to determine the existence of a leak. Should the leak occur at the same time as a penetration of the external panel a penetration through the double wall would be indicated. The size of hole would be indicated by the rate of pressure drop. Should no leaks occur from this cause during the 1-yr period, an effective bracket of structural requirements for missions of shorter periods being considered would be obtained.

Some additional instrumentation may be installed to obtain data of other events related to meteoroid penetrations or to obtain more complete instrumentation of the punctures. This could include:

- (1) Instrumentation to analyze the explosive effects of a meteoroid puncture in a large chamber with a high oxygen atmosphere.
- (2) Internal compartmentation could be installed to aid in detecting several punctures during the test life should they occur.
- (3) Variable panel thickness could be installed and may have some merit. However, a better simulation of a space station is believed possible with uniform panel thickness.



Fig. 3. Completed Expandable Space Structure Vehicle Fully Extended

Thermal Control Experiments

The thermal control of earth oriented orbital space stations is a most difficult problem to analyze precisely. The attitude and orbital variations and variations caused by structure and installed equipment all affect the thermal balance.

The extensive thermal analysis and laboratory tests of coatings conducted during the design of this expandable structure provide a basis for estimating the internal thermal environment in space.

More thorough analytical methods are available to determine the expected internal equipment and structural temperatures. However, the effect of the combined meteoroid and electromagnetic spectral environment over a 1-yr orbital life must be predicted. The need exists for data which verify these predictions and establish the validity of the experimental and analytical techniques. The expandable space structure provides a clean and uniform structure, yet complex enough to demonstrate applicability of analytical techniques. Coupled with the analyses and laboratory tests that have been conducted thus far, a test of the passive thermal control system devised for this vehicle would further verify the capability to design for similar space stations in the space environment.

The most enlightening data would be to verify the degradation of the passive thermal control coatings on a stabilized vehicle where one side receives greater exposure than others. The effect of the degradation of thermal control coatings on the internal temperature distribution (both on equipment and on a simulated astronaut) as well as on the internal atmosphere, should be determined. Such questions as the possibility of convection currents should be examined in this large volume to determine any possible secondary effects.

During the course of the test, the passive thermal control design would maintain inner wall temperatures within a specified temperature range determined analytically. This must be checked when internal heat sources are finalized. However, the time to recover from the initial cold internal atmosphere due to expansion by use of a stored gas system must be determined. To provide a satisfactory test, the forward dome must be insulated in the same manner as the side walls; the aft base plate may also be insulated, depending upon the equipment installed on its external surface.

Measurements would be taken of outer and inner skin temperatures, surface temperatures of critical equipment and the astronaut (if installed) and the internal vehicle atmospheric temperatures at various points. The thermal instrumentation would be designed to continue operation in the event of loss of pressure. A fan would be provided to circulate the air to provide uniform internal temperatures for equipment thermal control, if desired. The fan would be used when convection current testing was completed, or as soon as damaging hot spots were detected.

Since thermal variations would change only slowly over the 1-yr life of the vehicle, the sampling intervals could be quite large after the expansion and orbital transients had been recorded during the first few days.

Several variations are possible in addition to the simple recording of thermal levels and internal airflow. These include the following:

- (1) The thermal coatings could be varied at each telescoping section. While skin temperatures may vary, the internal atmosphere would keep the environment uniform for protection of equipment.
- (2) A semipassive cooling system could be installed in conjunction with a heat source. To do this, the aft base plate may be used for radiator installation as well as the outside panels of the aft telescoping section. An alternative cooling method would be to use an internal vehicle liquid-to-gas heat exchanger, pass the internal vehicle atmosphere through it and reject heat through the vehicle walls by selection of a suitable coating. However, in the event of a leak in the structure, radiative cooling would be necessary to continue a test.

The capability to perform these experiments was verified by defining several test configurations. While these configurations were defined for a particular launch vehicle, they also serve to illustrate the variations possible for application to other vehicles. A summary of the data required is given in Table 2.

TABLE 2
Summary of Data Required

<u>Configuration</u>			<u>Data Required</u>
<u>1</u>	<u>2</u>	<u>3</u>	
X	X	X	Expanded length of ESS
X	X	X	Internal pressure
X	X	X	Internal temperature
X	X	X	Gas supply pressure (structural leak rates)
X	X	X	ESS acoustical intensity and frequency
	X	X	Radiation measurements with plastinaut
	X	X	Radiation measurements without plastinaut
		X	Meteoroid count
X	X	X	Verify equipment operation
		X	Meteoroid penetration count
	X	X	Destruct system

Minimum Test Configuration

Figure 4 illustrates a minimum test configuration. This configuration is designed to test the operation of the structure itself. The launch vehicle would inject it into a 100-n mi orbit and provide initial stabilization in orbit. After separation from the injection stage, the structure would be expanded by a pressurization system. The expanded length, internal pressure and temperature would be measured. In addition, all acoustic noise would be recorded to indicate unusual occurrences. All data would be transmitted to a ground station once each orbit for a total mission time of 48 hr. In this test, the low orbital altitude precludes long duration measurements. Therefore, the extension of the structure is the primary test. For this configuration as well as those following, the injection altitude was a launch vehicle constraint. Higher injection altitudes would permit redesign to incorporate other test objectives.

For this test, only minor installations are required. An adapter is used to connect the structure to the launch vehicle, and the external equipment, such as antennas, is mounted on this adapter structure. All internal equipment is attached to the interior of the base bulkhead. This includes a pressurization system, telemetry and command communications and a battery power supply. The only modifications required for the structure are the installation of a hold-down system to retain the structure in the collapsed position during launch and the installation of pressure relief and equalization valves. The weight of the complete payload is 2145 lb.

Radiation Dosage Configuration

Figure 5 illustrates the use of the expandable structure for the radiation dosage test already discussed. This payload is also injected into a 100-n mi orbit. However, a complete test requires sampling over a wide range of altitudes so propulsion must be added to the payload to inject it into an elliptical orbit with approximately a 2000-n mi apogee. Due to the confines of the allowable payload envelope, and other launch vehicle constraints, the solid rocket propulsion is mounted in an inverted position. This requires rotating the structure before ignition of this motor for injection into the elliptical orbit.

The structure is expanded after injection into the elliptical orbit and pressurized to 11 psi. All data is recorded continuously and read out to the ground station on command approximately once each orbit. This operation is repeated for approximately 7 days. The alternative astronaut position may then be commanded and the mission repeated for an additional 7 days. Pressurization gas and power is supplied for a 14-day mission. Sufficient gas is supplied to make up for a loss of 2 lb/day which is assumed to give sufficient margin above test values for conservative design.

The design of this configuration requires several additional systems over those used for the minimum configuration. Propulsion necessitates the addition

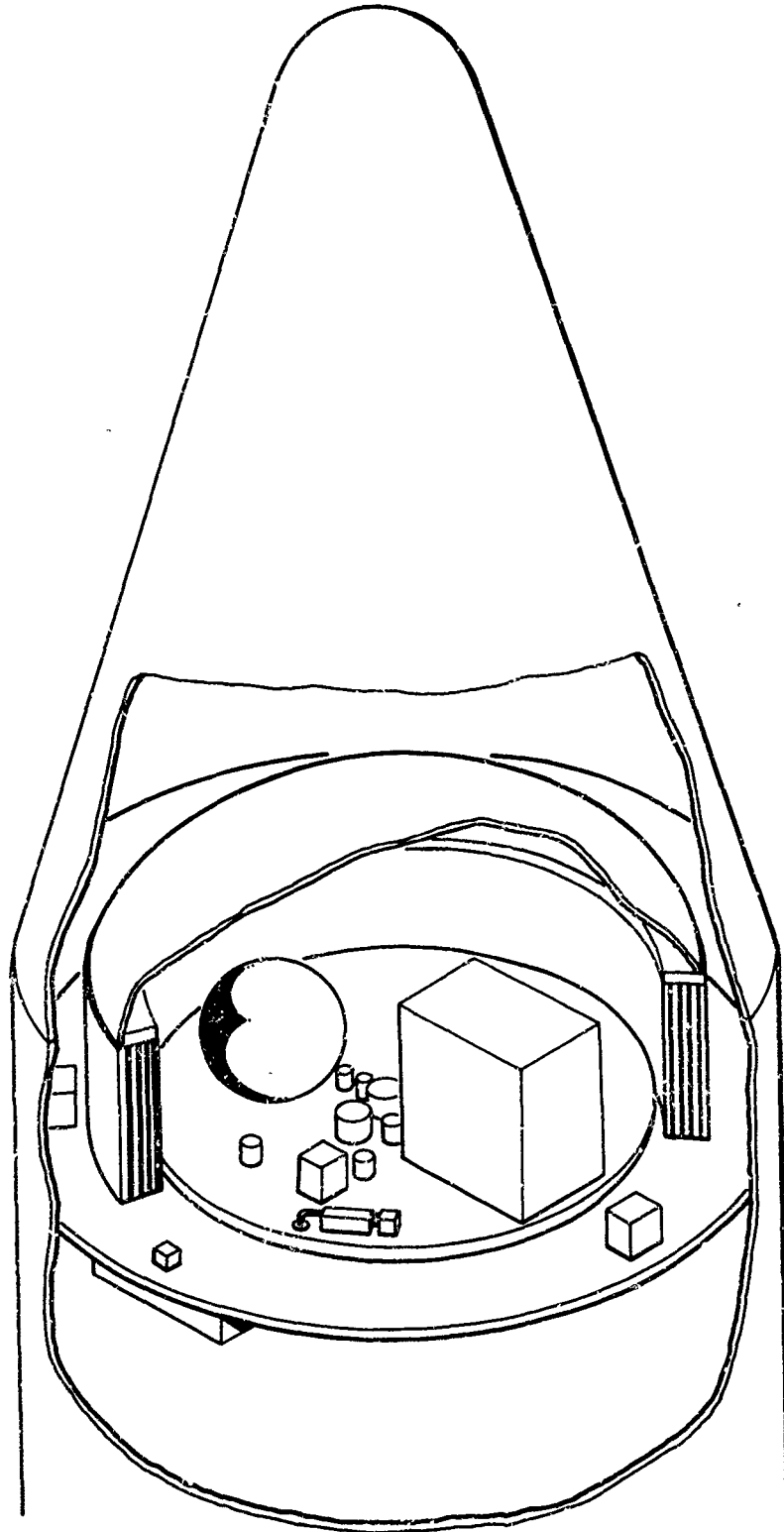


Fig. 4. Minimum Test Configuration

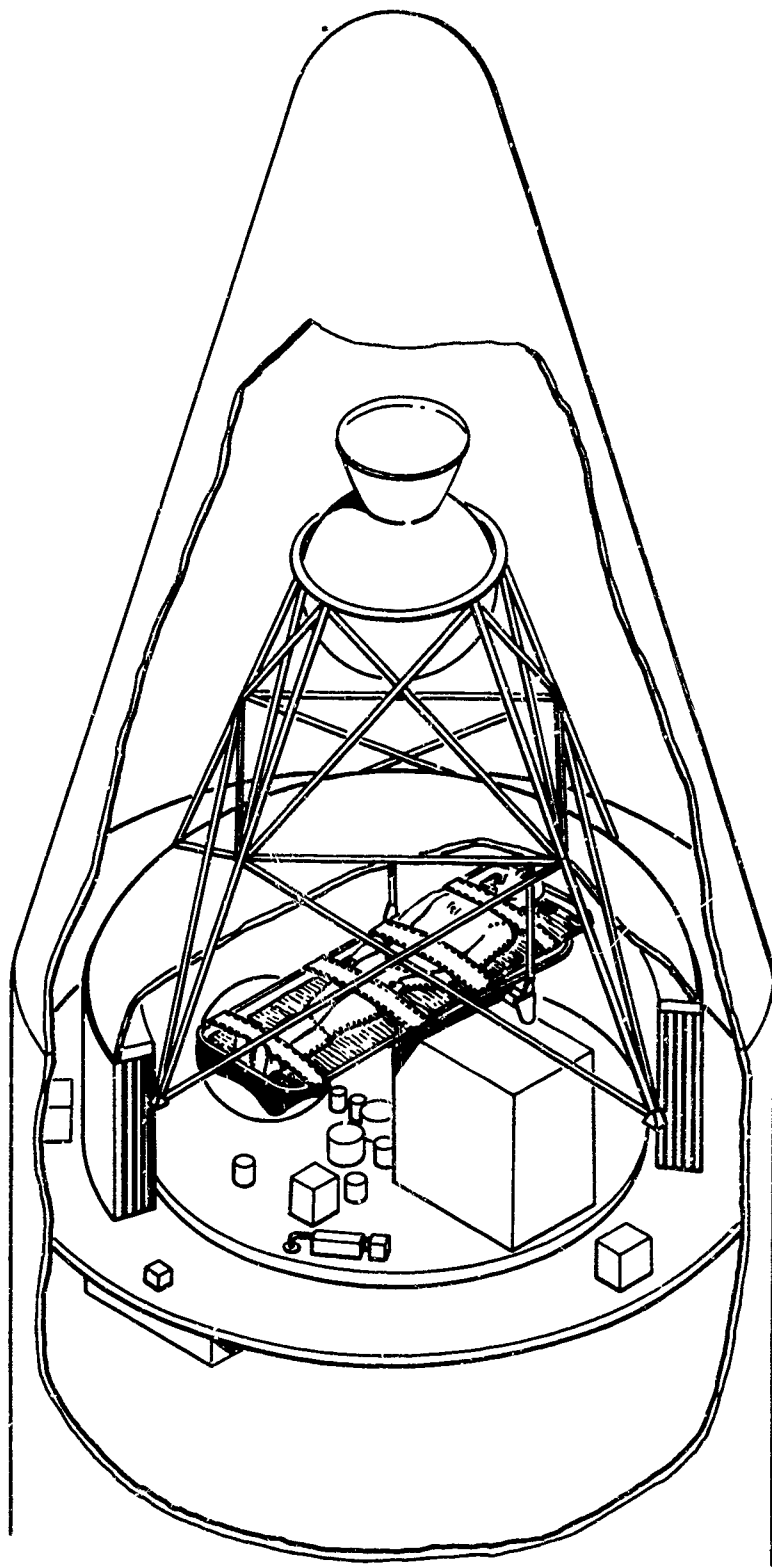


Fig. 5. Radiation Dosage Test Configuration

of stabilization and attitude control systems. These systems are also required to stabilize the structure during the 14-day mission and thereby assure a known position of the astronaut and his instrumentation within coarse limits. The instrumentation, telemetry and command, and power systems all are significantly increased in complexity over the minimum test configuration although the power supply still requires only batteries. Structure installations include supporting structure for the propulsion system; the design and installation of the astronaut couch assembly supported by the forward dome ring frame; installation of a propulsion separation system; installation of additional dome material as a false inside dome to increase shielding above the astronaut and installation of a locking system to lock the structure in the extended position in the event of a gas leak. These installations can be made with only very minor modifications of the structure. The total weight of the assembled payload is approximately 4500 lb.

Long Duration Test Configuration

Figure 6 illustrates a long duration test configuration which incorporates a wide variety of tests. This configuration is designed to provide a 1-yr mission in an orbit with perigee at 120 n mi and apogee at 500 n mi. After injection into orbit at 100 n mi and separation from the launch vehicle, an impulse transfers the vehicle into an orbit with a 120-n mi apogee. Another impulse then transfers it into the final orbit. The propulsion system is then jettisoned. An apogee of 500 n mi is used to decrease radiation effects over the 1-yr life but simulate a range of space station orbits. The perigee increase is necessary to attain a 1-yr life. This mission complexity may be alleviated by proper choice of launch vehicle trajectory, and the elimination of the propulsion and its attendant stabilization requirement. However, this complex system illustrates the possible application of propulsion to the payload.

To provide a test payload capable of accomplishing this mission, a number of minor modifications were made. The installed systems included the expansion and pressurization system, a passive thermal control with circulating fan, separation and hold-down, destruct and telemetry and communications systems. The installation of propulsion, stabilization and attitude control requires added adapter structures and increased volume within the selected payload envelope. The astronaut is installed to provide radiation dosage data over a long period. This test, however, cannot substitute for the highly eccentric orbit previously used for complete radiation data. Additional test equipment includes the installation of meteoroid test panels on all side panel sections and on the forward dome, and the installation of thermal instrumentation to conduct the thermal control test.

The pressurization gas is defined by leakage at 5.5 psi, and 708 lb are required for the 1-yr test. The power supply uses batteries for 31 w of nominal power over the 1-yr life for accomplishment of a minimum mission. A supplementary source from a solar cell panel provides an average of 45 w additional power to accomplish the complete mission. The solar panel is oriented to avoid

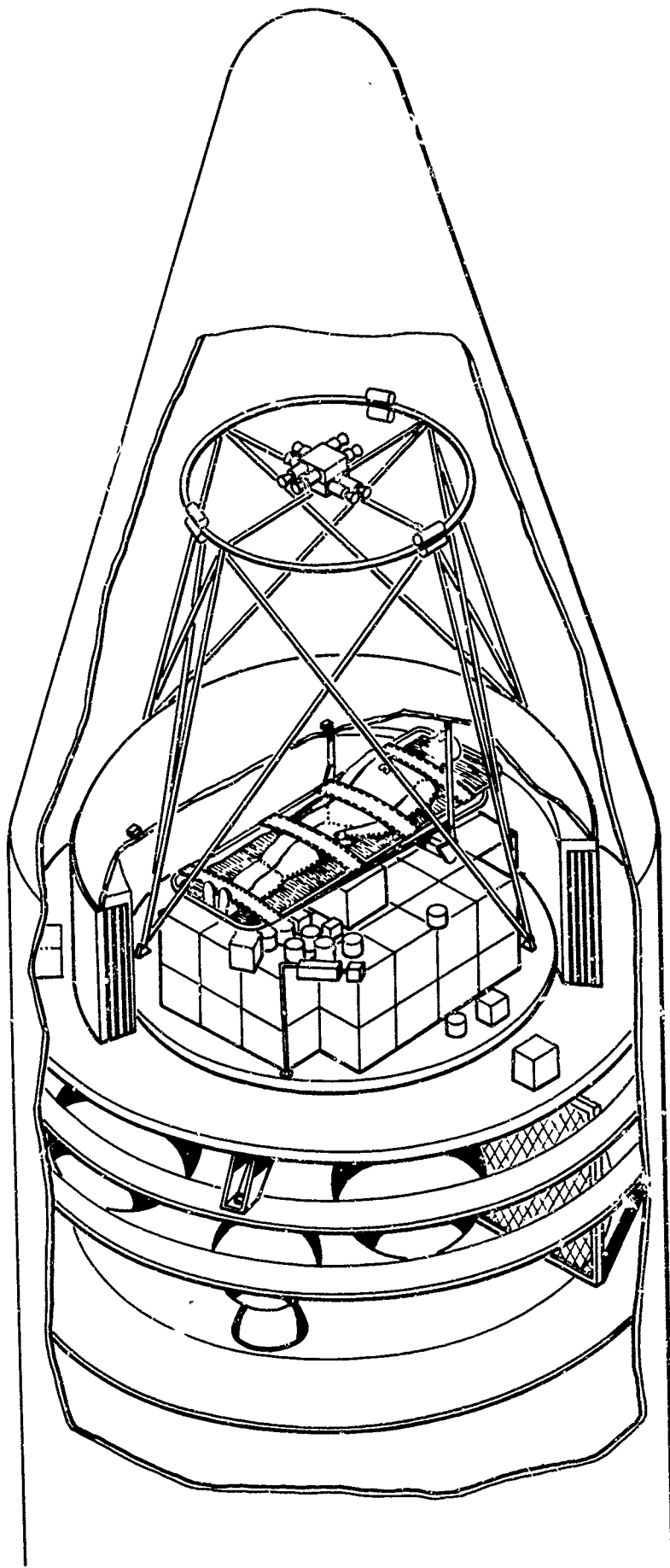


Fig. 6. Long Duration Test Configuration

shadowing any of the test structure panels and depends upon the attitude control of the structure to maintain correct solar orientation.

In general, the expandable space structure requires only minor modifications to accomplish this complex mission. The total payload weight is approximately 11,125 lb for the long duration mission.

Additional Applications

Although the utilization of this type of expandable structure for test purposes is an immediate potential application, the design for additional space applications is feasible and provides many advantages. The principal applications are found in conjunction with manned systems although several interesting unmanned versions have been defined.

Several types of manned space stations may use elongation along one axis to attain their design objectives. The question of the long term effects of zero gravity on man remains to be completely explored and, for missions requiring long periods between crew replacement, the need may exist for artificial gravity with low rotational rates. Several methods have been proposed to accomplish this, and the type of telescoping structure being considered herein is ideally suited for one of these methods.

In a two-body space station where permanent or temporary occupancy of both bodies is required, this structure provides a solution for moving the bodies far enough apart so that a low rotational rate will provide artificial gravity. This capability can be achieved without requiring any manual assembly in space. In this type of space station, a hub is usually required through which resupply and crew rotational functions are accomplished. This hub should be the rotational axis to allow docking of the resupply vehicles. The problem for the designer is to maintain this axis of rotation even though the mass of the two bodies may vary relative to each other during the mission. The capability of this type of expandable structure to retract as well as expand and still maintain its structural integrity allows a ready solution to the problem. In addition, the capability to transfer men between the elements of the space station without requiring movement through space outside of the station and air locks provides a major convenience for long term operations. If much transfer between station elements is required, the increased safety and reduced power and atmosphere losses due to air lock operations may be additional factors.

Another application is found when designing for long duration space station or space vehicle operations. The long duration requires stowage of an entry vehicle or vehicles for returning the crew. The need is self-evident that these vehicles must be maintained and protected from the space environment. External protection and maintenance, particularly of sensitive heat shields, appears to require some external covering of the entry body. Many types have been proposed. However, where a limited launch volume is restrictive, the

ability to expand over the attached entry vehicle may be an advantage. Also, the need for a rigid structure to provide protection and shielding may be a necessity, particularly when deep space missions are also considered. The type of structure which telescopes within or outside of a cylindrical body provides many advantages in arrangement as well as conservation of volume and offers a fine solution to these problems.

An additional advantage for this application is found in the capability to retract. This permits the docking system to be cleared for approach of the entry vehicle within broad maneuver limits without the danger of damaging either the entry vehicle or space station. Design of the end closure becomes the principal design problem.

One of the most interesting applications of this telescoping structure is its possible use as a combined retractable air lock and docking tube. The present docking requirements necessitate fine attitude and velocity regulation between the vehicles being joined in space. The problems involve reducing the relative motion to approximately zero at a fixed relative position without undue danger of shock loads being imposed on either vehicle. Many methods of making an initial connection and bringing these vehicles together have been explored. Standoff techniques become attractive when the masses involved become large.

This type of telescoping structure introduces some interesting characteristics into this docking operation. First, it requires only a small extended mass to join two very large bodies, thus reducing potential shock loads to a negligible value. The structure can be designed to be quite flexible when not fully expanded so that some relative motion between the bodies can be tolerated. Second, once the attachment has been made, the structure can be fully expanded and pressurized to form a rigid, load carrying link between the bodies. The rigidity of this load path aids considerably in maintaining an accurate attitude in the space station--a factor of extreme importance in some missions. Third, the structure can be designed, with a very small weight penalty, to perform the functions of an air lock between the vehicles. This requires a hatch at either end of the expandable tube. The sealing technique used permits such hatches, and since closures are normally required, the introduction of hatches is a simple matter. In operation, one hatch must remain closed at all times unless a mechanical locking system is used. A fourth advantage is the ability to stow this appendage to the space station in a small volume during launch and then use it in space without additional assembly operations. This stowage feature also allows considerable leeway in space station arrangement.

These applications are but a few of the many that can be devised. When such missions as interplanetary manned exploration, deep space stations and similar long duration missions are considered the range of applications increases. The principal characteristics that become of value are the ability to provide shielding from harmful radiation and meteoroids, the rigid load path, the increased operating volume or convenient stowage arrangements in normally cylindrical structures and the capability to retract after having been expanded.

RECENT APPLICATIONS OF INFLATED STRUCTURES TO AEROSPACE VEHICLES

R. Hoas

Good Year Space Corp. Akron, Ohio

Although expandable structures are generally considered for space applications primarily, because of their excellent packageability characteristics and the need for small volumes on the launch pad and large structural items once in space, there are quite a number of applications of expandable structures for aerospace vehicles which do function within the earth's atmosphere. In each of these instances the advantages of packageability, high structural integrity and low weight are paramount and result in a concept which is hard to match with a conventional rigid structure. In space, the prime object is often low weight without too great an emphasis on structural load. However, in most of the aerospace applications that operate on the earth's surface, high strength becomes of paramount importance. Developments in fabrics with high strength/weight ratios and good permeability characteristics are constantly opening new avenues for air inflated structures. The ability to utilize high strength materials in filament form - whether they be synthetic fibers, glass, metal or even the newly considered boron - makes work in this area a stepping stone toward even further improvements with normal development time. Advances in weaving technology, coating of fibers and special scuff resistant and abrasion resistant treatments, as well as finishes for protection from ultraviolet, all tend toward minimizing maintenance and increasing the life and reliability of such structures. This paper will deal with a few of the developments along these lines which have taken place recently and are now in use or being considered for current applications.

Ballutes

One of the most active applications of lightweight, high strength fabric material is the Ballute*, a combination balloon and parachute, which is a form of aerodynamic decelerator which provides stability and deceleration at a wide range of Mach numbers. The actual shape of a Ballute varies considerably depending on the specific application. Figure 1 shows three shapes that have been wind tunnel tested in order to determine their flight characteristics for future applications. These tests have been conducted by both the Air Force and NASA and the most promising ones are then evaluated in flight attached to a missile specifically designed for this purpose. The Air Force program on which this is done is known as ADDPEP (Aerodynamic Decelerator Development Performance Evaluation Program.)

From Figure 2 it can be seen that Ballutes are now available and have been tested over almost all speed ranges currently associated with earth atmosphere flights. These programs are continuing to extend the capability of the Ballute for application to re-entry vehicles and for extraterrestrial flight. As shown by the curve, "q" loadings as high as 3400 lb/sq ft have been achieved and this particular Ballute was about four feet in diameter and used for deceleration of a supersonic sled. It was made of Nomex - a high temperature nylon. Other Ballutes, however, have been made of stainless steel and Rene' 41 filaments and have been tested to temperatures up to 1500°F and speeds to Mach 10 in wind tunnel tests.

At the other end of the scale, Ballutes have been made as ultra low speed descent vehicles for use in the upper atmosphere where dynamic pressures as low as .05 lb/sq ft were used. Figure 3 is a picture of one of these Ballutes.

*T.M., Goodyear Aerospace Corporation, Akron, Ohio

approximately 14 feet in diameter, which utilizes a payload of about 7 1/2 pounds. This is made of a nylon film approximately .0004 inches thick. As in the case of most Ballutes, this is ram air filled so that it retains its structural integrity throughout its descent.

Perhaps the most popular Ballute is the 4 foot diameter unit shown in Figure 4, used by the Gemini astronaut. This particular unit is ram air filled from side inlets and has been completely tested and man rated for utilization at all escape conditions anticipated for the Gemini vehicle. In the event of an emergency the astronaut would utilize his ejection seat to escape from the capsule; the Ballute would then open and stabilize and orient the astronaut so that he would descend feet first to a sensible atmosphere where his normal recovery chute could be deployed. The main purpose for this Ballute is to prevent the man from going into a spin at altitude where his rate could become injurious or even fatal.

Sea Stilts

Expandable structures are also being considered for application to aerospace vehicles in forms other than for improvements of flight characteristics. A good example of this would be the retractable stabilizing floats now under study by Convair and the Navy for application to aircraft which would land on water and have to remain there in rough seas for extended periods of time. It has been found that an arrangement of vertical floats, "sea stilts", will considerably reduce the movement of the aircraft in wave action. As shown in Figure 5 tests have been conducted on a full sized aircraft using rigid hollow cylinders, proving the feasibility of the principle. At the present time these units are being made in a retractable form which will permit low drag during flight and yet provide the structural integrity for supporting the aircraft while on the water.

In order to permit retraction and extension of the inflatable floats, and maintain rigidity throughout the cycle, a special folding technique is employed. This is shown in Figure 6. The entire float is rolled up on a reel in the base of the unit and unreeled as needed. By providing torque to this reel, and holding a predetermined pressure inside the air tight fabric chamber, the structural properties of the float are retained. The technique is relatively simple, but extremely effective.

Airmat Applications

Airmat continues to provide a capability of expandable structures not possible with conventional bodies of revolution. Here the drop threads which tie together two surfaces of fabric can provide a shape control which is specifically applicable to areas where flat surfaces are required and variable geometry, and package-ability are also important. Weaving techniques have progressed from the modified carpet loom, on which the original Inflatoplane* was built, to a pilot type of R & D loom for more versatility and better control of weaving properties to the giant Air Force loom now available for weaving even large size metal structures.

Figure 7 shows the size of this facility as compared to a couple of automobiles. It is fully automatic and will weave to a contour as dictated by a scale model. New applications for Airmat are constantly being proposed where standard structural techniques are inadequate. The most current examples of this would be the following:

F-111 Wing Seal

In the General Dynamics concept where the wing changes sweep in order to obtain optimum performance at a wide variety of aircraft speeds, the intersection between the opening of the fuselage and the wing varies considerably for each wing setting. Attempts to seal this with an Airmat structure are considerably simpler than any other technique found so far. It is possible to predetermine the contours desired by weaving the Airmat with finite drop thread lengths that result in a wedge shape body with structural integrity maintained by an internal pressure. See Figure 8. When the wing moves from one position to another, this Airmat seal folds or extends as required to fill the gap. The fabric material is selected to withstand the temperatures and pressures expected and because of the almost infinite fatigue

*T.M.'s, Goodyear Aerospace Corporation, Akron, Ohio

characteristics of these structures, they should withstand a considerable number of wing movements. The inflatable components are serviced by bleed air from the jet engines and are equipped with a valving system so that changes in altitude are automatically handled to maintain the proper pressure differential across the structural walls. Each of the seals are preformed at manufacture and are readily attached to the hard structure of the airplane by conventional fastening methods. In Figure 9, can be seen the loom weaving the contoured Airmat for this application. This lightweight approach to filling the wing fuselage intersection should be applicable to any future airplane which considers the use of variable sweep wings. It may also be utilized in STOL type aircraft where increase in wing area could be handled with pneumatic sections instead of with multiple component complex metal segments.

Aircraft Modifications

The development of the new large Airmat weaving facility which is capable of fabricating components with a predetermined contour permits consideration of applications previously not even thought feasible. One such use of Airmat is for converting a land plane into a sea plane. By adding a special inflatable section to the bottom of the fuselage of a high wing airplane, it is possible to provide the necessary flotation and shape to permit the aircraft to operate from water bases. See Figure 10. When retracted, or deflated, the airplane shape returns to its original land configuration, and the fabric material is held tightly against the fuselage by a suction pump. For an aircraft the size of a C-130, this installation might weigh less than 500 pounds. The normal airplane is relatively unchanged, and it takes only about a minute to "lower" the water hull.

This concept might be applied to extra wing area when needed, external fuel supplies, spray tanks, and a wide number of other applications. It is interesting to note that this method of adding volume or structural area to an aircraft is readily performed on already existing vehicles, permitting them to attain increased capabilities without performance penalties. In the retracted form, the space taken by these components is almost imperceptible. Weight penalties are also surprisingly low. Each application, however, must be considered separately and evaluated on its own merits.

Inflatable Aircraft

The original Inflatoplane, which proved the feasibility of developing a complete aircraft structure out of pneumatic components, opened the door for other applications along similar lines. Two of these which might be of interest at the present are the inflatable glider and the inflatable communications drone. The fuel glider would be most applicable to uses at relatively low speeds, such as with helicopters and fixed wing aircraft in the subsonic speed range.

In the case of the fuel glider this can be used either as a delivery unit of fuel, food, water, cargo or possibly even people. Since the cargo compartment is pressurized in order to maintain the shape and integrity of the vehicle, it can be used for low altitude as well as high altitude work with equal ease.

The most immediate application would be with the helicopter as a means for range extension for this vehicle. See Figure 11. By towing an inflated fuel glider with a good L/D ratio and a sizeable payload, the helicopter could substantially increase its own range. At the end of the flight, or when the fuel supply is exhausted in the glider, it could be collapsed and carried back inside the helicopter.

Both the delivery unit and the range extension system have inherent qualities of packageability, resistance to damage and lightweight which are impossible to achieve with conventional construction. By carrying a small auxiliary air supply, which could be either ram air driven, electrically powered by the tow aircraft or by its own integral power supply, it should be possible to replace any air lost by small arms fire without effecting the aerodynamic or structural properties of the vehicle. As a matter of fact, once a source of air pressure is on board the fuel glider, it is possible to utilize this as a means for pumping the fuel, since the tanks are all collapsible and the retention of pressure in the fuselage will automatically force the fuel out if it is released.

As an inflatable drone, it is possible to employ an aircraft of this type as a high altitude relay link for range extension of communication systems. The main advantage for this drone is adaptability to field operations, practical indestructibility and ease of transportation. Preliminary analyses show that missions of 24 hours above 40,000 feet altitude are achievable, and that these can be increased as power plant selection improves. These aircraft have excellent payload to gross weight ratios, can operate from small unimproved fields, and are relatively low in initial cost. Maintenance on the aircraft structure itself is almost eliminated, since it is difficult to damage. Figure 12 is one configuration of such a vehicle utilizing the small Allison turboprop engine, and fabric structure that can be readily manufactured on the new loom.

Rotocraft

One of the first applications ever considered for Airmat was the rotor blade, because the centrifugal force maintains the tension and therefore, cone angle, and the internal pressure is merely required for shape retention. However, since most current helicopters are root driven and controlled, requiring more rigidity than easily obtained in the fabric blade, the work progressed slowly. The benefits of light weight and packageability still exist, however, and now that compound vehicles, giant flying cranes, and recovery systems are in demand, the Airmat re-interest has renewed.

When considering a compound helicopter, where a wing is used to unload the rotor during high speed flight, even before one considers the rotor, it becomes readily evident that an inflatable, retractable wing would be ideal. As shown in Figure 13, this wing could remain folded up into a small pod during hovering, when the rotor must be at its maximum efficiency, and then as the speed increases, it can be unrolled to take over much of the lift function. This capability is available today, and with normal development can become operational.

Another compound helicopter might be one in which the rotor remains stored in a retracted hub during high speed flight and is only deployed from a spinning hub for the landing and take-off position of the flight. Figure 14 illustrates such an aircraft. Here the interference of the wing during hovering would not be too important, because an extremely large radius could be employed to permit operation at a low disc loading. Naturally, during the high speed portion of the flight, which constitutes its major operating time, the aircraft would be performing in its most efficient mode.

Analytical studies of flying crane potential were also made and these showed that tip powered units of large rotor diameter are very promising for fabric blade construction. As shown in Figure 15, the larger the rotor the smaller the engine problem. Reasonably high tip speeds can be maintained at low rpm and hence vibratory problems from cyclic action are minimized. Blade weights look very good, especially with the tip mounted engines which assist in retaining a low coning angle.

Preliminary work has already been started along the lines of developing a blade which is completely collapsible so that it can be rolled up into the hub when not in use. The first unit, about 21 ft in diameter, is shown in Figure 16 mounted on a test truck. In this particular figure the blades are being pre-rotated prior to movement of the truck down the runway, at which time the blades go into autorotation, the rpm of which is set by the truck speed. In these particular tests it was found that these flexible blades work very well in the autorotative mode using only a root setting and a small tip tab to define the blade pitch angle.

As shown in Figure 17, the blades when not in motion are completely flexible and have no rigidity whatsoever. In these first units the inside of the blade was filled with soft plastic foam. In future blades the Airmat material will be employed and it will be possible to pressurize the blades to give a reasonable amount of stiffness when it is desired and by evacuating them to completely remove the stiffness when they must be stored. The vehicle shown in Figure 17 was merely used to check the blades in autorotation to see if they would actually lift the values indicated by the truck tests. This 600 lb vehicle "lifted off" at about 40 mi/hr and was very stable in operation.

Plans are now being made to wind tunnel test an Airmat blade in autorotation and to attempt to vary the pitch of the blades through tip controls.

At the present time this concept is sufficiently far along that it can be considered for recovery applications, utilizing large diameter blades, that can be stored in a small space and deployed slowly through spin up. It should be possible to achieve disc loadings which are low enough to permit zero velocity landings. Transferring the inertia of the blades just before impact to increased pitch of the rotors should completely eliminate the need for impact attenuators. This entire area of recovery is just now being investigated and it should become very fruitful because of the new loom developments which will permit weaving of a complete blade in practically a single operation.

Balloons

In the lighter-than-air field, it appears that the development of the very stable flying Vee-Balloon* has initiated a renewed interest in tethered balloon applications. These vary from the use of very small film constructed expendable units of a few cubic feet for marker applications to giant sized fabric units with long life expectancy in the 100,000 cu ft size for high altitude and heavy load carrying. Two of the most active uses are for communications and logging. See Figure 18.

The balloons used for communications - basically perform the function of elevating an antenna to extend line-of-sight range or to give it length and hence increased efficiency and range. These also have been used in a variety of sizes from 400 cu ft, flown at 500 ft altitude by the Army in Vietnam to 75,000 cu ft flown at 10,000 ft by the Navy. New developments in gas tight fabrics provide for increased endurance, minimizing operational costs and making time on station a reliable factor.

A commercial application of the Vee-Balloon is in the logging industry, here it has been found through studies for the Forest Service that a balloon can be utilized to good advantage to move timber from areas generally considered inaccessible or uneconomical using conventional logging methods. In experiments conducted by Bohemia Lumber Company on a Vee-Balloon, it was determined that by utilizing dynamic lift characteristics it is possible to actually fly the logs from the forest to the landing thus increasing productivity and decreasing chances for breakage. Besides the economical benefits of balloon logging, the Department of Agriculture is very much interested in the conservation effects which result from balloon logging. It is possible to clear areas without the need for extensive roads,

* T.M., Goodyear Aerospace Corporation, Akron, Ohio

disruption of the water sheds, soil erosion, etc. It is to be expected that as experience is gained in balloon logging, its utility will greatly increase. The aerospace industry will have to contribute to this field of endeavor by providing flight vehicles with increased performance for the specific properties required in balloon logging. These include high lift, good flight stability, quick turn around, survival in high winds, good bedding down characteristics, etc.

It becomes quite apparent that the advantages provided by new developments in fabrics opens a tremendous number of fields for application to aircraft where strength/weight ratios are so important. Actually the applications are so numerous that the only determining factor that justifies development in any particular area is a current need. From past experience with expandable structures, one can readily predict that wherever it appears feasible, the final application will be both economical and surprisingly effective in operation.

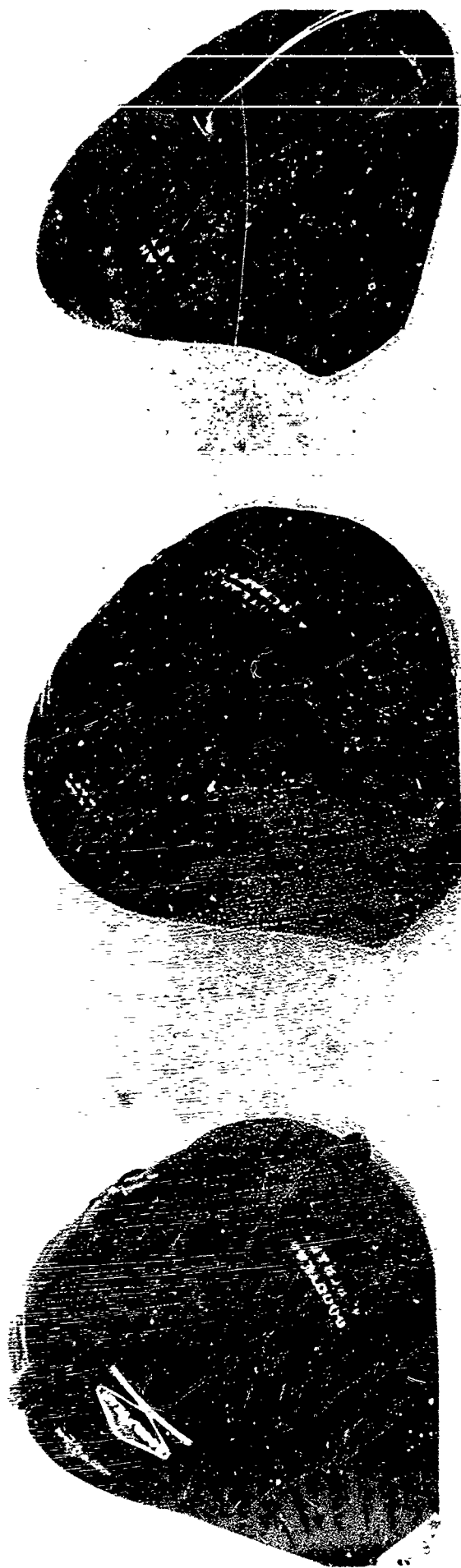


Figure 1. Typical Ballute Shapes for Wind Tunnel Testing

KEY: OCCURIT TESTED

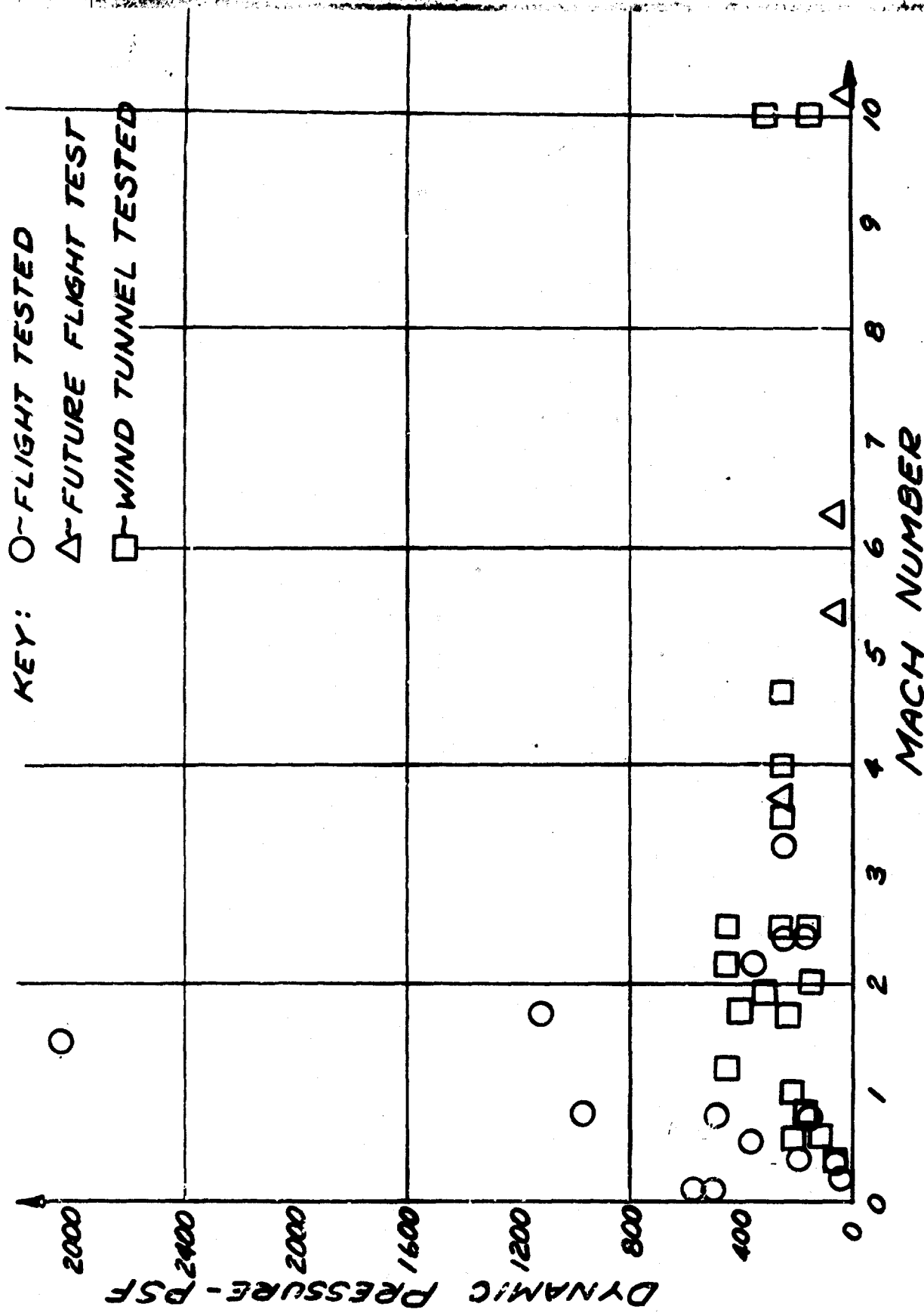


Figure 2. Ram Air Ballute Capabilities

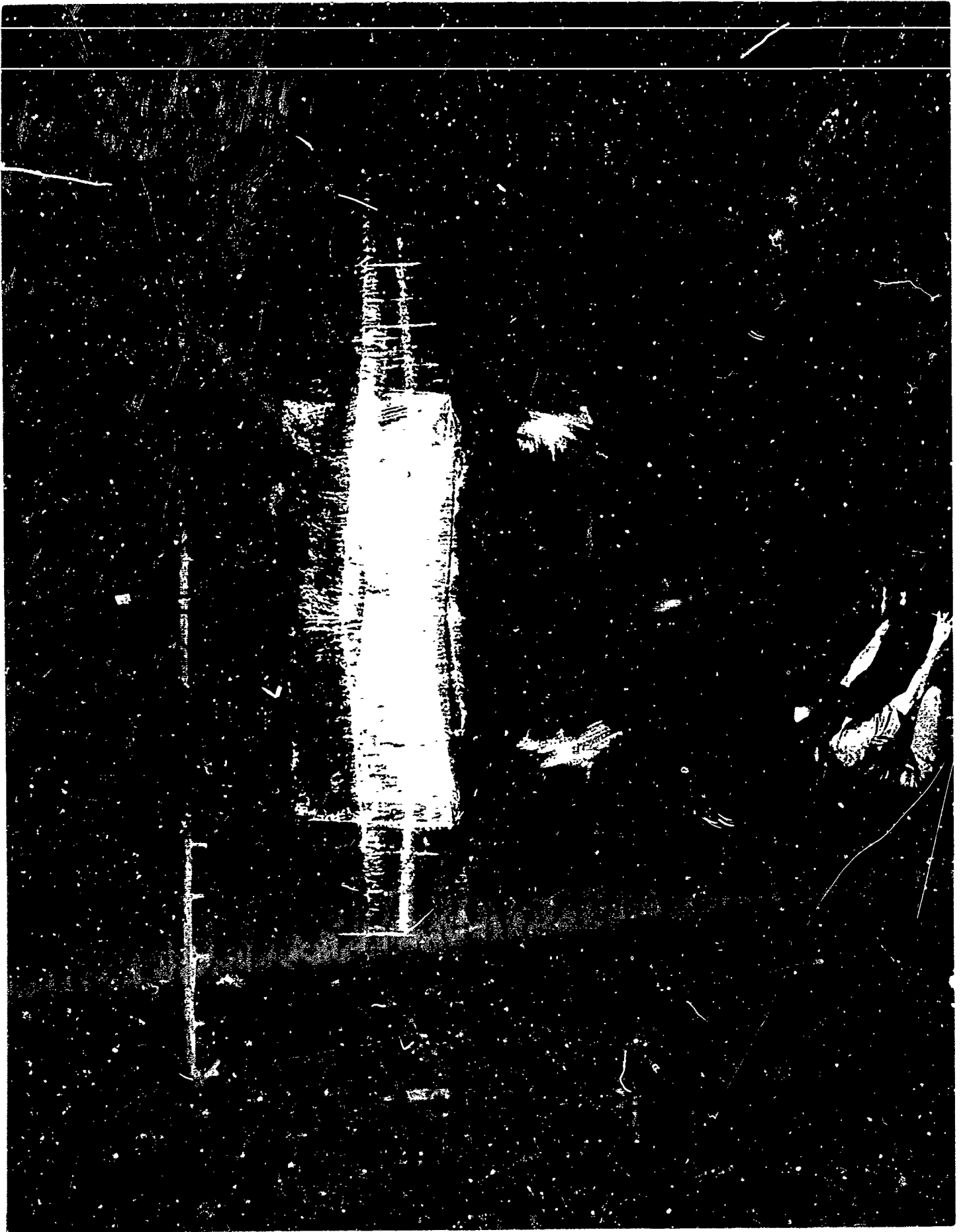


Figure 3. A Low "q" Supersonic Ballute for Upper Atmosphere Use



GEMINI BALLUTE (NASA)
1st LIVE JUMP
CWO CHARLES LAINE (TEST SUBJECT)
6511th TEST GROUP (P) AFFTC
NAF EL CENTRO, CALIFORNIA

Figure 4. Gemini Ballute in Jump Test



Figure 5. Vertical Floats Developed by General Dynamics

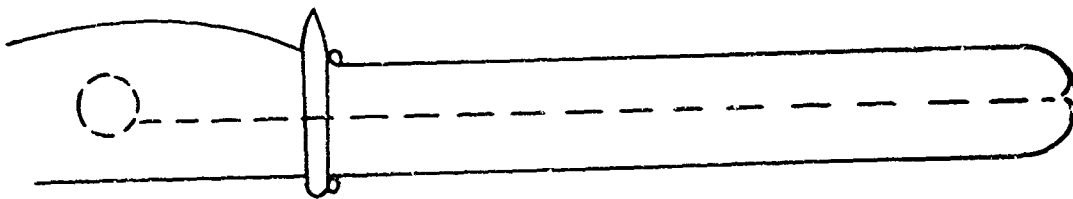
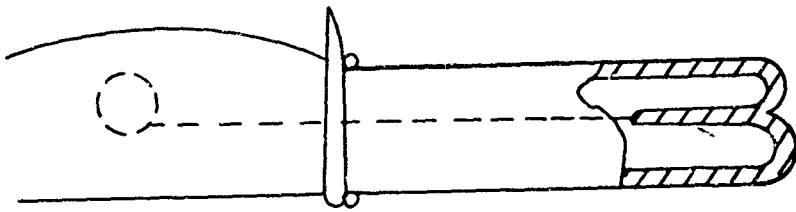
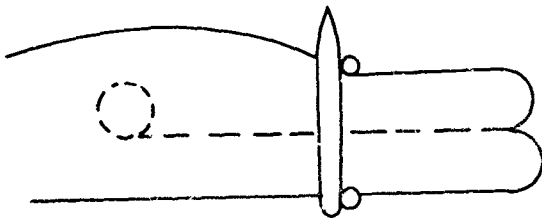
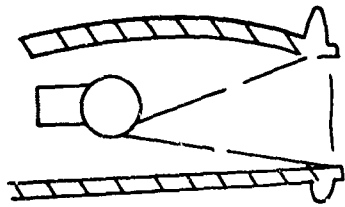


Figure 6. Vertical Float Retraction Concept
727

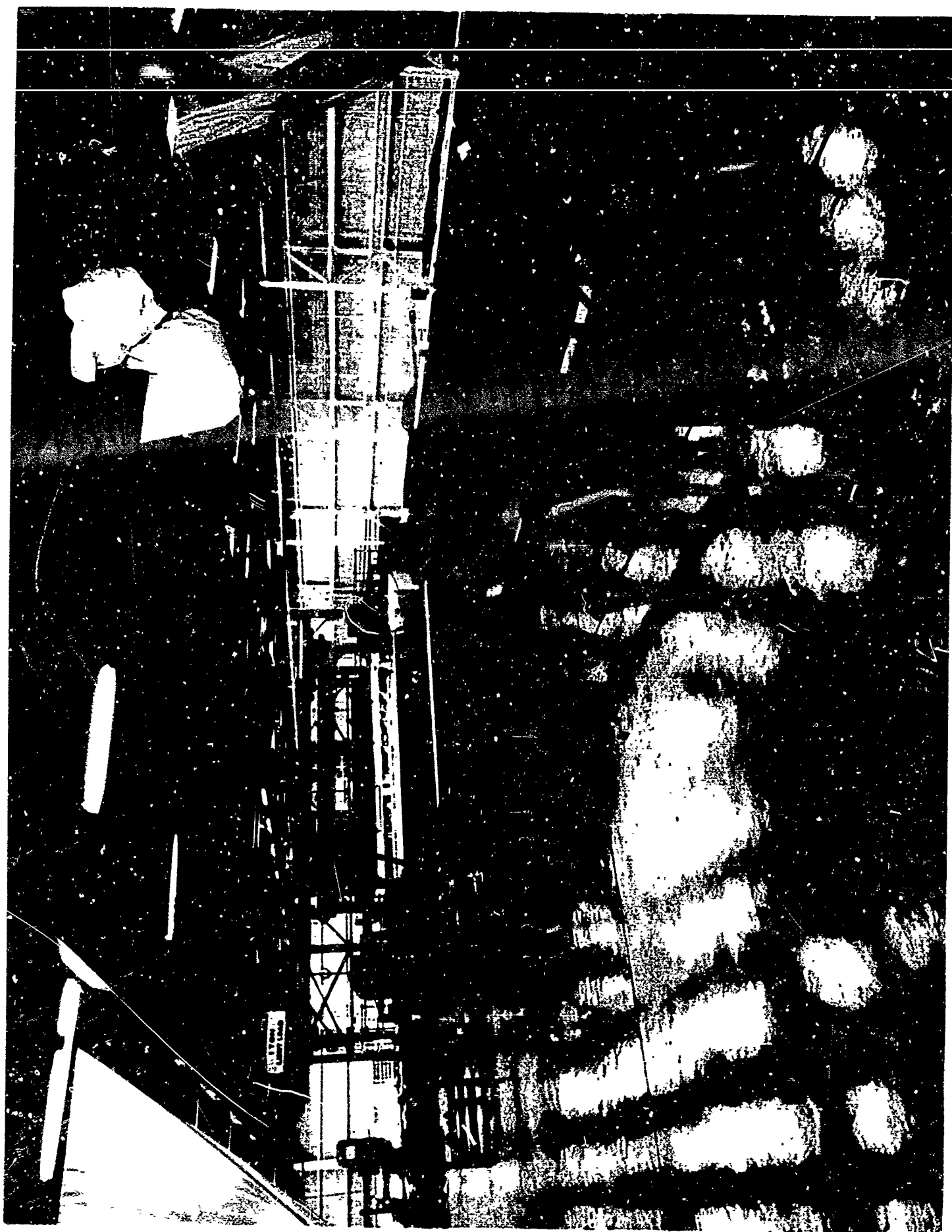


Figure 7. The Giant Air Force Airmat Loom

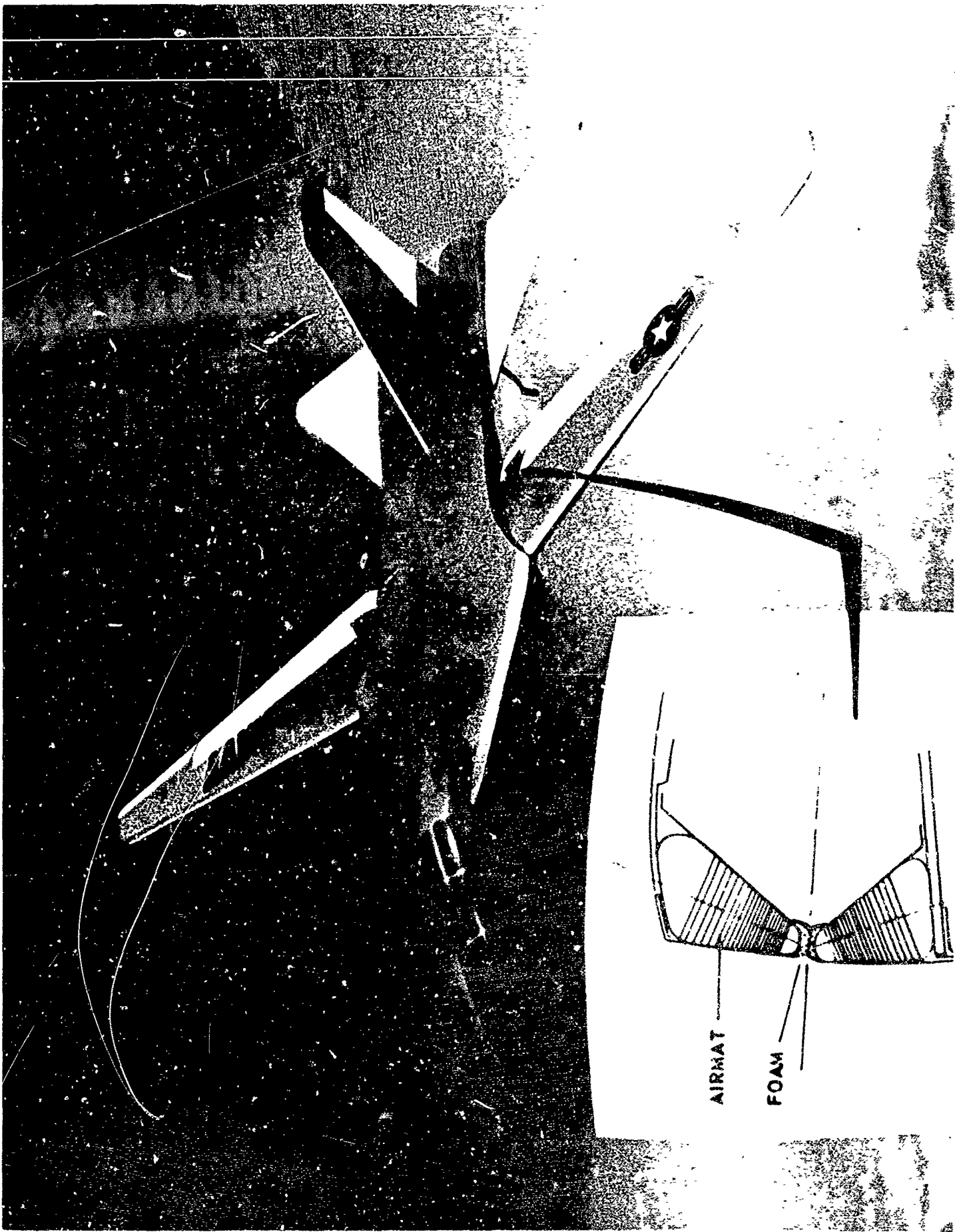


Figure 8. F-111 Wing Fuselage Intersection Seal
729

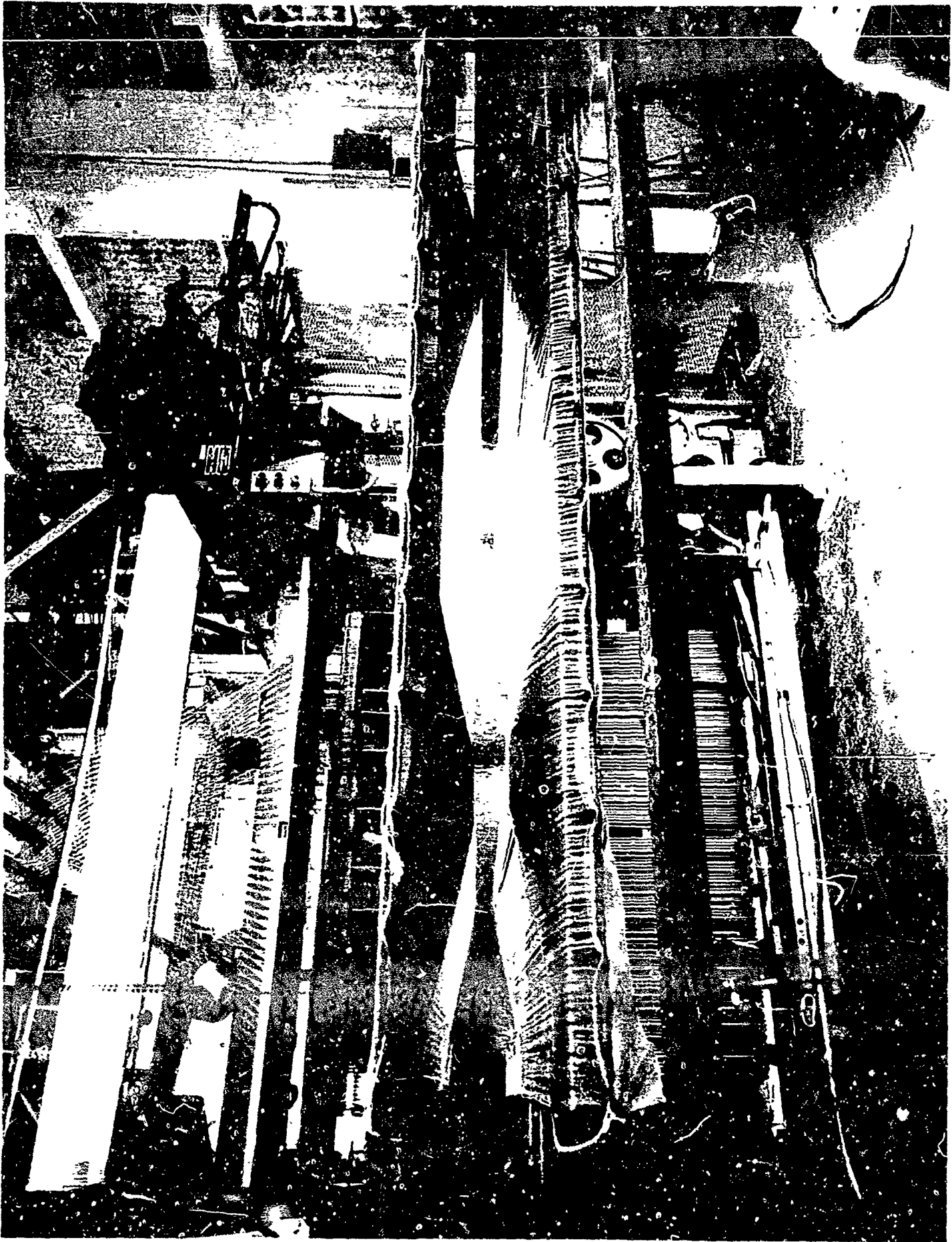


Figure 9. The GAC Airmat Loom weaving a Single Scal Contour.

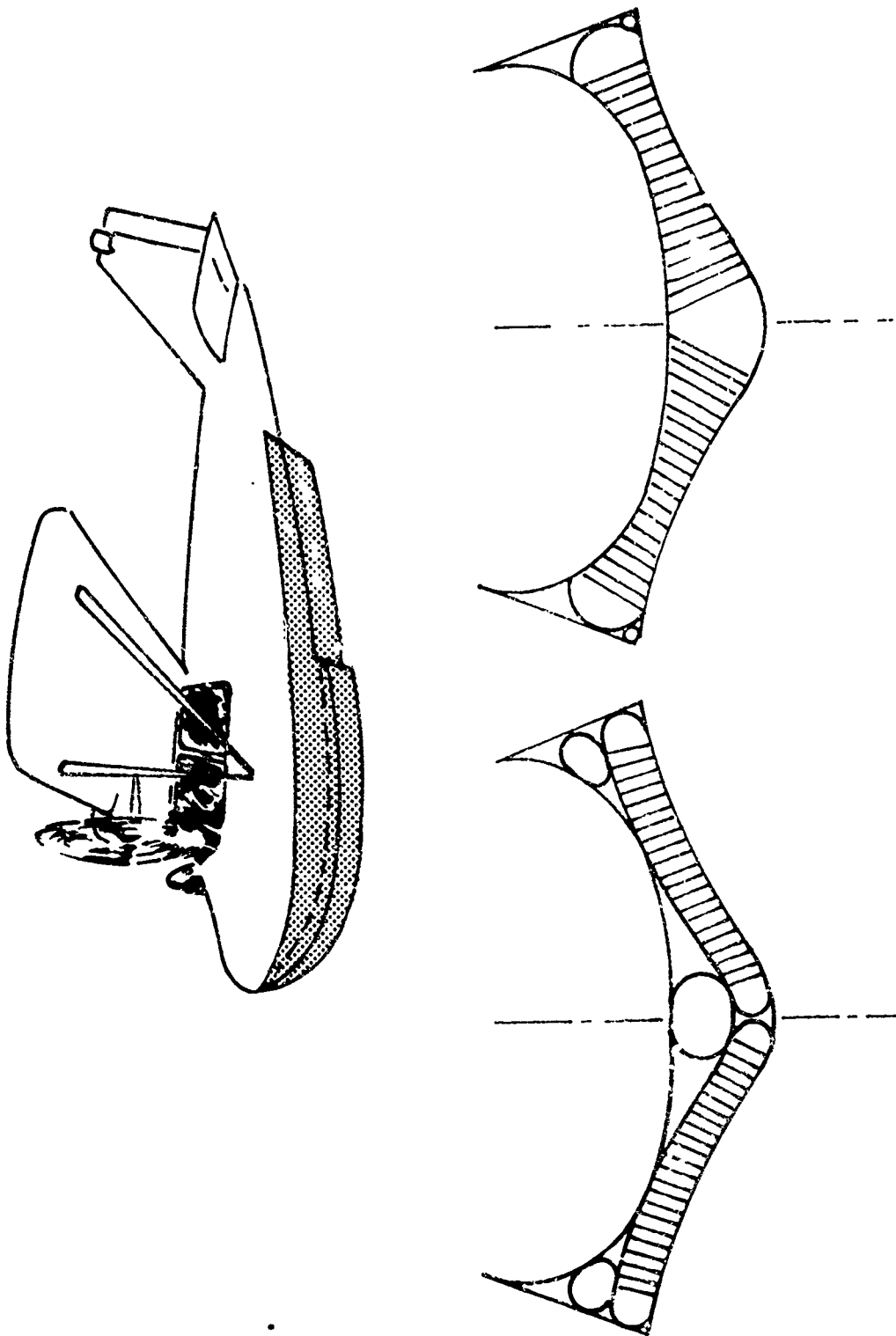


Figure 10. Water Configured Hull for Land Plane



Figure 11. Inflatable Helicopter Towed Glider for Range Extension

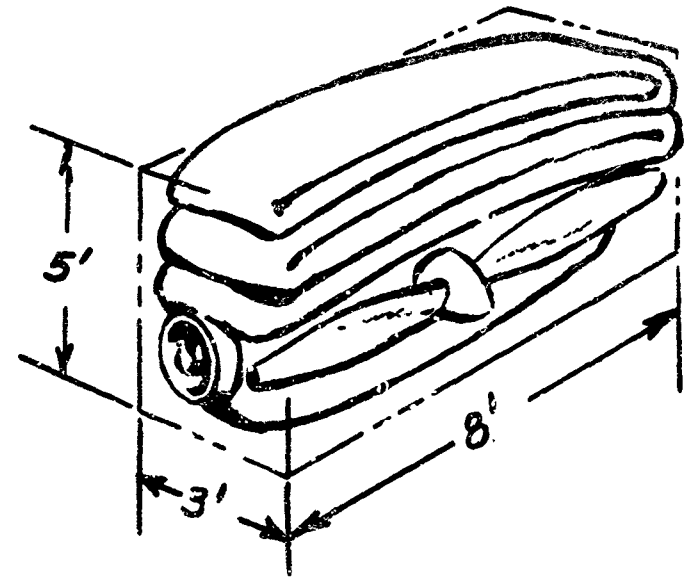
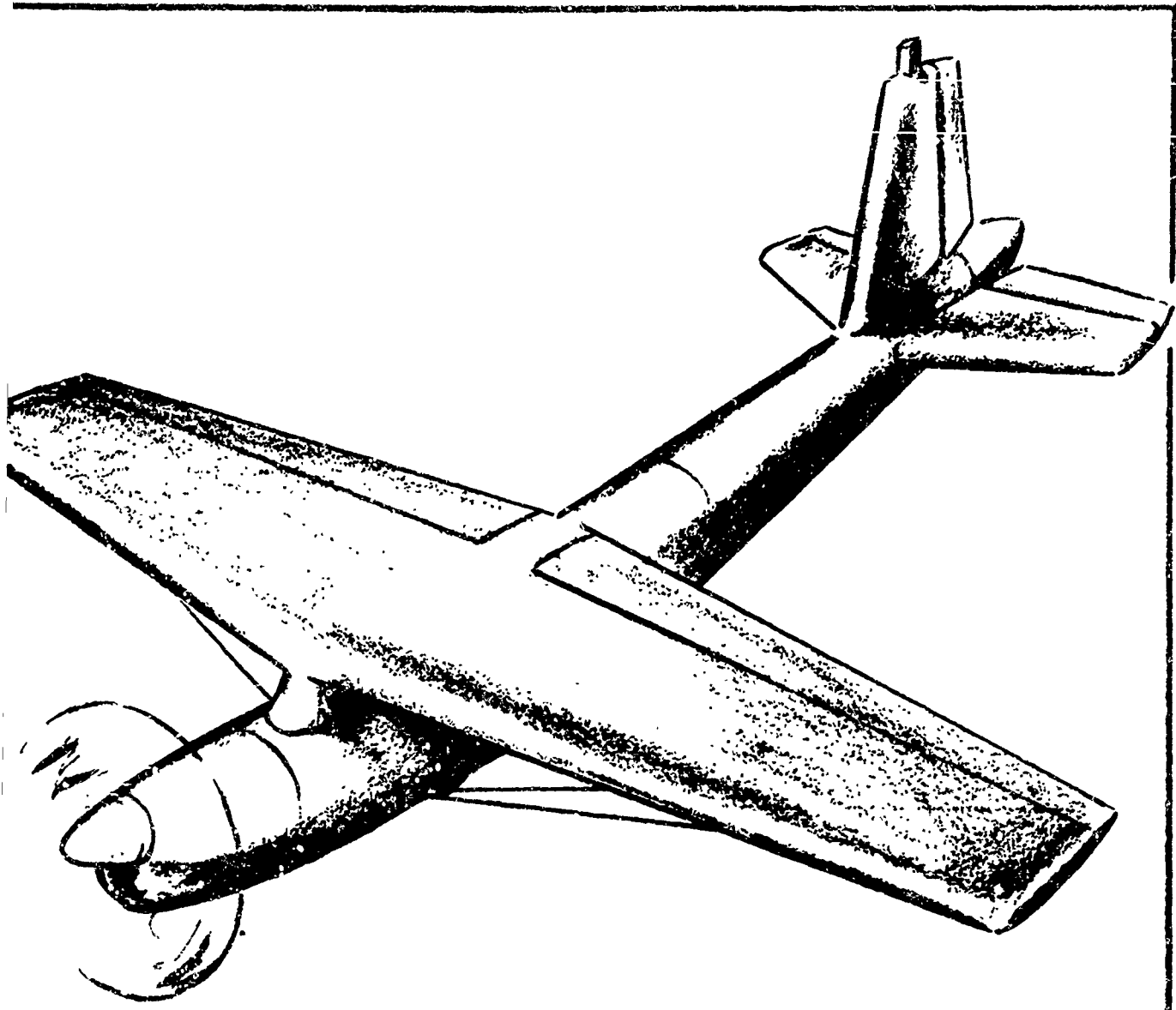


Figure 12. View Showing High Altitude Drone in Flight, Packaged

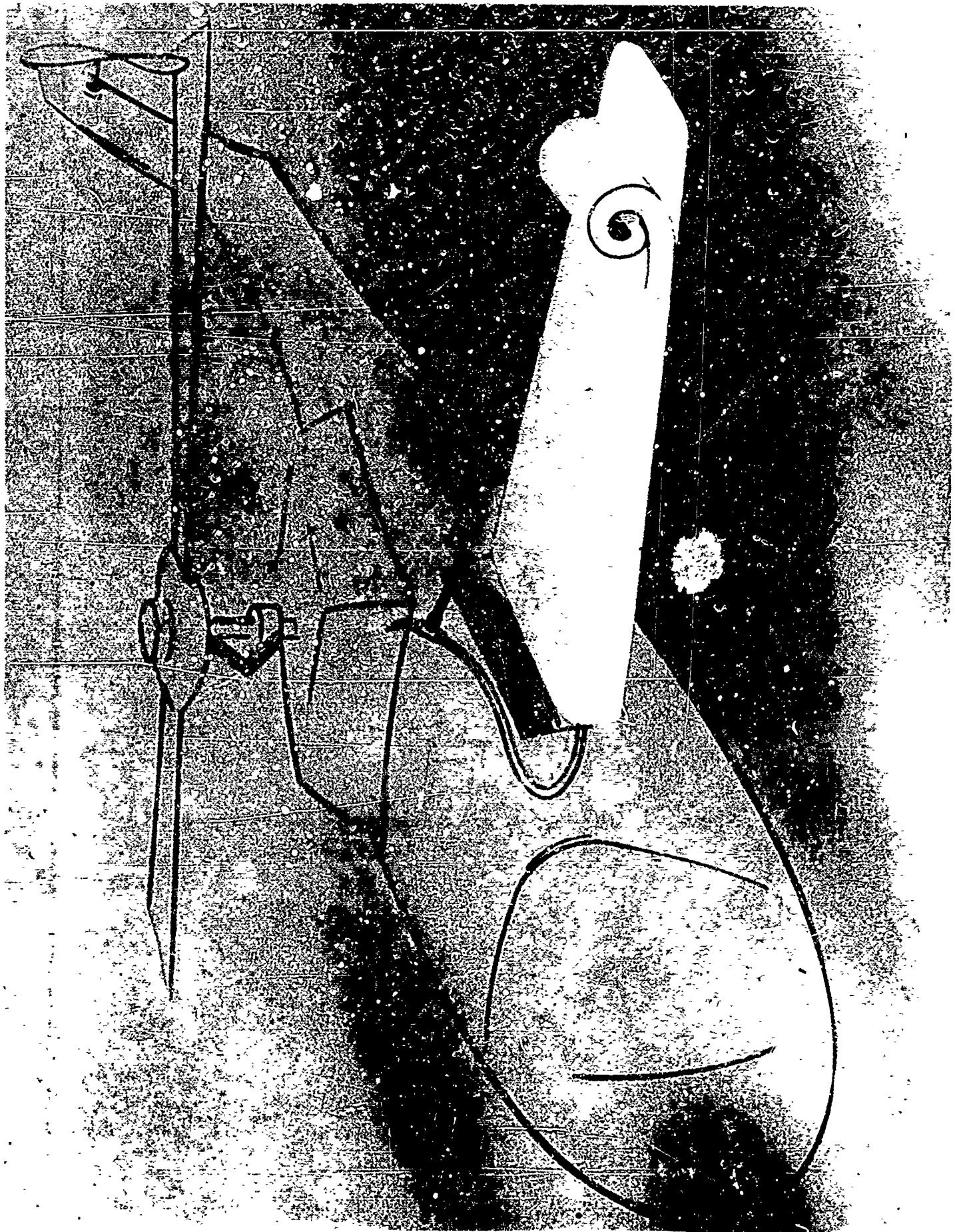


Figure 13. Compound Helicopter Using Inflatable Retractable Wing

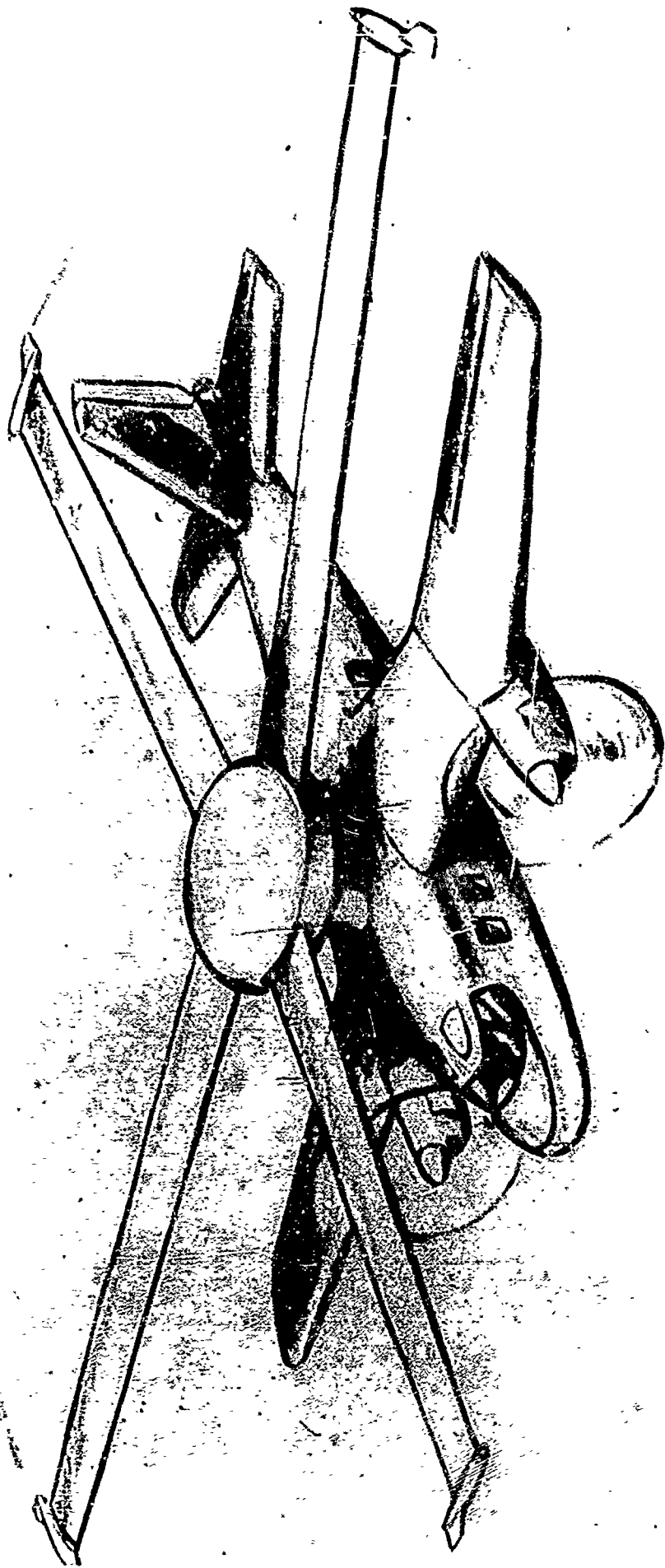


Figure 14. Convertible Aircraft with Retractable Fabric Rotors

ACCELERATION LOADS AT ROTOR TIP

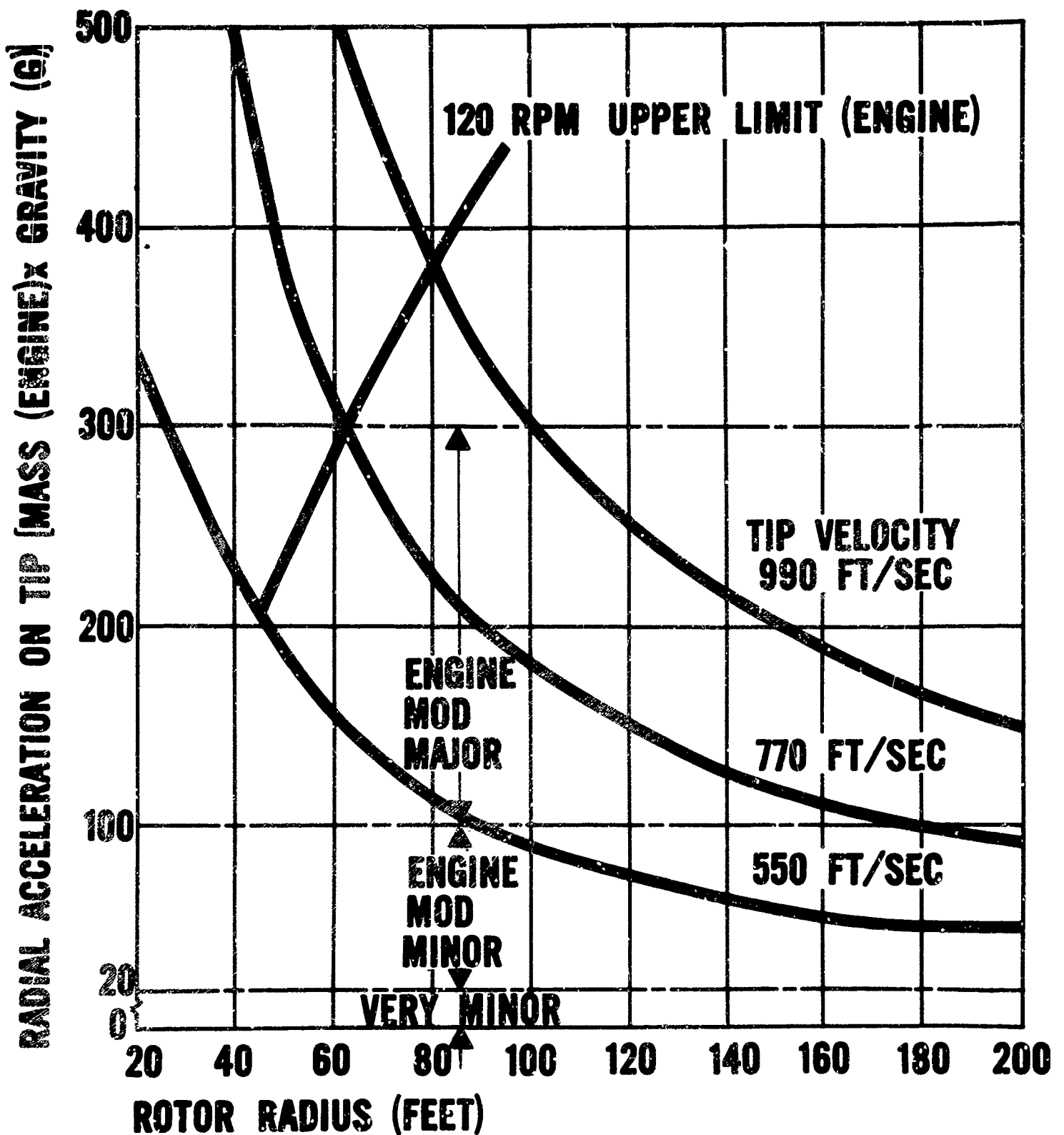


Figure 15. Relative Properties of Tip Powered Rotors

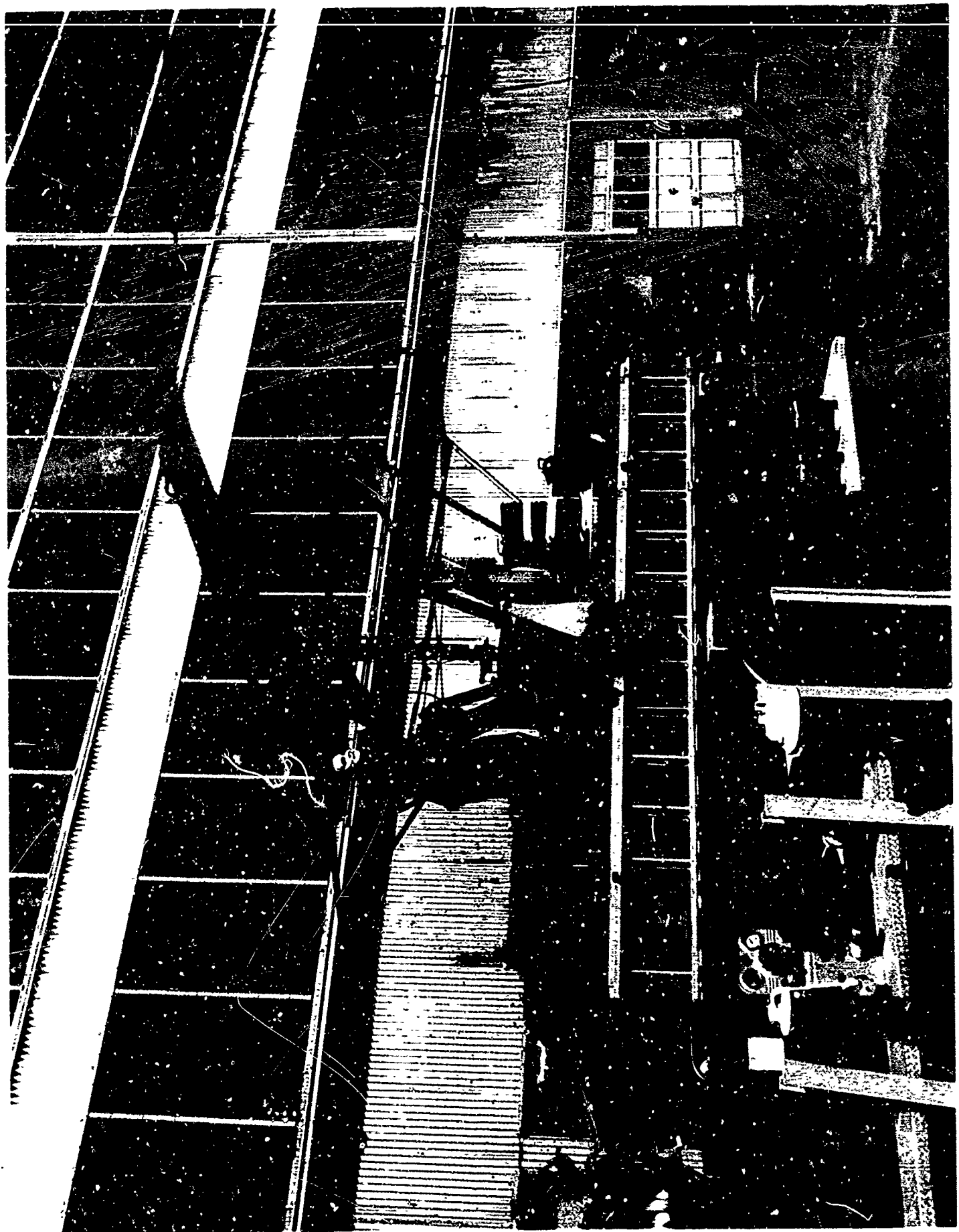


Figure 16. Fabric Rotor Mounted for Autorotation Truck Tests

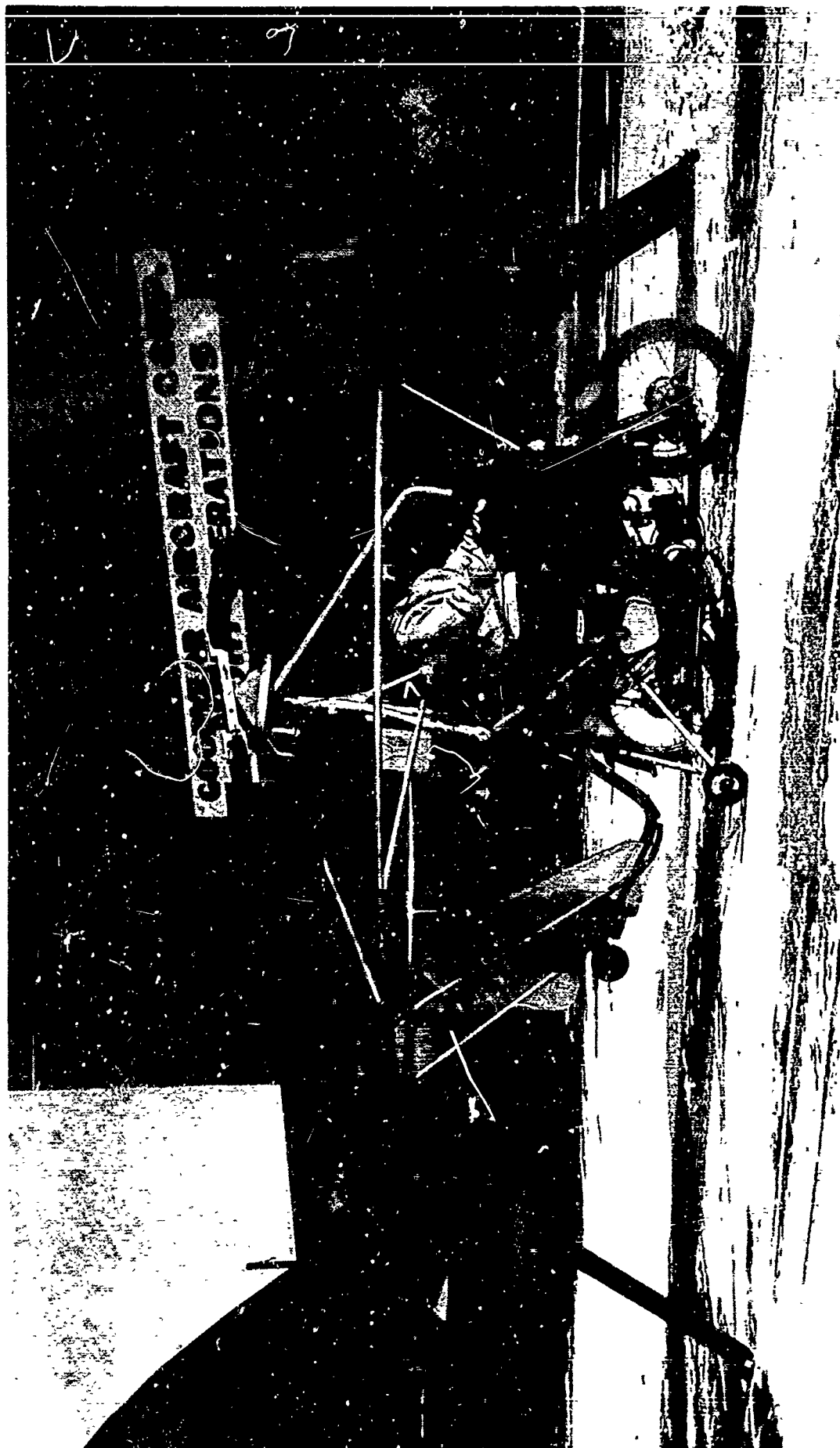


Figure 17. Six Hundred Pound Test Vehicle for Lift-Off Trials

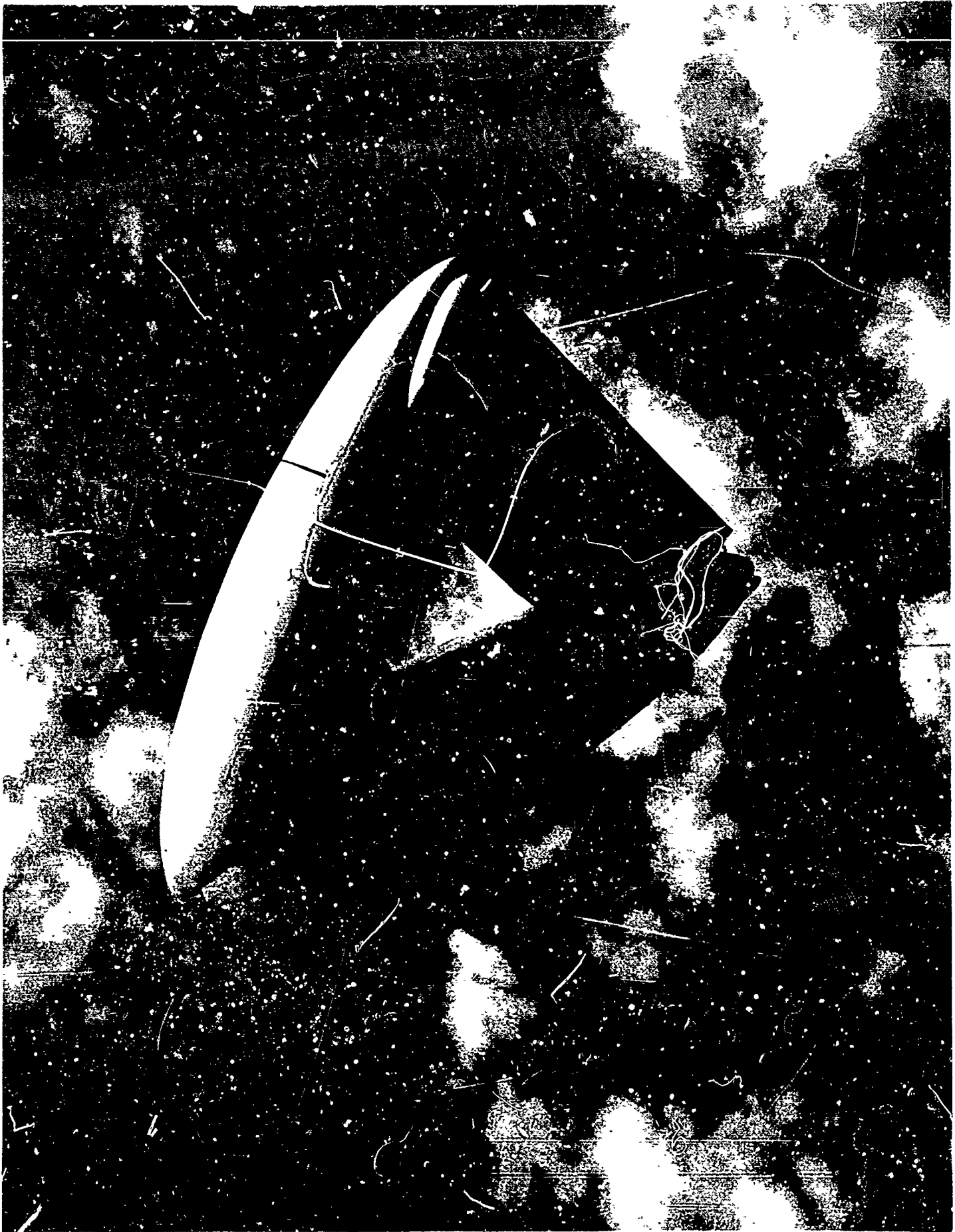


Figure 18. A Typical Stable Vee-Balloon for Tethered Operations

**CORRELATION OF ANALYTICAL AND EXPERIMENTAL
RESULTS OF CYLINDRICAL SHELLS UNDER NEWTONIAN
PRESSURE DISTRIBUTION**

by

Nicholas C. Lycurgus*
and
Wesley R. Midgley**

30 April 1965

Tests were performed to determine whether or not linear extensional shell theory is applicable to the analysis of cylindrical shells constructed of unfurlable wire cloth material and subjected to Newtonian type pressure distribution. Since the objective was to compare test results with results obtained through the application of linear extensional shell theory, the analysis and testing were performed on a stainless steel foil shell, which eliminated the problem of non-isotropy of the wire cloth material. It is expected that a similar comparison will be performed at a later date using wire cloth.

The comparison of analytical with test results, as well as the analytical results themselves, shows that linear extensional shell theory is applicable to the analysis of steel foil cylindrical shells under Newtonian pressure distribution.

* Assistant to the Chief, Analytical Mechanics
Avco Research and Advanced Development Division, Wilmington, Mass.

** Staff Engineer, Structures Laboratory
Avco Research and Advanced Development Division, Wilmington, Mass.

I. INTRODUCTION

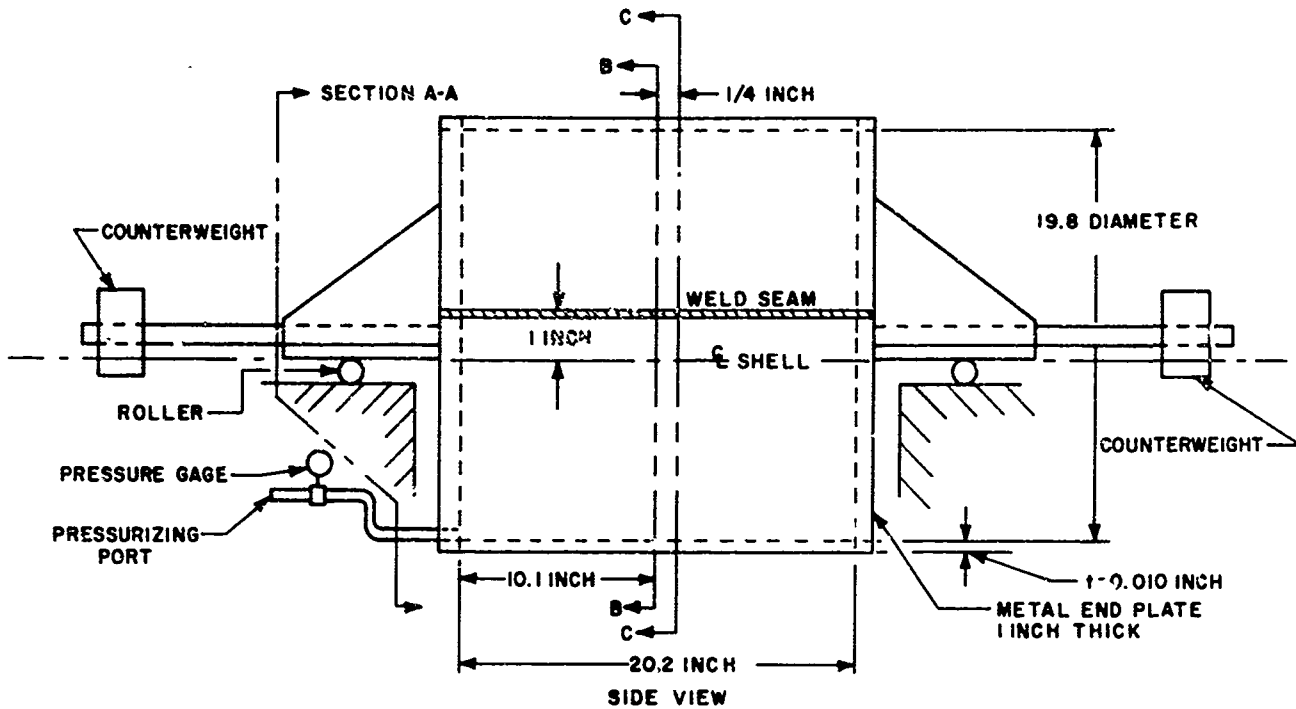
In the course of determining the feasibility of designing and manufacturing primary structural components in the area of advanced rocket vehicles partially constructed of unfurlable materials, investigations were conducted to assure that approximate analytical methods involving the application of linear extensional shell theory could be used in the design of this type of structures subjected to nonsymmetrical surface loadings. To demonstrate this, experimental tests were performed on a right circular cylindrical shell of stainless steel foil subjected to a normal loading of the form $A+B \cos \beta$. This was imposed through the use of liquid mercury by filling the shell completely and later on subjecting it to additional internal pressure. This type of loading simulates exactly the first two terms of a nonsymmetrical Newtonian Pressure Distribution, the difference existing only in the absolute values of the constants A and B.

This paper presents, first, the experimental testing performed on the cylindrical shell, second, the analytical procedure followed in the prediction of the quantities under consideration and third, a comparison of the experimental results obtained with the theoretical conclusions.

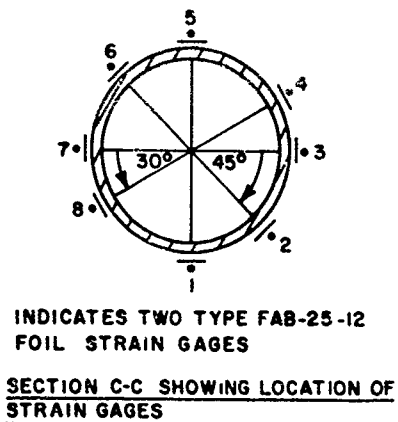
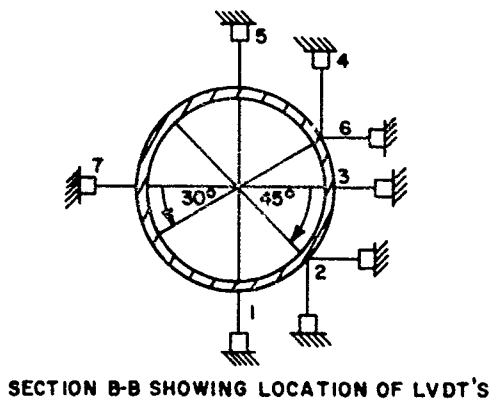
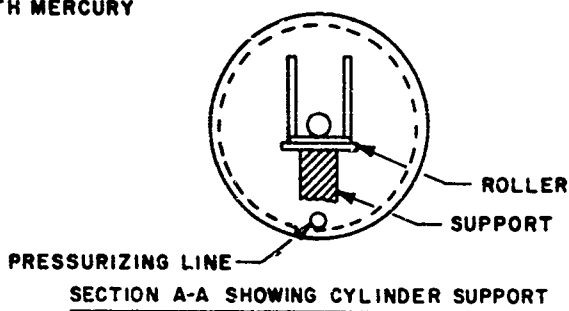
1. Experimental Testing

A 0.010-inch-thick, longitudinally welded, type 304 stainless-steel cylindrical shell having a modulus of elasticity $E = 25.9 \times 10^6$ psi average of 2 specimens with maximum error about $\pm 2.8 \times 10^6$ psi, and a Poisson's Ratio $\nu = 0.3$ was sealed at its ends and supported as shown in the schematic of the test setup of figure 1. The inner diameter was measured to be 19.8 inches, and the length between attached end plates 20.2 inches. The metal end-plates were counter weighted before the application of any loading, to remove any end force system they could impart to the shell before testing. At midlength of the shell, LVDT's (linearly variable differential transformers) were installed to measure displacement of the cross section and one quarter inch away from midlength, foil strain gages (type FAB-25-12) were installed to measure strains. Sections BB and CC of figure 1 show schematically the LVDT's and strain gages respectively. Figure 2 shows the cylindrical shell during installation. The instrumentation, is readily discernable in this photograph.

The cylinder was first filled and pressurized with water to locate any leaks, and also to preload the cylinder to yield local areas where residual stress might be high or where stress concentrations exist. About six small leaks were located, the water drained, and the holes repaired by bonding stainless steel shim stock over the full length of the weld bead with a room temperature vulcanizing rubber compound. The cylinder was then filled to depths of 4, 10, 15, and 19.8 inches, that is completely filled with mercury having



NOTE: COUNTERWEIGHT BALANCED BEFORE FILLING CYLINDER WITH MERCURY



65-5311

Figure 1 TEST SETUP FOR STAINLESS STEEL CYLINDRICAL SHELL

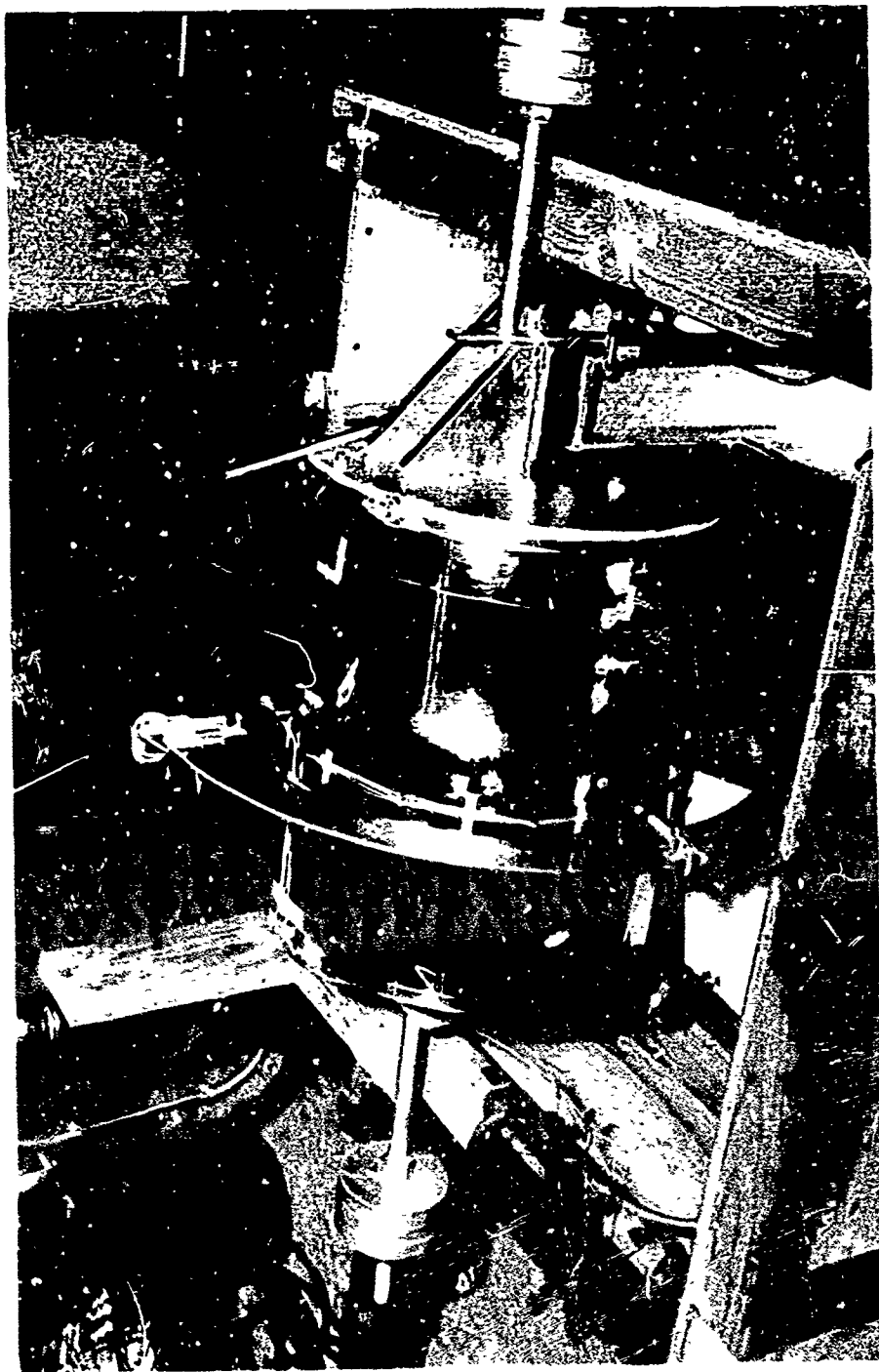


Figure 2 TEST SETUP DURING INSTALLATION OF INSTRUMENTATION

a density of $\gamma = 0.492 \text{ lb/in.}^3$. Deformations and strains were recorded at each depth of mercury. The shell was then pressurized to 8.8, 13.6, 18.4, 22.8, 0, 22.8, 28.2, and 0 psi. The load imposed by the liquid mercury together with the additional induced pressure simulated the first two terms, $A + B \cos \beta$, of a non-symmetric Newtonian Pressure Distribution. Figure 3 is a close-up view showing the instrumentation during the test. Deformations and strains were recorded for each LVDT and strain gage, at each loading condition.

It is interesting to note the deformations, shown in figure 4, of the cross section at midlength of the shell at different depths of mercury. At a depth of 10 inches of mercury, the shell deformed inwardly at the neutral axis of the cross section, and at a depth of 15 inches the deformation in the same direction at about 4 inches above the neutral axis of the cross section. When the cylindrical shell was completely filled with mercury and at 0 psi additional pressure, the cross section was close to the expected shape. At maximum pressurization, the maximum deformation was about 0.016 inch at the bottom of the cylindrical shell at LVDT gage 1.

Figure 5 shows plots of uniform internal pressure versus longitudinal and circumferential strains for gages 1, 5, and 3, 7 (this figure does not include strains due to hydrostatic head of mercury). As shown in figure 1, gages 1 and 5 are located at the bottom and top of the shell respectively and gages 3 and 7 on each side at the neutral axis. It is obvious from the plots that the structure behaved linearly and that the gages functioned properly. If the structure was perfectly symmetrical and the gages placed symmetrically, then, of course, the plots of the circumferential and longitudinal strains of gages 3 and 7, and 1 and 5 would be of the same magnitude. The maximum strain occurred in the circumferential direction and was about 800 micro-inches per inch tension.

Figures 6 and 7 show plots of pressure versus circumferential and longitudinal strains respectively of the cross section of the shell at midlength, including the hydrostatic head of mercury. The local effect of the weld seam is much more predominant in the longitudinal-strain plot than in the circumferential. The reason is probably due to the effect of the larger cross sectional area of the weld in the longitudinal direction, the weld bead not being ground off. The maximum circumferential strain shown in figure 6 was about 1250 microinches per inch tension, and the maximum longitudinal strain of figure 7 about 340 microinches per inch tension.

2. Analytical Procedure

The analysis of the test specimen was based on the approximate extensional theory of cylindrical shells. The field equations of cylindrical shells, as established in reference 1, are used to arrive at the equations of the extensional theory which then are solved explicitly for an arbitrary normal load

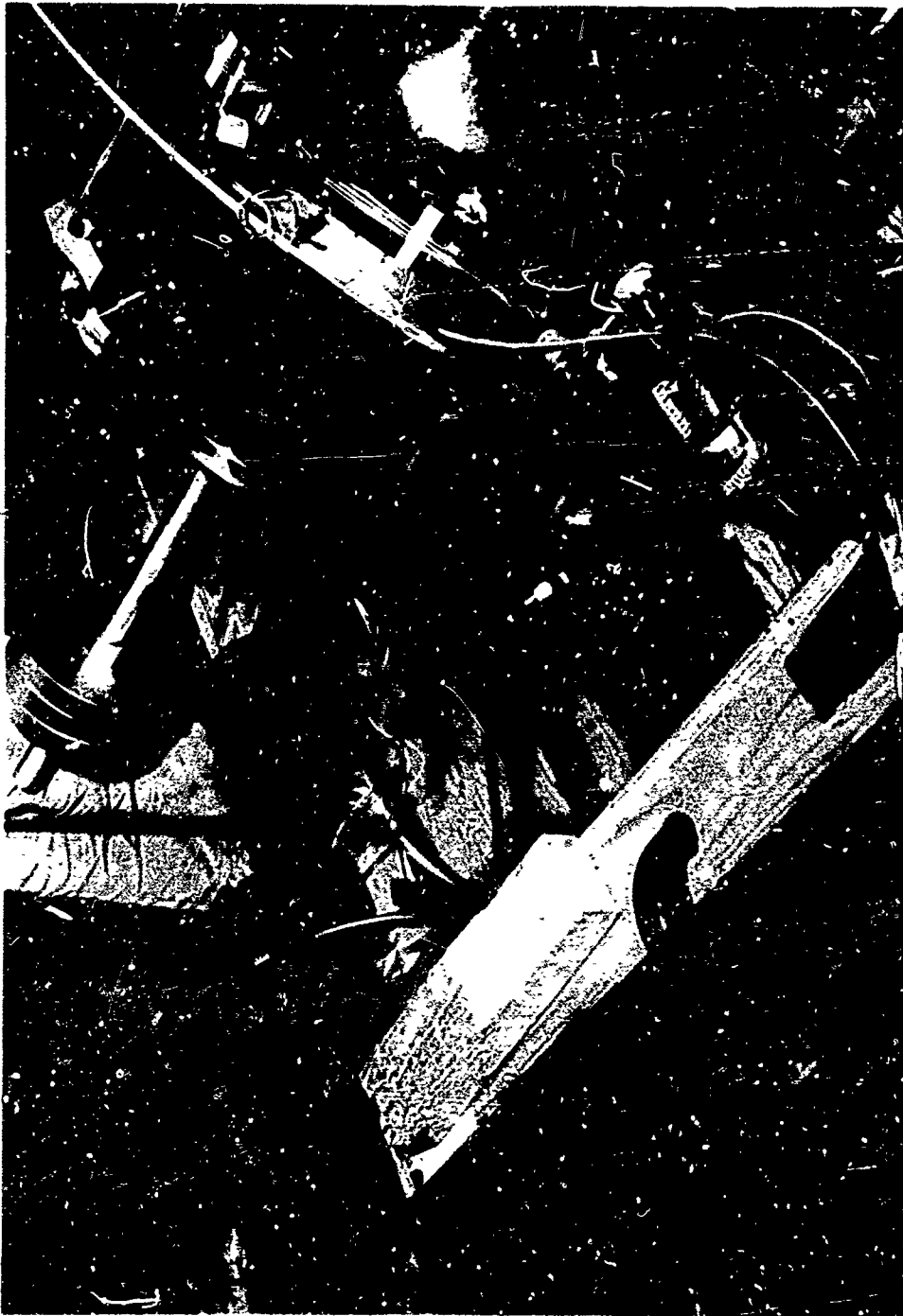
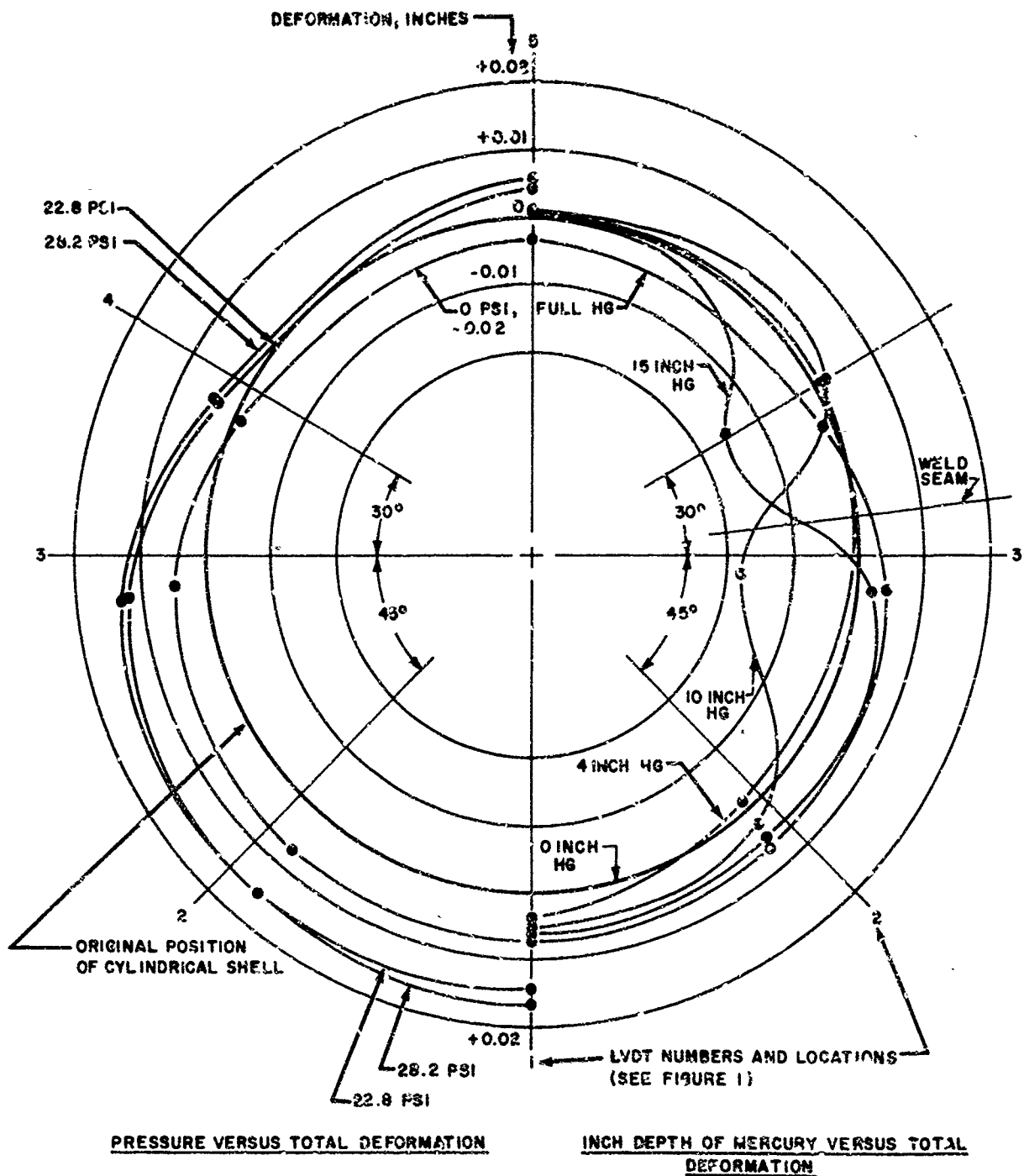
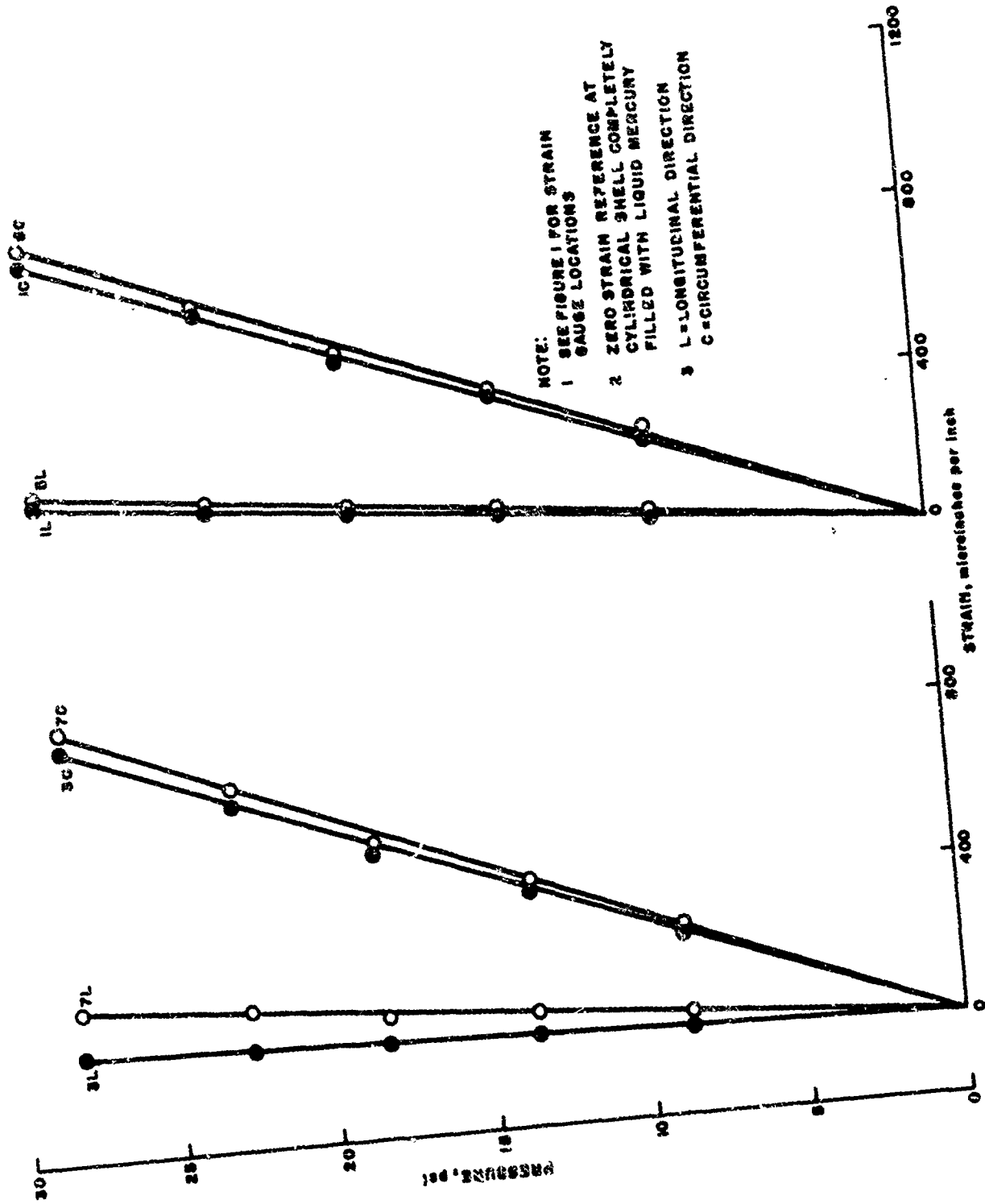


Figure 3 CLOSE-UP VIEW OF INSTRUMENTATION DURING TESTING



68-5814

Figure 4 TOTAL DEFORMATION OF CROSS SECTION AT MIDLENGTH OF CYLINDRICAL SHELL



65-3318

Figure 5 PRESSURE VERSUS STRAIN FOR GAGE LOCATIONS 1, 5 AND 3, 7

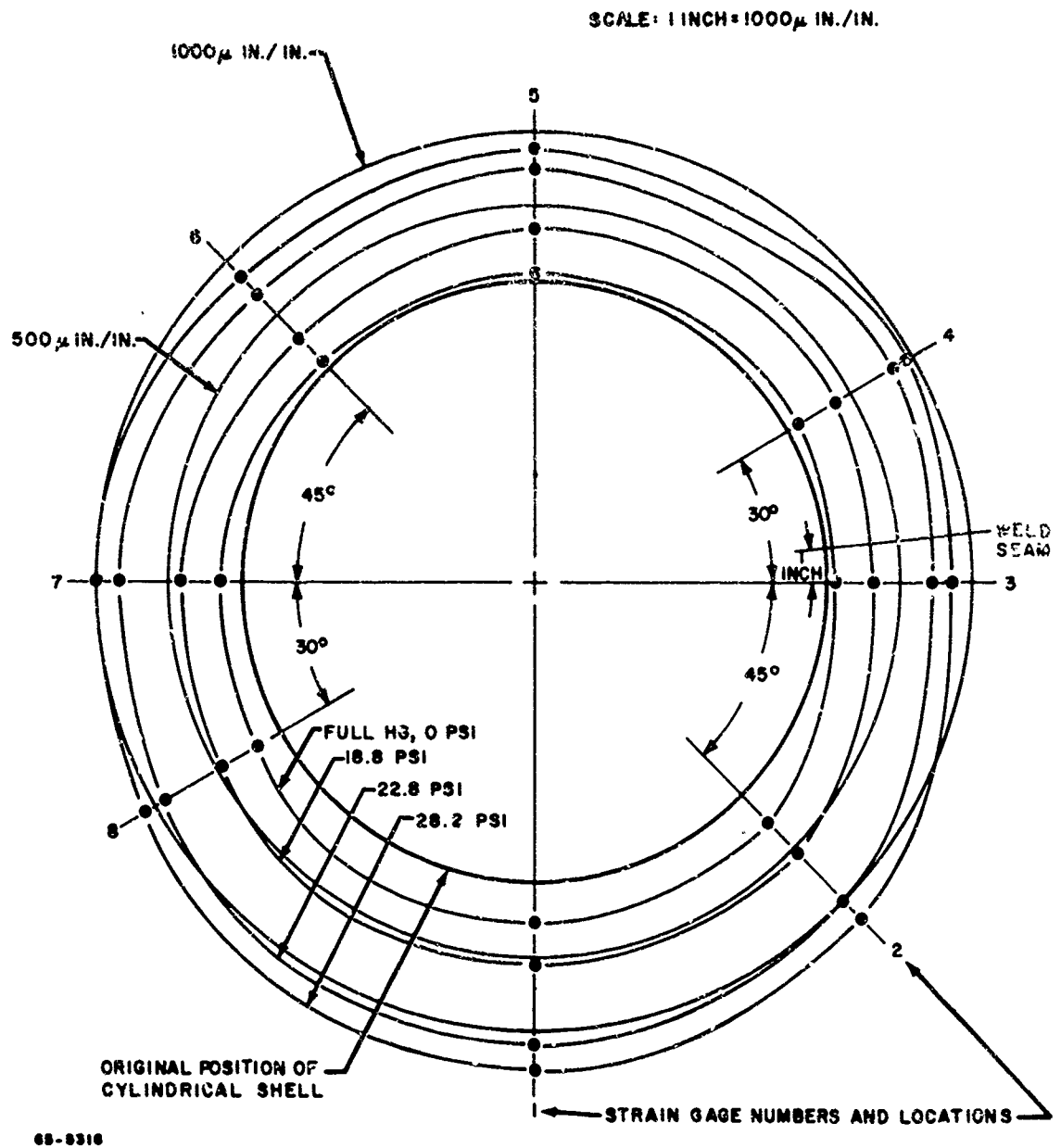


Figure 6 PRESSURE VERSUS CIRCUMFERENTIAL STRAIN OF THE CROSS SECTION
A' MIDLENGTH OF THE CYLINDRICAL SHELL

SCALE: 1 INCH = 400 μ IN./IN.

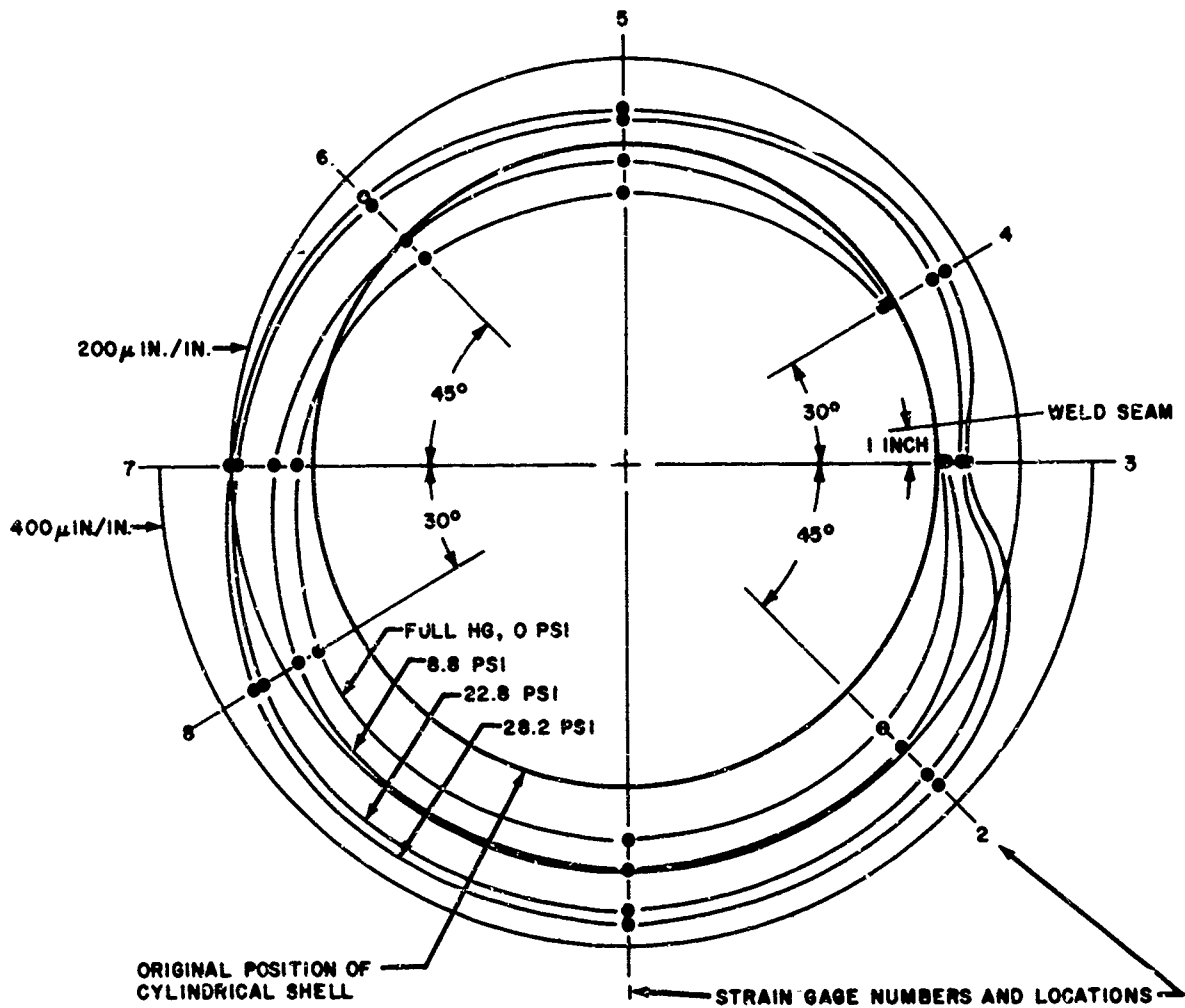


Figure 7 PRESSURE VERSUS LONGITUDINAL STRAIN OF THE CROSS SECTION AT MIDLNGTH OF THE CYLINDRICAL SHELL

acting on the shell surface. Within the limitation of the theory, results thus obtained represent the real state of stress in a cylindrical shell provided, that appropriate boundary conditions are applied, smoothly distributed surface loadings are imposed, and resulting bending stresses constitute a small percentage of the extensional stresses induced in the shell.

In general, and for thin shells, the stress resultants and displacements obtained by the extensional theory, in the case of smooth surface loadings normal to the shell and inplane boundary conditions, provide a satisfactory engineering approximation of the solution obtained from the field equations of cylindrical shells. Boundary conditions not of inplane nature, influencing a small zone in the neighborhood of the edges of the shell, can be dealt with effectively only through the theory of the edge effect.

The validity of the assumptions involved in arriving at the extensional shell theory depends on the magnitude of the quantities assumed originally to be zero and not included in the differential equations of equilibrium. Thus, the applicability of this approach into any specific problem is assured, for, if the quantities not included in the equilibrium equations assume a significant value for any loading this in itself would be proof of the inapplicability of the extensional theory.

The field equations of the linear shell theory of cylindrical shells are of the following form (see figure 3):

Equilibrium Equations

$$\frac{\partial T_1}{\partial \alpha} - \frac{1}{R} \frac{\partial S_2}{\partial \beta} + \bar{X} = 0$$

$$\frac{\partial S_1}{\partial \alpha} + \frac{1}{R} \frac{\partial T_2}{\partial \beta} - \frac{N_2}{R} + \bar{Y} = 0$$

$$\frac{T_2}{R} + \frac{\partial N_1}{\partial \alpha} + \frac{1}{R} \frac{\partial N_2}{\partial \beta} + \bar{Z} = 0$$

$$\frac{\partial H_1}{\partial \alpha} - \frac{1}{R} \frac{\partial G_2}{\partial \beta} + N_2 + \bar{E} = 0$$

$$\frac{\partial G_1}{\partial \alpha} + \frac{1}{R} \frac{\partial H_2}{\partial \beta} - N_1 - \bar{F} = 0$$

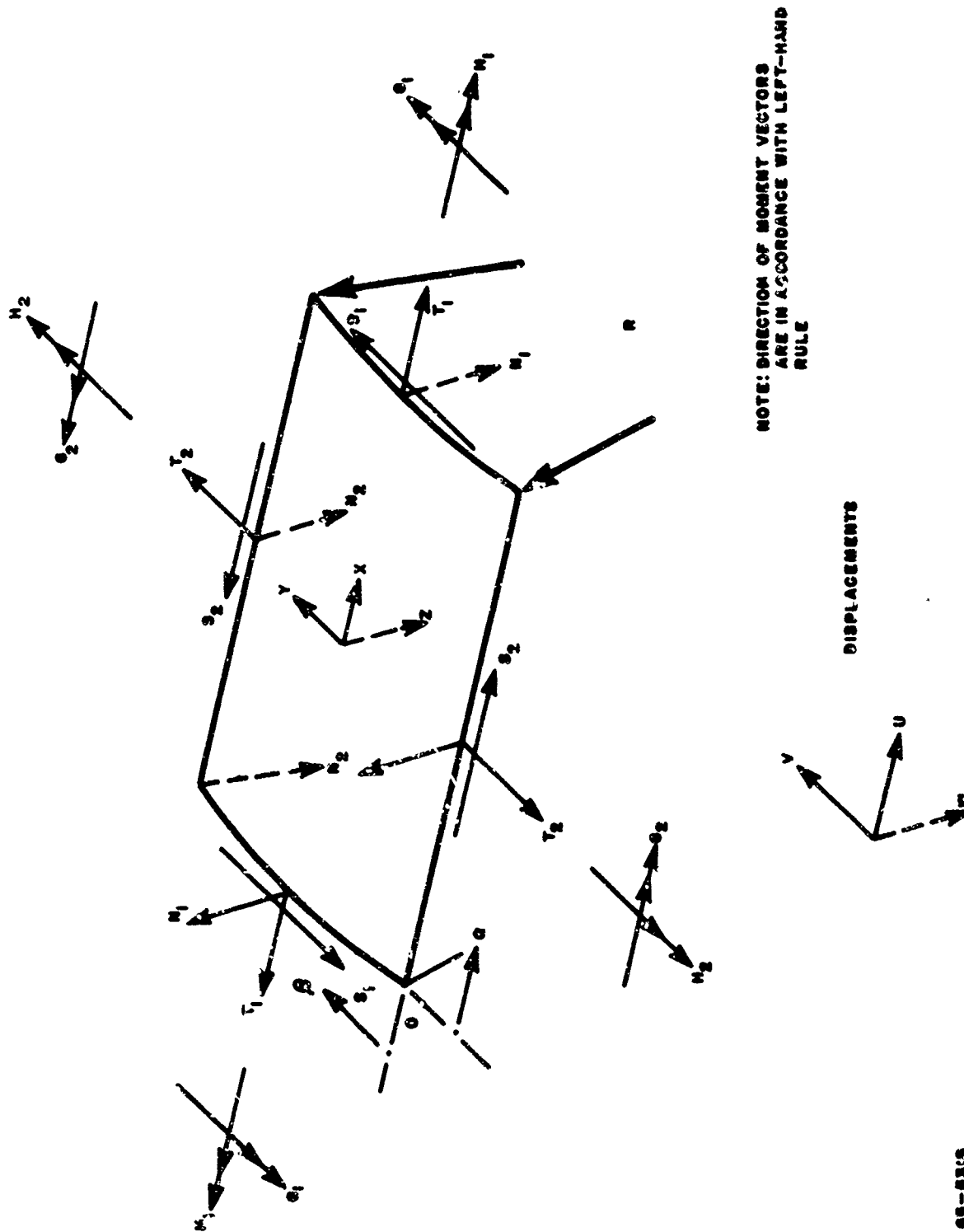


Figure 8 FREE-BODY DIAGRAM OF ELEMENT OF CYLINDRICAL SHELL

CS-3318

$$S_1 + S_2 + \frac{H_2}{R} = 0$$

Strain-Displacement Equations

$$\epsilon_1 = \frac{\partial u}{\partial \alpha}$$

$$\epsilon_2 = \frac{1}{R} \left(\frac{\partial v}{\partial \beta} - w \right)$$

$$\epsilon_{12} = \frac{1}{R} \frac{\partial u}{\partial \beta} + \frac{\partial v}{\partial \alpha}$$

$$\kappa_1 = \frac{\partial^2 w}{\partial \alpha^2}$$

$$\kappa_2 = \frac{1}{R^2} \left(\frac{\partial^2 w}{\partial \beta^2} + \frac{\partial v}{\partial \beta} \right)$$

$$\kappa_{12} = \frac{1}{R} \left(\frac{\partial^2 w}{\partial \alpha \partial \beta} + \frac{\partial v}{\partial \alpha} \right)$$

Stress-Strain Relations

$$T_1 = \frac{E t}{1 - \nu^2} (\epsilon_1 + \nu \epsilon_2)$$

$$T_2 = \frac{E t}{1 - \nu^2} (\epsilon_2 + \nu \epsilon_1)$$

$$S_1 = \frac{E t}{2(1 + \nu)} \left(\epsilon_{12} + \frac{t^2 \kappa_{12}}{6R} \right)$$

$$S_2 = - \frac{E t}{2(1 + \nu)} (\epsilon_{12})$$

$$G_1 = - \frac{E t^3}{12(1 - \nu^2)} (\kappa_1 + \nu \kappa_2)$$

$$G_2 = - \frac{E t^3}{12(1 - \nu^2)} (\kappa_2 + \nu \kappa_1)$$

$$H_1 = \frac{E t^3}{12(1 + \nu)} (\kappa_{12})$$

$$H_2 = - \frac{E t^3}{12(1 + \nu)} (\kappa_{12})$$

It can be easily seen that the 6th equilibrium equation is an identity, leaving a system of 19 equations in 19 unknowns.

The elimination of the transverse shears N_1 , N_2 , and their derivatives from the first three equilibrium equations, and the deletion of the term involving the t^2/R in the stress-strain relations, reduced the above equations into the field equations of the linear extensional theory. The following set of equations is obtained:

Equilibrium Equations

$$\frac{\partial T_1}{\partial \alpha} - \frac{1}{R} \frac{\partial S_2}{\partial \beta} + \bar{X} = 0$$

$$\frac{\partial S_1}{\partial \alpha} + \frac{1}{R} \frac{\partial T_2}{\partial \beta} + \bar{Y} = 0$$

$$\frac{T_2}{R} + \bar{Z} = 0$$

$$\frac{\partial H_1}{\partial \alpha} - \frac{1}{R} \frac{\partial G_2}{\partial \beta} + N_2 + \bar{E} = 0$$

$$\frac{\partial G_1}{\partial \alpha} + \frac{1}{R} \frac{\partial H_2}{\partial \beta} - N_1 - \bar{F} = 0$$

Strain Displacement Equations

$$\epsilon_1 = \frac{\partial u}{\partial \alpha}$$

$$\epsilon_2 = \frac{1}{R} \left(\frac{\partial v}{\partial \beta} - w \right)$$

$$\epsilon_{12} = \frac{1}{R} \frac{\partial u}{\partial \beta} + \frac{\partial v}{\partial \alpha}$$

$$\kappa_1 = \frac{\partial^2 w}{\partial \alpha^2}$$

$$\kappa_2 = \frac{1}{R^2} \left(\frac{\partial^2 w}{\partial \beta^2} + \frac{\partial v}{\partial \beta} \right)$$

$$\kappa_{12} = \frac{1}{R} \left(\frac{\partial^2 w}{\partial \alpha \partial \beta} + \frac{\partial v}{\partial \alpha} \right)$$

Stress Strain Relations

$$T_1 = \frac{Et}{(1-\nu^2)} (\epsilon_1 + \nu \epsilon_2)$$

$$T_2 = \frac{Et}{(1-\nu^2)} (\epsilon_2 + \nu \epsilon_1)$$

$$S_1 = \frac{Et}{2(1+\nu)} (\epsilon_{12})$$

$$S_2 = -\frac{Et}{2(1+\nu)} (\epsilon_{12})$$

$$G_1 = -\frac{Et^3}{12(1-\nu^2)} (\kappa_1 + \nu \kappa_2)$$

$$G_2 = \frac{E t^3}{12(1 - \nu^2)} (\kappa_2 + \nu \kappa_1)$$

$$H_1 = \frac{E t^3}{12(1 + \nu)} (\kappa_{12})$$

$$H_2 = - \frac{E t^3}{12(1 + \nu)} (\kappa_{12})$$

Noticing from the stress-strain relations that $S_1 = -S_2$ and considering the fact that $\bar{X} = \bar{Y} = \bar{E} = \bar{F} = 0$, the first three equilibrium equations reduce to a system of three equations in three unknowns whose solution in terms of the integration functions to be determined from the boundary conditions are:

$$T_1 = - \frac{1}{R} \int_{a_1}^a \frac{\partial}{\partial \beta} \int_{a_1}^a \left(\frac{\partial \bar{Z}}{\partial \beta} \right) da da - \frac{1}{R} \int_{a_1}^a \frac{\partial}{\partial \beta} f_1(\beta) da + f_2(\beta)$$

$$T_2 = - R \bar{Z}$$

$$S_1 = \int_{a_1}^a \left(\frac{\partial \bar{Z}}{\partial \beta} \right) da + f_1(\beta)$$

The three strains then, following from the stress-strain relations, are of the form:

$$\epsilon_1 = - \frac{1}{ERt} \int_{a_1}^a \frac{\partial}{\partial \beta} \int_{a_1}^a \left(\frac{\partial \bar{Z}}{\partial \beta} \right) da da - \frac{1}{ERt} \int_{a_1}^a \frac{\partial}{\partial \beta} f_1(\beta) da + \frac{1}{Et} f_2(\beta) + \frac{\nu R}{Et} \bar{Z}$$

$$\epsilon_2 = - \frac{R}{Et} \bar{Z} + \frac{\nu}{ERt} \int_{a_1}^a \frac{\partial}{\partial \beta} \int_{a_1}^a \left(\frac{\partial \bar{Z}}{\partial \beta} \right) da da + \frac{\nu}{ERt} \int_{a_1}^a \frac{\partial}{\partial \beta} f_1(\beta) da - \frac{\nu}{Et} f_2(\beta)$$

$$\epsilon_{12} = \frac{2(1+\nu)}{E_t} \int_{a_1}^a \left(\frac{\partial \bar{Z}}{\partial \beta} \right) da + \frac{2(1+\nu)}{E_t} f_1(\beta)$$

Having obtained these quantities, the strain-displacement relations can be integrated to give the following displacement in terms of the integration functions:

$$u = \frac{1}{ER_t} \int_{a_2}^a \int_{a_1}^a \frac{\partial}{\partial \beta} \int_{a_1}^a \left(\frac{\partial \bar{Z}}{\partial \beta} \right) da da da + \frac{\nu R}{E_t} \int_{a_2}^a \bar{Z} da -$$

$$\frac{1}{ER_t} \int_{a_2}^a \int_{a_1}^a \frac{\partial}{\partial \beta} f_1(\beta) da da + \frac{1}{E_t} \int_{a_2}^a f_2(\beta) da + \phi_1(\beta)$$

$$v = \frac{2(1+\nu)}{E_t} \int_{a_2}^a \int_{a_1}^a \left(\frac{\partial \bar{Z}}{\partial \beta} \right) da da + \frac{1}{ER_t^2} \int_{a_2}^a \int_{a_2}^c \frac{\partial}{\partial \beta} \int_{a_1}^a \frac{\partial}{\partial \beta} \int_{a_1}^a \left(\frac{\partial \bar{Z}}{\partial \beta} \right) da da da da -$$

$$\frac{\nu}{E_t} \int_{a_2}^a \int_{a_2}^a \left(\frac{\partial \bar{Z}}{\partial \beta} \right) da da + \frac{2(1+\nu)}{E_t} \int_{a_2}^a f_1(\beta) da + \frac{1}{ER_t^2} \int_{a_2}^a \frac{\partial}{\partial \beta} \int_{a_2}^a \int_{a_1}^a \frac{\partial}{\partial \beta} f_1(\beta) da da da -$$

$$\frac{1}{RE_t} \int_{a_2}^a \frac{\partial}{\partial \beta} \int_{a_2}^a f_2(\beta) da da - \frac{1}{R} \int_{a_2}^a \frac{\partial}{\partial \beta} \phi_1(\beta) da + \phi_2(\beta)$$

$$w = \frac{2(1+\nu)}{E_t} \frac{\partial}{\partial \beta} \int_{a_2}^a \int_{a_1}^a \left(\frac{\partial \bar{Z}}{\partial \beta} \right) da da + \frac{1}{ER_t^2} \frac{\partial}{\partial \beta} \int_{a_2}^a \int_{a_2}^a \frac{\partial}{\partial \beta} \int_{a_1}^a \frac{\partial}{\partial \beta} \int_{a_1}^a \left(\frac{\partial \bar{Z}}{\partial \beta} \right) da da da da -$$

$$\frac{\nu}{E_t} \frac{\partial}{\partial \beta} \int_{a_2}^a \int_{a_2}^a \left(\frac{\partial \bar{Z}}{\partial \beta} \right) da da + \frac{R^2}{E_t} \bar{Z} - \frac{\nu}{E_t} \int_{a_1}^a \frac{\partial}{\partial \beta} \int_{a_1}^a \left(\frac{\partial \bar{Z}}{\partial \beta} \right) da da +$$

$$\frac{2(1+\nu)}{E t} \frac{\partial}{\partial \beta} \int_{a_2}^a f_1(\beta) da + \frac{1}{ER^2 t} \frac{\partial}{\partial \beta} \int_{a_2}^a \frac{\partial}{\partial \beta} \int_{a_2}^a \int_{a_1}^a \frac{\partial}{\partial \beta} f_1(\beta) da da da -$$

$$\frac{1}{ER t} \frac{\partial}{\partial \beta} \int_{a_2}^a \frac{\partial}{\partial \beta} \int_{a_2}^a f_2(\beta) da da - \frac{\nu}{E t} \int_{a_1}^a \frac{\partial}{\partial \beta} f_1(\beta) da +$$

$$\frac{\nu R}{E t} f_2(\beta) - \frac{1}{R} \frac{\partial}{\partial \beta} \int_{a_2}^a \frac{\partial}{\partial \beta} \phi_1(\beta) da + \frac{\partial}{\partial \beta} \phi_2(\beta)$$

This completes the solution of the fourth order system comprising the extensional theory of cylindrical shells. The constants of integration have to be evaluated from the boundary conditions. The bending and torsional moments can then be evaluated from the curvature - moment expressions of the stress-strain relations, after the evaluation of the curvatures, which were obtained by successive differentiation of the displacements with respect of the independent variables a and β . Having thus evaluated the bending and torsional moments, the transverse shears N_1 and N_2 , that is, the quantities that were deleted from the equations of equilibrium in arriving at the extensional theory of shells, can now be evaluated from the fourth and fifth equilibrium equations. The validity of the extensional theory will be dependent upon the magnitude of these quantities since these were originally assumed to be negligible.

Analytical results for the meridional and circumferential strains and the radial displacement were determined, based on the following loading and boundary conditions:

Cylindrical Shell Completely Filled with Liquid Mercury

1) Loading

$$\bar{Z} = A + B \cos \beta, \text{ where}$$

$$A = -\gamma R = -4.864 \text{ psi}$$

$$B = +\gamma R = +4.864 \text{ psi}$$

2) Boundary conditions

Measuring a from the mid-shell, the boundary conditions are:

$$\begin{aligned}
S_{1\alpha=0} &= 0 \\
u_{\alpha=0} &= 0 \\
T_{1\alpha=\alpha_0} &= C + D \cos \beta \\
v_{\alpha=\alpha_0} &= 0, \text{ where (see appendix)} \\
C &= +18.058 \text{ lb/in} \\
D &= -24.077 \text{ lb/in}
\end{aligned}$$

The boundary conditions imposed by the end plates were determined by taking into account not only the pressure exerted by the liquid mercury on the end plates and subsequently on the shell in the meridional direction, but also the effect of the resultant force due to mercury and the support rollers in creating an additional force distribution in the meridional direction at the end of the shell. This force system was created since the metal end plates were not counter weighted after the application of the mercury loading, since rollers are not perfectly frictionless when their axes are not normal to the axis of the cylindrical shell, and since it is not possible to place the support rollers at the surface of the inner edge of the end plate, thereby eliminating the eccentricity involved in the test setup. These conditions have been incorporated in the values of the constants in determining the boundary conditions.

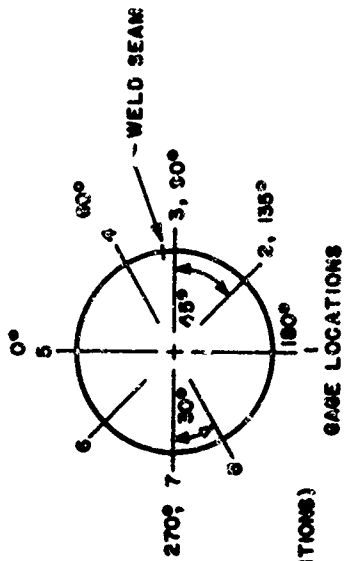
In the ideal case of a frictionless support hinge involving no eccentricity and a perfectly counter weighted test setup, the boundary conditions, if the end plates are plane elastic plates, would be of the form $\bar{E} + \bar{F} \cos \beta$. In the case of a cylindrical shell completely filled with liquid mercury the

constants \bar{E} and \bar{F} would assume, in this ideal case, the values $\frac{\gamma R^2}{2}$ and $-\frac{\gamma R^2}{4}$

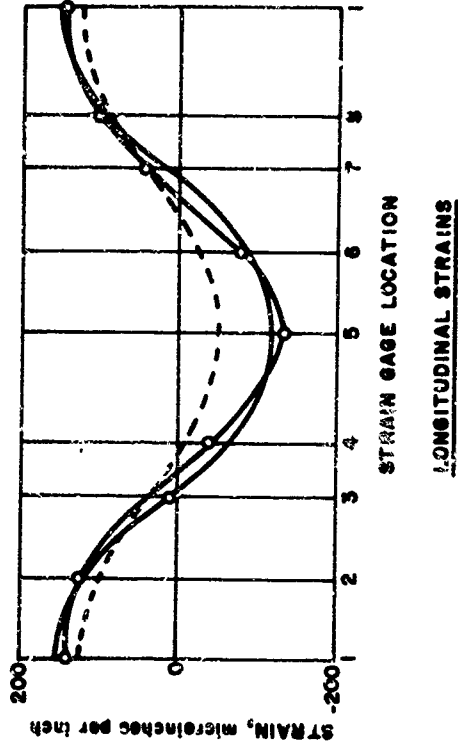
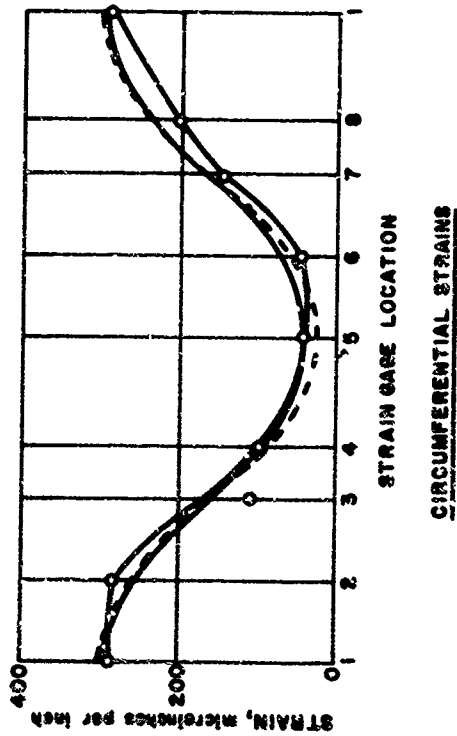
respectively. However, the laboratory boundary conditions imposed were of the form $C + D \cos \beta$, thus incorporating the actual force system created at the laboratory.

Making use of the appropriate loading and the corresponding boundary conditions meridional and circumferential strains and radial displacements were evaluated at the midlength of the shell and at different circumferential points. The results, obtained through Avco RAD IBM 7094 Program No. 1406 based on reference 2, are presented in graphical form in figures 9 and 10.

The values for the quantities N_1 and N_2 were found to be of the order of 1 to 10,000 or less throughout the shell, assuring the applicability, as far as the analysis is concerned, of the linear extensional theory used in the case under consideration.



- TEST RESULTS
- ANALYTICAL RESULTS (EXPERIMENTAL END-BOUNDARY CONDITIONS)
- - - ANALYTICAL RESULTS (IDEAL END-BOUNDARY CONDITIONS)



66-8519

Figure 9 ANALYTICAL CIRCUMFERENTIAL AND LONGITUDINAL STRAINS COMPARED WITH EXPERIMENTAL STRAINS; CYLINDRICAL SHELL AT MIDLNGTH FILLED WITH LIQUID MERCURY AND AT ZERO PSI APPLIED INTERNAL PRESSURE

β DEGREES	ANALYTICAL W INCHES	EXPERIMENTAL W INCHES
0	0.00274	0.00400
30	0.00218	---
60	0.00088	0.00238
90	-0.00163	-0.00460
135	-0.00473	-0.00742
180	-0.00900	-0.00870
270	-0.00163	-0.00200

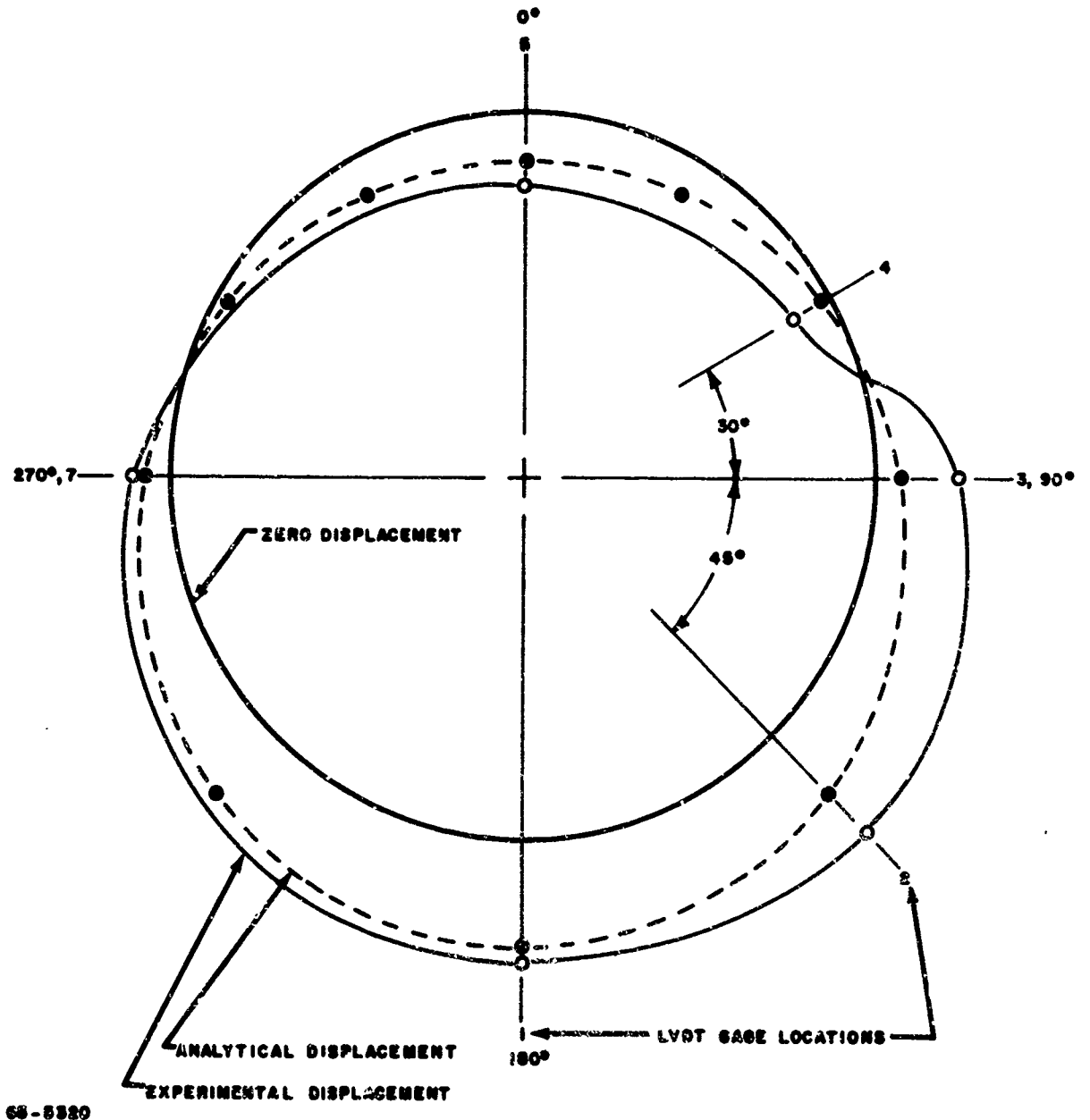


Figure 10 ANALYTICAL VERSUS EXPERIMENTAL RADIAL DISPLACEMENTS AT MIDLNGTH OF CYLINDRICAL SHELL FILLED WITH LIQUID MERCURY AND AT ZERO PSI APPLIED INTERNAL PRESSURE

3. Comparison of Experimental with Theoretical Results

Figure 9 shows plots of analytically obtained longitudinal and circumferential strains at mid-shell compared to the experimental points in the case of the cylindrical shell completely filled with liquid mercury and zero pressure. Figure 10 showing radial displacement, is an analogous plot to figure 9. Results are compared at the zero psi pressure rather than the maximum pressure of 28.2 psi because some permanent strain and deformation showed in the cylindrical shell at the 28.2 psi pressure level when repeated.

Figure 9 shows analytical results obtained for both ideal and laboratory-achieved boundary conditions (as mentioned in paragraph 2). As can be readily seen, the circumferential strains are not appreciably affected by the change in the boundary conditions. This is not so in the case of longitudinal strains. A careful review of the test setup after the application of the liquid mercury reveals the creation of an additional force system acting on the boundary of the cylindrical shell. An elementary free body diagram of the rod-plate assembly resting on the rollers accompanied by some analysis involving elementary statics (see appendix) shows plainly the creation of this additional force system. Under the boundary conditions imposed on the shell by this force system, the comparison of the meridional strains obtained analytically to the ones obtained experimentally are in good agreement. It is believed that if the analysis shown in the appendix was based on the true horizontal force developed at the rollers, and not on the analysis arrived at by assuming the value of μ , the agreement between theory and experiment would be much closer than that shown in figure 9.

The analytically obtained radial displacements shown in figures 10 agree very well with the experimentally obtained data, except in the 90 to 180 degree area. This obvious discrepancy is due to the weld bead (as would be expected) because of the pronounced stiffness of the shell in this area.

The structure behaved linearly with small deformations, substantiating the application of linear extensional theory in foil structures.

II. CONCLUSIONS

From the results obtained in this study, it can be concluded that linear extensional shell theory can be applied in the analysis of cylindrical shells under Newtonian pressure distribution, provided that the inplane boundary conditions are well defined. It is hoped that analogous studies involving unfurlable materials instead of foils can be carried out in the near future.

REFERENCES

1. Goldenveizer, A. L., Theory of Thin Elastic Shells, Pergamon Press, 1961.
2. Lycurgus, N. C., Solution of Field Equations - Extensional Theory of Cylindrical Shells Under Arbitrary Non-Symmetrical Surface Loading Distribution, Avco RAD-TR-S220-T-46, 1962.

APPENDIX

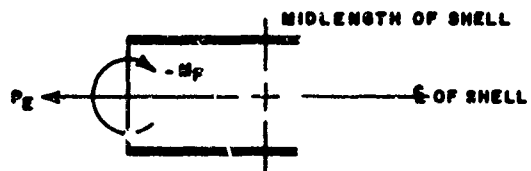
Cylindrical Shell Completely Filled with Liquid Mercury.
Boundary Conditions Incorporating Actual Force System
at the Laboratory.

$$\bar{E} = \frac{\gamma R^2}{2} = 24.077 \text{ lb/in.}$$

$$\bar{F} = -\frac{\gamma R^2}{4} = -12.039 \text{ lb/in.}$$

$$P_E = 2\pi R \bar{E} = 1497.685 \text{ lb.}$$

$$M_F = \pi R^2 \bar{F} = -3706.772 \text{ in.-lb.}$$



Free body of cylindrical shell - Ideal boundary conditions on shell showing acting resultant forces

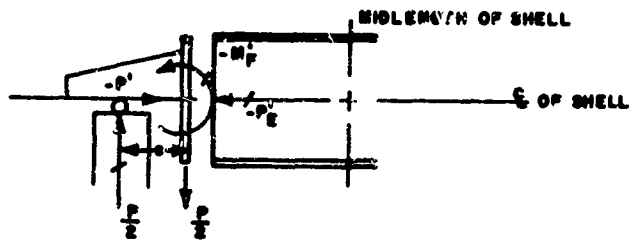
$$P = \pi R^2 (2 \alpha_0) \gamma = 3055.886 \text{ lb.}$$

$$\frac{P}{2} = 1527.943 \text{ lb.}$$

$$e = 2.426 \text{ in.}$$

Assuming $\mu = 0.245$ we obtain

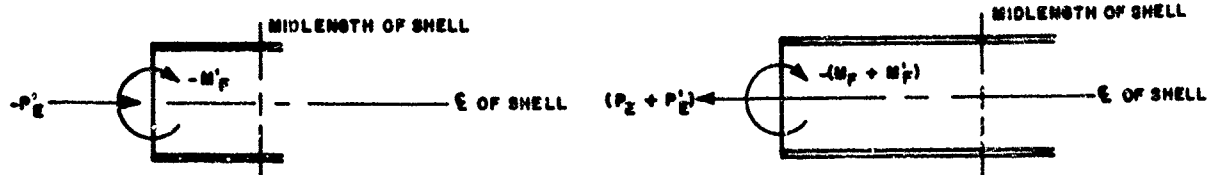
$$-P' = \left(\frac{P}{2}\right) \mu = 374.421 \text{ lb.}$$



Free body diagram - applied and reactive forces in Rod-Plate Assembly due to application of liquid mercury in the Cylindrical shell

$$M_F' = -\frac{P}{2} e = -3706.772 \text{ in.-lb}$$

$$P_E' = P' = -374.421 \text{ lb.}$$



Additional induced force system in shell
due to Laboratory Set-up

Total force system - ideal and induced -
acting on shell boundary

Therefore

$$-(M_F + M_F') = 3706.772 + 3706.772 = 7413.544 \text{ in.-lb.}$$

$$(P_E + P_E') = 1497.685 - 374.421 = 1123.264 \text{ lb.}$$

$$C = \frac{(P_E + P_E')}{2\pi R} = +18.058 \text{ lb./in.}$$

$$D = \frac{(M_F + M_F')}{\pi R^2} = -24.077 \text{ lb./in.}$$

NOMENCLATURE

- A Fourier coefficient of the zero harmonic for the \bar{Z} loading, psi
- B Fourier coefficient of the first harmonic for the \bar{Z} loading, psi
- C Fourier coefficient of the zero harmonic of the boundary condition in T_1 , actual force system, lb per in
- D Fourier coefficient of the first harmonic of the boundary condition in T_1 , actual force system, lb per in
- e Distance between roller and inner face of circular plate, inches
- E Modulus of elasticity, psi
- \bar{E} Fourier coefficient of the zero harmonic of the boundary condition in T_1 , ideal force system, lb per in
- \bar{E} External meridional bending moment, lb per in
- \bar{F} Fourier coefficient of the first harmonic of the boundary conditions in T_1 , ideal force system, lb per in
- \bar{F} External circumferential bending moment, lb per in
- G_1 Meridional bending moment, in-lb per in
- G_2 Circumferential bending moment, in-lb per in
- H_1 Meridional Torsional moment, in-lb per in
- H_2 Circumferential torsional moment, in-lb per in
- M_F Overall resultant moment due to \bar{F} , in-lb
- M_F Overall resultant moment due to $\frac{pe}{2}$, in-lb
- N_1 Meridional transverse shear, lb per in
- N_2 Circumferential transverse shear, lb per in
- P Resultant of mercury load, lb
- P' Force induced at rollers due to assumed coefficient of rolling-sliding friction, lb

NOMENCLATURE (Cont'd)

P_E	Overall resultant force due to \bar{E} , lb
P'_E	Overall resultant force due to P' , lb
R	Radius of cylindrical shell, in
S_1	Meridional inplane shear, lb per in
S_2	Circumferential inplane shear, lb per in
t	Thickness of cylindrical shell, in
T_1	Meridional stress resultant, lb per in
T_2	Circumferential stress resultant, lb per in
u	Meridional displacement, in
v	Circumferential displacement, in
w	Radial displacement, in
\bar{X}	Meridional surface loading on shell, psi
\bar{Y}	Circumferential surface loading on shell, psi
\bar{Z}	Normal surface loading on shell, psi
$f_1(\beta), f_2(\beta),$ $\phi_1(\beta), \phi_2(\beta)$	Integration functions to be determined from the boundary conditions
α	Meridional coordinate, in
α_0	Half length of cylindrical shell, in
α_1, α_2	Lower integration limits, fixed but of arbitrary choice
β	Circumferential coordinate, radians
γ	Density of mercury, lb per in ³
ϵ_1	Meridional extensional strain, in per in
ϵ_2	Circumferential extensional strain, in per in

NOMENCLATURE (Concl'd)

- ϵ_{12} Inplane shearing strain, in per in
- κ_1 Meridional bending strain, per in
- κ_2 Circumferential bending strain, per in
- κ_{12} Torsional strain, per in
- μ Coefficient of rolling-sliding friction, dimensionless
- ν Poisson's ratio, dimensionless

HIGH-TEMPERATURE PROTECTIVE RE-ENTRY COATINGS FOR EXPANDABLE STRUCTURES

by M. T. Conger and T. W. Chalmers

The Goodyear Tire & Rubber Co and its subsidiary, Goodyear Aerospace Corporation, were among the initial participants in the search for coatings that will make possible the successful re-entry of a structure rigidized by gases confined under pressure. This method of rigidization is not new. The list of commercially available products is long; e. g., tires, mattresses, beach balls, footballs, basketballs, toys, lighter-than-air vehicles of several types, and even an experimental heavier-than-air vehicle of the aeroplane geometry. You will notice immediately that most of these items are rubberized fabric products.

The portion of re-entry coating research that I wish to present to you is sponsored by the Research and Technology Division, Air Force Systems Command, United States Air Force, under Contract No. AF 33(657)-11257. One of the purposes of the work under this contract is to develop coatings for use in the manufacture of expandable structures. The structures of interest are those that, during re-entry, must be resistant to a peak skin temperature of 2000°F and are to be fabricated from a high-strength coated metal-fiber fabric composite. Only the coating portion of this composite and the application of the coating to the metal fabric are within the scope of this investigation. Such important tasks as the development of the metal-fiber fabric and the design and fabrication of the re-entry structure are not within the scope of this research program.

In this coatings research program, elevated temperature leak tests and visual inspection means were used as guides to coating quality. The type of coatings studied were inorganic coatings, chemical vapor-deposited coatings, coatings based upon elastomeric ablative insulation, and coatings containing silicone rubber in combination with fusible fillers. I will describe the techniques used in this program, and then summarize for you what has been discovered concerning the properties of the coatings.

A thermal screening apparatus (Figure 1) was used to determine the gross effect of re-entry heat on the coatings. Four specimens could be simultaneously subjected to a stagnant air re-entry heating cycle. The specimens, 1 x 8 inches, were held upon the metal frame using spring clamps. Radiant heat was supplied by two silicone carbide heating rods. The temperature was

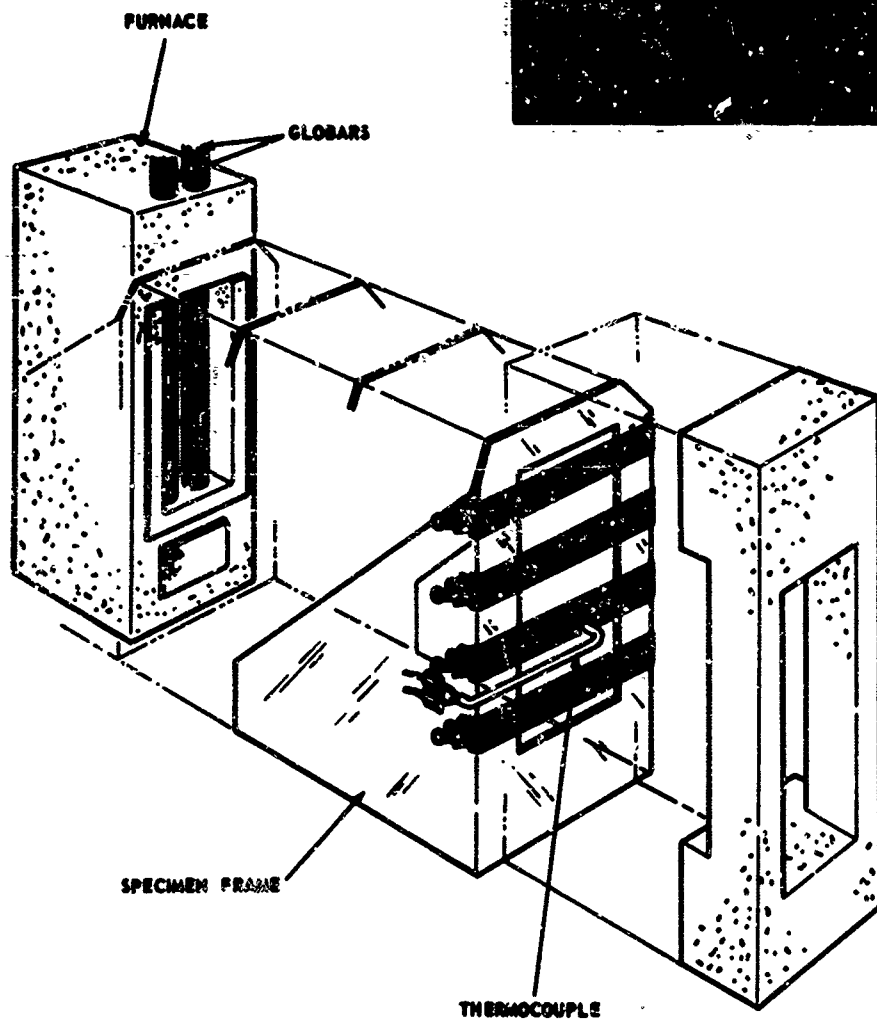
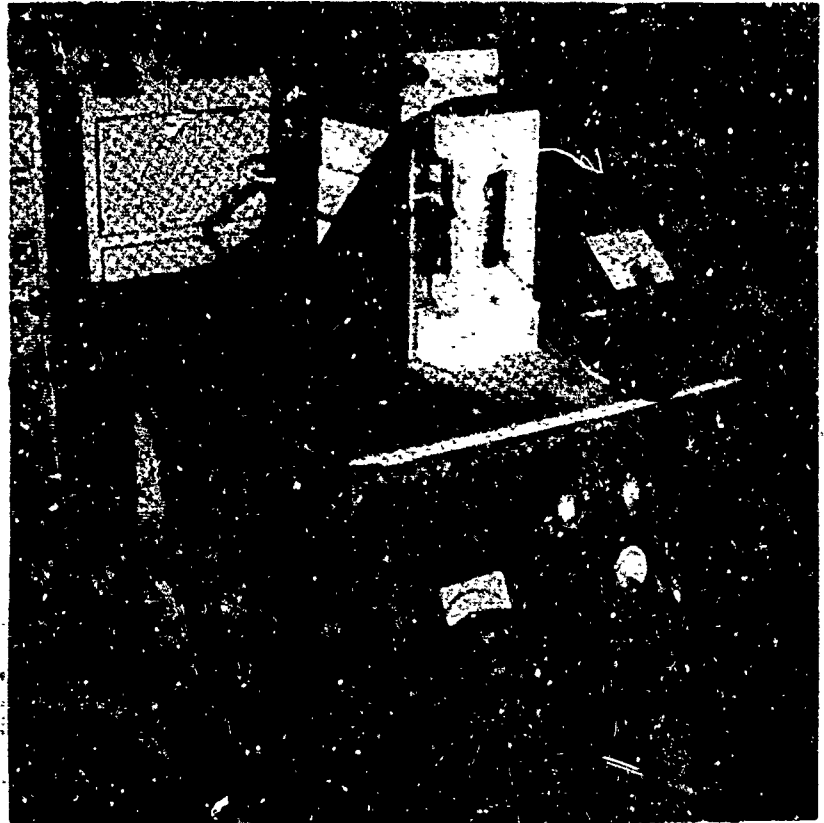


Figure 1. Thermal Screening Apparatus

varied in such a manner that there were 12-1/2 minutes from room temperature to 2000°F, 5 minutes at 2000°F, and 12-1/2 minutes from 2000°F to room temperature. Five specimens that have been subjected to this test are shown in Figure 2. If the coatings remained adhered to the substrate, were not visibly cracked, and were not visibly porous, they were judged to be worthy of further attention.

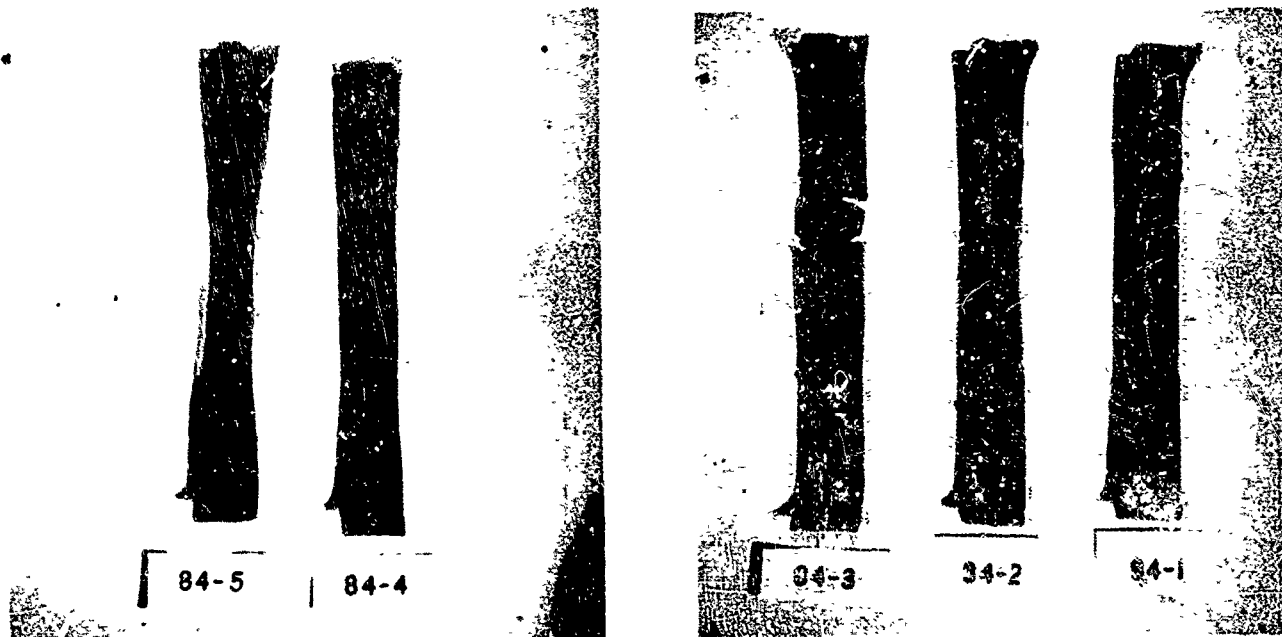


Figure 2. Specimens after Test

In most instances, further attention consisted of some form of leakage test conducted at high temperature and low inflation pressure. For this purpose, several apparatus designs were investigated. In the early work, these were used to determine the temperature at which coated metal fabric diaphragms from 1 to 6 inches in diameter leaked. The last of these designs was, at least in part, satisfactory (see Figure 3). Problems that arose in attempting to make gastight seals at the edge of the specimen during the high-temperature tests have been overcome through the use of focused radiant heating and water-cooled flanges.

However, instead of discussing diaphragm apparatus and tests further, I will discuss, in considerable detail, a much improved high-temperature test method that is now being used. This test is based on the testing of a 10-inch long by 3/8-inch diameter cylindrical specimen. Special features of this test are:

- (1) The ability to measure the effect of folding and creasing of the type that is associated with the packaged vehicle prior to ejection for re-entry.

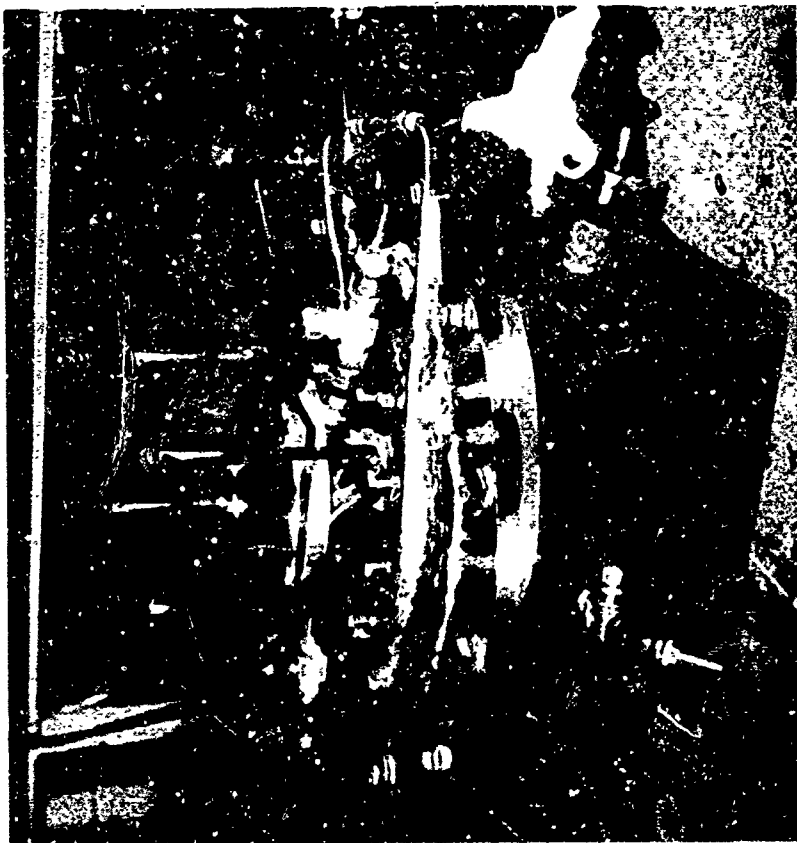
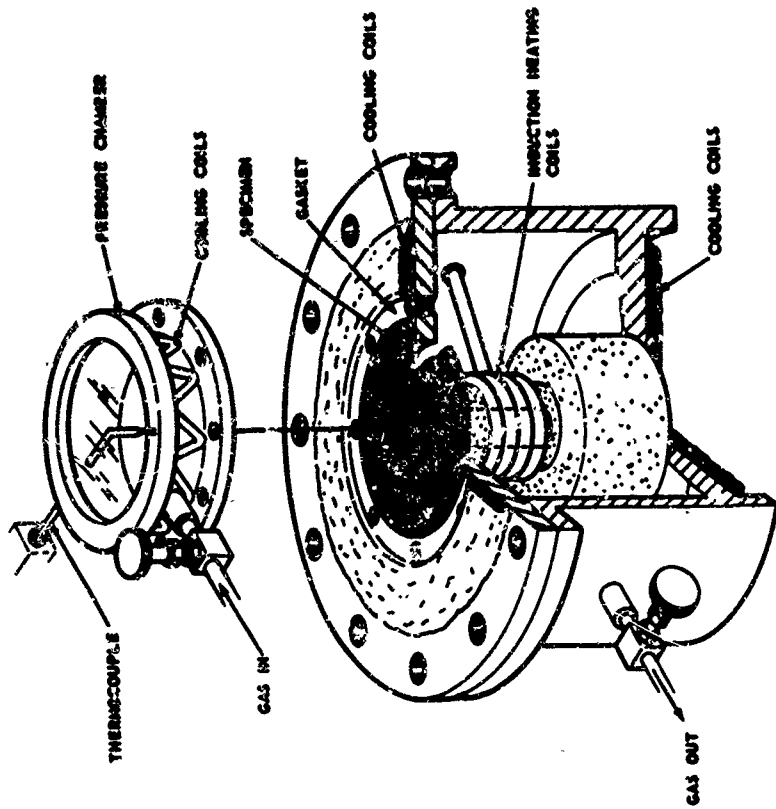
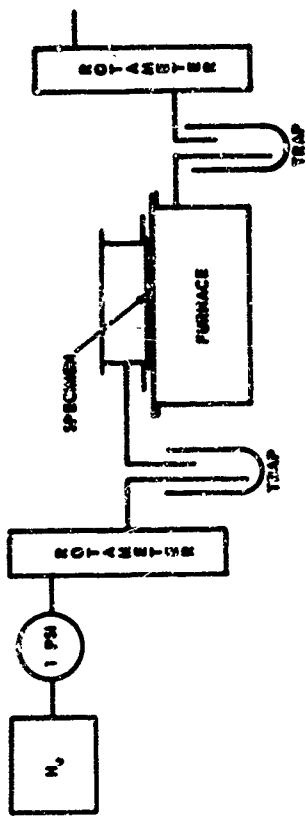


Figure 3. Diaphragm Leakage Apparatus

- (2) The ability to measure the effect of tension or torsion forces applied during simulation of re-entry heating.

The assembled apparatus that is used is shown in Figure 4. Items depicted are the test chamber, helium reservoir, flow indicator, rotameter, leakage tester, water manometer, liquid-nitrogen cold trap, and the temperature recorder. This apparatus uses a very unsophisticated heating source - two ordinary oxygen-acetylene torches. The torches are mounted in an adjustable device through which the operator can continuously and simultaneously change the position of both torches with respect to the specimen chamber.

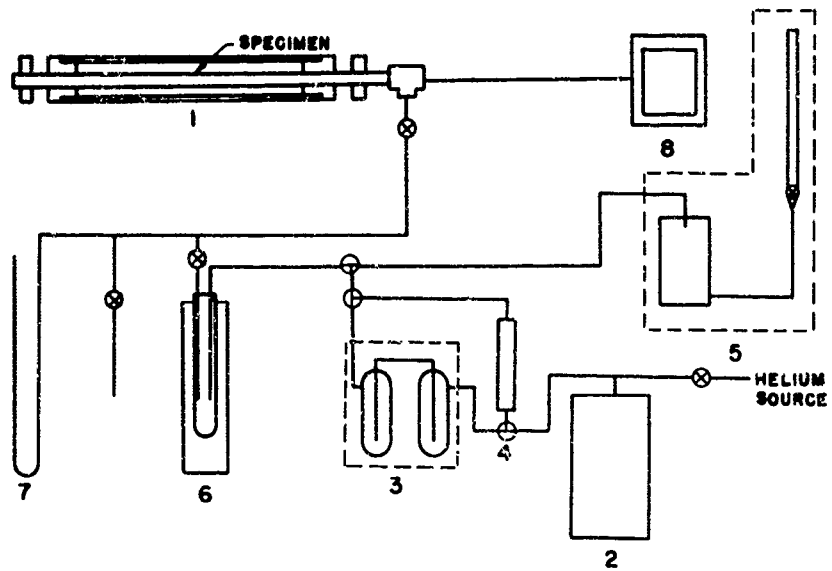
The test chamber itself is a one-inch stainless steel pipe with capped ends, which in turn have a centrally located hole 7/16 inch in diameter. A gas inlet tube in the chamber wall is used to introduce nitrogen or other gases to the space surrounding the test specimen. These gases, which simulate the re-entry atmosphere, escape from the chamber ends. Because of a large escape outlet, the pressure of the gas in the chamber is not measurably above atmospheric pressure at any time.

The stand that holds the test chamber also holds the specimen. This is possible because the specimen is several inches longer than the heating chamber, and this excess length projects through the holes in the capped ends. Devices that apply loads to the specimen can be readily attached to these projecting ends.

A bayonet-type chromel-alumel thermocouple inserted into the center of the specimen and terminating at the lengthwise center is assumed to measure the specimen temperature at that central point. Helium maintained at constant pressure is used inside the specimen. Suitable gages are provided to measure the rate at which the helium must be added to accomplish this. The last two items of the equipment are a liquid nitrogen trap for removal of volatile decomposition products and a device to determine the direction of flow of the inflation gas with respect to the specimen.

The test procedure normally used consists of two more or less independent operations, each of which investigates a separate property of the coating. In the first operation, the ability of the coating to withstand the stress imposed by the folds and creases in the preinflation package is investigated. To do this, the cylindrical test specimen is folded by bringing its ends together. Sufficient finger pressure is applied to the fold to exclude air from this area. The specimen is then unfolded and checked for leaks. If there are no leaks, it is assumed that the folding has caused no damage to the coating. Tensile tests after folding have shown considerable crease damage to the metal fabric substrate, however.

In the second operation, the ability of the coating to withstand re-entry heat while the cloth substrate is being subjected to cyclic distortions is investigated. To do this, the specimen is mounted in the heating chamber. Following



- | | |
|---------------------|-------------------------|
| 1. Test Chamber | 5. Leakage Tester |
| 2. Helium Reservoir | 6. Cold Trap |
| 3. Flow Indicator | 7. Manometer |
| 4. Rotameter | 8. Temperature Recorder |

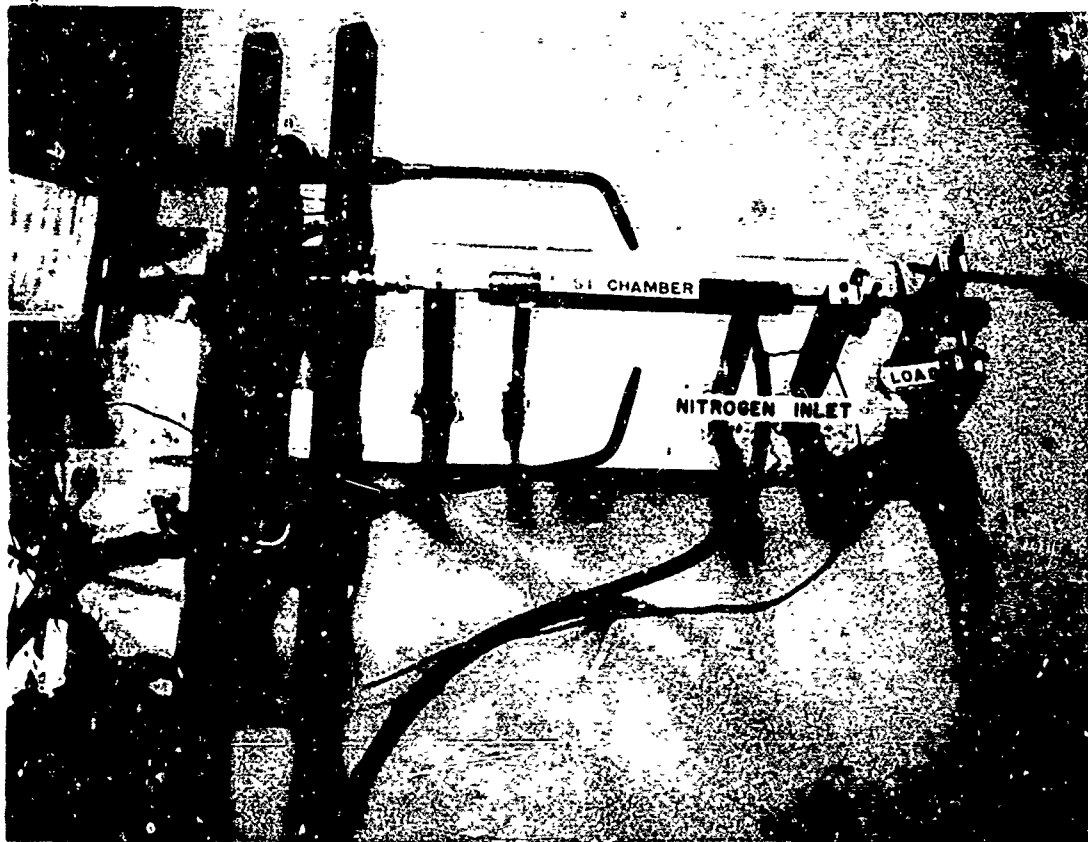


Figure 4. Cylinder Test Apparatus

purging of the specimen and the interconnected components with helium, the entire assembly is checked for leaks at one-psi helium pressure. After correcting leaks found, the cylindrical test specimen is heated to 2000°F in 12-1/2 minutes, held at 2000°F for 5 minutes, then cooled to room temperature in 12-1/2 minutes. During this time, the following steps are performed:

- (1) Either nitrogen or air is continuously added to the space surrounding the heated portion of the test specimen.**
- (2) An axial load of 50 percent of the braking load of the cylinder is applied for 30 seconds of each minute.**
- (3) A one-psi gage inflation pressure is maintained within the test specimen and the interconnected assembly, using helium.**
- (4) The direction of the gas flow is observed, and the temperature at which the gas first flows into the cylinder is noted.**
- (5) The rate of flow of the gas to the cylinder is measured as necessary, and the time at which this is done is recorded.**

We have used some of the many possible variations of this procedure to study the effects of (1) different peak temperatures, (2) different heating rates, (3) different inflation pressures, and (4) different tensile stresses. We can study, but have not studied, the effect of other types of loading such as torsional and compression and the combination of various loading means with each other and vibration. We believe that it is possible to study all the important conditions of re-entry with this single apparatus except those that are associated with the erosion of the coating caused by the vehicle's impingement upon the atmosphere at high velocity.

For those of you who are interested in some additional facts concerning the operating characteristics of this apparatus, your attention is directed to the fact that heating rates and cooling rates sufficiently high to change the temperature from between room temperature and 2000°F in 2-1/2 minutes can be achieved (see Figure 5). Your attention is also directed to Figure 6, a typical profile of temperatures that occurred at a particular instant along the length of the specimen. At the instant these temperatures occurred, the internally located thermocouple at the center had read 2000°F for 3 minutes. It will be noted that the 2000°F temperature is maintained only over a short length of the specimen and that the temperature decreases rapidly outside of this area. These data were obtained using a stainless steel tube as the test specimen. Due to the high rate of heat conduction along the length of this relatively thick walled stainless steel tube, the coated thin walled specimens used in the program will show a far greater lengthwise temperature variation. We have been told by aerodynamic experts that large, but not necessarily identical, temperature variations will exist on the surface of the re-entering structure.

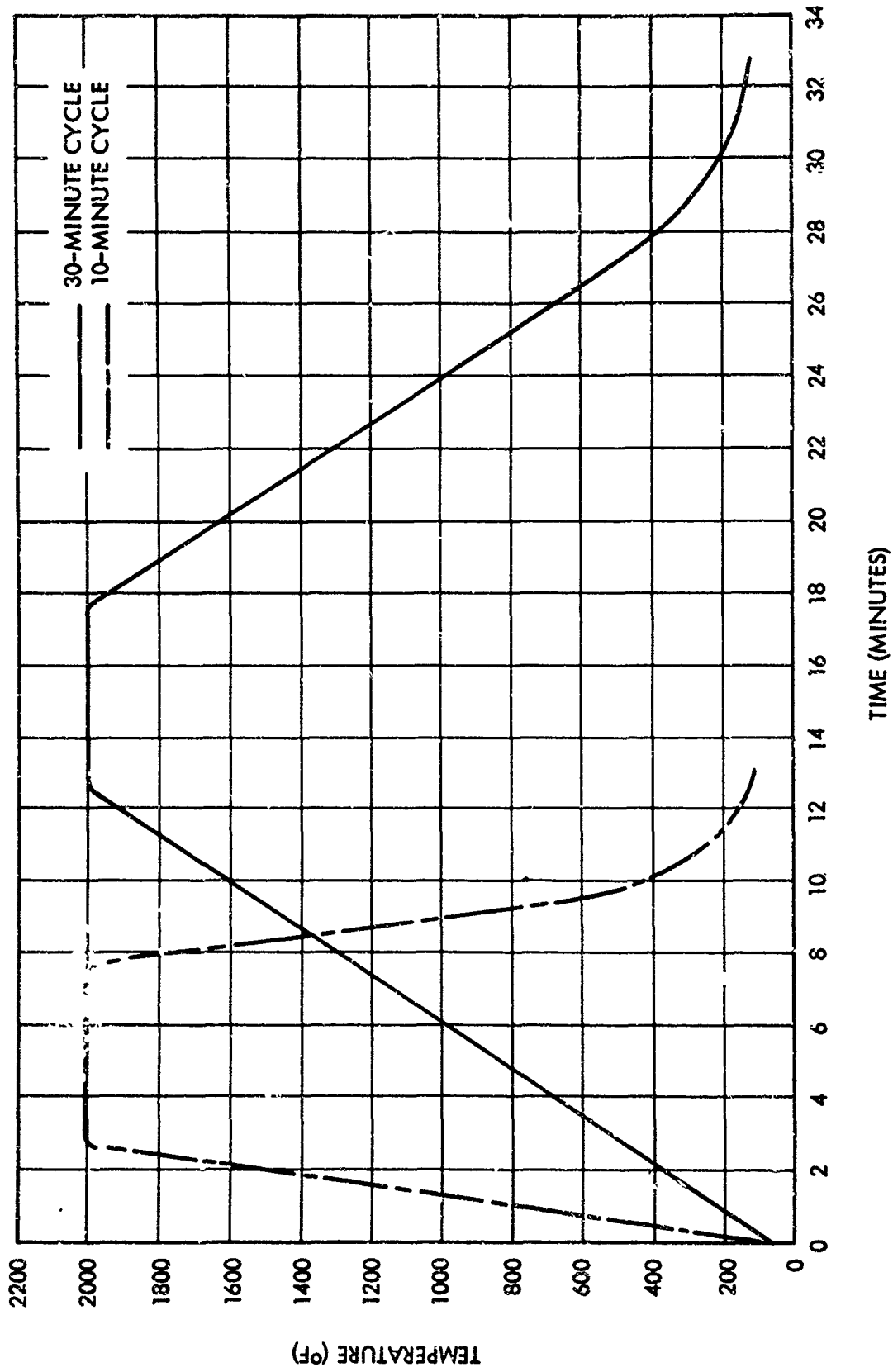


Figure 5. Heating Rate

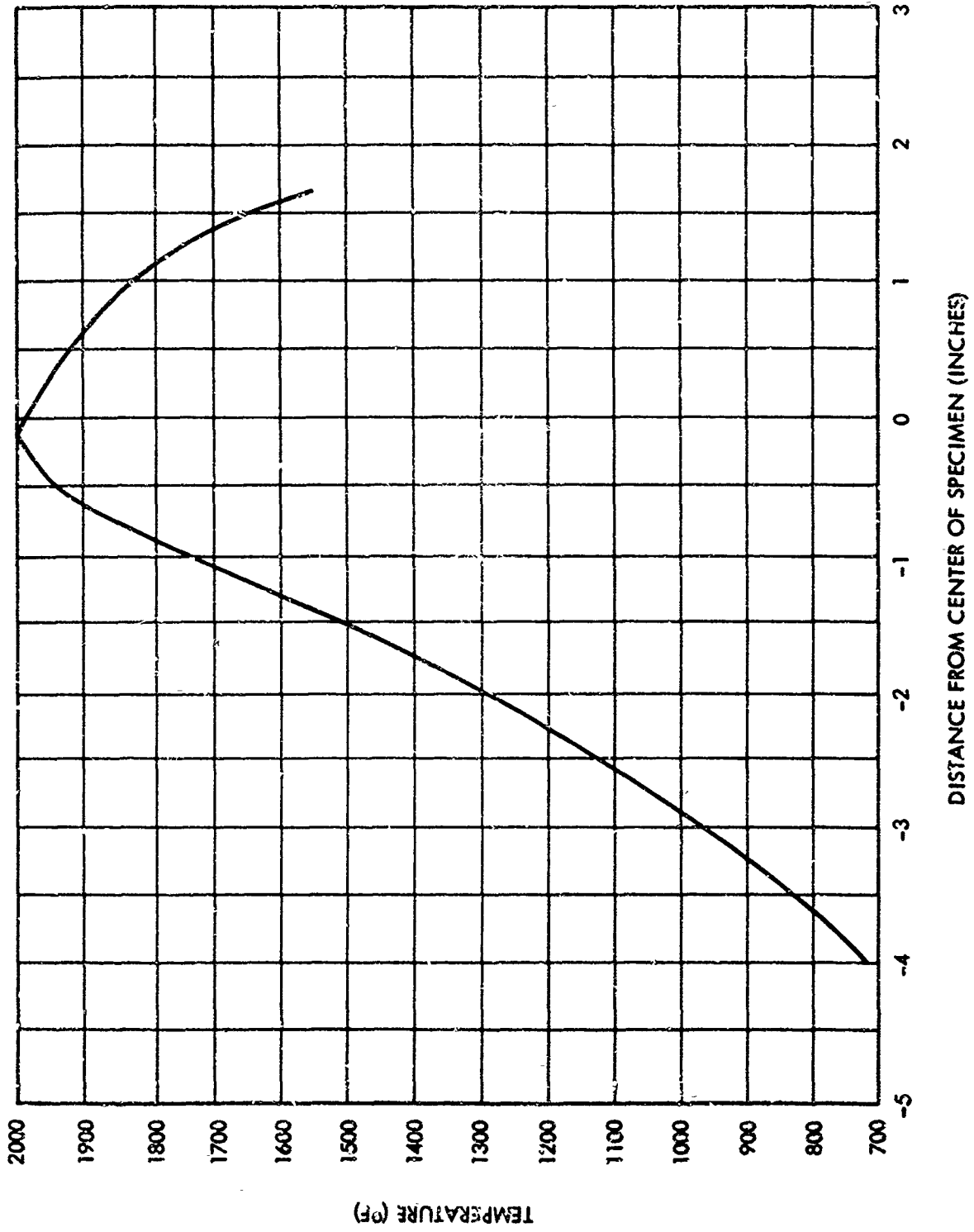


Figure 6. Temperature Profile

We have also been told that as heating occurs during re-entry, it may be necessary to remove inflation gases by special control mechanisms to maintain constant gage pressure. We know as a matter of experimental fact, that during a heating cycle in our apparatus at a constant pressure, it is necessary to bleed off some gas from the system because of the volume increase caused by thermal expansion of the gases. In the stainless steel tubing experiment previously described, the magnitude of the volume change due to thermal expansion was measured. The increase in volume was found to cause an outward flow of gas at a rate of 0.006 cc per second during the 12-1/2 minute heating cycle. If it is assumed that the 2000°F temperature is only that of the center one-inch length of the specimen and that the surface of this length is the entire surface of the test specimen, the point where the outward flow is observed to start during the re-entry cycle would identify the point where the leakage rate would be equal to the expansion rate of the gas; in other words, 0.006 cc/in.²/sec.

During the cooling cycle, the contraction of the gases makes it appear that the specimen is leaking at an insignificantly higher rate than it actually is. While it is obvious that a true leak rate can be measured only when the temperature is constant, the error introduced by neglecting this effect is small in our apparatus due to the smallness of the thermal expansion in relation to the size of the leakage rate of interest.

Error from another source is possible. During the heating cycle, the coatings tested in our program give off volatile products. While it is easy to show that there is a volume increase in the inflation gases due to these volatile products, it is difficult to determine their quantitative effect on a time basis. It is believed that for the purposes of determining a leak temperature and the order of magnitude of the leakage rate, this effect can be neglected.

I would now like to tell you how the cylindrical test specimens are made (see Figure 7). The first step in their fabrication is the welding of metal cloth to

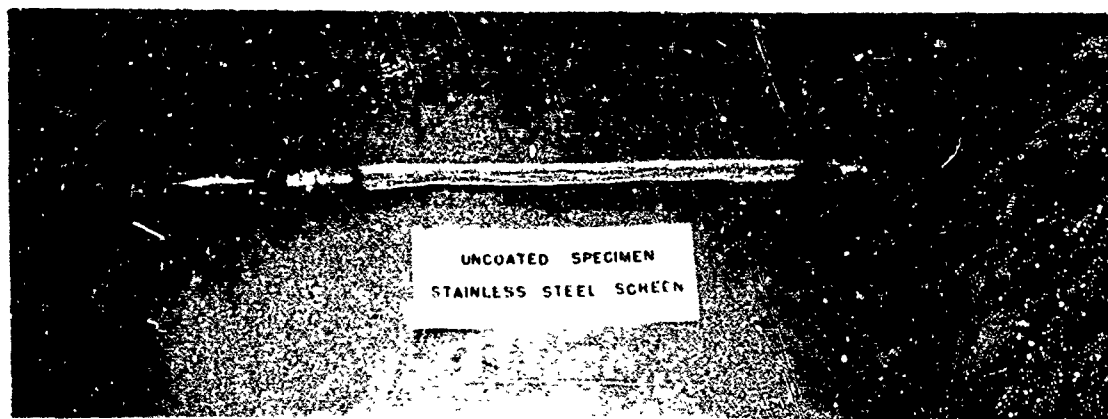


Figure 7. Uncoated Specimen

form a 3/8-inch diameter cylinder. This is accomplished using a jig designed and built by Goodyear Aerospace Corporation. While such factors are adjustable, we used a lapped seam having two weld lines 3/16 inch apart with each line consisting of 25 welds per inch.

In the second step of the cylinder fabrication, a 6-1/2 inch long piece of 3/8-inch diameter copper tubing is attached to each end of a 10-inch long piece of the metal cloth cylinder. A 1/2-inch long joining area is covered with a 1/4-inch length of 1/2-inch diameter copper tubing. This metal cover serves as a clamp to hold the cloth on the end of the 3/8-inch diameter copper tubing. It also acts as a heat sink during silver soldering. It would, in fact, be very difficult to make a gastight seal at the end joints and at the same time not burn a hole in the metal cloth if it were not for these external pieces of copper tubing.

After silver soldering, which is accomplished using an acetylene torch, excess soldering flux is removed with steam. The cleaning operation is completed with dichloroethylene degreasing solvent. After one hour in the solvent, the specimen is placed in a drying rack and allowed to air dry at ambient conditions.

The coating to be tested is applied by painting. Variable drying and vulcanization procedures were used that were dictated by the chemical nature of the coatings.

Figure 8 shows a finished specimen. The coating you see here is a 50/50 weight mixture of sodium silicate and silica.

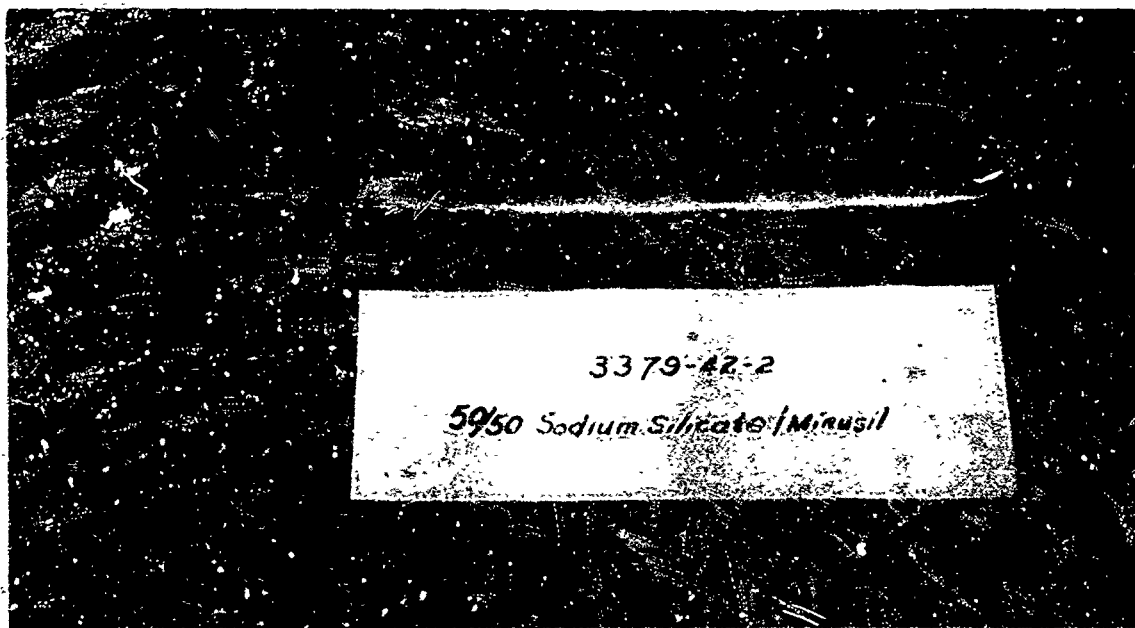


Figure 8. Coated Specimen

Using such test methods as have been described, more than 200 coatings have been evaluated, some of which were found to have interesting characteristics. These are coatings of sodium silicate reinforced with infusible fillers of several types, silicone rubber coatings containing fusible fillers, and coatings made from elastomeric ablative insulation containing fusible fillers.

A large amount of time was devoted to testing of coatings that used soluble silicates as binders. Such coatings attracted considerable attention because they were unique among the coatings; unique in that, neglecting the volatile water which is essential to achieving adequate flexibility, they were composed of materials that were chemically stable in the re-entry environment. It is now known that, unfortunately, the higher water solubility of these silicate coatings will restrict, if not completely prevent, their use.

The data in Table I shows the effect of various humidities upon a soluble sodium silicate coating at room temperature. The sodium silicate used is one that is commercially available and has a NaO_2 : SiO_2 ratio of 1:2. In the re-entry environment, this silicate reinforced with various filaments fails at a variety of temperatures depending upon the moisture content of the coating and the degree of exposure of the cold coating areas of the specimen to moisture driven from the coating areas heated to temperatures above 212°F . Data illustrating this is given in Table II. You will note that the completely unprotected coating leaks abruptly at 212°F when the coating contains 12 percent or more water. The drier but brittle coatings fail at higher temperatures. A flexible coating protected in the cold areas by a silicone rubber coating fails at higher temperatures. Inspection indicated that the leakage was along a path between the silicone rubber coating and the silicate coating.

Figure 9 shows the foam-like appearance of the moisture-blown silicate coatings after testing.

TABLE I
EFFECT OF ATMOSPHERIC MOISTURE ON A
SOLUBLE SILICATE COATING

Salt in Saturated Solution	Approximate Relative Humidity (%)	Condition of Coating	Moisture Content of Coating (%)
Sodium Sulfate	95	Liquid	Not measured
Ammonium Sulfate	81	Liquid	Not measured
Calcium Nitrate	51	Elastomeric	30
Calcium Chloride	31	Brittle	10

TABLE II
SODIUM SILICATE COATINGS CONTAINING
SILICA FILLER

Description	Leakage Temperature (°F)
Dry to 30% moisture	210
Dry to 12% moisture	210
Dry to 7.5% moisture	320
Dry to 5% moisture	400
Dry to 2.5% moisture	520
Ends, moisture barrier coated	1120
Ends, moisture barrier coated	2000

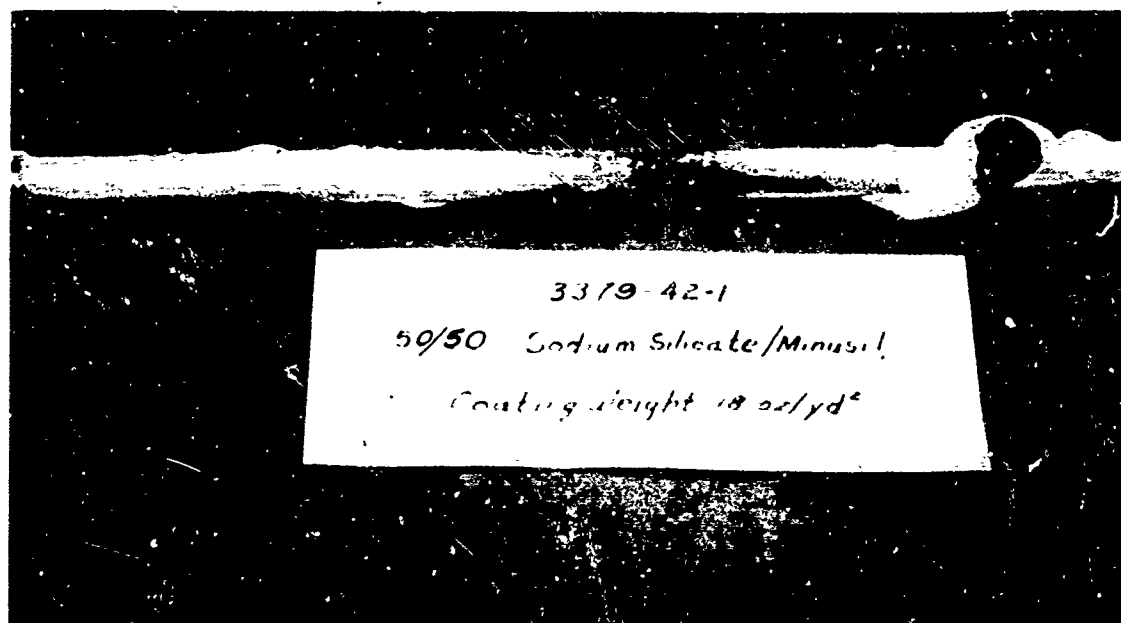


Figure 9. Sodium Silicate Coating after Test

Elastomeric ablative insulation might offer special advantages if its use would delay the time that peak skin temperature is reached and/or lower the peak skin temperature. Such compositions can, we believe, be made to have high leak temperatures. Data supporting this point of view are given in Table III. The high leak temperatures were achieved by the use of glass frits. The large amount required for 2000°F protection causes the coating to be undesirably stiff, however.

Silicone rubber of a special type combined with glass frit has long been recognized as a combination that has promise for expandable re-entry structures. Such coatings have been investigated in this program. They are considered to be the most promising of the coatings studied. Some of the data that have been obtained are given in Table IV to illustrate two important properties of these coatings. The first is that the coating weight necessary to obtain low leakage may be as high as 15 oz per sqyd when this coating is used in combination with an open-weave cloth. The second fact is that for reasons as yet not completely understood, this coating leaked during the re-entry heating cycle when air was used as the test atmosphere rather than the non-oxidizing nitrogen atmosphere normally used in this test program.

It is unfortunate that I must stop this discussion here. The final chapter of the story must await the publication of the final report covering this research. I urge you to read this report when it is published as a TDR in October. That a superior coating composition will be disclosed in this report is a distinct possibility.

TABLE III
NITRILE RUBBER
ELASTOMERIC ABLATIVE INSULATION

Description	Coating Wt (oz/yd ²)	Leakage Temp (°F)	Max Leak Rate (cc/sec)
Containing 75 % frit	11.6	>2000	0.13
Containing 50% frit	14.9	940	>7
Containing 25% frit	12.1	900	>7

TABLE IV
SILICONE RUBBER COATINGS*
CONTAINING GLASS FRIT

Coating Wt (oz/yd ²)	Leakage Temp (°F)	Max Leakage Rate (cc/sec)	Test Atmosphere
11.9	After Folding	> 7	Nitrogen
13.6	> 2000	0.16	Nitrogen
15.1	> 2000	0.24	Nitrogen
15.6	> 2000	0.12	Nitrogen
17.3	> 2000	0.06	Nitrogen
12.5	2000	> 7	Air
18.4	2000	> 7	Air
13.1	2000	> 7	Nitrogen/Air

*Dow Corning S2077 with equal weight (dry basis) Harshaw Chemical AW-35 on 200-mesh stainless steel screen.

ACKNOWLEDGMENTS

This report was prepared by The Goodyear Tire and Rubber Company and covers the work under Contract No. AF 33(657)-11257. This contract was initiated under Project No. 7320, "Fibrous Materials for Decelerators and Structures," Task No. 732002, "Fibrous Structural Materials." The work was administered under the direction of the Air Force Materials Laboratory, Research and Technology Division, Air Force Systems Command, with 1/Lt R. C. Cutright of the Elastomers and Coatings Branch acting as project engineer.

The Battelle Memorial Institute, a principal subcontractor, conducted the feasibility studies concerning inorganic coatings, chemical vapor deposition, and new elastomers.

"DUAL WALL INFLATABLE STRUCTURES FOR SPACE ORIENTED APPLICATIONS"

Herbert Q. Bair, Chief Engineer
Air Inflatable Products Corporation, East Haven, Connecticut

and

William H. Fischer, Technical Director
Air Inflatable Products Corporation, East Haven, Connecticut

(For presentation at the Second Aerospace Expandable
Structures Conference, Minneapolis, Minnesota, May 1965.)

INTRODUCTION

The problem of protecting high frequency radar antennas without degrading transmission or adding weight has led to the development of the wing tab technique. Dual-wall air-supported structures using the wing tab technique were pioneered and developed by Air Inflatable Products Corporation, a subsidiary of the National Union Electric Corporation. In wing tab construction, the attachment flange for the web is an integrally-woven portion of the skin material, thus stress concentrations are virtually eliminated. The ratio of the web width to web spacing has been established for equal loads in all members and may be varied to obtain specific characteristics in special applications.

The wing tab is especially applicable in structures, such as radomes, where the unit must be more stable, lighter weight, more versatile, and have less transmission interference than a single-skin unit. Such a unit is virtually self-erecting and may even be employed to erect the equipment being housed. In addition, individual sections of such a unit may be deflated and lowered, or raised, to permit easy movement of large equipment into or out of the area. Wing tab construction is currently being utilized on Contract No. DA-39-AMC-03744(s) for the Hughes Aircraft Company ComSat Satellite Radomes.

The geometry of wing tab structures may be readily varied and easily contoured in three planes at the same time. Since the materials are light and flexible, the structures are easily packaged and shipped. For example, a radome designed to withstand winds to 110 mph, 38' in diameter by 40' high, with an inside volume of 36,000 cubic feet, weighs less than 1800 $\frac{1}{2}$ and can be packed into less than 120 cubic feet. This radome also provides excellent insulation since it is essentially a rigid dead-air space thirty inches thick.

The ease with which a single radome panel is self-erecting is shown in Figure number 1. This multiple exposure shows the erection of a panel using only air pressure in the wall with no additional assistance.



Figure 1

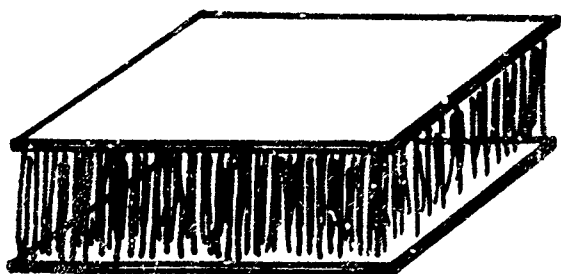
Currently, the materials used in wing tab structures range from the commonly-employed chloroprene-coated nylons and dacron to Kynar-coated fracture-resistant fiberglass, including metallized fibers for RF shielding. The horizontal web construction discussed here also lends itself to rigidization since, after erection, the unit is somewhat compartmentalized and therefore helps distribute any rigidizing material.

Potential uses for this type of structure include: radomes for satellite tracking stations; environmental control areas; housing or operations shelters; moon or planetary shelters; orbital repair or maintenance structures; etc. The unique features and advantages of dual-wall structures have been proven - - - opening new areas of operation to inflatable structures.

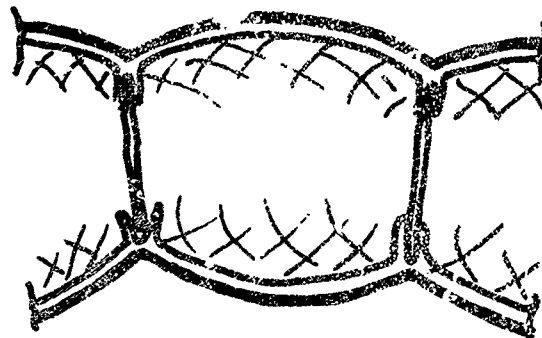
DUAL WALL CONCEPTS

The two main dual wall constructions are pile fabric and "Wing tab" or I-Beam ribs. Pile fabric, called "Airmat" by Goodyear and "Rigidair" by Air Inflatable Products Corporation, is basically a drop stitch fabric with threads tying two parallel faces together. The thread lengths are controlled to maintain a predetermined distance between the two plies of fabric. Wing tab fabric incorporates attachment flanges for the web as integrally-woven portions of the skin material. Two skins of this material, spaced by webs attached to the attachment flanges, form a dual-wall structure which provides adequate protection using a minimum of materials that interfere with the radar transmission. In general, wing tab fabric looks like a large air mattress with I-Beam webs holding the two surfaces parallel, but wing tab construction distributes the stress evenly. There is no possibility of stress concentrations by I-Beams or cross members.

Wing tab construction allows shaping of the structure into compound curves, such as spheres. The webs are contoured to provide the desired contour in their plane; varying the web spacing between the two surfaces provides the contouring in that plane.



RIGIDAIR



WING TAB

Figure 2

Since Goodyear is currently doing a great deal of development work on pile fabric, this presentation will be restricted to "Wing tab" construction. Wing tab utilizes an outer and inner skin of air-tight fabric with these skins held in position relative to each other by webs. The webs need not be air-tight since they only space the skins relative to each other and are not an air barrier. The webs can be either horizontal or vertical depending upon the structure configuration and operational requirements.

In radomes, the webs are usually horizontal for self erection, lifting capacity (to help erect the radar), and easy access (large sections of the wall open, permitting movement of large equipment into or out of the area). A dual wall radome (which is sectionalized into a number of easily transportable and handled components) can operate with alternate sections inflated, thus permitting a deflated portion to be raised as a large access opening for the removal or addition of equipment. In an eight section radome, it is possible to raise as many as three adjacent panels at one time for accessibility to the interior with the structure still remaining stable.

On the current contract for radomes, the inside dimensions are 60 feet in diameter by 54 feet high. The sections of these radomes are fastened together by a series of catenary panels along the walls and are under considerable compression when fastened together. This prevents any movement between sections as long as the operating pressure is maintained above six inches of water (up to a 100 knot wind). A static coefficient of friction of 1.3 between the surfaces has been attained and a compression of five inches for each face of the unit is used. This provides for a better than 26 inch flat contact between the panels. Thus the radome is one unit and may be treated as such relative to its resistance to torque and other extraneous loadings. A photograph of this assembly is included as Figure No. 3 for reference.

Previous tests indicate that the base angle of the radome should be at least 52° for stability without raising the pressure over that of the velocity pressure of the wind; this rule has been followed on the radome for the Comsat network, for example. The guy lines are only protection against excessive deflection, as opposed to actual support to fasten the radome to the ground. The radome will withstand 100 knot winds, $20\frac{1}{2}$ lb./ft.² snow load, 3" per hour rainfall and one-inch rime ice load. The guy cables are designed to withstand a 57 knot wind each while carrying the entire wind load against the structure. This provides for a more than adequate safety factor, since no one guy wire should be carrying the wind load independently.

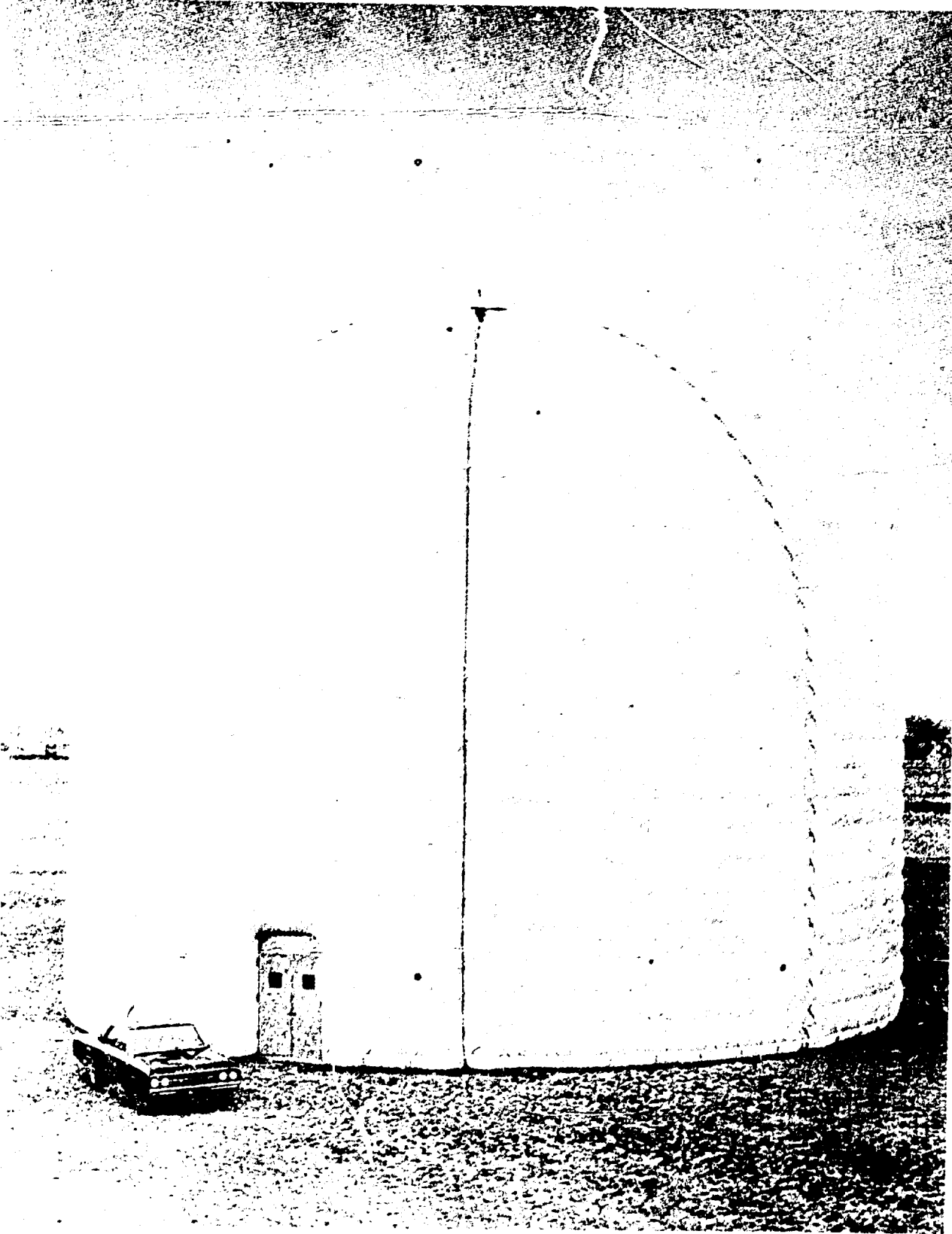


Figure 3

GENERAL DESIGN PARAMETERS

$A_{max} = 58"$ (Based on current weaving equipment capability.)

$L/W = 0.577$ (Not mandatory but used for equalization of stresses.)

When $L/W = 0.577$, $L = R$ and
 $F_1 = F_2 = R \times P$ (Where P equals the internal operating pressure of the wall.)

Inside radome diameter = 15
 W

$L/C = 5.4$

$W_C = 2.273 C$

$R = \sqrt{(L^2 + W^2)}/4$

$A = 0.0349 R \phi$

$H = R - \frac{1}{2} \sqrt{4R^2 - L^2}$

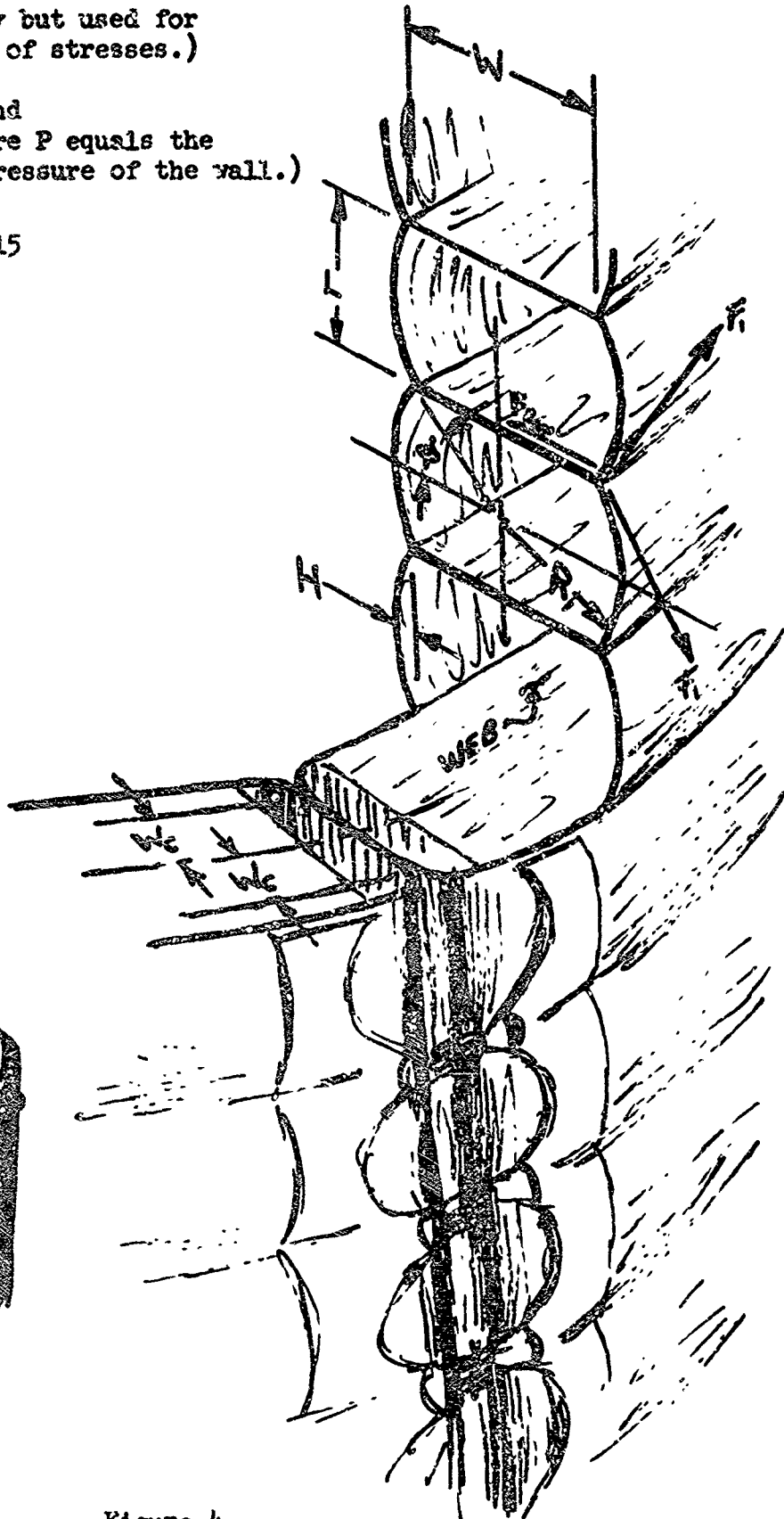
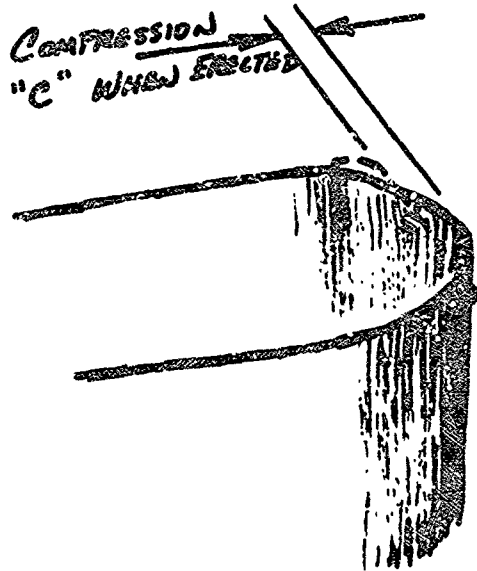


Figure 4

STRESS ANALYSES

As shown in Figure No. 4, the stresses involved in the wing tab and the outer skin are equal when L equals R. The stress in the fabric is then equivalent to the internal pressure in pounds per square inch times R or L as the case may be. To prevent deformation by wind loads the minimum operating pressure of the radome is as follows: $P = .00037V^2$ where P is pressure in pounds per square inch and V is the wind velocity in knots per hour.

Analysis of the load-lifting or load-carrying capabilities of the dual wall radome was conducted and confirmed by testing the initial unit. The equation evolved seems to omit radome size and wall thickness, but these are proportional and have been taken into account. The final equation is $D = .16\sqrt{W/P}$ where D is the diameter required to support the given load, W equals the load in pounds, and P equals the internal pressure of the unit in PSIG. This is based (see Fig. 5) on the premise that the load is lifted from a distance at least D over two below the point where the load is to be lifted, the maximum allowable deflection of the crown is one foot, and $R/W = 7.5$.

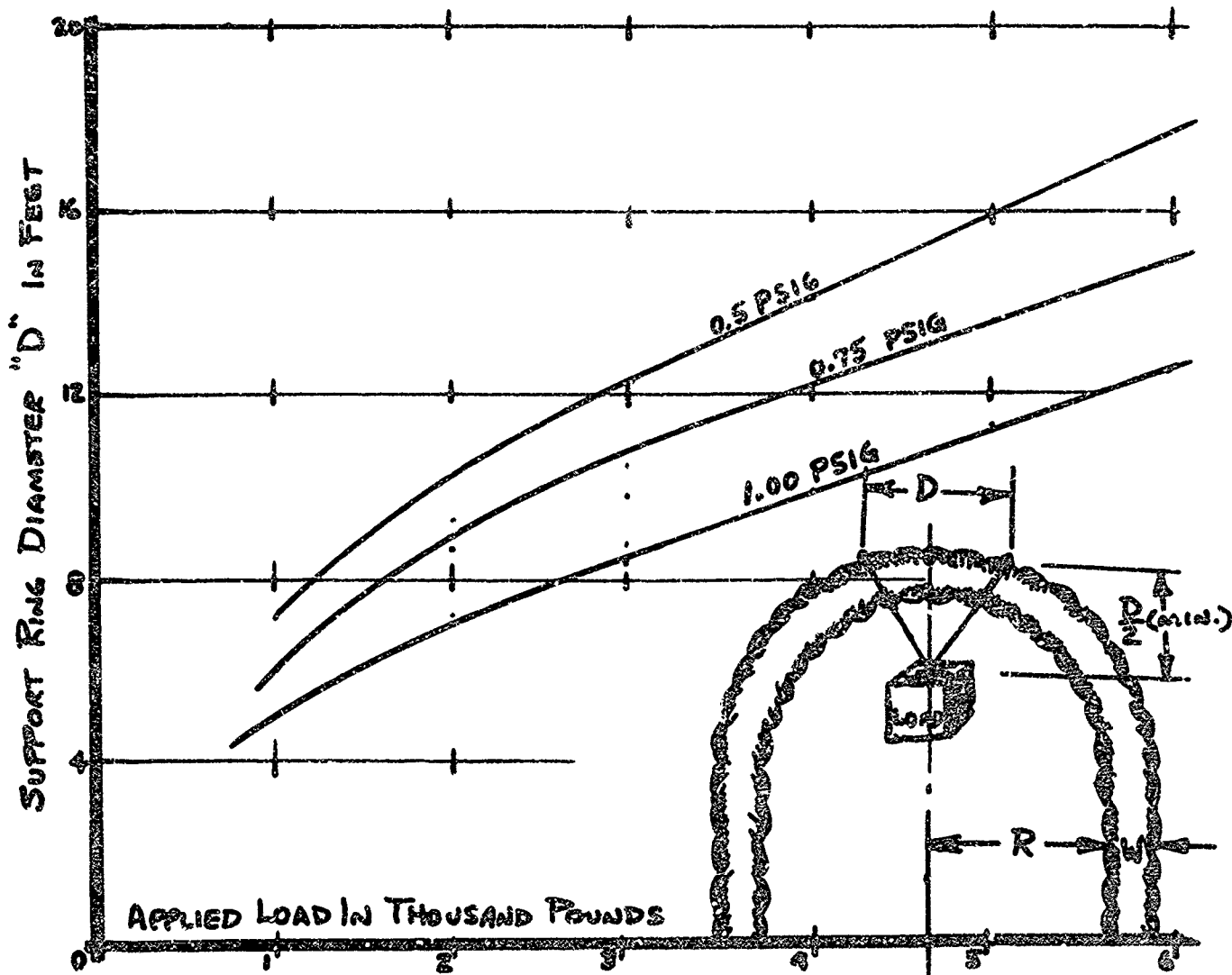


Figure 5

The maximum load lifting capability equals the projected horizontal area of the inflatable wall section at the largest diameter times the internal pressure. Of course the load-lifting capability at this point includes the weight of the radome itself. There could conceivably be some localized buckling of tubes in the areas to which the bridle is fastened (assuming it did not contain a continuous rigid ring) but, for the equation given, the shelter would support this load without collapsing or lowering the load. The radome for the Hughes Aircraft Company's ComSat system requires a lifting capability of approximately 2,000 pounds. In this unit there is a seven foot crown ring installed which can readily lift the required load at normal operating pressure.

Other applications have specified load lifting capabilities in the 5,000 to 6,000 pound range. For this, diameter D is extended to provide the required support.

The calculations for the operating pressure of dual wall radomes can be roughly simplified to $0.5 \times$ inside radome diameter \times pressure head caused by wind velocity equals fabric stress in #/inch. For single skin radomes this same type of analysis can be reduced to $3.32 \times$ (wind pressure head plus 0.5) \times radome diameter equals fabric stress in #/inch. These two equations are graphed in Fig. 6. The ratio of fabric stresses for the above equations is in the order of 1 to 7 depending on the wind velocity. Since the wind pressure is exponential with velocity, the ratio of the stresses for the radomes are also exponential relative to the maximum wind speed designed for.

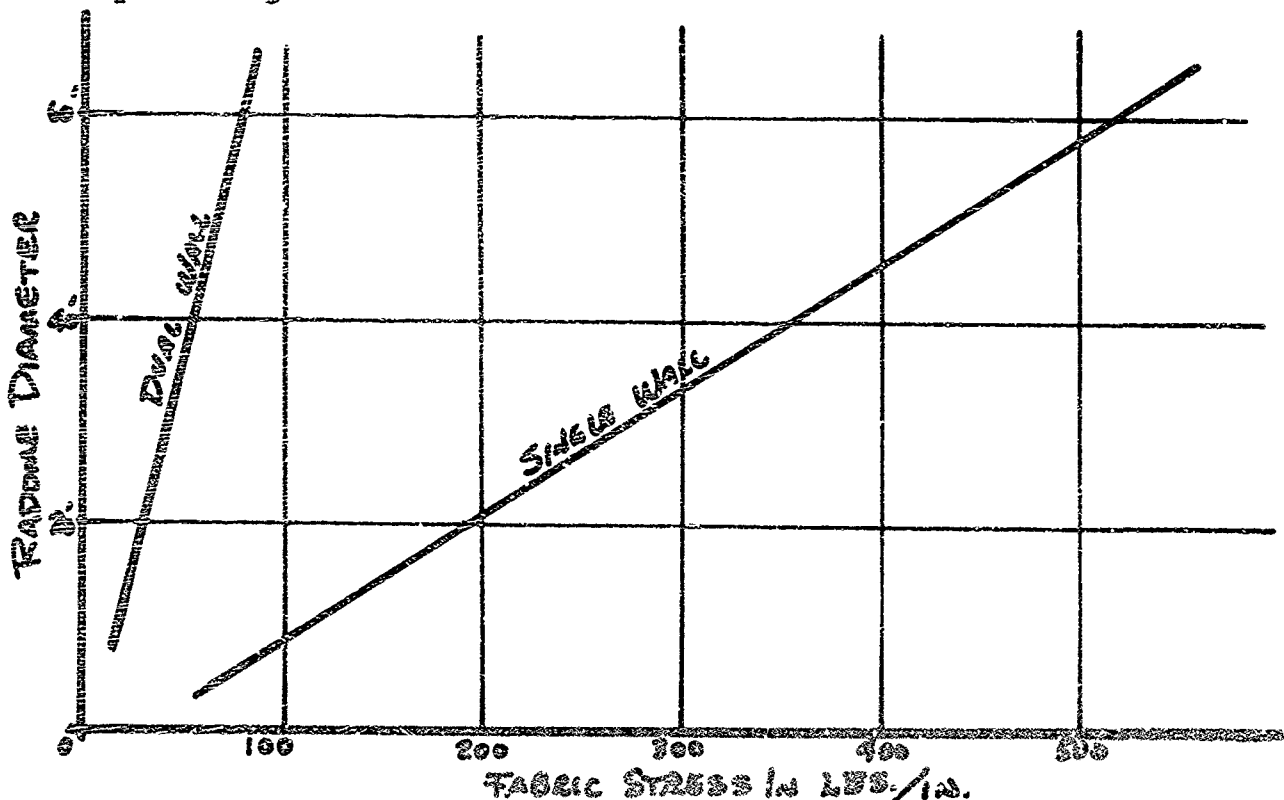


Figure 6

Advantages of dual wall over single wall include: the dual wall shelter can be easily reduced to small light-weight packages for easy handling and shipping; they provide for accessibility to the interior without airlocks; sections are readily replaceable and may be added for increased floor space; individual sections may be depressurized for repair and/or modification without putting the unit out of service; lighter weight fabrics can be utilized, thereby reducing total weight of the assembly; the unit is more versatile, since load-lifting bridles can be readily installed to lift virtually any load.

ELECTRICAL PROPERTIES

The electrical properties of dual wall radomes are very similar to single wall radomes in regard to the theoretical equations utilized to evaluate these properties. The equations are linearly related and are directly proportional to the number of plies of material utilized, the variations in the thickness of the material, the thickness of the fabric plies and the dielectric constant of the fabric. The equations are inversely proportional with the wavelength of the radar and the radius of the radar antenna.

Since the equations are virtually identical for single or dual wall assemblies, the only variables are fabric thickness, variations of fabric thickness, number of plies of material seen by the antenna, and the dielectric constant of the material.

A dual wall panel's webs introduce overall variation (thus producing a non-uniform wall for the antenna) therefore it appears that the single wall radome would give less boresight error. If extreme boresight accuracy is necessary, a single wall structure (assuming all other properties are equivalent) should be more accurate. But, boresight errors can be held to ± 0.10 milliradians with dual wall structures.

Pile fabric, from the tests performed on specimens of the fabric, exhibits excellent electrical properties due its uniformity. In essence, the pile is evenly distributed, as opposed to periodically spaced webs, therefore it gives more uniform transmission. Since the equations for boresight shift depend on thickness variations, this could be considerably reduced by using pile fabric but this could possibly cause related problems in regard to weight, packaging, and operating pressures. The above analysis was confirmed by tests on actual fabric specimens.

MATERIALS ANALYSIS

To provide a guaranteed life of at least seven trouble-free years, neoprene-coated dacron is used on the ComSat radome. Since dual wall structures use lighter fabric and need less elastomeric coating than a single skin structure for the same protection, a finer weave fabric and less elastomer may be used. This reduces the dielectric constant by 6.6%. Above a certain structure size, the coated fabric used for dual wall structures is less than half

as thick as for an equivalent single-skin unit. This then provides for better RF characteristics. Using the design ratio for the dual wall radomes, (the radome inside diameter divided by the wall-tube thickness equals 15) the dual wall radome theoretically provides identical protection with only 1/15 the fabric strength required of an equivalent single skin radome. Considering the stresses applied during erection and handling operations, this ratio is reduced to approximately 4 to 1. Currently, a dual wall radome which operates at a pressure of 1.48 PSIG requires a fabric strength of 160#/in. tensile which, coated, would not exceed .020" in thickness; a similar single skin radome would require fabric of 768#/in. tensile which would gauge .055". Approximately 20% less material is exposed to the radar antenna, even including the webs.

An advantage of dual wall radomes over single wall radomes is that wing tab dual wall fabrics have a standard carcass and coating on the exterior of the structure surface. This does not increase proportionally to the required strength, therefore a point is reached where the two plies of dual wall material are lighter in gauge thus exhibiting superior electrical properties to its single wall counterpart.

Figure No. 7 gives an indication of radome size to electrical properties by depicting the difference in the curve slopes of size to overall material gauge.

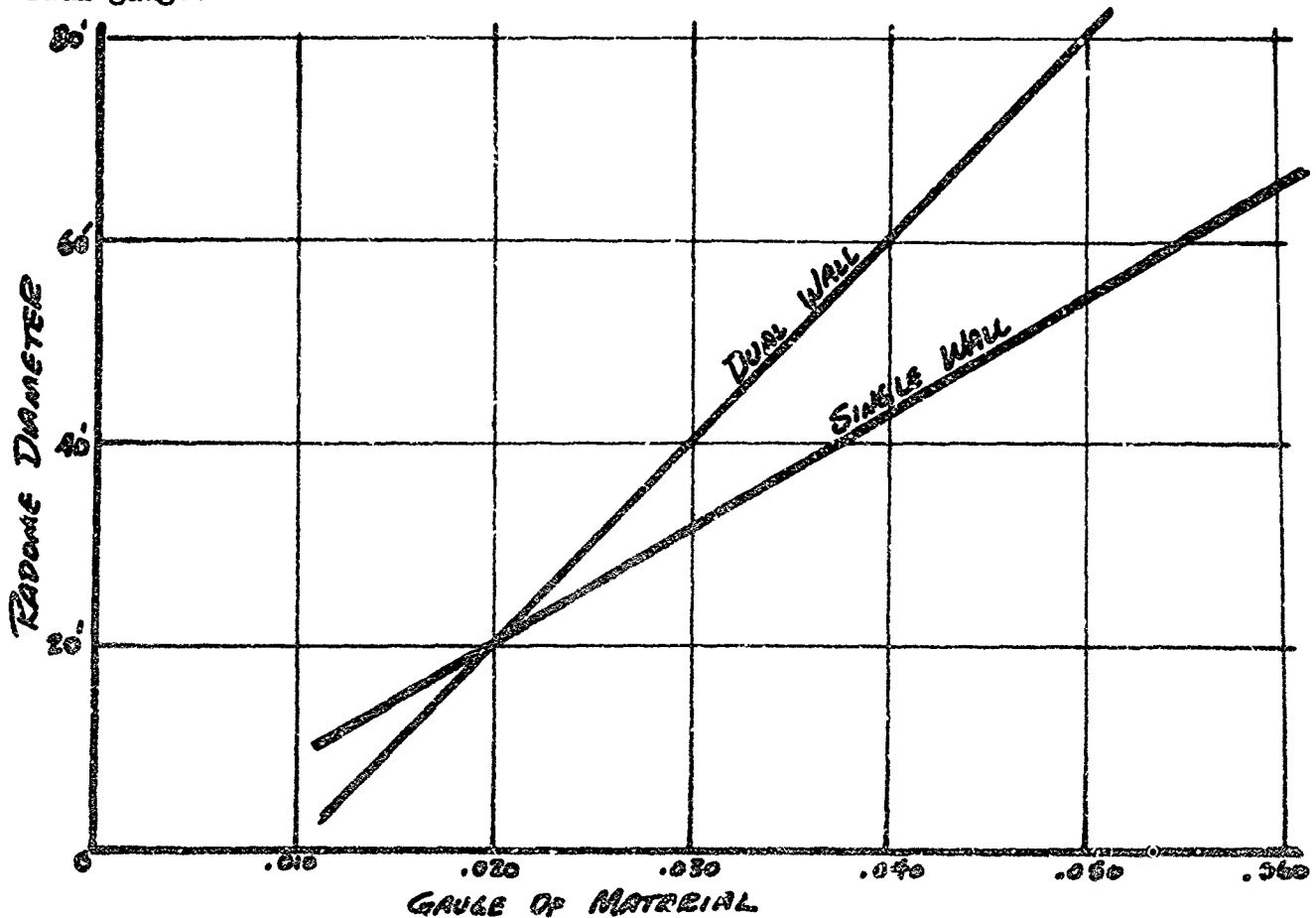


Figure 7

Dacron is chosen over Nylon due to its superior sunlight and UV resistance, excellent chemical resistance and higher melting temperatures. Neoprene is still the best all-purpose elastomer combining resistance to ozone, sunlight, oxidation and many petroleum derivatives; further, it has good resilience and tensile strength. A hypalon paint gives the surface color-stability, as well as weather and abrasion resistance.

The webs used for the ComSat radome are not coated with elastomer providing minimum material thickness for maximum transmissibility and minimum electrical interference. Similarly, seams in the webs have been sewn rather than cemented. The webs are bonded onto the integral wing tab as a final operation. Further, to maintain uniformity in the contours and stresses, the webs are segmentized to keep fabric fill threads within three degrees of the direction of the concentrated load application.

Experiments are currently being conducted to evaluate the possibility of using fracture-resistant fiberglass in higher temperature applications for longer life and better resistance to environmental hazards, including ultraviolet radiation. The Cordo Division of Ferro Corporation has been coating the glass filaments with vinyl (prior to weaving) for built-in chafing protection for the fibers. Work is also being conducted on laminating kynar film to the coated glass to provide maximum transparency (Ultraviolet light) with lightest weight. This technique is also under development with dacron.

Cordoglas-FR can take abuse and rough treatment since coating adhesion is mechanical rather than by adhesive primers that could break down during long term exposure. This material resists sunlight, weather, acids, mildew, and chemicals. It is also non-stretching and non-shrinking. Due to these characteristics and the use of glass fabric, seam wrinkles and puckers are virtually non-existent.

Tests show no degradation in breaking strength, even after two years outdoor aging. The heat-sealed adhesion and the tear strength degraded less than 5% for the same period. These materials are available in translucent and opaque colors with no sacrifice in UV degradation. The fabric is dimensionally stable with a minimum adhesion loss between the vinyl coating and the woven fiberglass substrate. At higher temperatures, silicone is used. With special compounding it has been used at over 1000 degrees Fahrenheit. The fabric substrate would then be fiberglass or metallic fibers depending on the operational requirements.

HEAT TRANSFER TESTS ON DUAL WALL RADOME OR WING TAB CONSTRUCTION

Wing tab panels have been tested to evaluate their thermal transmittance and to develop their "U" Factor. The tests were conducted on a panel three feet in thickness with the following result: the "U" factor is 0.41 BTU/hour/sq. ft./degree fahrenheit.

RF shielding tests conducted by York Research Corporation on specimens in which the fibers were plated with first copper then nickel, indicated a shielding effectiveness ranging from 80 db at .62 Mc to 50 db at 10,000 Mc, including a low point of 26 db at 15 Mc. These tests were conducted on specimens that were first metallized, then coated with neoprene.

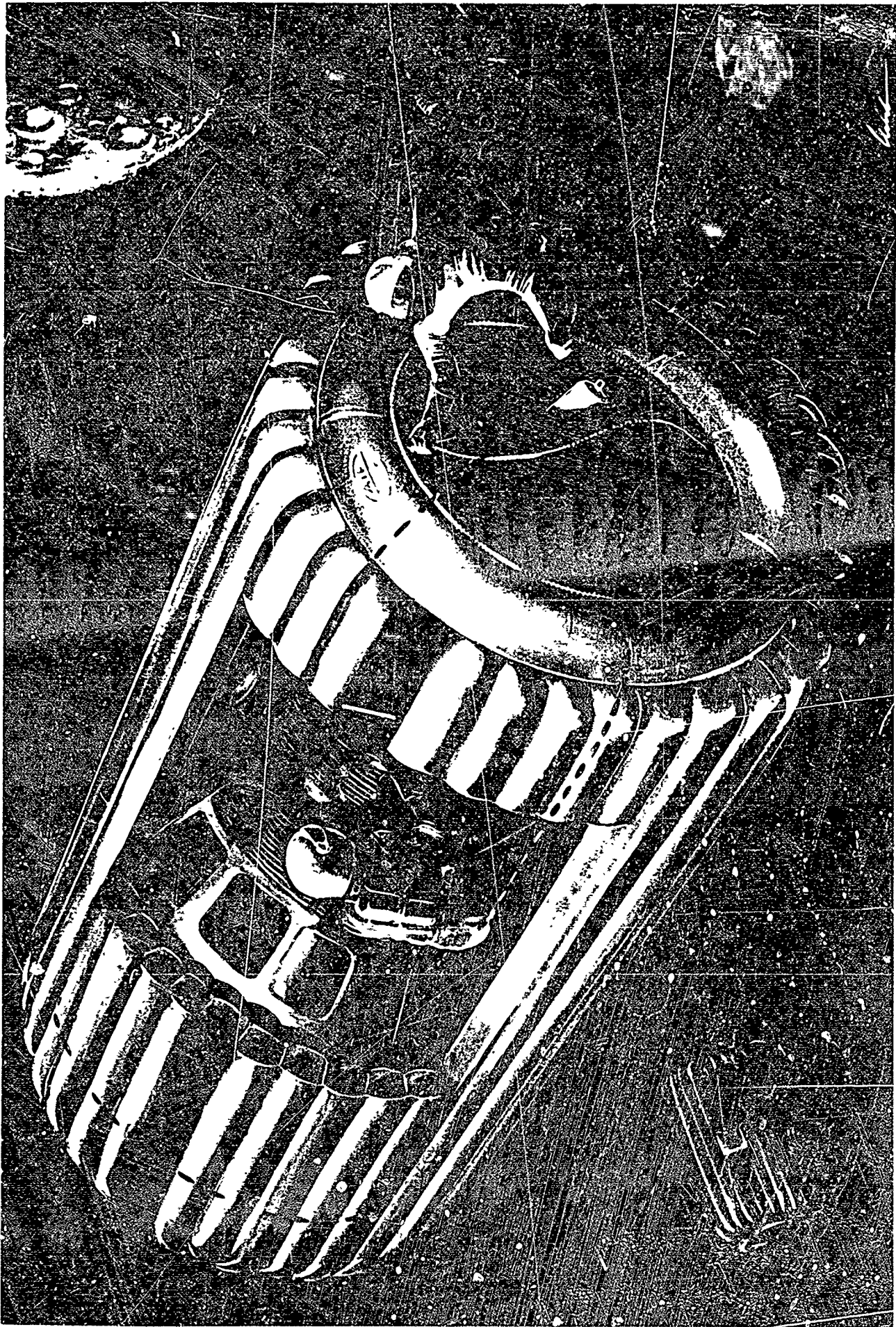
DESIGN CONCEPTS

A few applications of dual wall construction are as shown in the following six sketches with their description included on their respective pages. Dual wall structures (with possible rigidization included) are readily adaptable as emergency "repair garages" for orbiting space capsules or satellites. A pressure-sealing zippered end could be included for rapid entry with minimum effort and time.

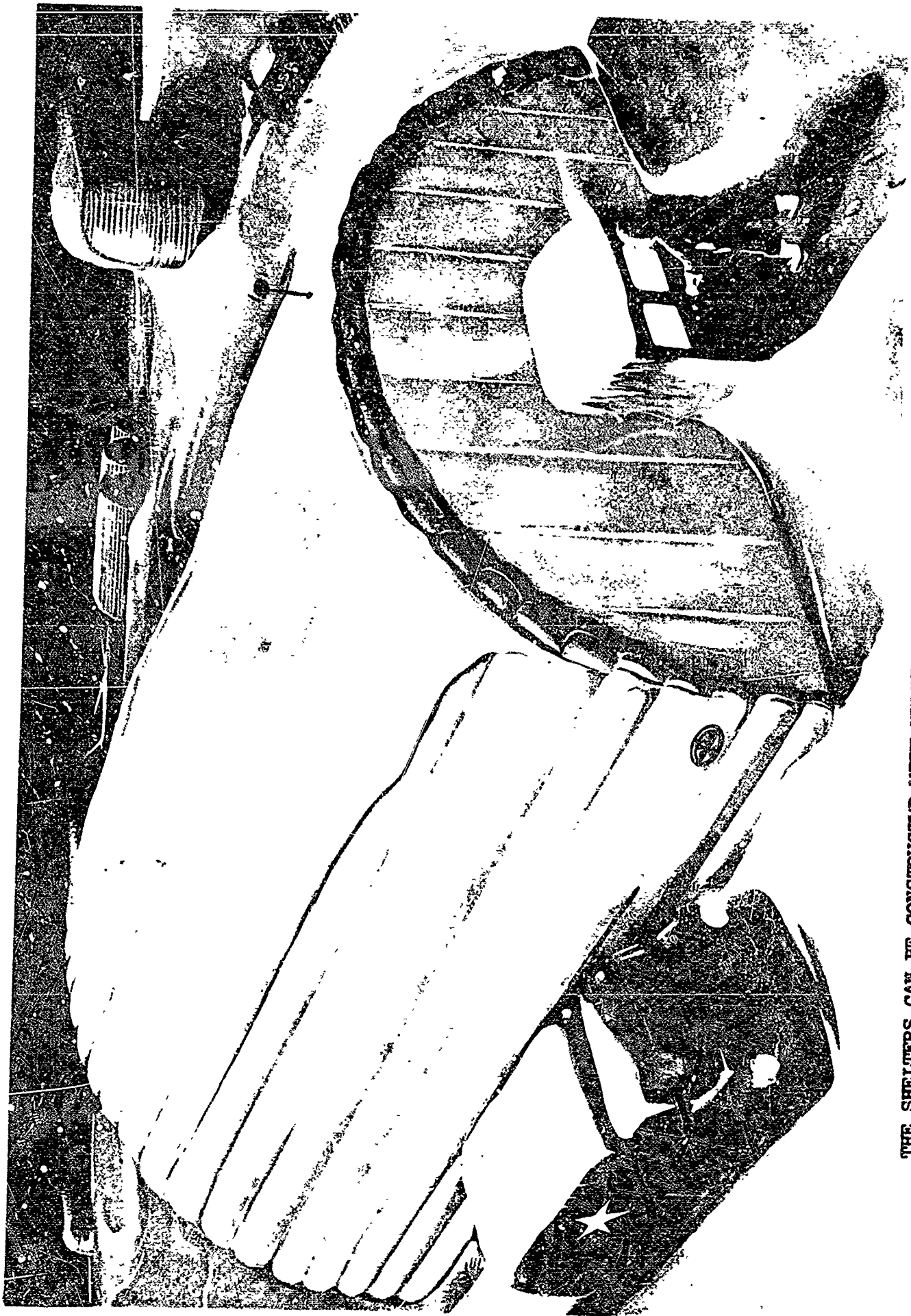
Another possible application of the wing tab dual wall structures is as an impact attenuator or support pad. The Impact Cushion Concept is currently being evaluated for sports activities such as a pole vaulters landing mat to replace the chopped or shredded sponge port-a-pit. Such a pad provides a much easier and improved landing, as the jumper cannot snag in a net or otherwise entangle himself.

A light-weight mat could be utilized for such things as landings on the moon, where it would spread out and distribute the load over an extended area (to overcome a possible dust layer or soft surface which would not support the concentrated load) thus providing, not only a support platform, but a work area adjacent to the craft.

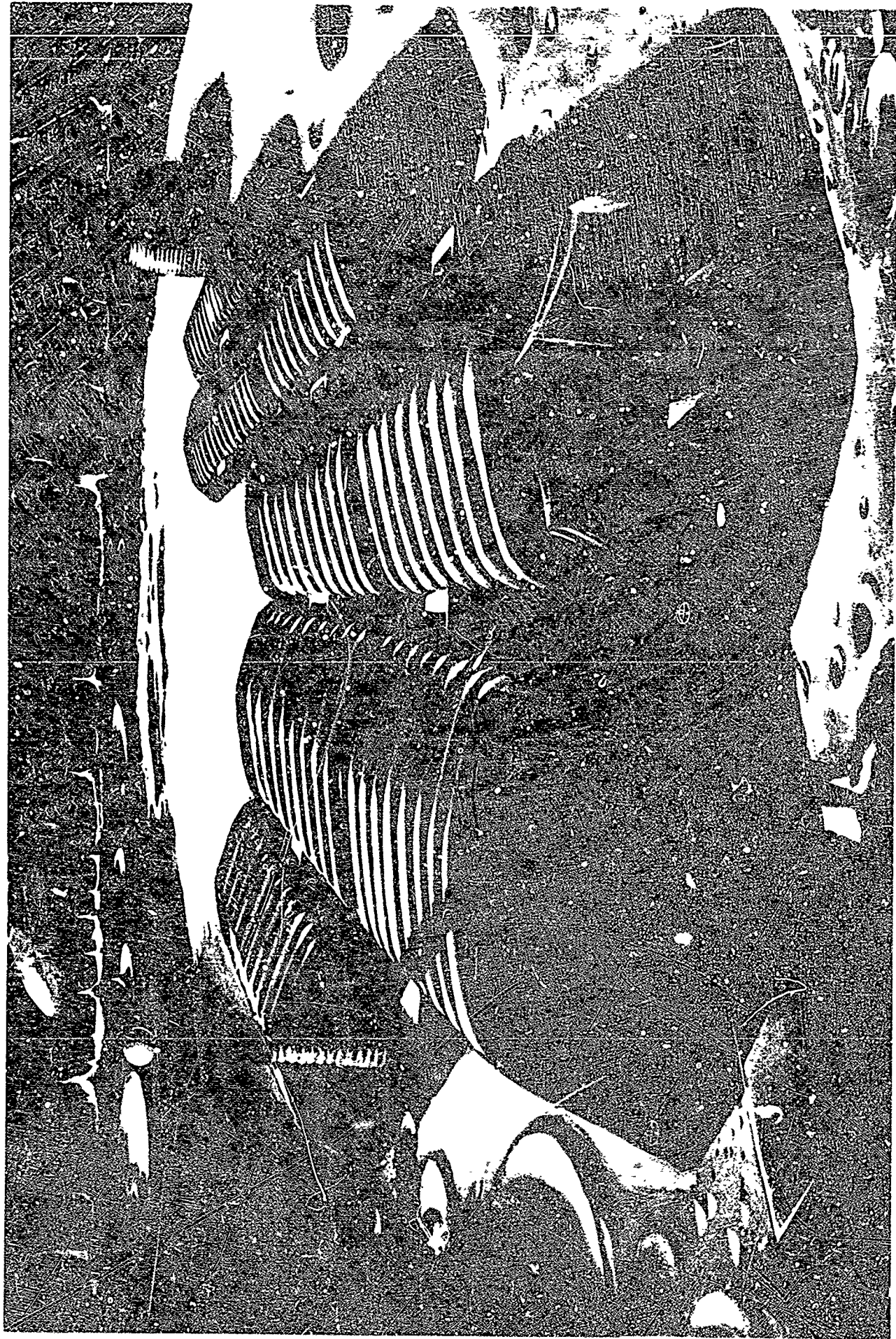
Dual wall wing tab could also be utilized in shelters for environment control, portable laboratories, greenhouses, and specialized applications such as RF shielded shelters. Potential uses are limited only by your own imagination.



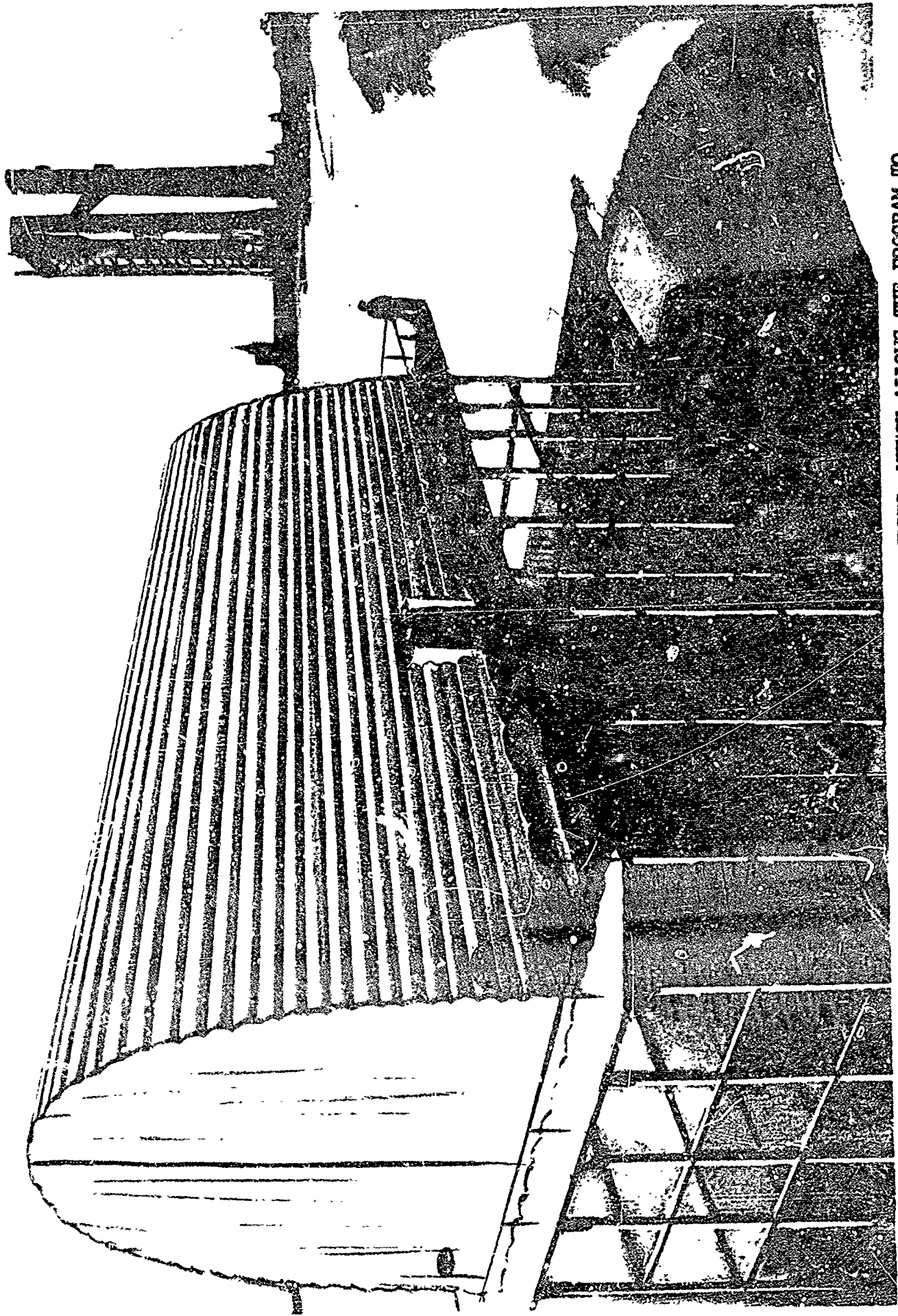
DUAL WALL STRUCTURES ARE ESPECIALLY SUITED TO USE IN OUTER SPACE BECAUSE THEY NEED LITTLE AIR TO INFLATE THEM COMPARED TO THE SINGLE SKIN STRUCTURES. THE DUAL WALL STRUCTURES ARE ALSO SUITED TO RIGIDIZATION IN SPACE SINCE THE BASIC DESIGN PROVIDES EXCELLENT GUIDES FOR DISTRIBUTING RIGIDIZERS.



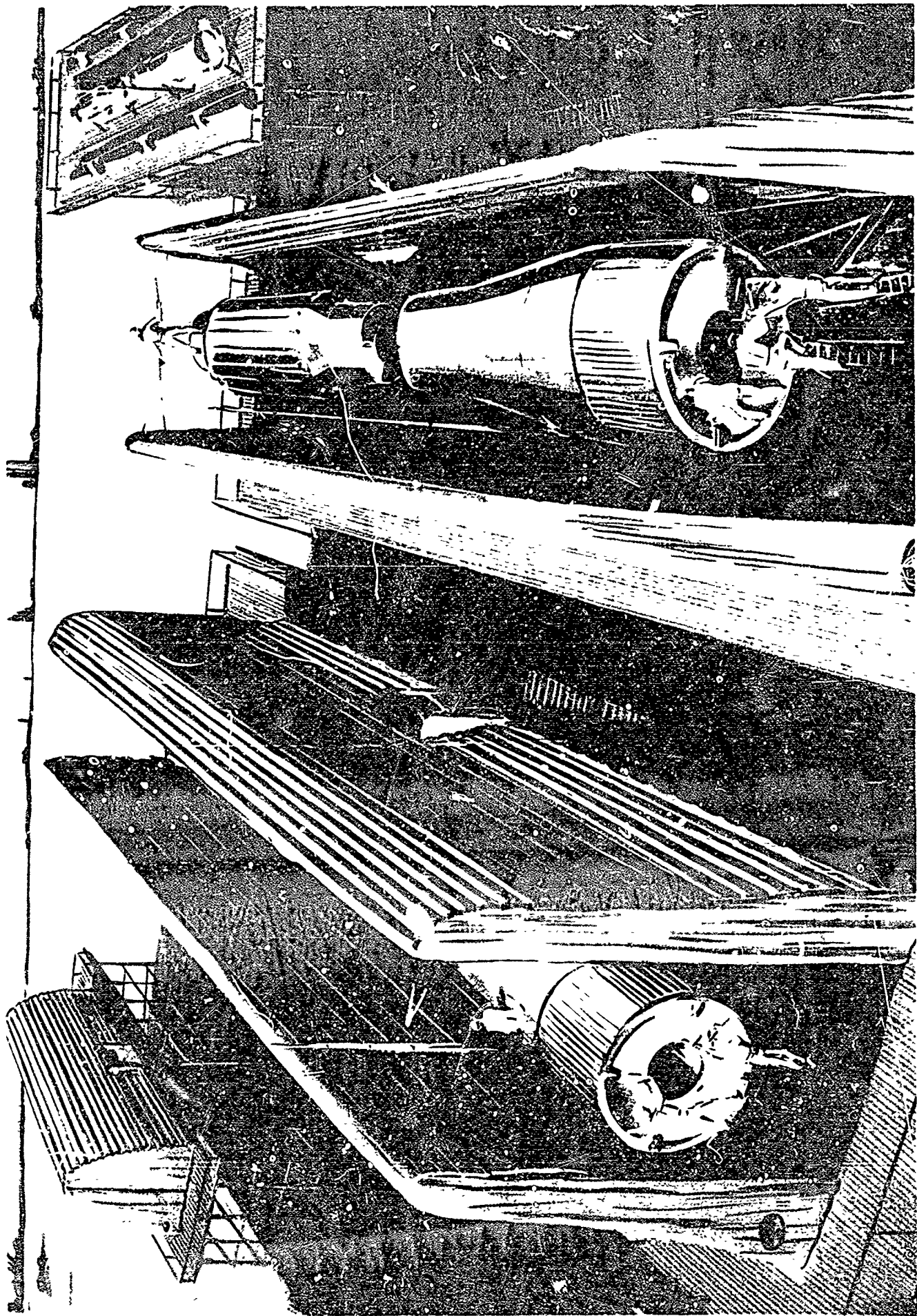
THE SHELTERS CAN BE CONSTRUCTED WITH VERTICAL OR HORIZONTAL WEBS, DEPENDING ON THE CHARACTERISTICS WANTED WITH HORIZONTAL WEBS SHOWN HERE. THE INSULATIVE QUALITIES OF THIS TYPE OF UNIT ARE FAR SUPERIOR TO MOST OTHERS MAKING IT SUITABLE FOR EITHER THE ARCTIC OR THE TROPICS.



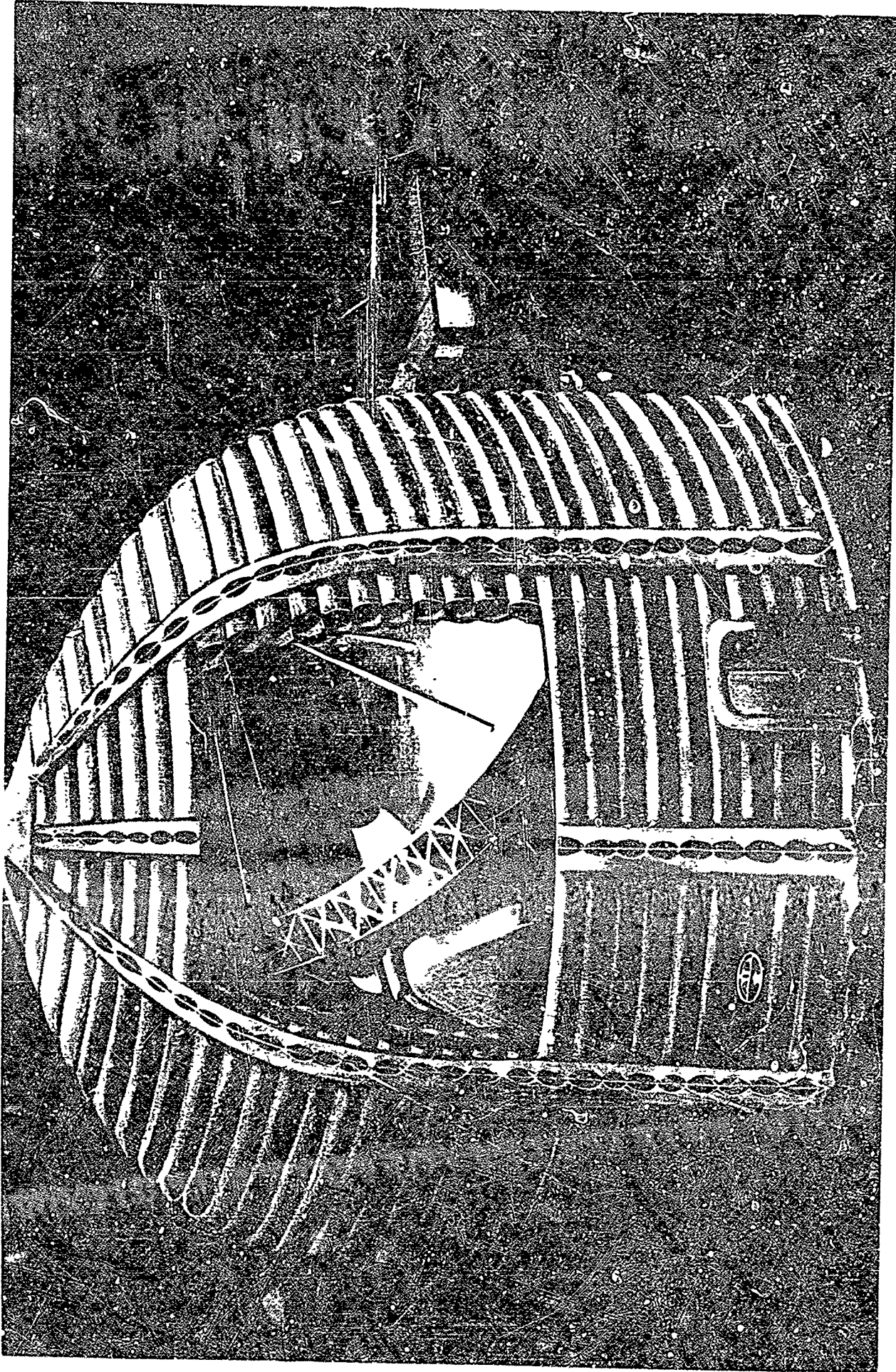
A CLUSTER OF UNIVERSAL SHELTERS POSSIBLY FOR USE IN SPACE OR ON THE MOON. THESE UNITS ARE INTERCHANGEABLE, CAN READILY BE DISCONNECTED AND USED AS INDIVIDUAL SHELTERS OR CAN BE JOINED TO FORM A LARGE COMPLEX. FOR OUTER SPACE WORK AN AIRTIGHT GROUND COVER AND INTERIOR PRESSURE, AS WELL AS THE PRESSURE TO SUPPORT THE STRUCTURE, ARE REQUIRED.



A TEST SHELTER FOR GROUND EXPERIMENTS AND PREFLIGHT TESTS, WHICH ALLOWS THE PROGRAM TO PROCEED DESPITE THE WEATHER. THE SHELTER IS ERECTED OR REMOVED WITHOUT ADDITIONAL EQUIPMENT. SPECIFICATIONS REQUIRE THAT THE UNIT MUST NOT COLLAPSE DURING REMOVAL OF THE SHELTER (REMOVAL IS EFFECTED WITHIN THIRTY MINUTES).



THE TEST SHELTER IN VARIOUS STAGES OF COLLAPSE IS PICTURED HERE. CONTROL OF THE AIR IN THE DUAL WALL ALLOWS DEFLATION BY COMPARTMENTS; THE SECTIONS ARE COLLAPSED OUT OF THE WAY WITHOUT DIFFICULTY.



THE RADOME UNDER CONSTRUCTION FOR THE COMSAT NETWORK IS DESIGNED FOR VERSATILITY, EASY-HANDLING AND RAPID ERECTION. THE COMPONENTS MAY BE ERECTED AROUND THE ASSEMBLED RADOME BUT IT IS EASIER TO ERECT THEM FIRST AND THEN ASSEMBLE THE RADAR INSIDE. THE EIGHT SECTIONS OR PANELS ARE SELF-ERECTING AND CAN BE DEFLATED AND RAISED TO ALLOW PASSAGE OF LARGE EQUIPMENT WITHOUT HINDERING THE OPERATION OF THE RADOME (ASSUMING THIS OPERATION TAKES PLACE WHILE THE WIND DOES NOT EXCEED 30 MPH).

UNCLASSIFIED

Security Classification

DOCUMENT CONTROL DATA - R&D

(Security classification of title, body of abstract and indexing annotation must be entered when the overall report is classified)

1. ORIGINATING ACTIVITY (Corporate author) Air Force Aero Propulsion Laboratory in Cooperation with Archer Daniels Midland Company, Minneapolis, Minnesota		2a. REPORT SECURITY CLASSIFICATION Unclassified	
		2b. GROUP	
3. REPORT TITLE SECOND AEROSPACE EXPANDABLE STRUCTURES CONFERENCE			
4. DESCRIPTIVE NOTES (Type of report and inclusive dates)			
5. AUTHOR(S) (Last name, first name, initials)			
6. REPORT DATE February 1966		7a. TOTAL NO. OF PAGES 802	7b. NO. OF REFS
8a. CONTRACT OR GRANT NO.		9a. ORIGINATOR'S REPORT NUMBER(S) AFAPL-TR-65-108	
b. PROJECT NO.		9b. OTHER REPORT NO(S) (Any other numbers that may be assigned this report)	
c.			
d.			
10. AVAILABILITY/LIMITATION NOTICES Distribution of this document is unlimited			
11. SUPPLEMENTARY NOTES		12. SPONSORING MILITARY ACTIVITY Air Force Aero Propulsion Laboratory Wright-Patterson Air Force Base, Ohio	
13. ABSTRACT <p>This report contains a presentation of technical contributions summarizing the status of current, significant research in the field of expandable structures. The report is based upon the discussions at the Second Aerospace Expandable Structures Conference held 25-27 May 1965 at the Lafayette Club, Minnetonka Beach, Minnesota. The subject matter has been arranged in six sessions in the order of presentation at the conference, followed by six papers which were not given at the conference.</p>			

Security Classification

<p>14. KEY WORDS</p> <p align="center">Expandable Materials</p> <p align="center">Structures for Reentry</p> <p align="center">Antennas</p> <p align="center">Solar Collectors</p> <p align="center">Space Stations</p>	LINK A		LINK B		LINK C	
	ROLE	WT	ROLE	WT	ROLE	WT

INSTRUCTIONS

1. **ORIGINATING ACTIVITY:** Enter the name and address of the contractor, subcontractor, grantee, Department of Defense activity or other organization (*Corporate author*) issuing the report.
- 2a. **REPORT SECURITY CLASSIFICATION:** Enter the overall security classification of the report. Indicate whether "Restricted Data" is included. Marking is to be in accordance with appropriate security regulations.
- 2b. **GROUP:** Automatic downgrading is specified in DoD Directive 5200.10 and Armed Forces Industrial Manual. Enter the group number. Also, when applicable, show that optional markings have been used for Group 3 and Group 4 as authorized.
3. **REPORT TITLE:** Enter the complete report title in all capital letters. Titles in all cases should be unclassified. If a meaningful title cannot be selected without classification, show title classification in all capitals in parenthesis immediately following the title.
4. **DESCRIPTIVE NOTES:** If appropriate, enter the type of report, e.g., interim, progress, summary, annual, or final. Give the inclusive dates when a specific reporting period is covered.
5. **AUTHOR(S):** Enter the name(s) of author(s) as shown on or in the report. Enter last name, first name, middle initial. If military, show rank and branch of service. The name of the principal author is an absolute minimum requirement.
6. **REPORT DATE:** Enter the date of the report as day, month, year, or month, year. If more than one date appears on the report, use date of publication.
- 7a. **TOTAL NUMBER OF PAGES:** The total page count should follow normal pagination procedures, i.e., enter the number of pages containing information.
- 7b. **NUMBER OF REFERENCES:** Enter the total number of references cited in the report.
- 8a. **CONTRACT OR GRANT NUMBER:** If appropriate, enter the applicable number of the contract or grant under which the report was written.
- 8b, 8c, & 8d. **PROJECT NUMBER:** Enter the appropriate military department identification, such as project number, subproject number, system numbers, task number, etc.
- 9a. **ORIGINATOR'S REPORT NUMBER(S):** Enter the official report number by which the document will be identified and controlled by the originating activity. This number must be unique to this report.
- 9b. **OTHER REPORT NUMBER(S):** If the report has been assigned any other report numbers (*either by the originator or by the sponsor*), also enter this number(s).
10. **AVAILABILITY/LIMITATION NOTICES:** Enter any limitations on further dissemination of the report, other than those

imposed by security classification, using standard statements such as:

- (1) "Qualified requesters may obtain copies of this report from DDC."
- (2) "Foreign announcement and dissemination of this report by DDC is not authorized."
- (3) "U. S. Government agencies may obtain copies of this report directly from DDC. Other qualified DDC users shall request through _____."
- (4) "U. S. military agencies may obtain copies of this report directly from DDC. Other qualified users shall request through _____."
- (5) "All distribution of this report is controlled. Qualified DDC users shall request through _____."

If the report has been furnished to the Office of Technical Services, Department of Commerce, for sale to the public, indicate this fact and enter the price, if known.

11. **SUPPLEMENTARY NOTES:** Use for additional explanatory notes.
12. **SPONSORING MILITARY ACTIVITY:** Enter the name of the departmental project office or laboratory sponsoring (*paying for*) the research and development. Include address.
13. **ABSTRACT:** Enter an abstract giving a brief and factual summary of the document indicative of the report, even though it may also appear elsewhere in the body of the technical report. If additional space is required, a continuation sheet shall be attached.

It is highly desirable that the abstract of classified reports be unclassified. Each paragraph of the abstract shall end with an indication of the military security classification of the information in the paragraph, represented as (TS), (S), (C), or (U).

There is no limitation on the length of the abstract. However, the suggested length is from 150 to 225 words.

14. **KEY WORDS:** Key words are technically meaningful terms or short phrases that characterize a report and may be used as index entries for cataloging the report. Key words must be selected so that no security classification is required. Identifiers, such as equipment model designation, trade name, military project code name, geographic location, may be used as key words but will be followed by an indication of technical context. The assignment of links, rules, and weights is optional.